AFRL-RQ-WP-TR-2012-0265

AIR VEHICLE INTEGRATION AND TECHNOLOGY RESEARCH (AVIATR)

Task Order 0023: Predictive Capability for Hypersonic Structural Response and Life Prediction: Phase II – Detailed Design of Hypersonic Cruise Vehicle Hot-Structure

Rob Quiroz, Jon Embler, Rich Jacobs, George Tzong, and Salvatore Liguore

The Boeing Company

FEBRUARY 2012
Final Report

Approved for public release; distribution unlimited.

See additional restrictions described on inside pages

STINFO COPY

AIR FORCE RESEARCH LABORATORY
AEROSPACE SYSTEMS DIRECTORATE
WRIGHT-PATTERSON AIR FORCE BASE, OH 45433-7542
AIR FORCE MATERIEL COMMAND
UNITED STATES AIR FORCE

NOTICE AND SIGNATURE PAGE

Using Government drawings, specifications, or other data included in this document for any purpose other than Government procurement does not in any way obligate the U.S. Government. The fact that the Government formulated or supplied the drawings, specifications, or other data does not license the holder or any other person or corporation; or convey any rights or permission to manufacture, use, or sell any patented invention that may relate to them.

This report was cleared for public release by the USAF 88th Air Base Wing (88 ABW) Public Affairs Office (PAO) and is available to the general public, including foreign nationals.

Copies may be obtained from the Defense Technical Information Center (DTIC) (http://www.dtic.mil).

AFRL-RQ-WP-TR-2012-0265 HAS BEEN REVIEWED AND IS APPROVED FOR PUBLICATION IN ACCORDANCE WITH ASSIGNED DISTRIBUTION STATEMENT.

*//Signature//

S. MICHAEL SPOTTSWOOD
Program Engineer
Sustainable Structures Branch

//Signature//

MICHAEL J. SHEPARD, Chief
Sustainable Structures Branch
Aerospace Structures Division

//Signature//

DAVID M. PRATT, Technical Advisor
Aerospace Structures Division
Aerospace Systems Directorate

This report is published in the interest of scientific and technical information exchange, and its publication does not constitute the Government's approval or disapproval of its ideas or findings.

*Disseminated copies will show "//Signature//" stamped or typed above the signature blocks.

REPORT DOCUMENTATION PAGE

Form Approved
OMB No. 0704-0188

The public reporting burden for this collection of information is estimated to average 1 hour per response, including the time for reviewing instructions, searching existing data sources, gathering and maintaining the data needed, and completing and reviewing the collection of information. Send comments regarding this burden estimate or any other aspect of this collection of information, including suggestions for reducing this burden, to Department of Defense, Washington Headquarters Services, Directorate for Information Operations and Reports (0704-0188), 1215 Jefferson Davis Highway, Suite 1204, Arlington, VA 22202-4302. Respondents should be aware that notwithstanding any other provision of law, no person shall be subject to any penalty for failing to comply with a collection of information if it does not display a currently valid OMB control number. **PLEASE DO NOT RETURN YOUR FORM TO THE ABOVE ADDRESS**.

1. REPORT DATE *(DD-MM-YY)*	2. REPORT TYPE	3. DATES COVERED *(From - To)*
February 2012	Final	01 September 2010 – 31 January 2012

4. TITLE AND SUBTITLE
AIR VEHICLE INTEGRATION AND TECHNOLOGY RESEARCH (AVIATR)
Task Order 0023: Predictive Capability for Hypersonic Structural Response and Life Prediction: Phase II – Detailed Design of Hypersonic Cruise Vehicle Hot-Structure

5a. CONTRACT NUMBER
FA8650-08-D-3857-0023

5b. GRANT NUMBER

5c. PROGRAM ELEMENT NUMBER
62201F

6. AUTHOR(S)
Rob Quiroz, Jon Embler, Rich Jacobs, George Tzong, and Salvatore Liguore

5d. PROJECT NUMBER
2401

5e. TASK NUMBER
N/A

5f. WORK UNIT NUMBER
Q068

7. PERFORMING ORGANIZATION NAME(S) AND ADDRESS(ES)
The Boeing Company
Boeing Research and Technology
5301 Bolsa Avenue
Huntington Beach, CA 92647

8. PERFORMING ORGANIZATION REPORT NUMBER

9. SPONSORING/MONITORING AGENCY NAME(S) AND ADDRESS(ES)
Air Force Research Laboratory
Aerospace Systems Directorate
Wright-Patterson Air Force Base, OH 45433-7542
Air Force Materiel Command
United States Air Force

10. SPONSORING/MONITORING AGENCY ACRONYM(S)
AFRL/RQSS

11. SPONSORING/MONITORING AGENCY REPORT NUMBER(S)
AFRL-RQ-WP-TR-2012-0265

12. DISTRIBUTION/AVAILABILITY STATEMENT
Approved for public release; distribution unlimited.

13. SUPPLEMENTARY NOTES
PA Case Number: 88ABW-2012-4343; Clearance Date: 09 Aug 2012. This report contains color.

14. ABSTRACT
Four panels from a representative Mach 7 hypersonic cruise vehicle were designed and analyzed with state-of-the-art standard methods and tools to verify structural response and life predictive capabilities. Several modifications were made to the Technology Experiment Vehicle (TX-V) to refine the structure and create a Mach 7 closed-concept configuration with an all-metallic, high-temperature airframe. Structural loads and environments from the TX-V were then used to size and design the four panels, and perform thermal, stress, acoustic, flutter, and fatigue analyses. An additional set of explicit dynamic analyses using an alternative method was performed on one of the four panels. Several analysis process and method findings based on these two analysis approaches are compared to previously identified knowledge gaps, confirming several while adding several more. The objectives of a validation test program are also reviewed, and a set of recommended test series are prioritized to best evaluate the accuracy of current structural response and life prediction capabilities.

15. SUBJECT TERMS
hypersonic, structural response, life prediction, structural analysis methods, explicit analysis, structural testing, combined environments, thermal analysis, stress analysis, acoustic analysis, flutter, fatigue, unit cell, flexible substructure, thermal loads

16. SECURITY CLASSIFICATION OF:			17. LIMITATION OF ABSTRACT:	18. NUMBER OF PAGES	19a. NAME OF RESPONSIBLE PERSON (Monitor)
a. REPORT	b. ABSTRACT	c. THIS PAGE			S. Michael Spottswood
Unclassified	Unclassified	Unclassified	SAR	762	19b. TELEPHONE NUMBER *(Include Area Code)* N/A

TABLE OF CONTENTS

1.0 EXECUTIVE SUMMARY 1
2.0 INTRODUCTION 4
2.1 Multi-Phase Program Overview and Objectives 4
2.2 Phase I – Identification of Knowledge Gaps 5
2.3 Phase II Program Overview 7
3.0 TECHNOLOGY X-VEHICLE REFINEMENT 9
3.1 Task 1 – Overview 9
3.2 Potential Solutions to "Close" the Design 11
3.3 Structural Sizing Results 13
3.4 Panel Sizing Results 15
3.5 Task 1 Summary 17
4.0 DETAILED PANEL DESIGN AND ANALYSIS 19
4.1 Task 2 Overview and Panel Selection 19
4.2 Detailed Design Approach 20
4.3 Panel 1 (862) Detailed Design 56
4.4 Panel 2 (780) Detailed Design 74
4.5 Panel 3 (816) Detailed Design 97
4.6 Panel 4 (1074) Detailed Design 122
4.7 Identified Detailed Design Process Limitations and Lessons Learned 142
5.0 VERIFICATION STUDIES 144
5.1 Panel Modeling and Validation 144
5.2 Panel Boundary Conditions and Vibration Analysis 145
5.3 Damping of Structure 148
5.4 Dynamic Explicit Analysis 150
5.5 Fatigue Life Prediction with Explicit Dynamic Analysis 170
5.6 Summary Knowledge Gap Related Findings 172
6.0 PHASE III TEST PLANNING 174
6.1 Background and Objectives 174
6.2 Testing Requirements 176
6.3 Test Facility Evaluations 178
6.4 Design Drivers and Test Recommendations 181
7.0 REVIEW OF PREDICTIVE CAPABILITY GAPS 187
7.1 Summary of Gaps Identified in Phase I 187
7.2 Confirmation of Phase I Gaps with Phase II Findings 188
7.3 Prioritized List of Revised Predictive Capability Knowledge Gaps 190
8.0 CONCLUSIONS 192
8.1 Technology X-Vehicle Refinement Conclusions 192
8.2 Detailed Design and Analysis Conclusions 192
8.3 Verification Study Conclusions 192
8.4 Phase III Test Conclusions 192
9.0 RECOMMENDATIONS FOR FUTURE WORK 194
9.1 Global Vehicle Loads and Sizing Recommendations 194
9.2 Detailed Panel Analysis Methods 194
10.0 REFERENCES 196

Approved for public release; distribution unlimited.

APPENDIX A: Panel 1 (862) Design and Analysis Package.....197
APPENDIX B: Panel 2 (780) Design and Analysis Package.....283
APPENDIX C: Panel 3 (816) Design and Analysis Package.....382
APPENDIX D: Panel 4 (1074) Design and Analysis Package.....528
APPENDIX E: Panel 1 (862) Verification Studies.....697

Approved for public release; distribution unlimited.

LIST OF FIGURES

Figure 1. This hypersonic cruise vehicle hot-structure design program provides actionable information for predictive capability development 1
Figure 2. Multi-phase program overview 4
Figure 3. Overview of Phase I 6
Figure 4. Overview of Phase II program tasks 8
Figure 5. TX-V Hypersonic Cruise Vehicle 9
Figure 6. Mach 7 Design Mission Trajectory 10
Figure 7. Temperatures for External Skin and Substructure 10
Figure 8. Modified TX-V Structure 12
Figure 9. Substructure Temperature Distribution 12
Figure 10. Modified Substructure Temperature Distribution 13
Figure 11. Baseline TX-V FEM Structural Sizing History 14
Figure 12. Modified TX-V FEM Structural Sizing History 15
Figure 13. Critical Panel Locations 16
Figure 14. Panel Concepts Investigated 16
Figure 15. Panel Unit Weights for Different Panel Concepts 17
Figure 16. Selected Panel Locations 19
Figure 17. Design and Analysis Flow for each panel 21
Figure 18. Unit cell boundary conditions 22
Figure 19. Temperature distributions for a bay cutout of the gloabl model (upper left) and the validation unit cell model (upper right), and a comparison of profiles through the depth (bottom) 23
Figure 20. Alternate sine-wave web and hybrid truss plus sine-wave substructure configurations 24
Figure 21. Panel 3 lofted unit cell surface geometry 27
Figure 22. Flight Trajectory 28
Figure 23. Thermal Model of Panel 2 and Temperature Distribution at t=2,520sec 31
Figure 24. Structural model of Panel 2 and temperature distribution at t=2,520 sec 31
Figure 25 Process flow to generate accurate loading and boundary conditions on the panel of interest 32
Figure 26. Inconel 718 material properties 34
Figure 27. Inconel 718 thermal knockdowns, Fty Ftu 35
Figure 28. Inconel 718 thermal knockdowns, E 36
Figure 29. Inconel 718 thermal knockdowns, G 36
Figure 30. Inconel 718 thermal knockdowns, μ 37
Figure 31. Simplified global vehicle load application to detailed unit cell 38
Figure 32. Example of global vehicle loads application to detailed unit cell 38
Figure 33. Rigid Body Motion unit cell Constraints 39
Figure 34. Example of Applied Loading for the Panel Level Analysis 40
Figure 35. Convection coefficient sensitivity to panel deflections into the flow 43
Figure 36. Trajectory Design Conditions 44
Figure 37. CFD++ Computed Flow Field 45
Figure 38. ADSAS Aero-acoustic Prediction 46
Figure 39. Historical Modal Structural Damping, ref AFWAL-TR-84-3089, Vol II 48

Approved for public release; distribution unlimited.

Figure 40. Example of empirically derived non-dimensional panel flutter 49
Figure 41. Aerodynamic model setup for piston theory flutter analysis..... 50
Figure 42. Plots of damping and frequency as a function of velocity for modes 1 and 2 of panel 4..... 51
Figure 43. Estimate of linear damage accumulation over a single flight..... 52
Figure 44. Acoustic fatigue margin of safety calculation for acoustic plus thermal stress 53
Figure 45. Process used in TMF margin evaluation for calculating a stress concentration at a fastener hole location 54
Figure 46. Free body loads calculation method from shell forces near a CFAST element 55
Figure 47. Best fit S/N curve used for thermal-mechanical fatigue life calculations (ref MMPDS-05 fig 6.3.5.1.8(c))..... 56
Figure 48 Location of Panel 1 (862) and the Corresponding unit cell..... 57
Figure 49. Corrugated core (top) and iso-grid (bottom) panel configurations 58
Figure 50. Ortho-grid panel configuration..... 59
Figure 51. Panel 1 unit cell 60
Figure 52. Panel 1 (862) Thermal Boundary Conditions..... 61
Figure 53. Panel 1 (862) Temperature Distributions 61
Figure 54. Panel 1 (862) Temperature Histories..... 62
Figure 55. Panel 1 (862) Temperature Gradients..... 63
Figure 56. Overlay of unit cell (Yellow) and global vehicle model (White/Blue) 64
Figure 57. The Stiffness of the Ortho-grid Skin Panels allow large deflections 65
Figure 58. Non-Linear Z-Component Deflection [in] Plot of Panel 1 (862) 66
Figure 59. Non-Linear Von Mises Stress [psi] Plot of Panel 1 (862)..... 67
Figure 60. 1st Buckling Mode [eigenvalue] of Panel 1 (862)..... 68
Figure 61. 2nd Buckling Mode [eigenvalue] of Panel 1 (862) 69
Figure 62. Condition Max Q, RMS Stress with listed Thermal Stresses, Details 71
Figure 63. Margin of safety calculation summary for Panel 1 acoustic fatigue 72
Figure 64. Free body diagram of FEM location with maximum bearing load 73
Figure 65. Calculated Ktσ at maximum bearing stress location 73
Figure 66. Location of Panel 2 (780) and the Corresponding unit cell..... 75
Figure 67. Panel 2 ortho-grid CAD model with 3” x 5” grid spacing 76
Figure 68. Panel 2 geometry with added stiffeners to reduce normal deflections 77
Figure 69. Panel 2 (780) Boundary Conditions 78
Figure 70. Panel 2 (780) Temperature Distributions 79
Figure 71. Panel 2 (780) Temperature Histories..... 80
Figure 72. Panel 2 (780) Temperature Gradients..... 80
Figure 73. Comparison of Thickness [in] for Surrounding Panels, Unit Cell for Panel 1 show uniform minimal thicknesses while Unit Cell for Panel 2 shows more variation in thickness 81
Figure 74. Comparison of Deformation Plots [in] Load case: Mechanical: 2.5g Ultimate (1.5), Unit Cell for Panel 2 shows minimal deflection compared to Unit Cell for Panel 1..... 82
Figure 75. Panel 2 (780) Panel Breakers (Highlighted in Blue) are Added to Reduce Flow-wise Deflection..... 82
Figure 76. Non-Linear Z-Component Deflection Plot [in] of Panel 2 (780) 83
Figure 77. Non-Linear Max Flow-wise Z-Component Deflection Plot [in] of Panel 2 (780)..... 84
Figure 78. Non-Linear Von Mises Stress Plot [psi] of Panel 2 (780)..... 85

Figure 79. Non-Linear Fastener Forces for Panel 2 (780) 86
Figure 80. 1st Buckling Mode of Panel 2 (780) 87
Figure 81. 2nd Buckling Mode of Panel 2 (780) 88
Figure 82. Unit cell view of constraints applied to static analyses compared to dynamic analyses 89
Figure 83. Panel 2 maximum principal stress fringe plot showing stress concentrated around panel stiffeners, 56.1ksi maximum stress 91
Figure 84. Plots of RMS Von Mises stress for Panel 2 and at maximum stress locations 92
Figure 85. Margin of safety calculation for maximum RMS stress on ortho-grid stiffener 93
Figure 86. Maximum stress location in Panel 2 skin with local free body diagram 94
Figure 87. Calculated stress at a worst case fastener hole in skin using detailed StressCheck FEM, Ktσ = 107 ksi (MS = 0.05) 95
Figure 88. Maximum stress location in Panel 2 ortho-grid with local free body diagram 96
Figure 89. Calculated stress at a worst case fastener hole in skin using detailed StressCheck FEM, Ktσ = 268 ksi (MS = -0.60) 96
Figure 90 Location of Panel 3 (816) and the Corresponding unit cell 98
Figure 91. Panel 3 (816) unit cell surface geometry with ortho-grid stiffeners and sine-wave substructure 99
Figure 92. Comparison of Panel 3 unit cell skin surfaces and Global FEM elements 100
Figure 93. Comparison of Panel 3 unit cell substructure and Global FEM elements 100
Figure 94. Panel 3 (816) Boundary Conditions 101
Figure 95. Panel 3 (816) Temperature Distributions 102
Figure 96. Panel 3 (816) Temperature Histories 103
Figure 97. Panel 3 (816) Temperature Gradients 103
Figure 98. Non-Linear Z-Component Deflection Plot [in] of Panel 3 (816) 105
Figure 99. Non-Linear Von Mises Stress Plot [psi] of Panel 3 (816) 106
Figure 100. 1st Buckling Mode of Panel 3 (816) 107
Figure 101. Unit cell boundary conditions for Panel 3 frequency response analysis (SOL 111) 109
Figure 102. Panel 3 deformed shape for non-linear thermal load case at t=900s (not to scale) 110
Figure 103. Panel 3 Von Mises stress plot for non-linear thermal load case at t=900s 110
Figure 104. RMS displacement response generated by MSC Random for Panel 3 SOL111 111
Figure 105. RMS Von Mises Stress fringe plot generated by MSC Random for Panel 3 SOL111 112
Figure 106. Altitude and Mach number shown for time, t=900s in vehicle flight profile 113
Figure 107. Design curve results for Panel 3 flutter 114
Figure 108. Comparison between flutter model and unit cell FEM for first three vibration modes 115
Figure 109. Structural model for Panel 3 flutter analysis using Piston Theory 116
Figure 110. Aerodynamic model for Panel 3 flutter analysis using Piston Theory 116
Figure 111. Plots of damping (G) and frequency (ω) as a function of air velocity for vibration modes that indicate Panel flutter 118
Figure 112. Locations checked for aero-acoustic fatigue 120
Figure 113. Worst case Ktσ calculation for skin to substructure joint 121
Figure 114 Location of Panel 4 (1074) and the Corresponding unit cell 122

Approved for public release; distribution unlimited.

Figure 115. Simplified 1/8 unit-cell models of the fuselage (a) and wing (b), and results (bottom) used to determine a thermal load scaling factor for Panel 4 123
Figure 116. Panel 4 ortho-grid and external stiffener geometry 124
Figure 117. Panel 4 unit cell geometry 125
Figure 118. Wing and Center Fuel Tank Schedules 126
Figure 119. Panel 4 (1074) Boundary Conditions 126
Figure 120. Panel 1 (862) Temperature Distributions 127
Figure 121. Panel 4 (1074) Temperature Histories 128
Figure 122. Panel 4 (1074) Temperature Gradients 129
Figure 123. Non-Linear Z-Component Deflection Plot [in] of Panel 4 (1074) 130
Figure 124. Non-Linear Von Mises Stress Plot [psi] of Panel 4 (1074) 131
Figure 125 Non-Linear Fastener Forces [lbs] for Panel 4 (1074) 132
Figure 126 1st Buckling Mode of Panel 4 (1074) 133
Figure 127. Boundary condition comparison between static and dynamic FEM 135
Figure 128. Fringe plot of out of plane RMS displacement and graph of PSD response as a function of frequency for Z displacement (Node 22701) 135
Figure 129. Fringe plot of RMS Von Mises Stress and graph of PSD response as a function of frequency for Von Mises Stress (Element 23364) 136
Figure 130. Panel 4 mode shape at 226 Hz from SOL 103 136
Figure 131. Design curve results for Panel 4 with Panel 3 results shown 137
Figure 132. Structural FEM for Panel 4 flutter analysis 138
Figure 133. Aerodynamic model for Panel 4 flutter analysis 138
Figure 134. Plots of damping (G) and frequency (ω) as a function of air velocity for vibration modes 1 and 2 (Alt=32.5kft, AoA= 6deg, No Preload) 139
Figure 135. Plots of Max RMS stress and mean stress (thermal) and MS calculation for Panel 4 141
Figure 136. Panel location and construction for explicit dynamic analysis 144
Figure 137. Temperature distribution at t=1,080 sec on Panel 1 145
Figure 138. Modes 1 thru 4 of Panel 1 146
Figure 139. Modes 5 thru 8 for Panel 1 146
Figure 140 Modes 5 Thru 8 of Panel 1 146
Figure 141. Modes 9 thru 12 of Panel 1 147
Figure 142. Comparison of first three modes between Panel 1 and unit-cell models 147
Figure 143. Rayleigh damping for transient dynamic analysis 149
Figure 144. Time history of acoustic pressure 150
Figure 145. Separated Turbulent Boundary Spectrum 151
Figure 146. Comparison of total displacements for static and quasi-dynamic cases with hinged BC and thermal loads 152
Figure 147. Comparison of Normal Displacements for Static and Quasi-dynamic Cases with Hinged BC and Thermal Loads 152
Figure 148. Comparison of von Mises stress for static and quasi-dynamic cases with hinged BC and thermal loads 152
Figure 149. Max principal stresses in panel due to thermal loads with hinged BC 153
Figure 150. Node and element locations for time history results 154
Figure 151. Snapshots of normal displacements (t=0.0 to 0.6sec) of panel with hinged BC and thermal loads 155

Approved for public release; distribution unlimited.

Figure 152. Snapshots of normal displacements (t=0.8 to 1.4sec) of panel with hinged BC and thermal loads 155
Figure 153. Snapshots of normal displacements (t=1.5 to 2.0sec) of panel with hinged BC and thermal loads 156
Figure 154. Time history of normal displacements at panel center with hinged BC 156
Figure 155. Time history of stress S11 of element 3117666 near panel center with hinged BC 157
Figure 156. Comparison of normal displacements of Node 3110916 at panel center 159
Figure 157. Comparison of stress S11 of Element 311766 on stiffener web and near panel center for hinged and fixed BC without thermal loads 160
Figure 158. Comparison of normal displacements of Node 3110916 at panel center for hinged and fixed BC with thermal loads 162
Figure 159. Comparison of stress S11 of Element 311766 on stiffener web and near panel center for hinged and fixed BC with thermal loads 163
Figure 160. Comparison of normal displacements of Node 3110916 at panel center 165
Figure 161. Comparison of stress S11 of Element 311766 on stiffener web and near panel center for hinged BC with and without thermal loads 166
Figure 162. Comparison of normal displacements of Node 3110916 at panel center 168
Figure 163. Comparison of stress S11 of Element 311766 on stiffener web and near panel center for fixed BC with and without thermal loads 169
Figure 164. Stress time history at Element ID=3117666 σ11 171
Figure 165. Fatigue life for center stiffener web 171
Figure 166. Inconel 718 RMS S-N data 172
Figure 167. Reference trajectory 176
Figure 168. AFRL Combined Environment Acoustic Chamber (CEAC) facility 179
Figure 169. CEAC Test Article Mounting Cart and Heat Lamp Bank 179
Figure 170. Panel 1 Overlay into CEAC Chamber 180
Figure 171. Combined thermal & structural curvature test fixture for a CMC TPS Panel [4] ... 184
Figure 172. NASP TMC Shear Panel test load fixture (lamps not shown) [6] 184
Figure 173 – Stiffened Panel Test in the AFRL CEAC Facility 185
Figure 174. Schematic and test photo for NASA LaRC 8-ft, Mach 7 HTT 186

Approved for public release; distribution unlimited.

LIST OF TABLES

Table 1. List of Phase I Gaps with confirmation by Phase II findings 2
Table 2. List of Gaps and associated Critical Regions identified in Phase I 7
Table 3. Overview of selected panel characteristics and analysis results 20
Table 4. Unit cell model approximately matched thermal loads from global model 23
Table 5. Summary of substructure trade results (Nx & Ny are the resulting panel thermal loads) 25
Table 6. Equivalent sine-wave web properties for flat shell elements 25
Table 7. Heat Transfer Analysis Methods and Assumptions 29
Table 8. Summary of Static Margins for All Panels 41
Table 9. Normalized Acoustic Loads for each panel 46
Table 10. Panel 1 sizing loads for a 2.5G turn at 1080 sec 59
Table 11. Summary of static margins of safety for Panel 1 (862) 69
Table 12. Margin of safety summary for Panel 1 thermal-mechanical fatigue 74
Table 13. Panel 2 sizing loads for a 2.5G turn at 1080 sec 76
Table 14. Summary of static margins of safety for Panel 2 (780) 89
Table 15. Summary of Finite Element Analyses Used for Acoustic and Thermal-Mechanical Fatigue 90
Table 16. Margin of safety summary table for Panel 2 acoustic fatigue 94
Table 17. Margin of safety summary for skin to substructure joint of Panel 2 95
Table 18. Margin of safety summary for ortho-grid to panel stiffener joint of Panel 2 97
Table 19. Panel 3 sizing loads for a 2.5G turn with Panel 1 thermal loads 99
Table 20 Summary of static margins of safety for Panel 3 (816) 107
Table 21. Finite Element Analyses Used for Acoustic and Thermal-Mechanical Fatigue 108
Table 22. Summary of flutter analyses to determine flutter altitude for a target flutter speed of Mach 6.25 119
Table 23. Margin of safety summary for Panel 3 AACF 120
Table 24. MS table for Panel 3 thermal-mechanical fatigue 122
Table 25. Panel 4 sizing loads for a 2.5G turn with scaled Panel 2 thermal loads 124
Table 26 Summary of static margins of safety for Panel 4 (1074) 133
Table 27. Analyses used for Panel 4 dynamic and fatigue evaluation 134
Table 28. Summary table for Panel 4 flutter analysis 140
Table 29 Comparison of modal frequencies for different boundary conditions 148
Table 30. Damping ratios for different frequency ranges 148
Table 31. Comparison of normal displacement at center of panel 157
Table 32. Comparison of dominant stress on stiffener web at center of panel 157
Table 33. Candidate Panel Summary 181
Table 34. List of Phase I Gaps with confirmation by Phase II findings 189

Approved for public release; distribution unlimited.

GLOSSARY

AACF	Aero-Acoustic Fatigue
ABAQUS	Finite Element Analysis Software
AFRL	Air Force Research Laboratory
ARAMIS	Non-contact strain measurement system.
ASET	Analysis Set, or degrees of freedom
BC	Boundary Conditions
BLAP	Boundary Layer Analysis Program
CAD	Computer Aided Design
CAEROS	NASTRAN Aerodynamic Panel Element Connection
CATIA	3D design software
CEAC	Combined Environmental Chamber
CEAS	NASTRAN spring element
CFAST	NASTRAN Fastener Element
CFD	Computational Fluid Dynamics
COV	Coefficient of Variance
CTE	Coefficient of Thermal Expansion
DIC	Digital Imaging Correlation
DOF	Degree of Freedom
DTIC	Defense Technical Information Center
FE	Finite Element
FEA	Finite Element Analysis
FEM	Finite Element Model
FOS	Factor of Safety
GAG	Ground-Air-Ground
GUI	Graphical User Interface
HCV	Hypersonic Cruise Vehicle
HIFiRE	Hypersonic International Flight Research and Experimentation
HTT	High Temperature Tunnel

Approved for public release; distribution unlimited.

I-DEAS/TMG	Thermal analysis software
IR	Initial Review
ITAR	International Traffic in Arms Regulation
LVD	Laser Displacement Measurement
LVDT	Linear Voltage Displacement Transducer
MINIVER	Aerothermal dynamic analysis software
MPC	Multipoint Constraints
MS	Margin of Safety
MSC	Software company that distributes NASTRAN
NASA	National Aeronautics & Space Administration
NASP	National Aerospace Plane
NASTRAN	Finite element analysis software
OASPL	Overall Sound Pressure Level
ODS	Overall Deflected Suface
PATRAN	User interface software for MSC/NASTRAN
PDS	Power Spectral Densities
RBE	Rigid Body Element
RMS	Root mean square
SME	Subject Matter Expert
SoA	State of Art
SPC	Special Programs Center
SSC	Structural Sciences Center
TBL	Turbulent Boundary Layer
TMF	Thermal-Mechanical Fatigue
TPS	Thermal Protection System
TX-V	Technology Experimental Vehicle

Approved for public release; distribution unlimited.

PREFACE

This final report of the Predictive Capability for Hypersonic Structural Response and Life Prediction: Phase II – Detailed Design of Hypersonic Cruise Vehicle Hot-Structure program summarizes work performed during the period from September 1, 2010 through January 31, 2012 under USAF Contract FA8650-08-D-3857-0023.

This project was funded by the Aerospace Structures Division of the Aerospace Systems Directorate of the AFRL. The Program Manager is Dr. Michael Spottswood. The contracts officer for the program has been Ms. Genet Stewart.

The Boeing team was composed of a core group consisting of Rob Quiroz, Rick Jacobs, George Tzong, Sal Liguore, Jon Embler, Pete Keller, Jim Ledesma, and Craig Masterson. The authors also wish to acknowledge the technical, business, and administrative contributions of the following individuals: Denise Boss, Ed Curry, Sharyn Garnett, Brian Foist, Mike Hand, Ryan Malawy, Keith McIver, Charlie Petrilla Jr., Pichuraman Sundaram, and Juliane Vossmeyer.

Additional support, interaction, and feedback during technical reviews along with other conversations with the following government agency personnel were appreciated: Dr. Tom Eason, AFRL/RQ; Dr. Michael Spottswood, AFRL/RQSS; Dr. Adam Culler, AFRL/RQ; Dr. Parthiv Shaw, ATA Engineering; and Travis Wyen, AFRL/RQ.

1.0 EXECUTIVE SUMMARY

Four panels from a representative Mach 7 hypersonic cruise vehicle were designed and analyzed with state-of-the-art standard methods and tools to verify structural response and life predictive capabilities. Several modifications were made to the Technology Experiment Vehicle (TX-V) to refine the structure and create a Mach 7 "closed-concept" configuration with an all metallic high temperature airframe. Structural loads and environments from the TX-V were then used to size and design the four panels, and perform thermal, stress, acoustic, flutter, and fatigue analyses. An additional set of explicit dynamic analyses using an alternative method was performed on one of the four panels. Several analysis process and method findings based on these two analysis approaches are compared to previously identified knowledge gaps, confirming several while adding several more. The objectives and requirements of a validation test program are also reviewed, along with the capabilities of available facilities, in the context of the design drivers of the analyzed panels. A set of recommended test series are identified and prioritized to best evaluate the accuracy of current structural response and life prediction capabilities. Finally, recommendations are made to further advance predictive capabilities for hypersonic structures as shown in Figure 1.

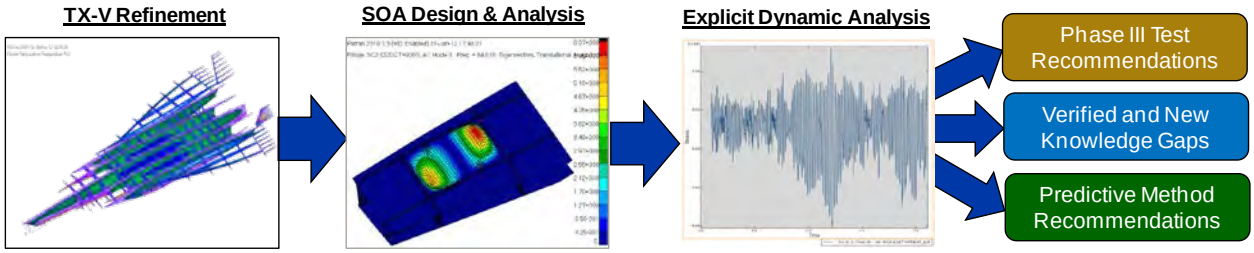

Figure 1. This hypersonic cruise vehicle hot-structure design program provides actionable information for predictive capability development

This program is the second phase of a larger three phase program led by the Structural Sciences Center (SSC) of the Air Force Research Laboratory (AFRL) to evaluate and improve the *Predictive Capability for Hypersonic Structural Response and Life Prediction*. In the first phase of this program, ten (10) predictive capability knowledge gaps were identified. The main objective of this Phase II program was to verify these knowledge gaps through the detailed design and analysis of representative panels. In Task 2, all four panels were designed and analyzed using standard practices for aerospace vehicles, while additional explicit dynamic analysis was performed on the first panel in Task 3. Eight of the ten knowledge gaps identified in Phase I were confirmed in Phase II as shown in Table 1. The two unconfirmed gaps were not however shown to be false. Rather, the first was not addressed by the selected analysis approach, while the second was not seen in the response of the selected panel.

Approved for public release; distribution unlimited.

Table 1. List of Phase I Gaps with confirmation by Phase II findings

Phase I Gap Description	Confirmation in Phase II
1. Difficult to identify critical thermo-mechanical and acoustic load combinations	Task 3 Explicit Analysis
2. Difficult to adopt temporal and spatial thermal gradients in panel level linear analysis	**Unconfirmed**: Uniform heating was assumed for each panel
3. Do not account for the coupling between transient thermal and acoustics in linear frequency response analysis	Task 3 Explicit Analysis
4. Cannot accurately include internal loads in panel level analysis	Task 2 Unit Cell Analysis
5. Cannot accurately define thermal and mechanical boundary conditions for detailed panel analysis	Task 2 Panel Sizing
6. Cannot simulate large deformation oscillation or dynamic snap-thru of panels	**Unconfirmed**: Not an issue with analyzed panels
7. Inadequately model accumulated damage and degradation due to high temperatures	Task 2 Panel Fatigue Allowables
8. Cannot accurately model damping in analysis	Task 3 Explicit Analysis
9. Can only approximate acoustic environment using empirical formulas until flight test data is available	Confirmed: All acoustic analyses used approximated environments
10. Lack the capability to analyze large-order high fidelity models to capture nonlinear, dynamic snap-thru, and high frequency response in coupled extreme environment	Task 3 Explicit Analysis

Several new knowledge gaps were also identified in addition to the original Phase I gaps. These new knowledge gaps are listed below:

11. Cannot adequately define panel level deflection criteria without an understanding of system level impacts to aero heating, drag, and performance. (Task 2)
12. Current practices are too cumbersome to allow rapid design iterations between detailed panel and vehicle load models, which is required to render the stiffness of the local panel consistent to the vehicle model. (Task 3)
13. Establishing initial conditions for explicit dynamic analysis require a quasi-dynamic step inconsistent with the actual time variant environment. (Task 3)
14. A separate labor intensive detailed tool is required to determine stress concentration factors and make life and stress predictions around design features (Tasks 2 & 3)

Approved for public release; distribution unlimited.

These 14 specific predictive capability knowledge gaps were then combined to create 3 high-level broad knowledge gaps that address the majority of the specific gaps. Additional discussion of all knowledge gaps can be found in Section 7.0 of this report.

I. Unable to accurately and efficiently perform multi-scale static and dynamic thermal-structural analysis with multiple types of loads.

II. Unable to accurately predict multiple basic physical phenomena, resulting in a reliance on scaling functions and the extrapolation of empirical data.

III. It is computationally impractical to perform transient thermal-mechanical analyses with radiation on large order models.

In Phase II, Boeing successfully confirmed eight of the ten previously identified predictive capability knowledge gaps and identified 4 additional gaps. This was accomplished through the refinement of the Mach 7 TX-V reference vehicle, the detailed design and analysis of 4 panels using standard design and sizing methods, as well as thermal, stress, acoustic, flutter, and fatigue analysis methods. Lastly, a high level test plan was developed to verify panel level response and life predictions. When combined with the Phase I effort, these findings provide the basis for several key recommendations:

1. Investigate the viability of using of equivalent orthotropic material properties to represent flexible sine-wave or corrugated substructures in loads models as a best practice
2. Explore analysis methods and processes for efficiently incorporating high fidelity thermal boundary conditions for the global vehicle model
3. Perform combined environment verification tests to determine the accuracy of structural response and life predictions
4. Develop methods for automatically mapping multiple loads and load types, from a global vehicle model to a detailed unit cell or panel model along its boundaries
5. Develop out-of-plane structural deflection sensitivities, sizing criteria and design guidelines for Mach 5 to 7 class cruise vehicles
6. Investigate coupled transient thermal-stress analysis methods for use on vehicle, unit cell, and panel level models; and if computationally reasonable, implement them in future detailed design efforts
7. Develop and validate analytical methods to predict allowables at design points of interest based on material failure mechanisms

Approved for public release; distribution unlimited.

2.0 INTRODUCTION

The United States Air Force (USAF) has identified a responsive hypersonic strike and reconnaissance aircraft as providing a potentially disruptive capability that would significantly enhance its ability to globally project force. Although there are several areas requiring significant technology advances in order to develop a hypersonic aircraft, one of the key challenges that has been identified is an operable and weight efficient, high temperature airframe. The AFRL and Boeing are actively engaged in developing the materials, structural concepts, and analytical capabilities required to develop such an airframe. The Structural Sciences Center (SSC) of the AFRL's Air Vehicles Directorate has been directed to research, develop, and transition analysis and simulation methods for these reusable extreme environment structures in order to more accurately define and expand the design space. This program is one part of a larger three-phased effort lead by the SSC to target acreage panel-level response and life prediction capabilities for a sustained, reusable, air-breathing, Mach 5-7 cruise, horizontal-takeoff platform [1].

2.1 Multi-Phase Program Overview and Objectives

An illustration of the three-phase *Predictive Capability for Hypersonic Structural Response and Life Prediction* program is shown in Figure 2. The first phase of the program was focused on uncovering knowledge gaps for detailed hypersonic structure design that most significantly restrict a truly predictive capability. A brief summary of Boeing's Phase I effort will be provided in the next section while the detailed final report can be obtained from the Defense Technical Information Center (DTIC) [2]. This report covers Boeing's effort under the second phase, in which detailed designs were created for selected regions of a "closed-concept" reference vehicle and accompanying trajectory, targeting the knowledge gaps delineated and documented in the Phase I. The third phase will proceed to build and test flight-weight panel-level hardware identified, detailed and documented in Phase II. [1]

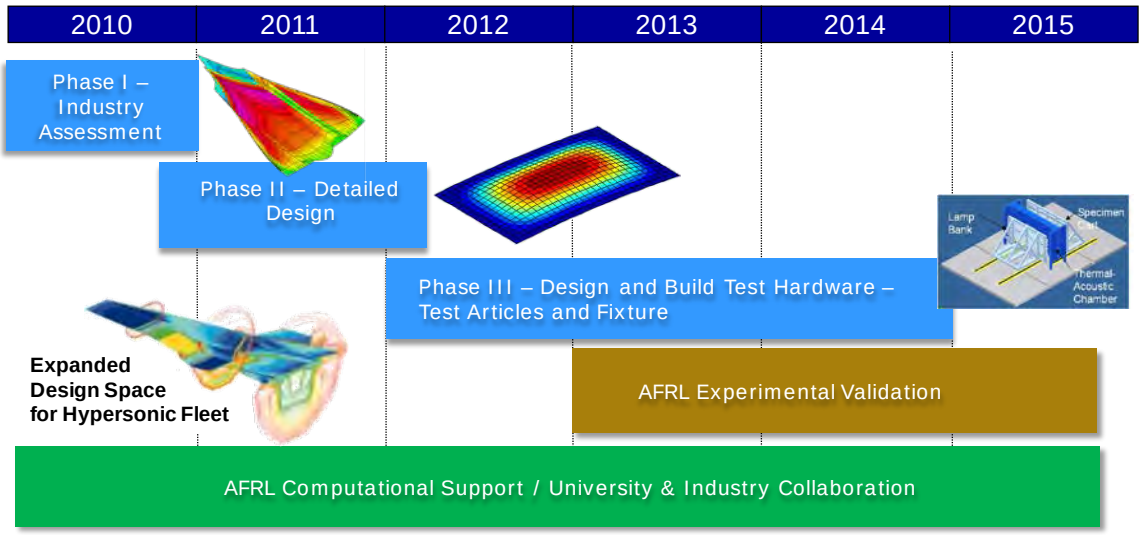

Figure 2. Multi-phase program overview

Approved for public release; distribution unlimited.

2.2 Phase I – Identification of Knowledge Gaps

The objective of the Phase I effort, *Identification of Knowledge Gaps*, was to identify gaps in structural analysis and life prediction methods applied to reusable, integrated air vehicle structures for sustained operations in a hypersonic environment. The program focused on areas of the structure where gaps exist in the state of the art (SoA) analysis methods and tools to accurately predict the response and life of the flight vehicle structure to the desired fidelity. Knowledge gaps were identified based on design and analysis issues of current production aircraft (including fighter, transport, and commercial aircraft), recent and past hypersonic vehicle experience (National Aerospace Plane (NASP), X-51A, and Hypersonic International Flight Research and Experimentation (HIFiRE)), and most importantly on a defined Mach 7 hypersonic cruise reference vehicle, called the Technology Experimental Vehicle (TX-V).

Boeing performed two major tasks in its Phase I program which is depicted in Figure 3. In the first task Boeing updated an existing hypersonic cruise vehicle conceptual design to create the TX-V and meet the needs of the overall multi-phase program. Major updates to create the TX-V included 1) scaling the vehicle to have a range consistent with an operational regional strike or reconnaissance aircraft, and 2) changing the structural definition to an all metallic hot structure. Prior Boeing studies looking at Mach 7+ vehicles had assumed aluminum or composite primary structure with parasitic TPS. Attempts to size the TX-V structure with super alloy skin panels and thermal loads for a Mach 7 trajectory were unsuccessful due to the large thermal gradients that develop between the substructure and skin panels. In order to close the vehicle, temperature gradients more representative of a Mach 5 trajectory were incorporated and used to size the structure. This Mach 5 structural configuration was later used as the starting point for Boeing's Phase II detailed design program.

Approved for public release; distribution unlimited.

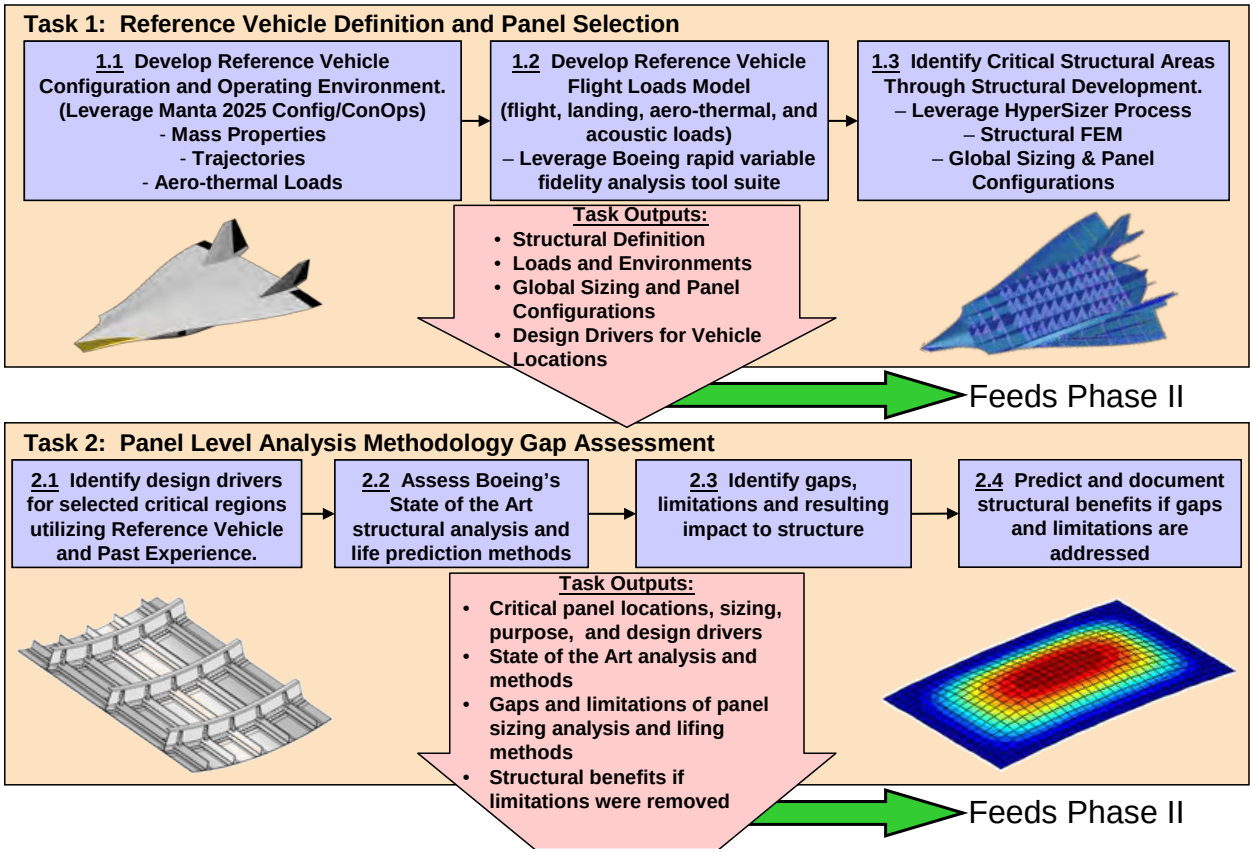

Figure 3. Overview of Phase I

In the second task, Boeing identified structural design drivers for various regions of the TX-V based on initial analysis of this vehicle and past experience on other programs. Issues involved in non-linear coupling between extreme hypersonic thermal-acoustic environments, evolving material attributes and the resulting structural response and failure modes were identified and documented. Limitations inherent in Boeing's SoA analysis and life prediction methods were then evaluated and used to identify gaps in our predictive capability. Also, the structural benefits that could be obtained through increased fidelity of the design of hot structures enabled by removal of the identified gaps and limitations were included. These gaps are discuss in detail in the final report for this effort [2] and are summarized in Table 2. An updated prioritized list of gaps that includes findings from the Phase II program can be found in the Sections 1.0 Executive Summary and 7.3 Prioritized List of Revised Predictive Capability Knowledge Gaps.

Table 2. List of Gaps and associated Critical Regions identified in Phase I

Gap Description	Critical Vehicle Region
1. Difficult to identify critical thermo-mechanical and acoustic load combinations	Engine nozzle, inlet and duct
2. Difficult to adopt temporal and spatial thermal gradients in panel level linear analysis	Engine nozzle, inlet and duct, wing leading edges, Fwd lower surface
3. Do not account for the coupling between transient thermal and acoustics in linear frequency response analysis	Engine nozzle, flaps and control surfaces, Fwd lower surface, Aft upper and lower surfaces
4. Cannot accurately include internal loads in panel level analysis	All acreage panels
5. Cannot accurately define thermal and mechanical boundary conditions for detailed panel analysis	All acreage panels
6. Cannot simulate large deformation oscillation or dynamic snap-thru of panels	Aft upper and lower surfaces, flaps and control surfaces
7. Inadequately model accumulated damage and degradation due to high temperatures	Engine nozzle, inlet and duct, wing leading edges, Fwd lower surface
8. Cannot accurately model damping in analysis	All acreage panels
9. Can only approximate acoustic environment using empirical formulas until flight test data is available	Wing leading edge , flaps and control surfaces, Aft upper and lower surfaces
10. Lack the capability to analyze large-order high fidelity models to capture nonlinear, dynamic snap-thru, and high frequency response in coupled extreme environment	Aft upper and lower surfaces, flaps and control surfaces

2.3 Phase II Program Overview

The overall objective of Phase II is to verify the most significant knowledge gaps identified in Phase I, by performing detailed analysis, design, and life prediction in regions of a reusable hot structure hypersonic cruise vehicle, where the panel-level structural analysis and life prediction knowledge gaps are known to exist [1]. In support of this objective, the AFRL requested that the following products be included in the design and analysis effort, and delivered in a non-proprietary package:

- Design and engineering intent, assumptions and rationale for the panel-level designs
- Design loading conditions

Approved for public release; distribution unlimited.

- Detailed CAD models of the selected panels
- Material properties/degradation, including assumptions regarding change with temperature
- Detailed finite element models (FEM) and analyses of the selected designs, including all assumptions and trade results
- Any thermal, aerodynamic models, or other detailed analyses used for the panel designs
- The associated limit-state and predicted life of the panel structural components
- All documentation of analyses conducted to support the component design

Boeing executed six tasks, summarized in Figure 4, to achieve these objectives. In *Task 1: Refine Reference Vehicle*, the TX-V reference vehicle structural sizing was modified to produce a "closed-concept" with panel level loads and environments. Four panels were then selected from different regions of the vehicle. Under *Task 2: Detailed Panel Design,* detailed designs were created for each panel, and analyses were performed to determine their response to thermal, mechanical, and acoustic loads using standard analysis methods. The design intent, detailed analyses, margins, and life predictions for each panel are documented in this report, while data packages of all computer aided design (CAD) and finite element (FE) models have been provided to AFRL and can be obtained from AFRL for use on related efforts. A series of explicit non-linear analyses was then performed in *Task 3: Verification Studies* to in order to compare these results to those obtained with the standard methods used in Task 2. Results were also used to verify previously identified knowledge gaps and quantify any potential benefits of these higher fidelity methods. Three additional tasks were performed to document and report findings, manage the program budget and schedule, and make recommendations for Phase III testing activities based on the results of this effort.

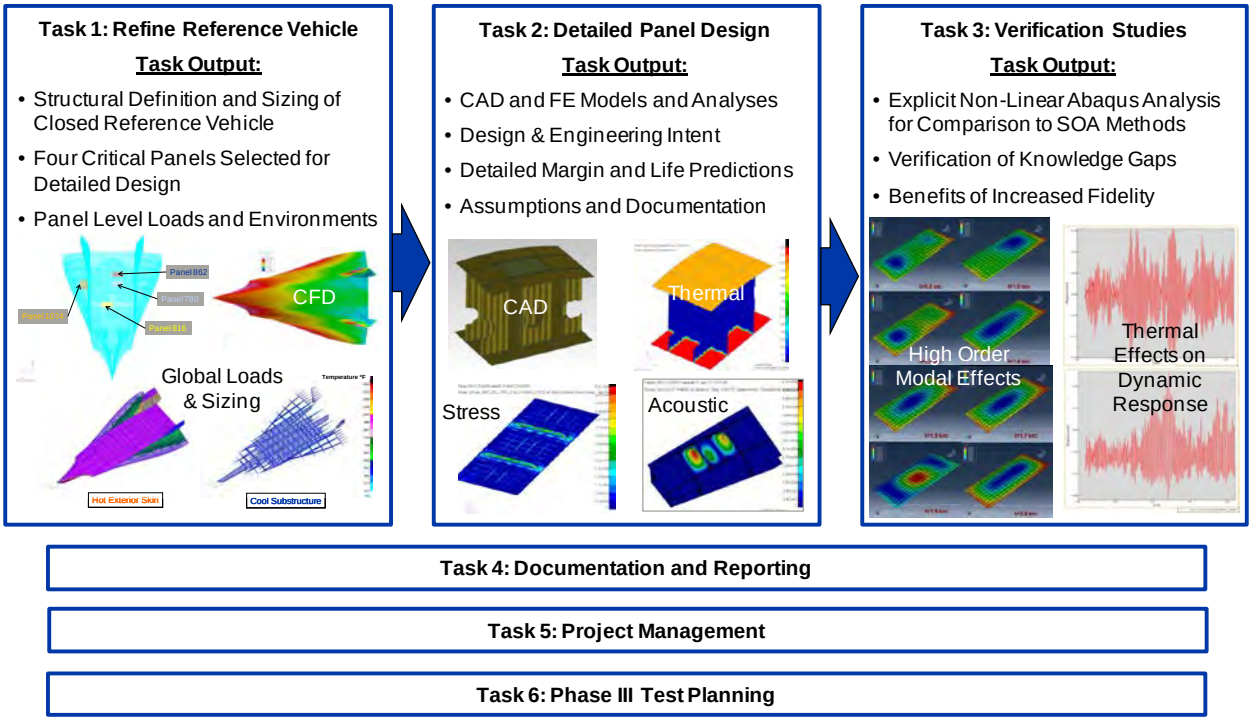

Figure 4. Overview of Phase II program tasks

Approved for public release; distribution unlimited.

3.0 TECHNOLOGY X-VEHICLE REFINEMENT

3.1 Task 1 – Overview

In Phase I, an aggressive approach was used for development of a Mach 7 hypersonic cruise vehicle using a metallic hot structure concept. To maximize value to the program, the existing Boeing Manta 2025 vehicle was selected as the basis from which the TX-V reference vehicle would be developed. The purpose of the reference vehicle is to assist in the identification of critical knowledge gaps for structures operating in extreme combined thermal-acoustic environments. Previously developed data such as a conceptual level Finite Element Model (FEM), aeroheating acreage database, mass properties, and trajectory data were extensively leveraged. Adapting the Manta data for the TX-V saved a great deal of effort, but required modifications and assumptions that scaling the existing data would not introduce excessive inaccuracies. The modifications included: uniformly scaling the vehicle FEM to increase the maximum length from 32 ft to 75 ft, removing the ceramic Thermal Protection System (TPS), replacing the structure with high temperature Inconel 718 materials, and adapting the aeroheating acreage database to the scaled vehicle. Specialty structures unique to hypersonic vehicles such as leading edges or inlet and exhaust ducts were not addressed in this conceptual level effort. Figure 5 presents the TX-V Hypersonic Cruise Vehicle and Figure 6 presents the design trajectory.

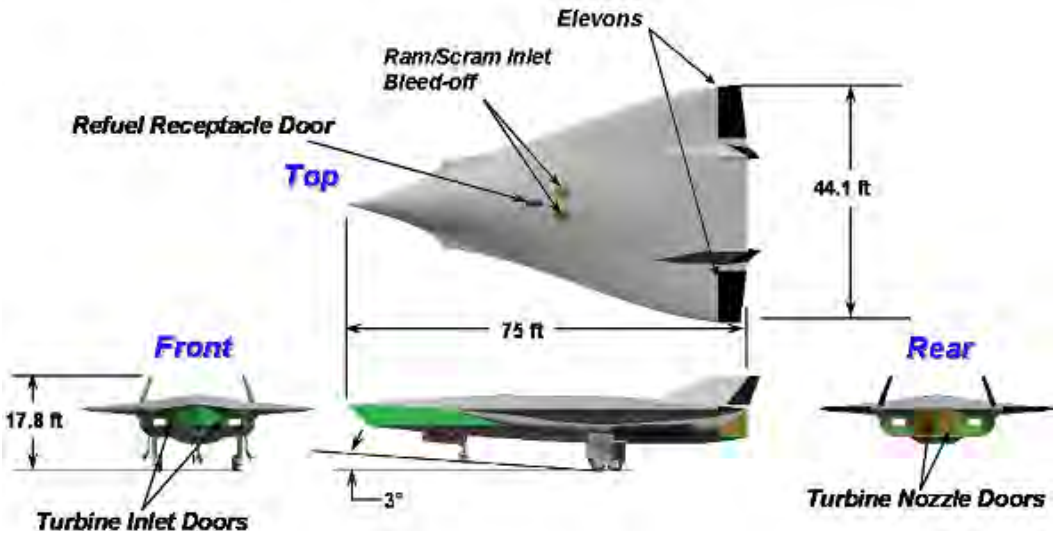

Figure 5. TX-V Hypersonic Cruise Vehicle

To support structural sizing of the new metallic hot structure, design loads and environments for the mission trajectory were determined by producing critical flight maneuver loads, performing transient thermal analysis, developing acoustics environments from which minimum panel frequency guidelines were established, and generating landing & ground handling loads.

Approved for public release; distribution unlimited.

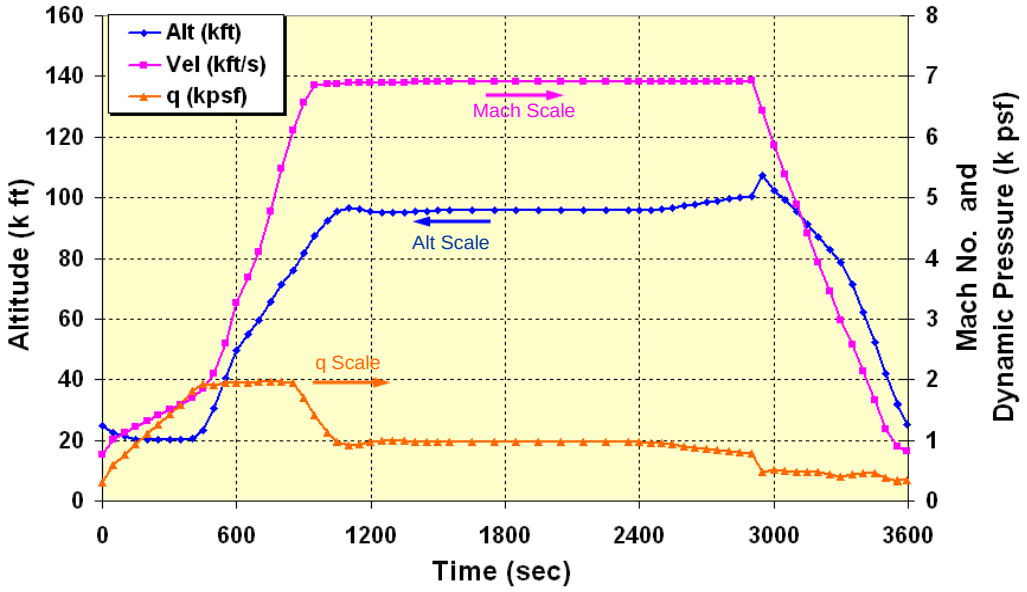

Figure 6. Mach 7 Design Mission Trajectory

Using the developed loads and environments structural sizing was performed for the new metallic hot structure. The initial sizing analysis failed to converge for the Mach 7 design trajectory. Failure to converge a sizing solution is also commonly referred to as not "closing" the vehicle. Investigation of the results showed that the thermal loads were driving the design and that increasing the panel gage failed to reduce stress levels since this also resulted in increased thermal loading. This was the result of attaching the hot external skin with a high CTE to a relatively cool substructure that did not expand with the skin. The mismatch in thermal expansion resulted in large thermal stresses. Figure 7 presents structural temperatures for the hot external skin and cool substructure. To complete the Phase I effort a reduced thermal load was used to obtain convergence by simply factoring the Mach 7 thermal temperatures. The resulting reduced thermal environment is roughly equivalent to reducing the cruise Mach number to between Mach 4 and 5.

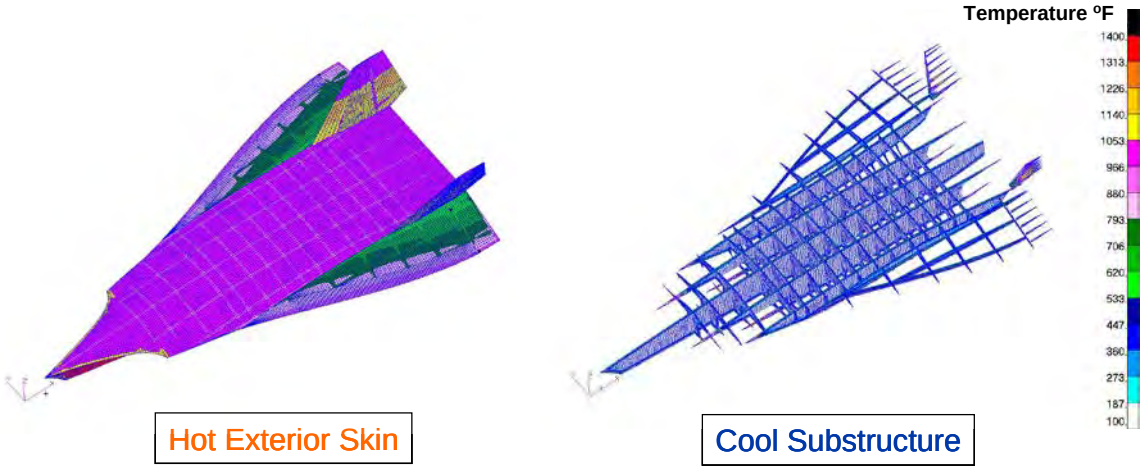

Figure 7. Temperatures for External Skin and Substructure

Approved for public release; distribution unlimited.

3.2 Potential Solutions to "Close" the Design

In this document the term "closed" design is used to signify that the resulting structure satisfies the strength, buckling, and panel frequency constraints, and meets the allocated weight target. At the vehicle level the term "closed" design would also include additional considerations of disciplines that would have specific requirements that would need to be satisfied. These might include propulsion structural deflection requirements, thermal management, and mold line deflection requirements.

To better support Phase II, several potential solutions to "close" the design, and improve results were identified. The primary shortcomings of the TX-V structural concept at this phase of the program were felt to be the excessive thermal stresses and unnecessary structural acreage in the bulkhead and keel structures which lead to an unrecoverable weight penalty. These characteristics are a consequence of using a converted TPS structural concept that was never intended for exposure to extreme Mach 7 thermal environments. As a result Phase I results showed that the structural sizing would not converge when subjected to the Mach 7 environments. For Phase II the focus was on reducing thermal loads, and reducing unnecessary structural acreage since Inconel 718 is nearly three times as dense as aluminum.

A preferred approach for producing an efficient lightweight structure is to employ a "clean-sheet" design with a structure specifically designed to accommodate high temperatures and thermal gradients while minimizing unnecessary structural area/weight. Structural concepts like those investigated for the National Aerospace Program (NASP) could be adapted for this application. This approach would require a new CAD model, FEM, and updated thermal and flight loads. Some iteration would likely be required to close the design, but the result would provide the most weight competitive structure. Unfortunately, this approach was not within the scope of this effort and a best effort attempt was made to reduce the weight of the existing design through simple modifications.

While the "clean-sheet" design was out of scope for the current effort it was decided that some of the concepts might be applied to the existing TX-V FEM within the program constraints to improve the results. The intent was to adapt the existing FEM to more of a semi-monocoque concept that would allow the structure to heat up and expand more uniformly. This approach was implemented by removing portions of the bulkhead and keel structures of the existing model. This also removes a significant amount of structural area and weight. Figure 8 presents a comparison between the baseline TX-V FEM and the modified FEM with structures removed to allow for more uniform expansion under thermal loading.

Approved for public release; distribution unlimited.

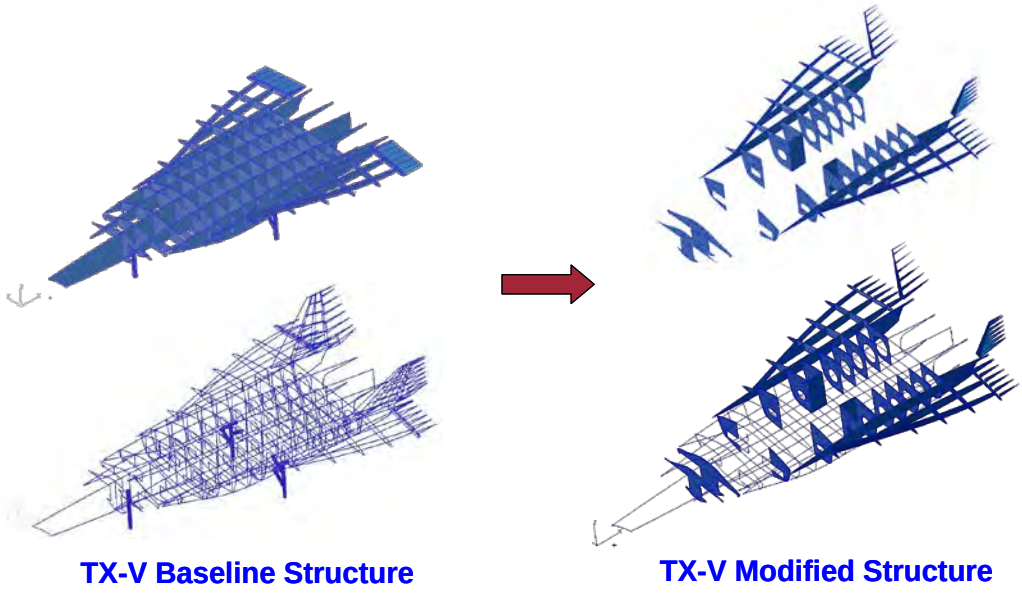

Figure 8. Modified TX-V Structure

Another option investigated was to determine the sensitivity of sizing results to variation in the internal substructure temperature distribution. The original thermal analysis showed that the temperature for most of the internal structure remained constant at the T_o initial temperature for the duration of the mission. In fact, the 1100°F external skin temperature only penetrated ~10 inches into the underlying structure before reaching the 100°F T_o initial temperature. Figure 9 shows the temperature penetration into the substructure at time = 2400s.

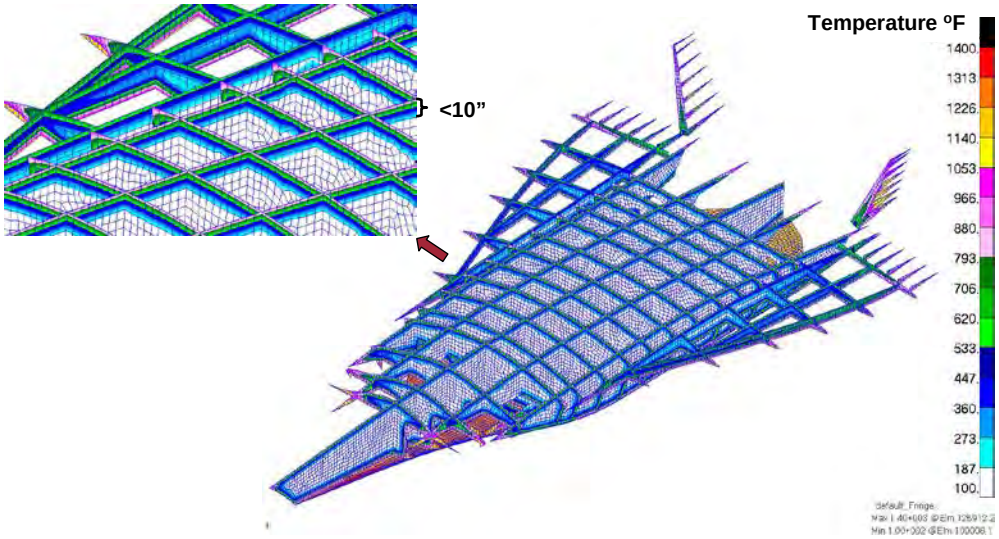

Figure 9. Substructure Temperature Distribution

The concern with the substructure temperature distribution was that several factors may have contributed to unrealistically low temperature results. First, internal heat sources such as engines and subsystems were not considered in the original thermal analysis nor were radiation effects

used for the internal structure. Radiation effects were included for the exterior skin. To investigate the impact of higher internal temperatures that might result from these affects, a modified internal temperature distribution was produced. The modified temperature distribution was produced by performing a steady state thermal analysis at time 2400s using the external skin temperature as a boundary condition. The heat transfer coefficient was then varied until the resultant temperature distribution between the upper and lower surfaces produced higher temperatures. Figure 10 presents the modified substructure temperature distribution for the baseline and modified structural configurations. The minimum substructure temperatures were increased from 100°F in the original thermal analysis to ~500°F. This type of simplified convective thermal boundary condition was used as the use of internal heating, insulation, and radiation would have been computationally prohibitive at the vehicle level (Recommendation #2, Page 3).

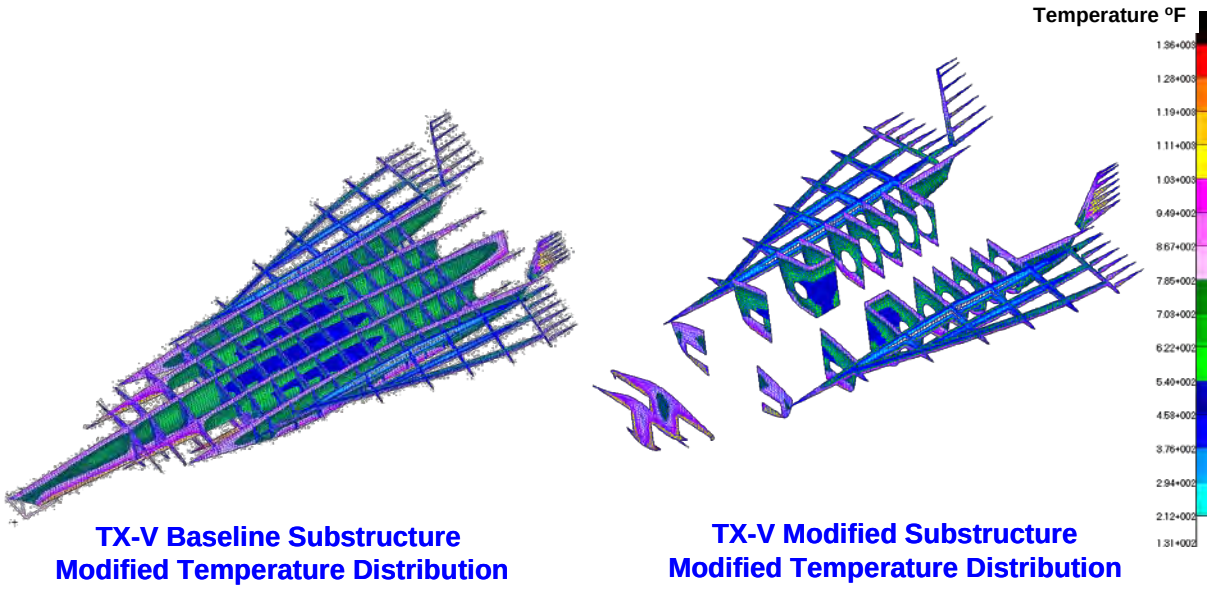

Figure 10. Modified Substructure Temperature Distribution

The third option investigated for improving the sizing results was to reduce the Coefficient of Thermal Expansion (CTE) of the Inconel material by 60%. The idea behind this approach was that panel attachment details along with implementation of sine wave web features could be added during the detail panel design activity to achieve reduced thermal stresses.

3.3 Structural Sizing Results

The initial structural sizing was performed for the baseline TX-V structure using a 60% CTE reduction with honeycomb sandwich construction throughout. The thermal loading was applied based on Mach 7 structural temperatures at time 2400s. Collier Research's HyperSizer structural analysis software was used to perform structural sizing subject to strength, panel frequency, and buckling constraints using the same process used in Phase I. The sizing converged after 12 iterations with a resulting total weight of ~65k lbs. This result is more than twice the ~25k lbs allocated for the structural weight. Next, sizing was continued but the original thermal

Approved for public release; distribution unlimited.

temperatures were replaced with the modified substructure temperature distribution. The sizing structural weight history for the baseline structure with a 60% CTE reduction, and modified internal temp distribution is shown in Figure 11. The affect of the modified substructure temperature was to reduce the structural weight from ~65k lbs to ~40k lbs. This is a significant reduction and shows the impact of reducing the thermal gradient between the exterior skin, and the substructure. Unfortunately, the weight is still significantly heavier than the weight allocation.

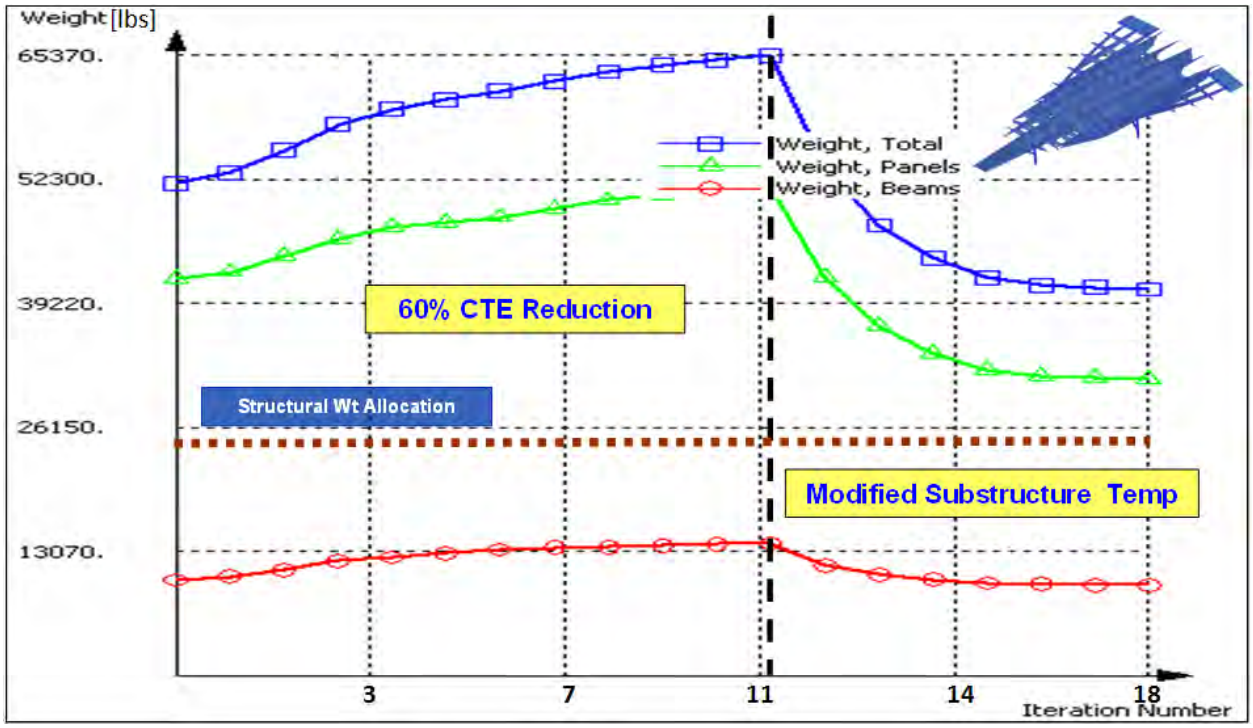

Figure 11. Baseline TX-V FEM Structural Sizing History

Structural sizing was also performed for the modified FEM that had some of the bulkhead and keel structures removed. Initially, sizing was performed using a 60% CTE reduction. This resulted in a total structural weight of ~30k lbs, which is close to the target structural weight of 25k lbs. Next, sizing was performed using the modified substructure temperature distribution. For the modified FEM this did not produce the significant weight reduction that was seen in the baseline FEM. This indicates the structure is now free to expand and does not benefit from the reduced thermal gradient. Finally, an unreduced 100% CTE value was used. This resulted in a structural weight of ~48k lbs. The structural weight histories for these three scenarios are presented in Figure 12. The modified FEM showed some promise, but requires additional design efforts to resolve the issue.

Approved for public release; distribution unlimited.

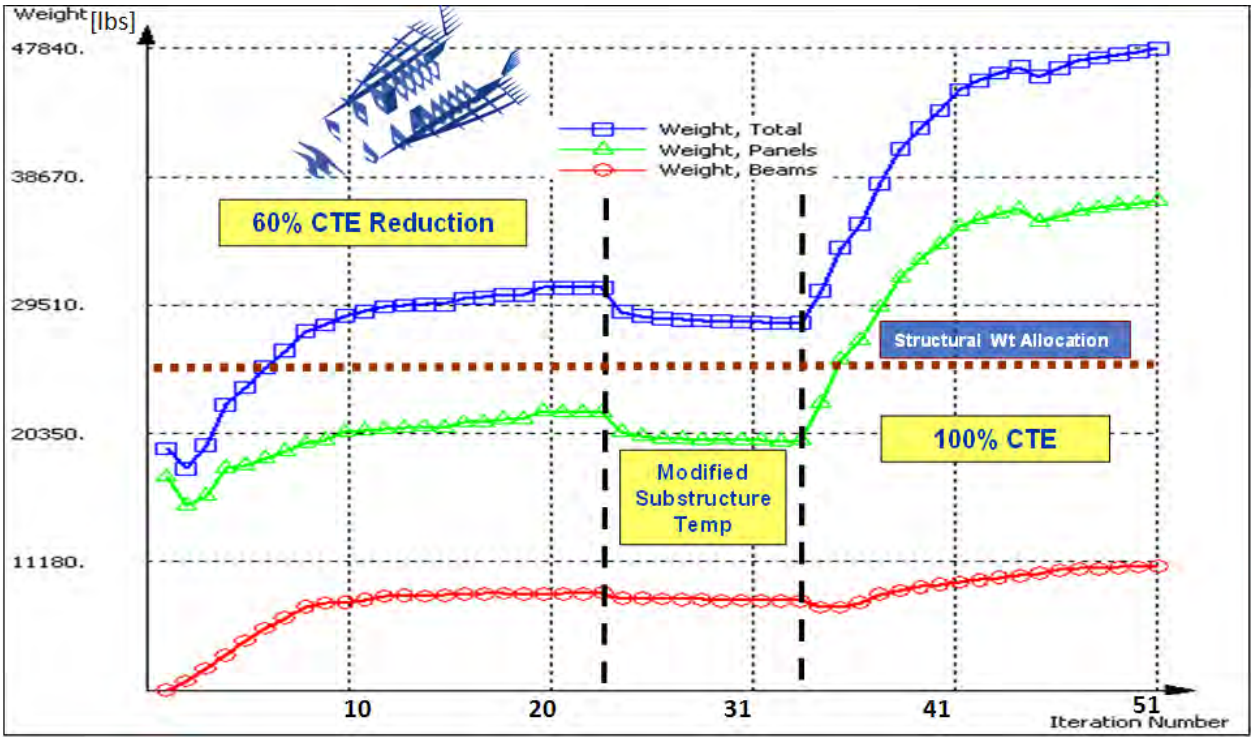

Figure 12. Modified TX-V FEM Structural Sizing History

Though all three of these options provided effective ways to reduce the vehicle weight, there were unaddressed uncertainties related to two of the options. The modified substructure option removed a large portion of primary structure. This modified the load paths of the vehicle, however revised mechanical load case was not created to capture this new load path. To do so would require substantial effort already performed in Phase I. Therefore, modifying the substructure is not a valid option. Additionally, the modified substructure temperature gradient was based on an engineering assumption. Its estimation is not well supported and should not be used to aid in closing the vehicle. With these restrictions in mind, the decision was made and discussed with the program managers at the AFRL to proceed with the full FEM configuration using a 60% CTE reduction. It was determined this solution would best support the objectives for Phase II.

3.4 Panel Sizing Results

A panel level trade study was performed for the four panel locations shown in Figure 13. The panel locations were selected in Phase I and represent critical thermal and acoustic environments for more detailed study. The panel numbers shown in Figure 13 correspond to the FEM panel property ID numbers. It should be noted that different panels were ultimately selected for detailed analysis in Task 2, although 3 of the 4 were in similar locations.

Approved for public release; distribution unlimited.

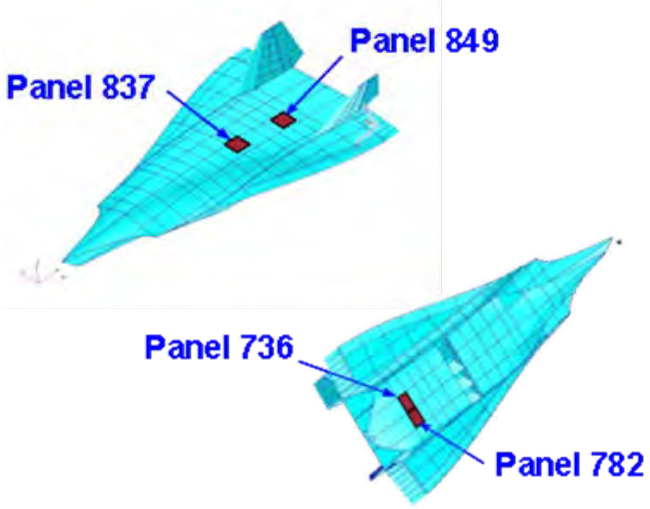

Figure 13. Critical Panel Locations

For each of the locations, panel sizing was performed for the four panel concepts illustrated in Figure 14. The panel concepts included; honeycomb sandwich, grid stiffened Isogrid, skin-stringer uniaxial, and a truss core panel. The panel internal loads N_x,N_y,N_{xy}, M_x,M_y,M_{xy}, Q_x, Q_y were obtained from the baseline TX-V vehicle FEM using a 60% CTE reduction, with the modified internal temperature distribution, and a NASTRAN sized honeycomb sandwich structure.

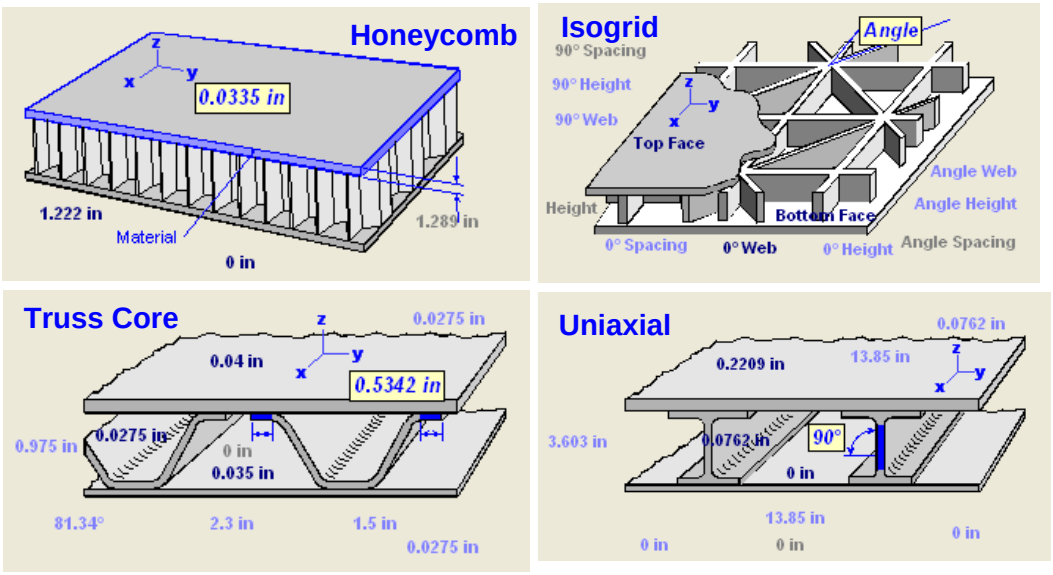

Figure 14. Panel Concepts Investigated

The results of the panel sizing study for each concept and location are shown in Figure 15. In general the results indicate that panels that are not able to efficiently support a biaxial load state produce the heaviest design. This is evident for the skin-stringer concept where the unit weight is significantly greater than the other panel concepts. For each location the honeycomb sandwich

panel produced the lightest results since it is capable of efficiently accommodating loading in any direction. It is believed that the biaxial load state is strongly influenced by the structural layout and attachment modeling of the current TX-V FEM. This would suggest that the current result trends would not necessarily hold for alternate structural concepts. It should also be noted that honeycomb sandwich panels often present the lightest solution for bi-axially loaded and stiffness driven structures. Bonded and brazed honeycomb sandwich panels tend to have poor damage arrestment capability however, and panel configurations with welded, fastened, or integral stiffeners are typically selected for operational aircraft. Iso-grid and truss (or fluted) sandwich panel configurations were thus initially evaluated in the Task 2 detailed design effort. Additional discussion about the merits of these two panel concepts can be found Section 4.3.1

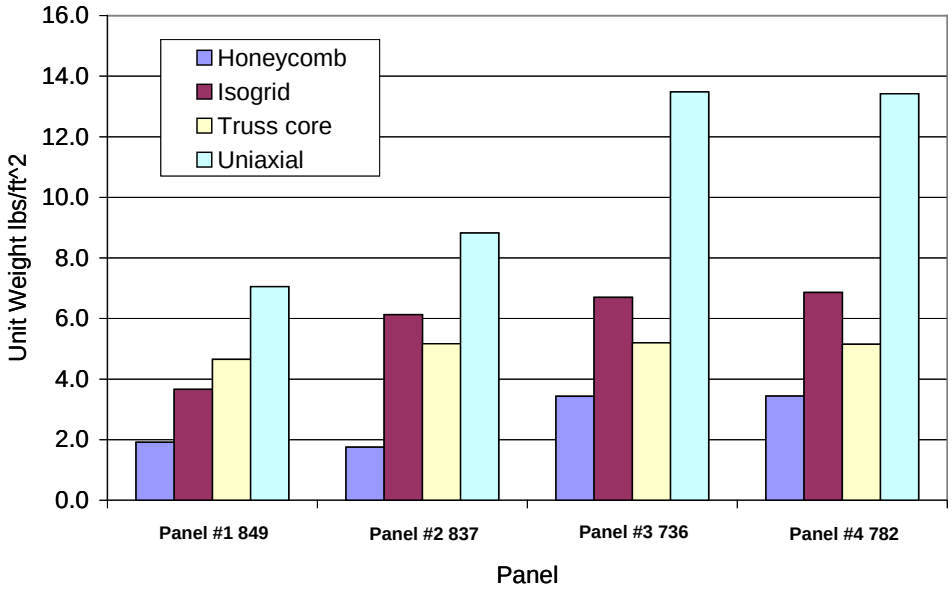

Figure 15. Panel Unit Weights for Different Panel Concepts

3.5 Task 1 Summary

In Phase I the TX-V reference vehicle was derived from the Boeing Manta 2025 by simply removing the TPS and using materials capable of withstanding Mach 7 hypersonic cruise environments. Flight maneuver, landing, and thermal loads along with acoustic panel frequency requirements were developed and applied to the structural model for sizing. The initial structural sizing failed to converge due to excessive thermal loading. A reduced thermal environment equivalent to cruise at Mach 4-5 was used to produce a converged result.

In Phase II several approaches to improve the efficiency of the TX-V structural design were investigated to "close" the design for Mach 7 environments. It is believed the best solution is to employ a “clean-sheet” design with a structure specifically designed to accommodate high temperatures and thermal gradients while minimizing unnecessary structural area to reduce weight. This approach would not have fit within the scope of this effort, so alternate methods were investigated to improve the existing design. The first approach attempted to modify the

existing TX-V FEM by removing bulkhead and keel structure to reduce thermal loading & save weight. This approach showed potential, but required further refinement to meet the weight target. Another approach that was investigated was to modify the internal temperature distribution of the substructure. The original thermal analysis did not include internal heat sources or radiation effects for the internal structure. The goal of this analysis was to examine the impact increased internal temperatures had on the sizing results. The last solution investigated to "close" the structural design was to use a reduced CTE as a way of simulating a more compliant structure for the global vehicle analysis. In the detailed panel design and analysis tasks, features such as sine wave webs and attachment details could then incorporated to obtain characteristics compatible with these global vehicle sizing assumptions.

Structural sizing was performed for the potential solutions identified. Based on the results it was decided to go forward with the reduced CTE approach. The revised CTE was applied to the TX-V FEM and was used for performing a panel trade study for a variety of panel concepts. The results of this analysis showed that panel concepts that could efficiently carry biaxial loading produced the lightest designs. Although the lightest concept, honeycomb panels were not considered in Task 2 due to concerns over damage tolerance. Iso-grid and truss (or fluted) sandwich panel configurations were thus initially evaluated in the Task 2 detailed design effort.

Approved for public release; distribution unlimited.

4.0 DETAILED PANEL DESIGN AND ANALYSIS

4.1 Task 2 Overview and Panel Selection

Task 2 includes the detailed design and analysis of 4 panels. The 4 panels were selected to provide a variation in which failure modes drive the design of each panel. The panels shown in Figure 16 represent both windward and leeward surface panels; fore, aft and wing panels; engine bay and fuel tank bay panels; and vary in temperature by more than 350° F. Panel 1 is located on the upper surface of the aft fuselage over the combustion region of the engines, has the lowest peak temperature, and was expected to be driven by acoustic and mechanical loads. Panel 2 is located on the lower surface beneath Panel 1, sees much higher temperatures, and was expected to be driven by thermally degraded material properties and thermal stresses. Panel 3 is located on the upper surface towards the center of the fuselage over a fuel tank and sees lower temperatures and acoustic loads. It was expected that Panel 3 would be sized to be one of the least stiff panels and would thus be driven by acoustic fatigue and flutter concerns. Lastly, Panel 4 is the largest panel and is located on the lower surface of the wing where. Panel 4 sees the highest peak temperatures, relatively high acoustic loads, but relatively low mechanical loads. It was thus expected that Panel 4 would be sized as a relatively flexible panel and that it would be driven by acoustic and thermal issues.

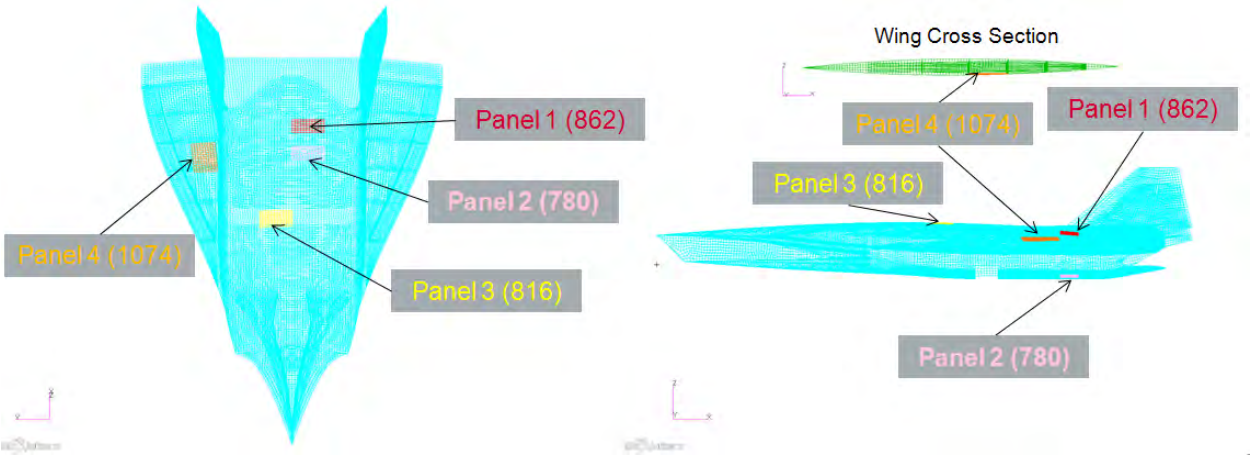

Figure 16. Selected Panel Locations

Table 3 lists the location and environments for each panel, along with the expected and actual panel response drivers. In general, thermal stresses, deflections, buckling and the low-cycle thermal-mechanical fatigue drove the design and life prediction of all panels. Acoustic fatigue was an issue while flutter margins were high for the two panels evaluated. It should be noted that the thermal loads for Panels 3 & 4 were initially under predicted and as a result these panels were undersized and have several low margins after this initial design and analysis cycle. Additional design iterations would provide the sizing modifications to mitigate these negative margins.

Approved for public release; distribution unlimited.

Table 3. Overview of selected panel characteristics and analysis results

Analysis Order	1	2	3	4
Global FEM ID	**862**	**780**	**816**	**1074**
Region	Aft fuselage	Aft fuselage	Mid fuselage	Wing
Surface	Upper	Lower	Upper	Lower
Airframe Feature	Engine Bay	Engine Bay	Fuel Tank	Fuel Tank
Appr Temperature	1100 F	1440 F	1230 F	1465 F
Appr Acoustic Level	161 dB	158dB	155 dB	161 dB
Expected Structural Integrity Drivers	Acoustic Fatigue Mechanical Fatigue	Thermal Stress Therm-Mech Fatigue	Acoustic Fatigue Flutter	Acoustic Thermal Stress
Actual Structural Integrity Drivers	Acoustic Fatigue Deflections	Therm-Mech Fatigue Buckling Deflections	Therm-Mech Fatigue Buckling Deflections	Thermal Stress Buckling Deflections
Static Margins	High	High	High	-0.27
Normal Deflection	0.19 in	0.12 in	0.45 in	0.51 in
Buckling Eigenvalue	High	0.99	0.83	0.61
Acoustic Fatigue Margin	-0.02	0.27	0.03	-.65
Therm-Mech Fatigue Margin	0.41	-0.6	-0.42	N/A
Flutter Margin	NA	NA	> 75,000 ft	31,000 ft

4.2 Detailed Design Approach

In order to represent the panel boundary conditions accurately, a unit cell analysis method was developed. This analysis included the panel of interest along with a half bay fore/aft and left/right through the entire depth of the vehicle. In this method, the panel is appropriately loaded thermally by the surrounding panels and the substructure. Additionally, the interaction between the panel and its surroundings can be tailored by modifying the surrounding structure. Each unit cell is representative of the panel location on the global vehicle.

All 4 panels utilize the unit cell analysis method; panel 1 (862) and 2 (780) share the same unit cell as they are windward and leeward panels of the same bay, while panel 3 (816) and panel 4 (1074) each have their own unit cells. The details of each unit cell vary slightly. Among the differences are: panel curvature, surrounding panels material type and thicknesses, substructure geometry, thermal boundary conditions and mechanical boundary conditions.

The following sections will provide a summary of how the unit cell was used to perform the panel analyses. Also included are the studies used to determine the unit cell design details and panel design concept. The same analysis process flow, outlined in Figure 17, was used for all four panels.

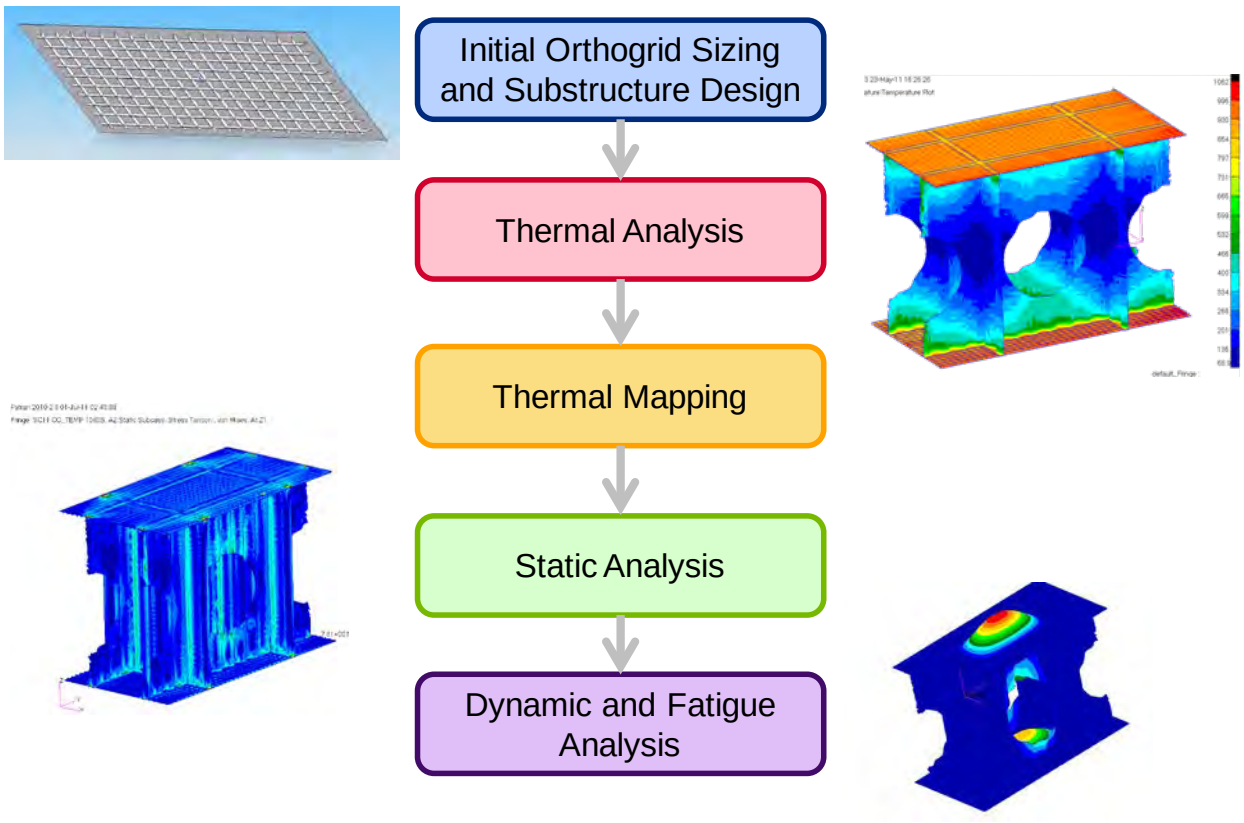

Figure 17. Design and Analysis Flow for each panel

4.2.1 Substructure Trade Study

The global vehicle sizing studies performed in Task 1 revealed that a weight efficient structure would not be achievable with heritage low expansion structural approaches using realistic sizing assumptions. Large thermal gradients through-the-thickness of the structure results in hot skin panels being restrained from expansion by a colder substructure. Initial discussions on how to address this challenge focused on flexible or sliding panel attachment designs which would allow the panels to expand relative to a fixed substructure. These concepts were seen as high risk for primary external structure due to the need to avoid steps, gaps, and leak paths in the aerodynamic surfaces of the vehicle. A small study was thus performed to evaluate substructure configurations which would allow the substructure to expand along with the skin while still effectively transferring shear and normal loads. The configurations evaluated include a) both keels and frames with sine-wave webs, and b) a hybrid approach with sine-wave keels and truss frames.

4.2.1.1 Unit Cell Approach and Validation

Evaluating multiple substructure concepts with the global FEM would have required significant resources. A unit cell analysis approach, shown in Figure 18, was thus proposed to study alternate substructure configurations. The unit cell includes the bay of the panel of interest and half of the surrounding bays. Since panel mechanical loads are small relative to thermal loads and these thermal loads are driven by local temperature gradients through the structure, it

was felt this unit cell was the minimum amount of modeled structure required to capture panel interaction with the substructure. The boundaries are constrained such that each side of the unit cell can expand uniformly in the XY plane. The panels were also assumed to be flat similar to the approach taken in the Panel 1 (862) and Panel 2 (780) Unit Cells.

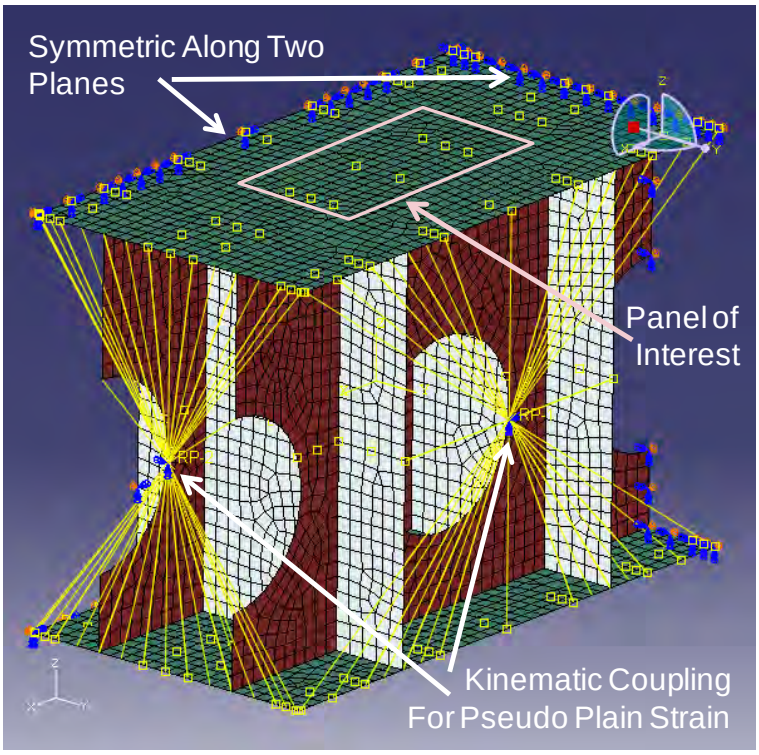

Figure 18. Unit cell boundary conditions

In order to verify the accuracy of a unit cell model, panel thermal load results from a unit cell were compared to those calculated with the global model. A unit cell model was built using the 60% CTE reduction assumption that the global model used and boundary temperatures were applied in a steady state thermal solution in an attempt to match the global model temperature distribution. Figure 19 shows the temperature distribution on a cutout from the global model and the approximate matched distribution on the unit cell validation model. Although the distribution through the unit cell was not exactly the same as the global model, the total ΔT was matched. The resulting thermal loads, shown in Table 4, show that the unit cell roughly matched the global FEM loads. It was thus decided to move forward with the unit cell for the purposes of the substructure trade.

Approved for public release; distribution unlimited.

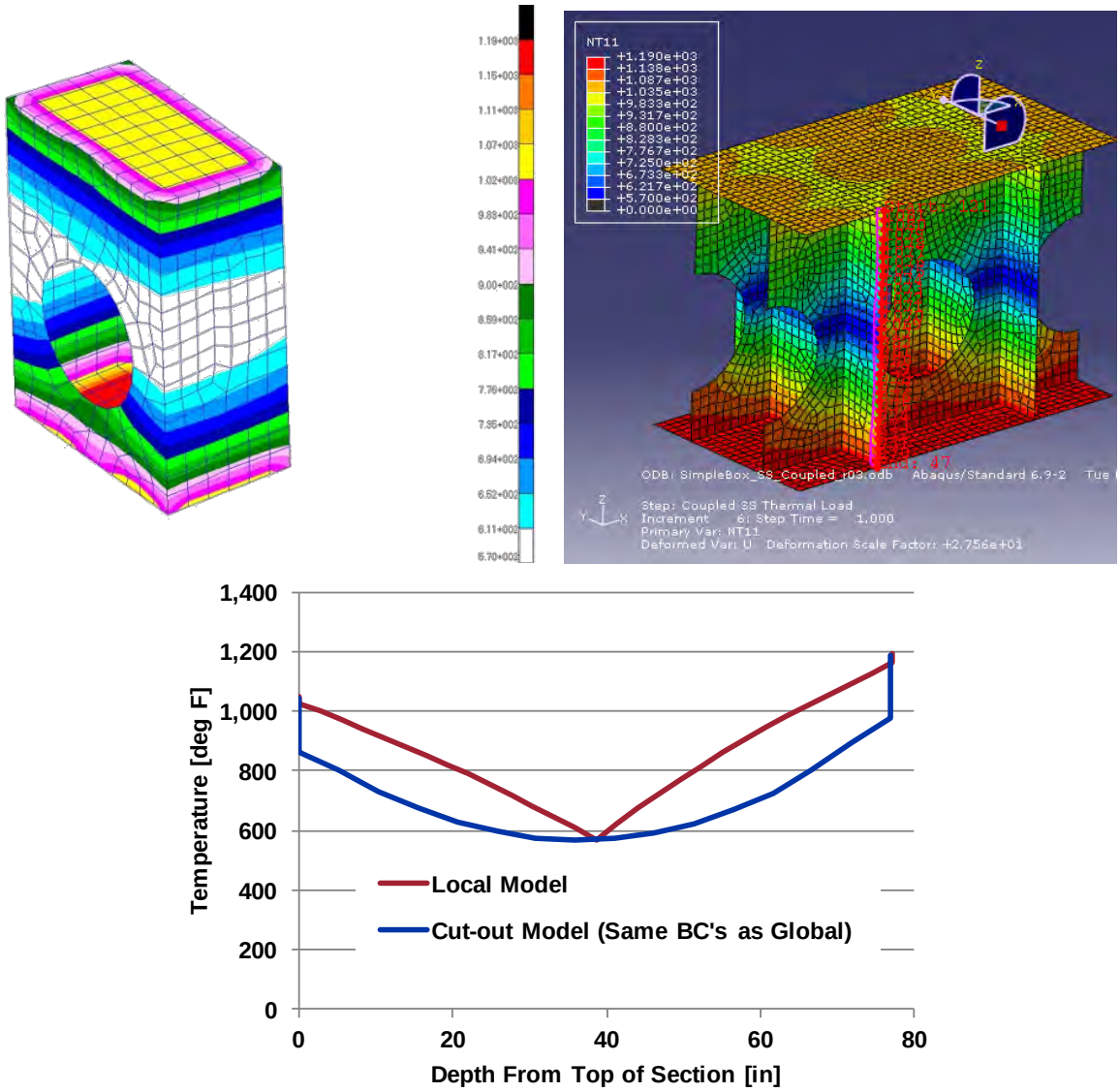

Figure 19. Temperature distributions for a bay cutout of the gloabl model (upper left) and the validation unit cell model (upper right), and a comparison of profiles through the depth (bottom)

Table 4. Unit cell model approximately matched thermal loads from global model

	Global Model	Local Model	% Difference
Nx [lbs/in]	782	757	3.2%
Ny [lbs/in]	624	558	10.6%

Approved for public release; distribution unlimited.

4.2.1.2 Alternate Configurations and Analysis Results

The two alternate substructure configurations evaluated in this study are shown in Figure 20. Both the sine-wave web and truss elements are meant to allow skin panel expansion while transferring shear across the structural box. Unlike the sine-wave keels and frames, the truss elements to do not effectively carry loads normal to the skin and a truss only substructure is likely impractical. The truss elements were expected to be significantly more flexible however, so a hybrid approach that uses truss frames and sine-wave keels was evaluated. This concept is similar to the Space Shuttle Orbiter wing which used corrugated web spars and truss element ribs. Although the Orbiter wing design was not developed specifically to relieve thermal loads, rather it was optimized for weight; it does illustrate the validity of the concept.

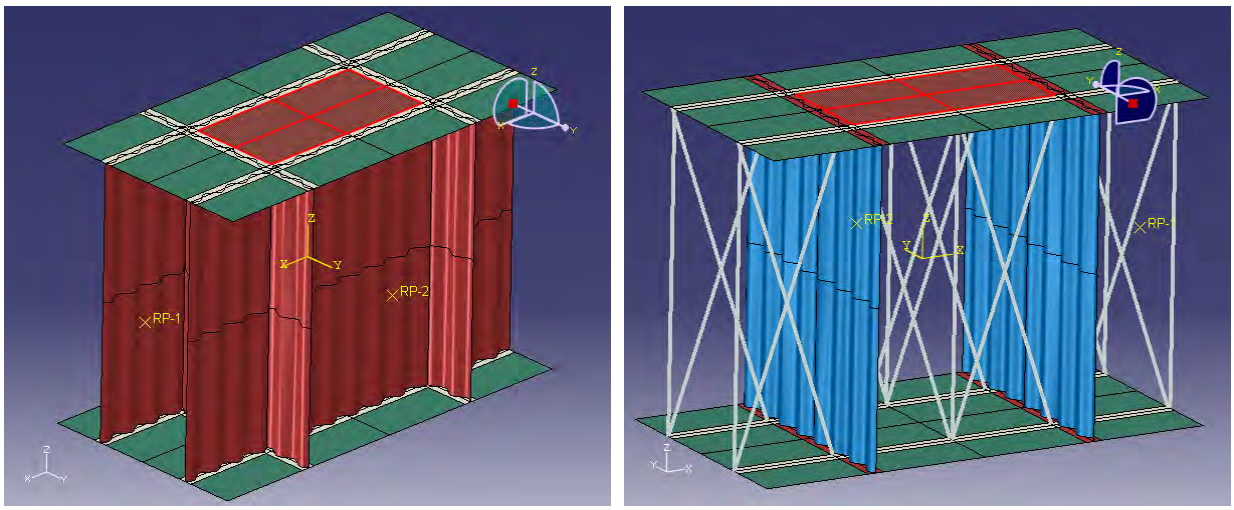

Figure 20. Alternate sine-wave web and hybrid truss plus sine-wave substructure configurations

A summary of analysis results for eight cases evaluated in the study is provided in Table 5. The first case shows the global model results with 40% CTE, while the 2nd and 3rd case show the equivalent flat-web unit cell results for a steady state (SS) thermal solution with 40% and 100% of the CTE of Inconel 718 used. These results show the resulting thermal loads (Nx and Ny) scale linearly with the material CTE. Although this is expected it is a good check on the functionality of the model. The next two cases apply a transient heat flux to the flat-web model with 40% and 100% CTE, while the final three cases looked at the all sine-wave unit cell with 40% and 100%, and the hybrid (combo) approach with both sine-wave webs and truss elements. A transient heat flux was applied in an attempt to create more realistic thermal gradients within the structure. Unfortunately, the heat flux data was incorrectly taken from leading edge body point and the resulting temperatures and loads are much higher than they should be. Although the absolute load results are skewed by these high temperatures, the relative difference in results between cases is still insightful and provides valuable information. As an additional check on the results, both the flat web and sine wave web results for the transient heating case show that the thermal loads maintain a linear scaling relationship with material CTE. Furthermore, the sine-wave web configurations show a significant drop in thermal load, by a factor of 16.5, for the same boundary conditions. Lastly, the hybrid case shows an additional 50% decrease in thermal load in the direction the truss elements are used (Nx).

Table 5. Summary of substructure trade results (Nx & Ny are the resulting panel thermal loads)

Case ->	Global Model	BC Mimic	BC Mimic + CTE	Simple Trans 01	Simple Trans 02	Sine Trans 02	Sine Trans 01	Combo Trans 01
Thermal Condition	SS, T & conv	SS, T only	SS, T only	Trans, 464 s	Trans, 464 s	Trans, 462 s	Trans, 462 s	Trans, 456 s
Material CTE	40%	40%	100%	40%	100%	40%	100%	100%
Substructure Design	Flat Web	Flat Web	Flat Web	Flat Web	Flat Web	Sine Web	Sine Web	Sine & Truss
Upper Surface Temp [F]	1045	1050	1050	1725	1725	1731	1731	1727
Lower Surface Temp [F]	1188	1190	1190	1761	1761	1767	1767	1762
Nx [lbs/in]	782	757	1,892	3,005	7,513	172	430	223
Ny [lbs/in]	624	558	1,394	2,954	7,382	189	473	464
Sine-wave web thermal load reduction factor, (flat web ave load / sine wave web ave load)						16.5	16.5	

It was decided to move forward with the sine-wave web configuration as it provided significant load relief and could be simulated with equivalent properties in the existing flat-web global model. In addition to concerns about high out of plane skin deflections, the truss structure approach would have been difficult to simulate in the global model and the additional load reduction was not significant enough to justify its use.

4.2.1.3 Equivalent Sine-Wave Web Properties

Equivalent sine-wave web properties for flat shell elements were developed for use in the existing global vehicle FEM. A sine-wave web model with an amplitude of 1 inch and wavelength of 8 inches was analyzed to determine its equivalent modulus in the skin expansion direction (E11) and its shear modulus (G12). The vertical direction modulus and density were estimated by the ratio of the sine-wave web chord length to its absolute length. These properties were then used in a flat model with a sandwich definition and the core thickness was varied until the bending stiffness of the sandwich panel roughly matched that of the sine-wave web. The resulting equivalent sandwich panel properties are provided in Table 6. These properties were incorporated into the global FEM and used to provide mechanical loads for detailed panel sizing.

Table 6. Equivalent sine-wave web properties for flat shell elements

Sine-Wave Web Thickens (in)	Equivalent Flat Sandwich Properties (Moduli are Skin Values)				
	Facesheet t (in)	Core t (in)	E11 (psi)	E22 (psi)	G12 (psi)
0.030	.015	1.25	120	33e6	9e6
0.104	.052	1.25	63e3	33e6	9e6

4.2.2 Design and Sizing Approach

All four panels were sized in HyperSizer and drawn along with their unit cells in SolidWorks. HyperSizer inputs included:

- Panel Construction
- Planform Dimensions
- Material Selection
- Minimum Gages

- Mechanical and Thermal Edge Loads
- Normal Pressure
- Panel Temperature
- Panel Temperature Gradient Through the Thickness
- Mechanical and Thermal Factors of Safety

Corrugated, or fluted, core sandwich, iso-grid, and ortho-grid panel constructions were initially compared for Panel 1. Ortho-grid construction was down selected for Panel 1 and was subsequently used for the remaining three panels. A detailed discussion of this down selection is provided in Section 4.3.1 Panel planform dimensions were taken from the Global FEM, while Inconel 718 was used for all panels due to high expected temperatures, and minimum gages were based on past experience and engineering judgment. Mechanical edge loads were taken from the Global FEM while thermal loads were estimated from prior analysis. For example, the Panel 1 thermal loads were initially based on the substructure trade study, while Panel 3 loads were estimated to be similar to the loads obtained from the Panel 1 detailed analysis. These estimates became a large source of error for Panels 3 & 4 and will be discussed thoroughly in the detailed results sections for these panels. Panel aero pressures were estimated from CFD surface contour plots and it was assumed the panels would see only atmospheric pressure thereby inducing no pressure differential across the panel. This assumption was based largely on the belief that we would not be able to develop a pressure seal that would operate at the expected skin temperatures. Panel temperatures and thermal gradients were estimated from prior results, while a FOS of 1.5 was used for mechanical ultimate loads, 1.15 was used for mechanical limit loads (yield criteria), and 1.0 was used for thermal loads.

Detailed solid geometry was initially created for all three Panel 1 constructions: corrugated sandwich, iso-grid, and ortho-grid. Discussions with the thermal and stress analysis teams later revealed that mid-plane surface geometry without any detailed features was desired for building analysis models. De-featured unit cell surface geometry, that did not include fastener holes or fillets, was thus created for Panel 1 and each subsequent panel. Unit cell geometry included the panel of interest with stiffening features, the surrounding panels, the substructure sine-wave webs with caps, and the skin surfaces on the opposing side of the vehicle. Unit cell geometry was initially provided with sized stiffening features included for adjacent panels, but these were not included after Panel 1 in order to more accurately represent the global vehicle model stiffness. The sized panels were around 0.6 inches in overall thickness where some of the global vehicle honeycomb panels were up to 4 inches in thickness resulting in a large difference in bending stiffness. It should also be noted that unit cell geometry for Panels 1 & 2 used flat skins. The use of flat skins significantly reduced geometry and analysis model generation time while allowing for simple geometry modifications from within the analysis program. This assumption was not thought to have a significant impact on stress results due to the very large radius of curvature in that region of the vehicle. Panels 3 & 4 were located in more lofted regions of the vehicle and curved geometry was created to match the Global FEM. Lofted Panel 3 unit cell geometry in shown in Figure 21.

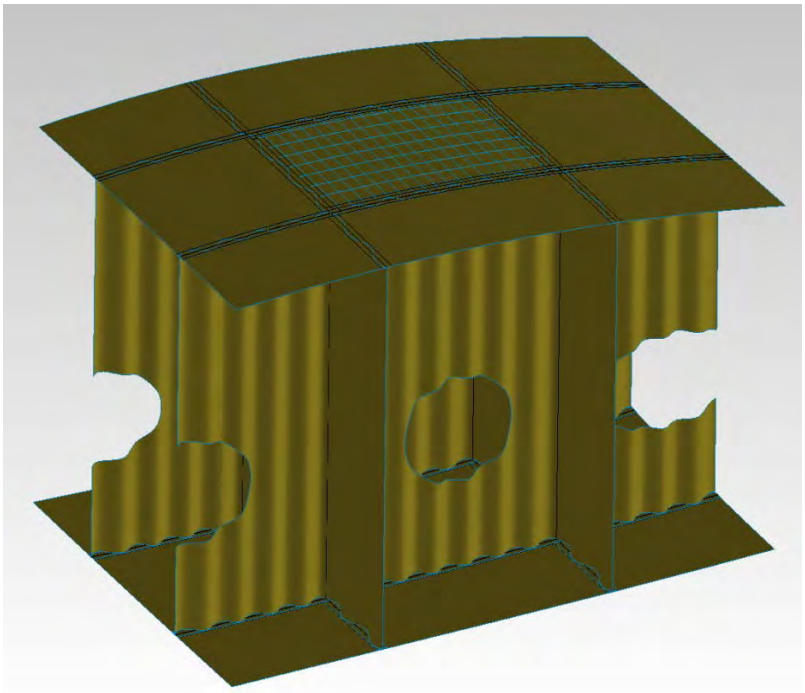

Figure 21. Panel 3 lofted unit cell surface geometry

4.2.3 Thermal Analysis Approach

Thermal analysis of the structural concepts was conducted with the finite element code I-DEAS/TMG. A mesh refinement study was conducted on the first panel to determine the mesh density required to accurately capture local temperature gradients. The results of this study were applied to all of the panels. Internal boundary conditions vary from panel to panel and were modeled by fixed temperatures or lumped mass heat capacities as appropriate. Initial structural temperatures were assumed uniform and equal to the recovery temperature at the initial flight conditions. External aerothermal environments were calculated using the 2D boundary layer code, MINIVER using the flight trajectory developed in Phase 1 shown in Figure 22. Heating variations over the panel surfaces are neglected. In converting the recovery enthalpies calculated by MINIVER to the recovery temperatures required in the finite element analysis, a constant room temperature value of specific heat was used. This resulted in an over-prediction of recovery temperatures of up to 15%. This is estimated to result in structural temperatures over-approximated by 5%. This error has inadvertently introduced conservatism in the thermal stress predictions. External upper and lower skin surfaces radiate to effective sky and earth temperatures respectively. Temperature dependent material properties are used in all cases. Analysis assumptions are summarized in Table 7. Resulting transient temperature predictions are then analyzed to determine time states of maximum temperature and gradients. These temperature distributions are then mapped to the structural FEM.

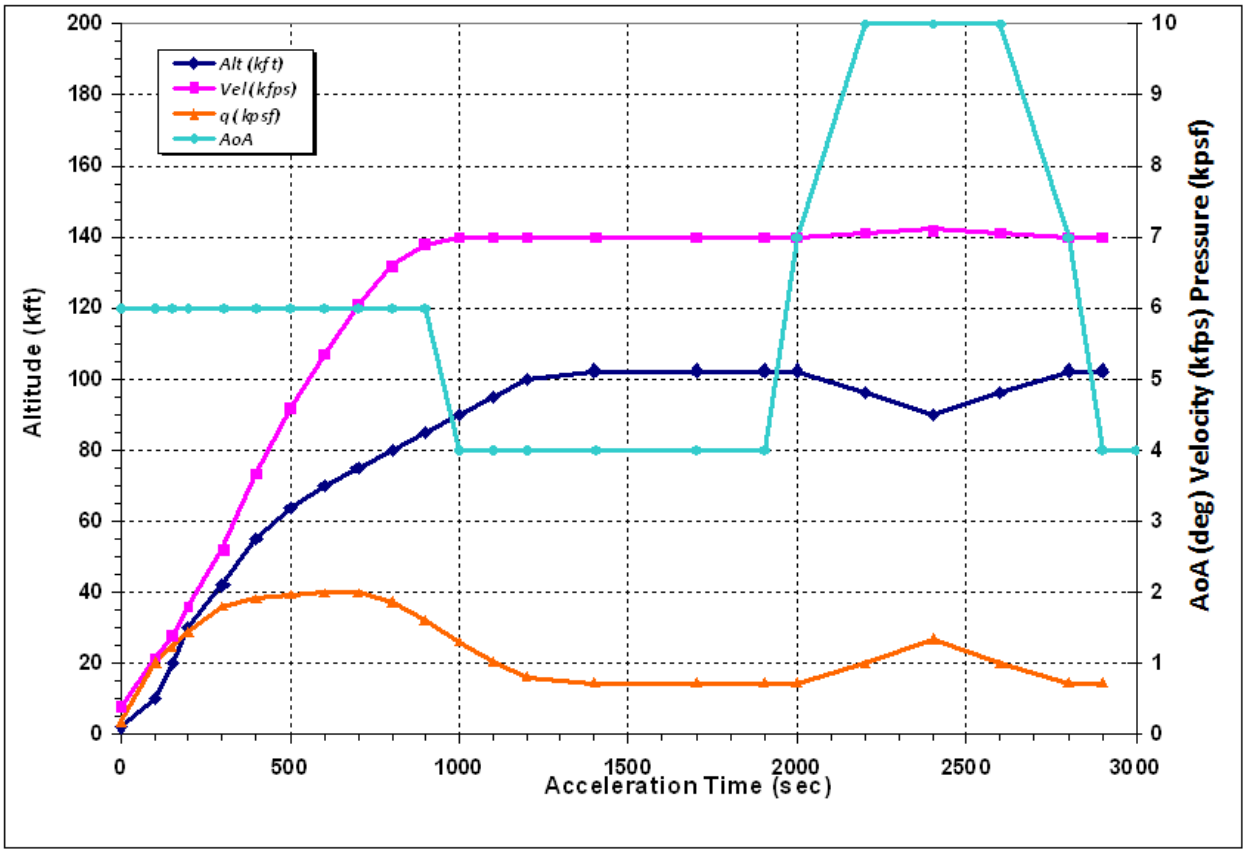

Figure 22. Flight Trajectory

Approved for public release; distribution unlimited.

Table 7. Heat Transfer Analysis Methods and Assumptions.

Issue	Approach	Source/Rationale
External Aero-heating	MINIVER analysis	Phase 1 analysis
Upper surface radiation	Radiation to effective sky temperature (Swinbank's method), view factor = 1	Preferred method:787, AWS, programs
Lower surface radiation	Radiation to earth surface (70 F), vf = 1	Standard conditions
Upper surface solar flux	Ignored	Insignificant w.r.t. aero-heating
Engine boundary condition	Uniform, time-dependant temperature inside 1" Min-K blanket	Lee Scuderi – previous programs
Internal cavity convection	Uniform natural convection at ambient pressure +1 psi	Kei Lau – previous programs
Internal radiation	Radiation enclosure in each cell	Symmetry in partially meshed cells
Initial temperature	Recovery temperature at time = 0.	Assumes uniform soak before flight 13°F, 25kft, M=0.75
Material properties	Temperature dependent	Material property databases
Finite element formulation	All shell elements	Conductive material, thin components result in insignificant through-thickness gradients
Thermal contact between webs and skin	100 Btu/ft^2-hr-F interface conductance No fasteners modeled	Typical metal-metal handbook value - conservative

4.2.4 Thermal Mapping Approach

The temperature distribution created by aero-heating, propulsion and other components internal to the structure is needed to assess the integrity of hypersonic structures. For efficiency of computation the thermal and structural analyses are generally performed using different solvers with models of different fidelities. A tool is therefore required to convert temperatures accurately from thermal to structural models for analysis, especially in areas with high thermal gradient. Boeing through its internal funding has developed a thermal mapping tool based on finite element (FE) formulation for this purpose. The tool aligns geometry of two models, and searches for the corresponding location of a structural node on the thermal model before assign temperature to the node with FE equations. Most element types are supported, including linear or quadratic and shell or solid elements, including quadrilateral, triangular, hexagon, tetrahedral and wedge, For example, the temperatures computed with a solid thermal model can be mapped to a plate-shell structural model. In the process, the user can request temperatures at different time steps for their analysis. A short description of the mapping method is as follows:

The location of a structural node mapped to a thermal finite element can be found with

$$x = \sum_{i=1}^{n} N_i(\xi,\eta,\varsigma)x_i$$

$$y = \sum_{i=1}^{n} N_i(\xi,\eta,\varsigma)y_i$$

$$z = \sum_{i=1}^{n} N_i(\xi,\eta,\varsigma)z_i$$

where N_i are the element shape functions, n is the number of nodes in the element, x_i , y_i and z_i are the ith nodal coordinates of element, and ξ, η and ζ are the local coordinates of the element, where the to-be-mapped structural node with coordinates of *x, y* and *z* refers to.

The temperature at the mapped node is then obtained from that at nodes of thermal element as

$$T = \sum_{i=1}^{n} N_i(\xi,\eta,\varsigma)T_i$$

Any deviation in geometry between two models can be overcome with an extrapolation to obtain a structural nodal temperature from that of a nearby thermal element. In addition, thermal nodal temperatures can be output from a thermal analysis or averaged from surrounding element temperatures.

The input required to pursue thermal mapping includes

- Structural FE models in either NASTRAN or ABAQUS format
- Thermal FE models in either NASTRAN or ABAQUS format
- Group files containing part of thermal or structural models for more accurate mapping
- Control parameters allowing extrapolations for voids due to mismatch between two models

The function module of the tool, which performs model matching, structural node and thermal element correlation, numerical search, and temperature data interpolation, was developed in FORTRAN. The execution of the module was facilitated by a PATRAN Graphical User Interface (GUI).

A demonstration and validation of the tool can be found with the mapping of Panel 2 in Figure 23 and Figure 24. These figures show the thermal model and temperature distribution at t=2520sec, and the structural model and corresponding temperature distribution. The thermal model is consisted of 23,800 nodes and 24,000 elements. The structural model is much finer and has 104,900 nodes and 98,900 elements.

One lesson learned during the exercise of the mapping tool under this program was that using nodal temperatures averaged from element temperatures led to an accuracy issue with the results. The nodal temperatures are now therefore directly output from thermal analysis for all subsequent analyses.

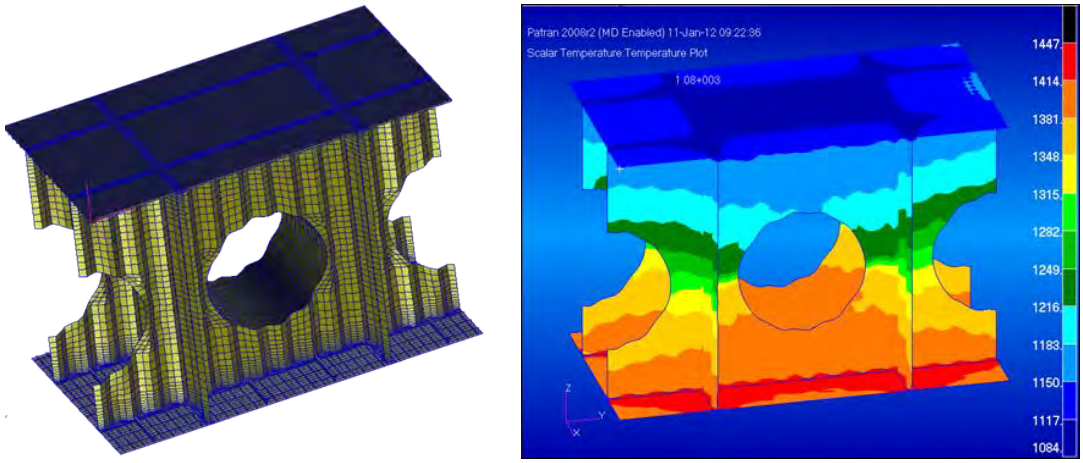

(a) Thermal Finite Element Model (b) Temperature Distribution

Figure 23. Thermal Model of Panel 2 and Temperature Distribution at t=2,520sec

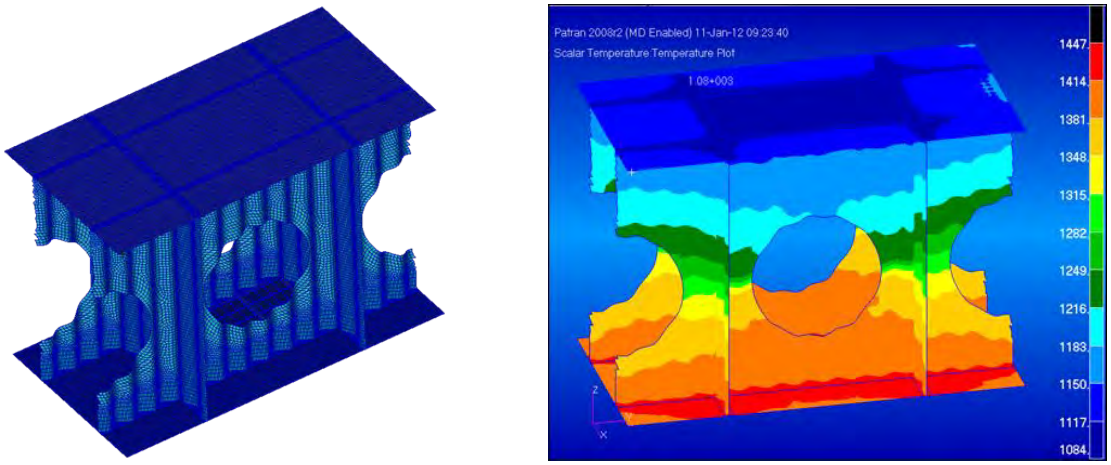

(a) Structural Finite Element Model (b) Temperature Distribution

Figure 24. Structural model of Panel 2 and temperature distribution at t=2,520 sec

4.2.5 Stress Analysis Approach

Each of the four panels follow the same stress analysis approach. There are slight variations as lessons learned are incorporated into subsequent analyses. These variations will be highlighted in the following sections along with the detailed results for each panel. All static analyses were performed using Patran 2010/Nastran 2010.1 FEA software.

The static analysis follows a three-part loads generation procedure that begins with the global vehicle model, continues with the unit cell model, then is completed with a panel level model. The global vehicle model, which was refined in Task 1, produces the mechanical loading and the geometry for the unit cell. The unit cell model incorporates the mechanical loading from the

global vehicle model and generates the thermal loading on the panel of interest by applying a temperature profile to the unit cell. Lastly, both mechanical and thermal loading is taken from the unit cell and is applied to the Panel level model through enforced displacements along the boundary of the panel. This process flow is shown in Figure 25.

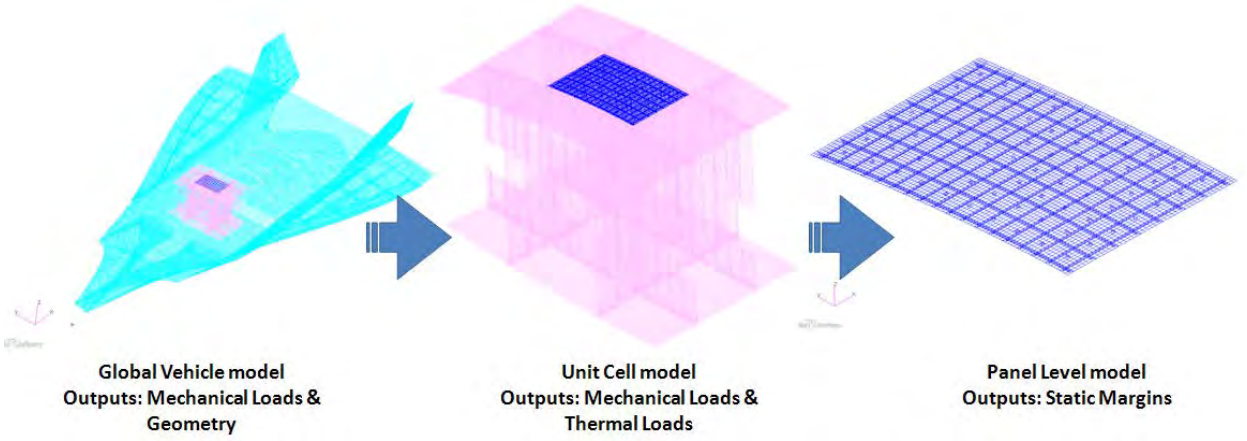

Figure 25 Process flow to generate accurate loading and boundary conditions on the panel of interest

No manipulation is done to the global vehicle model in Task 2 (Recommendation #1, Page 3). It is only referenced for geometry and mechanical loads.

The first step taken for each unit cell static analysis is to generate the finite element model. This process begins with the geometry creation. Each unit cell was modeled based on the global vehicle model geometry. Unit cell 1 (Panel 1 (862)) and unit cell 2 (Panel 2 (780)) are geometrically identical as the two panels share the same bay. Unit cell 1/2 has simplified geometry: the panel surfaces are represented as flat surfaces because the radius of curvature >> 1000"; the location of the frames and keels were estimated based on panel dimension. These simplifications make the geometry creation very quick, however it also causes the loading points from the global vehicle model to lie further than desired from the load application point within the unit cell. To provide a comparison, unit cell 3 (panel 3 (816)) and unit cell 4 (panel 4 (1074)) both used lofted surfaces that were extracted from the global vehicle Model. This eliminated the misalignment of nodes, however this process was quite difficult due to the availability of tools.

Several methods were tried unsuccessfully to extract the lofted surface from the global vehicle model and create the surface in SolidWorks. This technology gap proved cumbersome to overcome. Patran has several built in functions to export surfaces, elements, or nodes to a variety of CAD compatible formats. All of Patran's functionality, in this regard, did not create the desired result. The next method required an export of all the nodes in the surface which would be used to create the CAD surface. CATIA and SolidWorks do not have the capability to create a surface based on a set of points. Unigraphics does have a "Create Surface from Point Cloud" function which was successfully used to create the top and bottom skin CAD surfaces. Unfortunately, Unigraphics could not create some of the Keel and Frame CAD surfaces. Instead these surfaces were created using X, Y, Z node coordinates; a tedious and error prone process.

Once the geometry had been created, Inconel 718 material properties were applied to the elements. These material properties are based on MMPDS-05 [9], formerly Mil-Hdbk-5, (Figure 26). Since this analysis involved high temperatures, thermal knockdowns were applied to materials via Nastran MATT1 cards. These knockdowns were also referenced from MMPDS-05 [9] (Figure 27 - Figure 30). Figure 27 is valid for exposure for up to 30 minutes, while the TX-V flight profile is 60 minutes. Also, Figure 28 and Figure 29 show knockdown factors for dynamic modulus at temperature; no knockdown factors for static modulus at temperatures are available. Additional material data is required for a more accurate set of thermal knockdowns.

Approved for public release; distribution unlimited.

Table 6.3.5.0(c). Design Mechanical and Physical Properties of Inconel 718 Bar and Forging

Specification	AMS 5662 and AMS 5663								AMS 5664	
Form	Bar							Forging	Bar	Forging
Condition	Solution treated and aged per indicated specification									
Thickness, in.	0.250-1.000	1.001-1.500	1.501-2.000	2.001-2.500	2.501-3.000	3.001-4.000	4.001-5.000	≤5.000	≤10.000	≤10.000
Basis	S	S	S	S	S	S	S	S	S	S
Mechanical Properties:										
F_{tu}, ksi:										
L	185	185	185	185	185	185	185	185	185	180
LT[a]	180	180	180	180	180	180	180	180	180	180
ST[a]	...	...	...	...	180	180	180	...	...	180
F_{cy}, ksi:										
L	150	150	150	150	150	150	150	150	150	150
LT[a]	150	150	150	150	150	150	150	150	150	150
ST[a]	...	...	...	...	146	150	150	...	...	150
F_{cy}, ksi:										
L	156	156	156	156	156	156	156	...	...	...
ST	...	...	...	156	156	156	156	...	...	...
F_{su}, ksi	111	114	116	118	119	121	123	...	...	...
F_{bru}[b], ksi:										
(e/D = 1.5)	309	309	309	309	309	309	309	...	...	...
(e/D = 2.0)	394	394	394	394	394	394	394	...	...	...
F_{bry}[b], ksi:										
(e/D = 1.5)	216	216	216	216	216	216	216	...	...	...
(e/D = 2.0)	257	257	257	257	257	257	257	...	...	...
e, percent:										
L	12	12	12	12	12	12	12	12	10	12
LT[b]	6	6	6	6	6	6	6	10	10	12
ST[b]	...	...	...	...	6	6	6	...	10	12
RA, percent:										
L	15	15	15	15	15	15	15	15	12	15
LT[a]	8	8	8	8	8	8	8	12	12	15
ST[a]	...	...	...	...	8	8	8	...	12	15
E, 10^3 ksi:	29.4									
E_c, 10^3 ksi:	30.9									
G, 10^3 ksi	11.4									
μ	0.29									
Physical Properties:										
ω, lb/in.^{3}	0.297									
C, K, and α	See Figure 6.3.5.0									

a Applicable providing LT or ST direction is ≥2.500 inches.
b Bearing values are "dry pin" values per Section 1.4.7.1.

Figure 26. Inconel 718 material properties

Approved for public release; distribution unlimited.

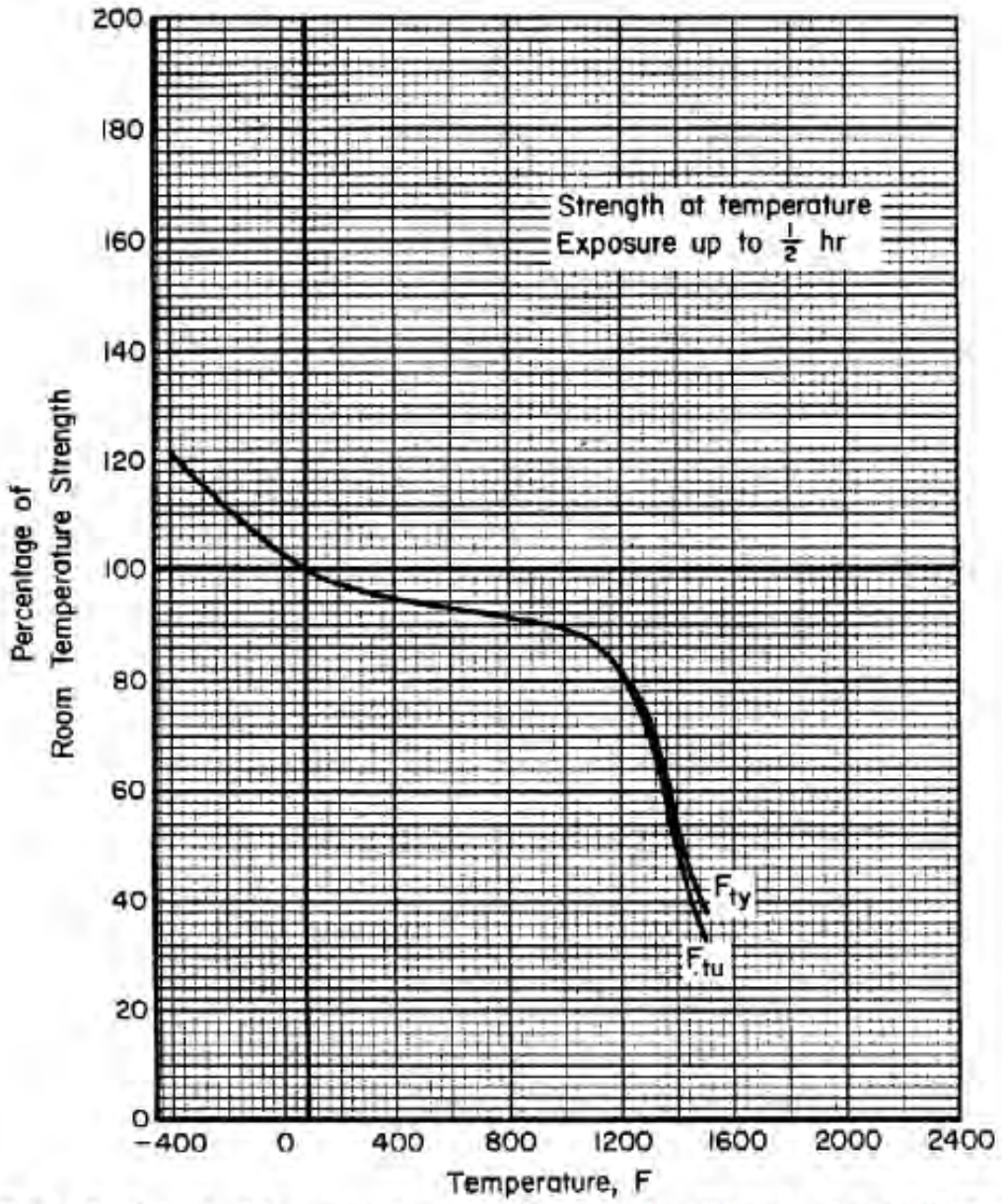

Figure 6.3.5.1.1. Effect of temperature on the tensile ultimate strength (F_{tu}) and tensile yield strength (F_{ty}) of solution-treated and aged Inconel 718.

Figure 27. Inconel 718 thermal knockdowns, Fty Ftu

Approved for public release; distribution unlimited.

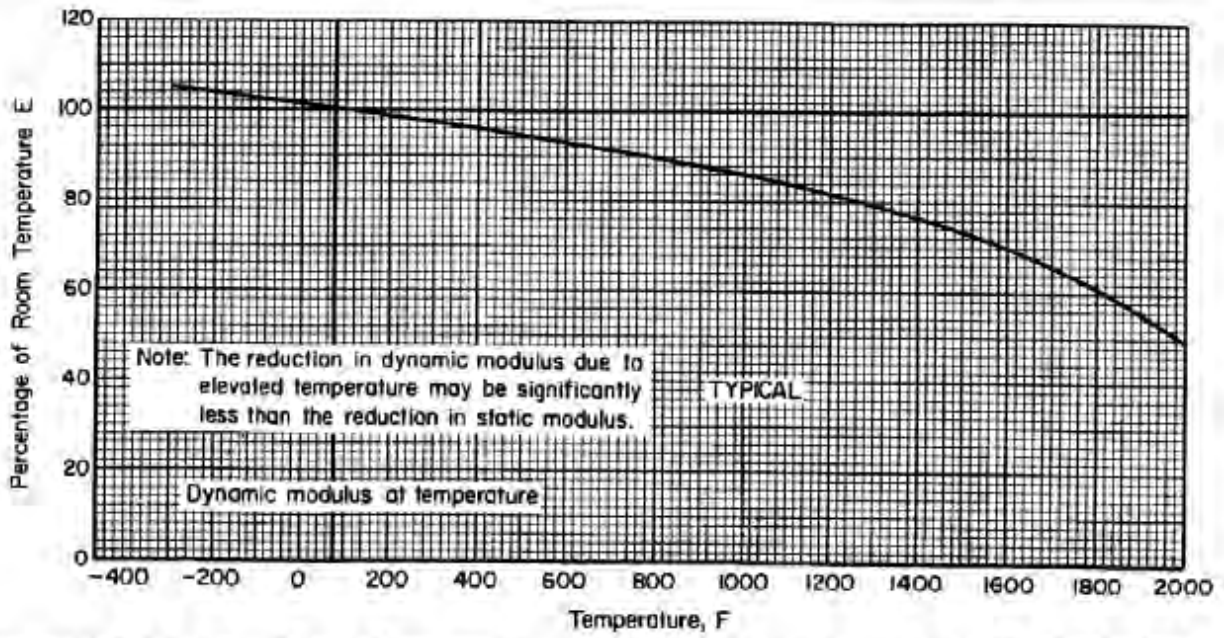

Figure 6.3.5.1.4(a). Effect of temperature on dynamic tensile modulus (E) of solution-treated and aged Inconel 718.

Figure 28. Inconel 718 thermal knockdowns, E

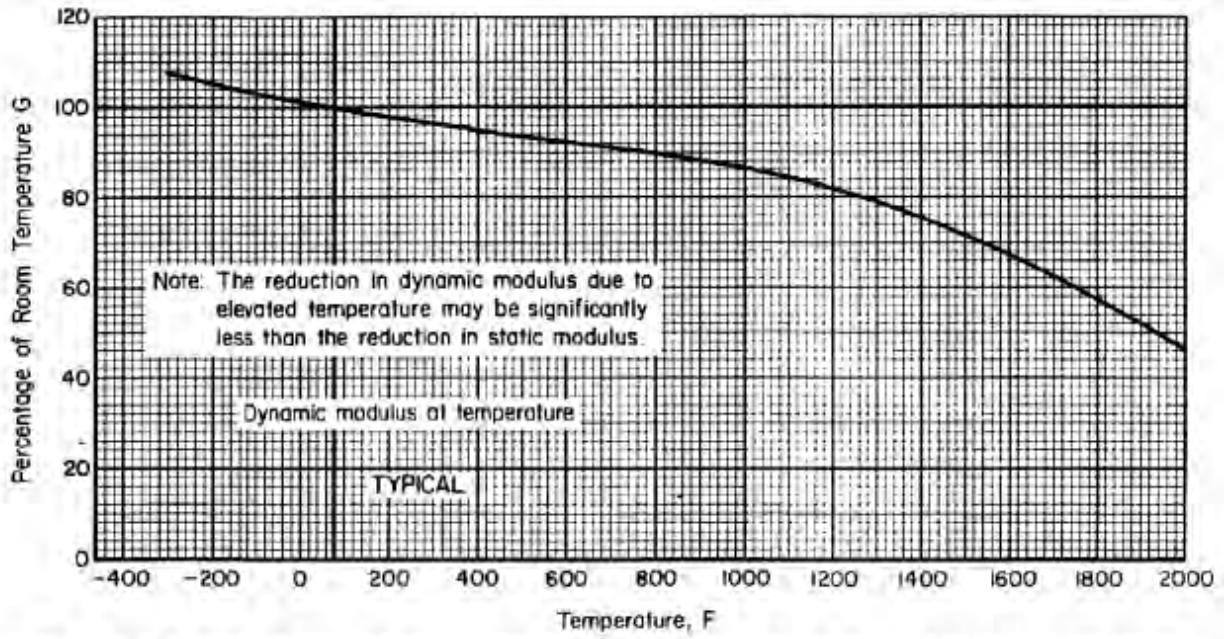

Figure 6.3.5.1.4(b). Effect of temperature on dynamic shear modulus (G) of solution-treated and aged Inconel 718.

Figure 29. Inconel 718 thermal knockdowns, G

Approved for public release; distribution unlimited.

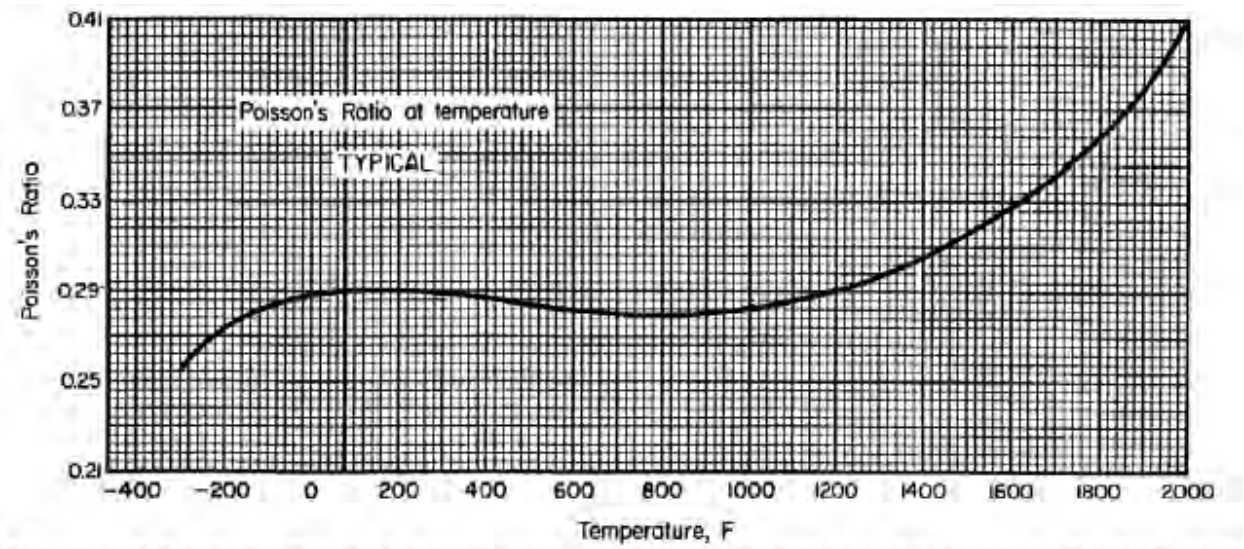

Figure 6.3.5.1.4(c). Effect of temperature on Poisson's ratio (μ) for solution-treated and aged Inconel 718.

Figure 30. Inconel 718 thermal knockdowns, μ

Elements thicknesses are applied at same time as the material properties. The thicknesses of the surrounding panels mimic the thicknesses in the vehicle model as composite materials. The thicknesses of the frames, keels, and panel of interest are based on either global FEM or panel level sizing results. The only exception to this is unit cell 1 where all the surrounding panels share the same ortho-grid panel concept and sizing as the panel of interest. The implications of this design are described in Section 4.3.3.

Now that the geometry has been created and assigned a material and thickness, the loads and boundary conditions are applied. The mechanical loads are extracted from the global vehicle model while the thermal loads are generated by applying a thermal profile to the unit cell. The thermal loads from the global vehicle model are not accurate because there was not enough thermal detail in that model. This model did not include radiation, insulation blankets, fuel tanks, engine temperatures, and other thermal boundary conditions.

Mechanical loading from the global vehicle model is extracted at every node within the unit cell. The applied mechanical loads include the aerodynamic pressures, inertial loads, running loads, and any system attachments. No additional surface pressure or inertial loads are added to the unit-cell because they are captured by the combined applied mechanical loads. These loads are applied to the detailed unit cell via MPCs (multipoint constraints) as shown in Figure 31 and Figure 32. RBE3's (Rigid body element) were used to allow the independent nodes on the detailed unit cell to move independently of each other. This is especially important since the elements will be deforming under heat.

Approved for public release; distribution unlimited.

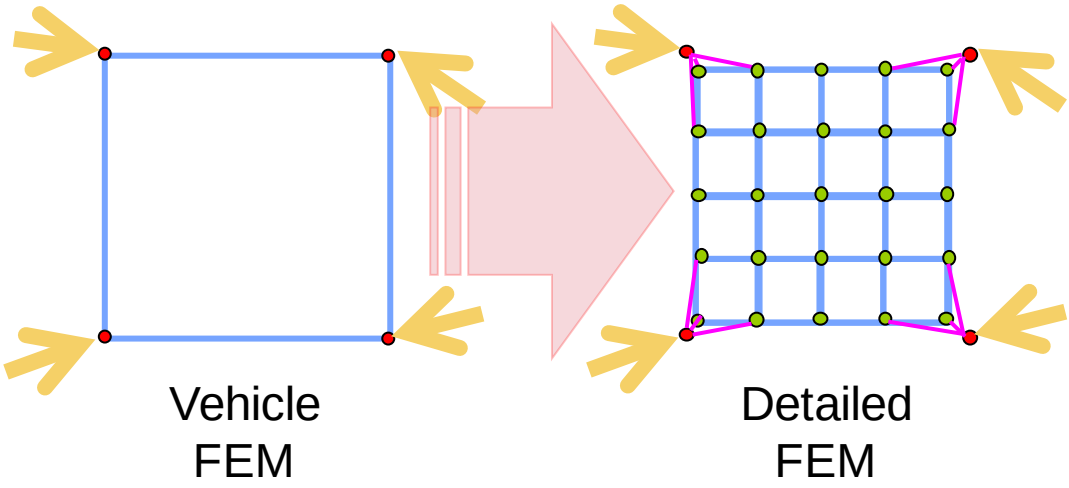

Figure 31. Simplified global vehicle load application to detailed unit cell

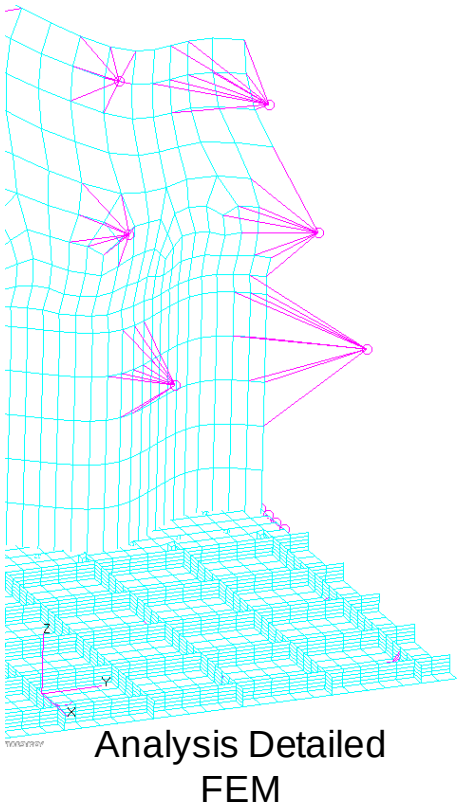

Figure 32. Example of global vehicle loads application to detailed unit cell

The critical mechanical load case was determined in Phase I as a 2.5g maneuver. For conservatism and simplicity, it was assumed that this maneuver can happen at any point in the reference trajectory as part of an evasion maneuver or abort scenario. The 2.5g load case is thus combined with each thermal load case at the unit cell level to create combined load cases. From these combinations, the load case that generated the highest Von Mises stress at the panel of

interest is selected as the most critical. All four panels have the same critical load case combination. The thermal load case that caused the highest Von Mises stress is the Maximum skin to substructure gradient. Note that this thermal load case occurs at different times in the flight profile for each panel.

Since the mechanical loading is balanced and the thermal load does not induce any external loading to the unit cell, it is only necessary to constrain the model's rigid body motion. Additionally it is necessary to not over constrain the model so that it may freely expand under heat. It is useful to remember that the purpose of the model is to replicate the mechanical and thermal loading on the panel of interest only, not the entire unit cell. By not over constraining the model, the unit cell is free to expand outwards, but still provides accurate local restraint forces on the center panel. Therefore, the model is constrained at 3 locations: <x, y, z> is constrained at location 1, <x, z> is constrained at location 2, <z> is constrained at location 3. These constraints are located along the frame/keel intersections. They vary across each unit cell and this variation has no implication on the analysis. An example of these constrains is shown in Figure 33.

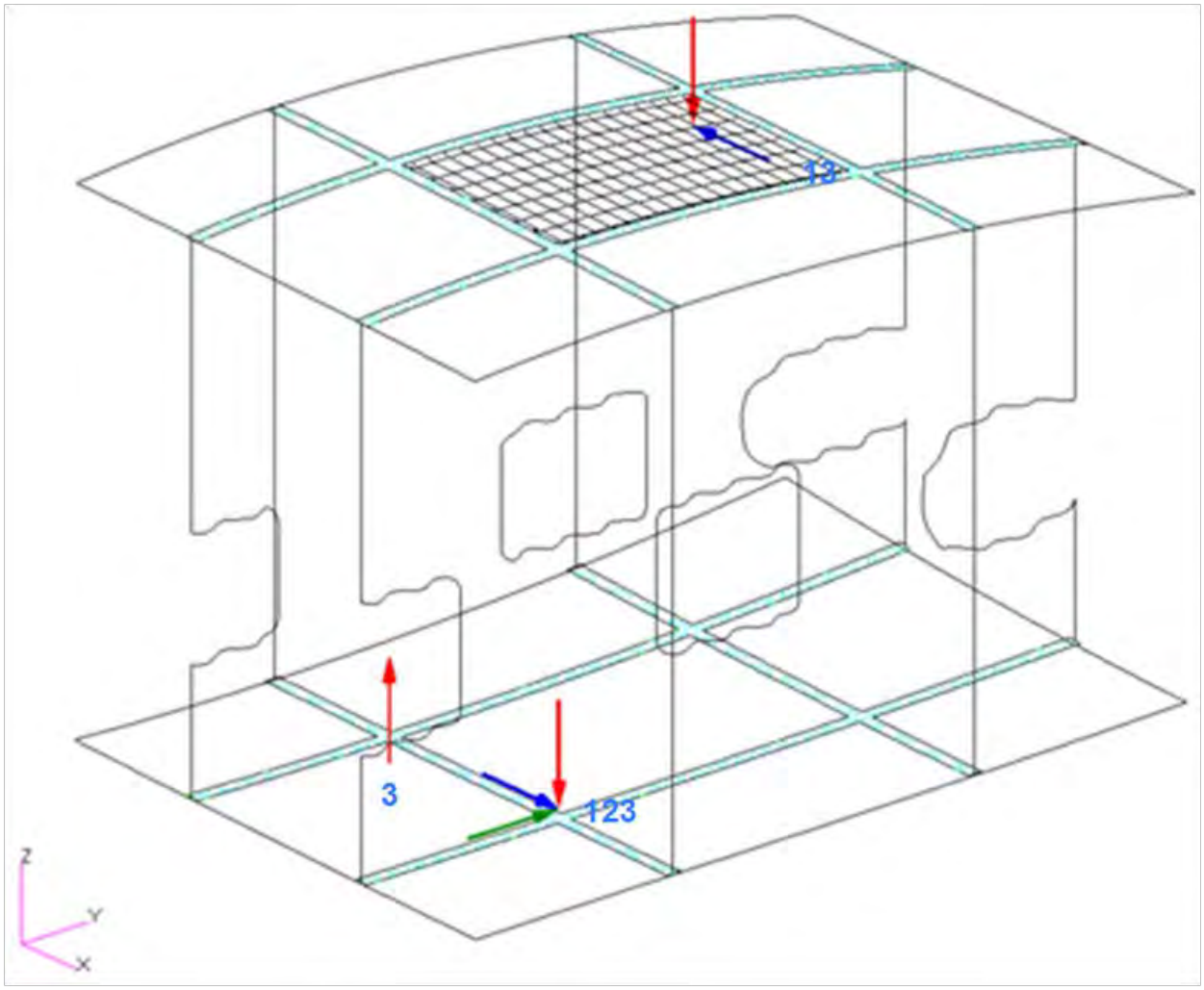

Figure 33. Rigid Body Motion unit cell Constraints

Approved for public release; distribution unlimited.

The unit cell model is then executed in Nastran and the results are validated by verifying that the constraint forces are near zero and that the displacements are representative of the loading conditions.

When validating the displacement plots of the unit cell for Panel 1 (862), it was observed that there were large displacements along the boundaries of the unit cell. These displacements are primarily due to a difference in stiffness of the surrounding panels from the detailed unit cell and the global vehicle model. For this reason, the unit cells for the following panels used panel stiffness that was representative of the global vehicle model. In addition, the misalignment of the global load application points and the local grid point also contributed to the large displacements.

The purpose of the unit cell is to provide accurate boundary conditions and thermal loading for the panel of interest. However, to run a non-linear solution for the entire unit cell is a resource intensive task. To utilize the computing resources more efficiently, the enforced displacement method is used to constrain and load the panel of interest only. There is an unmeasured approximation using enforced displacements generated from a linear run to constrain a non-linear solution. Linear, non-linear, and buckling analyses are performed at this panel level and provide the data which the margins of safety are written against. The boundary/loading conditions for the panel level analysis are shown in Figure 34.

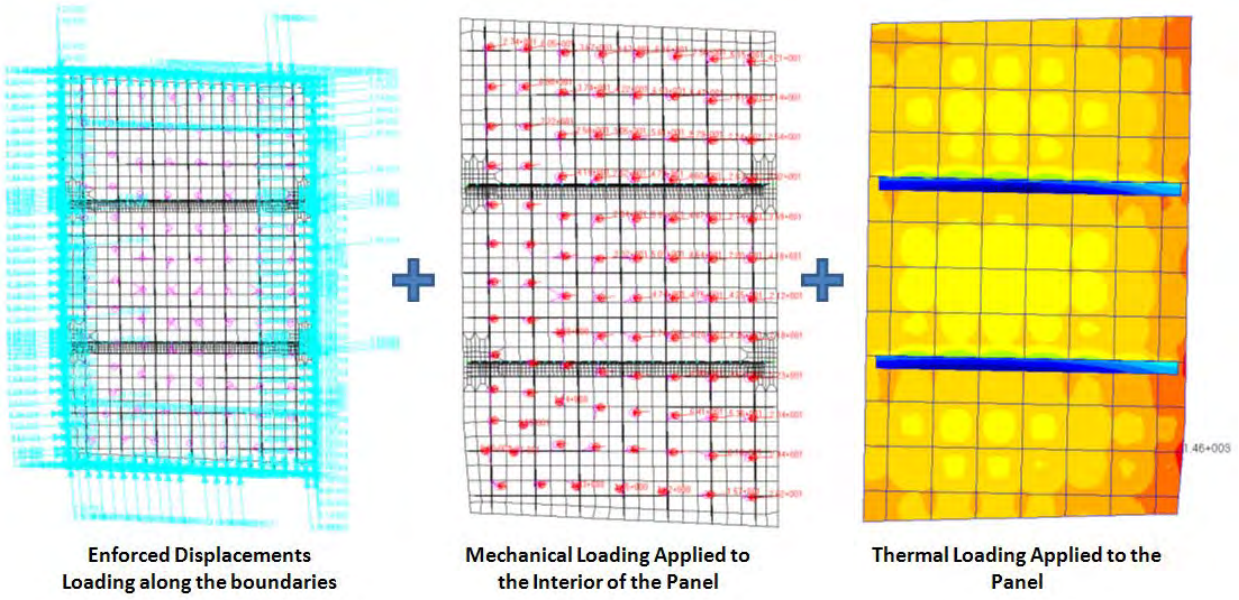

Figure 34. Example of Applied Loading for the Panel Level Analysis

Margins of safety are written for each panel for ultimate material failure, out of plane displacement, fastener bearing, and buckling. Fastener bearing margins of safety are only relevant for panels designed with panel breaker stiffeners. A summary of the margins for each panel is shown in Table 8. The detailed discussions for each panel are in the following sections.

Table 8. Summary of Static Margins for All Panels

Panel	Location	Failure Mode	Load Case	Allowable @ Temp	Units	Actual	Units	MS/RR
1 (862)	Panel Center	Deflection	2.5g Ult (1.5) + T=1080s	0.1	in	0.192	in	-0.48
1 (862)	Panel Boundary	Material Failure	2.5g Ult (1.5) + T=1080s	160.2	ksi	17	ksi	8.42
1 (862)	Panel Center	Buckling	2.5g Lim (1.15) + T=1080s	1		2.57		2.57
2 (780)	Panel Breaker/ Panel Intersection	Deflection	2.5g Ult (1.5) + T=720s	0.1	in	0.124	in	-0.19
2 (780)	Panel Breaker Scallop Edge	Material Failure	2.5g Ult (1.5) + T=720s	165.6	ksi	52.3	ksi	2.17
2 (780)	Panel Breaker/ Panel Intersection	Bearing	2.5g Ult (1.5) + T=720s	284.28	ksi	103	ksi	1.76
2 (780)	Panel Center	Buckling	2.5g Lim (1.15) + T=720s	1		0.998		0.998
3 (816)	Panel Center	Deflection	2.5g Ult (1.5) + T=900s	0.1	in	0.45	in	-0.78
3 (816)	Panel Boundary	Material Failure	2.5g Ult (1.5) + T=900s	144	ksi	46.3	ksi	2.11
3 (816)	Panel Center	Buckling	2.5g Lim (1.15) + T=900s	1		0.826		0.83
4 (1074)	Panel Center	Deflection	2.5g Ult (1.5) + T=2700s	0.1	in	0.514	in	-0.81
4 (1074)	Panel Breaker Runout	Material Failure	2.5g Ult (1.5) + T=2700s	64.8	ksi	88.5	ksi	-0.27
4 (1074)	Panel Breaker/ Panel Intersection	Bearing	2.5g Ult (1.5) + T=2700s	111.24	ksi	95.2	ksi	0.17
4 (1074)	Panel Center	Buckling	2.5g Lim (1.15) + T=2700s	1		0.609		0.609

4.2.6 Displacement Criteria Selection

After stress analysis for the first panel (862) predicted considerable surface deflections, a study was conducted to investigate the effects of waves and distortions in the skin on aerodynamic heating. A journal article was located that developed an empirical correlation between the magnitude of sine wave surface distortion and increases in aero-heating at Mach 7 flow conditions. This article, by Bertram and Wiggs [3] provides the following correlation.

$$\frac{h_{max}}{h_{flat\ plate}} = 1 + \frac{1}{5}\left(\frac{M_l}{\delta_l^*/_H}\right)^{1.3} \quad \text{(eqn. 2.1)}$$

Where: δ_l^* = local displacement thickness
H = maximum distortion height
M_l = local Mach number
h_{max} = peak convective coefficient due to distortions
$h_{flat\ plate}$ = convective coefficient on flat plate (undisturbed flow)

Evaluating this equation requires a value for the local boundary layer displacement thickness. Three methods were used to calculate this value:

1. MINIVER, an industry standard 2D boundary layer code used for aerothermal predictions for many years
2. BLAP (Boundary Layer Analysis Program) a Boeing 2D boundary layer code of a similar history
3. Theoretical equations from Schlichting's "Boundary Layer Theory" for a turbulent flat plate.

The three methods produce significantly different values and therefore result in the different heating amplification curves shown in Figure 35. After consulting with a Boeing subject matter expert (SME), it was determined that the predictions based on MINIVER (green curve in Figure 35) were the most accurate based on prior comparisons to wind tunnel data on other programs. The estimated temperature impact due to 10% and 20% increases in convective coefficients are noted on Figure 35 as 2% and 5% respectively. Therefore, if a 5% temperature increase is within the thermal stress margin, a maximum surface distortion of approximately 1/8 inch would be acceptable. However, note that this correlation is based on data from small coupons. The panels in the Phase II study are roughly 10 times in length. Therefore, it may be more appropriate to scale the maximum allowable surface distortion derived from this correlation such that the slope of the surface is consistent with the test cases. Exploring options for a slope correlation is recommended, however this effort is out of the scope of this contract. As a result, a draft design point of a 0.10 inch maximum deflection using linear analysis under limit loads was selected. This deflection criterion would be achievable while producing acceptable heating increases.

The inability to adequately define a panel deflection sizing and allowable criteria has been identified as a knowledge gap. Although this program defined a criteria for absolute deflection based on a predicted increase in heating, increased heating is more likely a function of the slope of the deflected panel. Furthermore, aerodynamic and vehicle performance effects were not considered. Understanding the sensitivity of deflected panel slope on heating, drag, and vehicle performance will be required to develop a robust deflection criterion. Due to the large potential panel and system design impacts of the selected criteria, developing these sensitivities for this class of aircraft, along with sizing criteria and design guidelines, was recommended for future work. It should be noted that extensive work was performed to develop criteria for the Space Shuttle and X-33 TPS systems. Although this work addresses a different flight regime, and in

some cases different phenomena (boundary layer transition), much of the developed data and methodology could be leveraged for Mach 7 cruise environments.

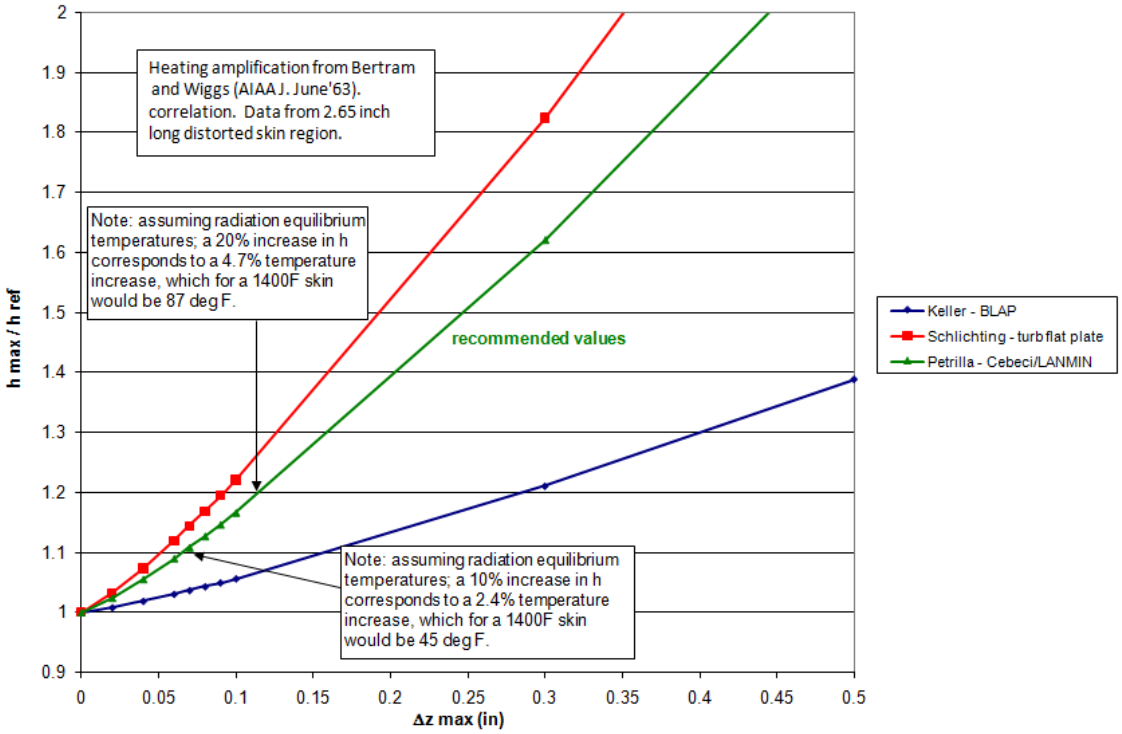

Figure 35. Convection coefficient sensitivity to panel deflections into the flow

4.2.7 Dynamic Analysis Approach

A standard structural development process was followed for Phase II dynamic analysis. Typically, all panels are sized to some rough frequency or other design requirements in the sizing analysis. This step was performed in the initial HyperSizer analysis. Then, a few critical panels are selected for refined analysis; such as the objective of this program. Detailed FEMs and loads cases are developed and a more refined level of structural analysis is performed. These analyses validate the initial sizing, and verify the integrity of certain panel/structural details. In this case, we are checking the margins of the joints and panel features under thermal/acoustic loads. This requires the development of FEM that models these features, and produces results that can be compared to allowables as required.

The Phase II dynamic analysis for the panel structure focused on fatigue margins for combined thermal and acoustic loads. Fatigue analysis consisted of low cycle thermal-mechanical fatigue (TMF) from cyclic flight loads and high cycle oscillations from acoustic loads, or aero-acoustic fatigue (AACF) under thermal load.

At the panel level stage of structural development it is necessary to look for critical combined load conditions where both thermal and acoustic loads are high. This occurs at max Q = 2000psf (V=Mach 6.25, Altitude = 75,000ft and AoA=6 deg), see Figure 36.

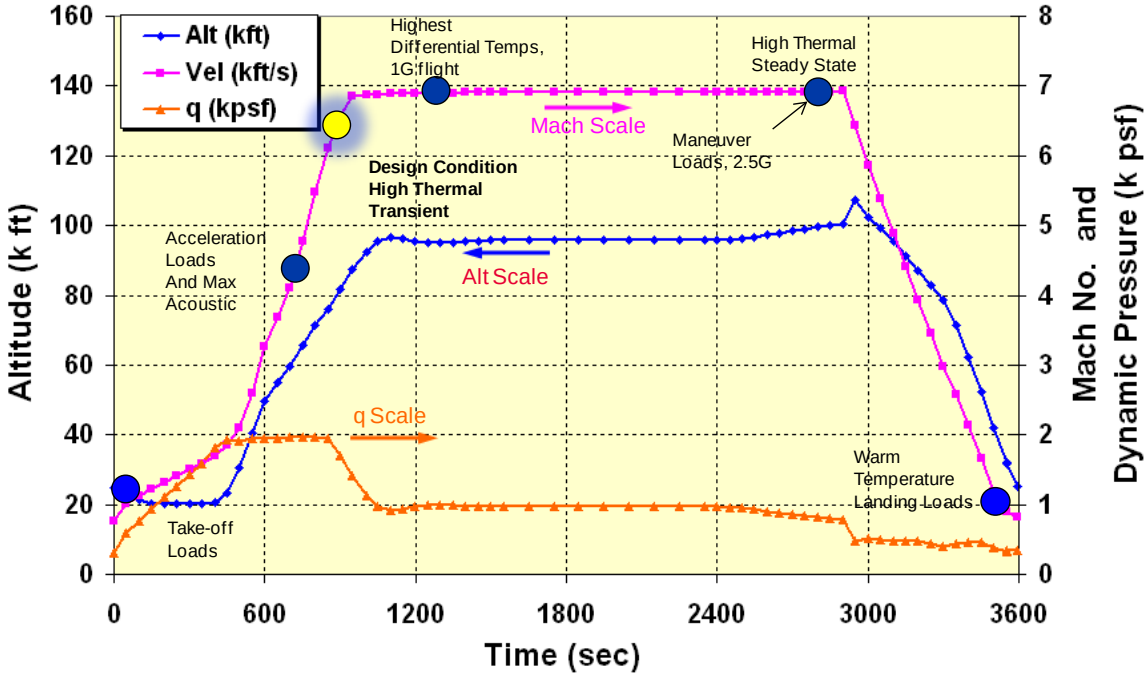

Figure 36. Trajectory Design Conditions

Acoustic loads were developed from steady state computational fluid dynamics (CFD) analysis performed at the trajectory point of interest, (Q=2000psf, Mach=6, Alt=75kft, AoA = 6deg) as illustrated in Figure 37.

Approved for public release; distribution unlimited.

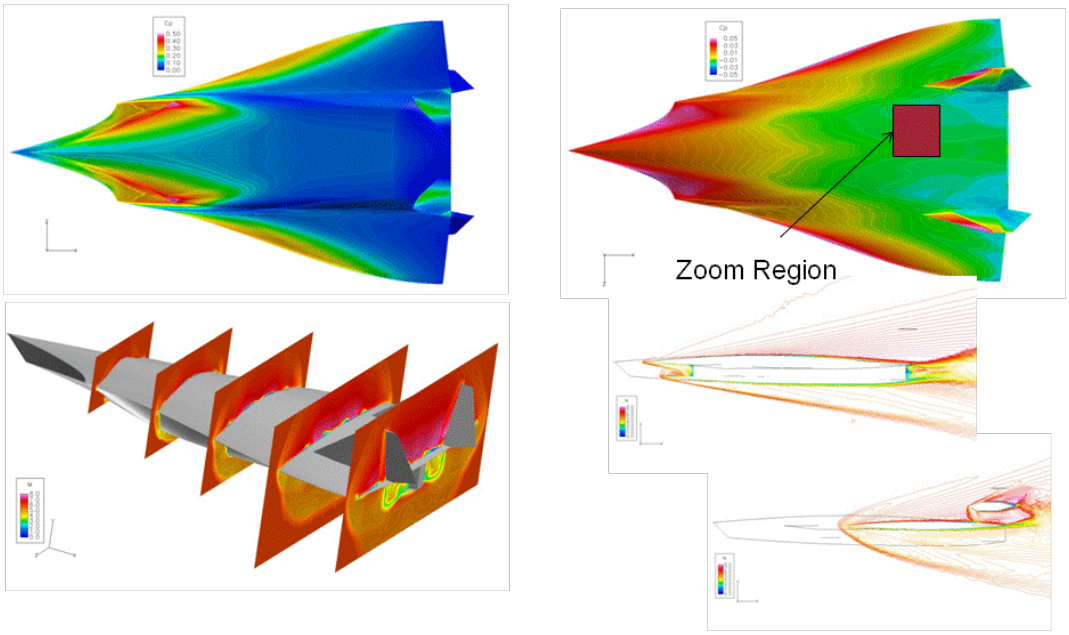

Figure 37. CFD++ Computed Flow Field

A semi-empirical, Turbulent Boundary Layer (TBL), aero-acoustic loads prediction model was used to generate the acoustic loads as a function of frequency. The primary CFD data used in the TBL model are TBL thickness, delta pressure, distance from leading edge, and flow field characteristics (attached, separated, shock, laminar). For this condition, the flow on the upper side is separated TBL type model while the flow on the lower surface is attached TBL. Acoustic spectra were predicted for the three different conditions. Condition 1 is the separated flow at max Q, Condition 2 is the attached flow condition on the lower side, and Condition 3 is the laminar flow condition for reference at this trajectory point. Whether separated TBL (Condition 1) or attached TBL (Condition 2) the acoustic load as a function of frequency behaves the same (Figure 38). Therefore, acoustic loads for each panel are simply scaled in magnitude from one another based on the Panel 1 curve shown in the figure.

Approved for public release; distribution unlimited.

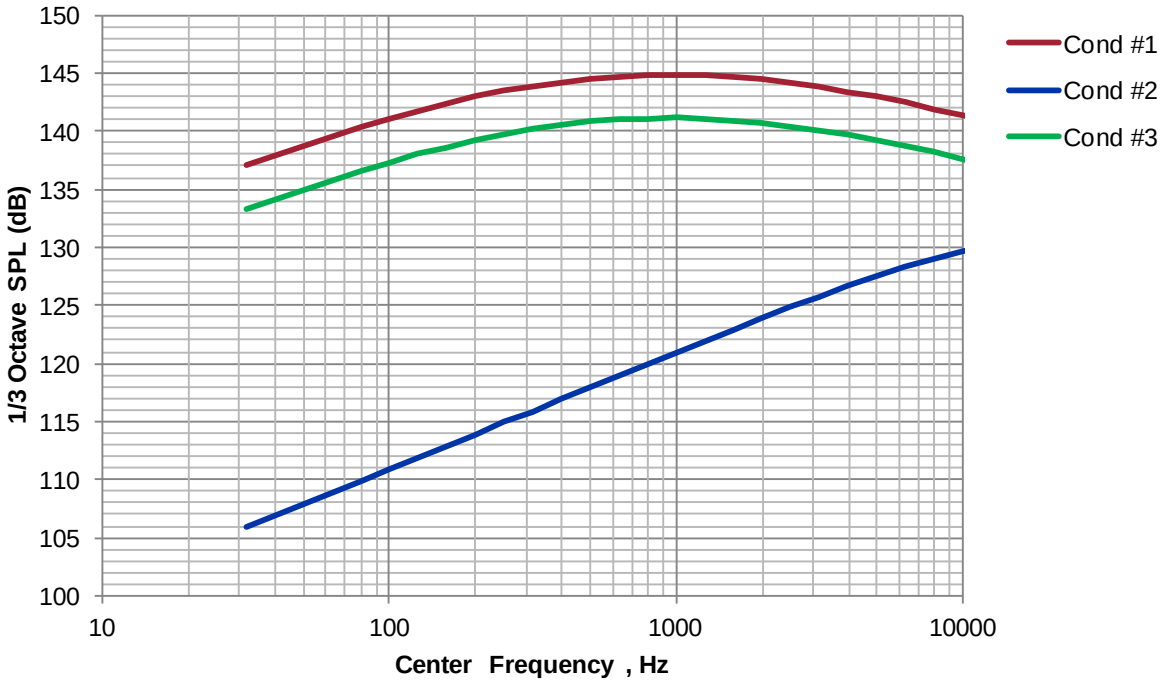

Figure 38. ADSAS Aero-acoustic Prediction

Panels on the upper surface (1 and 3) assumed a separated flow TBL model while panels on the lower surface (2 and 4) assumed an attached TBL model. Distance from the leading edge is another discriminator that scales the acoustic load in magnitude. Panel acoustic loads normalized to Panel 1 loads are shown in Table 9.

Table 9. Normalized Acoustic Loads for each panel

Panel	Normalized Acoustic Load	Surface Location
862	1.00	Upper
780	0.80	Lower
816	0.73	Upper
1074	0.80	Lower

The same detailed unit cell FEM used for structural analysis was used for dynamic analysis. Initially, the model produced several low order substructure and boundary modes. This issue would have made the subsequent dynamic analysis questionable in terms of accuracy and efficiency. Boundary conditions had to be modified from the static solution in order to prevent the undesirable vibration modes. Most commonly, SPCs were placed around the perimeter of the unit cell to model support from the surrounding structure and to restrict vibration modes that were not of interest. In addition to eliminating undesired vibration modes, the modified constraints also removed modal asymmetry caused by asymmetry in the constraints. In cases where unwanted substructure or surrounding panel modes persisted, the work around was to

filter out the unwanted substructure modes very simply by reducing the mass of the substructure and surrounding panels to near zero. This could have also been accomplished using other methods; such as, using ASETs. In fact the ASET approach was also tried and produced the same modal results.

Generally, the vibration modes for all panels occur at frequencies lower than our min frequency requirement of 150Hz at OASPL=157dB based on Phase I design requirements. Since the panels are out of the range of the program requirements set forth, standard development program procedures would be to verify the response (and fatigue life) using detailed analysis. In a large scale development program, we would normally be required to follow-up this detailed analysis with a validation test program. During structural development, usually several panels are identified for detailed analysis due to either not meeting initial sizing requirements or due to high risk (uncertainty) of structural details. The latter may be due to fact that no previous production parts have been certified (i.e. a new structural concept), which means that there are no coupon, sub-element, or sub-components test data. This is certainly the situation for this Inconel ortho-grid sine wave welded structural concept.

The next step was to perform acoustic response analysis. The standard process is to use linear modal frequency response in MSC/NASTRAN; i.e. SOL 111 with post-processing in MSC/RANDOM. The previous acoustic loads were applied as three zones across the panel (Fwd to Aft). The flow was assumed to have some level of temporal correlation in the flow direction, but fully correlated in the cross direction. This generally considered is a best initial guess within our design practices. Generally, complete fully correlated is considered to be conservative, and complete fully uncorrelated in considered to be less conservative. Within Boeing we have developed validated models for aero-acoustic TBL spatial correlation and we apply this approach when we have high confidence that we understand the flow physics either thru test or CFD. A general practice is to apply a 3.5 dB factor of safety if there is a lack of flight test data. This is accepted practice for highly maneuverable fighter/attack aircraft which have considerable uncertainty in the aero-acoustic loads (reference, Liguore S.L. “Identification of Uncertainties and Application of Probabilistic Analysis in Acoustic Fatigue Design,” Recent Advances in Structural Dynamics, 2006.) In this case of hypersonic cruise vehicles, we can deviate from the 3.5dB FOS because the flight profile is simple, and assumed the same for every mission. Hence, uncertainty in the flight conditions that can possibly produce extreme loads is low. Plus, we have a well validated aero-acoustic model and supporting CFD data.

Another critical parameter to account for in any dynamic analysis is the modal structural damping. In the above reference, the damping is by far the greatest source of uncertainty in any analysis with a COV~0.5 for some structural concepts. We have no available data for our structural concept, but we do have historical data on a range of structures and materials shown in Figure 39. In this analysis, the dark black curve is used for the response analysis.

Approved for public release; distribution unlimited.

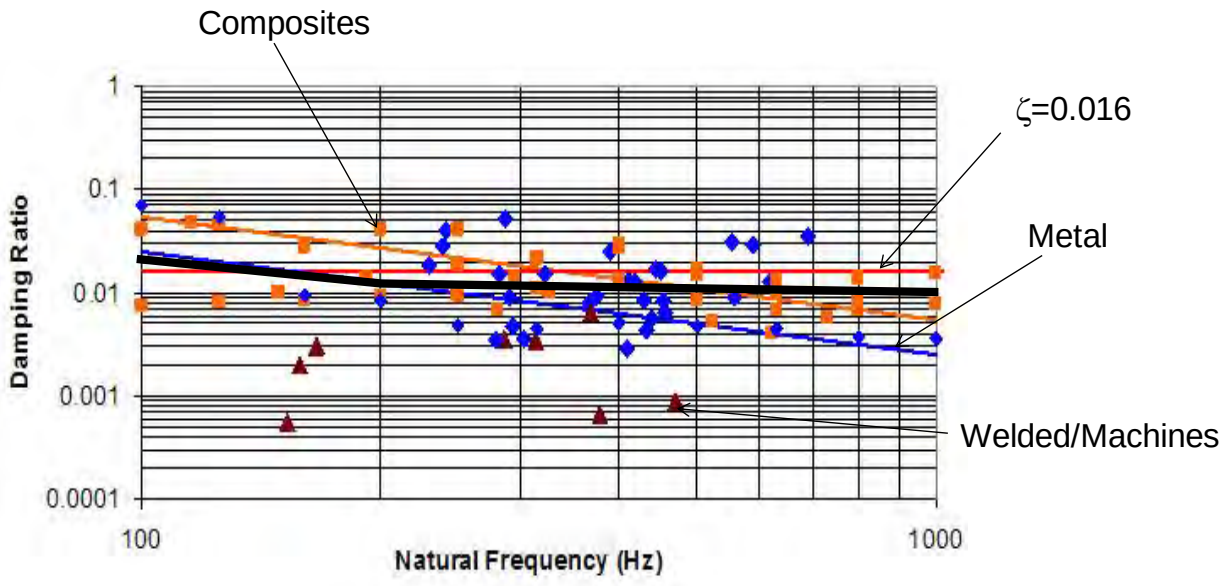

Figure 39. Historical Modal Structural Damping, ref AFWAL-TR-84-3089, Vol II

In addition to fatigue, aeroelastic stability (flutter) was evaluated for Panels 3 and 4 (MSC/Nastran SOL 145). For the flutter analyses of Panel 3 and 4 a case near max Q was selected at t=900s, (V=Mach 6.25, Altitude = 75,000ft and AoA=6 deg). An empirical based method was first tried to get a sense of how close the panel was to being unstable. This method is used as a design tool but is intended for flow up to Mach 3.0. The design curve could serve as a "rule of thumb" check but does not give the fidelity required at this level of structural detail. An example is shown in Figure 40.

Approved for public release; distribution unlimited.

Nondimensional Panel Flutter Parameter

$\Phi = [\, f(M) \times E / q \,]1/3 \times (t / l)$

where:

- Φ = Non-dimensional panel flutter parameter; a function of panel length-to-width ratio, l/w
- E = Young's modulus
- f(M) = Mach number correction factor; a function of Mach number and l/w ratio;
- l = Panel length (stream wise)
- q = Dynamic pressure
- t = Panel thickness
- w = Panel width

Correction Factors for:

- Curvature
- Mach Number
- Flow Angle
- In-plane stress
- Differential Pressure
- Differential Temperature

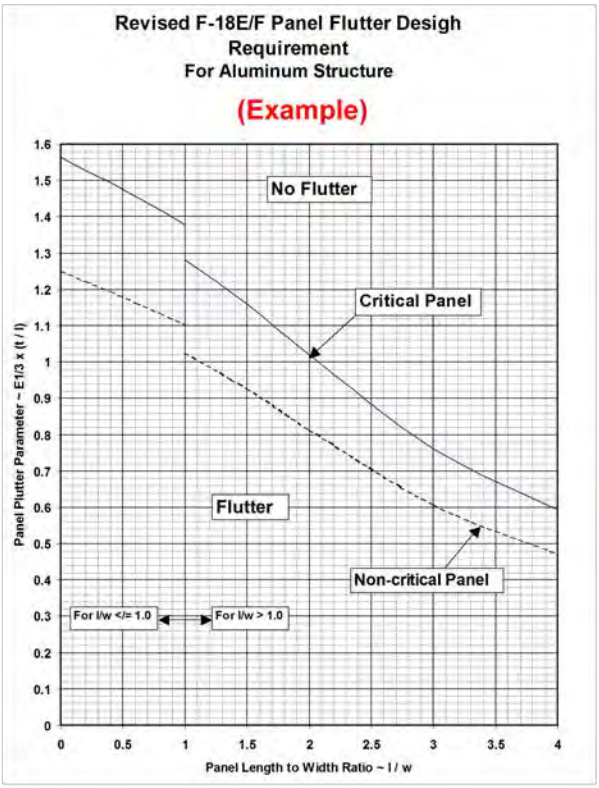

Figure 40. Example of empirically derived non-dimensional panel flutter

To analyze the panels to a much greater degree of precision, an aeroelastic FEA solution was created. For hypersonic flow, a "Piston Theory" panel flutter analysis method was used which is valid for velocities as low as Mach 1.5. The flutter analysis couples an aerodynamic (aero) model (Figure 41) with the structural FEM and recomputes the stiffness matrix based on response of the aero model to changes in air velocity.

Approved for public release; distribution unlimited.

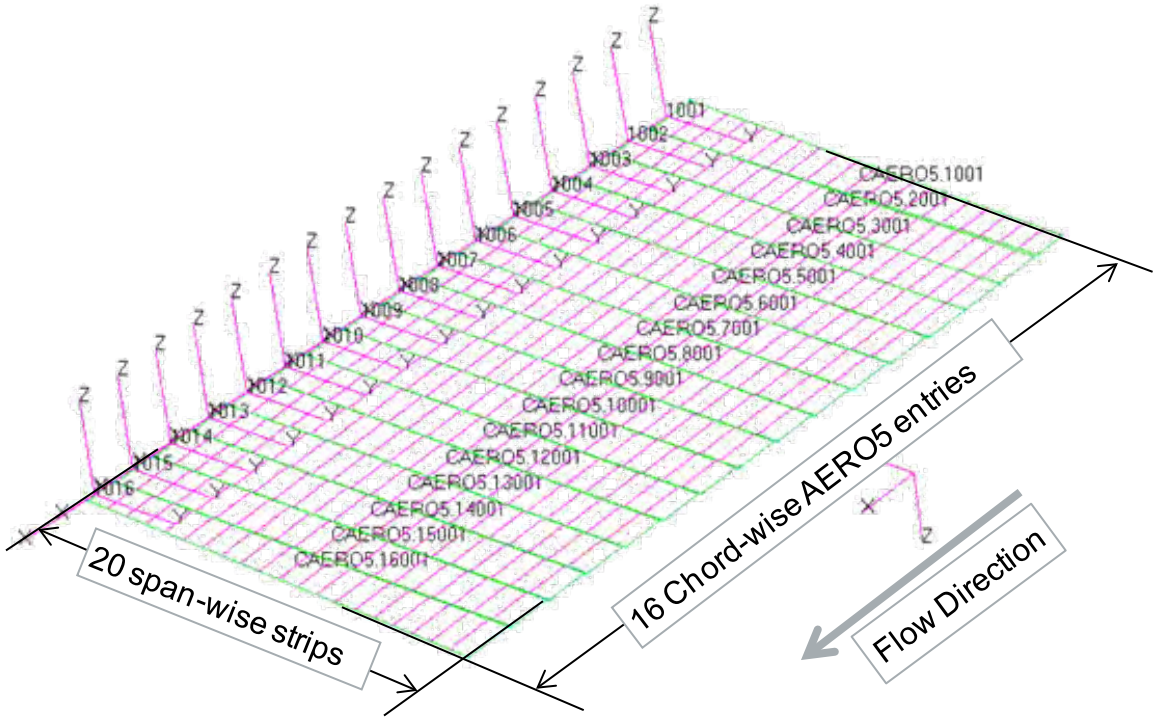

Figure 41. Aerodynamic model setup for piston theory flutter analysis

The analysis calculates a critical damping value and natural frequency over a range of velocities input for the analysis. In this case the velocities ranged from M=3.0 to M=14.0. The velocity range can be narrowed more tightly around a particular air speed. Other important analysis input parameters include analysis Mach number, reduced frequencies, air density (altitude), air density factor (equal to 0.5 for single-sided flow), angle of attack, and panel length. Since damping of the system is unknown, the panel is considered unstable for any value greater than 0.02. Figure 42 shows a typical plot of damping and frequency as a function of velocity for two modes.

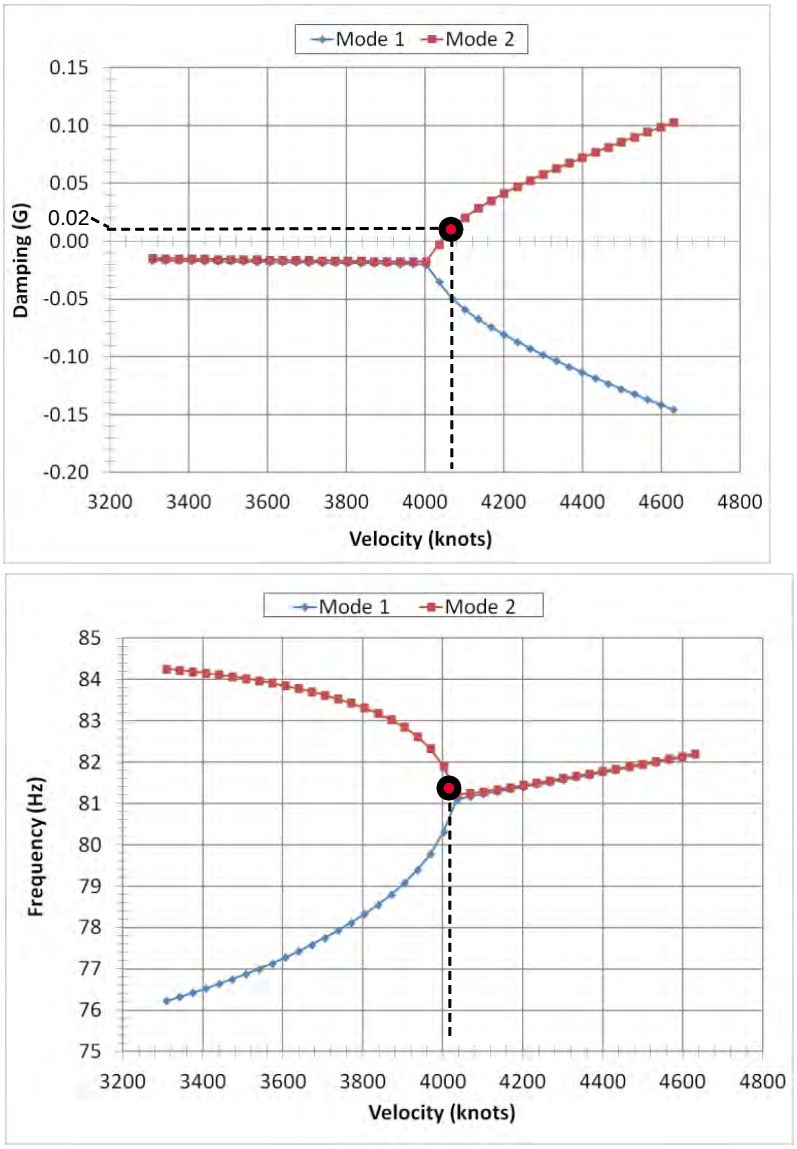

Figure 42. Plots of damping and frequency as a function of velocity for modes 1 and 2 of panel 4.

As shown in the figure vibration modes 1 and 2 have the same frequency at approximately 4040 knots. This coalescence of vibration modes causes the panel to become unstable indicated by the damping curve for Panel 2 exceeding the 0.02 damping limit. For this example, the flutter speed would be approximately 4040 knots (M=6.10).

4.2.8 Fatigue Margin Evaluation Approach

The thermal-mechanical fatigue (TMF) was analyzed separately from the aero-acoustic fatigue (AACF) for the four Phase II panels. Panel 1 was limited by AACF while the other panels were limited by TMF. The method for calculating fatigue margins was similar for thermal-mechanical or aero-acoustic fatigue. TMF pulled results from the unit cell linear static solutions for Limit mechanical loads (2.5g*1.15) combined with worst case thermal loads. AACF ignored

mechanical loads since a 2.5g pull-up is not likely to happen during the acceleration phase of flight (maximum Q).

The AACF analysis process is as follows. Run dynamic response analysis and locate critical stress locations. Run static thermal/maneuver load condition, and document stress/loads and same locations. Find applicable S-N data and/or adjust for random, thermal and mean load effects as required (Refer to Inconel 718 data from MIL-HDBK-5J, Section 6.3.5). The next step is to determine fatigue allowables based on time at condition, and expected stress cycles. We have assumed a fairly conservative endurance limit allowable based on the following:

Required Life = 5,000 hrs
Ave Frequency = 100 hz
Cycles = 1.8e9 (endurance limit)
Ref $K_t\sigma_e$ = 19 ksi (RMS, Kt=1.0, R=-1, LT)

For a combined thermal/acoustic response at the Max-Q condition, it is necessary to determine how long the aircraft is exposed to high temperature and noise. This was estimated based on a linear damage accumulation calculation. It was found that for all panels about 400 sec per 1 hr mission can be assumed to account for 99% of the acoustic fatigue damage. This calculation is fairly simple and implements a spreadsheet to determine the normalized damage level based on ratio of Acoustic Level to RMS stress and time at condition

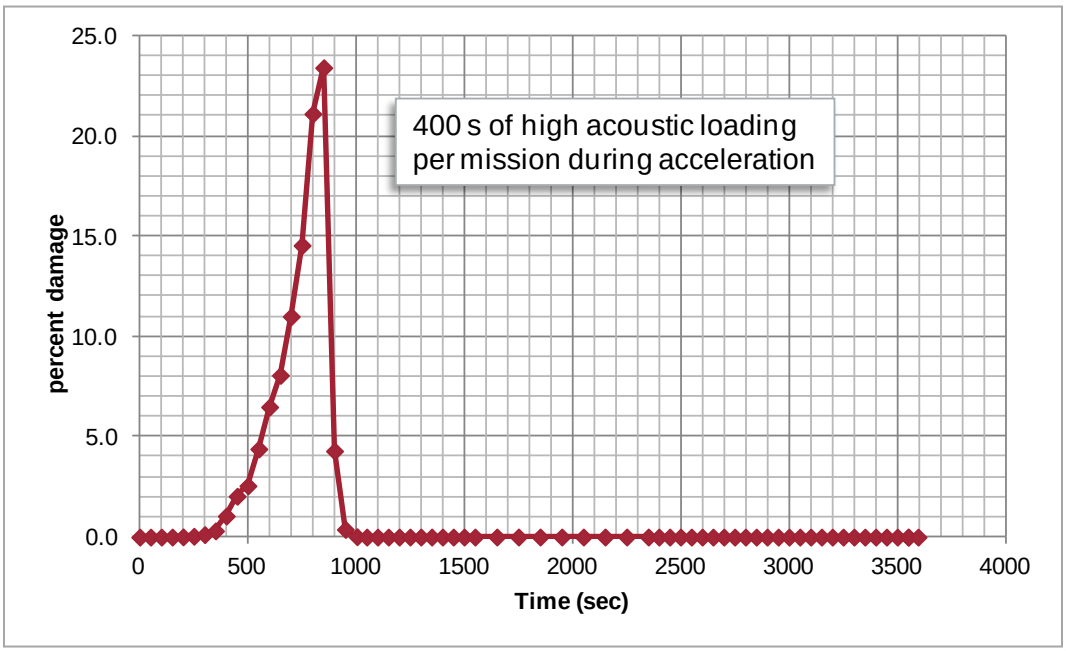

Figure 43. Estimate of linear damage accumulation over a single flight

Approved for public release; distribution unlimited.

The baseline allowables are adjusted for temperature and stress ratio to calculate a corrected fatigue allowable (S_n). The fatigue allowable is assumed to be proportional to Fty as a function of temperature (ref. MMPDS-05 Figure 6.3.5.1.1). For Panel 1 the following method was used to perform a life analysis for AACF at temperature: read in the Stress PSD from MSC/Random and generate a peak/valley stress spectrum, adjust the spectrum for thermal/static mean stress at the location of interest, and perform linear strain-life analysis using Smith, Watson, and Topper equation. Panels 2 thru 4 used a linear interpolation between the constant stress ratio curves (ref. MMPDS-05 Figures 6.3.5.1.8c-e). Stress ratio has a significant impact on the fatigue allowable. Fatigue curves for Inconel at constant stress ratios, ranging from R= -1 to R=0.60 result in endurance limit allowables ranging from approximately 55ksi to 150ksi respectively (ref MMPDS-05 Figure 6.3.5.1.8(c)).

The last step is to write detailed fatigue (endurance limit) margins for critical details. Stress concentrations factors for critical details were either derived from handbook references or assumed based on the type and geometry of the stress riser detail. The figure below gives an example of combining a margin calculation for a combined acoustic and thermal stress.

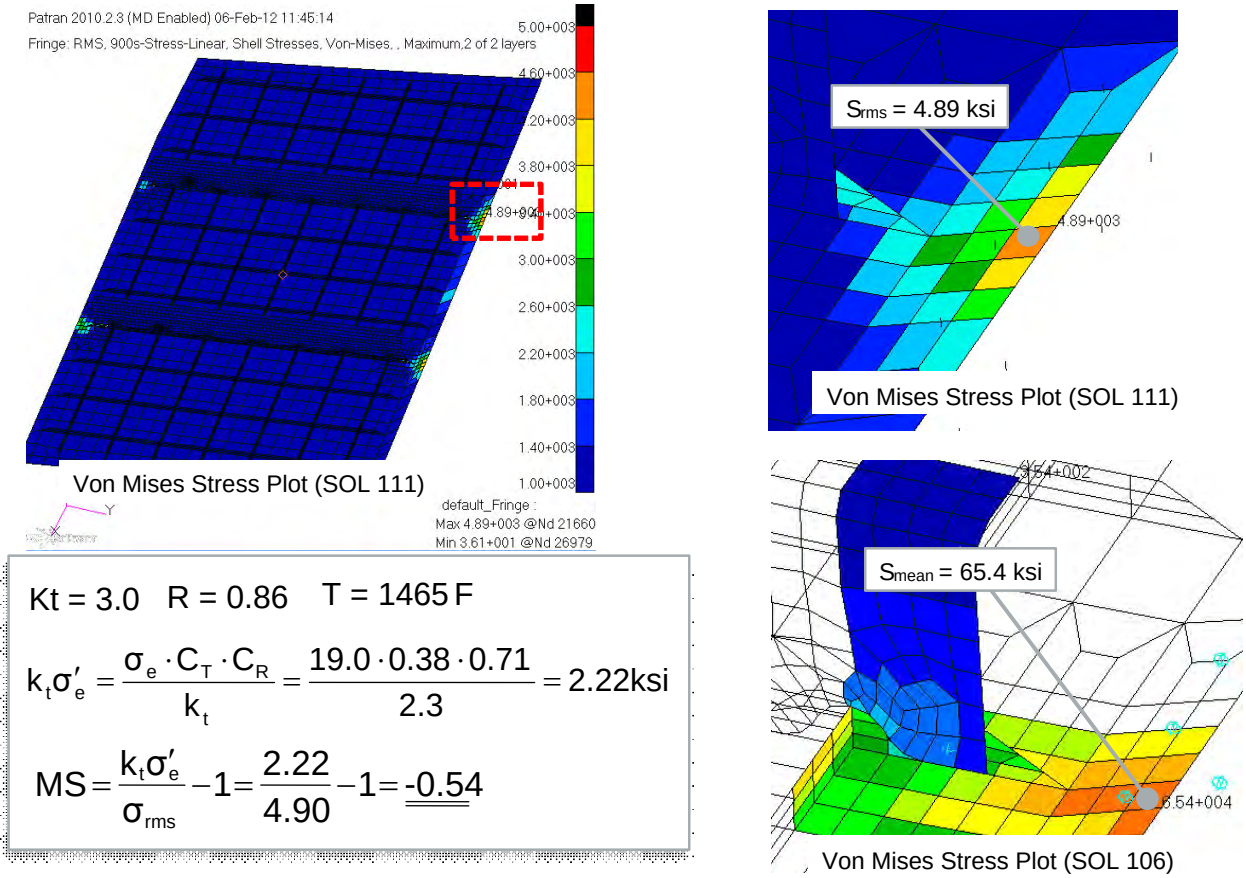

Figure 44. Acoustic fatigue margin of safety calculation for acoustic plus thermal stress

Approved for public release; distribution unlimited.

Thermal-mechanical fatigue from cyclic ground-air-ground (GAG) flight cycles used results from linear static FEA at the worst case combination of thermal and limit mechanical loads (LF = 1.15*2.5g maneuver). A ground-air-ground load cycle was calculated assuming 9,600 cycles over operational lifetime and a lifetime safety factor of 4, totaling to 38,400 cycles for design life. Since only discrete points along the flight profile are analyzed, using a combination of worst case at limit load should be adequately conservative for sizing structure at this level of detail. TMF fatigue evaluation was performed fastener hole stress concentration details only. Other design details such as thickness steps, stiffener terminations and radii were not considered for TMF.

Fastener hole stress concentrations for TMF were calculated by transferring loads from the unit cell FEM to a parametric StressCheck handbook solution FEM that is auto-generated using a web based GUI. Figure 45 below shows the process of extracting loads from the unit cell FEM and the resulting Ktσ calculated by the StressCheck solution.

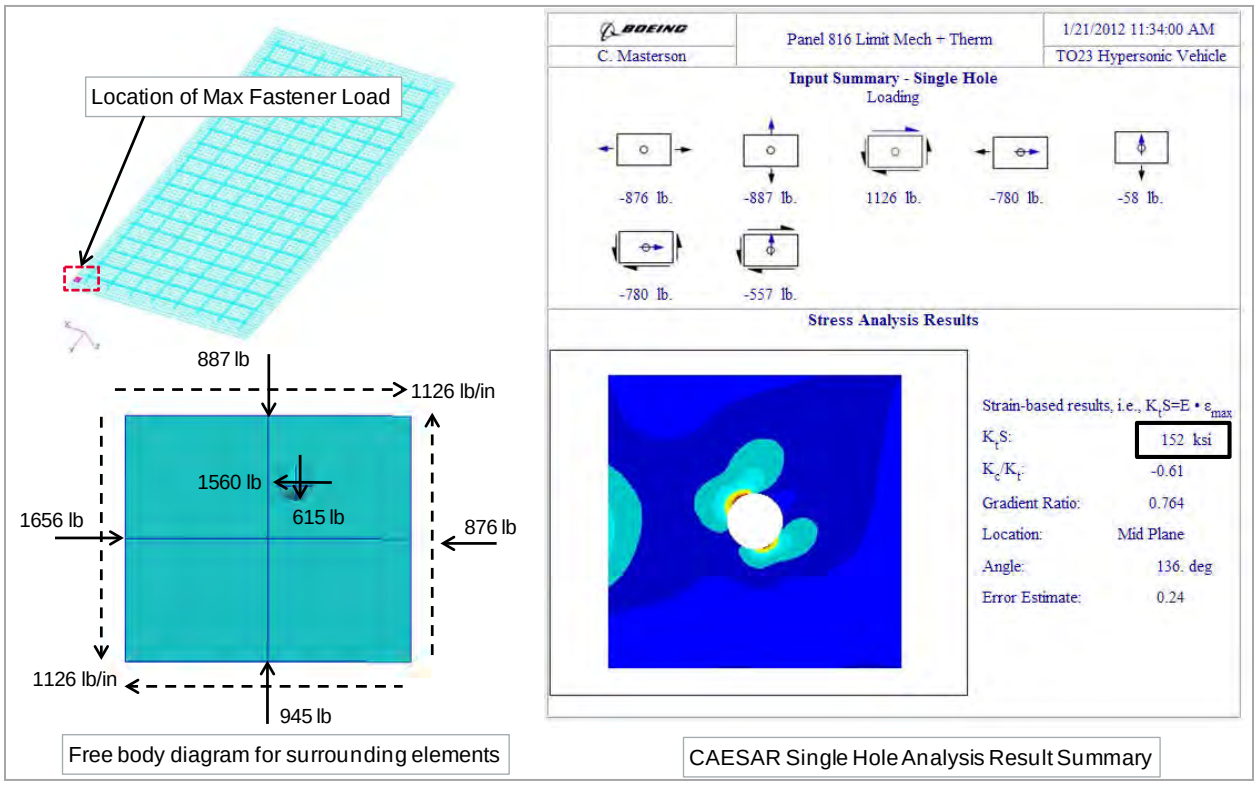

Figure 45. Process used in TMF margin evaluation for calculating a stress concentration at a fastener hole location

The free body loads at the fastener hole were calculated in a process equivalent to the one showed in Figure 46 below where shell forces surrounding the fastener are used to develop a state of stress for a free body diagram.

Approved for public release; distribution unlimited.

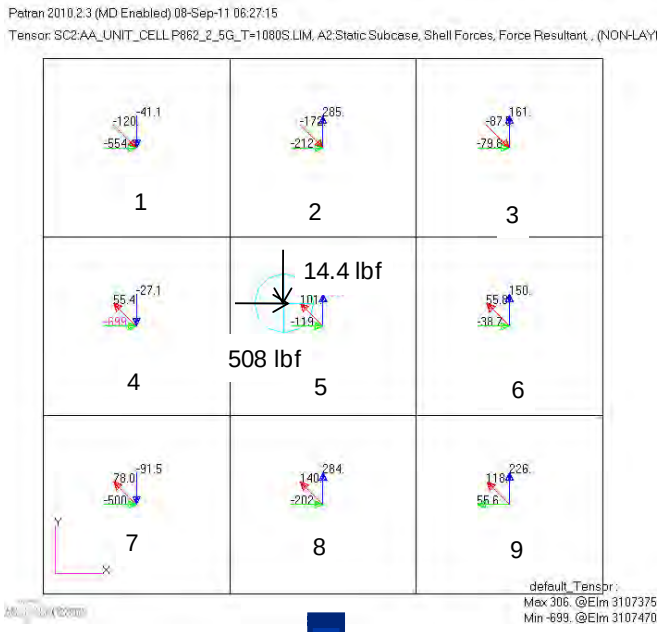

$$Nx_{BY} = \frac{Nx_3 + Nx_6 + Nx_9}{3} \qquad Ny_{BY} = \frac{Ny_1 + Ny_2 + Ny_3}{3}$$

$$Nx_{GR} = \frac{Nx_1 + Nx_4 + Nx_7}{3} \qquad Ny_{GR} = \frac{Ny_7 + Ny_8 + Ny_9}{3}$$

$$Nxy_{BY} = \frac{Nxy_1 + Nxy_2 + Nxy_4 + Nxy_5}{4} \leftarrow \text{4 Nearest Elements}$$

Fastener Load (Pbr)	508	lbf
Bypass Load in X-direction (Nx By)	-20.9	lb/in
Gross Load in X-direction (Nx Gr)	-584	lb/in
Bypass Load in Y-direction (Nyby)	135	lb/in
Gross Load in Y-direction (NyGr)	140	lb/in
Bypass shear load (Nxyby)	-33.9	lb/in

Figure 46. Free body loads calculation method from shell forces near a CFAST element

Approved for public release; distribution unlimited.

The next step is to calculate a fatigue margin by comparing the maximum stress at the fatigue detail ($K_t\sigma$) to a fatigue allowable of 110ksi taken from MMPDS-05 figure 6.3.5.1.8(c) for a stress ratio (R) of zero and temperature of 1000˚F. The fatigue allowable was adjusted for panel temperature for the selected load case based on the curve shown in MMPDS-05 figure 6.3.5.1.1. Alternatively to a margin of safety, a fatigue life for the maximum $K_t\sigma$ can be calculated based on the equation for the S/N curves in MMPDS-05 figure 6.3.5.1.8(c) (Figure 47 below). The equation allows us to plug in a maximum stress and solve for a number of fatigue cycles to failure.

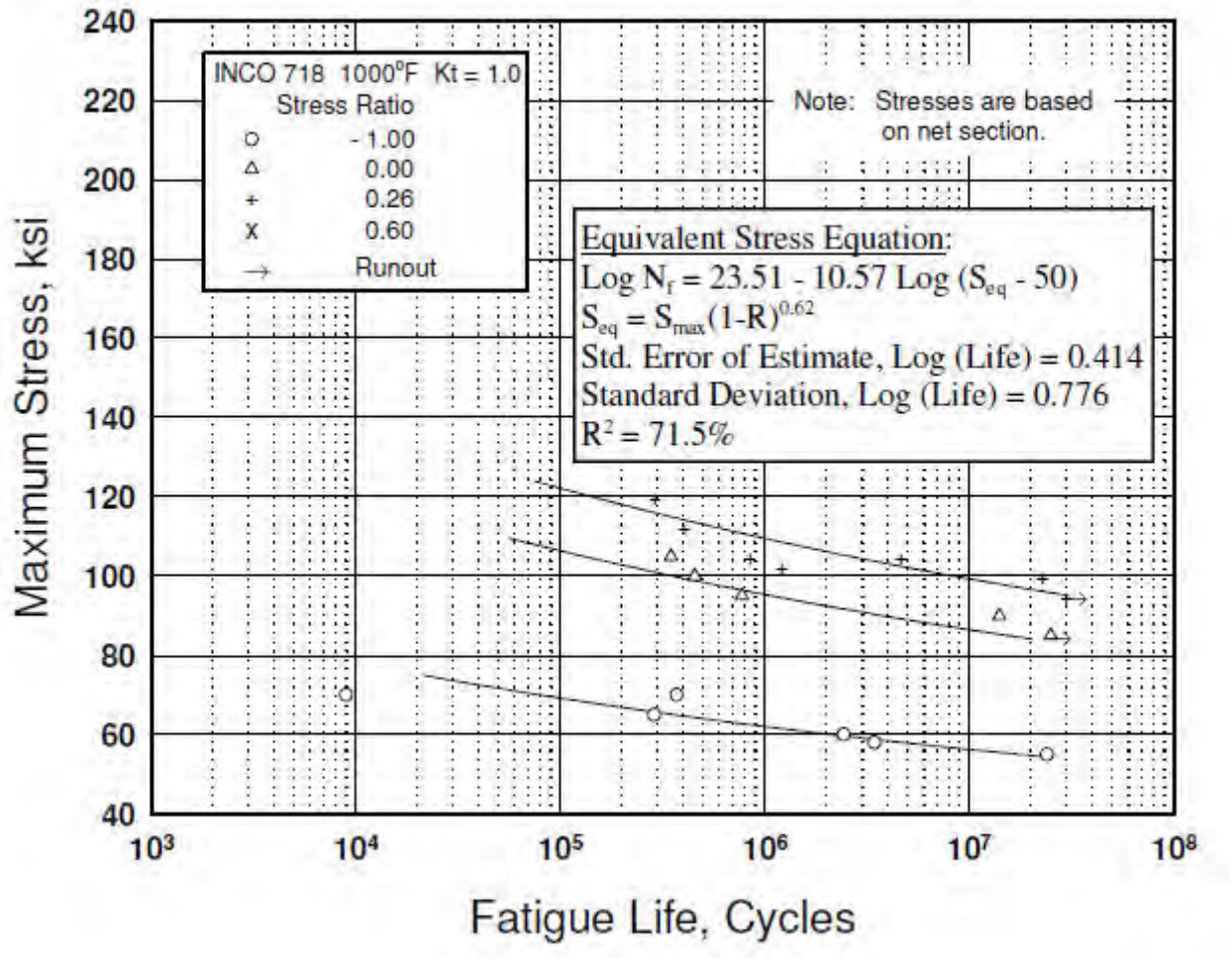

Figure 47. Best fit S/N curve used for thermal-mechanical fatigue life calculations (ref MMPDS-05 fig 6.3.5.1.8(c))

4.3 Panel 1 (862) Detailed Design

Panel 1 (862), Figure 48, is located on the leeward surface of the TX-V. It lies above an engine bay in the rear of the vehicle just left of the vehicle centerline.

Approved for public release; distribution unlimited.

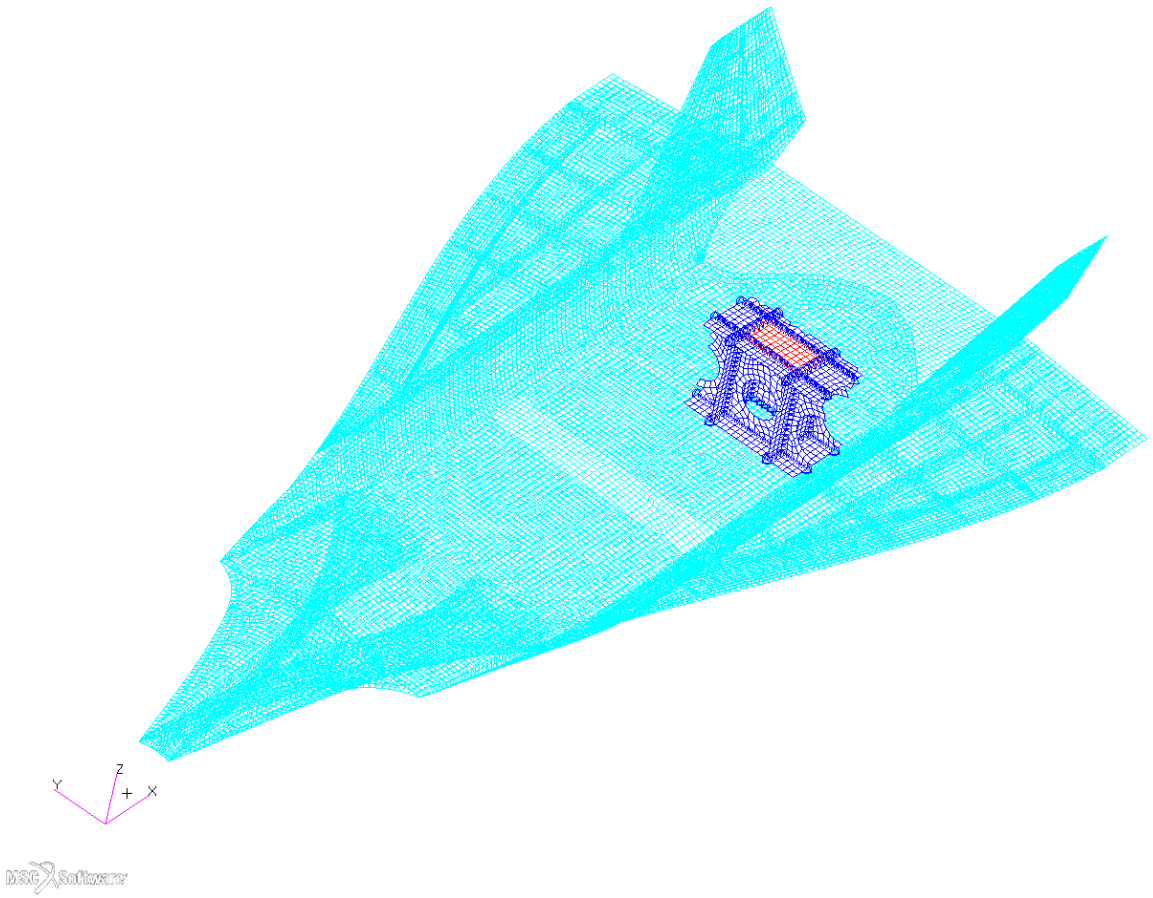

Figure 48 Location of Panel 1 (862) and the Corresponding unit cell

4.3.1 Panel 1 (862) Sizing and Design

Multiple panel configurations were initially explored for the first panel. Although the global vehicle FEM sizing was based on honeycomb sandwich for computational simplicity, there are several fabrication and damage tolerance issues with super alloy honeycomb panels and they were not considered in detail under Task 2. Initial focus was placed on the corrugated core sandwich and machined iso-grid panel configurations shown in Figure 49. Titanium corrugated sandwich panels had traded well in prior high speed transport studies and it was thought that fabricating such panels with Inconel 718 sheet, though challenging, could be achieved for reasonable costs. Iso-grid panel configurations were considered as they typically trade well for bi-axially loaded structures, can be optimized for various ratios of directional and shear loads, and can be readily machined from plate material. When evaluated for Inconel 718 and the loads estimated for Panel 1 however, both of these concepts were driven by minimum gage constraints and ended up being quite heavy; 4.0 psf for the corrugated sandwich panel and over 6 psf for the iso-grid panel. This was a good lesson of how design experience with aluminum and titanium structures does not necessarily apply to higher density metallic structures. A minimum gage for .030 inches was assumed for sheet, .050 inches for machined skins and .070 inches for machined

stiffening features. The .030 inches for sheet was based on a prior aircraft program while the machining limitations were based on the X-51A Inconel 718 control fin body.

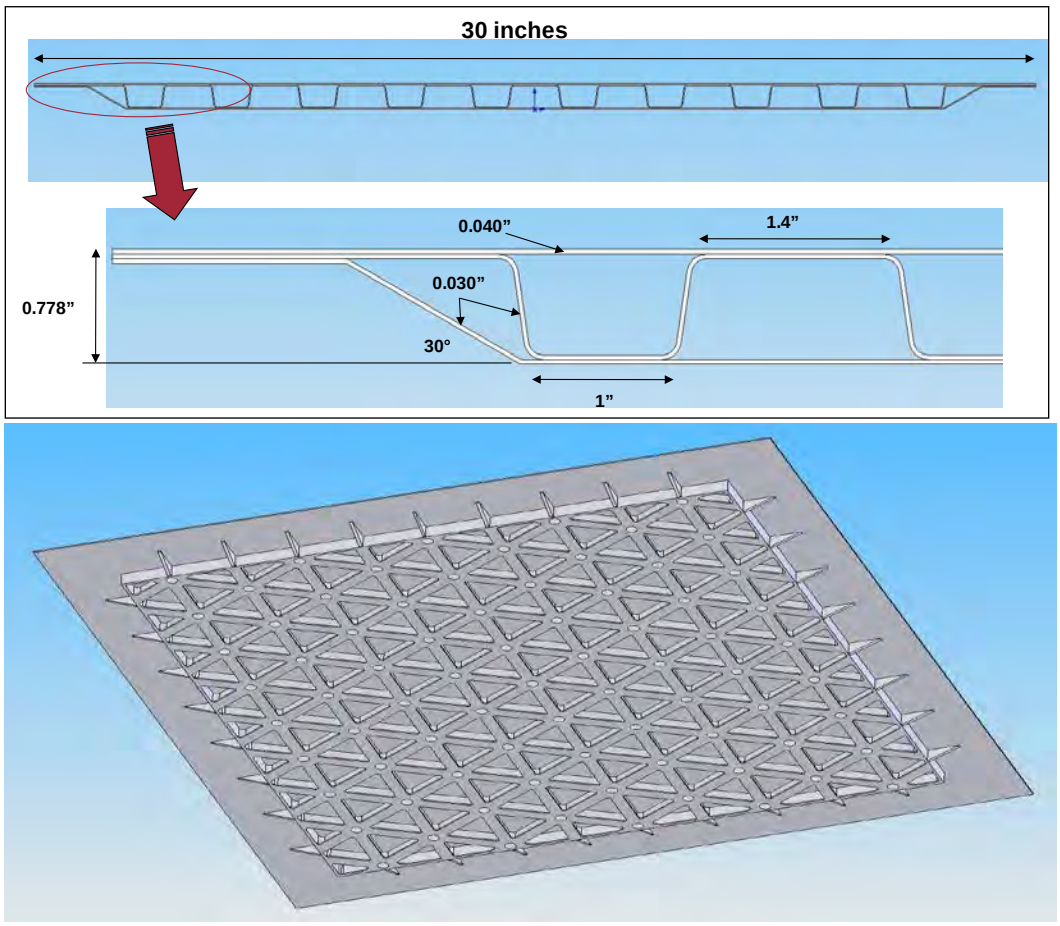

Figure 49. Corrugated core (top) and iso-grid (bottom) panel configurations

A large portion of the weight of the iso-grid is in the diagonal members, and since it was expected that TX-V panel shear loads would be small relative to principal direction thermal loads, an ortho-grid configuration was evaluated. Like the iso-grid, the ortho-grid panel can also be optimized for various ratios of principal direction loads without the need for the diagonal members and can be machined from plate material. Using similar minimum gage constraints as the iso-grid panel, the ortho-grid panel was sized at 3.2 psf for Panel 1 loads. Shown in Figure 50, the panel has a 3 inch x 3 inch stiffener spacing, a 0.61 inch total height, and minimum gage skin and stiffener thickness of .050 and .070 inches.

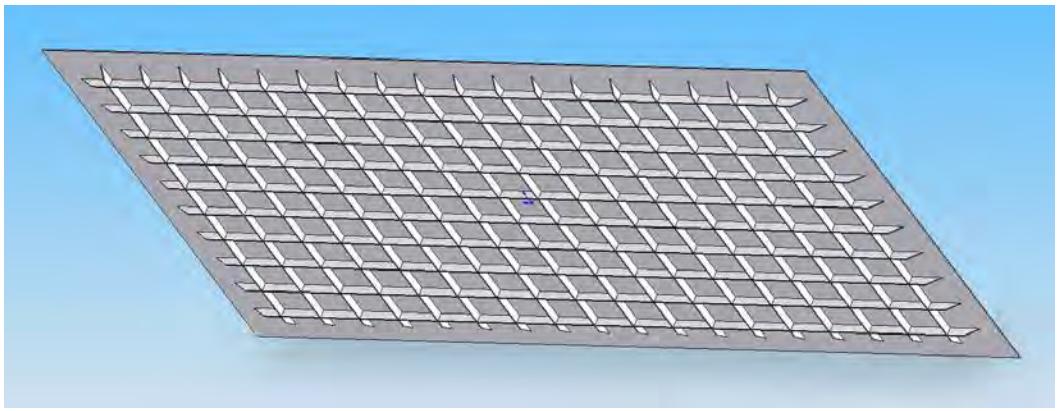

Figure 50. Ortho-grid panel configuration

Mechanical loads for sizing Panel 1 were extracted from HyperSizer from the Task 1 sizing study discussed in Section 3.4, while thermal loads were based on the sub-structure trade study results. These sizing loads are provided in Table 10. The listed buckling loads are lower than the strength sizing loads due to the way HyperSizer was linked to the FEM in Task 1. When mechanical loads are pulled from a linked FEM as they were in Task 1, HyperSizer applies a statistical knockdown factor for buckling loads. Sizing loads for Panels 2-4 were input manually and buckling sizing loads were set equal to the strength sizing loads. Relatively high factors of safety of 2.0 for Ultimate and 1.6 for Limit, which are consistent with experimental aircraft, were also used for sizing Panel 1. Discussions with the AFRL later revealed that they would prefer the use of safety factors more consistent with a production program, and factors of 1.5 for Ultimate and 1.15 for Limit were used for the Panels 2 through 4. High factors of safety are often used for experimental aircraft where structural qualification by analysis with large safety factors is acceptable and often preferred in order to avoid the cost of extensive airframe testing.

Table 10. Panel 1 sizing loads for a 2.5G turn at 1080 sec

	Nx	Ny	Nxy	Mx	My	Mxy	Qx	Qy
	[lbs / in]			[in-lbs / in]			[lbs / in]	
Strength from Global FEM	-73.9	-29.1	-23.7	22.5	8.7	-1.7	-0.2	-0.2
Buckling with HyperSizer Knockdown	-67.7	-25.6	-15.2	22.5	8.7	-1.0	-0.2	-0.1
Thermal from Substructure Study	-430	-473						

Additional inputs: 1350F temperature, 100F/in temperature gradient, 1.5 psi normal pressure

The completed ortho-grid panel unit cell geometry is shown in Figure 51. It should be noted that the sized ortho-grid configuration for Panel 1 was used for the other skin panels in this unit cell. Geometry for subsequent unit cells was created with simple surfaces for the remaining panels

and these were later given equivalent sandwich properties from the Global FEM during detailed analysis (Gap #5 Page 2).

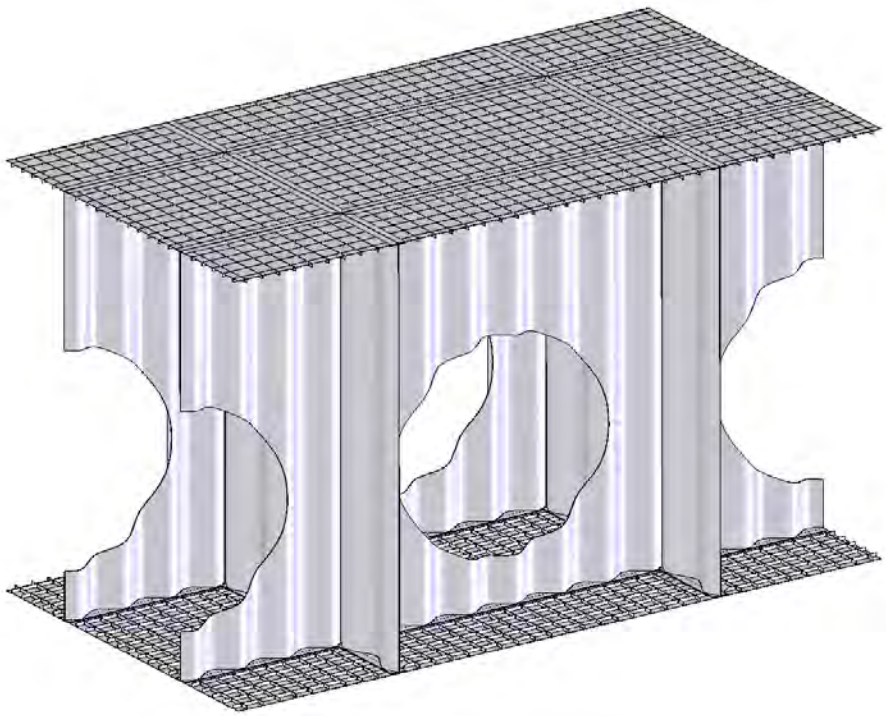

Figure 51. Panel 1 unit cell

4.3.2 Panel 1 (862) Thermal Analysis

Thermal analysis of Panel 1 (862) was conducted under the assumptions discussed in section 4.2.3 . This panel is located above the engine bay. The engine surface is modeled by a specified transient temperature profile based on previous hypersonic studies. The engine case is assumed to be surrounded by a 1 inch thick Min-k insulation blanket. Internal radiation between the blanket surface and surrounding structure is included in the analysis. The boundary conditions used for this panel including the external aerothermal and engine case conditions are illustrated in Figure 52. Figure 53 shows temperature distributions at critical load conditions during the flight. The first image represents temperatures during acceleration when maximum temperature gradients between the panel skin and ortho-grid occur. The second image shows the maximum flight temperatures. The third image shows the greatest negative temperature gradients which occur at the end of flight when the lower flight velocities and enthalpies cause external cooling.

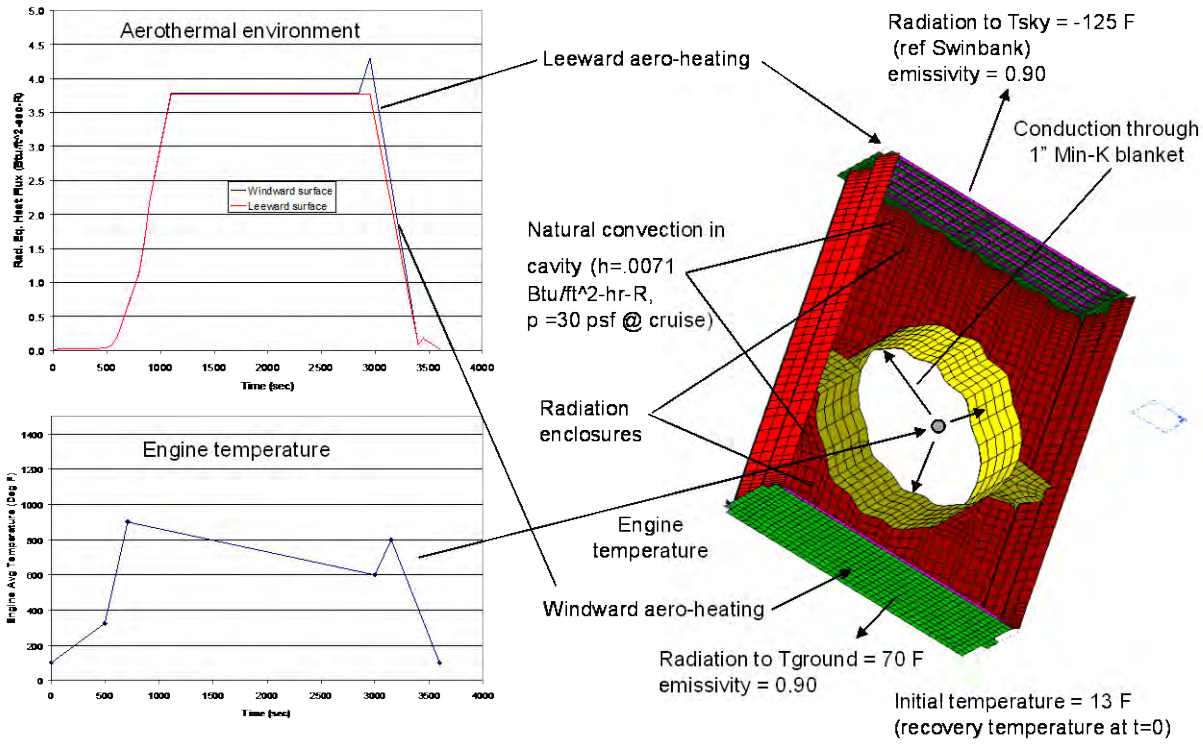

Figure 52. Panel 1 (862) Thermal Boundary Conditions

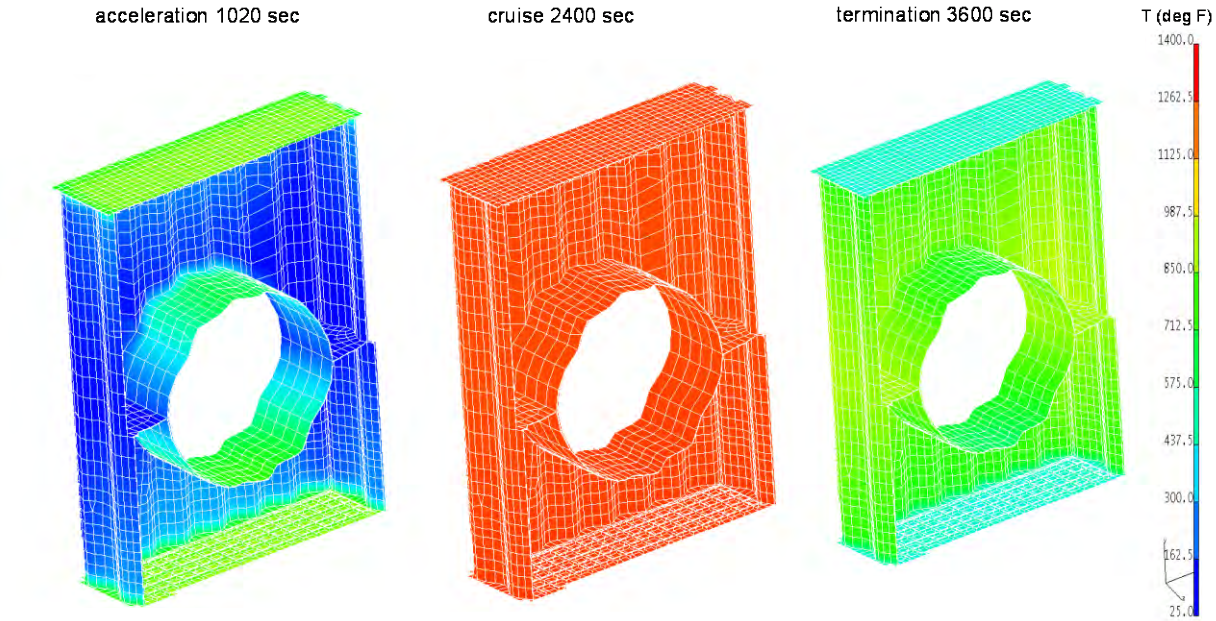

Figure 53. Panel 1 (862) Temperature Distributions

Transient temperature profiles at locations on all the major structural components are plotted in Figure 54. The engine case temperature is also included for reference. The temperature lag between the panel and the web substructure is easily seen during the initial phase of the flight.

Approved for public release; distribution unlimited.

By the end of the cruise, the entire structure has approached a uniform and maximum temperature. Figure 55 shows maximum temperature difference between structural components. These results are used to identify the time states corresponding to maximum temperatures and temperature gradient conditions. The four conditions: maximum gradient in the panel, maximum gradient between panel and substructure, maximum temperatures and maximum reverse gradient are specified.

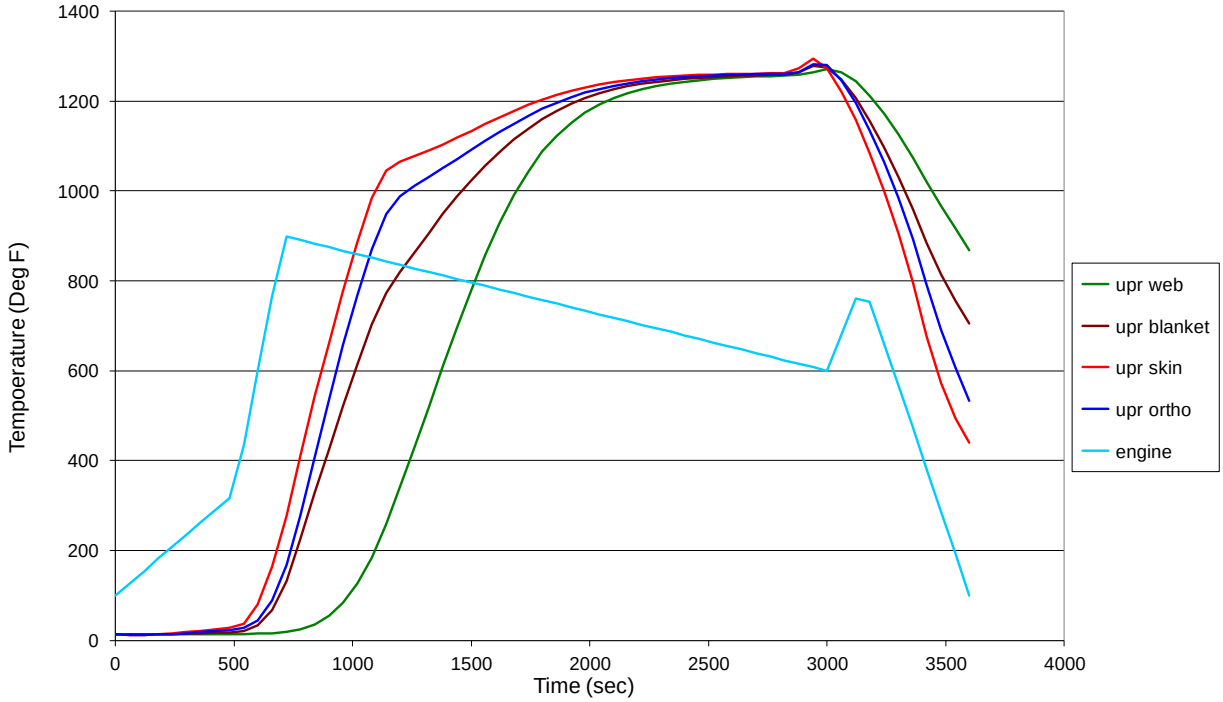

Figure 54. Panel 1 (862) Temperature Histories

Approved for public release; distribution unlimited.

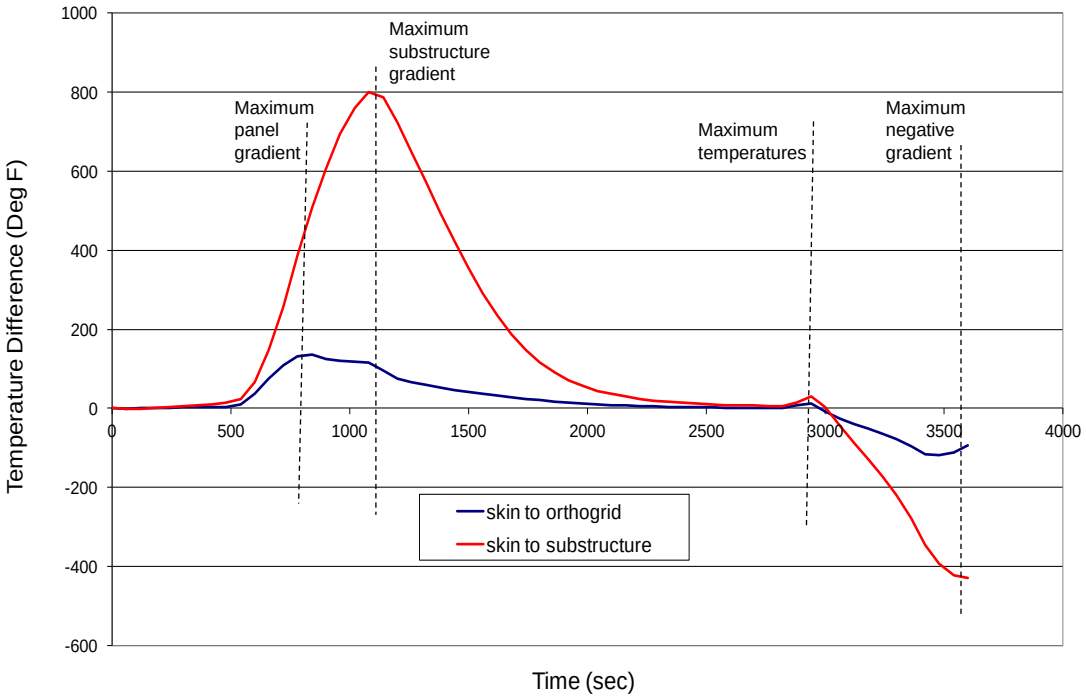

Figure 55. Panel 1 (862) Temperature Gradients

4.3.3 Panel 1 (862) Stress Analysis

The first attempt for any analysis usually encounters many issues and as that analysis is repeated, lessons learned allow the process to become more efficient. For this reason, Panel 862 was selected as Panel 1 because it had the least stringent static loading conditions.

There were two major simplifications incorporated into the design: flat panels and simplified substructure geometry. The radius of curvature for Panel 1 is much greater than 1000 inches, which can be assumed to be flat. There are several implications to this simplification. First, because the panel is flat, the CAD geometry is very simple to create and can be set up with parametric dimensioning to allow rapid modification of geometry. Second, finite element modeling is also simple and quick to create and modify. The panel was created using dimensions determined in the design stage; as opposed to using imported CAD geometry. This ability allowed the FEM generation to begin at the same time as the CAD geometry and thermal FEM creation, thereby saving time. There were some disadvantages to a flat panel. Because the flat panel did not follow the curvature of the vehicle, the boundaries of the unit cell along the leeward surface did not coincide with the vehicle model. The maximum distance between points on the two models is 4.2 inches. This discrepancy could have been minimized by angling the unit cell leeward surface to correlate more closely to the vehicle model, however this added complexity was not incorporated. Figure 56 shows an overlay of the unit cell model and the relevant global vehicle model.

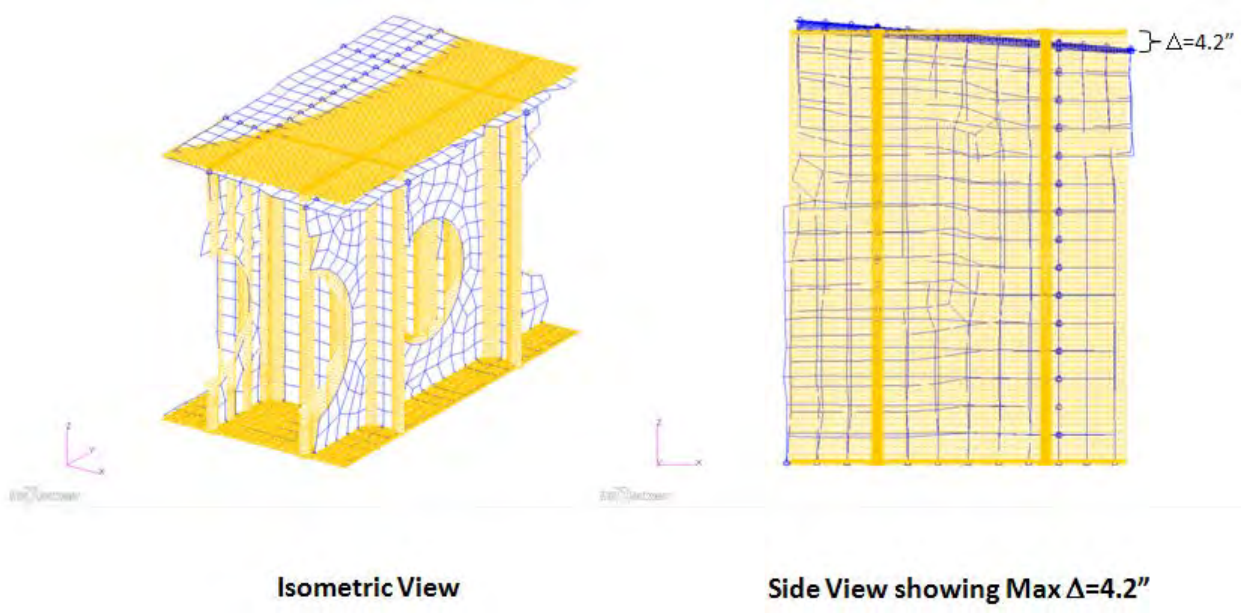

Figure 56. Overlay of unit cell (Yellow) and global vehicle model (White/Blue)

The second simplification made in this model was the estimation of the substructure location. Engine bay cutouts, unit cell height, frame and keel location and intersections, and unit cell boundaries were all approximated separately from the CAD model and Thermal FEM. This allowed the static analysis FEM to be generated quickly without having to wait for the CAD model to be complete. However, there are small discrepancies between the three models. The effects of these discrepancies were determined to be acceptable though the results showed that this simplification could have contributed to the large deflection at the unit cell boundaries.

This first unit cell was modeled using the same ortho-grid pattern and sizing for all skin panels. This was done to represent a vehicle utilizing all ortho-grid panels. However, when the loads are applied from the global vehicle model, there are large deflections in the unit cell surrounding skin panels which do not match the displacements in the global vehicle model. This is because the skin panels in the global vehicle model are modeled as honeycomb sandwich panels which have a much higher bending stiffness than the ortho-grid panels. Therefore the loads that are generated from the global vehicle model are based on a very stiff structure which deflects the much less stiff ortho-grid structure. These deflections are mostly at the unit cell boundaries which has little effect on the loading at the boundaries of the panel of interest. Figure 57 shows a deflection plot of the unit cell with the critical load case, Mechanical: 2.5g Ultimate (1.5) + Thermal: T=1080s, applied.

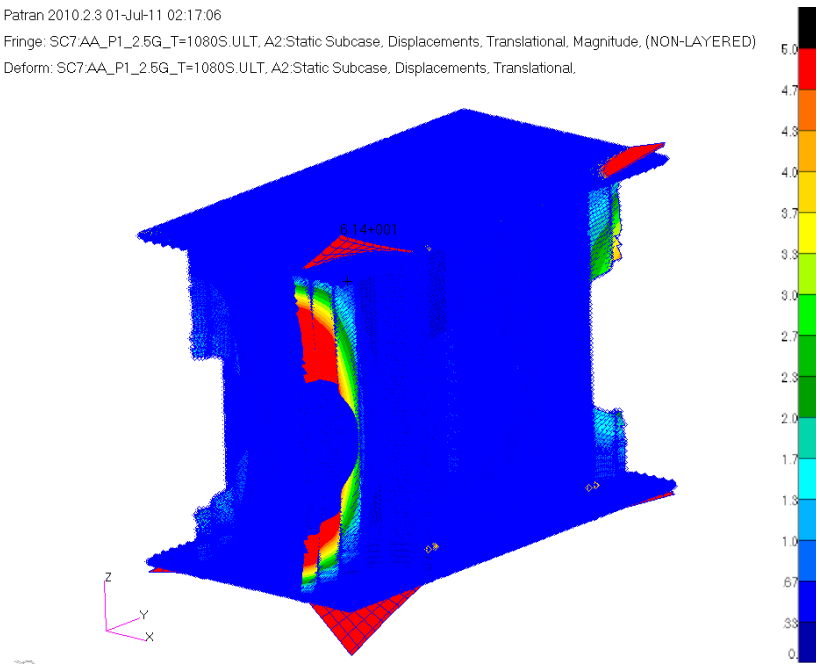

Figure 57. The Stiffness of the Ortho-grid Skin Panels allow large deflections

Results from the panel level analysis are discussed below. The critical load case is Mechanical: 2.5g Ultimate (1.5) + Thermal: T=1080s. These analyses are non-linear.

The maximum relative displacement in the Z direction is calculated as follows:

$$\Delta = \text{Maximum deflection} - \text{Minimum deflection} = (0.0729) - (-0.119") = 0.192"$$

The allowable for deflection is 0.1" as defined the thermal analysis section. Therefore the deflection margin of safety (MS) is calculated as follows:

$$MS = \text{Allowable/Actual} - 1 = 0.1/0.192 - 1 = -0.48$$

The displacement plot of Panel 1 (862) is shown in Figure 58.

.

Approved for public release; distribution unlimited.

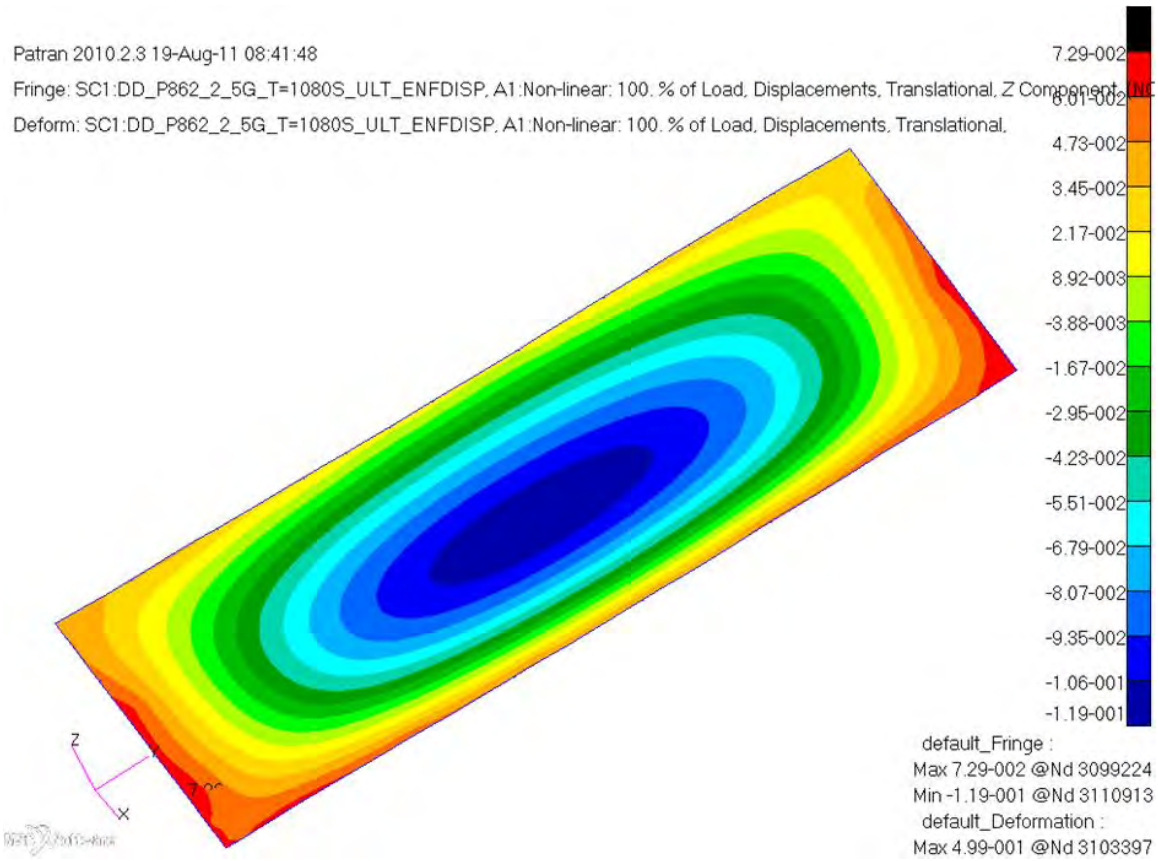

Figure 58. Non-Linear Z-Component Deflection [in] Plot of Panel 1 (862)

Load Case Mechanical - 2.5g Ultimate (1.5) + Thermal - T=1080s

The maximum Von Mises stress of 17 ksi is located near the boundary of the panel. The allowable for Ultimate Material Failure for Inconel at room temperature is Ftu = 185 Ksi. At T = 1080s, the maximum temperature of the unit cell is 1060°F which dictates a thermal knockdown factor 89% of room temperature allowable. The allowable is calculated as follows:

$$F_{tu@1060°F} = F_{tu@70°F} * \text{Thermal Knockdown} = 180 \text{ Ksi} * 0.89 = 160.2 \text{ Ksi}$$

Therefore the Ultimate Material Failure margin of safety (MS) is calculated as follows:

$$MS = \text{Allowable/Actual} - 1 = 160.2/17 - 1 = 8.42$$

The Von Mises Stress plot of Panel 1 (862) is shown in Figure 59.

Approved for public release; distribution unlimited.

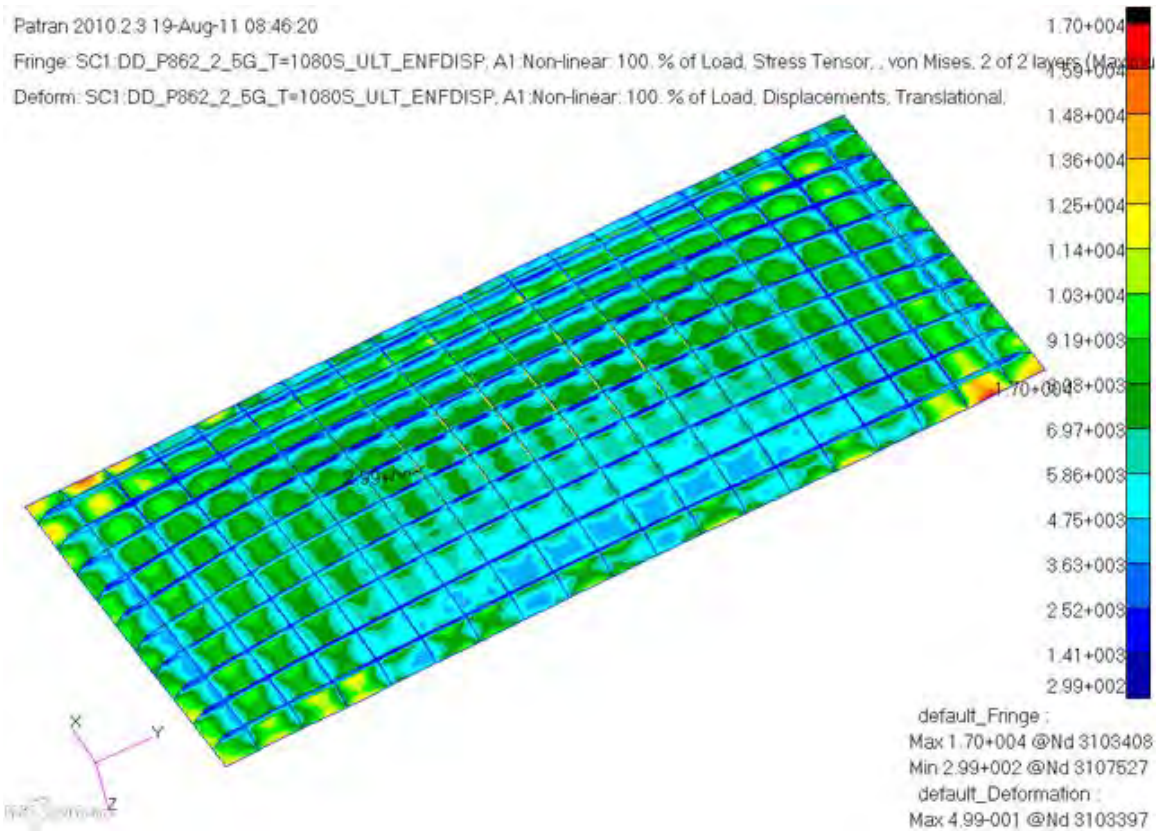

Figure 59. Non-Linear Von Mises Stress [psi] Plot of Panel 1 (862)

Load Case Mechanical - 2.5g Ultimate (1.5) + Thermal - T=1080s

The last static check performed on Panel 1 (862) is a buckling analysis. Limit loads are applied to the panel rather than Ultimate loads since the panel is expected to buckling during normal flight loads and return to its undeformed state with no plastic deformation. The first buckling mode is at an eigenvalue of 2.57. The minimum eigenvalue allowable is 1.0. The buckling Ratio to Requirement (RR) is calculated as follows:

$$RR = \text{Actual/Allowable} = 2.57 / 1.0 = 2.57$$

The plots for the first two buckling modes of Panel 1 (862) are shown in Figure 60 and Figure 61.

Approved for public release; distribution unlimited.

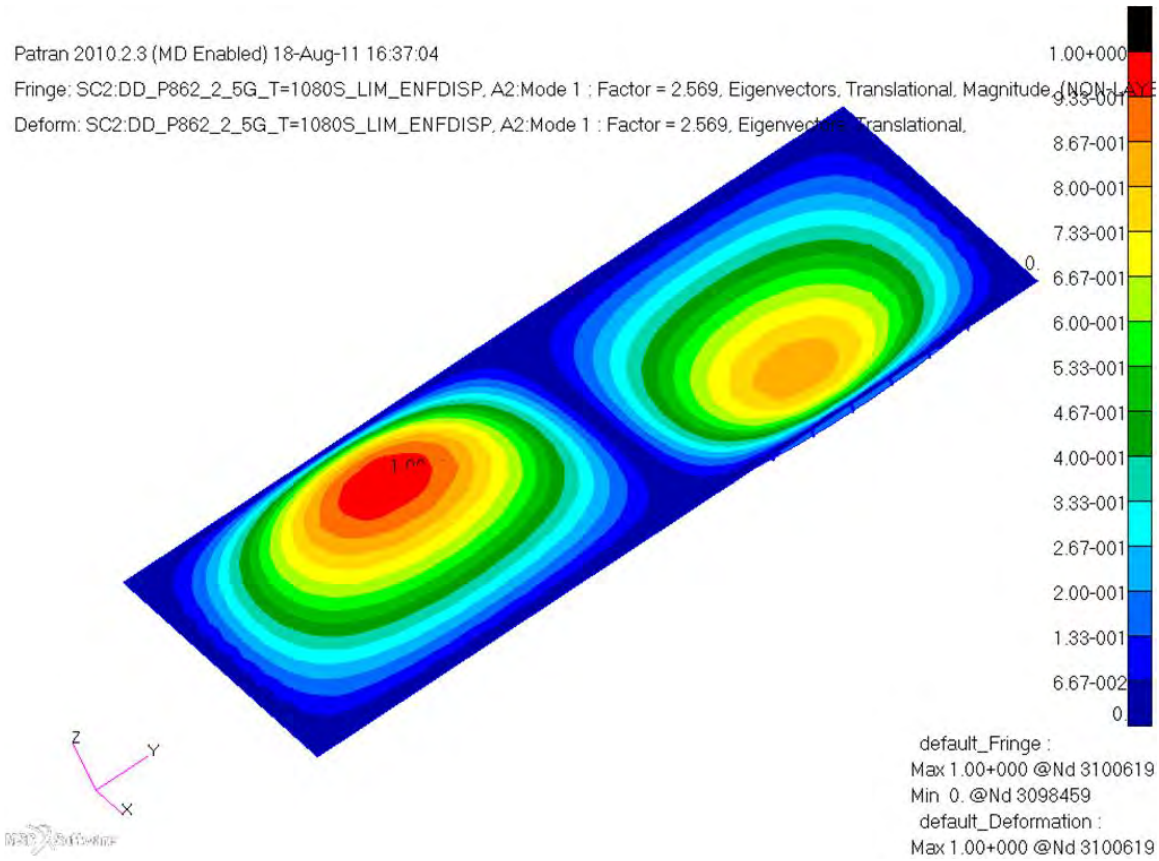

Figure 60. 1st Buckling Mode [eigenvalue] of Panel 1 (862)

Load Case Mechanical - 2.5g Limit (1.15) + Thermal - T=1080s

Approved for public release; distribution unlimited.

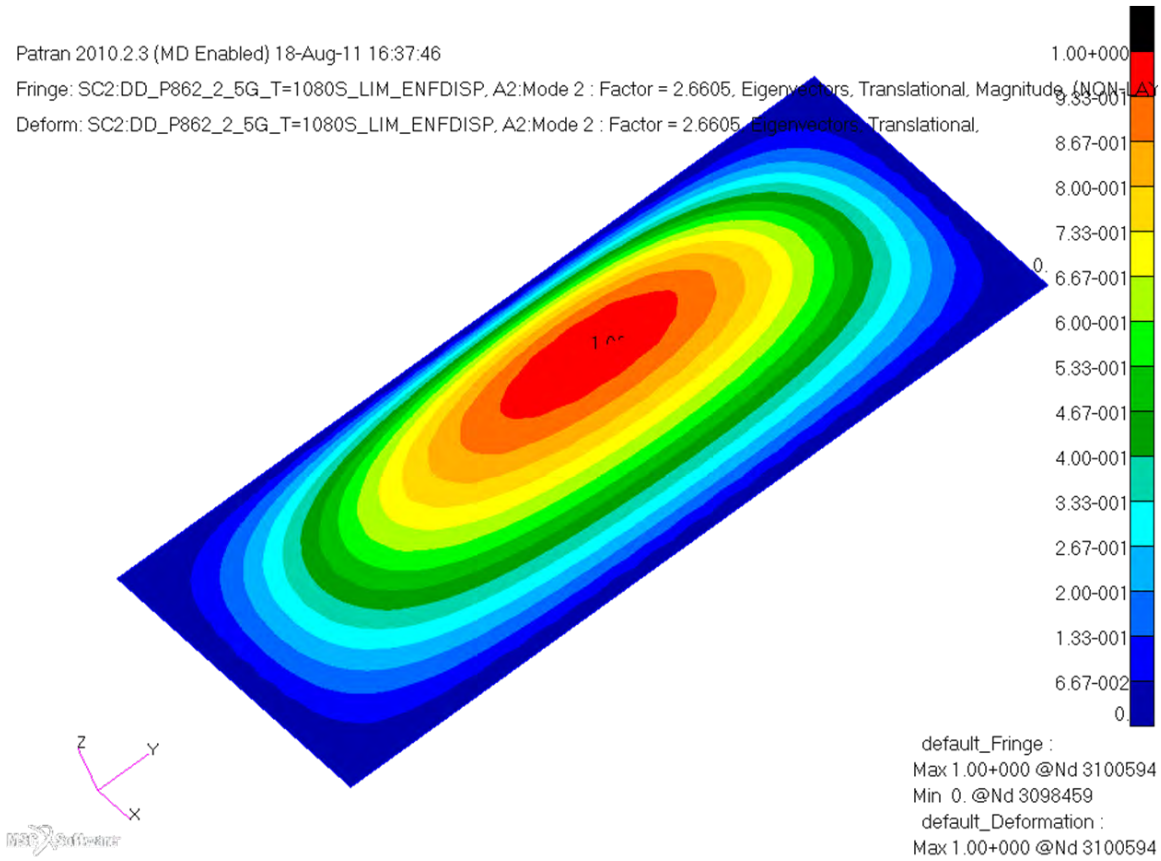

Figure 61. 2nd Buckling Mode [eigenvalue] of Panel 1 (862)

Load Case Mechanical - 2.5g Limit (1.15) + Thermal - T=1080s

As expected there are high margins for material failure and buckling at this panel location with lower loads. The displacements for this panel are over the allowable; however it is not certain whether the leeward surface should share the same deflection requirement as the windward surface (Recommendation #5, Page 3). Additionally, the deflection requirement would need more development to determine if it is too stringent. Iterations can be performed to reduce the high margins, but the negative deflection margin indicates that a raise in margin is likely. A summary of the static margins of safety is in Table 11.

Table 11. Summary of static margins of safety for Panel 1 (862)

Panel	Location	Failure Mode	Load Case	Allowable @ 70° F	Units	Temp	Units	Knock-down	Allowable @ Temp	Units	Actual	Units	MS/RR
1 (862)	Panel Center	Deflection	2.5g Ult (1.5) + T=1080s	0.1	ksi	1060	° F	1	0.1	in	0.192	in	-0.48
1 (862)	Panel Boundary	Material Failure	2.5g Ult (1.5) + T=1080s	180	ksi	1060	° F	0.89	160.2	ksi	17	ksi	8.42
1 (862)	Panel Center	Buckling	2.5g Lim (1.15) + T=1080s	1		1060	° F	1	1		2.57		2.57

4.3.4 Panel 1 (862) Dynamic Analysis

As discussed in Section 4.2.7, Panel 1 is the aft-most panel and experiences greater acoustic loads than the other panels. The thermal loads at this location are low relative to the other panels producing larger than adequate margins for thermal-mechanical fatigue. The high acoustic loads coupled with the low thermal loads make the panel critical in acoustic fatigue. In the case of acoustic fatigue, low thermal stress tends to reduce mean stress. A reduction in mean stress leads to a reduction in the stress ratio and subsequently, reduction in allowable RMS stress.

Thermal acoustic fatigue for Panel 1 was evaluated at highly loaded fasteners and elements at the skin to substructure joint. Stress concentration design details outside of the skin to substructure joint were ignored for Panel 1 analysis. Fastener loads were exported and then sorted to determine the location of maximum bearing stress. Shell forces were sorted within Patran to select maximum and minimum element forces to analyze. Kt factors were calculated for each case selected. KtS was compared with a temperature adjusted allowable to determine margin of safety.

4.3.5 Panel 1 (862) Fatigue Margin Evaluation

The acoustic fatigue evaluation of Panel 1 resulted in a near zero margin of safety at the "flange hole" at the skin to substructure joint. The figure below shows RMS and thermal stress for locations analyzed for aeroacoustic fatigue (AACF).

Approved for public release; distribution unlimited.

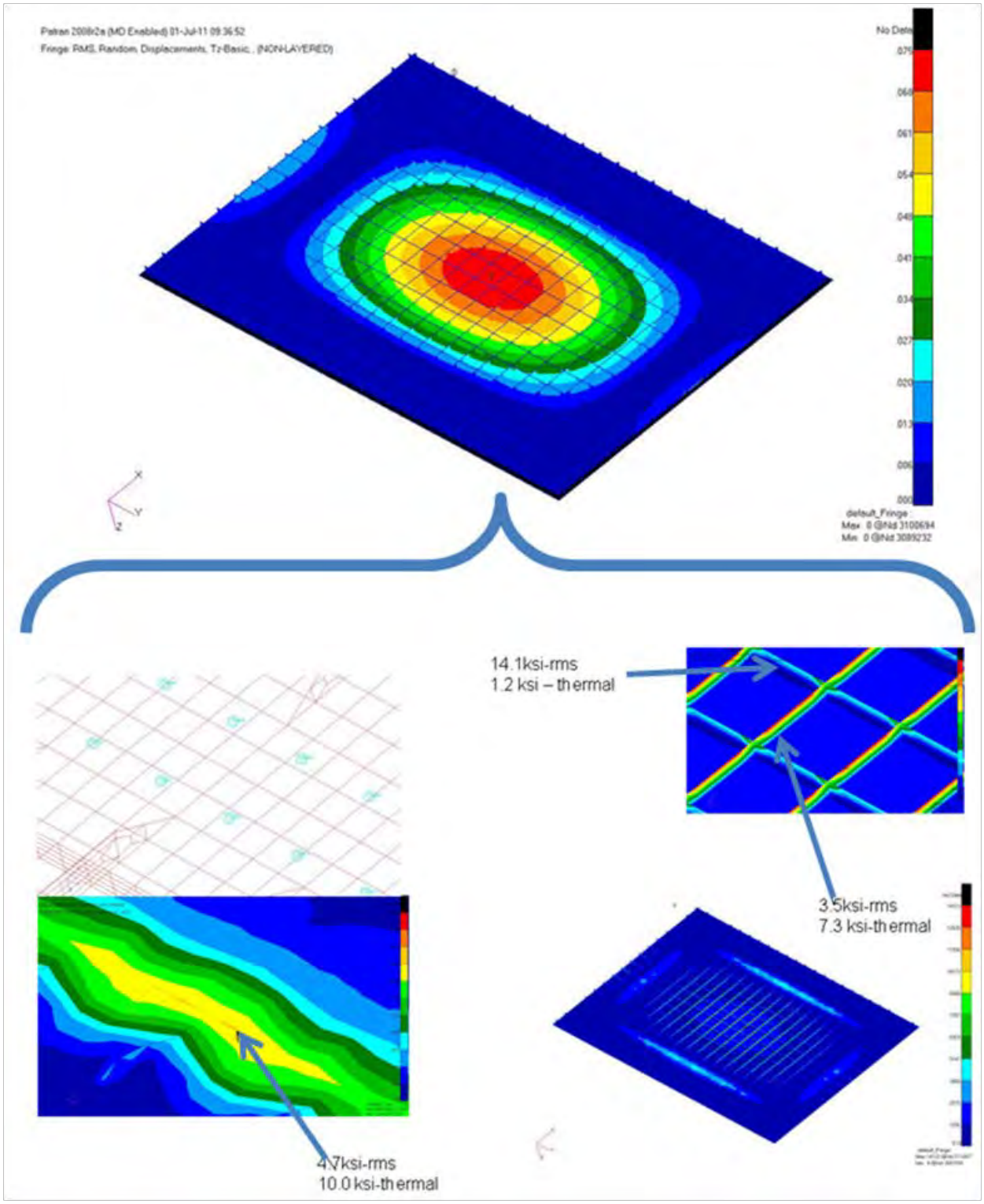

Figure 62. Condition Max Q, RMS Stress with listed Thermal Stresses, Details

Approved for public release; distribution unlimited.

An allowable stress of 14.6 ksi was calculated for T = 850˚F and R=0.35. Results showed an RMS stress of 14.0 ksi (using Kt = 2.97). The margin of safety calculations for a combined thermal acoustic condition at all three locations is given in Figure 62.

ENGINEER	The Boeing Company	PAGE
S. Liguore		2
CHECKER	TITLE	DRAWING NO
DATE		MODEL
July 6, 2011		TO 23

Allowables:

Material: Inconel 718

Ref KtS = 19ksi, RMS, Kt=1, R=-1, RT
(ref. MIL-HDBK-5J section 6.3.5

Adjustments:
1.) KtS = 17.0 ksi, RMS, Kt=1.00, R=-1, T=1050F
2.) KtS = 11.9 ksi, RMS, Kt=1.22, R=0.35, T=1050F
3.) KtS = 4.90 ksi, RMS, Kt=2.97, R=0.35, T=850F

Thermal Loads

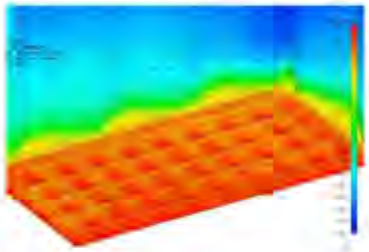

2.) Check RMS Thermal/Acoustic response

Location: Stiffener Web
Element ID = 311530
Stress = Max of Surface VM
MS = (17/14.1 - 1) = 0.21

Location: Stiffener Fillet Radius
Element ID = 311293
Stress = Max of Surface VM
MS = (11.9/3.5 - 1) = 2.40

Location: Frame Flange Hole
Element ID = 310671
Stress = Max of Surface Sx
MS = (4.9/4.8 - 1) = 0.02

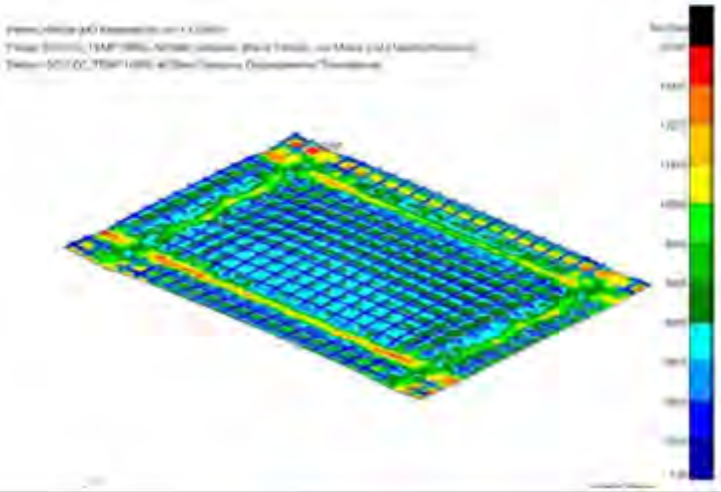

Figure 63. Margin of safety calculation summary for Panel 1 acoustic fatigue

Thermal-mechanical fatigue margins were adequate for Panel 1 due to a relatively low thermal stress. The state of stress at the location of maximum skin to substructure fastener load is shown in Figure 64 and Figure 65. A maximum $K_t\sigma$ of 64.6 ksi occurs for the maximum bearing load case at the skin to substructure joint.

Approved for public release; distribution unlimited.

Max Bearing Case		
Pbr	508	lbf
Nx By	-20.9	lb/in
NxGr	-584	lb/in
Nyby	135	lb/in
Nygr	140	lb/in
Nxyby	-33.9	lb/in

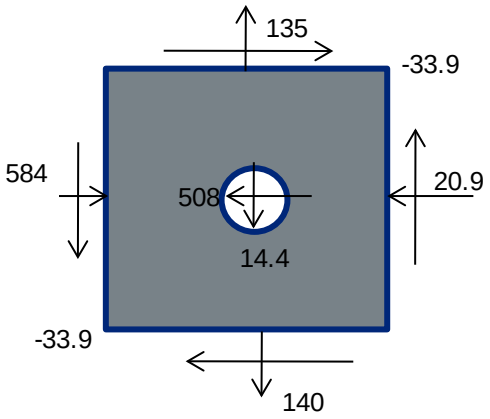

Figure 64. Free body diagram of FEM location with maximum bearing load

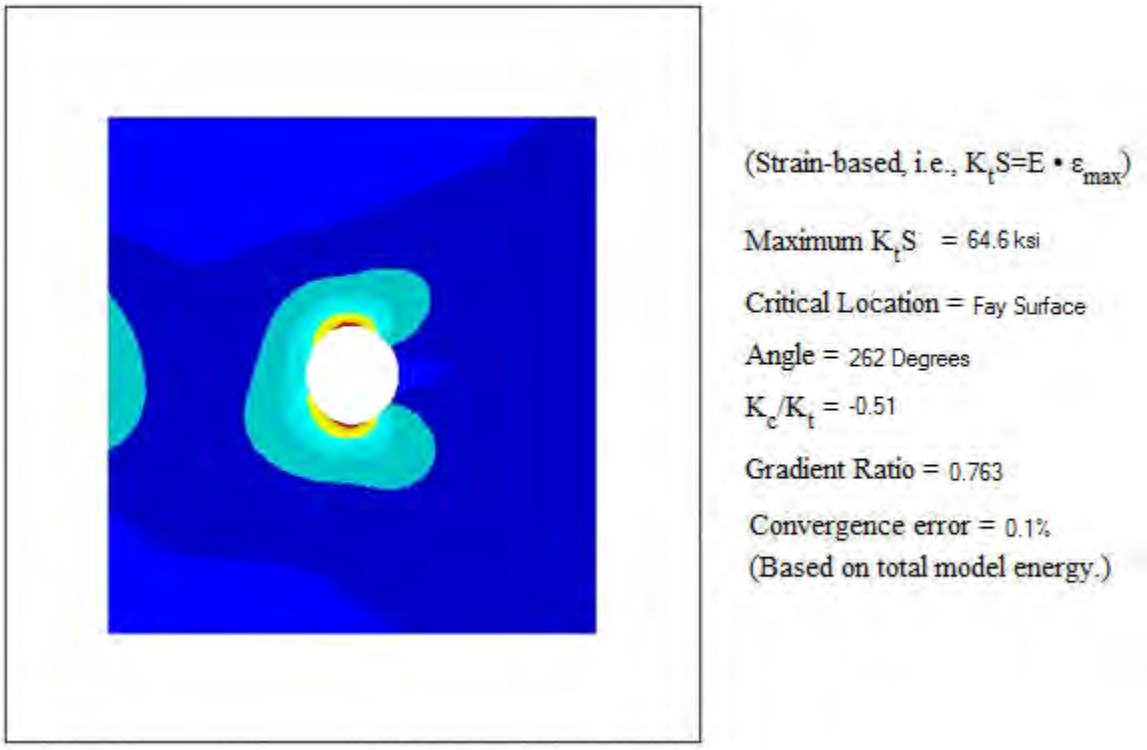

Figure 65. Calculated Ktσ at maximum bearing stress location

A summary of the thermal-mechanical fatigue MS calculations is shown in Table 12.

Approved for public release; distribution unlimited.

Table 12. Margin of safety summary for Panel 1 thermal-mechanical fatigue

	Max Brg	Max Shr	Min Nx	Min Ny	Max Ny	
Pbr	508	259	274	163	87.3	lbf
Nx By	-20.9	-446	-342	-414	-436	lb/in
Nx Gr	-584	-254	-698	-396	-513	lb/in
Nyby	135	-110	122	-339	189	lb/in
Nygr	140	-62	111	-464	244	lb/in
Nxyby	-33.9	-113	62.7	0.98	74.6	lb/in
KT Sigma	**64.6**	**31.6**	**47.9**	**4.7**	**33.1**	**ksi**
Fatigue Margin	**0.41**	**0.71**	**0.56**	**0.95**	**0.69**	
Cycles to failure	**Endurance Limit**	**Endurance Limit**	**Endurance Limit**	**Endurance Limit**	**Endurance Limit**	

4.4 Panel 2 (780) Detailed Design

Panel 1 (862), shown in Figure 66, is located on the leeward surface of the TX-V. Panel 2 (780), located on the windward surface, shares the same unit cell as Panel 1 (862). It lies below an engine bay in the rear of the vehicle just left of the vehicle centerline.

Approved for public release; distribution unlimited.

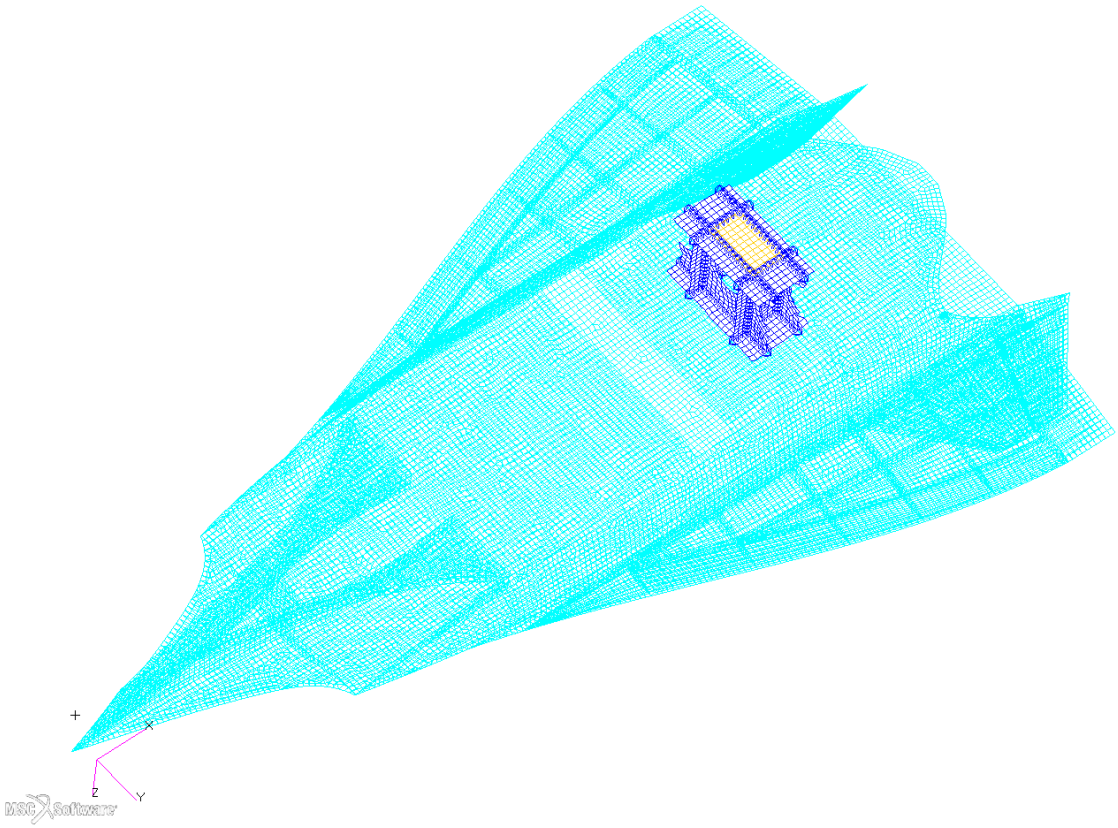

Figure 66. Location of Panel 2 (780) and the Corresponding unit cell

4.4.1 Panel 2 (780) Sizing and Design

Panel 2 was located on the bottom surface of the same unit cell as Panel 1, allowing the direct extraction of both thermal and mechanical loads which are shown in Table 13. Based on Panel 1 sizing results, only an ortho-grid configuration was evaluated for Panel 2. Sizing resulted in a 0.61 inch tall panel with a 3.2 inch by 5.6 inch grid and minimum gage skin and stiffener thicknesses. Fitting this larger grid pattern on the panel with gussets and enough room for substructure attachment fasteners proved difficult and the grid spacing was reduced to 3 x 5 inches in the analyzed design that is shown in Figure 69.

Table 13. Panel 2 sizing loads for a 2.5G turn at 1080 sec

	Nx	Ny	Nxy	Mx	My	Mxy	Qx	Qy
	lbs/in			in-lbs/in			lbs/in	
Strength and Buckling from Panel 1 unit cell	-339	-46.6	-20.0	0.0	0.0	-5.9	-7.2	2.1
Thermal from Panel 1 unit cell	-385	-369	-6.2	0.0	0.0	-0.9	0.7	1.4

Additional inputs: 1154F temperature, 325F/in temperature gradient, 1.0 psi normal pressure

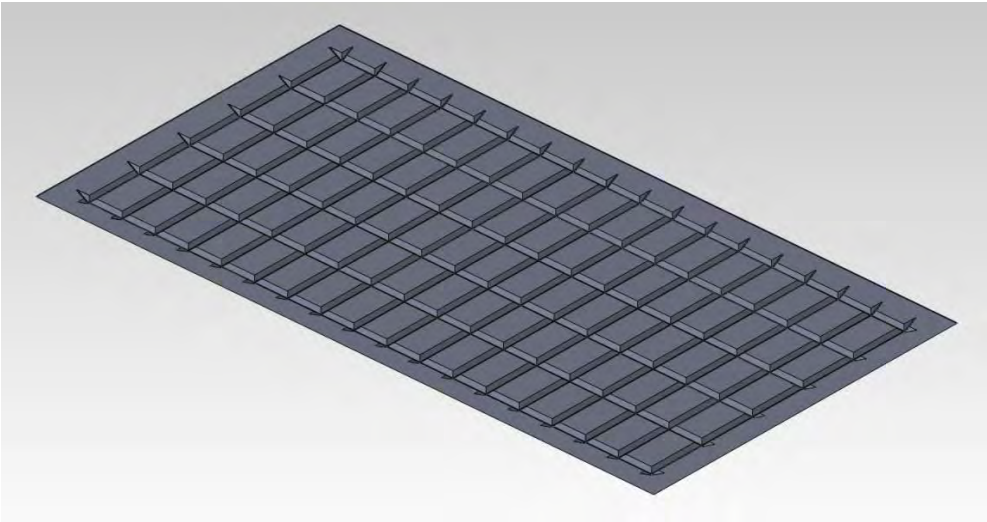

Figure 67. Panel 2 ortho-grid CAD model with 3” x 5” grid spacing

Initial analysis of Panel 2 showed large out of plane deflections of approximately 0.36 inches. A small study was thus performed to evaluate options for stiffening the panel and the panel breaker approach shown in Figure 68 was selected. In this approach, external stiffeners, or panel breakers, are fastened to the ortho-grid stiffeners to add additional out of plane stiffness to the panel and limit normal deflections. The stiffeners would be formed out of sheet material and could be attached with slotted fasteners if needed to limit an in-plane thermal stresses. This panel geometry was then incorporated into the existing unit cell for detailed analysis.

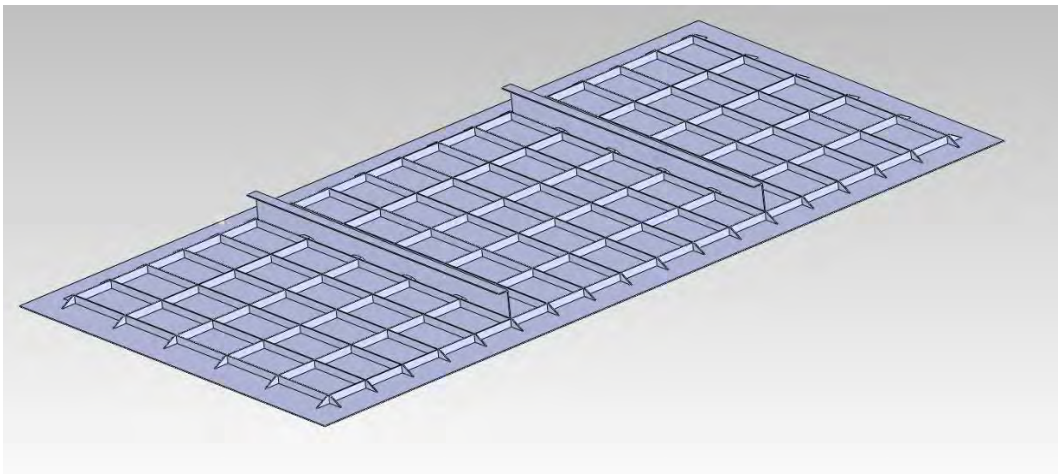

Figure 68. Panel 2 geometry with added stiffeners to reduce normal deflections

4.4.2 Panel 2 (780) Thermal Analysis

Panel 2 (780) is located directly below Panel 1 (862). Therefore the same internal boundary conditions are used in this analysis. The boundary conditions are summarized below in Figure 69. The only changes in boundary conditions are the aerothermal environments. This and subsequent panels made use of a different mission trajectory with variable angle of attack. This results in more typical temperature gradients between windward and leeward surfaces. Unlike the previous panel, Panel 2 (780) includes two panel breaker stiffeners. These introduce additional thermal mass and therefore additional thermal gradients. Figure 70 shows temperature distributions at critical load conditions during the flight. The first image represents temperatures during acceleration when maximum temperature gradients between the panel skin and ortho-grid occur. The next two images illustrate the maximum temperature gradients between skin and substructure and skin and panel breakers respectively. The fourth image shows the maximum flight temperatures, and the fifth the greatest negative temperature gradients which occur at the end of flight when the lower flight velocities and enthalpies cause external cooling.

Approved for public release; distribution unlimited.

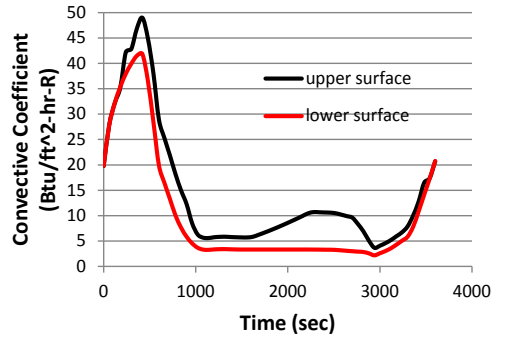

Panel 780 Aerothermal Environment

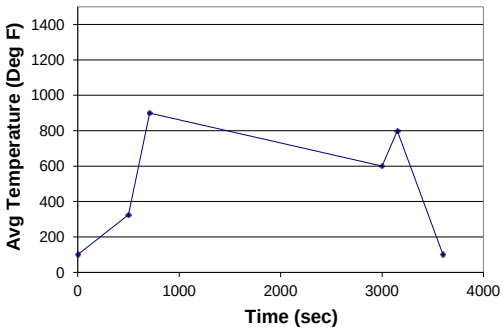

Engine temperature

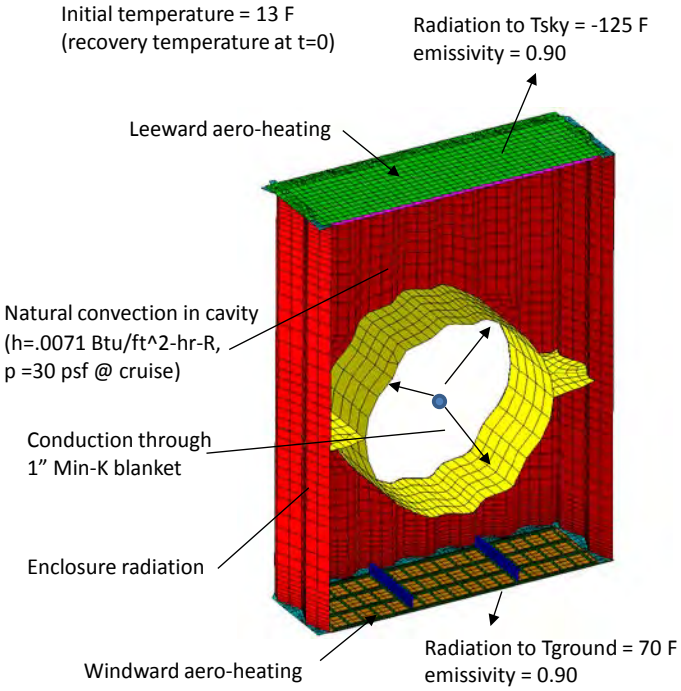

Figure 69. Panel 2 (780) Boundary Conditions

Approved for public release; distribution unlimited.

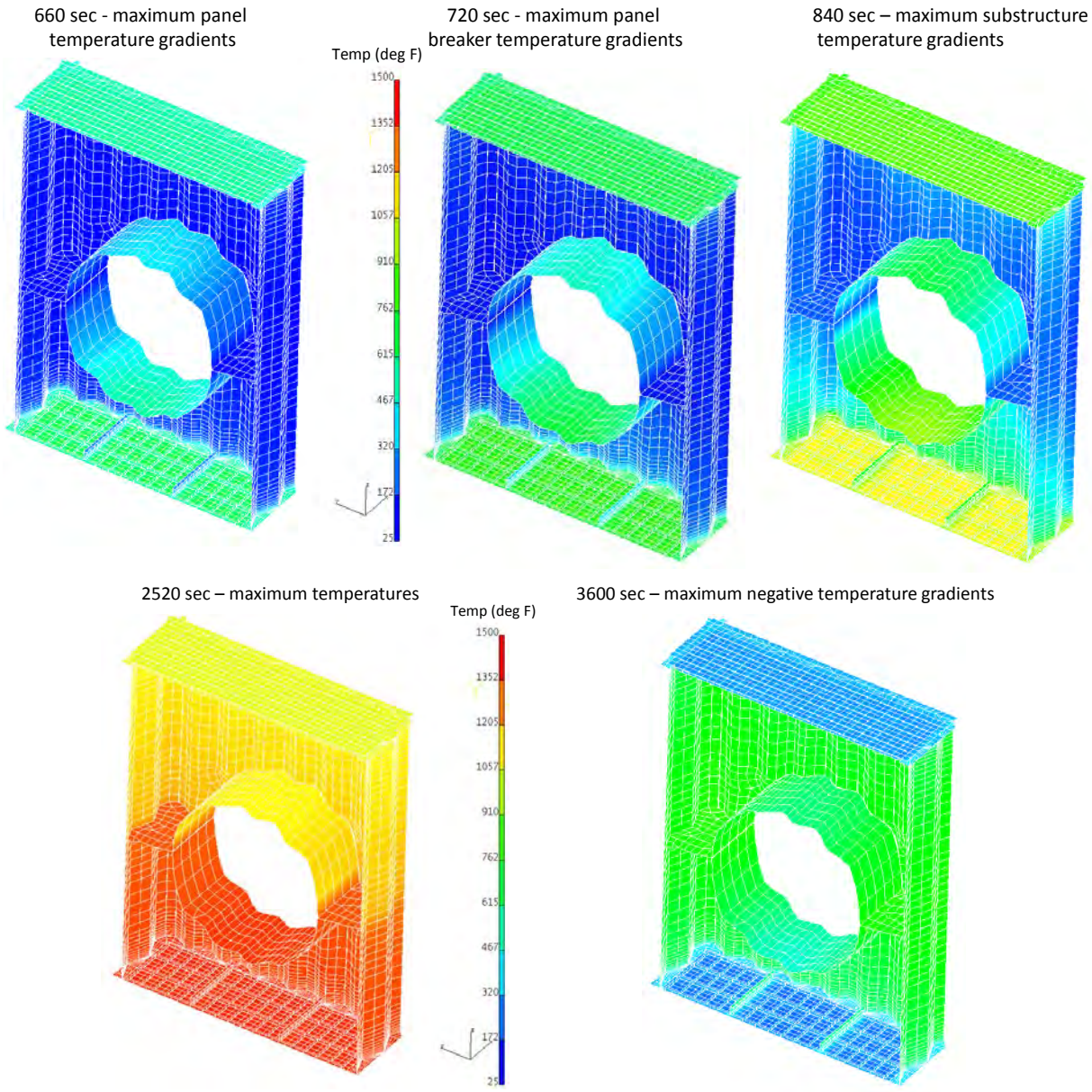

Figure 70. Panel 2 (780) Temperature Distributions

Transient temperature profiles at locations on all the major structural components are plotted in Figure 71. The temperature lag between the panel and the web substructure is easily seen during the initial phase of the flight. By the end of the cruise, the entire structure has approached steady state. Figure 72 shows maximum temperature difference between structural components. These results are used to identify the time states corresponding to maximum temperatures and temperature gradient conditions. The five conditions: maximum gradient in the panel, maximum gradient between skin and substructure, maximum gradient between skin and panel breaker maximum temperatures and maximum reverse gradient are specified. Since Panels 1 (862) and 2 (780) are located at the same station and experience the same internal engine case temperature, structural temperatures and gradients are similar.

Approved for public release; distribution unlimited.

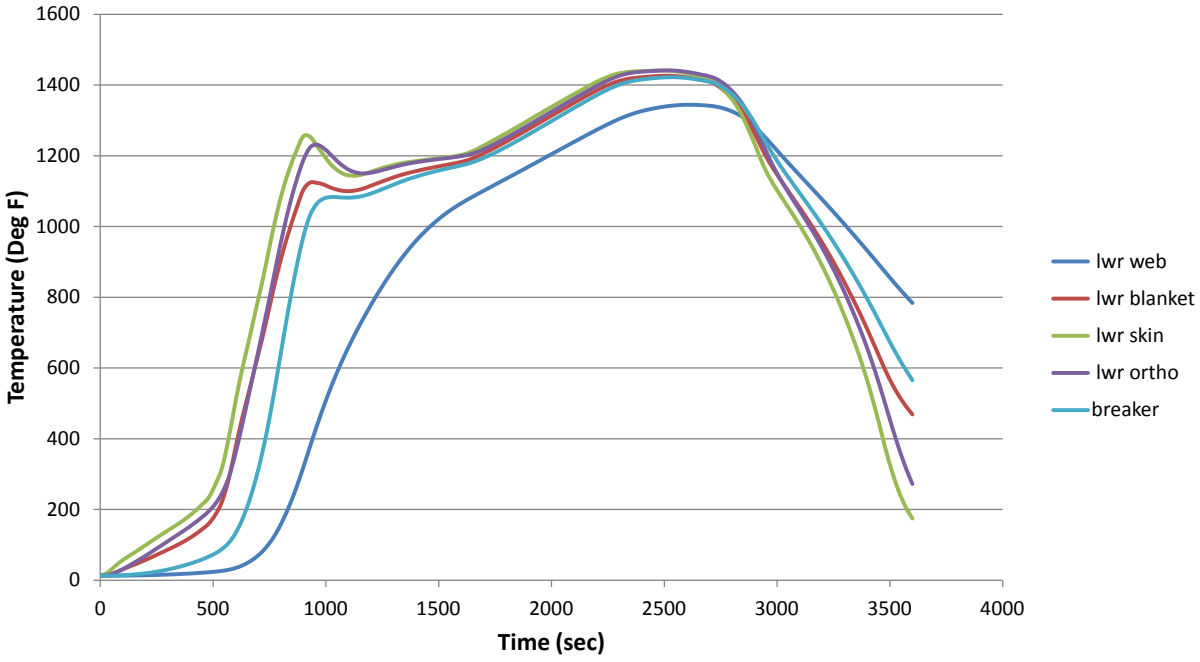

Figure 71. Panel 2 (780) Temperature Histories

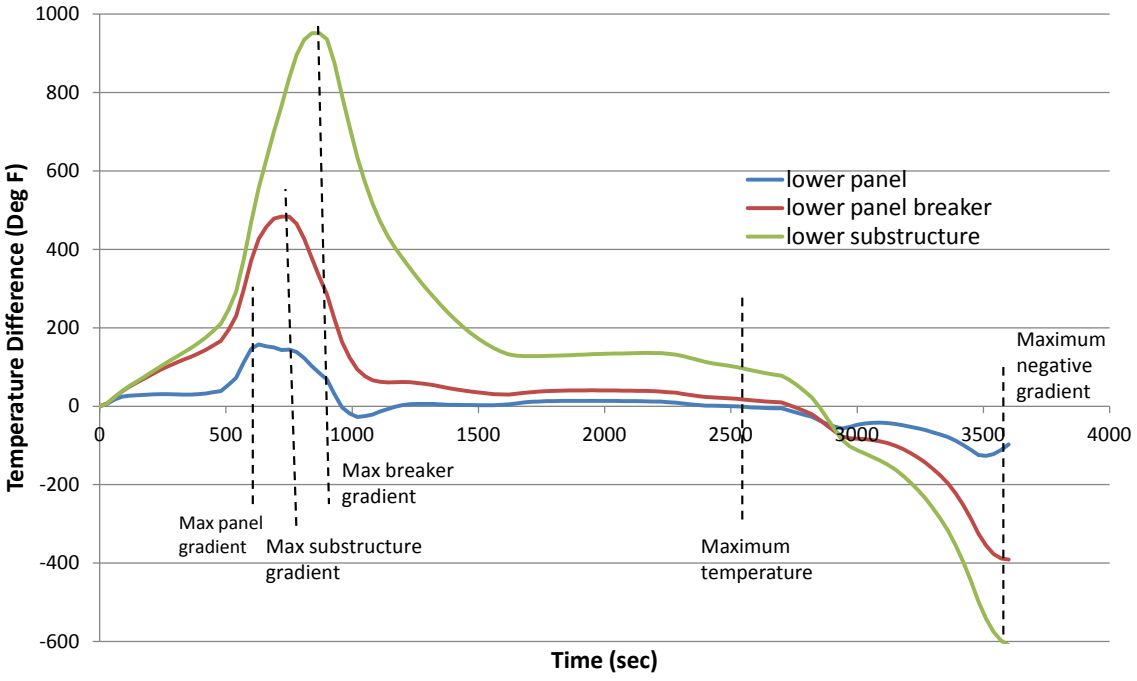

Figure 72. Panel 2 (780) Temperature Gradients

Approved for public release; distribution unlimited.

4.4.3 Panel 2 (780) Stress Analysis

Because Panel 2 (780) lies directly below Panel 1 (862), the same unit cell created for Panel 1 (862) was utilized for Panel 2 (780). This technique saved many hours of FEM creation. The only major change made to the Panel 2 (780) unit cell was to represent all the skin panels, with the exception of the panel of interest, with the same stiffnesses dictated in the global vehicle model, Figure 73. This was done to reduce the large deflections near the boundary of the unit cells. Since the 2.5g mechanical loading was the main driver for the large deflections and the mechanical loading is the same for Panel 1 (862) and Panel 2 (780) as they are part of the same unit cell, a direct comparison can be made between the two versions of the same unit cell as shown in Figure 74. This change in stiffness reduced the overall deflection of the skin panels from 10 inches to less than 1 inch.

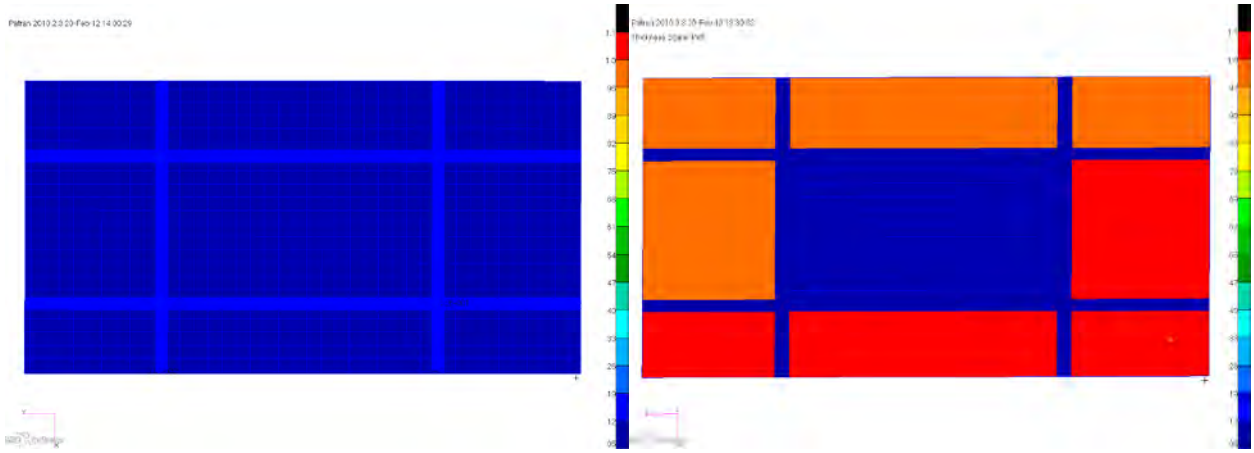

Unit Cell for Panel 1 (862) **Unit Cell for Panel 2 (780)**

Figure 73. Comparison of Thickness [in] for Surrounding Panels, Unit Cell for Panel 1 show uniform minimal thicknesses while Unit Cell for Panel 2 shows more variation in thickness

Approved for public release; distribution unlimited.

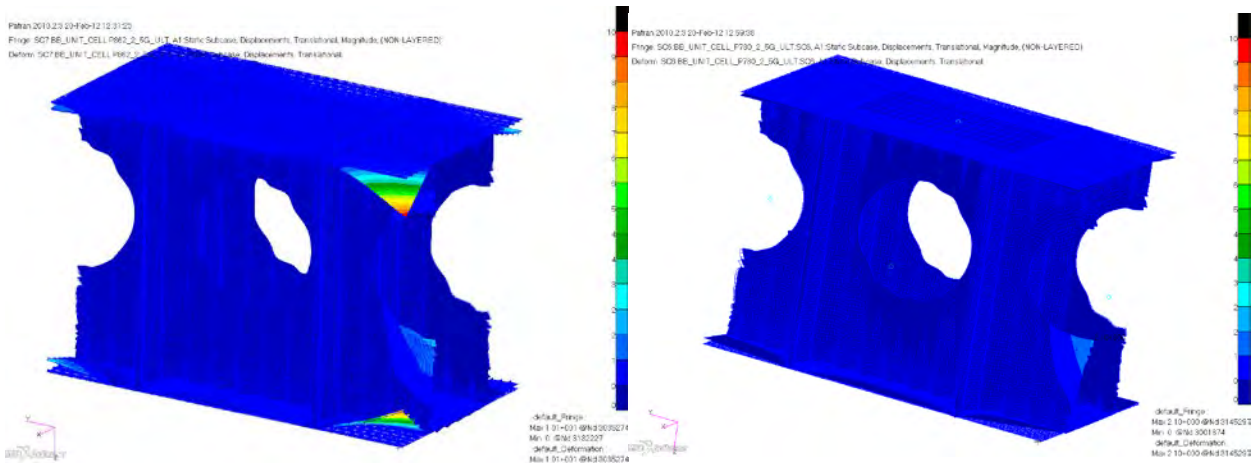

Unit Cell for Panel 1 (862) **Unit Cell for Panel 2 (780)**

Figure 74. Comparison of Deformation Plots [in] Load case: Mechanical: 2.5g Ultimate (1.5), Unit Cell for Panel 2 shows minimal deflection compared to Unit Cell for Panel 1

In addition to this change in skin panel stiffness, panel breaker stiffeners, shown in Figure 75, were also incorporated into the Panel 2 (780) design to help meet the maximum flow-wise deflection requirement. Panel breakers were only added to the windward panels as they have more severe aeroheating impacts due to deformation than the leeward panels. The number of stiffeners, spacing, and sizing were determined by performing a trade study.

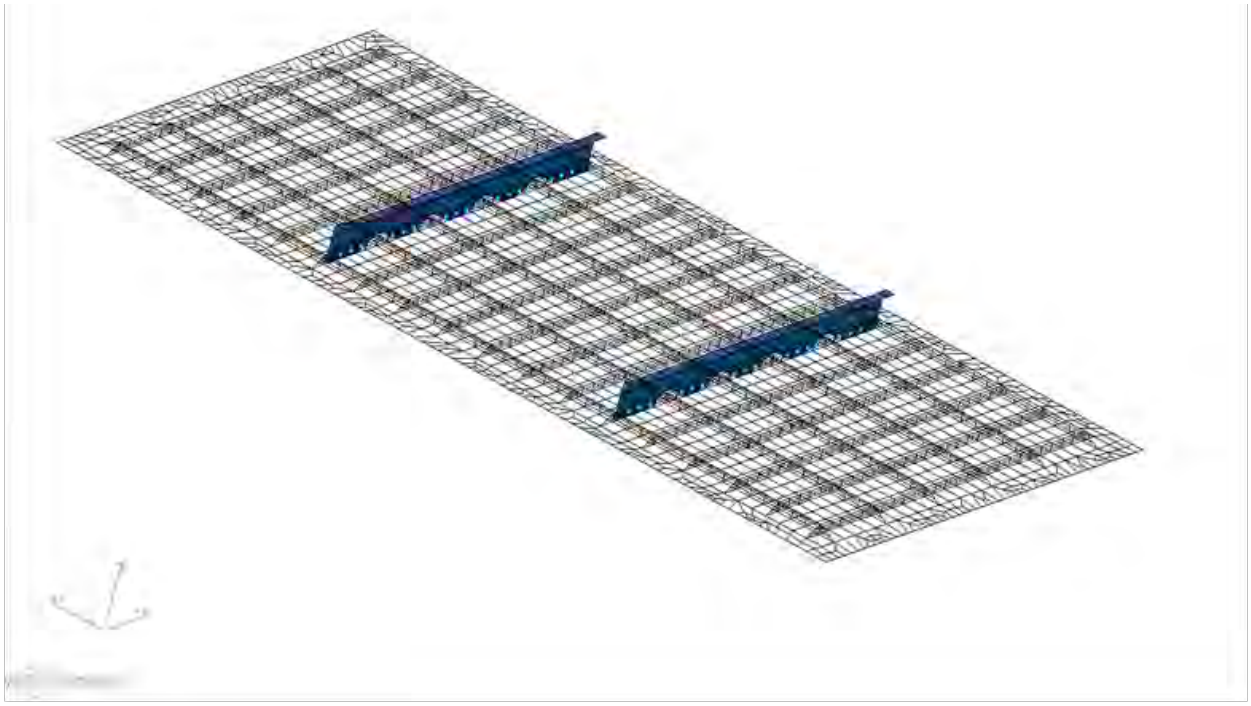

Figure 75. Panel 2 (780) Panel Breakers (Highlighted in Blue) are Added to Reduce Flow-wise Deflection

Approved for public release; distribution unlimited.

The critical load case was determined similarly to the other panels and was selected as Mechanical: 2.5g Ultimate (1.5) + Thermal: T=720s. This temperature profile is at the maximum temperature gradient between the skin and the keel/frame substructure. Results from the panel level analysis are discussed below. These analyses are non-linear.

The maximum relative displacement in the Z direction is calculated as follows:

$$\Delta = \text{Maximum deflection} - \text{Minimum deflection} = (0.0202") - (-0.104") = 0.124"$$

The allowable for deflection is 0.1" as defined the thermal analysis section. Therefore the deflection margin of safety (MS) is calculated as follows:

$$MS = \text{Allowable/Actual} - 1 = 0.1/0.124 - 1 = -0.19$$

The displacement plot of Panel 2 (780) is shown in Figure 76.

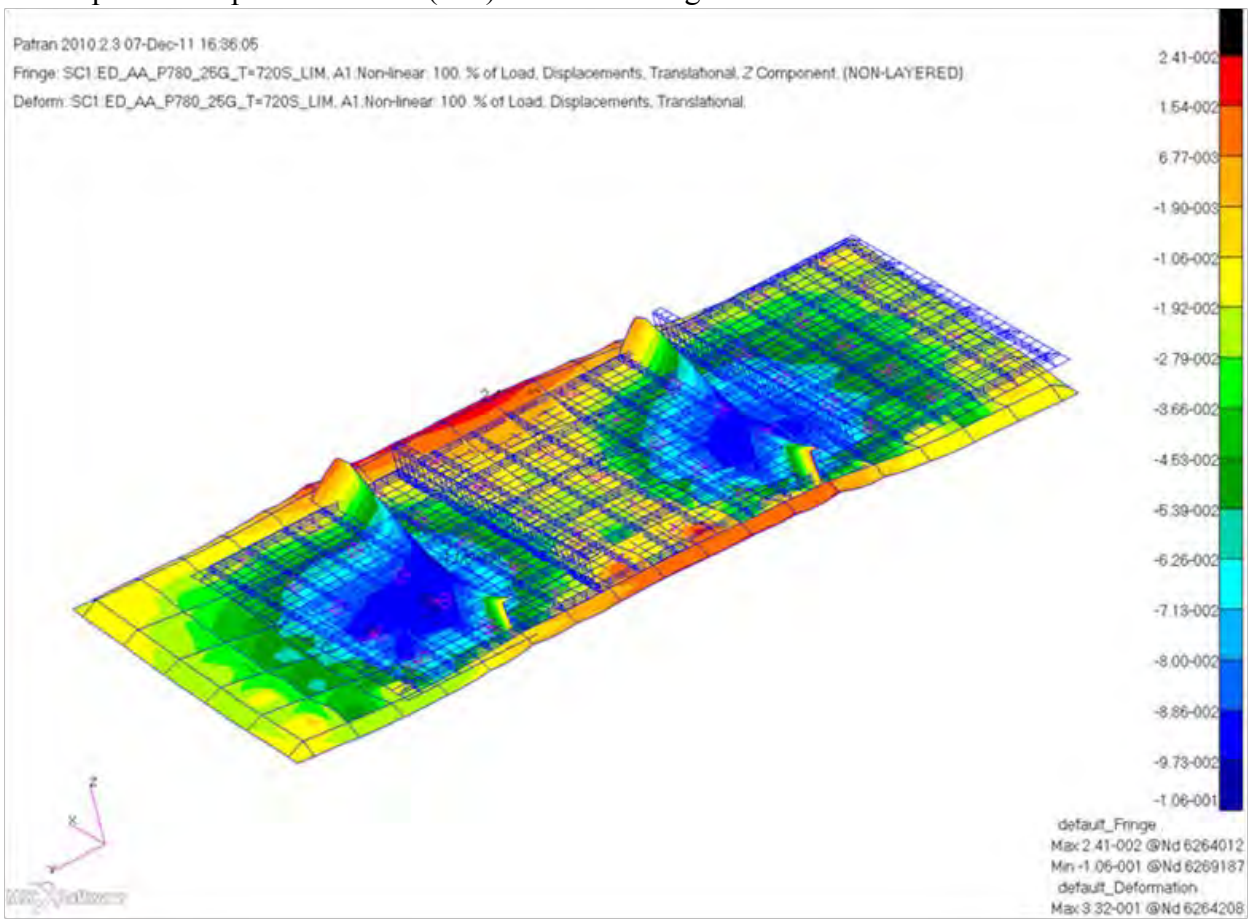

Figure 76. Non-Linear Z-Component Deflection Plot [in] of Panel 2 (780)

Load Case Mechanical - 2.5g Limit (1.15) + Thermal - T=720s

Since the deflection requirement is meant to represent flight conditions that will be experienced by the structure periodically through the flight profile, limit loads are used to write the margins of safety rather than ultimate loads. Additionally, the deflection requirement applies to the

Approved for public release; distribution unlimited.

maximum relative out of plane displacement in the flow-wise direction. The most severe flow-wise section is shown in Figure 77.

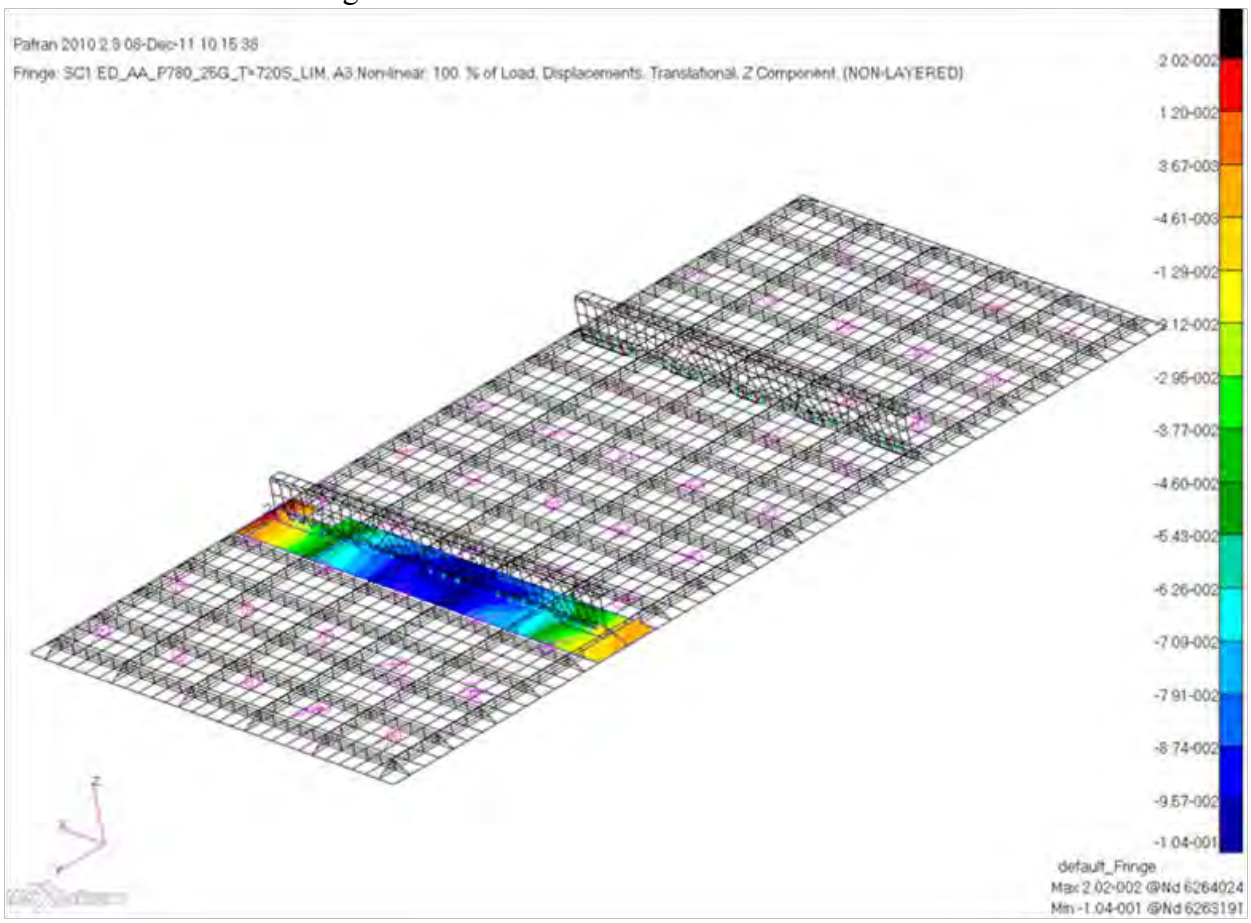

Figure 77. Non-Linear Max Flow-wise Z-Component Deflection Plot [in] of Panel 2 (780) Load Case Mechanical - 2.5g Limit (1.15) + Thermal - T=720s

The maximum Von Mises stress of 52.3 ksi is located near the one of the scalloped edges of the panel breaker stiffeners.

The allowable for Ultimate Material Failure for Inconel at room temperature is Ftu = 185 Ksi. At T = 720s, the maximum temperature of the unit cell is 850°F which dictates a thermal knockdown factor 92% of room temperature allowable. The allowable is calculated as follows:

$$F_{tu@850°F} = F_{tu@70°F} * \text{Thermal Knockdown} = 180 \text{ Ksi} * 0.92 = 165.6 \text{ Ksi}$$

Therefore the Ultimate Material Failure margin of safety (MS) is calculated as follows:

$$MS = \text{Allowable/Actual} - 1 = 165.6/52.3 - 1 = 2.17$$

The Von Mises Stress plot of Panel 2 (780) is shown in Figure 78.

Approved for public release; distribution unlimited.

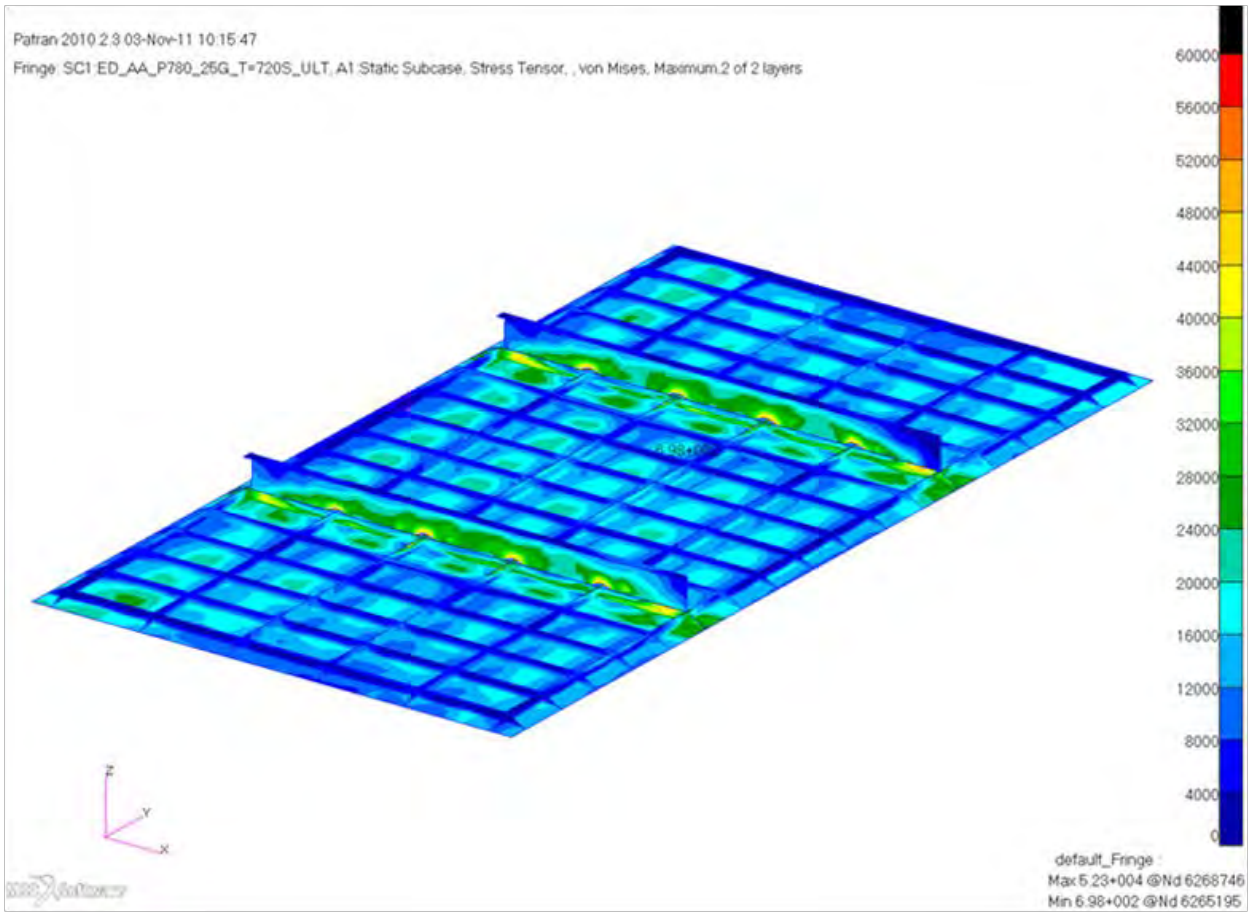

Figure 78. Non-Linear Von Mises Stress Plot [psi] of Panel 2 (780)
Load Case Mechanical - 2.5g Ultimate (1.5) + Thermal - T=720s

Because this panel incorporates panel breaker stiffeners, which are attached with fasteners to the ortho-grid, a fastener bearing analysis must be performed.

The maximum fastener load is P = 1370 lbs. The bearing stress is calculated as follows:

$$\sigma_{brg} = P/(d*t) = 1370 / (0.19*.07) = 103 \text{ ksi}$$

The allowable for Ultimate Bearing for Inconel at room temperature is Fbru = 309 Ksi (e/D = 1.5). At T = 720s, the maximum temperature of the unit cell is 850°F which dictates a thermal knockdown factor 92% of room temperature allowable. The allowable is calculated as follows:

$$F_{bru@850°F} = F_{bru@70°F} * \text{Thermal Knockdown} = 309 \text{ Ksi} * 0.92 = 284.2\text{Ksi}$$

Therefore the Ultimate Material Failure margin of safety (MS) is calculated as follows:

$$MS = \text{Allowable/Actual} - 1 = 284.2/103 - 1 = 1.76$$

The fastener forces plot for Panel 2 (780) is shown in Figure 79.

Approved for public release; distribution unlimited.

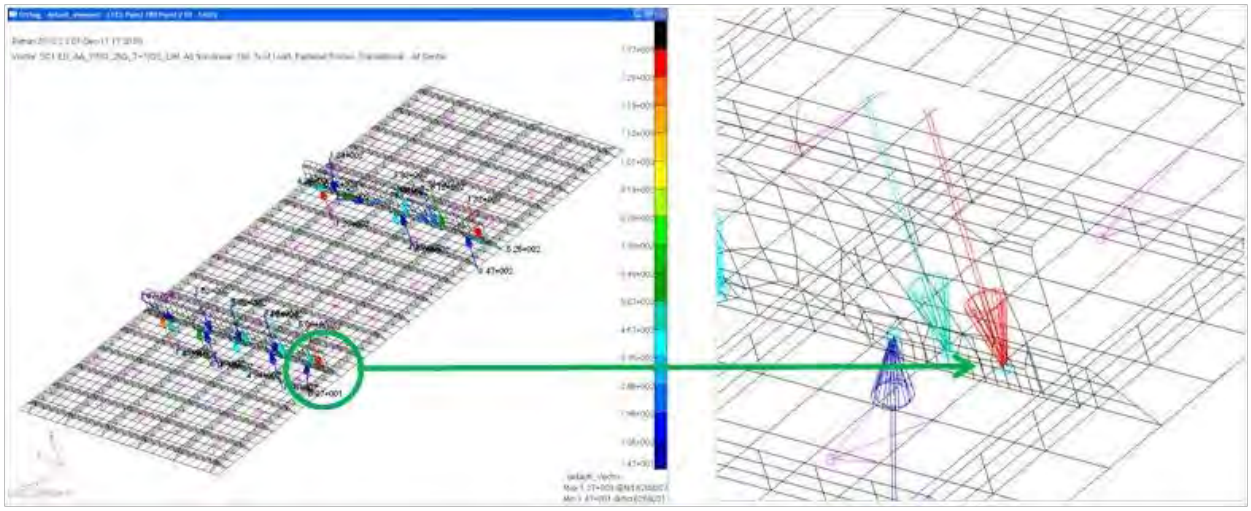

Figure 79. Non-Linear Fastener Forces for Panel 2 (780)

Load Case Mechanical - 2.5g Ultimate (1.5) + Thermal - T=720s

The last static check performed on Panel 2 (780) is a buckling analysis. Limit loads are applied to the panel rather than Ultimate loads. Solution 105 in Nastran provides the eigenvalues. The first buckling mode is at an eigenvalue of 0.998. The minimum eigenvalue allowable is 1.0. The buckling Ratio to Requirement (RR) is calculated as follows:

$$RR = \text{Actual/Allowable} = 0.998 / 1.0 = 0.998$$

The plots for the first two buckling modes of Panel 2 (780) are shown in Figure 80 and Figure 81.

Approved for public release; distribution unlimited.

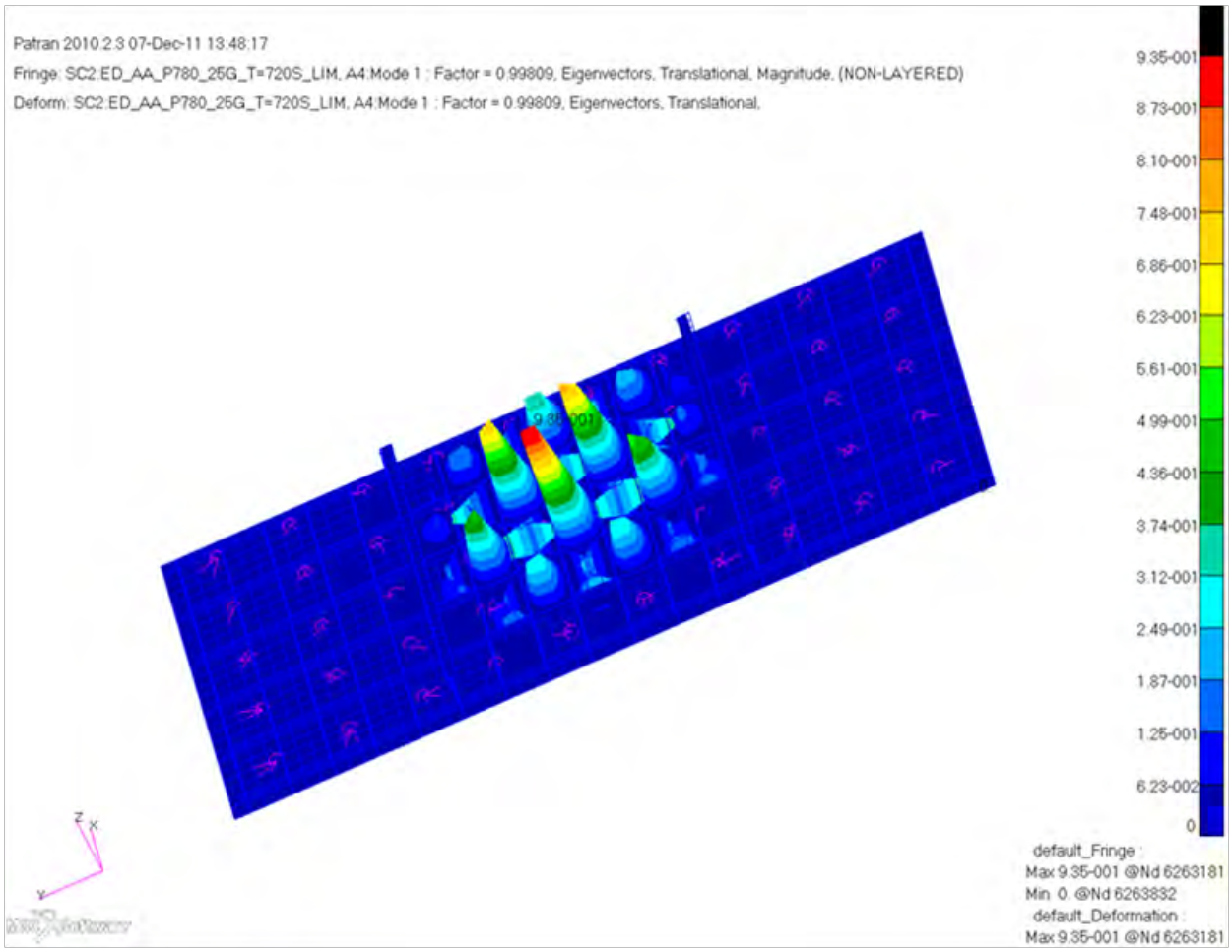

Figure 80. 1st Buckling Mode of Panel 2 (780)

Load Case Mechanical - 2.5g Limit (1.15) + Thermal - T=720s

Approved for public release; distribution unlimited.

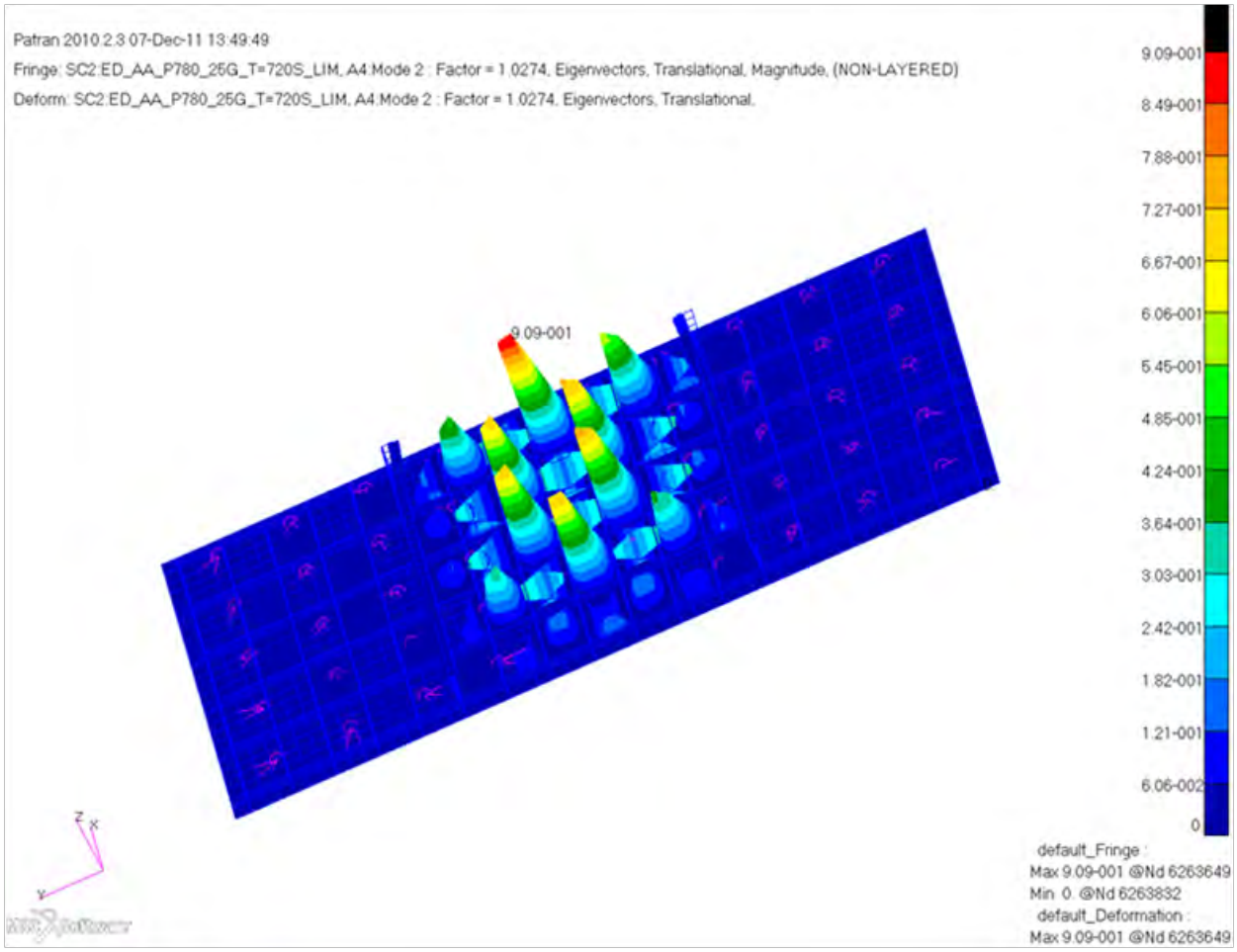

Figure 81. 2nd Buckling Mode of Panel 2 (780)

Load Case Mechanical - 2.5g Limit (1.15) + Thermal - T=720s

The addition of the panel breaker stiffeners reduced the deflection of the panel and increased the buckling eigenvalue. However, the panel still does not meet both of these analysis requirements by a small margin. The buckling analysis can be assumed to be satisfactory for this design maturity. The deflection requirements should be better defined before adjusting designs to meet the criteria. Both the Bearing and Ultimate Material Failure analysis checks have high margins. A summary of the static margins of safety is in Table 14.

Approved for public release; distribution unlimited.

Table 14. Summary of static margins of safety for Panel 2 (780)

Panel	Location	Failure Mode	Load Case	Allowable @ 70° F	Units	Temp	Units	Knock-down	Allowable @ Temp	Units	Actual	Units	MS/RR
2 (780)	Panel Breaker/ Panel Intersection	Deflection	2.5g Ult (1.5) + T=720s	0.1	ksi	850	° F	1	0.1	in	0.124	in	-0.19
2 (780)	Panel Breaker Scallop Edge	Material Failure	2.5g Ult (1.5) + T=720s	180	ksi	850	° F	0.92	165.6	ksi	52.3	ksi	2.17
2 (780)	Panel Breaker/ Panel Intersection	Bearing	2.5g Ult (1.5) + T=720s	309	ksi	850	° F	0.92	284.28	ksi	103	ksi	1.76
2 (780)	Panel Center	Buckling	2.5g Lim (1.15) + T=720s	1		850	° F	1	1		0.998		0.998

4.4.4 Panel 2 (780) Dynamic Analysis

The static analysis for Panel 2 (780) determined the 2.5g mechanical combined with thermal load at t=720s (maximum skin to substructure gradient) to be the critical load case. The dynamic analysis for Panel 2 (780) ignored the mechanical load but used the thermal load at t=720s as a preload for acoustic response analysis. Mechanical loads were left out of the dynamic analysis because they had little impact on stress compared to the thermal load and it was felt that a 2.5g maneuver was a low probability over the maximum Q period of flight. The preload state was from a nonlinear static solution for the entire unit cell. This methodology was used for Panel 2 and all subsequent panels. Large deformations present in the Panel 1 (862) unit cell FEM caused the non-linear solution to fail, which prevented the Panel 1 (862) frequency response analysis with pre-load. (Recommendation #6, Page 3) As was the case for most panels, the dynamic analyses featured a different set of boundary conditions to better simulate the support from surrounding structure and eliminate unwanted vibration modes, see Figure 82.

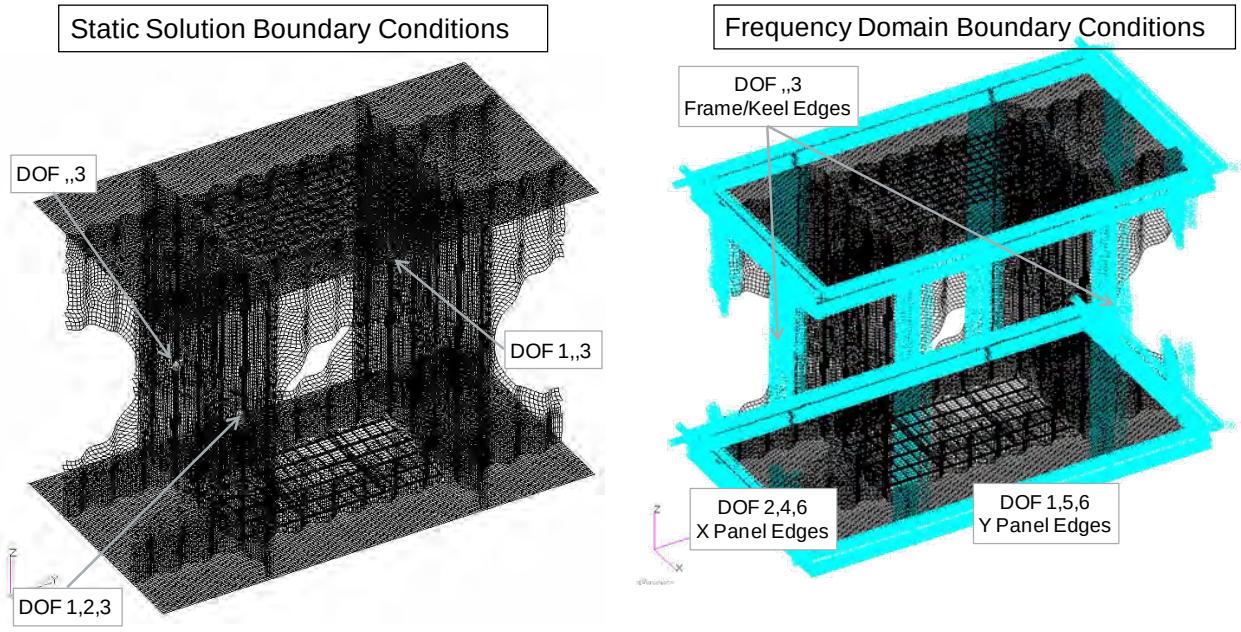

Figure 82. Unit cell view of constraints applied to static analyses compared to dynamic analyses

Approved for public release; distribution unlimited.

Thermal mechanical fatigue checked the Limit 2.5g (LF=1.15) + Thermal load for two different thermal cases: maximum skin to substructure gradient (t=720s) and maximum temperature (t=2520s). The maximum gradient load case was the dominant thermal case. The results used to compute thermal-mechanical fatigue were from linear static solutions. Table 15 shows the analyses used for Panel 2 dynamic and fatigue.

Table 15. Summary of Finite Element Analyses Used for Acoustic and Thermal-Mechanical Fatigue

Analysis Type	Preload	Load	Boundary Conditions	Output	Solution File(s)
Linear Static (SOL 101)	None	Mechanical (2.5G) Thermal (All times)	RBM Constraint at 3 nodes	> Stress for thermal-mechanical loads fatigue analysis	panel_2_2_5g_all_temps.xdb
Normal Modes (SOL 103)	None	Thermal (t=720s) Material Property Only	Symmetry along unit cell boundary	> Normal Modes and Mode Shapes > Provides frequency range of interest for SOL 111	sol103_unitcell_t720s_111222-02-symm.xdb
Non-linear Static (SOL 106)	None	Thermal (t=720s) Material + Load	RBM Constraint at 3 nodes	> Non linear stress and displacement > Preload for SOL111 > Stress results used as mean stress in fatigue calculations	panel2_sol106_1203-01.xdb
Frequency Response (SOL 111)	SOL 106	Thermal (t = 720s) Material Property Only	Symmetry along unit cell boundary	> RMS stress	panel2_sol111_1222-02_symm.xdb

Panel 2 features two large panel stiffeners fastened to the integral ortho-grid stiffeners. The panel stiffeners were configured to limit out of plane deflection of the panel into the airflow caused by the thermal gradients between skin and substructure. While the panel stiffeners were effective in reducing out of plane deflection, they also produce a stress concentration due to the large out of plane stiffness they introduce. Figure 83 shows a fringe plot of maximum principal stress for Panel 2 for a combined load case of 2.5g Limit (LF=1.15). The stress in the panel is focused around the panel stiffeners and the stiffeners themselves are subjected to the maximum stress of 56.1ksi. As will be shown in the fatigue margin evaluation, the concentration of stress around the panel stiffeners resulted in high $K_t\sigma$ values at fastener holes near the panel stiffener termination point.

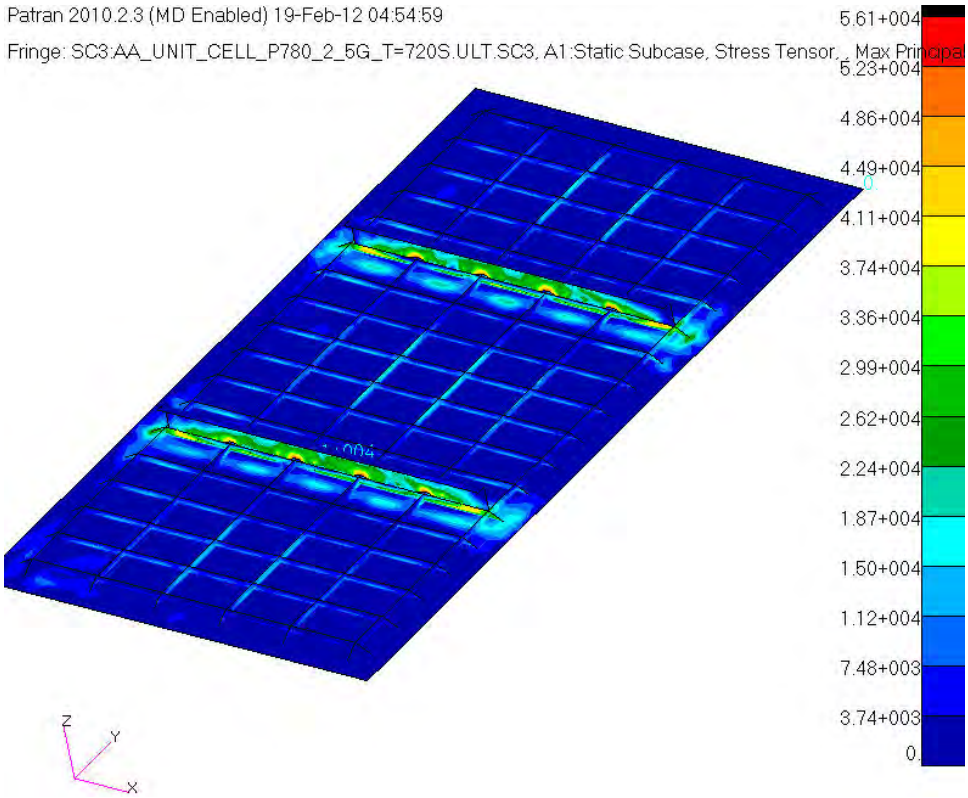

Figure 83. Panel 2 maximum principal stress fringe plot showing stress concentrated around panel stiffeners, 56.1ksi maximum stress

4.4.5 Panel 2 (780) Fatigue Margin Evaluation

The acoustic fatigue analysis included areas of high stress with Kt=1 and filled fastener holes with an assumed Kt=2.3. RMS stress was highest in the ortho-grid stiffener near the panel stiffener termination. Figure 84 shows a plot of the RMS Von Mises stress for Panel 2 as well as the maximum stress locations for the ortho-grid stiffener, the skin, and the panel stiffeners. The FEM mesh density was later increased for Panel 4 (1074) in these same areas to increase the result fidelity.

Approved for public release; distribution unlimited.

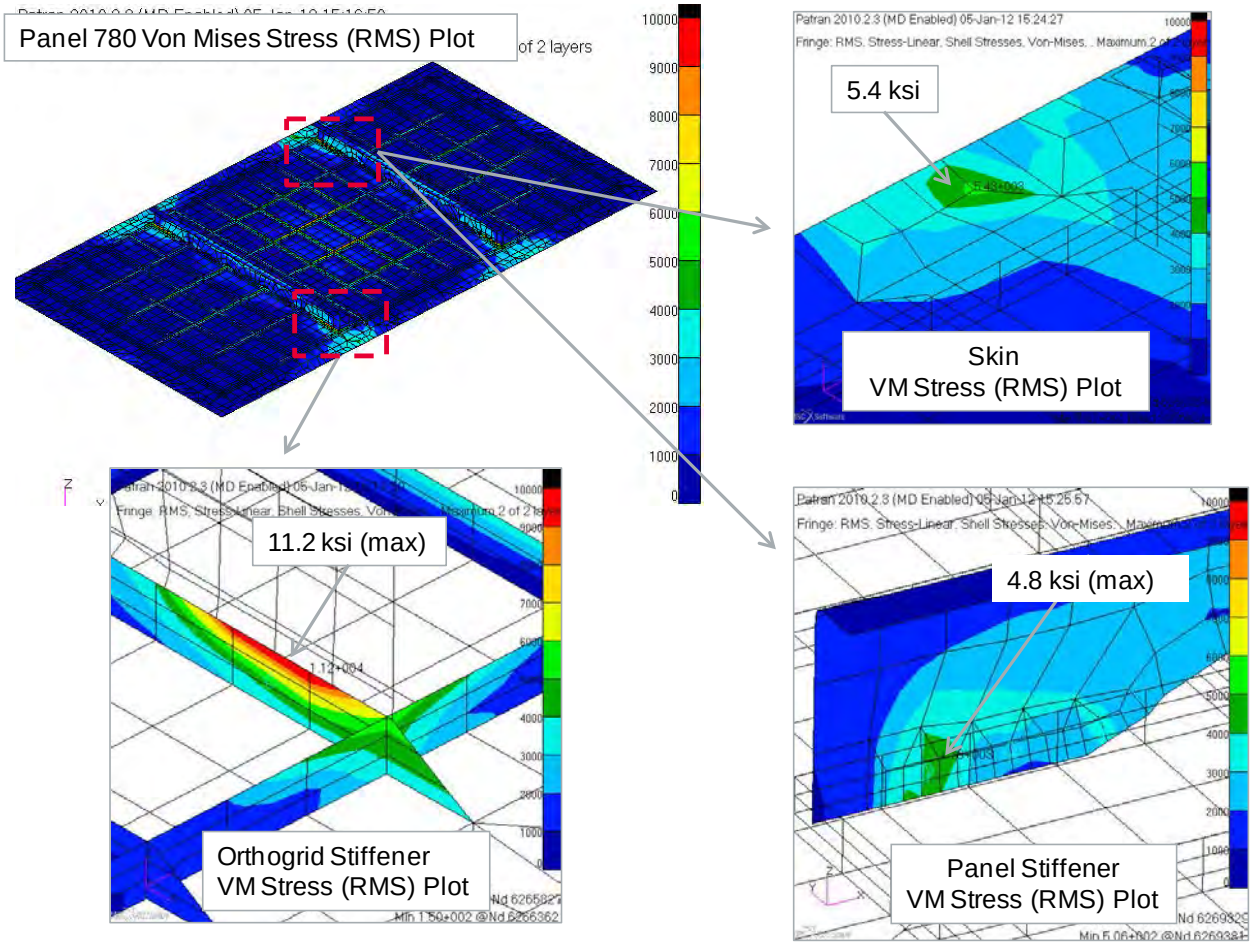

Figure 84. Plots of RMS Von Mises stress for Panel 2 and at maximum stress locations

A margin of safety was calculated for acoustic fatigue at the locations shown as well as for the ortho-grid stiffeners at the center of the panel. The minimum margin of safety (MS = 1.17) occurs at the center panel location due to an RMS stress value of 9.6 ksi and only a 3.5 ksi mean stress from thermal load (see Figure 85). The small amount of mean stress at this point creates a stress ratio of -0.47, resulting in a stress ratio factor of 0.98.

Approved for public release; distribution unlimited.

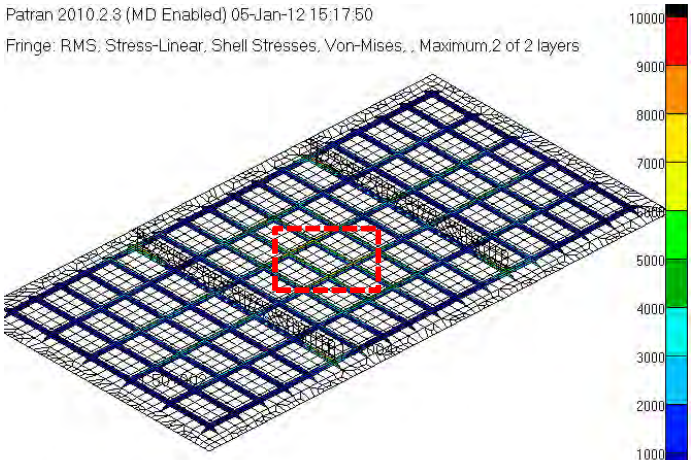

Von Mises Stress Plot (SOL 111)

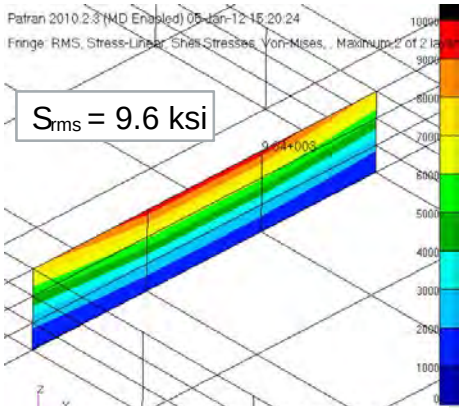

Von Mises Stress Plot (SOL 111)

Kt = 1.0 R =-0.47 T = 750F

$$k_t\sigma'_e = \frac{\sigma_e \cdot C_T \cdot C_R}{k_t} = \frac{19.0 \cdot 0.91 \cdot 0.98}{1.0} = 16.9\text{ksi}$$

$$MS = \frac{k_t\sigma'_e}{\sigma_{rms}} - 1 = \frac{16.9}{9.6} - 1 = \underline{0.76}$$

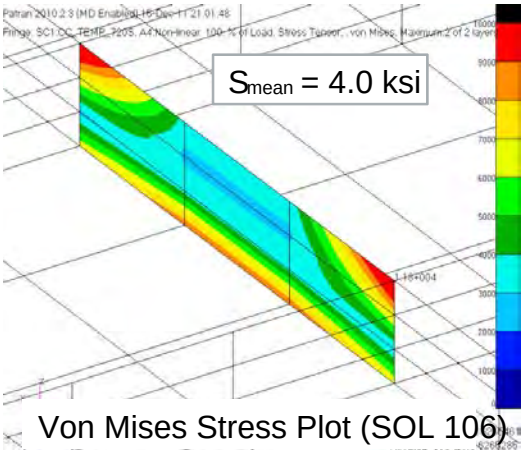

Von Mises Stress Plot (SOL 106)

Figure 85. Margin of safety calculation for maximum RMS stress on ortho-grid stiffener

The Panel 2 MS for acoustic fatigue indicate that damage associated with acoustic fatigue is not a critical concern for this panel. A summary of the acoustic fatigue margin checks is given in Table 16.

Approved for public release; distribution unlimited.

Table 16. Margin of safety summary table for Panel 2 acoustic fatigue

Location of Stress Concentration	Stress Conc. Type	Structural Temp (°F)	Temp Factor	Stress Ratio	Stress Ratio Factor	Kt	Allowable Stress (ksi)	RMS Stress Result (ksi)	Mean Stress Thermal Load (ksi)	Marginof Safety
Orthogrid Stiffener Near Panel Breaker Termination	None	600	0.93	0.15	0.93	1.0	16.4	11.2	15.0	0.48
Orthogrid Stiffener to panel breaker fastener hole	Filled Hole	600	0.93	0.55	0.91	2.3	6.99	5.5	19.0	0.27
Orthogrid Stiffener at panel center	None	750	0.91	-0.47	0.98	1.0	16.9	9.6	3.5	0.76
Skin Near Panel Breaker Termination	Filled Hole	750	0.91	0.44	0.94	2.3	7.06	5.4	14.0	0.30
Panel Breaker to Orthogrid Connection	Filled Hole	750	0.91	0.60	0.91	2.3	6.84	4.8	19.0	0.42

*Baseline Allowable = 19ksi (Kt=1,R=-1, T=RT) Results file: panel2_sol111_122202_symm.xdb

Results from thermal-mechanical fatigue (TMF) indicate the panel is not properly configured to handle the stress imparted from the cyclical flight profile anticipated for a vehicle of this type. As was discussed in Section 4.4.2 the large out of plane stiffness provided by the panel stiffeners induces an area of high stress concentrated at each stiffener. Maximum stress locations in the skin to substructure joints occur at the termination of the panel stiffener, see Figure 86.

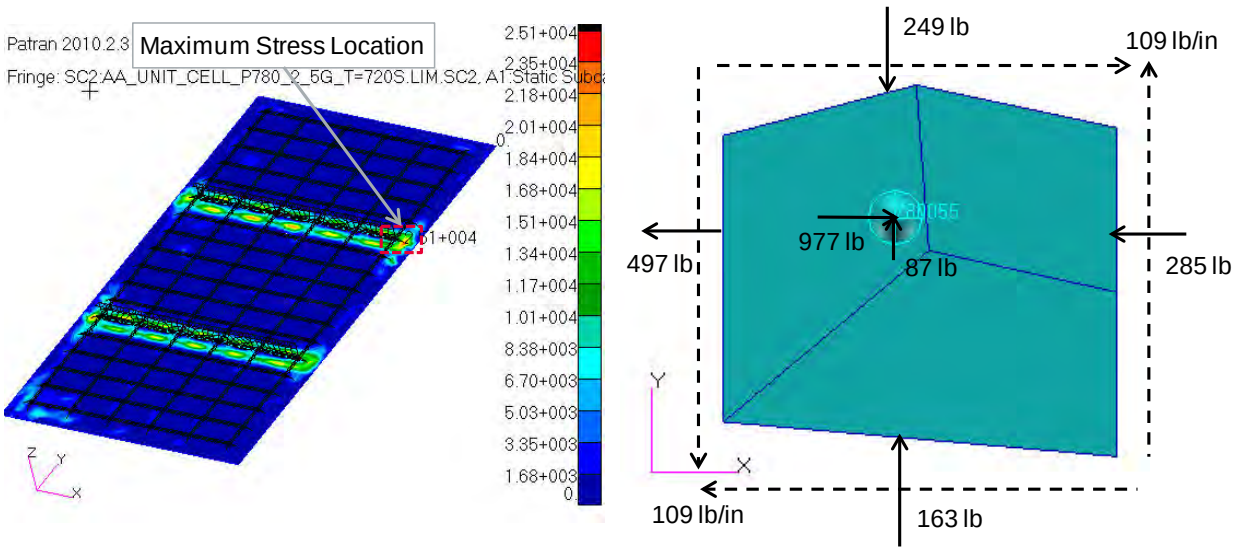

Figure 86. Maximum stress location in Panel 2 skin with local free body diagram

Approved for public release; distribution unlimited.

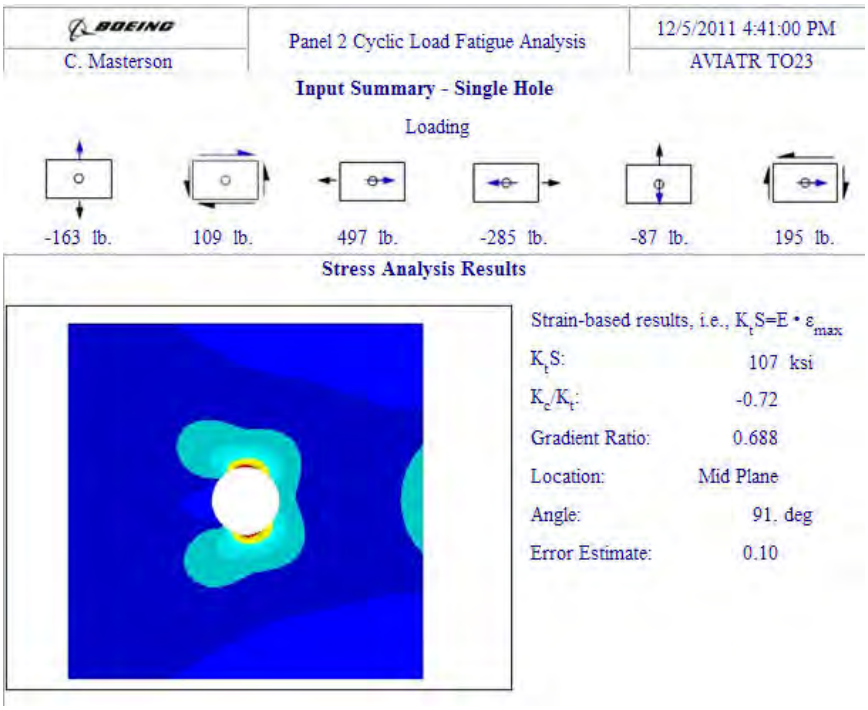

Figure 87. Calculated stress at a worst case fastener hole in skin using detailed StressCheck FEM, Ktσ = 107 ksi (MS = 0.05)

A summary of fatigue margins for the skin to substructure joint is given in Table 17. A minimum MS of 0.05 occurred at fastener 780055 for the limit 2.5g + Thermal (t=720s) case. An adequate MS was found for all checks for the limit 2.5g+Thermal (t=2520s) case.

Table 17. Margin of safety summary for skin to substructure joint of Panel 2

Load Case		2.5g + Therm (t=720s)	2.5g +Therm (2520s)
Element Loads	PxLH	-497	308
	PxRH	-285	443
	PyLwr	163	434
	PyUpr	-249	-346
	Nxy	109	37.67
Fastener Load	Fastener ID	780055	780005
	Px	-977	94
	Py	-87	70
	Pz	0	307
Stress Result	**KTs**	**107**	**27.8**
	MS	**0.05**	**1.22**
Calculated Fatigue Life	**Load Cycle**	**112050**	**Endur. Limit**

Approved for public release; distribution unlimited.

The worst case fatigue was calculated for the panel stiffener to ortho-grid joint, particularly near the termination of the panel stiffeners. Resulting fastener loads indicate a large vertical load near the stiffener termination point that must be sheared out from the panel stiffener and into the ortho-grid stiffener. A large portion of the stress in the ortho-grid stiffener is caused by the high bearing loads. Figure 88 and Figure 89 below shows the analysis for the worst case ortho-grid to stiffener fastener location.

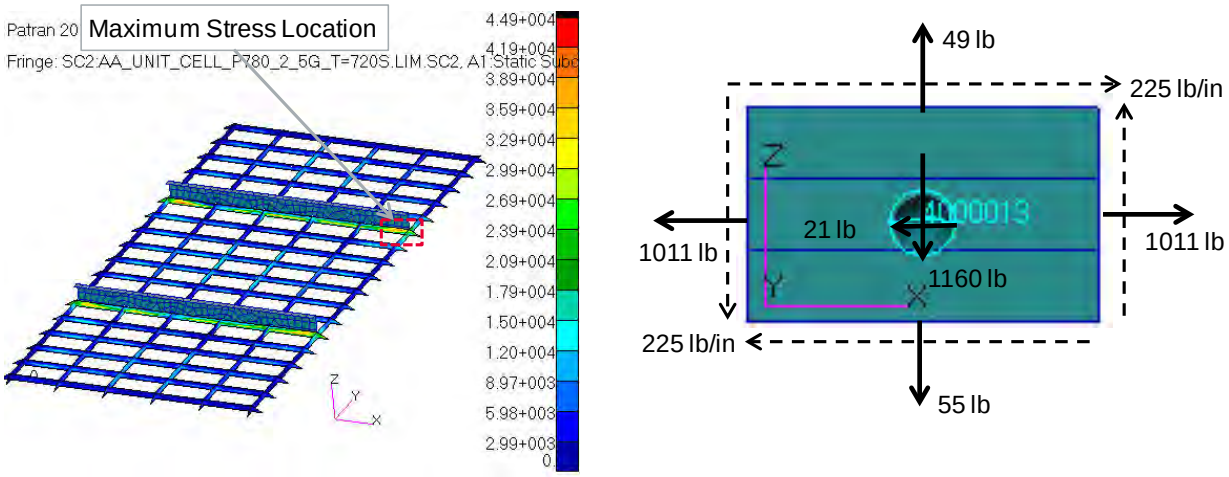

Figure 88. Maximum stress location in Panel 2 ortho-grid with local free body diagram

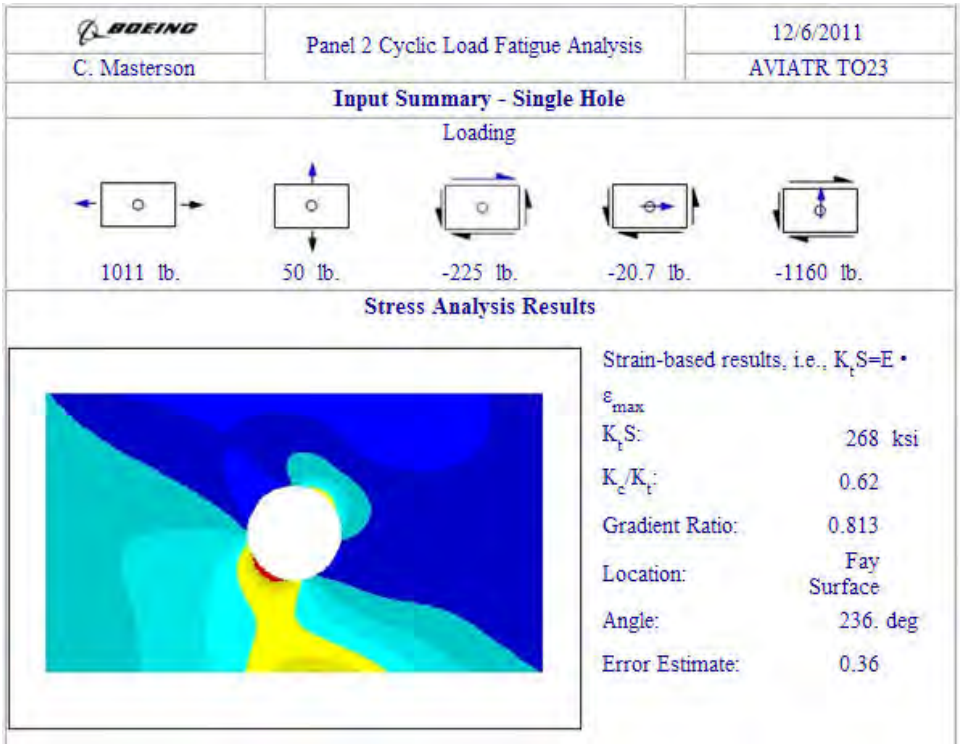

Figure 89. Calculated stress at a worst case fastener hole in skin using detailed StressCheck FEM, Ktσ = 268 ksi (MS = -0.60)

Approved for public release; distribution unlimited.

Table 18 below lists the margin of safety checks at various ortho-grid to panel stiffener locations. The persistent negative margins for both the maximum gradient (t=720s) and the maximum temperature (t=2520s) cases indicate that design improvements are needed for this panel concept to be viable. There are several design ideas that would reduce the fatigue stress without dramatic modifications of the design: the panel stiffeners should be extended to the point at which the ortho-grid stiffeners terminate with increases to local stiffener gages in the termination locale, fastener hole edge distance needs improvement (an increase in ortho-grid stiffener height would result), reduce fastener spacing, design joint to allow for thermal expansion in plane. A good portion of the stress is caused by the thermal gradient between the ortho-grid stiffener and the large panel stiffeners. Increasing thickness in the panel stiffeners could exacerbate the thermal gradient issue.

Table 18. Margin of safety summary for ortho-grid to panel stiffener joint of Panel 2

Load Case		2.5g + Therm (t=720s)	2.5g +Therm (2520s)
Element Loads	PxLH	-1011	-730
	PxRH	1011	730
	PzLwr	-55	-69
	PzUpr	49	35
	Nzx	-225.33	20.33
Fastener Load	Fastener ID	4000013	4000002
	Px	20.7	1
	Pz	1160	-382
	Py	364	-427
Stress Result	**KTs**	**286**	**96.2**
	MS	**(0.60)**	**(0.36)**
Calculated Fatigue Life	**Load Cycle**	**0**	**1416849**

4.5 Panel 3 (816) Detailed Design

Panel 3 (816), shown in Figure 90, is located on the leeward surface of the TX-V. It lies above a fuel tank in the forward section of the vehicle just left of the vehicle centerline.

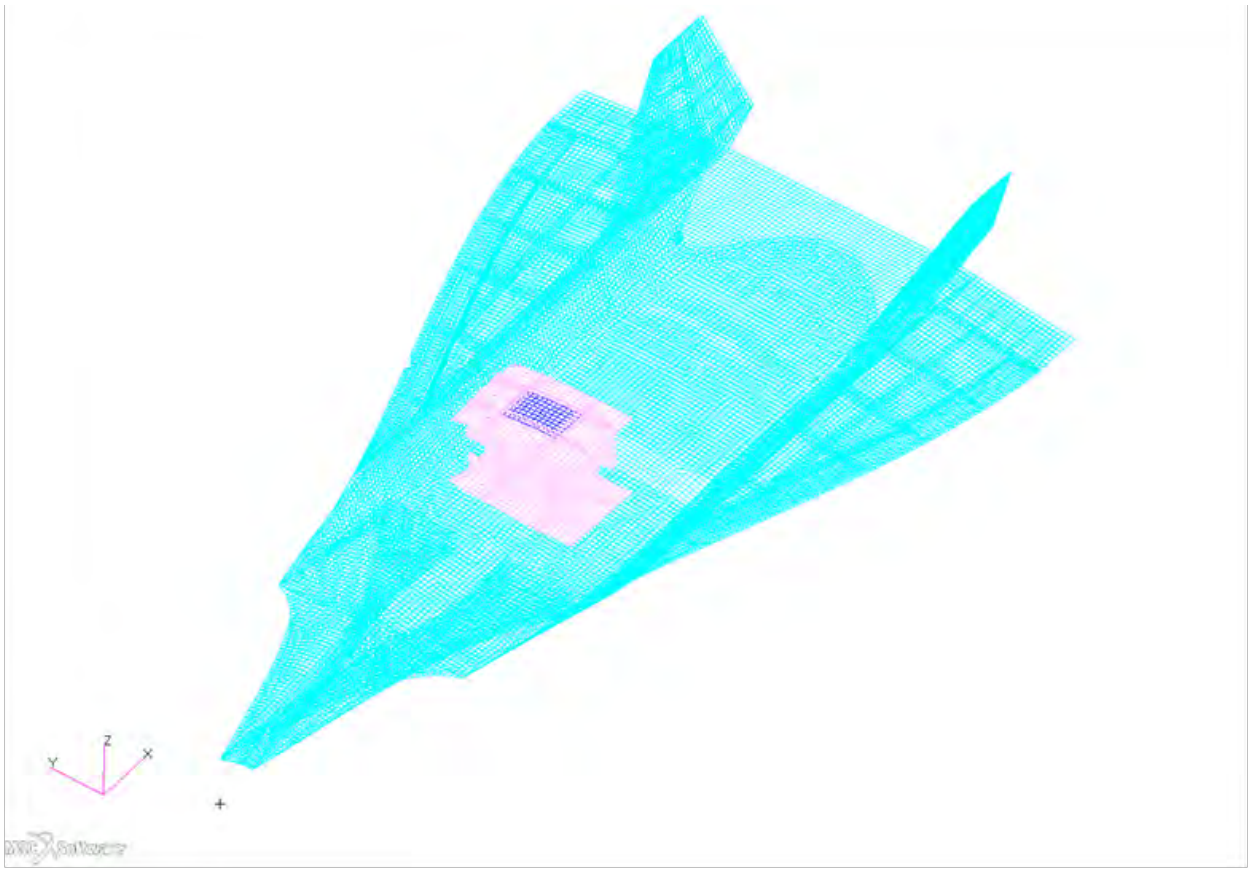

Figure 90 Location of Panel 3 (816) and the Corresponding unit cell

4.5.1 Panel 3 (816) Sizing and Design

Panel 3 internal thermal loads were estimated as being similar to Panel 1, since both were on the upper surface, and were thus taken from the Panel 1 unit cell results. Though Panel 3 is both upstream and over the intake duct for the engine rather than the engine itself, this estimation was considered sufficient for initial design. These are shown along with mechanical loads taken from the global FEM in Table 19. Similarly to Panel 2, HyperSizer sizing resulted in a panel with 3 x 5 inch ortho-grid spacing, a 0.61 inch total height and minimum gage skin and stiffener thicknesses.

Approved for public release; distribution unlimited.

Table 19. Panel 3 sizing loads for a 2.5G turn with Panel 1 thermal loads

	Nx	Ny	Nxy	Mx	My	Mxy	Qx	Qy
	lbs/in			in-lbs/in			lbs/in	
Strength and Buckling from Global FEM	-269	9.2	-41.2	150.1	-20.3	-0.5	9.7	1.6
Thermal from Panel 1 unit cell	-357	-277	-4.6	-20.4	-6.2	0.0	-2.0	-0.5

Additional inputs: 715°F temperature, 204°F/in temperature gradient, 1.0 psi normal pressure

Unlike the first two panels, Panel 3 was selected for a region of the vehicle with a contoured surface and it was not felt the flat surface approximation used for the first unit cell would have been accurate. Nodal coordinates for the upper and lower surfaces were thus extracted and a point cloud interpolation was used to generate lofted CAD surface geometry. Ortho-grid stiffening geometry and substructure features were added to these lofted surfaces to create the unit cell geometry shown in Figure 91. These surfaces were then imported back into the global FEM and compared the elements in this region to verify the surfaces aligned as shown in Figure 92 and Figure 93.

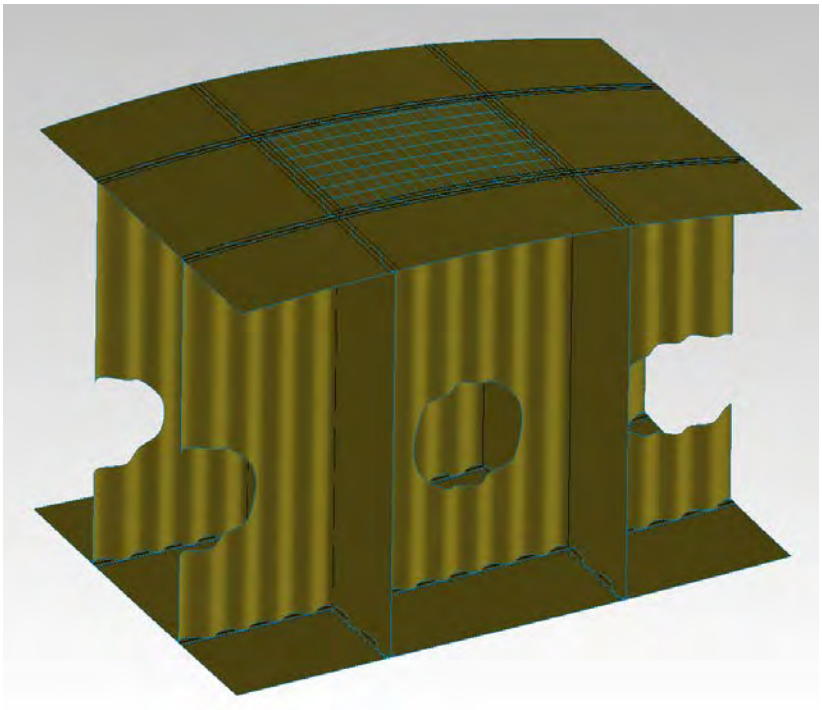

Figure 91. Panel 3 (816) unit cell surface geometry with ortho-grid stiffeners and sine-wave substructure

Approved for public release; distribution unlimited.

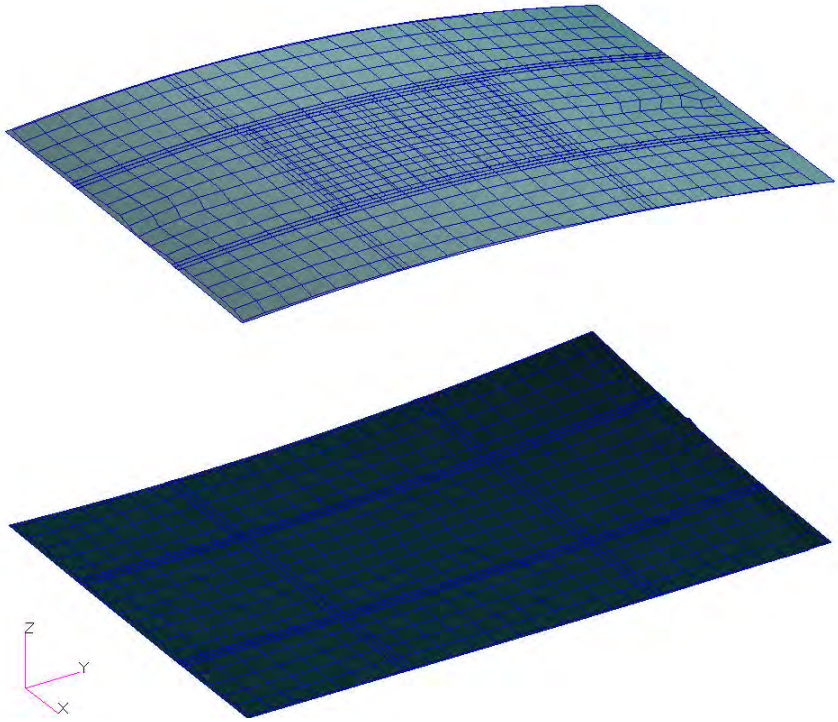

Figure 92. Comparison of Panel 3 unit cell skin surfaces and Global FEM elements

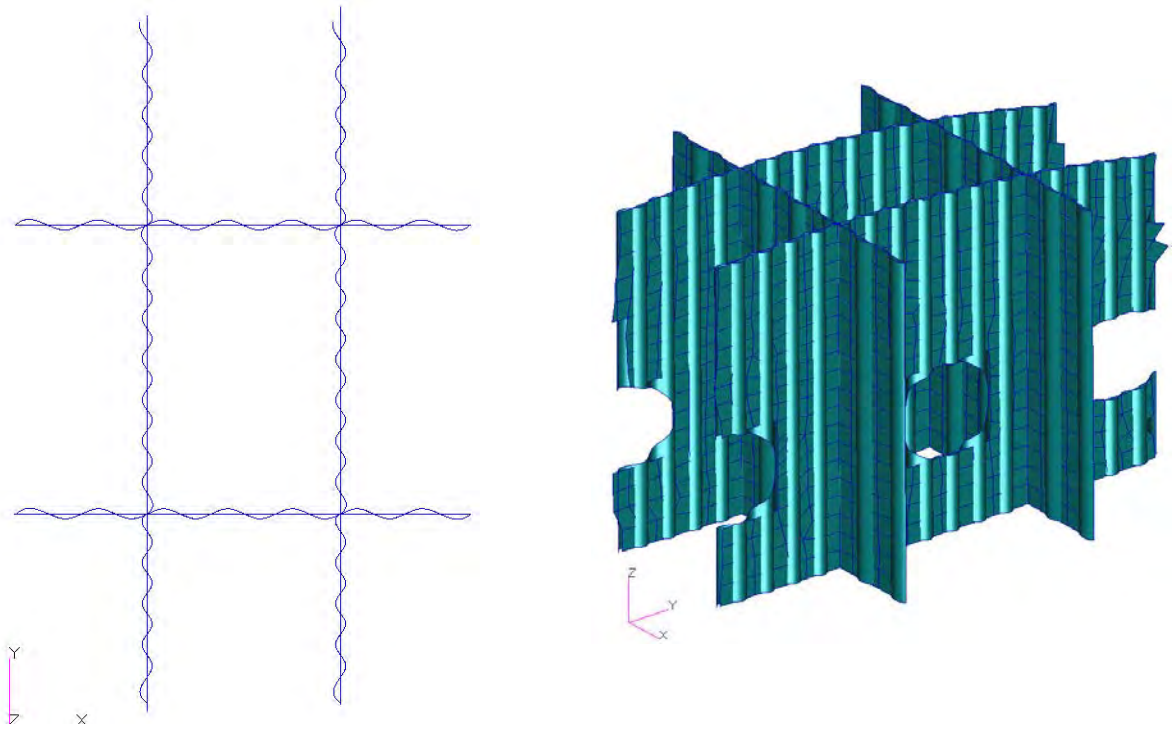

Figure 93. Comparison of Panel 3 unit cell substructure and Global FEM elements

4.5.2 Panel 3 (816) Thermal Analysis

Panel 3 (816) is located above the center fuel tank. This results in a much different temperature distribution than on Panels 1 and 2. The fuel is modeled by a lumped heat capacity which decreases over the course of the flight as fuel is consumed. The fuel levels in the center tank are taken from previous hypersonic vehicle studies. In these studies, maximum fuel temperatures were required to remain below 120 F. A layer of insulation sufficient to achieve this requirement was included in this analysis. Internal radiation between the insulation surface and surrounding structure results in heat flux into the fuel. Convection on the engine inlet duct, which runs through this bay, provides another source of heating to the fuel. These boundary conditions are shown in Figure 94.

Figure 95 shows temperature distributions at critical load conditions during the flight. The first image shows the maximum temperature gradients between the panel skin and ortho-grid occurring during acceleration. The next image illustrates the maximum temperature gradients between skin and substructure. The third image shows the maximum flight temperatures, and the fourth, the greatest negative temperature gradients which occur when the lower flight velocities and enthalpies cause external cooling. These temperature distributions are very different from those predicted for Panels 1 and 2. The requirement of maintaining the fuel temperature below 120 F and the absence of radiative heat transfer between panel and substructure due to the fuel tank causes substructure temperatures to remain relatively cool as well.

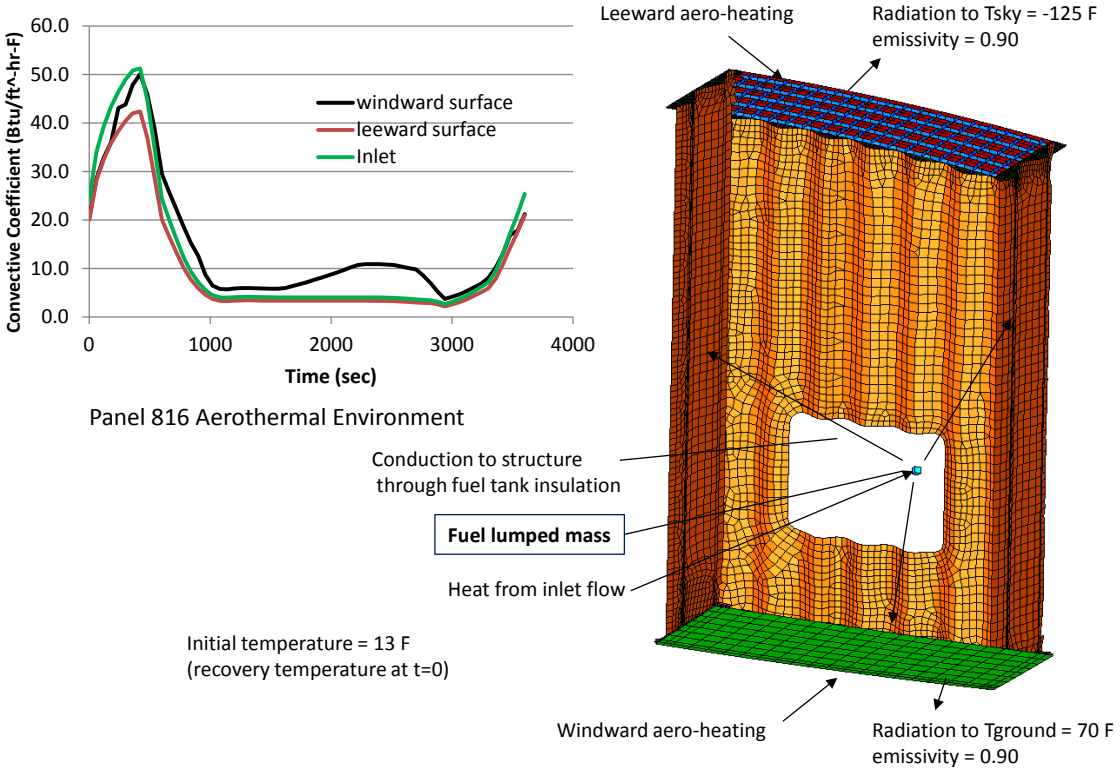

Figure 94. Panel 3 (816) Boundary Conditions

Approved for public release; distribution unlimited.

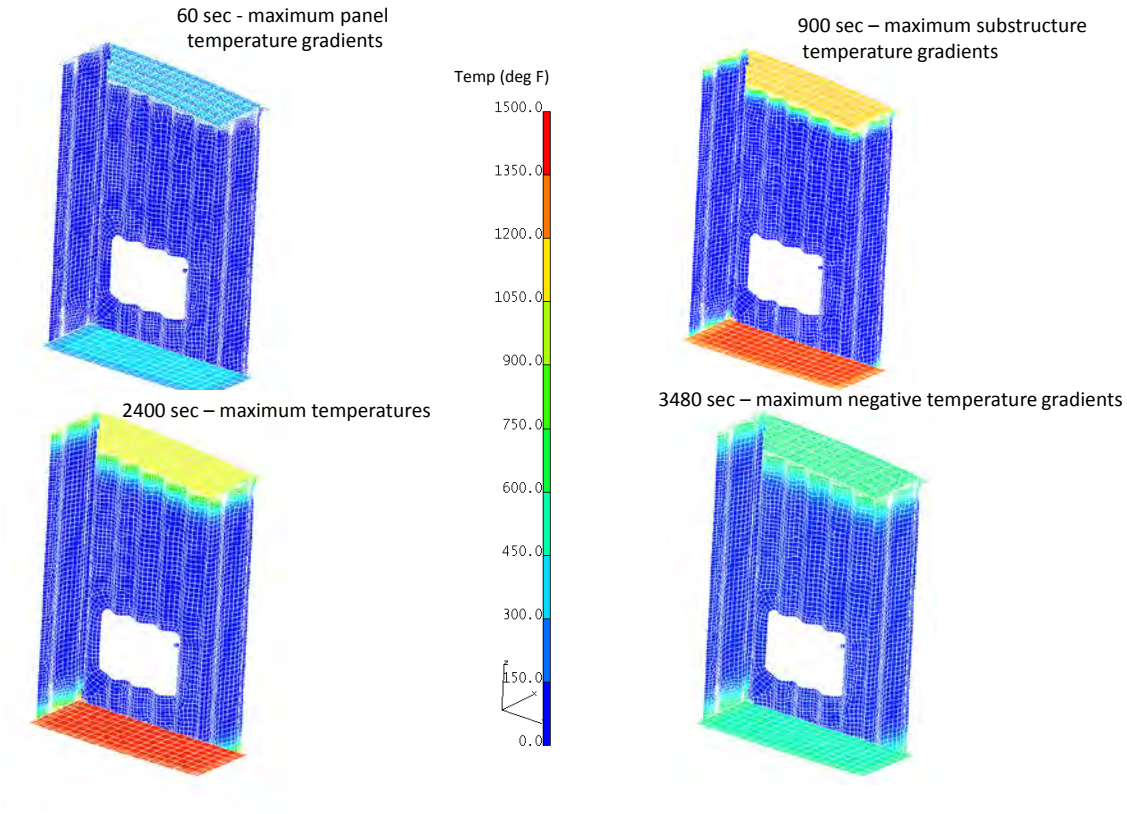

Figure 95. Panel 3 (816) Temperature Distributions

Transient temperature profiles at locations on all the major structural components are plotted in Figure 96. In addition to the temperature histories at skin, ortho-grid, and substructure locations, the results of a brief trade study regarding fuel tank capacity are shown. The baseline analysis was conducted assuming 50% of the internal volume was occupied by fuel. Since detailed design of the fuel tank and other internal features was beyond the scope of this study, another case assuming fuel occupied 80% of the volume was considered. Comparison of the solid and dashed curves shows that the fuel volume assumption has a limited effect on the analysis results. When a greater mass of fuel is present, the insulation required to maintain the temperature requirement decreases. Thus, the change in one variable is partially compensated for by the other. Figure 97 shows maximum temperature difference between structural components. These results are used to identify the time states corresponding to maximum temperatures and temperature gradient conditions. The five conditions: maximum gradient in the panel, maximum gradient between skin and substructure, maximum gradient between skin and panel breaker maximum temperatures and maximum reverse gradient are specified. As discussed above, the presence of the fuel results in much larger temperature gradients and therefore thermal stress between the panel and substructure. The consideration of skin panels located over engine and fuel tank bays provides a wide range of conditions to exercise the analysis methods.

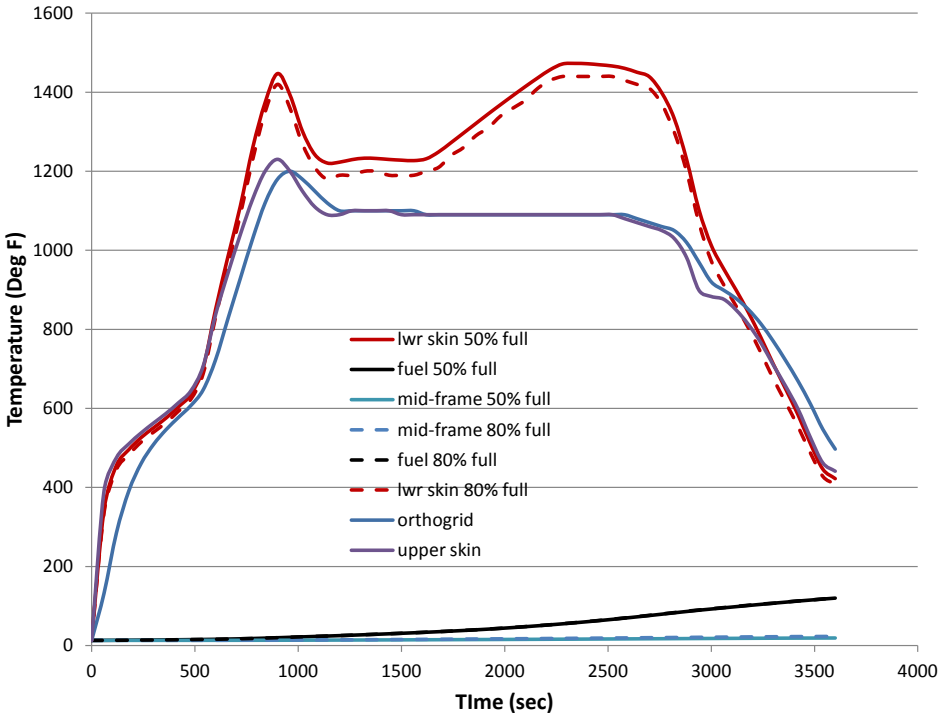

Figure 96. Panel 3 (816) Temperature Histories

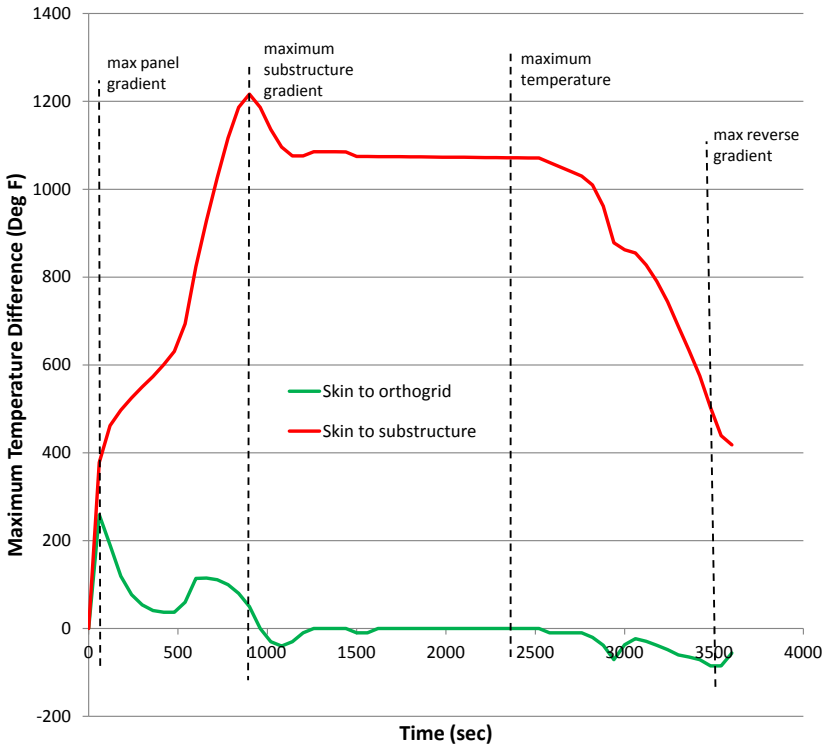

Figure 97. Panel 3 (816) Temperature Gradients

Approved for public release; distribution unlimited.

4.5.3 Panel 3 (816) Stress Analysis

Panel 3 (816) is similar to Panel 1 (862) in that it is does not use panel breaker stiffeners. This was done because it lies on the leeward side of the vehicle where the impact to aero-thermal due to deflection is not as critical as on the windward side. However, the unit cell geometry was created directly from the CAD model, which was created directly from the global vehicle model. This ensured consistency across the global vehicle FEM, CAD, Thermal FEM, and unit cell FEM.

Additionally, the thermal gradient for this unit cell is much higher than anticipated. This severe thermal gradient is caused by the fuel tank and its max temperature requirement of 120° F. The gradient causes high thermal loading on the panel of interest resulting in large deflections and low buckling eigenvalues, similar to what was seen in Panel 2 (780).

The critical load case was determined similarly to the other panels and was selected as Mechanical: 2.5g Ultimate (1.5) + Thermal: T=900s. This temperature profile is at the maximum temperature gradient between the skin and the keel/frame substructure. The temperature difference at this time step is 1200°F. Results from the panel level analysis are discussed below. These analyses are non-linear.

The maximum relative displacement in the Z direction is calculated as follows:

$$\Delta = \text{Maximum deflection} - \text{Minimum deflection} = (0.0") - (-0.45") = 0.45"$$

The allowable for deflection is 0.1" as defined the thermal analysis section. Therefore the deflection margin of safety (MS) is calculated as follows:

$$MS = \text{Allowable/Actual} - 1 = 0.1/0.45 - 1 = -0.78$$

The displacement plot of Panel 3 (816) is shown in Figure 76.

Approved for public release; distribution unlimited.

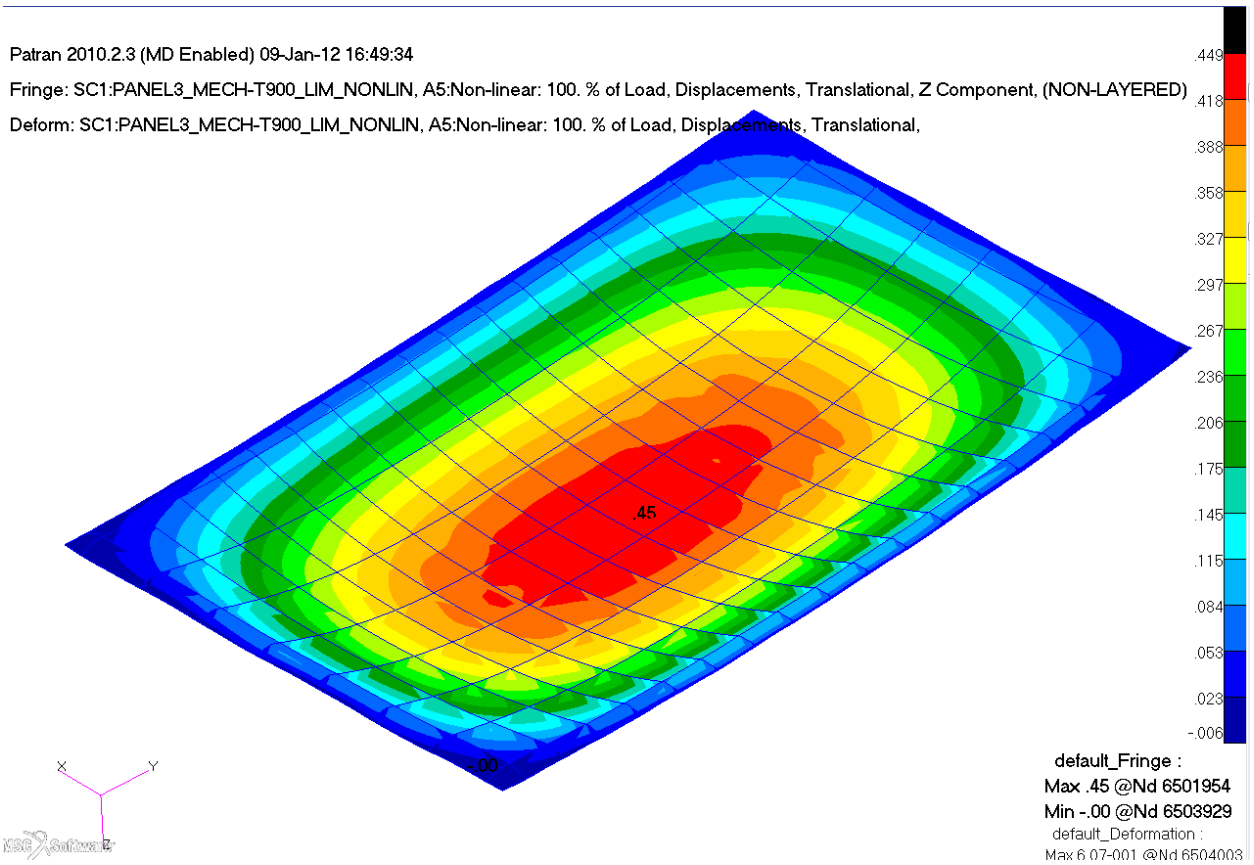

Figure 98. Non-Linear Z-Component Deflection Plot [in] of Panel 3 (816)
Load Case Mechanical - 2.5g Limit (1.15) + Thermal - T=900s

Since the deflection requirement is meant to represent flight conditions that will be experienced by the structure periodically through the flight profile, limit loads are used to write the margins of safety rather than ultimate loads.

The maximum Von Mises stress of 46.3 ksi is located near the boundaries of the panel of interest.

The allowable for Ultimate Material Failure for Inconel at room temperature is Ftu = 185 Ksi. At T = 900s, the maximum temperature of the unit cell is 1220°F which dictates a thermal knockdown factor 80% of room temperature allowable. The allowable is calculated as follows:

$$F_{tu@900°F} = F_{tu@70°F} * \text{Thermal Knockdown} = 180 \text{ Ksi} * 0.80 = 144.0 \text{ Ksi}$$

Therefore the Ultimate Material Failure margin of safety (MS) is calculated as follows:

$$MS = \text{Allowable/Actual} - 1 = 144.0/46.3 - 1 = 2.11$$

The Von Mises Stress plot of Panel 3 (816) is shown in Figure 99.

Approved for public release; distribution unlimited.

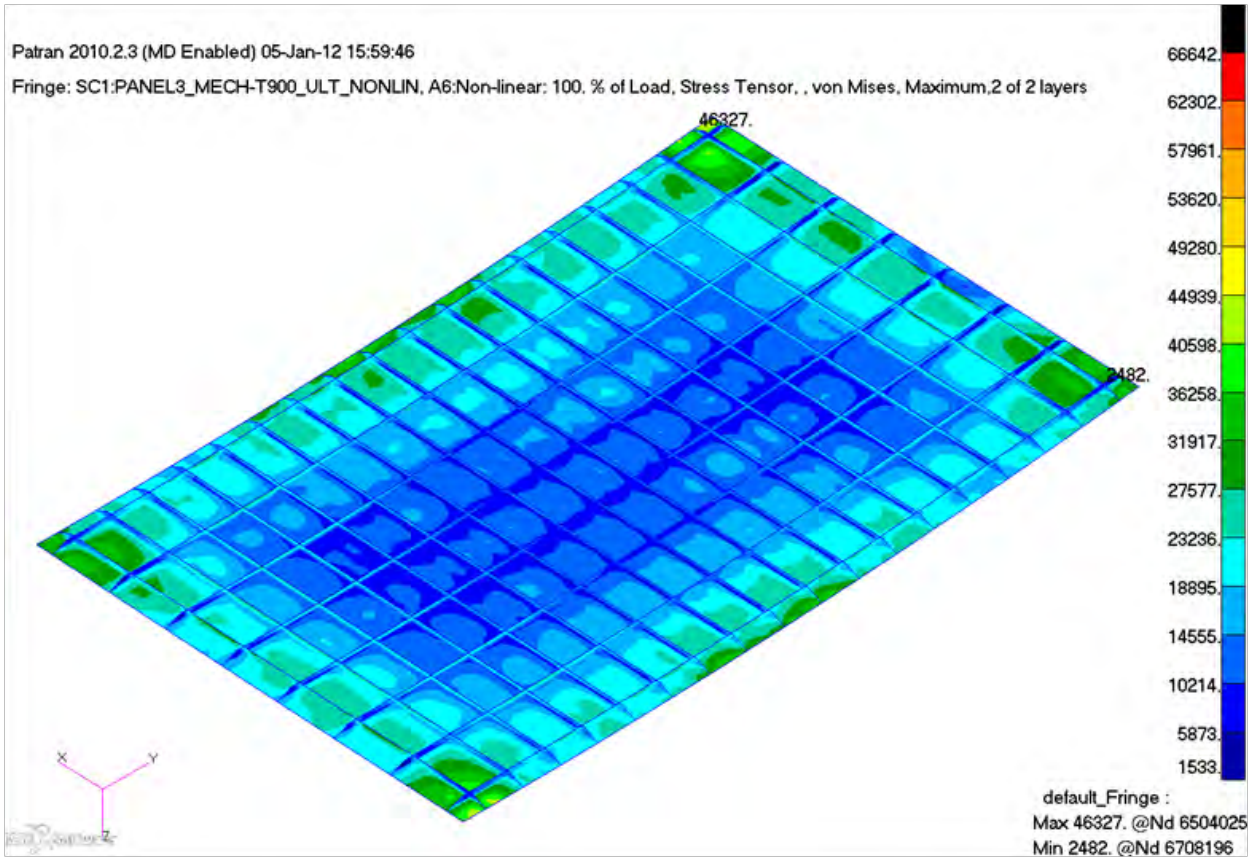

Figure 99. Non-Linear Von Mises Stress Plot [psi] of Panel 3 (816)

Load Case Mechanical - 2.5g Ultimate (1.5) + Thermal - T=900s

The last static check performed on Panel 3 (816) is a buckling analysis. Limit loads are applied to the panel rather than Ultimate loads. The first buckling mode is at an eigenvalue of 0.826. The minimum eigenvalue allowable is 1.0. The buckling Ratio to Requirement (RR) is calculated as follows:

$$RR = Actual/Allowable = 0.826 / 1.0 = 0.826$$

The plots for the first buckling mode of Panel 3 (816) is shown in Figure 100.

Approved for public release; distribution unlimited.

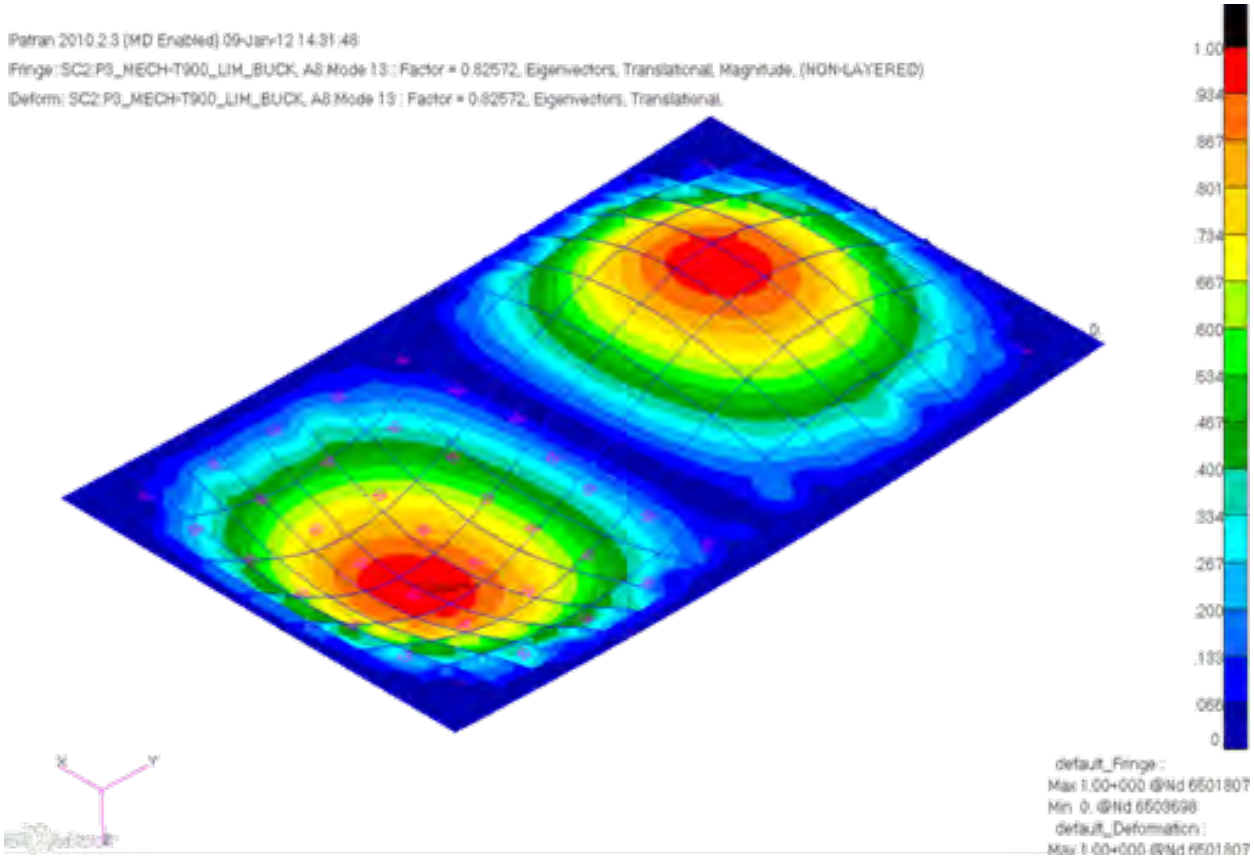

Figure 100. 1st Buckling Mode of Panel 3 (816)

Load Case Mechanical - 2.5g Limit (1.15) + Thermal - T=900s

The assumption that this panel would not need panel breaker stiffeners was incorrect. Panel breaker stiffeners would aid in reducing the deflection of the panel and increasing the buckling eigenvalue. In its current design, Panel 3 (816) has significant negative margins of safety for deflection along with inadequate bucking stiffness. Both the Bearing and Ultimate Material Failure analysis checks have high margins. A summary of the static margins of safety is in Table 20.

Table 20 Summary of static margins of safety for Panel 3 (816)

Panel	Location	Failure Mode	Load Case	Allowable @ 70° F	Units	Temp	Units	Knock-down	Allowable @ Temp	Units	Actual	Units	MS/RR
3 (816)	Panel Center	Deflection	2.5g Ult (1.5) + T=900s	0.1	ksi	1220	° F	1	0.1	in	0.45	in	-0.78
3 (816)	Panel Boundary	Material Failure	2.5g Ult (1.5) + T=900s	180	ksi	1220	° F	0.8	144	ksi	46.3	ksi	2.11
3 (816)	Panel Center	Buckling	2.5g Lim (1.15) + T=900s	1		1220	° F	1	1		0.826		0.83

Approved for public release; distribution unlimited.

4.5.4 Panel 3 (816) Dynamic Analysis

Panel 3 (816) is an upper skin panel over fuel tank and is the forward most of the four Task II panels. It was determined to be a good candidate for a region in which the combination of high aerodynamic loads, thermally induced stress, and material property change cause aeroelastic stability to be of primary concern. Analysis shows that the structure is not driven by aero-acoustic fatigue (AACF) or aeroelastic stability (flutter). Instead, the panel is dominated by high stress due to thermal loads. The thermal stress is enough to make the panel buckling critical and induce mean stress levels that wash out any RMS stress due to acoustic loads. Static analysis determined the combined mechanical plus thermal load case (t=900s) to be the worst case load condition. This case is within the envelope of maximum Q and was used for AACF as well as thermal mechanical fatigue (TMF).

Analysis for Panel 3 followed the prescribed steps detailed in Section 4.2.6. The table below documents the fatigue and dynamic analyses performed on Panel 3.

Table 21. Finite Element Analyses Used for Acoustic and Thermal-Mechanical Fatigue

Analysis Type	Preload	Load	Boundary Conditions	Output
Linear Static (SOL 101)	None	Mechanical (2.5G) Thermal (t = 900s)	RBM Constraint at 3 nodes	> Stress for thermal-mechanical loads fatigue analysis
Normal Modes (SOL 103)	None	Thermal (t=900s) Material Property Only	Symmetry along unit cell boundary	> Normal Modes and Mode Shapes > Provides frequency range of interest for SOL 111
Non-linear Static (SOL 106)	None	Thermal (t=900s) Material + Load	RBM Constraint at 3 nodes	> Non linear stress and displacement > Preload for SOL111 > Stress results used as mean stress in fatigue calculations
Frequency Response (SOL 111)	SOL 106	Thermal (t = 900s) Material Property Only	Symmetry along unit cell boundary	> RMS stress
Flutter (SOL 145)	None	Thermal (t = 900s) Material Property Only	Symmetry at fwd and aft edges, Z pin at frame locations	> Damping and modal frequency vs. velocity

Approved for public release; distribution unlimited.

Panel 3 constraints were similar to those for Panel 2 with separate boundary conditions for static load analyses and dynamic load analyses. Figure 101 shows the unit cell model boundary conditions for the frequency response solutions. The upper surface is separated into three pressure zones for the uncorrelated plane wave acoustic load.

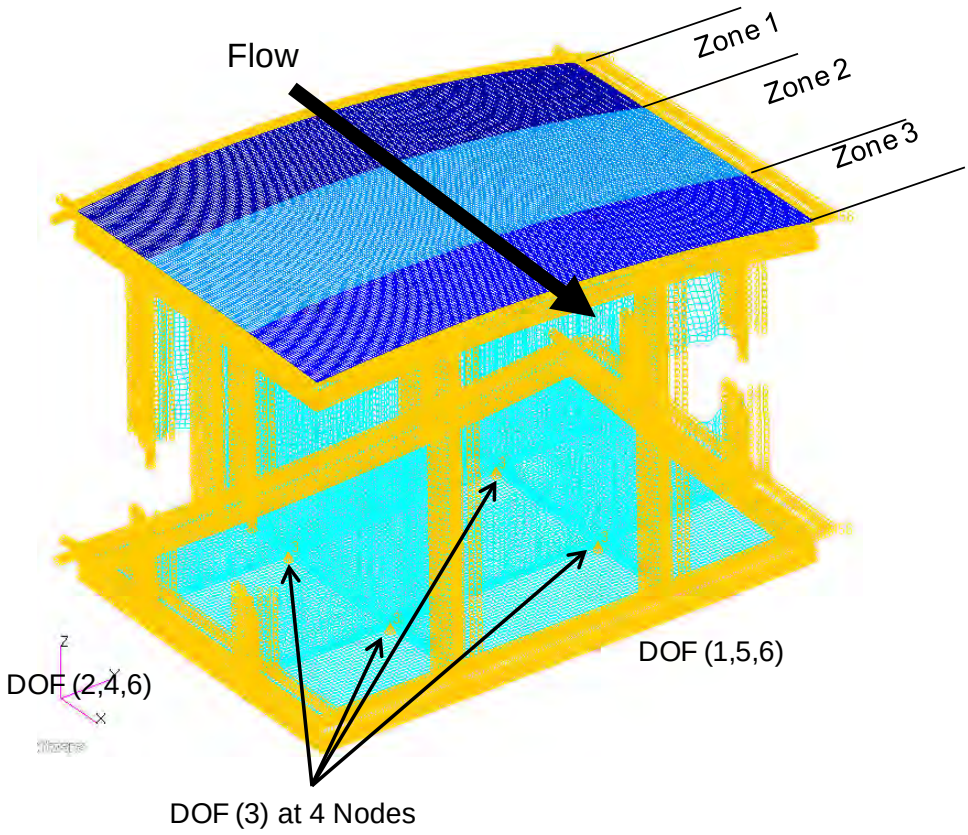

Figure 101. Unit cell boundary conditions for Panel 3 frequency response analysis (SOL 111)

The non-linear thermal only solution used as a preload for the frequency response analysis produced some interesting results that indicated some local buckling may be occurring between ortho-grid stiffeners. Local buckling of skin panels below ultimate load is common for some applications. It was assumed that this type of structural behavior at limit load would be acceptable. Figure 102 and Figure 103 show the location of deformation and stress respectively.

Approved for public release; distribution unlimited.

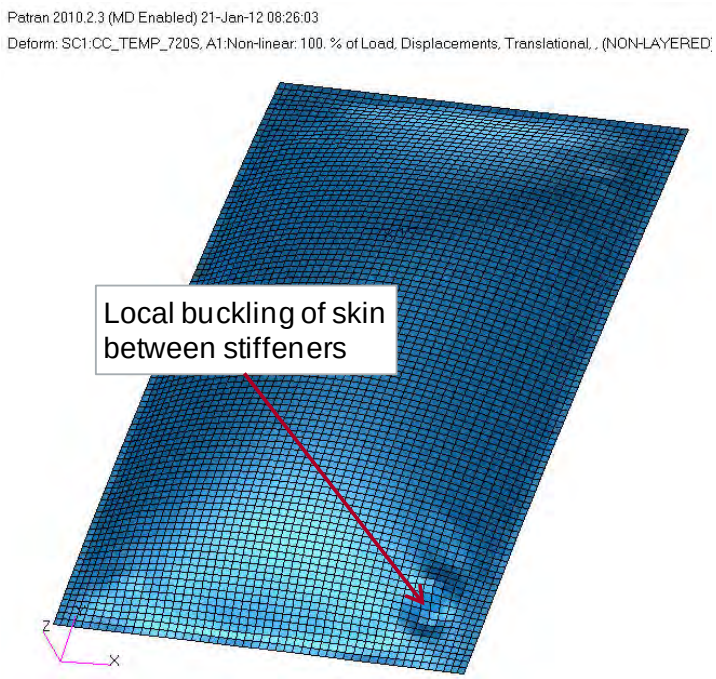

Figure 102. Panel 3 deformed shape for non-linear thermal load case at t=900s (not to scale)

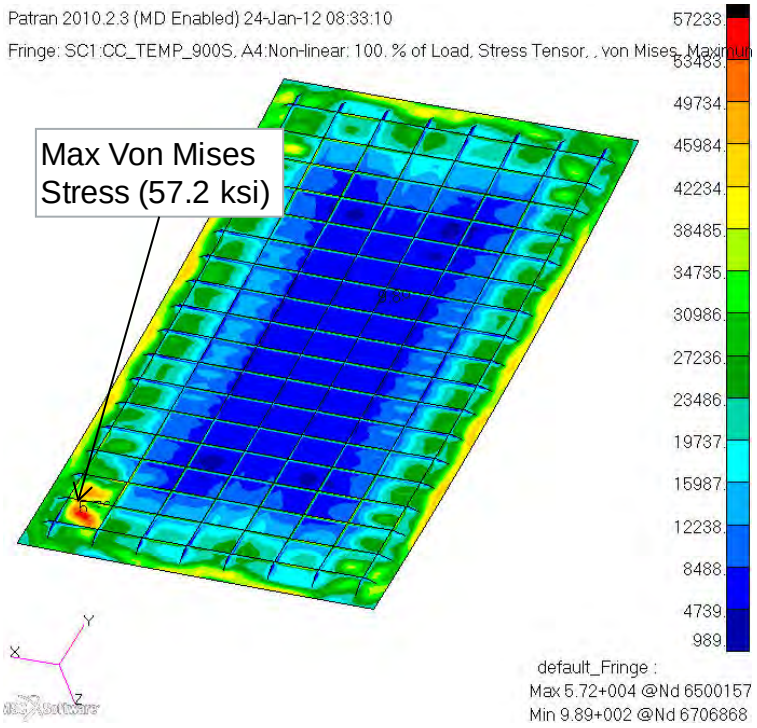

Figure 103. Panel 3 Von Mises stress plot for non-linear thermal load case at t=900s

Approved for public release; distribution unlimited.

Frequency response analysis was started from the non-linear static results. The displacement response of the panel is shown in Figure 104. The maximum PSD response is centered around the first vibration mode (approximately 48Hz).

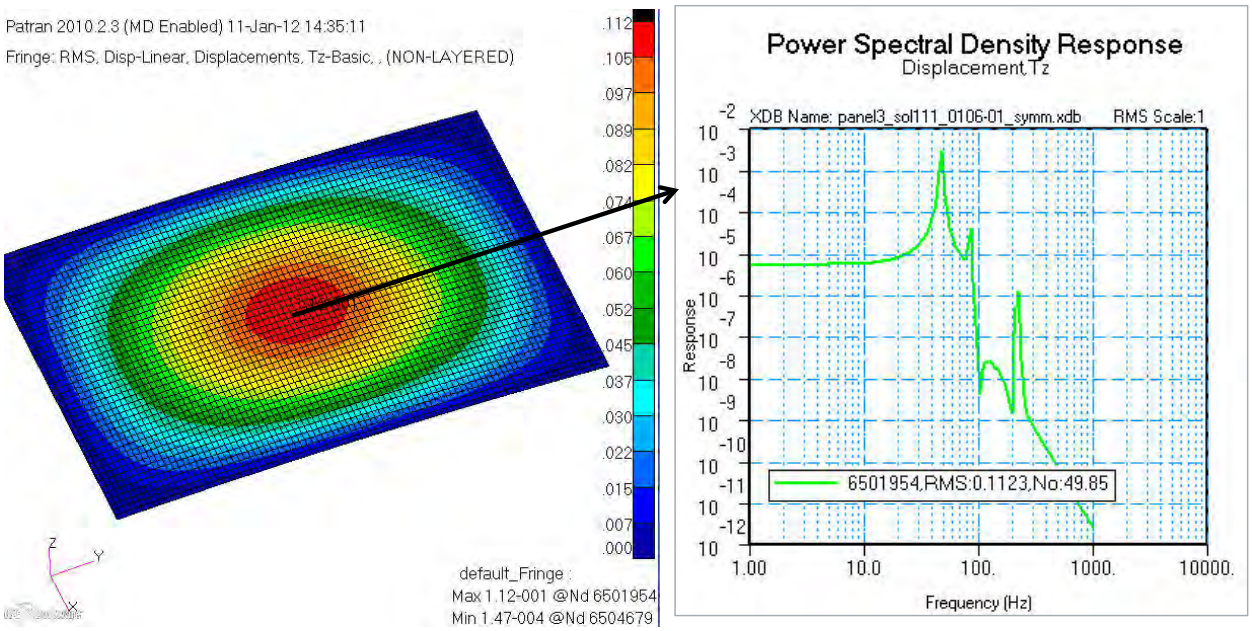

Figure 104. RMS displacement response generated by MSC Random for Panel 3 SOL111

The RMS stress results peaked at 10.1ksi at the extreme fiber of the ortho-grid stiffener near the center of the panel. The stress in this case was low in comparison to the mean stress on the panel due to thermal load. A fringe plot of RMS Von Mises stress is shown in Figure 105.

Approved for public release; distribution unlimited.

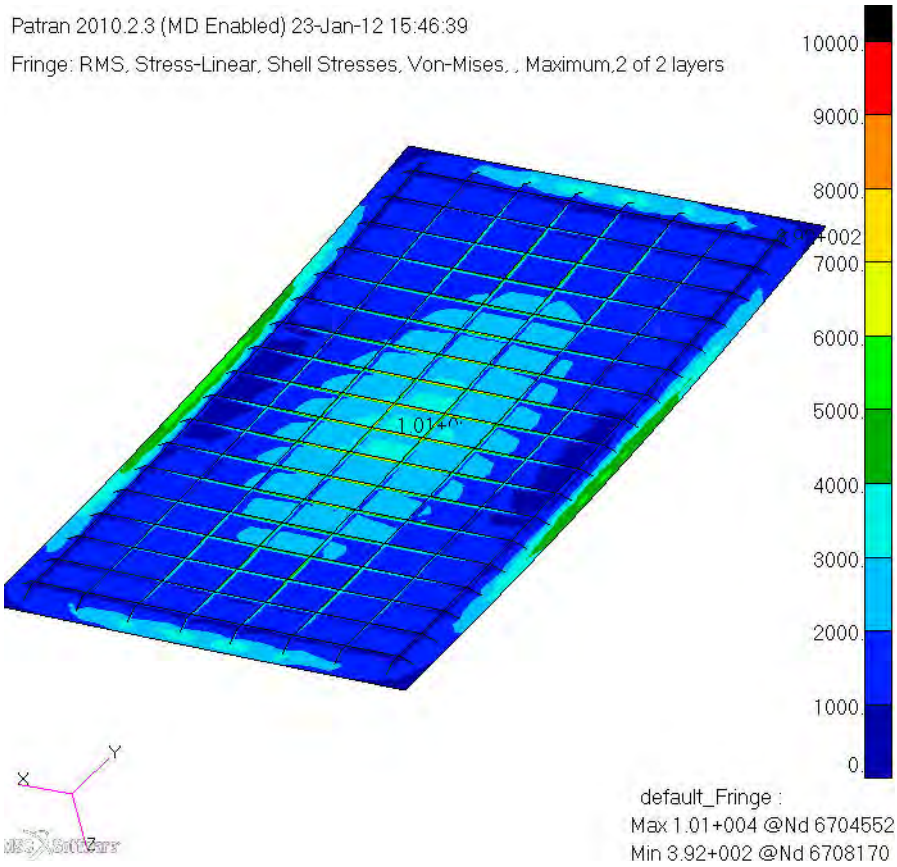

Figure 105. RMS Von Mises Stress fringe plot generated by MSC Random for Panel 3 SOL111

Panel flutter analysis is generally performed at the worst case combination of highest Mach number during the maximum Q portion of flight. For Panel 3, maximum thermal load and maximum Q occur at the 900s time point on during flight at approximately 75kft and Mach 6.25. Figure 106 shows the flight profile for the vehicle as well as the point in the sky information.

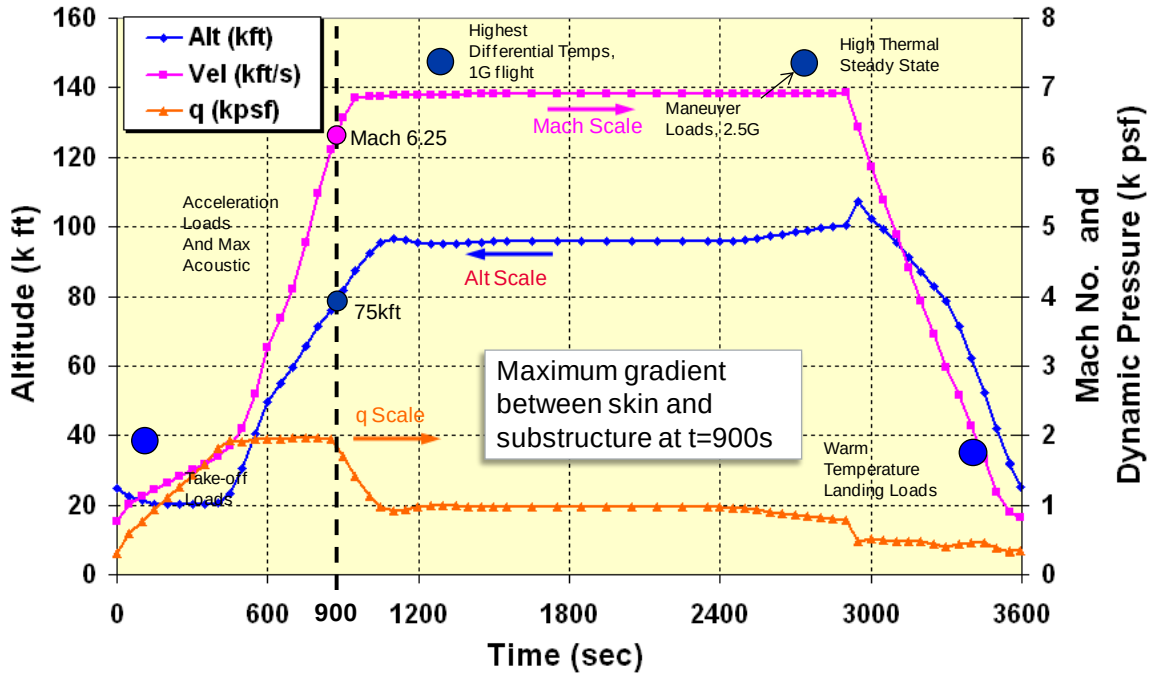

Figure 106. Altitude and Mach number shown for time, t=900s in vehicle flight profile

An empirical method was tried as a rough check of the panel. This method uses a non-dimensional parameter to develop a design curve for panel flutter. The panel flutter parameter is a function of material stiffness, panel aspect ratio, and thickness. The thickness input is an equivalent thickness to produce a first mode vibration equal to the frequency of the first panel mode from SOL103. Figure 107 shows Panel 3 plotted against the design curves. The curve indicates the panel is above the threshold for panel flutter. It should be noted that this particular curve was developed for flow of $M \leq 3.0$. It would require further study to determine if a curve could be computed for velocities up to $M = 7.0$.

Approved for public release; distribution unlimited.

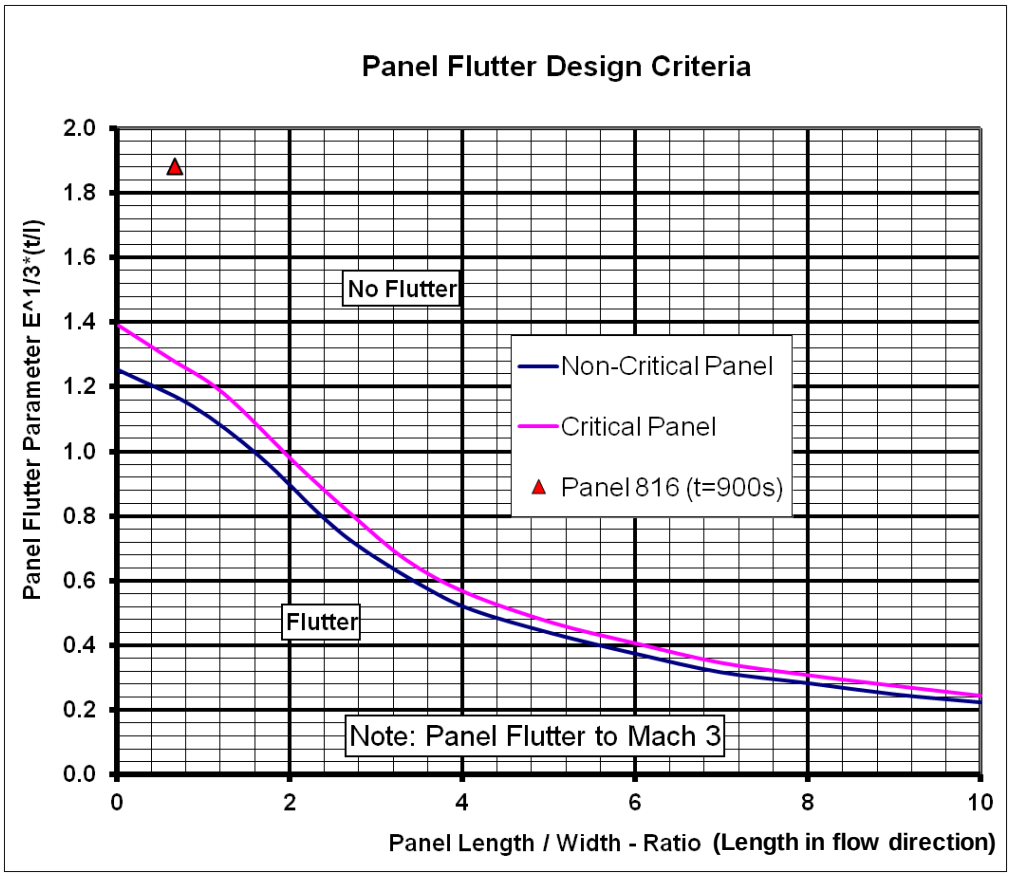

Figure 107. Design curve results for Panel 3 flutter

A FEA approach was also tried to predict flutter for Panel 3. It was thought that a unit cell FEM would take a long time to run, so a model of just the upper surface was developed that had very similar modal characteristics as the unit cell FEM, Figure 108 through Figure 110. It was later learned for Panel 4 that a panel flutter analysis on a unit cell sized model would be feasible.

	Unit Cell FEM	Panel 816 Flutter FEM
Mode 1	47.9	45.6
Mode 2	51.4	49
Mode 3	86.6	83.1

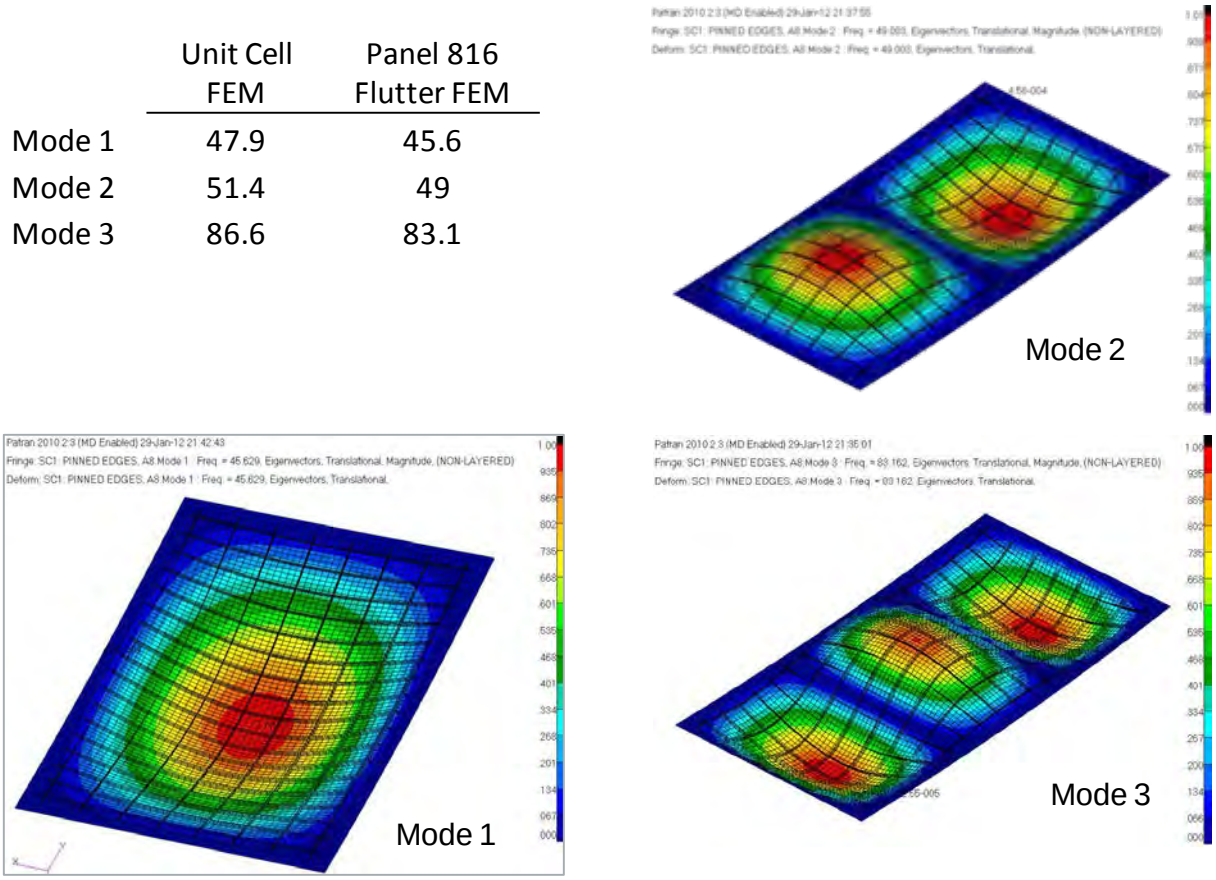

Figure 108. Comparison between flutter model and unit cell FEM for first three vibration modes

A separate aerodynamic FEM had to be created. This FEM is coupled with the structural FEM to calculate the interaction between aerodynamic loads and structural stiffness (vibration modes shapes) as a function of velocity. The structural FEM and AERO FEM are shown below respectively. The AERO FEM is constructed of 10 chord-wise CAERO5 elements divided into 20 span-wise strips.

Approved for public release; distribution unlimited.

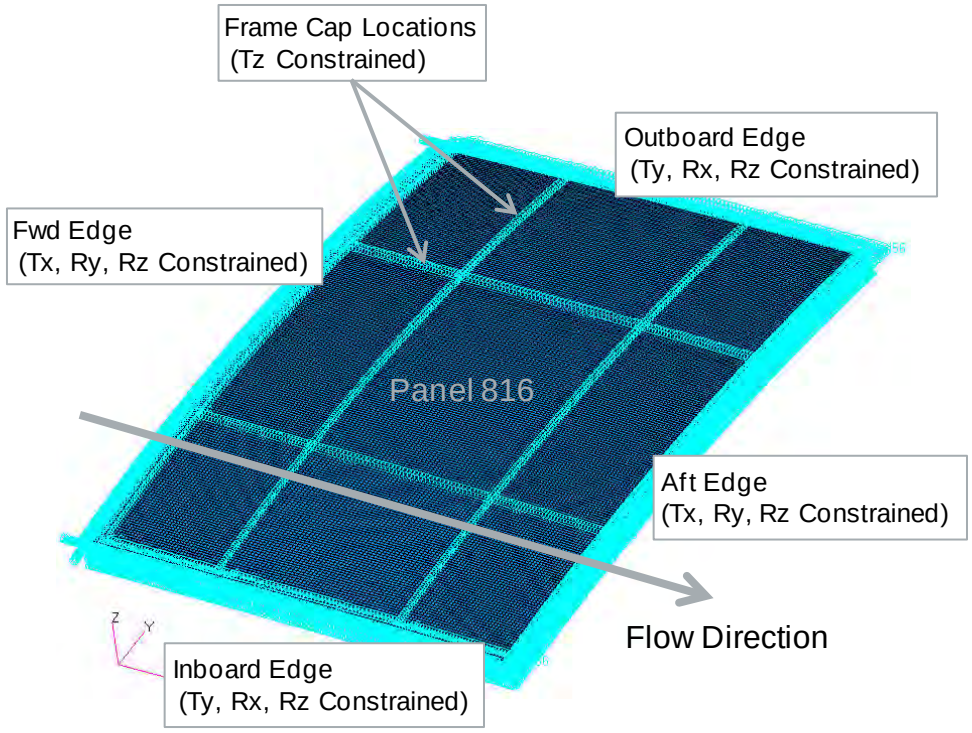

Figure 109. Structural model for Panel 3 flutter analysis using Piston Theory

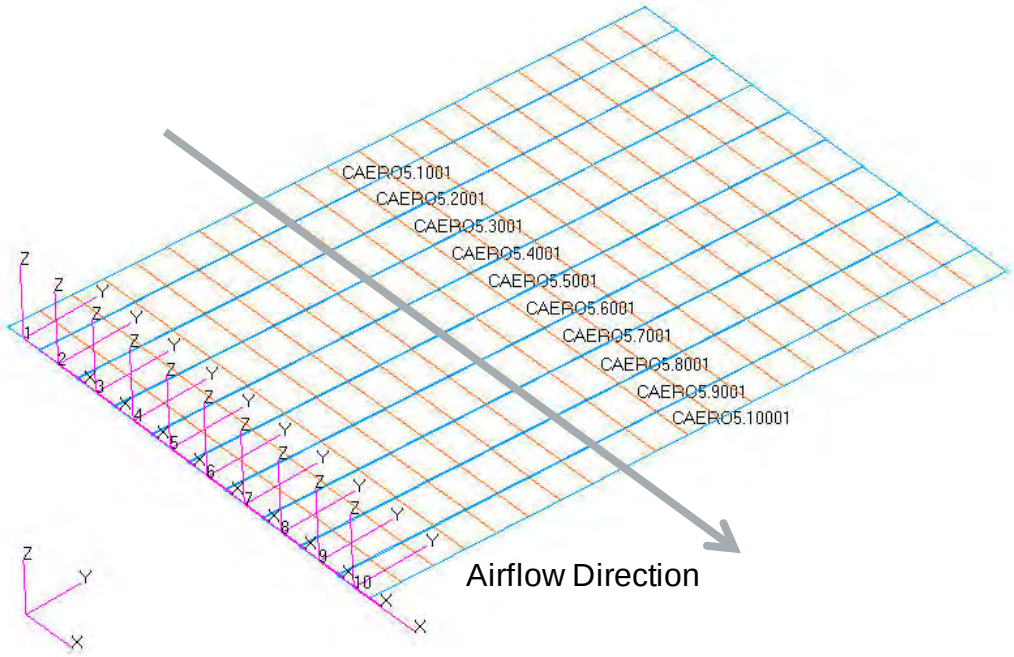

Figure 110. Aerodynamic model for Panel 3 flutter analysis using Piston Theory

The flutter analysis calculates modal frequency and damping for a given number of vibration modes and a given number of velocities. The basic process was to hold the analysis Mach number constant at M = 6.25 and adjust the altitude (air density) until a panel flutter speed could be approximated. The baseline analysis was run for a velocity range of Mach 3.0 to Mach 14.0.

Approved for public release; distribution unlimited.

A narrower band of velocities is used once an approximate flutter speed is determined to get a more refined value for flutter speed. Figure 111 shows results plotted for Panel 3 for negative 10,000 ft equivalent air density and a velocity range of M = 5.0-7.0.

Approved for public release; distribution unlimited.

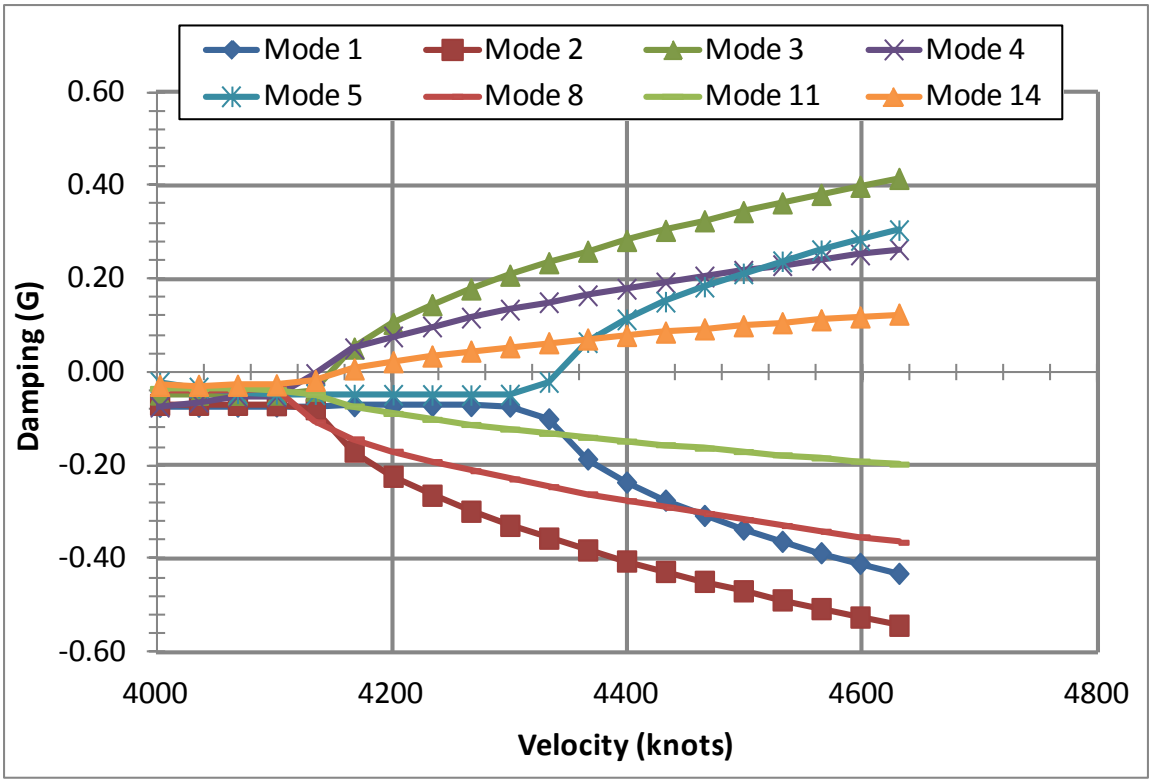

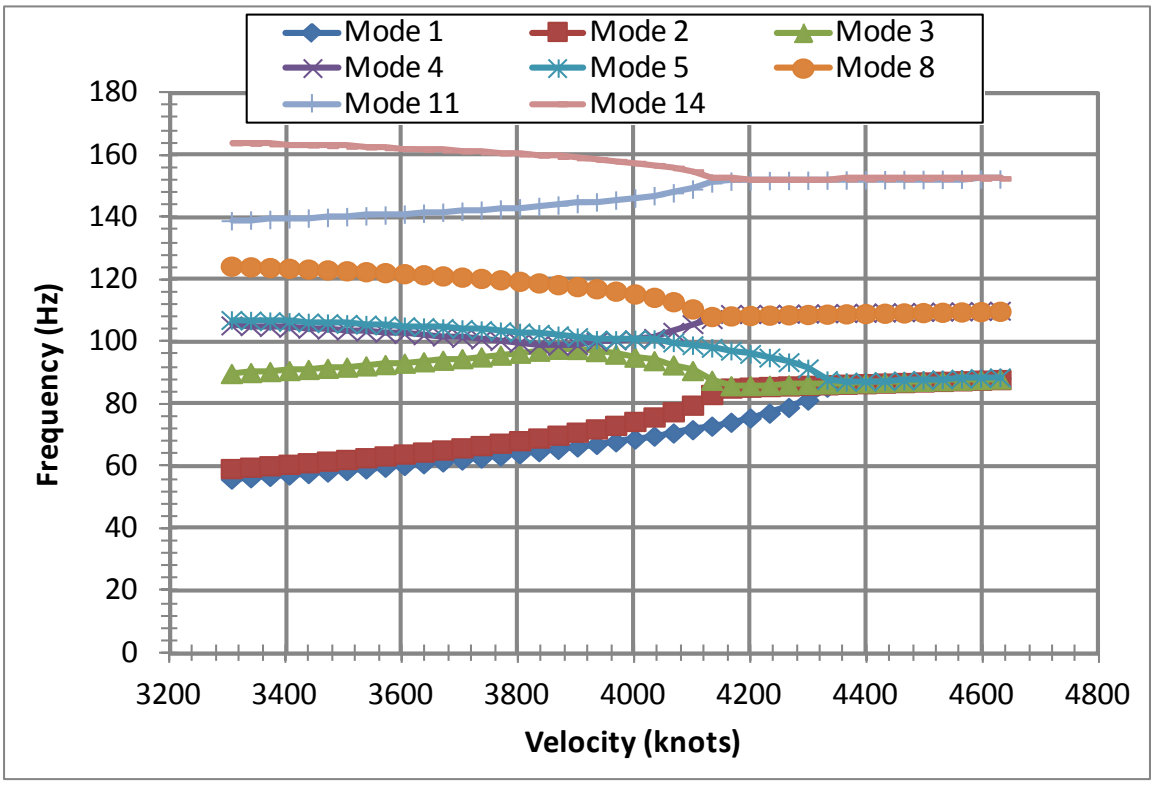

Figure 111. Plots of damping (G) and frequency (ω) as a function of air velocity for vibration modes that indicate Panel flutter

Approved for public release; distribution unlimited.

A critical damping (G) value above 0.02 is considered an unstable mode. The velocity at which G = 0.02 is considered the flutter speed. The table below summarized the progression of the flutter analysis as a flutter speed is determined. This analysis shows Panel 3 to have a flutter margin of approximately 80 kft. This value is calculated by taking the difference between the vehicle altitude at that point in the flight trajectory (75kft) and the equivalent altitude at which flutter occurred (-5kft).

Table 22. Summary of flutter analyses to determine flutter altitude for a target flutter speed of Mach 6.25

Altitude of Air Density	Solution Mach Number	Air Density	Velocity Range	Material Properties	First Flutter Mode	Flutter Speed (Knots)	Flutter Speed Mach Number	Frequency (Hz)
75,000 ft	6.25	5.26E-09	M3 - M14	Temp Adj. (t=900s)	-----	-----	-----	-----
Sea Level	6.25	1.147E-07	M3 - M14	Temp Adj. (t=900s)	Mode 3	4498.2	6.80	109.0
-10,000	6.25	1.522E-07	M3 - M14	Temp Adj. (t=900s)	Mode 3	3903	5.90	86.0
-5000	6.25	1.3238E-07	M3 - M14	Temp Adj. (t=900s)	Mode 3	4167	6.30	86.0
-5000	6.25	1.3238E-07	M5 - M7	Temp Adj. (t=900s)	Mode 3	4167	6.30	86.0

4.5.5 Panel 3 (816) Fatigue Margin Evaluation

As discussed above, the large mean stress due to the thermal load at t=900s makes aero-acoustic fatigue an issue for Panel 3. Figure 112 shows four locations of high RMS stress that were checked for AACF. Two locations are peak stresses in the ortho-grid stiffeners. The other two locations are near stiffener terminations at the skin to substructure joint. At these locations, a stress concentration factor is used. At the stiffener termination, there is a radius fillet with an Kt=1.15. At location 4, the Kt at the fastener hole is Kt=2.3 in bending. At the fastener hole (Location 4), there is only slight positive margin.

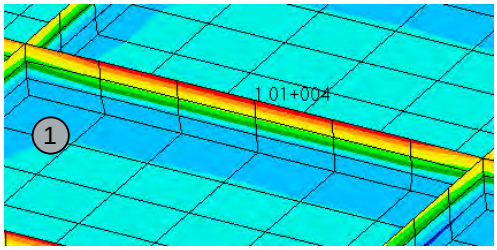

RMS Von Mises Stress =10.1ksi
Short Direction Orthogrid

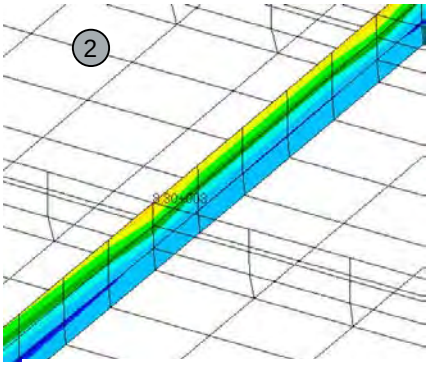

RMS Von Mises Stress =8.3ksi
Long Direction Orthogrid

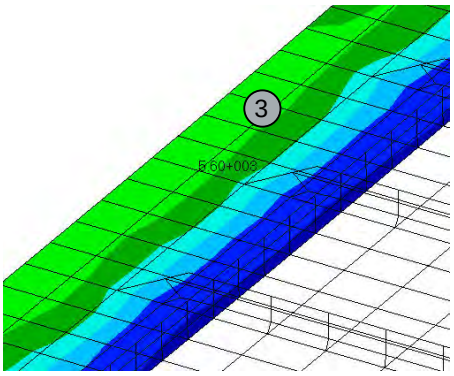

RMS Von Mises Stress =5.6ksi
Aft Skin to Substructure Joint

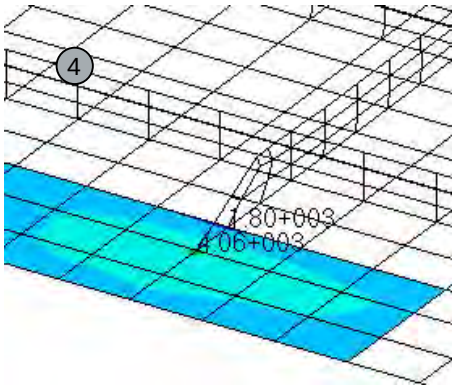

RMS Von Mises Stress =4.1ksi
Aft Skin to Substructure Joint

Figure 112. Locations checked for aero-acoustic fatigue

The table below gives a summary of results for AACF analysis. The results show all positive margins with thermal stress.

Table 23. Margin of safety summary for Panel 3 AACF

Location of Stress Concentration	Stress Conc. Type	Struct. Temp (℉)	Temp. Factor	Stress Ratio	Stress Ratio Factor	Kt	Allowable Stress (ksi)	RMS Stress Result (ksi)	Mean Stress (ksi)	**MS**
Orthogrid (Short direction)	None	1180	0.82	0.58	0.82	1.0	12.8	10.1	38.5	**0.26**
Orthogrid (Long Direction)	None	1180	0.84	0.00	0.97	1.0	15.5	7.0	7.0	**1.21**
Aft Skin edge at Skin to Substructure Joint	Filled Hole	1150	0.84	0.74	0.83	2.3	4.96	5.6	37.0	**0.03**
Outboard Skin at Skin to Substructure Joint	Filled Hole	1150	0.84	0.77	0.86	1.15	9.04	4.1	32	**1.91**

Approved for public release; distribution unlimited.

Thermal-mechanical fatigue analysis used results from the linear static unit cell FEA. The maximum Ktσ calculated for the Limit mechanical + Thermal (t=900s) load case was 177ksi. This is well above the calculated allowable of 103ksi.

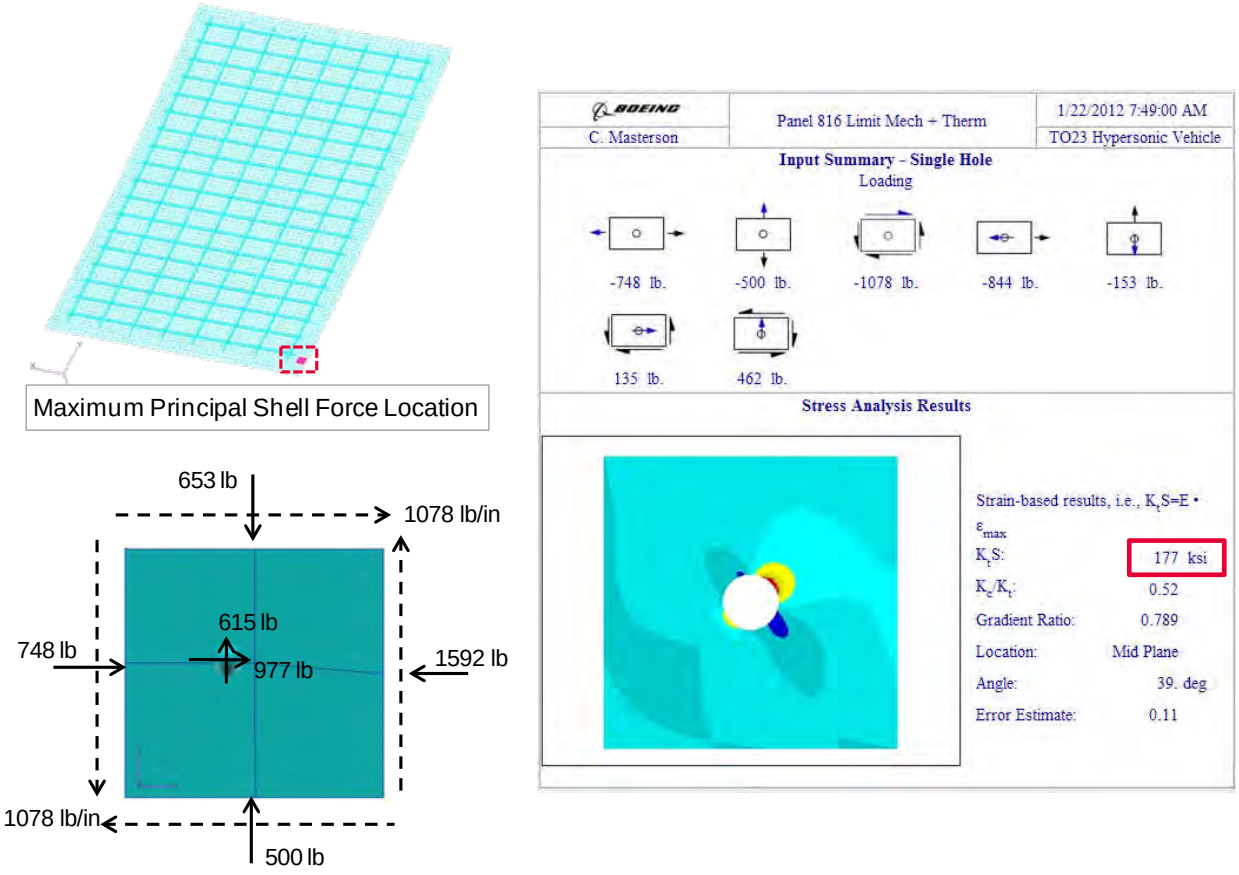

Figure 113. Worst case Ktσ calculation for skin to substructure joint

A summary of margin of safety calculations for TMF is given in Table 24. All fatigue checks are for skin to substructure fastened joints. Additional sizing iterations will alleviate the negative margins shown in Table 24.

Approved for public release; distribution unlimited.

Table 24. MS table for Panel 3 thermal-mechanical fatigue

Load Case	Limit Mechanical (1.15*2.5g) + Thermal (t=900s)		
Location	Max Brg	Max Princ	Min Princ
Elem ID	----	4004919	4005926
Nearest Fastener	13626813	13626974	13626813
Temperature	1150	1150	1150
KT Sigma (ksi)	**152**	**177**	**152.0**
Allowable Stress (ksi)	**103.4**	**103.4**	**103.4**
MS	**(0.32)**	**(0.42)**	**(0.32)**
Calculated Fatigue Life (N Cycles)	**139**	**16**	**139**

4.6 Panel 4 (1074) Detailed Design

Panel 4 (1074), shown in Figure 114, is located on the windward surface of the TX-V. It lies below a fuel tank in the right wing section of the vehicle just right of the vehicle body.

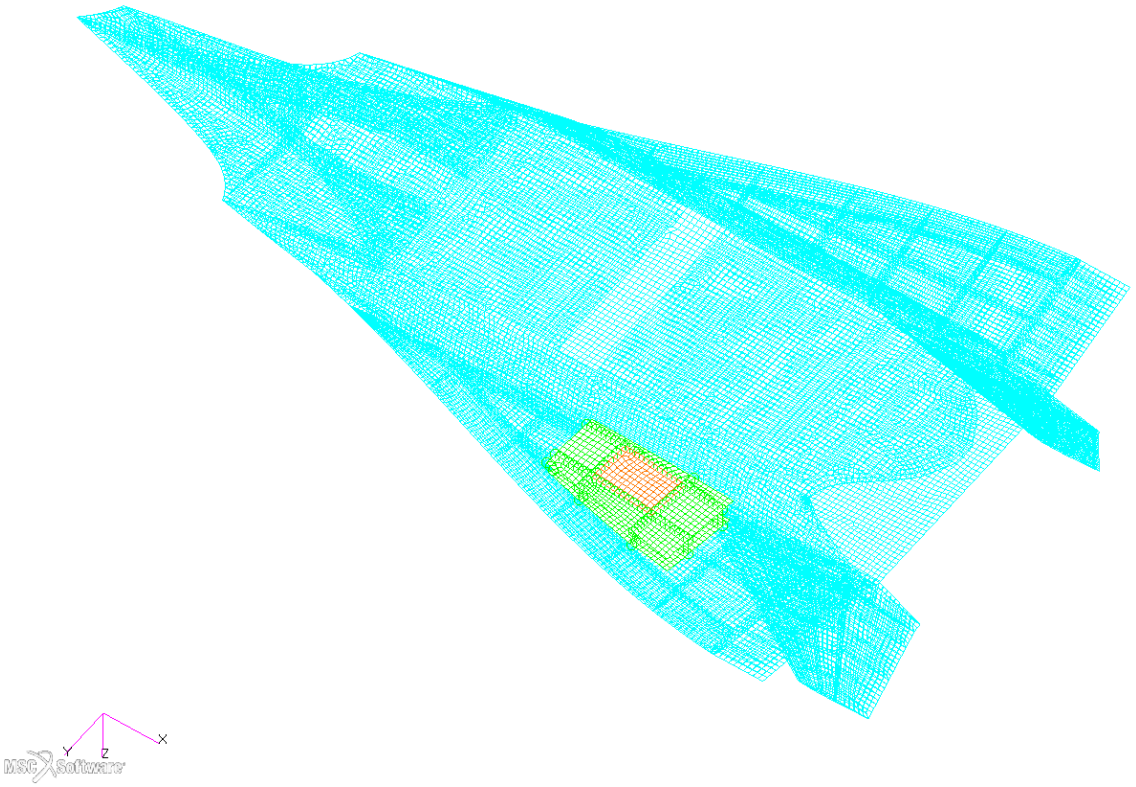

Figure 114 Location of Panel 4 (1074) and the Corresponding unit cell

Approved for public release; distribution unlimited.

4.6.1 Panel 4 (1074) Sizing and Design

Unlike the first 3 panels which were part of the TX-V fuselage, Panel 4 is part of the wing structure which has a much lower total depth. It had been assumed that thermal loads were being driven primarily by the differential expansion between the substructure and skin panels, and that a reduction in substructure cross-sectional area would provide a corresponding reduction in stiffness and thus thermal loads. A quick study was even performed on a flat 1/8 unit cell model (symmetric about 3 principal planes) and confirmed that thermal loads scale with overall bay depth as shown in Figure 115. Furthermore, since this panel is part of a wing fuel tank that is emptied early in the trajectory prior to the structure reaching high temperatures, it was assumed that no internal insulation would be required and that radiative heat transfer inside the bay would limit the magnitude of any thermal gradients. As a result, thermal loads for Panel 4 were estimated by scaling Panel 2 thermal loads by the ratio of unit cell bay depths (20 vs 70 inches). These estimated thermal loads are provided along with mechanical loads from the global FEM in Table 25. Unfortunately, it was later discovered that the total ΔT across the bay (skin-to-skin) make a large contribution to thermal loads and the 1/8 unit cell used for the scaling study was unable to capture this effect. As a result, Panel 4 was significantly undersized for its thermal load condition and has several negative margins. More discussion on the thermal boundary conditions and resulting thermal loads is provided in the following sections.

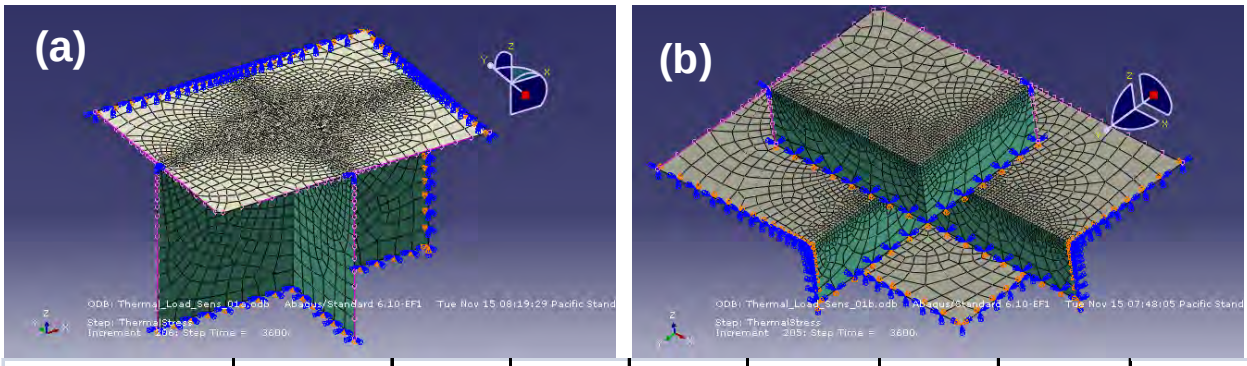

	Lz (depth)	Lx	Ly	Fx	Fy	Nx	Ny	time
	Inches			lbs		lbs/in		sec
Wing Bay	20	22	29	669	687	30	24	913
Fuselage Bay	70	22	29	2336	2.35E+03	106	81	928
Depth Ratio	**3.5**			**Nx and Ny Ratios**		**3.5**	**3.4**	

Figure 115. Simplified 1/8 unit-cell models of the fuselage (a) and wing (b), and results (bottom) used to determine a thermal load scaling factor for Panel 4

Approved for public release; distribution unlimited.

Table 25. Panel 4 sizing loads for a 2.5G turn with scaled Panel 2 thermal loads

	Nx	Ny	Nxy	Mx	My	Mxy	Qx	Qy
	lbs/in			in-lbs/in			lbs/in	
Strength and Buckling from Global FEM	-91.3	69.9	-29.2	29.7	-45.5	-1.5	0.2	-13.4
Thermal Scaled from Panel 2	-110	-106	-1.8	0.0	0.0	-0.3	0.2	0.4

Additional inputs: 1154°F temperature, 325°F/in temperature gradient, 1.0 psi normal pressure

HyperSizer sizing resulted in a 5.75 x 5.75 inch ortho-grid where the X-direction (or long) stiffeners are 0.085 inches thick, while the Y-direction stiffener and skin were minimum gage (.070 and .050 inches). To limit normal deflections, a set of external stiffeners was sized and added to the panel as shown in Figure 116. In order to further limit deflections and mitigate external stiffener induced thermal loads, the stiffeners were extended over the ortho-grid gussets and all grid run-out gussets were given sections 50% thicker than the acreage grid in the analysis models. It should be noted that the external stiffeners were sized with the underestimated thermal loads and unit cell deflection results despite the added stiffeners. As with Panel 3, the Panel 4 unit cell, shown in Figure 117, was generated from lofted surface geometry interpolated from a point cloud of global FEM nodal coordinates. Furthermore, a comparison of the generated geometry to the global FEM also showed good alignment.

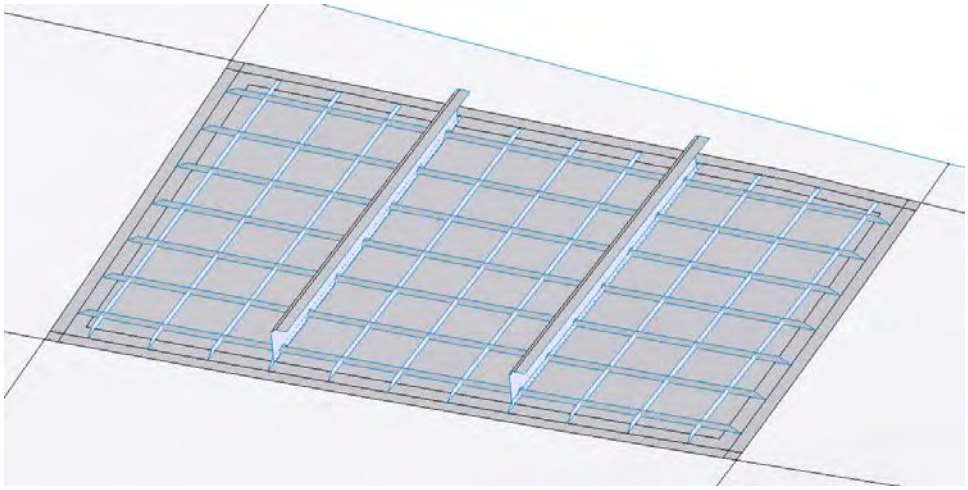

Figure 116. Panel 4 ortho-grid and external stiffener geometry

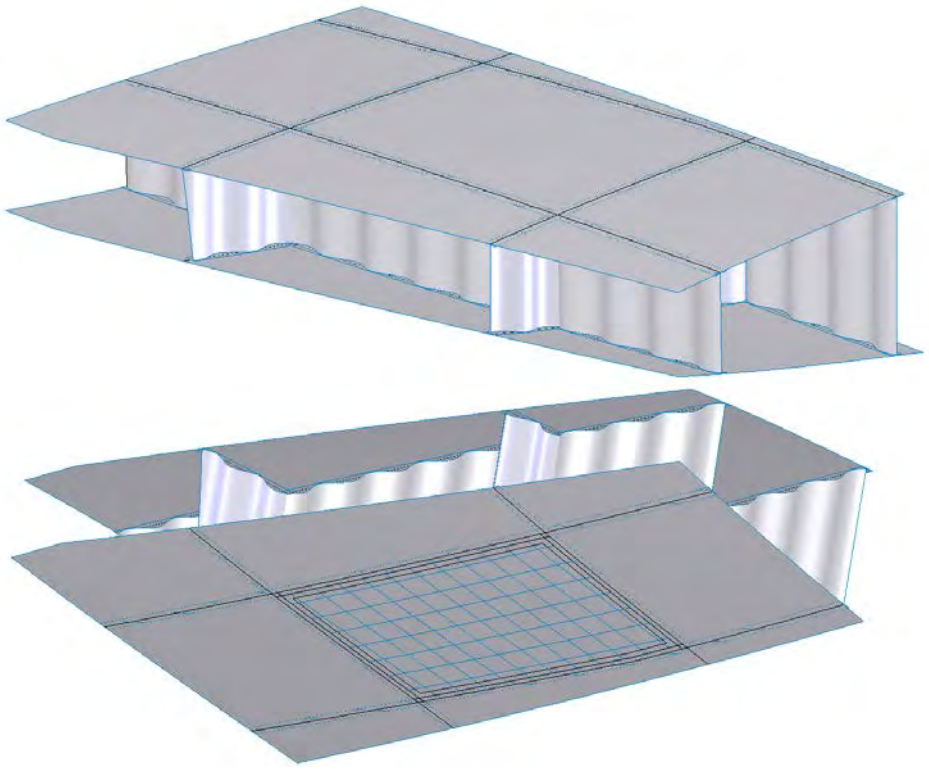

Figure 117. Panel 4 unit cell geometry

4.6.2 Panel 4 (1074) Thermal Analysis

Panel 4 is located on the windward surface of the starboard wing. This bay includes the wing fuel tank. As with Panel 3, the fuel is modeled as a lumped mass which decreases during the flight according to the fuel use schedule developed on a previous program, Figure 118. However, since the wing tanks are smaller and are first to be emptied the fuel mass decreases to insignificant values before the structure reaches high temperatures. The bay is therefore assumed to be a flooded structure without an additional bladder or insulation, and the fuel is essentially ignored in the boundary conditions. This results in a very different temperature response than seen for Panel 3. Since the fuel tank is empty during the high temperature portion of the flight, internal radiation was included in this analysis. Additional boundary conditions are shown in Figure 119. Figure 120 shows temperature distributions at critical load conditions during the flight. The first image shows the maximum temperature gradients between the panel skin and ortho-grid occurring early in the flight. The second image shows maximum flight temperatures. The next image illustrates the maximum temperature gradients between skin and substructure, and the fourth, the greatest negative temperature gradients. The thermal behavior of this model is quite different from the previous three due to the lack of either an internal heat source or constrained fuel temperature. This allows the substructure temperatures to follow the panel temperatures more closely.

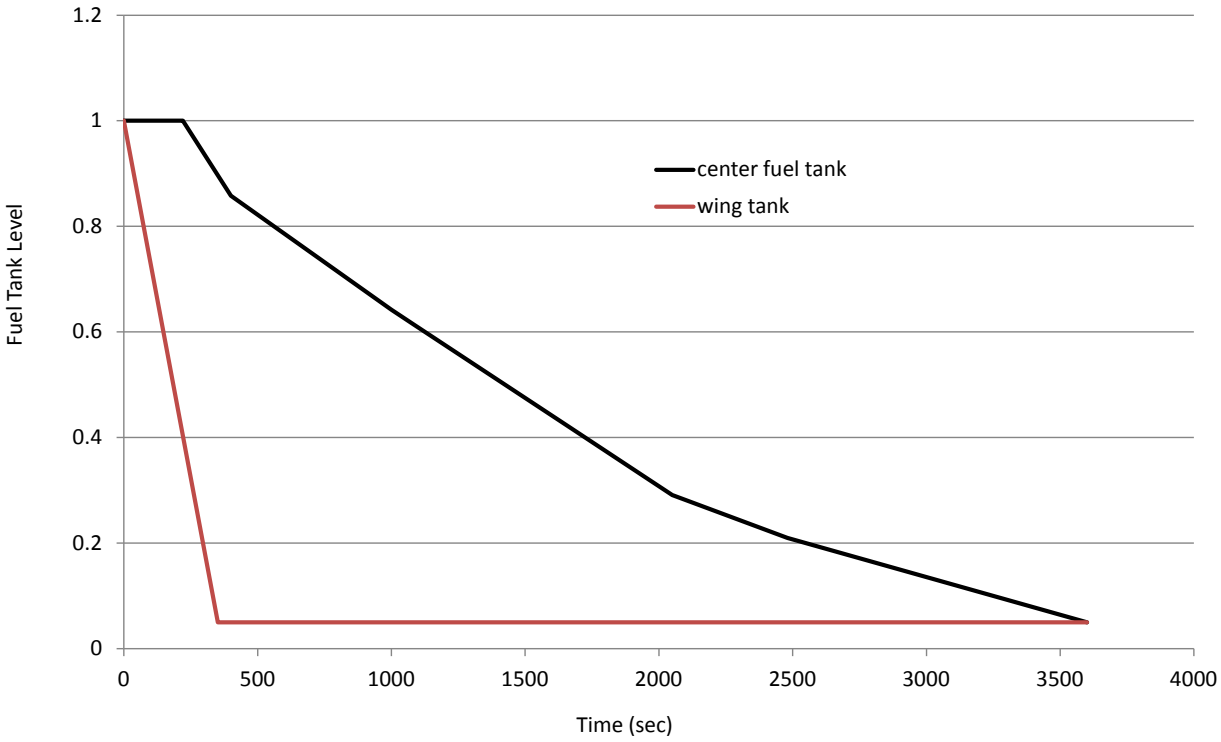

Figure 118. Wing and Center Fuel Tank Schedules

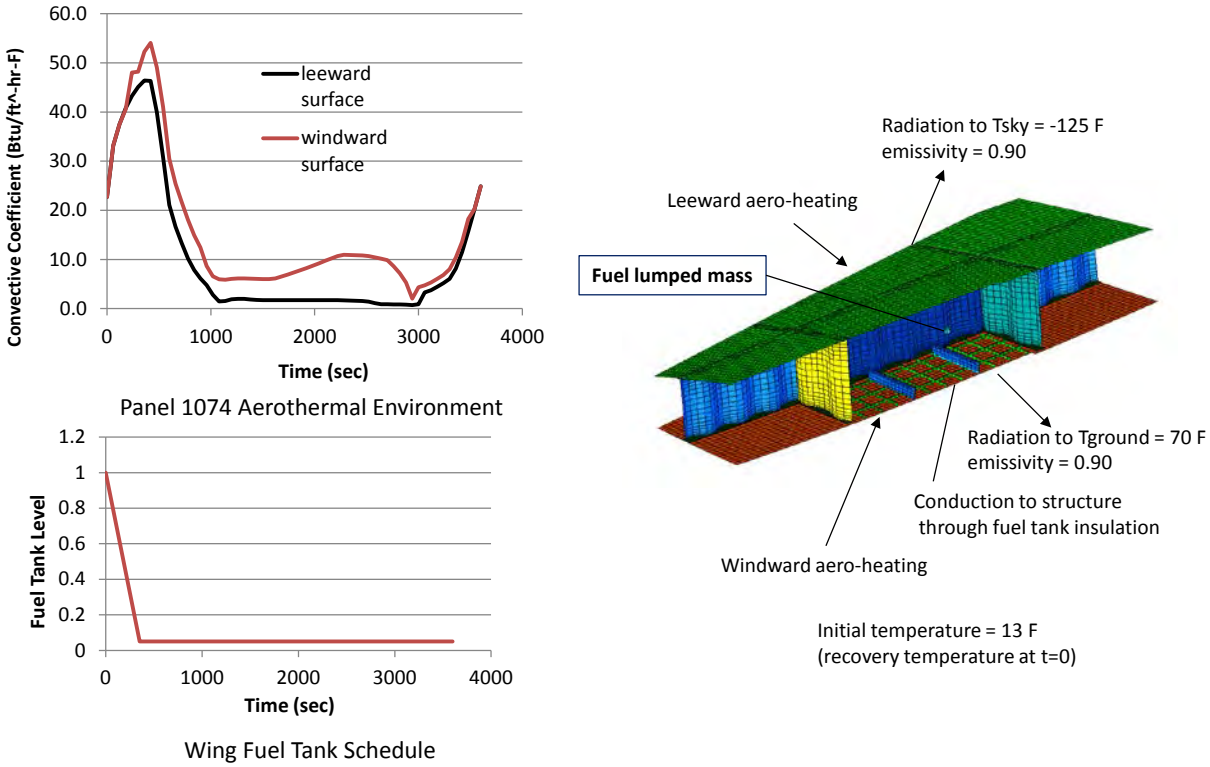

Figure 119. Panel 4 (1074) Boundary Conditions

Approved for public release; distribution unlimited.

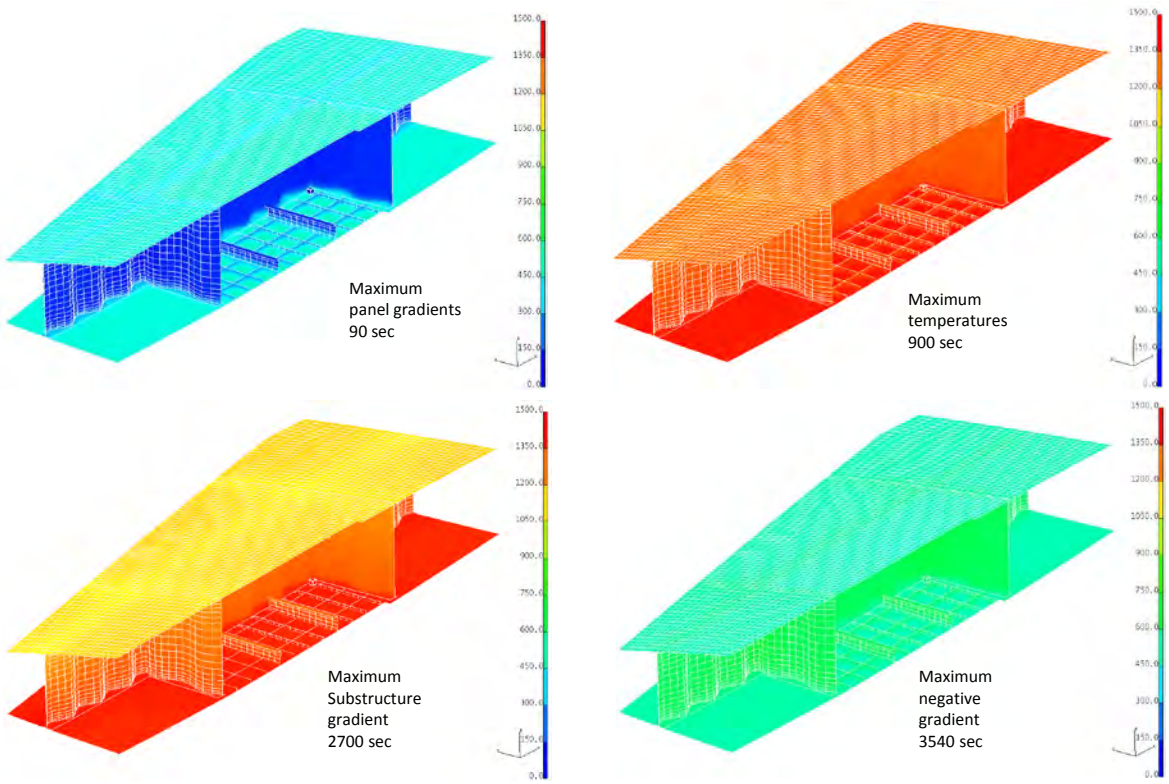

Figure 120. Panel 1 (862) Temperature Distributions

Transient temperature profiles at locations on all the major structural components are plotted in Figure 121. As mentioned above, the absence of fuel and engine allows substructure temperatures to follow the panel temperatures much more closely. Figure 122 shows maximum temperature differences between structural components. These results are used to identify the time states corresponding to maximum temperatures and temperature gradient conditions. The five conditions: maximum gradient in the panel, maximum gradient between skin and substructure, maximum gradient between skin and panel breaker, maximum temperatures and maximum reverse gradient are specified. This panel location provides another diverse condition to exercise the analysis methods and more rigorously investigate the design process.

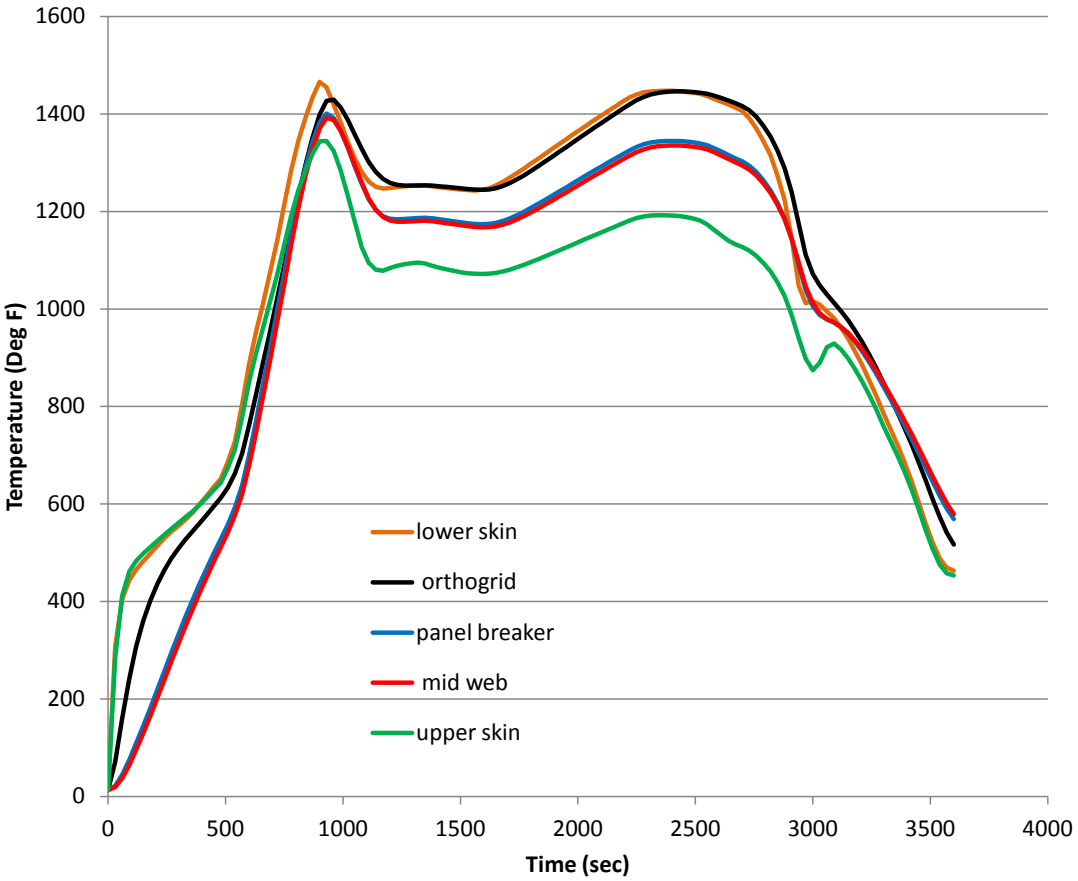

Figure 121. Panel 4 (1074) Temperature Histories

Approved for public release; distribution unlimited.

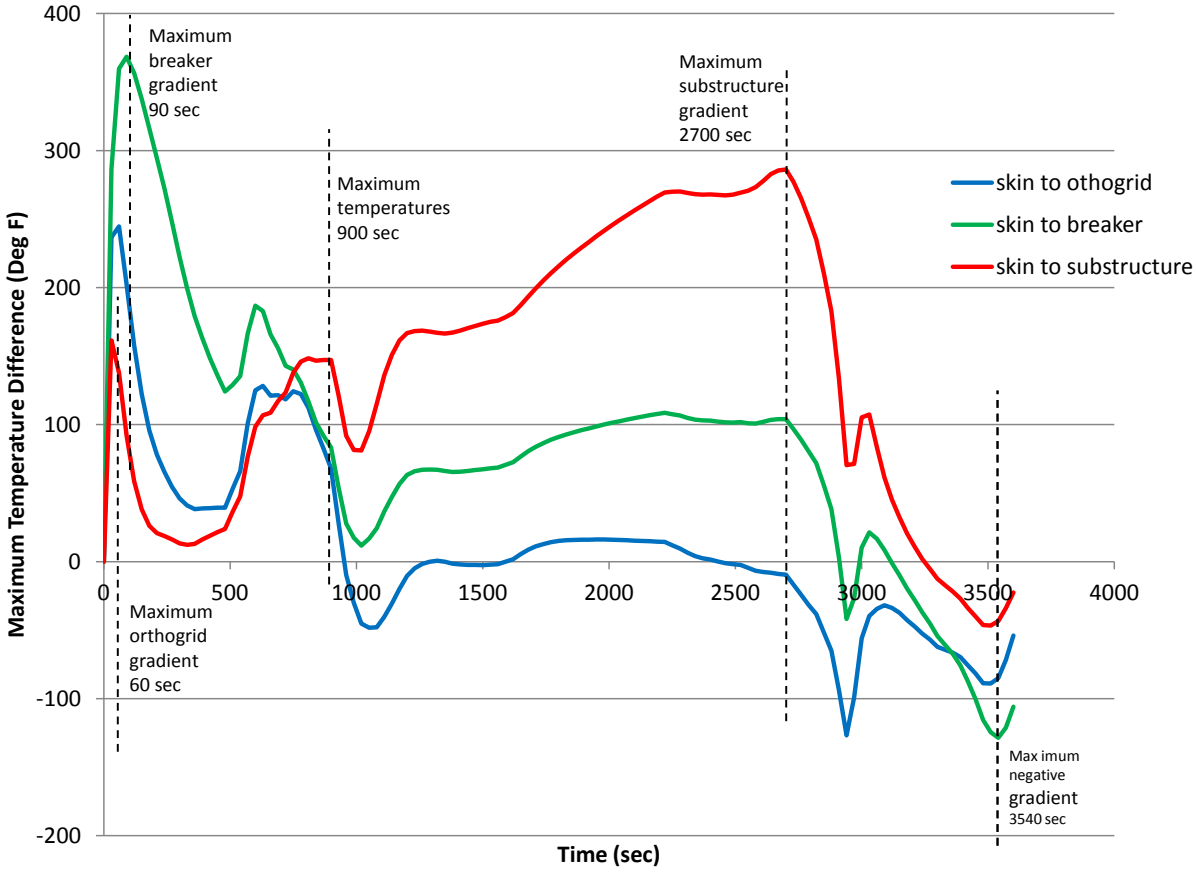

Figure 122. Panel 4 (1074) Temperature Gradients

4.6.3 Panel 4 (1074) Stress Analysis

Similarly to Panel 2 (816), Panel 4 (1074) is also a windward panel therefore panel breakers were utilized in the design. Because this is a wing panel, the unit cell is roughly 1/3 the depth of the previous three panels. This geometrical difference was used to proportion the thermal loads used for initial sizing as discussed in Section 4.6.1. However, the study performed to establish this relationship did not account for the difference in the thermal profile between the previous unit cells and the unit cell of a wing section. Since, there is no thermal insulation like a fuel tank full of fuel or a large amount of substructure, the lowest temperature of a wing section unit cell is not in the center of the substructure like it is on a fuselage section unit cell. Rather, the unit cell cools or heats almost linearly from the windward side to the leeward side. This provides an overall bending of the wing. This unanticipated heating profile and thermal loading during initial sizing provided undersized structure, most notably large ortho-grid spacing compared to the previous panels. The undersized structure contributed severely negative displacement margins of safety in addition to eigenvalues well below the buckling requirements. Additionally, because this is a windward wing panel, the maximum temperature of this panel is very high at 1470°F. This results in a very low material allowable which provides negative margins of safety for Ultimate Material Failure.

The critical load case was determined similarly to the other panels and was selected as Mechanical: 2.5g Ultimate (1.5) + Thermal: T=2700s. This temperature profile is at the maximum temperature gradient between the skin and the keel/frame substructure. Results from the panel level analysis are discussed below. These analyses are non-linear.

The maximum relative displacement in the Z direction is calculated as follows:

$$\Delta = \text{Maximum deflection} - \text{Minimum deflection} = (0.122") - (-0.392") = 0.514"$$

The allowable for deflection is 0.1" as defined the thermal analysis section. The large deflection could cause a variation in the thermal loading which would be captured in a coupled thermal and mechanical analysis. (Recommendation #6, Page 3) Therefore the deflection margin of safety (MS) is calculated as follows:

$$MS = \text{Allowable/Actual} - 1 = 0.1/0.514 - 1 = -0.81$$

The displacement plot of Panel 4 (1074) is shown in Figure 123.

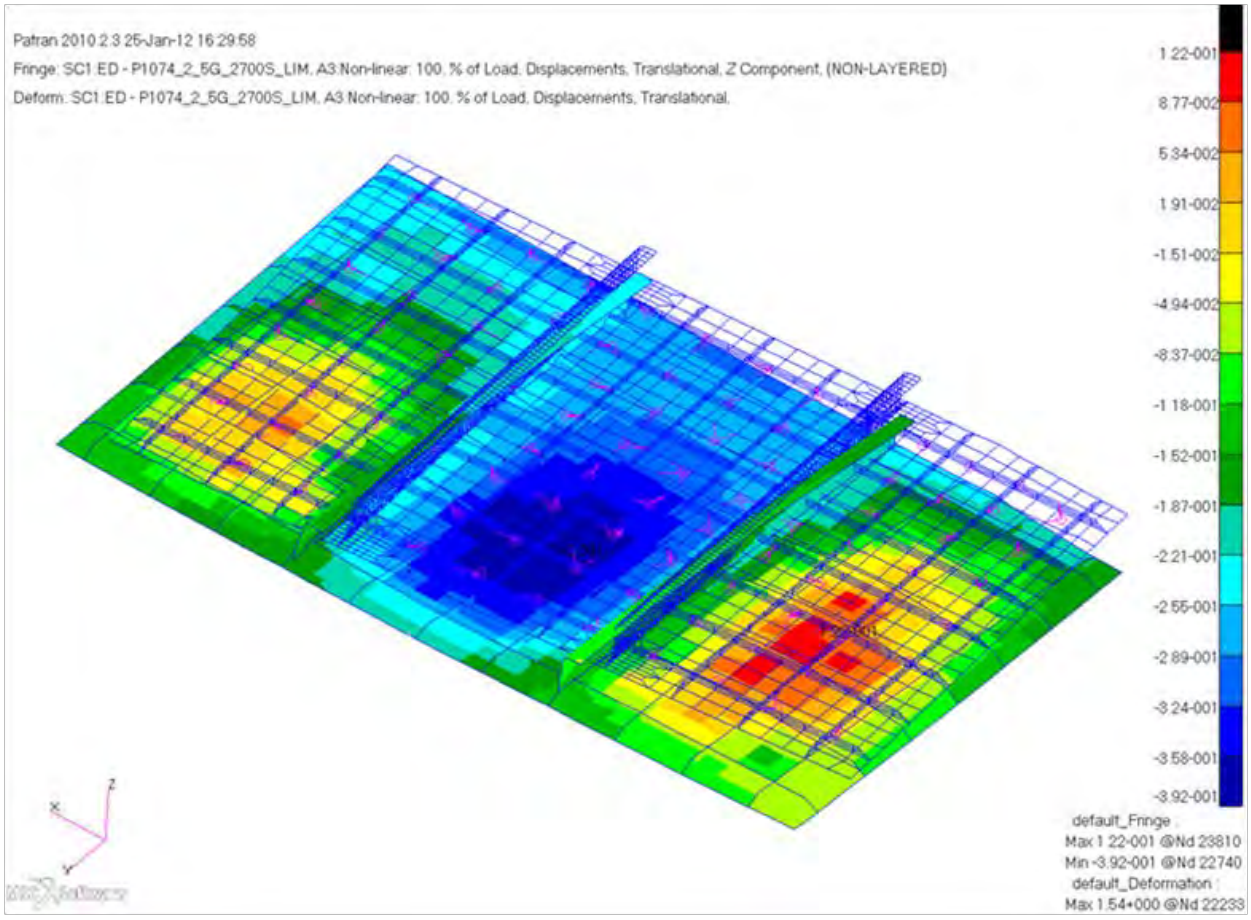

Figure 123. Non-Linear Z-Component Deflection Plot [in] of Panel 4 (1074)

Load Case Mechanical - 2.5g Limit (1.15) + Thermal - T=2700s

Approved for public release; distribution unlimited.

Since the deflection requirement is meant to represent flight conditions that will be experienced by the structure periodically through the flight profile, limit loads are used to write the margins of safety rather than ultimate loads

The maximum Von Mises stress of 85.5 ksi is located near the one of the scalloped edges of the panel breaker stiffeners.

The allowable for Ultimate Material Failure for Inconel at room temperature is Ftu = 185 Ksi. At T = 2700s, the maximum temperature of the unit cell is 1470°F which dictates a thermal knockdown factor 36% of room temperature allowable. The allowable is calculated as follows:

$$F_{tu@2700°F} = F_{tu@70°F} * \text{Thermal Knockdown} = 180 \text{ Ksi} * 0.36 = 64.8 \text{ Ksi}$$

Therefore the Ultimate Material Failure margin of safety (MS) is calculated as follows:

$$MS = \text{Allowable/Actual} - 1 = 64.8/88.5 - 1 = -0.27$$

The Von Mises Stress plot of Panel 4 (1074) is shown in Figure 124.

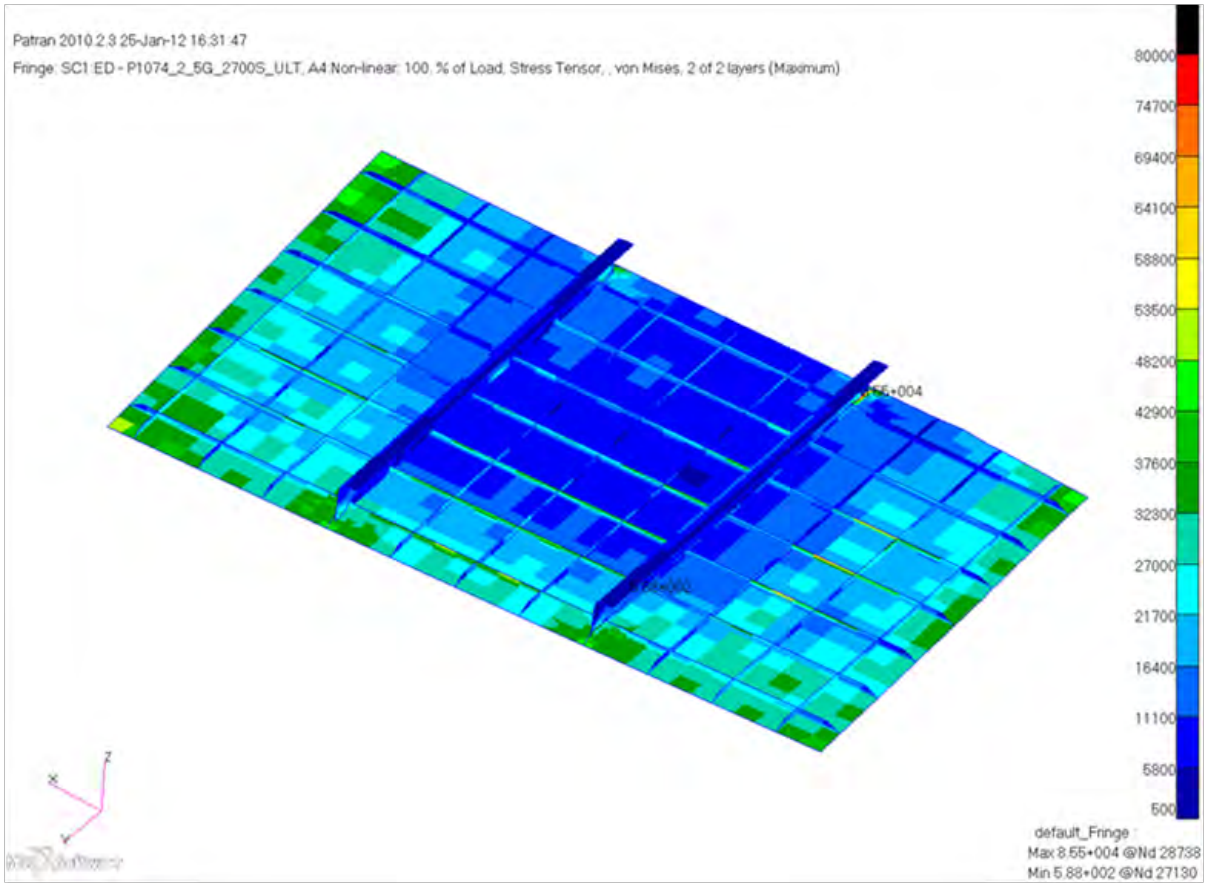

Figure 124. Non-Linear Von Mises Stress Plot [psi] of Panel 4 (1074)

Load Case Mechanical - 2.5g Ultimate (1.5) + Thermal - T=2700s

Approved for public release; distribution unlimited.

Because this panel incorporates panel breaker stiffeners, which are attached with fasteners to the ortho-grid, a fastener bearing analysis must be performed.

The maximum fastener load is P = 1140. The bearing stress is calculated as follows:

$$\sigma_{brg} = P/(d*t) = 1140 / (0.19*.063) = 95.2 \text{ ksi}$$

The allowable for Ultimate Bearing for Inconel at room temperature is Fbru = 309 Ksi (e/D = 1.5). At T = 2700s, the maximum temperature of the unit cell is 1470°F which dictates a thermal knockdown factor 36% of room temperature allowable. The allowable is calculated as follows:

$$F_{bru@2700°F} = F_{bru@70°F} * \text{Thermal Knockdown} = 309 \text{ Ksi} * 0.36 = 111 \text{ Ksi}$$

Therefore the Ultimate Material Failure margin of safety (MS) is calculated as follows:

$$MS = \text{Allowable/Actual} - 1 = 111/95.2 - 1 = 0.17$$

The fastener forces plot for Panel 4 (1074) is shown in Figure 125.

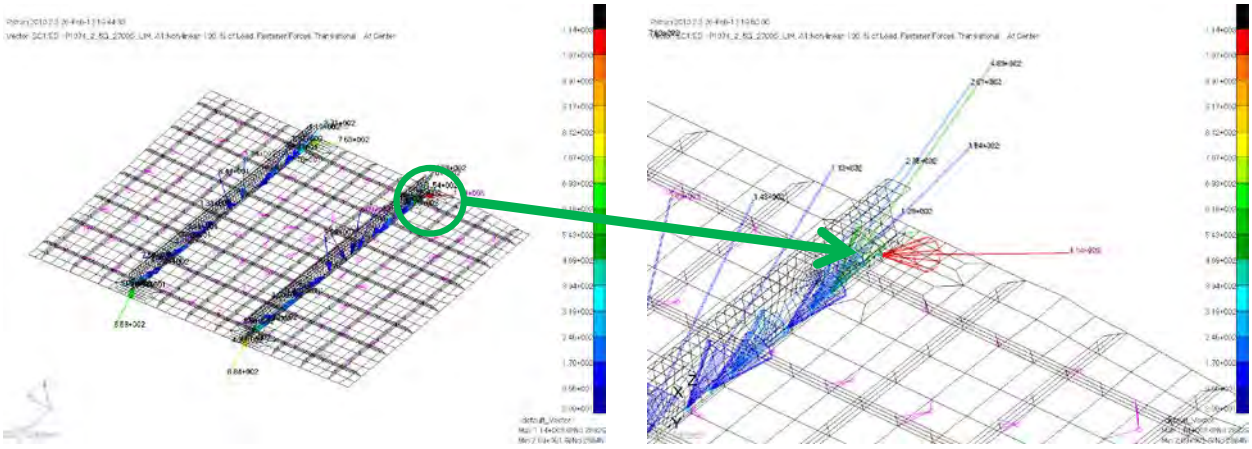

Figure 125 Non-Linear Fastener Forces [lbs] for Panel 4 (1074)

Load Case Mechanical - 2.5g Ultimate (1.5) + Thermal - T=2700s

The last static check performed on Panel 4 (1074) is a buckling analysis. Limit loads are applied to the panel rather than Ultimate loads. There are many local buckling modes that were not considered critical in the preliminary panel design, which however need to be resolved in the detailed part design. Local buckling still allows the panel to carry the overall load of the panel w/o significant change to the global load paths. The first buckling mode that was considered is a mixed local and global buckling mode with an eigenvalue of 0.609. The minimum eigenvalue allowable is 1.0. The buckling Ratio to Requirement (RR) is calculated as follows:

$$RR = \text{Actual/Allowable} = 0.609 / 1.0 = 0.609$$

The plot for the first buckling mode of Panel 4 (1074) is shown in Figure 126.

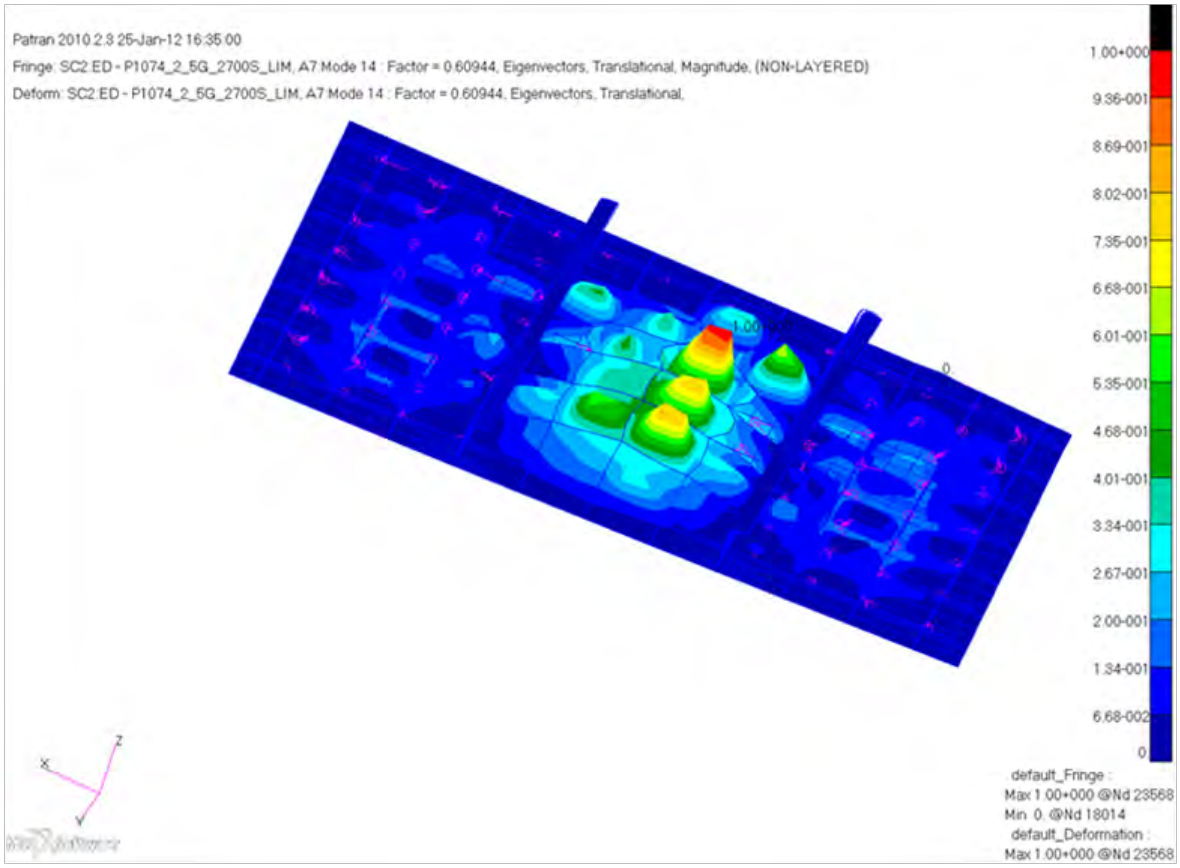

Figure 126 1st Buckling Mode of Panel 4 (1074)

Load Case Mechanical - 2.5g Limit (1.15) + Thermal - T=2700s

In this panel, the addition of the panel breaker stiffeners was effective in the reduction of the deflection of the panel and increase of the buckling eigenvalue. However, the undersizing of the panels still remains an issue that requires additional design iteration. Additionally the temperature at which this panel operates severely limits the load this panel can sustain. Development of more mature allowable for Inconel 718 could provide some marginal relief. The bearing analysis check has adequate margin. A summary of the static margins of safety is in Table 26.

Table 26 Summary of static margins of safety for Panel 4 (1074)

Panel	Location	Failure Mode	Load Case	Allowable @ 70° F	Units	Temp	Units	Knock-down	Allowable @ Temp	Units	Actual	Units	MS/RR
4 (1074)	Panel Center	Deflection	2.5g Ult (1.5) + T=2700s	0.1	ksi	1470	° F	1	0.1	in	0.514	in	-0.81
4 (1074)	Panel Breaker Runout	Material Failure	2.5g Ult (1.5) + T=2700s	180	ksi	1470	° F	0.36	64.8	ksi	88.5	ksi	-0.27
4 (1074)	Panel Breaker/ Panel Intersection	Bearing	2.5g Ult (1.5) + T=2700s	309	ksi	1470	° F	0.36	111.24	ksi	95.2	ksi	0.17
4 (1074)	Panel Center	Buckling	2.5g Lim (1.15) + T=2700s	1		1470	° F	1	1		0.609		0.609

Approved for public release; distribution unlimited.

4.6.4 Panel 4 (1074) Dynamic Analysis

Panel 4 is a lower wing panel that was selected as a candidate to have several potential structural integrity drivers including acoustic fatigue. Static analysis indicated that this panel is driven by thermal load to the point where negative margins were calculated for static loads. The panel was analyzed for aeroacoustic fatigue (AACF) as well as flutter. The table below lists the analyses that were used to evaluate Panel 4 for AACF and flutter.

Table 27. Analyses used for Panel 4 dynamic and fatigue evaluation

Analysis Type	Preload	Load	Boundary Conditions	Output	Solution File(s)
Normal Modes (SOL 103)	None	Thermal (t=900s) Material Property Only	SPC at 5 nodes restricting rigid body motion and global vibration modes	> Normal Modes and Mode Shapes > Provides frequency range of interest for SOL 111	sol103_p1074_unit_cell_t900s_spc103.xdb
Nonlinear Static (SOL 106)	None	Thermal (t=900s) Material + Load	SPC at 5 nodes restricting rigid body motion and global vibration modes	> Non linear stress and displacement > Preload for SOL111 > Stress results used as mean stress in fatigue calculations	panel4_sol106_0131-03_t900s.xdb
Frequency Response (SOL 111)	SOL 106	Thermal (t = 900s) Material Property Only	SPC at 5 nodes restricting rigid body motion and global vibration modes	> RMS stress	panel4_sol106_0131-03_t900s.MASTER panel4_sol106_0131-03_t900s.dball panel4_sol111_0131-06.xdb
Flutter (SOL 145)	None	Thermal (t = 900s) Material Property Only	SPC at 5 nodes restricting rigid body motion and global vibration modes	> Damping and modal frequency vs. velocity	P4UCt_XFlow_Temp900s_15Mds_M5to7_k1_32p5k.dat

For dynamic analysis of the other panel structures a symmetry condition was applied along the boundary of the unit cell to simulate the support from surrounding structure. The way in which the unit cell for Panel 4 is situated presents more of a challenge for creating a similar symmetry boundary condition as the opposite edges are not parallel. An alternate constraint approach was developed for this panel which was effective in restricting unit cell vibration modes while allowing the panel of interest to vibrate. Figure 127 compares the static and dynamic set of single point constraints for the unit cell. There were multiple reasons separate boundary conditions were required for dynamic models. The static boundary conditions proved insufficient at reducing undesired modes of vibration particularly in the substructure. Secondly, the asymmetry of the static boundary conditions caused asymmetry in the vibration modes of panel where there should not have been.

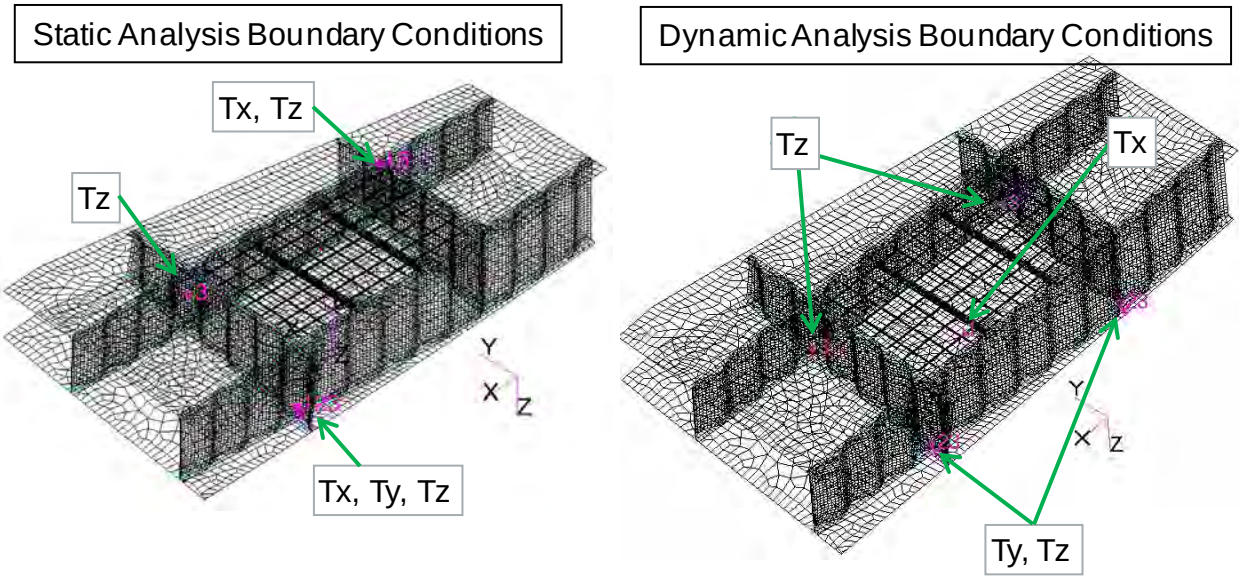

Figure 127. Boundary condition comparison between static and dynamic FEM

Frequency response results for this panel differed from other panels in that the maximum response did not occur near the first vibration mode (74Hz) but instead occurred near 224Hz. Figure 128 and Figure 129 show the displacement and stress PSD response as a function of frequency for Panel 4 results. The RMS Von Mises stress plot indicated only one area of high stress near the panel stiffener termination and the skin to substructure joint.

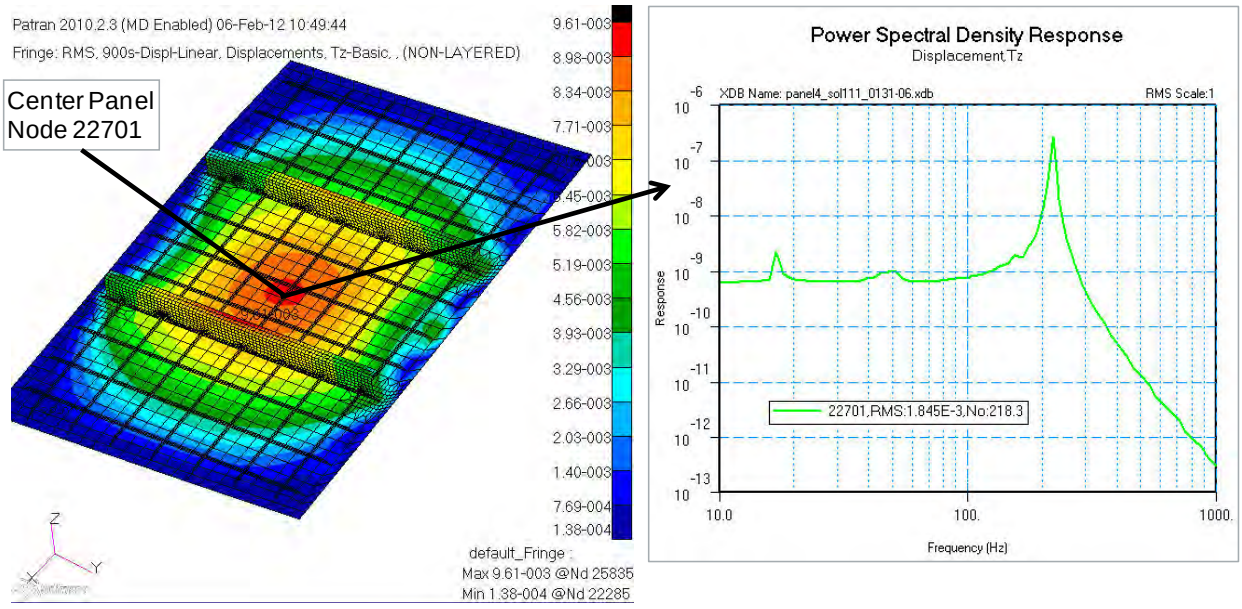

Figure 128. Fringe plot of out of plane RMS displacement and graph of PSD response as a function of frequency for Z displacement (Node 22701)

Approved for public release; distribution unlimited.

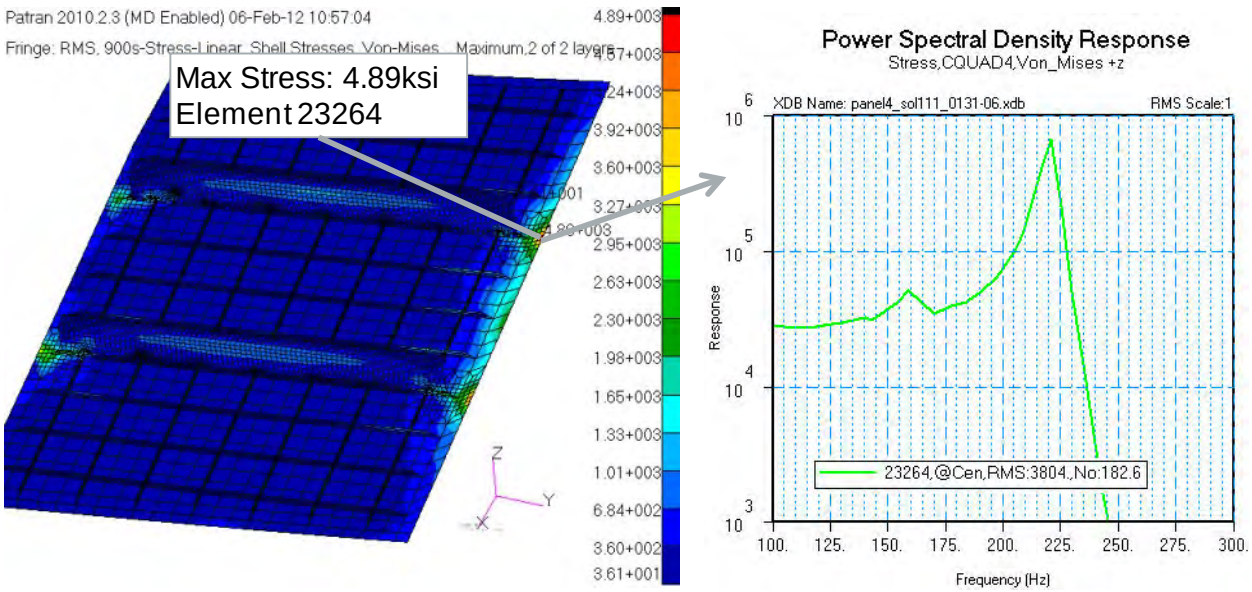

Figure 129. Fringe plot of RMS Von Mises Stress and graph of PSD response as a function of frequency for Von Mises Stress (Element 23364)

It is not clear why the maximum response occurs near 224Hz. The nearest mode shape at 226Hz (Figure 130) indicates large vibrations of the panel stiffeners near the stiffener termination. This could explain the high stress response for that frequency, but it doesn't represent well the displacement response near the center of the panel at the same frequency. If this condition produced a near negative margin of safety, more investigation would be required.

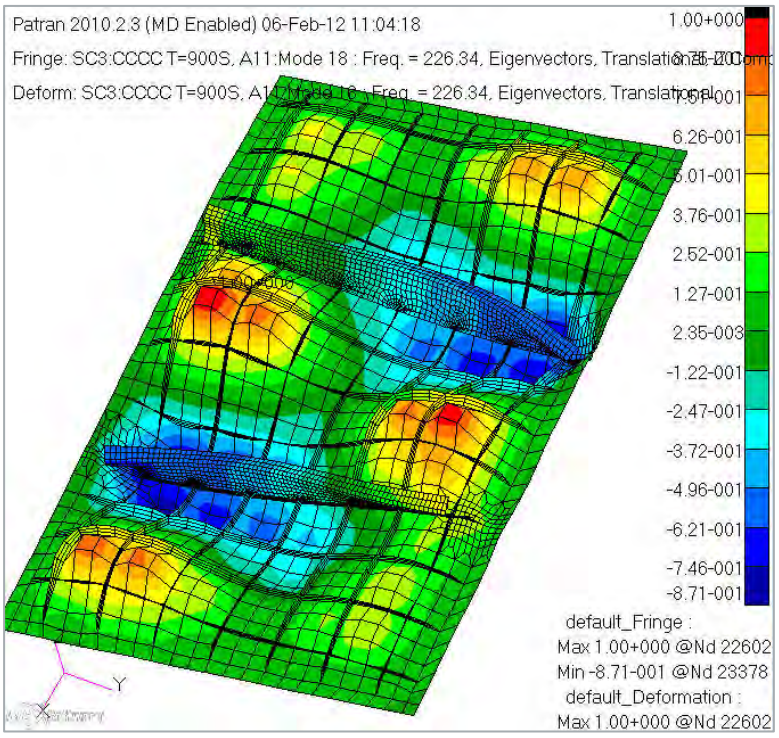

Figure 130. Panel 4 mode shape at 226 Hz from SOL 103

Approved for public release; distribution unlimited.

Panel flutter analysis followed the method used for Panel 3 with employing a first cut check with an empirical based method as well as a FEA approach. Figure 131 shows results for the panel check against the non-dimensional panel flutter design criteria. Panel 4 shows a higher margin above the critical panel curve. In this case the longer aspect ratio makes the panel less likely to flutter. The panel also has a higher first vibration mode (74Hz for panel 4 v. 48Hz for Panel 3) giving it a greater equivalent thickness value.

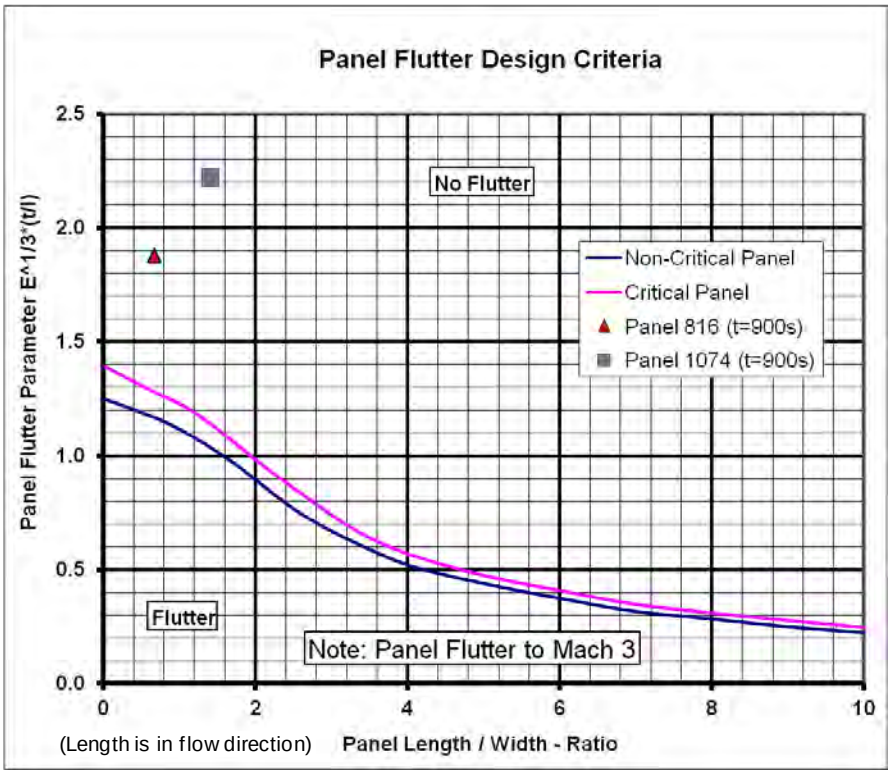

Figure 131. Design curve results for Panel 4 with Panel 3 results shown

The panel flutter FEA used the entire unit cell FEM for the structural model. The extra degrees of freedom (DOF) of the unit cell FEM did not affect run times substantially and saved time by not having to create a separate model for the panel flutter.

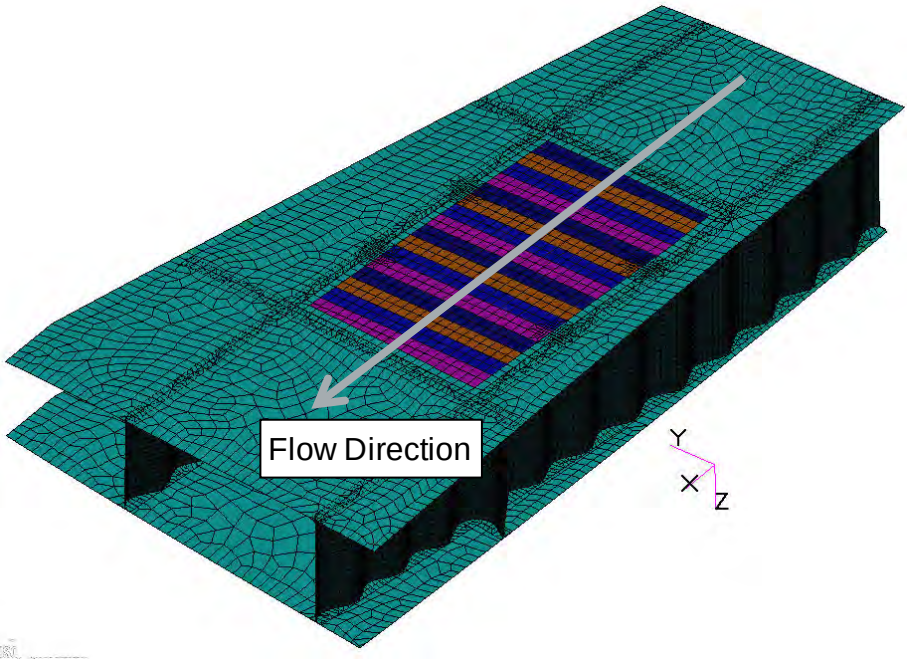

Figure 132. Structural FEM for Panel 4 flutter analysis

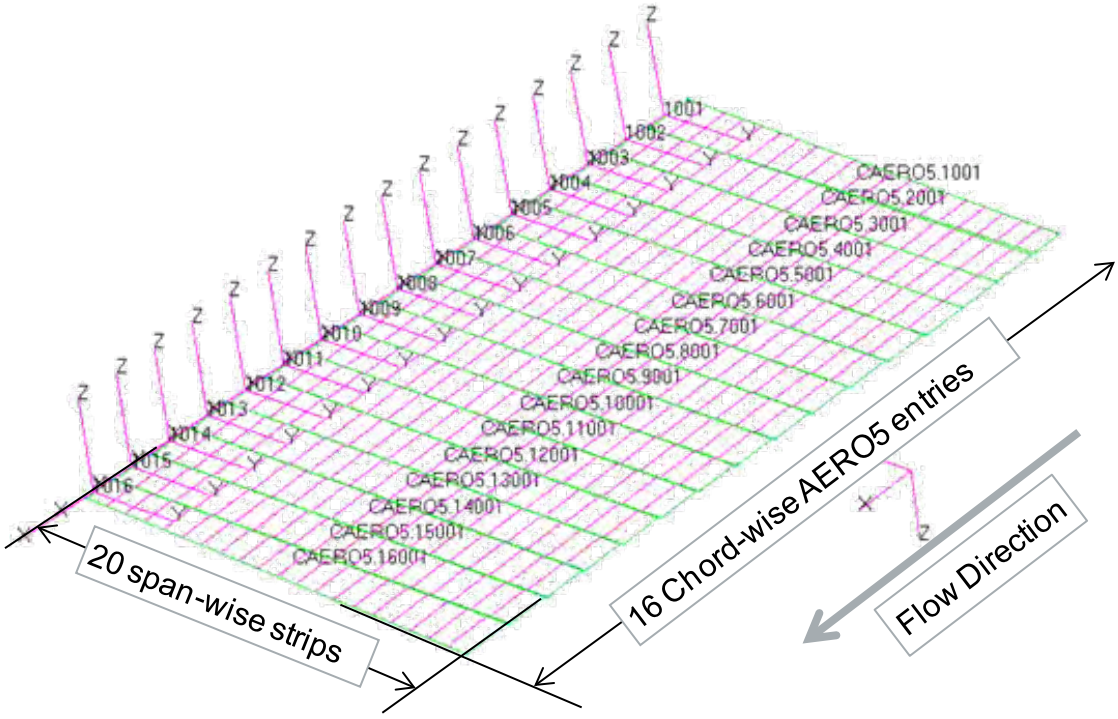

Figure 133. Aerodynamic model for Panel 4 flutter analysis

For Panel 4 the flutter analysis was approached in the same way as Panel 3 where Mach number was held constant at M = 6.25 and the altitude (air density) was adjusted until a panel flutter speed could be approximated. However, for Panel 4 the analysis was run with a SOL 106 preload as well as an angle of attack (AoA) of 6˚. Figure 134 below shows results for Panel 4

Approved for public release; distribution unlimited.

without preload, at an altitude of 32,500 ft, M=6.25, AoA=0deg. The analysis shows that over a range of air velocity from Mach 5 to 7, only Modes 1 and 2 interact to produce instability at a velocity of approximately 4100 knots (Mach 6.20).

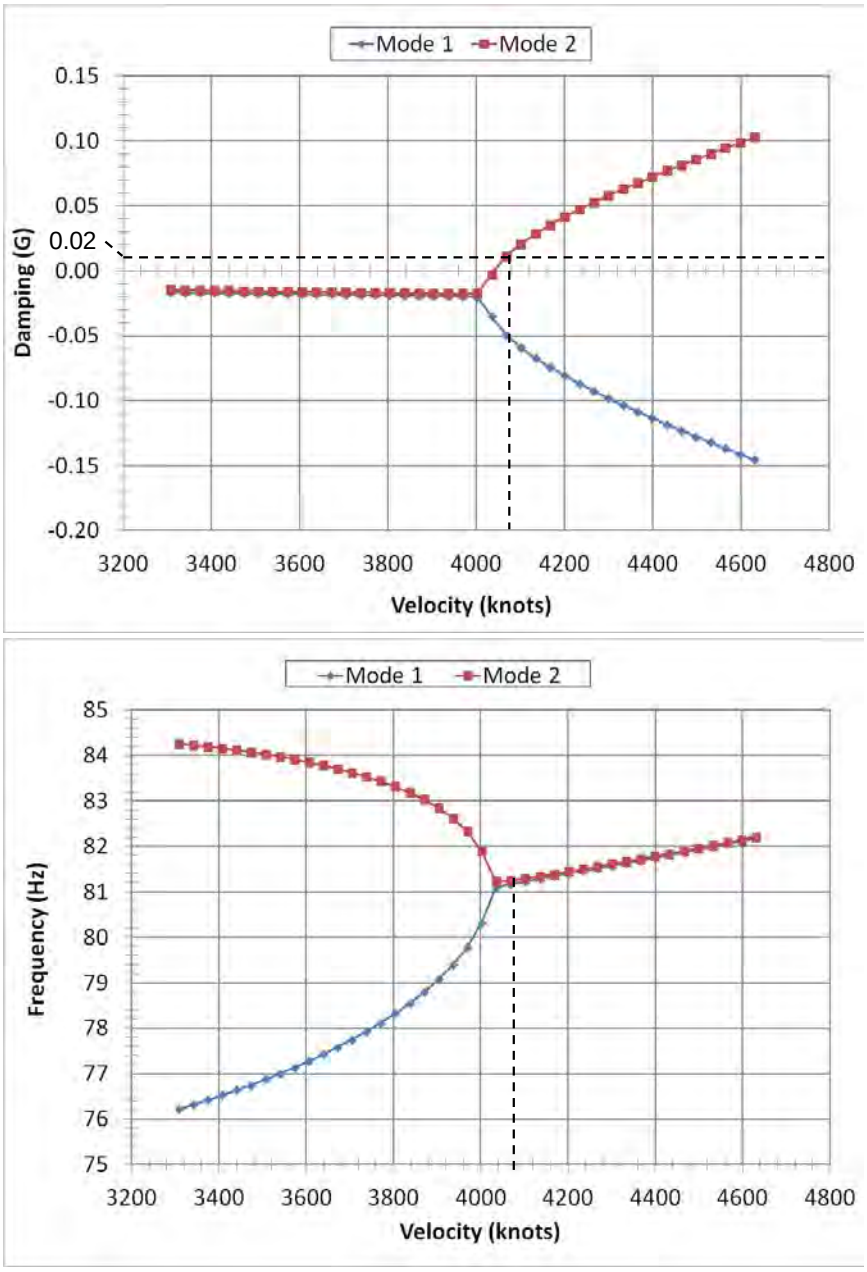

Figure 134. Plots of damping (G) and frequency (ω) as a function of air velocity for vibration modes 1 and 2 (Alt=32.5kft, AoA= 6deg, No Preload)

The table below summarizes the flutter results for Panel 4. The non-linear static preload did not have an effect on the flutter speed. Sea level runs with and without preload yielded the same results. Angle of attack had a moderate effect on flutter speed. Comparing sea level flutter speeds for an AoA of 0deg and an AoA of 6deg, the flutter speed was reduced by approximately

Approved for public release; distribution unlimited.

11% for the 6deg AoA case (from 2448knots to 2183knots). Minimum flutter margin is calculated as 37,000ft for the case with AoA=6.0deg.

Table 28. Summary table for Panel 4 flutter analysis

Preload	Altitude (ft)	Air Density	Solution Mach Number	Velocity Range	Material Properties	Angle of Attack (deg)	Unstable Mode	Frequency (Hz)	Flutter Speed (Knots)	Flutter Speed Mach Number
No	75,000	5.262E-09	6.25	M3 - M14	Temp Adj. (t=900s)	0	None	-----	-----	-----
No	50,000	1.750E-08	6.25	M3 - M14	Temp Adj. (t=900s)	0	Mode 2	81.2	6086	9.2
No	35,000	3.549E-08	6.25	M3 - M14	Temp Adj. (t=900s)	0	Mode 2	81.3	4300	6.5
No	32,500	3.904E-08	6.25	M3 - M14	Temp Adj. (t=900s)	0	Mode 2	81.4	4161	6.3
No	30,000	4.286E-08	6.25	M3 - M14	Temp Adj. (t=900s)	0	Mode 2	81.4	3969	6
No	25,000	5.1338E-08	6.25	M3 - M14	Temp Adj. (t=900s)	0	Mode 2	81.4	3638	5.50
No	Sea Level	1.147E-07	6.25	M3 - M14	Temp Adj. (t=900s)	0	Mode 2	81.4	2448	3.70
No	**32,500**	**3.904E-08**	**6.25**	**M5-M7**	**Temp Adj. (t=900s)**	**0**	**Mode 2**	**81.3**	**4101**	**6.20**
No	50,000	1.750E-08	6.25	M3 - M14	Temp Adj. (t=900s)	6	Mode 2	81.2	5490	8.30
No	40,000	2.8299E-08	6.25	M3 - M14	Temp Adj. (t=900s)	6	Mode 2	81.3	4300	6.50
No	38,500	3.0414E-08	6.25	M5 - M7	Temp Adj. (t=900s)	6	Mode 2	81.3	4167	6.30
No	**38,000**	**3.1154E-08**	**6.25**	**M5 - M7**	**Temp Adj. (t=900s)**	**6**	**Mode 2**	**81.3**	**4101**	**6.20**
No	37,500	3.191E-08	6.25	M3 - M14	Temp Adj. (t=900s)	6	Mode 2	81.2	4101	6.20
No	37,500	3.191E-08	6.25	M5 - M7	Temp Adj. (t=900s)	6	Mode 2	81.3	4035	6.10
No	32,500	3.904E-08	6.25	M3 - M14	Temp Adj. (t=900s)	6	Mode 2	81.2	3638	5.50
No	37,500	3.191E-08	6.25	M3 - M14	Temp Adj. (t=900s)	6	Mode 2	81.2	4101	6.20
Yes	Sea Level	1.147E-07	6.25	M3 - M14	Temp Adj. (t=900s)	0	Mode 2	81.4	2448	3.70
Yes	Sea Level	1.147E-07	6.25	M3 - M14	Temp Adj. (t=900s)	6	Mode 2	81.4	2183	3.30

It was expected that a preload would have an effect on the behavior of the panel. The same method was used for flutter as was used for frequency response. The method for applying a preload to a flutter solution needs further study.

4.6.5 Panel 4 (1074) Fatigue Margin Evaluation

Fatigue margins for Panel 4 were written only for aeroacoustic fatigue (AACF). Since static analysis determined that Panel 4 produced negative margins due to thermal load, it was decided

not to evaluate the panel in thermal-mechanical fatigue (TMF). Panel 4 is governed by the extreme temperatures with a maximum panel temperature of 1480˚F causing a reduction in stress allowables to approximately 35% of the room temperature values. The severe reduction in allowable stress produces negative margins against linear static stress.

RMS stress results indicate the only areas of high stress are near the panel stiffener termination points. The RMS stress results are generated by MSC Random from the frequency response solution and the PSD developed for Panel 4. The margin of safety for AACF is positive but is less than what was found for Panels 2 and 3. This is mostly due to the strength knockdown due to the extreme temperatures. Figure 135 gives the location of maximum stress as well as the margin of safety calculations for this panel. The negative static fatigue margins also produce negative sonic fatigue margins as well.

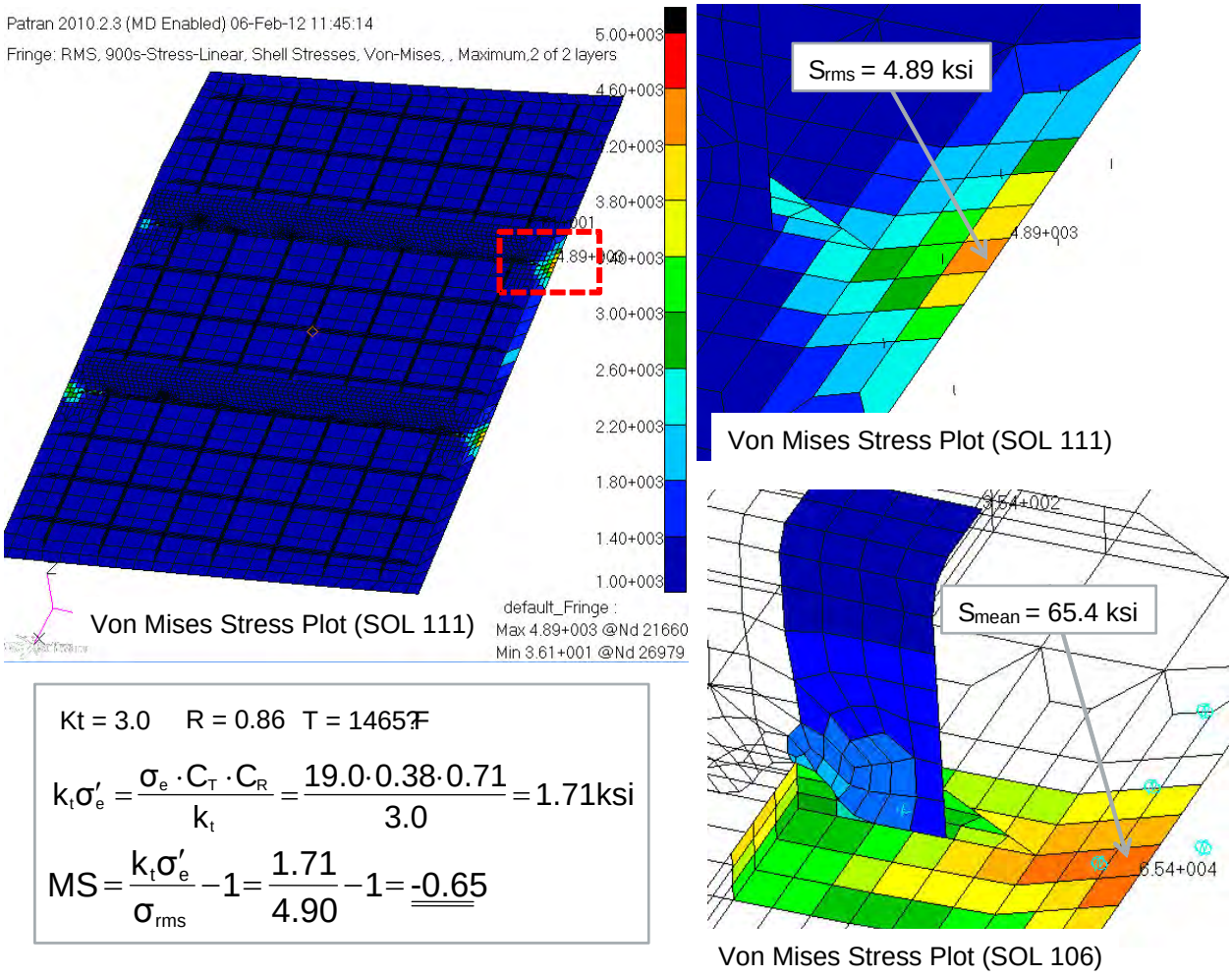

Kt = 3.0 R = 0.86 T = 1465?F

$$k_t\sigma'_e = \frac{\sigma_e \cdot C_T \cdot C_R}{k_t} = \frac{19.0 \cdot 0.38 \cdot 0.71}{3.0} = 1.71 ksi$$

$$MS = \frac{k_t\sigma'_e}{\sigma_{rms}} - 1 = \frac{1.71}{4.90} - 1 = \underline{\underline{-0.65}}$$

Figure 135. Plots of Max RMS stress and mean stress (thermal) and MS calculation for Panel 4

Approved for public release; distribution unlimited.

4.7 Identified Detailed Design Process Limitations and Lessons Learned

Key findings, process limitations and lessons learned identified in this task, and their associations with knowledge gaps identified in the Phase I report (Appendix 1) [2], as well as in Section 7.1 of this report, are summarized as follows:

1. **Ability to iterate quickly to design for thermal loads**

   Phase I Gap Association: Gap 5
   When deciding on a substructure or panel concept to reduce thermal loads, a better method is needed to quickly iterate these designs and evaluate their effectiveness. Much effort was spent on time consuming full detailed analyses in order to evaluate a concepts response to sustain thermal loads.

2. **Better estimation of thermal loads in initial sizing**

   Phase I Gap Association: Gap 5
   The main driver for this study is thermal loading; unfortunately thermal loading is the most uncertain portion of this study. Initial estimates for thermal loading proved to be insufficient to mature in detailed design. While it is possible to perform an additional design iteration after the detailed design and analysis reveals the need, this process is highly time consuming and inefficient. A method is required to quickly iterate the thermal load which includes all relevant boundary conditions before detailed design and analysis. Additionally, rules of thumb for thermal boundary conditions and cell dimensions and their relation to thermal loads would be extremely useful.

3. **Better definition of deflection criteria**

   Phase I Gap Association: Not Identified in Phase I; New Gap 11
   Since these analyses all deal with thermal conditions causing significant thermal growth at the Mach speed of this vehicle's flight profile, panel deflection has proven to be a design concern for each panel. The deflection criteria developed for this study is driving negative margins of safety for all panels. Before extensive effort can be spent to resolve these negative margins, the deflection requirement should be further investigated for relaxation and maturation.

4. **A simpler, more transparent way to transfer global vehicle loads to the unit cell and correlate back to the global vehicle**

   Phase I Gap Association: Gap 4
   As a product of how the loads are applied to the global vehicle model, loaded at every node, the application of global vehicle loads to the unit cell is very complicated. Additionally, once the loads are applied, it is difficult to decipher the overall direction and magnitude of the applied loads. This makes interpreting and verifying results difficult.

5. **Additional material test data, or analytical methods for estimating allowables, at design points of interest (temperature, R-ratios, kt factors, and cycles)**

   Phase I Gap Association: Gap 7
   The tabulated allowables for the design points incurred in both static and dynamic analysis are limited. Often, design allowables are developed by combining separate factors to represent the specific situation. While this may be acceptable, the actual interaction of these factors may be different from the basic linear superposition used. Although an actual empirical value for the specific condition would be the most reliable, an analytical method based on the micro-mechanics of the material would be a significant improvement.

6. **Separate the panel connectivity in the unit cell**

   Phase I Gap Association: Not a Gap; Analysis Lesson Learned
   In the global vehicle model, the vehicle skin is model as a continuous surface per common analysis best practice. However, in actual practice, separate panels will be manufactured and fastened to the substructure. The unit cell includes these fasteners and should also have separated panel surfaces thereby transferring all loads from the panels into the substructure, with no direct load transfer between panels.

7. **Panel temperatures should be limited to prevent excessive strength loss**

   Phase I Gap Association: Not a Gap; Design Lesson Learned
   In the case of Panel 4 (1074), the static material allowable is knocked down to a third of its allowable at its operating temperature. Even at stresses that are comparable to the other panels, Panel 4 has negative margins of safety for ultimate material failure. This constraint creates an issue where either the stresses need to be lowered or the operating temperature needs to be lowered. Max panel use temperatures should be limited to above the "knee in the curve" of the strength vs temperature graph. For example, a limit of 1250°F for Inconel 718 would help ensure robust allowables. Such a max temperature constraint would dictate a different material or design approach, such as parasitic TPS, would need to be used for this class of Mach 7 cruise vehicle.

8. **Prior experience designing panels with aluminum and titanium alloys does not directly apply to higher density nickel alloy panels.**

   Phase I Gap Association: Not a Gap; Design Lesson Learned
   Nickel alloy panels were chosen for this study due to their capability to sustain high temperatures. However, design concepts used previously for aluminum and titanium perform poorly due to the higher density and CTE of Inconel. Additionally, rules of thumb for design and manufacturing used for aluminum and titanium do not apply to nickel alloys. Testing is required to determine minimum gages for machining as well as optimum machining, forming and welding parameters.

5.0 VERIFICATION STUDIES

The objective of this task is to verify the knowledge gaps of current design analysis methods based on linear frequency response analysis in tackling thermal-acoustic fatigue problems in extreme environment. The approach is to compare analysis results of a panel with two different methods, i.e., the linear frequency response and nonlinear explicit transient dynamic analyses with un-deformed (excluding elastic effect) thermal and acoustic loads.

In order to show the impact of thermal loads to response, two analysis conditions were defined, one with temperature-dependent material properties and thermal loads for the structure, and another one with temperature-dependent materials only. The temperature-dependent-material-only case was used to compare directly with that of linear response analysis. The thermal loads cases will reveal the impact of the loads to response.

5.1 Panel Modeling and Validation

The analysis region was is the upper center panel of Panel 1 (862), which is part of a unit-cell structure of the vehicle, shown in Figure 136. The panel and surrounding panels are of an ortho-grid construction. Details of Panel 1 design can be found in Section 4.34.2.2 . The panel was analyzed for the maximum dynamic pressure condition (Q=2000psf) with maneuver loads (Lf=2.5g) in combination with thermal loads at 1,080 sec in a flight trajectory. However, combining worst flight and mechanical loads with worst case thermal loads at different trajectory points is overly conservative (Finding 1).

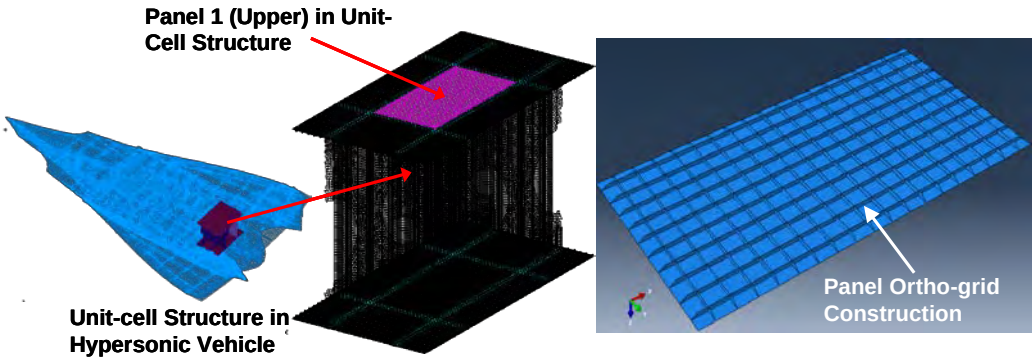

Figure 136. Panel location and construction for explicit dynamic analysis

Since the ortho-grid panels are more flexible than the original honeycomb design in the vehicle model, the internal loads transferred from the vehicle result in excessive large deflection and unrealistic high stresses in some locations of unit-cell structure that prevent a nonlinear dynamic analysis from being conducted. (Finding 2: Design iteration between panel and vehicle models to render the stiffness of local/panel design consistent to the vehicle model is important in the design process.) In addition, the geometry of the panel shown in Figure 136 contains no fastener that attaches the surface panel to sub-structure. (Finding 3: Critical thermal-mechanical-

fatigue/crack initiation locations utilize special tools such as Boeing Lifeworks to predict life/stress.)

The thermal/mechanical analysis model of Panel 1 is modified to enable the explicit dynamic analysis by reducing the number of elements through stiffener web height from 5 to 3 elements. This mesh modification increases the stable time step size by 40% in explicit analysis and hence reduces the computational effort. The validation of the modified model was made by comparing modal frequencies with the panel in unit cell model, which reveals a maximum difference of 1.2% for the 1st nine modes.

In the explicit dynamic analysis, the temperature distribution at t=1,080sec, illustrated in Figure 137, is used for thermal loads and temperature-dependent materials. The displacements from the unit-cell analysis with thermal loads along the edges of panel were extracted and imposed on the modified model prior to the explicit dynamic analysis. The displacements include deflections and rotations at panel edges, which cause a minor asymmetry of the panel.

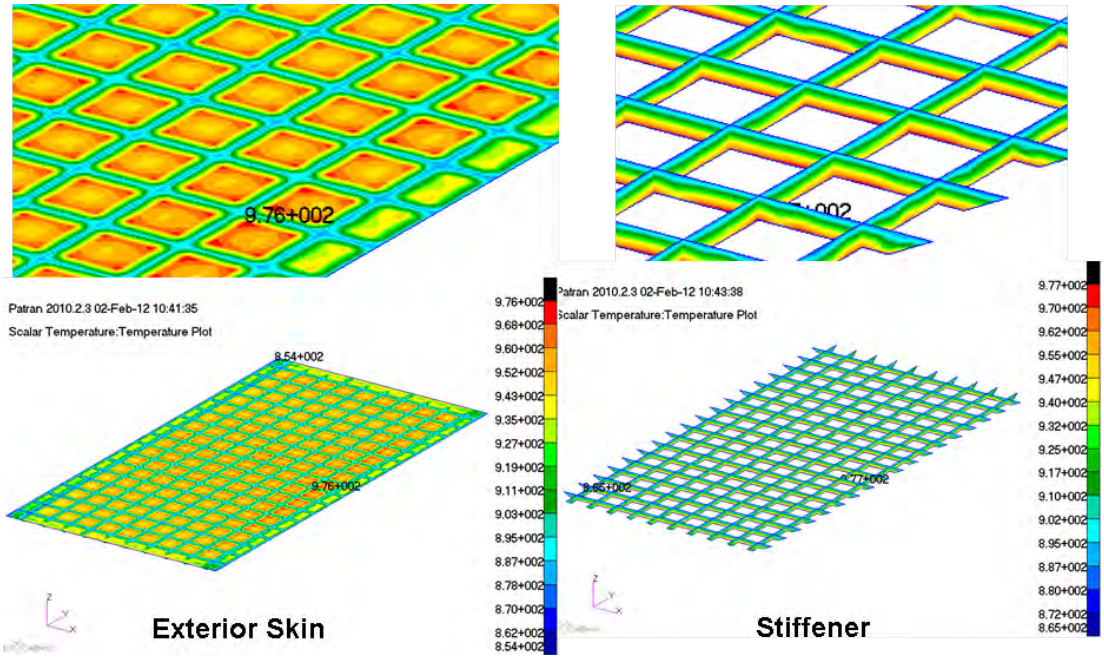

Figure 137. Temperature distribution at t=1,080 sec on Panel 1

5.2 Panel Boundary Conditions and Vibration Analysis

The boundary conditions (BC) that simulates energy transmission or elastic wave propagation between the center panel and surrounding structures, including neighboring panels, keels and frames, is difficult to define. An engineering approach has been adopted by using two different boundary conditions to bound the extent of the compliance of the unit cell structure: (1) a fully restrained or fixed one; and (2) a hinged (pinned) one, for this study. It is expected that unit cell structural panel response will be enveloped by that of the two BC. (Finding 4: Design is

Approved for public release; distribution unlimited.

generally evaluated by results approximated with the two BC.) Modal analysis was performed for the panel with two different BC to study their effects to dynamic response. Figure 138 to Figure 141 show the first 12 vibration modes of the panel.

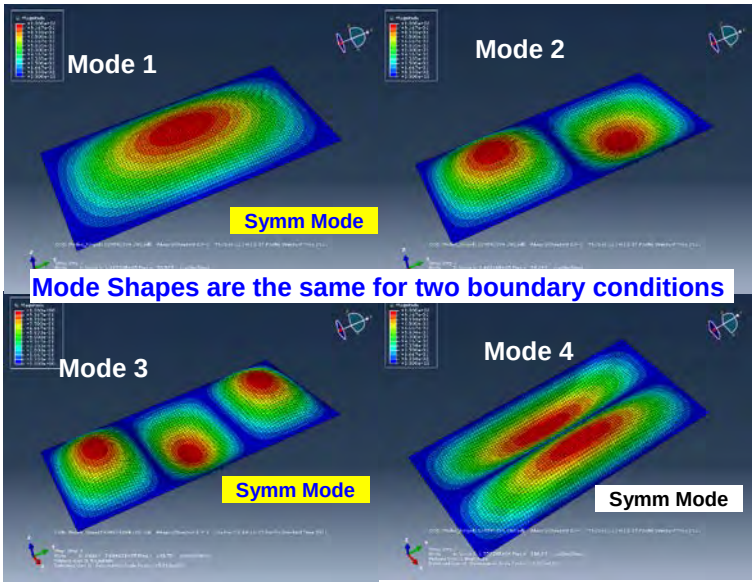

Figure 138. Modes 1 thru 4 of Panel 1

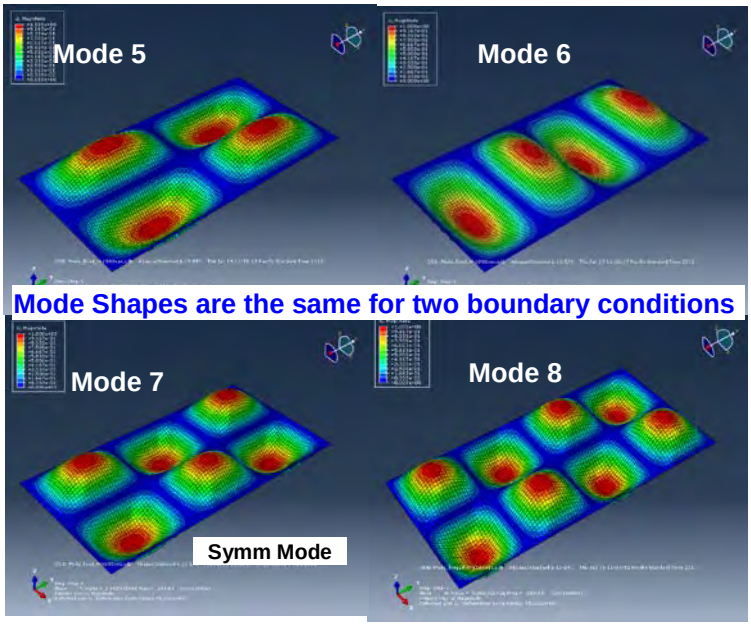

Figure 139. Modes 5 thru 8 for Panel 1

Approved for public release; distribution unlimited.

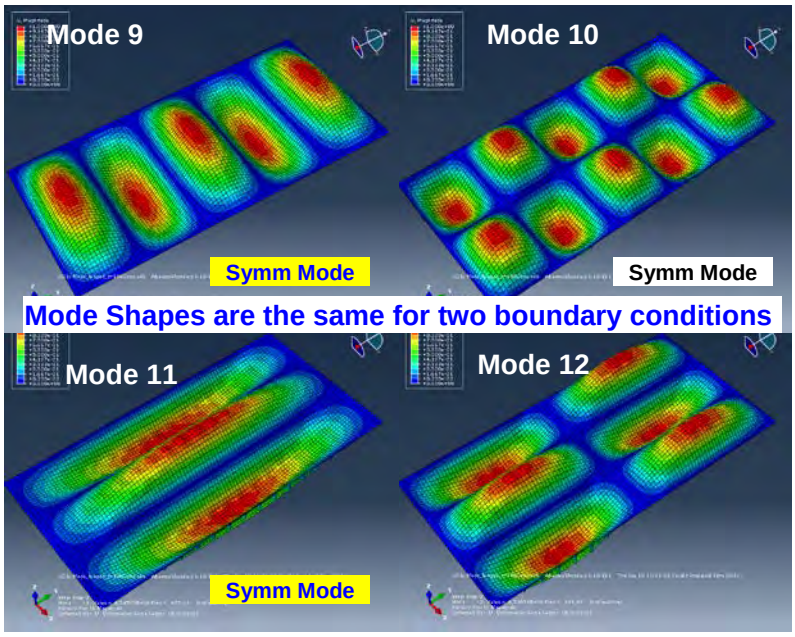

Figure 141. Modes 9 thru 12 of Panel 1

The mode shapes of the two BC cases are identical, and symmetric modes with respect to the centerline of short panel direction are identified in Figure 138 to Figure 141. The ones symmetric in both short and long directions are highlighted in yellow. In addition, the first three mode shapes compare well between the Abaqus panel model and Nastran unit-cell model in Figure 142.

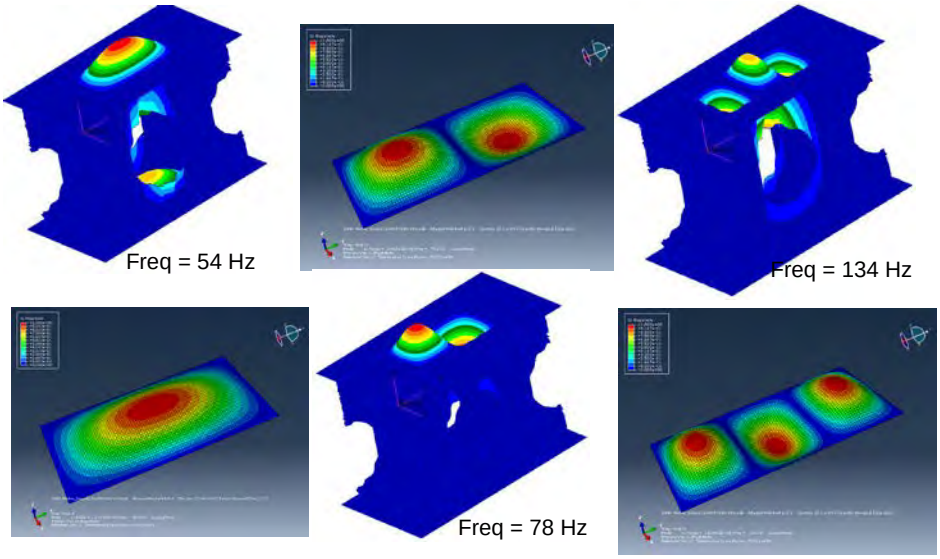

Figure 142. Comparison of first three modes between Panel 1 and unit-cell models

The modal frequencies for the two BC at room temperature and elevated temperature at t=1,080sec, used to adjust the material properties, are listed in Table 29.

Table 29 Comparison of modal frequencies for different boundary conditions

Mode No.	Hinged (Hz, T=75o)	Hinged (Hz, t=1080sec)	Fixed (Hz, T=75o)	Fixed (Hz, t=1080sec)	Linear Response w/ Unit-cell (t=1080sec)
1 (symm)	55.5	51.7	72.1	67.4	54
2	79.2	73.9	96.8	90.4	78
3 (symm)	138.7	129.5	155.4	145.1	134
4	198.2	184.9	220.7	205.9	
5	209.5	195.4	232.8	217.2	
6	229.5	214.1	245.9	229.5	
7	244.0	227.6	267.4	249.6	
8	310.1	289.4	333.0	310.8	
9 (symm)	347.9	324.7	364.4	340.1	
10 (symm)	409.1	381.7	431.3	402.5	
11	436.5	407.1	463.5	432.4	
12	441.6	411.9	469.4	437.9	

It can be seen from Columns 3, 5 and 6 that the frequencies of first three modes of the unit-cell model are enclosed by that of hinged and fixed BC. The stiffness softening by materials is shown by comparing with the modal frequencies at room temperature. In addition, the fundamental frequency of the panel is relatively low, i.e., 51.7 Hz for hinged BC and 67.4 Hz for fixed BC at temperature of 1,080sec in the flight.

5.3 Damping of Structure

Table 30 illustrates the critical damping ratios used for linear response analysis for frequencies ranging from 10 to 1000Hz. The damping is adopted for this study. The alpha and beta coefficients in the Rayleigh damping matrix shown in Eq. 3.1 are determined by Eq. 3.2 for explicit dynamic analysis.

Table 30. Damping ratios for different frequency ranges

Frequency (Hz)	Damping Ratio
10	0.025
100	0.02
1000	0.01

$$\mathbf{C} = \alpha\mathbf{M} + \beta\mathbf{K} \tag{3.1}$$

$$\xi_n = \frac{1}{2}\left(\frac{\alpha}{\omega_n} + \beta\omega_n\right) \tag{3.2}$$

M, **C** and **K** are mass, viscous damping and stiffness matrices of the panel. α and β are coefficients determined by damping ratio ξ_n and frequency ω_n of selected modes.

However, including the β term or stiffness-proportional damping will significantly reduce the stable time increment. For example, the time step size for the panel will get smaller by a factor of 50, which translates into 50 times more computation. The β term is therefore excluded from Eq. 3.1. Moreover, use of the α or mass-proportional term only will noticeably under-damp higher frequency modes, as shown in Figure 143. For example, using the first mode to compute α for the case of hinged BC will result in the damping ratio for the 2nd mode being reduced from 2.14%, interpolated from the damping in Table 30, to 1.59%, and for the 3rd mode reduced from 1.97% to .91%.

Since the responses of panel are dominated by the lower frequency modes, e.g., first three modes, the effect of under-damping are not considered significant. (Finding 5: a high computation requirement and approximation of viscous damping with the α term only dissuade the use of more advanced analysis methods, e.g., explicit dynamic analysis, for panel design.)

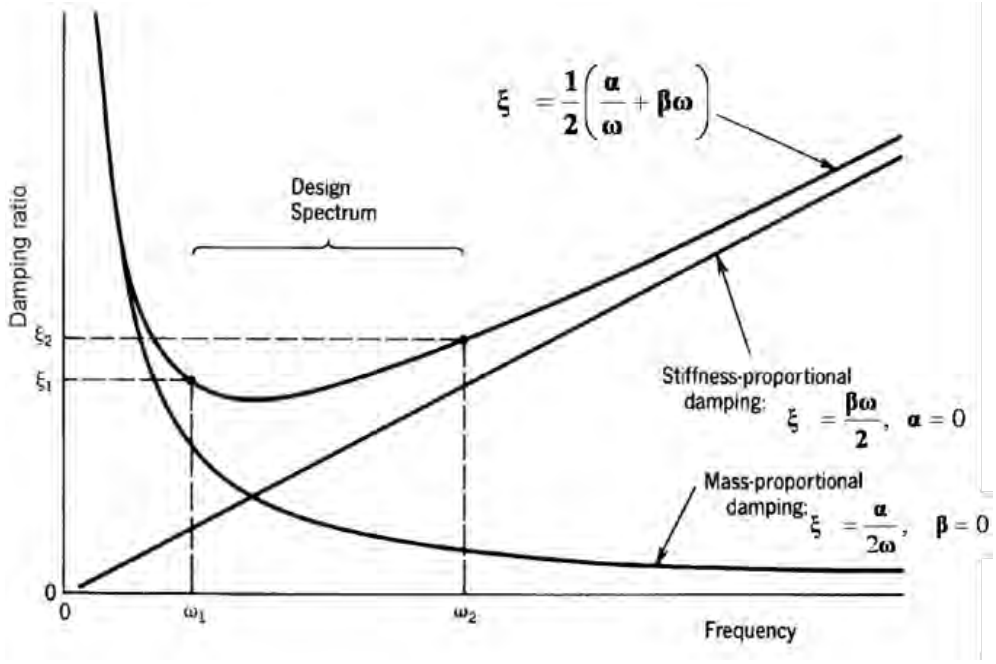

Figure 143. Rayleigh damping for transient dynamic analysis

Approved for public release; distribution unlimited.

Moreover, Coefficient α is different for two boundary condition cases. It is 18.5 for the hinged BC and 14.8 for the fixed BC.

5.4 Dynamic Explicit Analysis

The dynamic explicit analysis includes temperature-dependent materials, thermal loads, time varying acoustic pressure, and large deformation. However, the coupling effect between acoustic, thermal and elasticity cannot be addressed (Finding 6). In addition, no static aeroelastic loads are included since defining the loads consistent with the time of thermal loads is difficult. The effect of steady state aero loads to this panel is however minor compared to thermal loads. Since there will only be a short-time simulation, the variation of thermal loads is insignificant and the loads are treated as constant.

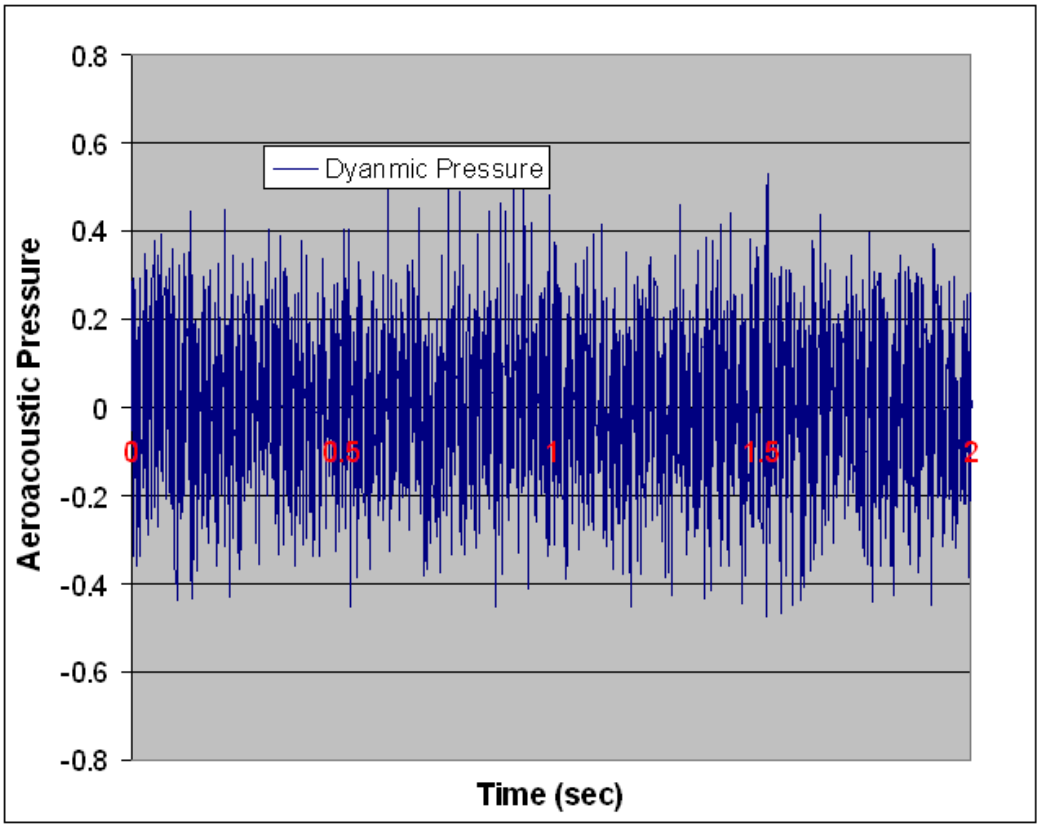

Figure 144. Time history of acoustic pressure

The study focuses on investigating the effects of thermal loads (or preload), geometrical nonlinearity, and boundary conditions to thermal-acoustic response with the goal to quantify the gaps of current analysis methods. The analysis started with a quasi-dynamic analysis step by imposing displacements from the unit-cell analysis and thermal loads to the panel. The analysis step with a time period of 0.1 sec is to establish the initial conditions by ramping up thermal

loads and displacements to minimize the impact of inertia of panel (Finding 7). Then, 2-second time history simulation of panel is conducted with acoustic pressure.

The analysis includes oscillation of acoustic pressure (Figure 144) generated by separated turbulent boundary spectrum, Figure 145, at trajectory point of 1,080 sec. This condition is at the end of vehicle accent or transition from maximum Q (aerodynamic pressure) to maximum T (temperature) conditions. The acoustic pressure is applied uniformly and normal to the panel surface. No coupling effect of the panel dynamics to these pressure loads is accounted for.

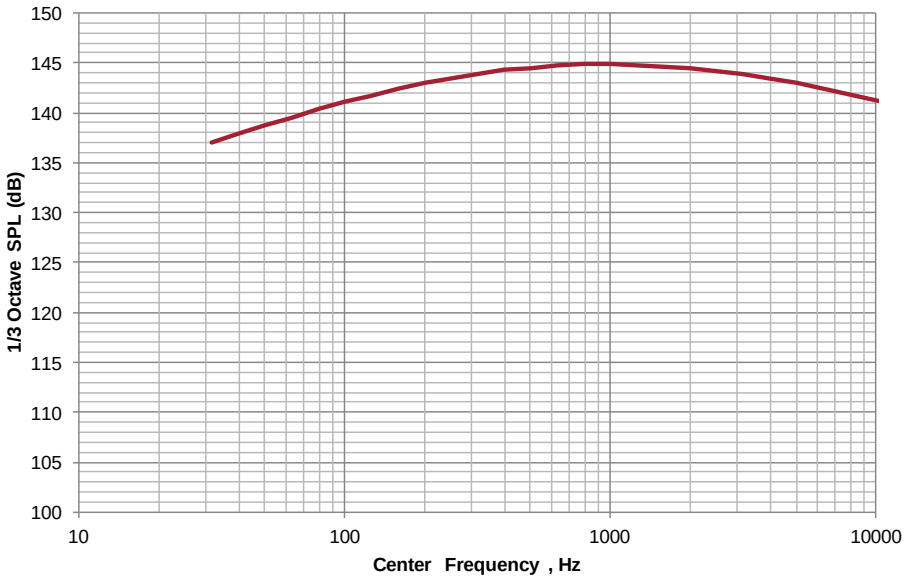

Figure 145. Separated Turbulent Boundary Spectrum

To validate the initial conditions, the results of quasi-dynamic analysis of the panel are compared with the static analysis with thermal loads and imposed boundary displacements. For the case of fixed BC, both translational and rotational displacements from the unit-cell analysis are imposed to the panel boundaries. Only translational displacements are enforced on the boundaries for hinged BC. Figure 146 to Figure 148 show good comparisons of total displacement, normal displacement and Von Mises stress for the panel with hinged BC, in which the difference for maximum normal displacement between static and quasi-dynamic analyses is about 4.5% and that for stress is 0.2%. However, the comparisons for panel with fixed BC are not impressive. The difference for maximum normal displacement between two analyses is about 19% and that for stress is more acceptable at 4.5%. The large deviation of normal displacements for fixed BC may be reduced by increasing the 0.1-sec initial simulation time step to further alleviate the inertia effect and stabilize the solution.

Approved for public release; distribution unlimited.

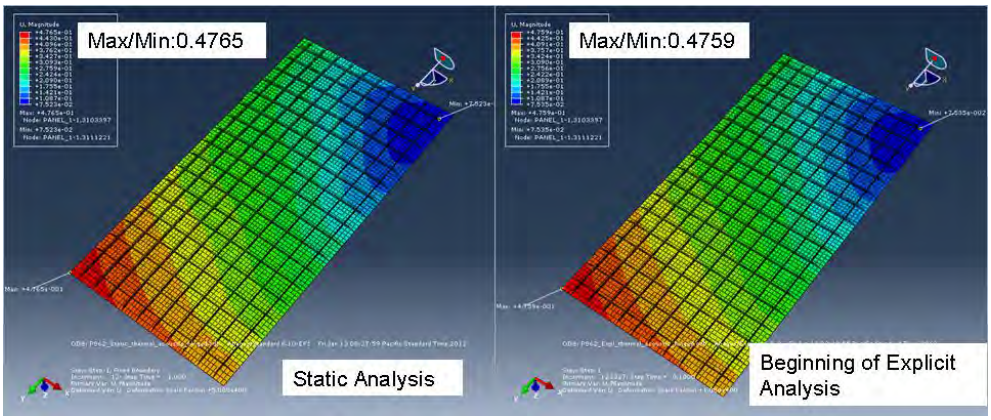

Figure 146. Comparison of total displacements for static and quasi-dynamic cases with hinged BC and thermal loads

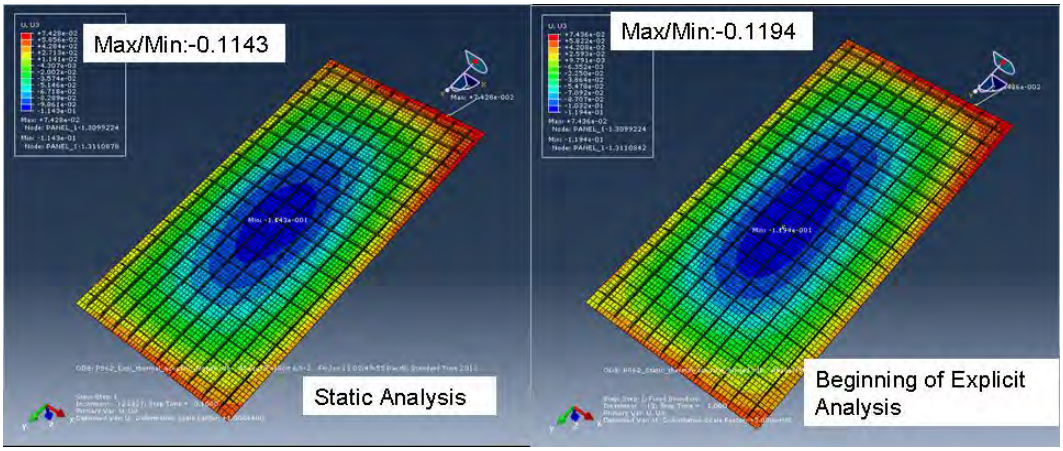

Figure 147. Comparison of Normal Displacements for Static and Quasi-dynamic Cases with Hinged BC and Thermal Loads

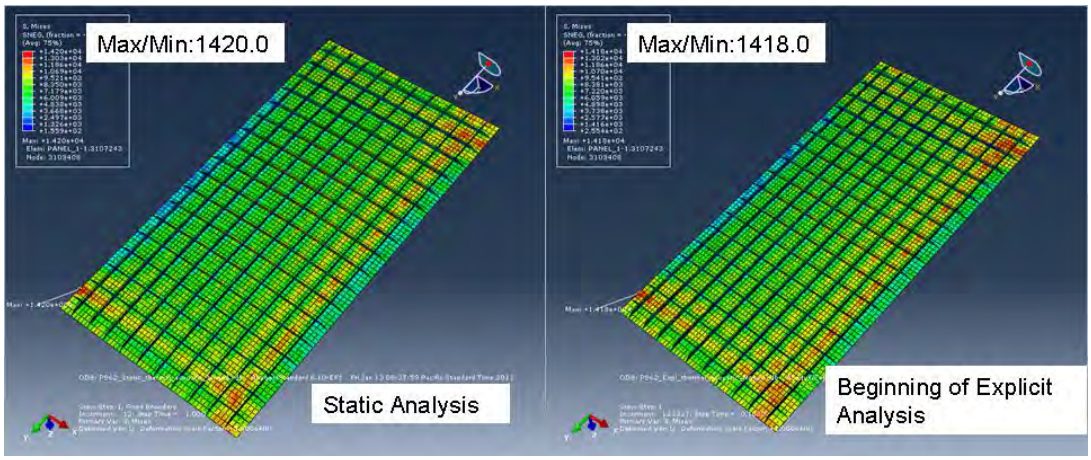

Figure 148. Comparison of von Mises stress for static and quasi-dynamic cases with hinged BC and thermal loads

The Max principal stresses induced by thermal loads are shown in Figure 149, which indicates that the panel skin is in compression and the stiffener webs are in tension. The stresses altered the stiffness and the vibration characteristics of panel.

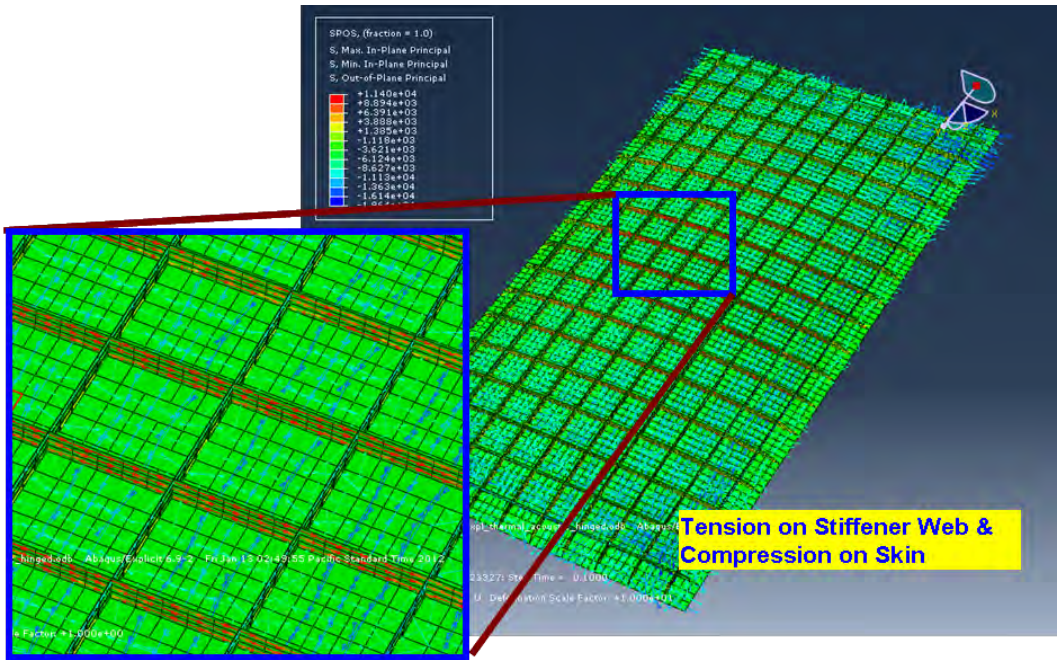

Figure 149. Max principal stresses in panel due to thermal loads with hinged BC

Four analysis cases with different boundary conditions (BC) and thermal load considerations were conducted. These are listed below:

1. Fixed BC without thermal loads
2. Fixed BC with thermal loads
3. Hinged BC without thermal loads
4. Hinged BC with thermal loads

The cases without thermal loads are used to compare with the linear frequency response analysis in Task 2, which did not include thermal loads. The cases with thermal loads focus on the thermal-acoustic response. All analysis cases contain temperature-dependent material properties. For the cases without thermal loads, zero thermal expansion coefficients were used in structure for analysis.

A few sample locations were selected to monitor the time history response of panel. Figure 150 shows the node and element locations and their corresponding identification number (ID), in which time histories of displacements at node and stresses in element are output.

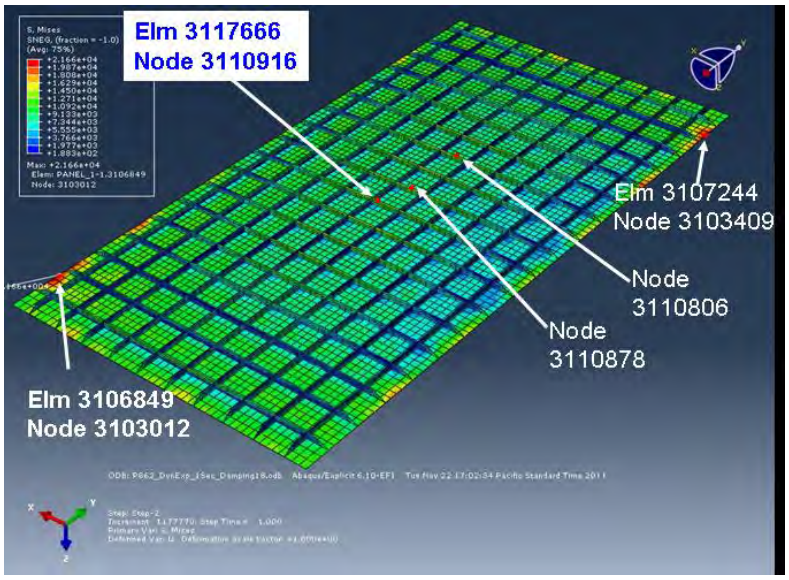

Figure 150. Node and element locations for time history results

5.4.1 Panel Response of Hinged Boundary Conditions

To illustrate the dynamic analysis results, the snapshots of normal displacements of panel with hinged BC and with thermal loads at different time steps are included in Figure 151 to Figure 153. The figures show the asymmetric response of panel, e.g., at t=0.2s, 0.8s, 1.0s etc., which is caused by thermal loads and associated boundary displacements from the unit-cell analysis. The normal displacement at t=1.9s indicates the reverse of displacement, i.e., dynamic displacement exceeding the initial displacement due to thermal loads, at the panel center, which is however not a snap-through of panel.

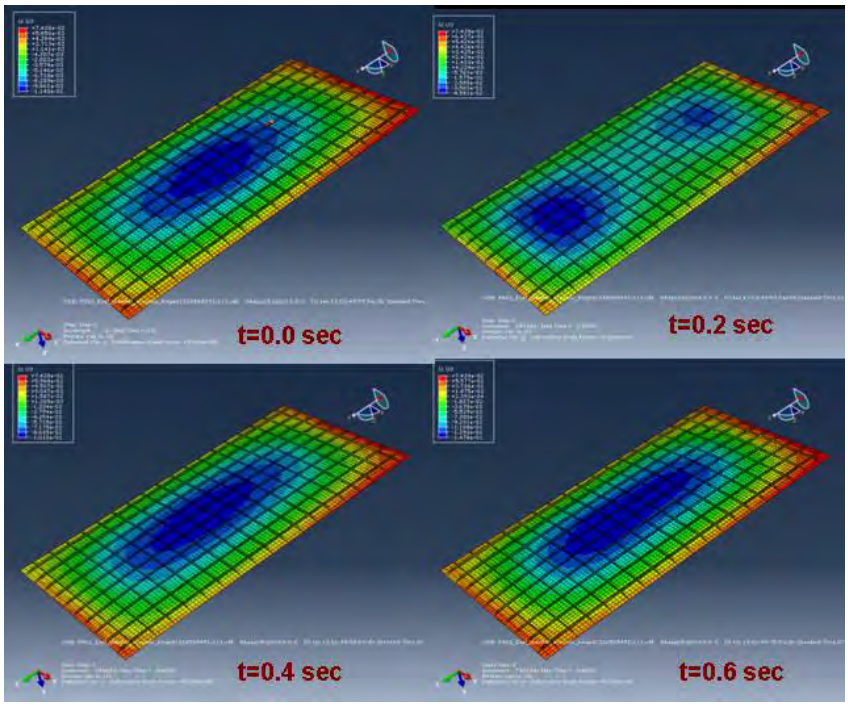

Figure 151. Snapshots of normal displacements (t=0.0 to 0.6sec) of panel with hinged BC and thermal loads

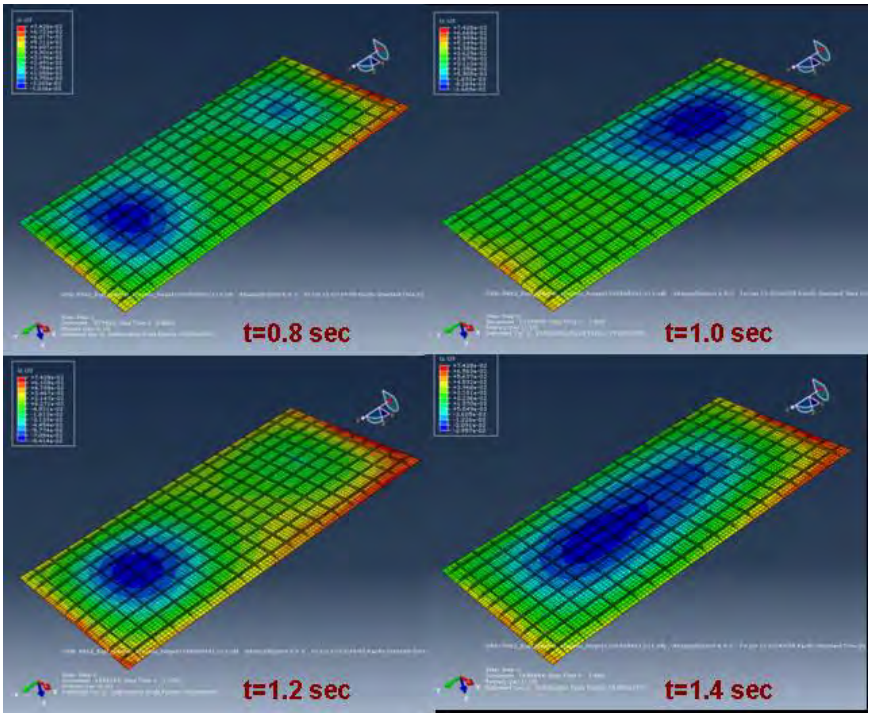

Figure 152. Snapshots of normal displacements (t=0.8 to 1.4sec) of panel with hinged BC and thermal loads

Approved for public release; distribution unlimited.

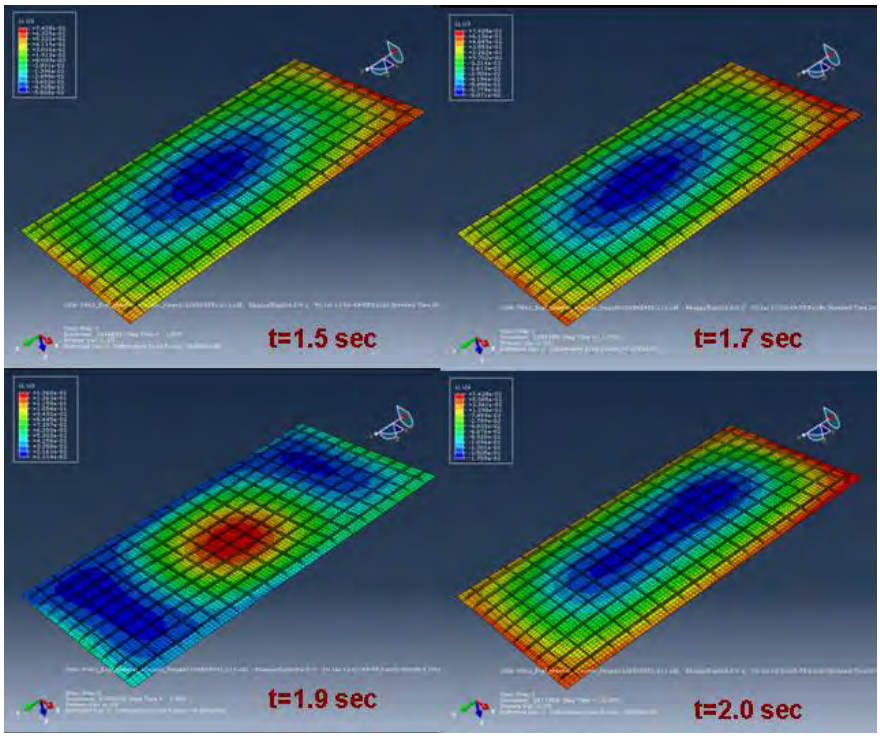

Figure 153. Snapshots of normal displacements (t=1.5 to 2.0sec) of panel with hinged BC and thermal loads

The time histories of Node ID of 3110916 on stiffener web near the panel center without and with thermal loads are shown in Figure 154. Besides the difference of initial displacement between two cases, the response characteristics are different. This will be discussed with their corresponding power spectral density (PSD) in the next section. The stress time histories for Element ID of 3117666, on the stiffener web and close to the panel center, are shown in Figure 155 for cases without and with thermal loads.

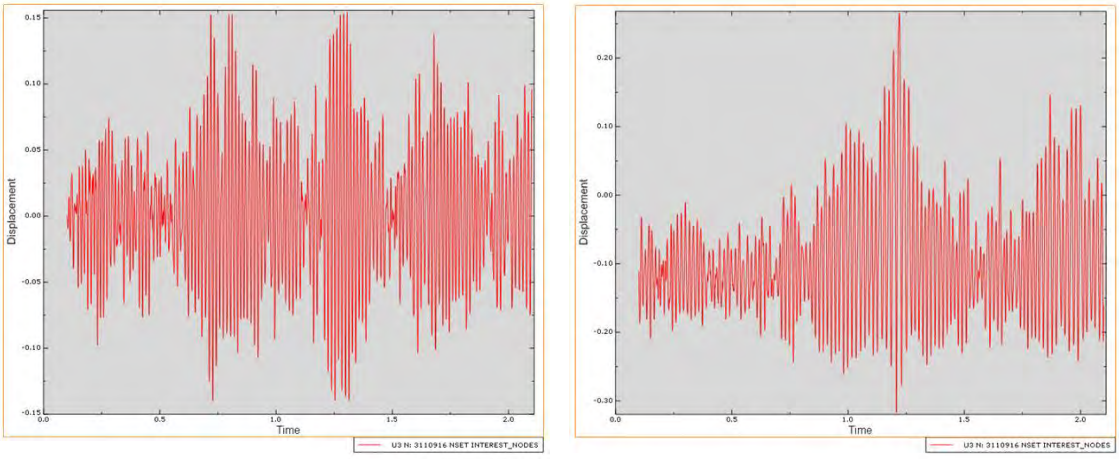

(a) No Thermal Loads **(b) Thermal Loads Included**

Figure 154. Time history of normal displacements at panel center with hinged BC

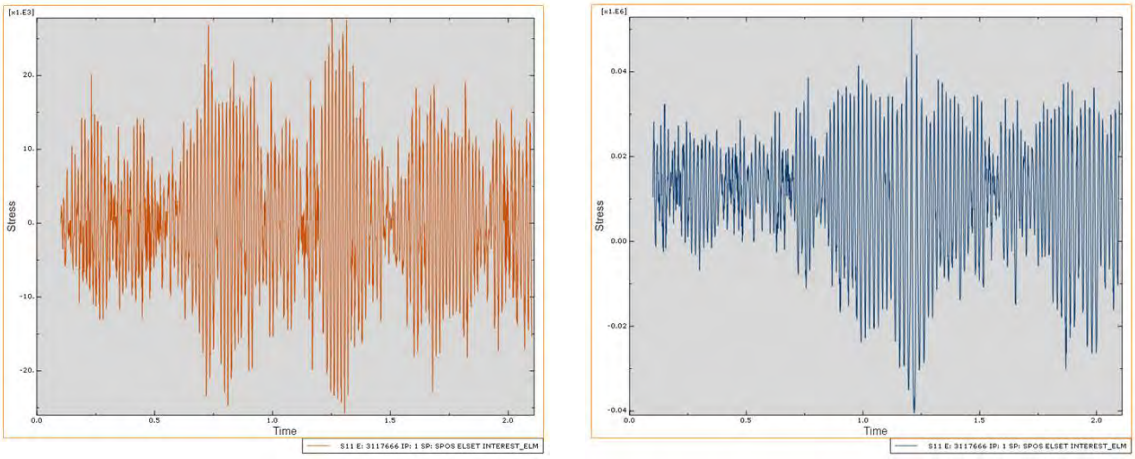

(b) No Thermal Loads **(b) Thermal Loads Included**

Figure 155. Time history of stress S11 of element 3117666 near panel center with hinged BC

Table 31 and Table 32 list the mean, standard deviation and root-mean-square (RMS) values of each time history output.

Table 31. Comparison of normal displacement at center of panel

Analysis Case	Mean	Standard Deviation	RMS
Fixed BC w/o Thermal Loads	.0027	0.051	.0511
Hinged BC w/o Thermal Loads	.0105	0.077	.0777
Fixed BC w/ Thermal Loads	-.0931	0.050	.1055
Hinged BC w/ Thermal Loads	-0.0941	0.084	.1262

Table 32. Comparison of dominant stress on stiffener web at center of panel

Analysis Condition	Mean	Standard Deviation	RMS
Fixed BC w/o Thermal Loads	-201	8681	8683
Hinged BC w/o Thermal Loads	-979	11440	11479
Fixed BC w/ Thermal Loads	9562	9554	13515
Hinged BC w/ Thermal Loads	9475	14198	17066

In the tables, the initial condition for cases with thermal loads increases the mean values of the response. The standard deviations of normal displacement for the same BC for cases with and without thermal load are relatively close, which differs by 2.0% for fixed BC and 9.1% for hinged BC. The difference of standard deviations for stress is higher for both hinged BC (24%) and fixed BC (10%). RMS values are obtained by simply manipulating the mean and standard deviation values.

5.4.2 Response of Displacement and Stress at Center of Panel

The power spectral densities (PSD) of normal displacement and stress at the center of panel are illustrated in Figure 156 thru Figure 163. The natural frequencies primarily for modes symmetric in the short panel direction are marked on the PSD plots for the convenience of discussion. Since both the structure and acoustic pressure are symmetric with respect to the centerline of panel, the expectation is that the symmetric modes will dominate the panel response. Figure 156 and Figure 157 compare the PSD for cases of hinged BC, fixed BC, and linear response without thermal loads. The following lists the observations of this comparison:

- The dominant PSD response of each case, i.e., hinged BC, fixed BC, and linear response analysis, matches their corresponding fundamental frequency. In other words, the system responds linearly to the acoustic pressure;
- The responses of fixed and hinged BC enclose that from linear response analysis;
- The acoustic pressure doesn't seem to excite the 2nd mode, which is the first anti-symmetrical mode of panel;
- Responses of 3rd mode also show that the linear response falls between two BC cases;
- The displacement response (Figure 156) of fixed BC better correlates to the case of linear response for frequencies ranging from180Hz to 300Hz;
- Symmetric mode No. 4 and 7 are not excited by the acoustic pressure, which is due to the anti-symmetric nature of the modes in the long direction of panel (Figure 138 and Figure 139);
- Peak response of both BC cases has minor shift in frequency, possibly due to the geometric nonlinearity of panel response;
- There are some noticeable responses for frequencies higher than 310 Hz, which correspond to Modes 9 and 11. The two modes are symmetric in both long and short directions of panel.

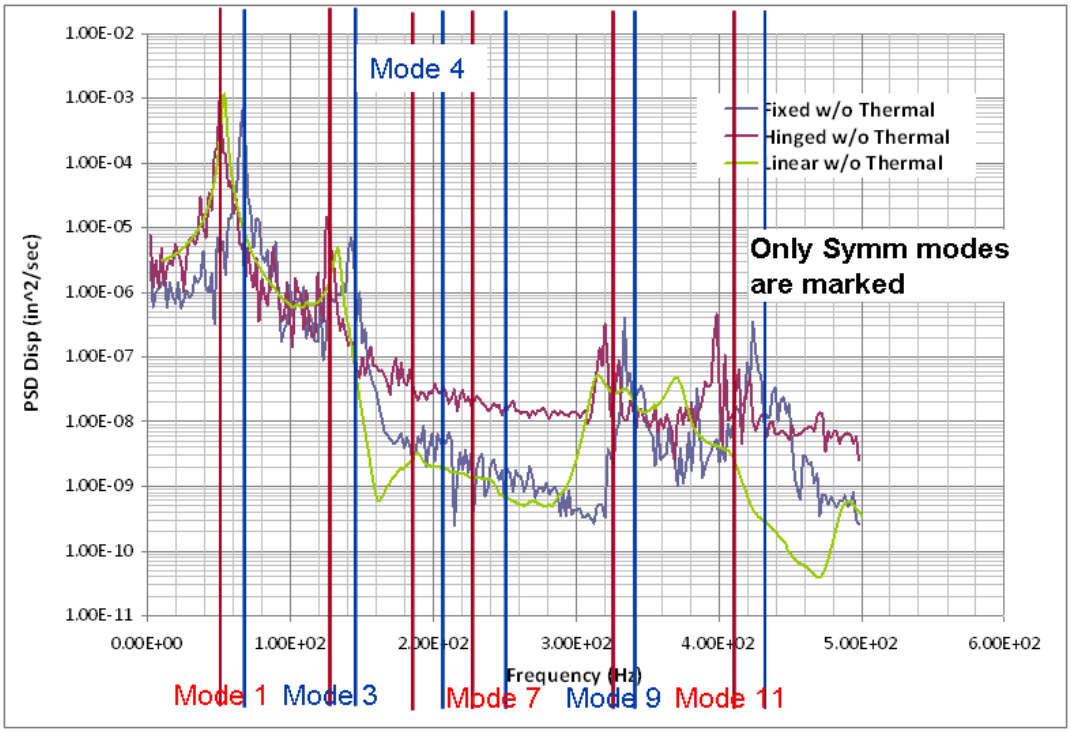

a. Displacement Response Spectrum

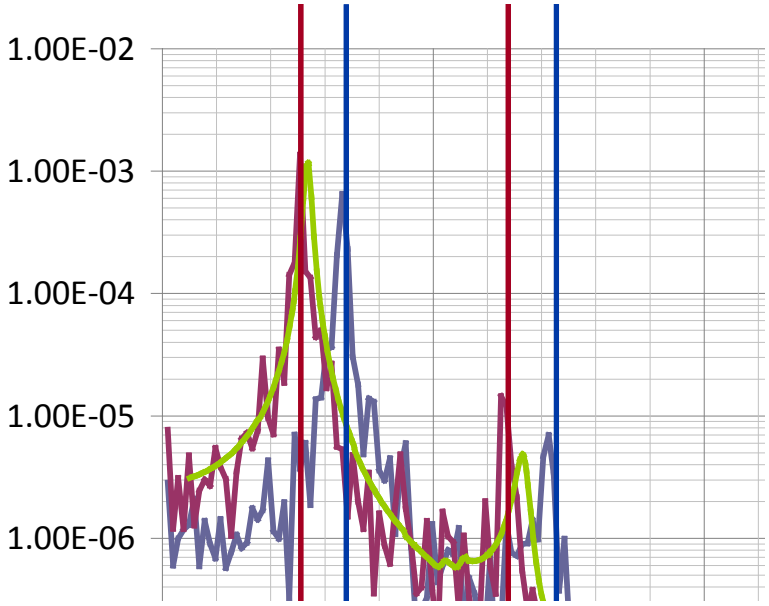

(b) Enlarged View at Peak Response

Figure 156. Comparison of normal displacements of Node 3110916 at panel center

Approved for public release; distribution unlimited.

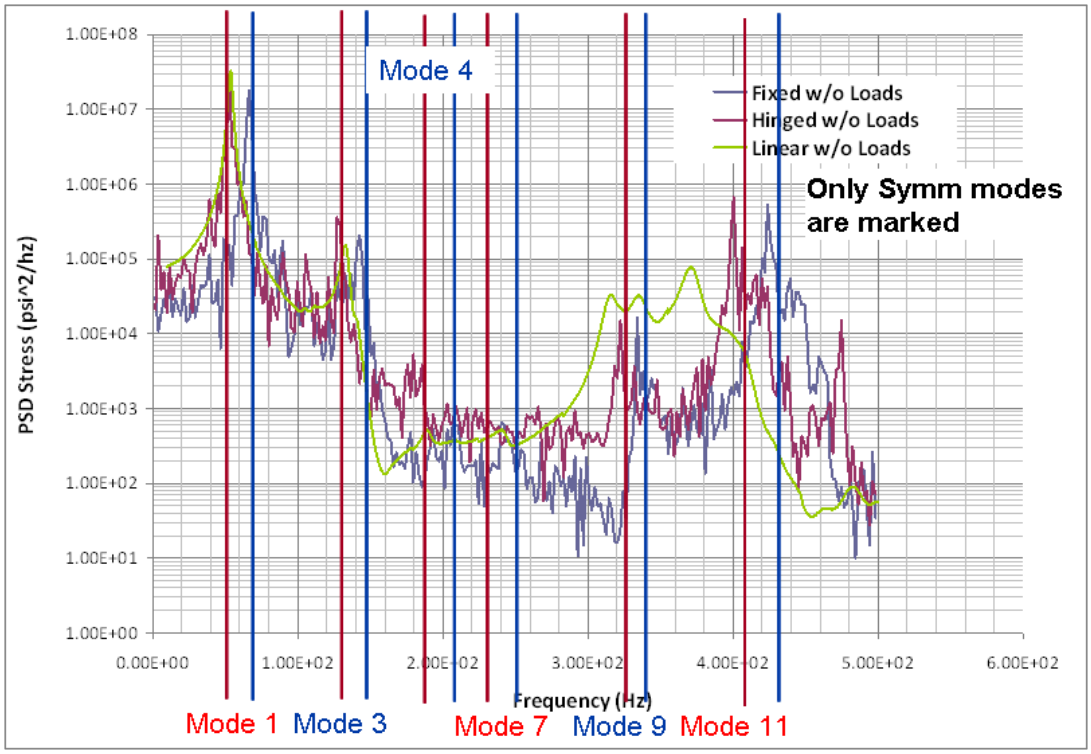

(a) Stress Response Spectrum

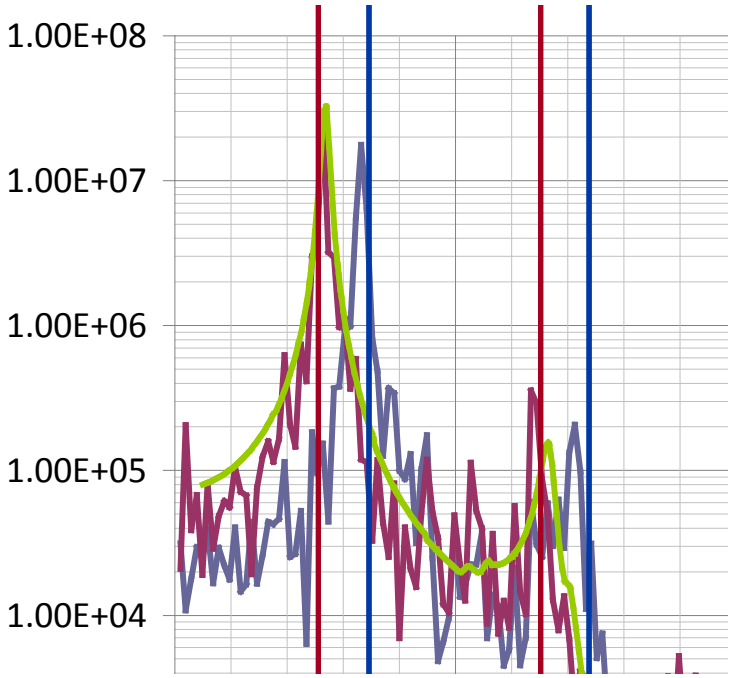

(b) Enlarged View at Peak Response

Figure 157. Comparison of stress S11 of Element 311766 on stiffener web and near panel center for hinged and fixed BC without thermal loads

Approved for public release; distribution unlimited.

The PSD for cases of hinged and fixed BC with thermal loads are compared in Figure 158 and Figure 159. Some observations of the comparison are:

- The responses near the 1st mode for both BC still enclose that from the linear response analysis. However, the bandwidth of response for each BC is wider and the peak is lower than that without thermal loads, which is more obvious for hinged BC than for fixed BC. It is likely the result of the panel stiffness change due to geometric nonlinearity by thermal loads and geometrical stiffness effects, which are more significant for hinged BC than for fixed BC;
- The peak response of both BC shifts to lower frequency ranges as a result of geometric nonlinear effects, which is more significant for higher modes including the 3^{rd} , 9^{th} and 11^{th} modes;
- A minor asymmetry of the system caused by the inclusion of boundary displacements may contribute to the difference between dynamic explicit and linear responses;
- There is a high response for very low frequencies for hinged BC.

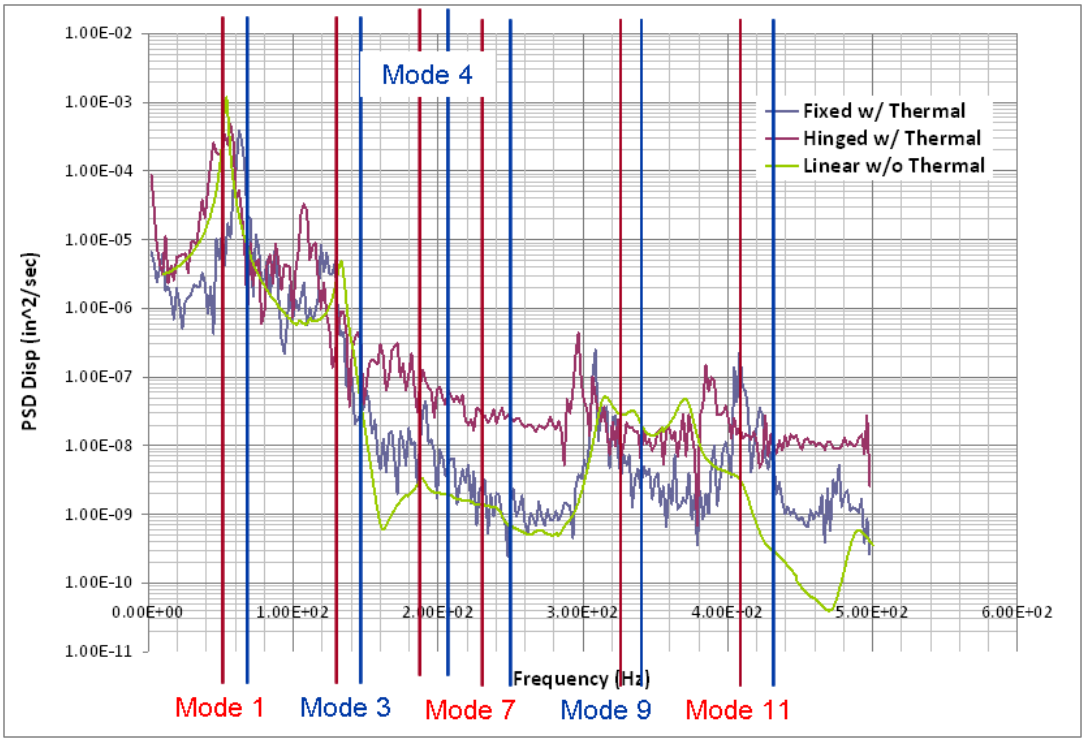

(a) Displacement Response Spectrum

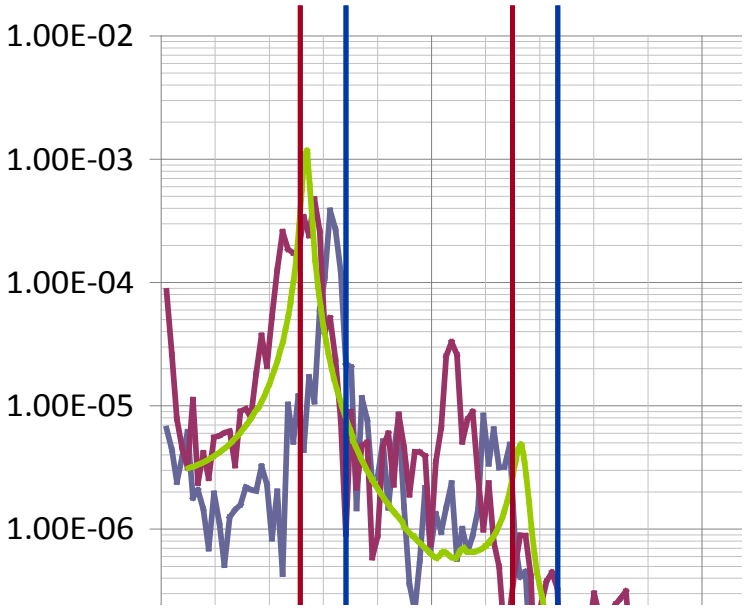

(b) Enlarged View at Peak Response

Figure 158. Comparison of normal displacements of Node 3110916 at panel center for hinged and fixed BC with thermal loads

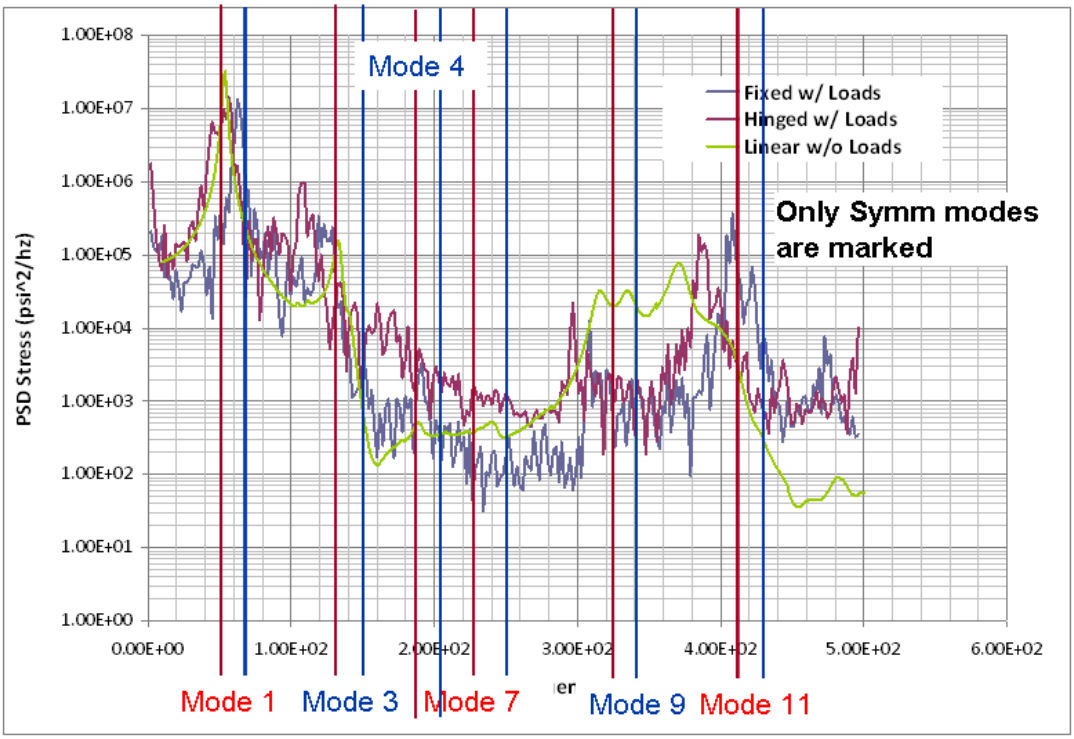

(a) Stress Response Spectrum

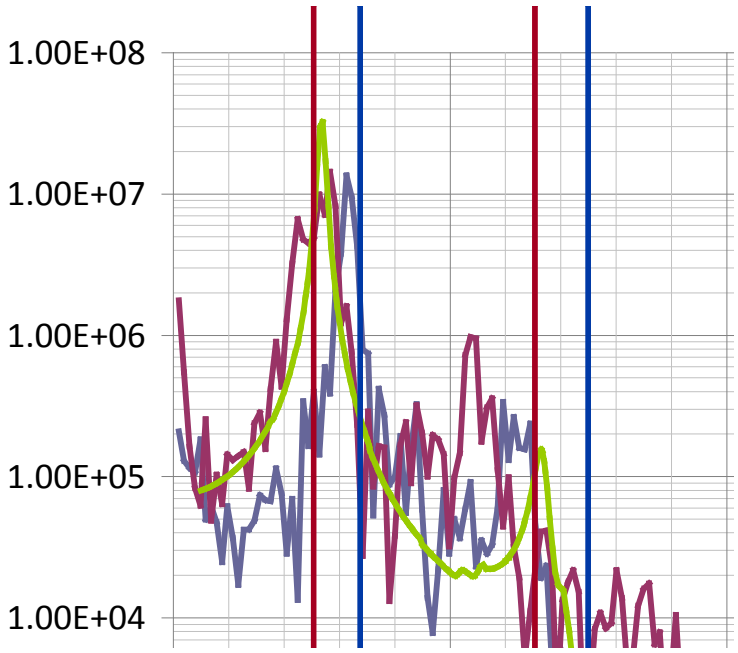

(b) Enlarged View at Peak Response

Figure 159. Comparison of stress S11 of Element 311766 on stiffener web and near panel center for hinged and fixed BC with thermal loads

Approved for public release; distribution unlimited.

To show the effect of thermal loads to panel response, two PSD of hinged BC, one with and one without thermal loads, are included in Figure 160 and Figure 161. Observations for the comparison are listed as follows:

- The PSD plots show that the shift of peak response for 1st mode is relatively minor. This indicates that the stiffness softening due to compression of panel skin may offset stiffness increase due to geometric or deflection effect from thermal loads.
- The effects of thermal loads to the response of 1st mode include wider bandwidth and lower peak of the response;
- There is a noticeable shift of response corresponding to the 3rd mode from 129 Hz to about 107 Hz. Again a wider bandwidth of the response is observed;
- The displacement response of frequencies higher than 140 Hz deviates from the linear analysis result. Comparing with displacement response the stress is closer to the linear response analysis in the higher frequency range.

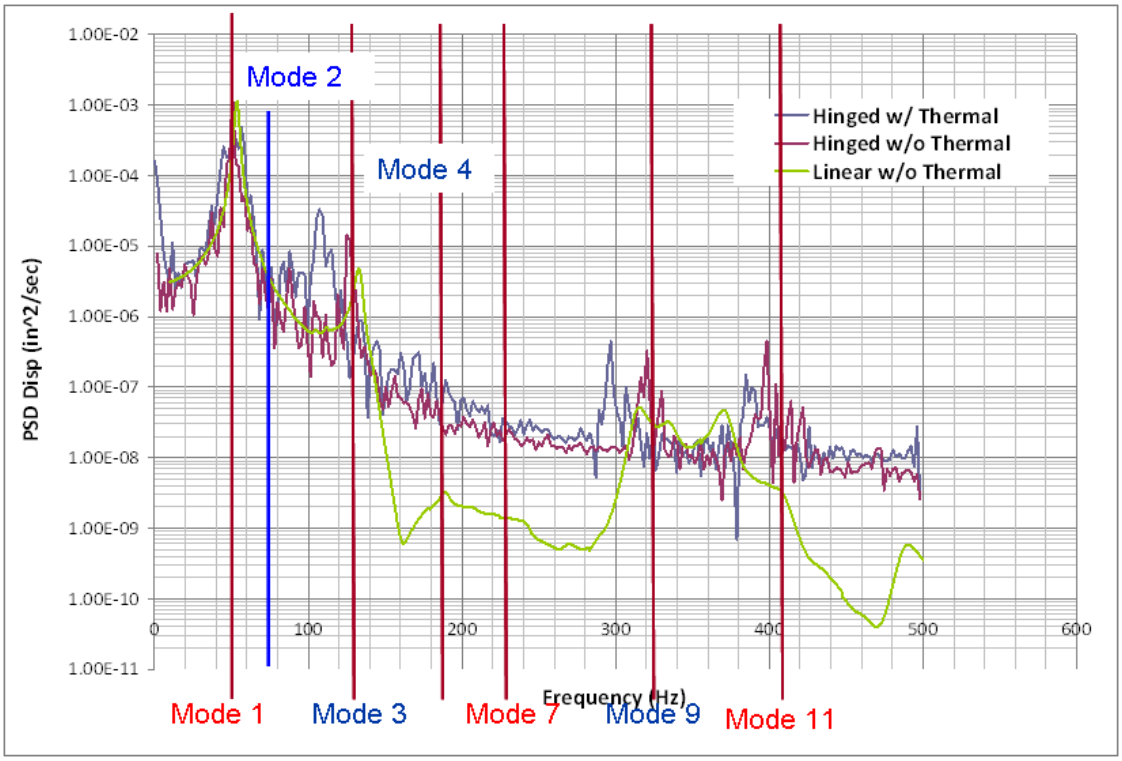

(a) Displacement Response Spectrum

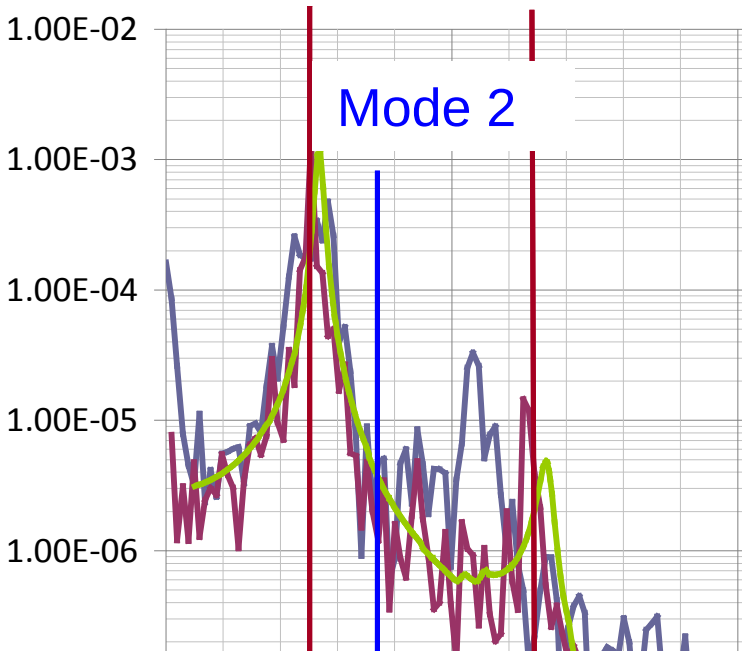

(b) Enlarged View at Peak Response

Figure 160. Comparison of normal displacements of Node 3110916 at panel center

Approved for public release; distribution unlimited.

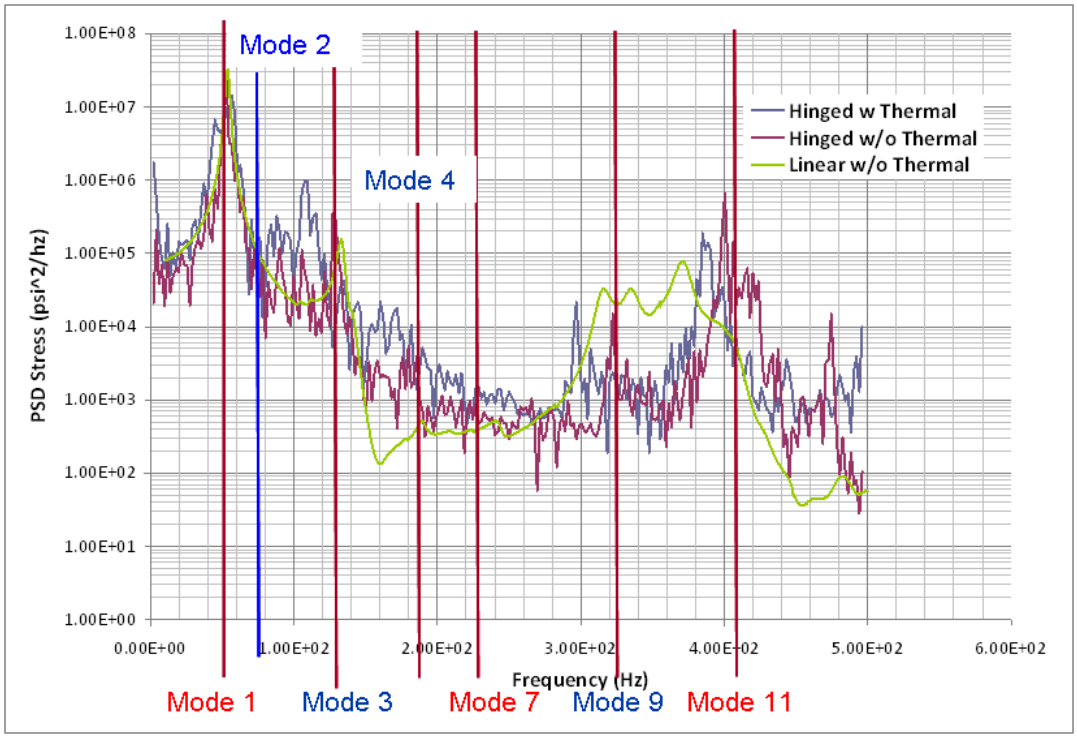

(a) Stress Response Spectrum

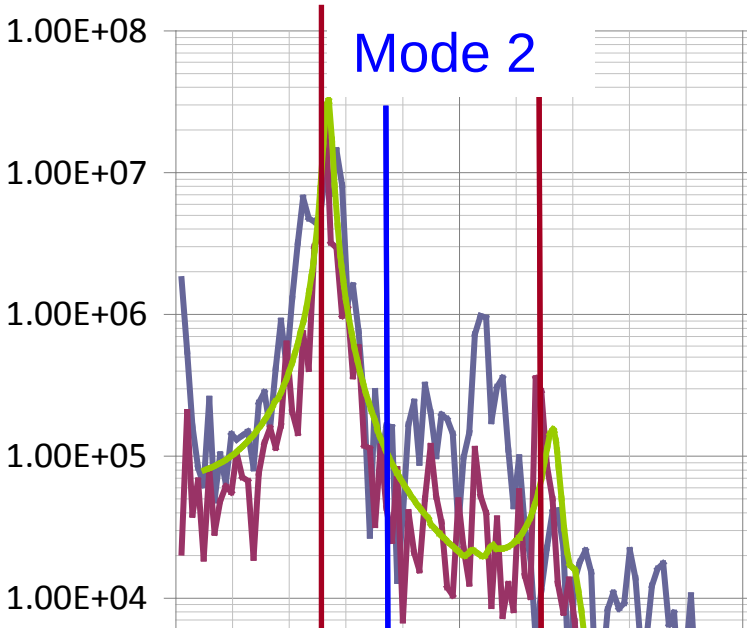

(b) Enlarged View at Peak Response

Figure 161. Comparison of stress S11 of Element 311766 on stiffener web and near panel center for hinged BC with and without thermal loads

The comparison of cases with and without thermal loads for fixed BC in Figure 162 and Figure 163 is included as:

- For the 1st mode the shift of peak response is minor and is similar to the case of hinged BC. The bandwidth increase of fixed BC with thermal loads is not as much as that of hinged BC (due to smaller displacement effect). However, the shift of response for the 3rd mode is significant, and again is similar to the hinged BC case.
- For frequencies ranging from 180 to 290 Hz, the displacement responses for cases with and without thermal loads are closer than that for hinged BC. However, the stress response is not in good agreement;
- Higher responses at frequencies higher than 300 Hz are primarily contributed by Modes 9 and 11, both are symmetric in long and short directions of panel. The magnitude is however small compared to Mode 1.

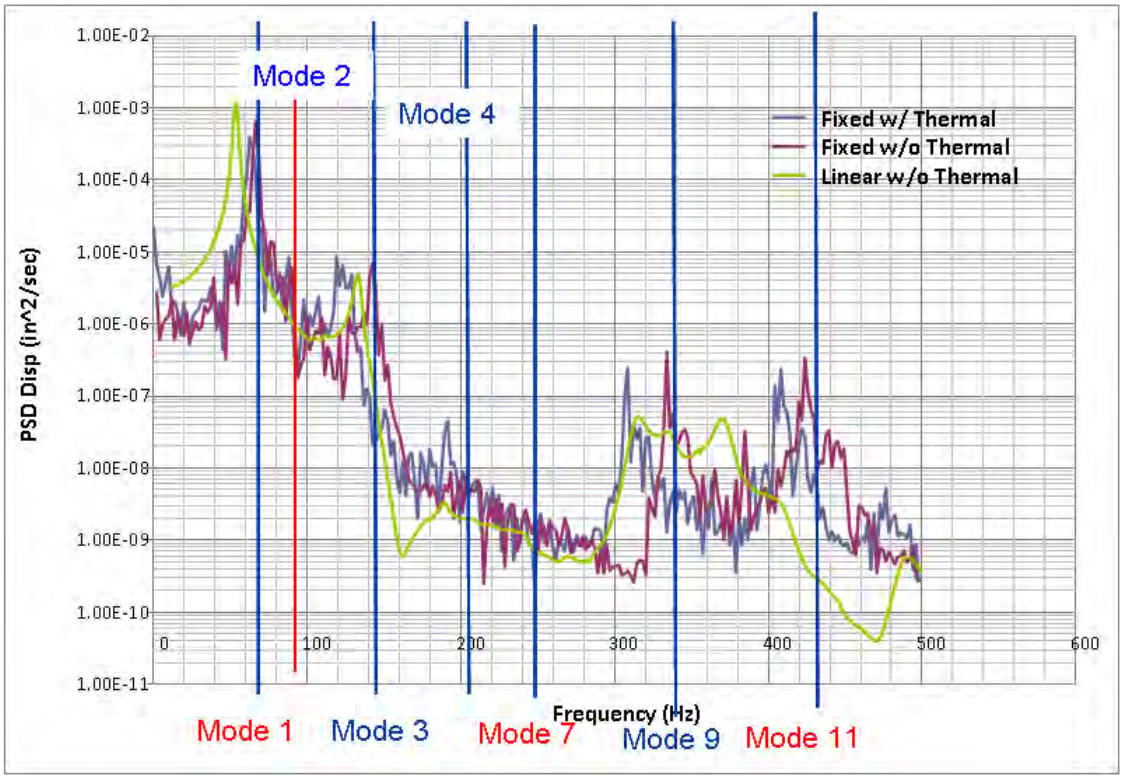

(a) Displacement Response Spectrum

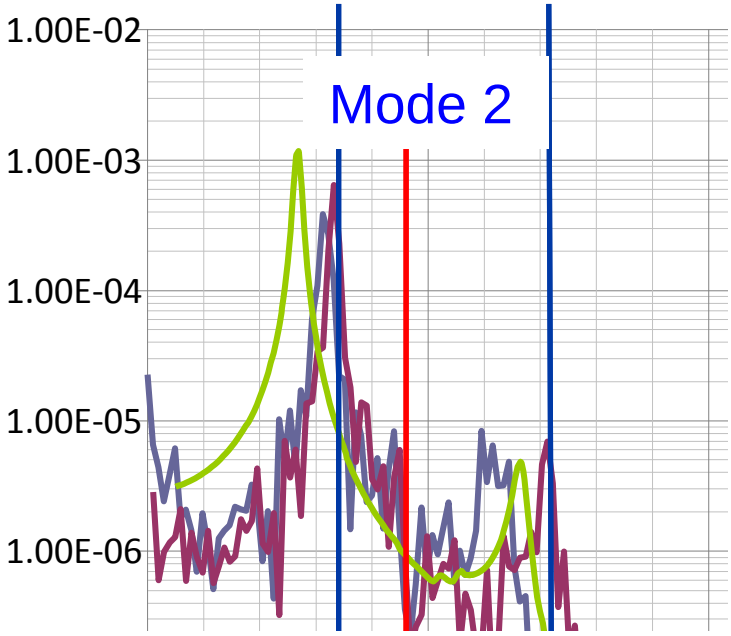

(b) Enlarged View at Peak Response

Figure 162. Comparison of normal displacements of Node 3110916 at panel center

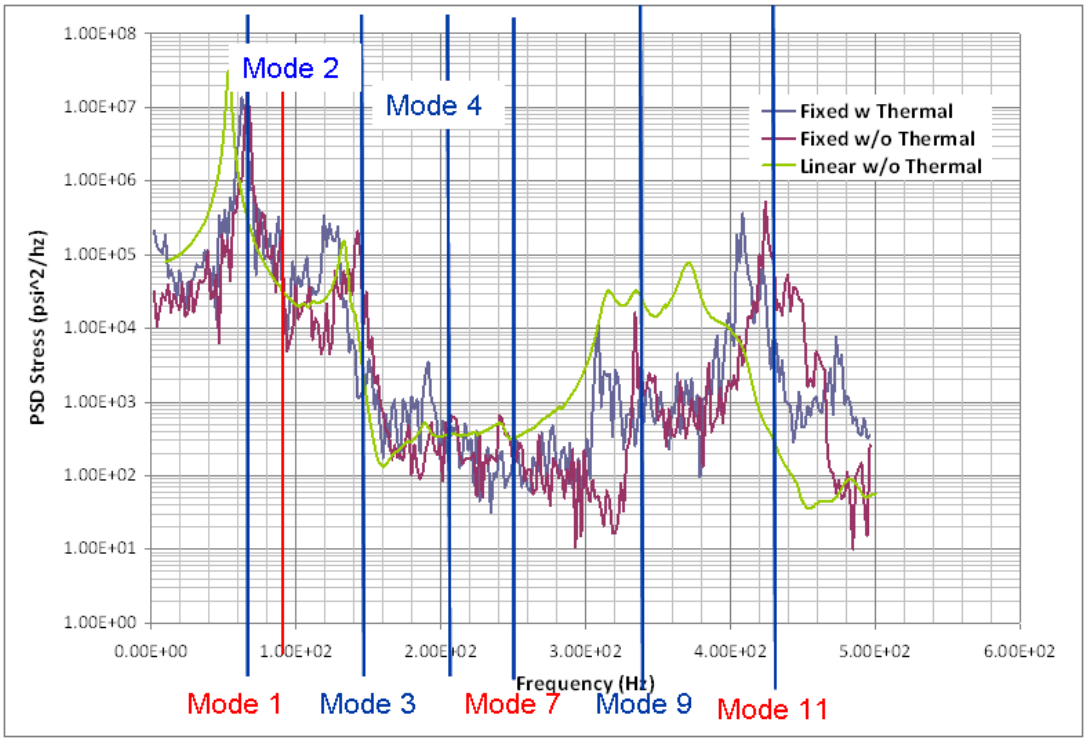

(a) Displacement Response Spectrum

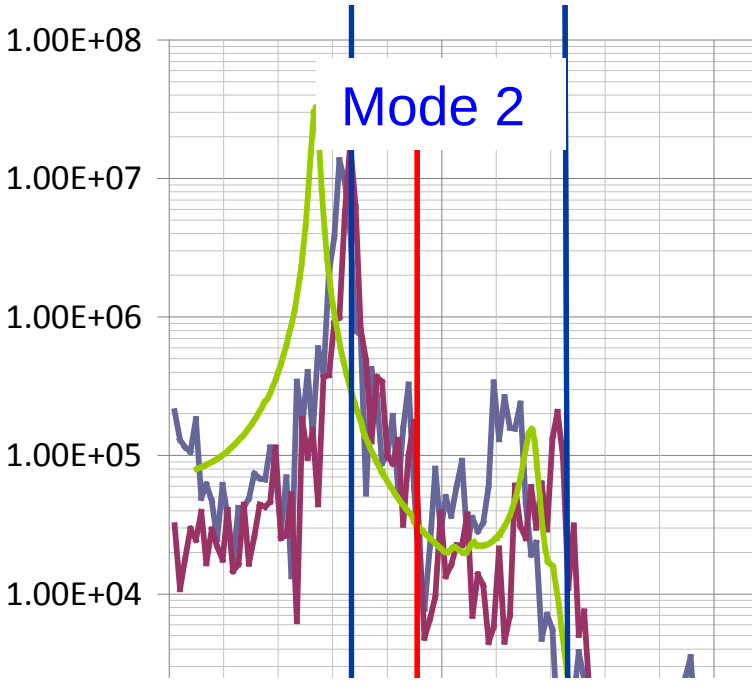

(b) **Enlarged View at Peak Response**

Figure 163. Comparison of stress S11 of Element 311766 on stiffener web and near panel center for fixed BC with and without thermal loads

Approved for public release; distribution unlimited.

5.5 Fatigue Life Prediction with Explicit Dynamic Analysis

The last comparison is the prediction of fatigue life from the linear frequency response analysis and nonlinear explicit dynamic analysis. The fatigue is calculated at the center panel stiffener for comparison to the linear random frequency response approach. The hinged/pinned boundary conditions case is used for comparison, since this case better matches the unit cell analysis.

For the center panel location, these stresses were the highest predicted by the dynamic solution. The stress time at Element ID=3117666 was used for the fatigue analysis. This stress is on the center stiffener. For the explicit analysis, the mean stress was calculated as σ_{11}=9.48ksi and RMS stress σ_{11}-rms = 14.19ksi at the element centriod. The time history is shown below in Figure 164. This time history was then filtered into a peaks and valleys (P-V) table. Once in a P-V table format, then a cycle counting fatigue analysis is performed.

For the fatigue analysis, an Inconel 718 RT, Kt=1.0 s-N curve is used, Figure 166. The stresses are not scaled for Kt at this location. The damage is calculated for the 2 sec time history. Then, the damage is scaled to a Damage Index of D=1.0. This results in the plot in Figure 165. The blue curve represents the fatigue life at different scale factors of the applied stress. For instance, at a relative (Re) stress of 1.0, this would the fatigue assuming no knock downs, Kt adjustments, etc. Hence, the intersection of the red and blue curves are the fatigue life without factors, and the intersection of the green and blue curves represent the knock-down in the s-N properties due to elevated temperature at this location. The fatigue life is 1e6 seconds to failure or 277 hrs. If this part is exposed to 400 seconds of high intensity noise and temperature per flight, then this part is good for 2500 flights. This is well beyond the design life for a replaceable component. The design requirement was for 1600 flights for a non-critical replaceable exterior skin panel. Hence, this panel is good for almost 1.5x the design life requirement.

This is total fatigue due to acoustic and thermal loads. In this fatigue analysis, the mean stress is a type of ground-air-ground (GAG) cycle. This is a worst case scenario, since the max thermal stresses and acoustic stresses are assumed to occur simultaneously. In this case, the acoustic stresses are much higher than the thermal mean stress, and the acoustic stresses are the primary contributor to the fatigue damage index.

For the linear random frequency response analysis, fatigue life is predicted from an RMS s-N fatigue allowable. The elevated temperature allowable is σ_e = 17ksi, with a knock down and adjusted for mean stress effects. This represents the RMS stress limit for a Fatigue Life of 1e9 cycles. The RMS stress was $\sigma_{11\text{-rms}}$ =14.1 ksi in the linear analysis, hence the margin to the endurance limit is

Stiffener Web, Margin = 17.ksi/14.1ksi – 1 = 0.21

In conclusion, the fatigue life calculated from the nonlinear simulation does yield a more conservative fatigue life estimate. But, in general the predicted response is fairly similar for both the linear random frequency response analysis and the nonlinear explicit transient analysis, hence the fatigue life prediction demonstrates a similar result.

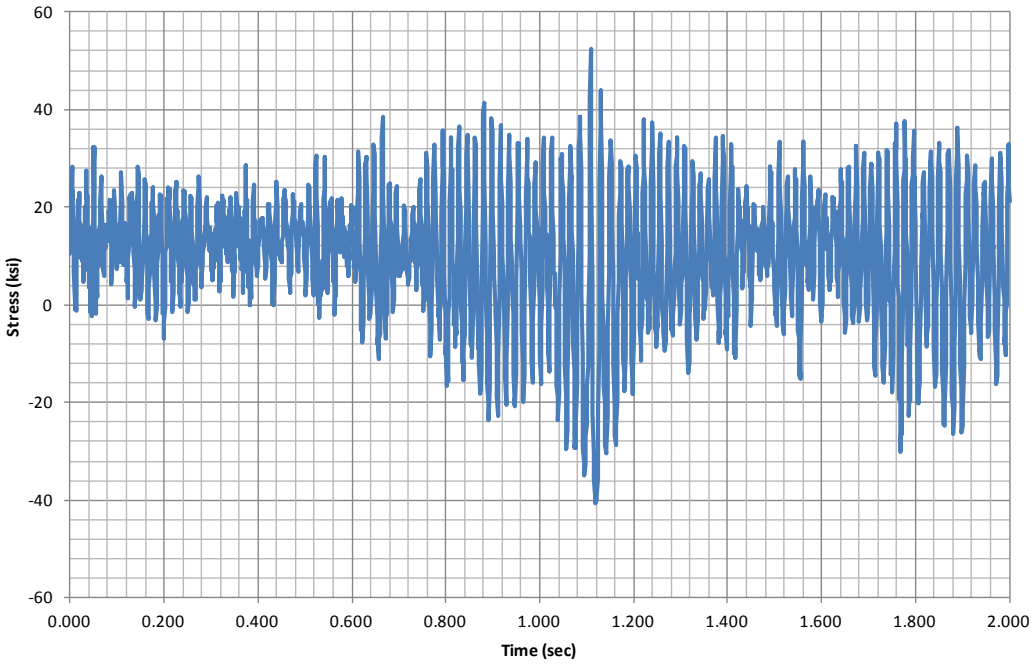

Figure 164. Stress time history at Element ID=3117666. σ_{11}

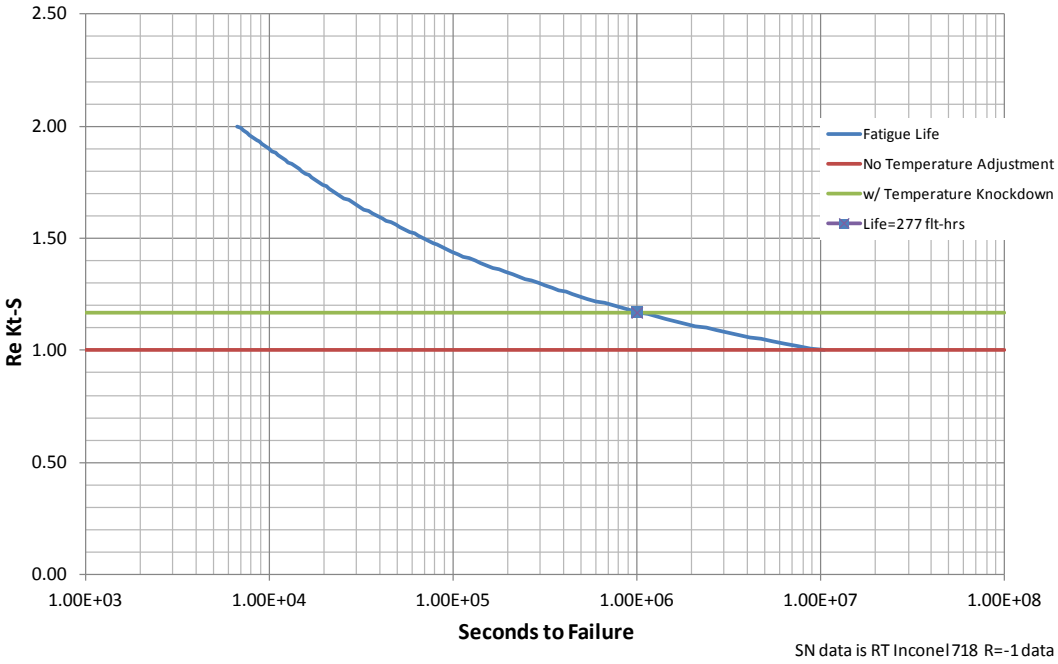

Figure 165. Fatigue life for center stiffener web

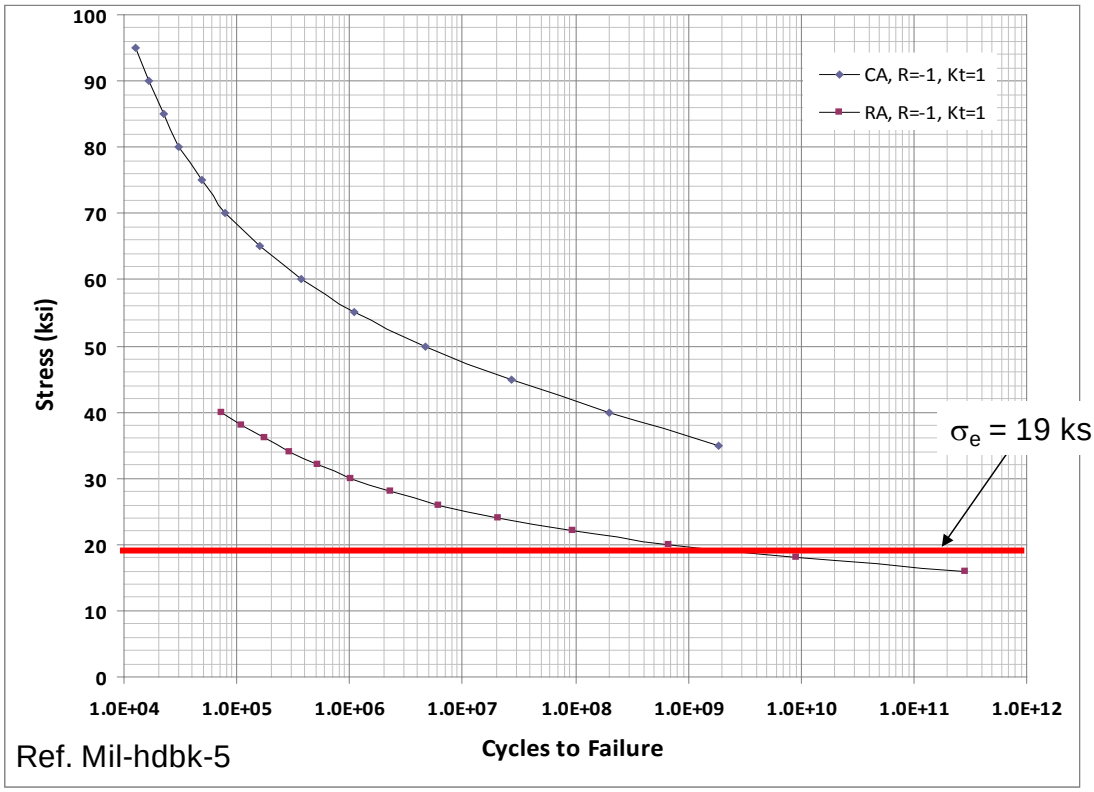

Figure 166. Inconel 718 RMS S-N data

5.6 Summary Knowledge Gap Related Findings

Key findings identified in this task, and their associations with knowledge gaps identified in the Phase I report [2], as well as in Section 7.1 of this report, are summarized as follows:

1. **Combining worst flight/mechanical loads with worst thermal loads at different trajectory points for structural design is conservative.**

   Phase I Gap Association: Gap 1

   Potential Impact: In this study, it was shown that this practice will generate a feasible but conservative design**. As a result, steady-state aerodynamic loads are not included.**

2. **Design iterations between detailed panel and vehicle load model are required to render the stiffness of local panel consistent to the vehicle model.**

   Phase I Gap Association: Not included in Phase I gaps; New Gap 12

   Potential Impact: Since the ortho-grid-construction panels are more flexible than the honeycomb design in the vehicle model, the internal loads transferred from the vehicle to the unit-cell structure result in excessive large deflection and unrealistic high stresses that prevent a nonlinear dynamic analysis of unit-cell from being conducted.

3. **The life/stress prediction relies on special tool to determine stress concentration factors**

   Phase I Gap Association: Not included in Phase I gaps, New Gap 13

   Potential Impact: Critical thermal-mechanical-fatigue locations such as fasteners, fillet radii, weld butts, are not represented in exact detail in the panel model. Hence, this type of analysis requires either a secondary analysis step to determine local stress response in the neighborhood of these features, or there needs to be available Design Values, Allowables, and DaDT data specific to the features.

4. **The engineering approach is used to evaluate structures with two different boundary conditions: (1) a fully restrained or fixed one; and (2) a hinged (pinned) one.**

   Phase I Gap Association: Gap 5

   Potential Impact: Representative boundary conditions, which can simulate energy transmission or elastic wave propagation between panel and surrounding structures, can not be modeled with simple restraints. These more representative boundary conditions are difficult to obtain.

5. **A high computation cost and approximation of damping with the α term only dissuade engineers from using advanced analysis methods, e.g., explicit dynamic analysis, for the panel design.**

   Phase I Gap Association: Gap 8 and Gap 10

   Potential Impact: Direct integration response methods have limited options for modeling the damping. The methods available can not accurately represent the true or expected frequency dependent damping behavior.

6. **The coupling between thermal, acoustics and elasticity is not addressed.**

   Phase I Gap Association: Gap 3

   Potential Impact: The dynamic explicit analysis includes temperature-dependent materials, thermal loads, time varying acoustic pressure, and large deformation. However, all loads do not include structural deformation. Co-simulation while feasible for certain loads is an expensive option. Also, there is no reliable co-simulation capability for acoustics i.e. high frequency unsteady aerodynamic.

7. **The initial conditions were established with an engineering approach for explicit dynamic analysis, e.g., a dummy/quasi-dynamic analysis step.**

   Phase I Gap Association: Not included in Phase I gaps, New Gap 14
   Potential Impact: The quasi-dynamic analysis ramping up thermal loads in a time period of 0.1 sec led to the approximation of initial conditions.

6.0 PHASE III TEST PLANNING

Under *Task 6: Test Planning*, Boeing reviewed the key design drivers for each panel, discussed appropriate methods to experimentally validate analyses of this effect, compared these to AFRL ground test facilities, and provides testing recommendations for future development. The output of this task will be used to guide planning activities for the Phase III Validation Testing program. This section will step through the test planning thought process by discussing the

- Background and Objectives
- Test Requirements
- Facility Evaluations
- Design Drivers and Test Recommendations

6.1 Background and Objectives

Considerable progress has been made on advancing key elements of critical future war-fighting capabilities, such as rapid, responsive, and reusable space access and hypersonic flight. Such structures experience environments that consist of combinations of *thermal, acoustic, and mechanical loading*, and are characterized by high magnitudes, spatial and temporal gradients, and with coupled interactions. Currently, these structures: (1) contain external thermal management designs, (2) are designed using different tools and separate analyses for the three enumerated loadings, and (3) are based on end-of-life coupon test allowables.

Significant technological breakthroughs are essential to enable the development, qualification, and deployment of robust and durable structural solutions capable of operating reliably under extreme operating conditions and in combined, extreme environments. These include the development and use of (1) thermal protection imbedded in the structure or heat tolerant structure, (2) combined loading analysis tools, simulations, and tests, (3) variable scale mechanical modeling, and (4) computationally estimated material and design detail allowables based on limited coupon test data. Additionally, this design approach must yield improved economics in both cost and time.

Analytic tools of the required type are being developed, and several structural concepts are being proposed to fulfill these needs. Test approaches and techniques are needed to support and correlate these design tools. This section is intended to pose requirements and alternatives for such tests.

This program is a three phased effort targeting acreage panel-level response and life prediction capabilities for a sustained, reusable, air-breathing, Mach 5-7 cruise, horizontal takeoff platform. The first phase uncovered those knowledge gaps for detailed hypersonic structure design that most significantly restrict a truly predictive capability. The second phase entailed detailed design of selected regions of a “closed concept” reference hypersonic vehicle and accompanying trajectory, targeting the knowledge gaps delineated and documented in Phase I. The third phase will proceed to build and test flight-weight panel-level hardware identified, detailed, and documented from Phase II, with the testing to be performed at USAF combined, extreme environment facilities.

Approved for public release; distribution unlimited.

For Phase II, four panel-level structural components were selected for detailed design, one for each of the following loading scenarios:

1. Panel 1 - A vehicle region where material property changes and aeroacoustic fluctuating pressures resulting for separate/turbulent boundary layer flow and shock interaction are of a primary concern.

2. Panel 2 - A vehicle region where transient, quasi-static thermal and mechanical loading and material property changes drive the design.

3. Panel 3 - A vehicle region where the combination of high dynamic pressure, thermally-induced stress and material stress and material property change causes aeroelastic stability to be of primary concern

4. Panel 4 - A vehicle region where the combination of all extreme-environments (acoustic, material change, thermally induced stress, and mechanical loading) drive the design.

Therefore, in Phase II the outcome from the detailed design analysis studies are preliminary design of aircraft structure designed to actual flight conditions. In Phase III, the objective will be to adapt these panel designs into test articles and fixtures that can simulate the boundary conditions, predict the panel response to expected test conditions. Additional tests will also need to be performed to ensure adequate data is available to predict the response and life of panels (properties, design values, and fatigue curves). The keys to success will be:

1. Setup a well characterized experiment
2. Replicate actual design to conditions, but with controllable loading levels
3. Collect sufficient data on loads and response
4. Validate thermal, acoustic, mechanic load limit states, advanced combined loads structural response models, and
5. Quantify the uncertainty in all measurements

The test program will have these objectives:

1. Develop a test regimen and data for response prediction of aerospace structures operating in extreme, combined environments, with emphasis on spatially-tailored aero-thermo-structures. This involves tests at the subcomponent level that expose a specimen to thermal, mechanical, and acoustic loads.
2. Develop techniques and processes for computational model validation. This requires the test article to be sufficiently simple to create an accurate mathematical model whose results can be directly compared to test data. Modeling of portions of the test fixture may be required.
3. Obtain specimen response and fatigue data to correlate the computational methods for modeling and predicting damage initiation and evolution.

6.2 Testing Requirements

The goal of the test program is to verify identified predictive capability knowledge gaps by evaluating the accuracy of predicted thermal and mechanical structural responses for the panels designed and analyzed in Task 2. The test program will likely also help to identify additional shortcomings in current analysis methods.

The primary requirement to accomplish this goal is to be able to simulate loads (Thermal, Aero, Maneuver, and Acoustic) and environment during critical trajectory points. For this Phase II study, five critical design points have been identified. Additional design points were also considered during the study, but these five represent a consistent set for discussion of the validation test program.

From the HCV trajectory shown in Figure 167, these five flight conditions have been selected to provide critical design loads.

- Max Q =2000 psf, Mach = 6, AoA=6 deg, when highest external aero-acoustic loads occur
- Max T Transient (Temperature up 1500F), when highest differential temperatures occur between internal and external structure
- Max T steady state (Mach 7, Alt=100K), when highest temperature occurs, hot soaked to max duration
- Max G, 2.5g maneuver, at 90K, and Mach 7, when highest mechanical (aero and maneuver) loads occur.
- Max Temperature for internal structure and max negative temperature gradient at landing.

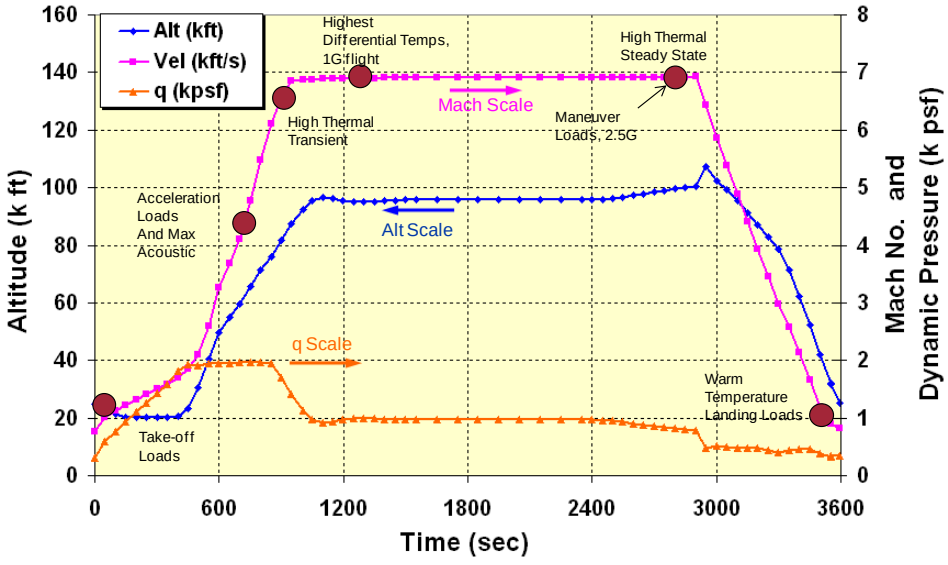

Figure 167. Reference trajectory

Approved for public release; distribution unlimited.

Considering these flight conditions, then the test facility requirements are:

- Aero-Acoustic spectrum up to OASPL=165dB controllable from 20Hz to 500Hz
- Steady pressure loading up to +/-1.5psi
- Mechanical loading (bending and in-plane loads) due to 2.5 g Maneuver loads
- Thermal Transients of up to 3 deg/sec skin temp, controllable heating/cooling rates
- Sustained High Temperature and Acoustic Load Testing – Simulate Trajectory (~1 hr) and accelerated acoustic life testing (~16 hrs), thermal load controllable over test article

The instrumentation requirements are listed below:

Static Loads/Response:
- Low sample rate
- Max channels at low SR: up to 96
- Temperature measurements – Calibrated IR cameras, thermocouples, heat rate controls
- Thermal Induced Displacements and Loads – Digital Imaging Correlation (DIC), LVDTs, LVD
- High temperature strain gages (1500F) and wiring
- Thermal compensated strain measurements

Dynamic Loads/Response:
- High sample rate (up to 40kHz)
- Max channels at high SR: up to 48
- High temperature accelerometers and displacement transducers (1500F rated)
    - Non-Contacting Disp Probes (1500F)
    - Accels are limited in temperature and size
- High temperature, thermally compensated strain measurement
- Laser displacement measurement (LVD) – Point and ODS

Based on the test paradigm that experiments are used to explore mechanics of system and validate predictions. There is a need for accurate IR images to indirectly verify the applied and secondary loading (with respect to radiation, convection, conduction heat transfer). A lab test can not exactly duplicate the complex aero-thermal design loads, so a necessary step is to verify the test environment and reanalyze after the test. This is required to understand if the structure was over or under tested.

For some tests, there also needs to be verification of performance of the Thermal Management System (such as cooling concepts). Hence, for this type of tests a full – field IR is necessary in order to verify the thermal response. Note, point measurements with TCs are limited. All sides of the test article need to be imaged (front, back, internal, sides).

Non-contacting measurements are necessary for component testing and analysis. One of the better tools for understanding the response behavior under real-use conditions is the ARAMIS

Approved for public release; distribution unlimited.

system by GOM. The measure is also independent of material, size, and geometry of the test article. These measurements allow us to link back to CAD/CAE models for direct correlation, comparisons, and visualization of the difference between test and analysis response.

The second critical piece of information is the response measurements. This is required to verify Thermal Expansion deformation, to confirm FEM boundary conditions, to observe static buckling deformation shapes, and high speed dynamic operating deflection shapes (ODS) and strains; and to examine nonlinear deformation behavior and characterize creep.

6.3 Test Facility Evaluations

This section will provide an evaluation of the AFRL Combined Environmental Chamber (CEAC) at Wright Patterson AFB, Figure 168.

Two of the four loading scenarios mentioned above involve acoustic noise (or more specifically aero-acoustic noise generated from separated flow and shock induced turbulent boundary layer interaction) at high temperature combined with thermal and mechanical loads. The AFRL CEAC facility is capable of combined thermal and acoustic loads. The heating capability is up to 90 BTU/ft^2-sec and the acoustic load capability is up to 170 dB overall sound pressure level (OASPL) at frequency range of 50-500 Hz flat spectrum. The max opening to the test chambers is up to 8 ft x 4 ft. The facility can also accommodate up to 96 low sample rate channels and up to 64 high sample rate (40 Khz) channels.

The facility is setup to provide front side (exterior skin side) heating. The quartz heater bank is of similar size to the specimen opening. The heat bank consists of eight 12 inch wide individually controllable quartz heaters. The heater bank can provide uniform heat for up to a full 4 ft by 8 ft surface. The heat profile can be tailored thru individual controls on each of the eight banks or by removing individual lamps.

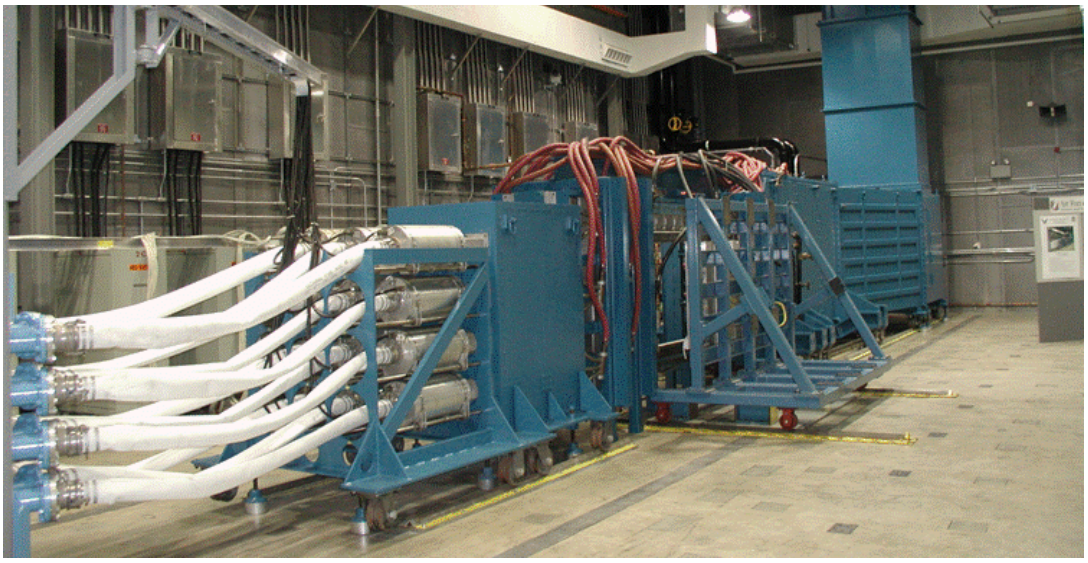

Figure 168. AFRL Combined Environment Acoustic Chamber (CEAC) facility

The test facility uses a strong back cart to position the test specimen within the acoustic chamber, and shown in Figure 169. A similar strong back cart is used to position the quartz lamp banks on the opposing side of the chamber. The specimen cart allows test panels to be securely mounted, independent of the test section, to minimize transmission of vibration from the chamber walls. The cart system also allows for the test specimen to be removed from the chamber between test runs for inspection.

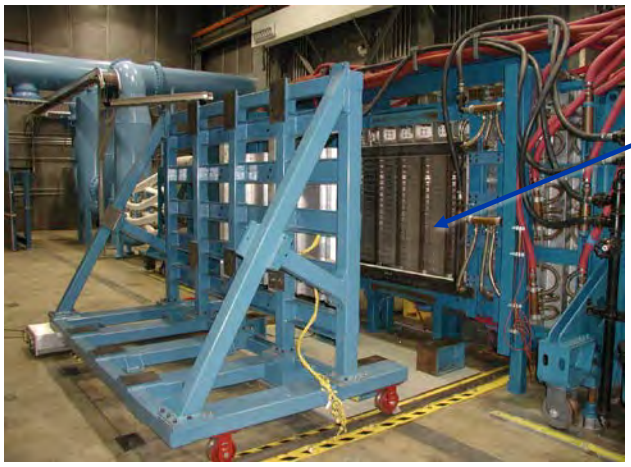

Figure 169. CEAC Test Article Mounting Cart and Heat Lamp Bank

The specimen panel is to be representative of an ortho-grid type structure with a bay size of 56 in. by 32 in. See Figure 170. In order to fit the 108 in. by 48 in. or 96 in. by 72 in. aperture in the CEAC facility the most desirable nine-bay unit cell configuration cannot be accommodated at full-scale. Therefore, two alternatives exist; (1) a nine-bay panel of reduced-scale, or (2) a single-bay panel with sufficient portions of the surrounding bays to provide proper boundary conditions on the center panel.

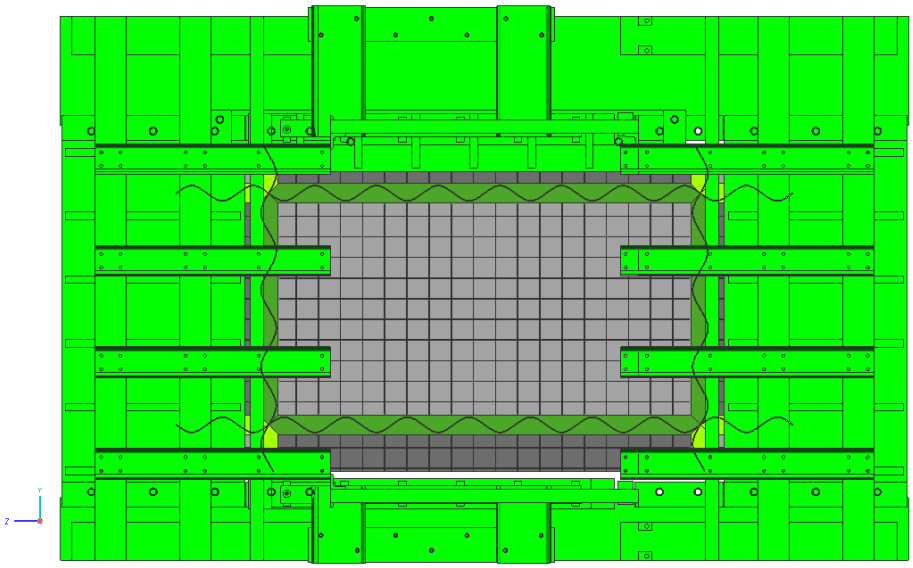

Figure 170. Panel 1 Overlay into CEAC Chamber

Reduced Scale Panel – A nine-bay panel of ½ or ¾ scale can be accommodated. With such a specimen the loads would be reduced by the square of the scale factor to obtain the same stress levels as a full-scale specimen. This would be a useful and economic tool for structure development; however, this approach contains several risks. Among these are: (1) the assumption of linear load scaling, and (2) the possibility that reduced scaling may require details thinner than minimum machining thicknesses.

Single Bay Panel – This option consists of a single bay with the same surrounding substructure that would be found in an airframe. These structural details continue into adjacent panel bays, which gradually transition into edges of increased thickness, including substructure terminations, to attach to test fixturing without the unintended creation of weak fatigue details adjacent thereto. Transition areas of 26 in. length are available in the long dimension and 8 in. length in the transverse dimension.

If the panel is to represent a 500 in radius of curvature in the long dimension, a 3 in. depth will be created in the panel, which will cause many complications in the test fixturing. It is recommended that for a test, which is primarily for design analysis tool development and correlation, that the specimen panel be flat, and not curved in either dimension.

General observations about the facility:

- Thermal/Acoustic Loads - Chamber can simulate equivalent fuselage HCV M7+ environments, although the number of zones and zone control scheme can make achieving desired temperature distributions difficult
- Test Chamber size is large enough for HCV candidate panels (8’ wide exposed is max size, due to chamber bulkhead

- Mechanical static loads - Capability can be added but there will be limits imposed on the temperature and acoustic levels unless the mechanical equipment and actuators can be shielded and isolated.
- Pressurized Loads - Back side pressure is possible, but with limits
- Low flow – No aero-elastic effects or flow/heating/structure coupling
- Instrumentation and Measurements – Adequate high and low sample rate channels, advanced ARAMIS/DIC (Digital Image Correlation) , and laser vibrometer (LDV) capability.

Much of the test process will be bounded by the size and complexity of the test article that can be constructed economically, and that can be accommodated in the CEAC facility. Attempting a single test that includes all four types of loads (mechanical, acoustic, thermal, and pressure) will be extremely expensive and technically difficult. Therefore, performing two tests on a single specimen is recommended; (1) a thermal-acoustic test in the CEAC facility; and (2) a thermal load strain survey test in a separate facility. The thermal acoustic test could include the addition of a constant aerodynamic pressure load by applying elevated or reduced air pressure in a chamber attached to the back side of the specimen panel.

6.4 Design Drivers and Test Recommendations

A summary of the loads, drivers, and margins for each panel is given in Table 33.

Table 33. Candidate Panel Summary

Analysis Order	1	2	3	4
Global FEM ID	862	780	816	1074
Region	Aft fuselage	Aft fuselage	Mid fuselage	Wing
Surface	Upper	Lower	Upper	Lower
Airframe Feature	Engine Bay	Engine Bay	Fuel Tank	Fuel Tank
Appr Temperature	1100 F	1440 F	1230 F	1465 F
Appr Acoustic Level	161 dB	158dB	155 dB	161 dB
Expected Structural Integrity Drivers	Acoustic Fatigue Mechanical Fatigue	Thermal Stress Therm-Mech Fatigue	Acoustic Fatigue Flutter	Acoustic Thermal Stress
Actual Structural Integrity Drivers	Acoustic Fatigue Deflections	Therm-Mech Fatigue Buckling Deflections	Therm-Mech Fatigue Buckling Deflections	Thermal Stress Buckling Deflections
Static Margins	High	High	High	-0.27
Normal Deflection	0.19 in	0.12 in	0.45 in	0.51 in
Buckling Eigenvalue	High	0.99	0.83	0.61
Acoustic Fatigue Margin	0.02	0.27	0.03	-.65
Therm-Mech Fatigue Margin	0.41	-0.6	-0.42	N/A
Flutter Margin	NA	NA	> 75,000 ft	31,000 ft

Approved for public release; distribution unlimited.

Specific panel design drivers include:

- Thermal-stresses dominate over mechanical & acoustic stresses for most panels
- Resulting compression loads drive deflections, buckling and panel-to-substructure joint fatigue
- Panel breakers help limit buckling and deflection, but create breaker-to-panel joint fatigue issues
- If large deflections from flexible panels without breakers are acceptable, these panels may have acoustic fatigue issues
- Flutter does not appear to be an issue for acreage structural panels

The following is a summary of loading requirements from the four panels studies described in the earlier sections of this report.

Thermal Loads:
- Max temperature up to 1500F
- Non-uniform heating (surface temperature) control – (Panel surface temperature can vary by 100 deg/ft)
- Thermal (isolation) load path control to facility – maintain uniform gradients to panel edges and reduce any heat loss to fixtures.
- Applied Thermal Transients (Induce Structural Temp ~ 3 degs per sec)
- Heating and Cooling transients in trajectory

Acoustic Loads:
- Spectrum control from 50 to 500Hz – aero- acoustic type
- Max levels up to OASPL = 167dB
- Long duration testing up to 8hrs per test segment
- Constant acoustic level monitoring up to 4 high temp microphones

Static Loads:
- Uniform steady pressure up to +/- 1.5 psi – due to external aerodynamic flow and/or internal pressurization – backside pressure box
- Line loads (in-plane static loads 1200 lbs/in) – due to maneuver loads

Test Article Size:
- Size: Height = 40”, Width = 60”-90”, Depth = 20”
  - Support and load introduction fixture may require up to 30” on each side of panel
- Slight Curvature ~ 500” – during acoustic testing in CEAC test article may protrude into chamber
- Materials: Titanium and Inconel, stainless steel fixture

<u>Test Priorities:</u>
1. As a minimum, a radiant thermal test of a panel attached to a flexible substructure should be performed to validate thermal stress & deflection predictions.

2. A thermal-acoustic test of a panel w/ & w/o a panel breaker attached to a flexible substructure would help verify acoustic response predictions and combined load effects
    - This could be the same panel and substructure as the thermal only test
    - Thermal only test would allow better temperature control than the CEAC and thus adds value
3. A thermal-mechanical test of a panel (w/o substructure) with active load control would allow for additional thermal and combined load cases, but superposition of flight loads is not a driver
4. A wind tunnel test that would verify heating, deflections, acoustic levels and flow interactions

6.4.1 Thermal and Thermal-Mechanical Testing

The thermal-mechanical is required to verify thermal response, and the thermal compliance features of the design. For this type of test, a special load introduction fixture needs to be built with a heat lamp bank mounted over the test panel for the high temperature thermal runs. A photo of a similar test rig with the panel installed is shown in Figure 171.

Thermal Only

Setup: Panel with flexible sub-structure under quartz lamps (no mechanical loads)

Goal: Validate thermal stress/strain predictions; sub-structure joint modeling; thermal-mechanical fatigue

Other: This is a non-destructive test, hence the specimen can be designed to be used in a second test; such as, thermal-acoustic testing.

Thermal-Structural

Setup: Panel mounted in high temperature load fixture (uni or bi-axial) with quartz lamps

Goal: Validate thermal load/stress/strain; mechanical load/stress/strain; non-linear deflection impact on loads; thermal-mechanical fatigue

Other: High temperature test fixture will be complicated; ensure panel design has robust attachments to drive acreage failure; investigate methods to accelerate low-cycle fatigue

Approved for public release; distribution unlimited.

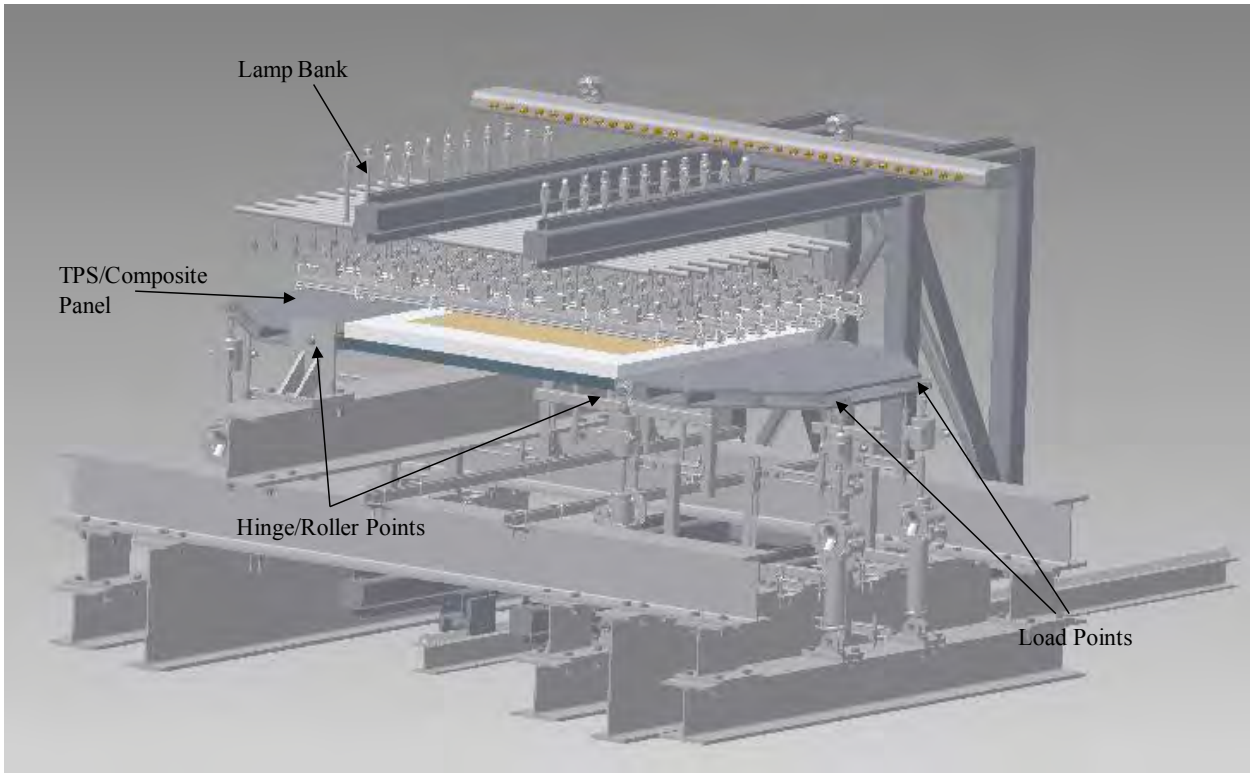

Figure 171. Combined thermal & structural curvature test fixture for a CMC TPS Panel [4]

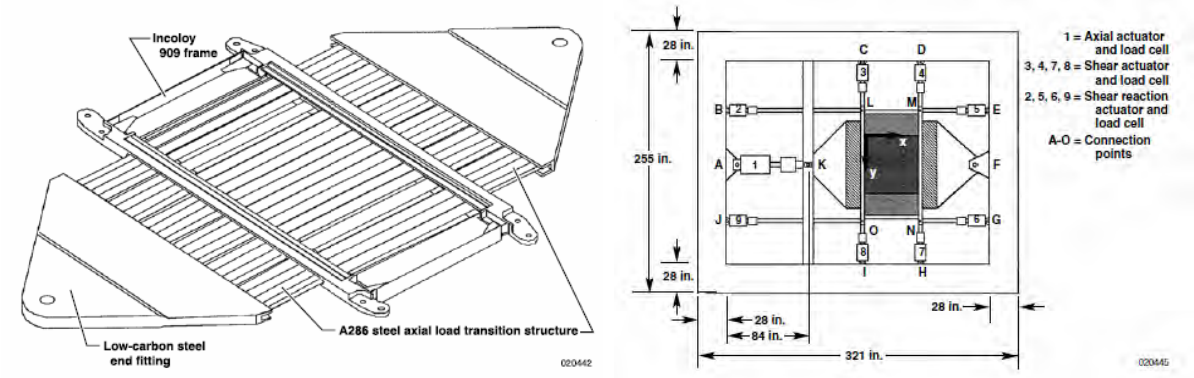

Figure 172. NASP TMC Shear Panel test load fixture (lamps not shown) [6]

6.4.2 Thermal-Acoustic Testing

The thermal-acoustic test is required to verify durability analyses. Also, the test will verify any nonlinearity geometric behavior due to thermal and acoustic loads. For the four candidate panels, neither static pressure nor mechanical loading is required for these tests. A typical setup is shown in Figure 173, reference (2).

Setup: Panel with flexible sub-structure mounted in CEAC (no mechanical or pressure loads)

Goal: Validate thermal loads; sub-structure joint modeling; how thermal loads affect dynamic response; and acoustic fatigue predictions at elevated temperatures

Other: Perform accelerated test based on material S-N curves; ensure panel design has robust attachments to drive acreage failure;

Figure 173 – Stiffened Panel Test in the AFRL CEAC Facility

6.4.3 High Temperature Wind Tunnel Tests

A hypersonic wind tunnel test in a facility like the NASA Langley Research Center (LaRC) High Temperature Tunnel (HTT) would validate aero-heating predictions; deflection due to heating; and increased heating due to deflections. A slightly reduced-size panel could fit on existing sleds into the 8 ft Mach 7 tunnel, shown in Figure 174. Flow conditions that can be achieved in the facility should be compared to the reference trajectory and available CFD results to select test conditions that best match the panel design conditions listed in Section 6.2.

Setup: Panel mounted on existing sled for Langley 8-ft Mach 7 tunnel

Goal: Validate aero heating predictions; deflection due to heating and flow; and increased heating due to deflections.

Other: Leverage TPS Integration Program sled modifications and instrumentation; access panel gapping issues.

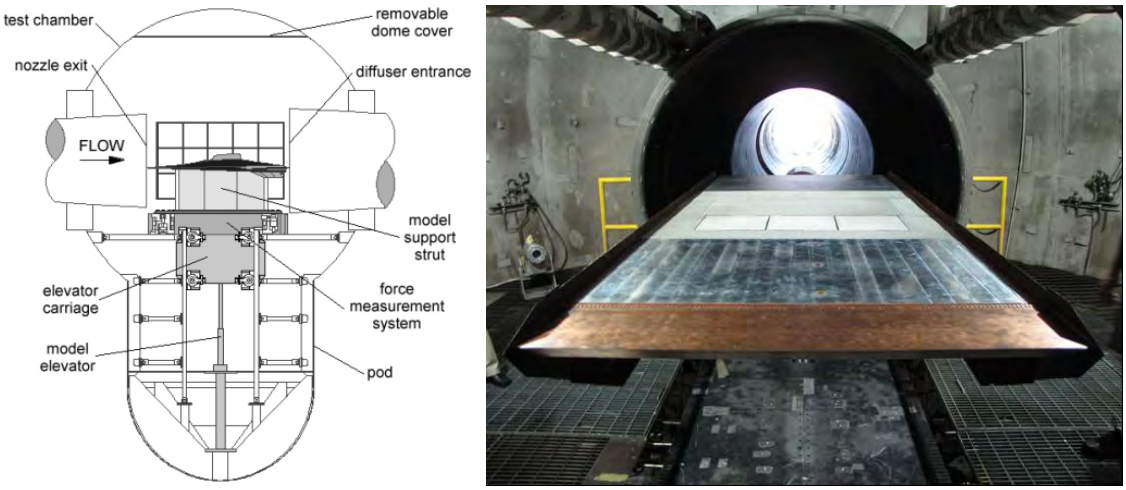

Figure 174. Schematic and test photo for NASA LaRC 8-ft, Mach 7 HTT

Approved for public release; distribution unlimited.

7.0 REVIEW OF PREDICTIVE CAPABILITY GAPS

The predictive capability knowledge gaps identified in Boeing's Phase I program [2] are reviewed and compared to findings from this Phase II effort in the following sections.

7.1 Summary of Gaps Identified in Phase I

Predictive capability knowledge gaps identified by Boeing in the Phase I program include:

1. It is difficult to identify the critical design load combination for thermo-mechanical and acoustic loads. The SoA assumes that the worst case loading scenario meets and exceeds the design requirements. The workaround is accomplished by using the worst combinations of loads from different trajectory points.
2. The temporal and spatial thermal gradients are difficult to adopt in the panel level linear analysis. The assumption causing the gap in this SoA method is that the maximum temperature and thermal gradient are used for the critical thermal load conditions. The work-around is to use maximum temperature or thermal gradient for the panel.
3. The linear frequency response analysis adopted in SoA does not account for the coupling between transient thermal and vibro-acoustic analyses. The linear analysis is conducted with the assumption of a constant thermal condition. The workaround is to ignore the coupling, use the thermal as the preload, and then factor in the acoustic response.
4. The panel evaluation and FE analysis need to properly include internal loads. The assumption is to use uniformly distributed loads along the boundaries of the panel FEM. The workaround is to ignore the internal loads in the panel evaluation process and the effect of using uniformly distributed loads along the boundaries of panel FEM.
5. Defining the thermal and mechanical boundary conditions for the detailed panel analysis remains a challenge due to primary reliance on subject matter experts (SME) past experience on similar analyses/efforts. The assumption is using prior experience and test scenarios will establish a conservative condition if the test scenarios show results below the allowable. A typical workaround would allow the SME to perform test scenarios and use experience to guide a boundary condition selection. For a project like X-51A, both fixed and hinged boundary conditions were used to ensure the response of structure was bounded. The two boundary conditions were both below the allowable.
6. The linear frequency response analysis does not account for large deformation oscillation or dynamic snap-thru of panel. The assumption is that the response will be linear and that there will not be large deformation oscillation or dynamic snap-thru. The workaround is to superimpose the static and dynamic solutions.
7. The accumulated damage and degradation due to exposure to high temperature environments is inadequately modeled in the SoA approach. The assumption is that degradation and accumulated damage can be simulated by knockdown factors. The workaround is to use knockdown factors for both materials and allowable.

8. Accurately predicting damping for analysis is a challenge due to lack of data. The assumption is that a low damping value, such as 1.6%, over-predicts the structural response. The workaround is to use a low damping value and accept the conservatism.
9. The acoustics can only be approximated using established empirical formulas at the beginning of the design phase until flight test can be conducted. The assumption is that the empirical formulas will provide sufficient data for initial panel sizing. The workaround for the preliminary design phase is to add a factor of safety (FS) to be conservative.
10. An efficient design and analysis method to analyze large-order models with a high fidelity mesh to capture nonlinear, dynamic snap-thru, and high frequency response in coupled thermal-acoustic environment is cost and schedule prohibitive for programs. The assumption is a heavier weight design will account for these factors in an effort to save time and cost. The workaround is to use the linear response analysis approach.

7.2 Confirmation of Phase I Gaps with Phase II Findings

Eight of the ten knowledge gaps identified in Phase I were confirmed in Phase II as shown in Table 34. The two gaps that were not confirmed, Gaps 2 and 6, were not however shown to be false. The panel level and unit cell analyses performed in Phase II ignored spatial aero heating gradients as these gradients were expected to have a small impact relative to the large gradients created by conduction and radiation within the structure. Furthermore, the explicit analysis performed on Panel 1 did not identify snap through as an issue, which however could occur if other panels were used in the study.

Table 34. List of Phase I Gaps with confirmation by Phase II findings

Phase I Gap Description	Confirmation in Phase II
1. Difficult to identify critical thermo-mechanical and acoustic load combinations	Task 3 Explicit Analysis
2. Difficult to adopt temporal and spatial thermal gradients in panel level linear analysis	**Unconfirmed**: : Uniform heating was assumed for each panel
3. Do not account for the coupling between transient thermal and acoustics in linear frequency response analysis	Task 3 Explicit Analysis
4. Cannot accurately include internal loads in panel level analysis	Task 2 Unit Cell Analysis
5. Cannot accurately define thermal and mechanical boundary conditions for detailed panel analysis	Task 2 Panel Sizing
6. Cannot simulate large deformation oscillation or dynamic snap-thru of panels	**Unconfirmed**: Not an issue with analyzed panel
7. Inadequately model accumulated damage and degradation due to high temperatures	Task 2 Panel Fatigue Allowables
8. Cannot accurately model damping in analysis	Task 3 Explicit Analysis
9. Can only approximate acoustic environment using empirical formulas until flight test data is available	Confirmed: All acoustic analyses used approximated environments
10. Lack the capability to analyze large-order high fidelity models to capture nonlinear, dynamic snap-thru, and high frequency response in coupled extreme environment	Task 3 Explicit Analysis

In addition to the eight Phase I gaps that were confirmed in this effort, several additional knowledge gaps have been identified:

11. Cannot adequately define panel level deflection criteria without an understanding of system level impacts to aero heating, drag, and performance. (Task 2)
12. Design iterations between detailed panel and vehicle load models are required to render the stiffness of the local panel consistent to the vehicle model. (Task 3)
13. Life and stress predictions around design features relies on a detailed tool to determine stress concentration factors (Tasks 2 & 3)

14. Establishing initial conditions for explicit dynamic analysis require a quasi-dynamic step inconsistent with the actual time variant environment. (Task 3)

7.3 Prioritized List of Revised Predictive Capability Knowledge Gaps

Through the execution of the detailed panel design and analysis effort, and subsequent evaluation of Phase I and new knowledge gaps, it became apparent that several of the previously identified and new gaps share similar themes and could be combined. The revised gaps listed below combine the previously identified specific gaps into three broad predictive capability knowledge gaps. This revised list has also been prioritized to aid future planning efforts.

I. Unable to accurately and efficiently perform multi-scale static and dynamic thermal-structural analysis with multiple types of loads. Common practices include the distributed loading of boundary edges and mapping combined nodal forces onto detailed models. Applying distributed loads to boundary edges ignores the effect internal loads including applied pressures, inertial loads, and attached systems. Conversely, mapping combined nodal forces, as was done on this program, can be labor intensive and makes it difficult to separate the effects of each load and trace the causality of the predicted structural response. This is particularly important when trying to debug or verify the response of a new model. Both of these methods also rely on the stiffness of the panel or feature being analyzed in the detailed model being consistent with the representation of that feature in the loads model. As a result, if significant design changes are required to improve margins for the panel or feature of interest, both models need to be updated to reflect these changes. Lastly, the accurate application of thermal loads requires that the stiffness and thermal-strain of the surrounding structure be included in detailed analyses. The assumption that acreage panel thermal stresses are mostly influenced by nearby structures allowed the application of the unit-cell analysis approach in this study. This assumption however will not be valid for more detailed analyses of design critical features with high in-plane thermal gradients along the propulsion flow path and near the leading edges. This revised gap addresses Phase I gaps 4 and 5, as well as new gaps 12 and 14.

II. Unable to accurately predict multiple basic physical phenomena, resulting in a reliance on scaling functions and the extrapolation of empirical data. Physical phenomena not currently addressed by commonly used methods include: a) the degradation of materials due to high temperatures, cyclic loading, and notch features; b) material and structural damping; c) aerodynamic and propulsion system acoustic environments; and d) hypersonic flow parameters near or around surface imperfections. Structural and material life predictions are typically evaluated with allowables calculated by multiplying several knockdown factors, each with built in conservatism. Material and structural damping assumptions are typically taken from prior testing of similar structures. Acoustic environments are scaled from flight or wind tunnel test data at similar flow conditions and the prediction of hypersonic flow conditions around surface features remains an active area of investigation. In order to ensure robust margins once test data is available, excessive conservatism is often incorporated in the design to counter the uncertainty of these scaled and extrapolated values. This revised gap addresses Phase I gaps 7, 8, and 9, as well as new gap 13.

III. It is computationally impractical to perform transient thermal-mechanical analyses with radiation on large order models. To overcome this, separate models are commonly built to determine flight loads, thermal gradients, and component level static and dynamic responses. Results from the loads and thermal models are mapped onto component models, and any component design changes will require updates to each model. The more integrated and sensitive the design is to coupled-loads, the more cumbersome and lengthy this iteration process becomes. To simplify the problem, the number of combined load cases is often limited to expected worse case conditions. Peak temperature and gradient thermal cases are superimposed with worse case maneuvering and acoustic loads. Although this is typically conservative, there are often intermediate transient thermal-load cases, in between the peak gradient and thermal soak condition, where reduced strength at temperature results in a lower margin than the peak gradient or thermal soak cases. Furthermore, it can be difficult to accurately apply combined thermal and mechanical preloads to dynamic models and these interactions are often ignored. Several hot structure and TPS component design efforts have overcome this challenge by using a single model to perform detailed transient thermal-mechanical analysis. This is possible because these components tend to be relatively isolated cantilevered parts with limited interaction with the primary structure such as a control surface, exhaust nozzle, or parasitic TPS standoff panel. Because of their relative size and isolation, these components can be accurately represented with a low order model (< 25,000 linear elements) for which a full trajectory thermal-mechanical simulation can be completed in a few hours. Dynamic analysis can also be run with the same model using quasi-static thermal-mechanical solutions for the transient analysis as an initial condition. If a similar approach were taken with a high order model (> 200,000 elements) several days would be required to complete each simulation, which is considered impractical for preliminary design efforts. This revised gap addresses Phase I gaps 1, 2, and 3, as well as new gap 14.

8.0 CONCLUSIONS

8.1 Technology X-Vehicle Refinement Conclusions

Attempts to modify the TX-V structural FEM to create a "closed-concept" using realistic material and thermal assumptions, while not changing the basic structural concept, were unsuccessful. Large thermal gradients between the skin and substructure coupled with the high CTE of the high-temperature alloys considered create significant thermal stresses which cannot be reduced through structural sizing. Global vehicle sizing required a 60% reduction in skin panel CTE to achieve closure. Equivalent orthotropic material properties for a flexible sine-wave substructure were later developed and incorporated into the global FEM reducing the thermal loading significantly. Incorporation of these or similar properties in future high speed vehicle studies will likely improve global sizing results for thermal load cases.

8.2 Detailed Design and Analysis Conclusions

High thermal loads require not only advanced materials, but also a different design methodology. Compliant structure that allows for thermal growth is necessary for all metallic vehicles. In order to design this structure, several iterations are required to achieve positive margins of safety for all analysis checks. A large portion of these iterations are due to the inability to accurately estimate thermal loads during initial sizing and the inability to quickly iterate design trades w/o completing the entire analysis process. Also contributing to this difficulty is the unavailability of relevant panel deflection sizing criteria and requirements. While it is possible to achieve a flight worthy design for the acreage panels, significant effort will be needed to address panels with extremely high temperatures, therefore very low material allowables.

8.3 Verification Study Conclusions

Panel behaviors in the explicit dynamic analysis were fairly linear and can be explained with the linear vibration modes. Moreover, no panel snap-thru was observed. This is likely due to the high static buckling margin for the selected panel. The other three panels had negative buckling margins and may exhibit a more non-linear response if analyzed with explicit methods. Flight loads were also not applied to the explicit model and their inclusion may have influenced the dynamic response. The comparison of nonlinear explicit dynamic solution with a cycle counting fatigue analysis to that of the linear response concludes that the fatigue life predicted at the center of panel by the explicit dynamic solution is more conservative but similar to the linear response solution with fatigue allowable.

8.4 Phase III Test Conclusions

Full scale, or near full scale, panel level testing will advance the goals of the *Predictive Capability for Hypersonic Structural Response and Life Prediction* program. Existing government ground test facilities can simulate multiple relevant combined environments and provide the data required to verify structural response and life predictions. A panel test program

consisting of a combination of thermal, thermal-acoustic, thermal-mechanical, and wind tunnel test series, supported by select coupon and element tests, will be able to validate several critical predictions required to design hypersonic acreage structure. In doing so, such a test program will build trust in the analytical methods being used, effectively reducing the risk of implementing an all-metallic Mach 7 airframe.

Approved for public release; distribution unlimited.

9.0 RECOMMENDATIONS FOR FUTURE WORK

In order to further advance hypersonic structural response and life prediction capabilities, the following recommendations are made for process and method development. These recommendations are organized into two sections by the scale and fidelity at which they occur: at the global vehicle level and at the panel or unit cell level.

9.1 Global Vehicle Loads and Sizing Recommendations

Investigate the viability of using of equivalent orthotropic material properties to represent flexible sine-wave or corrugated substructures in large scale loads models as a best practice. Although this program determined it was possible to represent the stiffness of one web configuration, multiple configurations should be explored along with the ability to correlate stress results. Furthermore, design curves or equivalent property estimating guidelines should be published to facilitate incorporation of flexible substructure concepts in early vehicle level analysis iterations.

Explore analysis methods and processes for efficiently incorporating high fidelity thermal boundary conditions at the global vehicle. Transient thermal effects due to engine heating, fuel use, internal insulation, and internal radiation significantly impact peak thermal gradients and the resulting thermal loads. Incorporation of these effects in the global vehicle FEM is currently perceived as being computationally prohibitive. This is particularly true of internal radiation, which is a principal source of heat transfer with the unit cell at the temperatures of interest.

9.2 Detailed Panel Analysis Methods

Perform combined environment verification tests to determine the accuracy of structural response and life predictions. Testing should be performed at or near full scale for a given panel and should explore the combination and interaction of thermal, mechanical, acoustic, and aero-heating loads. Although combining all critical flight environments would be cost prohibitive with existing ground test facilities, thermal-structural, thermal-acoustic, and wind tunnel tests would provide valuable data.

Develop methods for automatically mapping multiple loads, and load types, from a global vehicle model to a detailed unit cell or panel model along its boundaries. Under the executed program Boeing used a nodal forces mapping technique that ensures all internal and external loads are accounted for. This process however, makes is difficult to determine free body forces along a boundary of interest, and thus difficult to determine the cause of a given structural response. Ideally, global FEM loads, including mechanical, thermal, pressure, and inertial loads, could be mapped separately to a detailed unit cell or panel over the appropriate edge or surface boundaries.

Develop out-of-plane structural deflection sensitivities, sizing criteria and design guidelines for Mach 5 to 7 class cruise vehicles. This class of vehicles will inherently see high thermal gradients across the structure, and the resulting out-of-plane deflections can significantly reduce

the in-plane loads and stresses created by these gradients. Unfortunately, these deflections can also increase local surface heating, potentially creating a vicious feedback cycle of increased deflections and heating. Furthermore, large panel deflections may also impact vehicle aerodynamic performance and total system performance. In order to effectively design for these effects and balance the competing desires to reduce thermal loads and minimize aerodynamic interactions, deflection or deflection slope criteria or design guidelines based on heating, drag and performance sensitivities are needed.

Investigate coupled transient thermal-stress analysis methods for use on vehicle, unit cell, and panel level models; and if computationally reasonable, implement these methods in future detailed design efforts. Coupled transient thermal-mechanical analysis has many advantages and is widely used for hot structure components such as exhaust structures, control surfaces, and parasitic TPS. These analyses can evaluate margins at all time steps ensuring no critical combinations of load and temperature degraded allowables are missed. Coupled models also eliminate the need to build two separate models (thermal and stress) and map nodal temperatures, reducing potential sources of error and the number of steps required to iterate the design and update the analysis.

Develop and validate analytical methods to predict the evolution of material properties and strengths for conditions of interest, over the life of the vehicle, based on material failure mechanisms. Current design practice involves multiplying knockdown factors for thermal degradation, notch configuration (kt factors), load reversal ratio (R-ratios), and number of cycles. This creates a great deal of uncertainty in the allowable and additional conservatism is added to each prediction or factor to ensure that initial designs meet their life requirement. For example, 4 equivalent lifetimes is often assumed when determining the number of cycles to be used in a fatigue knockdown factor. Material testing at design points of interest is often performed later in a program to ensure positive margins, but this data is typically available too late in a program for it to be incorporated in a more efficient design. A trusted analytical method that could predict material evolution and end-of-life allowables would thus enable more weight efficient designs while reducing total testing costs.

10.0 REFERENCES

1. Spottswood, M., & Eason, T., *Statement of Objective, Predictive Capability for Hypersonic Structural Response and Life Prediction: Phase II – Detailed Design of Sustained Hypersonic Cruise Vehicle Hot-Structure*, May 2010

2. Tzong, G., Jacobs, R., & Liguore, S., *Final Report, Predictive Capability for Hypersonic Structural Response and Life Prediction: Phase I – Identification of Knowledge Gaps*, AFRL-RB-WP-TR-2010-3068, V1, The Boeing Company, Huntington Beach, CA, Contract Number FA8650-080D-3857-0015, September 2010

3. Bertram, M., & Wiggs, M., *Effect of Surface Distortions on the Heat Transfer to a Wing at Hypersonic Speeds*, AIAA J No6., June 1963

4. Embler, J., et al*., Final Report, AVTIP Delivery Order 0085: Thermal Protection System (TPS) Attachments for High-Temperature Composites*, AFRL-RB-WP-TR-2009-3227, October 2009

5. Liguore, S., et al., *Final Report, AVIATR Task Order 0013: Nonlinear Low Order Reduced Order Modeling Applications and Demonstrations*, AFRL-RB-WP-TR-2011-3102, December 2011.

6. Fields, R., et al., *Combined Loads Test Fixture for Thermal-Structural Testing Aerospace Vehicle Panel Concepts*, NASA/TM-2004-212039, February 2004

7. Embler, J., et al., *Final Report, AVIATR Task Order 0006: Windward Blanket Integration and Validation*, AFRL-RB-WP-TR-2011-3023, January 2011

8. R. Rackl, and A. Weston, *Modeling of Turbulent Boundary Layer Surface Pressure Fluctuation Auto and Cross Spectra - Verification and Adjustments Based on TU-144LL Data*, NASA/CR-2005-213938, 2005

9. Joint, *Metallic Materials Properties Development and Standardization (MMPDS),* MMPDS-05, April 2010

Engineering, Operations & Technology
Boeing Research & Technology

Panel 862 Heat Transfer Analysis

July 7, 2011

Pete Keller
206-544-7528
peter.c.keller@boeing.com

Approved for public release; distribution unlimited.

Thermal Analysis Methods and Approach

- heat transfer analysis conducted with I-DEAS/TMG
  - exercises mapping of temperatures to stress FEM using differing mesh and analysis tools (TMG to nastran)

- external aerothermal and internal component boundary conditions taken from previous studies

- simplified modeling of internal component details and attachments consistent with scope of current study

- model one complete cell and half of neighboring cells to accurately account for radiation from both sides of webs

Approved for public release; distribution unlimited.

Thermal Analysis Assumptions

Issue	Approach	Source/Rationale
External Aero-heating	MINIVER analysis	Phase 1 analysis
Upper surface radiation	Radiation to effective sky temperature (Swinbank's method) , view factor = 1	Preferred method:787, AWS, programs
Lower surface radiation	Radiation to earth surface (70 F), vf = 1	Standard conditions
Upper surface solar flux	Ignored	Insignificant w.r.t. aero-heating
Engine boundary condition	Uniform, time-dependant temperature inside 1" Min-K blanket	Lee Scuderi – previous programs
Internal cavity convection	Uniform natural convection at ambient pressure +1 psf	Kei Lau – previous programs
Internal radiation	Radiation enclosure in each cell	Symmetry in partially meshed cells
Initial temperature	Recovery temperature at time = 0.	Assumes uniform soak before flight
Material properties	Temperature dependent	Material property databases
Finite element formulation	All shell elements	Conductive material, thin components result in insignificant through-thickness gradients
Thermal contact between webs and skin	100 Btu/ft^2-hr-F interface conductance No fasteners modeled	Typical metal-metal handbook value - conservative

Approved for public release; distribution unlimited.

Orthogrid Panel 849 Finite Element Model

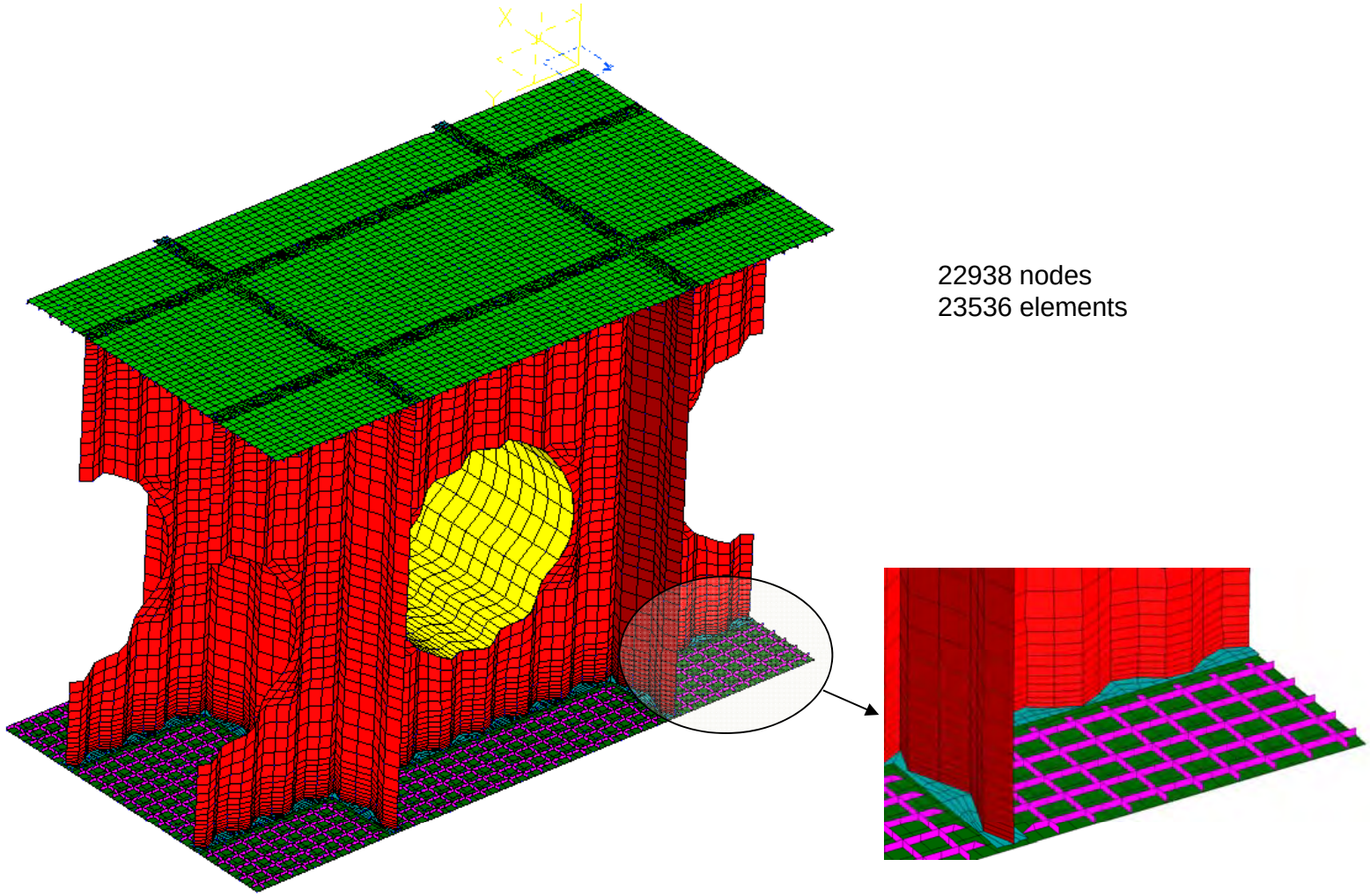

22938 nodes
23536 elements

Approved for public release; distribution unlimited.

Thermal Analysis Boundary Conditions

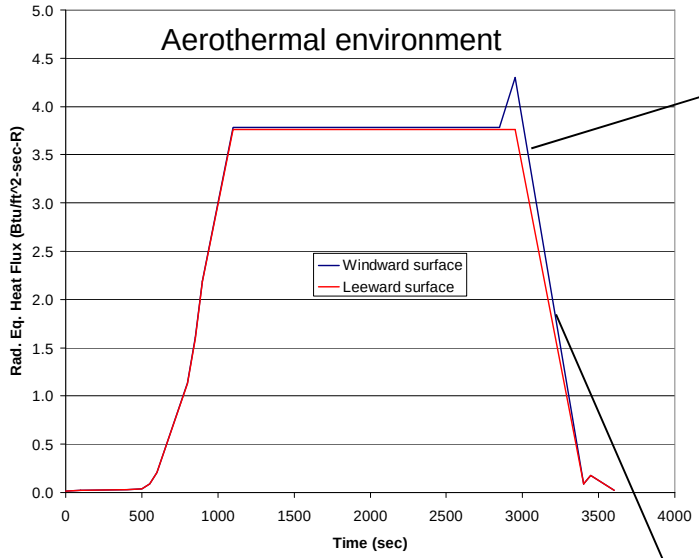

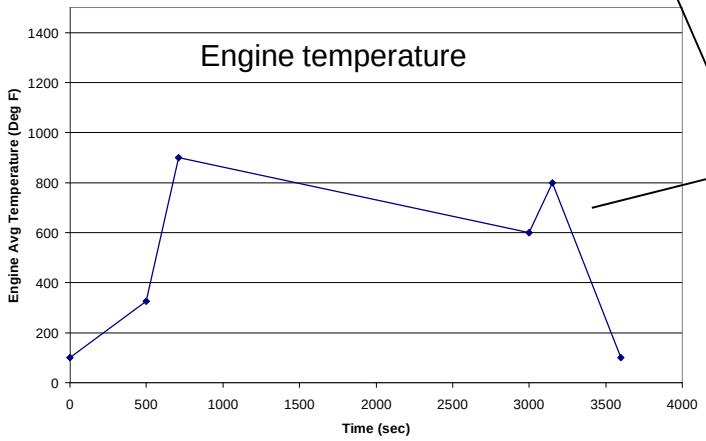

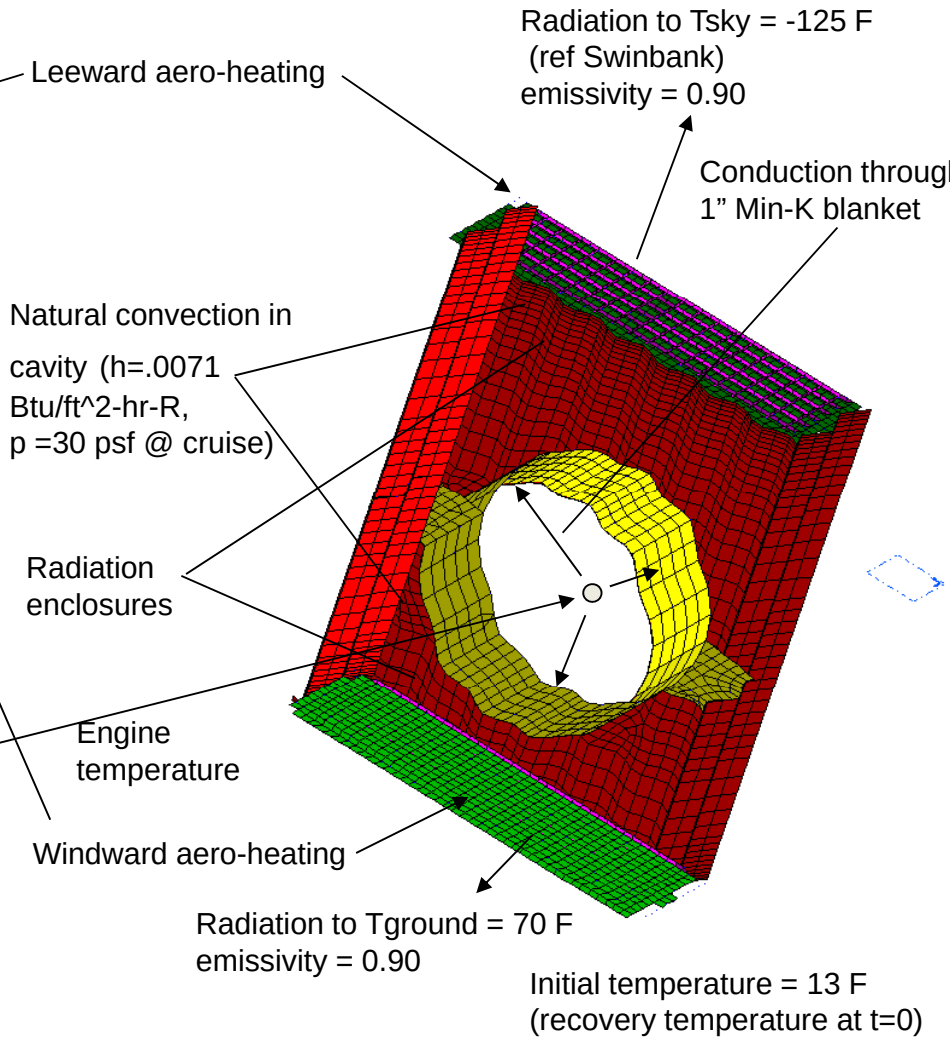

Approved for public release; distribution unlimited.

Panel 849 Temperature Distributions

acceleration 1020 sec

cruise 2400 sec

termination 3600 sec

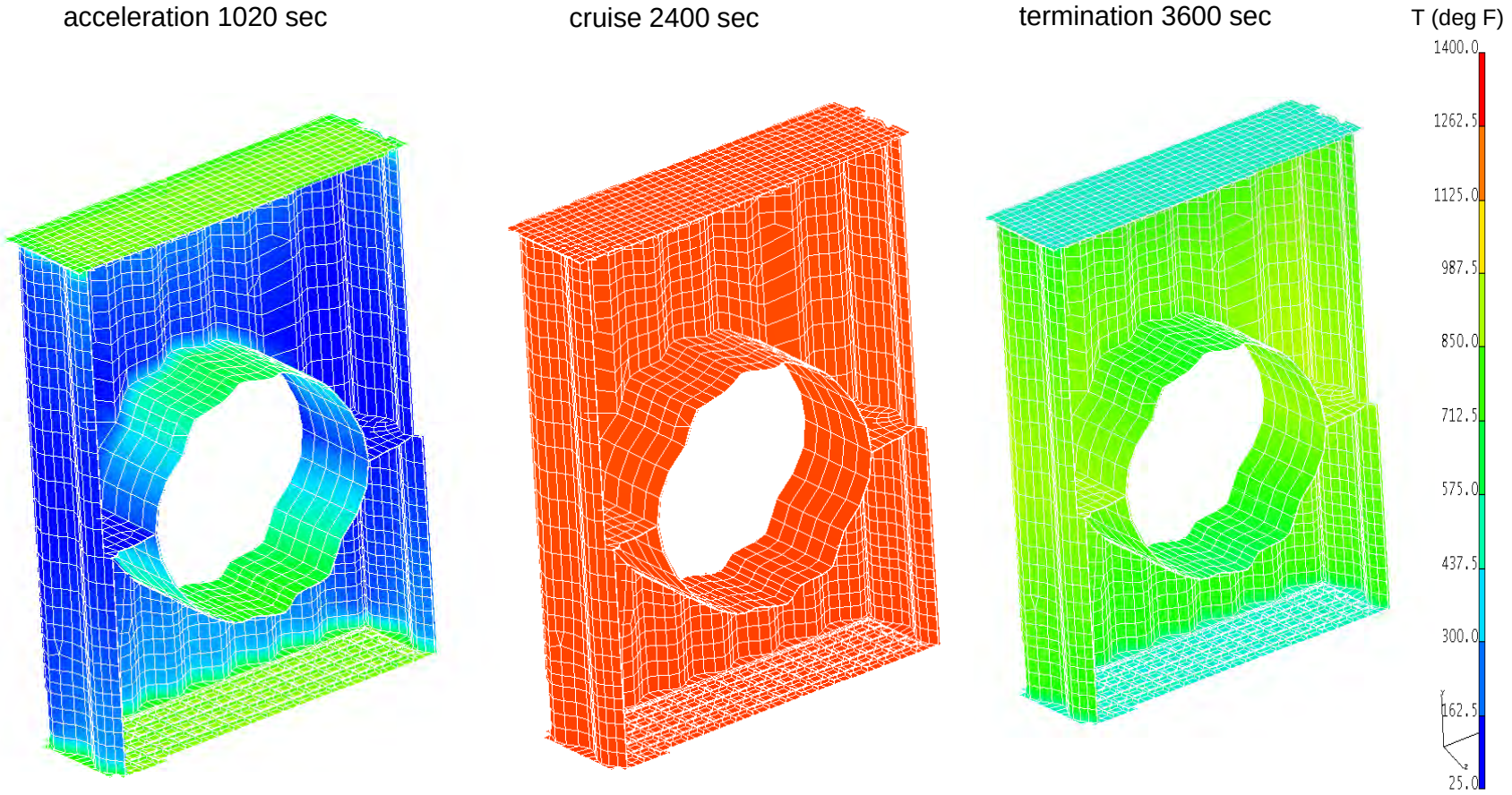

Approved for public release; distribution unlimited.

Transient Temperature Profile Locations

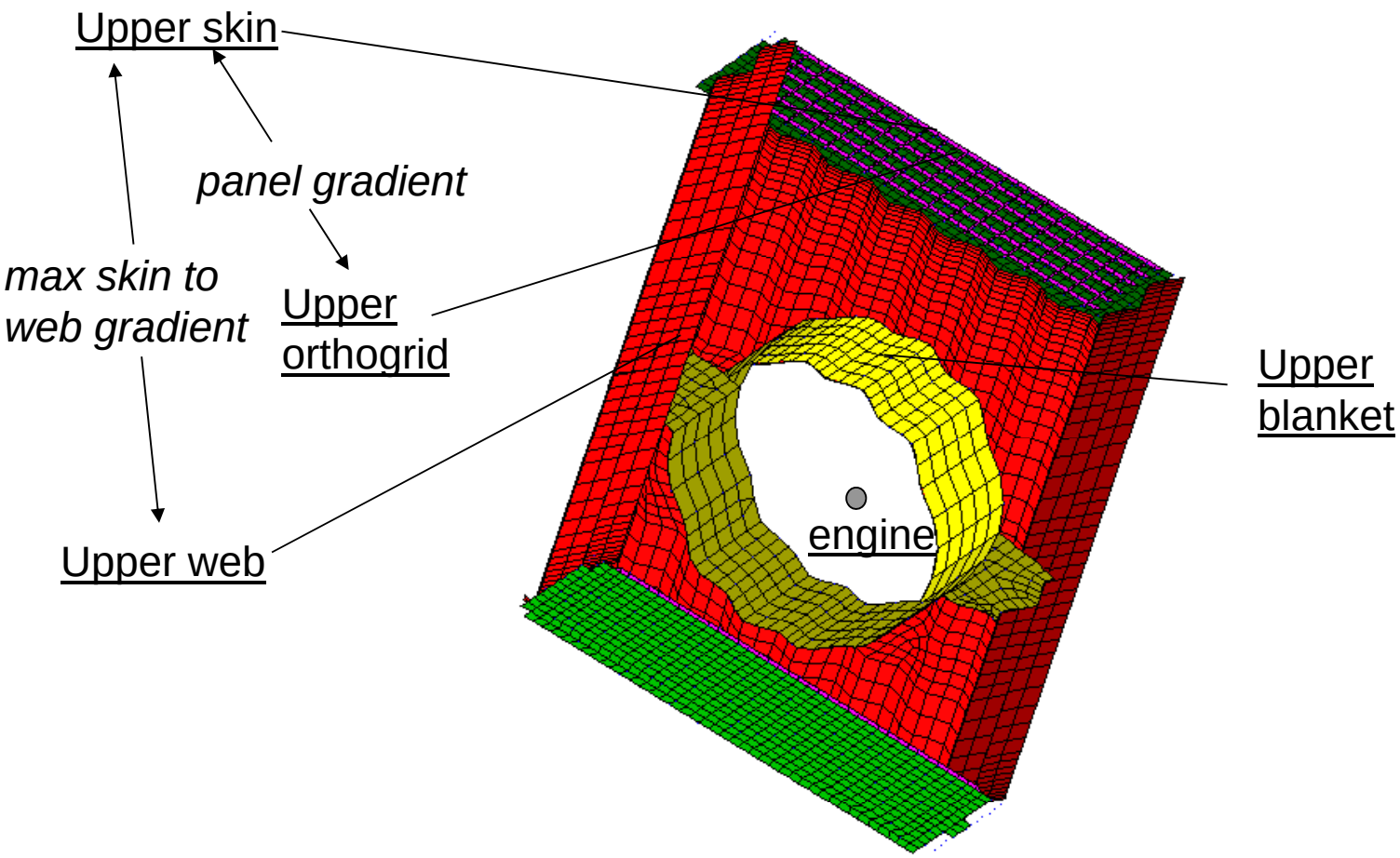

Approved for public release; distribution unlimited.

Orthogrid Panel 849 Concept Temperature History

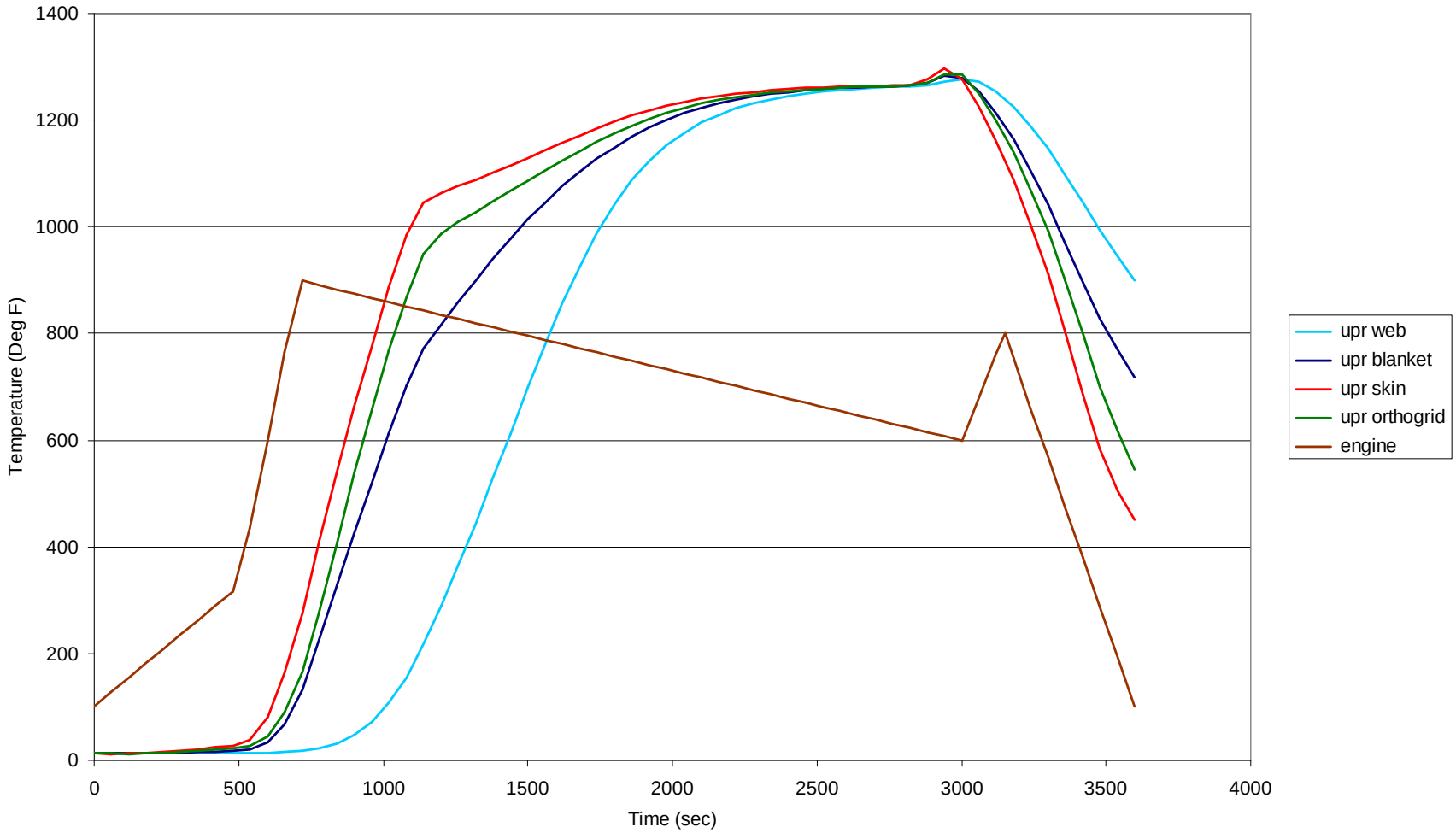

Approved for public release; distribution unlimited.

Orthogrid Panel 849 Concept Temperature Gradient History

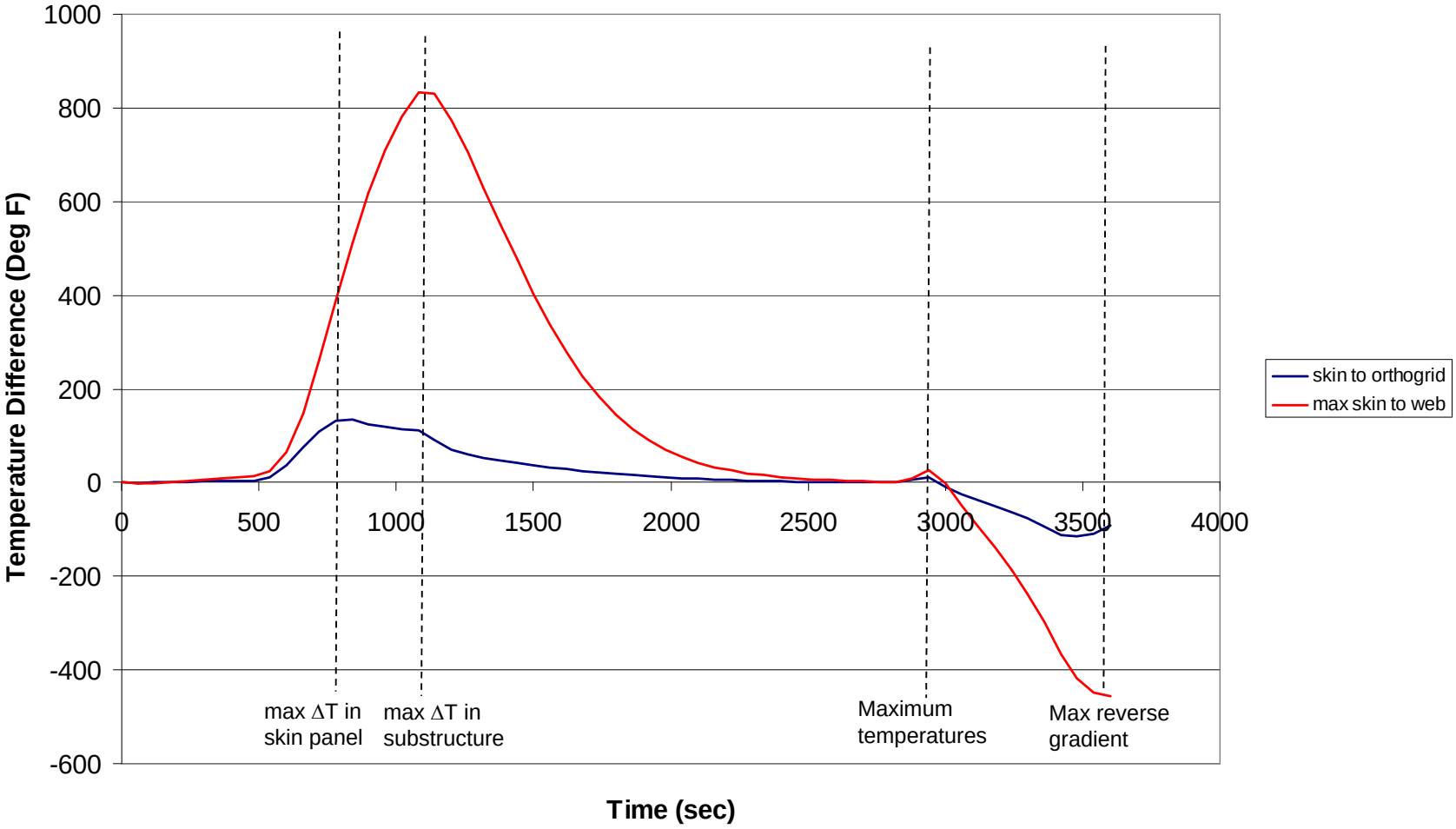

Approved for public release; distribution unlimited.

Summary

- maximum skin temperatures = 1298 F at 2940 sec
- maximum temperature gradient in the orthogrid = 135 F at 840 sec
- maximum temperature gradient between skin and web = 832 F at 1080 sec
- temperature distributions provided for thermal stress and acoustic analysis at all time states

Approved for public release; distribution unlimited.

Sensitivity of Temperature Gradients to Grid Refinement

Grid refinement at web/skin interface

The original FE mesh was found to be too coarse in the web/skin interface region, resulting in inaccurate temperature gradients and therefore thermal stress predictions.
A brief mesh refinement study was conducted to determine the density required for accurate thermal stress analysis.

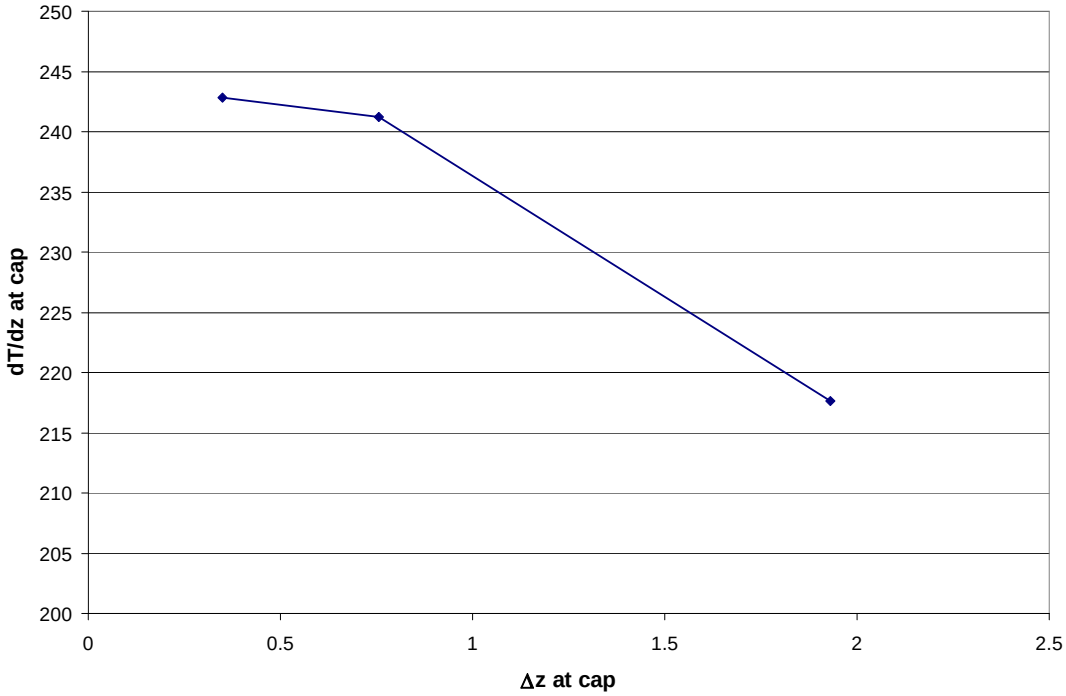

Approved for public release; distribution unlimited.

Heat Transfer Analysis Grid Refinement

Calculation of radiation view factors in internal enclosures increases greatly with model size. Therefore, limiting run time and memory requirements requires optimizing mesh density.

The original and refined mesh temperature predictions at 1080 seconds are shown below.

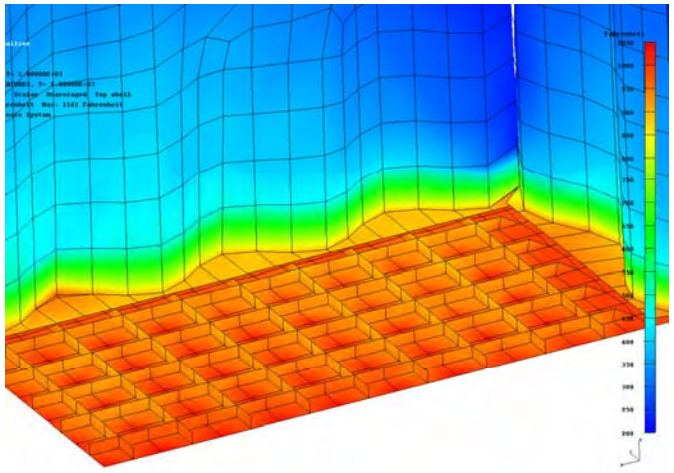

Original mesh
$\Delta z = 1.93$
$\Delta T/\Delta z = 217.6$ deg F/ in

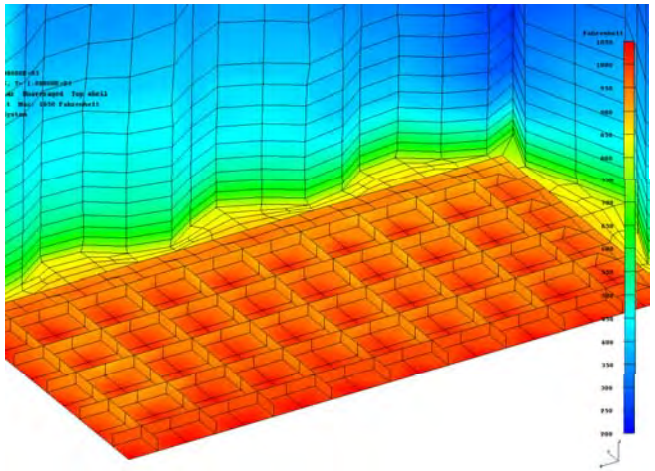

Refined mesh
$\Delta z = 0.35$
$\Delta T/\Delta z = 242.9$ deg F/ in

Approved for public release; distribution unlimited.

Heat Transfer Analysis Lessons Learned

- **Internal heat sources and sinks**
  - Temperatures, heat flux and heat capacity and of internal components can strongly effect internal structural temperatures
  - Additional complexity of detailed modeling of avionics, fuel tanks and engines can exceed the scope of studies

Lesson: Include simplified representation of all internal heat sources and sinks

- **Computational mesh density**
  - Mapping temperatures between dissimilar heat transfer and stress meshes can be very sensitive to differences in mesh density in critical locations.
  - radiation view factor calculations for fine mesh models can be extremely memory and CPU intensive.

Lesson: Use grid refinement study results to guide mesh size in critical regions.

Approved for public release; distribution unlimited.

Future Activities

Heat transfer analysis of panel 734

Windward skin panel also located in engine region

- create finite element mesh for panel
- integrate with existing web mesh
- apply windward surface aerothermal environment
- apply radiation to ground temperatures to surface
- create radiation enclosure with web and engine insulation blanket surface
- provide transient temperature predictions for stress and acoustic analysis

Approved for public release; distribution unlimited.

Panel 1 (862) Static Stress Analysis

August 19, 2011

Rob Quiroz
Robert.Quiroz@boeing.com
714-916-2577
BR&T Structures Technology

Approved for public release; distribution unlimited.

Panel Analysis Study

Static Analysis of unit-cell: 2.5G ultimate (FS=1.5) + Temp @ 1080 sec

1. Structure was imposed w/ rigid-body constraints; loads were balanced, i.e., zero reactions @ supports
2. Linear analysis revealed large corner deformations due to skin construction changed from H/C (vehicle model) to Orthogrid (panel model)
3. A constraint on out-of-plane rotation was then applied to better simulate support from surrounding panels to reduce corner deflection (not sufficient to eliminate the deformation)
4. Unable to converged a nonlinear analysis solution due to large deformation of the deep and flexible structure
5. Buckling analysis led to modes of keel and frame webs

Static Analyses using center panel model on upper surface (Panel 862) only

1. Applied displacement from unit-cell model as boundary conditions to center panel for 2.5G ultimate + Temp(1080s); an approximation for nonlinear analysis
2. Linear analysis; good comparison with unit-cell model
3. Converged nonlinear analysis unveiled slightly larger out-of-plane deflection of panel and lower stress
4. Buckling loads of center panel much higher than HyperSizer design

Approved for public release; distribution unlimited.

Model Constraints

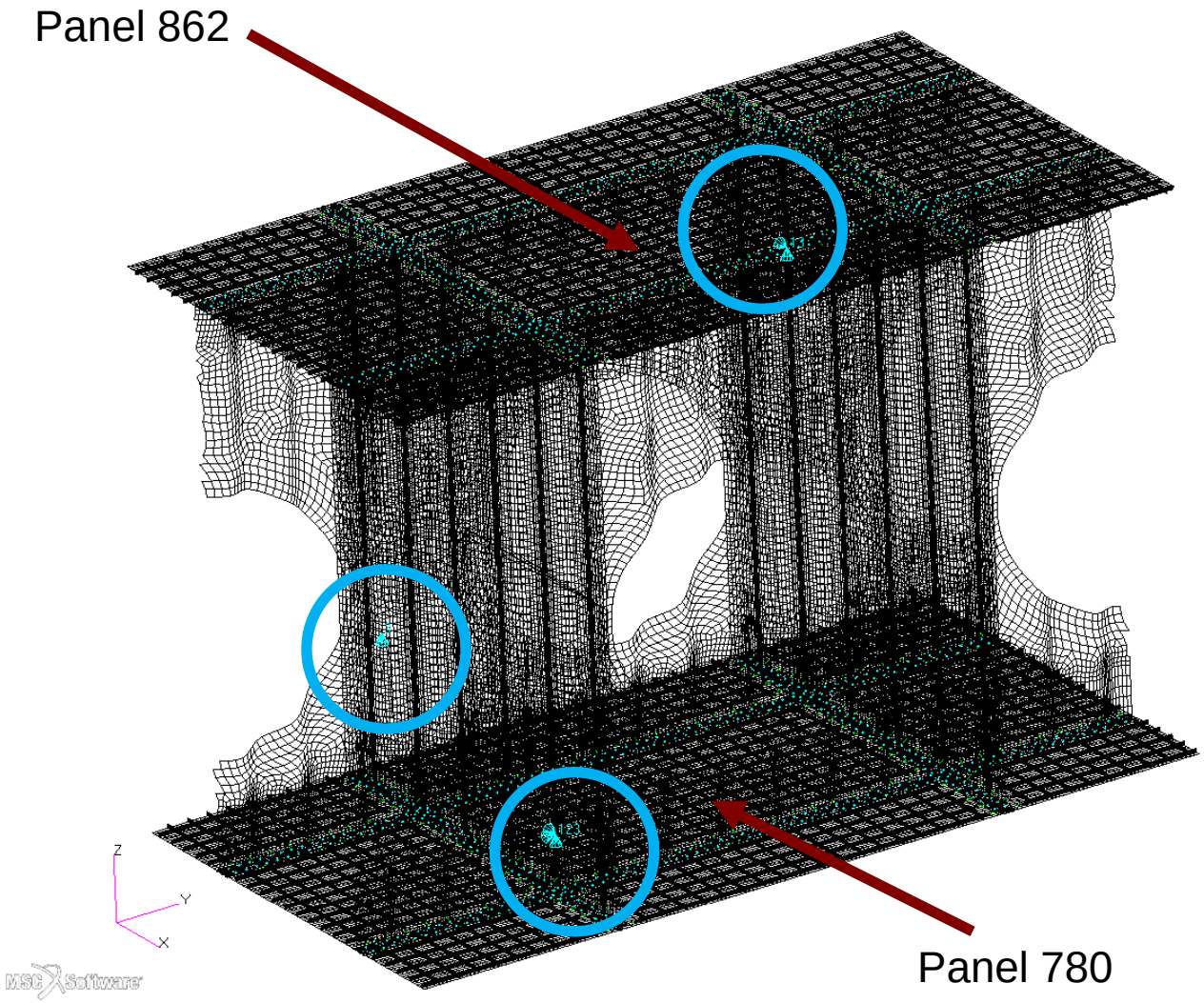

Approved for public release; distribution unlimited.

Normal Rotation Constraints Along Edges of Panel and Web

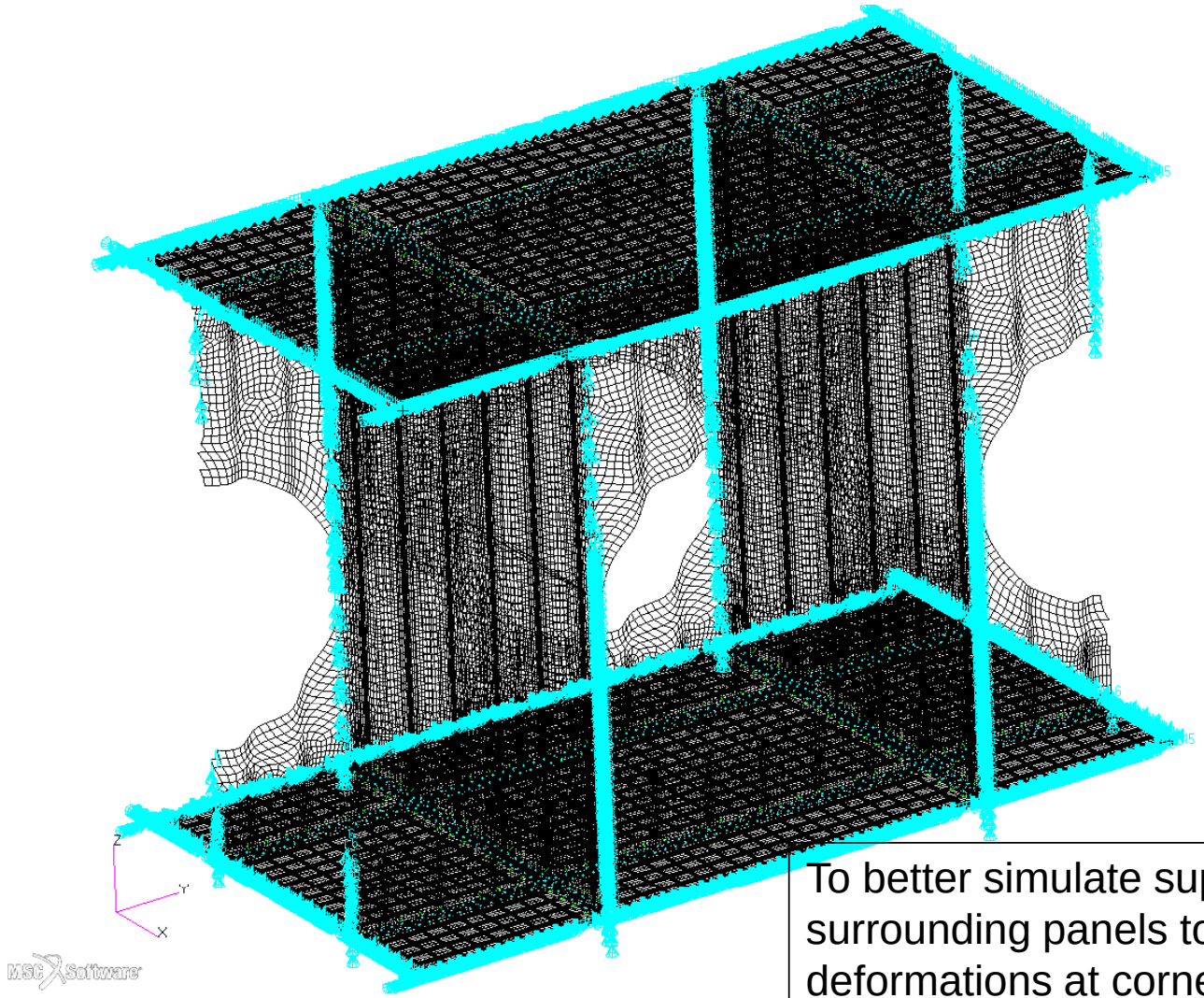

To better simulate support from surrounding panels to reduce large deformations at corners ~86” vs. 11.4”

Approved for public release; distribution unlimited.

Temperature Profile @ t =1080s

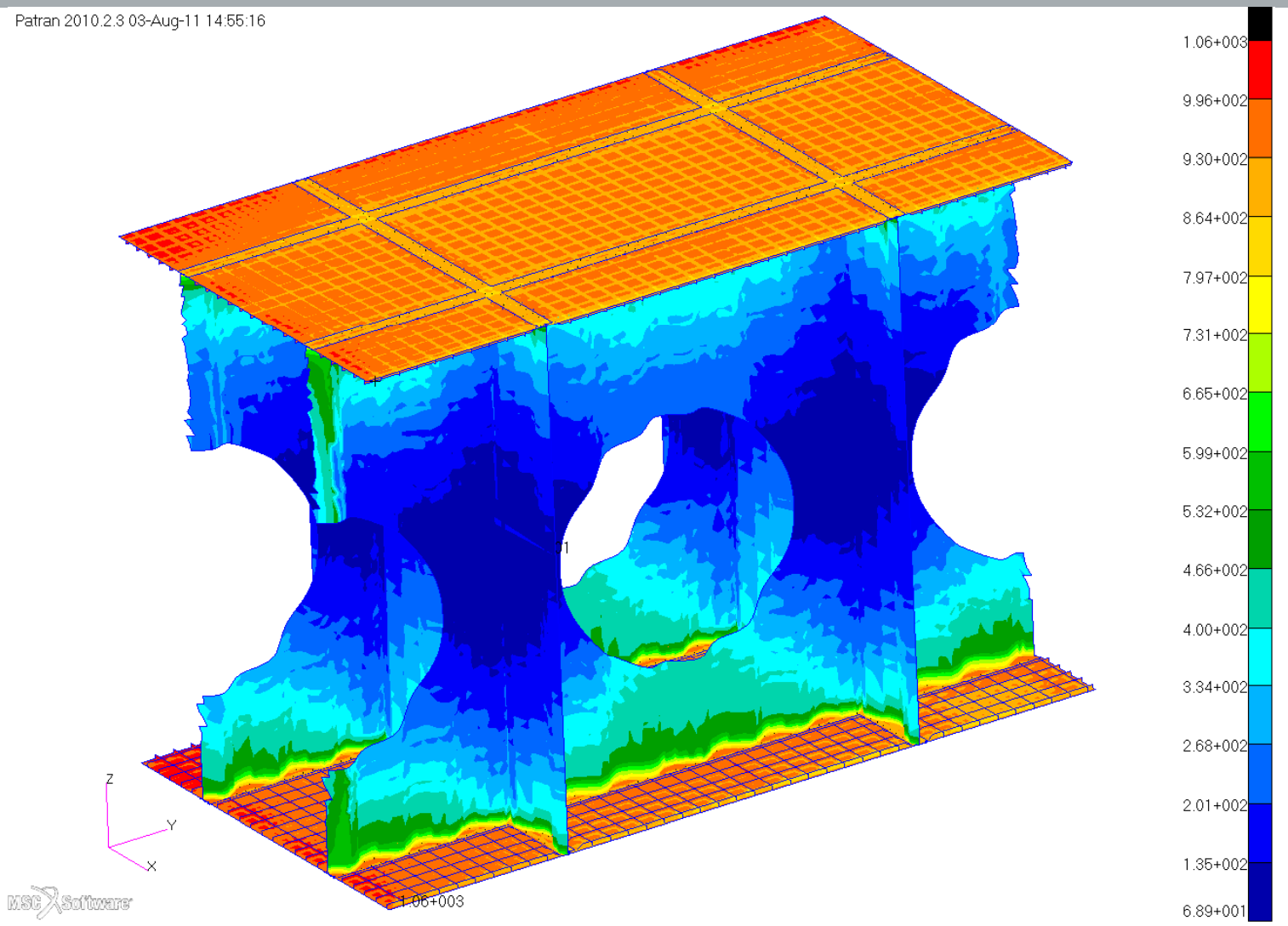

Approved for public release; distribution unlimited.

2.5g Mechanical Free-body Loading

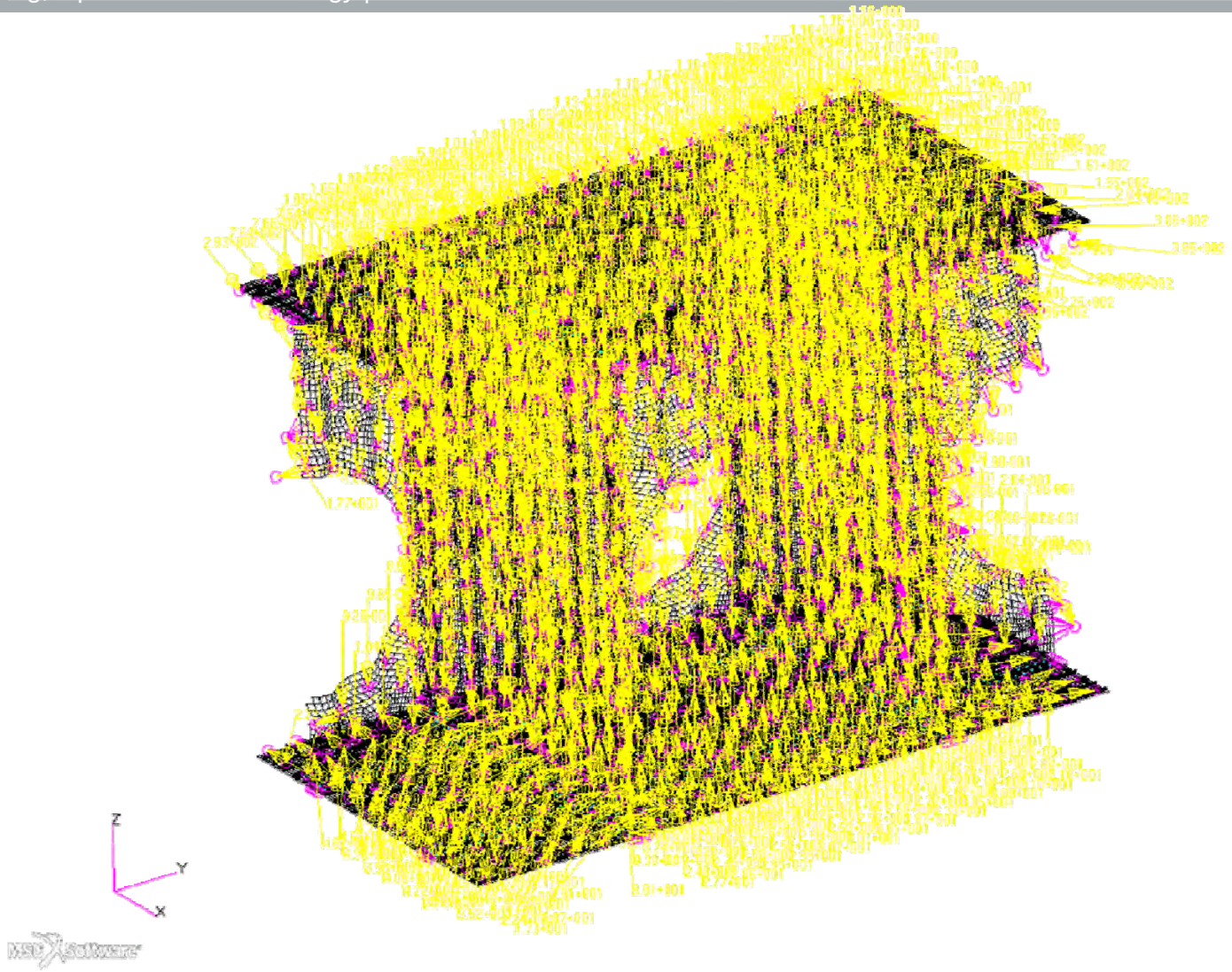

Approved for public release; distribution unlimited.

Unit Cell, 2.5g, Highest loaded corner nodes, 100% DLL

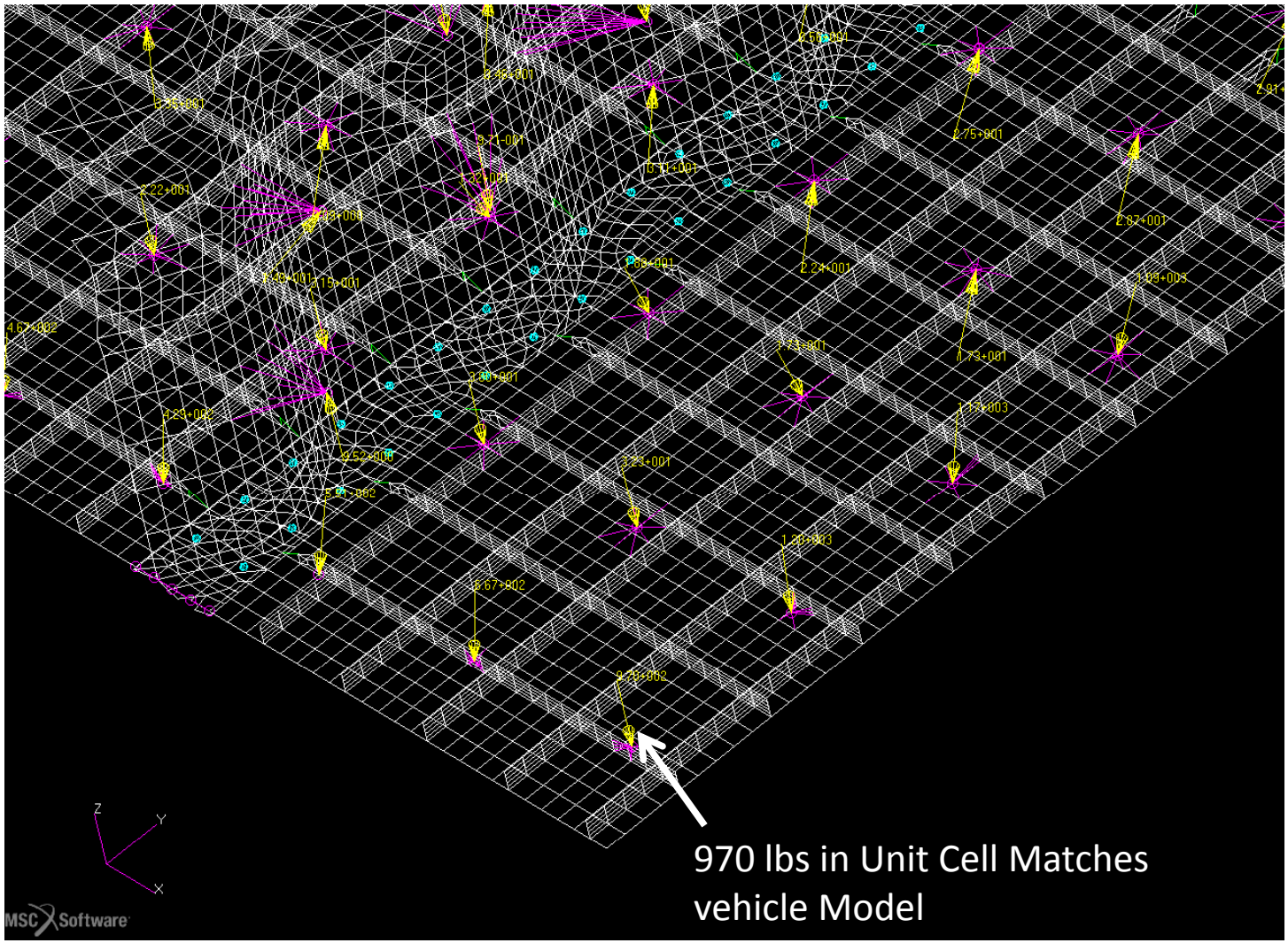

Approved for public release; distribution unlimited.

Displacements, Unit Cell, 2.5g Ult 1.5, T=1080s, Linear

Magnitude of Displacements

11.4” deflection at the unit cell corner Primarily due to Orthogrid construction with high loads from vehicle FEM (Vehicle H/C skin is much stiffer than Orthogrid skin in bending)

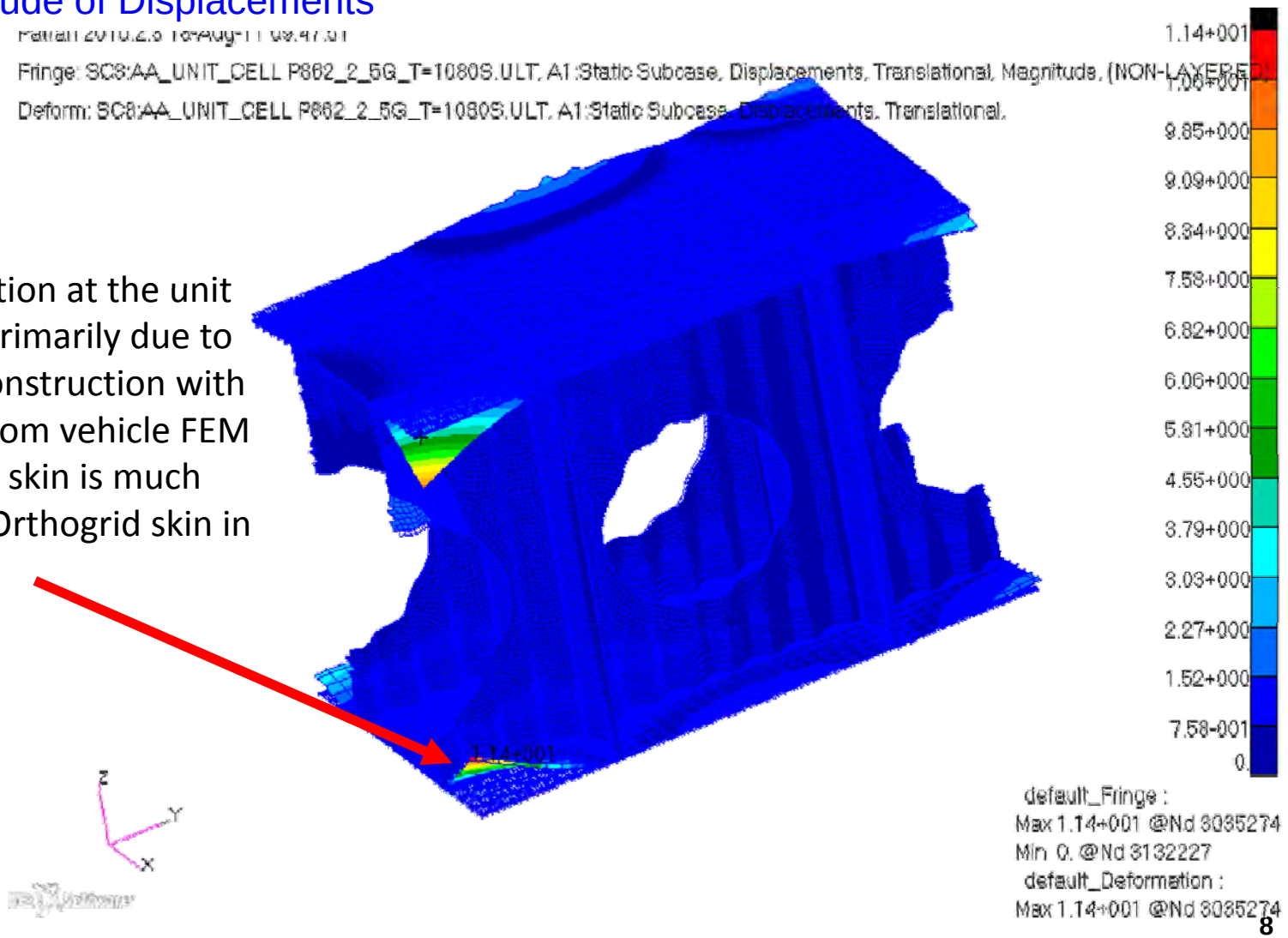

Approved for public release; distribution unlimited.

Von Mises, Unit Cell, 2.5g Ult 1.5, T=1080s, Linear

Stress Peaking at unit cell boundaries and at highly loaded corners of unit cell.

These concentrations may have minor effect to stresses in the center panel

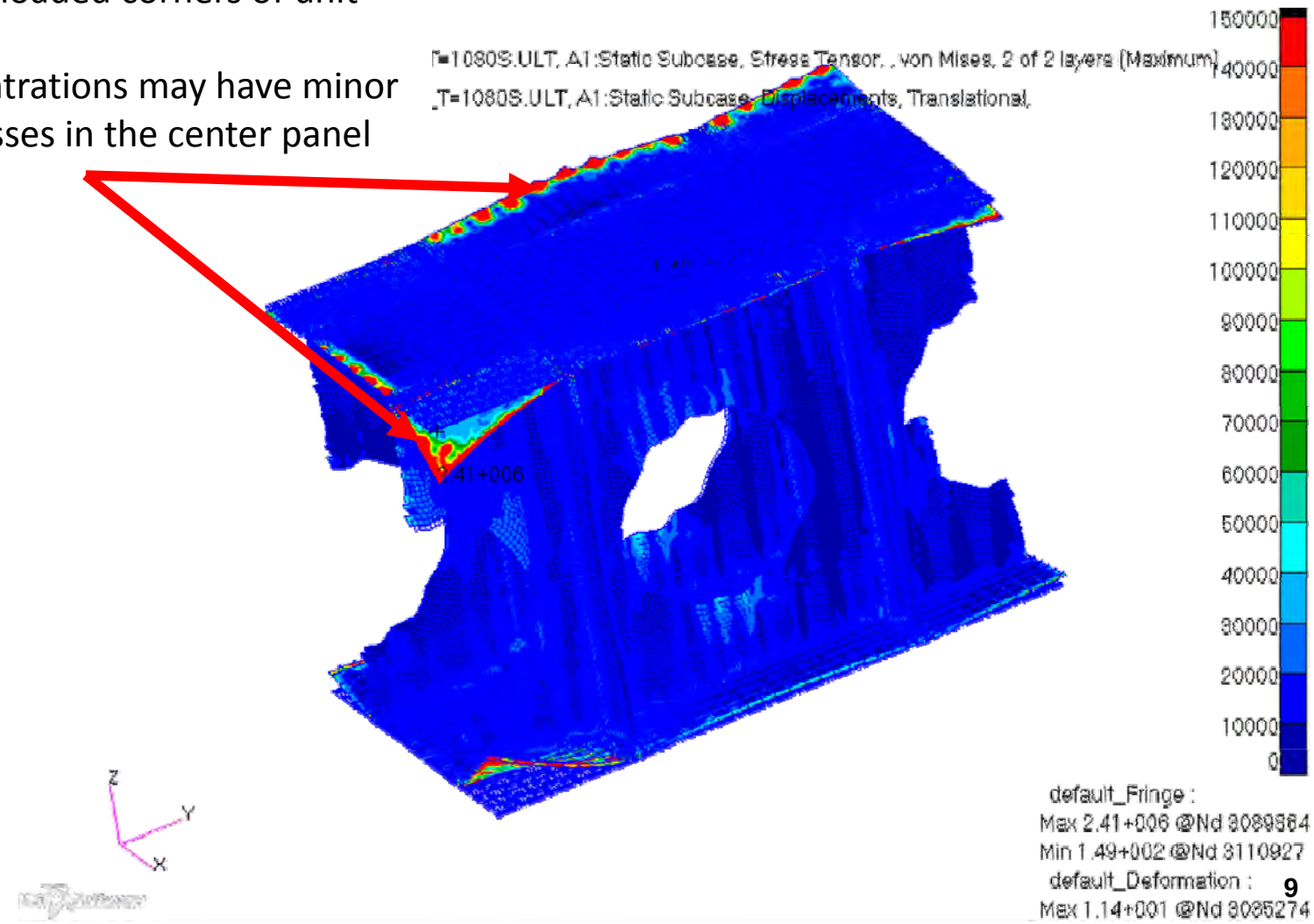

Approved for public release; distribution unlimited.

Von Mises, Unit Cell, 2.5g Ult 1.5, T=1080s, Linear

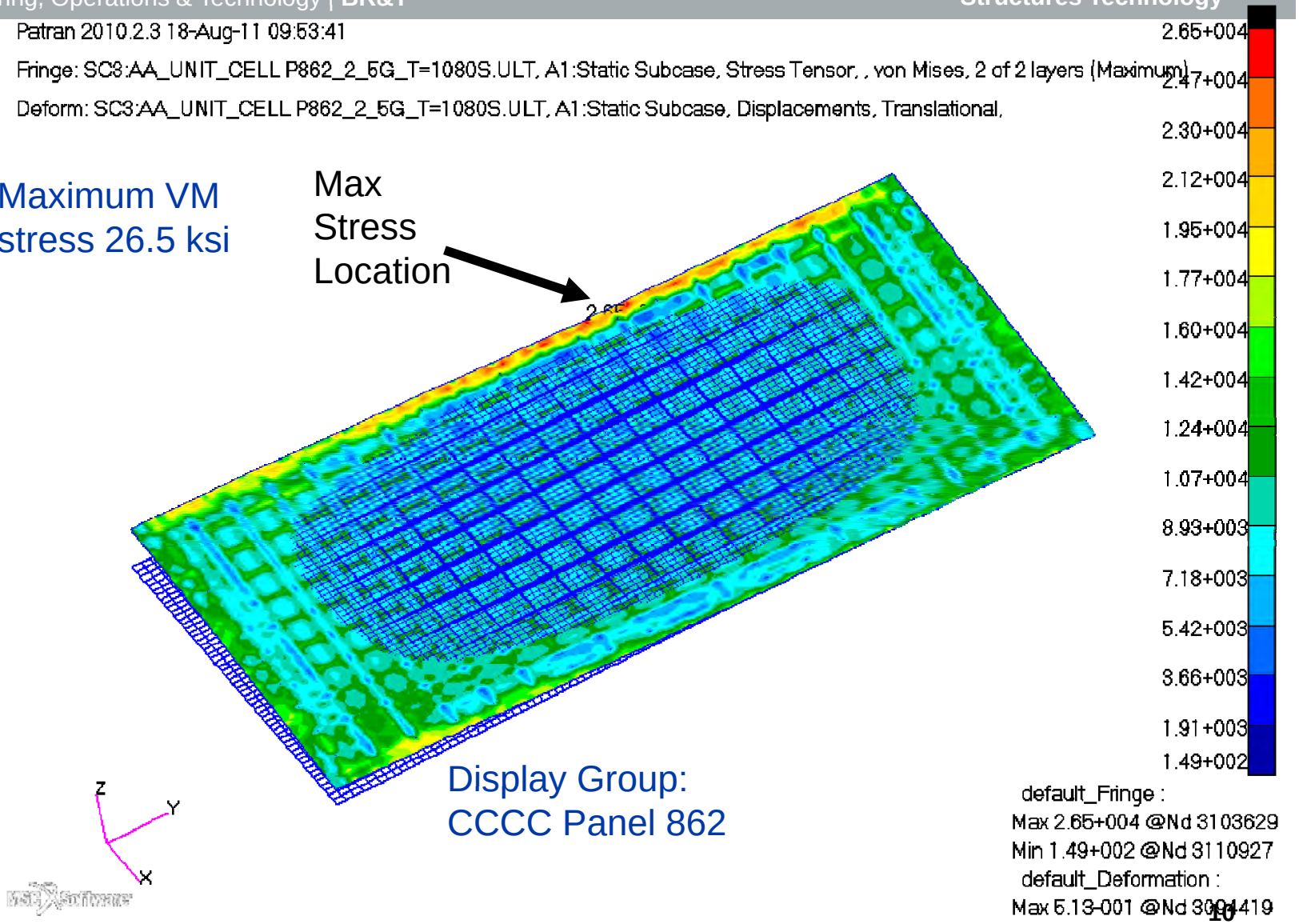

Approved for public release; distribution unlimited.

Von Mises, Unit Cell, 2.5g Ult 1.5, T=1080s, Linear

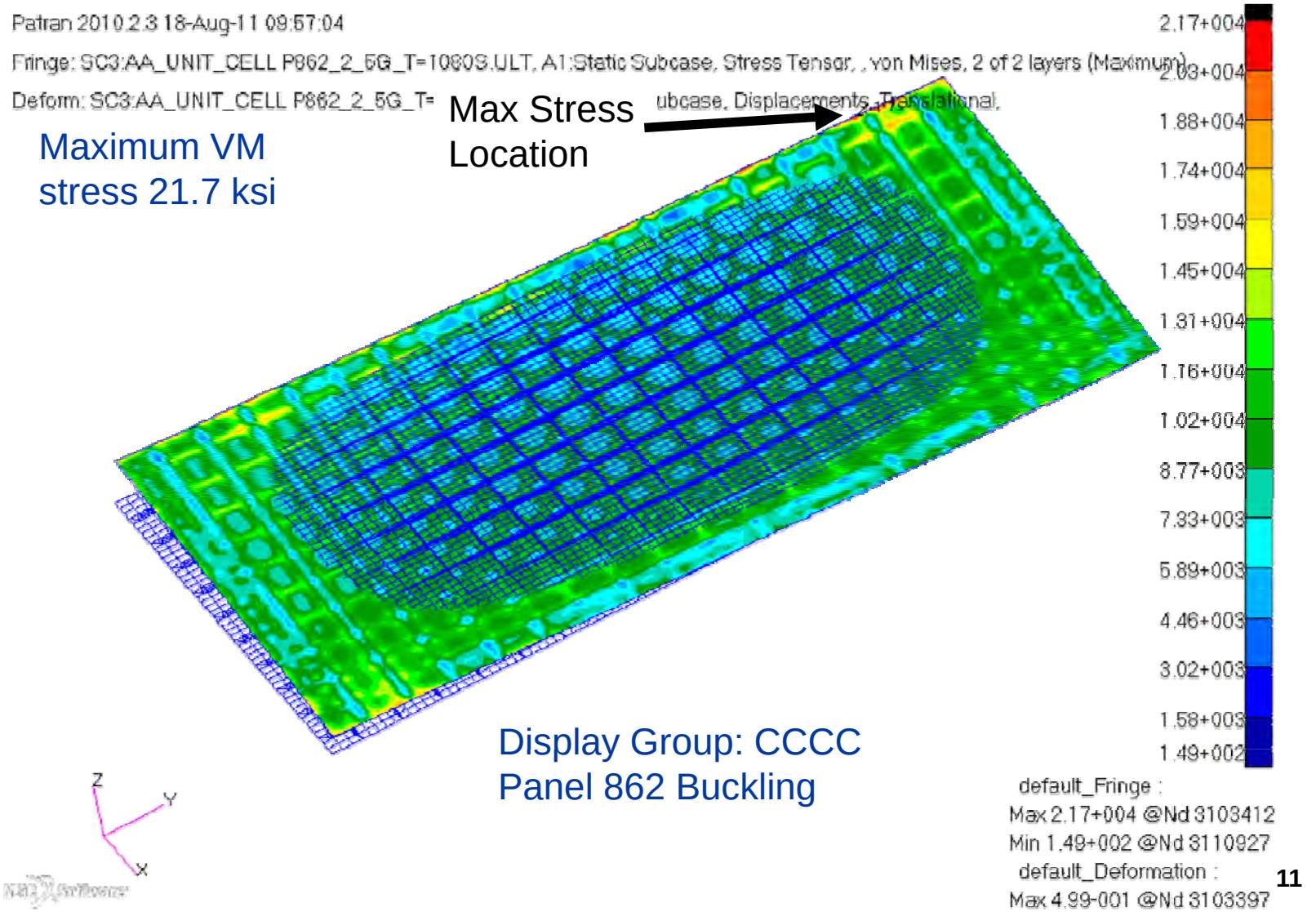

Approved for public release; distribution unlimited.

Von Mises, Panel, 2.5g Ult 1.5, T=1080s, Linear

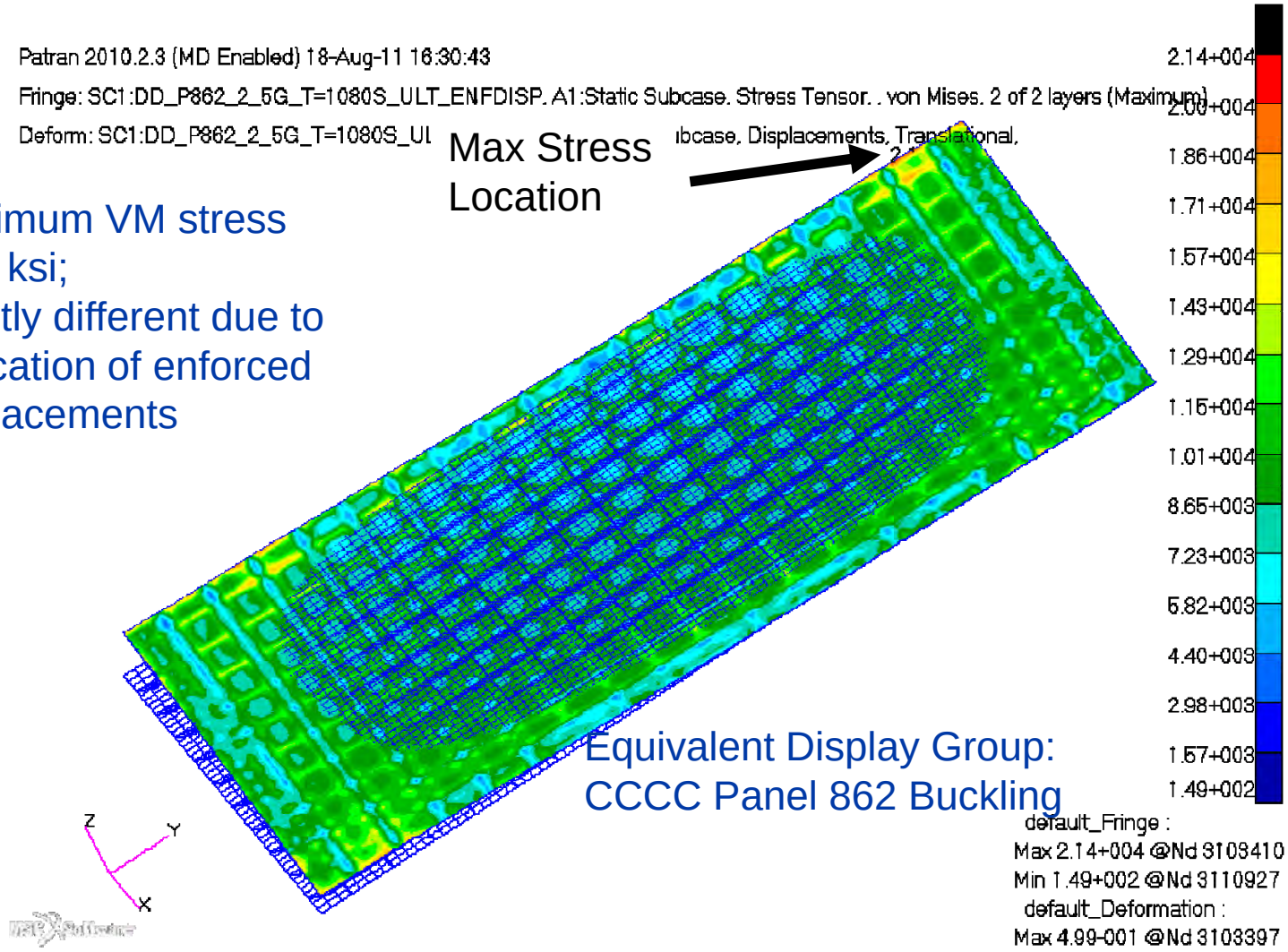

Approved for public release; distribution unlimited.

Displacements, Unit Cell, 2.5g Ult 1.5, T=1080s, Linear

Magnitude of Displacements

Maximum resultant deformation is 0.513”

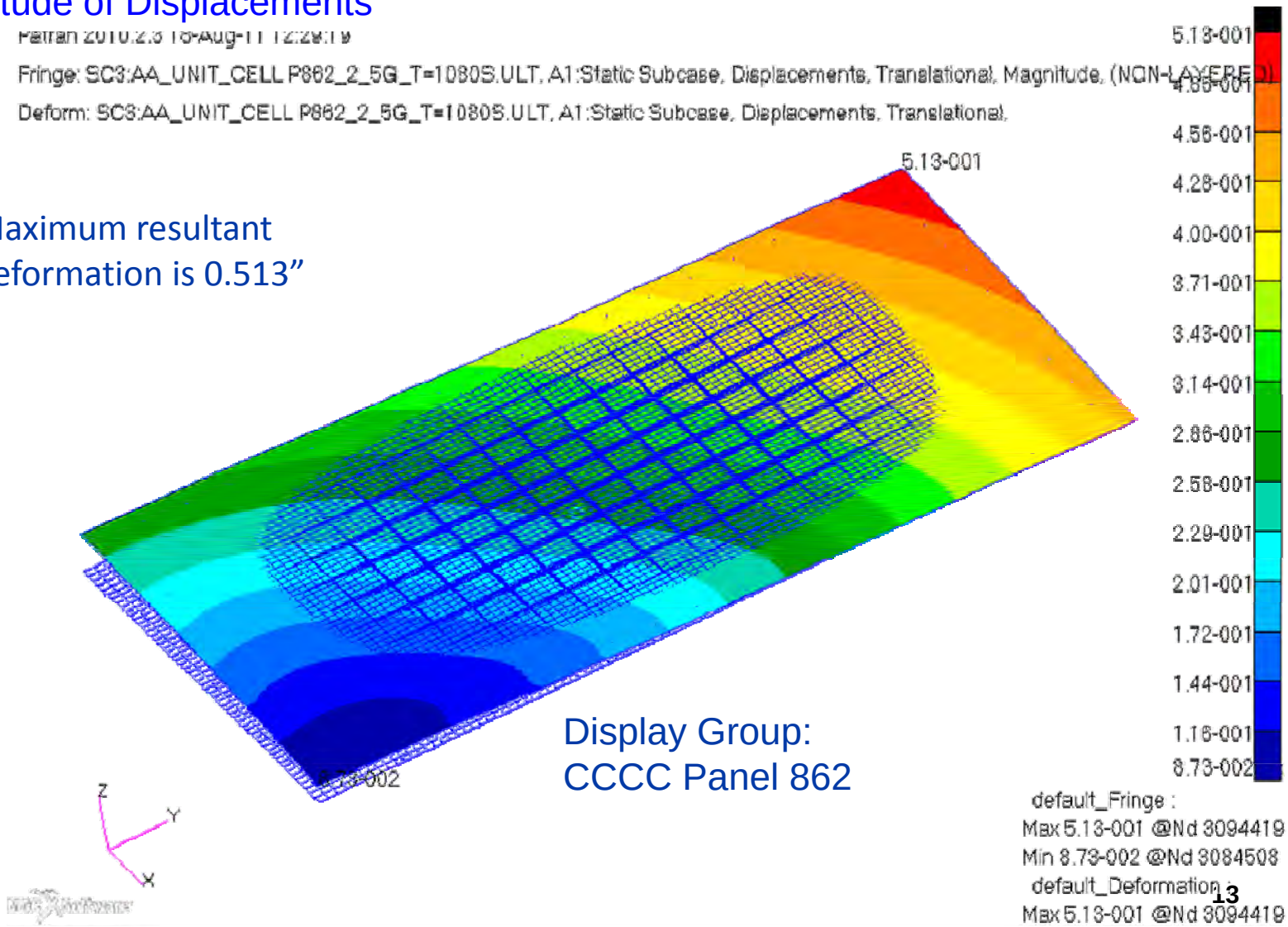

Display Group:
CCCC Panel 862

Approved for public release; distribution unlimited.

Displacements, Unit Cell, 2.5g Ult 1.5, T=1080s, Linear

Magnitude of Displacements

Maximum resultant deformation is 0.499”

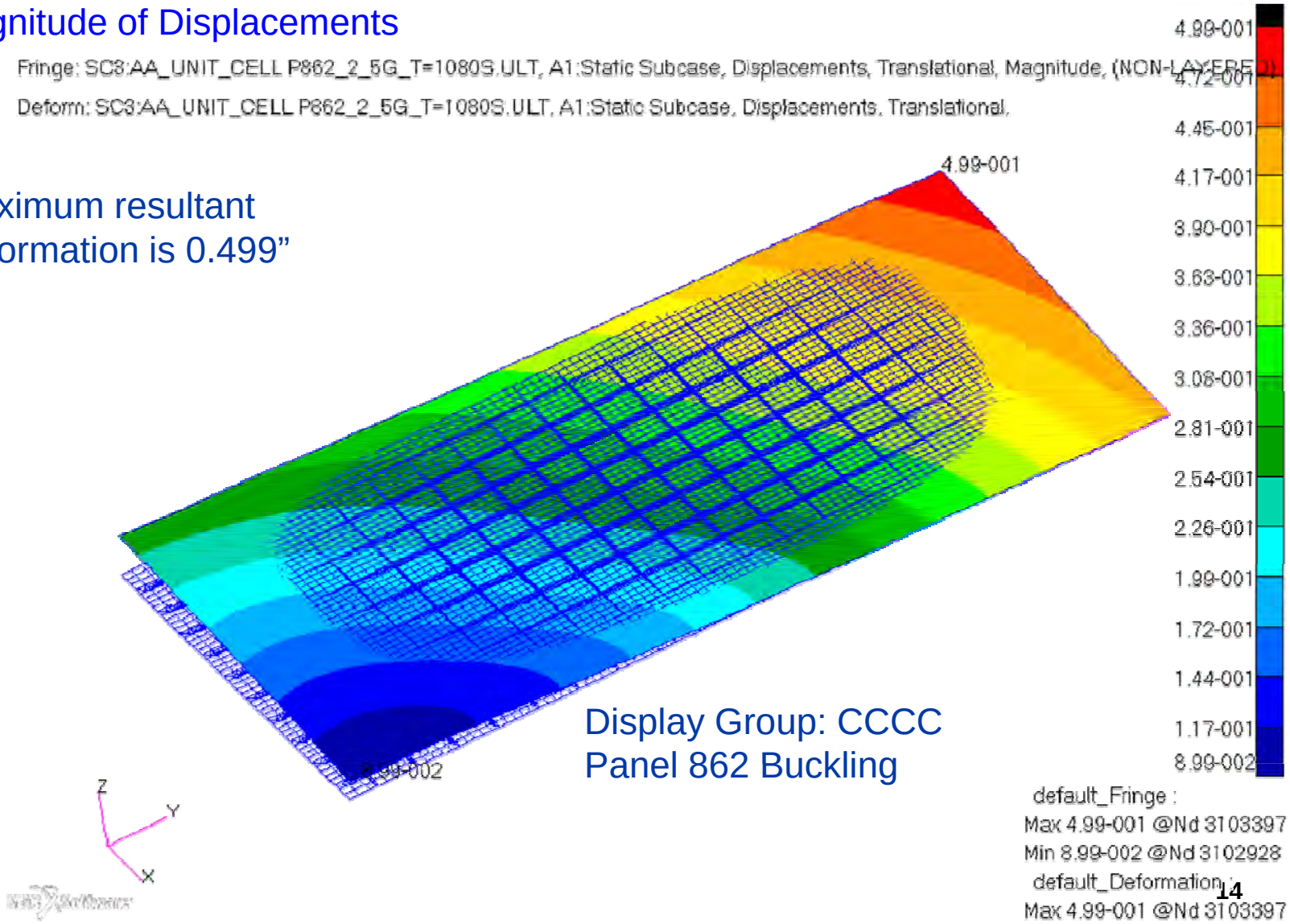

Display Group: CCCC Panel 862 Buckling

Approved for public release; distribution unlimited.

Displacements, Unit Cell, 2.5g Ult 1.5, T=1080s, Linear

Z-Displacements (Normal to Panel Surface)

Maximum relative Z-displacement is 0.0729-(-.0701)= 0.143”

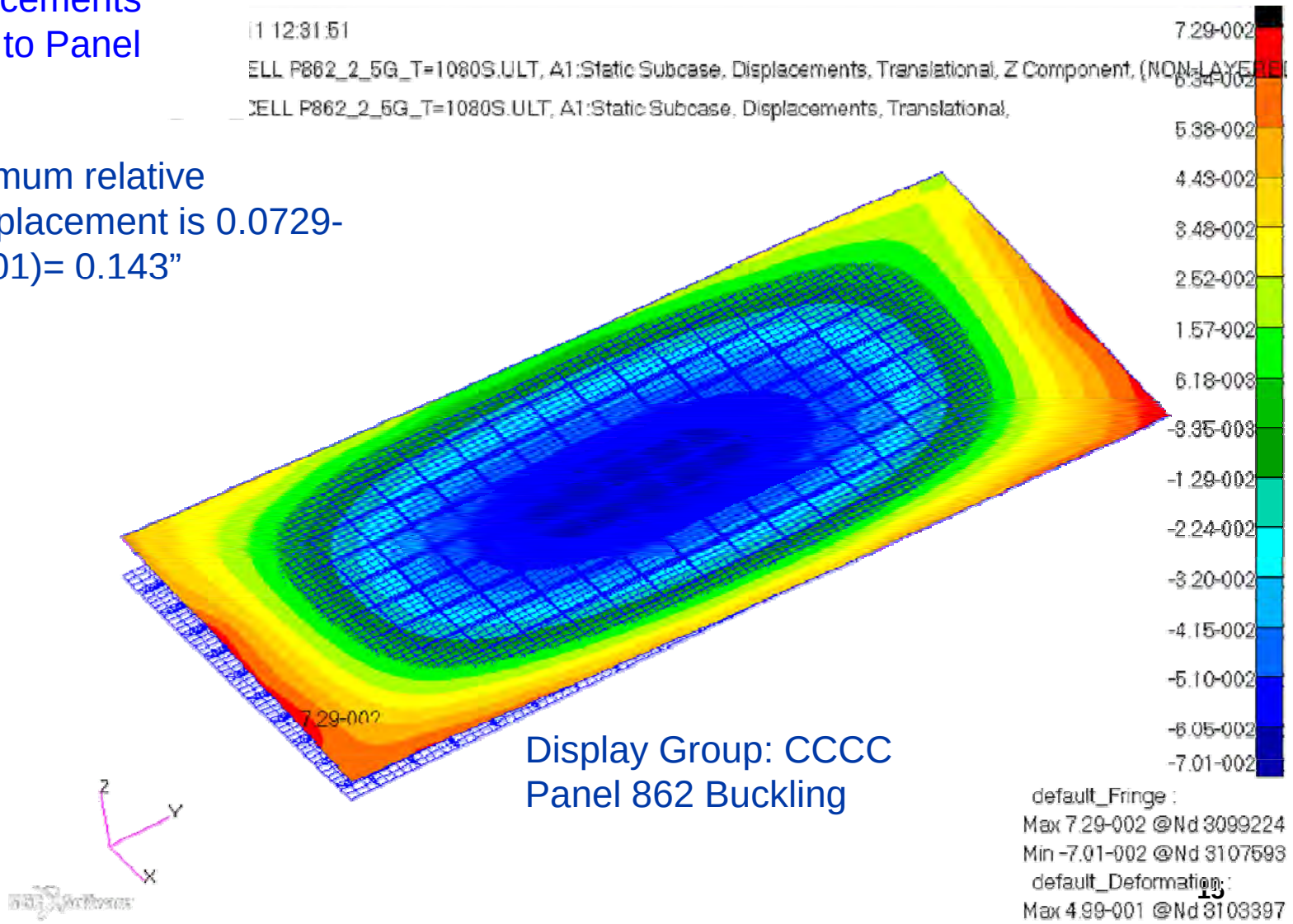

Display Group: CCCC Panel 862 Buckling

Approved for public release; distribution unlimited.

Displacements, Panel, 2.5g Ult 1.5, T=1080s, Linear

Magnitude of Displacements

Maximum resultant deformation is 0.499", matching Unit-Cell Model

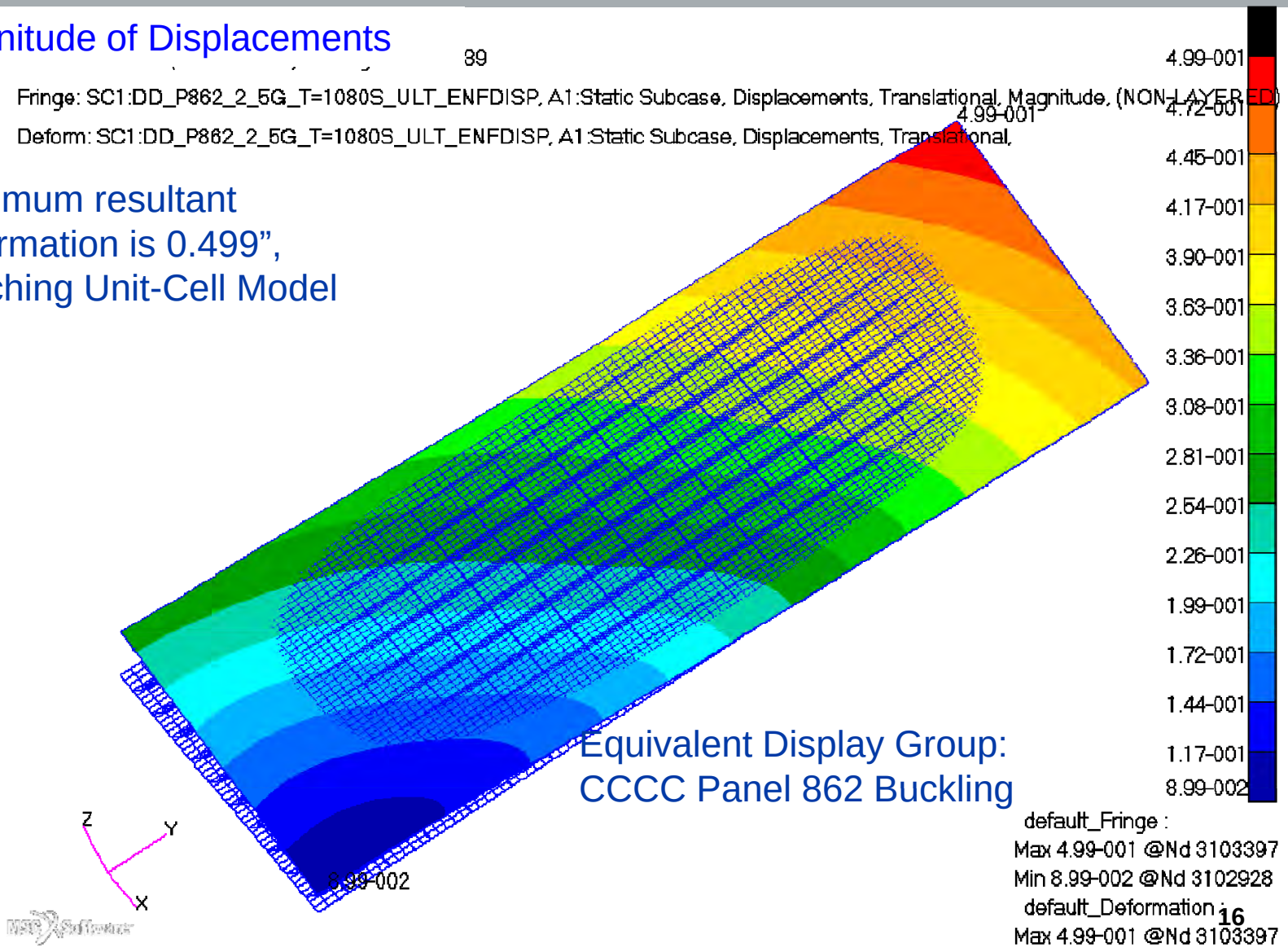

Equivalent Display Group: CCCC Panel 862 Buckling

Approved for public release; distribution unlimited.

Displacements, Panel, 2.5g Ult 1.5, T=1080s, Linear

Z-Displacements (Normal to Panel Surface)

Maximum relative z-displacement is 0.0729-(-.0701)= 0.143", matching Unit-Cell Model

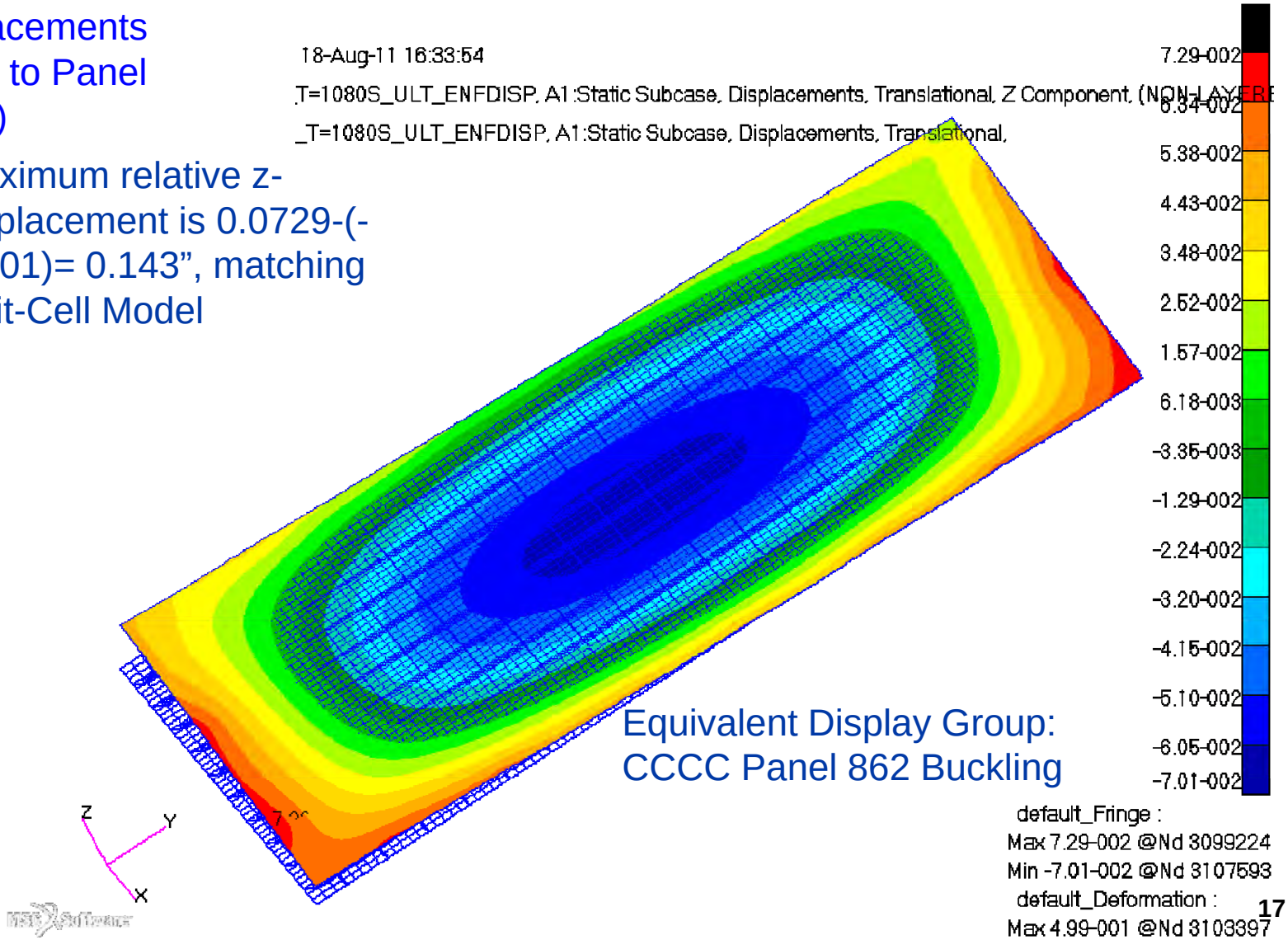

Equivalent Display Group: CCCC Panel 862 Buckling

Approved for public release; distribution unlimited.

Displacements, Panel, 2.5g Ult 1.5, T=1080s, Non-Linear

Magnitude of Displacements

Deflected shape driven by Thermal (T=1080sec) & Mechanical loads; 2.5% load increment

Maximum Displacement = 0.499”

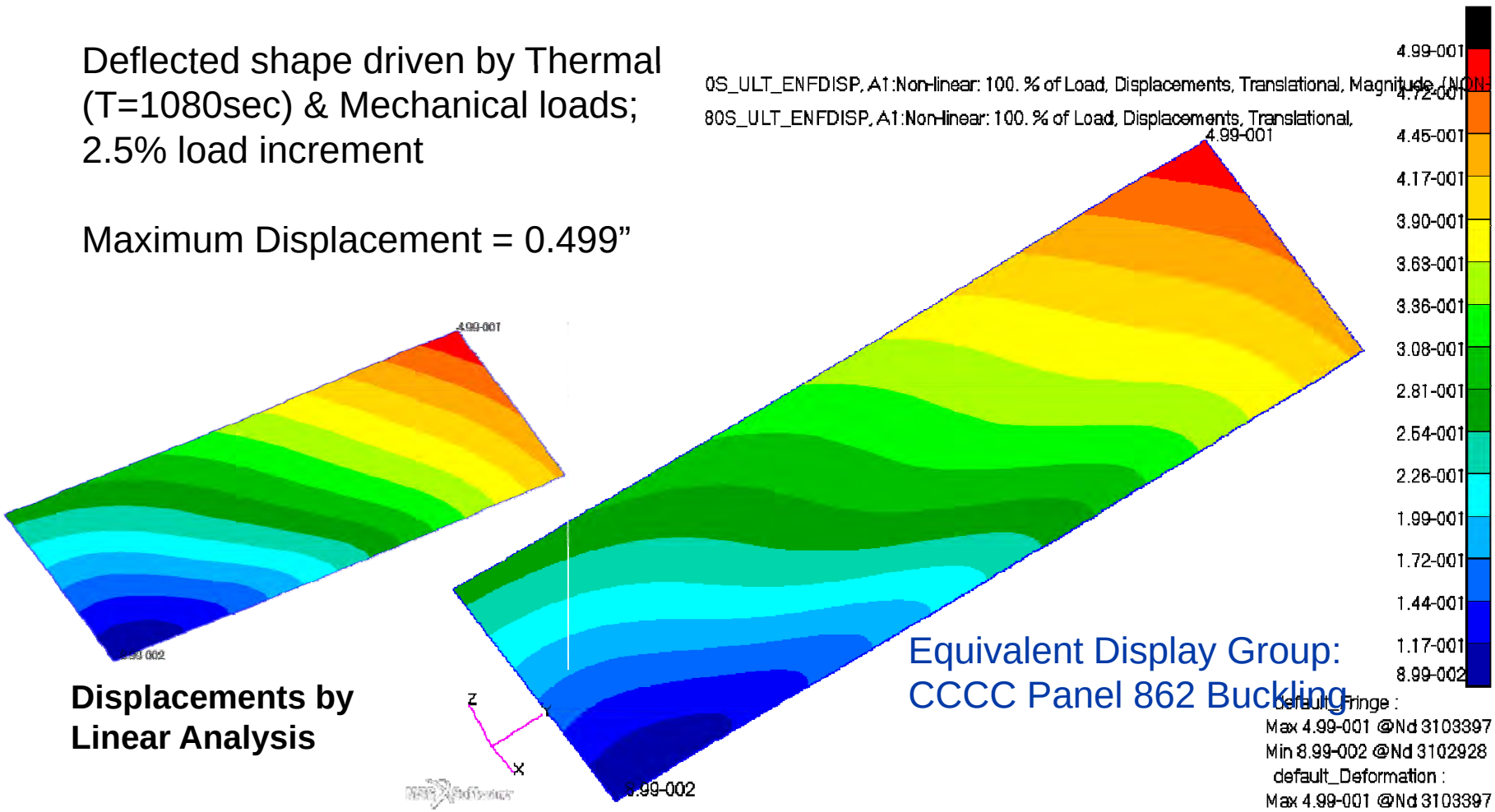

Displacements by Linear Analysis

Equivalent Display Group: CCCC Panel 862 Buckling

Approved for public release; distribution unlimited.

Displacements, Panel, 2.5g Ult 1.5, T=1080s, Non-Linear

Z-Displacements (Normal to Panel Surface)

Deflected shape driven by Thermal (t=1080sec) & Mechanical loads: 2.5% load increment

Maximum Relative Z-Displacement = 0.0729-(-.119) = 0.192”

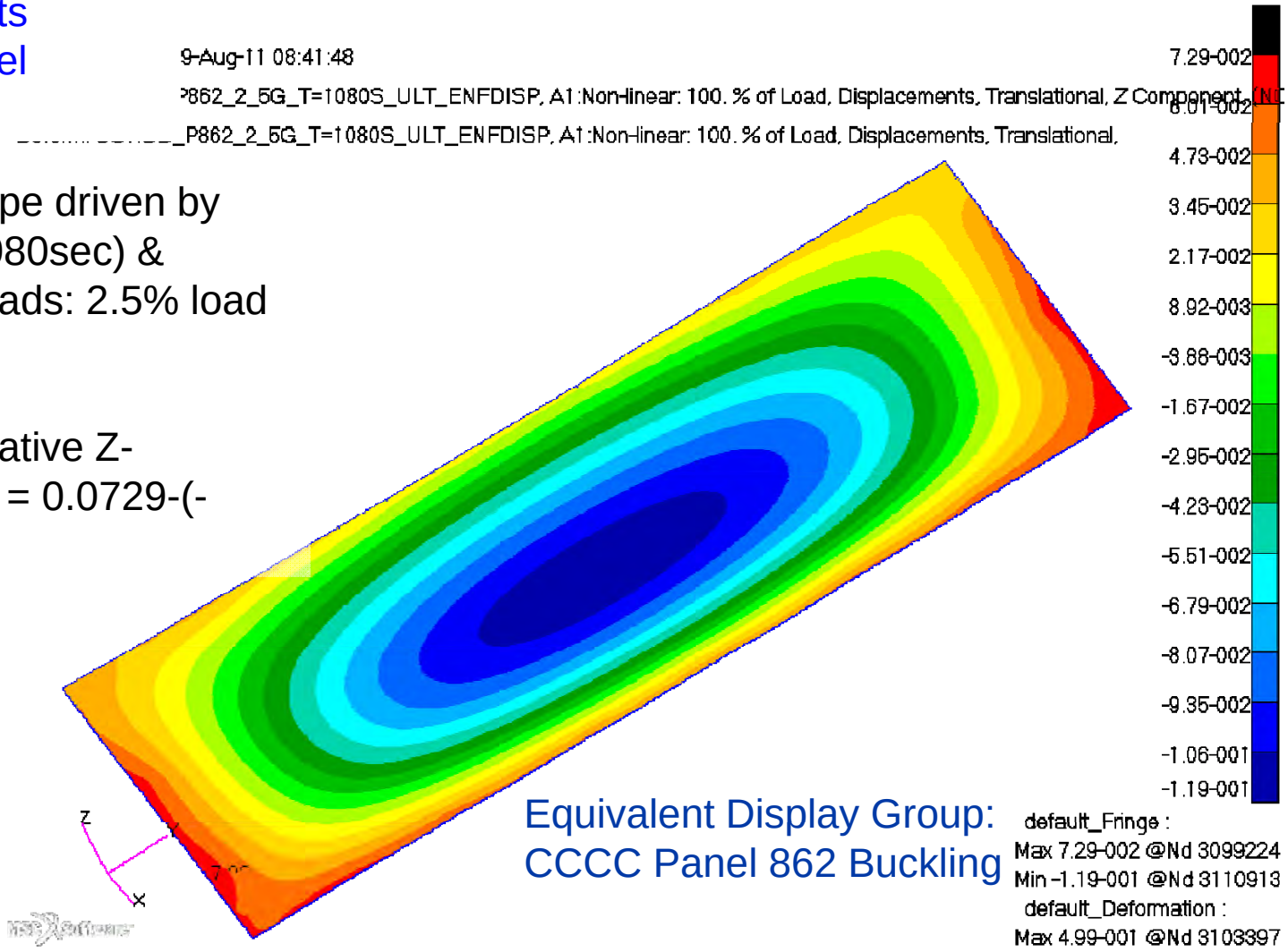

Equivalent Display Group: CCCC Panel 862 Buckling

Approved for public release; distribution unlimited.

Von Mises, Panel, 2.5g Ult 1.5, T=1080s, Non-Linear

Thermal (t=1080sec) & Mechanical loads; 2.5% load increment

Maximum Stress = 17 ksi

Equivalent Display Group:
CCCC Panel 862 Buckling

Exterior Surface

Max Stress Location

Interior Surface

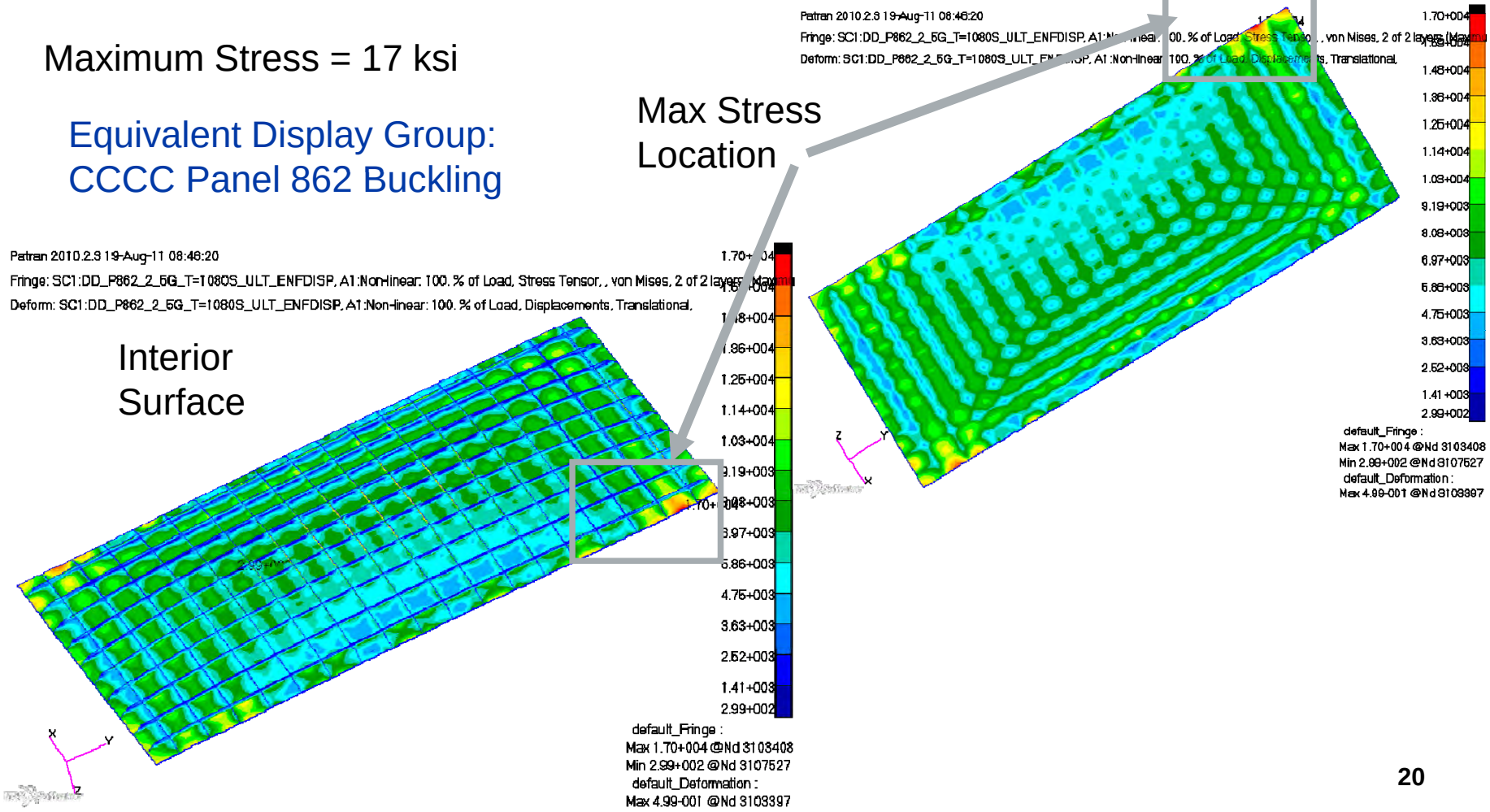

Approved for public release; distribution unlimited.

Buckling Mode 1, Panel, 2.5g Lim 1.15, T=1080s

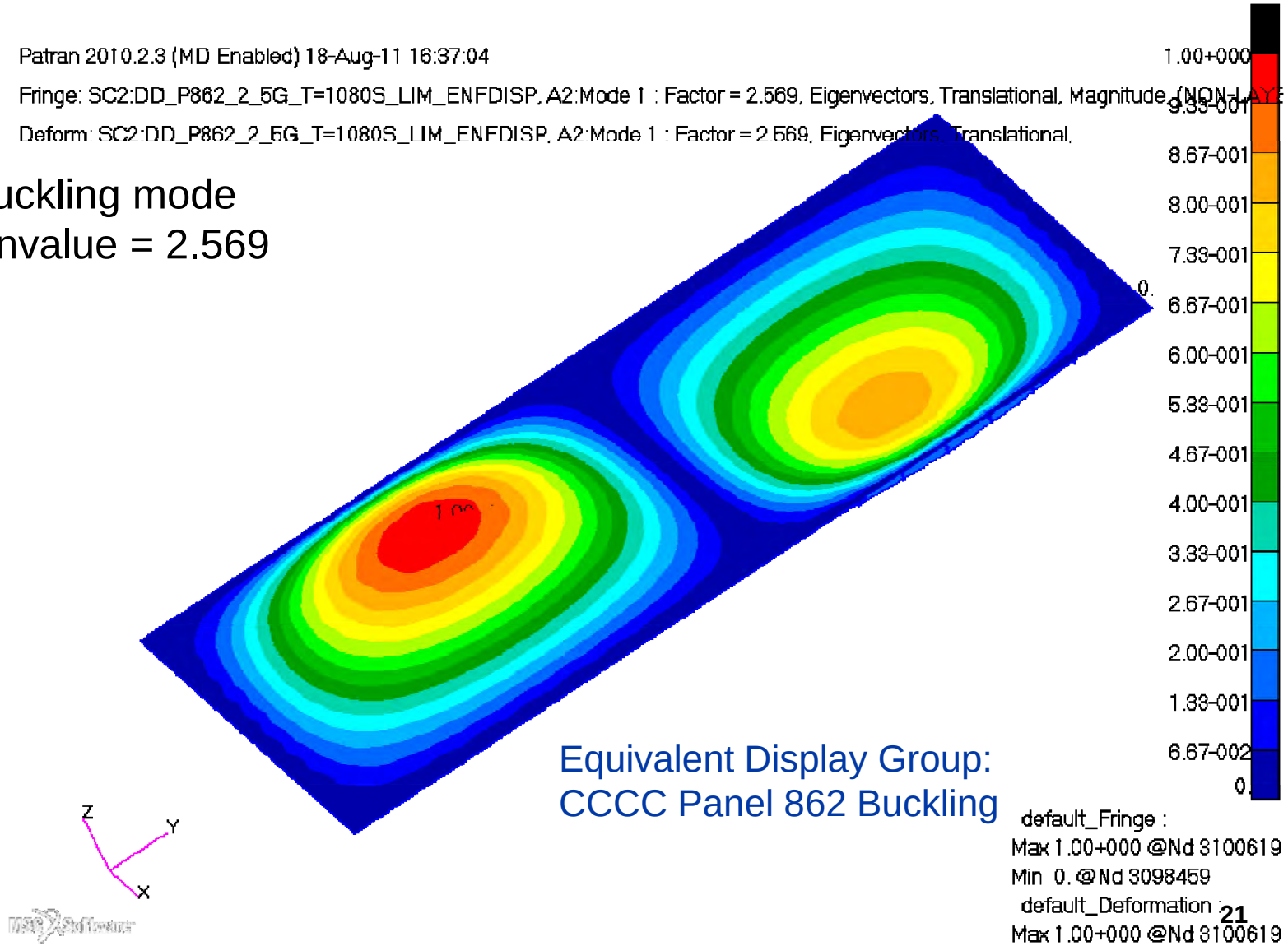

1st buckling mode
Eigenvalue = 2.569

Equivalent Display Group:
CCCC Panel 862 Buckling

Approved for public release; distribution unlimited.

Buckling Mode 2, Panel, 2.5g Lim 1.15, T=1080s

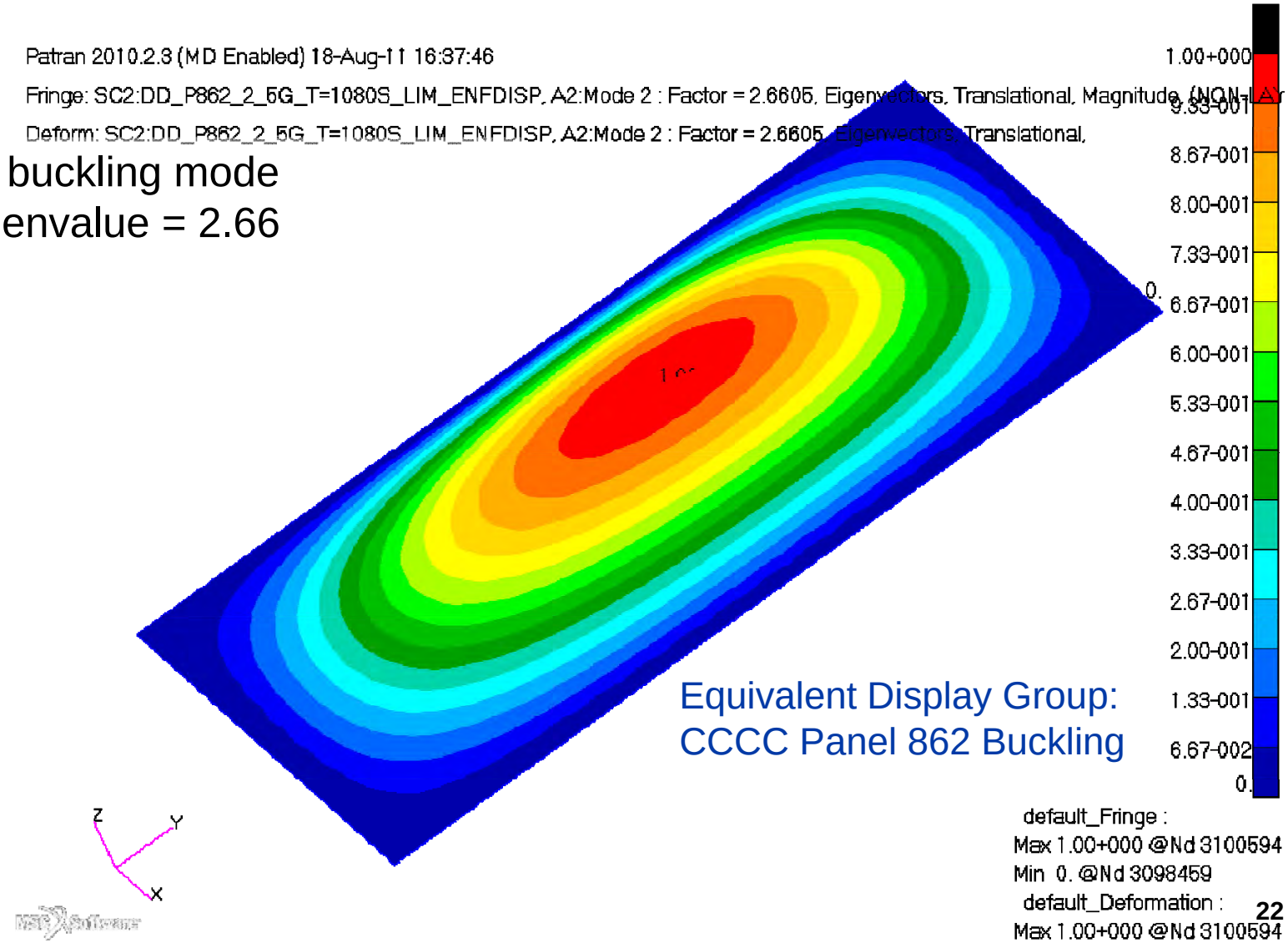

2nd buckling mode
Eigenvalue = 2.66

Equivalent Display Group:
CCCC Panel 862 Buckling

22

Approved for public release; distribution unlimited.

Buckling Mode 3 & 4, Panel, 2.5g Lim 1.15, T=1080s

Higher modes are local modes

Equivalent Display Group:
CCCC Panel 862 Buckling

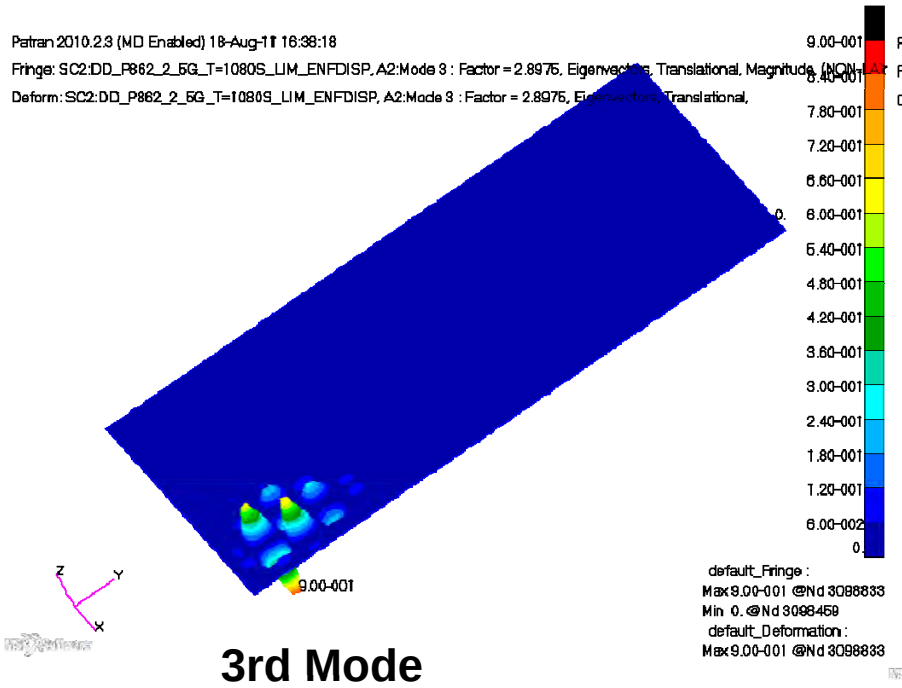

3rd Mode
Eigenvalue = 2.90

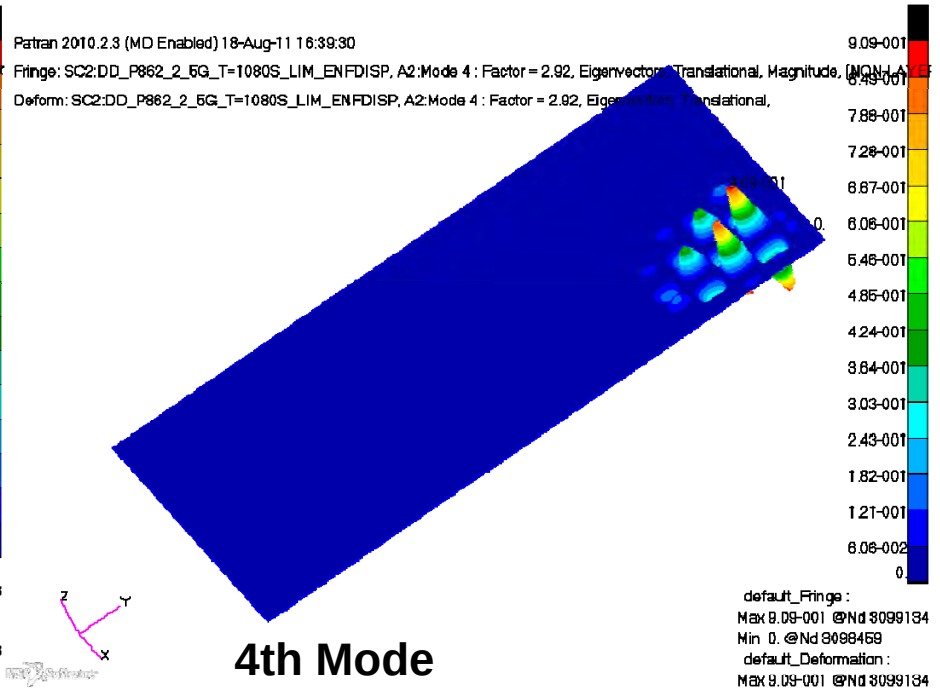

4th Mode
Eigenvalue = 2.92

Approved for public release; distribution unlimited.

PATRAN Database and NASTRAN Analysis Files

Approved for public release; distribution unlimited.

Location of files

Contact AFRL/RBSM Structural Sciences Center
WPAFB, OH, 45433

POC: Dr. S. Michael Spottswood, 937.904.6789, stephen.spottswood@wpafb.af.mil

PATRAN Database for Unit-Cell and Panel Models

Orthogrid.db

Flight Loads

Mach 7, +2.5g, symmetric pull up maneuver

Thermal

Temperature @
T = 780 sec, Maximum thermal gradient between panel skin and stiffener
T = 1080 sec, Maximum thermal gradient between panel and substructure
T = 2880 sec, Maximum temperature
T = 3600 sec, Maximum reverse thermal gradient

Boundary Conditions for Unit-Cell Model

Rigid Body Constraints plus constraints on normal rotation along all free edges

Approved for public release; distribution unlimited.

Linear Stress Analysis of Unit-Cell Model for 2.5G and Thermal (T=1080s)

Load Cases

AA_Unit_Cell_P862_2.5G_T=1080s
2.5g loading * 1.0 (F.S.), Temp @ 1080s, Rigid body and normal rotation web edge constraints

AA_Unit_Cell_P862_2.5G_T=1080s.LIM
2.5g loading * 1.15 (F.S.), Temp @ 1080s, Rigid body and normal rotation web edge constraints

AA_Unit_Cell_P862_2.5G_T=1080s.Ult
2.5g loading * 1.5 (F.S.), Temp @ 1080s, Rigid body and normal rotation web edge constraints

CC_TEMP_1080S
Temp @ 1080s, Rigid body and normal rotation web edge constraints

Analysis Files

Unit_Cell_P862_2.5g_T1080.dat
Unit_Cell_Model_Load_Thermal.bdf: FE Model of Unit Cell with loads, BCs & thermal
MATT8 Inconel 718.MAT8: Temperature dependent materials

Results

unit_cell_p862_2.5g_t1080.xdb

Approved for public release; distribution unlimited.

Linear Stress Analysis of Unit-Cell Model for 2.5G

Load Cases

BB_Unit_Cell P862_2_5G
2.5g loading * 1.0 (F.S.), Rigid body and normal rotation web edge constraints

BB_Unit_Cell P862_2_5G_Lim
2.5g loading * 1.15 (F.S.), Rigid body and normal rotation web edge constraints

BB_Unit_Cell P862_2_5G_Ult
2.5g loading * 1.5 (F.S.), Rigid body and normal rotation web edge constraints

Analysis Files

Unit_Cell_P862_2.5g_only.dat
Unit_Cell_Model_Load_Thermal.bdf: FE Model of Unit Cell with loads, BCs & thermal
MATT8 Inconel 718.MAT8: Temperature dependent materials

Results

unit_cell_p862_2.5g_only.xdb

Approved for public release; distribution unlimited.

Linear Stress Analysis of Unit-Cell Model for Thermal

Load Cases

CC_TEMP_2880S
Temp @ 2880s, Rigid body and normal rotation web edge constraints

CC_TEMP_3600S
Temp @ 3600s, Rigid body and normal rotation web edge constraints

CC_TEMP_780S
Temp @ 780s, Rigid body and normal rotation web edge constraints

Analysis Files

Unit_Cell_P862_T2880.dat
Unit_Cell_P862_T3600.dat
Unit_Cell_P862_T780.dat
Unit_Cell_Model_Load_Thermal.bdf: FE Model of Unit Cell with loads, BCs & thermal
MATT8 Inconel 718.MAT8: Temperature dependent materials

Results

unit_cell_p862_t2880.xdb
unit_cell_p862_t3600.xdb
unit_cell_p862_t780.xdb

Approved for public release; distribution unlimited.

Linear Stress Analysis of Panel Model

Flight Loads
Mach 7, +2.5g, symmetric pull up maneuver

Thermal
Temperature @
T = 1080 sec, Maximum thermal gradient between panel and substructure

Load Case
For 2.5g loading *1.5 (F.S.), Temp @ 1080s

Boundary Conditions for Panel Model
Enforced displacements from unit-cell analysis for 2.5G flight (FS=1.5) + thermal (T=1080 sec)
patran_endisp_ult.csv: enforced displacements on panel boundaries
patran_endRot_ult.csv: enforced rotations on panel boundaries

Analysis Runs
P862_2.5g_T_1080s_101.dat
P862_Model_BC_Lod_Therm_NoSPCD.bdf: FE Model of Panel 862 with loads, BCs & thermal
MATT8 Inconel 718.MAT8: Temperature dependent materials

Results
p862_2.5g_t_1080s_101.xdb

Approved for public release; distribution unlimited.

Buckling Analysis of Panel Model

Flight Loads
Mach 7, +2.5g, symmetric pull up maneuver

Thermal
Temperature @
T = 1080 sec, Maximum thermal gradient between panel and substructure

Load Case
For 2.5g loading *1.15 (F.S.), Temp @ 1080s

Boundary Conditions for Panel Model
Enforced displacements from unit-cell analysis for 2.5G flight (FS=1.15) + thermal (T=1080 sec)
patran_endisp_lim.csv: enforced displacements on the panel boundaries
patran_endRot_lim.csv: enforced rotations on the panel boundaries

Analysis Runs
P862_2.5g_T_1080s_105.dat
P862_Model_BC_Lod_Therm_NoSPCD.bdf: FE Model of Panel 862 with loads, BCs & thermal
MATT8 Inconel 718.MAT8: Temperature dependent materials

Results
p862_2.5g_t_1080s_105.xdb

Approved for public release; distribution unlimited.

Non-Linear Stress Analysis of Panel Model

Flight Loads
Mach 7, +2.5g, symmetric pull up maneuver

Thermal
Temperature @
T = 1080 sec, Maximum thermal gradient between panel and substructure

Load Case
2.5g loading *1.5 (F.S.), Temp @ 1080s

Boundary Conditions for Panel Model
Enforced displacements from unit-cell analysis for 2.5G flight (FS=1.5) + thermal (T=1080 sec)
patran_endisp_ult.csv: enforced displacements on the panel boundaries
patran_endRot_ult.csv: enforced rotations on the panel boundaries

Analysis Runs
P862_2.5g_T_1080s_106_081811.dat
P862_Model_BC_Lod_Therm_NoSPCD.bdf: FE Model of Panel 862 with loads, BCs & thermal
MATT8 Inconel 718.MAT8: Temperature dependent materials

Results
P862_2.5g_T_1080s_106_081811.xdb

Approved for public release; distribution unlimited.

Groups in PATRAN Database

AAAA Unit Cell Analysis Group
: Elements, Nodes, and MPC's required to analyze the Unit Cell

AAAA Unit Cell Elements and Nod
: Elements, Nodes, and no MPC's for Unit Cell

AAAA Unit Cell MPCs
: MPC's for Unit Cell

BBBB Caps
: Sinewave Keel and Frame Caps

BBBB Freebody Nodes
: Nodes for Applying Freebody Loads from Vehicle FEM

BBBB Stiffeners
: Panel Stiffeners

BBBB Substructure Web
: Sinewave Keel and Frame Webs

CCCC Panel 780
: FEM for Panel 780 (Panel 2 on windward surface)

CCCC Panel 862
: FEM for Panel 862 (Panel 1 on leeward surface)

CCCC Panel 862 Buckling
: Analysis Group for Panel 862 w/o elements overlapping Sinewave Caps for Panel Level analyses

CCCC Panel 862 Edge Nodes
: Boundary Nodes to apply enforced displacement for Panel level Analysis

FEM Connectors
: CFASTs

Approved for public release; distribution unlimited.

Panel 1 (862) Dynamic & Fatigue Analysis

September 9, 2011

Craig Masterson
314-232-9424
Craig.Masterson@boeing.com

Approved for public release; distribution unlimited.

Panel 862 Dynamic Analysis

- Methods and Approach
- Analysis Assumptions
- Finite Element Model and Boundary Conditions
- Results
  - Modal
  - Response
  - Fatigue
- Lessons Learned
- Summary
- Current /Future Activities

Approved for public release; distribution unlimited.

Methods & Approach

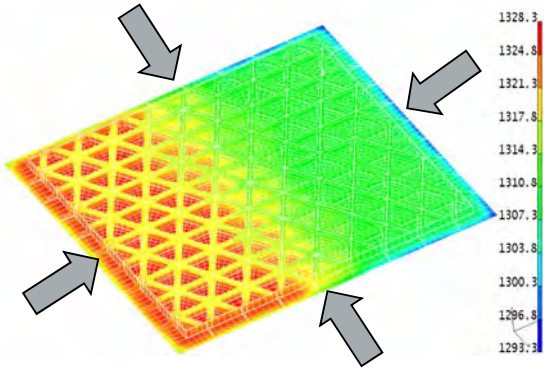

- Check fatigue at stress critical locations
- and Determine Flights to Failure
- Apply thermal knockdowns to fatigue S-N data
- Build combined spectrum and perform fatigue analysis

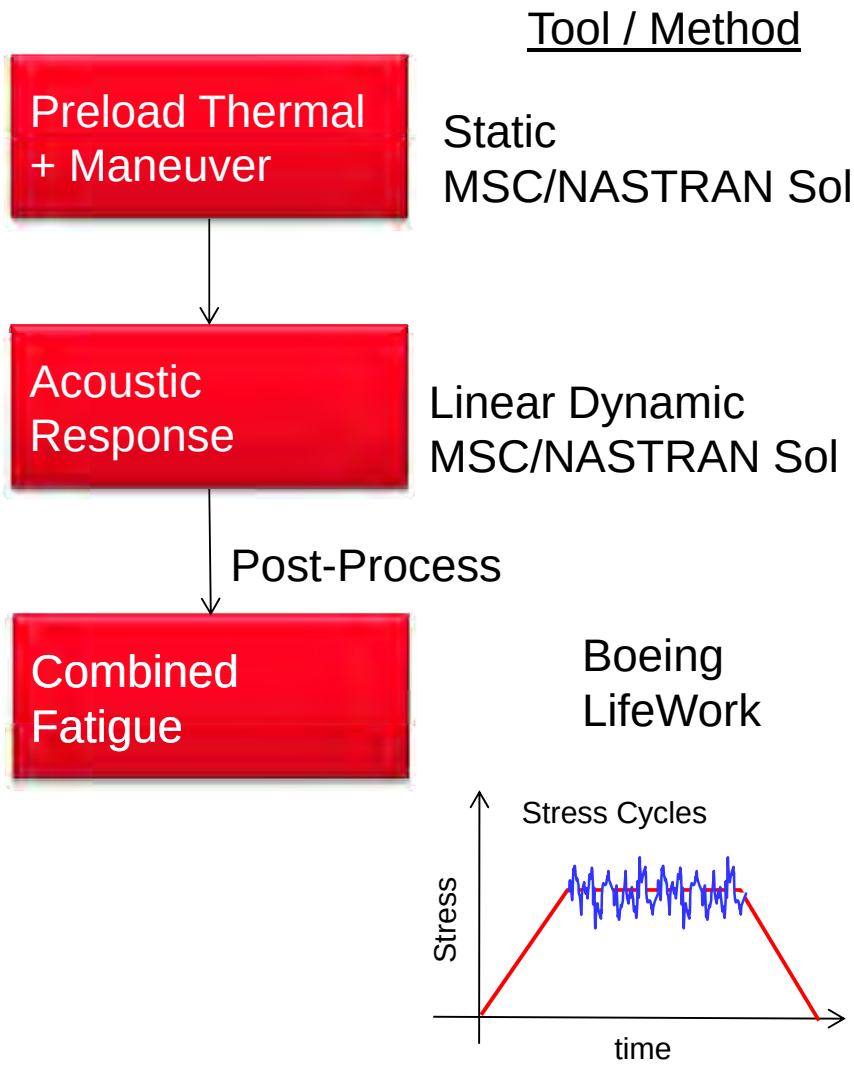

Approved for public release; distribution unlimited.

Analysis Issues

Issue	Approach	Source/Rationale
External Aero-acoustic Loads	Empirical with CFD guidance	Efimtsov Models, Boeing Best Practice, no hypersonic flight test data, or predictive capability available
Damping	Empirical Data	USAF Damping Design Guide, Boeing Best Practices, no inconel sine wave , iso-grid test data available
S-N Data for In 718	Convert Constant Amplitude Data to RMS Data, Adjust based for Temperature based on Strength	Mil-5, Best Practices, only source of reliable data
Sub-structure Modes	Filtered most Sub-structure modes	Concentrating on Panel Structure, also allows for quicker turn around
Choosing Worst Case Design Conditions	Using Max Thermal , matched to Max Acoustic for Fatigue Margin Checks	Dissimilar loads from different points in the trajectory, points are close, but not exact. This accounts for possible difference in trajectories
Combined Spectrum	Assuming a single trajectory	Don't have other trajectories, but a real vehicle will have many different possible missions.
Joint Allowables	Similarity to other material, joints	Boeing Best Practice, Need to test specific joints – welds, machine, fastened, etc…

Approved for public release; distribution unlimited.

Dynamic Model - Loading & Boundary Conditions

Acoustic Loads (3 - Zones)
- Flow Direction - Partially Correlated
- Cross Flow – Fully Correlated

Boundary Conditions
- Pinned all Free Edges on Skin and Keels

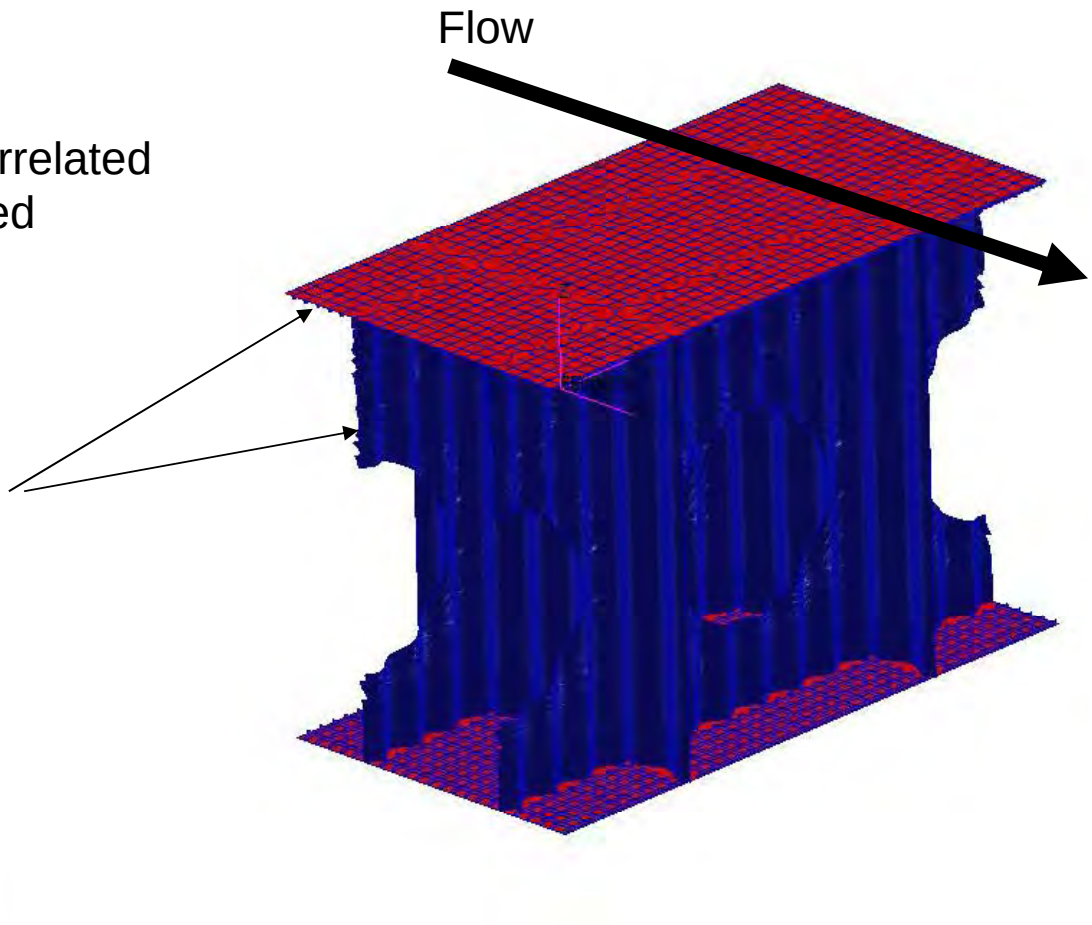

Approved for public release; distribution unlimited.

Translation/Rotation Constraints Along Edges of Panel and Web

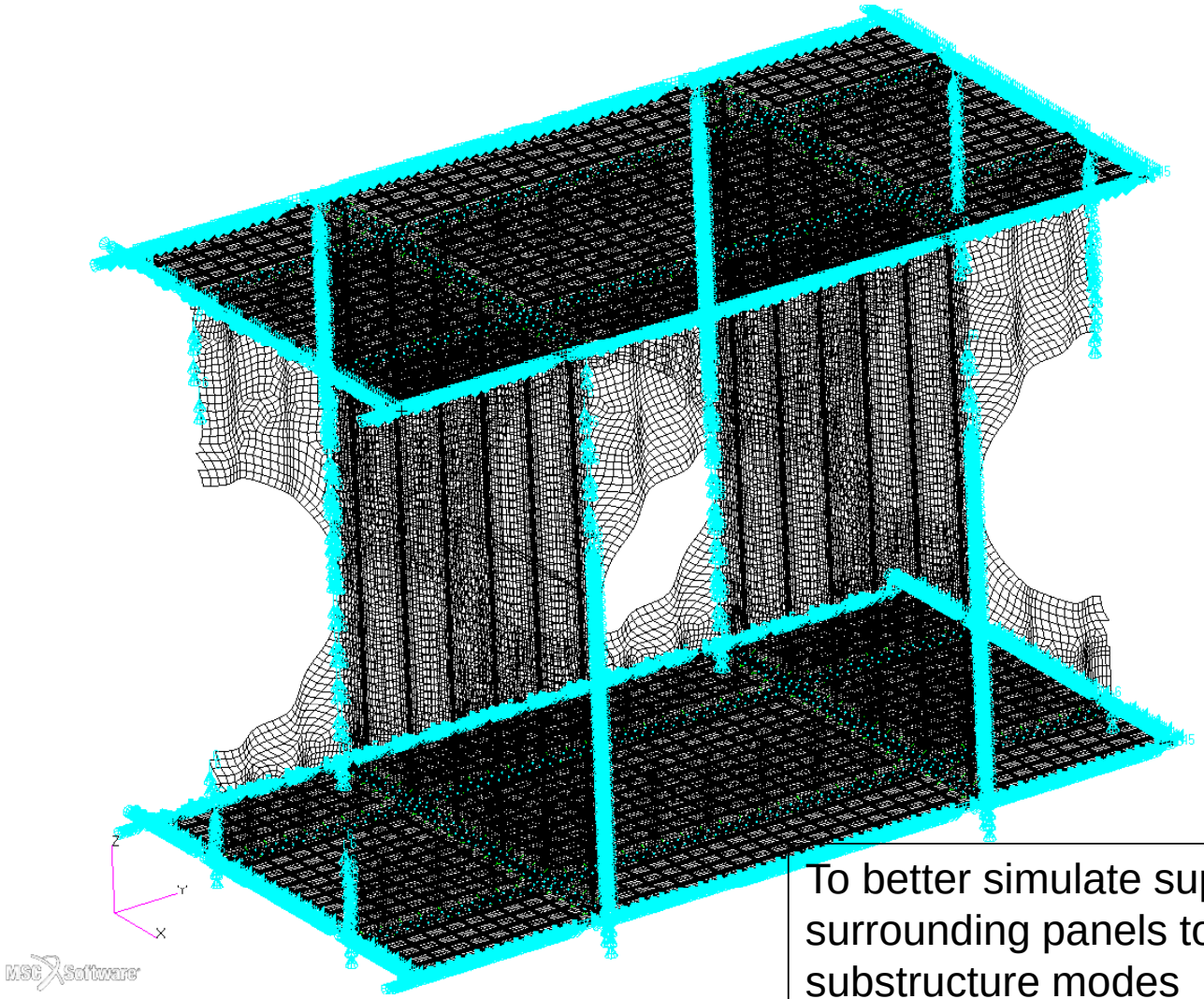

To better simulate support from surrounding panels to minimize substructure modes

Approved for public release; distribution unlimited.

Panel 862 Location

Define acoustic levels for each panel and critical conditions:

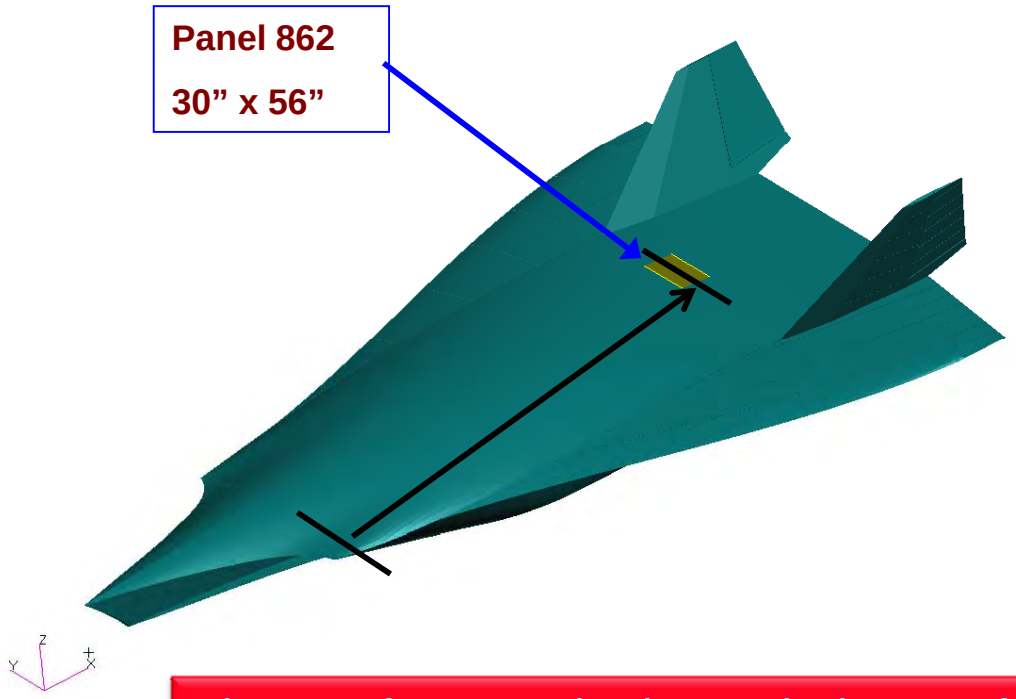

Distance from Lead Edge and Distance from Point of Separation are inputs to aero-acoustic models

Approved for public release; distribution unlimited.

Trajectory – Design Conditions of Interest

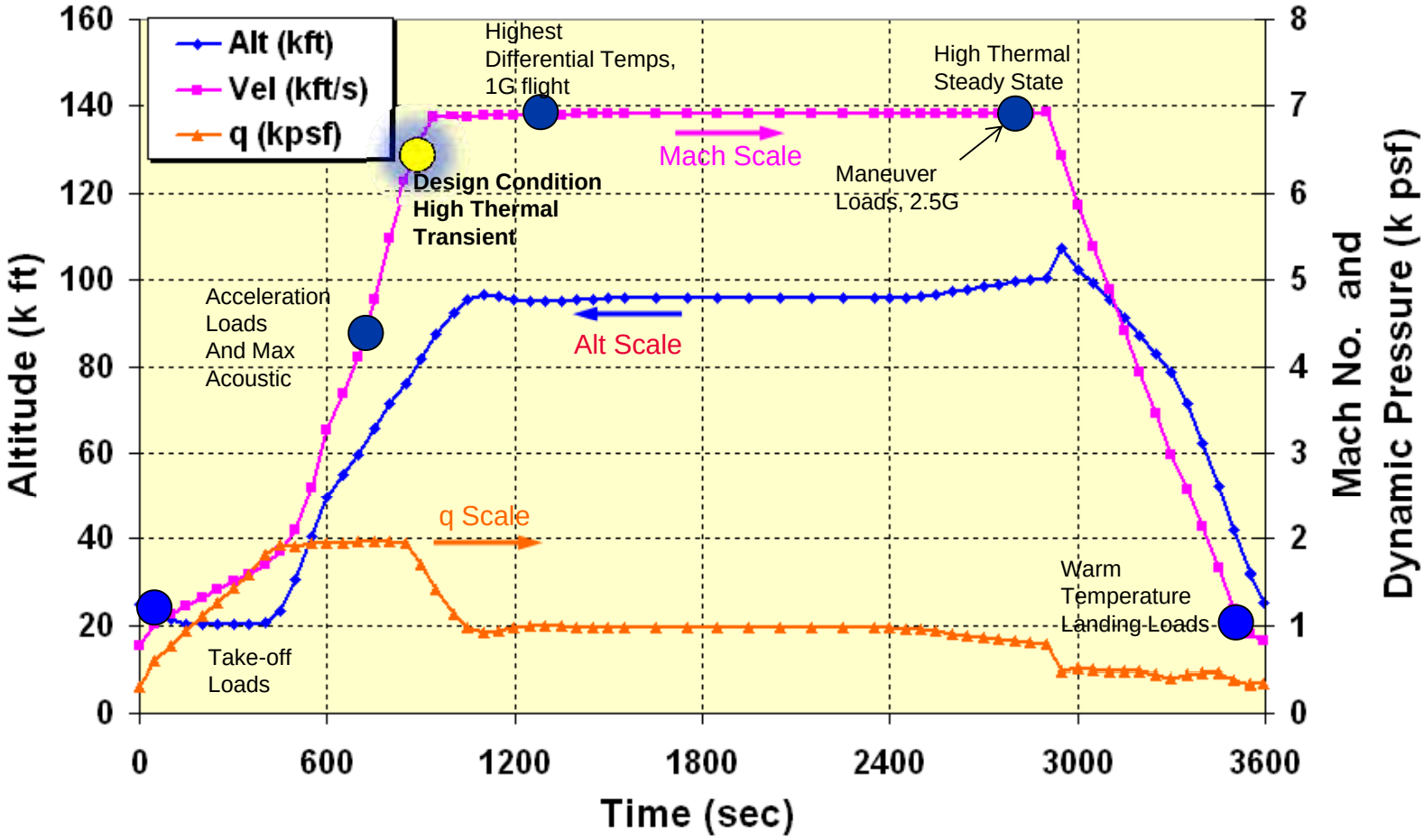

These are the Design Conditions of Interest for Dynamic & Fatigue Analysis.

Approved for public release; distribution unlimited.

CFD Results

CFD++ N-S Flow Field for M=7.0, α = 10 deg., Alt.=90Kft

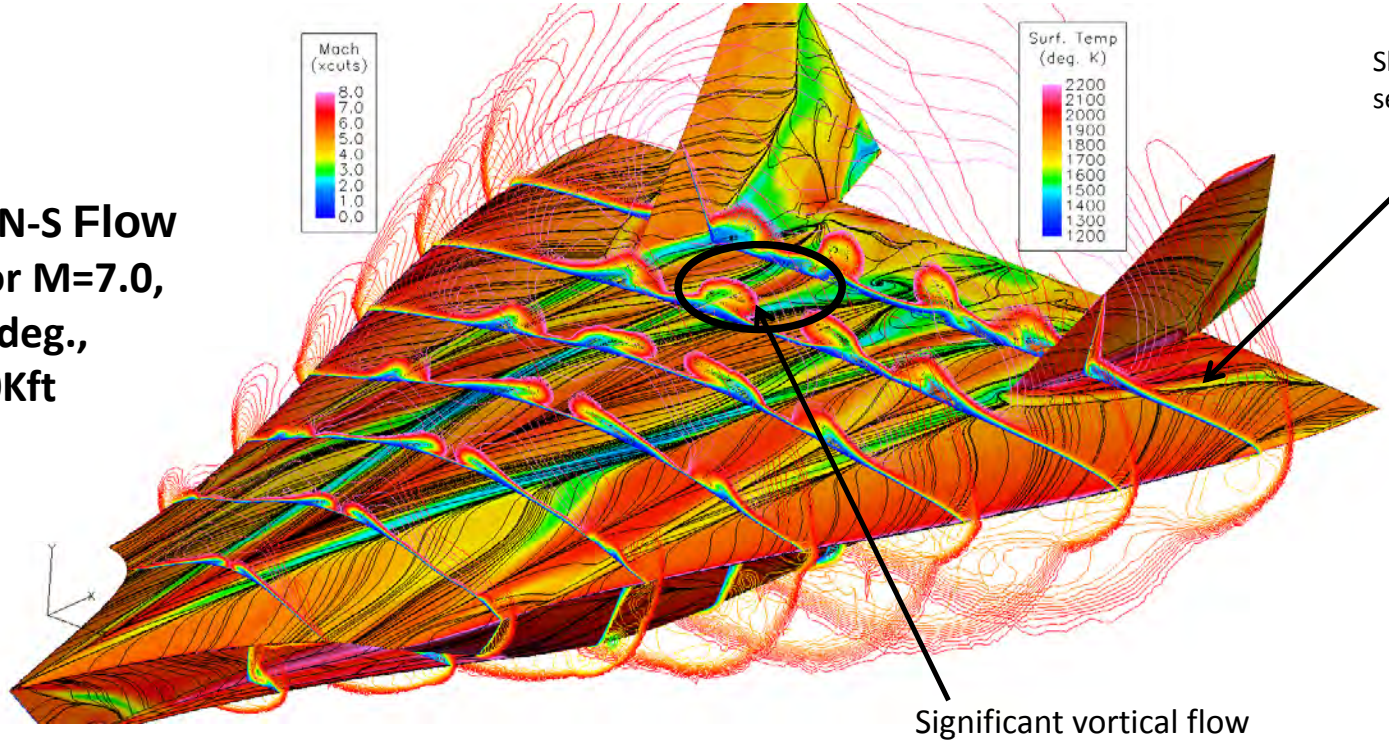

CFD was used to determine local flow features. This information was used in our Empirical models to predict acoustic loading spectrum

Approved for public release; distribution unlimited.

CFD Runs for Acoustic Loads

1.) Mach 7, 2.5g, AoA=10 deg, turn , Alt=90kft, q=1340 psf, Highest Maneuver and thermal loads (max G)

2.) Mach 7, 1.0g, AoA=4 deg, Cruise, Alt=100Kft, q=730 psf, High thermal loads and transient conditions (max T)

3.) Mach 6, 1.0g, AoA=6 deg, Accel, Alt= 75kft, q=2000 psf, Highest acoustic and thermal loads (max Q)

The load conditions for the detailed analysis was based on these are the three trajectory.

Approved for public release; distribution unlimited.

Required Data from CFD for Aero-acoustic Models

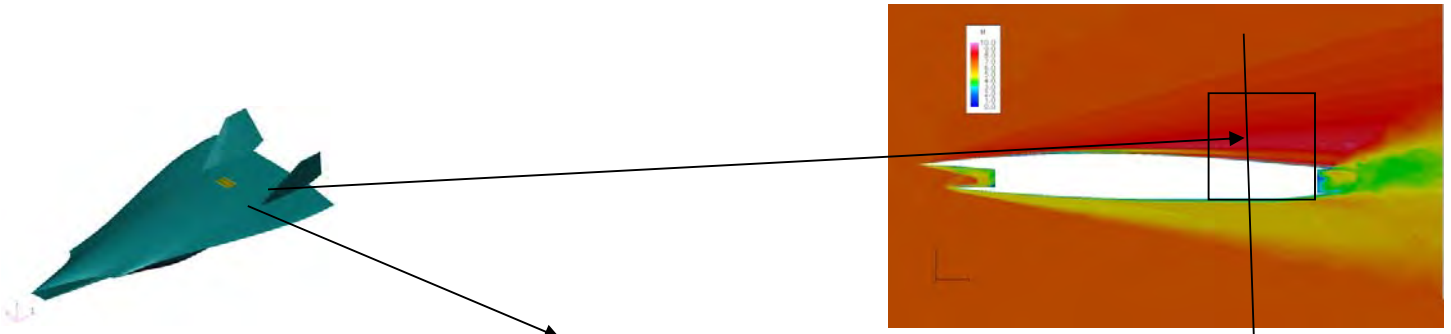

Streamline at center of panel

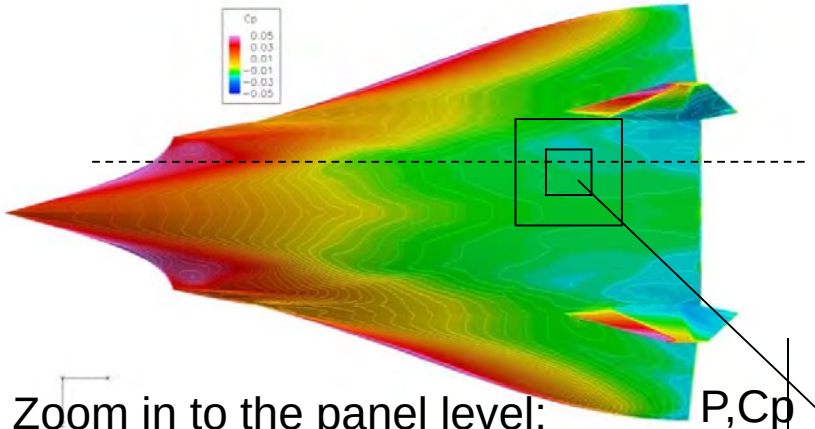

Zoom in to the panel level:

Graph of the pressure across
The panel at the Ctr line

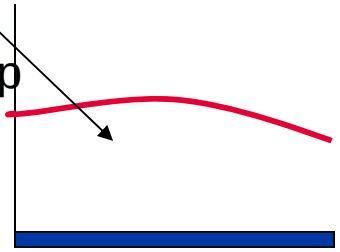

Velocity Profile

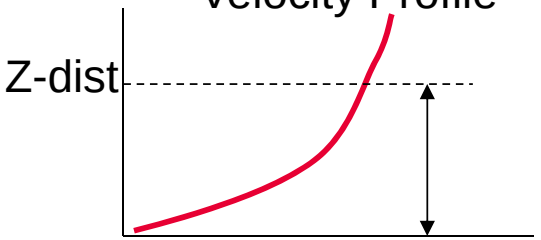

M,vel

An estimate of BL thick
At the leading edge of
the panel

Approved for public release; distribution unlimited.

CFD++ Computed Flow Field, M=6.0, a=6.0 deg., Alt.=75 Kft

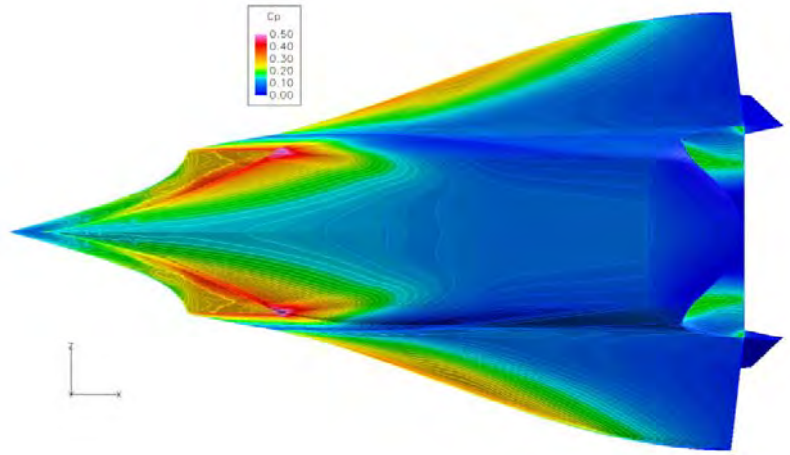

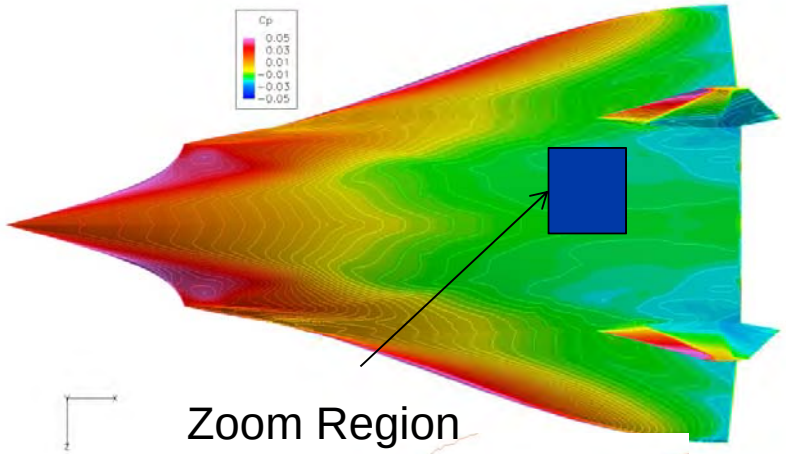

Zoom Region

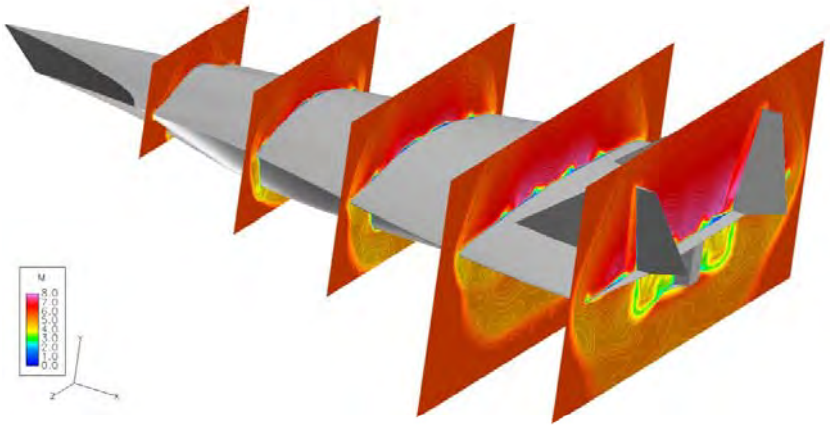

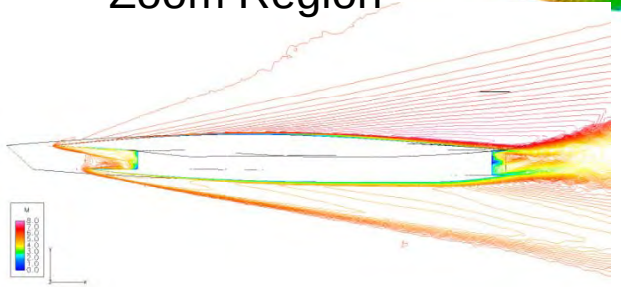

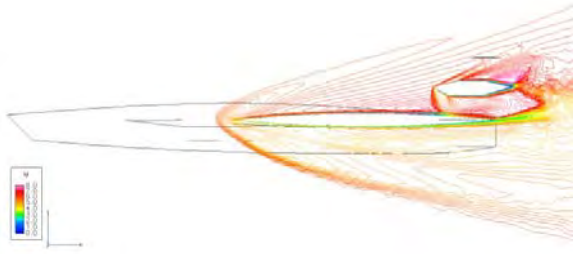

Approved for public release; distribution unlimited.

Computed Surface Pressures on the Panels

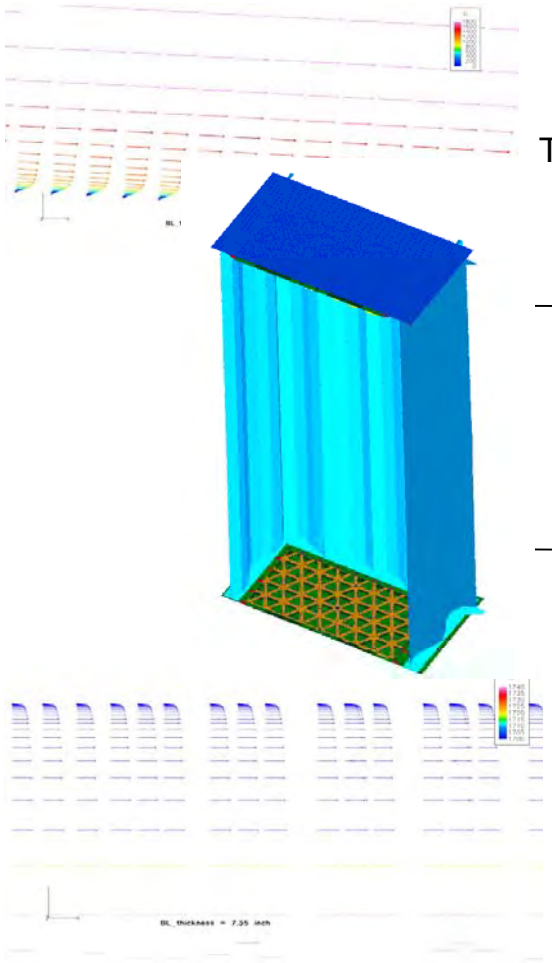

TBL_{ave}~11”

TBL_{ave}~7”

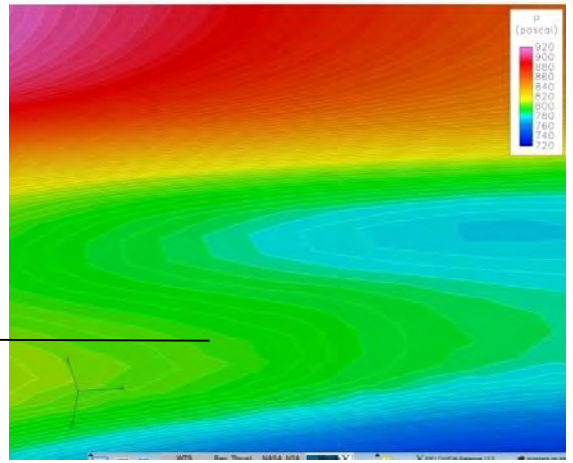

Panel 862
(Upper Surf)
ΔPy ~ 200 pa/m

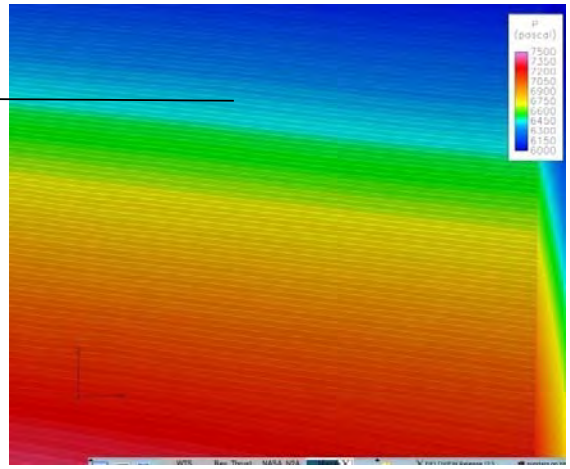

Panel 782
(Lower Surf)
ΔPy~1500 pa/m

Approved for public release; distribution unlimited.

Empirical Model Acoustic Prediction

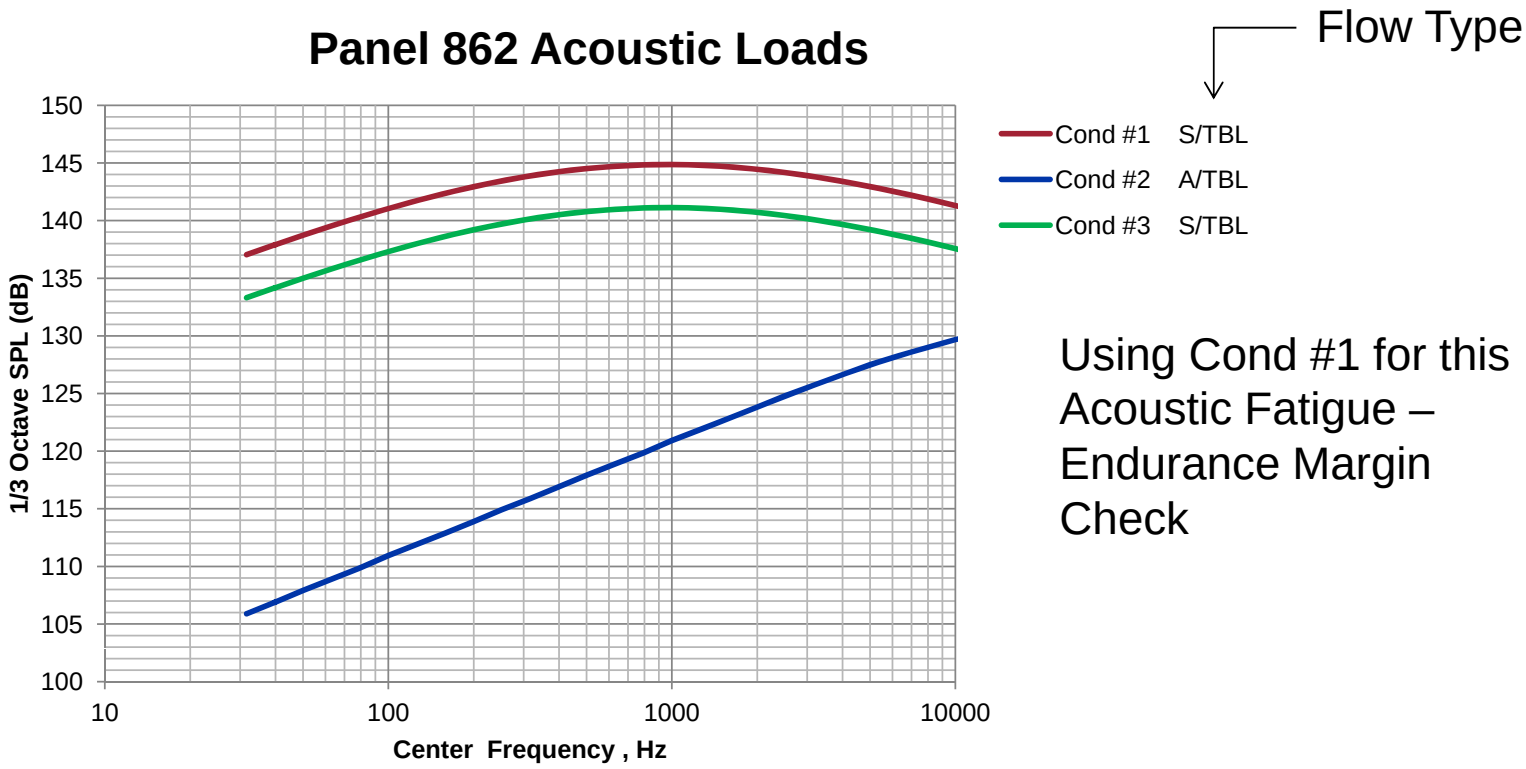

Using Cond #1 for this Acoustic Fatigue – Endurance Margin Check

Based on CFD input into Efimtsov TBL Models

Ref. R. Rackl, and A. Weston, "Modeling of Turbulent Boundary Layer Surface Pressure Fluctuation Auto and Cross Spectra - Verification and Adjustments Based on TU-144LL Data," NASA/CR-2005-213938.

Approved for public release; distribution unlimited.

Results - Modal , No Preload

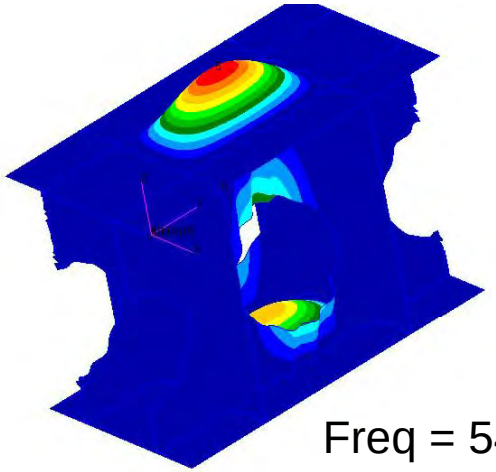

Freq = 54 Hz

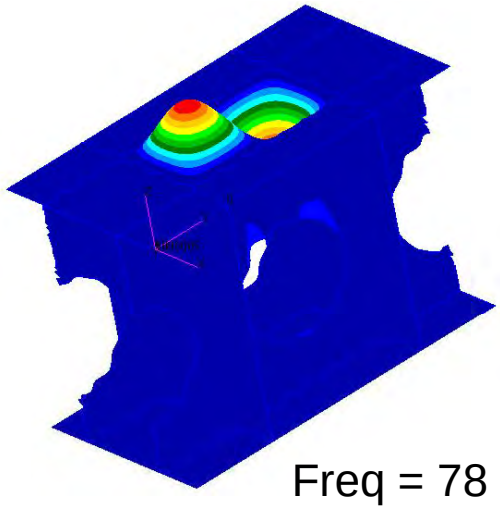

Freq = 78 Hz

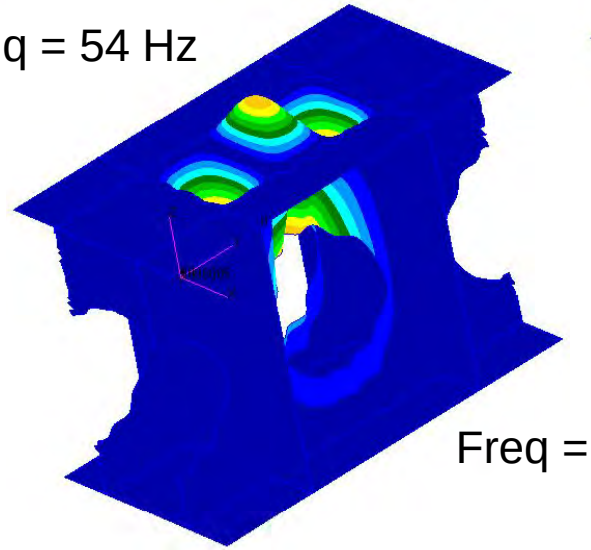

Freq = 134 Hz

These are the modes of interest for Acoustic Fatigue. Note: They are fairly low frequency.

Approved for public release; distribution unlimited.

Structural Damping

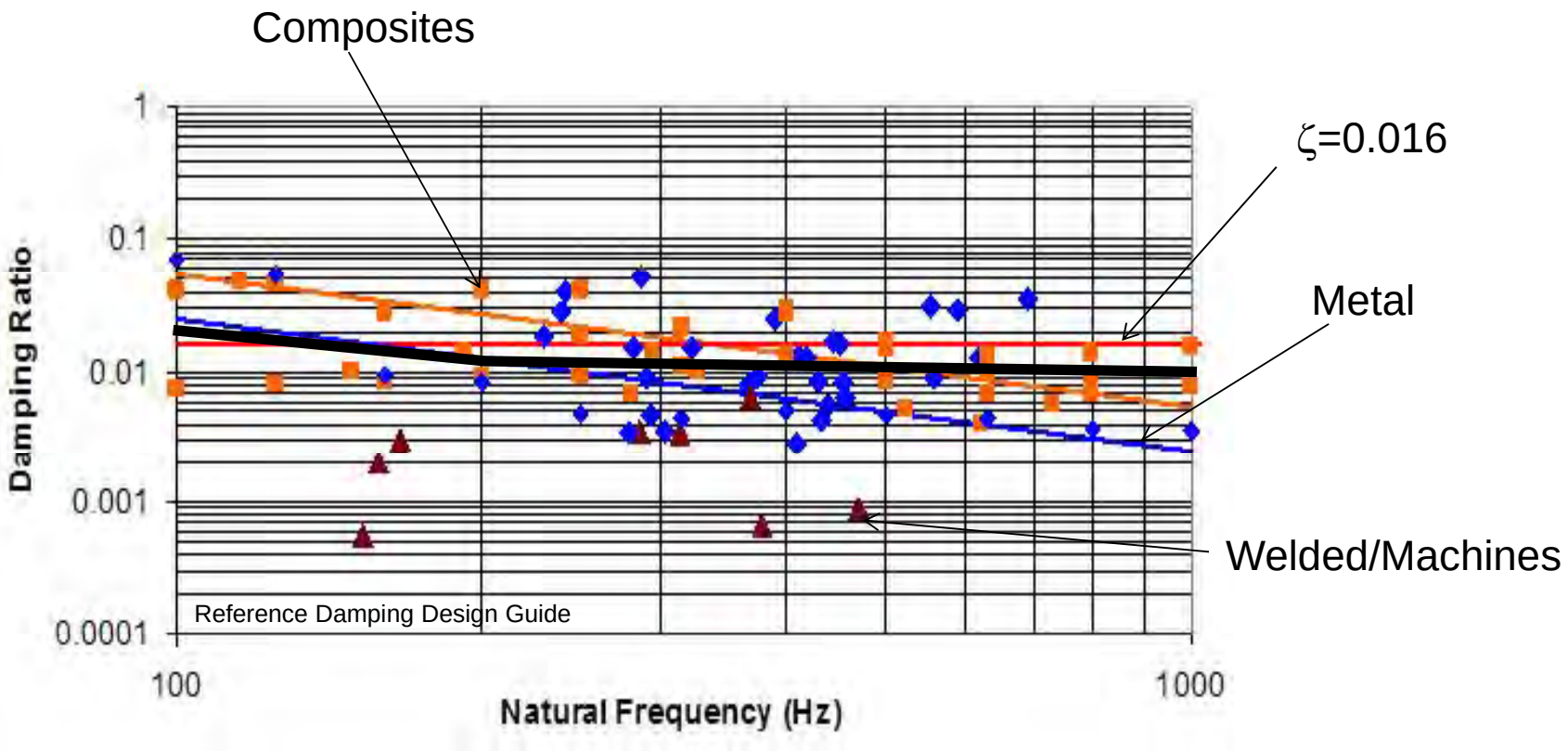

Dynamic Analysis uses the black curve

Approved for public release; distribution unlimited.

Results – Acoustic Response, RMS Disp

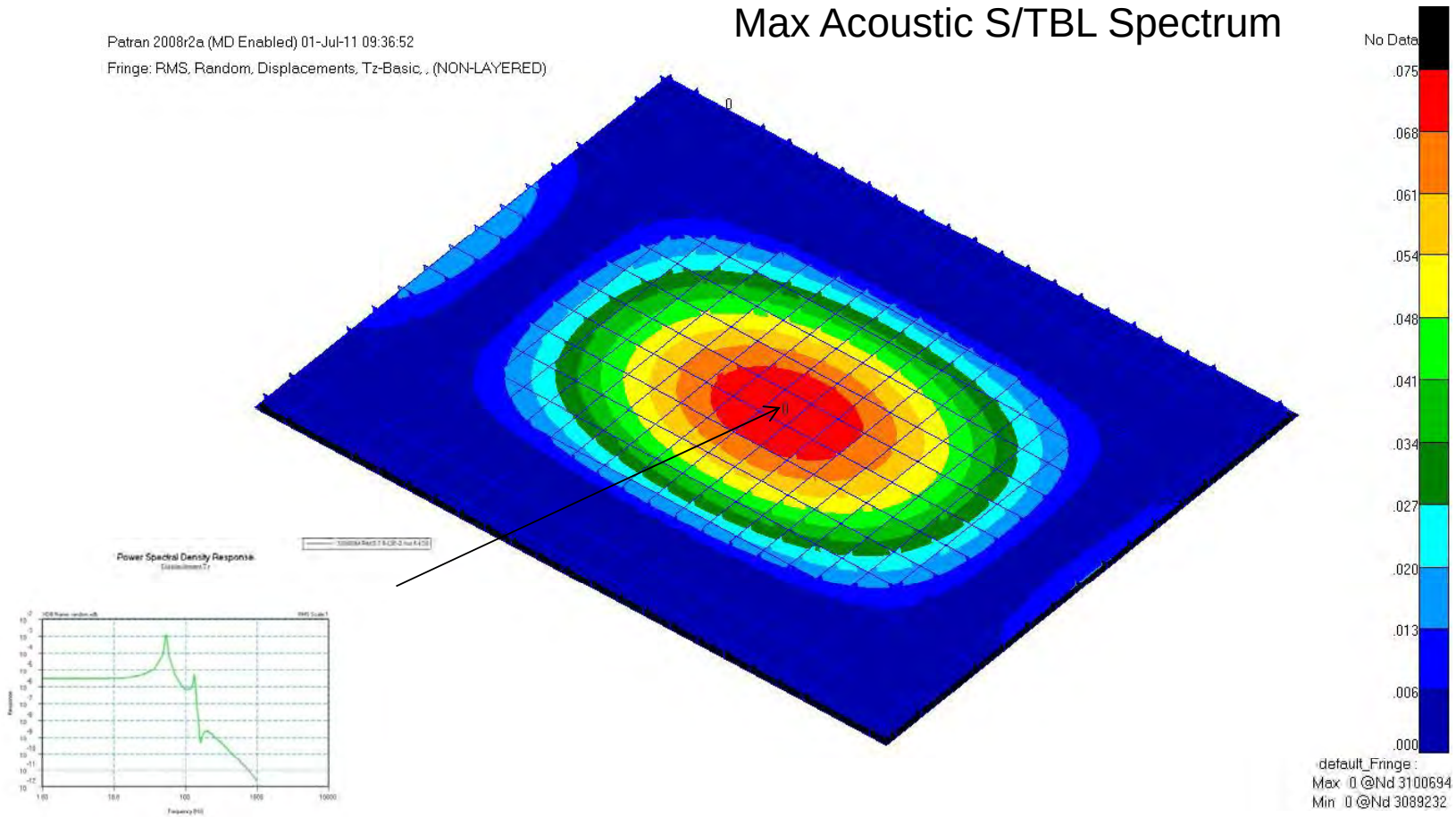

Approved for public release; distribution unlimited.

Max Acoustic –RMS Stress and Thermal Stress

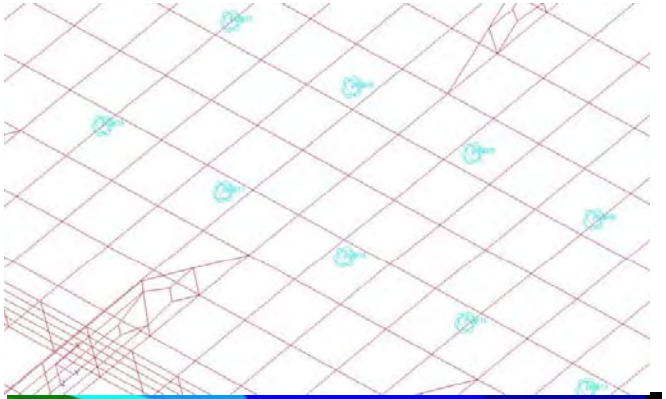

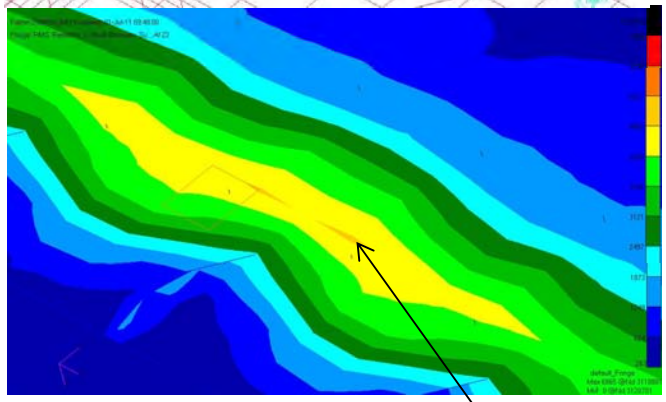

4.7ksi-rms
10.0 ksi-thermal

14.1ksi-rms
1.2 ksi – thermal

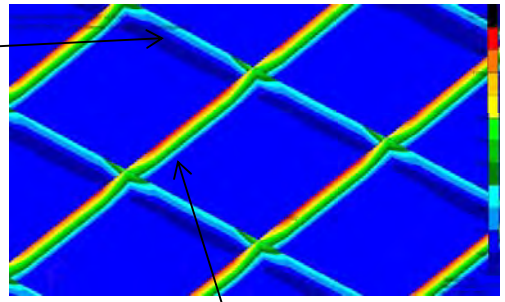

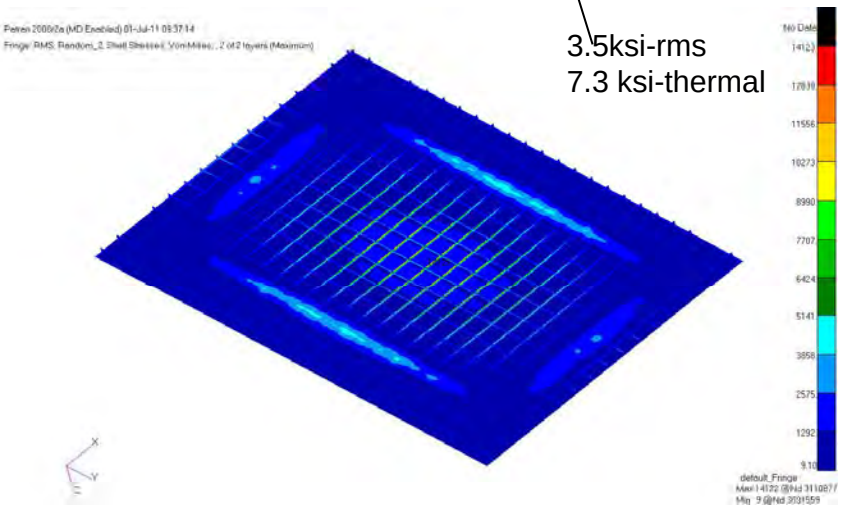

3.5ksi-rms
7.3 ksi-thermal

Note: These Plots are RMS only

Approved for public release; distribution unlimited.

Orthogrid Panel 862 Temperature Gradient History

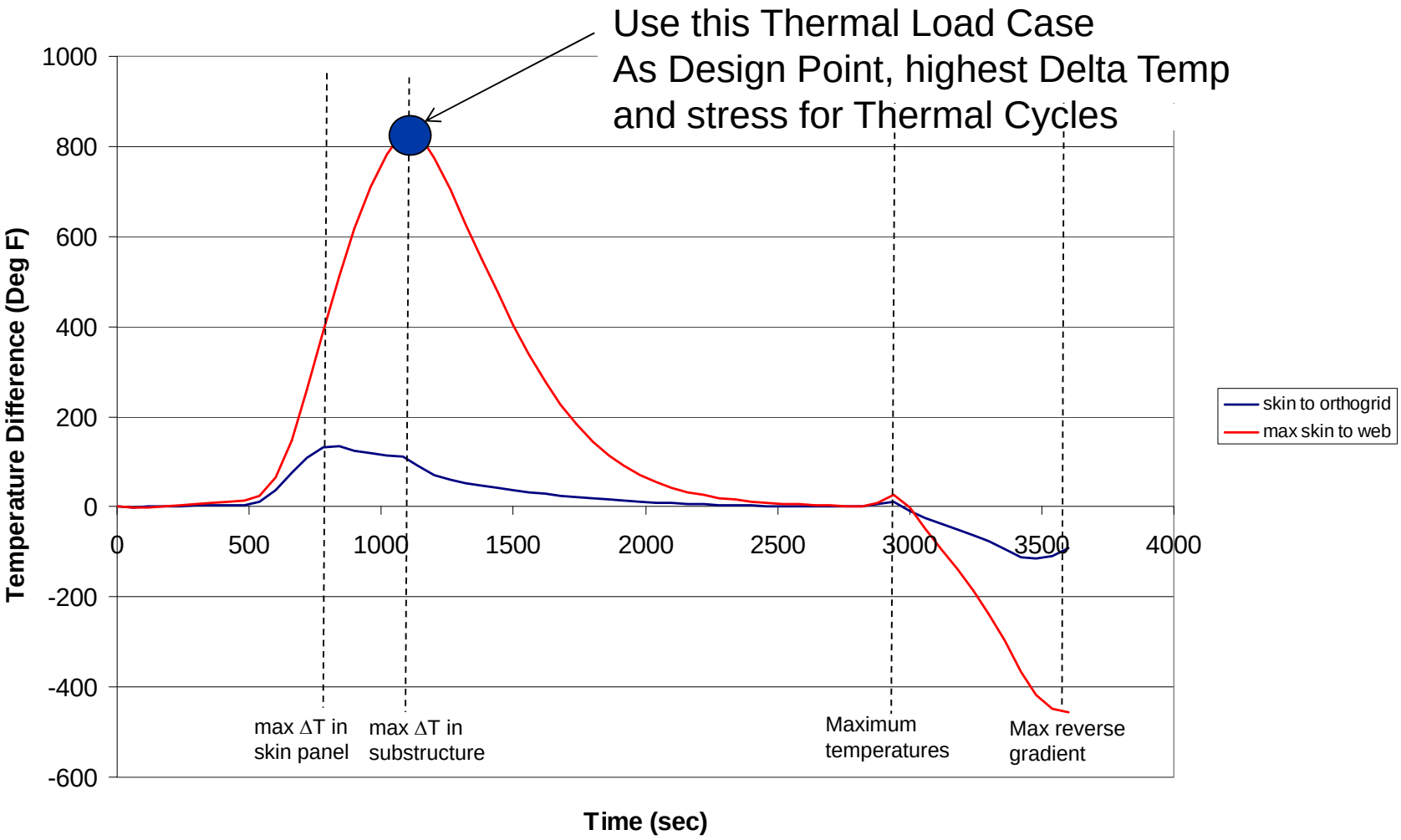

Approved for public release; distribution unlimited.

Results – Thermal Load at 1080 sec

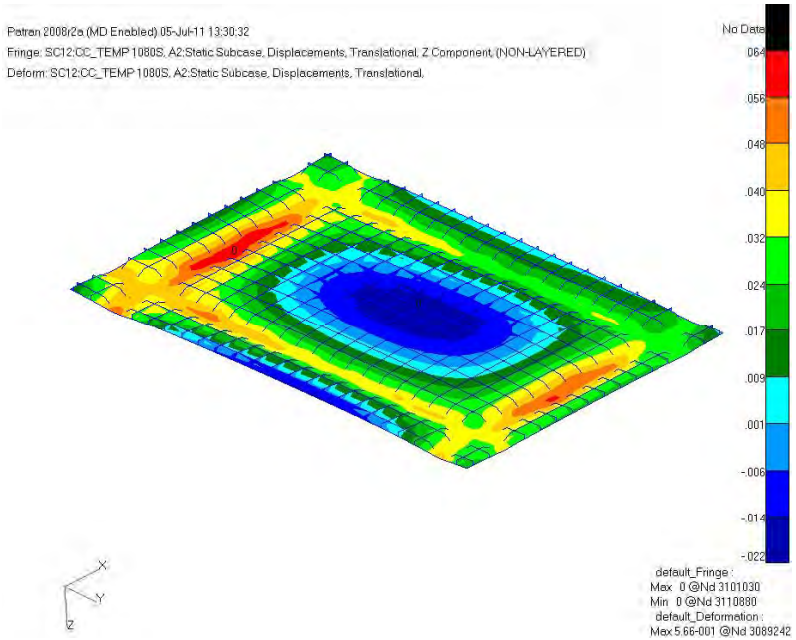

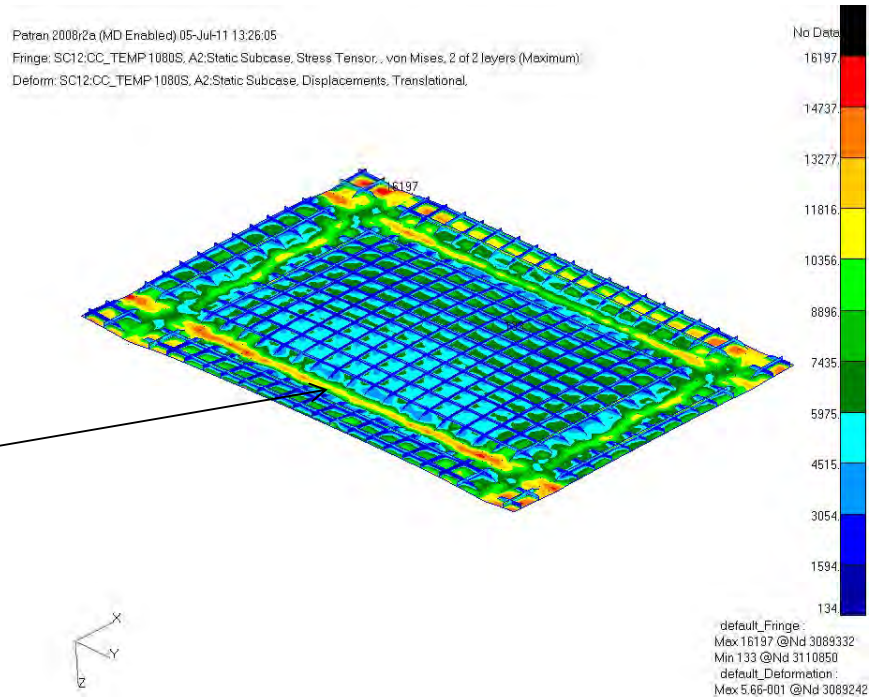

Record stress at same hot spots as acoustic locations

Approved for public release; distribution unlimited.

RMS Stress Allowable - Inconel 718

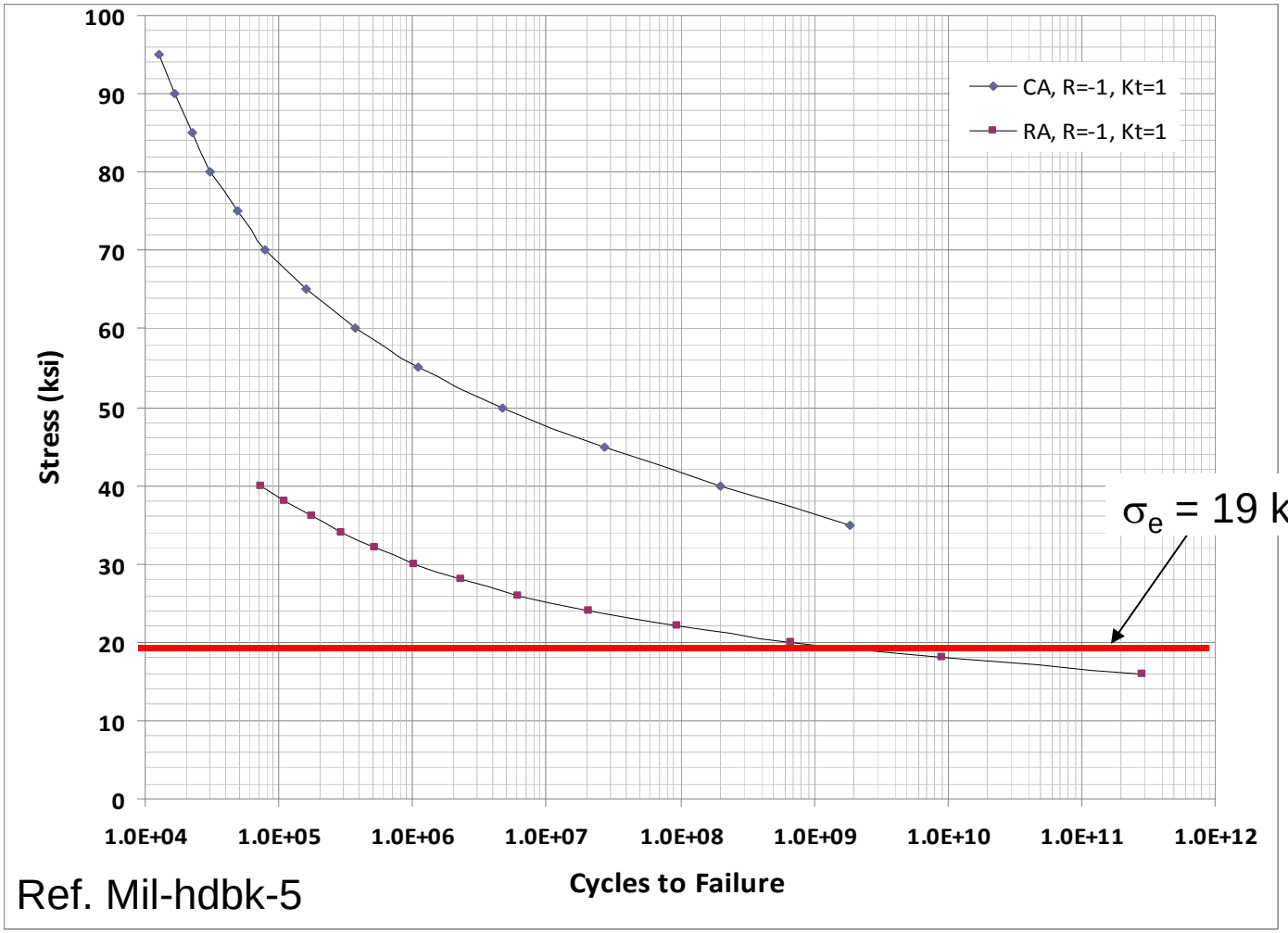

Approved for public release; distribution unlimited.

Hypersonic Strike Vehicle Operational Thermal Cycles

Assumptions:
1.0-hr cruise per fuel load
Average two air refuels, hence three thermal cycles per sortie
(Fly to theater, Engage, Return to base)
Average Three sorties per week over 20 year operational life
(Includes training flights and strike missions)
Critical highly-loaded exterior panels designed for 25% of the primary structure life
Other less loaded areas designed for 50% of the primary structure life

Primary Structure Design Implications:
3200 Sorties over operational life
3200 x 3 hrs flight = 9,600 operational hours
3200 x 3 cycles per flight = 9,600 thermal cycles

Exterior Panel Design Implications:
Critical Panels: 800 Sortie operational life
Other Panels: 1600 Sortie operational life
Critical Panels: 800 x 3 hrs flight = 2,500 operational hours
Other Panels: 1600 x 3 hrs flight = 5,000 operational hours
Critical Panels: 800 x 3 cycles = 2,500 thermal cycles
Other Panels: 1600 x 3 cycles = 5,000 thermal cycles

Approved for public release; distribution unlimited.

Acoustic Damage Accumulation

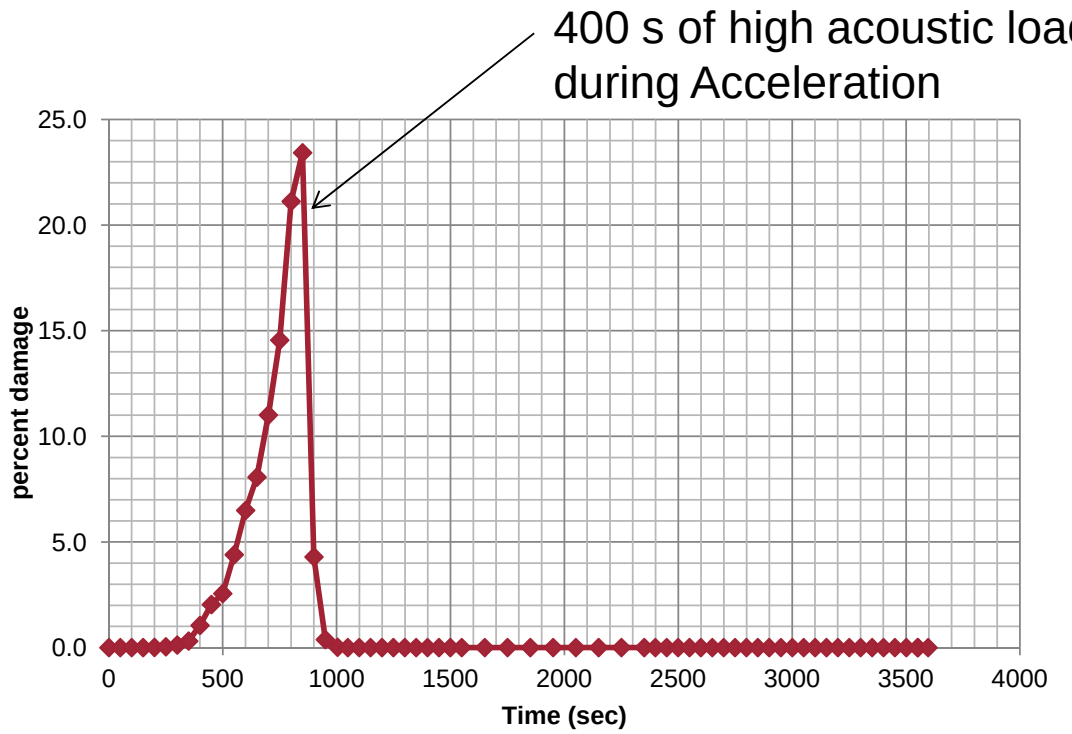

Acoustic Loads only critical during acceleration, add these stress cycles to fatigue spectrum

Approved for public release; distribution unlimited.

Temperature Profile @ t=1080 sec

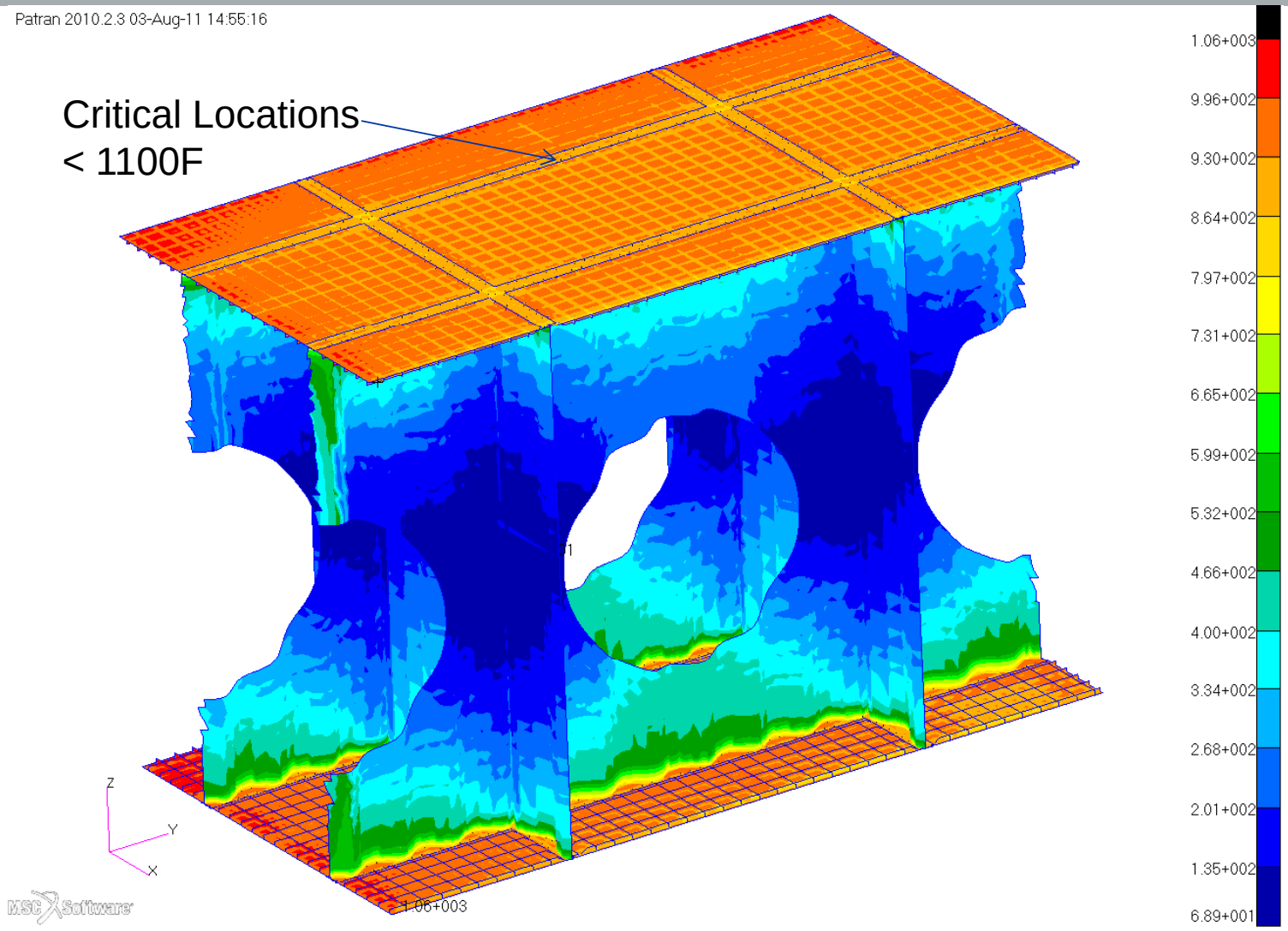

Approved for public release; distribution unlimited.

Acoustic Fatigue Results

For Endurance Limit, Based on analysis, 5000 hrs * 3600 sec/hr * 100 cycles/sec = 1.8e9.

Allowables Endurance Limit,
Ref. $K_t\sigma_e$ = 19.ksi – rms (K_t=1.00, R=-1, RT)
Stiffener Web, $K_t\sigma_e$ = 17.ksi – rms (K_t=1.00, R=-1, 1050)
Fillet Radius, $K_t\sigma_e$ = 14.1ksi – rms (K_t=1.22, R=.35, 1050F)
Flange Hole, $K_t\sigma_e$ = 5.7ksi – rms (K_t=2.97, R=.35, 850F)

2.) Check RMS thermal/acoustic response versus Se ➔

$$R = \frac{-\sigma_{rms} + \sigma_{mean}}{\sigma_{rms} + \sigma_{mean}}$$

Stiffener Web, Margin = 17.ksi/14.1ksi – 1 = 0.21
Fillet Radius , Margin = 11.9ksi/3.5ksi – 1 = 2.4
Flange Hole, Margin = 4.9ksi/4.8ksi – 1 = 0.02

$$S_g = S_{dyn}\left(1 - \frac{S_{mean}}{S_{ult}}\right)$$

Approved for public release; distribution unlimited.

Static Thermal Fatigue Method & Assumptions

- **Define Spectrum (load cycles)**
- **Define Material Fatigue Allowable & knockdowns**
- **Determine Spectrum Fatigue $K_t\sigma$ Allowable**
- **Check Margins in Analysis**

Approved for public release; distribution unlimited.

Hypersonic Strike Vehicle Operational Thermal Cycles

Assumptions: First Pass Fatigue Analysis, Use simple worst case scenario (G-A-G)

Primary Structure Design :

9600 x 1hr Sorties over operational life

Hence, 9,600 Ground-Air-Ground thermal cycles (2.5g Maneuver @ Max Thermal)

Design Life Factor of Safety = 4 life times or 38,400 cycles

Fatigue Spectrum uses, R-Ratio = 0 Inconel 718 s-N data.

Approved for public release; distribution unlimited.

Fatigue Analysis Approach

- **Use Mil-hd-bk 5 Inconel 718 Constant Amplitude Data**
- **Adjust for Temperature**
- **Calculate Design Feature Kts – Holes, Welds, Radii**
- **Post-process results – references stress value**
- **Calculate Margins – Compare predicted RMS Stress (KtS) to RMS Allowable (Endurance Limit)**
- **Assembly Stress Spectrum – Include Maneuver Loads, Temperature Ground Air Ground Cycles**
- **Perform acoustic damage (Dynamic Cycles) separate**
- **Calculate Total Fatigue Life – Combined Damage**

Approved for public release; distribution unlimited.

Inconel 718 S-N Data

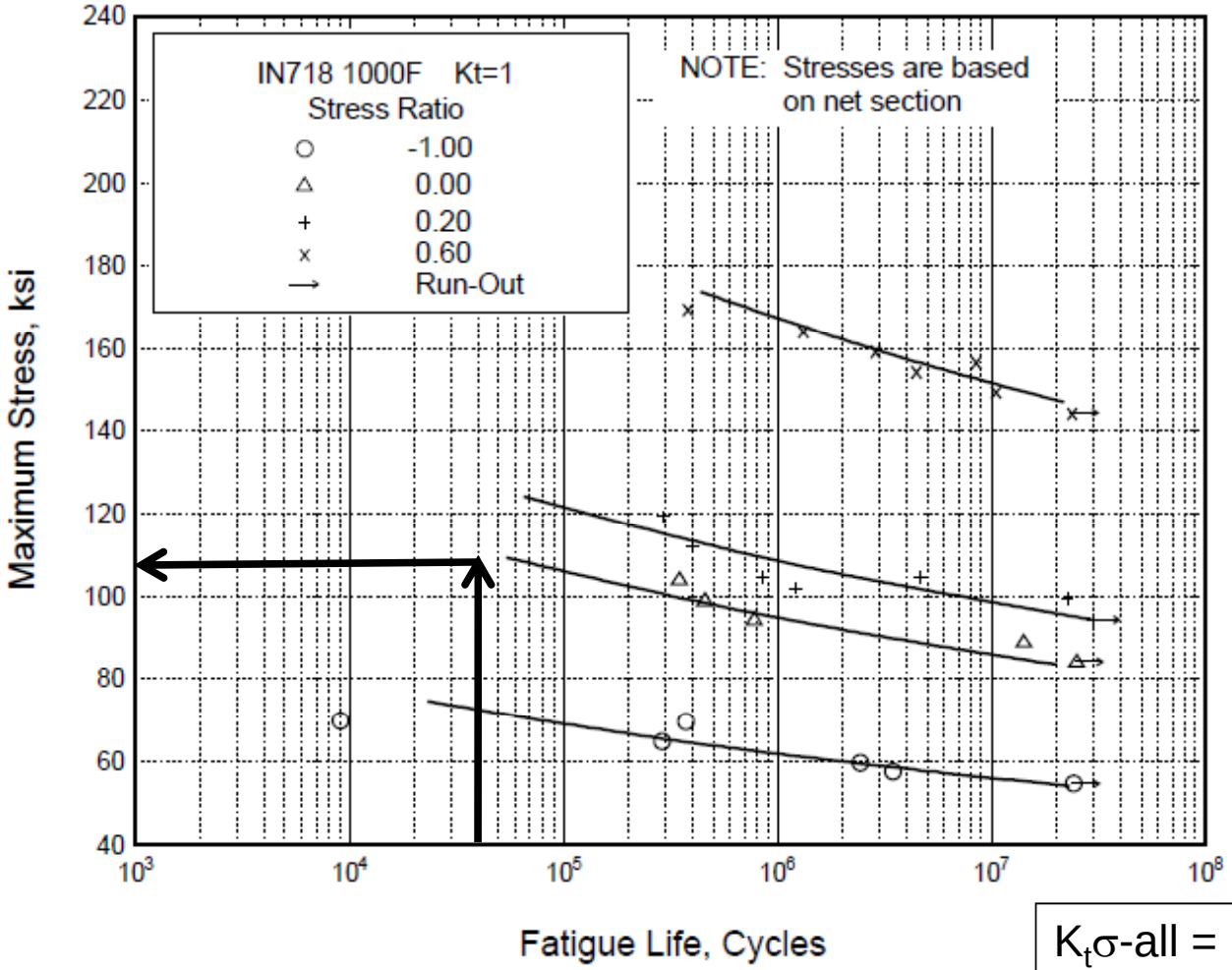

$K_t\sigma$-all = 110ksi
At 1000F, R=0

Ref. Mil-hdbk-5 J, section 6.3.5

Approved for public release; distribution unlimited.

Static FEA Information

Database

Orthogrid.db

Analysis Runs

Unit_Cell_P862_2.5g_T1080.dat (From .. \Delivered Analysis Files and Results\Panel_1)
Unit_Cell_Model_Load_Thermal.bdf

Load Case(s)

AA_Unit_Cell P862_2_5G_T=1080S.LIM

Results

'Bdf name'.xdb

Approved for public release; distribution unlimited.

Group Locations

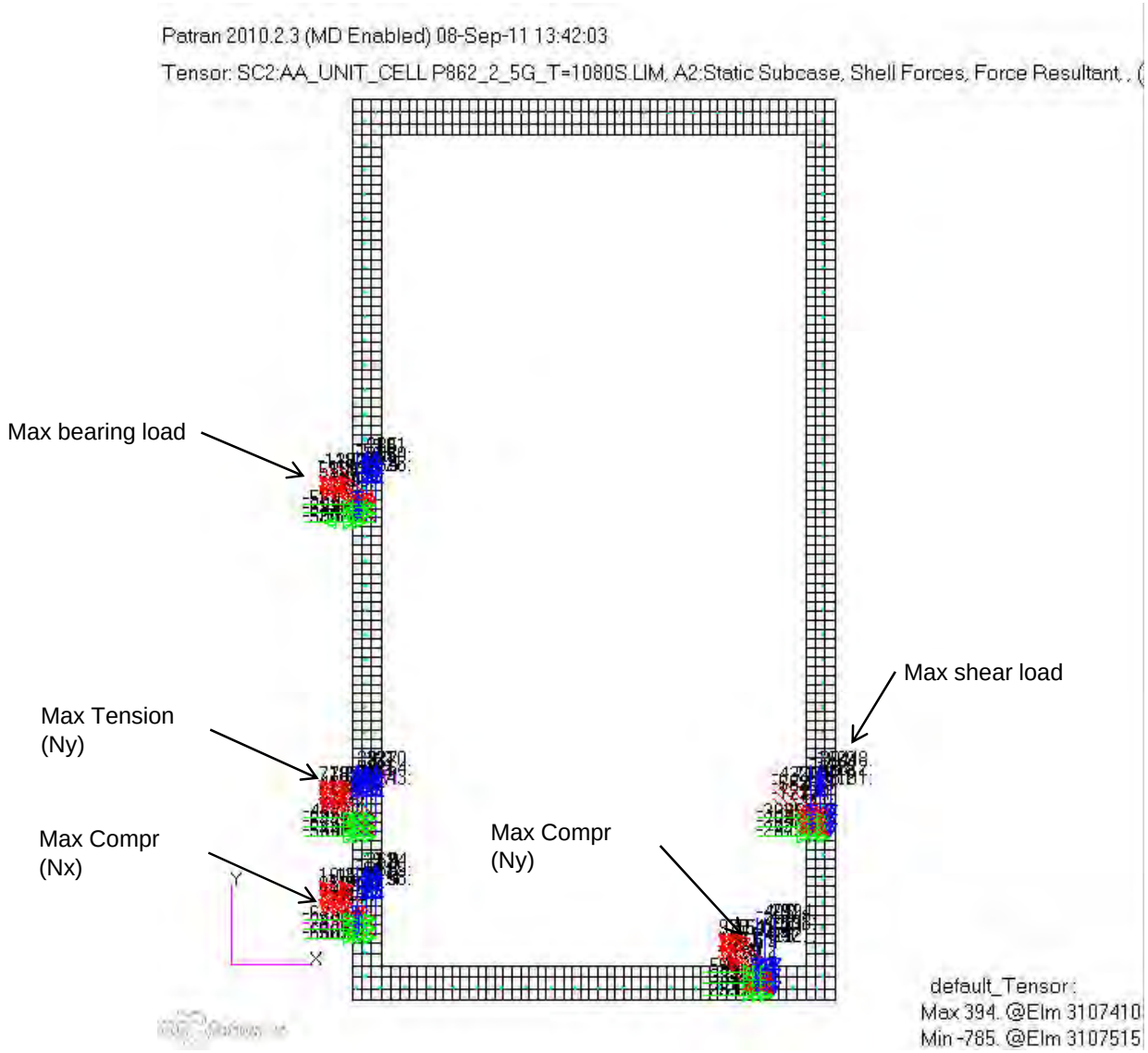

Approved for public release; distribution unlimited.

Stress and Margin Summary

	Max Brg	Max Shr	Min Nx	Min Ny	Max Ny	
Pbr	508	259	274	163	87.3	lbf
Nx By	-20.9	-446	-342	-414	-436	lb/in
Nx Gr	-584	-254	-698	-396	-513	lb/in
Nyby	135	-110	122	-339	189	lb/in
Nygr	140	-62.0	111	-464	244	lb/in
Nxyby	-33.9	-113	62.7	0.98	74.6	lb/in
KT Sigma	64.6	31.6	47.9	4.7	33.1	ksi
Fatigue Margin	0.41	0.71	0.56	0.95	0.69	

Load Case: AA_Unit_Cell P862_2_5G_T=1080S.LIM

Note: Load for max Nx load was small

Supporting documentation to follow

$$\text{Margin of Safety} = \frac{\text{Failure Load}}{\text{Design Load}} - 1$$

Approved for public release; distribution unlimited.

Example CAESAR INPUT (Max Bearing Case)

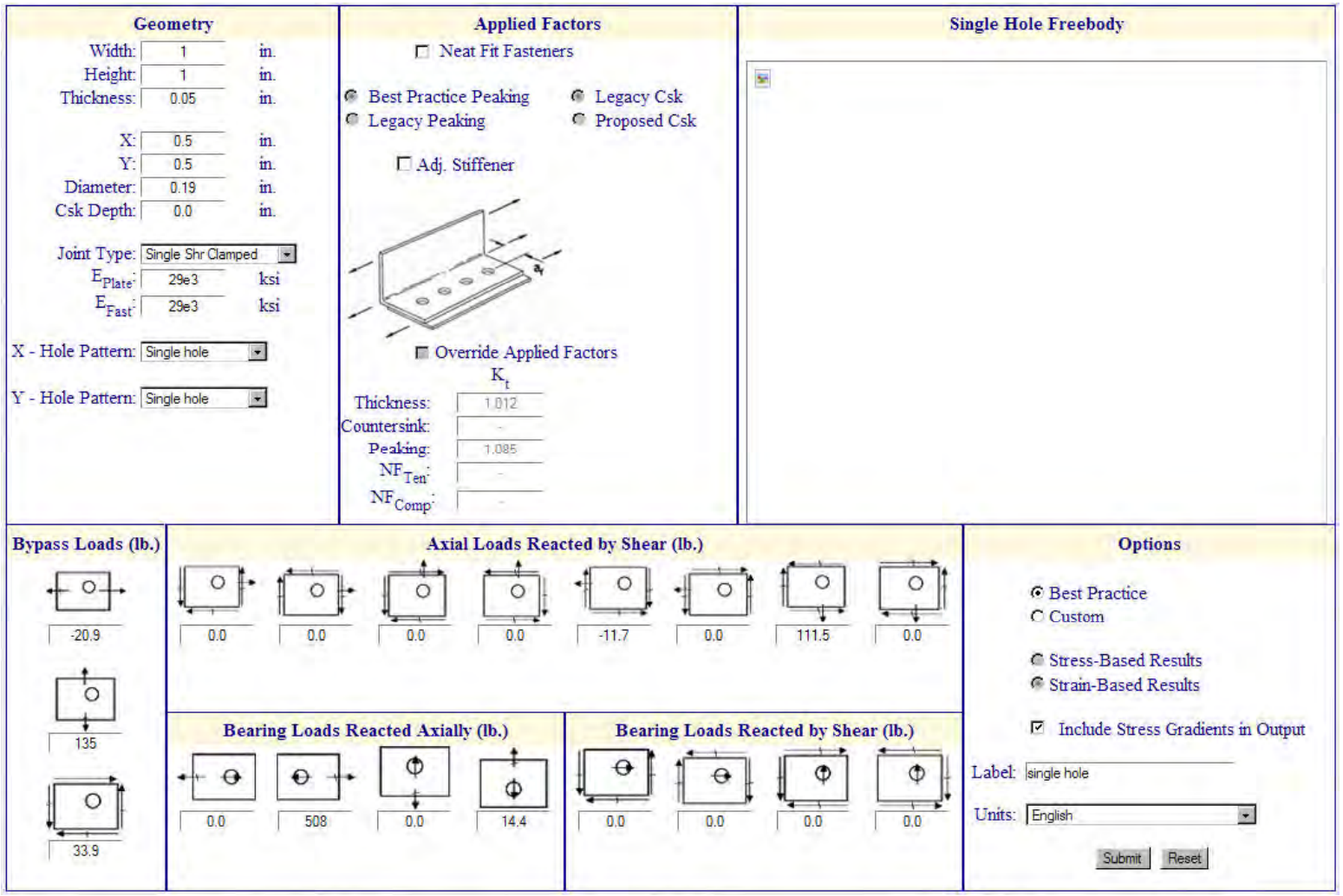

Approved for public release; distribution unlimited.

Maxima locations for P862 - Max Bearing

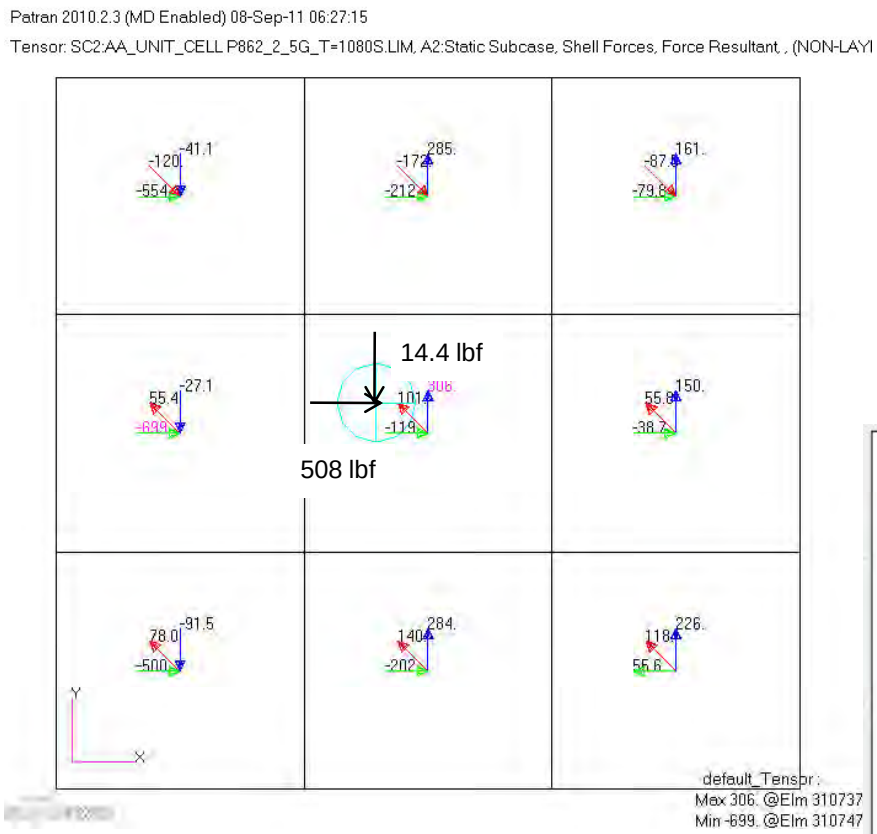

	Max Brg	
Pbr	508	lbf
Nx By	-20.9	lb/in
Nx Gr	-584	lb/in
Nyby	135	lb/in
Nygr	140	lb/in
Nxyby	-33.9	lb/in

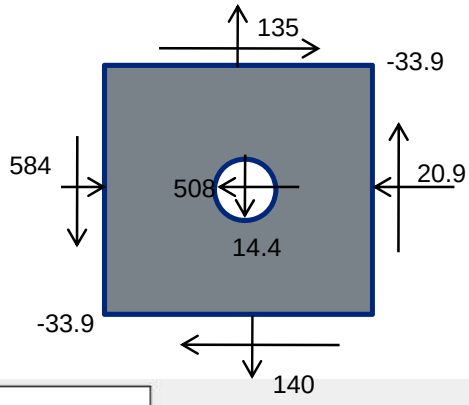

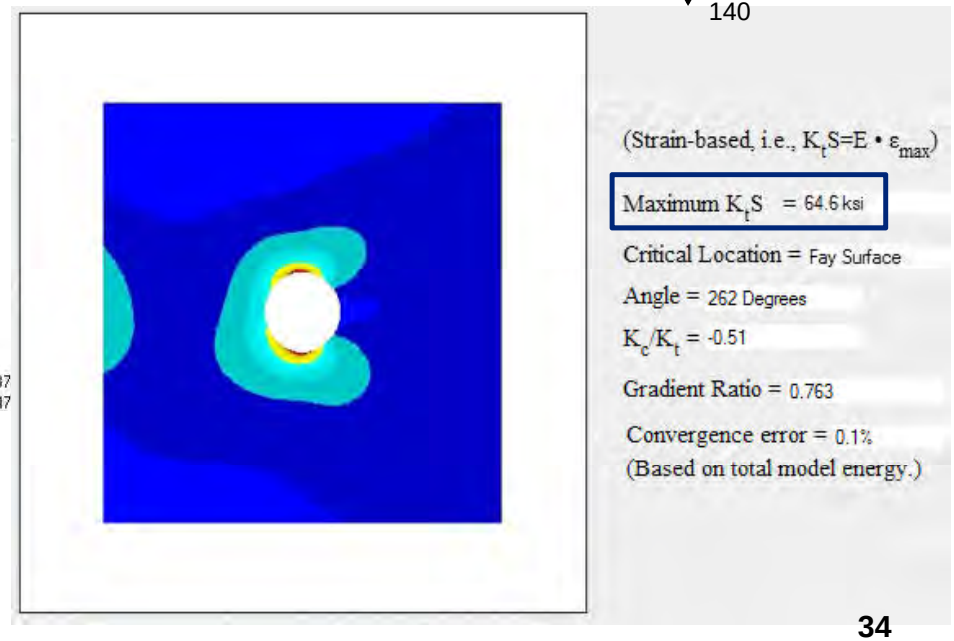

Approved for public release; distribution unlimited.

Maxima locations for P862 - Max Shear

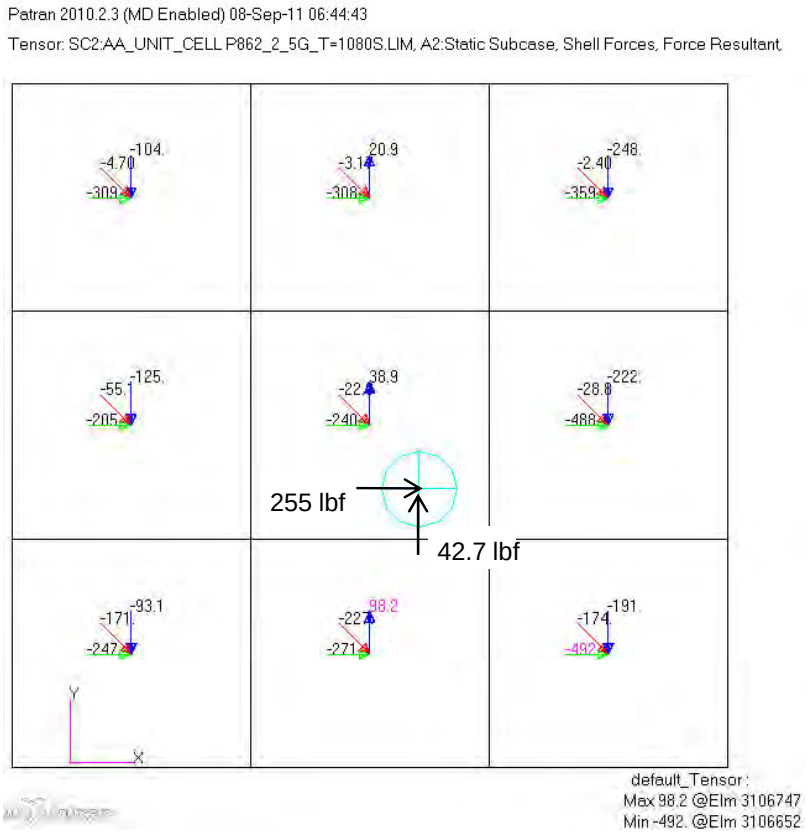

	Max Shr	
Pbr	259	lbf
Nx By	-446	lb/in
Nx Gr	-254	lb/in
Nyby	-110	lb/in
Nygr	-62.0	lb/in
Nxyby	-113	lb/in

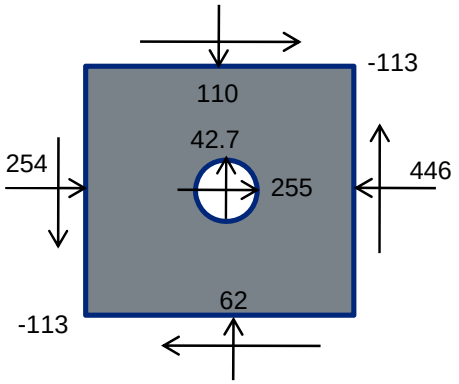

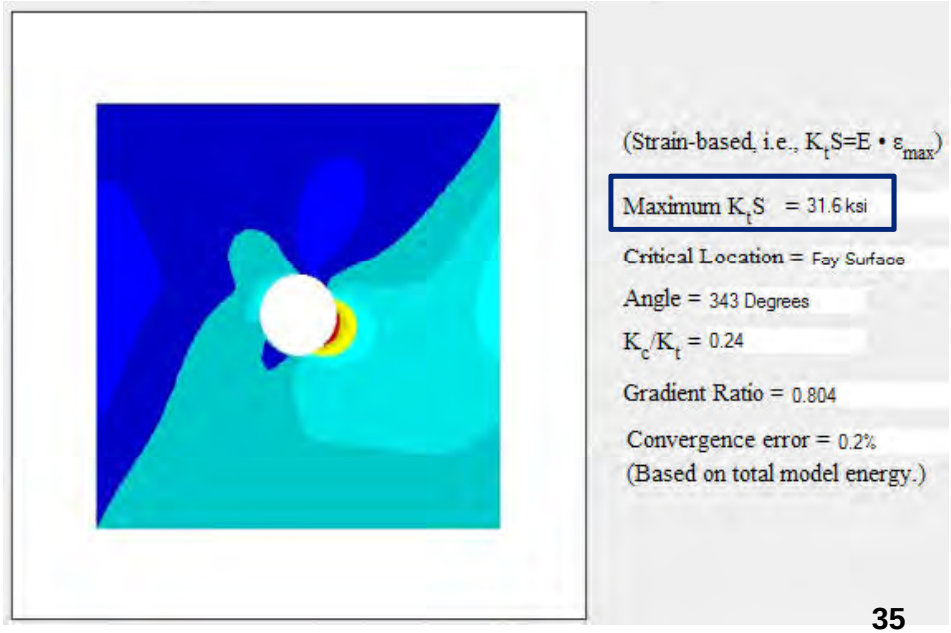

Approved for public release; distribution unlimited.

Maxima locations for P862 - Min Nx

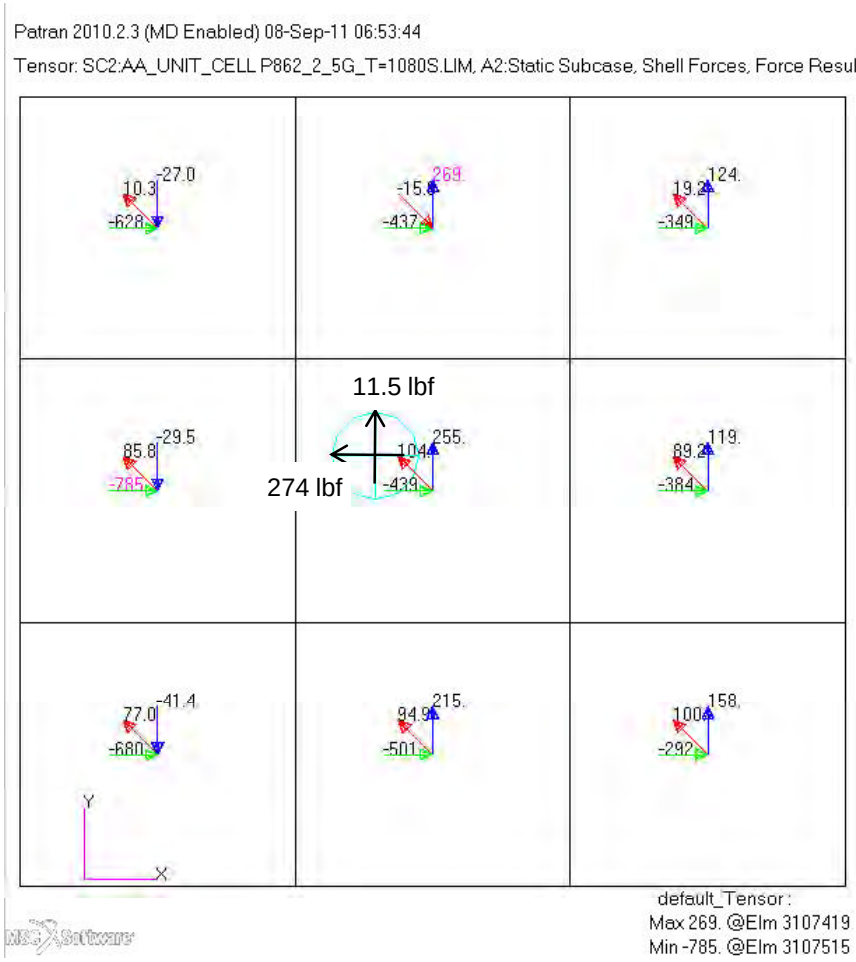

	Min Nx	
Pbr	274	lbf
Nx By	-342	lb/in
Nx Gr	-698	lb/in
Nyby	122	lb/in
Nygr	111	lb/in
Nxyby	62.7	lb/in

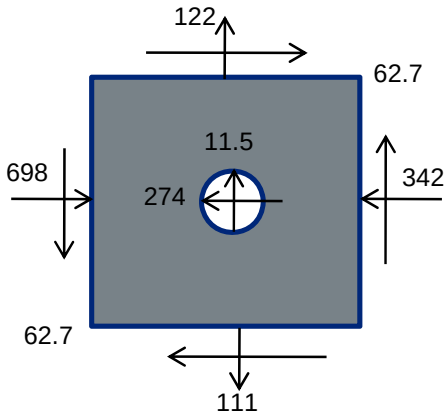

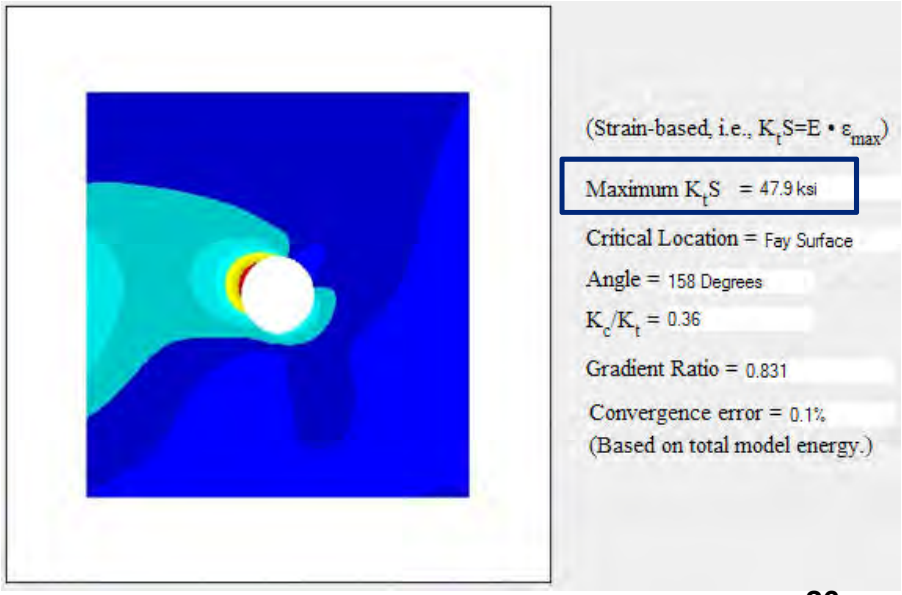

Approved for public release; distribution unlimited.

Maxima locations for P862 - Min Ny

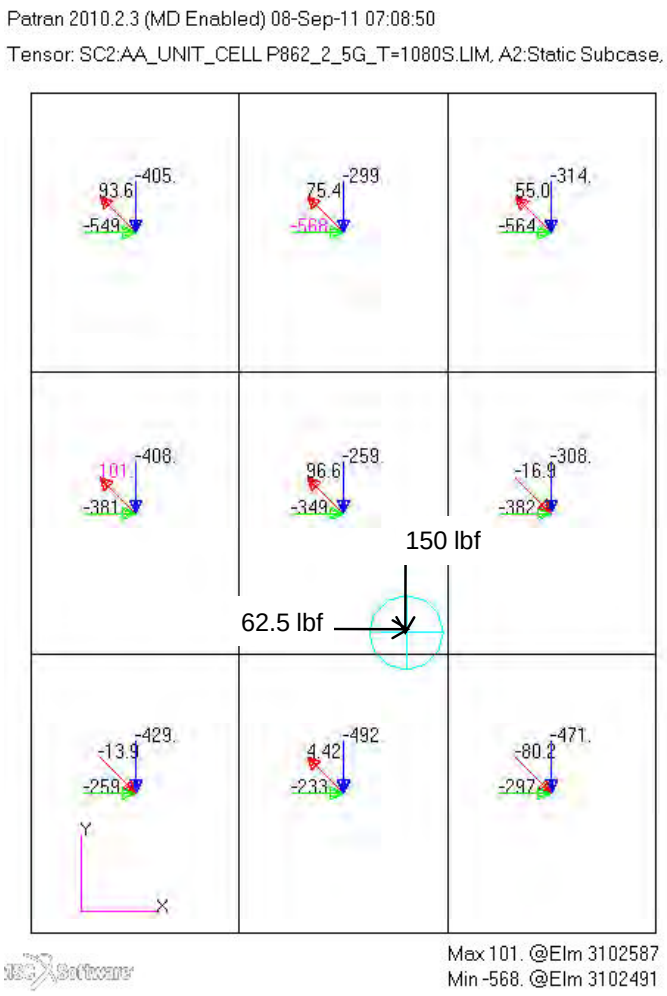

	Min Ny	
Pbr	163	lbf
Nx By	-414	lb/in
Nx Gr	-396	lb/in
Nyby	-339	lb/in
Nygr	-464	lb/in
Nxyby	0.98	lb/in

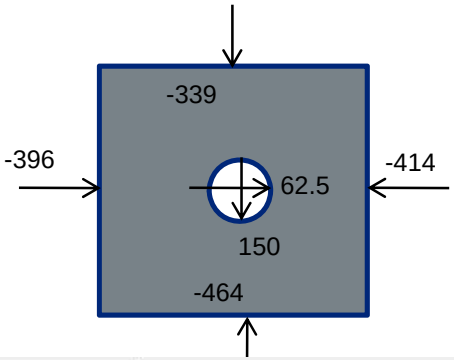

(Strain-based, i.e., $K_t S = E \cdot \varepsilon_{max}$)

Maximum $K_t S$ = 4.69 ksi

Critical Location = Fay Surface

Angle = 359 Degrees

K_e/K_t = -4.70

Gradient Ratio = 0.371

Convergence error = 0.1%
(Based on total model energy.)

Approved for public release; distribution unlimited.

Maxima locations for P862 - Max Ny

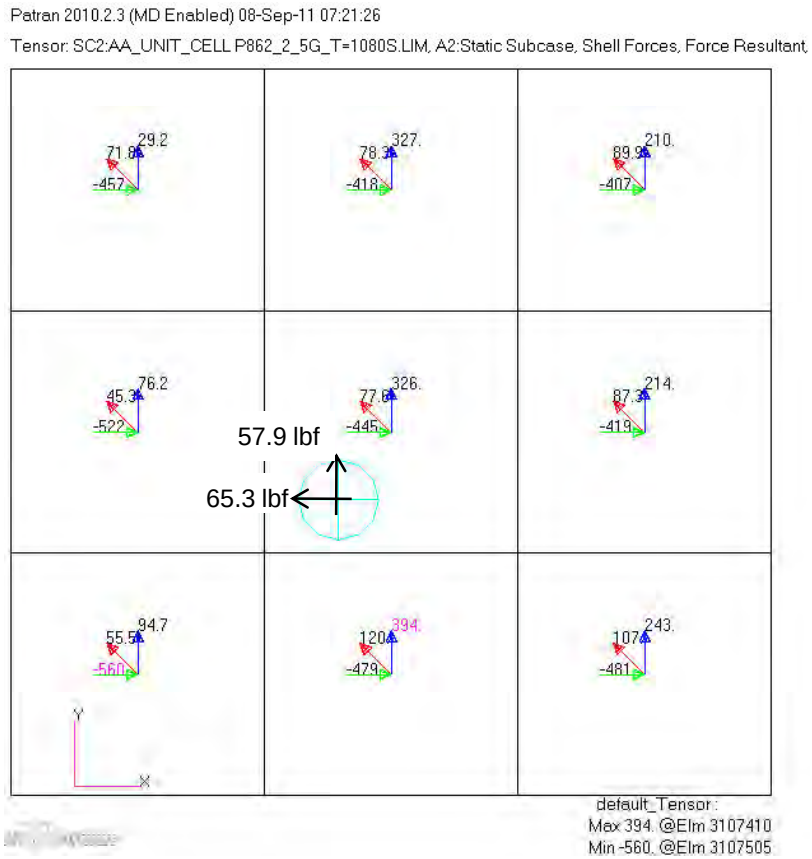

	Max Ny	
Pbr	87.3	lbf
Nx By	-436	lb/in
Nx Gr	-513	lb/in
Nyby	189	lb/in
Nygr	244	lb/in
Nxyby	74.6	lb/in

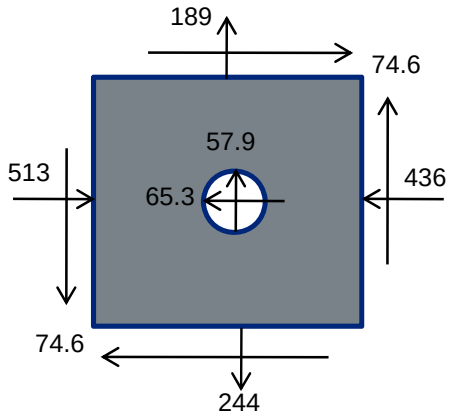

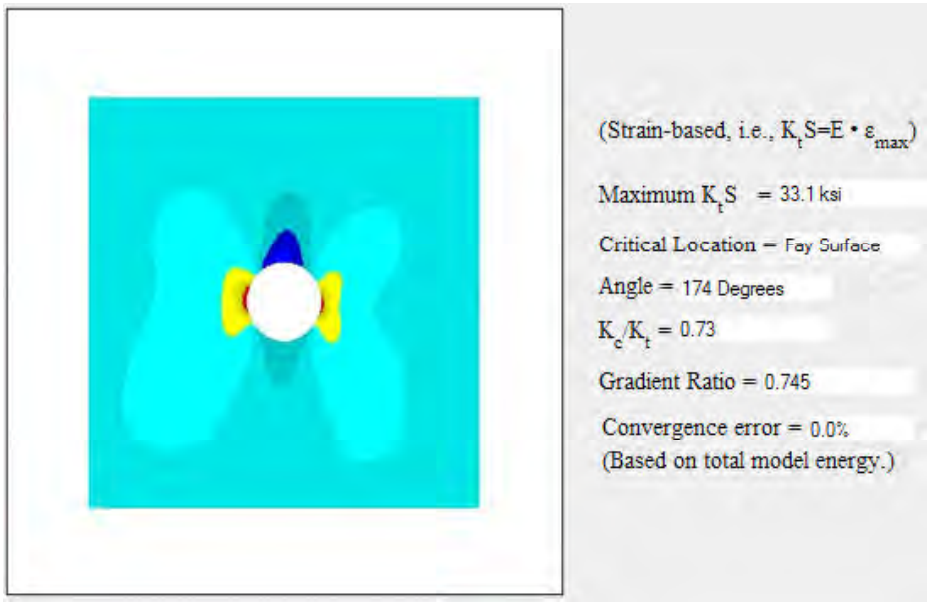

Approved for public release; distribution unlimited.

Bearing Calculations

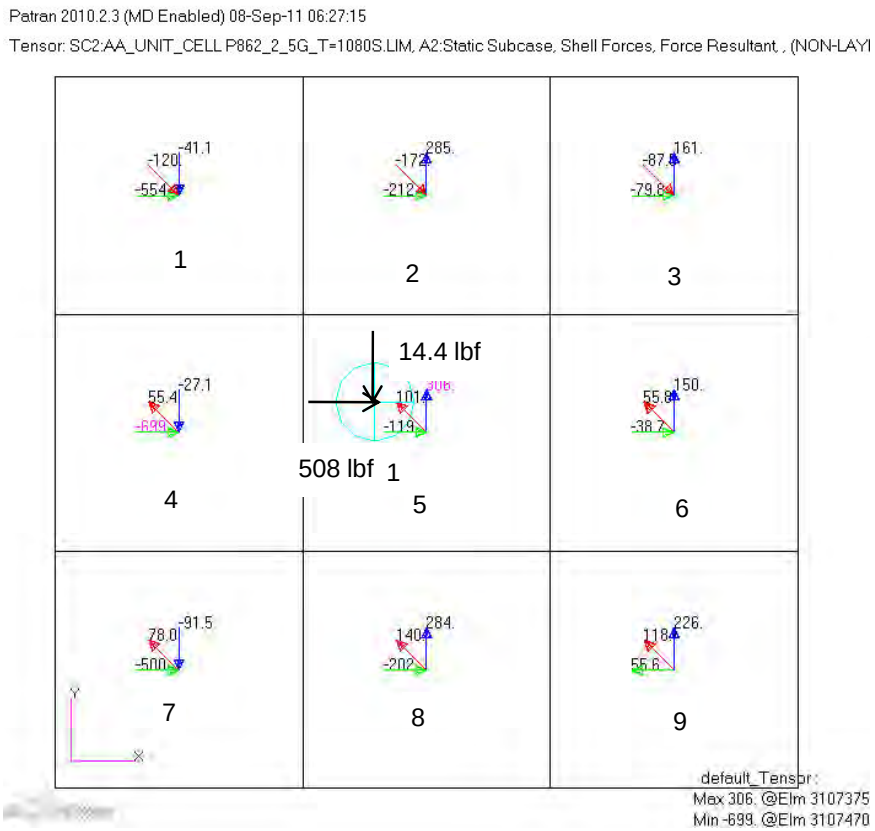

	Max Brg	
Pbr	508	lbf
Nx By	-20.9	lb/in
Nx Gr	-584	lb/in
Nyby	135	lb/in
Nygr	140	lb/in
Nxyby	-33.9	lb/in

$$Nx_{BY} = \frac{Nx_3 + Nx_6 + Nx_9}{3} \qquad Ny_{BY} = \frac{Ny_1 + Ny_2 + Ny_3}{3}$$

$$Nx_{GR} = \frac{Nx_1 + Nx_4 + Nx_7}{3} \qquad Ny_{GR} = \frac{Ny_7 + Ny_8 + Ny_9}{3}$$

$$Nxy_{BY} = \frac{Nxy_1 + Nxy_2 + Nxy_4 + Nxy_5}{4}$$

4 Nearest Elements

Approved for public release; distribution unlimited.

Summary

Flight Loads
Mach 7, +2.5g, symmetric pull up maneuver

Thermal
Temperature @
T = 1080 sec, Maximum thermal gradient between panel and substructure

Load Case
For 2.5g loading *1.15 (F.S.), Temp @ 1080s

Boundary Conditions for Panel Model
Translational/Rotational Constraints

Analysis Runs
Ctr_panel_1080_random.bdf (sol 111, setup)

Acoustic Loads
Rand_panel.rnd (acoustic input PSDs), average separated flow spectrum, uncorrelated loads

Approved for public release; distribution unlimited.

Engineering, Operations & Technology
Boeing Research & Technology

Panel 780 Heat Transfer Analysis

April 5, 2011

Pete Keller
206-544-7528
peter.c.keller@boeing.com

Approved for public release; distribution unlimited.

Assumptions

- Transient analysis, temperature dependant material properties
- All structure modeled with shell elements: through-thickness gradients not significant
- Engine insulation blanket between upper and lower panel regions
- Aerothermal environment provided from MINIVER Mach 7 trajectory analysis
- Natural convection inside cavity – pressurized to ambient +1 psf
- Uniform initial temperature = recovery temperature at M=0.75, 25kft
- Internal radiation exchange between skin, isogrid, panel breakers, web and engine insulation

Approved for public release; distribution unlimited.

Panel 780 Unit Cell

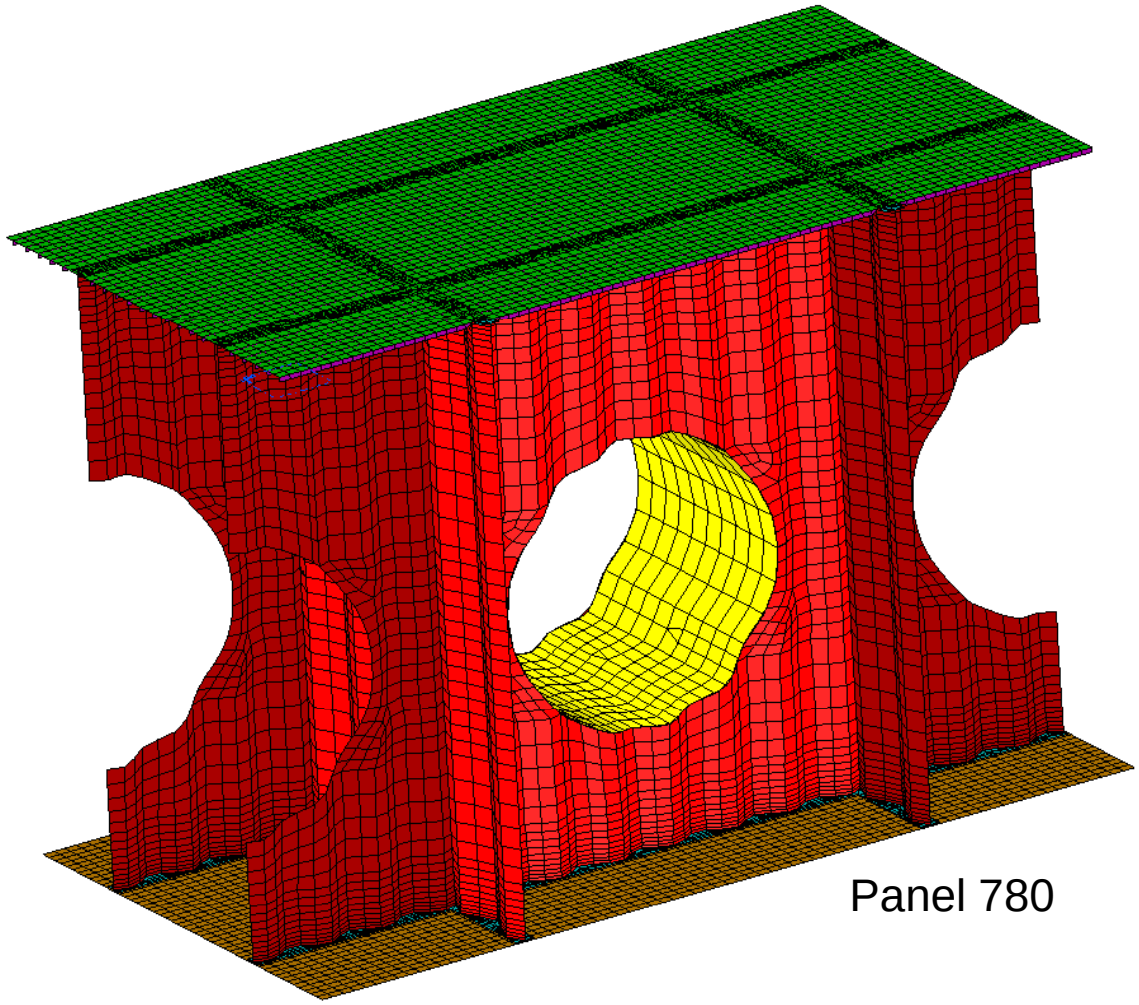

Panel 780

26553 nodes
26448 element

Approved for public release; distribution unlimited.

Panel 780 Thermal Boundary Conditions

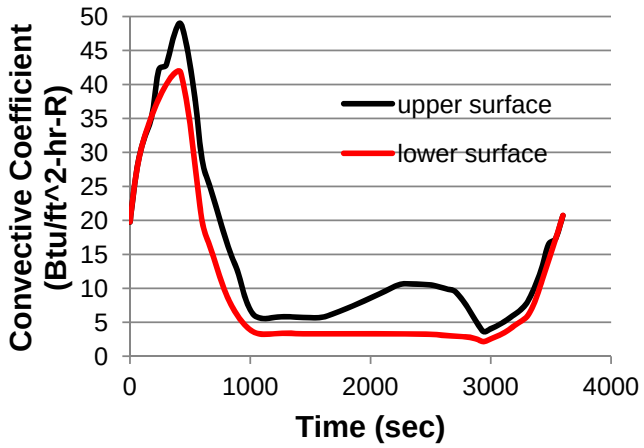

Panel 780 Aerothermal Environment

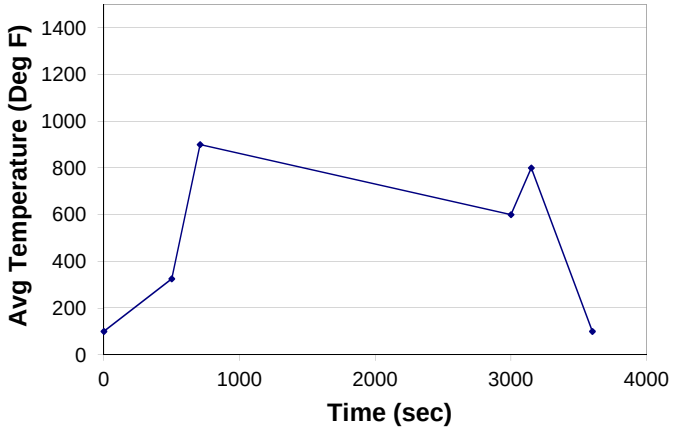

Engine temperature

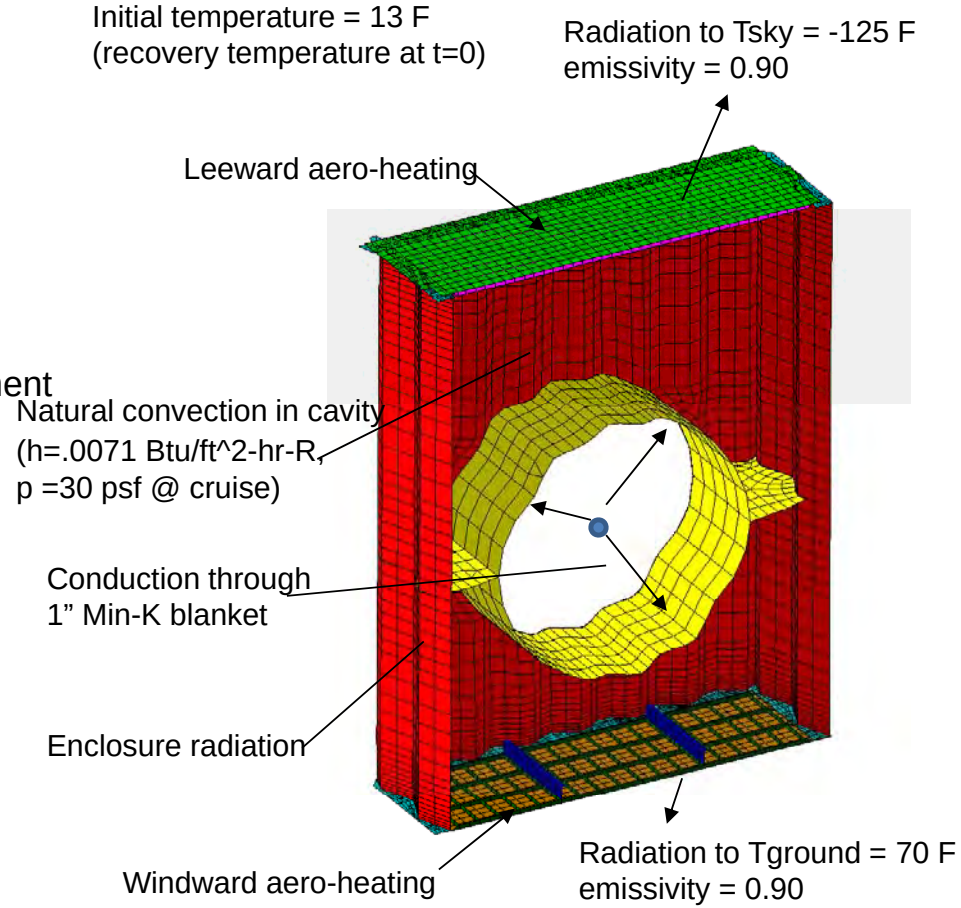

Approved for public release; distribution unlimited.

Panel 780 Temperature Distributions

660 sec - maximum panel temperature gradients

720 sec - maximum panel breaker temperature gradients

840 sec – maximum substructure temperature gradients

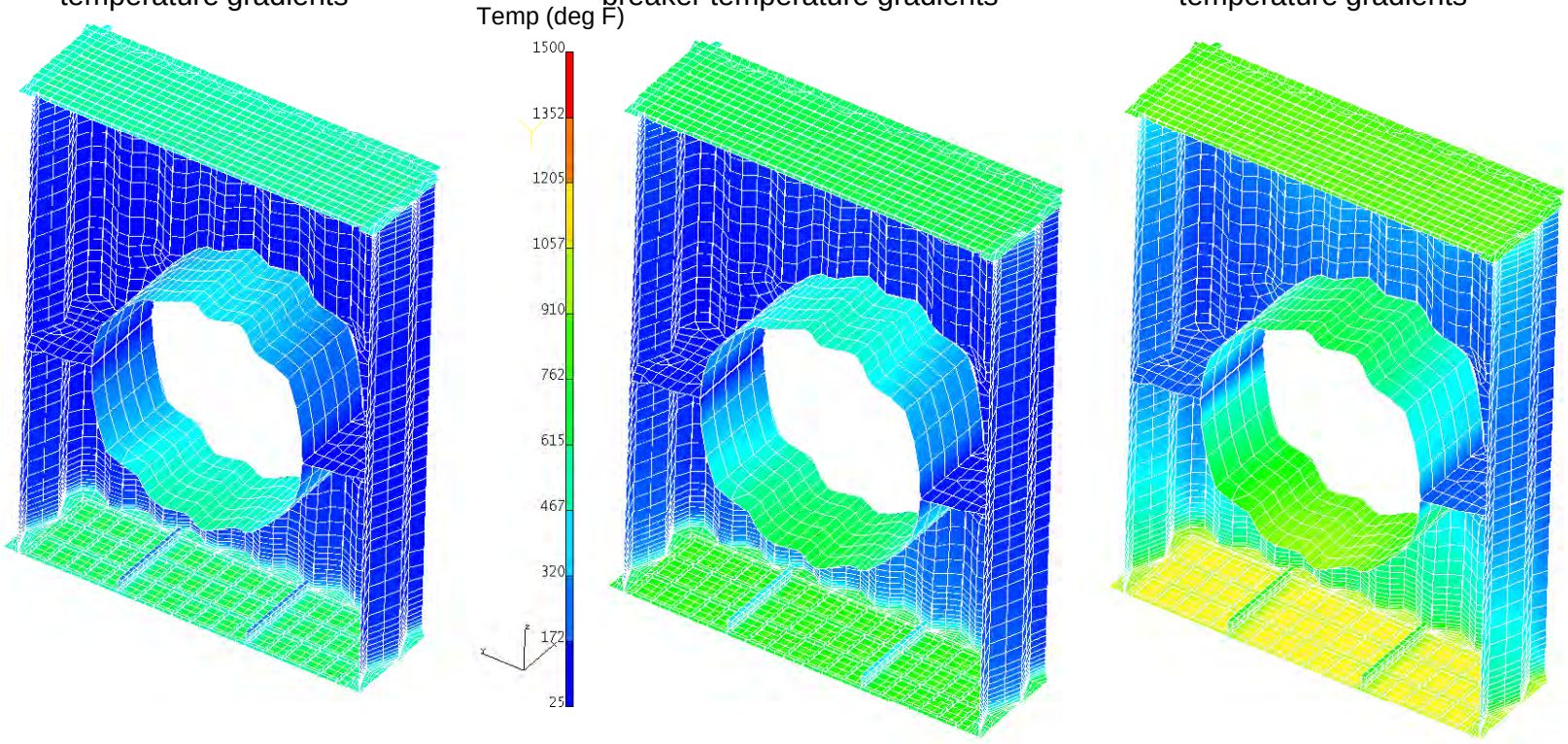

Approved for public release; distribution unlimited.

Panel 780 Temperature Distributions

2520 sec – maximum temperatures

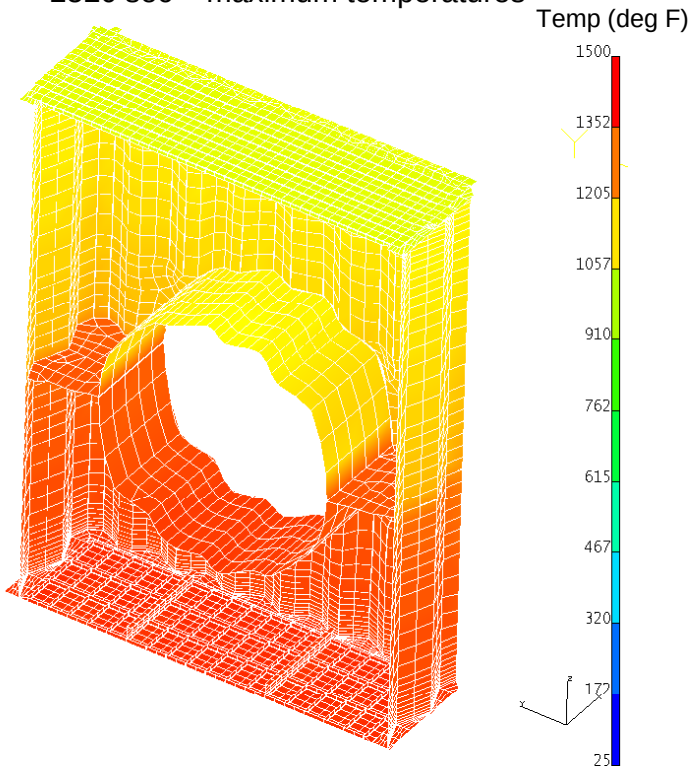

3600 sec – maximum negative temperature gradients

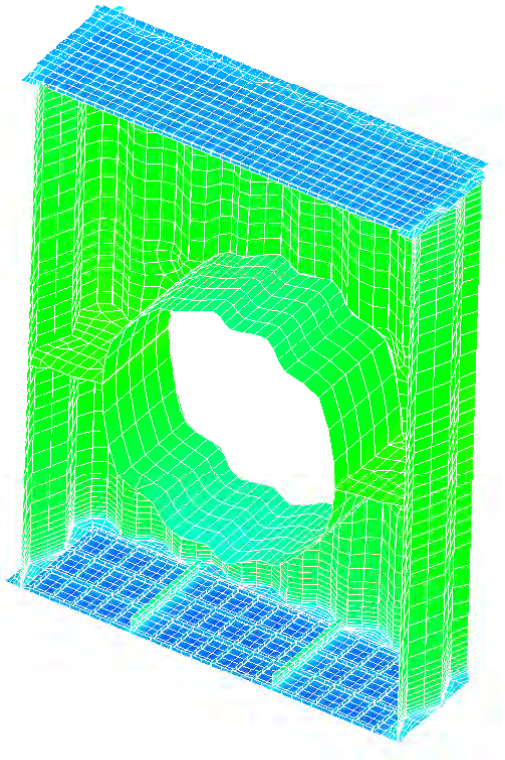

Approved for public release; distribution unlimited.

Panel 780 Temperature History

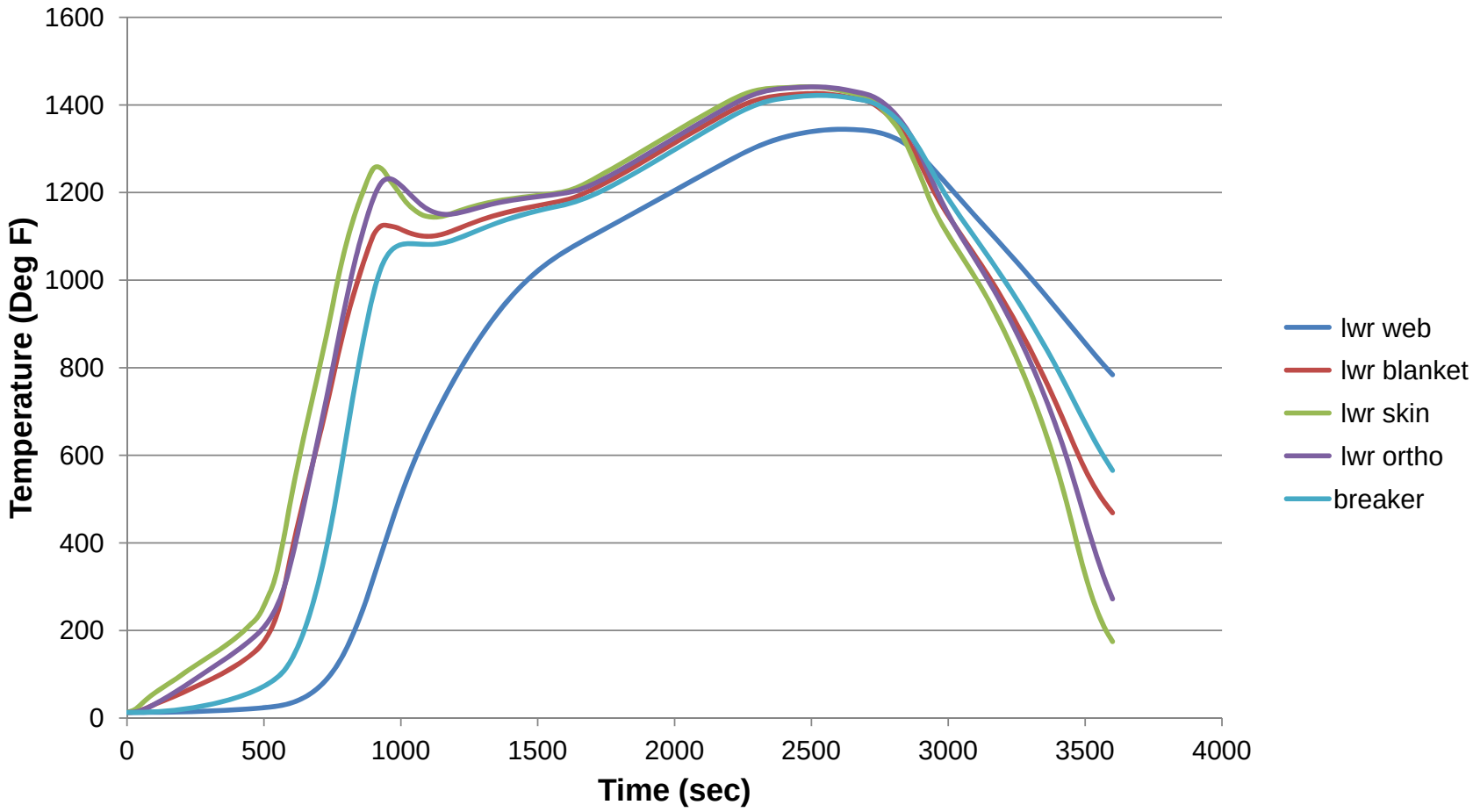

Approved for public release; distribution unlimited.

Panel 780 Temperature Gradient History

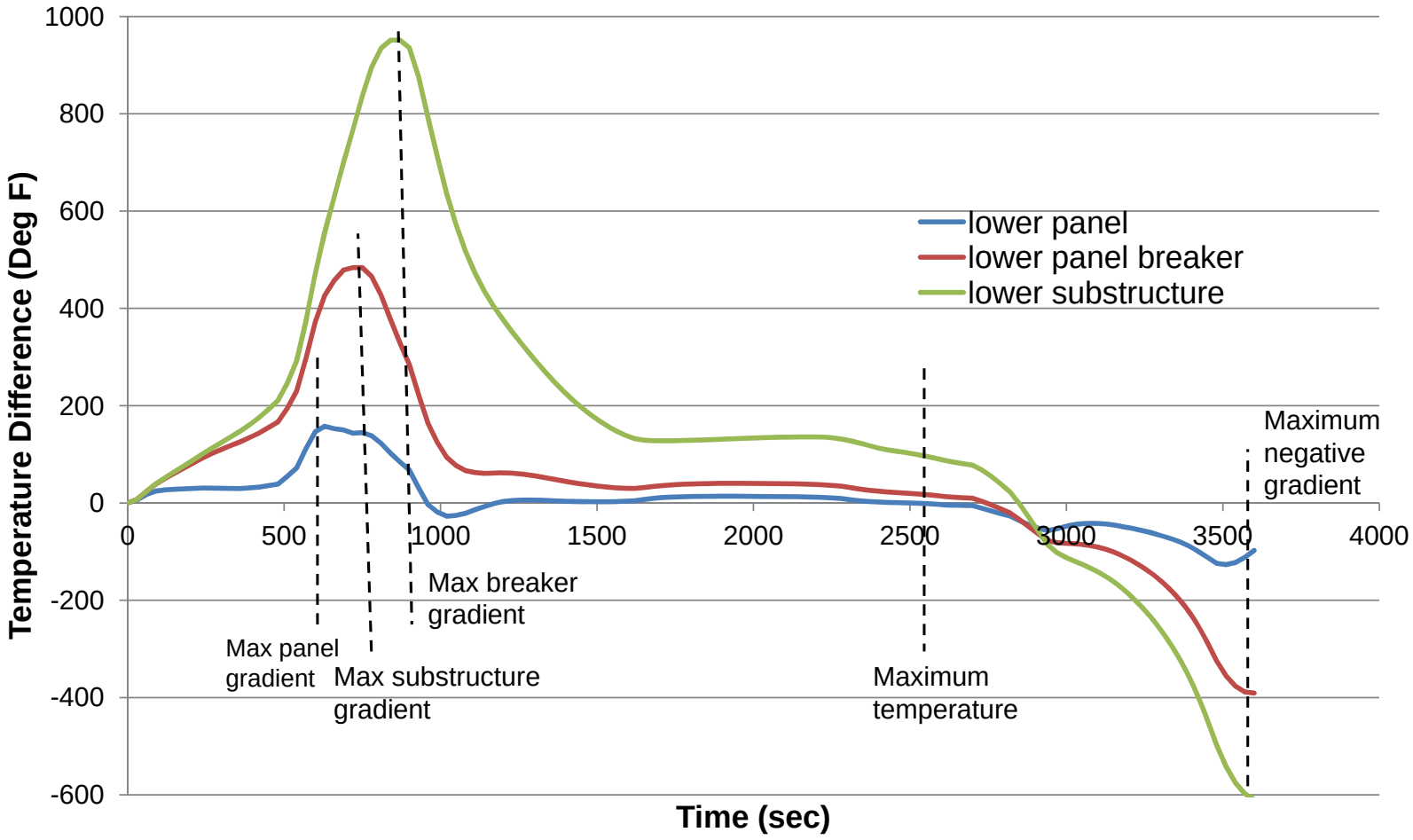

Approved for public release; distribution unlimited.

Summary of Results

- maximum skin temperatures = 1441 F at 2520 sec
- maximum temperature gradient in the isogrid = 158 F at 630 sec
- maximum temperature gradient between skin and breaker = 484 F at 720 sec
- maximum temperature gradient between skin and web = 951 F at 840 sec

Approved for public release; distribution unlimited.

Panel 2 (780) Static Stress Analysis

November 14, 2011

Rob Quiroz
Robert.Quiroz@boeing.com
714-916-2577
BR&T Structures Technology

Approved for public release; distribution unlimited.

Panel Analysis Study

Static Analysis of unit-cell: 2.5G ultimate (FS=1.5) + Temp @ 720 sec

1. Structure was imposed w/ rigid-body constraints; loads were balanced, i.e., zero reactions @ supports
2. Linear analysis revealed large corner deformations due to a large moment arm between the unit cell node boundaries and the load application point from the global FEM due to offset of frame web locations between vehicle and unit-cell models.
3. Nonlinear analysis solution only performed for the panel level analysis because the unit cell model utilizes honeycomb structure which is not representative of the orthrogrid skin of interest.

Static Analyses using center panel model on Lower surface (Panel 780) only

1. Applied displacement from linear unit-cell analysis as boundary conditions to center panel for 2.5G ultimate + Temp(720s). The same displacements are used as an approximation for nonlinear panel analysis
2. Linear analysis; good comparison with unit-cell model
3. Converged nonlinear analysis unveiled slightly larger out-of-plane deflection of panel and lower stress than the linear analysis

Approved for public release; distribution unlimited.

Constraints on Rigid Body Motion

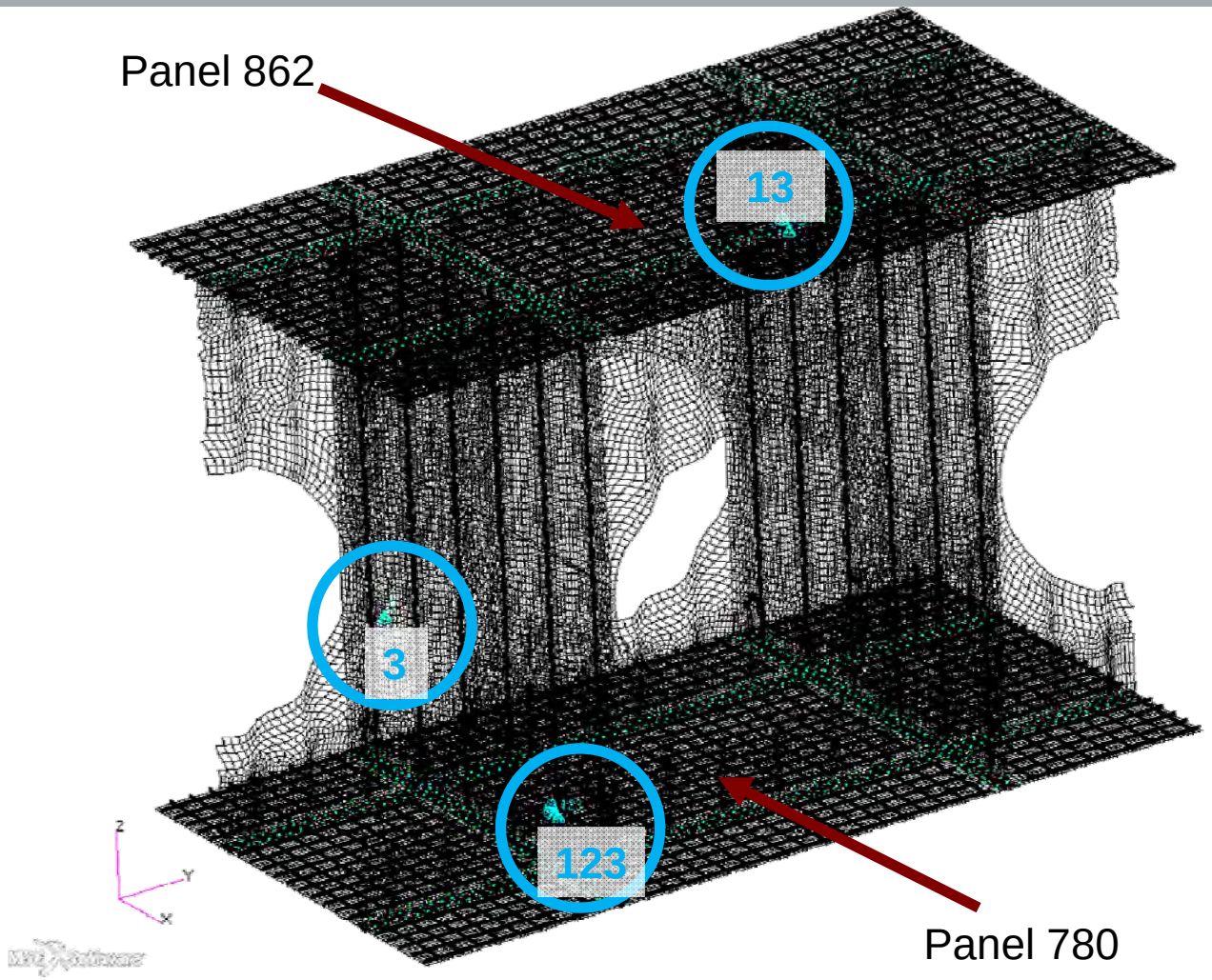

Rigid body motion constraints were applied to allow the model to deflect freely

Approved for public release; distribution unlimited.

Temperature Profile @ t =720s

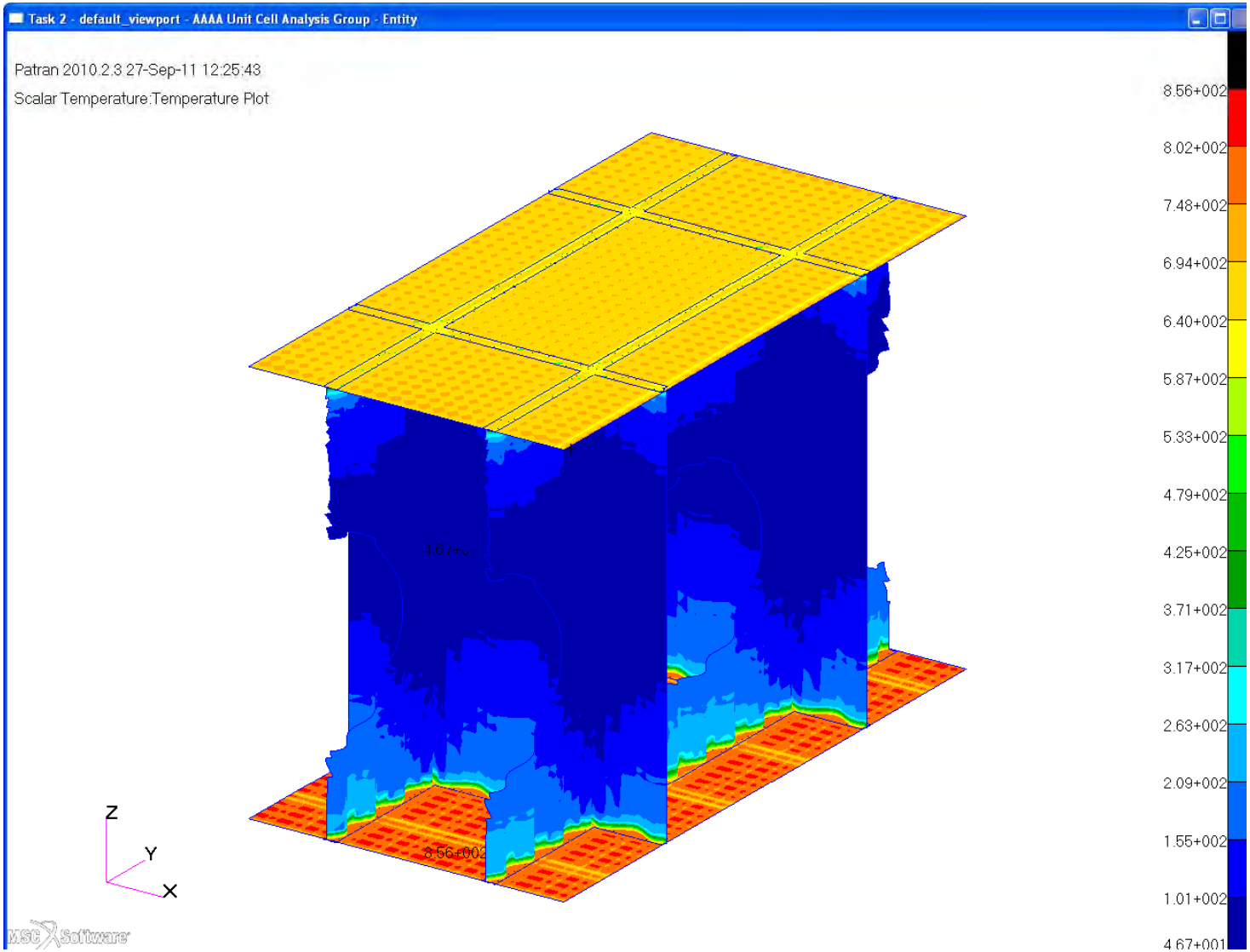

Approved for public release; distribution unlimited.

Inconel 718 Allowables @ 850º F

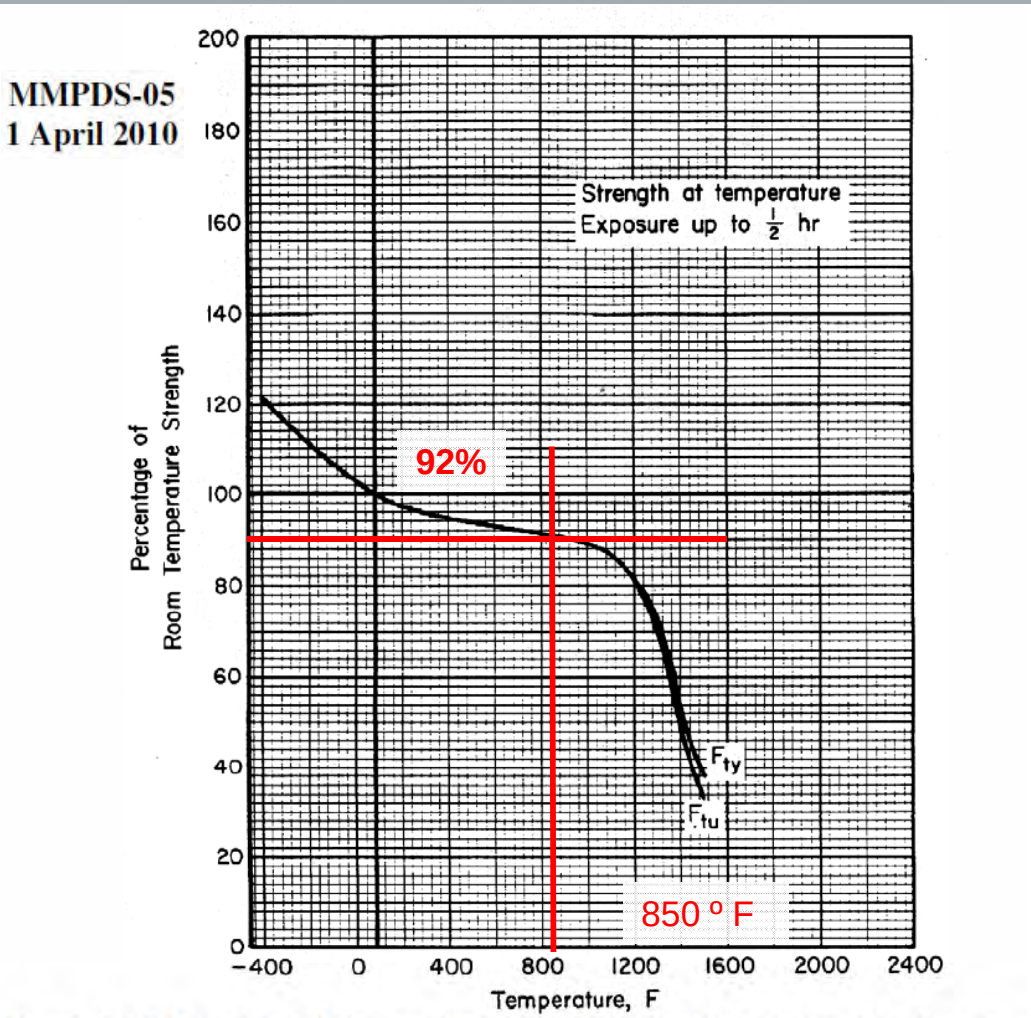

Figure 6.3.5.1.1. Effect of temperature on the tensile ultimate strength (F_{tu}) and tensile yield strength (F_{ty}) of solution-treated and aged Inconel 718.

Allowables @ 850º F	
F_{tu}	165.6 ksi
F_{bru}	284.28 ksi

Approved for public release; distribution unlimited.

Displacements, Unit Cell, 2.5g Ult 1.5, Linear

2.08” deflection at the unit cell corner Primarily due to moment arm created by load application point offset dictated by the global FEM and the compliant sine wave web structure.

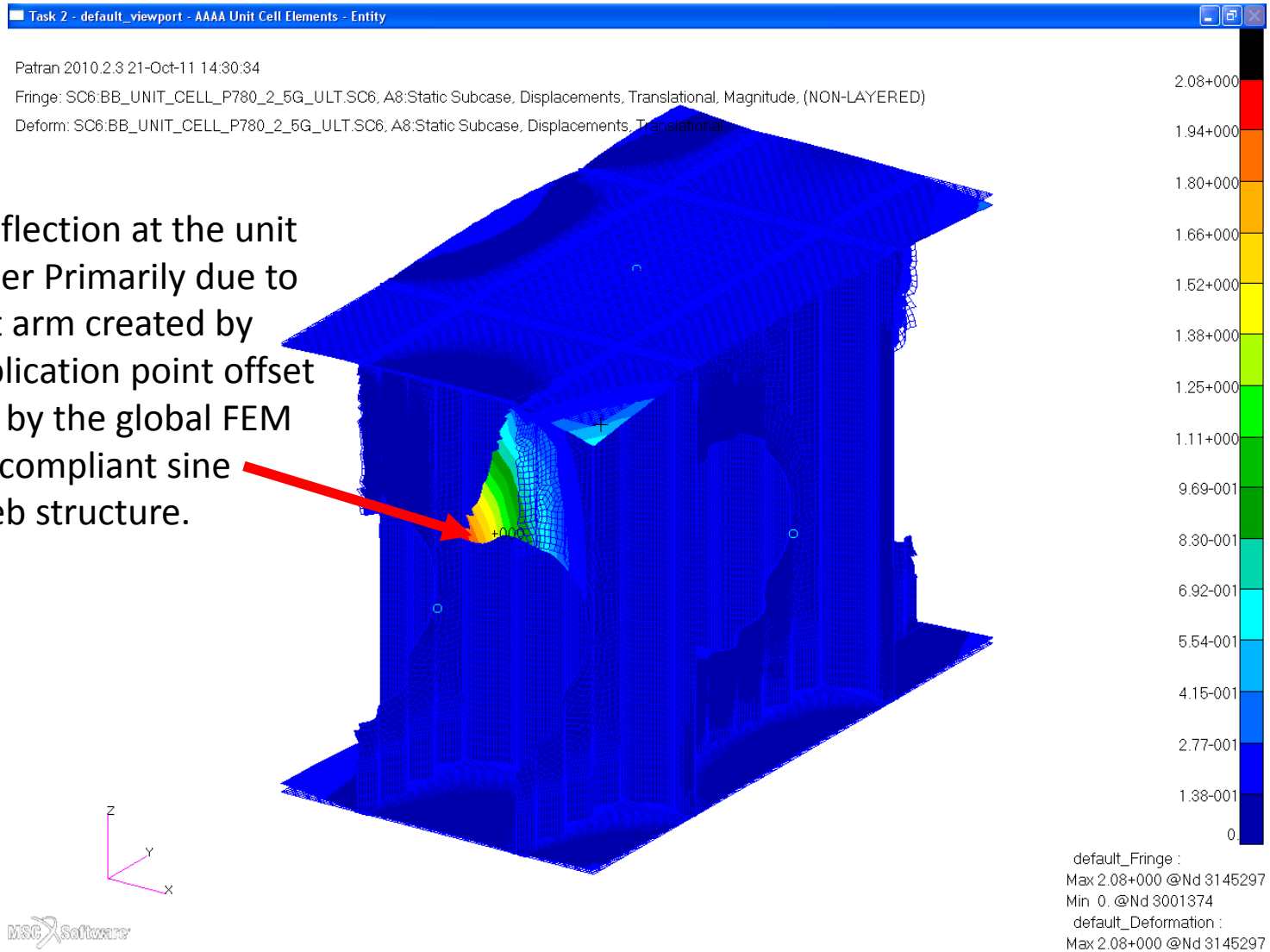

Approved for public release; distribution unlimited.

Von Mises, Unit Cell, 2.5g Ult 1.5, Linear

Stress peaking at roots of large displacements.

These concentrations may have minor effect to stresses in the center panel

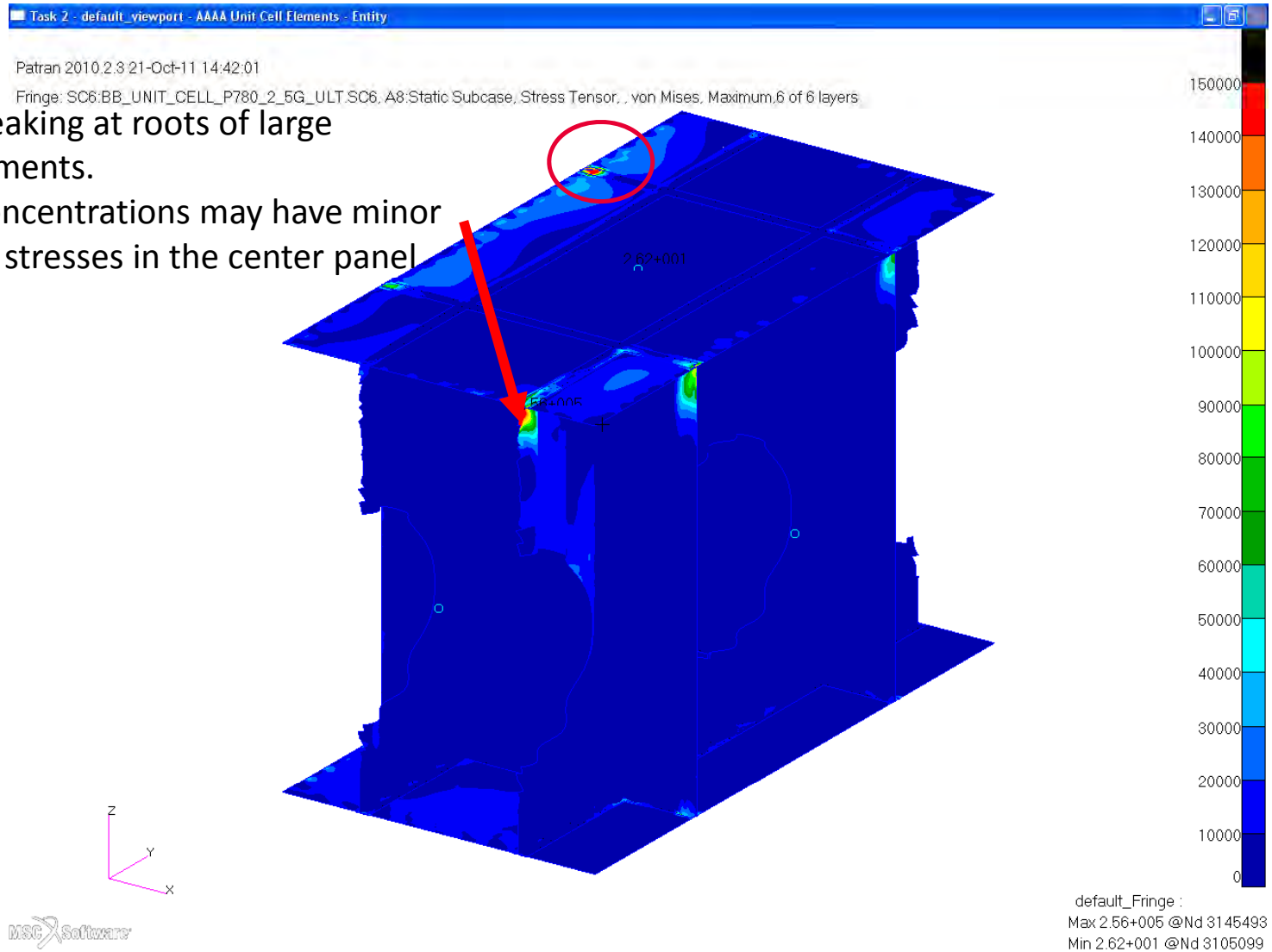

Approved for public release; distribution unlimited.

Von Mises, Panel, 2.5G Ult 1.5+T=720s Linear

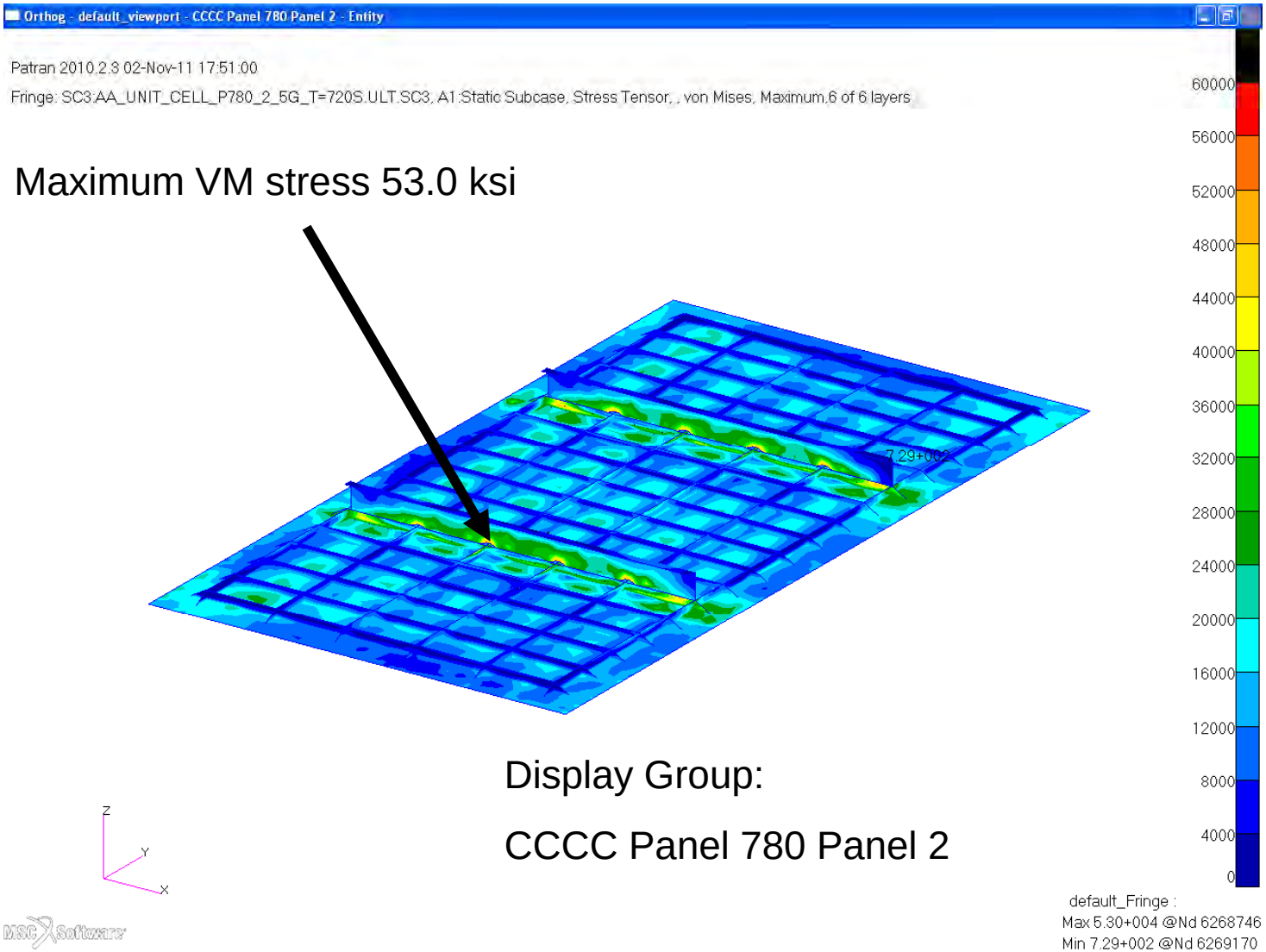

Maximum VM stress 53.0 ksi

Display Group:

CCCC Panel 780 Panel 2

Approved for public release; distribution unlimited.

Von Mises, Panel, 2.5G Ult 1.5+T=720s Linear

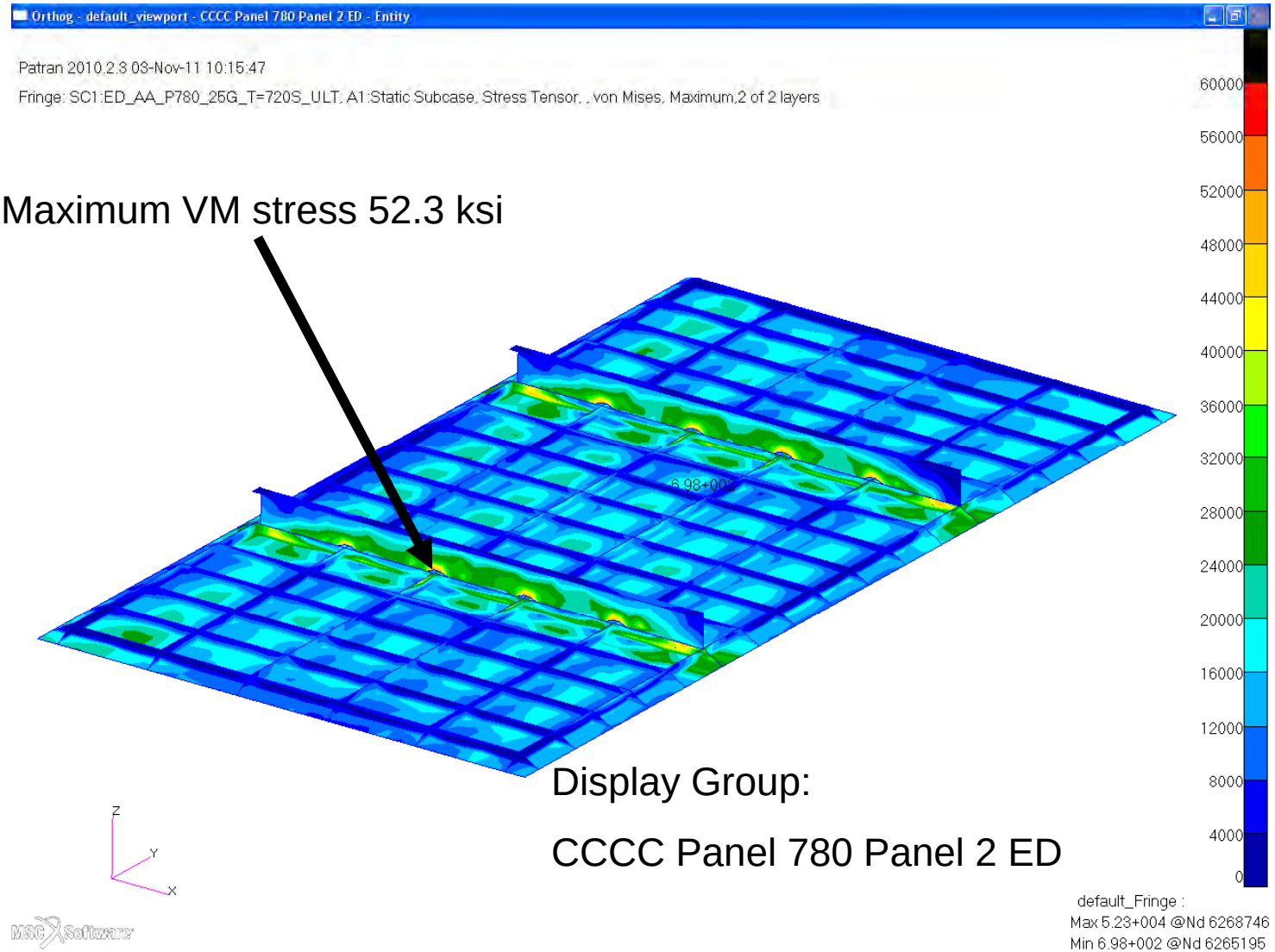

Approved for public release; distribution unlimited.

Von Mises, Panel, 2.5G Ult 1.5+T=720s Non-Linear

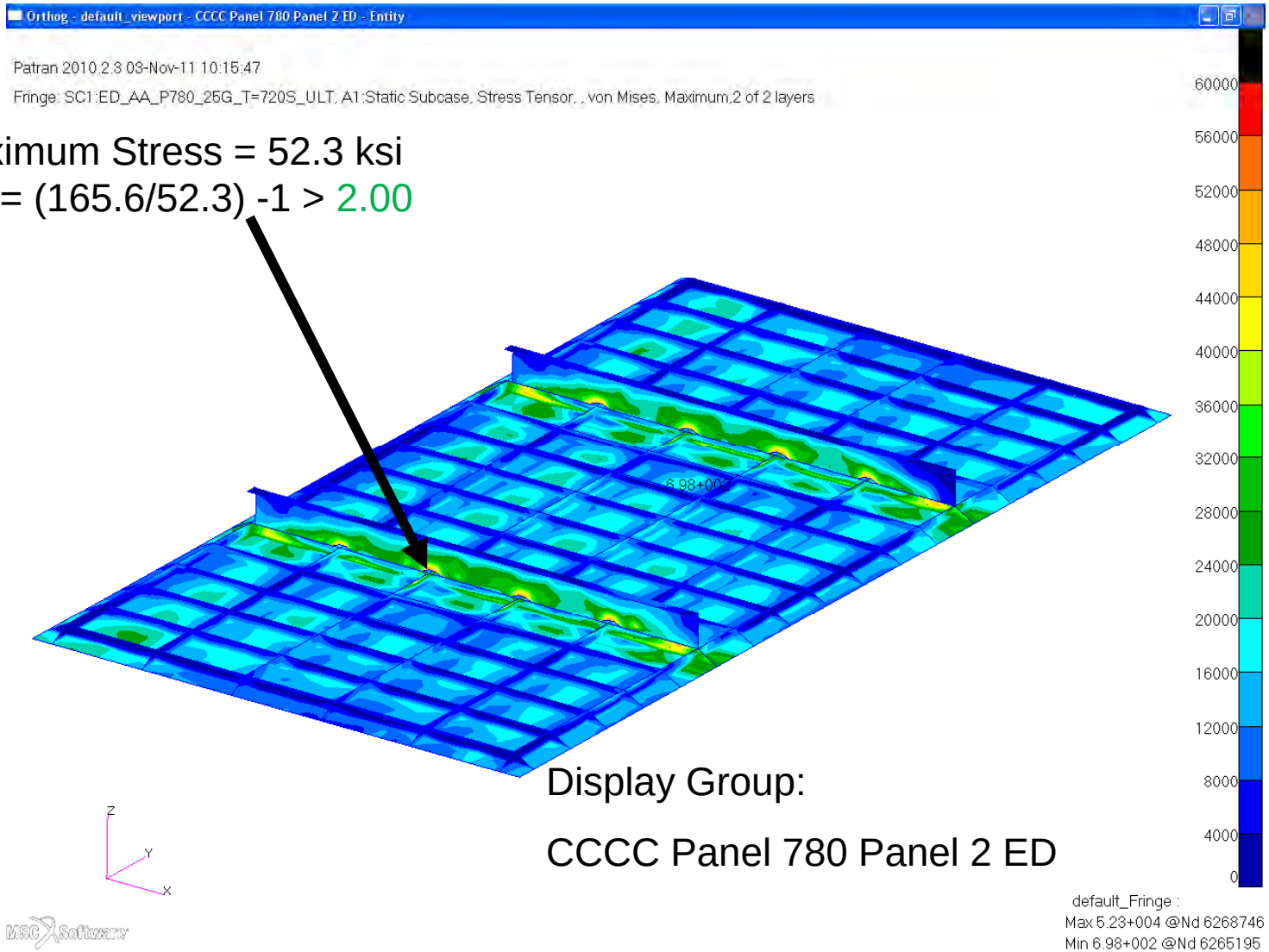

Maximum Stress = 52.3 ksi

MS = (165.6/52.3) -1 > 2.00

Display Group:

CCCC Panel 780 Panel 2 ED

Approved for public release; distribution unlimited.

Displacements, Unit Cell, 2.5G Lim 1.15+T=720s Linear

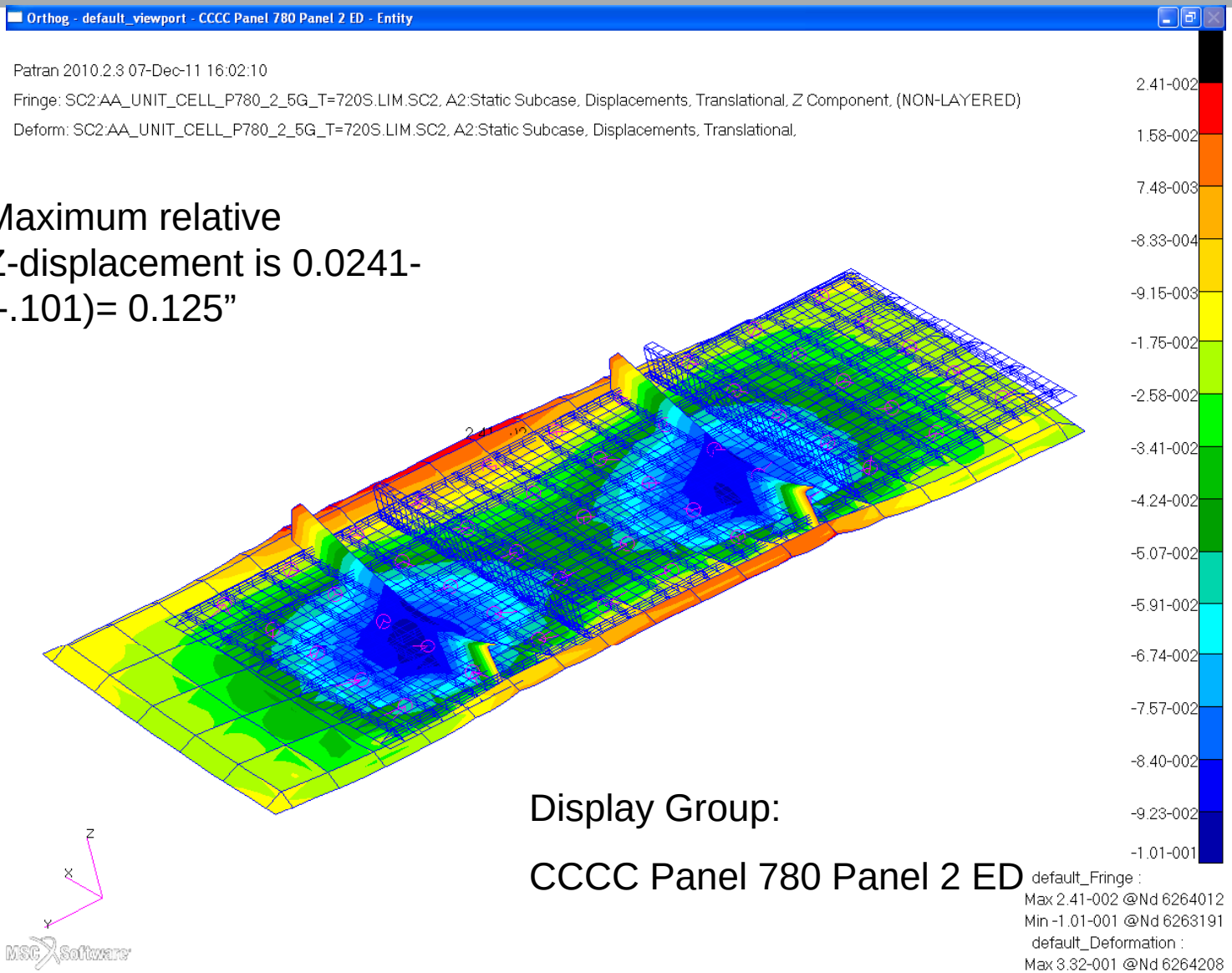

Maximum relative Z-displacement is 0.0241-(-.101)= 0.125”

Display Group:

CCCC Panel 780 Panel 2 ED

Approved for public release; distribution unlimited.

Displacements, Panel, 2.5G Lim 1.15+T=720s Linear

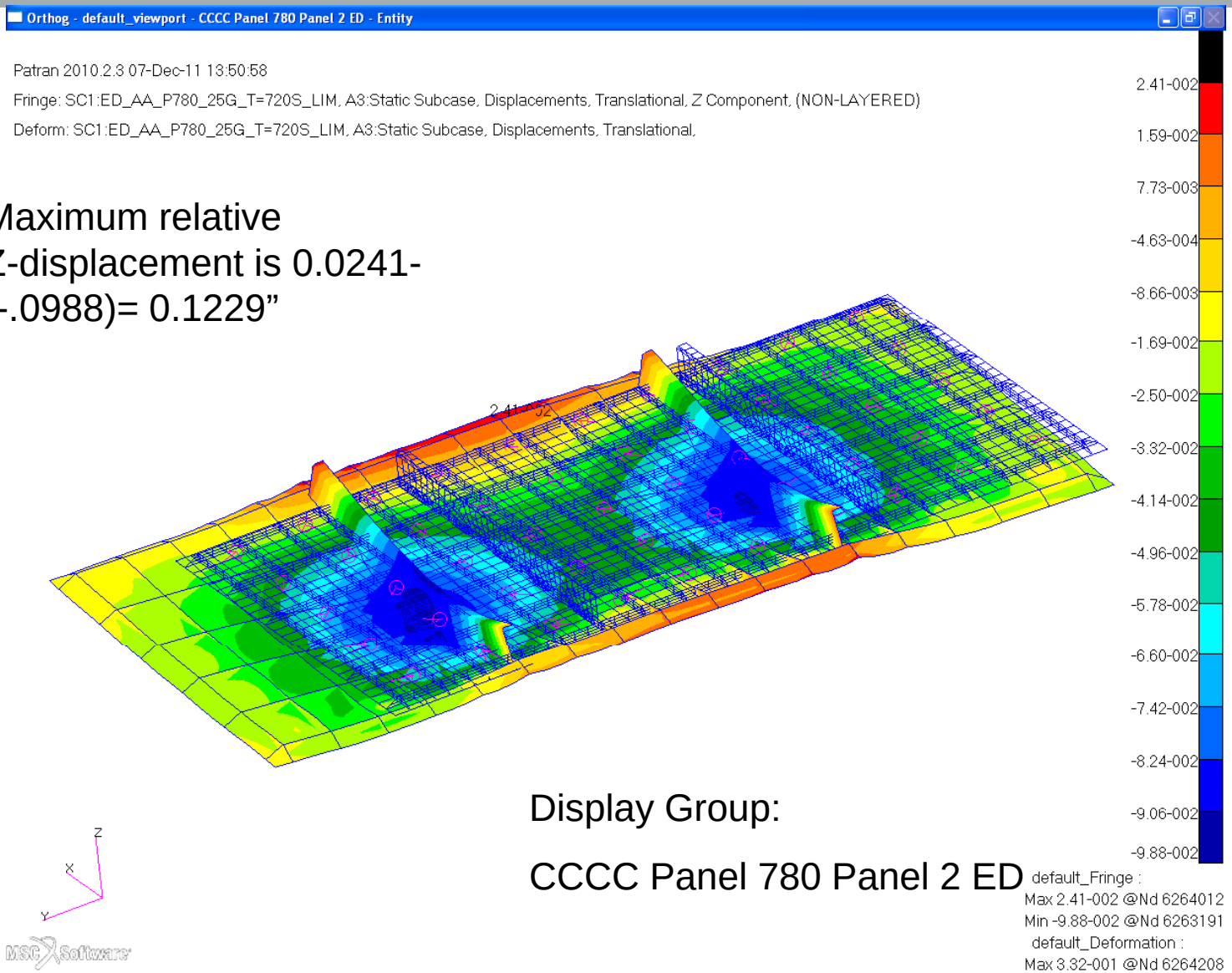

Maximum relative Z-displacement is 0.0241-(-.0988)= 0.1229”

Display Group:

CCCC Panel 780 Panel 2 ED

Approved for public release; distribution unlimited.

Displacements, Panel, 2.5G Lim 1.15+T=720s Non-Linear

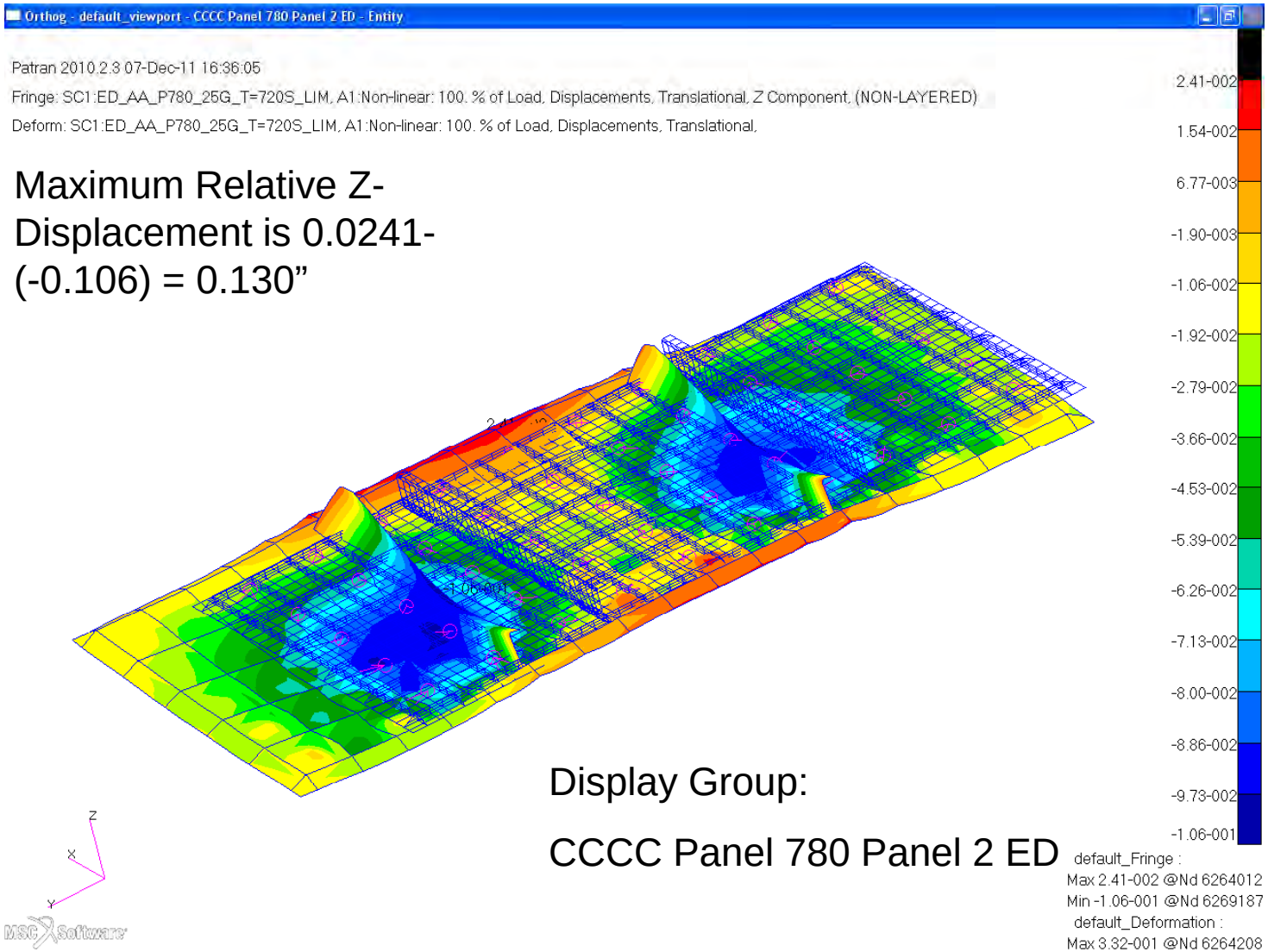

Maximum Relative Z-Displacement is 0.0241-(-0.106) = 0.130”

Display Group:

CCCC Panel 780 Panel 2 ED

Approved for public release; distribution unlimited.

Displacements, Panel, 2.5G Lim 1.15+T=720s Non-Linear, Flow-wise Direction

Maximum Relative Z-Displacement
= 0.0202-(-0.104) = 0.124”
Margin of Safety = 1/0.124-1 = -0.19
*There is a 15% margin for Limit
*The 0.1” max deflection requirement may be relaxed

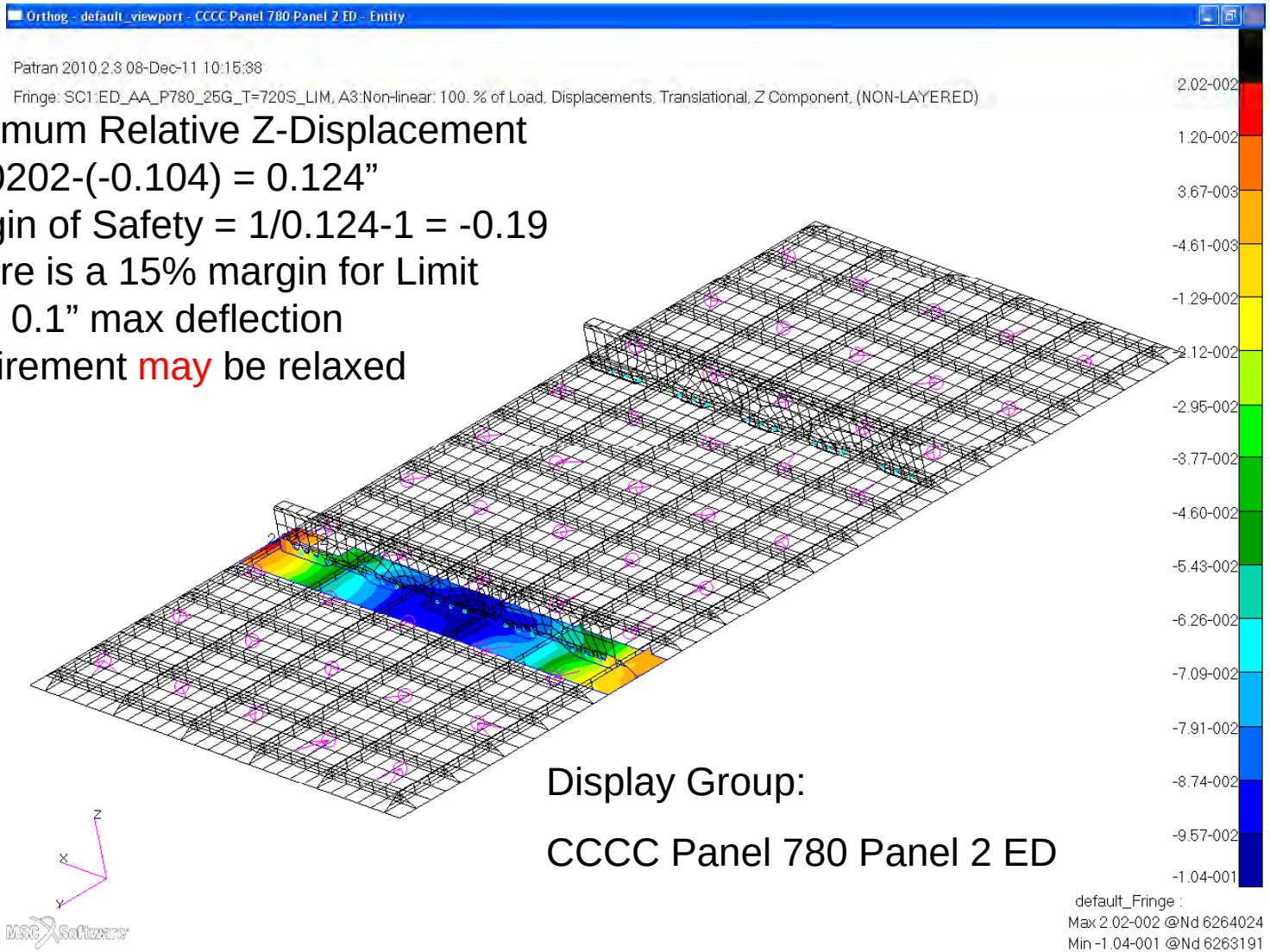

Display Group:

CCCC Panel 780 Panel 2 ED

Approved for public release; distribution unlimited.

Buckling Mode 1, Panel, 2.5G Lim 1.15+T=720s

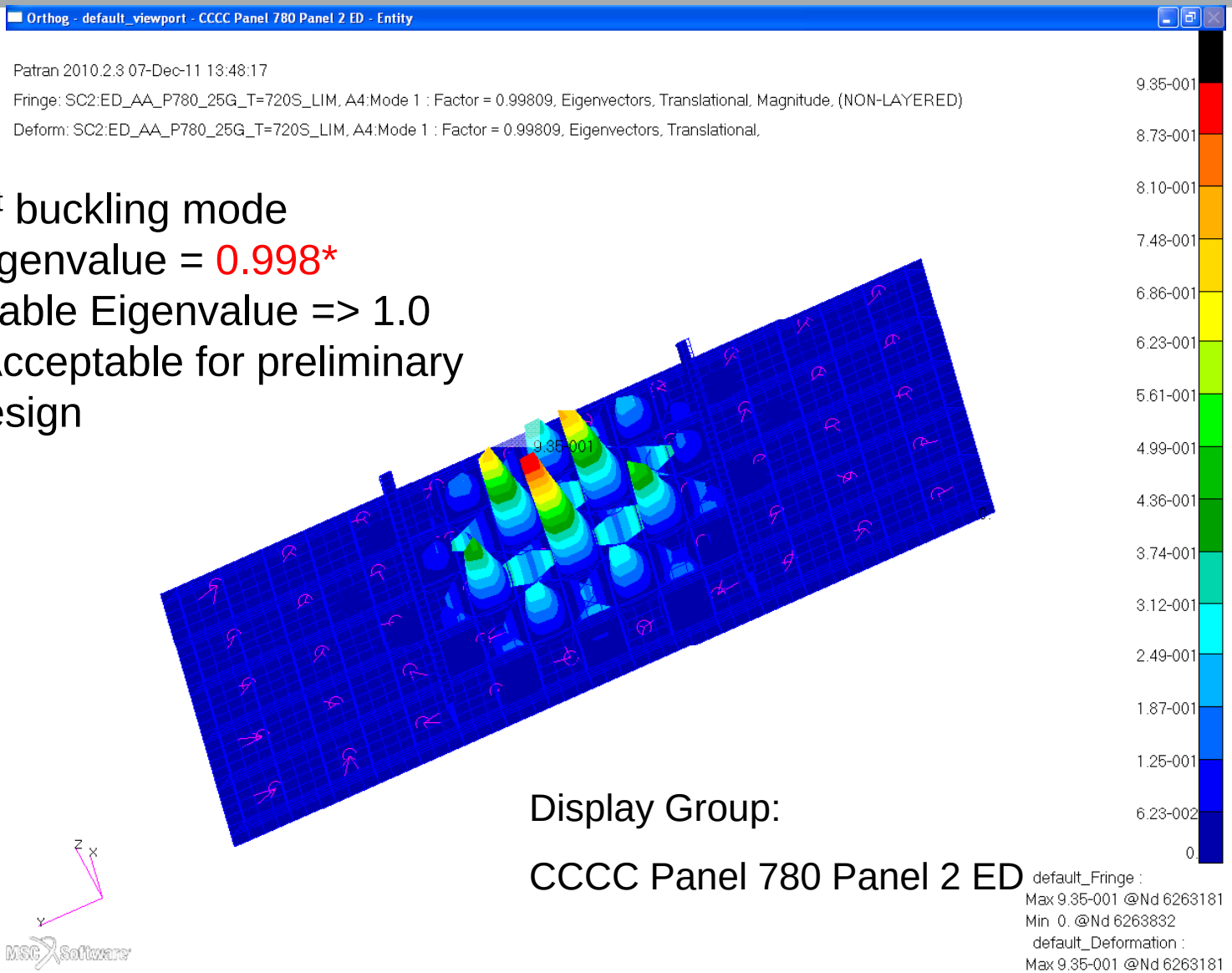

1st buckling mode
Eigenvalue = 0.998*
Stable Eigenvalue => 1.0
*Acceptable for preliminary design

Display Group:

CCCC Panel 780 Panel 2 ED

Approved for public release; distribution unlimited.

Buckling Mode 2, Panel, 2.5G Lim 1.15+T=720s

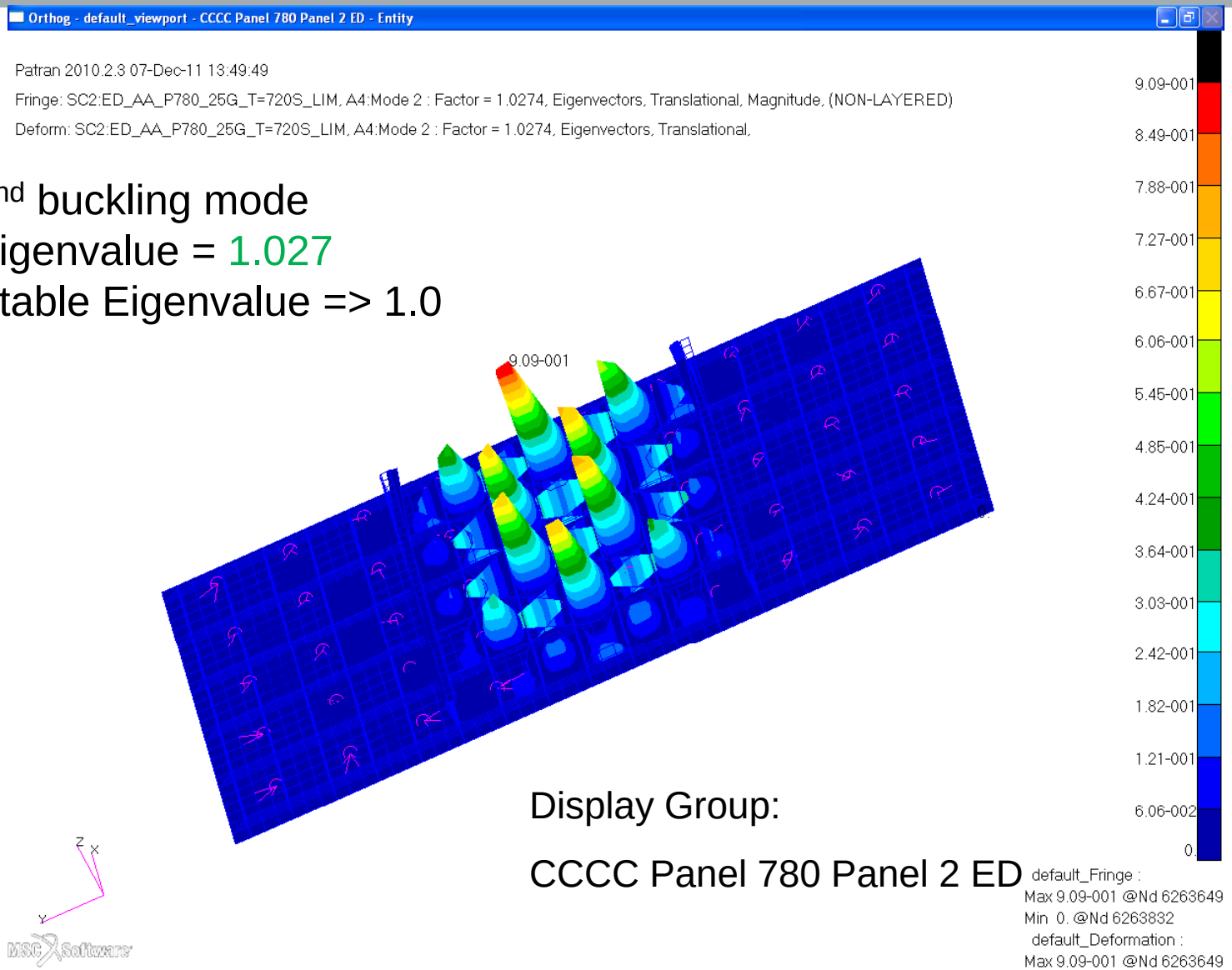

2nd buckling mode

Eigenvalue = 1.027

Stable Eigenvalue => 1.0

Display Group:

CCCC Panel 780 Panel 2 ED

Approved for public release; distribution unlimited.

Fastener Bearing, Panel, 2.5G Ult 1.5+T=720s

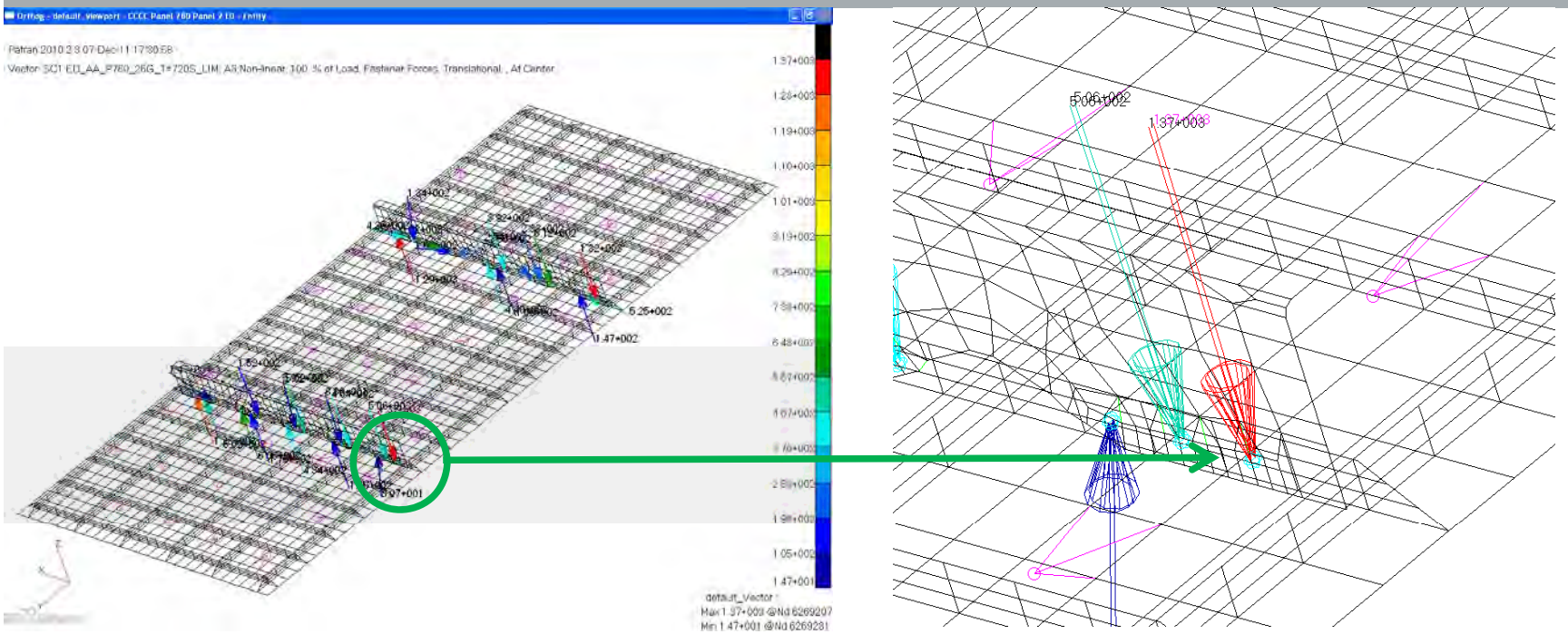

Maximum Fastener Load = 1370 lbs

σ_{brg} = P/(d*t) = 1370 / (0.19*.07) = 103 ksi

MS = (278/103)-1 =1.69

Approved for public release; distribution unlimited.

Summary

Failure Mode	Solution Type	Thermal Load	Thermal FoS	Mechanical Load	Mechanical FoS	Allowable	Actual	Units	Margin of Safety or Ratio to Requirement
Ultimate Material Failure	Non-Linear	t=720s	1	2.5g	1.5	165.6	52.3	Ksi	2.17
Displacement	Non-Linear	t=720s	1	2.5g	1.15	0.1	0.124	inches	-0.19
Buckling	Buckling	t=720s	1	2.5g	1.15	1	0.998	eigenvalue	1.00
Bearing	Non-Linear	t=720s	1	2.5g	1.5	284.28	103	Ksi	1.76

- High positive stress margins
- Small negative margins for Buckling, acceptable for this stage of design
- Displacements Allowable to be refined, predicted values may be acceptable

Approved for public release; distribution unlimited.

PATRAN Database and NASTRAN Analysis Files

Approved for public release; distribution unlimited.

Location of files

Contact AFRL/RBSM Structural Sciences Center
WPAFB, OH, 45433

POC: Dr. S. Michael Spottswood, 937.904.6789, stephen.spottswood@wpafb.af.mil

PATRAN Database for Unit-Cell and Panel Models

Orthogrid Panel 2.db

Flight Loads

Mach 7, +2.5g, symmetric pull up maneuver

Thermal

Temperature @
T = 660 sec, Maximum thermal gradient between panel skin and orthogrid stiffener
T = 720 sec, Maximum thermal gradient between panel skin and panel breaker stiffener
T = 840 sec, Maximum thermal gradient between panel and substructure
T = 2520 sec, Maximum temperature
T = 3600 sec, Maximum reverse thermal gradient

Boundary Conditions for Unit-Cell Model

Rigid Body Constraints

Approved for public release; distribution unlimited.

Linear Stress Analysis of Unit-Cell Model for 2.5G and Thermal (T=720 sec)

Load Cases

AA_Unit_Cell_P780_2_5G_T=720s
2.5g loading * 1.0 (F.S.), Temp @ 720s, Rigid body constraints

AA_Unit_Cell_P780_2_5G_T=720s.LIM
2.5g loading * 1.15 (F.S.), Temp @ 720s, Rigid body constraints

AA_Unit_Cell_P780_2_5G_T=720s.Ult
2.5g loading * 1.5 (F.S.), Temp @ 720s, Rigid body constraints

Analysis Files

Panel_2_2_5g_T720s.dat – Nastran Control Deck
Panel 2 Nodes Elements.bdf – Nastran elements and nodes
Panel 2 RBEs.bdf – Nastran RBE's
Panel 2 SPCs.bdf – Nastran constraints
Panel 2 Forces.bdf – Nastran Force Cards
Panel 2 Temps.bdf – Nastran Nodal Temperatures
Panel 2 Coordinate Frames.bdf – Nastran Coordinate frames

Results

Panel_2_2_5g_t720s.xdb

Approved for public release; distribution unlimited.

Linear Stress Analysis of Unit-Cell Model for 2.5G only

Load Cases

BB_Unit_Cell P780_2_5G
2.5g loading * 1.0 (F.S.), Rigid body constraints

BB_Unit_Cell P780_2_5G_Lim
2.5g loading * 1.15 (F.S.), Rigid body constraints

BB_Unit_Cell P780_2_5G_Ult
2.5g loading * 1.5 (F.S.), Rigid body constraints

Analysis Files

Panel_2_2_5g.dat - Nastran Control Deck

Results

Panel_2_2_5g.xdb

313
Approved for public release; distribution unlimited.

Linear Stress Analysis of Unit-Cell Model for Thermal only

Load Cases

CC_TEMP_660S
Temp @ 660s, Rigid body constraints
CC_TEMP_720S
Temp @ 720s, Rigid body constraints
CC_TEMP_840S
Temp @ 840s, Rigid body constraints
CC_TEMP_2520S
Temp @ 2520s, Rigid body constraints
CC_TEMP_3600S
Temp @ 3600s, Rigid body constraints

Analysis Files

Panel_2_T660s.dat
Panel_2_T840s.dat
Panel_2_T720s.dat
Panel_2_T2520s.dat
Panel_2_T3600s.dat

Results

Panel_2_T660s.xdb
Panel_2_T840s.xdb
Panel_2_T720s.xdb
Panel_2_T2520s.xdb
Panel_2_T3600s.xdb

Approved for public release; distribution unlimited.

Linear Stress Analysis of Panel Model

Flight Loads
Mach 7, +2.5g, symmetric pull up maneuver

Thermal
Temperature @
T = 720 sec, Maximum thermal gradient between panel and panel breaker stiffener

Load Case
For 2.5g loading *1.5 (F.S.), Temp @ 720s

Boundary Conditions for Panel Model
Enforced displacements from unit-cell analysis for 2.5G flight (FS=1.5) + thermal (T=720 sec)

Analysis Files
Panel_P780_2_5g_T720s_ED_101.bdf

Results
Panel_P780_2_5g_T720s_ED_101.xdb

315
Approved for public release; distribution unlimited.

Buckling Analysis of Panel Model

Flight Loads
Mach 7, +2.5g, symmetric pull up maneuver

Thermal
Temperature @
T = 720 sec, Maximum thermal gradient between panel and panel breaker stiffener

Load Case
For 2.5g loading *1.15 (F.S.), Temp @ 720s

Boundary Conditions for Panel Model
Enforced displacements from unit-cell analysis for 2.5G flight (FS=1.15) + thermal (T=720 sec)

Analysis Runs
Panel_P780_2_5g_T720s_ED_105.bdf

Results
Panel_P780_2_5g_T720s_ED_105.xdb

Approved for public release; distribution unlimited.

Linear Stress Analysis of Panel Model

Flight Loads
Mach 7, +2.5g, symmetric pull up maneuver

Thermal
Temperature @
T = 720 sec, Maximum thermal gradient between panel and substructure

Load Case
2.5g loading *1.5 (F.S.), Temp @ 720s

Boundary Conditions for Panel Model
Enforced displacements from unit-cell analysis for 2.5G flight (FS=1.5) + thermal (T=720 sec)

Analysis Runs
Panel_P780_2_5g_T720s_ED_106.bdf

Results
Panel_P780_2_5g_T720s_ED_106.xdb

Approved for public release; distribution unlimited.

Groups in PATRAN Database

AAAA Unit Cell Analysis Group
    Elements, Nodes, and MPC's required to analyze the Unit Cell
AAAA Unit Cell Elements and Nodes
    Elements, Nodes, and no MPC's for Unit Cell
AAAA Unit Cell MPCs
    MPC's for Unit Cell
BBBB Caps
    Sinewave Keel and Frame Caps
BBBB Freebody Nodes
    Nodes for Applying Freebody Loads from Vehicle FEM
BBBB Panel Breaker Stiff CFAST
    Connectors for the Panel Breaker Stiffener
BBBB Panel Breaker Stiffeners
    Panel Breaker Stiffeners
BBBB Skin Lands
    Skin Elements which overlap the Keel and Frame Caps
BBBB Stiffeners
    Panel Stiffeners
BBBB Substructure Web
    Sinewave Keel and Frame Webs
CCCC Panel 780 Panel 2
    FEM for Panel 780 (Panel 2 on windward surface)
CCCC Panel 780 Panel 2 ED
    FEM for Panel 780 used for enforced displacement panel level analysis
CCCC Panel 862
    FEM for Panel 780 (Panel 1 on leward surface)
FEM Connectors
    CFASTs

Approved for public release; distribution unlimited.

Panel 2 (780) Dynamic & Fatigue Analysis

January 5, 2012

Craig Masterson
314-232-9424
Craig.Masterson@boeing.com

Approved for public release; distribution unlimited.

Panel 2 Dynamic Solution Corrections

- **It was discovered on 21 December that the incorrect density for Inconel 718 was used in the previous Panel 2 dynamic analyses**
- **The density for the results presented have been updated to the correct value of 0.297lb/in^3, from 0.3386 lb/in^3**
- **The structural damping table was also updated to be consistent with panel 1 dynamic analysis:**
  - Damping changes increase RMS stress results from SOL 111 by approximately 5%. Margins for acoustic fatigue remain adequate

WAS

```
$
TABDMP1  1        CRIT
         10.     .025     200.     .02       1000.    .01      ENDT
$
```

IS

```
$
TABDMP1  1        CRIT
         10.     .025     100.     .02       1000.    .01      ENDT
$
```


Approved for public release; distribution unlimited.

Panel 780 Dynamic Analysis

- Methods and Approach
- Analysis Assumptions
- Finite Element Model and Boundary Conditions
- Results
  - Modal
  - Response
  - Fatigue
- Lessons Learned
- Summary
- Current /Future Activities

321
Approved for public release; distribution unlimited.

Methods & Approach

Tool / Method

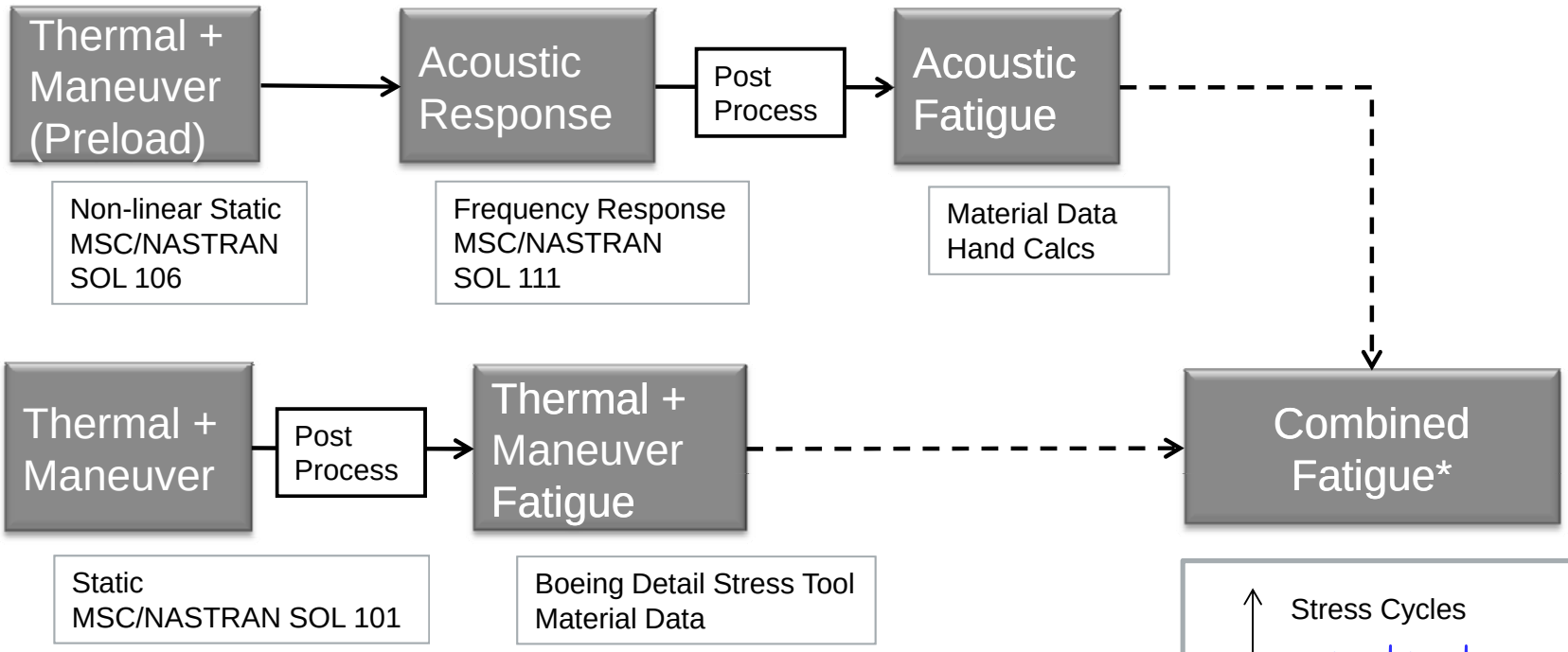

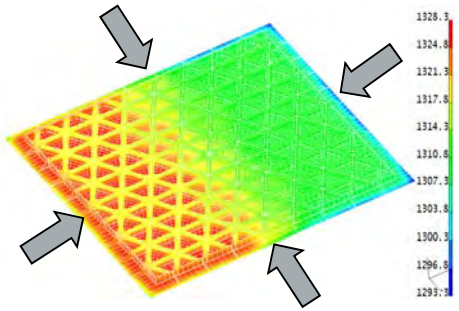

- Check fatigue at stress critical locations and Determine Flights to Failure
- Apply thermal knockdowns to fatigue S-N data
- Build combined spectrum and perform fatigue analysis

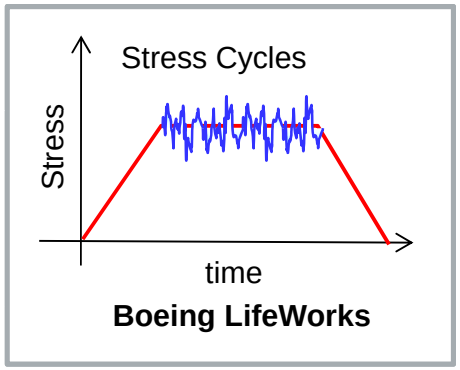

*Combined fatigue analysis not performed for panel 780

Approved for public release; distribution unlimited.

Fatigue Analysis Approach

- **Use Mil-hd-bk 5 Inconel 718 constant amplitude data**
- **Adjust for temperature and stress ratio if applicable**
- **Calculate design feature $k_t\sigma$ – holes, welds, radii**
- **Post-process results – references stress value**
- **Calculate Acoustic Margins – Compare predicted RMS Stress (KtS) to RMS Allowable (Endurance Limit)**
- **Assembly stress spectrum – Include maneuver loads, temperature for ground-air-ground (GAG) Cycles**
- **Calculate thermal-mechanical fatigue margins**
- **Perform acoustic damage (Dynamic Cycles) separate***
- **Calculate Total Fatigue Life – Combined Damage***

*A total fatigue life based on combined damage accumulation was not calculated for this panel
Margin of safety calculations will show panel is dominated by thermal-mechanical cyclic fatigue

Approved for public release; distribution unlimited.

General Fatigue Analysis Assumptions

- **A combined total fatigue life based on accumulated damage from aero-acoustic loads and cyclic thermal-mechanical fatigue was not performed for this panel (fatigue life dominated by thermal-mechanical stress)**
- **Thermal exposure effect on Fty is proportional to temperature effect on fatigue allowable**
- **Boundary conditions are dependent on the type of analysis being performed**
  - Linear and non-linear static solutions: 3 nodes are pinned to constrain rigid body motion
  - Modal and frequency response solutions: symmetry boundary condition imposed along unit cell interface nodes to simulate support from surrounding bays

Approved for public release; distribution unlimited.

Analysis Summary Table

- **Unit cell FEM used for all analyses**

Analysis Type	Preload	Load	Boundary Conditions	Output	Solution File(s)
Linear Static (SOL 101)	None	Mechanical (2.5G) Thermal (All times)	RBM Constraint at 3 nodes	> Stress for thermal-mechanical loads fatigue analysis	panel_2_2_5g_all_temps.xdb
Normal Modes (SOL 103)	None	Thermal (t=720s) Material Property Only	Symmetry along unit cell boundary	> Normal Modes and Mode Shapes > Provides frequency range of interest for SOL 111	sol103_unitcell_t720s_111222-02-symm.xdb
Non-linear Static (SOL 106)	None	Thermal (t=720s) Material + Load	RBM Constraint at 3 nodes	> Non linear stress and displacement > Preload for SOL111 > Stress results used as mean stress in fatigue calculations	panel2_sol106_1203-01.xdb
Frequency Response (SOL 111)	SOL 106	Thermal (t = 720s) Material Property Only	Symmetry along unit cell boundary	> RMS stress	panel2_sol111_1222-02_symm.xdb

Approved for public release; distribution unlimited.

Unit Cell Boundary Conditions

Static Solution Boundary Conditions

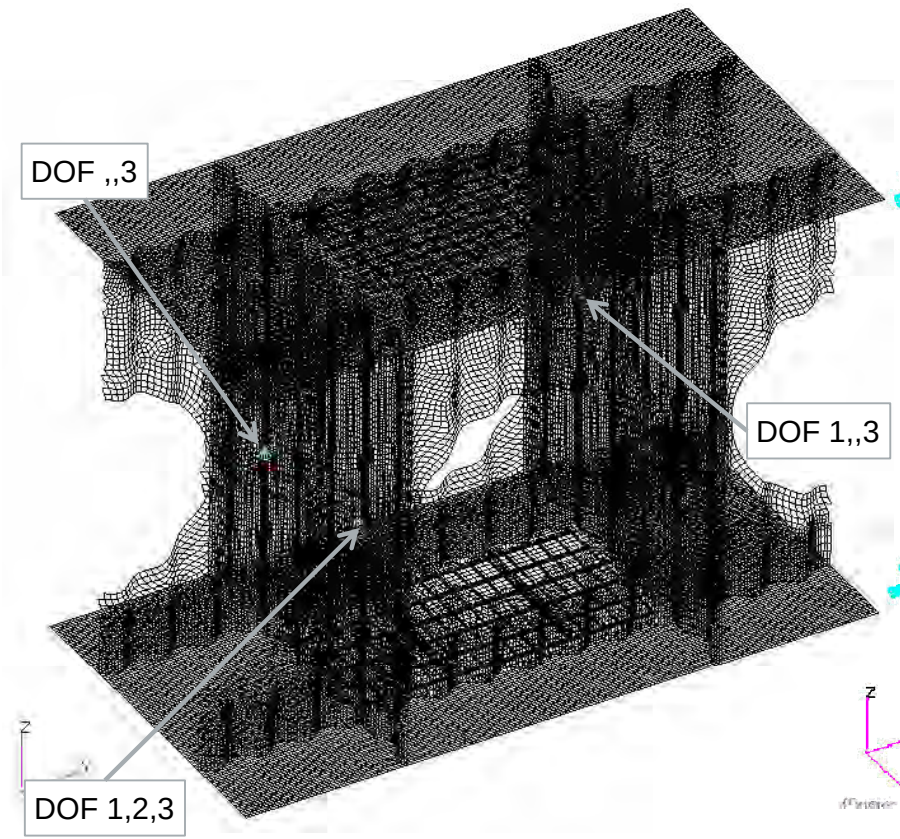

Constrained at 3 nodes on keel webs to prevent rigid body motion

Frequency Domain Boundary Conditions

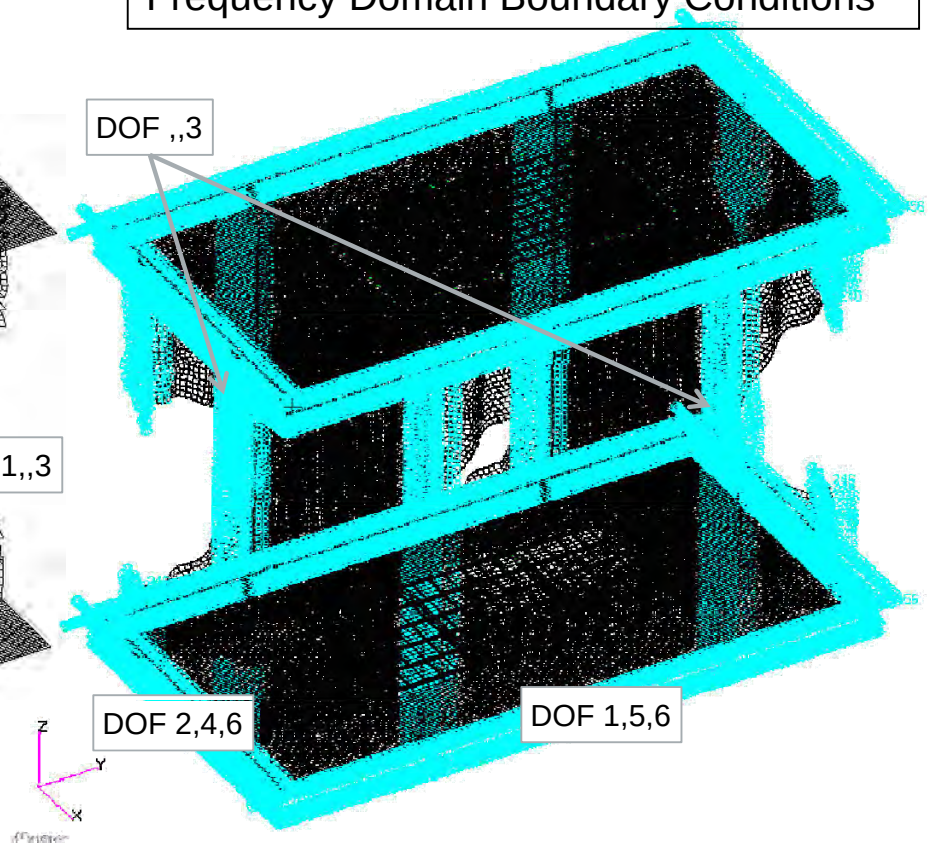

Symmetry boundary condition used to simulate support from surrounding panels to minimize substructure modes

Z-dir SPC applied to nodes 3005532 3012172

Approved for public release; distribution unlimited.

SOL 103 Documentation

- **Preload**
  - None
- **Material Properties**
  - Inconel properties at mapped temperatures for t=720s thermal load
  - Remove mass from all structure excluding panel 780
- **Boundary Conditions**
  - Symmetry Applied to Edges
  - Z-dir SPC applied to nodes 3005532 3012172
- **SOL 103**
  - Group: AAAA Unit Cell Elements (No MPCs)
  - Input File: SOL103_UnitCell_T720s_111222-02-Symm.bdf
  - Results File: SOL103_UnitCell_T720s_111222-02-Symm.xdb

```
$ Normal Modes Analysis, Database
SOL 103
CEND
$ Direct Text Input for Global Case Control Data
TITLE = MSC.NASTRAN JOB CREATED ON
ECHO = NONE
RESVEC = YES
SUBCASE 1
$ Subcase name : CC_TEMP_720S.SC8
   SUBTITLE=CC_TEMP_720S.SC8
   METHOD = 1
   SPC = 2
   TEMPERATURE(MATERIAL) = 124
   VECTOR(SORT1,REAL)=ALL
   SPCFORCES(SORT1,REAL)=ALL
BEGIN BULK
$ Direct Text Input for Bulk Data
PARAM    POST    0
PARAM    WTMASS .0026
PARAM   PRTMAXIM YES
EIGRL    1                       10      0
$Damping Table
TABDMP1  1       CRIT
         10.    .025    100.    .02      1000.
.01     ENDT
$
```

Excerpt of SOL 103 Nastran Deck

Approved for public release; distribution unlimited.

SOL 103 Results

Patran 2010.2.3 (MD Enabled) 05-Jan-12 13:05:26
Fringe: SC1:CC_TEMP_720S.SC8, A7:Mode 1 : Freq. = 88.121, Eigenvectors,

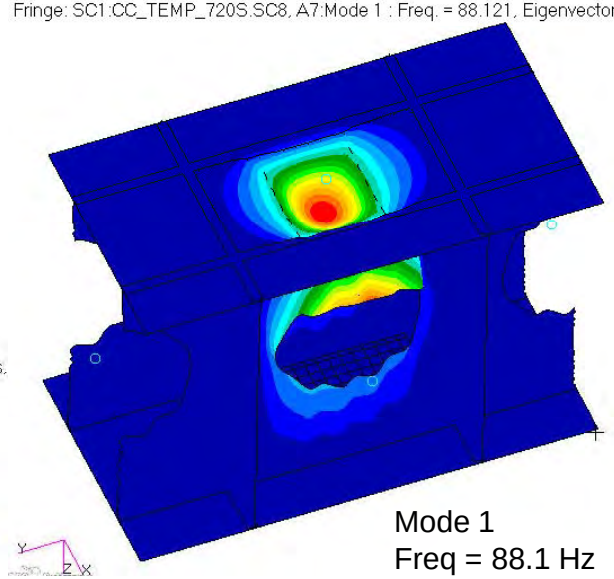

Mode 1
Freq = 88.1 Hz

Mode 2
Freq = 113.7 Hz

Patran 2010.2.3 (MD Enabled) 05-Jan-12 13:06:19
Fringe: SC1:CC_TEMP_720S.SC8, A7:Mode 2 : Freq. = 113.73, Eigenvectors,

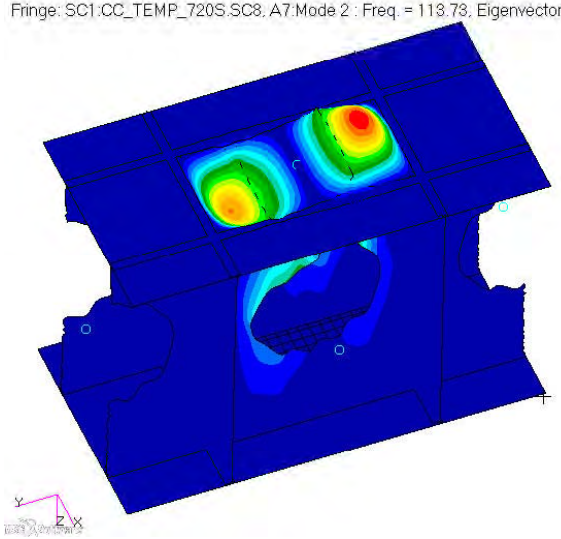

Mode 3
Freq = 123.8 Hz

Patran 2010.2.3 (MD Enabled) 05-Jan-12 13:06:51
Fringe: SC1:CC_TEMP_720S.SC8, A7:Mode 3 : Freq. = 123.75, Eigenvectors,

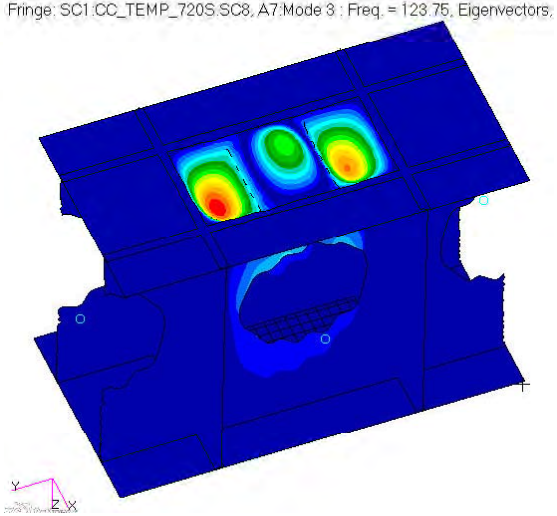

Approved for public release; distribution unlimited.

Acoustic Fatigue Analysis Approach

- **Use Mil-hdbk-5 Inconel 718 Constant Amplitude Data**
  - Adjust for Temperature and Stress Ratio
- **Calculate Design Feature Ktσ – Holes, Welds, Radii**
- **Post-process results – references stress value**
- **Calculate Margins – Compare predicted RMS Stress (KtS) to RMS Allowable (Endurance Limit)**

Approved for public release; distribution unlimited.

Acoustic Fatigue Analysis Assumptions

- **Mechanical Loads negligible during max Q flight envelope**
  - Limit Case of 1G * 1.15 did not affect stress results
- **Kt = 3.0 for filled fastener hole**
- **Thermal exposure effect on Fty is proportional to temperature effect on fatigue allowable**

Approved for public release; distribution unlimited.

Dynamic Model - Loading & Boundary Conditions

- Preload
  - SOL 106: panel2_sol106_1203-01.master
- Material Properties
  - Inconel properties at mapped temperatures for t=720s thermal load
- Boundary Conditions
  - Symmetry Applied to Edges
  - Z-dir SPC applied to nodes 3005532 3012172
- Acoustic Loads (3 - Zones)
  - Flow Direction – Uncorrelated (Panels vibrate independently)
  - Cross Flow – Fully Correlated (Panel vibration is in phase)
  - 1 psi plane wave acoustic load (Orthogonal to panel)
  - 0.1 to 1000hz forcing frequency
  - Damping function of frequency
- SOL 111
  - Input File: panel2_sol111_1222-02_symm.xdb
  - Results File: panel2_sol111_1222-02_symm.xdb

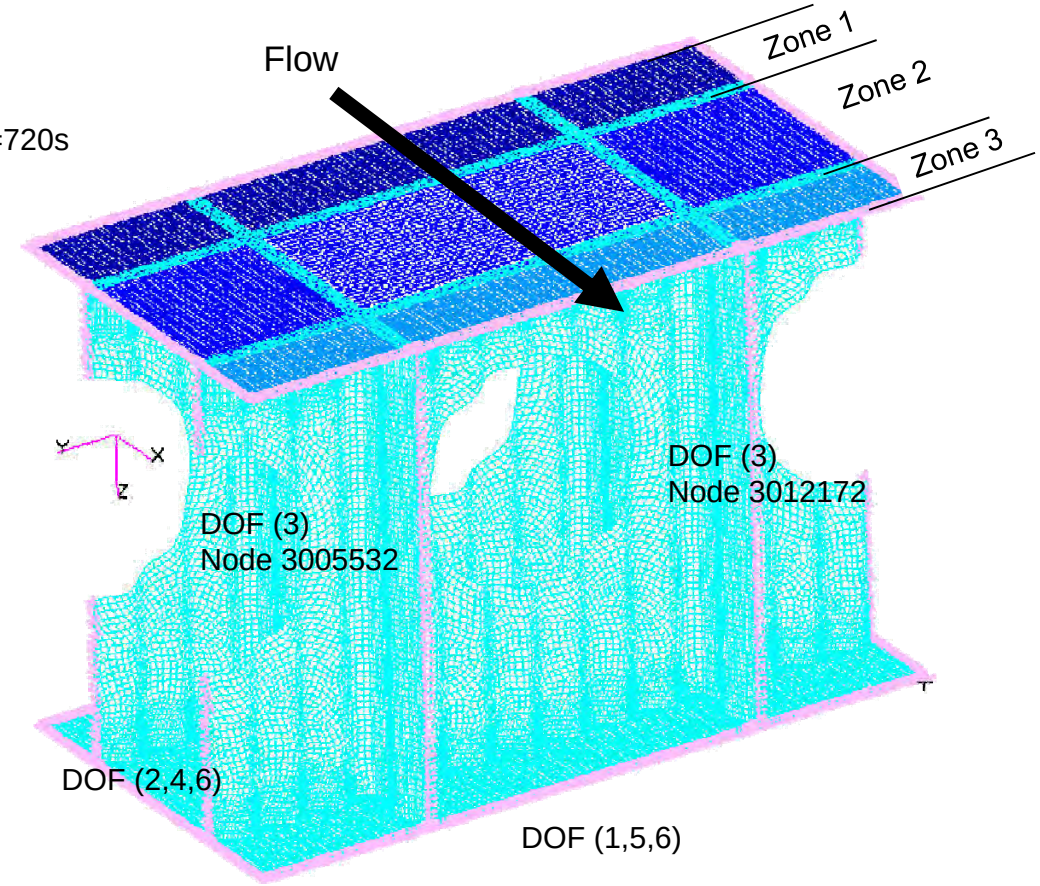

331
Approved for public release; distribution unlimited.

Acoustic Response – RMS Displacement Result

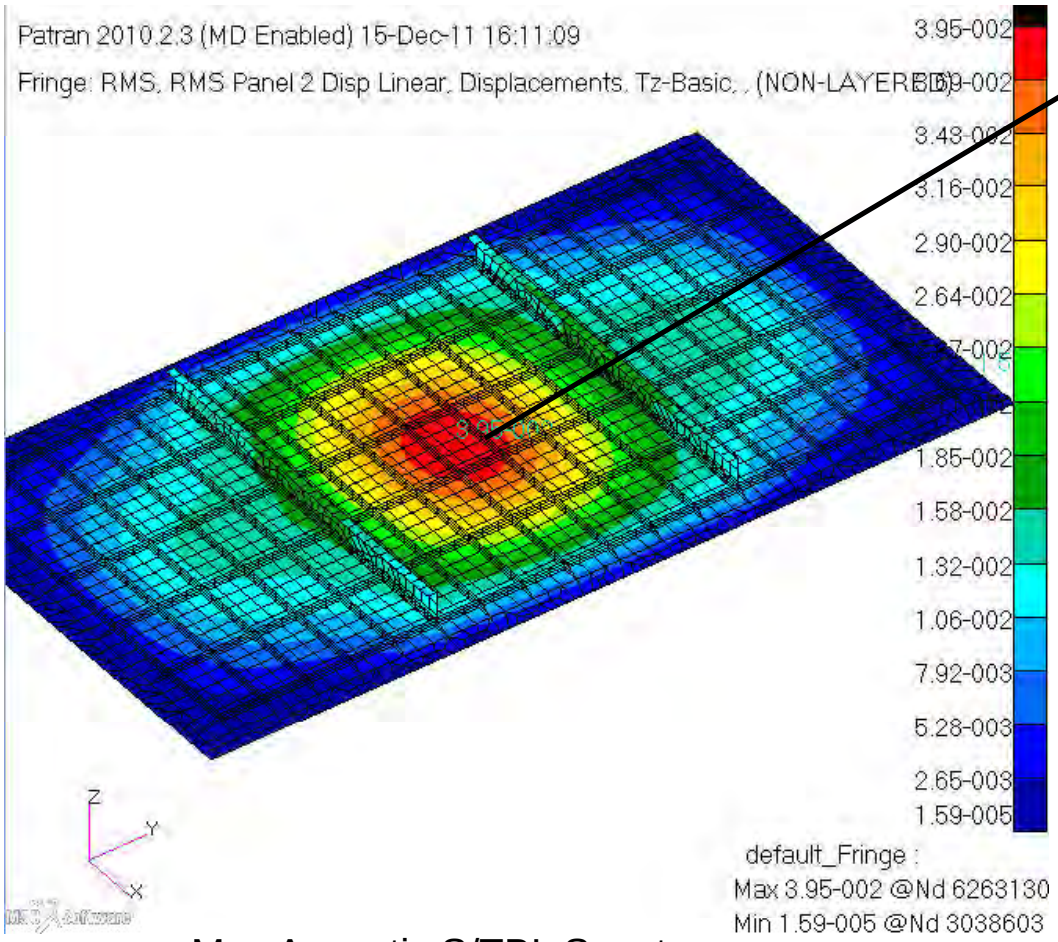

Max Acoustic S/TBL Spectrum
(Max TZ, node 6263130)

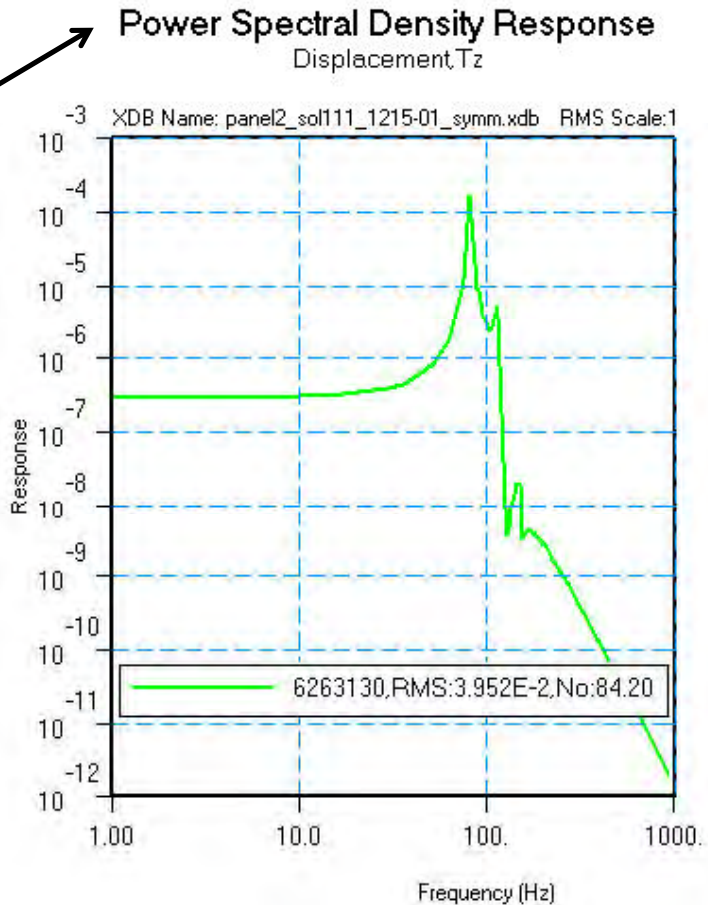

PSD Displacement Response:
Node 6263183

Approved for public release; distribution unlimited.

RMS Stress Allowable - Inconel 718

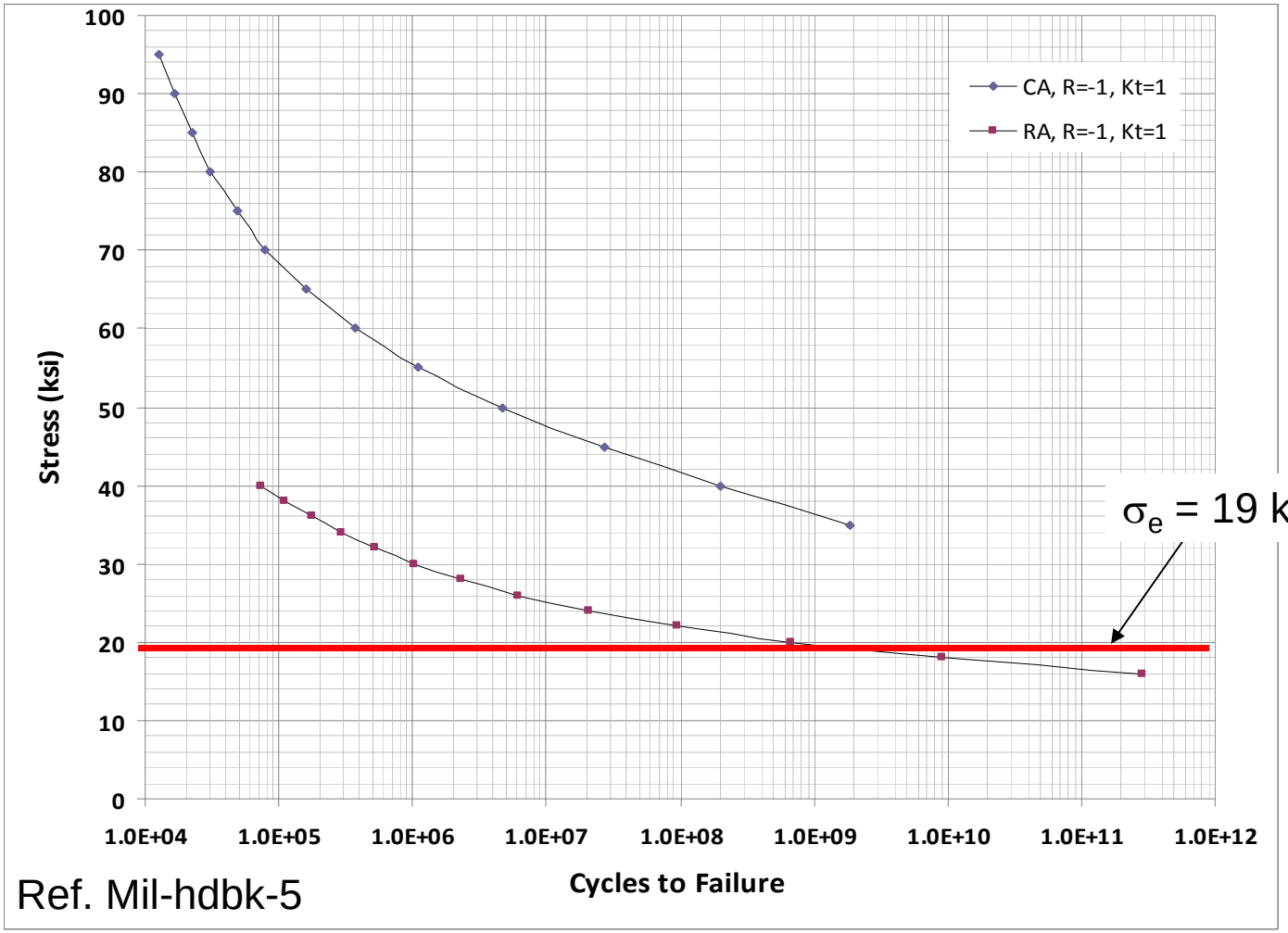

Approved for public release; distribution unlimited.

MMPDS – Inconel 718 – Fty v. Temp

- **Assume fatigue allowable follows trend of Fty as a function of temperature exposure**

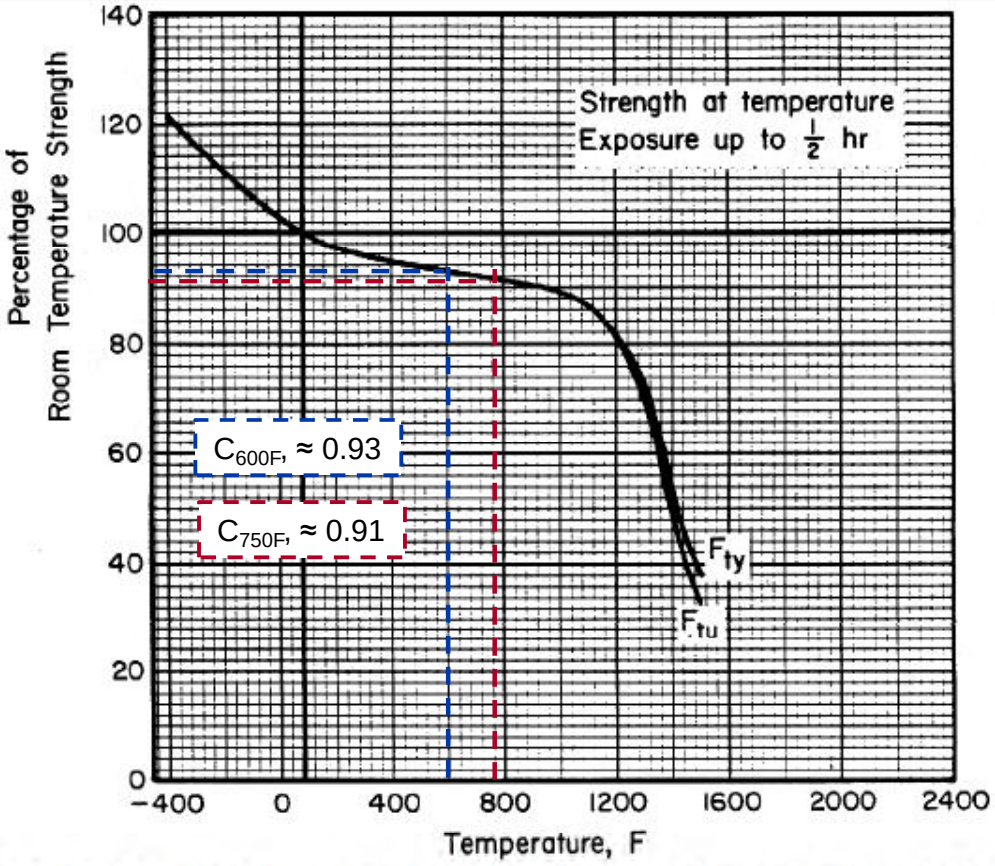

Figure 6.3.5.1.1. Effect of temperature on the tensile ultimate strength (F_{tu}) and tensile yield strength (F_{ty}) of solution-treated and aged Inconel 718.

Approved for public release; distribution unlimited.

MMPDS – Inconel 718 – S/N Curve

- **For locations with Kt < 1.5 use Fig 6.3.5.1.8.c (Best-fit S/N curves for un-notched Inconel 718 sheet at 1000F)**

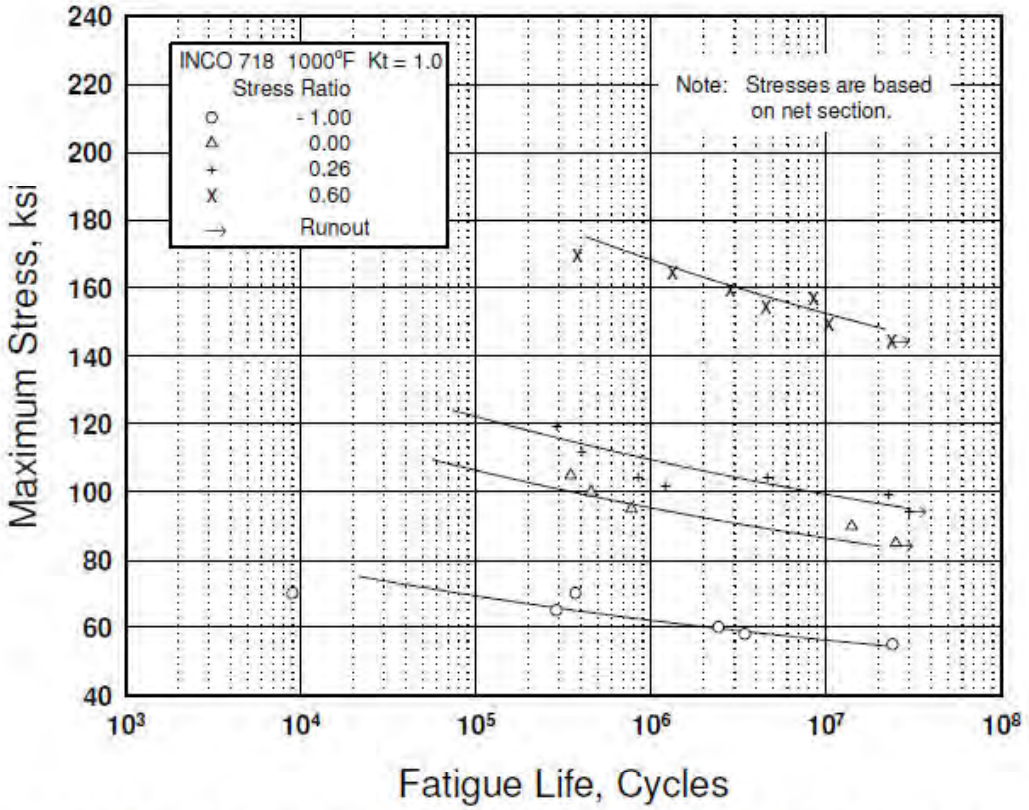

Equivalent Stress Equation:

$\text{Log } N_f = 23.51 - 10.57 \text{ Log } (S_{eq} - 50)$

$S_{eq} = S_{max}(1\text{-}R)^{0.62}$

Std. Error of Estimate, Log (Life) = 0.414

Standard Deviation, Log (Life) = 0.776

$R^2 = 71.5\%$

Figure 6.3.5.1.8(c). Best-fit S/N curves for unnotched Inconel 718 sheet at 1000°F, long transverse direction.

Approved for public release; distribution unlimited.

MMPDS – Inconel 718 – S/N Curve

- **For locations with Kt > 1.5 use Fig 6.3.5.1.8.c (Best-fit S/N curves for un-notched Inconel 718 sheet at 1000F)**

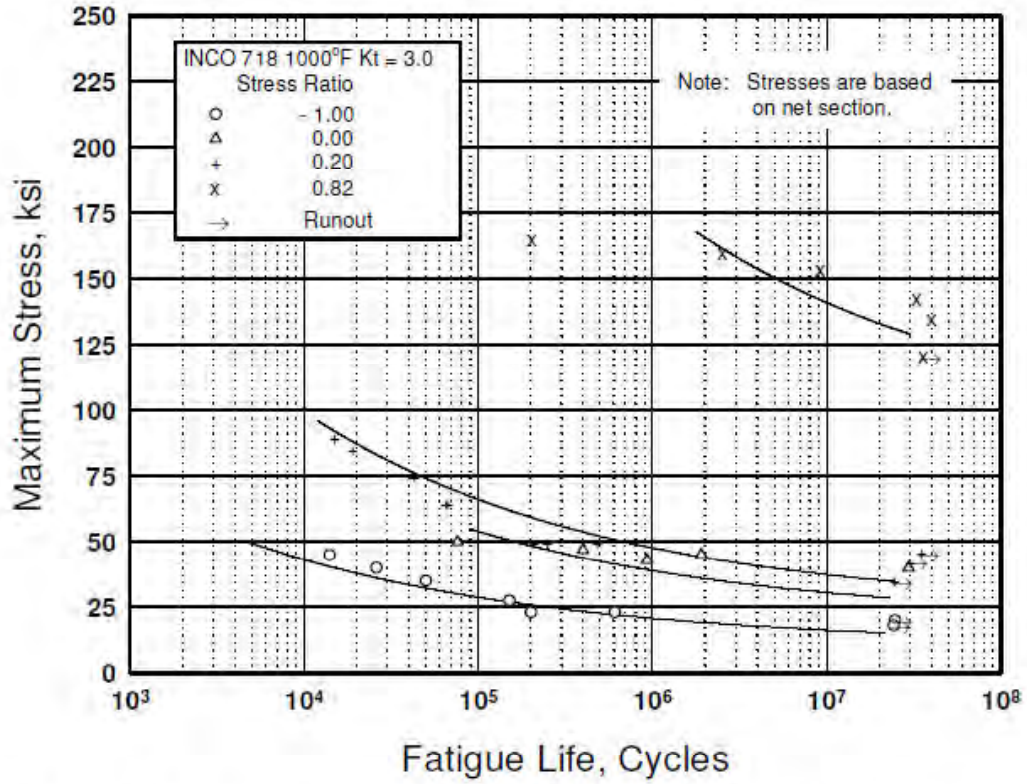

Equivalent Stress Equation:

$\text{Log } N_f = 11.02 - 3.93 \text{ Log } (S_{eq} - 20)$

$S_{eq} = S_{max}(1\text{-}R)^{0.91}$

Std. Error of Estimate, Log (Life) = 0.404

Standard Deviation, Log (Life) = 0.988

$R^2 = 83.3\%$

Sample Size = 23

[Caution: The equivalent stress model may provide unrealistic life predictions for stress ratios beyond those represented above.]

Figure 6.3.5.1.8(d). Best-fit S/N curves for notched, K_t = 3.0, Inconel 718 sheet at 1000°F, long transverse direction.

Approved for public release; distribution unlimited.

Locations of Max Acoustic Stress (T=720s)

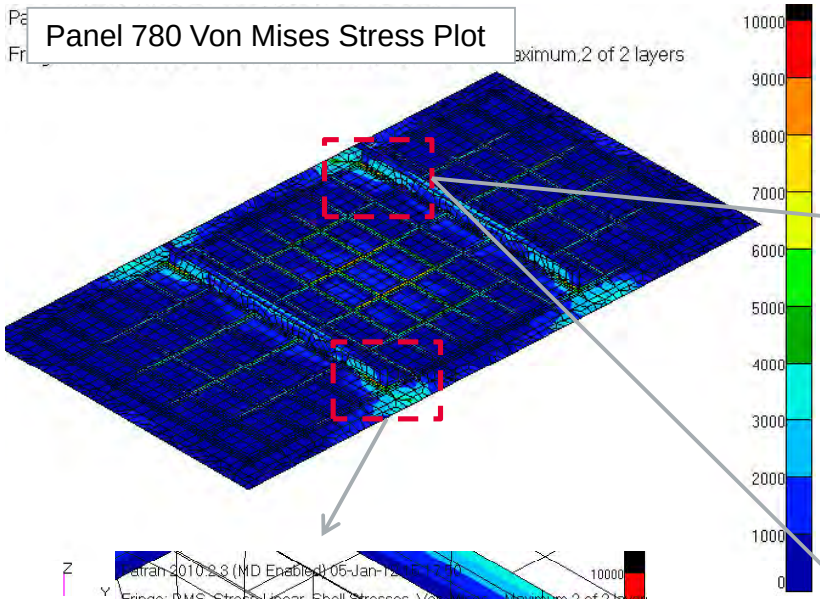

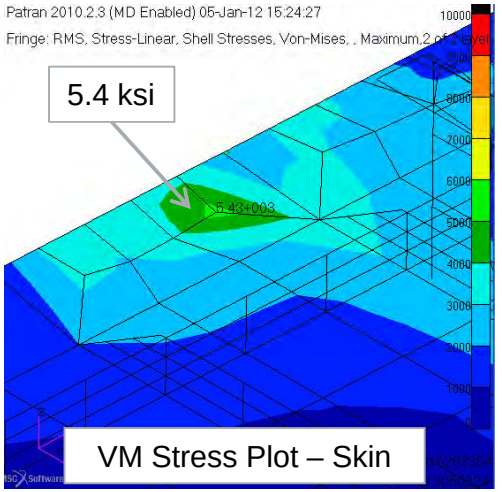

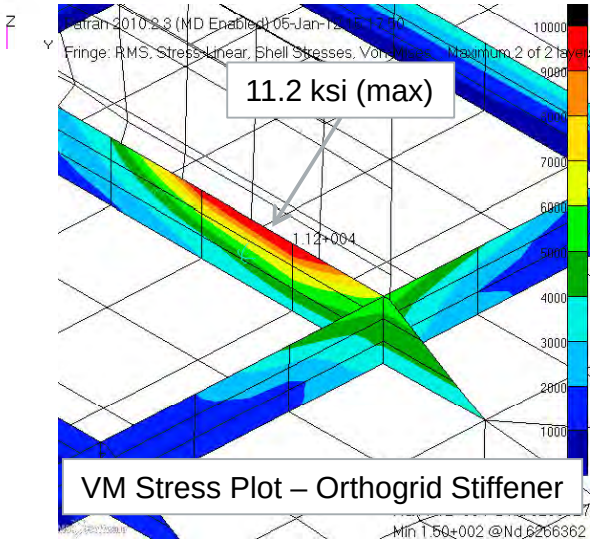

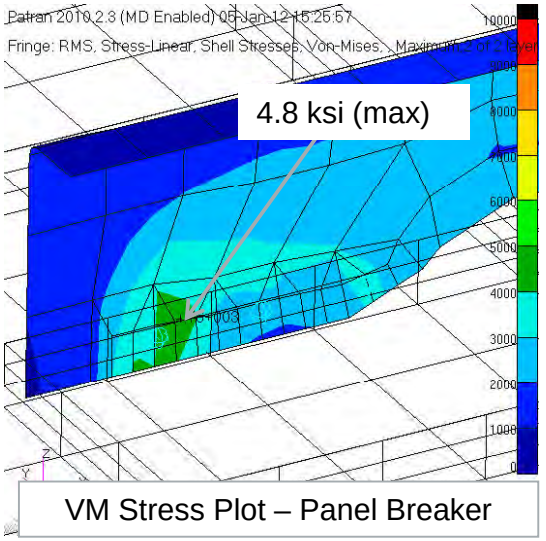

337
Approved for public release; distribution unlimited.

Orthogrid Stiffener Max Stress Location

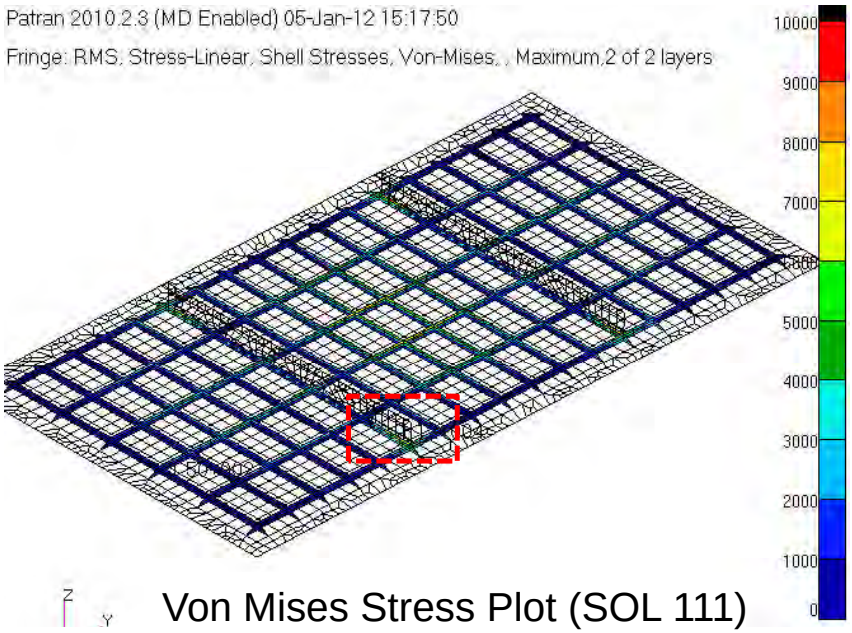

Von Mises Stress Plot (SOL 111)

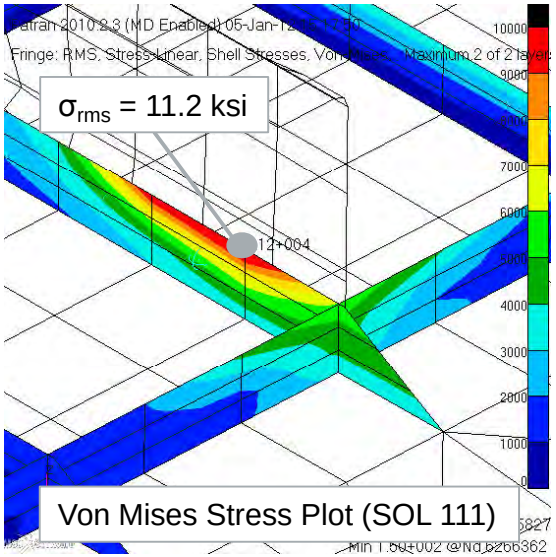

Kt = 1.0 R = 0.15 T = 600F

$$k_t\sigma'_e = \frac{\sigma_e \cdot C_T \cdot C_R}{k_t} = \frac{19.0 \cdot 0.93 \cdot 1.70}{1.0} = 30.0\text{ksi}$$

$$MS = \frac{k_t\sigma'_e}{\sigma_{rms}} - 1 = \frac{30.0}{11.2} - 1 = \underline{\underline{1.68}}$$

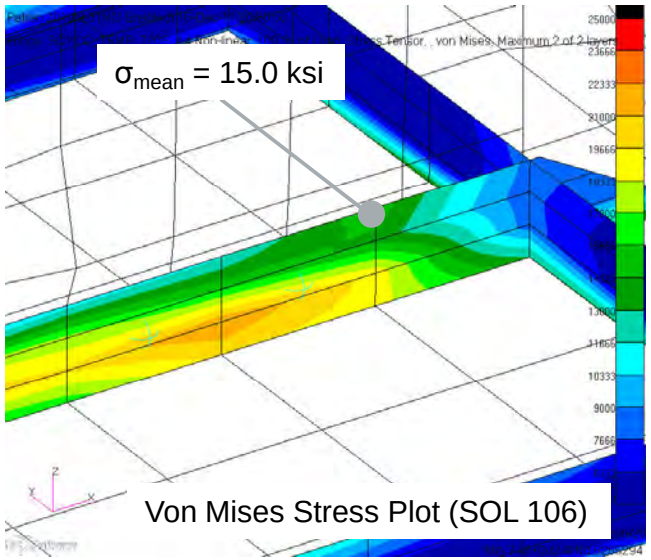

Approved for public release; distribution unlimited.

Orthogrid Stiffener at Panel Breaker Fastener Hole

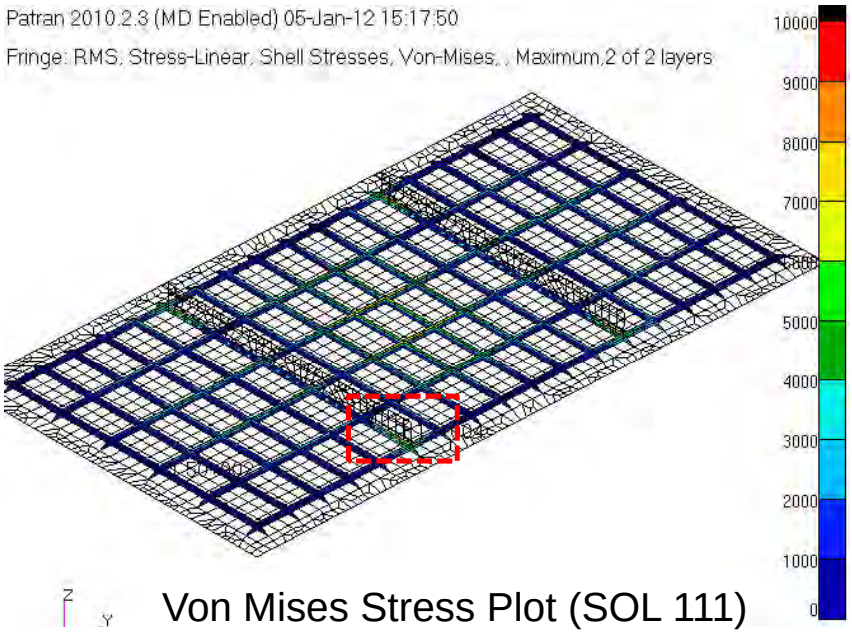

Von Mises Stress Plot (SOL 111)

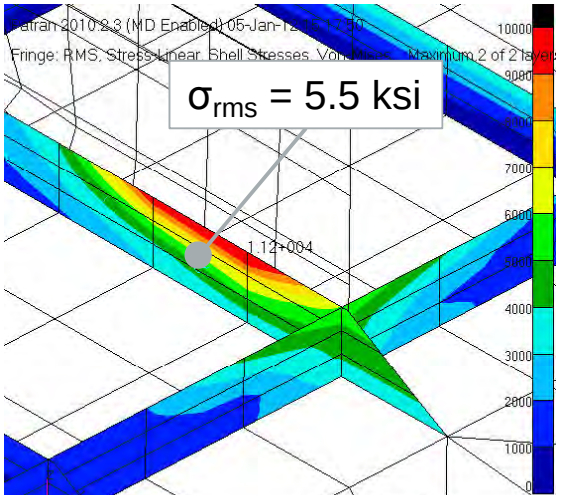

Von Mises Stress Plot (SOL 111)

Kt = 3.0 R = 0.55 T = 600F

$$k_t\sigma'_e = \frac{\sigma_e \cdot C_T \cdot C_R}{k_t} = \frac{19.0 \cdot 0.93 \cdot 3.53}{3.0} = 20.8\text{ksi}$$

$$MS = \frac{k_t\sigma'_e}{\sigma_{rms}} - 1 = \frac{20.8}{5.5} - 1 = \underline{\underline{2.78}}$$

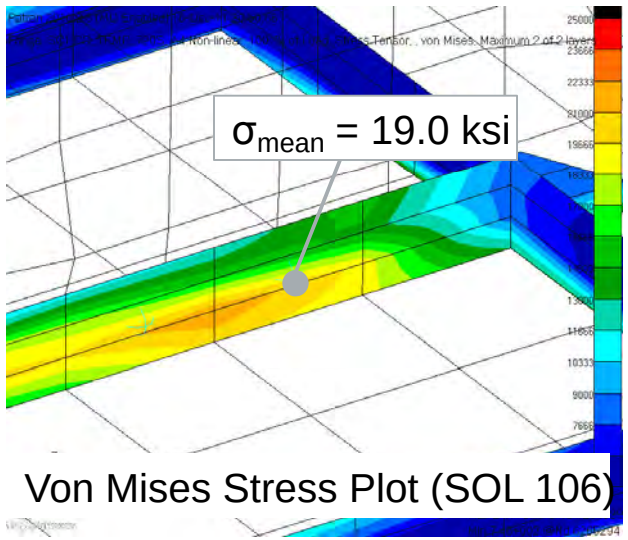

Von Mises Stress Plot (SOL 106)

Approved for public release; distribution unlimited.

Orthogrid Stiffener Center Panel Location

Von Mises Stress Plot (SOL 111)

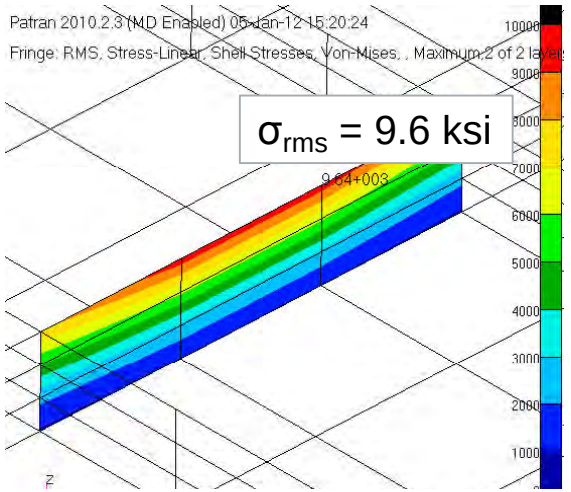

Von Mises Stress Plot (SOL 111)

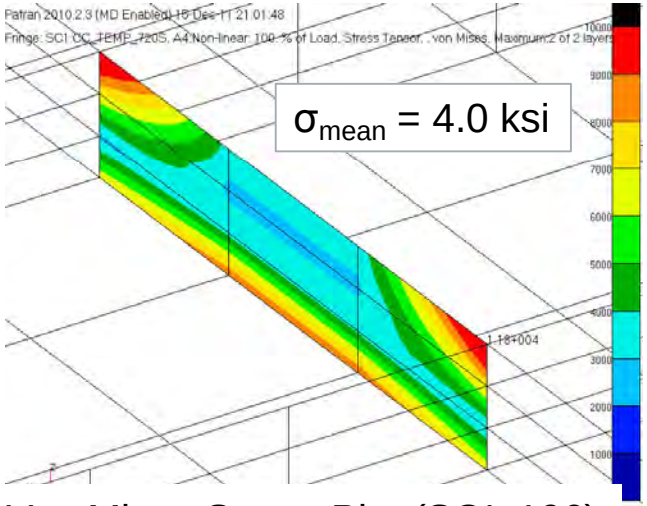

Von Mises Stress Plot (SOL 106)

Kt = 1.0 R = -0.47 T = 750F

$$k_t\sigma'_e = \frac{\sigma_e \cdot C_T \cdot C_R}{k_t} = \frac{19.0 \cdot 0.91 \cdot 1.21}{1.0} = 20.9\text{ksi}$$

$$MS = \frac{k_t\sigma'_e}{\sigma_{rms}} - 1 = \frac{20.9}{9.6} - 1 = \underline{\underline{1.17}}$$

Approved for public release; distribution unlimited.

Skin to Substructure Fastener Hole near Panel Stiffener Termination

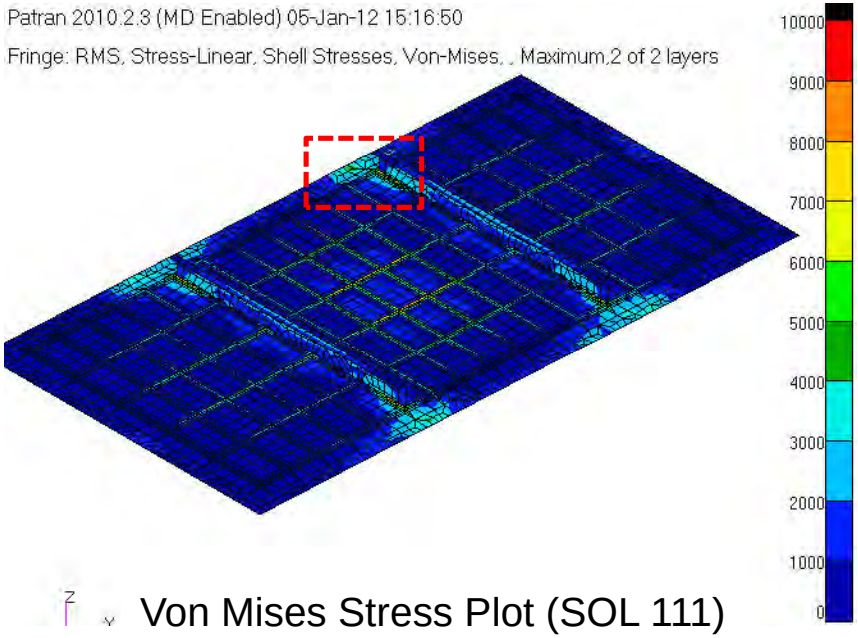

Von Mises Stress Plot (SOL 111)

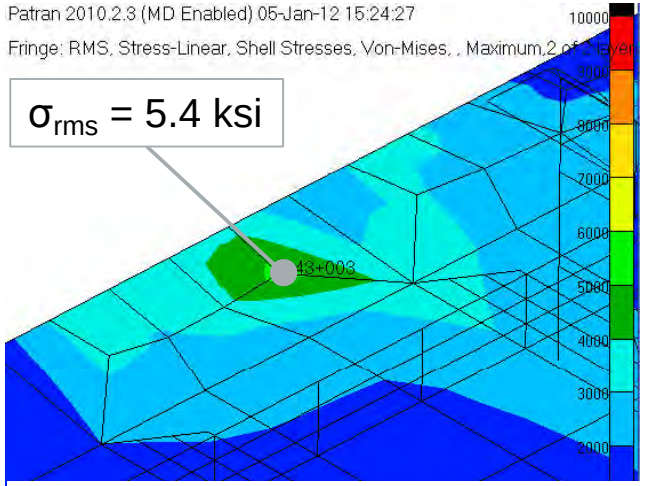

Von Mises Stress Plot (SOL 111)

Kt = 3.0 R = 0.44 T = 750F

$$k_t\sigma'_e = \frac{\sigma_e \cdot C_T \cdot C_R}{k_t} = \frac{19.0 \cdot 0.91 \cdot 3.18}{3.0} = 18.4\text{ksi}$$

$$MS = \frac{k_t\sigma'_e}{\sigma_{rms}} - 1 = \frac{18.4}{5.4} - 1 = \underline{\underline{2.38}}$$

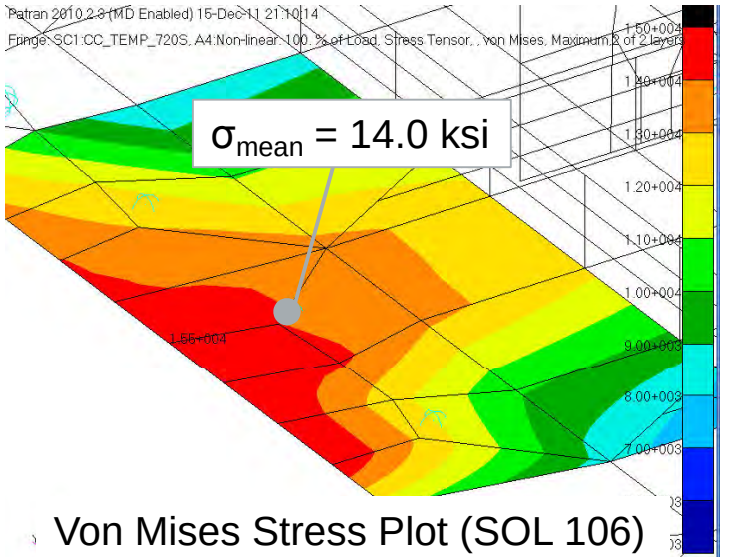

Von Mises Stress Plot (SOL 106)

Approved for public release; distribution unlimited.

Panel Stiffener to Orthogrid Fastener Hole

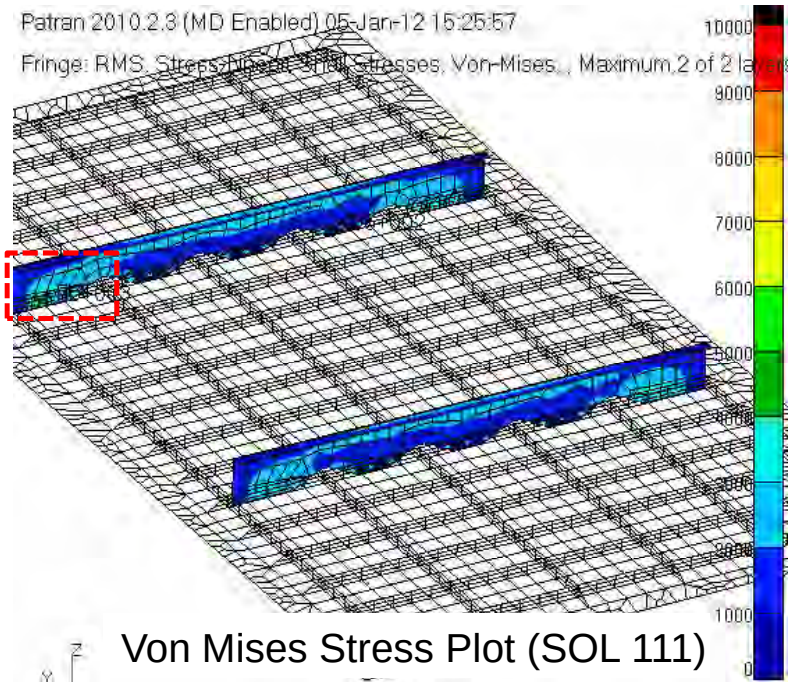

Von Mises Stress Plot (SOL 111)

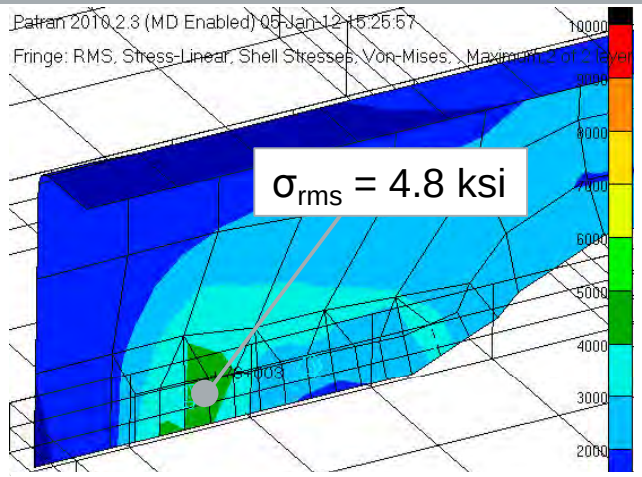

Von Mises Stress Plot (SOL 111)

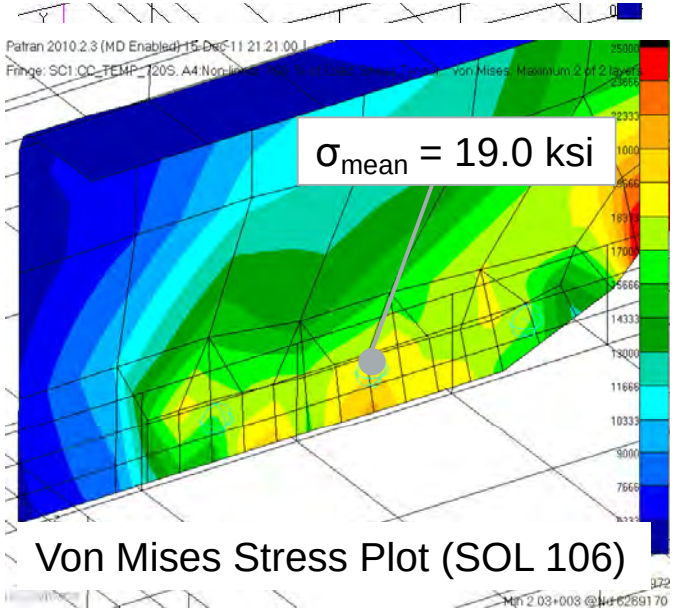

Von Mises Stress Plot (SOL 106)

Kt = 3.0 R = 0.60 T = 750F

$$k_t\sigma'_e = \frac{\sigma_e \cdot C_T \cdot C_R}{k_t} = \frac{19.0 \cdot 0.91 \cdot 3.53}{3.0} = 20.3\text{ksi}$$

$$MS = \frac{k_t\sigma'_e}{\sigma_{rms}} - 1 = \frac{20.3}{4.8} - 1 = \underline{\underline{3.27}}$$

Approved for public release; distribution unlimited.

Acoustic Fatigue Summary Table

Location of Stress Concentration	Stress Concentration Type	Structural Temperature (˚F)	Temp. Factor	Stress Ratio	Stress Ratio Factor	Kt	Allowable Stress (ksi)	RMS Stress Result (ksi)	Mean Stress Thermal Load (ksi)	MS
Orthogrid Stiffener Near Panel Breaker Termination	None	600	0.93	0.15	1.70	1.0	30.0	11.2	15.0	1.68
Orthogrid Stiffener to panel breaker fastener hole	Filled Hole	600	0.93	0.55	3.53	3.0	20.8	5.5	19.0	2.78
Orthogrid Stiffener at panel center	None	750	0.91	-0.47	1.21	1.0	20.9	9.6	3.5	1.17
Skin Near Panel Breaker Termination	Filled Hole	750	0.91	0.44	3.18	3.0	18.4	5.4	14.0	2.38
Panel Breaker to Orthogrid Connection	Filled Hole	750	0.91	0.60	3.53	3.0	20.3	4.8	19.0	3.27

*Baseline Allowable = 19ksi (Kt=1,R=-1, T=RT) Results file: panel2_sol111_1222-02_symm.xdb

Approved for public release; distribution unlimited.

Fatigue Analysis Approach for Thermal Mechanical Loads

- **Define Spectrum**
  - Assume lifetime of 9600 GAG cycles and 4x safety factor = 38,400 load cycles
- **Define Fatigue Allowables & Knockdowns**
  - Use Mil-hdbk 5 Inconel 718 Constant Amplitude Data
    - Adjust for Temperature
- **Determine Spectrum Fatigue $K_t\sigma$**
  - Post-process results – references stress value
    - Use Max/Min sort to determine maximum and minimum principal stress locations
    - Sort fastener loads to determine maximum bearing location
  - Calculate Design Feature Ktσ using Boeing CAESAR Tool
    - CAESAR (ComputAtional Engineering Structural Analysis Routines) is a web based tool for determining detail stresses
    - User entered Input variables are submitted to stress check model templates which are executed on a remote server
- **Calculate Margin of Safety**

344
Approved for public release; distribution unlimited.

Hypersonic Strike Vehicle Operational Thermal Cycles

- **Assumptions: First Pass Fatigue Analysis, Use simple worst case scenario (G-A-G)**
- **Primary Structure Design :**
  - 9600 x 1hr Sorties over operational life
  - *Hence, 9,600 Ground-Air-Ground thermal cycles (2.5g Maneuver @ Max Thermal)*
  - *Design Life Factor of Safety = 4 life times or 38,400 cycles*
  - Fatigue Spectrum uses, R-Ratio = 0 Inconel 718 s-N data.

345
Approved for public release; distribution unlimited.

Thermal-Mechanical Fatigue Analysis Summary

- **Flight Loads**
  - Mach 7, +2.5g symmetric pull up maneuver
- **Thermal**
  - Temperature @
    - t = 720 sec, Maximum thermal gradient between panel and substructure, max stress
    - t = 2520 sec, Maximum structural temperature, reduced fatigue allowable
- **Load Cases**
  - Limit flight load 1.15*2.5g, Temp @ 720s (max stress / temp. gradient)
  - Limit flight load 1.15*2.5g, Temp @ 2520s (max temperature)
- **Boundary Conditions for Panel Model**
  - Translational/Rotational Constraints on frame webs
- **Analysis Runs**
  - Panel_2_2_5g_All_Temps.bdf (sol 101)

Approved for public release; distribution unlimited.

Orthogrid Panel 780 Temperature Gradient History

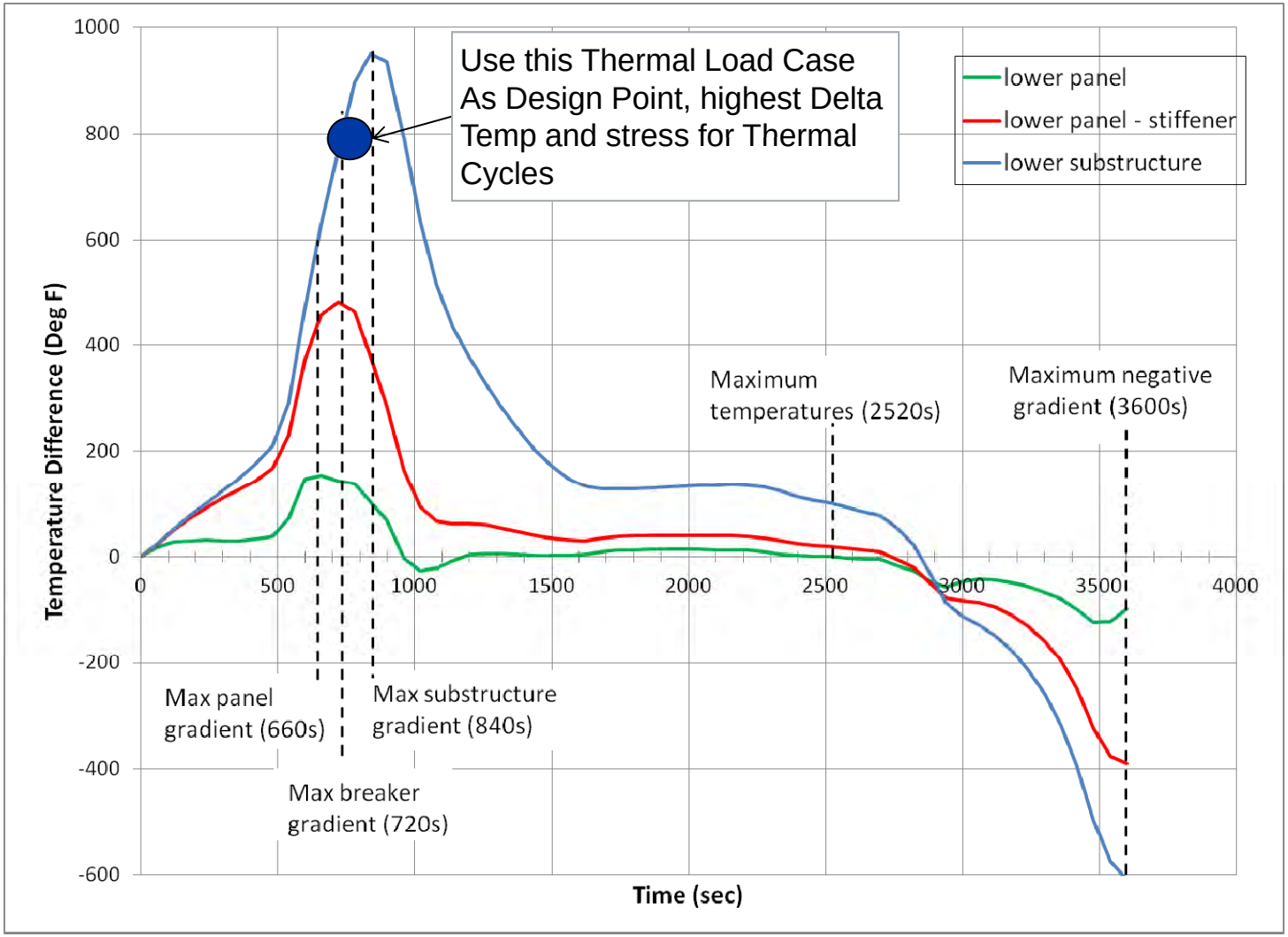

Approved for public release; distribution unlimited.

Inconel 718 S-N Data

$K_t\sigma$-all = 110ksi
At 1000F, R=0

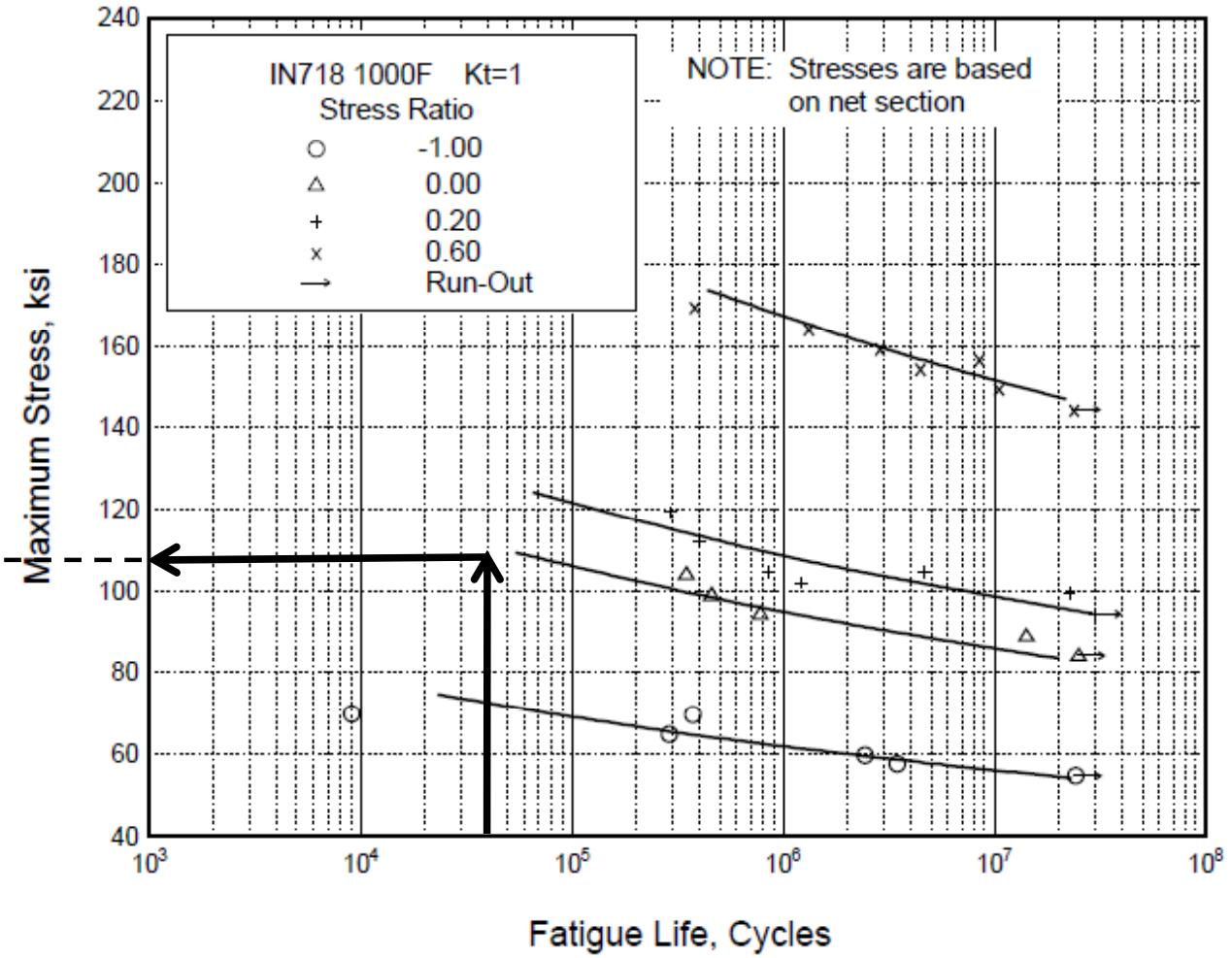

Ref. MMPDS-05 Figure 6.3.5.1.8(d)

Approved for public release; distribution unlimited.

Temperature Adjusted Fatigue Allowables

- **Temperature adjusted allowable stress were calculated for each trajectory point based on Fty as a function of temperature**
  - Ref. MMPDS-05 Fig 6.3.5.1.1
  - Max thermal stress occurs at t=720s
  - Maximum temperature (≈ 1400˚F) occurs at t=2520s

	Panel 2 Skin to Substructure				Panel 2 Ogrid to Panel Stiffnr			
Time (s)	Temp. (F)	RT Temp Factor	Adj. Temp Factor	Temp Adj. Allowable (KSI)	Temp. (F)	RT Temp Factor	Adj. Temp Factor	Temp Adj. Allowable (KSI)
660	650	0.93	1.04	114.4	450	0.94	1.06	116.6
720	800	0.91	1.02	112.2	650	0.93	1.04	114.4
840	1100	0.86	0.97	106.7	950	0.9	1.01	111.1
2520	1400	0.5	0.56	61.6	1400	0.5	0.56	61.6
3600	400	0.95	1.07	117.7	400	0.95	1.07	117.7
	ref allowable =		110	ksi				
	ref 1000 F factor =		0.89					

Significant knockdown at 1400˚F

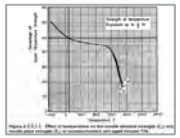

Fty v. Temp

Approved for public release; distribution unlimited.

Fastened Joints for Thermal-Mechanical Fatigue Analysis

- **Panel 2 has fastened joints at two locations**
  - skin panel to substructure cap
  - orthogrid to panel stiffener

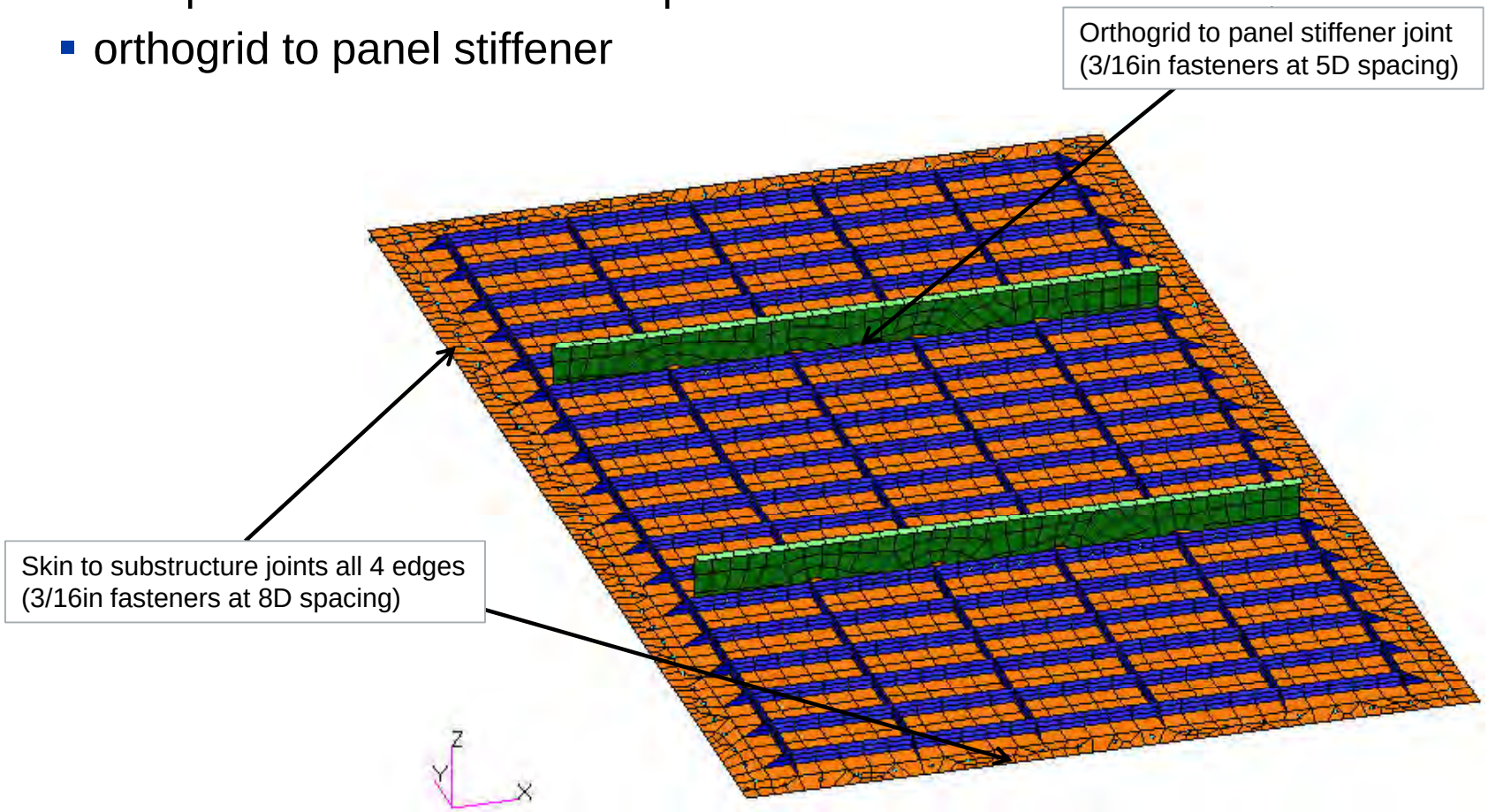

Approved for public release; distribution unlimited.

Skin to Substructure Joint – Max Stress Location

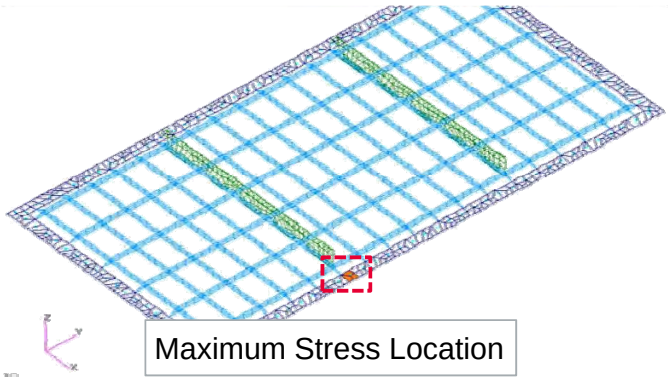

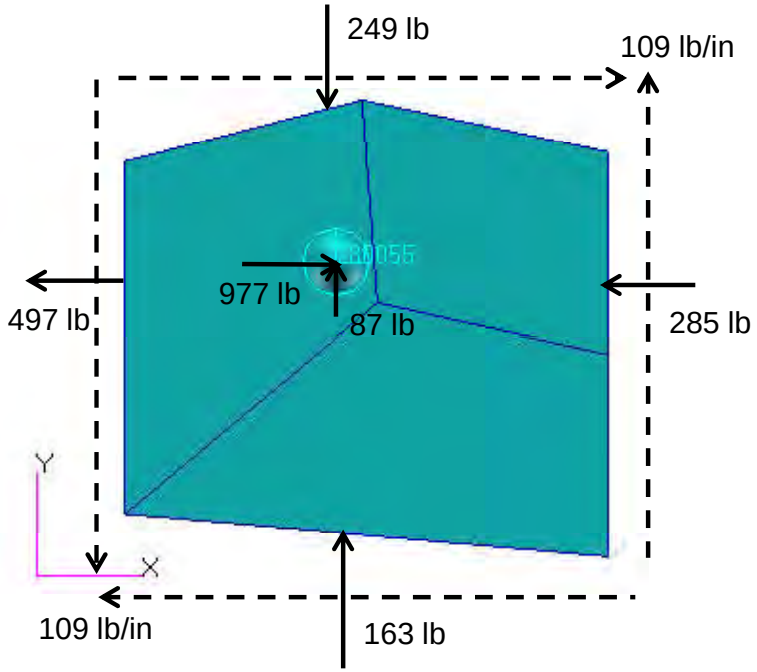

CAESAR Single Hole Input Screen (expand to view)

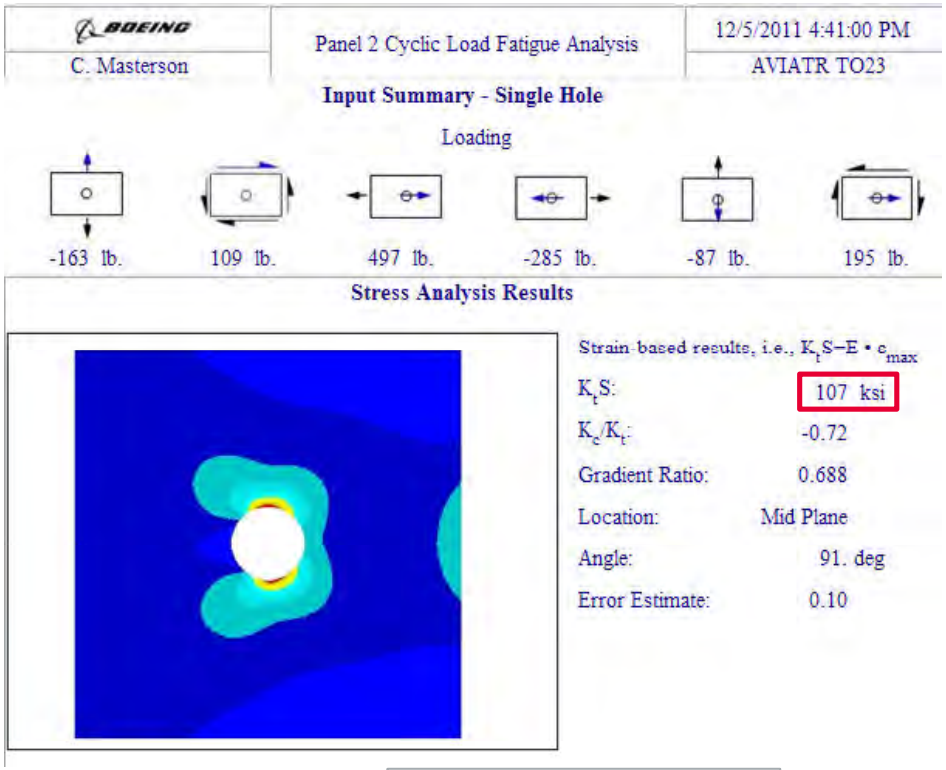

Ktσ = 107 ksi
Allowable Stress = 112 ksi
MS = 0.05

Approved for public release; distribution unlimited.

Skin to Substructure – Joint Loads and MS Summary

- **Min MS of 0.05 at Fastener 780055 for 2.5g+Thermal(t=720s)**
- **Adequate MS for all checks at t=2520s**

Skin to Substructure Joint		Min Nx	Max Nx	Min Ny	Max Ny	Max Nxy	Max Brg	Max Princ	Min Princ	Max Shear	Max Brg
Load Case		2.5g + T(720s)	2.5g + 720s	2.5g + 720s	2.5g + 720s	2.5g + 720s	2.5g + 720s	2.5g +T(2520s)	2.5g +T(2520s)	2.5g +T(2520s)	2.5g +T(2520s)
Element Loads	PxLH	570	-497	211	381	600	-497	263	306	263	308
	PxRH	-1300	-285	-167	-486	-196	-285	-114	179	-114	443
	PyLwr	23	163	788	96	-86	163	-130	303	-130	434
	PyUpr	-100	-249	908	168	171	-249	130	-245	130	-346
	Nxy	-121	109	47	-168	-284.5	109	-85.5	-76.75	-85.5	37.67
Fastener Load	Fastener ID	780070	780055	780090	780058	780020	780055	780020	780029	780020	780005
	Px	-770	-977	-46	-267	593	-977	19	29	19	94
	Py	-47	-87	-153	186	29	-87	8.4	-45	8.4	70
	Pz	29	0	2.5	38	9.5	0	71	260	71	307
Stress Result	KTs	81.7	107	21.4	41	85.1	107	15.4	7.4	15.4	27.8
	MS	0.37	0.05	LARGE	1.74	0.32	0.05	LARGE	LARGE	LARGE	1.22

Approved for public release; distribution unlimited.

Orthogrid to Stiffener Joint – Max Principal Stress Location

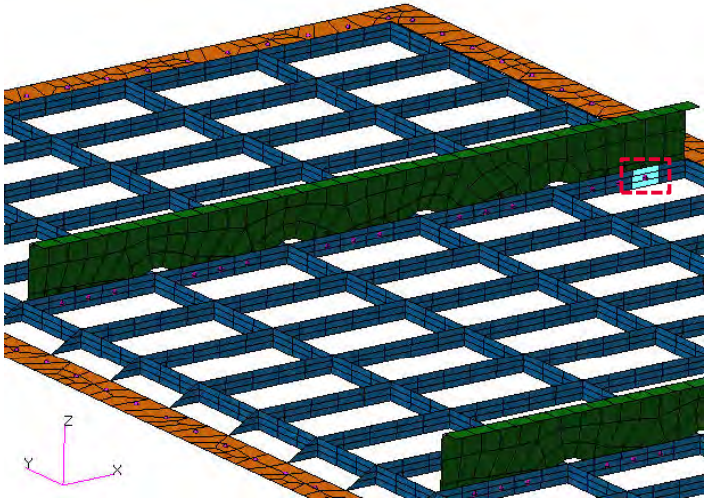

Maximum Stress Location

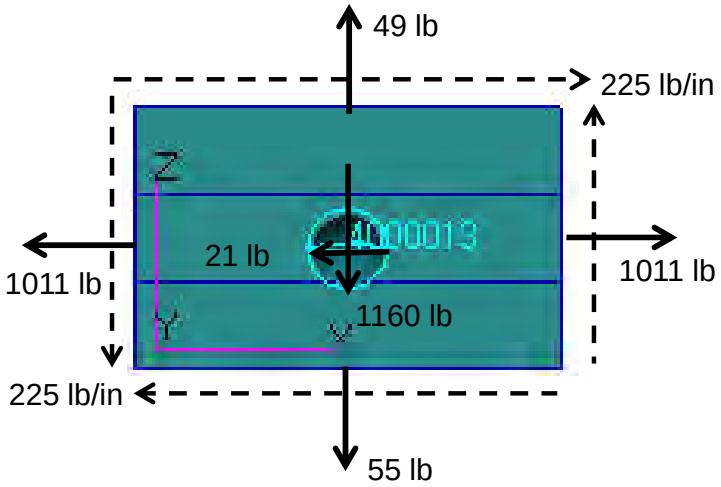

CAESAR Single Hole Input Screen (expand to view)

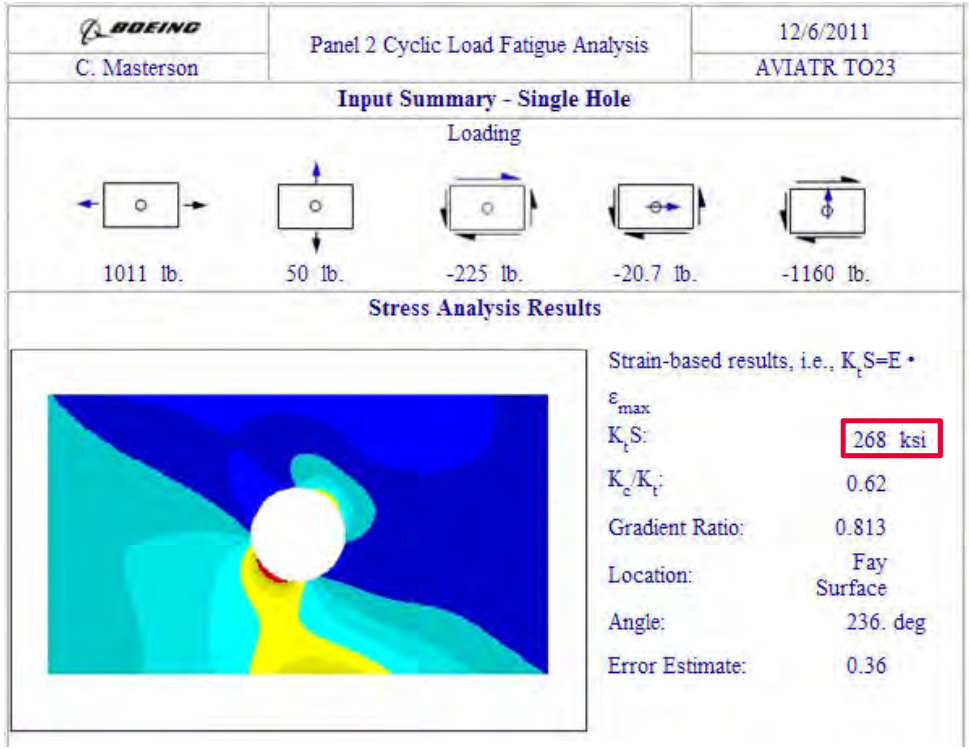

Ktσ = 268 ksi
Allowable Stress = 114 ksi
MS = -0.60

Approved for public release; distribution unlimited.

Orthogrid to Stiffener – Joint Loads and MS

- **Large bearing loads contribute to negative MS at orthogrid to stiffener joint**
  - Allowable stress = 114 ksi
  - Max Ktσ = 286 ksi

Panel Stiffener to Orthogrrid Joint		Max Princ	Min Princ	Max Shr	Max Brg	Max Princ	Min Princ	Max Shr	Max Brg
Load Case		2.5g + T(720s)	2.5g + T(720s)	2.5g + T(720s)	2.5g + T(720s)	2.5g +T(2520s)	2.5g +T(2520s)	2.5g +T(2520s)	2.5g +T(2520s)
Element Loads	PxLH	-1011	-1011	-1011	-1039	-745	-377	-381	-730
	PxRH	1011	1011	1011	1039	745	377	381	730
	PzLwr	-55	-55	-55	-49	-64	6	6	-69
	PzUpr	49	49	49	34	34	-3	-4	35
	Nzx	-225.33	-225.33	-225.33	10	-14.6	260	-129.26	20.33
Fastener Load	Fastener ID	4000013	4000013	4000013	4000001	4000028	4000027	4000000	4000002
	Px	20.7	20.7	20.7	25	2.93	0.7	-0.2	1
	Pz	1160	1160	1160	-1240	380	206	-211	-382
	Py	364	364	364	380	-426	86	88.9	-427
Stress Result	KTs	286	286	286	236	107	71.8	66.8	96.2
	MS	(0.60)	(0.60)	(0.60)	(0.52)	(0.42)	(0.14)	(0.08)	(0.36)

Approved for public release; distribution unlimited.

Orthogrid to Stiffener Joint – Fastener Loads

- **First and last fasteners of joint transfer nearly double load of next most highly loaded fastener**
- **Some fasteners are lightly loaded**

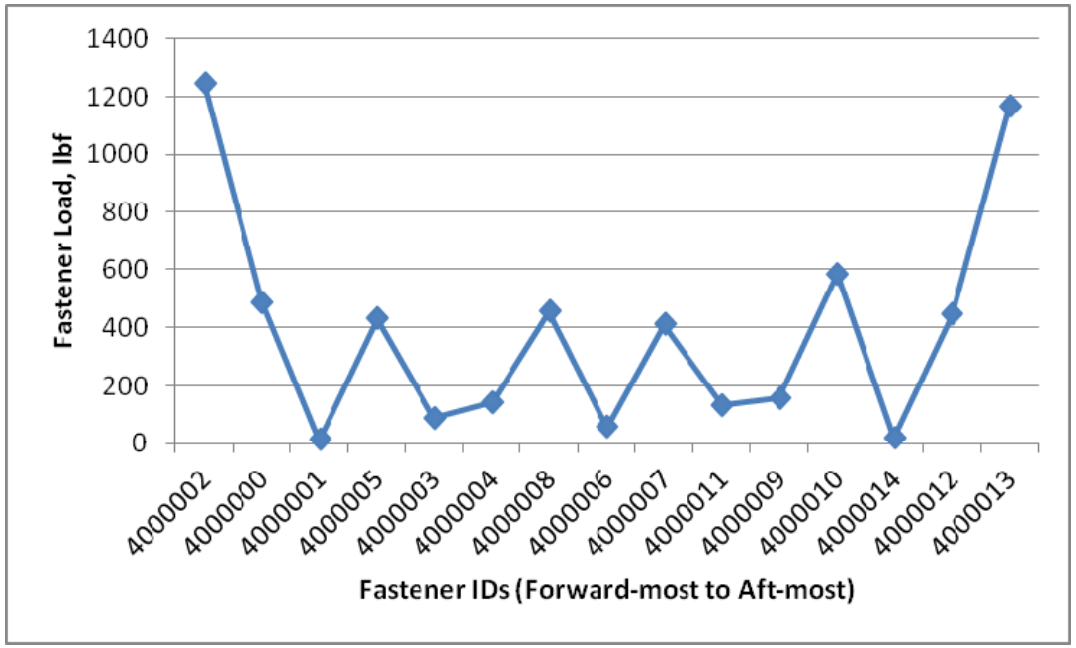

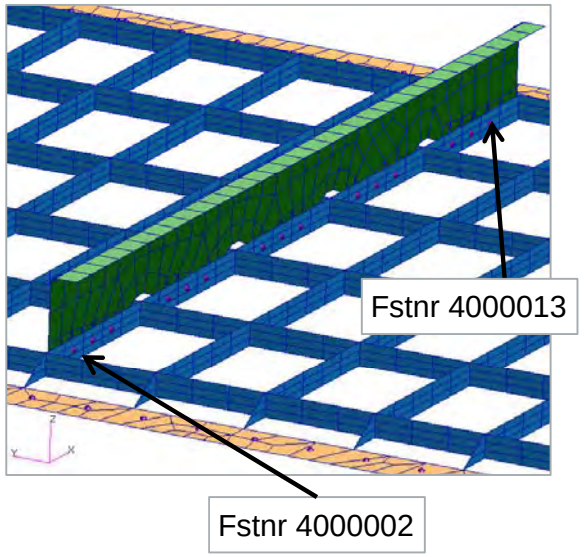

Fastener loads for 2.5g Limit + T(720s)

Approved for public release; distribution unlimited.

Orthogrid to Stiffener Joint - Improvements

- **High stress due to thermal mechanical loads can be mitigated through design improvements and are NOT considered concept inhibitors**
- **Design improvement ideas**
  - Extend panel stiffener beyond last IB-OB orthogrid stiffener and increase gage in grid termination region (similar to panel 4 design)
  - Increase fastener hole edge distance (bumps orthogrid height)
  - Reduce fastener spacing from 5D to 4D
  - Slotted fastener holes allowing for thermal expansion in-plane while preventing normal direction deflection

NOTE: It is likely that a thickness increase of the stiffeners will drive up thermal stress proportionally and prove to be an ineffective solution

Approved for public release; distribution unlimited.

Lessons Learned

- **Stress at fatigue details cannot be pulled directly from FEM results and need to be calculated using closed-form, empirical solutions, or a detailed FEA**
  - The process used for Panel 780 involved manually transferring free body loads to the Boeing CAESAR detailed stress analysis program. (This a very time consuming process)
  - Frequency response results are in terms of stress which are not easily input into the CAESAR tool. In this case a conservative Kt was assumed and applied to the stress read from the unit cell FEM
- **Calculated stress ratio can significantly affect fatigue allowables**
- **In many cases for the panel 780 FEM, mesh could be improved at fatigue details**
- **Large FEMs can execute for a long time before a solution failure occurs, making failed solutions more expensive than for FEMs with fewer DOF**

Approved for public release; distribution unlimited.

BACKUP CONTENT

Approved for public release; distribution unlimited.

SOL 103 Results (Wrong Density)

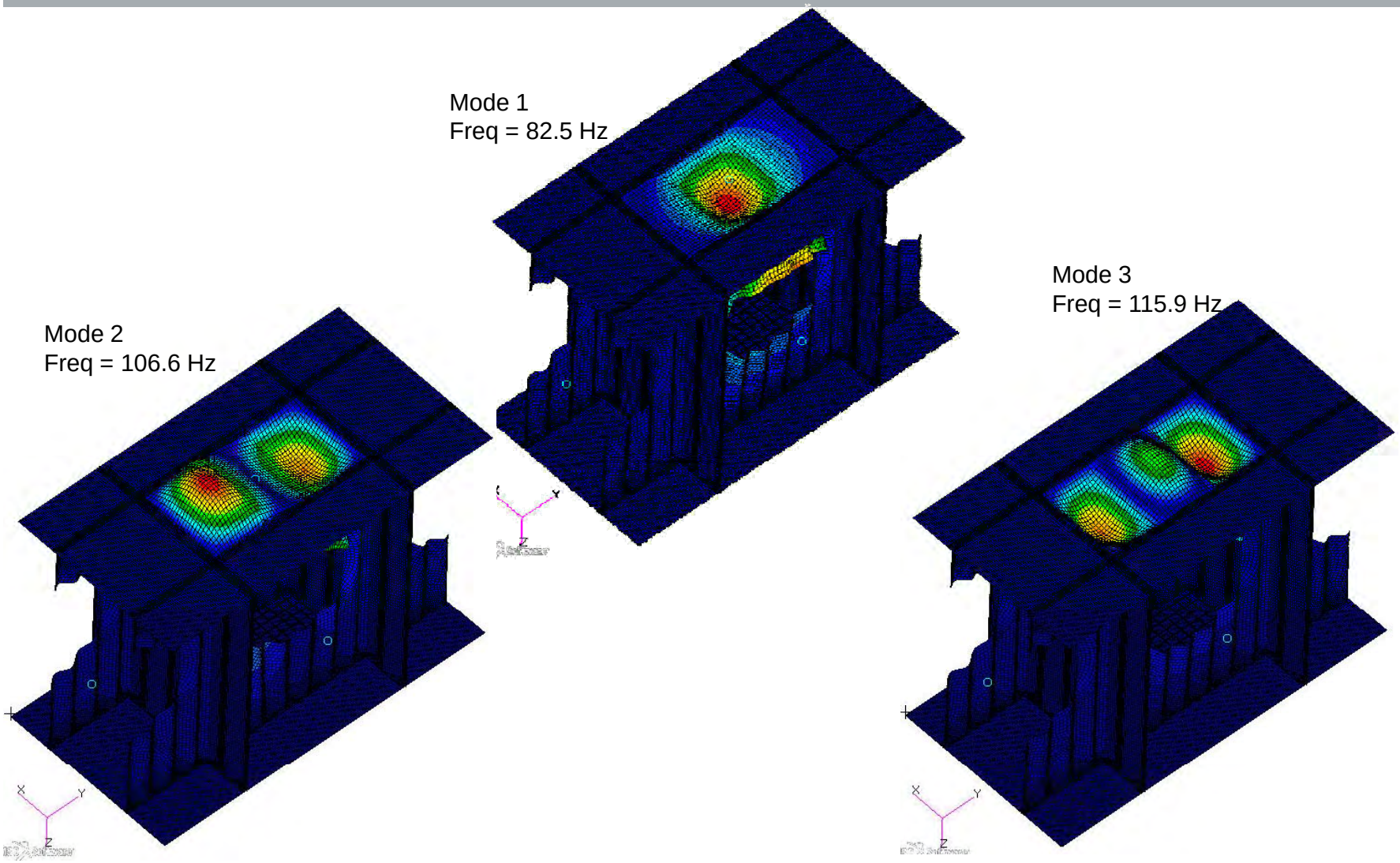

Approved for public release; distribution unlimited.

Asymmetry Fix

Was

SPC (3)
Node 3005532

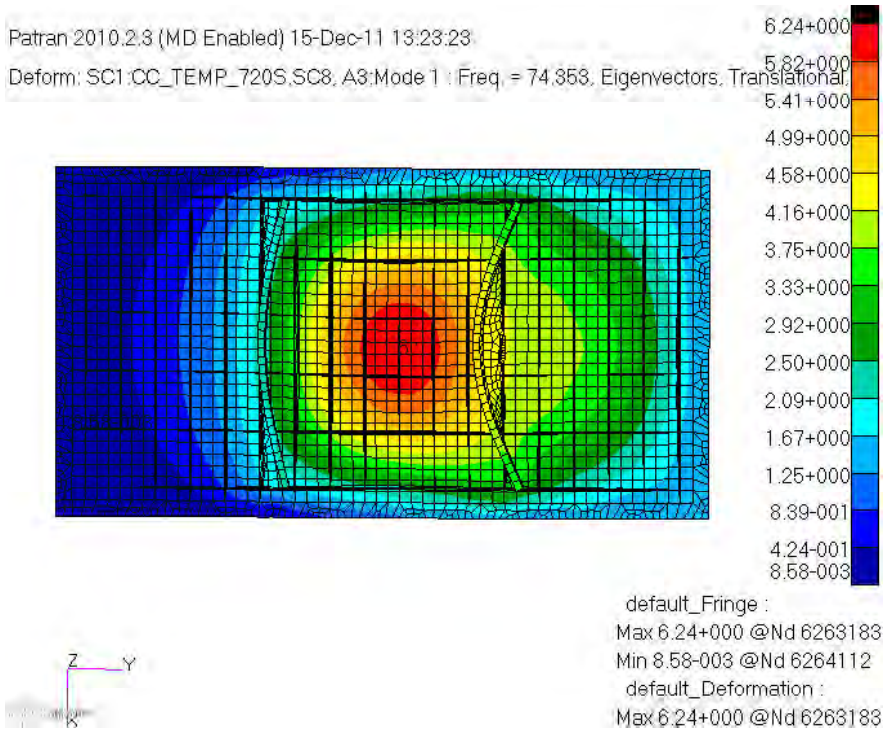

Is

SPC (3)
Node 3005532
Node 3012172

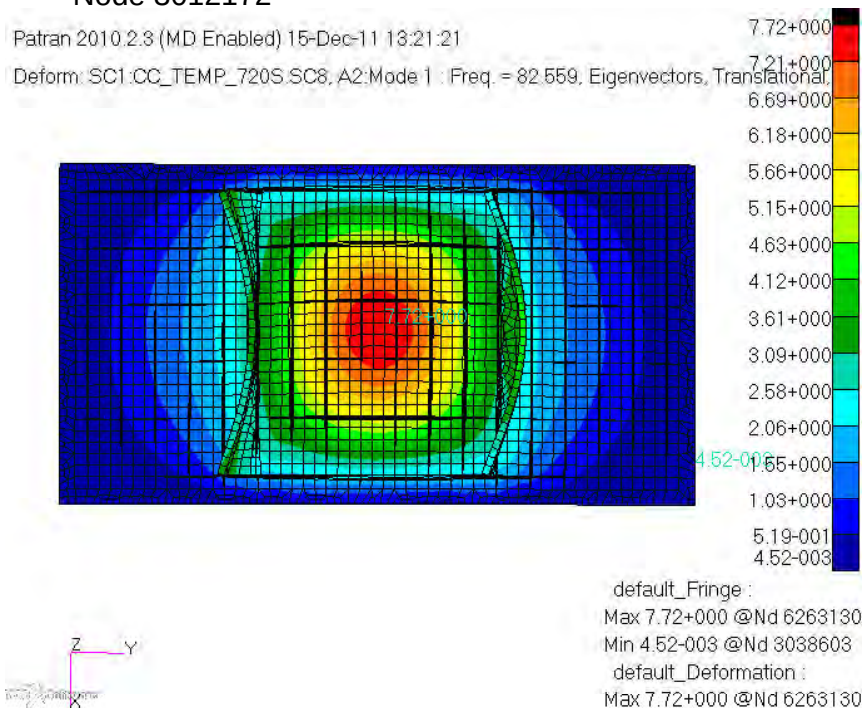

Approved for public release; distribution unlimited.

Analysis Issues

Issue	Approach	Source/Rationale
External Aero-acoustic Loads	Empirical with CFD guidance	Efimtsov Models, Boeing Best Practice, no hypersonic flight test data, or predictive capability available
Damping	Empirical Data	USAF Damping Design Guide, Boeing Best Practices, no inconel sine wave , iso-grid test data available
S-N Data for In 718	Convert Constant Amplitude Data to RMS Data, Adjust based for Temperature based on Strength	Mil-5, Best Practices, only source of reliable data
Sub-structure Modes	Filtered most Sub-structure modes	Concentrating on Panel Structure, also allows for quicker turn around
Choosing Worst Case Design Conditions	Using Max Thermal , matched to Max Acoustic for Fatigue Margin Checks	Dissimilar loads from different points in the trajectory, points are close, but not exact. This accounts for possible difference in trajectories
Combined Spectrum	Assuming a single trajectory	Don't have other trajectories, but a real vehicle will have many different possible missions.
Joint Allowables	Similarity to other material, joints	Boeing Best Practice, Need to test specific joints – welds, machine, fastened, etc…

Approved for public release; distribution unlimited.

ACOUSTIC MODEL DEVELOPMENT

Approved for public release; distribution unlimited.

Trajectory – Design Conditions of Interest

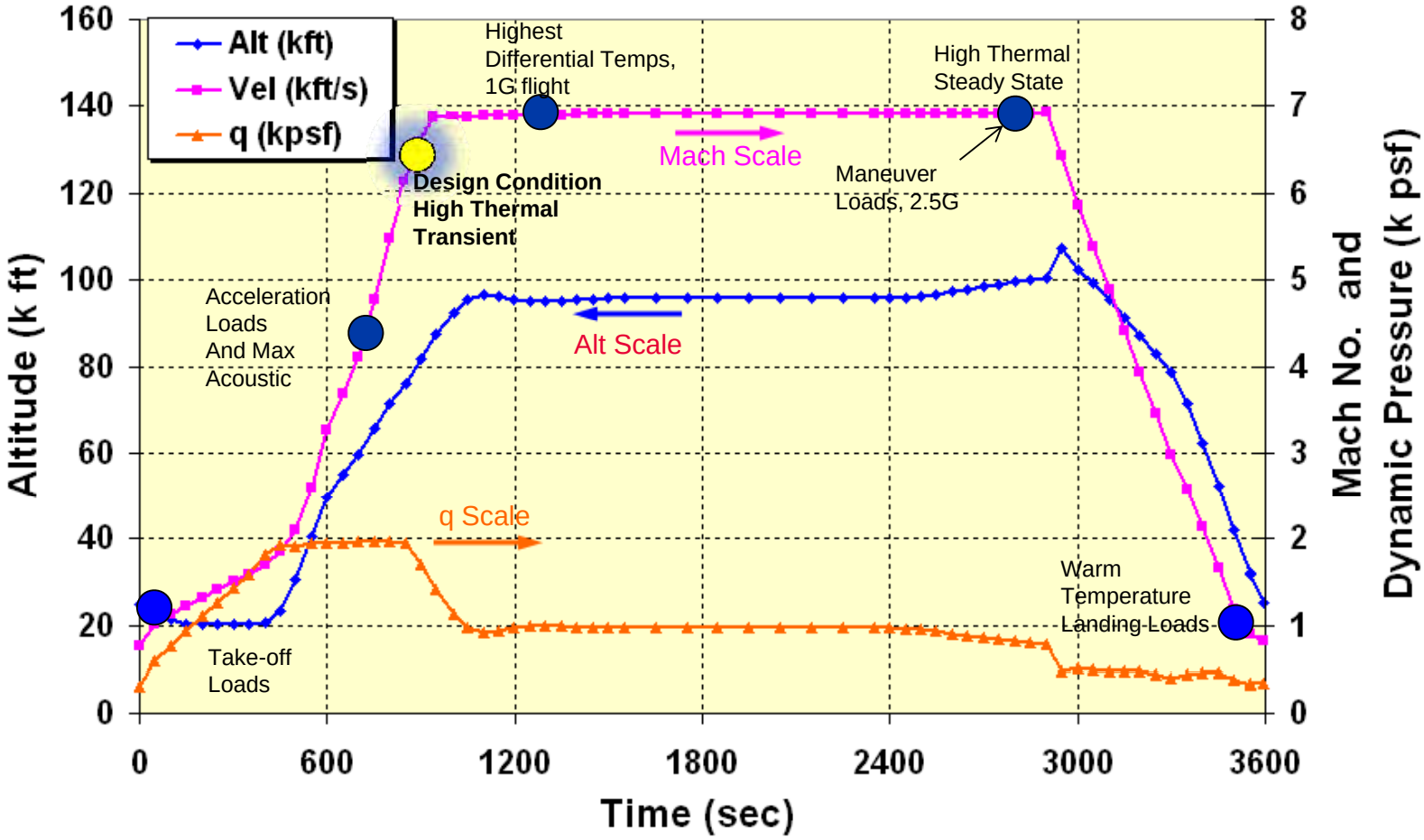

These are the Design Conditions of Interest for Dynamic & Fatigue Analysis.

Approved for public release; distribution unlimited.

Structural Damping

Frequency (Hz)	Damping Ratio, ζ
10	0.025
200	0.02
1000	0.01

```
$
TABDMP1  1        CRIT
         10.     .025     200.     .02       1000.
.01      ENDT
```

Nastran Damping Table Card

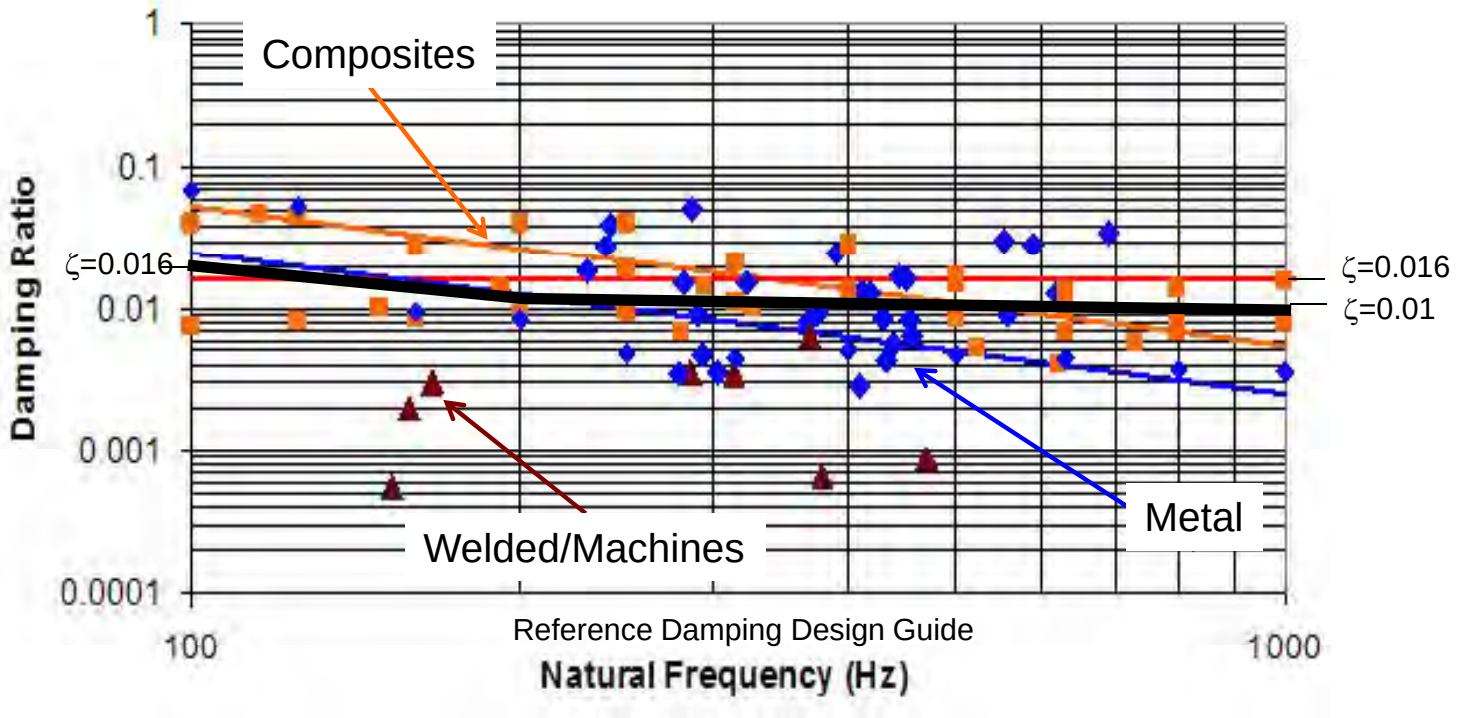

Dynamic Analysis uses the black curve

Approved for public release; distribution unlimited.

Panel 862 Location

Define acoustic levels for each panel and critical conditions:

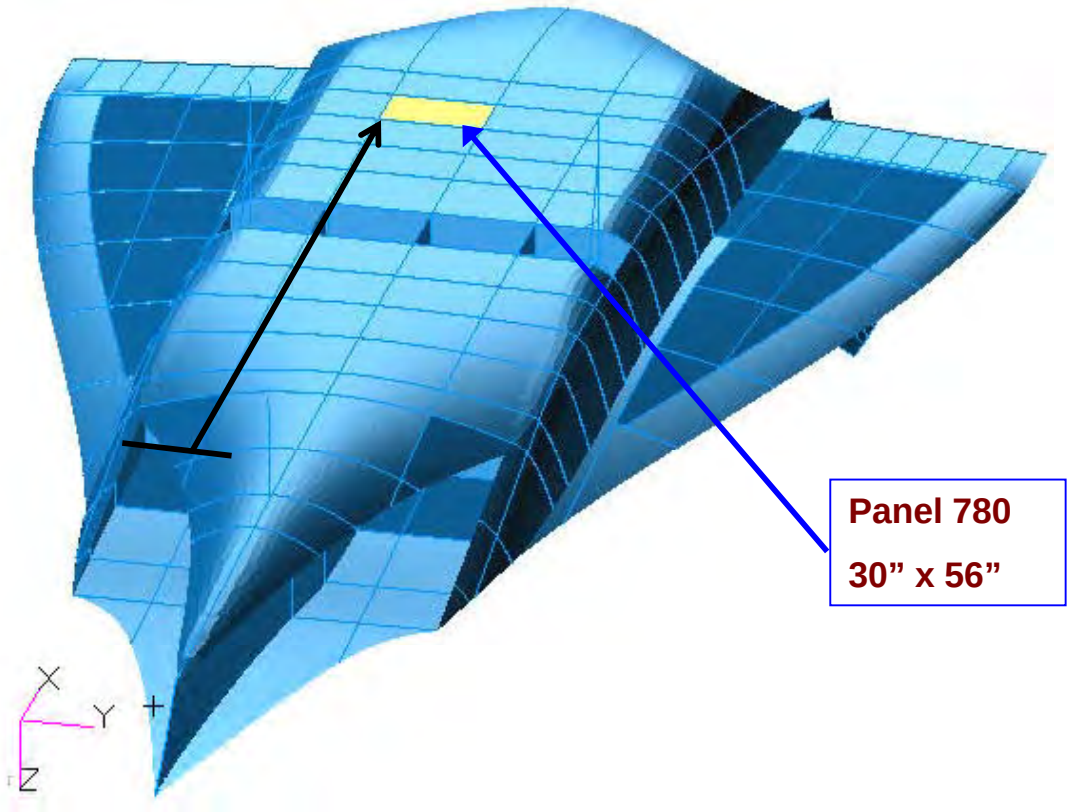

Distance from Lead Edge and Distance from Point of Separation are inputs to aero-acoustic models

Approved for public release; distribution unlimited.

CFD Results

CFD++ N-S Flow Field for M=7.0, α = 10 deg., Alt.=90Kft

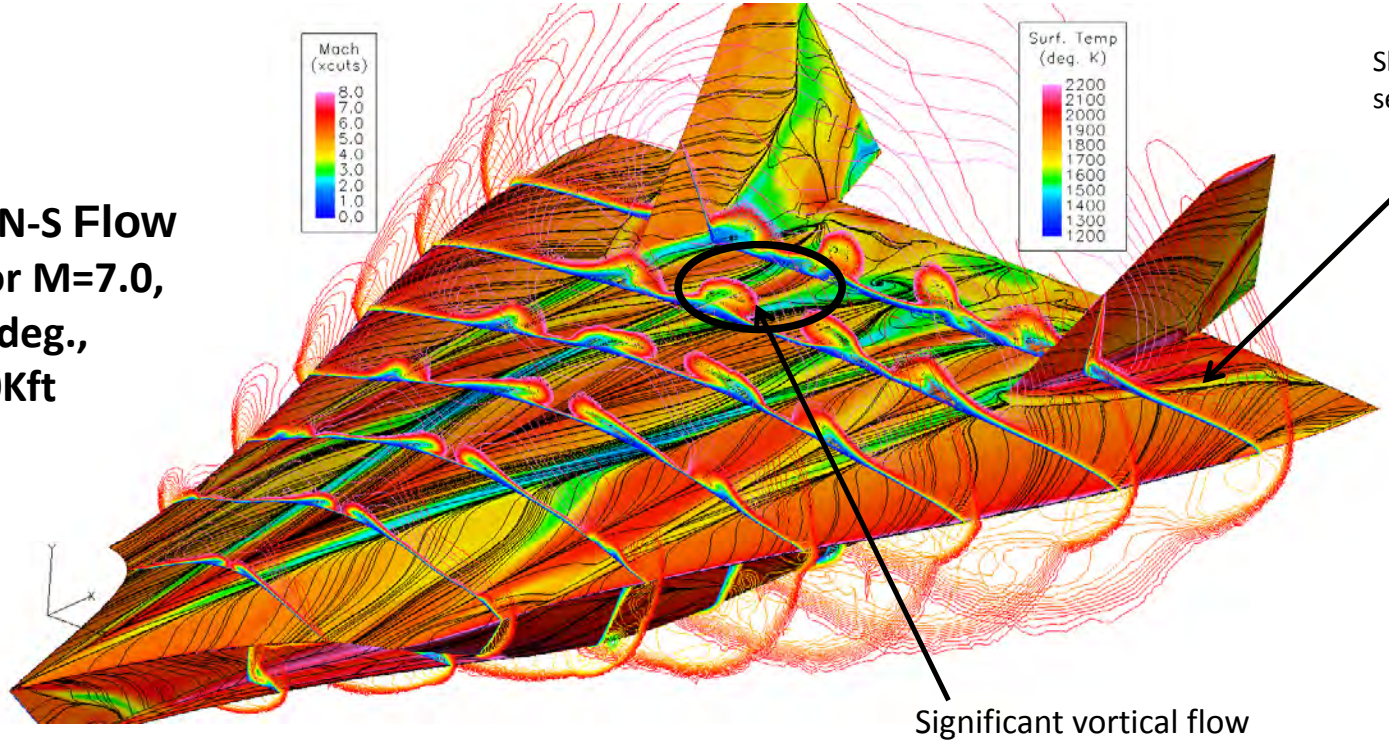

CFD was used to determine local flow features. This information was used in our Empirical models to predict acoustic loading spectrum

Approved for public release; distribution unlimited.

CFD Runs for Acoustic Loads

1.) Mach 7, 2.5g, AoA=10 deg, turn , Alt=90kft, q=1340 psf, Highest Maneuver and thermal loads (max G)

2.) Mach 7, 1.0g, AoA=4 deg, Cruise, Alt=100Kft, q=730 psf, High thermal loads and transient conditions (max T)

3.) Mach 6, 1.0g, AoA=6 deg, Accel, Alt= 75kft, q=2000 psf, Highest acoustic and thermal loads (max Q)

The load conditions for the detailed analysis was based on these are the three trajectory.

Approved for public release; distribution unlimited.

Required Data from CFD for Aero-acoustic Models

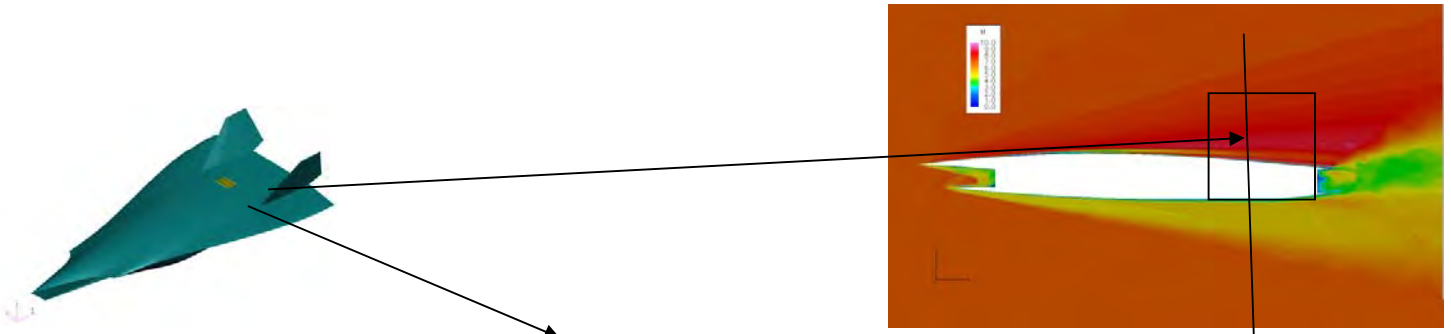

Streamline at center of panel

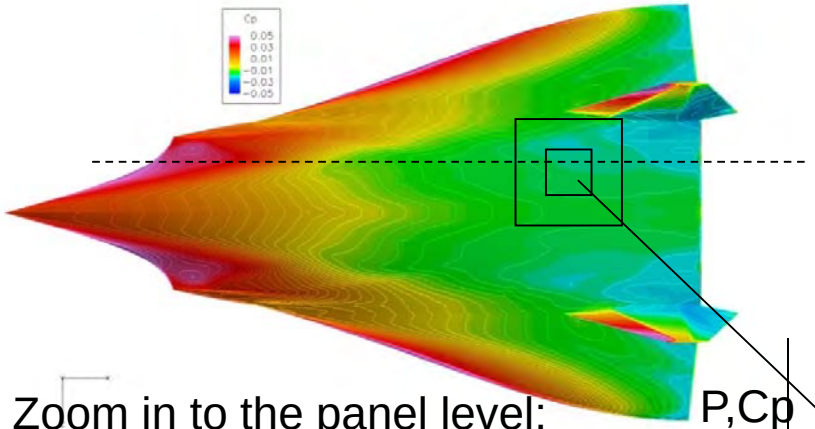

Zoom in to the panel level:

Graph of the pressure across
The panel at the Ctr line

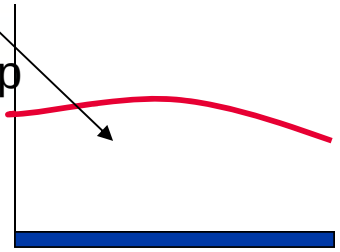

Velocity Profile

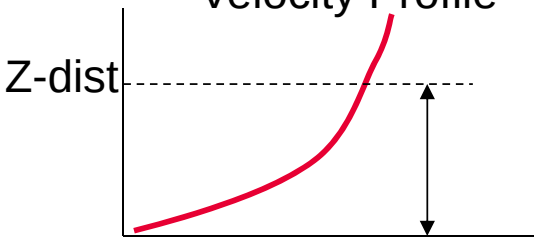

M,vel

An estimate of BL thick
At the leading edge of
the panel

Approved for public release; distribution unlimited.

CFD++ Computed Flow Field, M=6.0, a=6.0 deg., Alt.=75 Kft

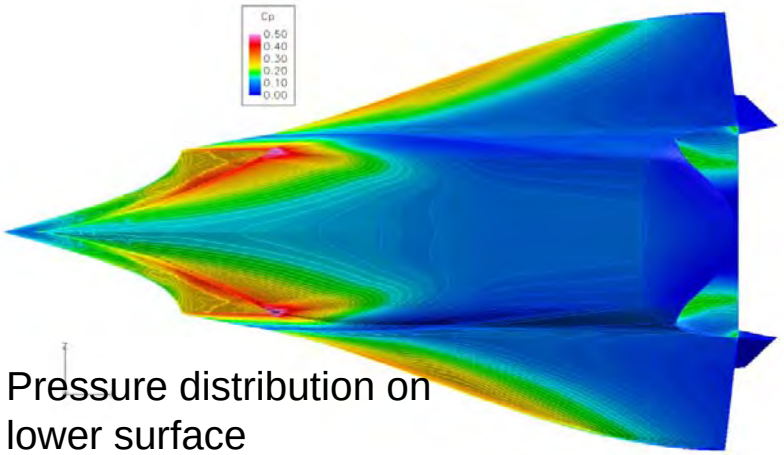

Pressure distribution on lower surface

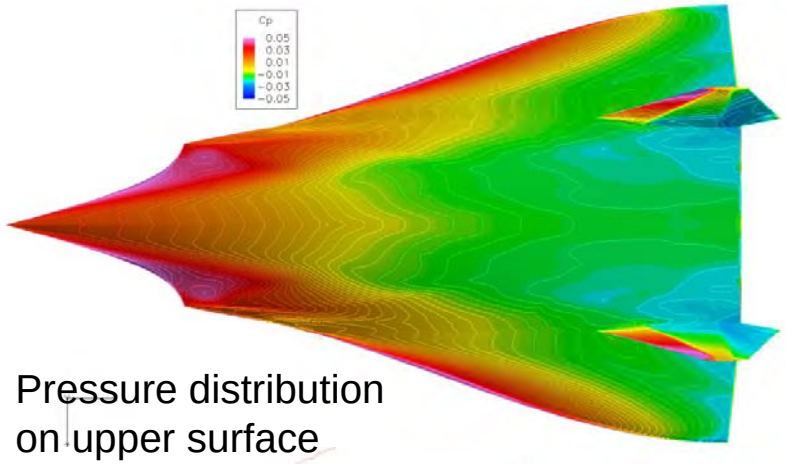

Pressure distribution on upper surface

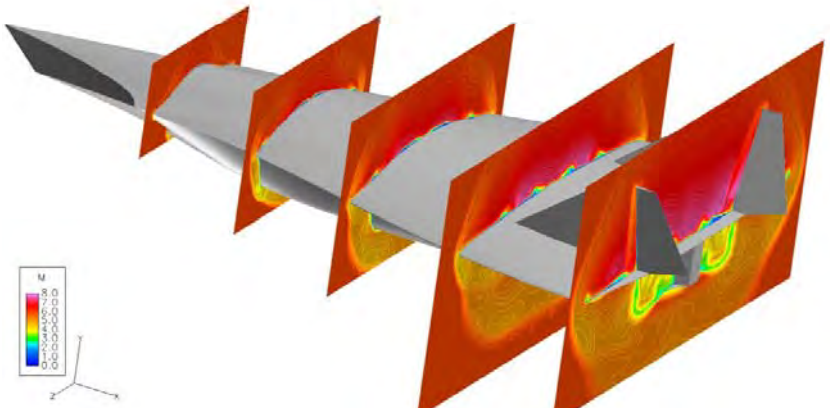

Mach No. at section cuts

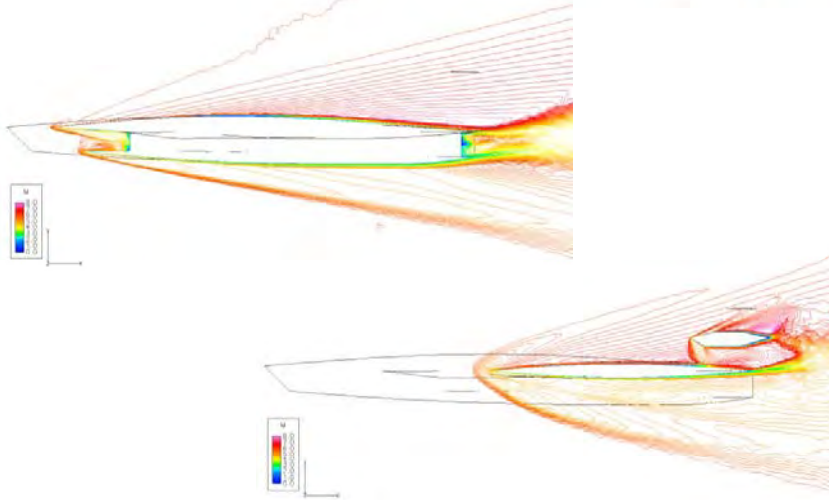

Approved for public release; distribution unlimited.

Computed Surface Pressures on the Panels

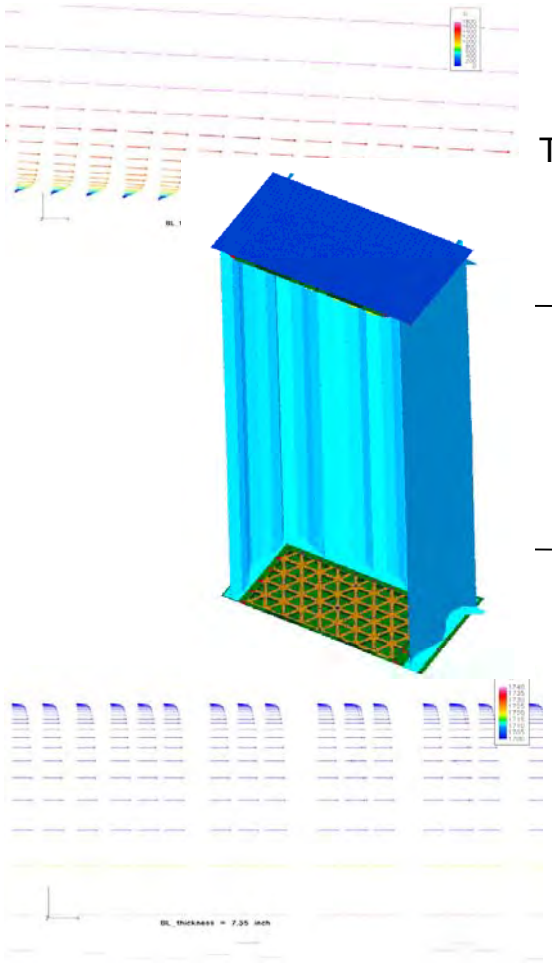

TBL_{ave}~11”

TBL_{ave}~7”

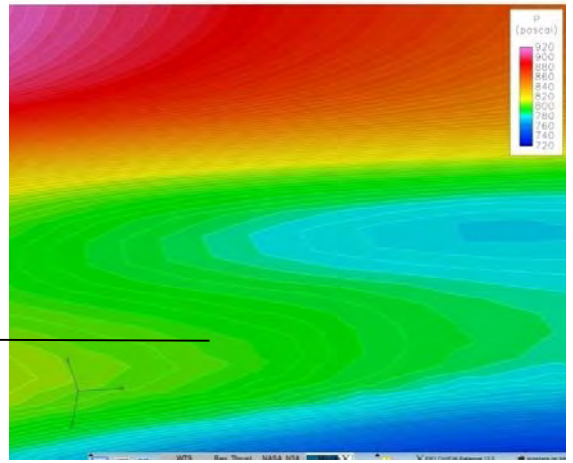

Panel 862
(Upper Surf)
ΔPy ~ 200 pa/m

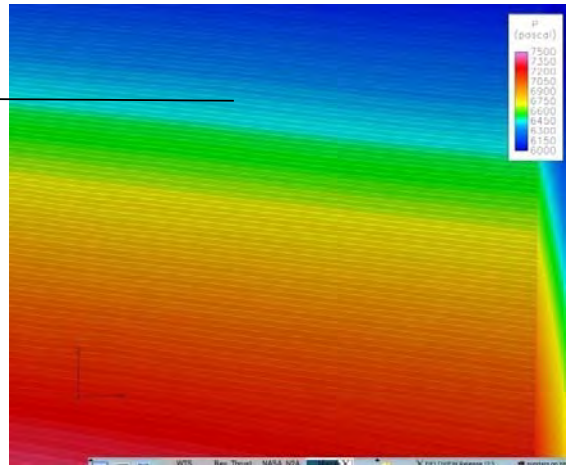

Panel 782
(Lower Surf)
ΔPy~1500 pa/m

Approved for public release; distribution unlimited.

Empirical Model Acoustic Prediction

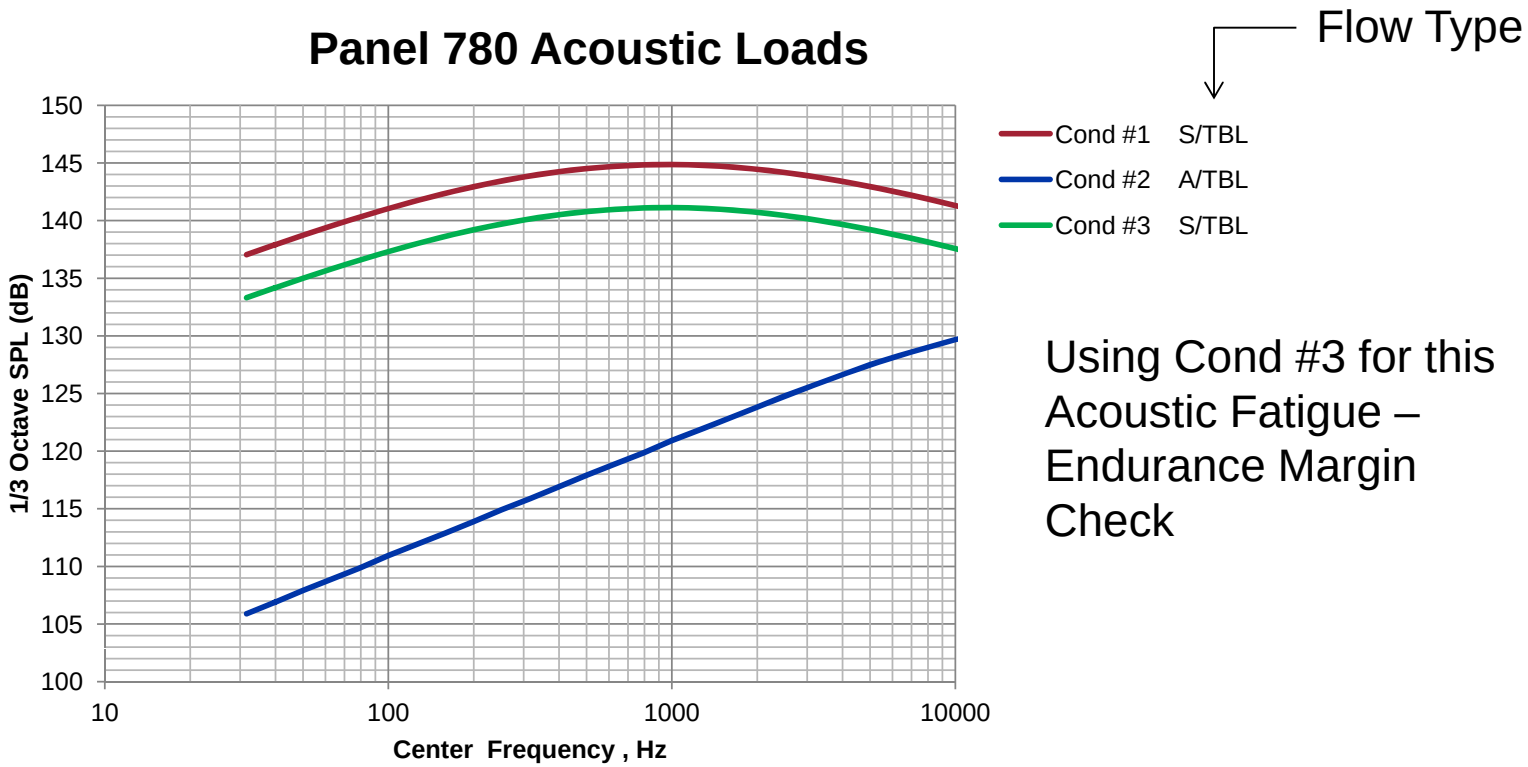

Using Cond #3 for this Acoustic Fatigue – Endurance Margin Check

Based on CFD input into Efimtsov TBL Models

Ref. R. Rackl, and A. Weston, "Modeling of Turbulent Boundary Layer Surface Pressure Fluctuation Auto and Cross Spectra - Verification and Adjustments Based on TU-144LL Data," NASA/CR-2005-213938.

Approved for public release; distribution unlimited.

Acoustic Damage Accumulation

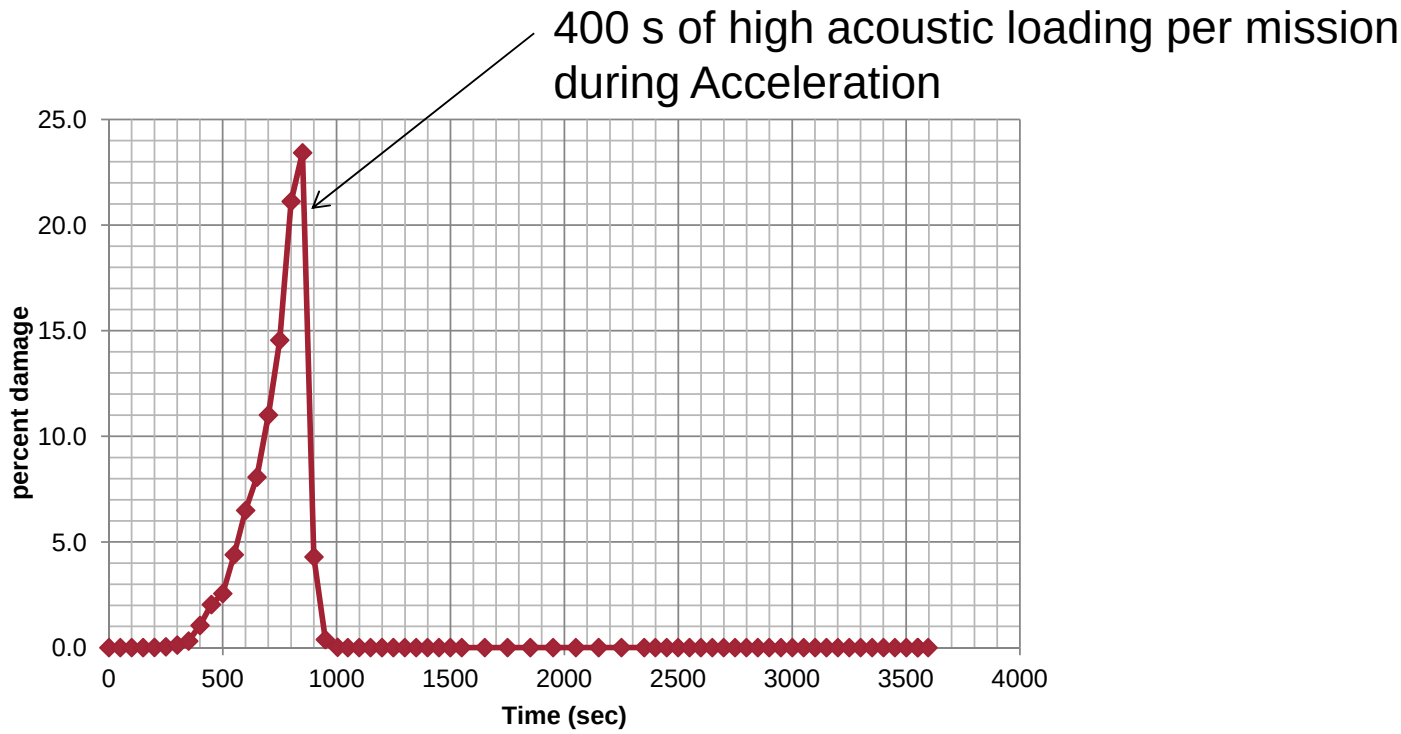

Acoustic Loads only critical during acceleration, add these stress cycles to fatigue spectrum

Approved for public release; distribution unlimited.

CAESAR DETAIL STRESS TOOL

Approved for public release; distribution unlimited.

CAESAR Description

- CAESAR (ComputAtional Engineering Structural Analysis Routines)
- CAESAR is a web based tool for determining detail stresses for open holes, filled holes, notches, fillets, etc
- User entered Input variables are submitted to stress check model templates which are executed on a remote server
- Results can be retrieved in multiple formats
- Details are given on stress check model and results calculations
- XML files and stress check model files can be saved for future runs

Approved for public release; distribution unlimited.

CAESAR Home Screen

Holes	Detail Stress Analysis	Notches, Fillets, etc.
Single Hole Cold Worked Single Hole Multi-Hole Multi-Loaded Holes Lug Rod End Cutout in Shear Reinforced Cutout (2D) Reinforced Cutout (3D) Reinforced Hole (3D) Nutplate	 *Please use Microsoft's Internet Explorer* Download SVG Install Package (Does not require admin privileges.)	Single Notch Double Notch Shallow Gradient Specimen Shoulder Fillet Web Fillet Stepped Flange (3D) Tension Fittings Multi-Hole Plate Buckling Reinforced Hole Plate Buckling Reinforced Cutout Plate Buckling
Questions or Problems? Email: CaesarSupport@Boeing.com Pager: 314-507-0531	First Time Users: Download Overview Charts	Change Log: • Functional change 12/19/2007

375
Approved for public release; distribution unlimited.

Example CAESAR INPUT – Single Hole Detail

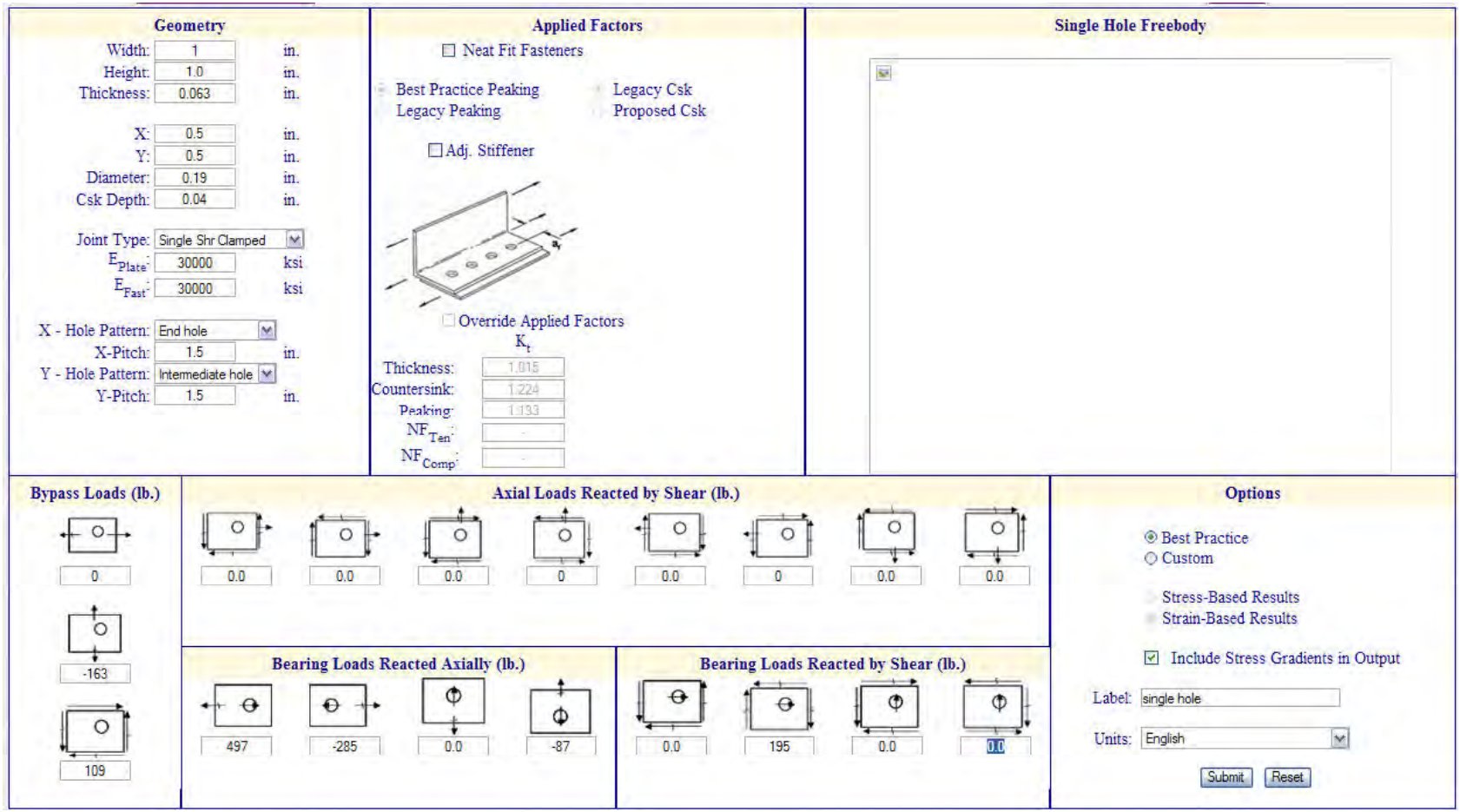

Approved for public release; distribution unlimited.

Example CAESAR Result – Single Hole Detail

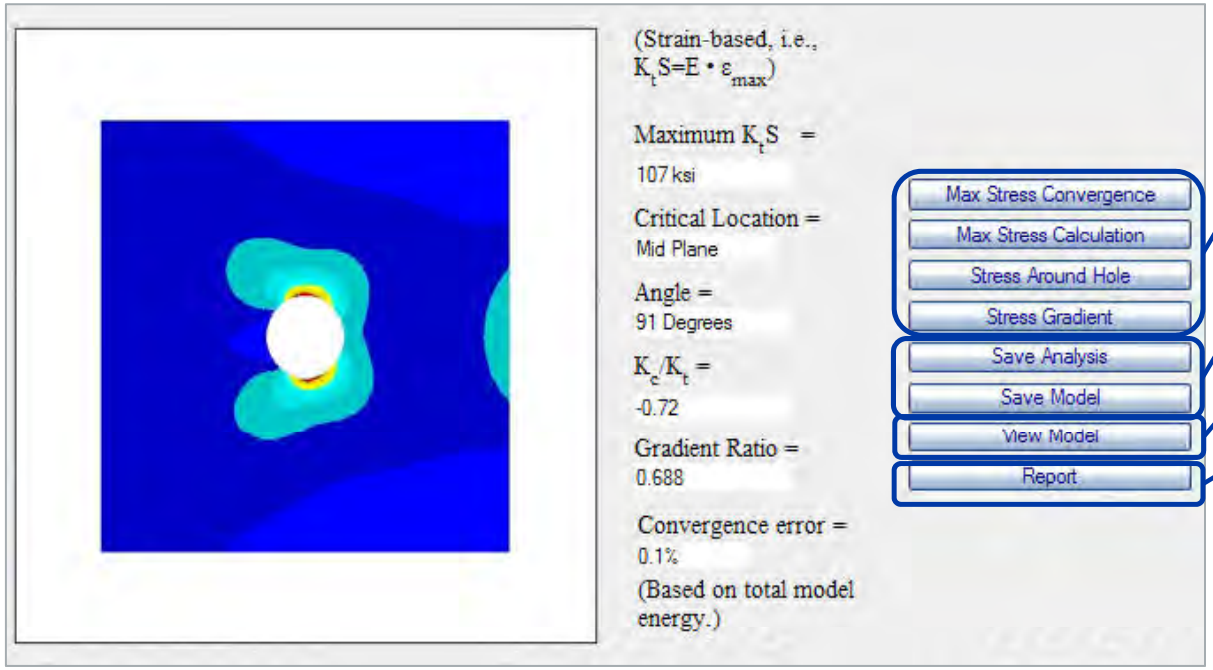

Details on solution and calculation of maximum stress

Options to save the solution or stress check model files

Interactive view of stress check model

Create a report in html or MS Word formats

377
Approved for public release; distribution unlimited.

STATIC RESULTS

Approved for public release; distribution unlimited.

Global Displacement SOL 101 v. SOL 106

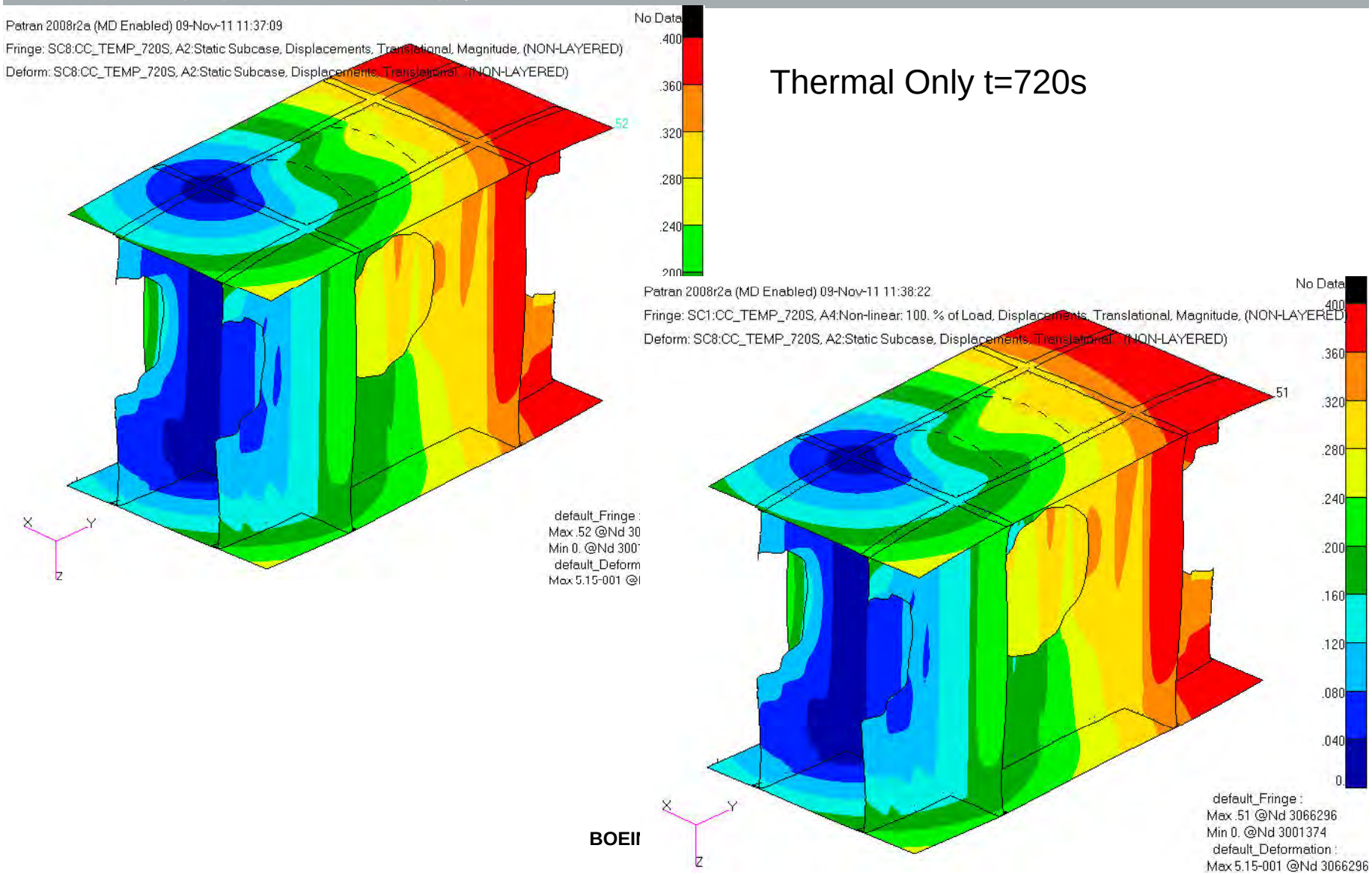

Approved for public release; distribution unlimited.

Panel Displacement SOL 101 v. SOL 106

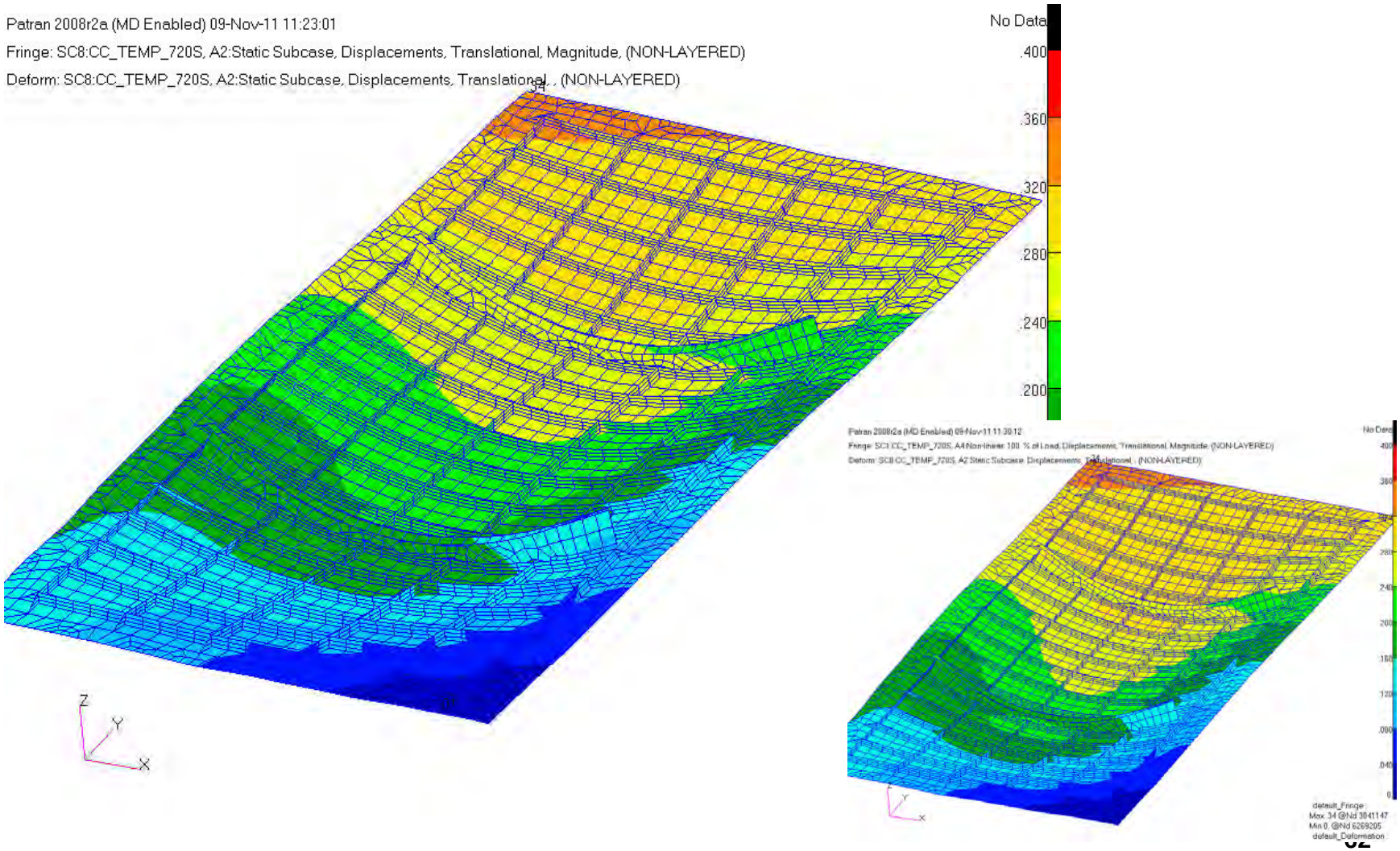

Approved for public release; distribution unlimited.

Panel 2 Stress: SOL 101 v. SOL 106

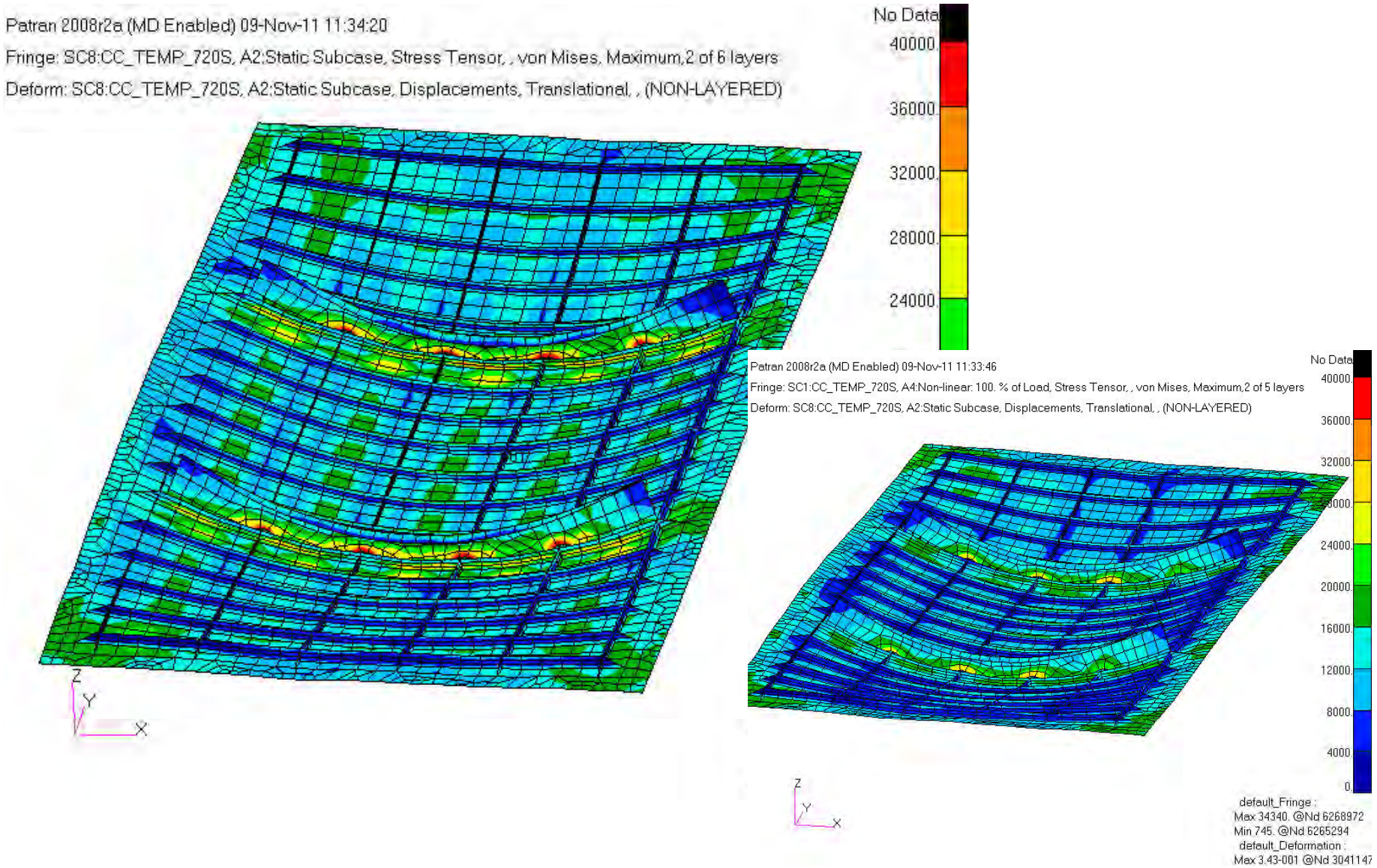

Approved for public release; distribution unlimited.

Engineering, Operations & Technology
Boeing Research & Technology

Panel 816 Heat Transfer Analysis

November 7, 2011

Pete Keller
206-544-7528
peter.c.keller@boeing.com

Approved for public release; distribution unlimited.

Analysis Approach and Assumptions

- Transient analysis, temperature dependant material properties
- All structure modeled with shell elements: through-thickness gradients not significant
- Uniform initial temperature = recovery temperature at M=0.75, 25kft
- Aerothermal environment provided from MINIVER Mach 7 trajectory Analysis
- Fuel assumed to occupy 80% of internal volume, modeled as lumped mass
- Uniform insulation thickness between fuel and inlet,frames and lower panel
- No internal radiation or convection between panel and substructure. Volume assumed to be occupied by fuel and surrounding insulation.

Approved for public release; distribution unlimited.

Panel 816 Thermal Boundary Conditions

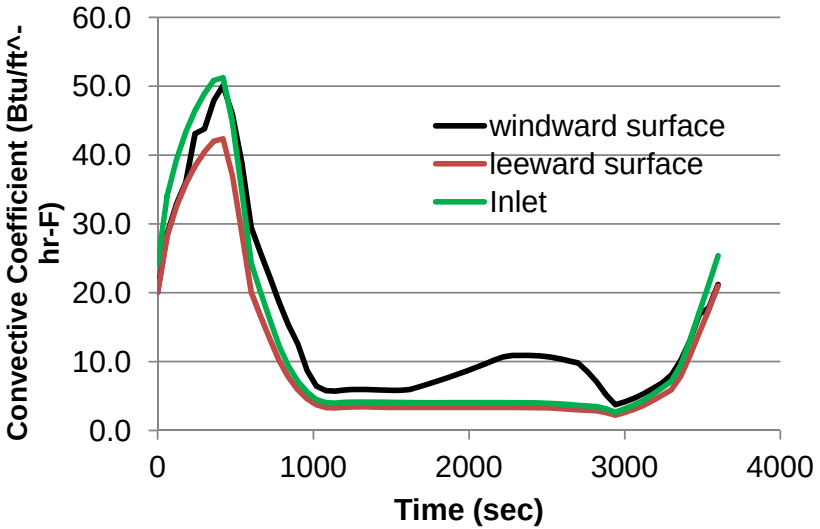

Panel 816 Aerothermal Environment

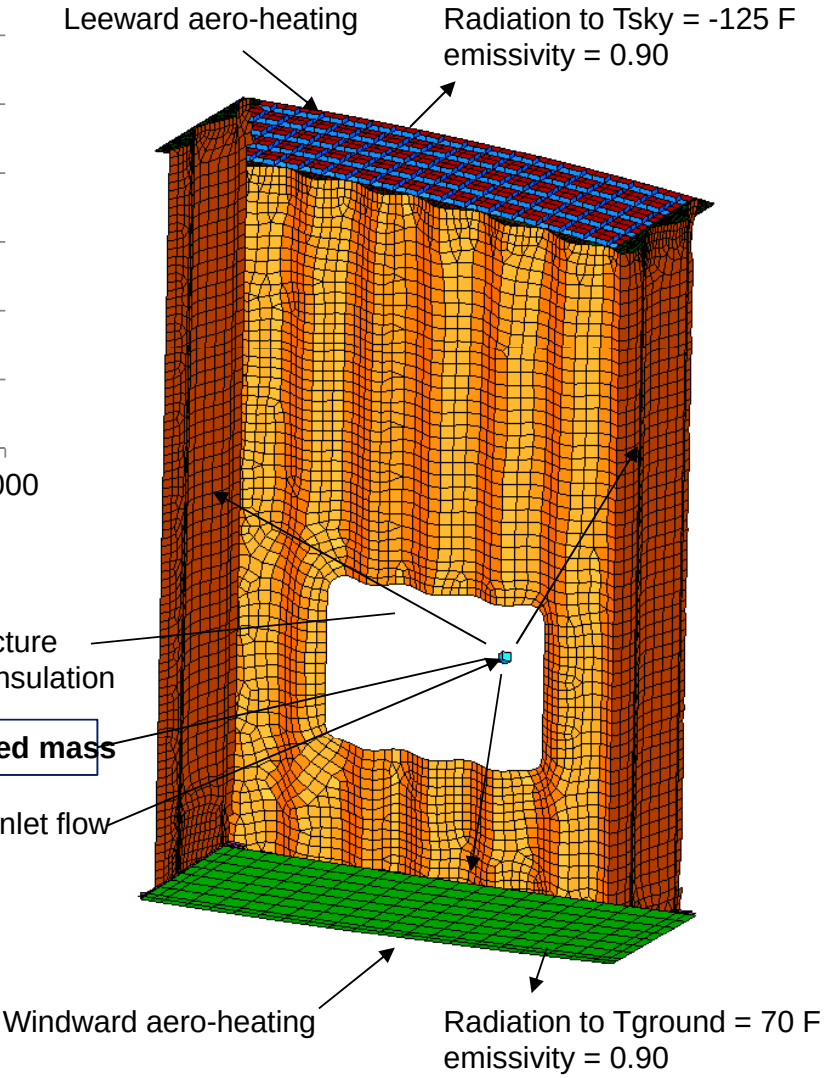

Approved for public release; distribution unlimited.

Panel 816 Thermal Analysis

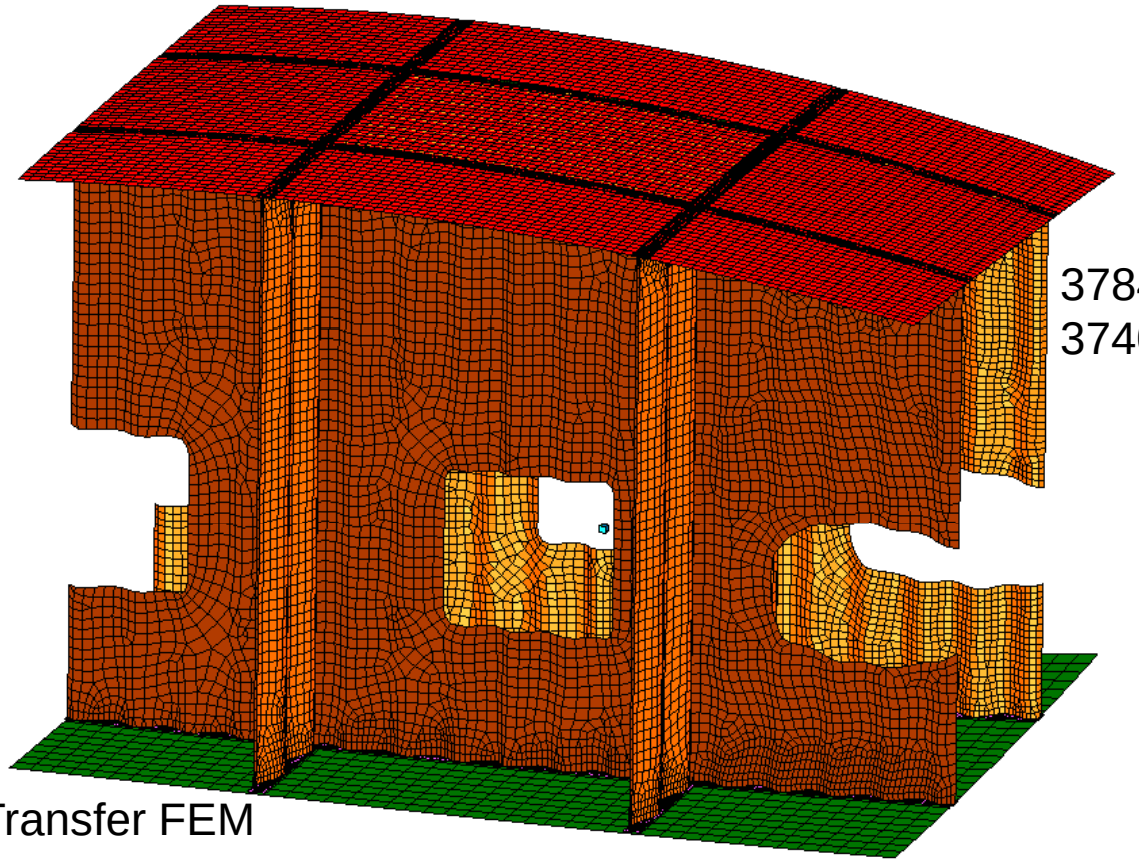

37849 nodes
37409 elements

Heat Transfer FEM

Approved for public release; distribution unlimited.

Panel 816 Temperature Distributions

60 sec - maximum panel temperature gradients

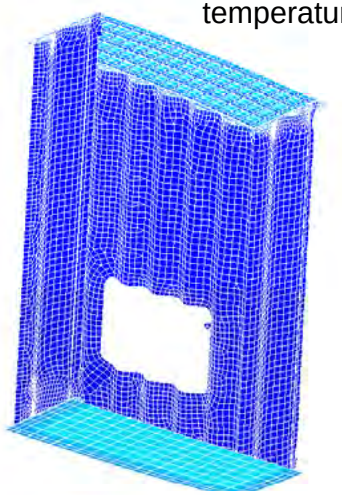

900 sec – maximum substructure temperature gradients

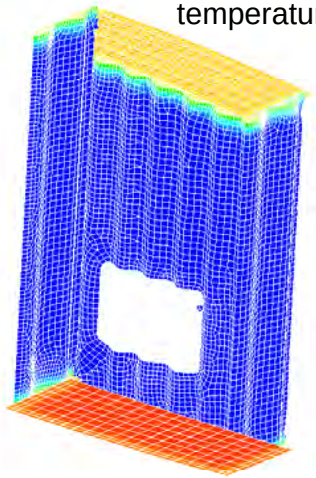

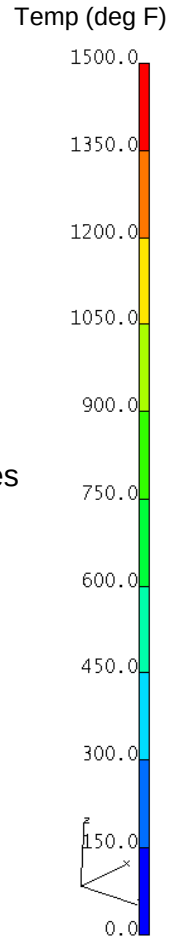

2400 sec – maximum temperatures

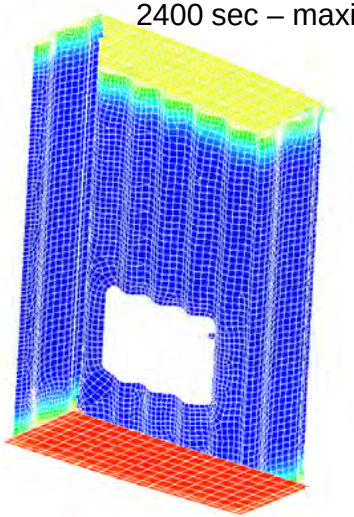

3480 sec – maximum negative temperature gradients

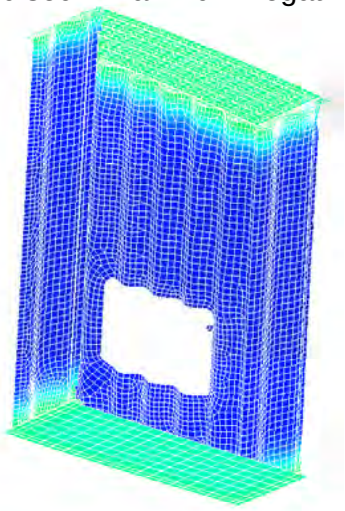

Approved for public release; distribution unlimited.

Panel 816 Temperature History

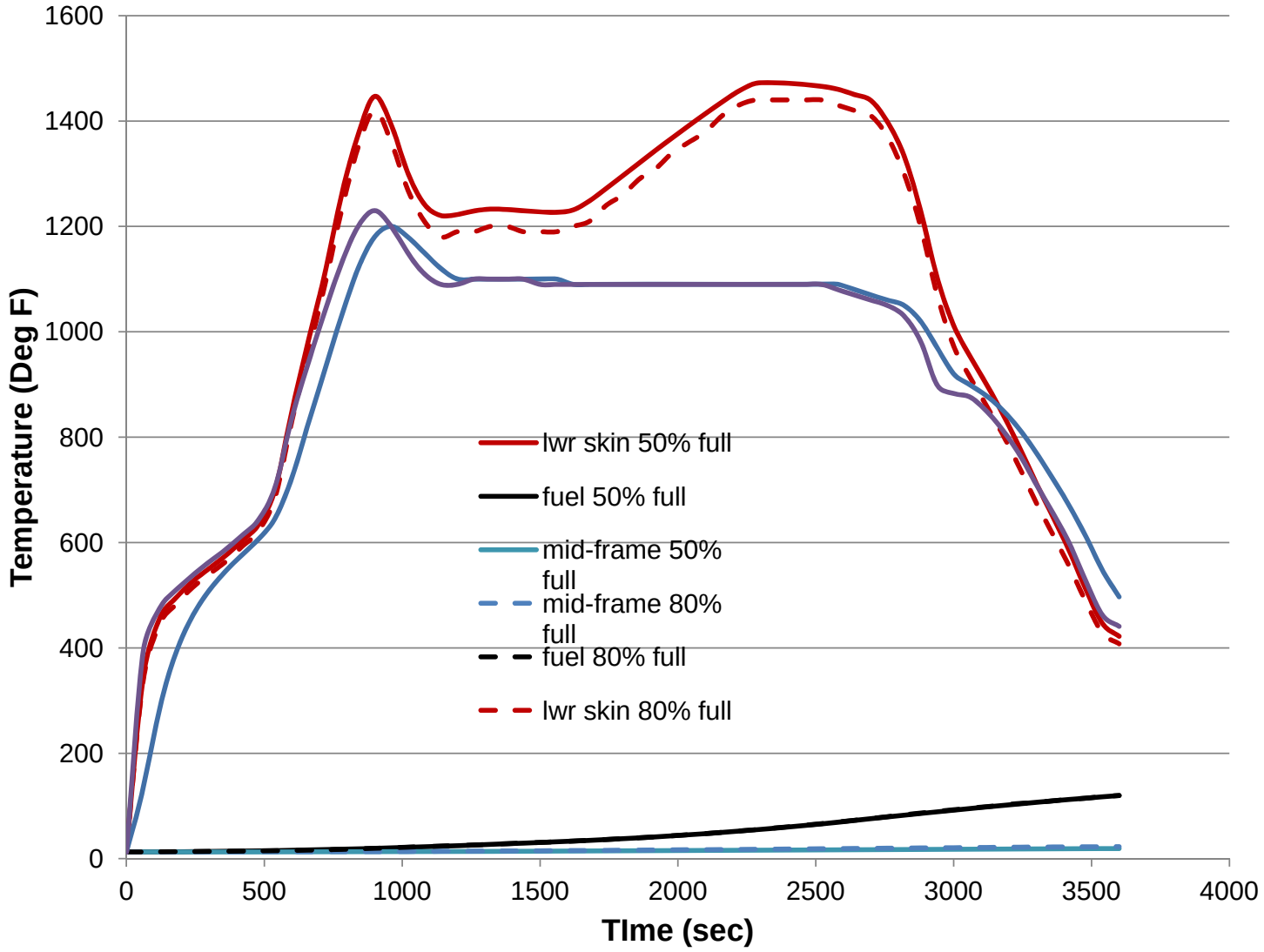

Approved for public release; distribution unlimited.

Panel 816 Temperature Gradient History

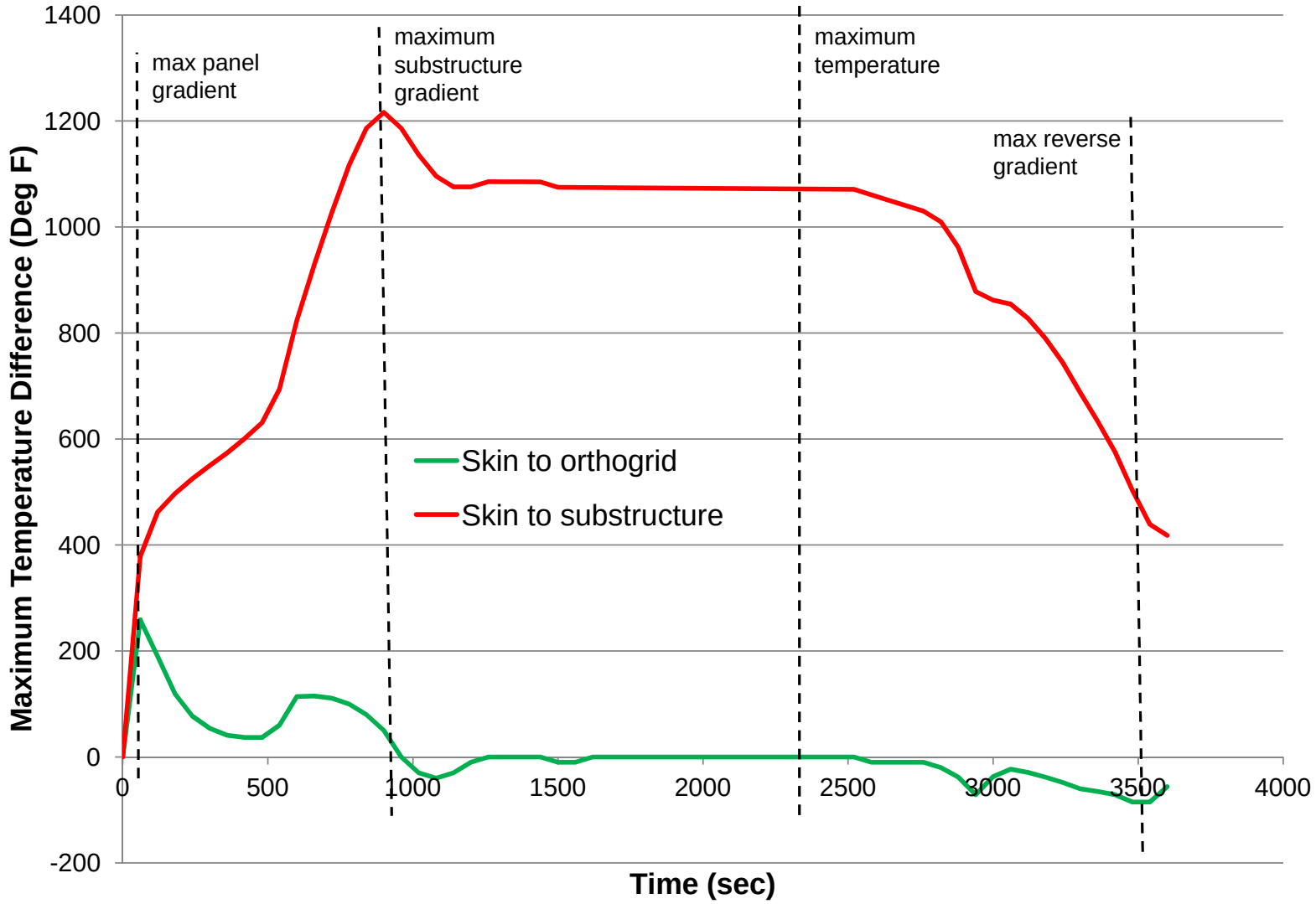

Approved for public release; distribution unlimited.

Summary of Results

- maximum skin temperatures = 1230 F at 900 sec
- maximum allowable fuel temperature = 120 F
- maximum temperature gradient in the panel = 378 F at 60 sec
- maximum temperature gradient between skin and substructure = 1216 F at 900 sec
- assumed fraction of internal volume occupied by fuel has little effect on results - 5 deg F substructure temperature difference between 80% and 50% fuel capacity

Approved for public release; distribution unlimited.

Research & Technology

Panel 3 (816) Static Stress Analysis

January 11, 2012

Tricia Carr
Patricia.J.Carr@boeing.com
562-797-2862
BR&T Structures Technology

Approved for public release; distribution unlimited.

Panel Analysis Study

Unit Cell Static Analysis (linear): 2.5G ultimate (FS=1.5), no Temp

1. P3 run with mech loads from global model and SPC's to remove rigid-body motion; loads are balanced (reactions at supports ≈ zero)
2. Large deformation in center frame web, due to large skin loads and the fact that the web is not restrained at mid-cutout.

Unit Cell Static Analysis (linear): 2.5G ULT, T(900s)

1. Timestep T(900s) is critical case, max displacement and stress.

Panel local model Static Analyses:

Static linear: 2.5G ULT, T(900s)

1. Applied displacement from unit-cell model as boundary condition to center panel for 2.5G ULT + Temp(900s)
2. Results match Unit Cell model

Static nonlinear: 2.5G ULT, T=900s

1. Max stress lower than linear analysis
2. Out of plane displacement greater than design criterion

Buckling analysis: 2.5G LIM (LF=1.15), T=900s

1. First panel eigenvalue < 1

Approved for public release; distribution unlimited.

Unit Cell

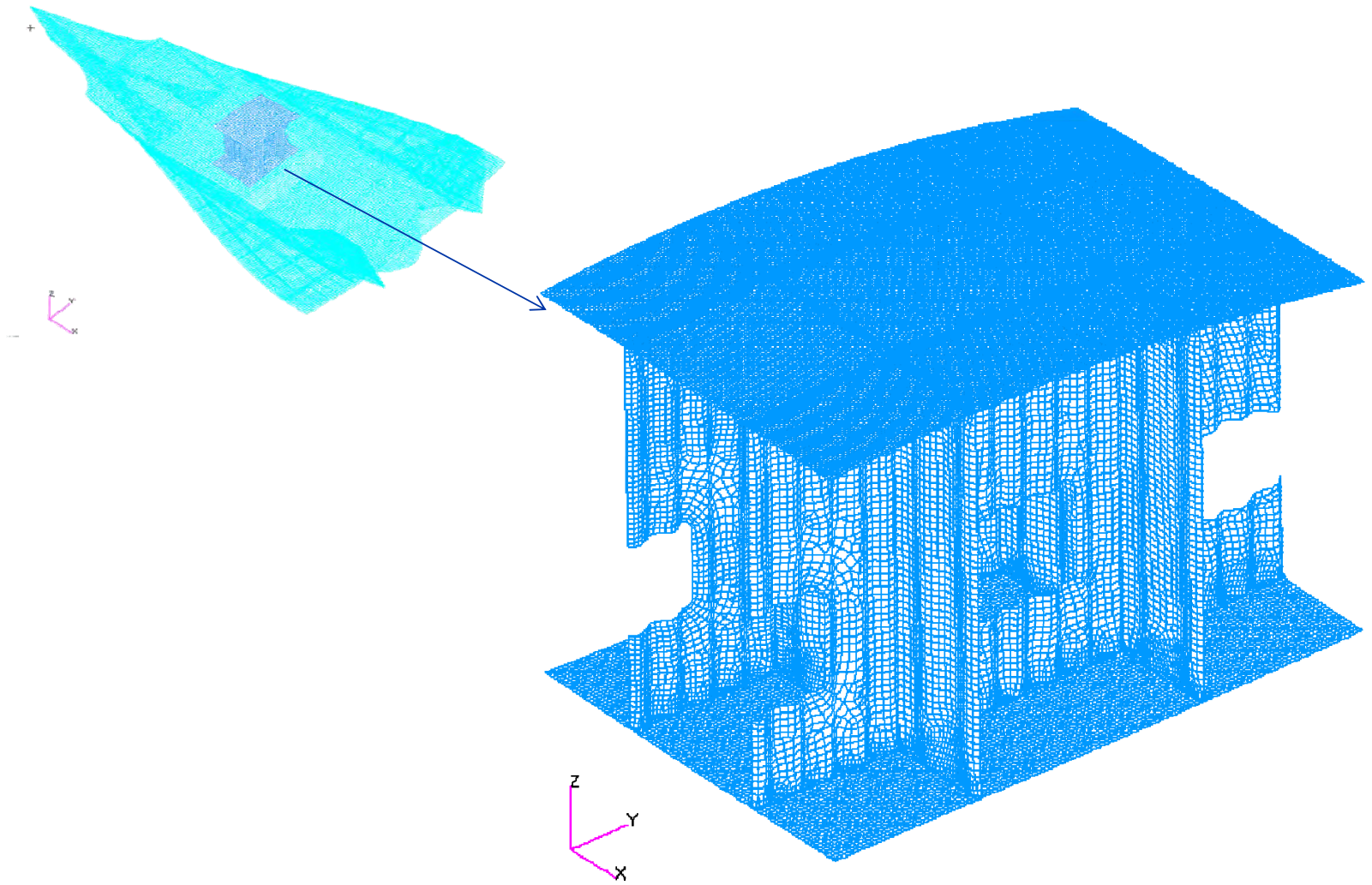

Approved for public release; distribution unlimited.

Constraints on Rigid Body Motion

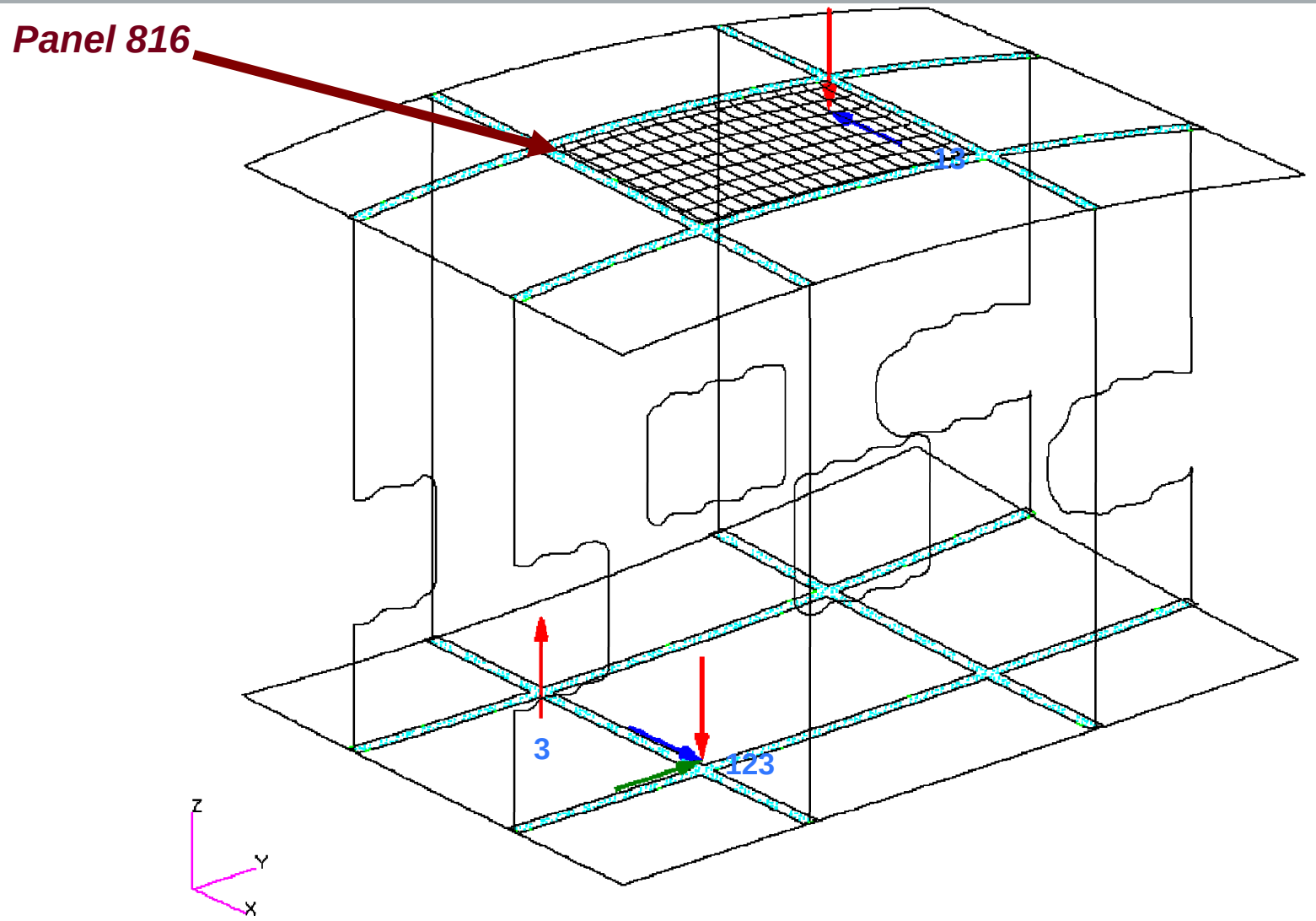

Approved for public release; distribution unlimited.

SPC force — Rigid Body Constraints

Load case: 2.5g mechanical loads

Load case is balanced (RB motion constraint forces are small)

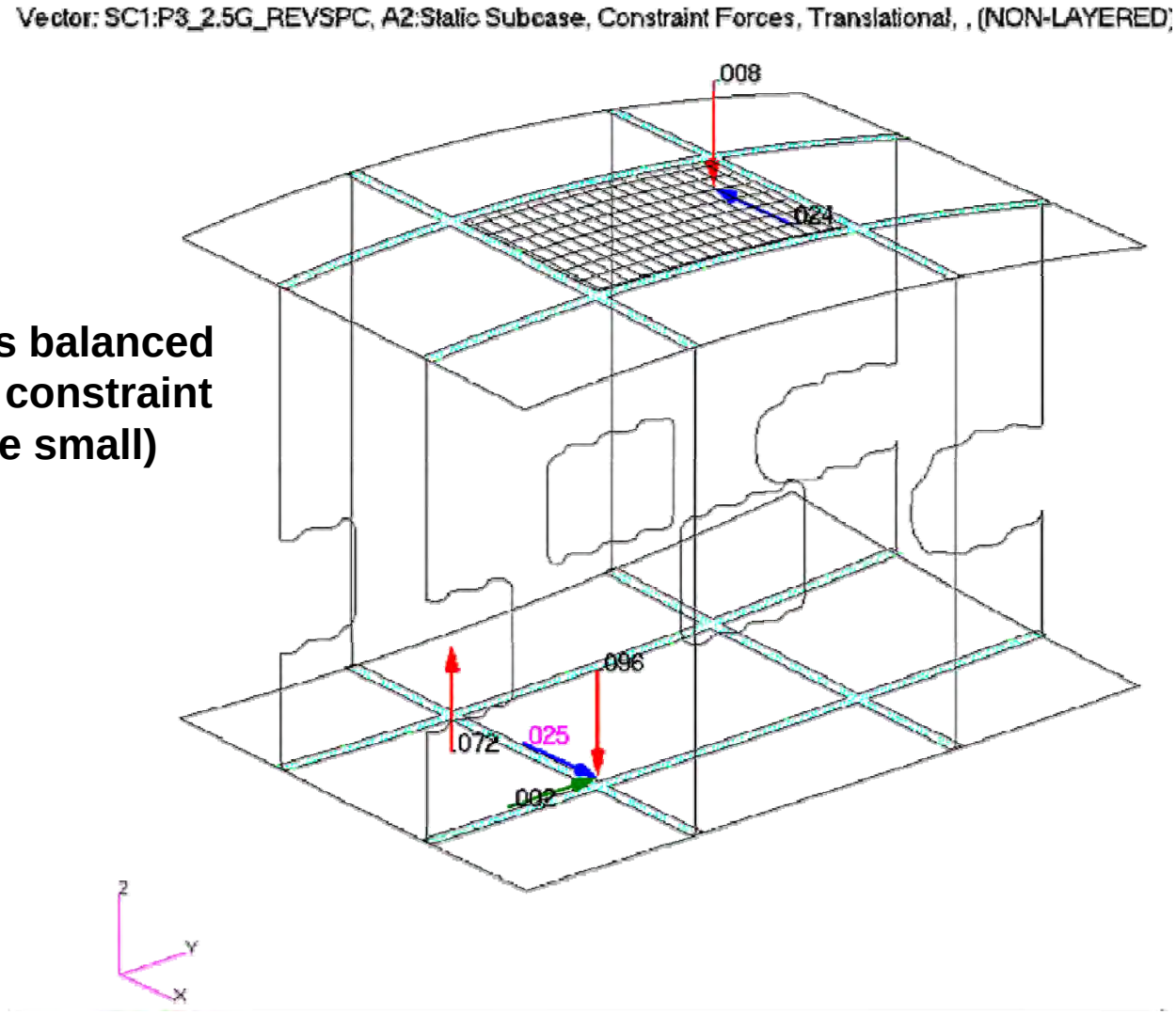

Approved for public release; distribution unlimited.

Unit Cell – Loading Conditions: Mechanical

2.5 G Mechanical Loads extracted from Vehicle FEM are applied to RBE3's which spread the load to Unit Cell nodes

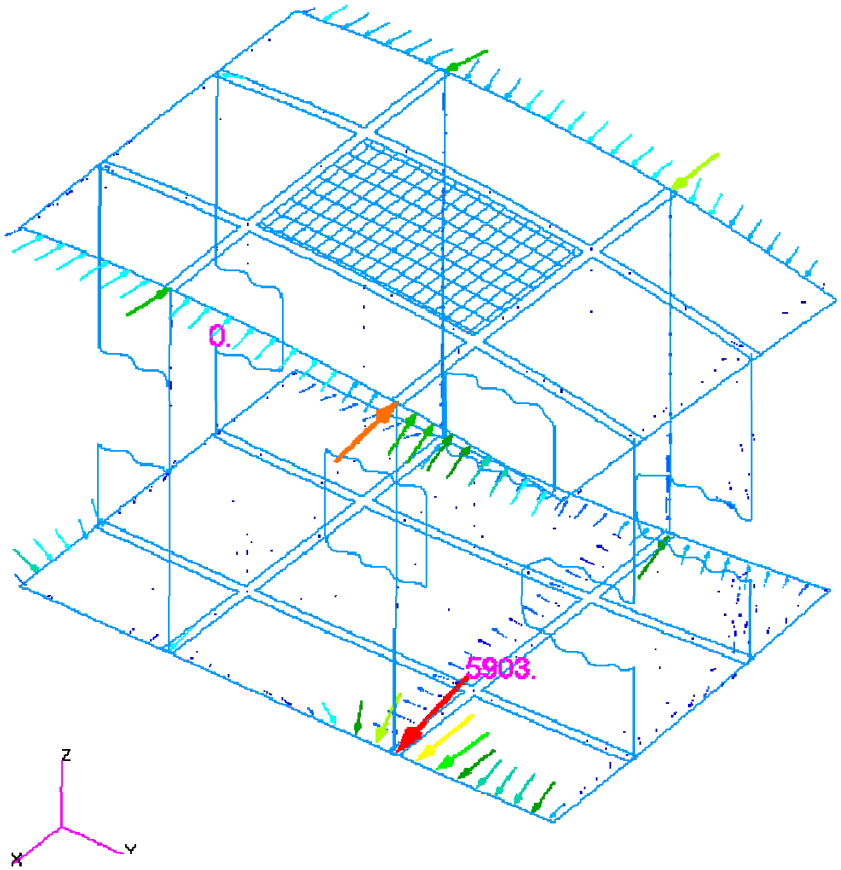

forces

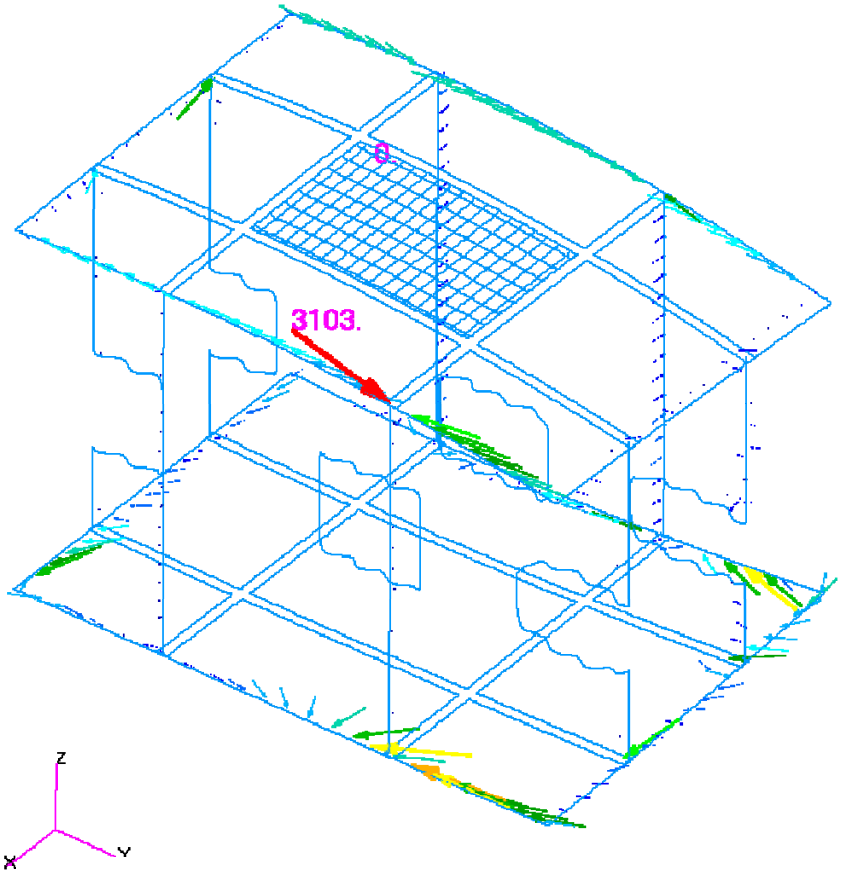

moments

Approved for public release; distribution unlimited.

SLL8

Inconel 718 Allowables @ 1220º F

MIL-HDBK-5H
1 December 1998

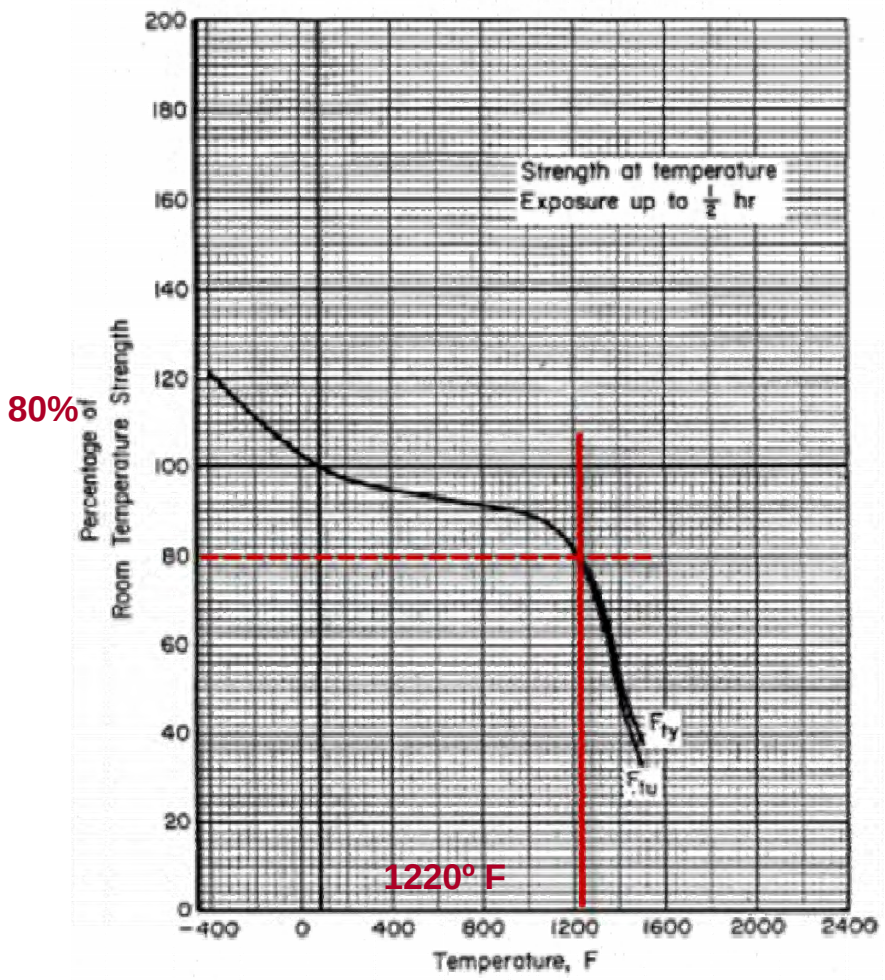

Figure 6.3.5.1.1. Effect of temperature on the tensile ultimate strength (F_{tu}) and tensile yield strength (F_{ty}) of solution-treated and aged Inconel 718.

Allowables @ 1220º F *80% knockdown*	
F_{tu}	144 ksi
F_{bru}	247 ksi

(1220° is temperature for skin only; conservative)

Approved for public release; distribution unlimited.

SLL8 What the significance of 850F?
Salvatore L Liguore, 12/8/2011

Approved for public release; distribution unlimited.

Panel 816 Temperature Gradient History

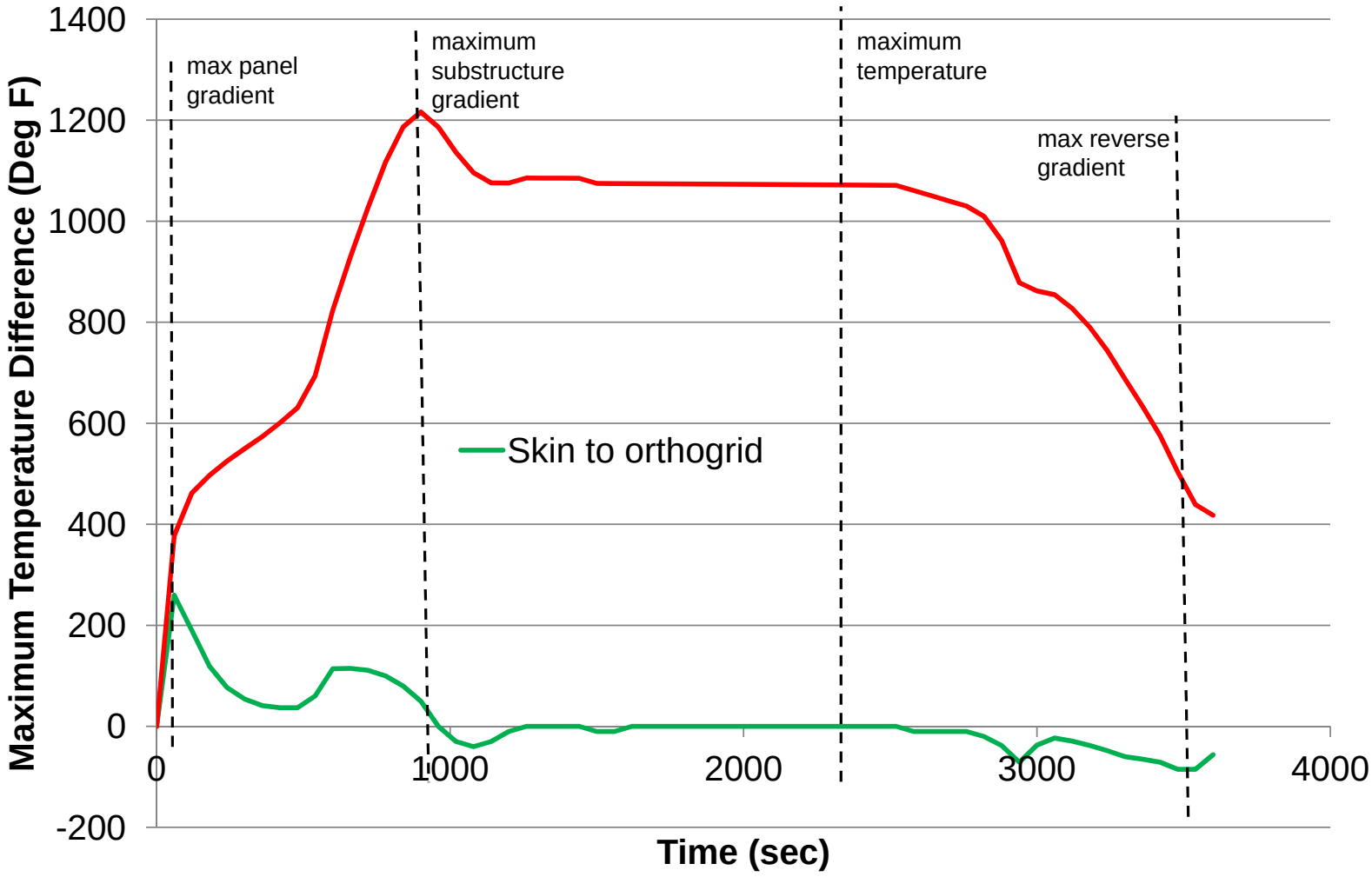

Approved for public release; distribution unlimited.

Unit Cell – Loading Conditions: Thermal

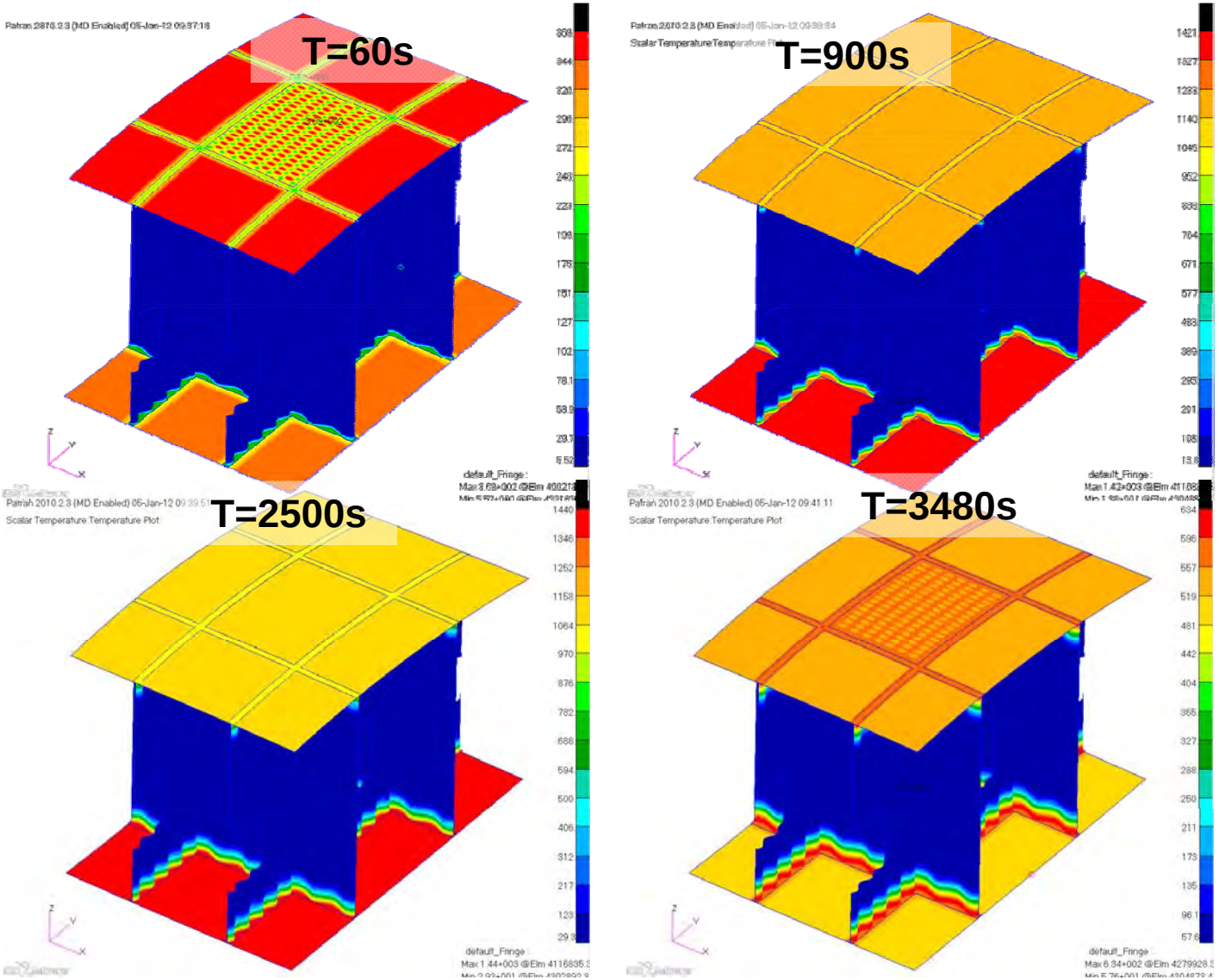

Approved for public release; distribution unlimited.

Unit Cell – Loading Conditions

Thermal Load T=60s

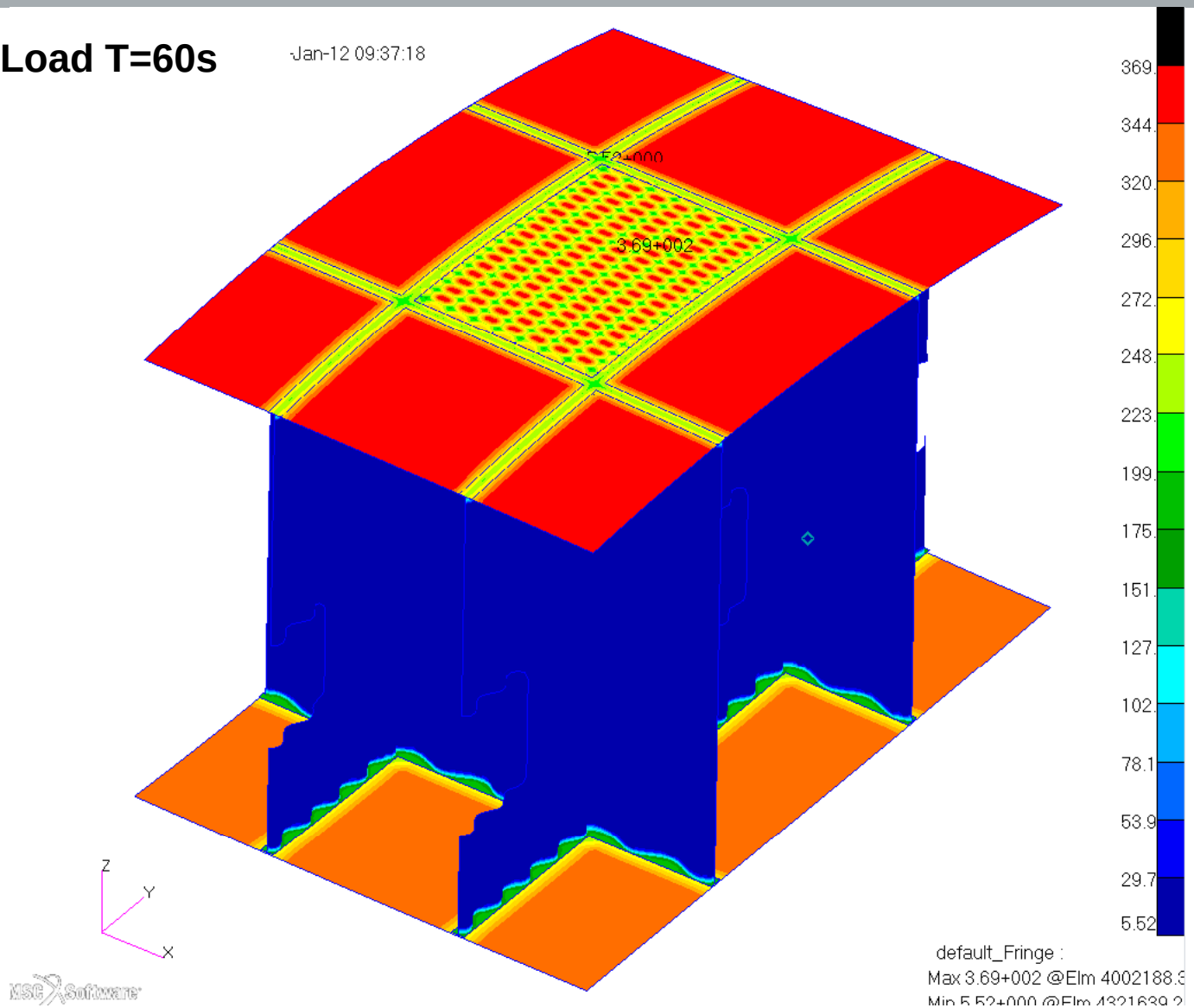

Approved for public release; distribution unlimited.

Unit Cell – Loading Conditions

Thermal Load T=900s

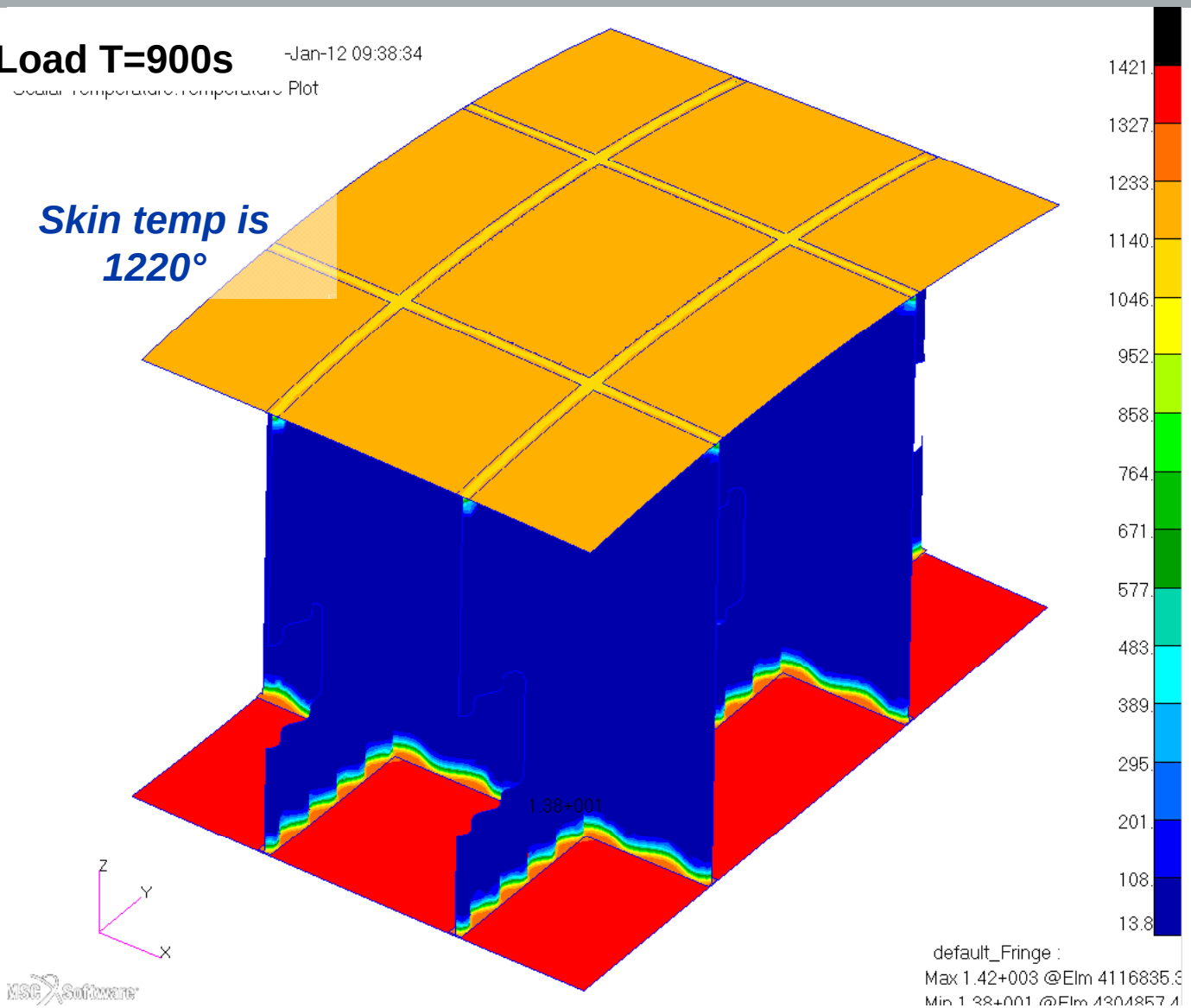

Approved for public release; distribution unlimited.

Unit Cell – Loading Conditions

Thermal Load T=2500s

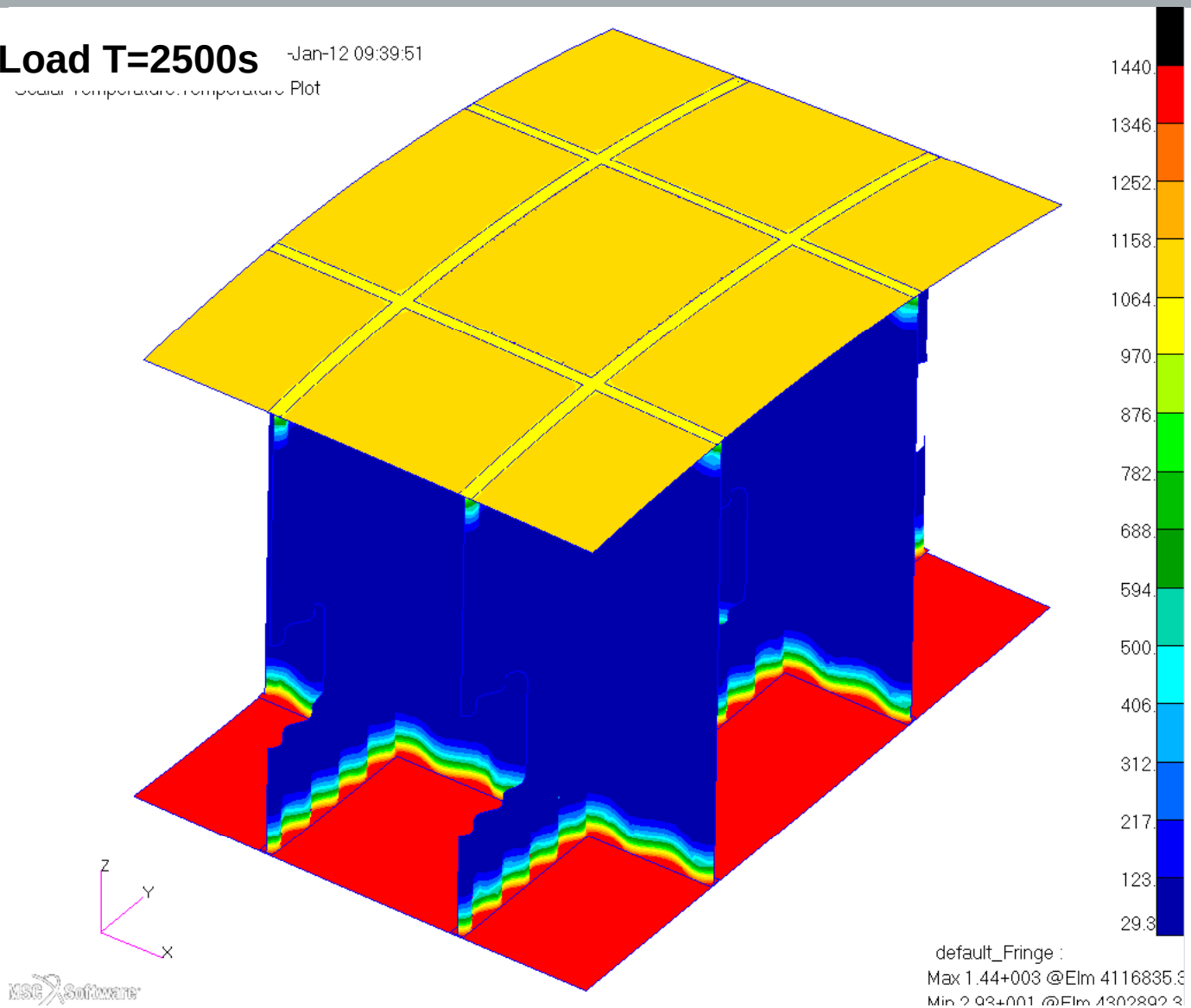

Approved for public release; distribution unlimited.

Unit Cell – Loading Conditions

Thermal Load T=3480s

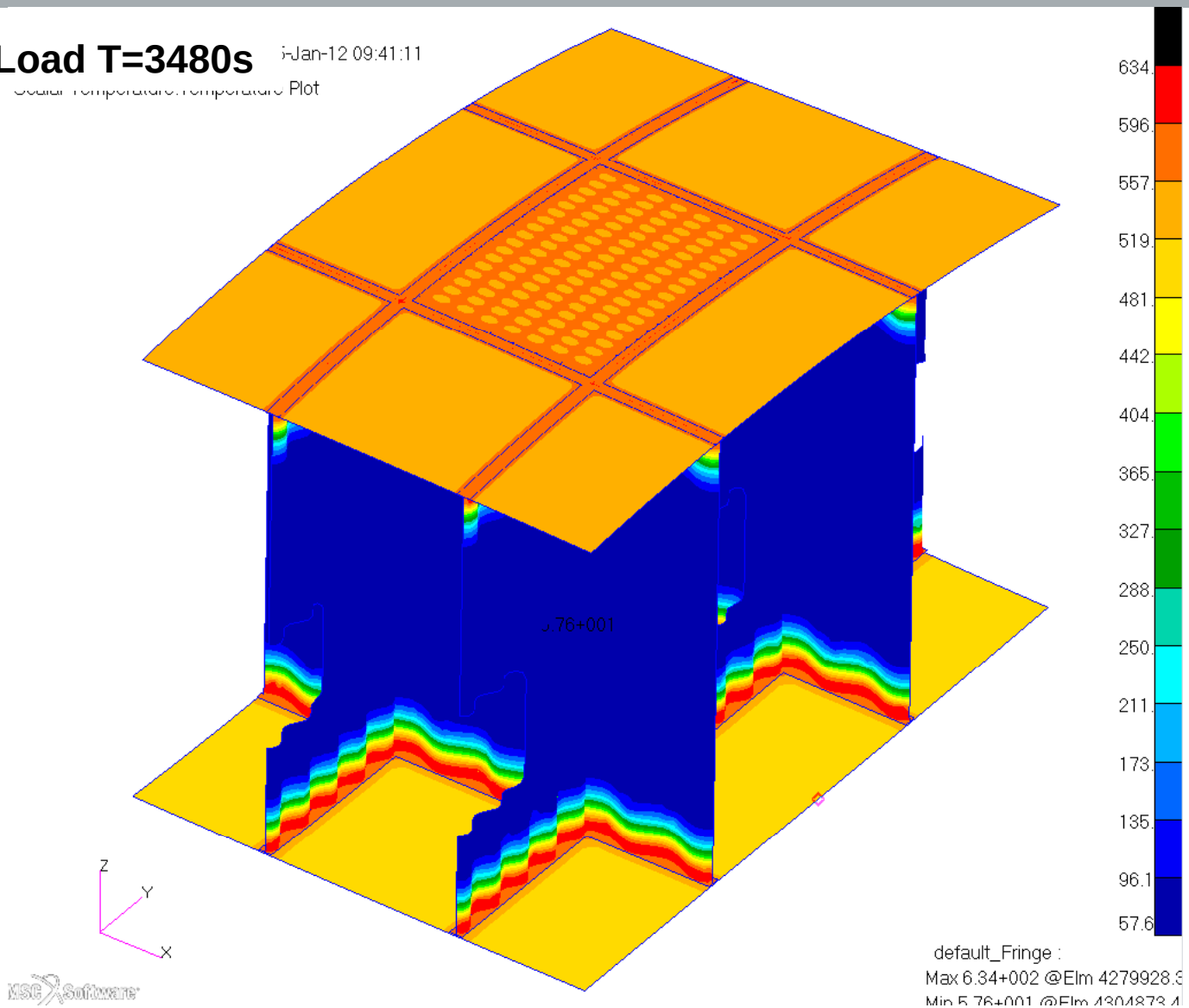

Approved for public release; distribution unlimited.

Orthogrid– Loading Conditions

Thermal Load T=60s

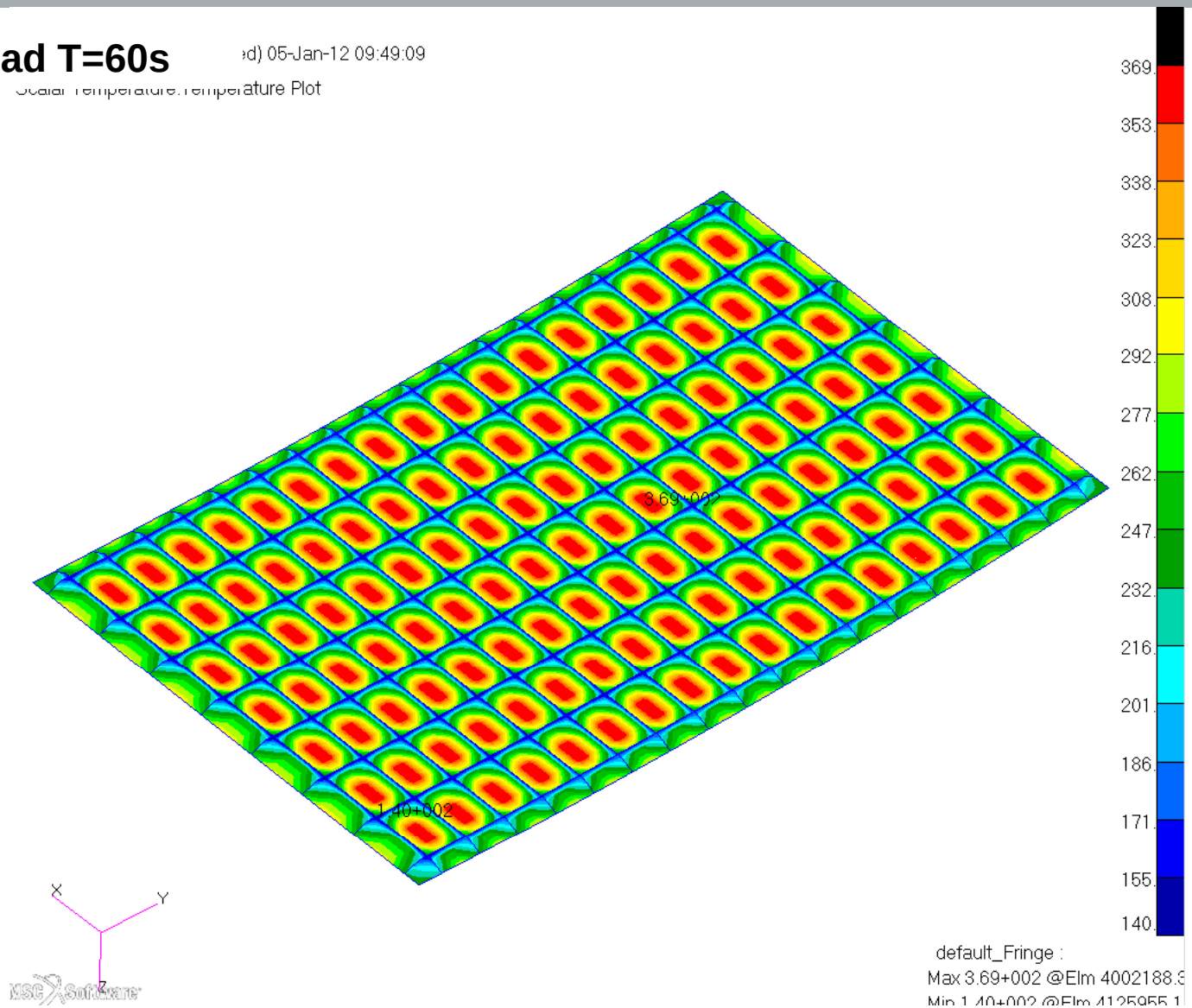

Approved for public release; distribution unlimited.

Orthogrid– Loading Conditions

Thermal Load T=900s

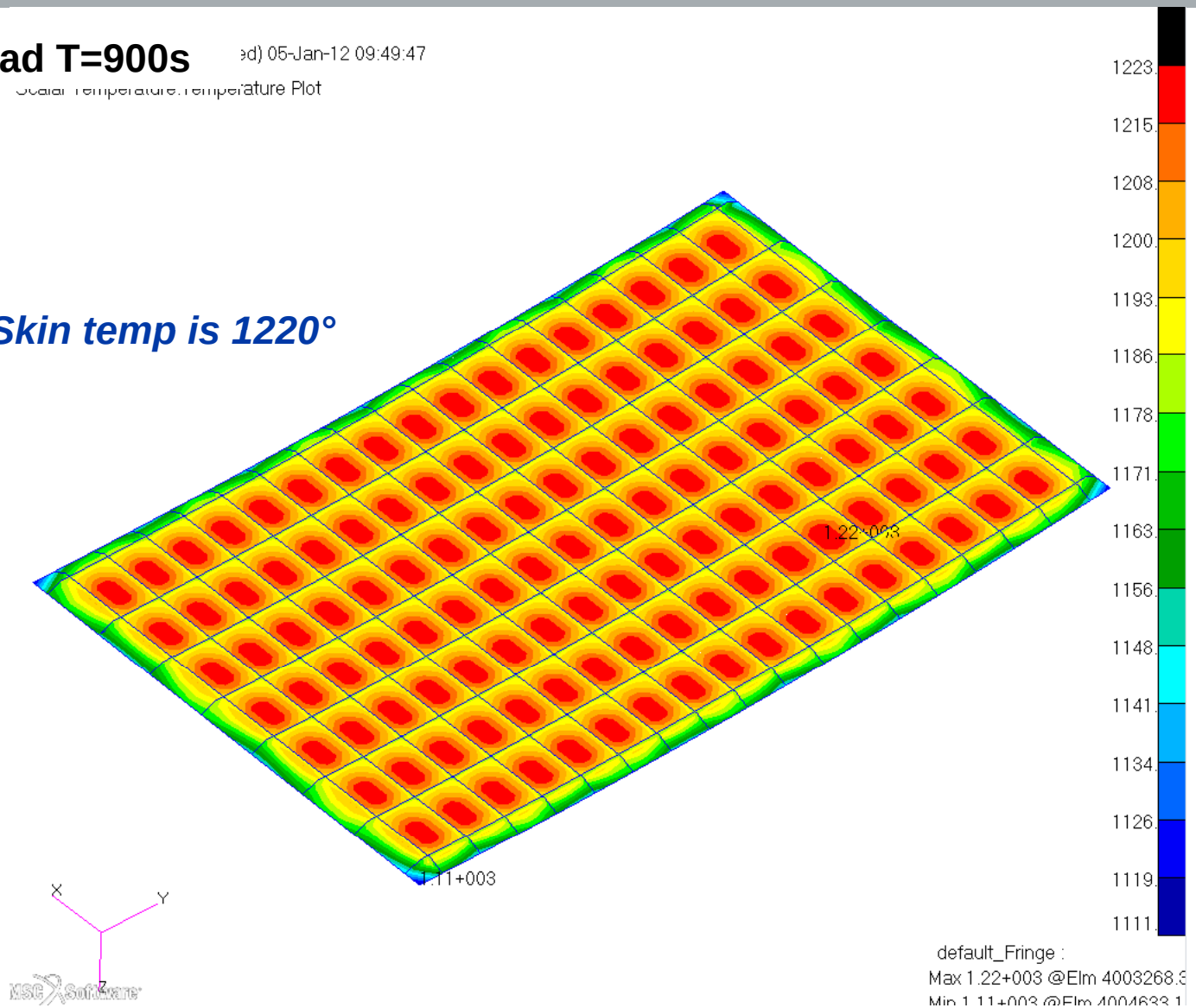

Skin temp is 1220°

Approved for public release; distribution unlimited.

Orthogrid– Loading Conditions

Thermal Load T=2500s

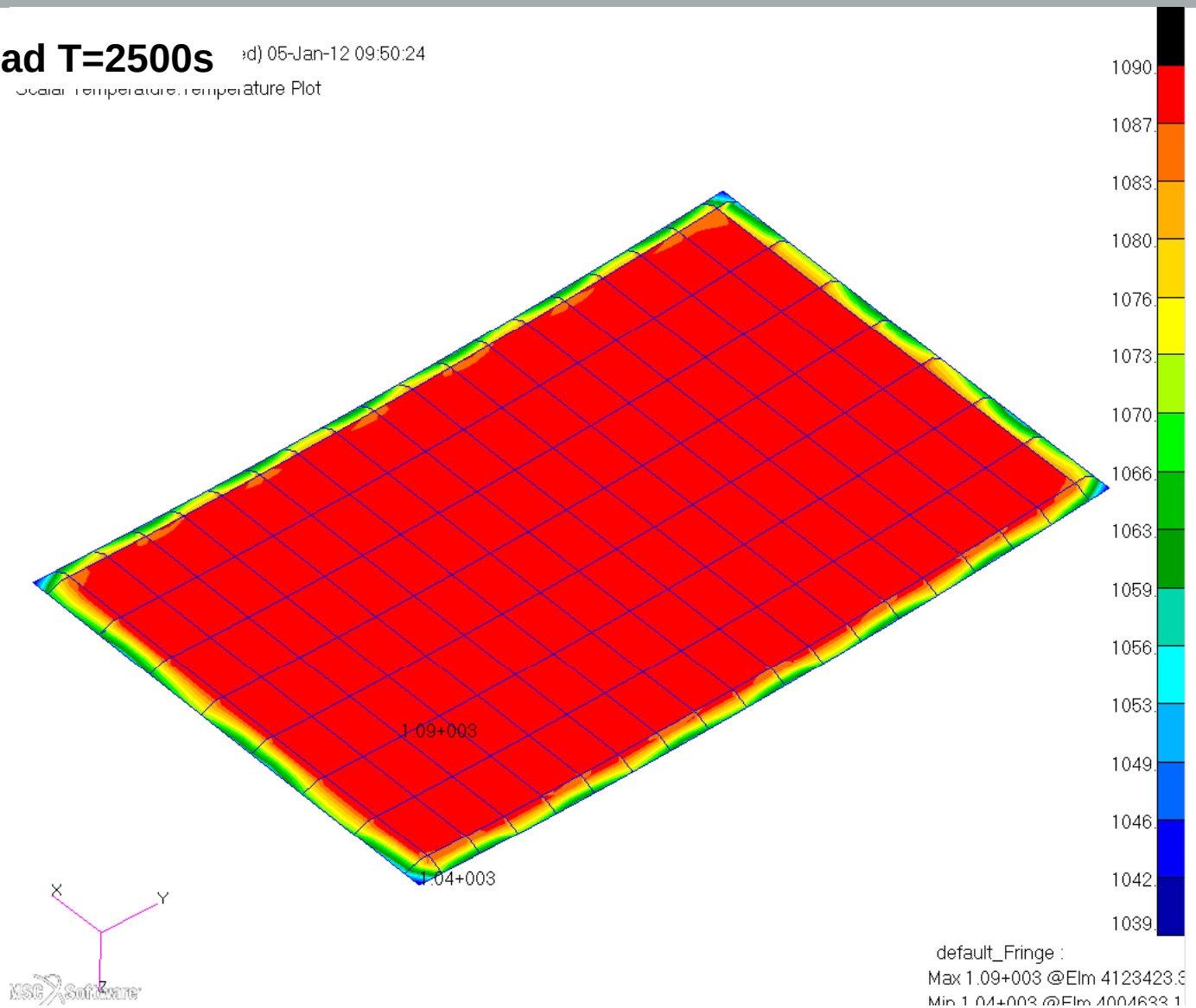

Approved for public release; distribution unlimited.

Orthogrid– Loading Conditions

Thermal Load T=3480s

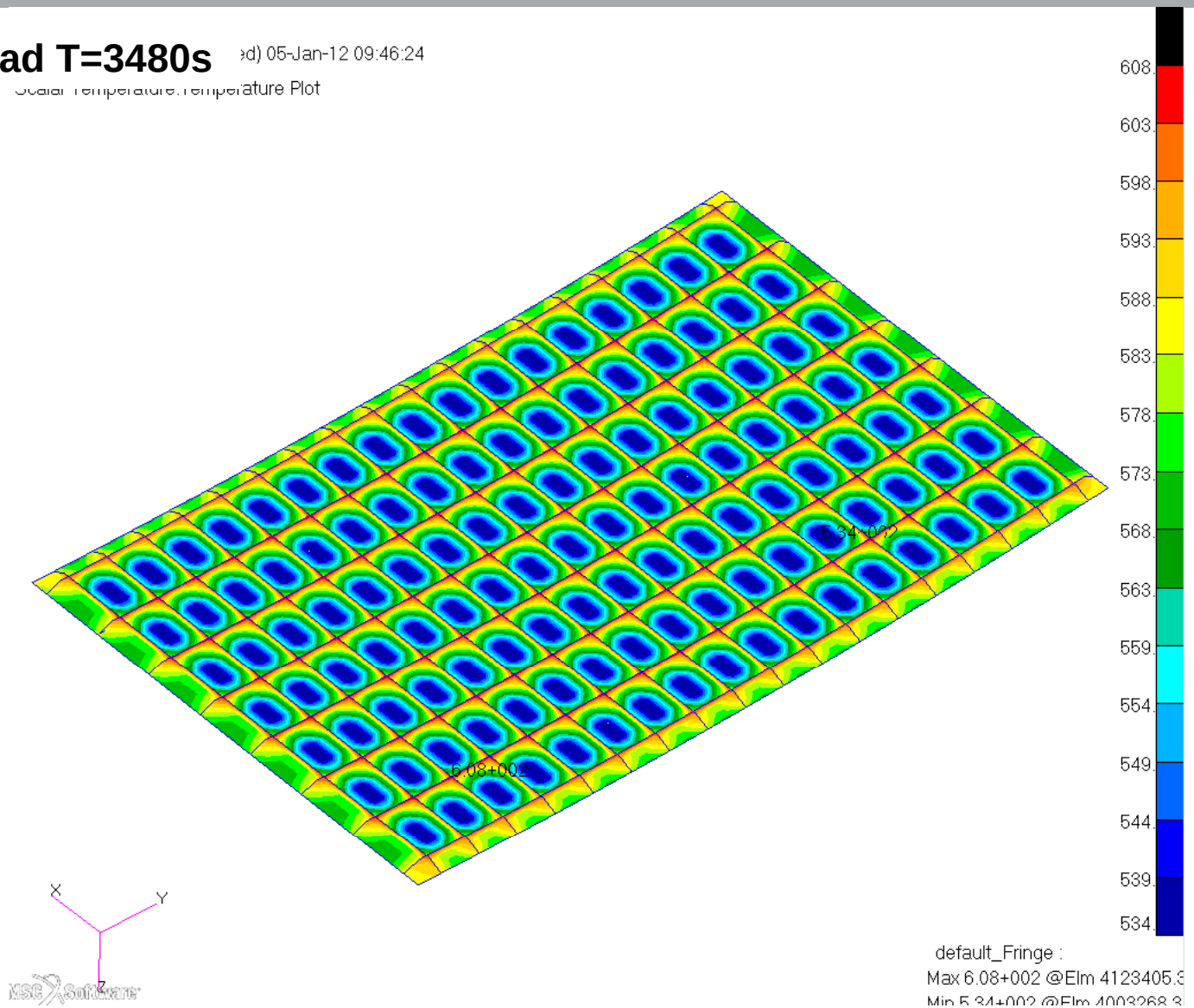

Approved for public release; distribution unlimited.

Unitcell

Mech only

Approved for public release; distribution unlimited.

Displacements, Unit Cell, 2.5g ULT 1.5, Linear

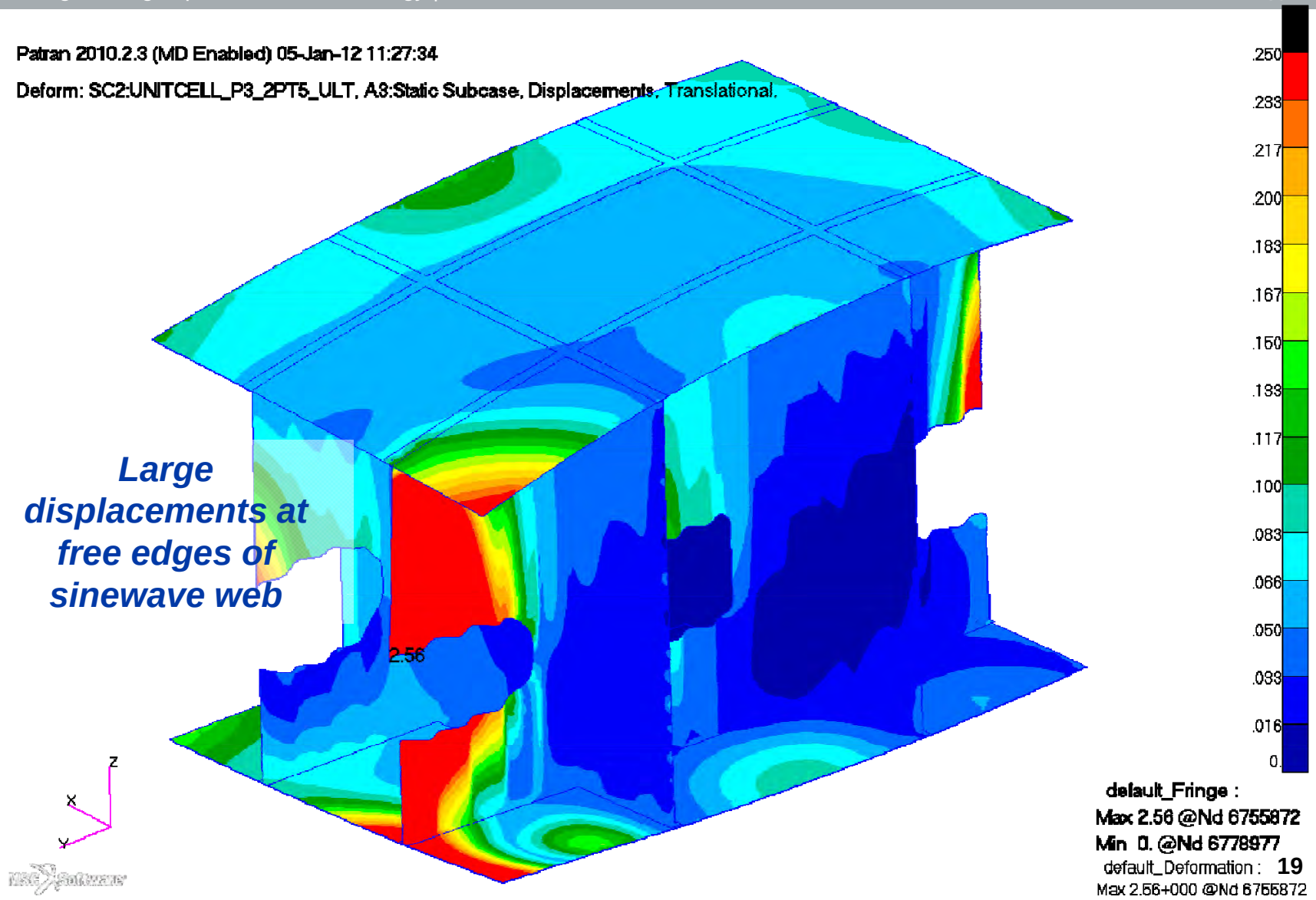

Approved for public release; distribution unlimited.

Von Mises, Unit Cell, 2.5g ULT 1.5, Linear

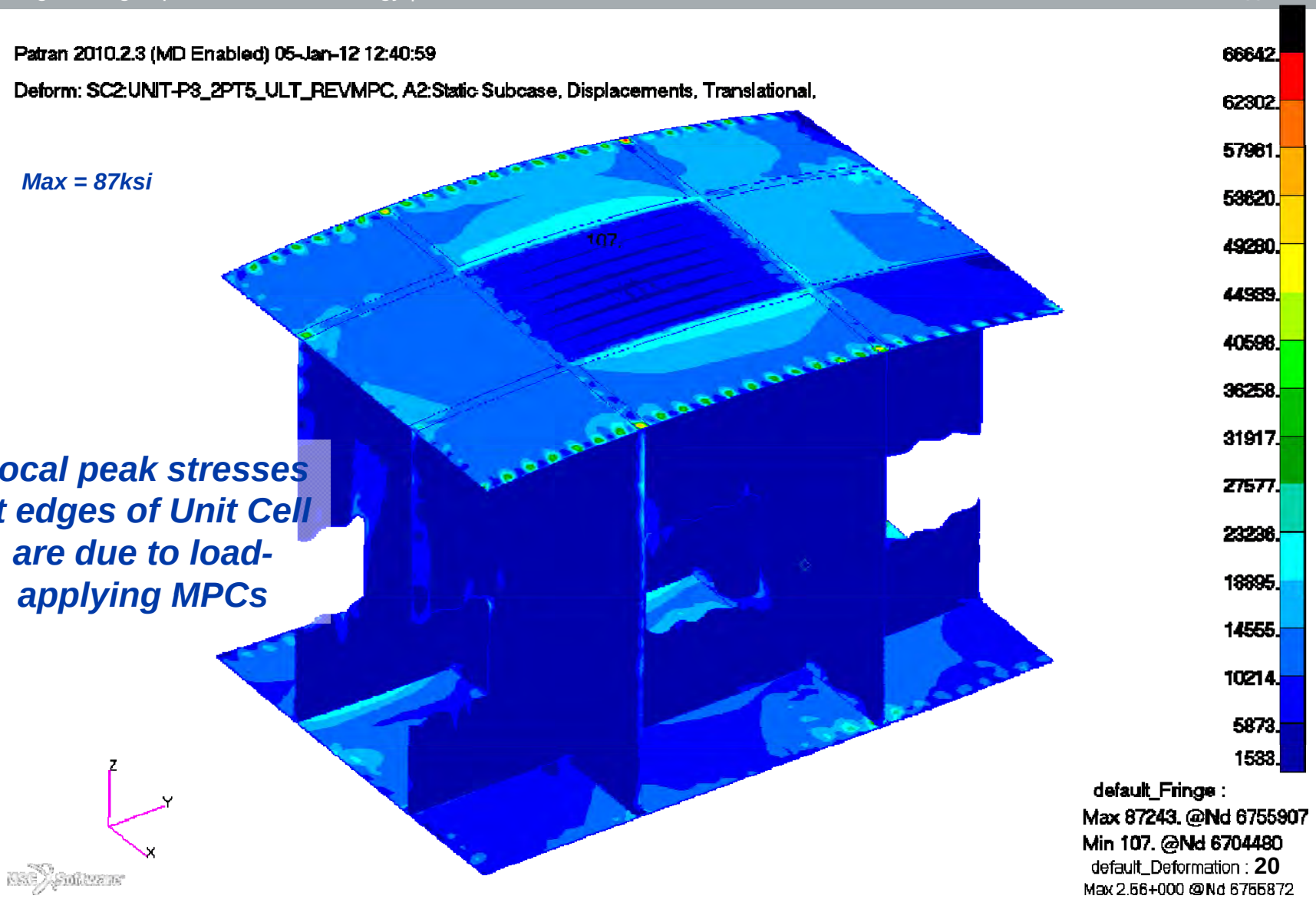

Local peak stresses at edges of Unit Cell are due to load-applying MPCs

Approved for public release; distribution unlimited.

Von Mises, Unit Cell, 2.5g ULT 1.5, Linear

Local peak stresses at edges of Unit Cell are due to load-applying MPCs; Spreading out MPCs reduces local peak stresses

Max = 163ksi

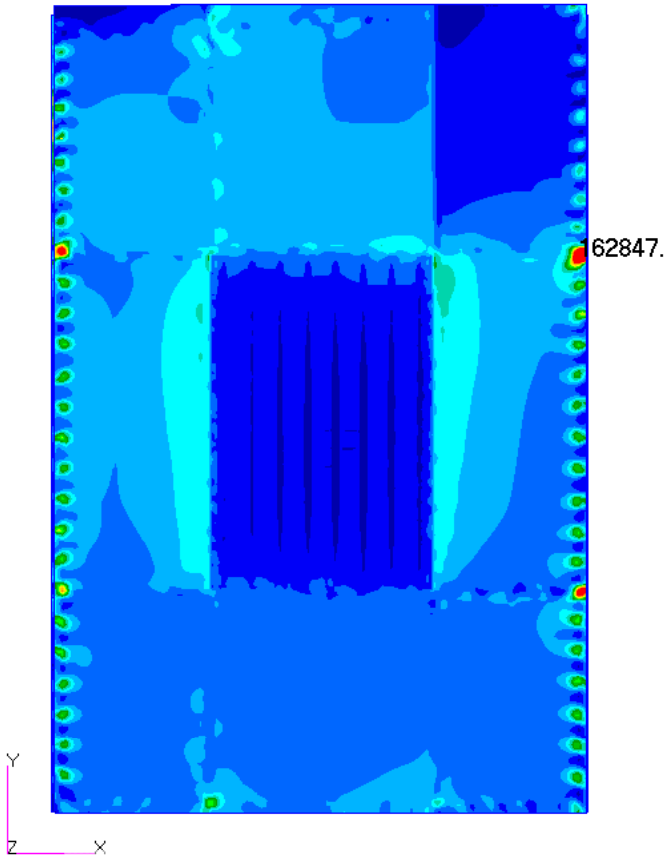

1st iteration MPCs

Max = 87ksi

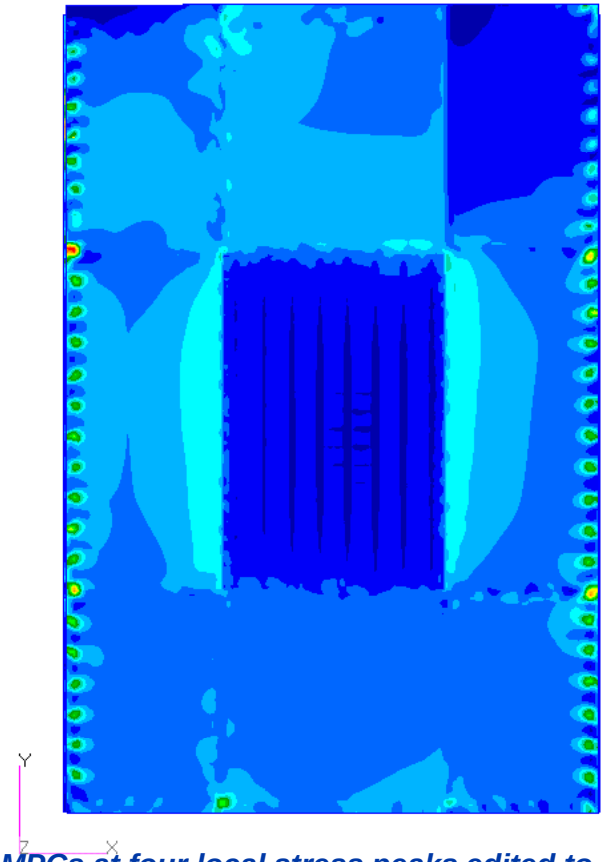

MPCs at four local stress peaks edited to spread load to more grids

Approved for public release; distribution unlimited.

Displacements, Unit Cell, 2.5g Lim 1.15, Linear

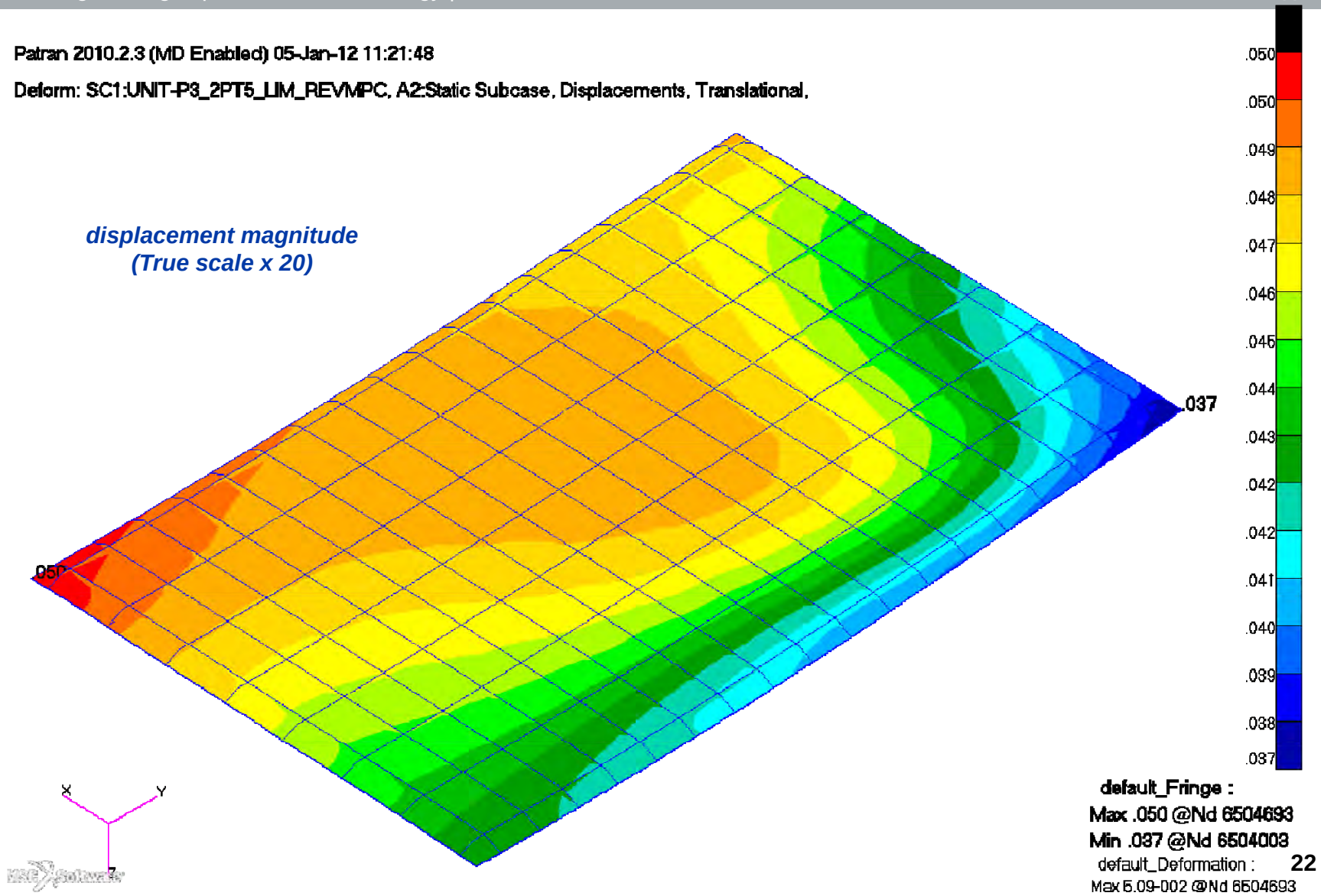

Approved for public release; distribution unlimited.

Displacements, Unit Cell, 2.5g Ult 1.5, Linear

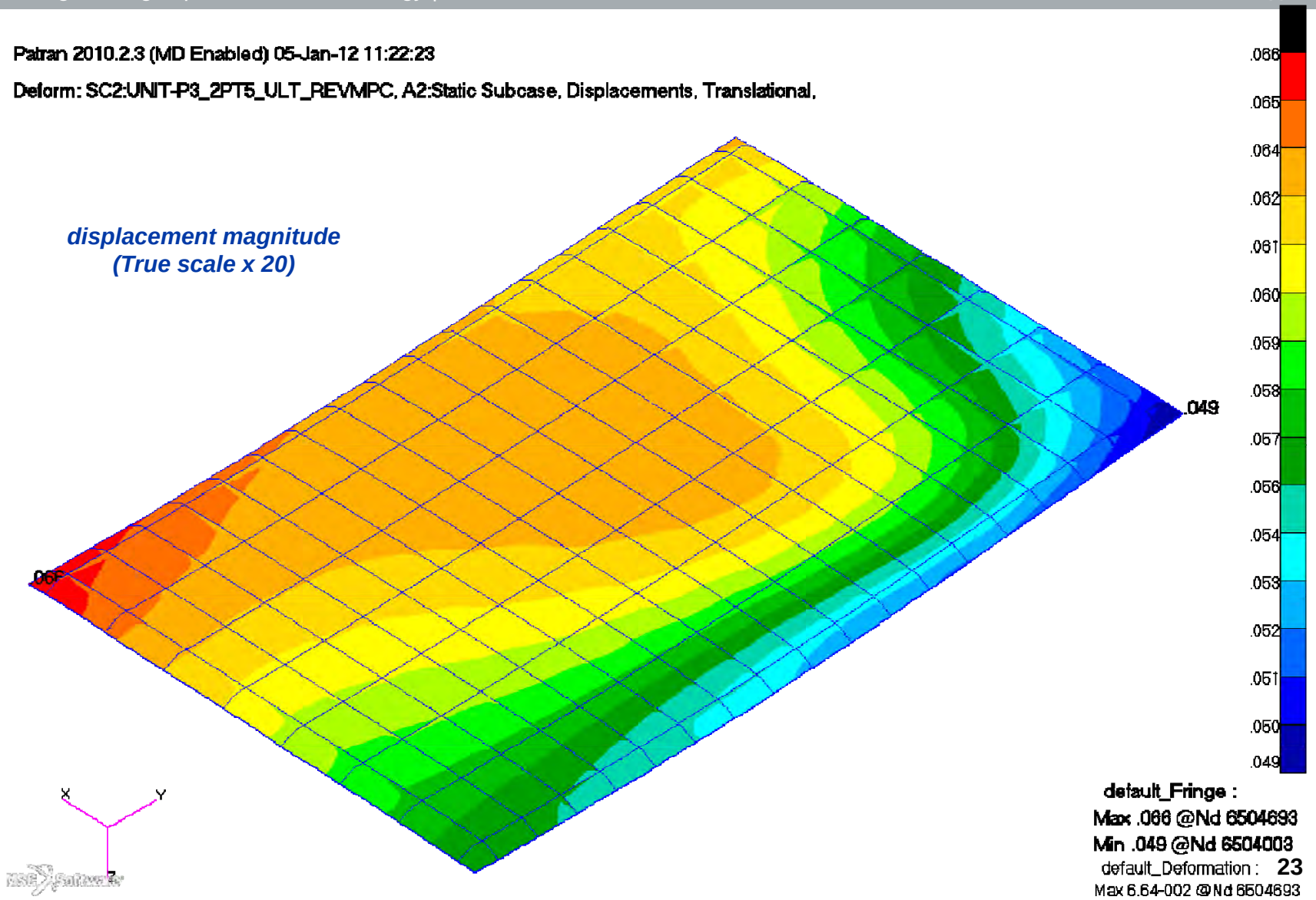

Approved for public release; distribution unlimited.

Displacements, Unit Cell, 2.5g Ult 1.5, Linear

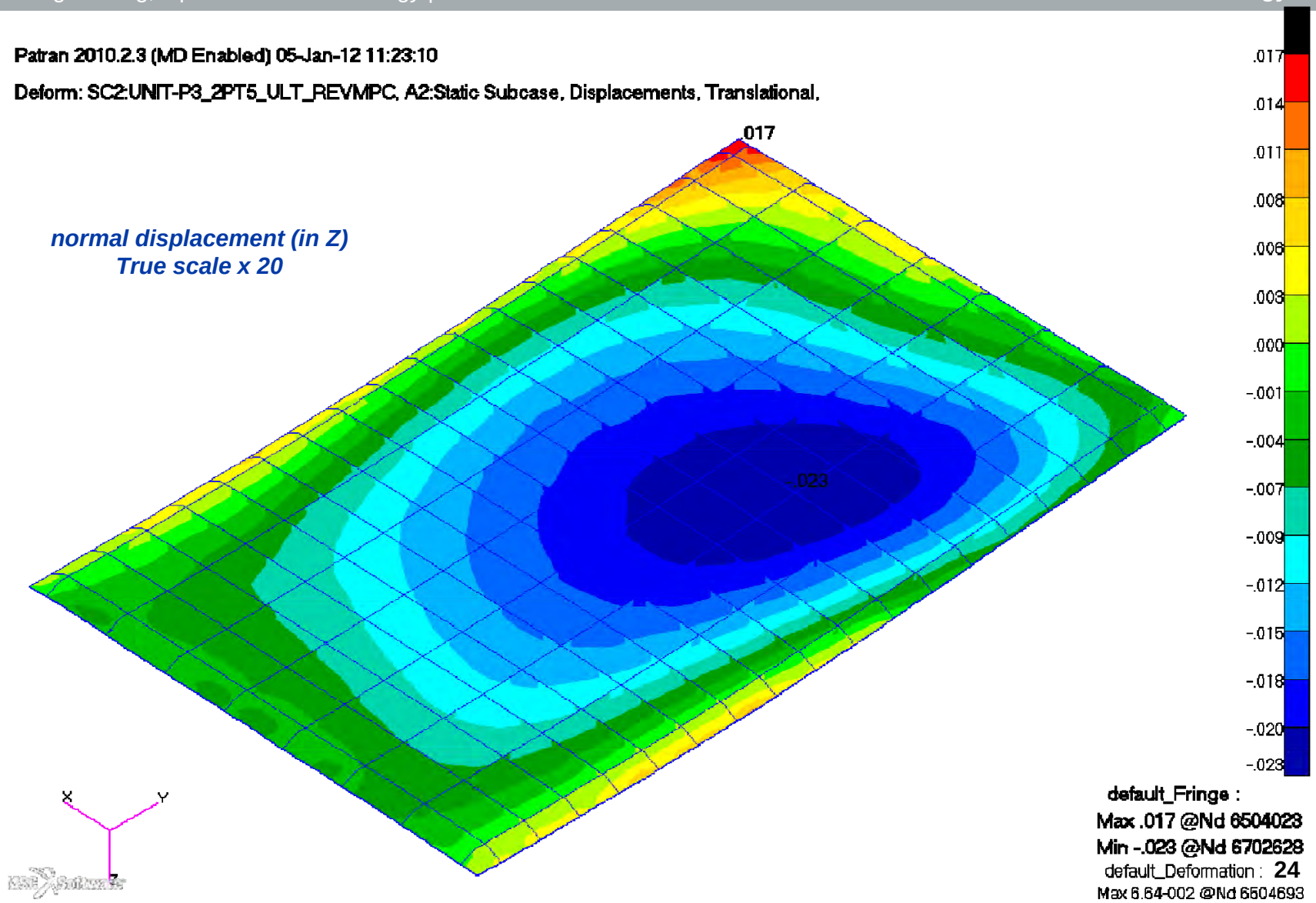

Approved for public release; distribution unlimited.

Von Mises, Unit Cell, 2.5g Ult 1.5, Linear

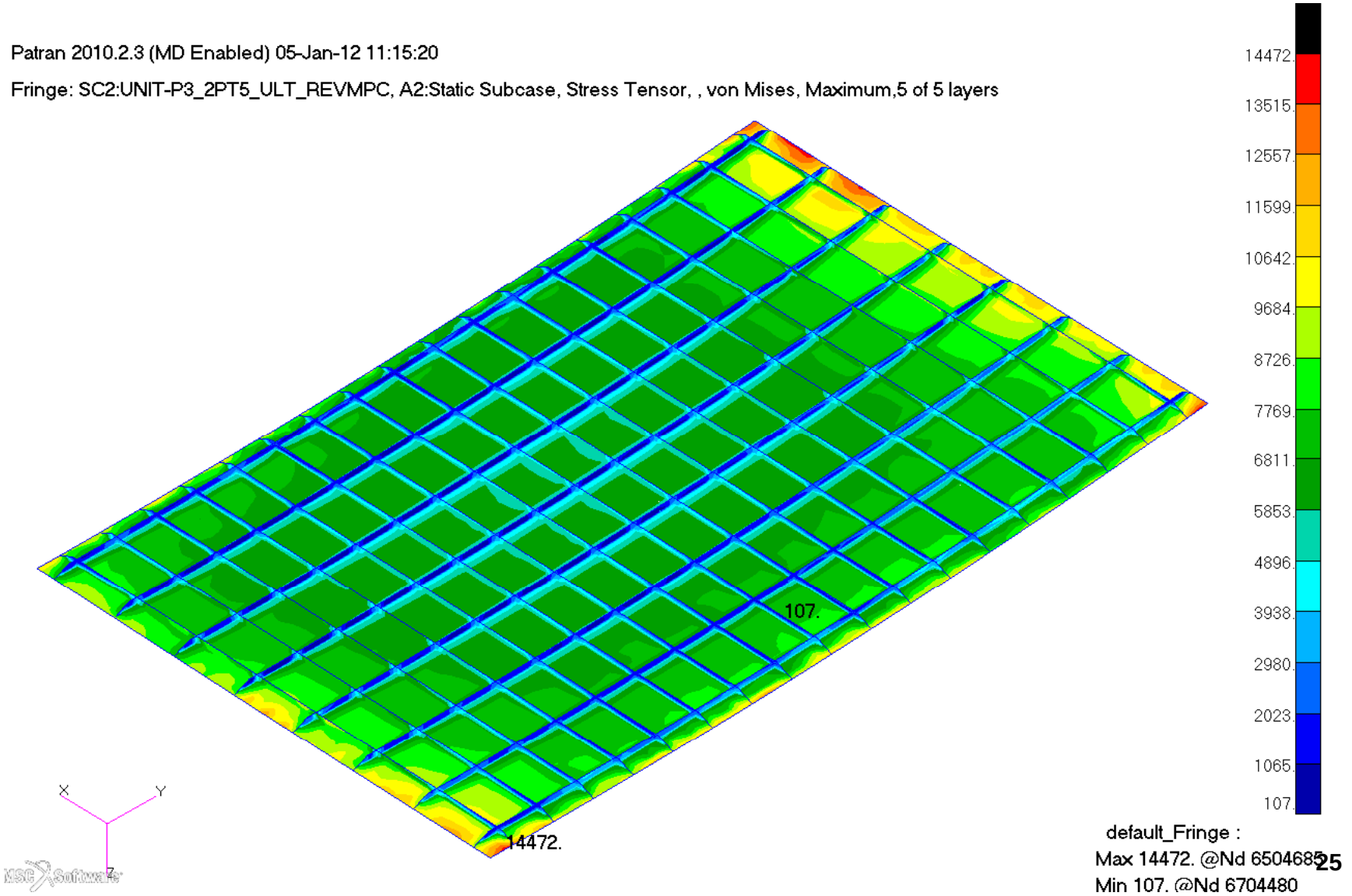

Approved for public release; distribution unlimited.

Unitcell

Temp only

Approved for public release; distribution unlimited.

Displacements, Unit Cell, T=900s Linear

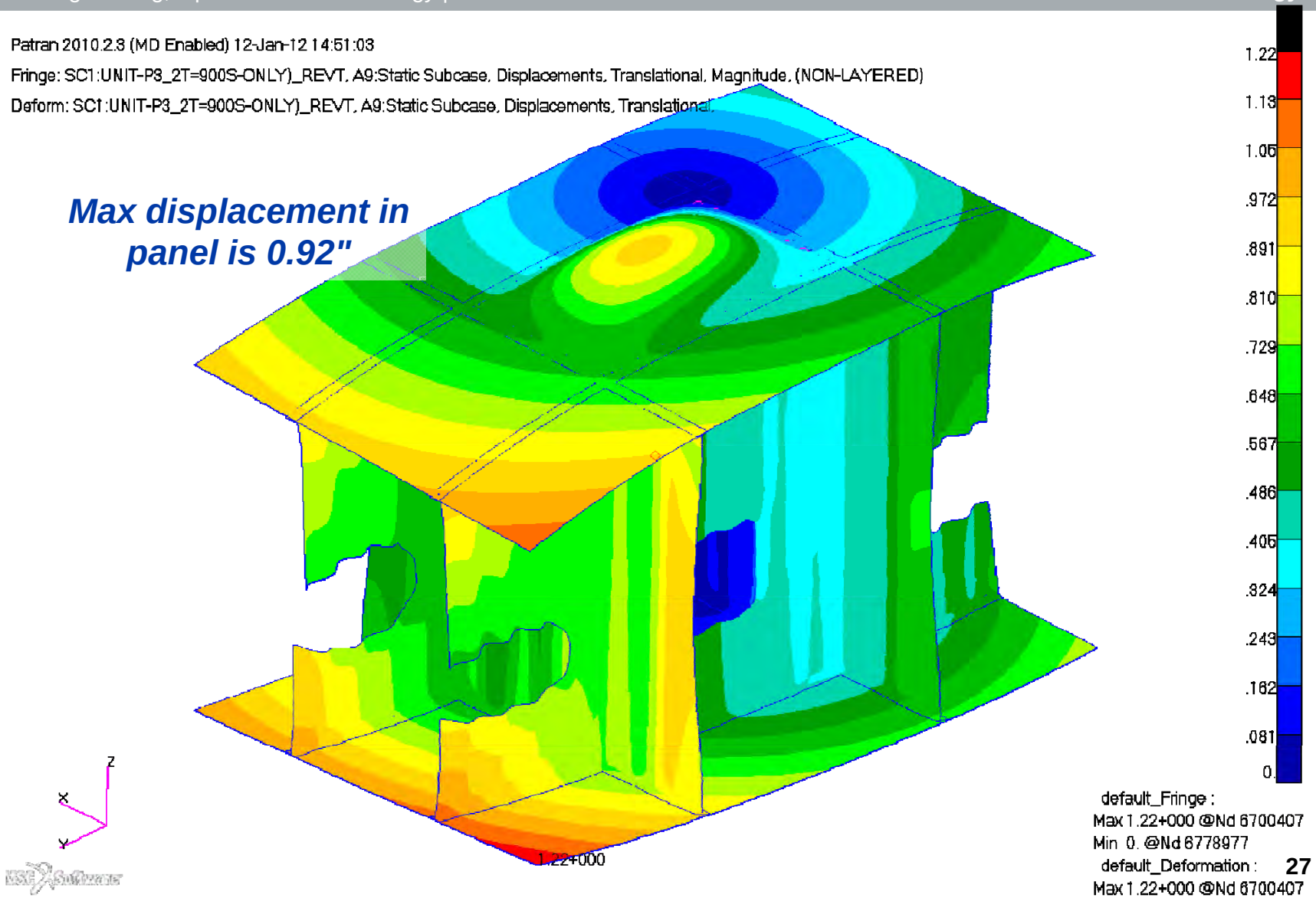

Approved for public release; distribution unlimited.

Von Mises, Unit Cell, T=900s Linear

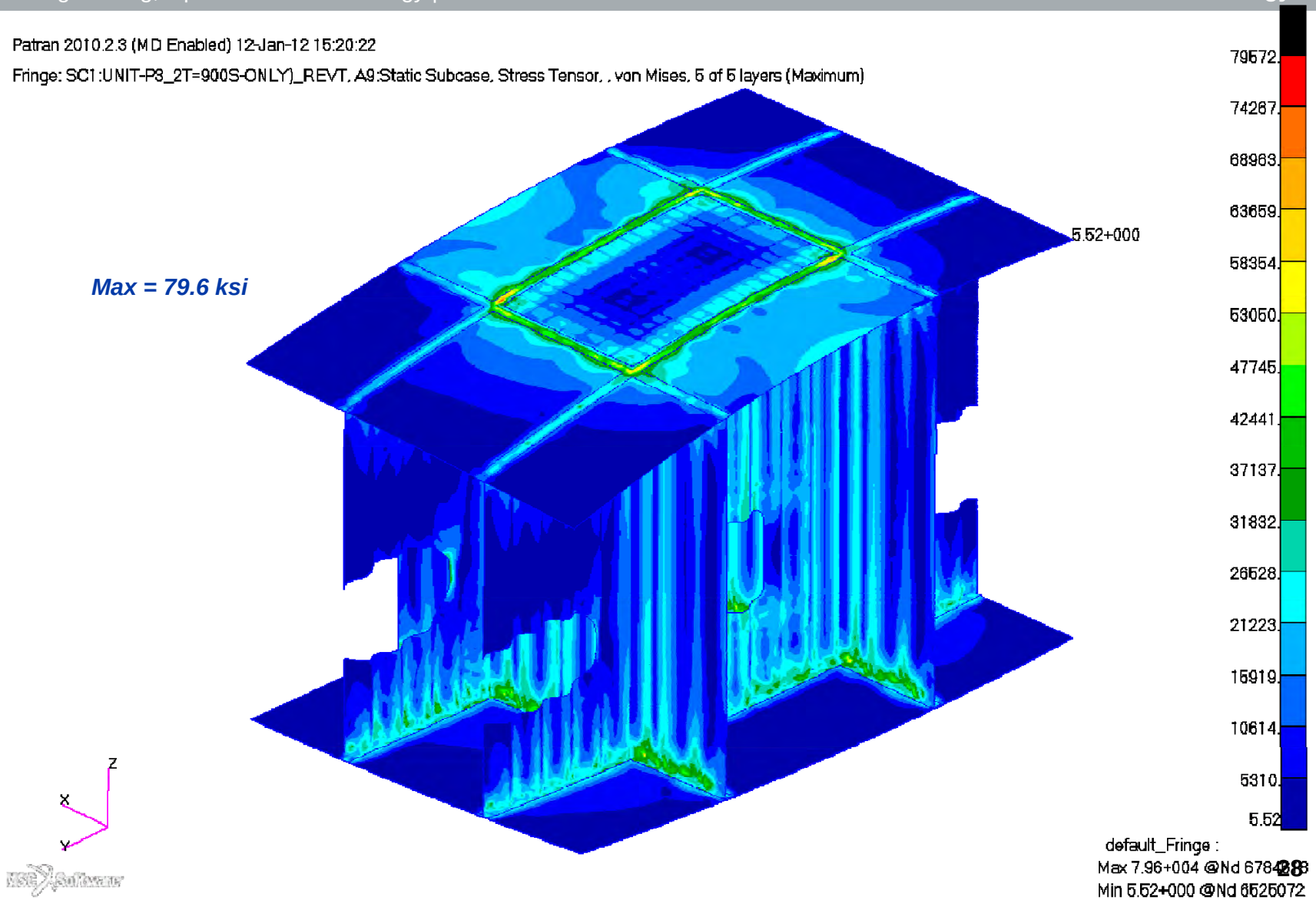

Approved for public release; distribution unlimited.

Unitcell

Mech (2.5g) + Temp (T=900s)

Approved for public release; distribution unlimited.

Displacements, Unit Cell, 2.5G Ult 1.5, T=900s Linear

Critical case for displacement and stress is Mech + T(900s)

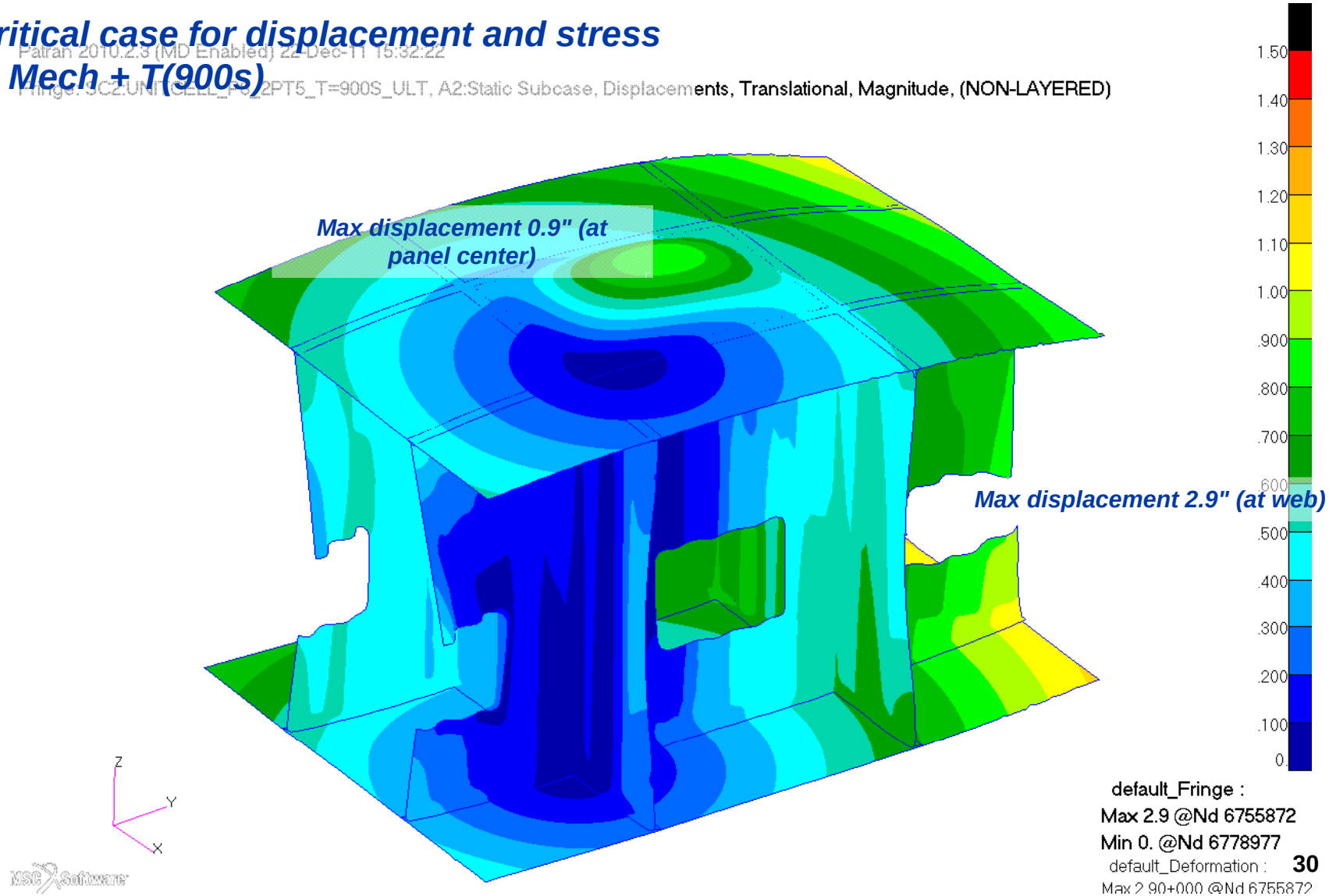

Approved for public release; distribution unlimited.

Von Mises, Unit Cell, 2.5G Ult 1.5, T=900s Linear

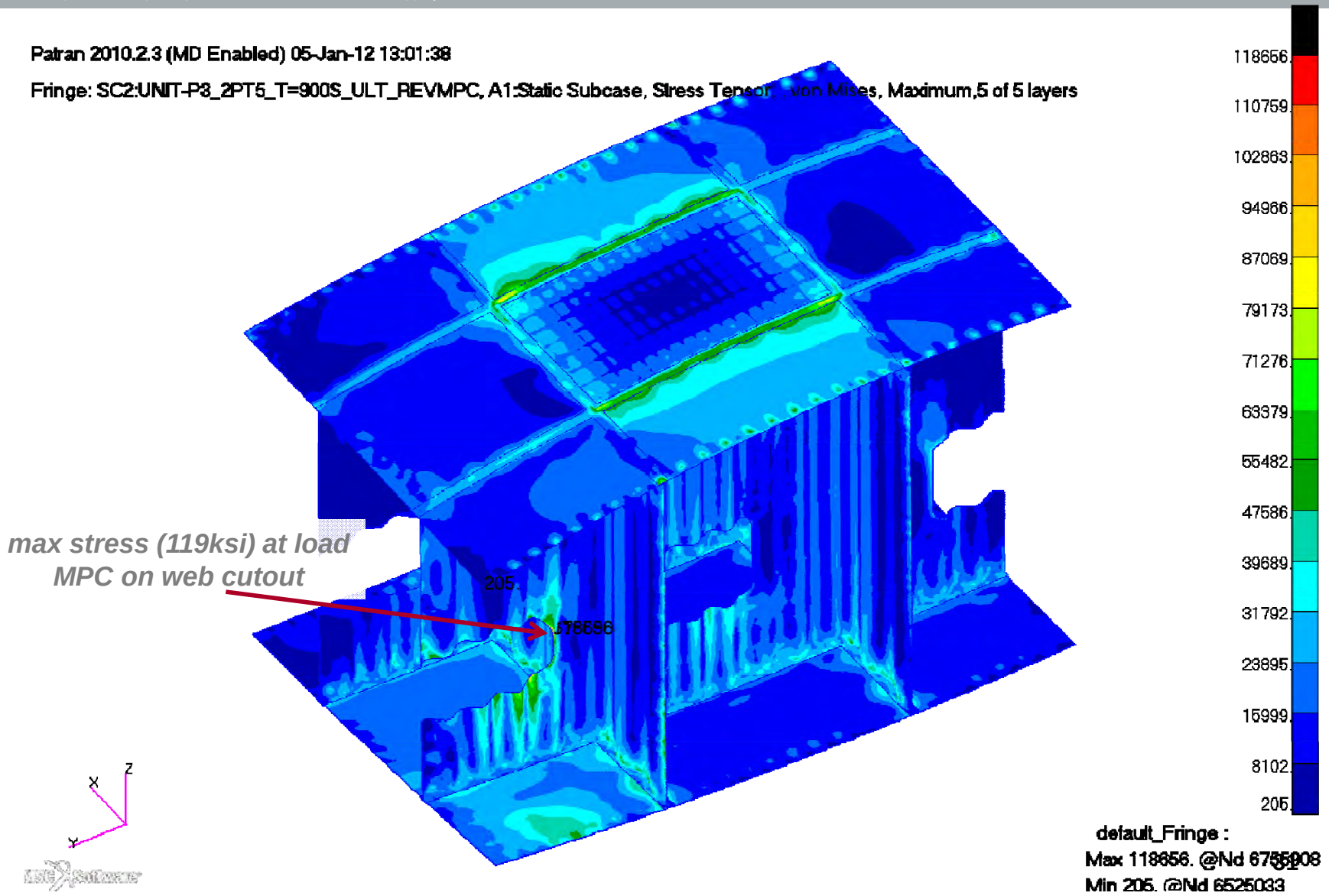

Approved for public release; distribution unlimited.

Displacements, Unit Cell, 2.5G Ult 1.5, T=900s Linear

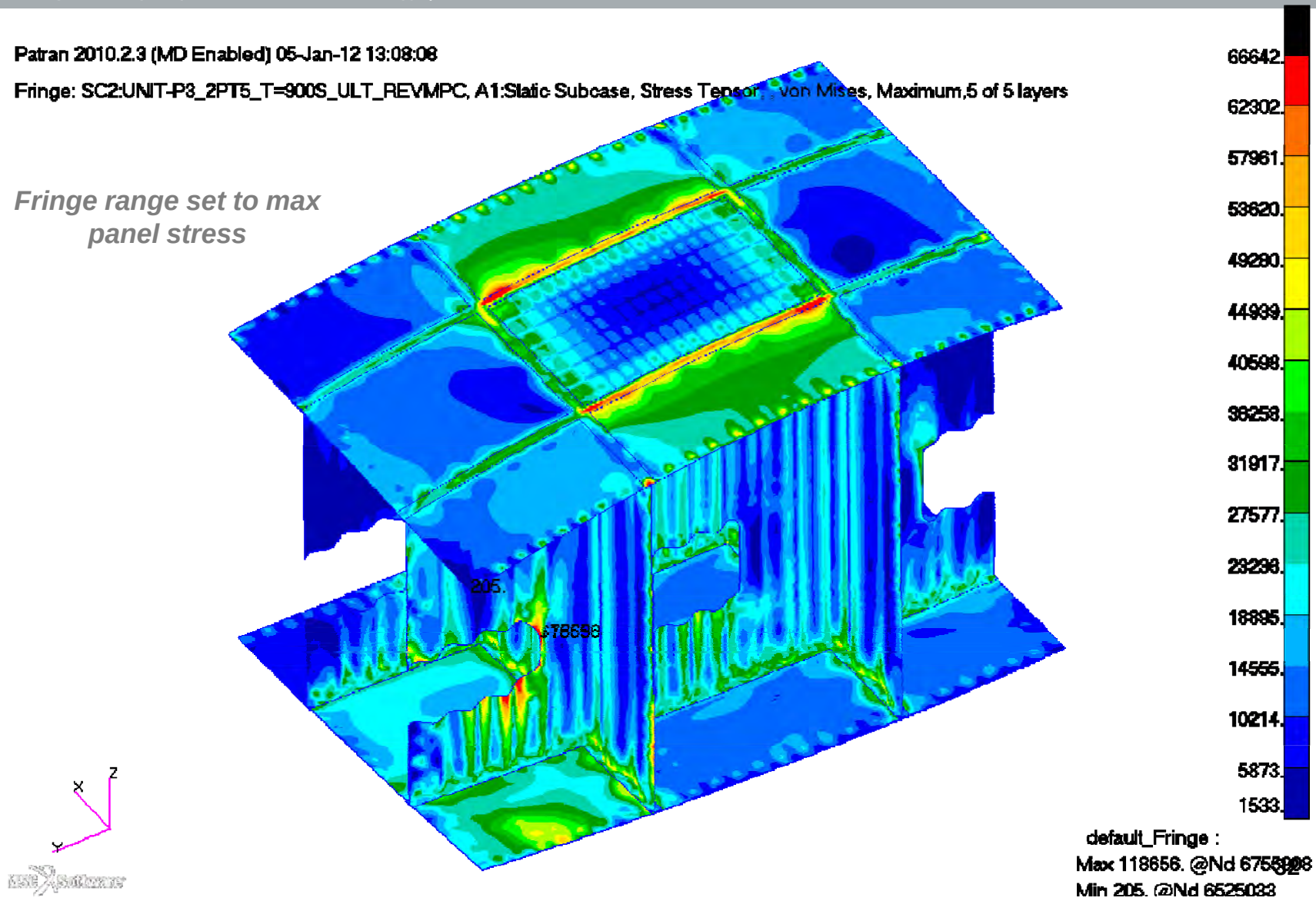

Approved for public release; distribution unlimited.

Displacements, Unit Cell, 2.5G Ult 1.5, T=900s Linear

Critical case for displacement and stress is Mech + T(900s)

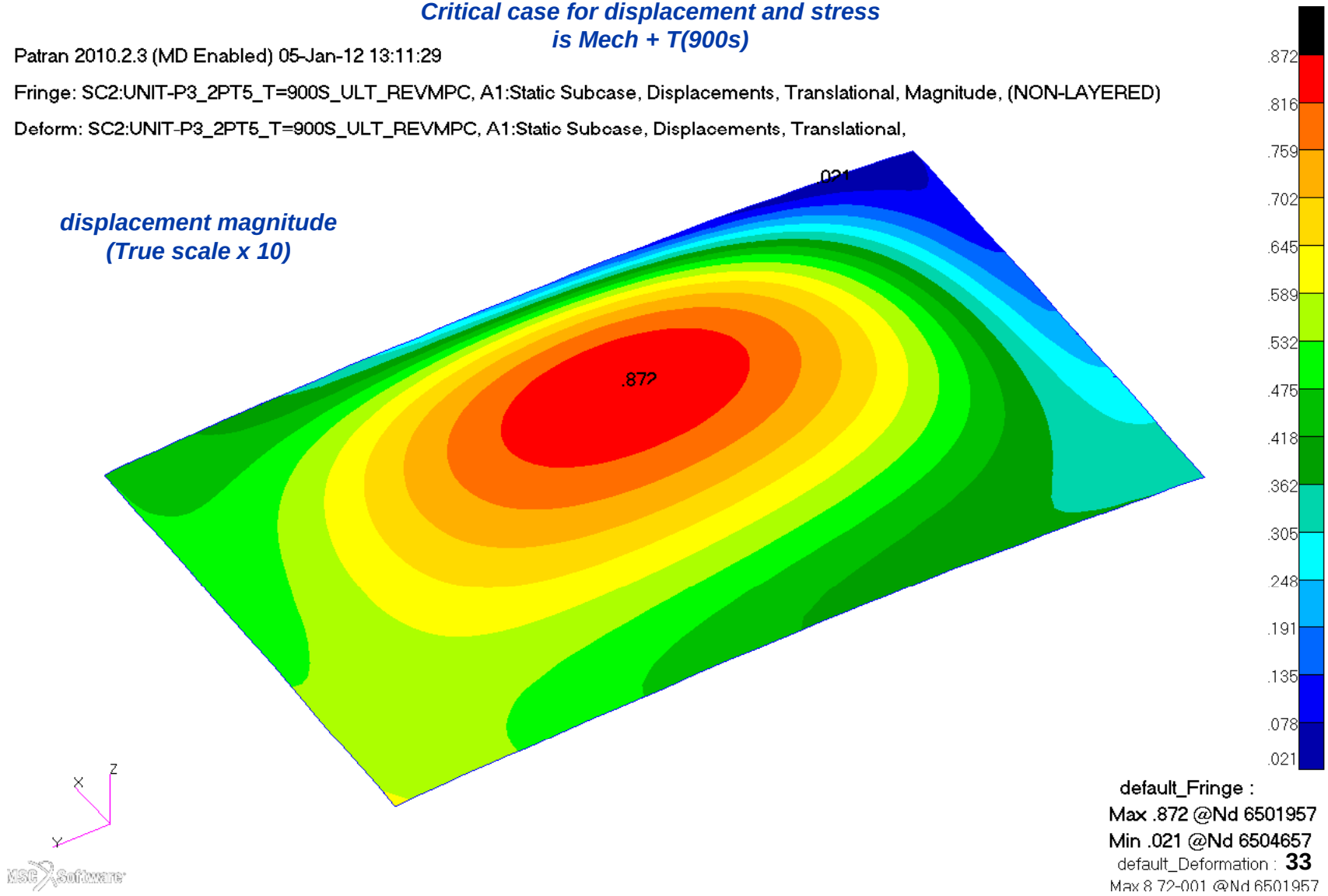

Approved for public release; distribution unlimited.

Displacements, Unit Cell, 2.5G Ult 1.5, T=900s Linear

Critical case for displacement and stress is Mech + T(900s)

Patran 2010.2.3 (MD Enabled) 05-Jan-12 13:16:11

Fringe: SC2:UNIT-P3_2PT5_T=900S_ULT_REVMPC, A1:Static Subcase, Displacements, Translational, Z Component, (NON-LAYERED)

Deform: SC2:UNIT-P3_2PT5_T=900S_ULT_REVMPC, A1:Static Subcase, Displacements, Translational,

Normal displacement (in Z)
True scale x 10

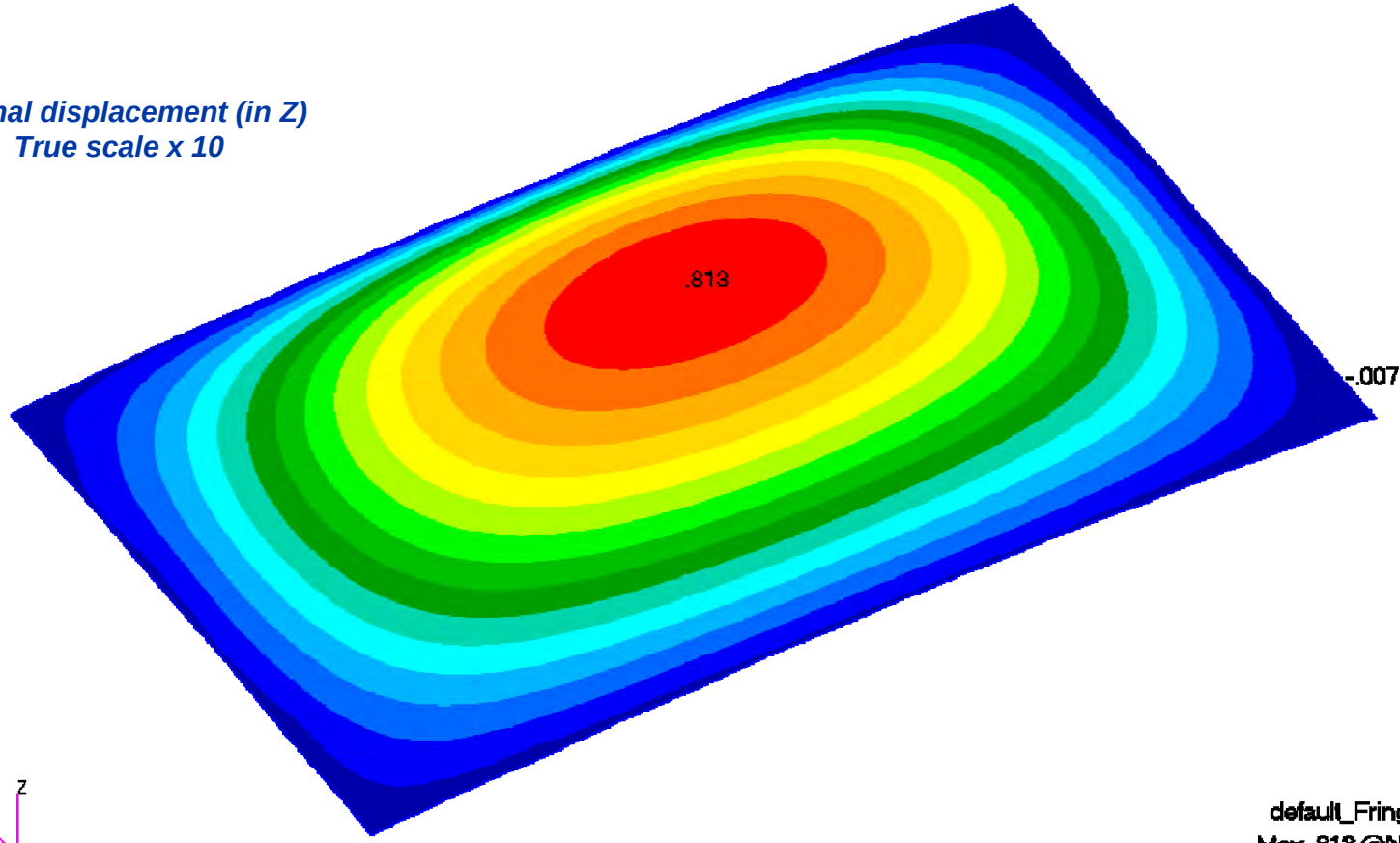

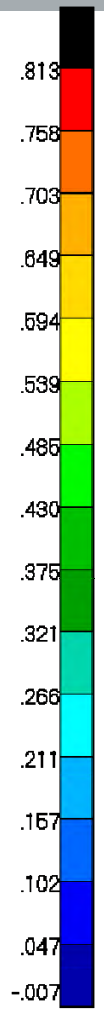

default_Fringe :
Max .813 @Nd 6501954
Min -.007 @Nd 6503929
default_Deformation : 34
Max 8.72-001 @Nd 6501957

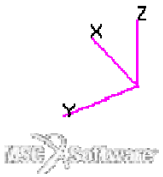

Max normal displacement (in Z) = 0.813"

Approved for public release; distribution unlimited.

Displacements, Unit Cell, 2.5G Lim 1.15, T=900s Linear

Critical case for displacement and stress is Mech + T(900s)

Patran 2010.2.3 (MD Enabled) 05-Jan-12 13:13:50

Fringe: SC1:UNIT-P3_2PT5_T=900S_LIM_REVMPC, A1:Static Subcase, Displacements, Translational, Magnitude, (NON-LAYERED)

Deform: SC1:UNIT-P3_2PT5_T=900S_LIM_REVMPC, A1:Static Subcase, Displacements, Translational,

displacement magnitude (True scale x 10)

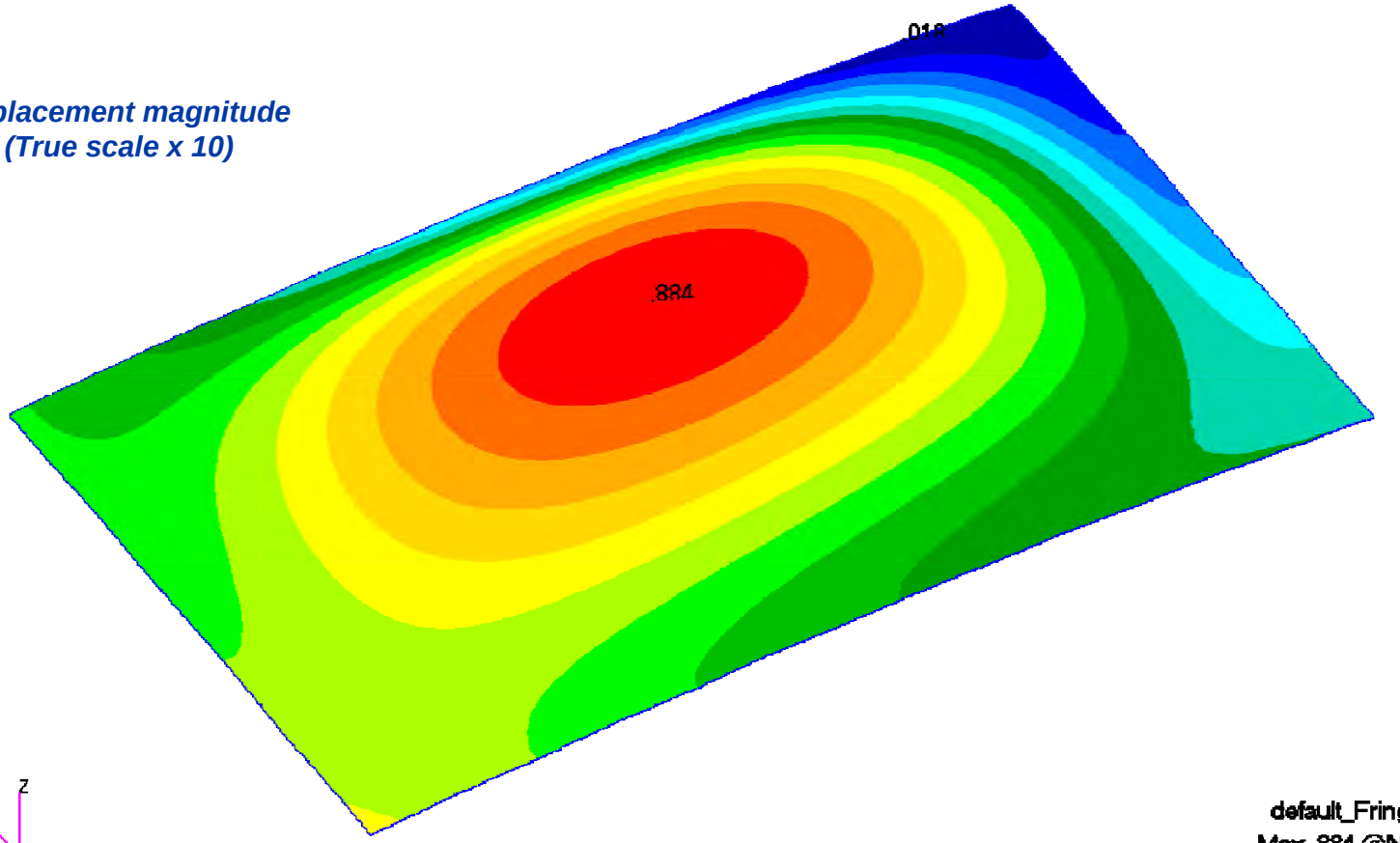

Approved for public release; distribution unlimited.

Displacements, Unit Cell, 2.5G Lim 1.15, T=900s Linear

Critical case for displacement and stress is Mech + T(900s)

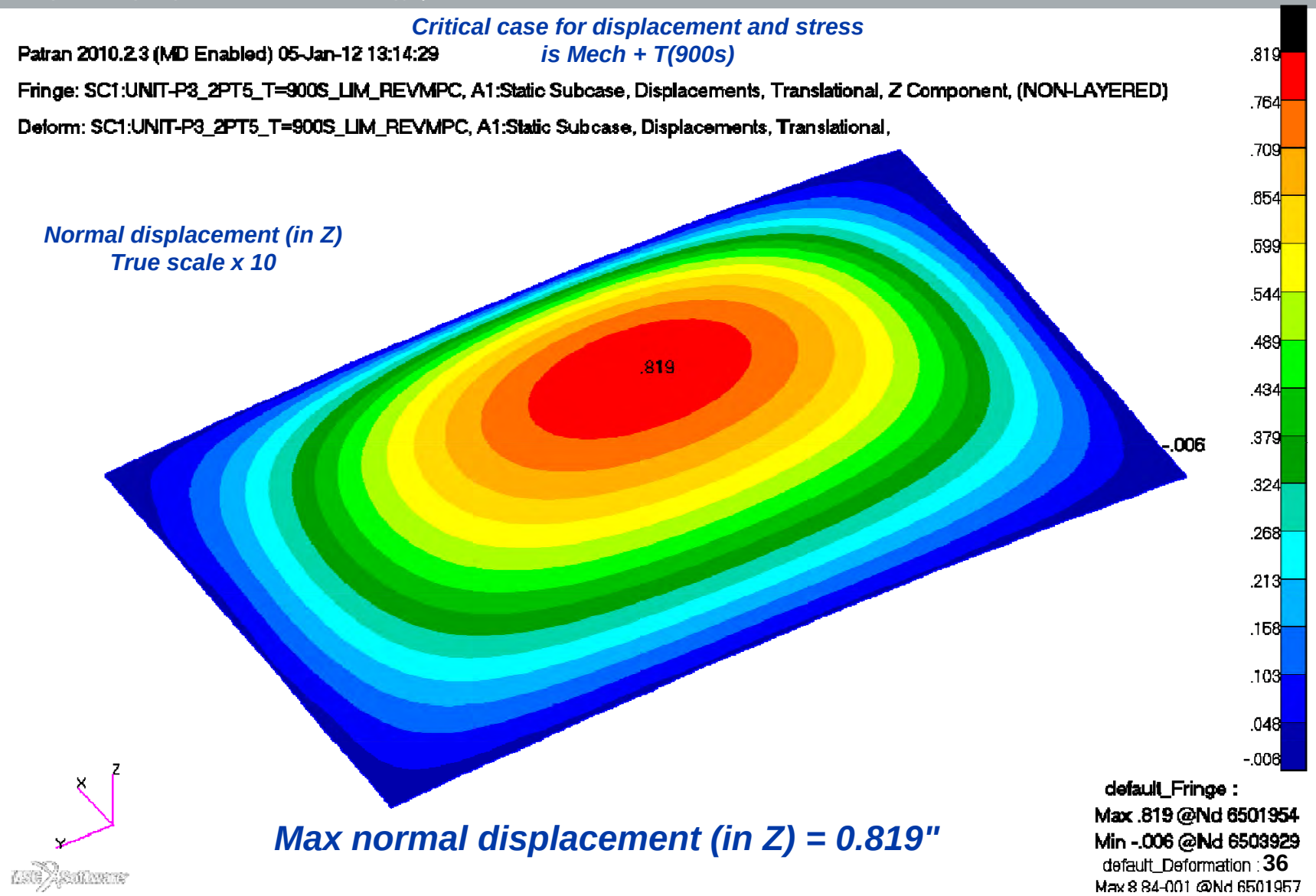

Normal displacement (in Z)
True scale x 10

Max normal displacement (in Z) = 0.819"

Approved for public release; distribution unlimited.

Von Mises, Unit Cell, 2.5G Ult 1.5, T=900s Linear

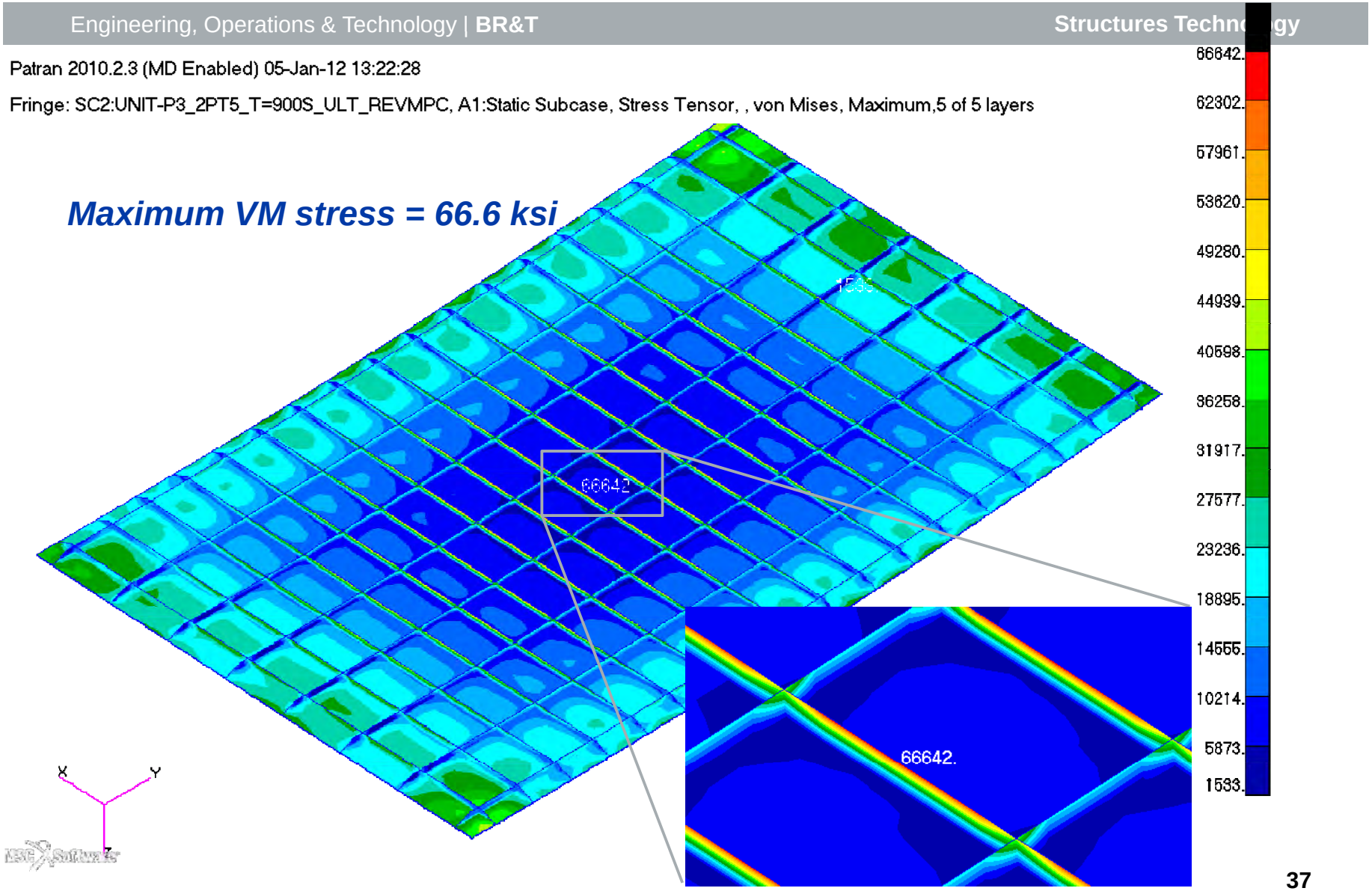

Approved for public release; distribution unlimited.

Panel model

Temp (T=900s) only

Approved for public release; distribution unlimited.

Displacements, Panel, T=900s Linear

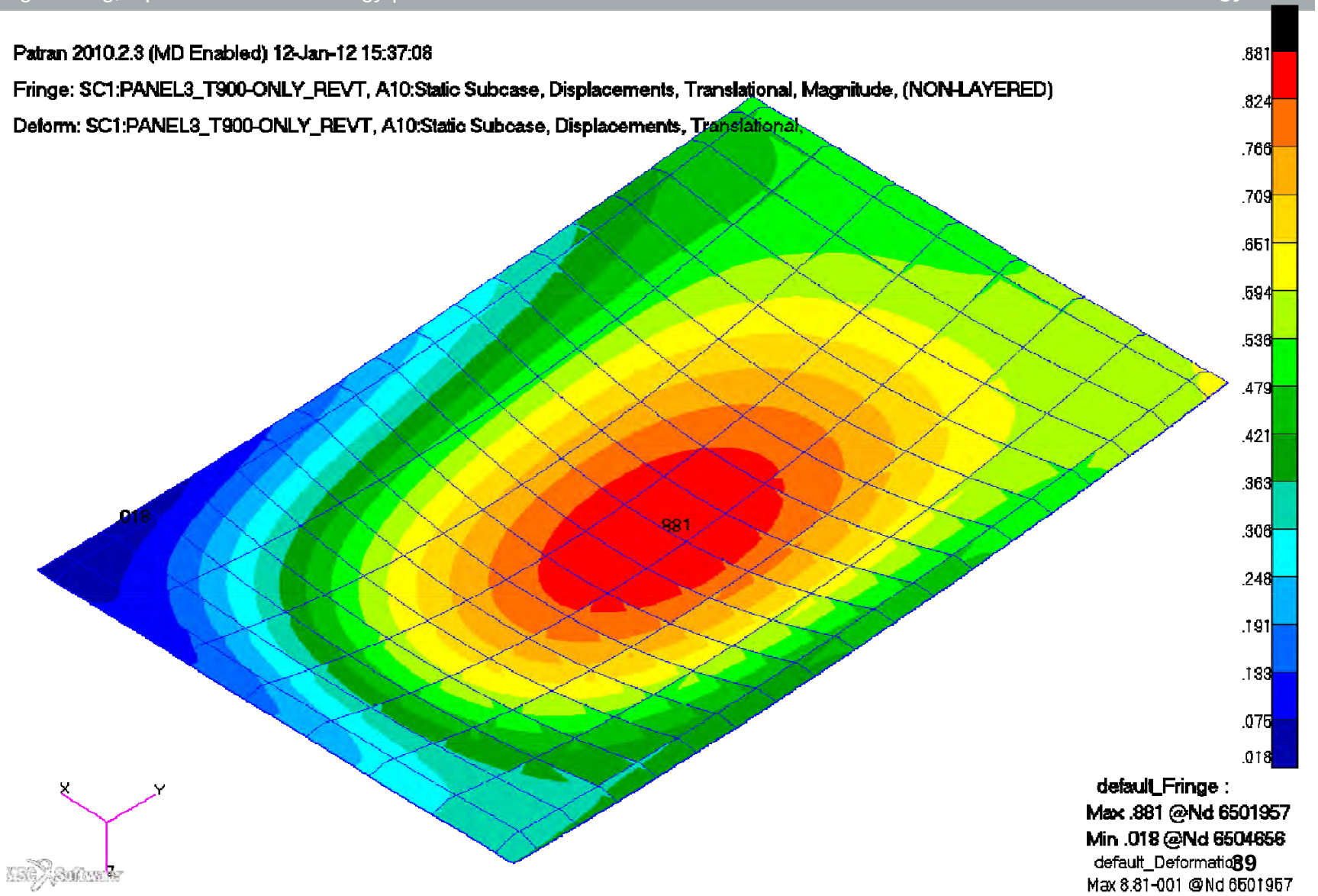

Approved for public release; distribution unlimited.

Von MIses, Panel, T=900s Linear

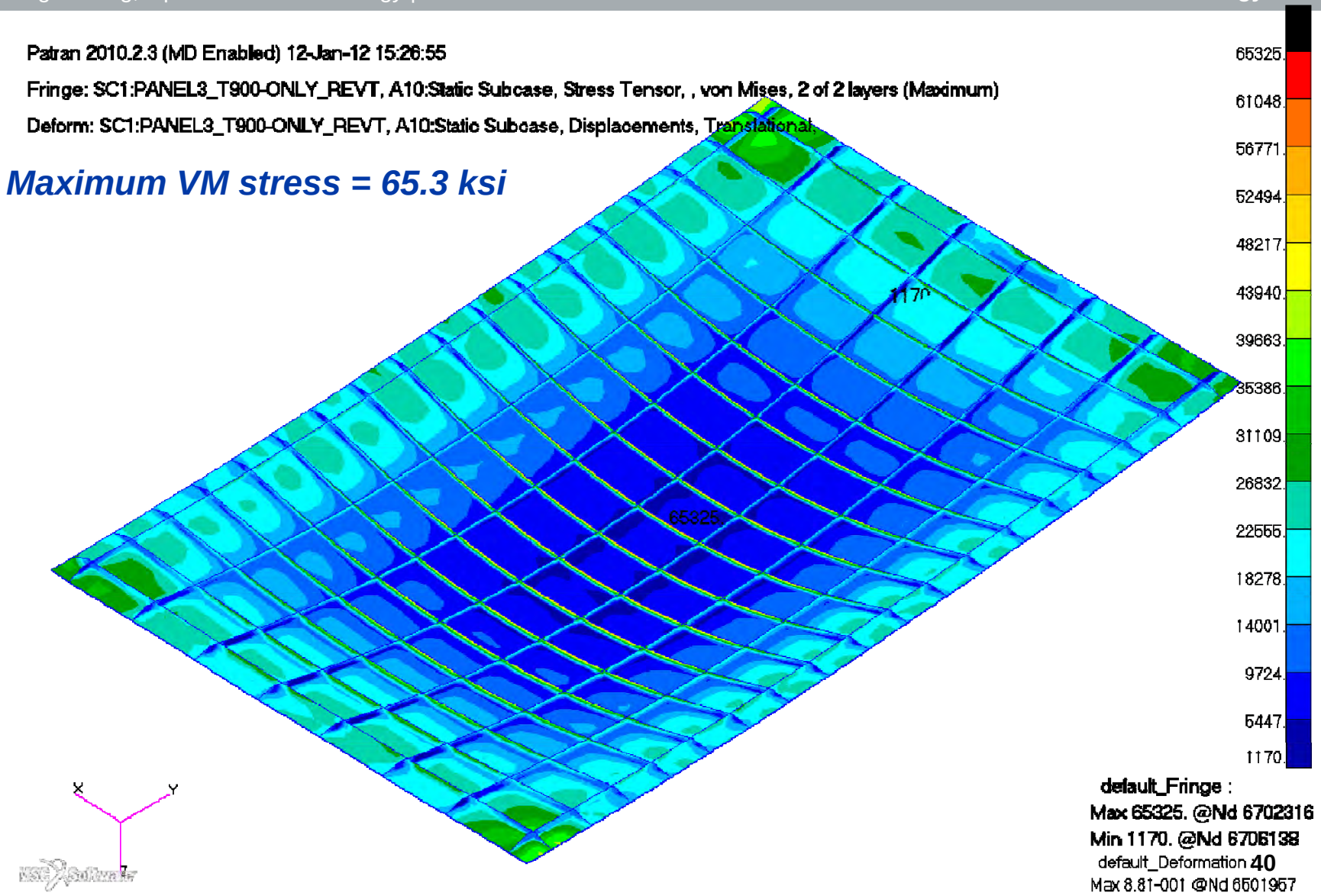

Maximum VM stress = 65.3 ksi

Approved for public release; distribution unlimited.

Panel model

Mech (2.5g) + Temp (T=900s)

431
Approved for public release; distribution unlimited.

Von Mises, Panel, 2.5G Ult 1.5, T=900s Linear

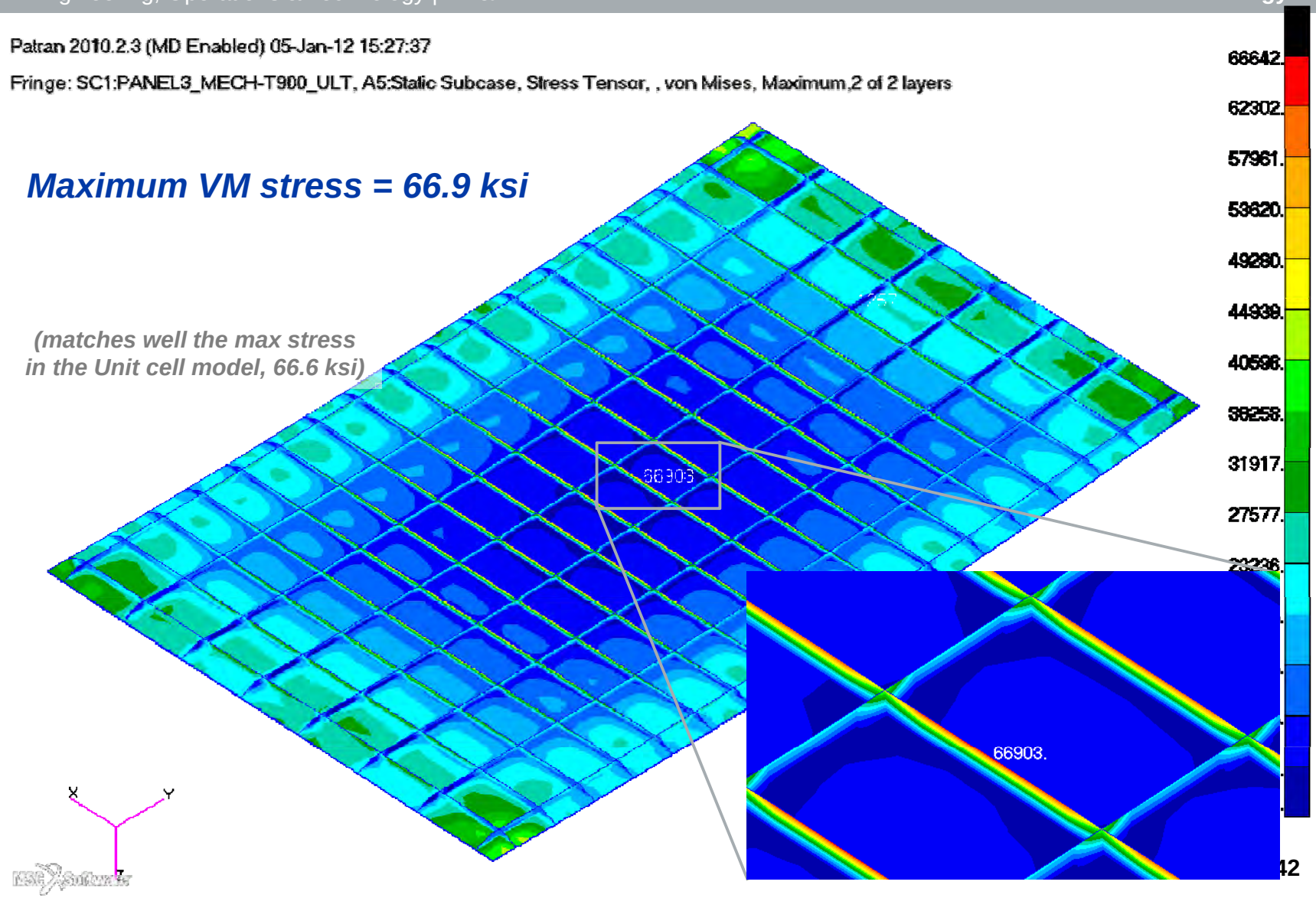

Maximum VM stress = 66.9 ksi

(matches well the max stress in the Unit cell model, 66.6 ksi)

Approved for public release; distribution unlimited.

Von Mises, Panel, 2.5G Ult 1.5, T=900s Linear

COMPARISON: Unit Cell v. Panel local model

Stresses plotted w/ same fringe range

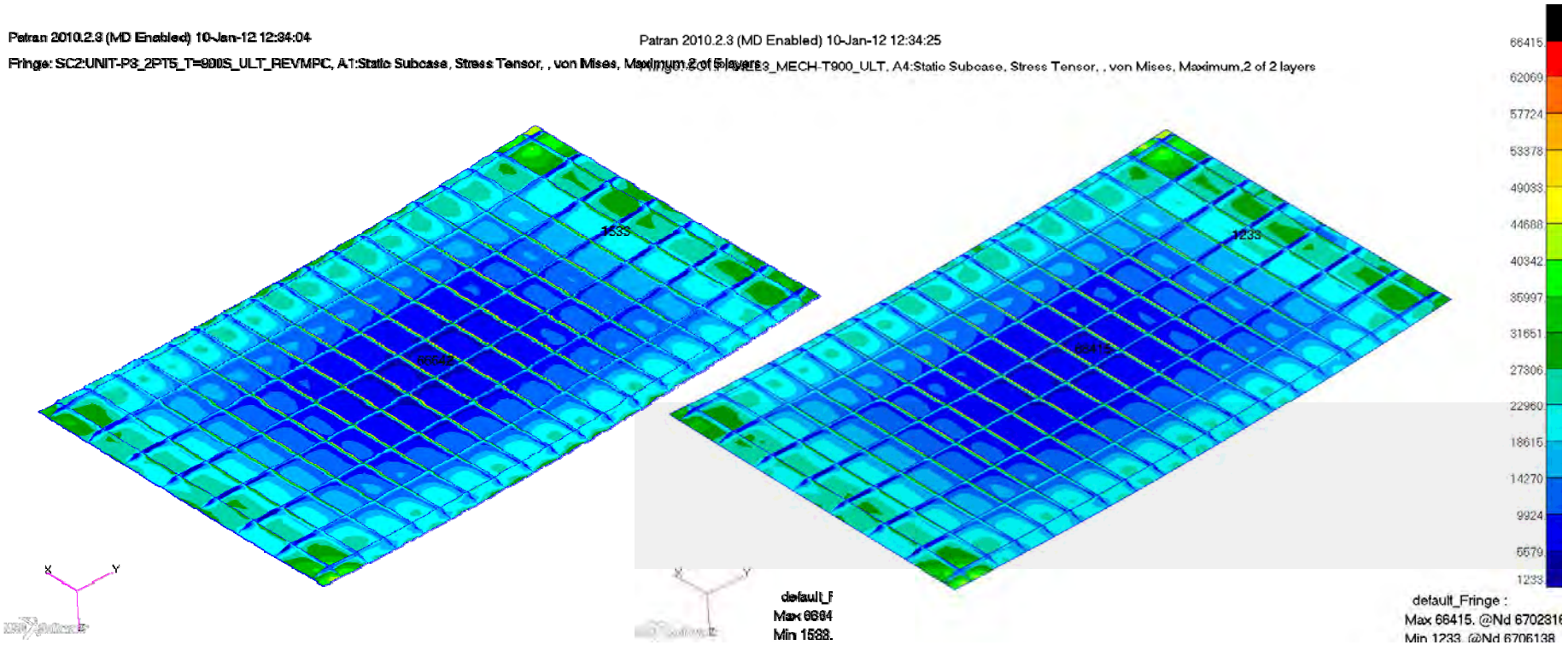

Unit Cell model
max stress = 66.6 ksi

Panel local model
max stress = 66.4 ksi

Approved for public release; distribution unlimited.

Von Mises, Panel, 2.5G Ult 1.5, T=900s Non-Linear

Local panel model

Stresses plotted w/ same fringe range

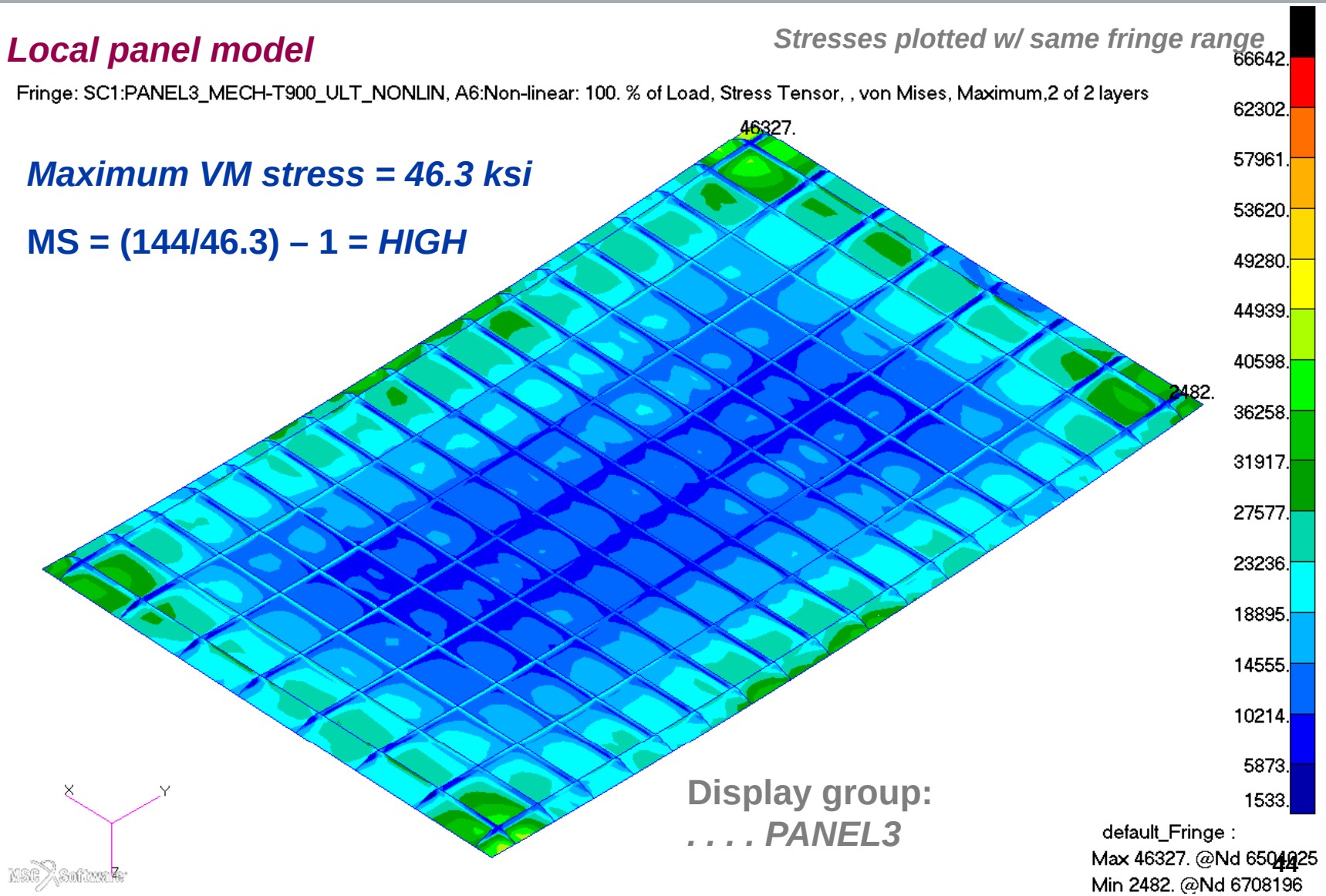

Maximum VM stress = 46.3 ksi

MS = (144/46.3) – 1 = *HIGH*

Display group:
. . . . PANEL3

Approved for public release; distribution unlimited.

Von Mises, Panel, 2.5G Lim 1.15, T=900s Non-Linear

Stresses plotted w/ same fringe range as linear run

Local panel model

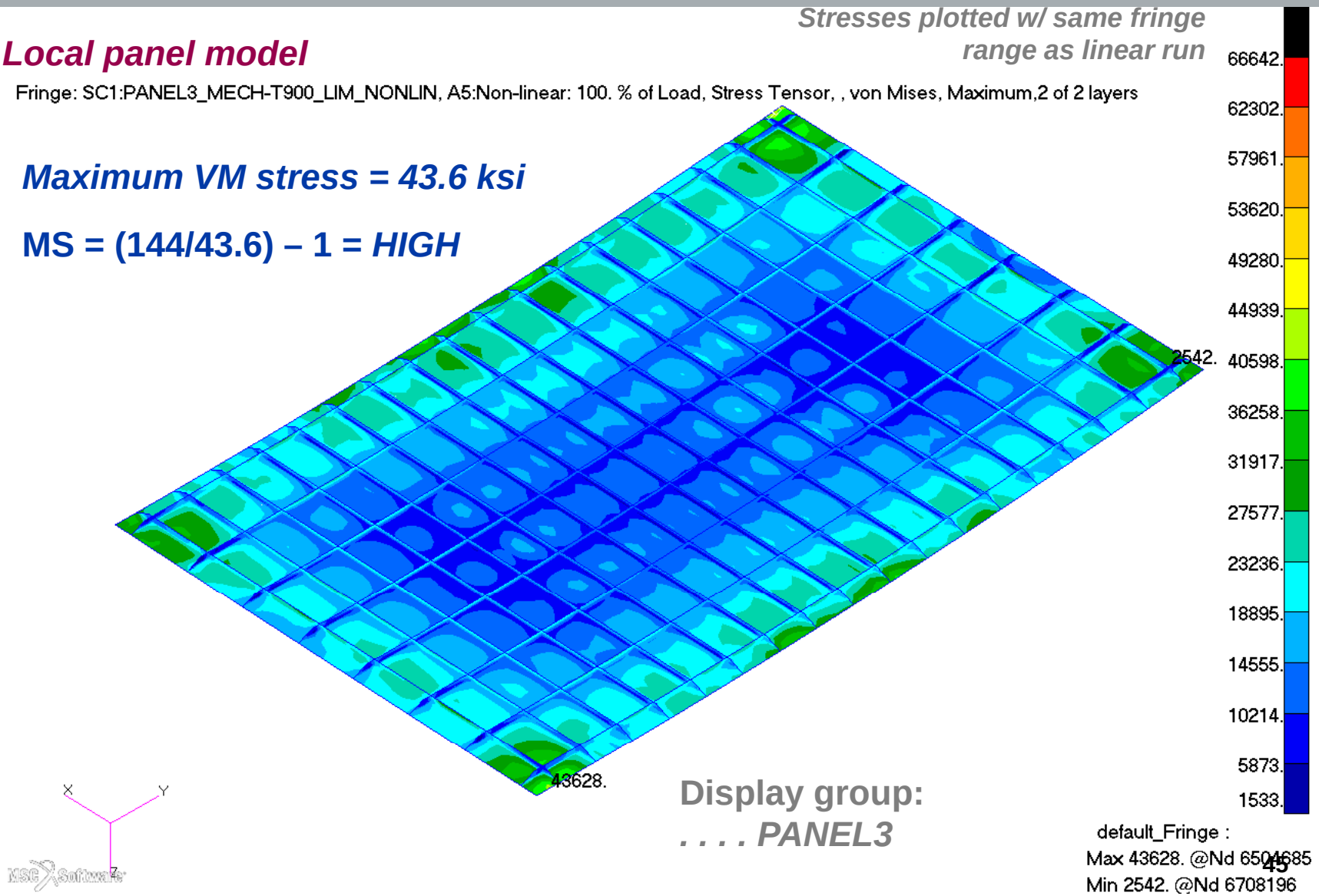

Maximum VM stress = 43.6 ksi

MS = (144/43.6) – 1 = *HIGH*

Display group:
. . . . PANEL3

Approved for public release; distribution unlimited.

Von Mises, Panel, 2.5G Ult 1.5, T=900s

Local panel model
Comparison, linear vs nonlinear

Stresses plotted w/ same fringe range

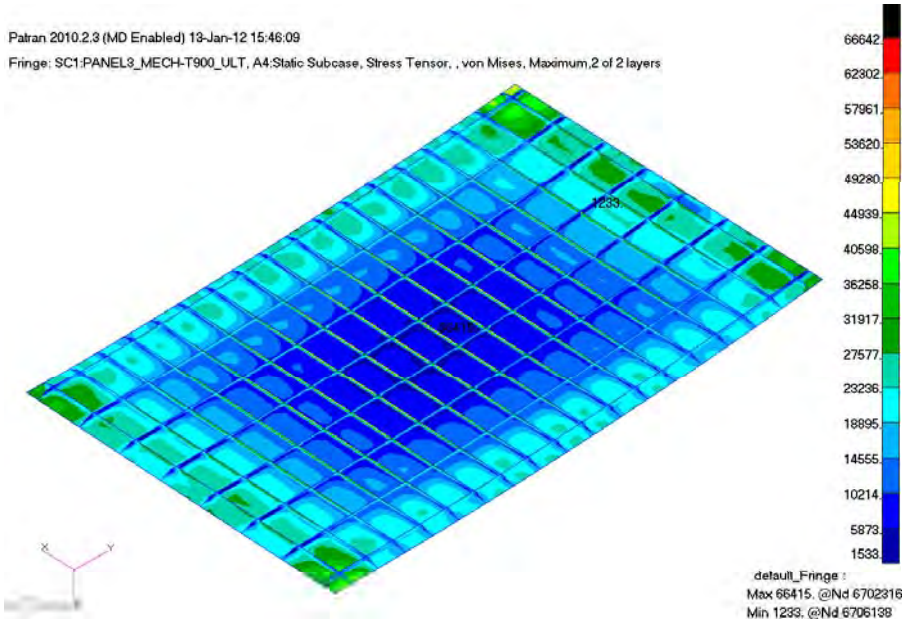

Linear

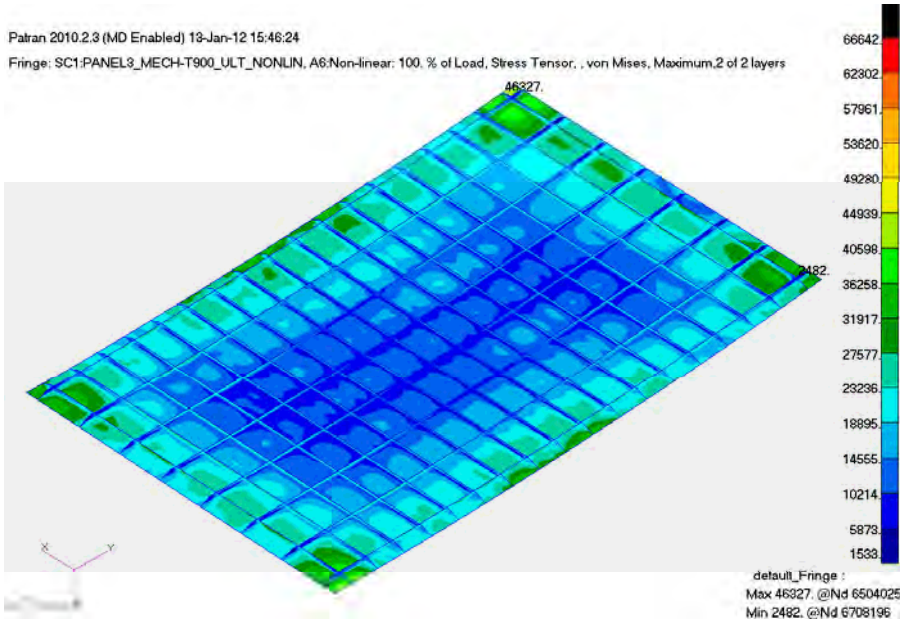

Non-linear

Approved for public release; distribution unlimited.

Displacements, Panel, 2.5G Lim 1.15, T=900s Non-Linear

Local panel model

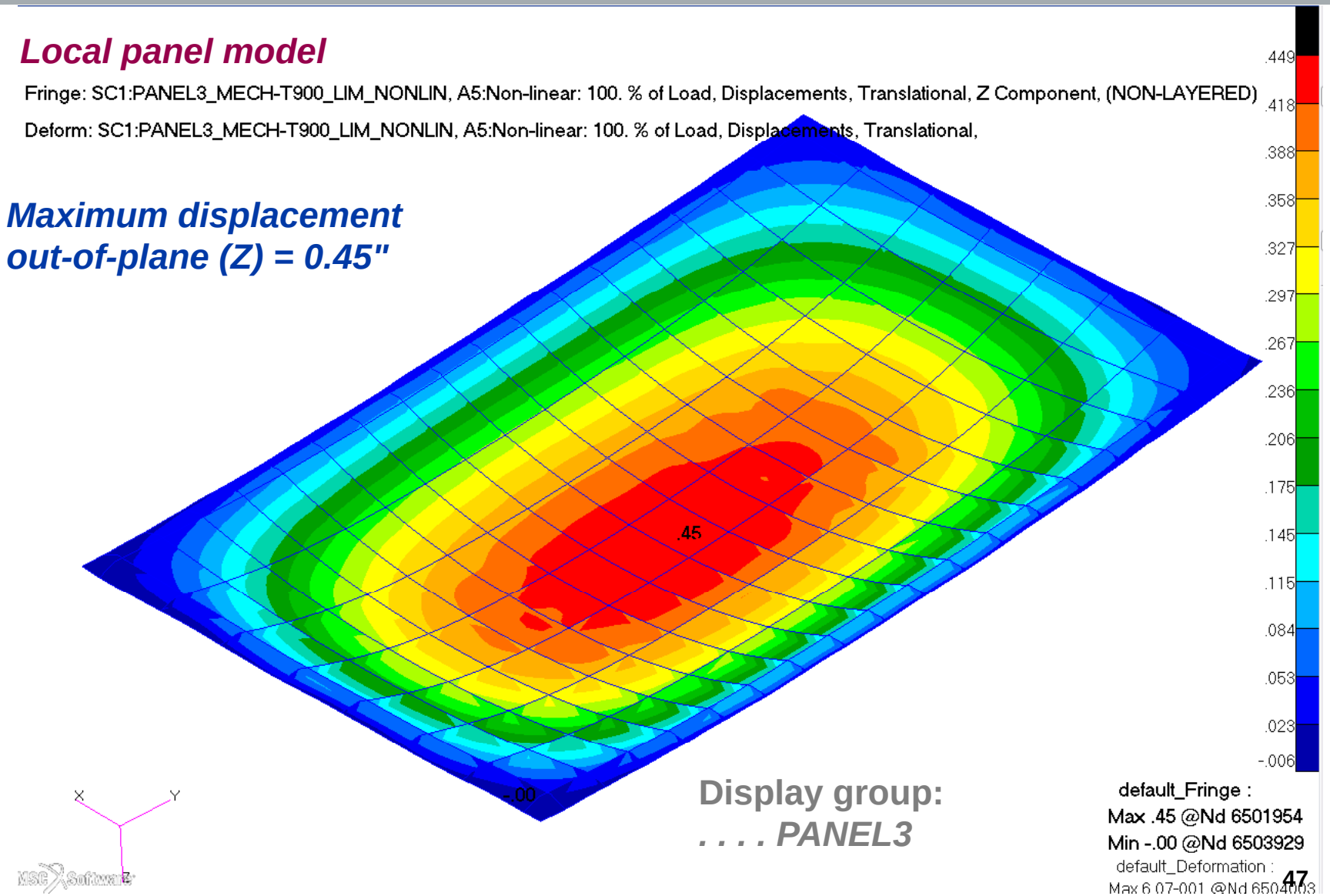

Maximum displacement out-of-plane (Z) = 0.45"

Display group:
. . . . PANEL3

Approved for public release; distribution unlimited.

Buckling, Panel, 2.5G Lim 1.15, T=900s

Local panel model

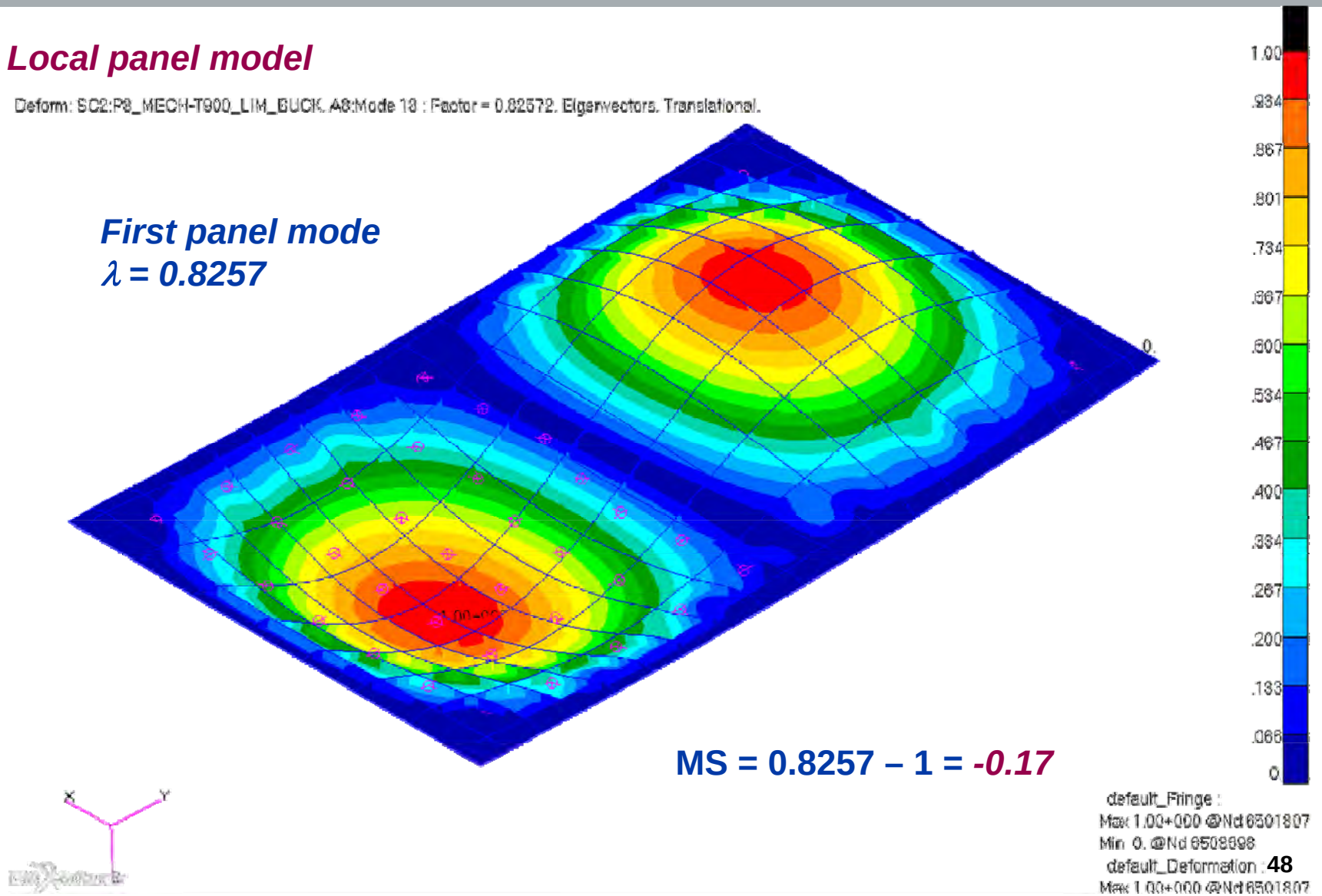

First panel mode
λ = 0.8257

MS = 0.8257 – 1 = *-0.17*

Approved for public release; distribution unlimited.

Margin of Safety Summary

Failure Mode	Solution Type	Thermal Load	Thermal F.S.	Mechanical Load	Mechanical F.S.	Allowable	Actual	Units	M.S.
Ultimate Material Failure	Non-Linear	T=900s	1	2.5g	1.5	144	46.3	ksi	***HIGH***
Displacement	Non-Linear	T=900s	1	2.5g	1.15	0.1	0.45	in.	***NEG***
Buckling	Buckling	T=900s	1	2.5g	1.15	1	0.83	eigenvalue	***-0.17***

- **Good static stress margins.**
- **Large normal displacements do not meet preliminary windward panel sizing criteria of 0.10".**
- **Negative buckling margins.**
- **This panel location was chosen and sized before thermal boundary conditions were fully developed. The effect of the fuel temperature constraints on structural thermal gradients was underestimated resulting in significantly higher thermal gradients and loads. Panel breakers were not initially considered necessary, but should be evaluated in future design iterations to improve stability and decrease normal deflection.**

Approved for public release; distribution unlimited.

PATRAN Database and NASTRAN Analysis Files

Approved for public release; distribution unlimited.

File Location:
Contact AFRL/RBSM Structural Sciences Center
WPAFB, OH, 45433

POC: Dr. S. Michael Spottswood, 937.904.6789, stephen.spottswood@wpafb.af.mil

Name of .zip file:
Panel_3_delivery_stress.zip

PATRAN Database for Unit-Cell and Panel Models
Orthogrid_P3.db

Flight Loads
Mach 7, +2.5g, symmetric pull up maneuver

Thermal
Temperature @
T = 60 sec, Maximum thermal gradient between panel skin and orthogrid stiffener
T = 900 sec, Maximum thermal gradient between panel and substructure
T = 2500 sec, Maximum temperature
T = 3480 sec, Maximum reverse thermal gradient

Boundary Conditions for Unit-Cell Model
Rigid Body Constraints

Approved for public release; distribution unlimited.

Linear Stress Analysis of Unit-Cell Model for 2.5G Only

Load Cases

UNITCELL

UNIT-P3_2PT5_LIM

2.5g * 1.15 (F.S.), Rigid body constraints

UNIT-P3_2PT5_ULT

2.5g * 1.5 (F.S.), Rigid body constraints

Analysis Files

010512_UNIT-P3_2p5_revMPC.dat

Results

010512_UNIT-P3_2p5_revMPC.xdb

Approved for public release; distribution unlimited.

Linear Stress Analysis of Unit-Cell Model for Thermal Only

Load Cases

UNITCELL

UNIT-P3_2T=900S)_REVT

Temp @ 900s, Rigid body constraint

Analysis Files

011112_UNIT-P3_T900s_ONLY_revT.dat

Results

011112_UNIT-P3_T900s_ONLY_revT.xdb

Approved for public release; distribution unlimited.

Linear Stress Analysis of Unit-Cell Model for 2.5G and Thermal (T=900s)

Load Cases

UNITCELL

UNIT-P3_2PT5_T=900S_LIM

2.5g * 1.15 (F.S.), Temp @ 900s, Rigid body constraint

UNIT-P3_2PT5_T=900S_ULT

2.5g * 1.5 (F.S.), Temp @ 900s, Rigid body constraint

Analysis Files

010512_UNIT-P3_2p5_T900s_revT_revMPC.dat

Results

010512_UNIT-P3_2p5_T900s_revT_revMPC.xdb

Approved for public release; distribution unlimited.

Linear Stress Analysis of Panel Model for Thermal (T=900s) Only

Load Cases

LOCAL PANEL

PANEL3_T900-ONLY_REVT

Temp @ 900s, Enforced displacements from Unit Cell at panel edges

Analysis Files

011112_PANEL_T900_ONLY_revT.bdf

Results

011112_panel_t900_only_revt.xdb

445
Approved for public release; distribution unlimited.

Linear Stress Analysis of Panel Model for 2.5G and Thermal (T=900s)

Load Cases

LOCAL PANEL

PANEL3_MECH-T900_LIM

2.5g * 1.15 (F.S.), Temp @ 900s, Enforced displacements from Unit Cell at panel edges

PANEL3_MECH-T900_ULT

2.5g * 1.5 (F.S.), Temp @ 900s, Enforced displacements from Unit Cell at panel edges

Analysis Files

010512_PANEL_MECH-T900_LIM.bdf
010512_PANEL_MECH-T900_ULT.bdf

Results

010512_panel_mech-t900_lim.xdb
010512_panel_mech-t900_ult.xdb

Approved for public release; distribution unlimited.

Non-Linear Stress Analysis of Panel Model for 2.5G and Thermal (T=900s)

Load Cases

LOCAL PANEL

PANEL3_MECH-T900_LIM_NONLIN

2.5g * 1.15 (F.S.), Temp @ 900s, Enforced displacements from Unit Cell at panel edges

PANEL3_MECH-T900_ULT_NONLIN

2.5g * 1.5 (F.S.), Temp @ 900s, Enforced displacements from Unit Cell at panel edges

Analysis Files

010512_PANEL_MECH-T900_LIM_NONLIN.bdf
010512_PANEL_MECH-T900_ULT_NONLIN.bdf

Results

010512_panel_mech-t900_lim_nonlin.xdb
010512_panel_mech-t900_ult_nonlin.xdb

447
Approved for public release; distribution unlimited.

Buckling Analysis of Panel Model for 2.5G and Thermal (T=900s)

Load Cases

LOCAL PANEL

P3_MECH-T900_LIM_BUCK

2.5g * 1.15 (F.S.), Temp @ 900s, Enforced displacements from Unit Cell at panel edges

Analysis Files

010612_PANEL_MECH-T900_BUCK_2.bdf

Results

010612_panel_mech-t900_buck_2.xdb

Approved for public release; distribution unlimited.

Panel 3 (816) Dynamic & Fatigue Analysis

January 20, 2012

Craig Masterson
314-232-9424
Craig.Masterson@boeing.com

Approved for public release; distribution unlimited.

Unit Cell

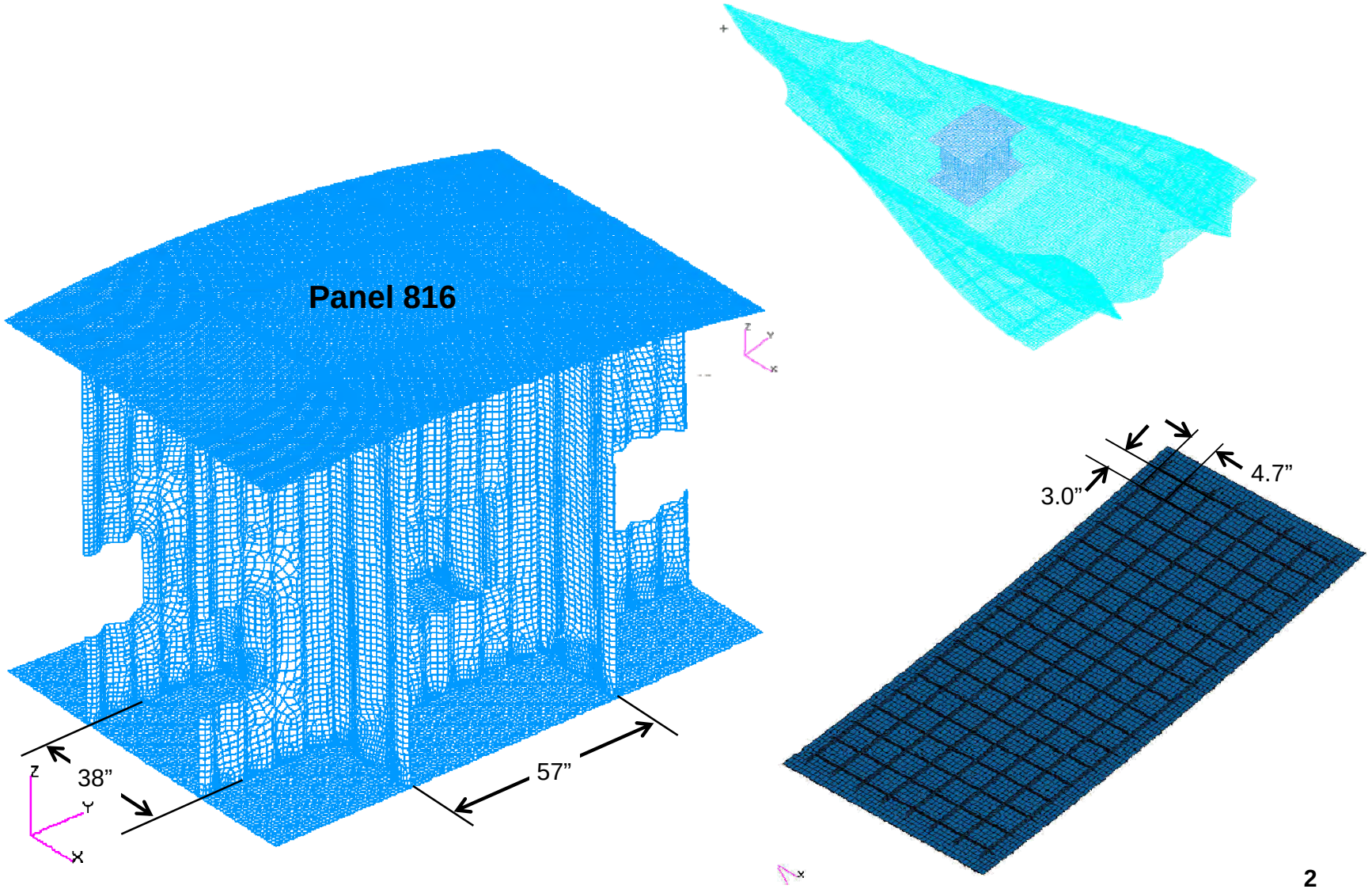

Approved for public release; distribution unlimited.

Panel 816 Dynamic Analysis

- Methods and Approach
- Analysis Assumptions
- Finite Element Model and Boundary Conditions
- Results
  - Modal
  - Response
  - Fatigue
  - Flutter
- Lessons Learned
- Summary
- Current /Future Activities

451
Approved for public release; distribution unlimited.

Methods & Approach

Tool / Method

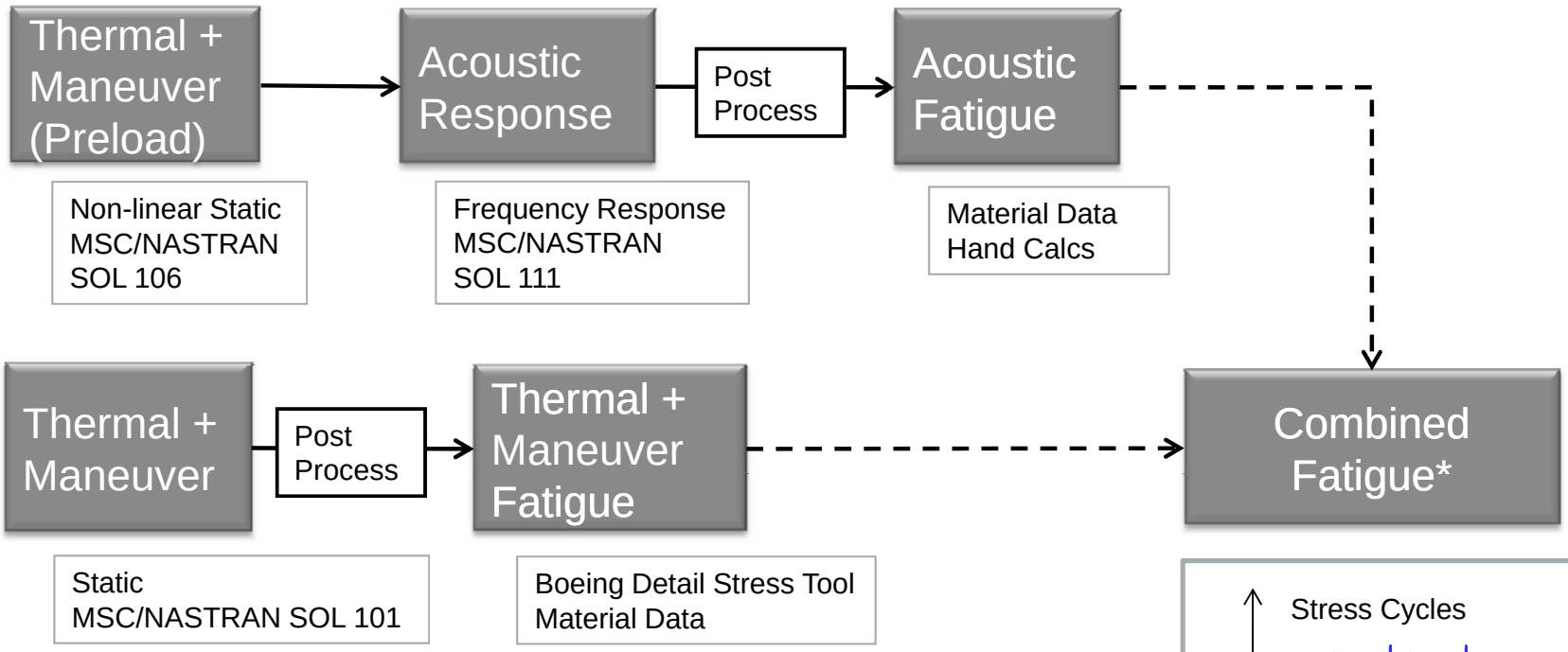

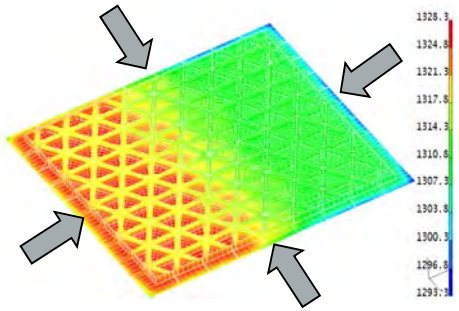

- Check fatigue at stress critical locations and Determine Flights to Failure
- Apply thermal knockdowns to fatigue S-N data
- Build combined spectrum and perform fatigue analysis

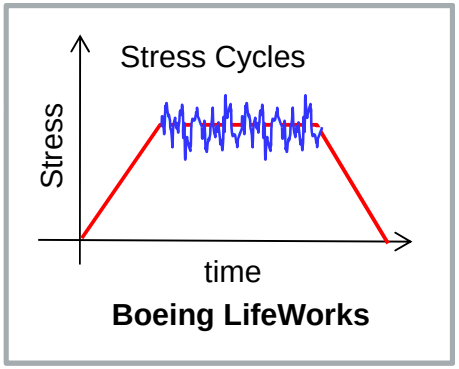

*Combined fatigue analysis not performed for panel 816

Approved for public release; distribution unlimited.

Fatigue Analysis Approach

- **Use Mil-hd-bk 5 Inconel 718 constant amplitude data**
- **Adjust for temperature and stress ratio if applicable**
- **Calculate design feature $k_t\sigma$ – holes, welds, radii**
- **Post-process results – references stress value**
- **Calculate Acoustic Margins – Compare predicted RMS Stress (KtS) to RMS Allowable (Endurance Limit)**
- **Assembly stress spectrum – Include maneuver loads, temperature for ground-air-ground (GAG) Cycles**
- **Calculate thermal-mechanical fatigue margins**
- **Perform acoustic damage (Dynamic Cycles) separate***
- **Calculate Total Fatigue Life – Combined Damage***

*A total fatigue life based on combined damage accumulation was not calculated for this panel
Margin of safety calculations will show panel is dominated by thermal-mechanical cyclic fatigue

Approved for public release; distribution unlimited.

General Fatigue Analysis Assumptions

- **A combined total fatigue life based on accumulated damage from aero-acoustic loads and cyclic thermal-mechanical fatigue was not performed for this panel (fatigue life dominated by thermal-mechanical stress)**
- **Thermal exposure effect on Fty is proportional to temperature effect on fatigue allowable**
- **Boundary conditions are dependent on the type of analysis being performed**
  - Linear and non-linear static solutions: 3 nodes are pinned to constrain rigid body motion
  - Modal and frequency response solutions: symmetry boundary condition imposed along unit cell interface nodes to simulate support from surrounding bays

Approved for public release; distribution unlimited.

Analysis Summary Table

- **Unit cell FEM used for all analyses except for flutter analysis**

Analysis Type	Preload	Load	Boundary Conditions	Output	Solution File(s)
Linear Static (SOL 101)	None	Mechanical (2.5G) Thermal (t = 900s)	RBM Constraint at 3 nodes	> Stress for thermal-mechanical loads fatigue analysis	010512_UNIT-P3_2p5_T900s_revT_rev MPC.xdb
Normal Modes (SOL 103)	None	Thermal (t=900s) Material Property Only	Symmetry along unit cell boundary	> Normal Modes and Mode Shapes > Provides frequency range of interest for SOL 111	p3_uc_sol103_temp-900s-materal.xdb
Non-linear Static (SOL 106)	None	Thermal (t=900s) Material + Load	RBM Constraint at 3 nodes	> Non linear stress and displacement > Preload for SOL111 > Stress results used as mean stress in fatigue calculations	panel3_sol106_0106-01.xdb
Frequency Response (SOL 111)	SOL 106	Thermal (t = 900s) Material Property Only	Symmetry along unit cell boundary	> RMS stress	Panel3_SOL111_0106-01_Symm.xdb
Flutter (SOL 145)	None	Thermal (t = 900s) Material Property Only	Symmetry at fwd and aft edges, Z pin at frame locations	> Damping and modal frequency vs. velocity	P3Ext_XFlow_Temp900s_15Mds_M6to9_k1_SL_M7p5.dat

Approved for public release; distribution unlimited.

Unit Cell Boundary Conditions

Static Solution Boundary Conditions

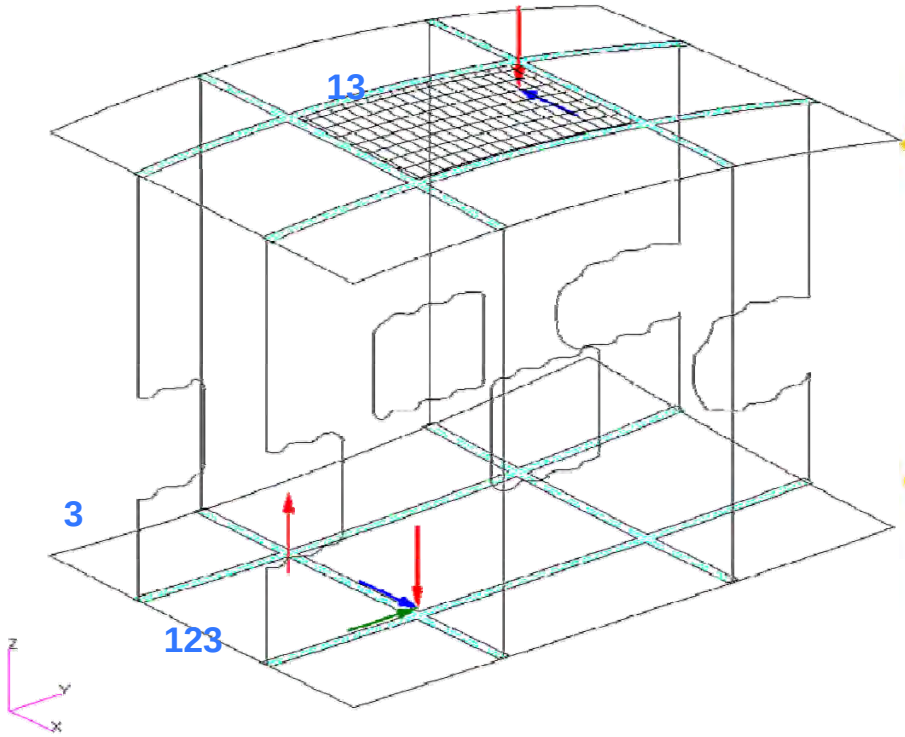

Constrained at 3 nodes on keel webs to prevent rigid body motion

Frequency Domain Boundary Conditions

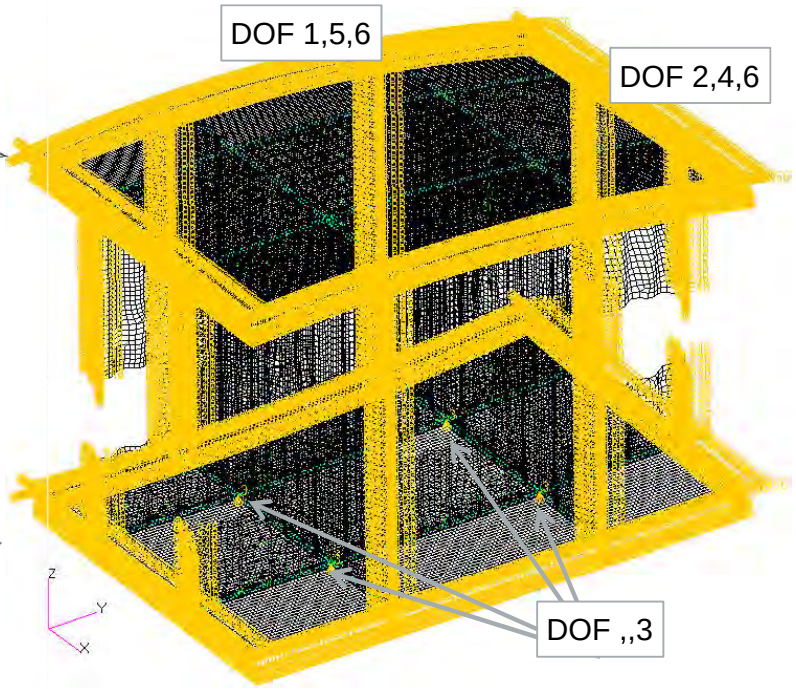

Symmetry boundary condition used to simulate support from surrounding panels to minimize substructure modes

Z-dir SPC applied to nodes: 6748377, 6748597, 6763840, 6778597

Approved for public release; distribution unlimited.

MODAL ANALYSIS

457
Approved for public release; distribution unlimited.

SOL 103 Documentation

- **Preload**
  - None
- **Material Properties**
  - Inconel properties at mapped temperatures for t=900s thermal load
  - Remove mass from all structure excluding panel 816
- **Boundary Conditions**
  - Symmetry Applied to Edges
  - Z-dir SPC applied to nodes: 6748377, 6748597, 6763840, 6778597
- **SOL 103**
  - Group: "…RUN_FEM_NEW_120711a_noMPC"
  - Input File: P3_UC_SOL103_Temp-900s-Materal.dat
  - Results File: P3_UC_SOL103_Temp-900s-Materal.xdb

```
$ Normal Modes Analysis, Database
SOL 103
CEND
$ Direct Text Input for Global Case Control Data
TITLE = MD NASTRAN JOB CREATED ON 11-NOV-11 AT
13:00:52
ECHO = NONE
RESVEC = YES
SUBCASE 1
   SUBTITLE=P3_UC_Temp-900s_Symm
   METHOD = 1
   SPC = 901
   TEMPERATURE(MATERIAL) = 900
   VECTOR(SORT1,REAL)=ALL
   SPCFORCES(SORT1,REAL)=ALL
$ Direct Text Input for this Subcase
BEGIN BULK
$ Direct Text Input for Bulk Data
PARAM    POST    0
PARAM    WTMASS .0026
PARAM   PRTMAXIM YES
EIGRL    1       .1      1000.    10      0
MASS
$
TABDMP1  1       CRIT
         10.     .025    100.     .02     1000.
.01      ENDT
$
```

Excerpt of SOL 103 Nastran Deck

Approved for public release; distribution unlimited.

SOL 103 Results

Mode 1
Freq = 47.9 Hz

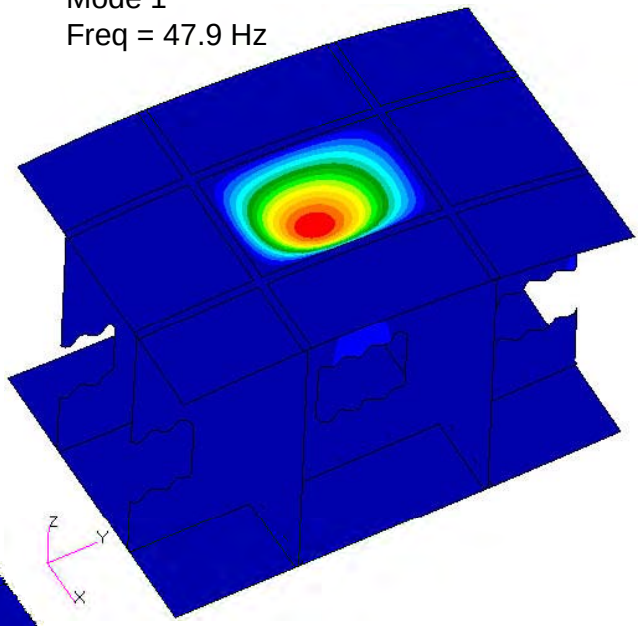

Mode 2
Freq = 51.4 Hz

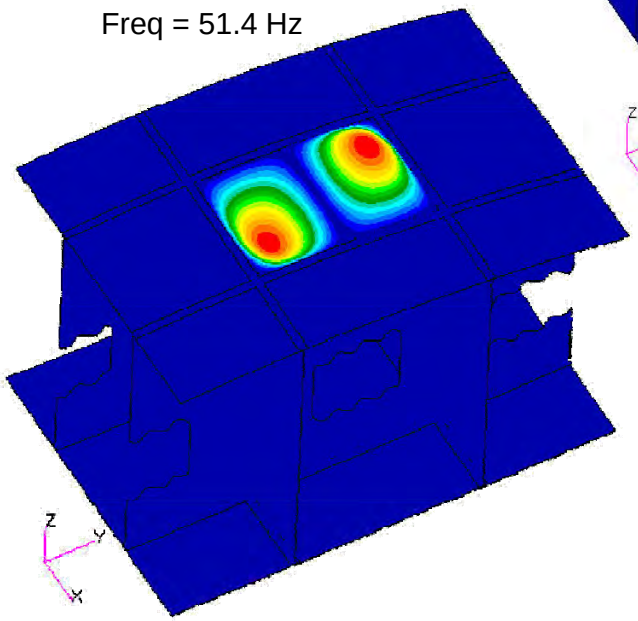

Mode 3
Freq = 86.6 Hz

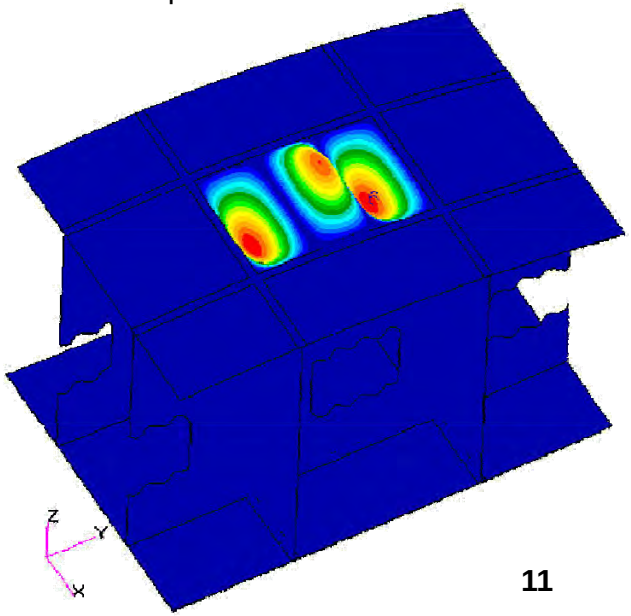

P3_UC_SOL103_Temp-900s-Materal.dat

Approved for public release; distribution unlimited.

SOL 103 Panel Results (Flutter Analysis)

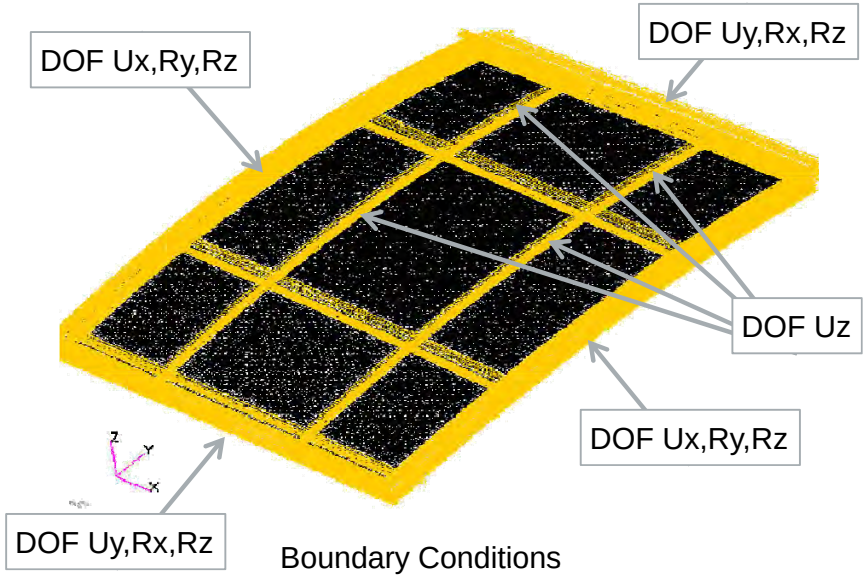

Boundary Conditions

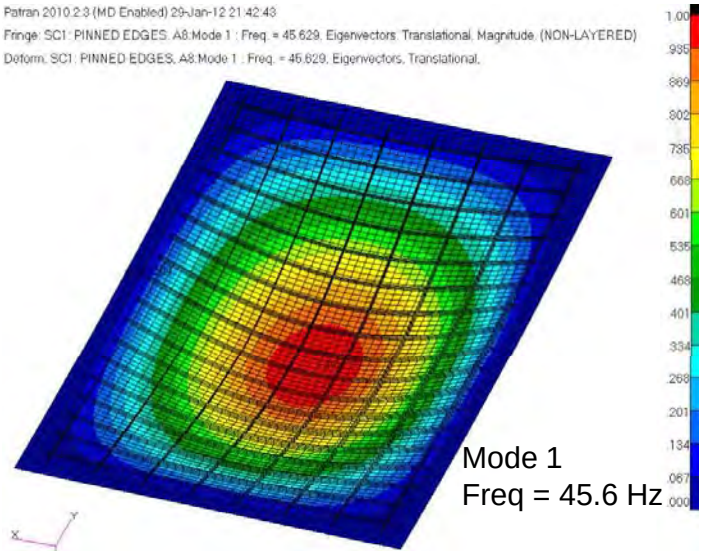

Mode 1
Freq = 45.6 Hz

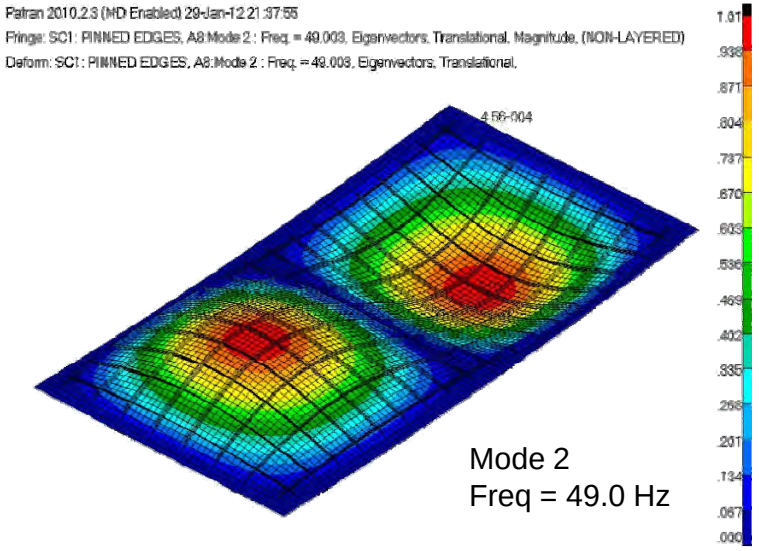

Mode 2
Freq = 49.0 Hz

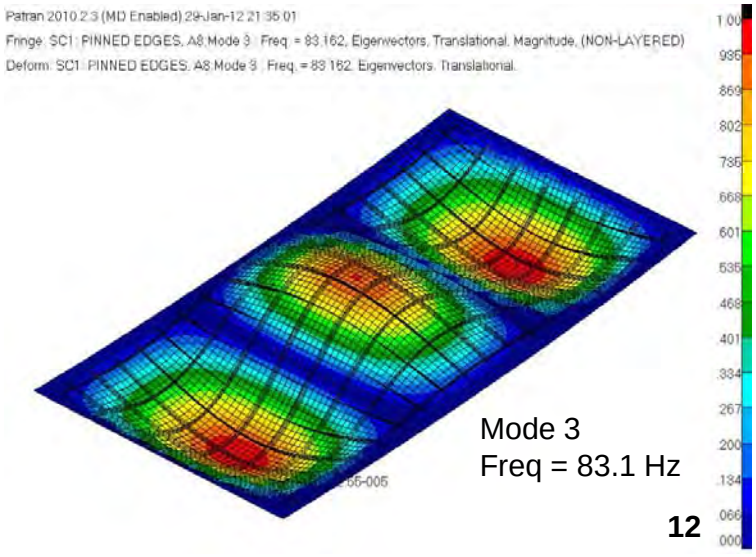

Mode 3
Freq = 83.1 Hz

Approved for public release; distribution unlimited.

AERO-ACOUSTIC FATIGUE

461
Approved for public release; distribution unlimited.

Acoustic Fatigue Analysis Approach

- **Use Mil-hdbk-5 Inconel 718 Constant Amplitude Data**
  - Adjust for Temperature and Stress Ratio
- **Calculate Design Feature Ktσ – Holes, Welds, Radii**
- **Post-process results – references stress value**
- **Calculate Margins – Compare predicted RMS Stress (KtS) to RMS Allowable (Endurance Limit)**

Approved for public release; distribution unlimited.

Acoustic Fatigue Analysis Assumptions

- **Mechanical Loads negligible during max Q flight envelope**
  - Limit Case of 1G * 1.15 did not affect stress results
- **Kt = 3.0 for filled fastener hole**
- **Thermal exposure effect on Fty is proportional to temperature effect on fatigue allowable**
- **Stress concentrations at orthogrid stiffener terminations will be ignored due to the time constraints of this study**

463
Approved for public release; distribution unlimited.

Dynamic Model - Loading & Boundary Conditions

- Preload
  - SOL 106: Panel3_SOL106_0106-01.dat
- Material Properties
  - Inconel properties at mapped temperatures for t=900s thermal load
- Boundary Conditions
  - Symmetry Applied to Edges
  - Z-dir SPC applied to nodes 6748377, 6748597, 6763840, 6778597
- Acoustic Loads (3 - Zones)
  - Flow Direction – Uncorrelated (Panels vibrate independently)
  - Cross Flow – Fully Correlated (Panel vibration is in phase)
  - 1 psi plane wave acoustic load (Orthogonal to panel)
  - 0.1 to 1000hz forcing frequency
  - Damping function of frequency
- SOL 111
  - Input Files: Panel3_SOL106_0106-01.dat, FME_UC_SOL103_Temp-900s.bdf, test_T3D_Str_Thermal_ld_900.nas
  - Results File: Panel3_SOL111_0106-01_Symm.xdb

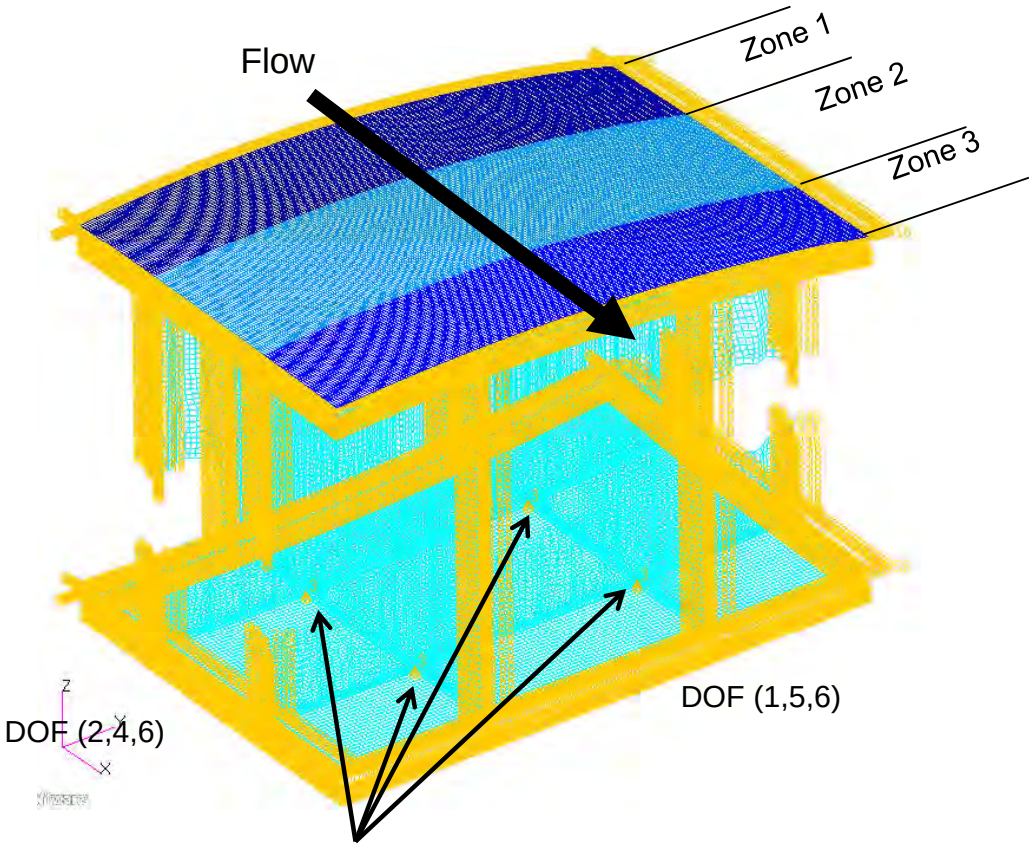

Approved for public release; distribution unlimited.

Acoustic Response – RMS Displacement Result

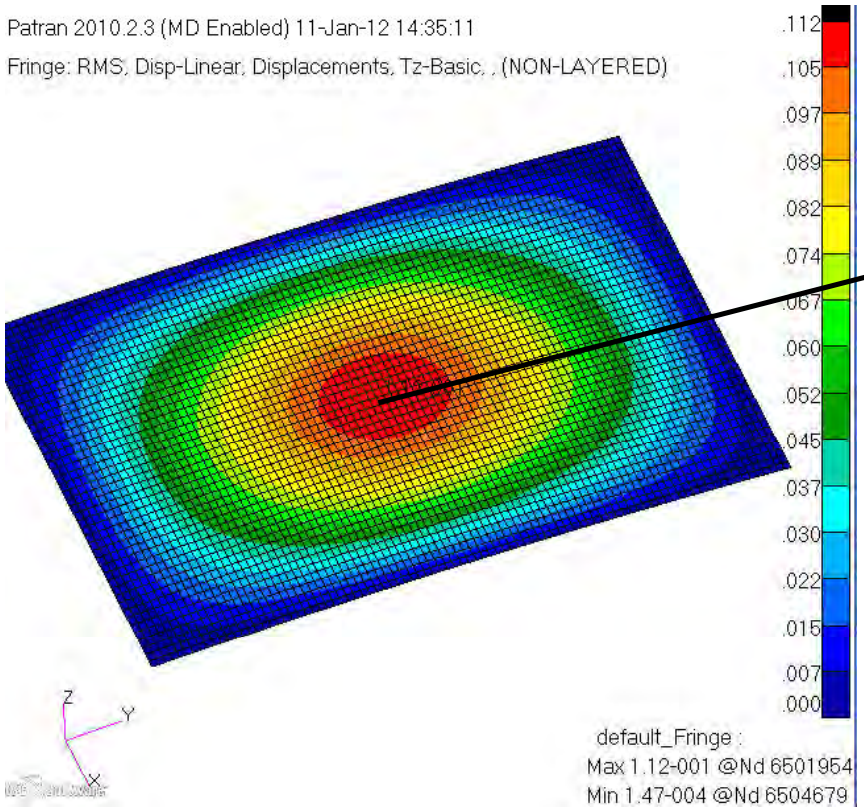

Max Acoustic S/TBL Spectrum
(Max TZ, node 6501954)

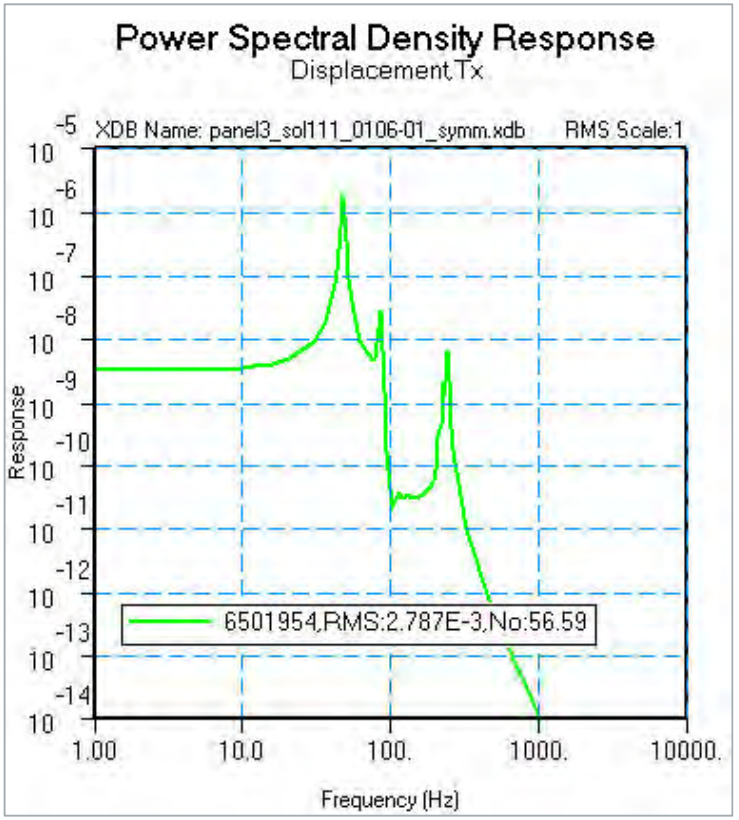

PSD Displacement Response:
Node 6501954

Approved for public release; distribution unlimited.

RMS Stress Allowable - Inconel 718

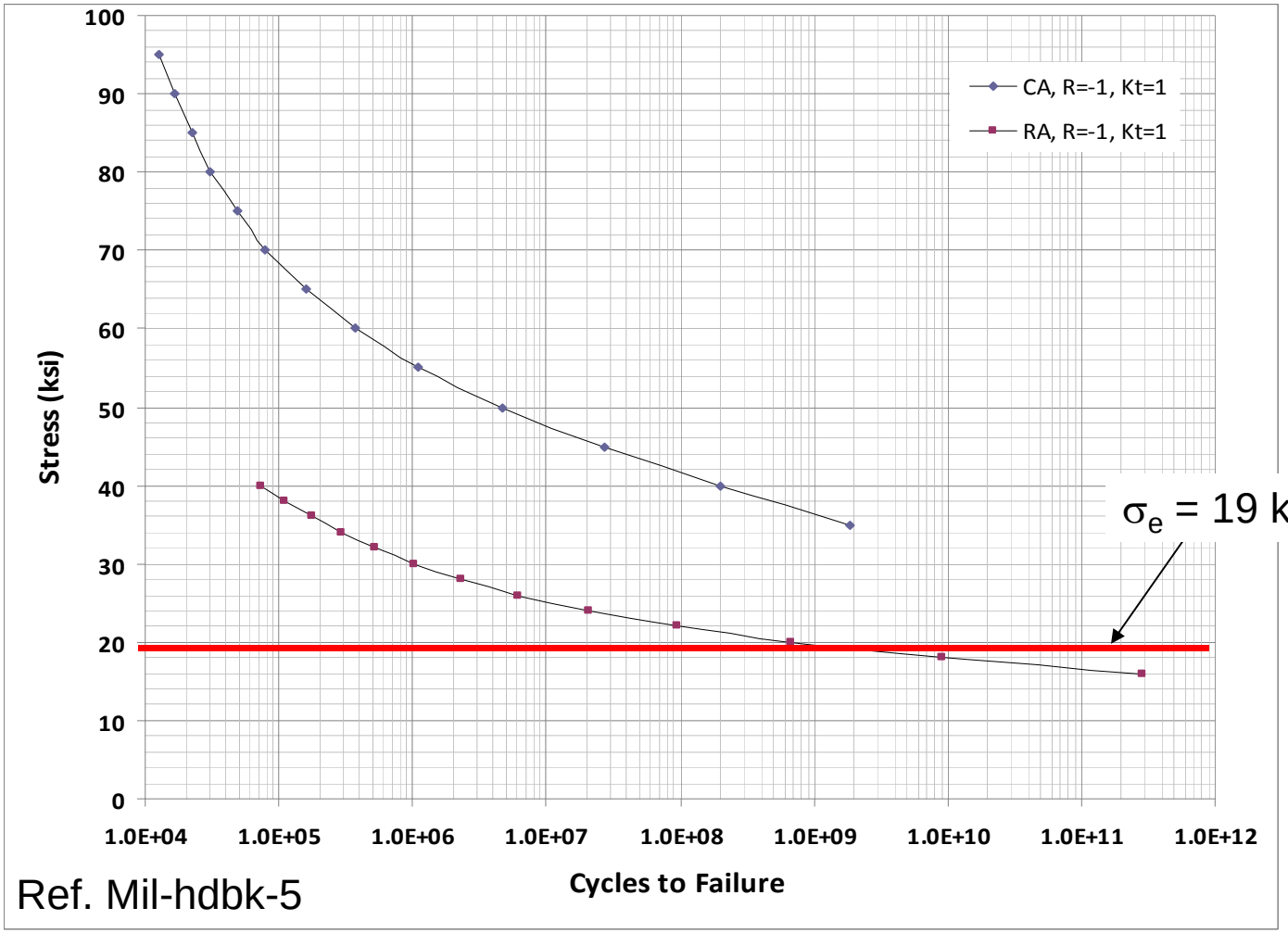

Approved for public release; distribution unlimited.

MMPDS – Inconel 718 – Fty v. Temp

- **Assume fatigue allowable follows trend of Fty as a function of temperature exposure**

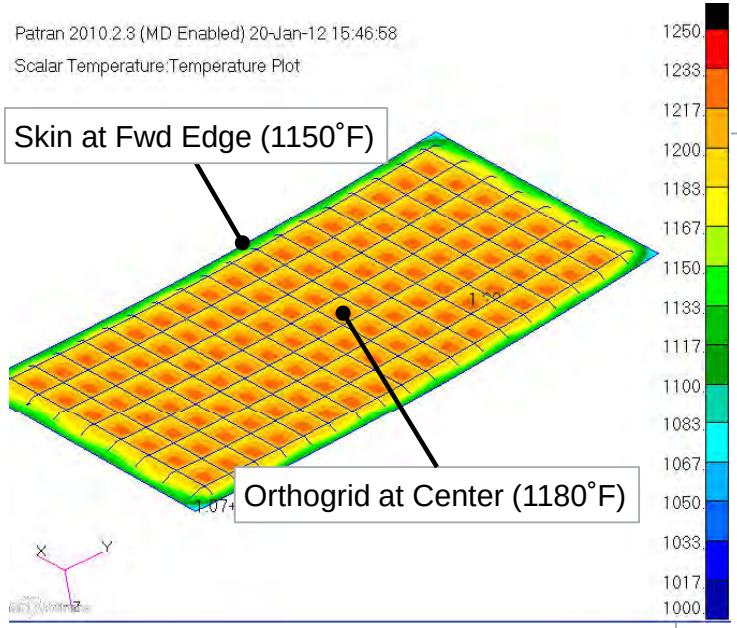

Applied Thermal Load for maximum panel to substructure gradient (t=900s)

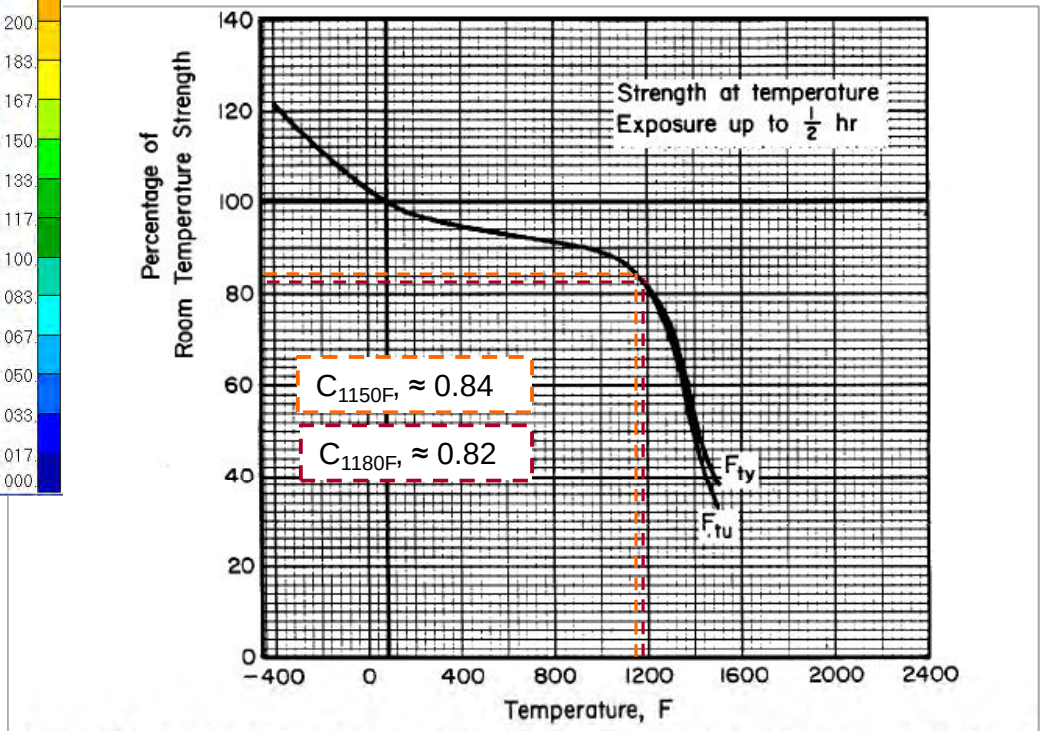

Figure 6.3.5.1.1. Effect of temperature on the tensile ultimate strength (F_{tu}) and tensile yield strength (F_{ty}) of solution-treated and aged Inconel 718.

Approved for public release; distribution unlimited.

MMPDS – Inconel 718 – S/N Curve

- **For locations with Kt < 1.5 use Fig 6.3.5.1.8.c (Best-fit S/N curves for un-notched Inconel 718 sheet at 1000F)**

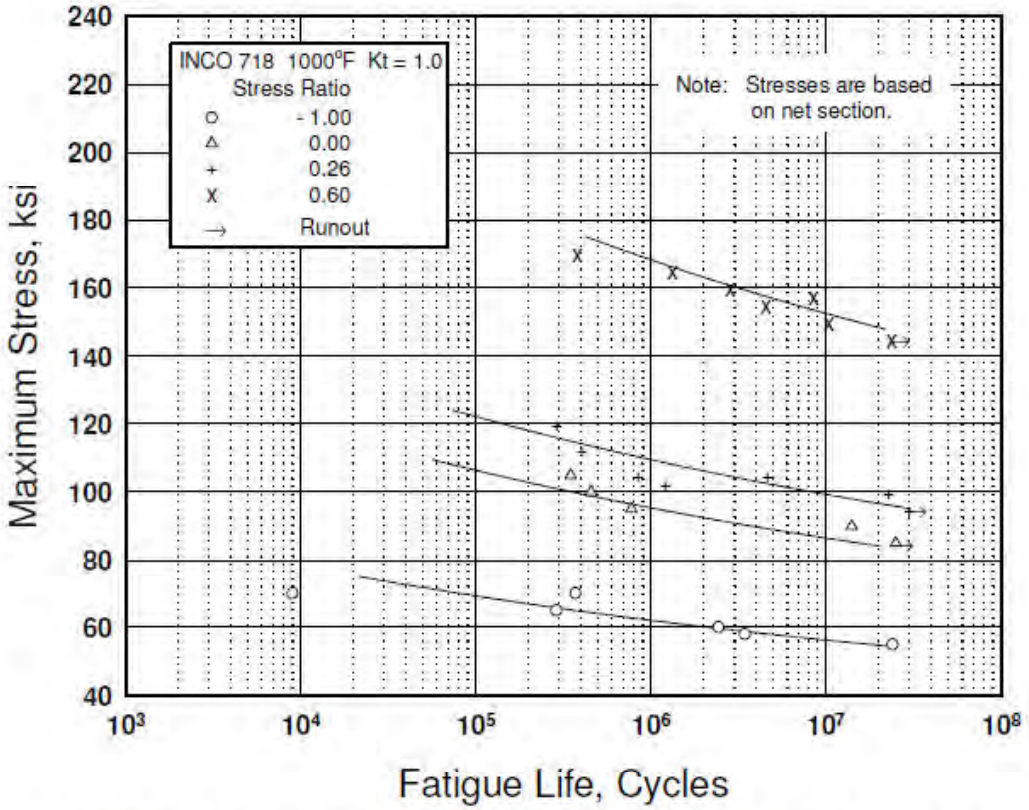

Equivalent Stress Equation:

$\text{Log } N_f = 23.51 - 10.57 \text{ Log } (S_{eq} - 50)$

$S_{eq} = S_{max}(1\text{-}R)^{0.62}$

Std. Error of Estimate, Log (Life) = 0.414

Standard Deviation, Log (Life) = 0.776

$R^2 = 71.5\%$

Figure 6.3.5.1.8(c). Best-fit S/N curves for unnotched Inconel 718 sheet at 1000°F, long transverse direction.

Approved for public release; distribution unlimited.

MMPDS – Inconel 718 – S/N Curve

- **For locations with Kt > 1.5 use Fig 6.3.5.1.8.c (Best-fit S/N curves for un-notched Inconel 718 sheet at 1000F)**

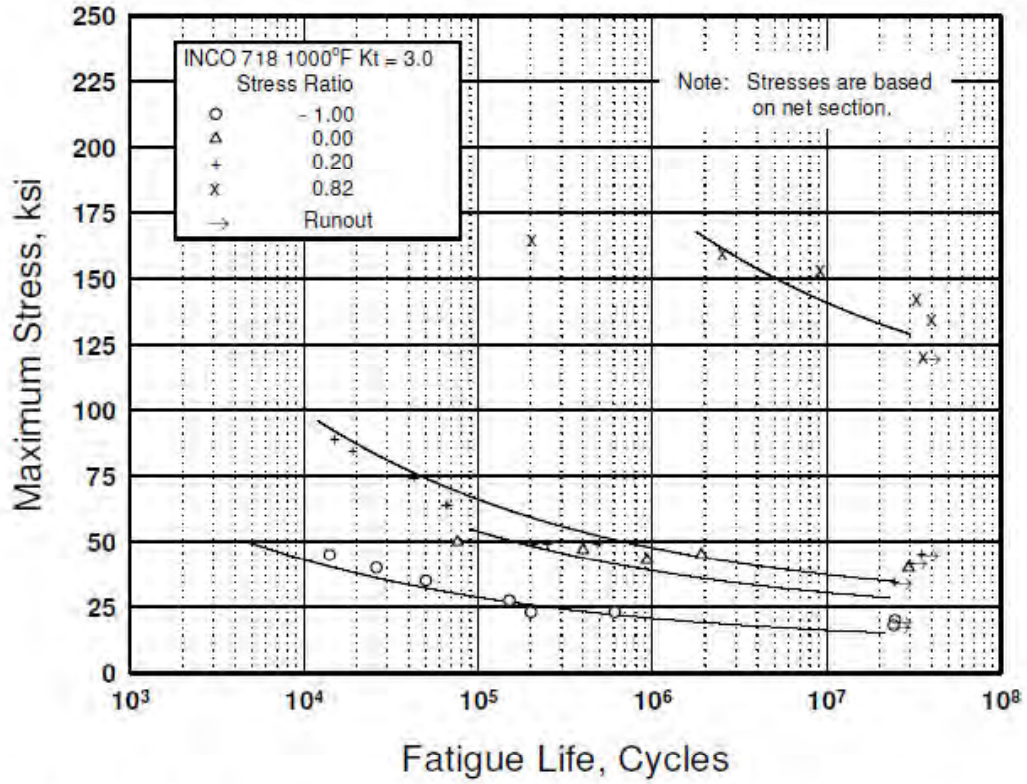

Equivalent Stress Equation:

$\text{Log } N_f = 11.02 - 3.93 \text{ Log } (S_{eq} - 20)$

$S_{eq} = S_{max}(1\text{-}R)^{0.91}$

Std. Error of Estimate, Log (Life) = 0.404

Standard Deviation, Log (Life) = 0.988

$R^2 = 83.3\%$

Sample Size = 23

[Caution: The equivalent stress model may provide unrealistic life predictions for stress ratios beyond those represented above.]

Figure 6.3.5.1.8(d). Best-fit S/N curves for notched, K_t = 3.0, Inconel 718 sheet at 1000°F, long transverse direction.

Approved for public release; distribution unlimited.

Unit Cell Model, Panel Results, Frequency Response, Thermal Only Preload (t=900s)

- **RMS stress plot shows peak stress along orthogrid stiffeners and near skin to substructure**

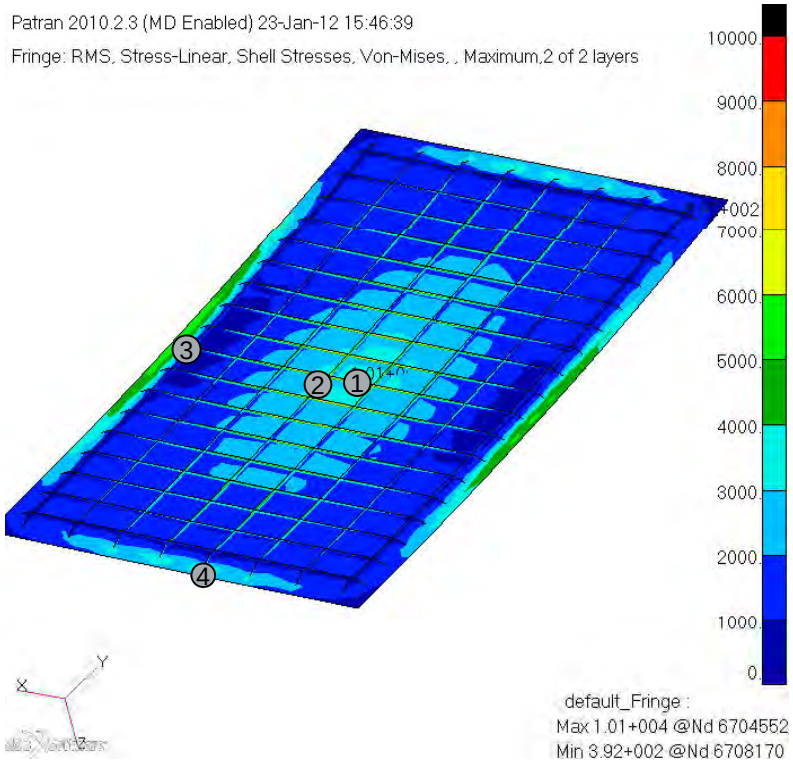

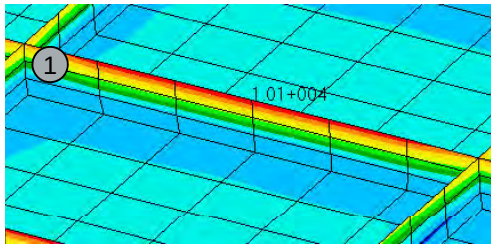

RMS Von Mises Stress =10.1ksi
X-dir Orthogrid

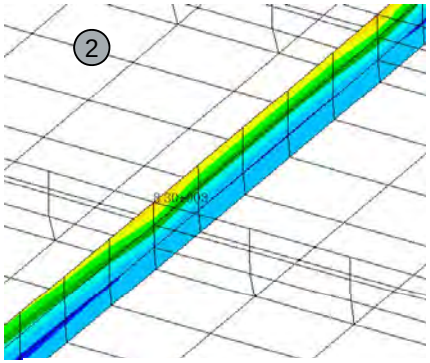

RMS Von Mises Stress =8.3ksi
Y-dir Orthogrid

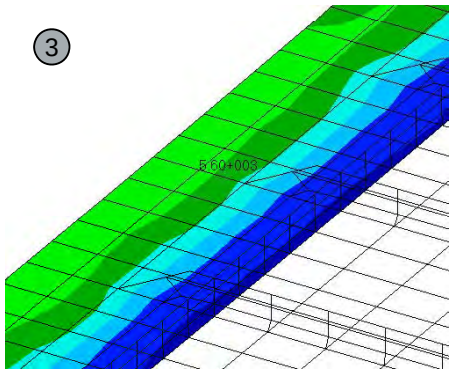

RMS Von Mises Stress =5.6ksi
Aft Skin to Substructure Joint

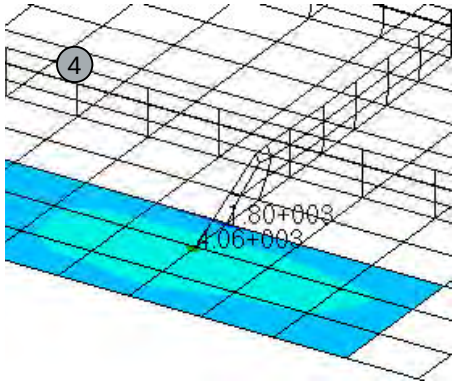

RMS Von Mises Stress =4.1ksi
Aft Skin to Substructure Joint

Approved for public release; distribution unlimited.

Skin to Substructure Fastener Hole near Panel Stiffener Termination

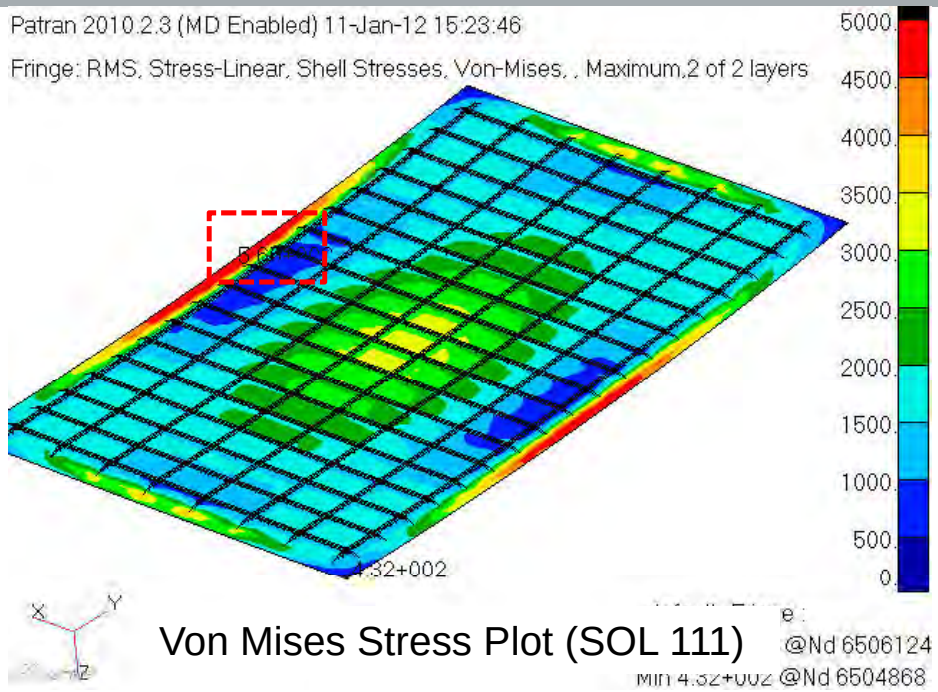

Von Mises Stress Plot (SOL 111)

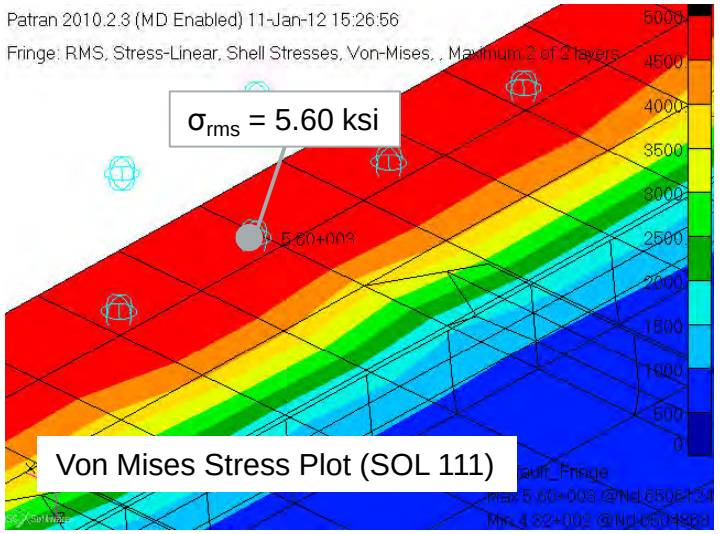

Von Mises Stress Plot (SOL 111)

Kt = 3.0 R = 0.74 T = 1150F

$$k_t\sigma'_e = \frac{\sigma_e \cdot C_T \cdot C_R}{k_t} = \frac{19.0 \cdot 0.84 \cdot 3.53}{3.0} = 18.8\text{ksi}$$

$$MS = \frac{k_t\sigma'_e}{\sigma_{rms}} - 1 = \frac{18.8}{5.60} - 1 = \underline{\underline{2.35}}$$

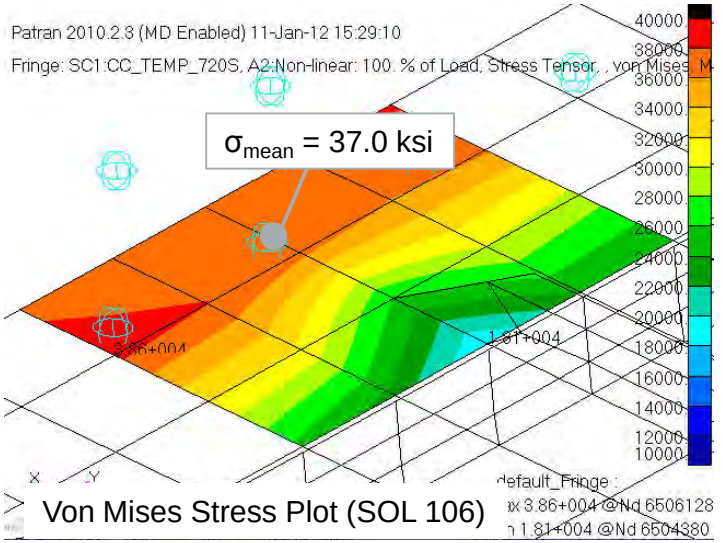

Von Mises Stress Plot (SOL 106)

Approved for public release; distribution unlimited.

Skin to Substructure Fastener Hole near Panel Stiffener Termination

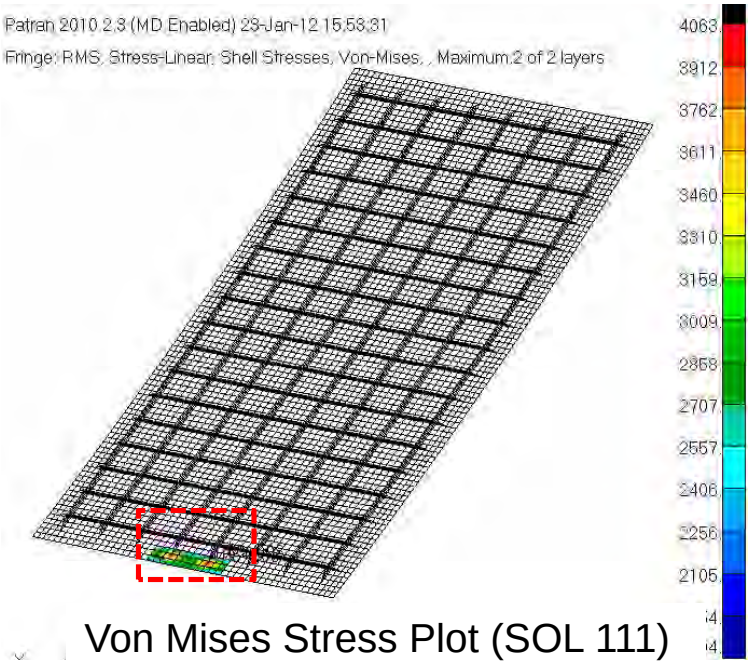

Von Mises Stress Plot (SOL 111)

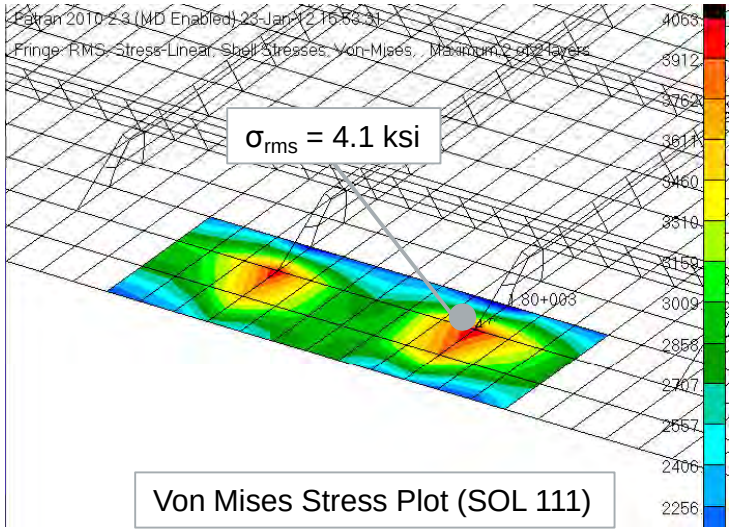

Von Mises Stress Plot (SOL 111)

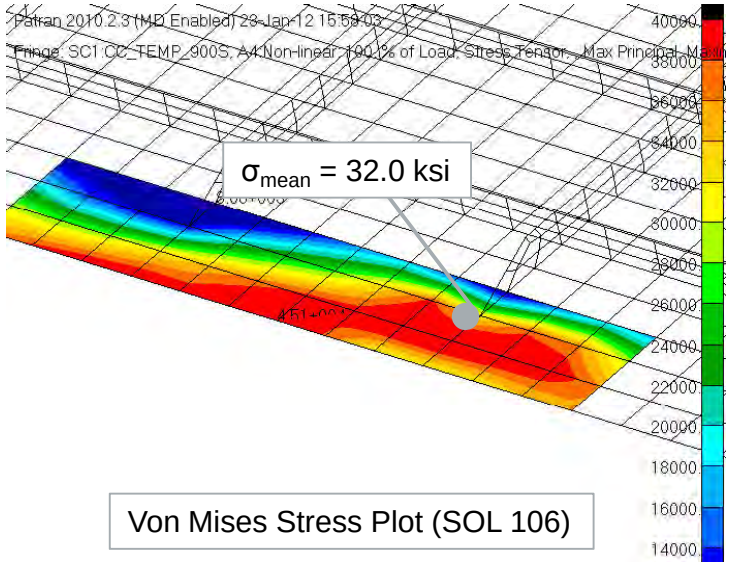

Von Mises Stress Plot (SOL 106)

Kt = 3.0 R = 0.77 T = 1150F

$$k_t\sigma'_e = \frac{\sigma_e \cdot C_T \cdot C_R}{k_t} = \frac{19.0 \cdot 0.84 \cdot 3.53}{3.0} = 18.8\text{ksi}$$

$$MS = \frac{k_t\sigma'_e}{\sigma_{rms}} - 1 = \frac{18.8}{4.1} - 1 = \underline{\underline{3.63}}$$

Approved for public release; distribution unlimited.

X-direction Orthogrid, Max RMS Stress, Non-linear Static Thermal (t=900s)

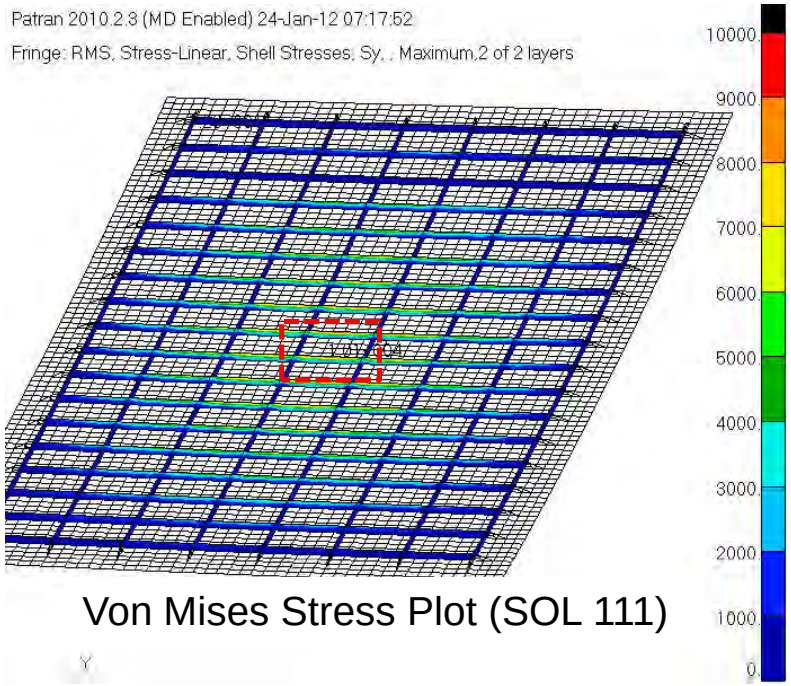

Von Mises Stress Plot (SOL 111)

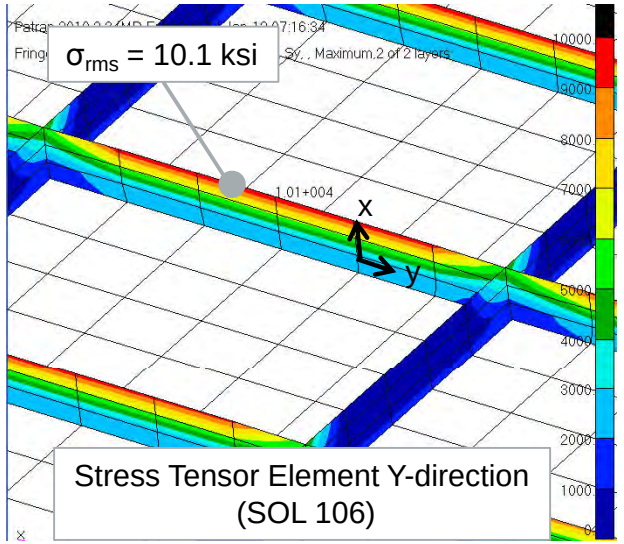

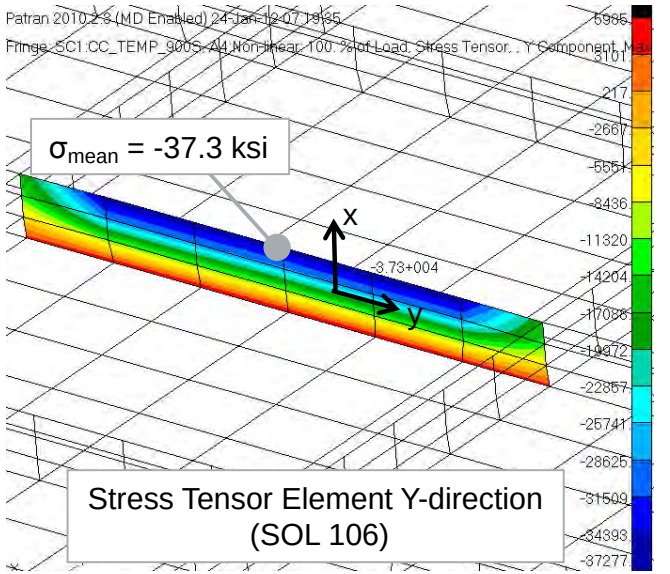

Kt = 1.0 R = 0.57 T = 1180F

$$k_t\sigma'_e = \frac{\sigma_e \cdot C_T \cdot C_R}{k_t} = \frac{19.0 \cdot 0.82 \cdot 2.36}{1.0} = 36.8\text{ksi}$$

$$MS = \frac{k_t\sigma'_e}{\sigma_{rms}} - 1 = \frac{36.8}{10.1} - 1 = \underline{\underline{2.64}}$$

Approved for public release; distribution unlimited.

Y-direction Orthogrid, Max RMS Stress, Non-linear Static Thermal (t=900s)

Von Mises Stress Plot (SOL 111)

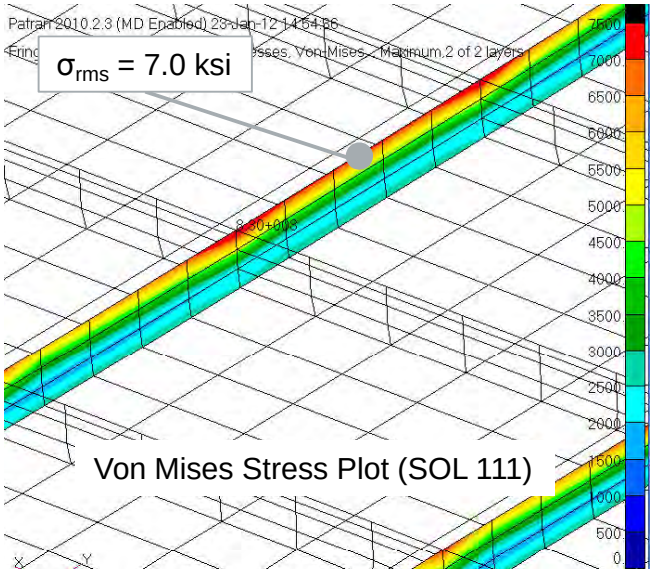

Kt = 1.0 R = 0.0 T = 1180F

$$k_t\sigma'_e = \frac{\sigma_e \cdot C_T \cdot C_R}{k_t} = \frac{19.0 \cdot 0.82 \cdot 1.54}{1.0} = 23.9\text{ksi}$$

$$MS = \frac{k_t\sigma'_e}{\sigma_{rms}} - 1 = \frac{23.9}{7.0} - 1 = \underline{\underline{2.42}}$$

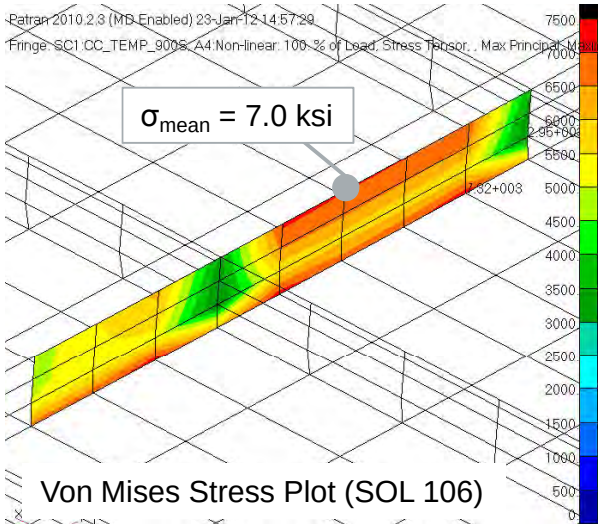

Approved for public release; distribution unlimited.

Acoustic Fatigue Summary Table

Location of Stress Concentration	Stress Conc. Type	Struct. Temp (°F)	Temp. Factor	Stress Ratio, R	Stress Ratio Factor	Kt	Allowable Stress* (ksi)	RMS Stress Result (ksi)	Mean Stress Thermal Load (ksi)	MS
Orthogrid at panel center	None	1180	0.82	0.57	2.36	1.0	36.8	10.1	-37.3	2.64
Orthogrid Y-direction	None	1180	0.82	0.00	1.54	1.0	23.9	7.0	7.0	2.42
Aft Skin edge at fastener hole	Filled Hole	1150	0.84	0.74	3.53	3.0	18.8	5.6	37.0	2.35
Outboard Skin edge at fastener hole	Filled Hole	1150	0.84	0.77	3.53	3.0	18.8	4.1	32.0	3.63

Results file(s): panel3_sol106_0106-01.xdb
panel3_sol111_0106-01_symm.xdb

*Baseline Allowable = 19ksi (Kt=1,R=-1, T=RT)

- RMS stress from acoustic loads are small in magnitude compared to the thermal stress at t=900s.
- The fatigue life of this panel is not greatly impacted by aero-acoustic loading.

$$R = \frac{-\sigma_{rms} + \sigma_{mean}}{\sigma_{rms} + \sigma_{mean}}$$

Approved for public release; distribution unlimited.

Aeroacoustic Fatigue Conclusions

- **Panel 816 Conclusions**
  - RMS stress is well below baseline allowable of 19.0ksi
  - Based on fatigue curves in MMPDS references, a positive stress ratio will bump allowables up, counteracting the effects of high temperatures or stress concentrations.
- **Analysis Issues**
  - Non-linear static solution needed as a preload case to frequency response solution
  - RMS results are in terms of stress, Ktσ at fatigue details are usually calculated from element or grip point forces. In this case, a Kt was assumed for the fastened joints analyzed

Approved for public release; distribution unlimited.

THERMAL-MECHANICAL FATIGUE

477
Approved for public release; distribution unlimited.

Fatigue Analysis Approach for Thermal Mechanical Loads

- **Define Spectrum**
  - Assume lifetime of 9600 GAG cycles and 4x safety factor = 38,400 load cycles
- **Define Fatigue Allowables & Knockdowns**
  - Use Mil-hdbk 5 Inconel 718 Constant Amplitude Data
    - Adjust for Temperature
- **Determine Spectrum Fatigue $K_t\sigma$**
  - Post-process results – references stress value
    - Use Max/Min sort to determine maximum and minimum principal stress locations
    - Sort fastener loads to determine maximum bearing location
  - Calculate detail or joint Ktσ
- **Calculate Margin of Safety**

478
Approved for public release; distribution unlimited.

Hypersonic Strike Vehicle Operational Thermal Cycles

- **Assumptions: First Pass Fatigue Analysis, Use simple worst case scenario (G-A-G)**
- **Primary Structure Design :**
  - 9600 x 1hr Sorties over operational life
  - *Hence, 9,600 Ground-Air-Ground thermal cycles (2.5g Maneuver @ Max Thermal)*
  - *Design Life Factor of Safety = 4 life times or 38,400 cycles*
  - Fatigue Spectrum uses, R-Ratio = 0 Inconel 718 s-N data.

479
Approved for public release; distribution unlimited.

Thermal-Mechanical Fatigue Analysis Summary

- **Flight Loads**
  - Mach 7, +2.5g symmetric pull up maneuver
- **Thermal**
  - Temperature @ t = 900 sec,
    Maximum thermal gradient between panel and substructure
- **Load Cases**
  - Limit flight load 1.15*2.5g, Temp @ 900s (max stress / temp. gradient)
- **Boundary Conditions for Panel Model**
  - Rigid Body motion constraints at 3 nodes
    - Node 6778977 (DOF 1,2,3), Node 6757185 (DOF 1,3), Node 6754569 (DOF3)
- **Analysis File(s)**
  - 010512_UNIT-P3_2p5_T900s_revT_revMPC.bdf
  - test_T3D_Str_Thermal_ld_900.nas

480
Approved for public release; distribution unlimited.

Panel 816 Temperature Gradient Profile

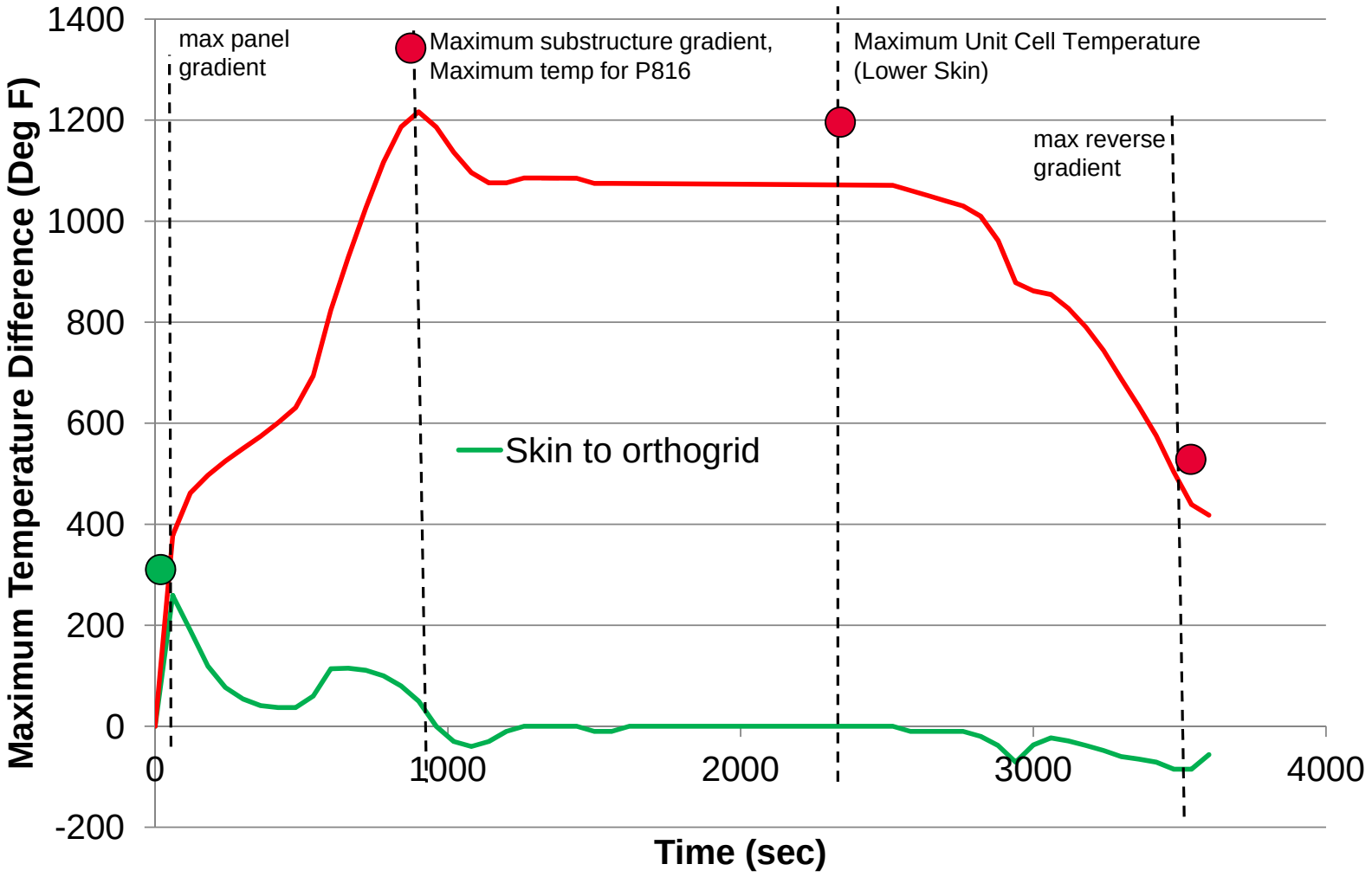

Approved for public release; distribution unlimited.

Inconel 718 S-N Data

$K_t\sigma$-all = 110ksi
At 1000F, R=0

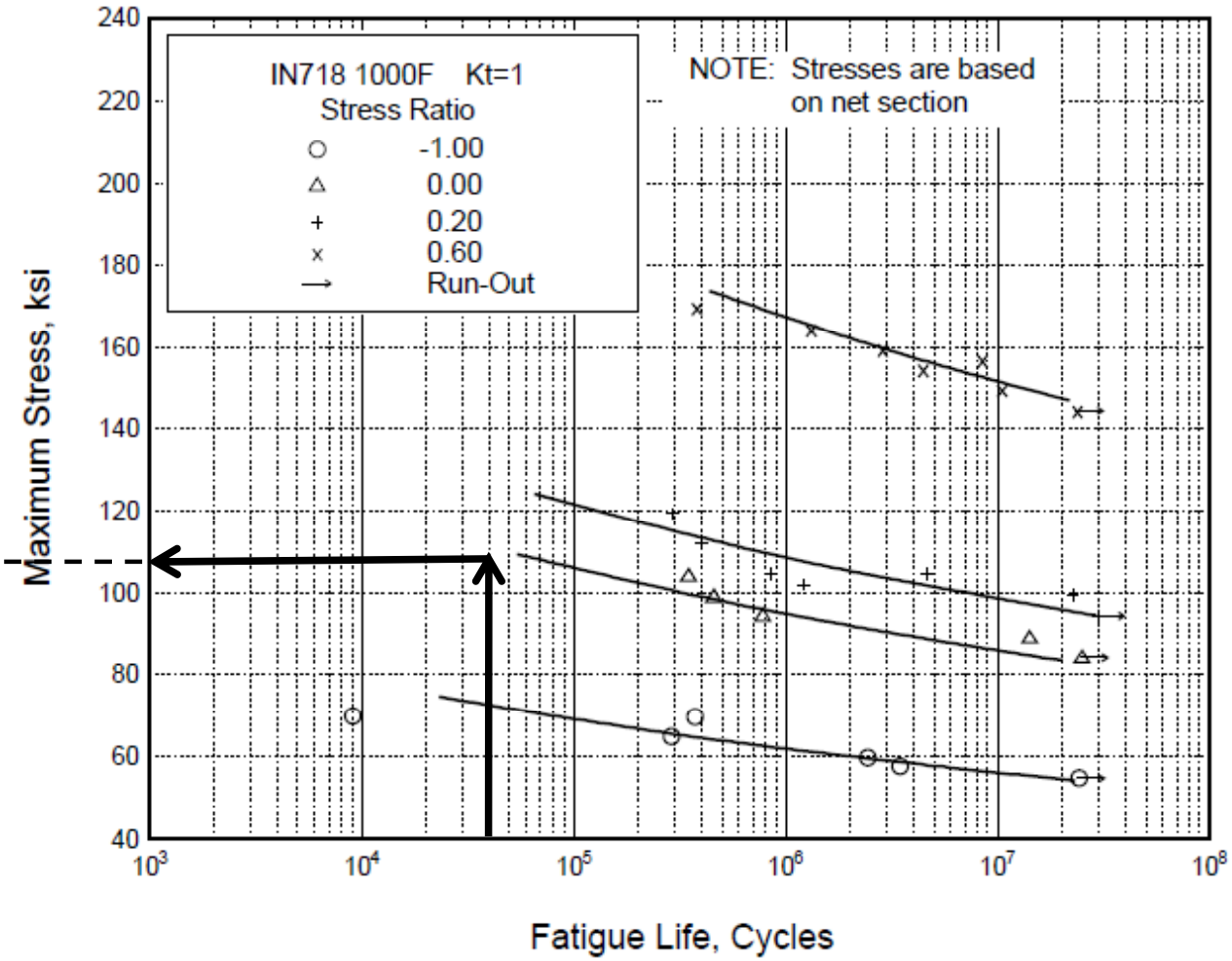

Ref. MMPDS-05 Figure 6.3.5.1.8(d)

482
Approved for public release; distribution unlimited.

Temperature Adjusted Fatigue Allowables

- **Temperature adjusted allowable stress was calculated for thermal loads at t=900spoint based on Fty as a function of temperature (Ref. MMPDS-05 Fig 6.3.5.1.1)**
  - Baseline allowable of 110 ksi at T=1000˚F
  - Critical Skin to substructure joint temperature ≈ 1150˚F
  - Temperature adjusted allowable of 103 ksi for skin to substurcture joint

	Panel 3 Skin to Substructure		
Time (s)	Temp. (F)	Adj. Temp Factor	Temp Adj. Allowable (KSI)
900	1150	0.94	103.4
ref allowable =		110	ksi
ref 1000 F factor =		0.89	

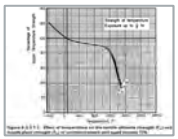

Fty v. Temp

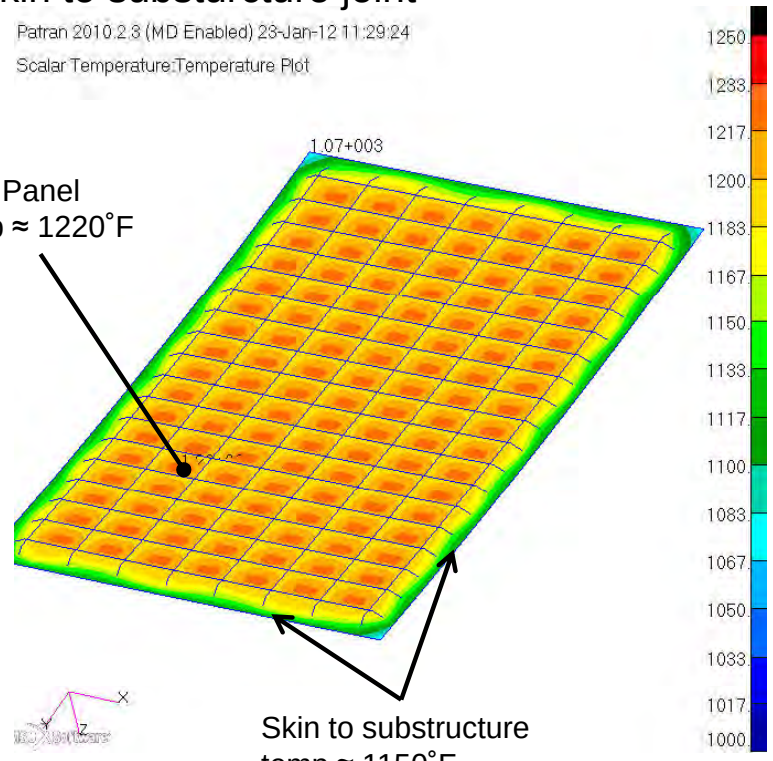

Fringe Plot of Applied Thermal Load at t=900s

Approved for public release; distribution unlimited.

Unit Cell FEM, Thermal Only (t=900s), Von Mises Stress

Linear Static Solution

- **Higher stress results on stiffeners, lower stress in skin**
- **Min principal stress on orthogrid stiffener (59.6 ksi compression)**
- **Max principal stress at skin to substructure joint (51.3 ksi tension)**

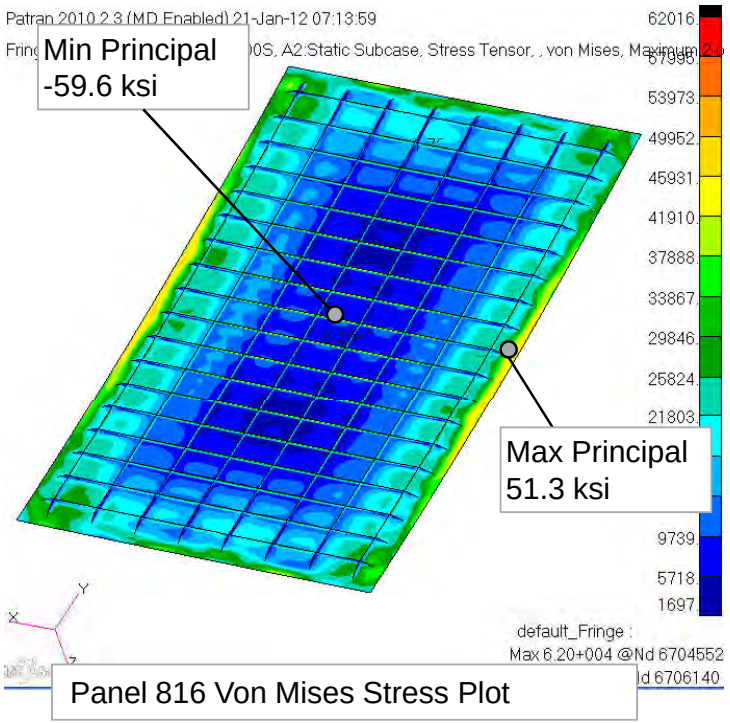

Non-linear Static Solution

- **Lower stress on stiffeners, higher stress in skin**
- **Skin appears to cripple in two panel bays**
- **Min principal stress on orthogrid stiffener (43.6 ksi compression)**
- **Max principal stress at skin to substructure joint (56.8 ksi tension)**

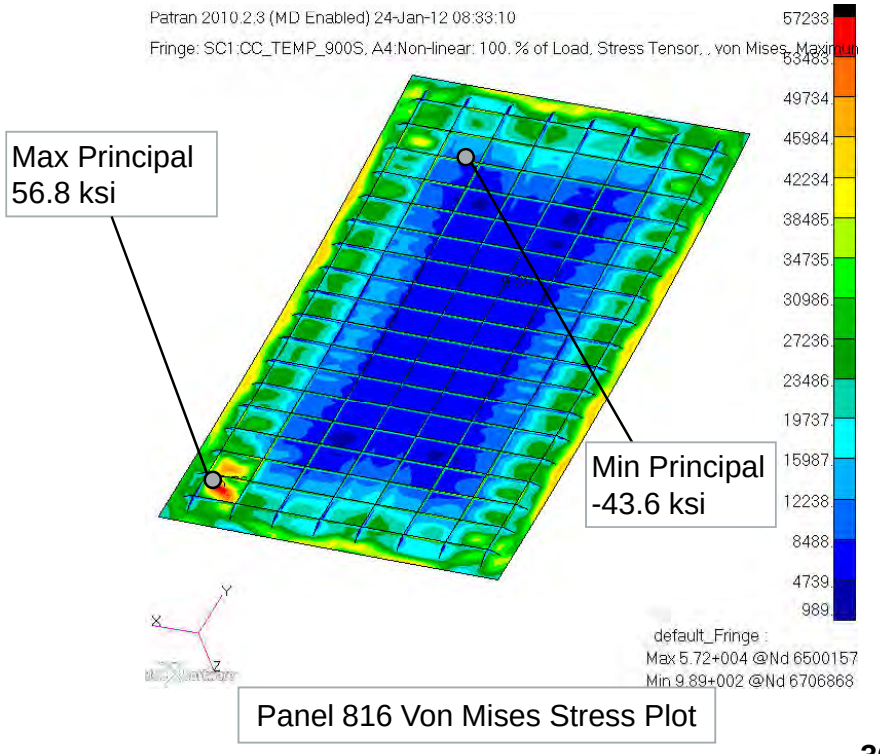

Approved for public release; distribution unlimited.

Unit Cell, Non-linear Static, Thermal Only (t=900s)

- **High stress in corner seem to be caused by localized buckling of skin panels between stiffeners**
- **This occurs between 90% and 100% thermal load**

Patran 2010.2.3 (MD Enabled) 21-Jan-12 08:27:14
Deform: SC1:CC_TEMP_720S, A1:Non-linear: 90. % of Load, Displacements, Translational, , (NON-LAYERED)

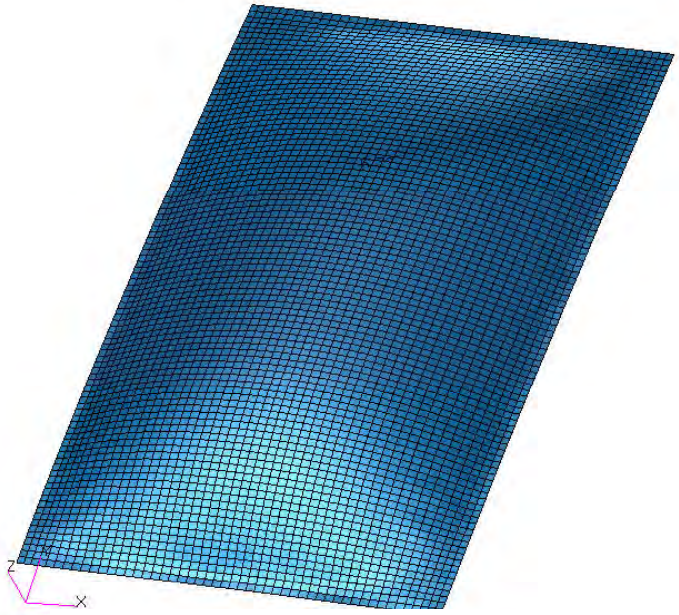

Deformed shape at Load Factor = 0.9

Patran 2010.2.3 (MD Enabled) 21-Jan-12 08:26:03
Deform: SC1:CC_TEMP_720S, A1:Non-linear: 100. % of Load, Displacements, Translational, , (NON-LAYERED

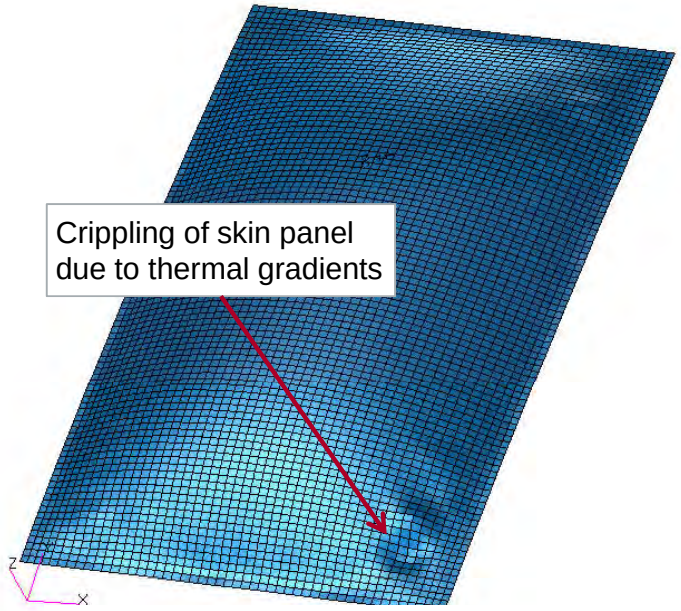

Deformed shape at Load Factor = 1.0

P3_UC_NLThermONLY_900s_DeformedSHape_SHD_ANIM_ISO.wmv

Approved for public release; distribution unlimited.

Unit Cell FEM, Lim 2.5g (LF=1.15) + Thermal (t=900s),

Linear Static Solution

- **Higher stress results on orthogrid stiffener**
- **Min Stress location on orthogrid stiffener (63.1 ksi compression)**
- **Max Stress location at aft skin to substructure joint (52.4 ksi Tension)**

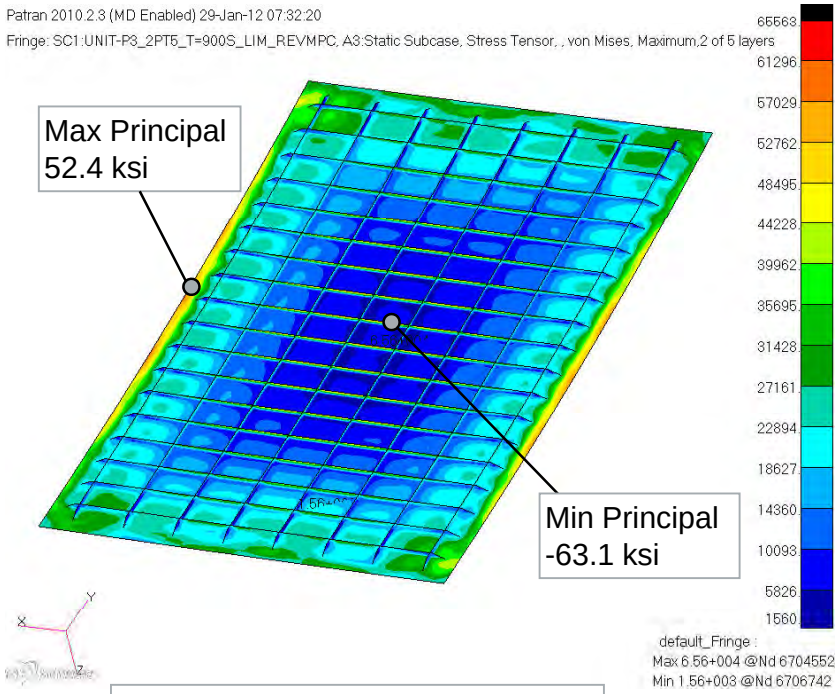

Panel 816 Von Mises Stress Plot

Non-linear Static Solution

- **Lower stress for orthogrid stiffeners**
- **Higher stress at skin to substructure attachments**
- **Min Stress location on orthogrid stiffener (54.6 ksi compression)**
- **Max Stress location at aft skin to substructure joint (54.3ksi Tension)**

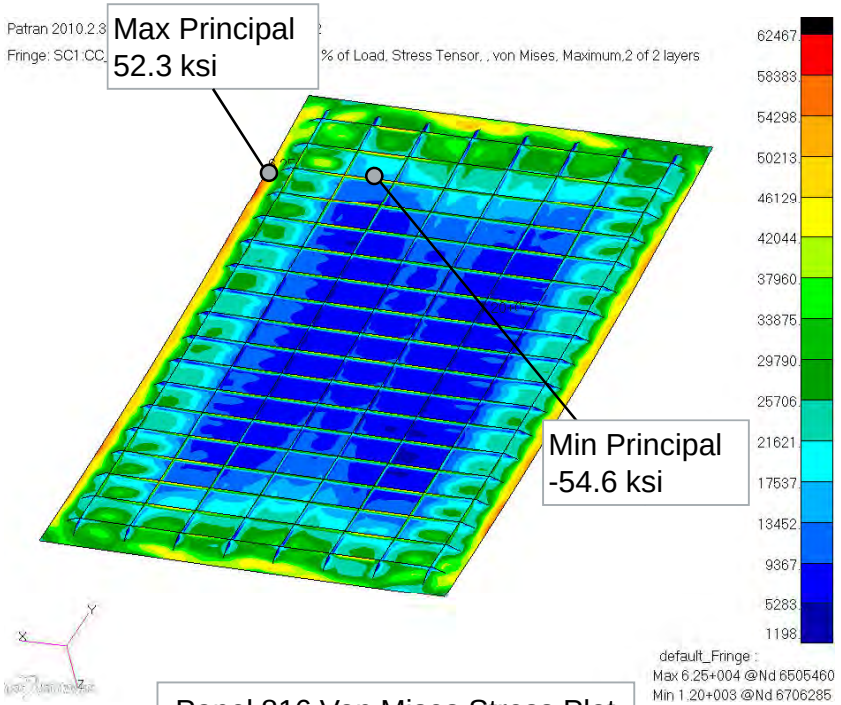

Panel 816 Von Mises Stress Plot

Approved for public release; distribution unlimited.

Unit Cell FEM, Non-linear Static, Thermal Only (t=900s)

- **Non-linear thermal load only solution presents unique stress in skin panel due to local buckling of skin**
- **A positive margin of safety is maintained at this location**

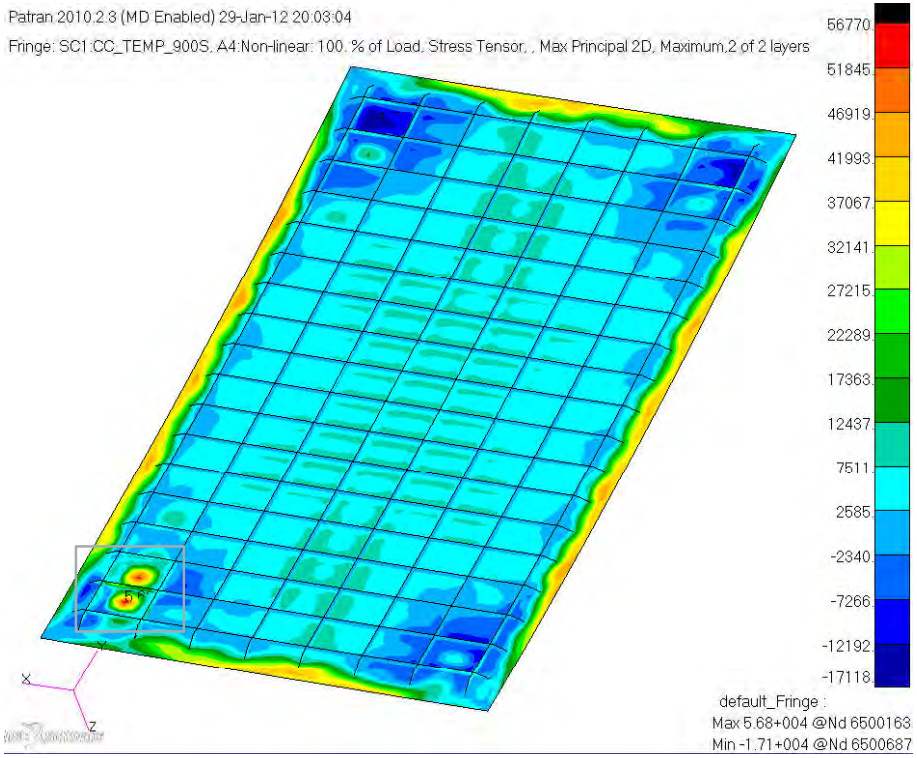

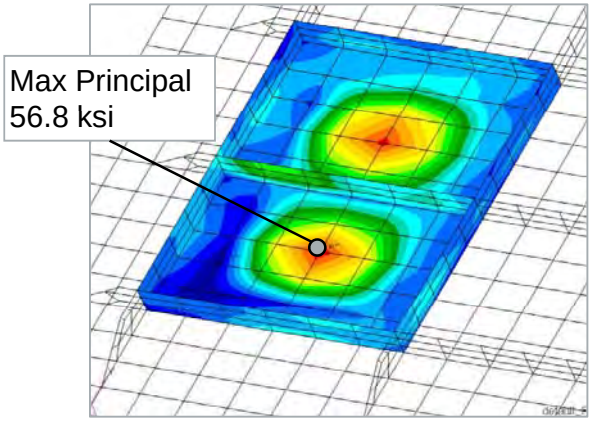

Fatigue Check at Non Linear Local Panel Crippling		
Max Princ. Stress	56.8	ksi
Stress Conc.	1	----
Ktσ	56.8	ksi
Baseline Allowable	110	ksi
Temp Knockdown	0.88	(1000°F - 1220°F)
Temp Adj Allowable	96.8	ksi
MS	0.70	----

Approved for public release; distribution unlimited.

Unit Cell, 2.5g LIM (LF=1.15), Linear, Detail Stress Results

CAESAR Single Hole
Input Screen
(expand to view)

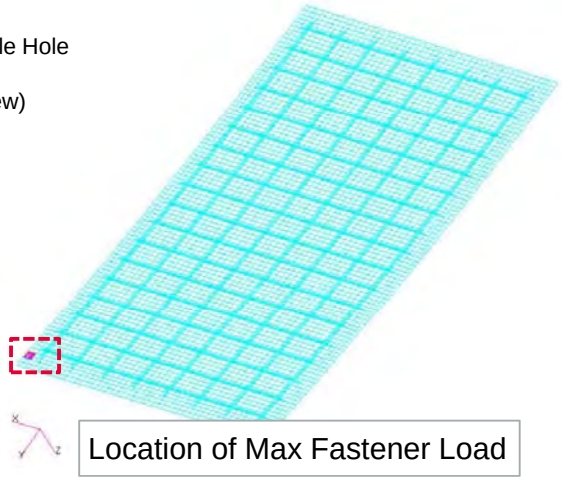

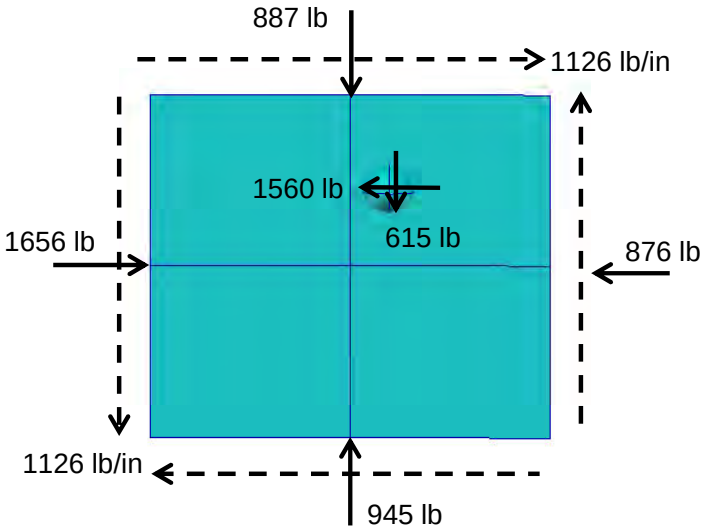

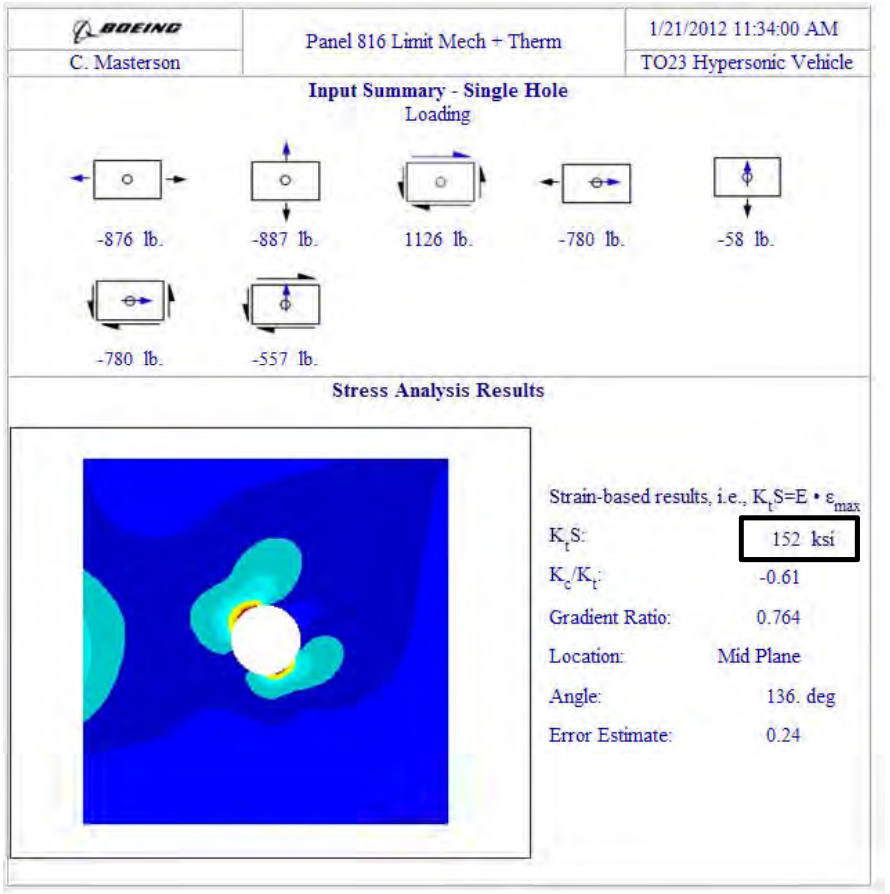

CAESAR Single Hole Analysis Result Summary

Ktσ = 152 ksi
Allowable Stress = 103 ksi
MS = -0.32

Approved for public release; distribution unlimited.

Unit Cell, 2.5g LIM (LF=1.15), Linear, Detail Stress Results

CAESAR Single Hole
Input Screen
(expand to view)

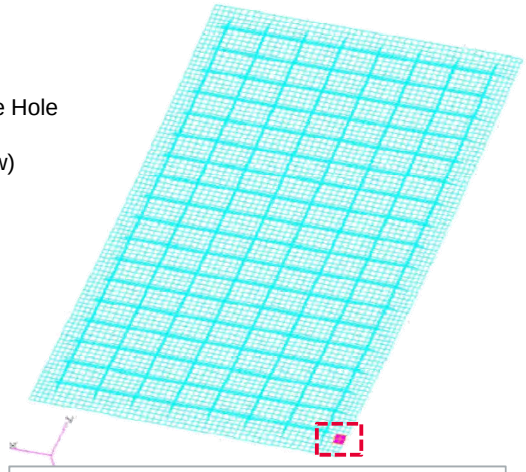

Maximum Principal Stress Location

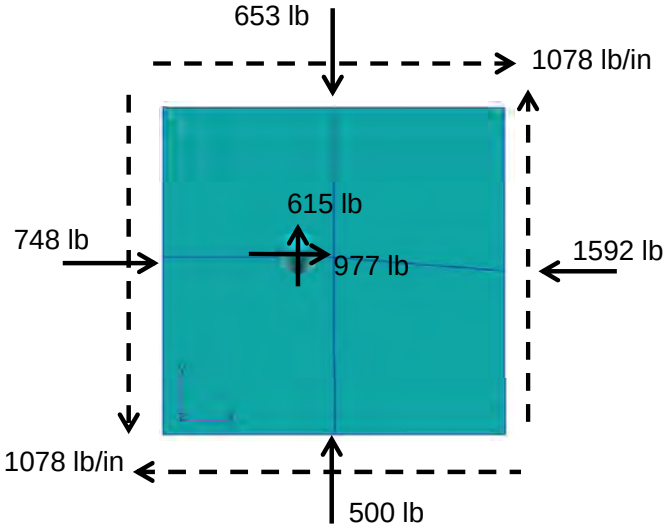

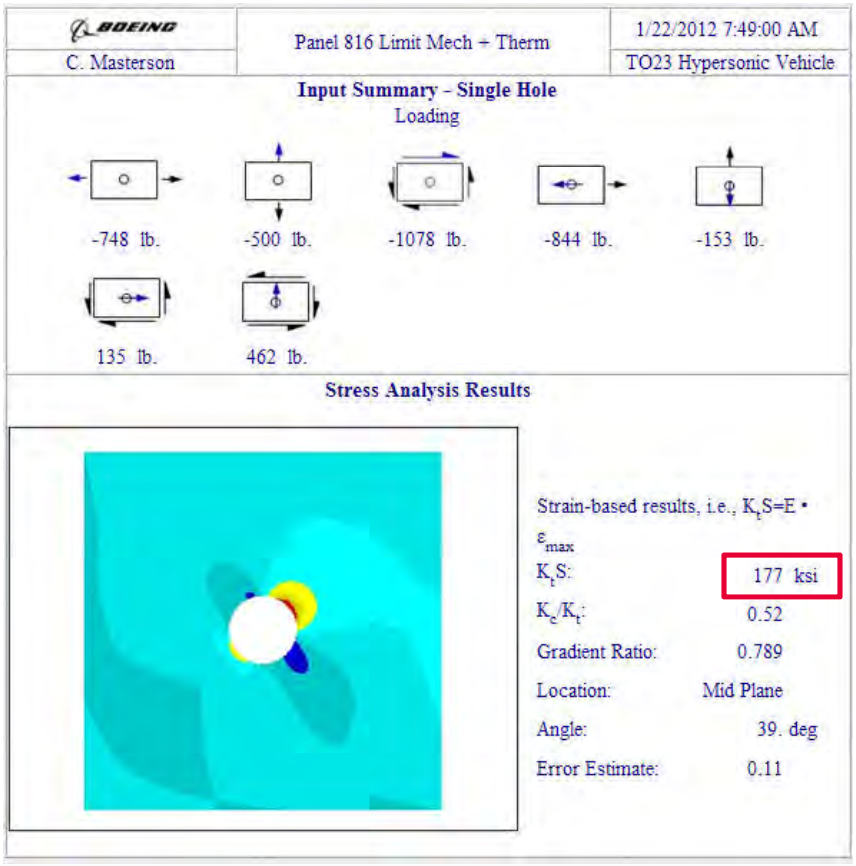

CAESAR Single Hole Analysis Result Summary

Ktσ = 177 ksi
Allowable Stress = 103 ksi
MS = -0.42

Approved for public release; distribution unlimited.

Skin to Substructure – Joint Loads and MS Summary

- **Fatigue checks at skin to substructure joints show significant negative margin at highly loaded fasteners**
- **Contributing factors to the high stresses due to thermal gradient are:**
  - Large panel size
  - Presence of insulation drives higher gradient between skin and substructure
  - Single fastener row
  - Joints do not allow for thermal expansion
- **These issues can be mitigated through design improvements**

	Max Brg	Max Princ	Min Princ
Elem ID	----	4004919	4005926
Nearest Fastener	13626813	13626974	13626813
Temperature	1150	1150	1150
Pbrx	-1560	979	-1560
Pbry	-615	615	-615
Nx LH	-1655.5	-747.5	-1655.5
Nx RH	-876	-1592	-876.0
NyUp	-887	-653	-887.0
NyDwn	-945	-500	-945.0
Nxyby	1126.0	-1078.0	1126.0
KT Sigma	152	177	152.0
Allowable	103.4	103.4	103.4
MS	(0.32)	(0.42)	(0.32)

Panel 816 Thermal-Mechanical Fatigue (Temperature Knockdown)			
Time (s)	Temp. (˚F)	Temp Factor (1000˚F)	Temp Adj. Allowable (KSI)
900	1150	0.94	103.4
900	1180	0.92	101.2
900	1220	0.8	88.0
ref allowable =		110	ksi
ref 1000 F factor =		0.89	

Approved for public release; distribution unlimited.

Unit Cell, 2.5g LIM (LF=1.15), X-Dir Results, Linear

- **Ktσ is typically calculated using average loads from nearby elements**
- **In the area of the skin to substructure joint, many of the elements with worst case stress are in bending and the average shell forces are near zero**
- **Location of shell force maxima do not correspond with shell stress maxima**

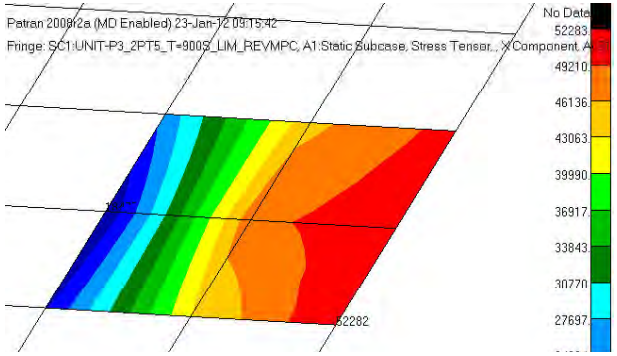

X-direction Stress Plot at extreme fiber Z1 (IML)
(Maximum stress = 52.2 ksi Tension)

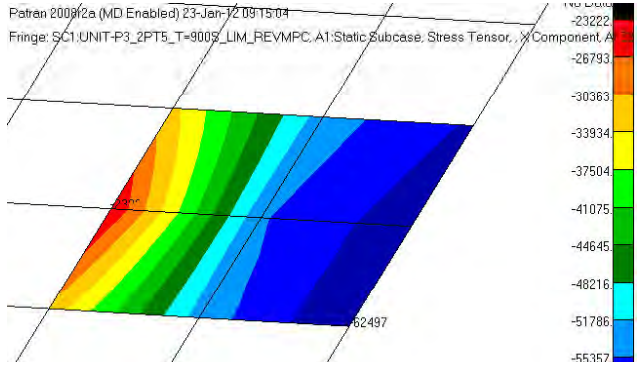

X-direction Stress Plot at extreme fiber Z2 (OML)
(Maximum stress = 62.5 ksi Compression)

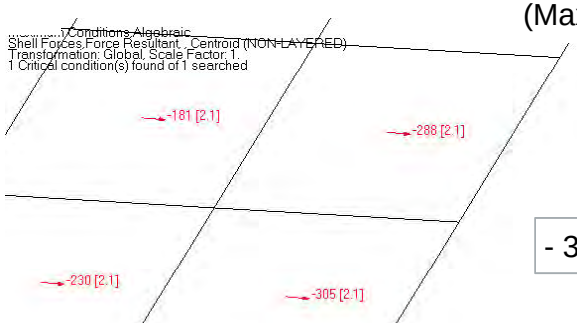

X-direction Shell Forces
(Maximum = 305 lb/in Compression)

- 305lb/in ≈ 4.8 ksi (compression)

Approved for public release; distribution unlimited.

Thermal-Mechanical Fatigue Conclusions

- Panel 816 experiences high stresses at skin to substructure joints due to thermal gradients between panel and substructure causing negative margins for fatigue
- Factors contributing to high stress include large panel size, fuel insulation (increasing ΔT between skin and substructure), joints that prohibit thermal expansion, single row of fasteners
- It would be helpful if thermal loads could be incorporated at a higher level to get proper panel sizing before analyzing at a panel level
- Shell forces or grid point forces are typically used to determine stress at fatigue details
  - In cases of shell elements under bending, element forces can be averaged out to show net zero load

492
Approved for public release; distribution unlimited.

PANEL FLUTTER ANALYSIS

493
Approved for public release; distribution unlimited.

Trajectory – Design Conditions of Interest

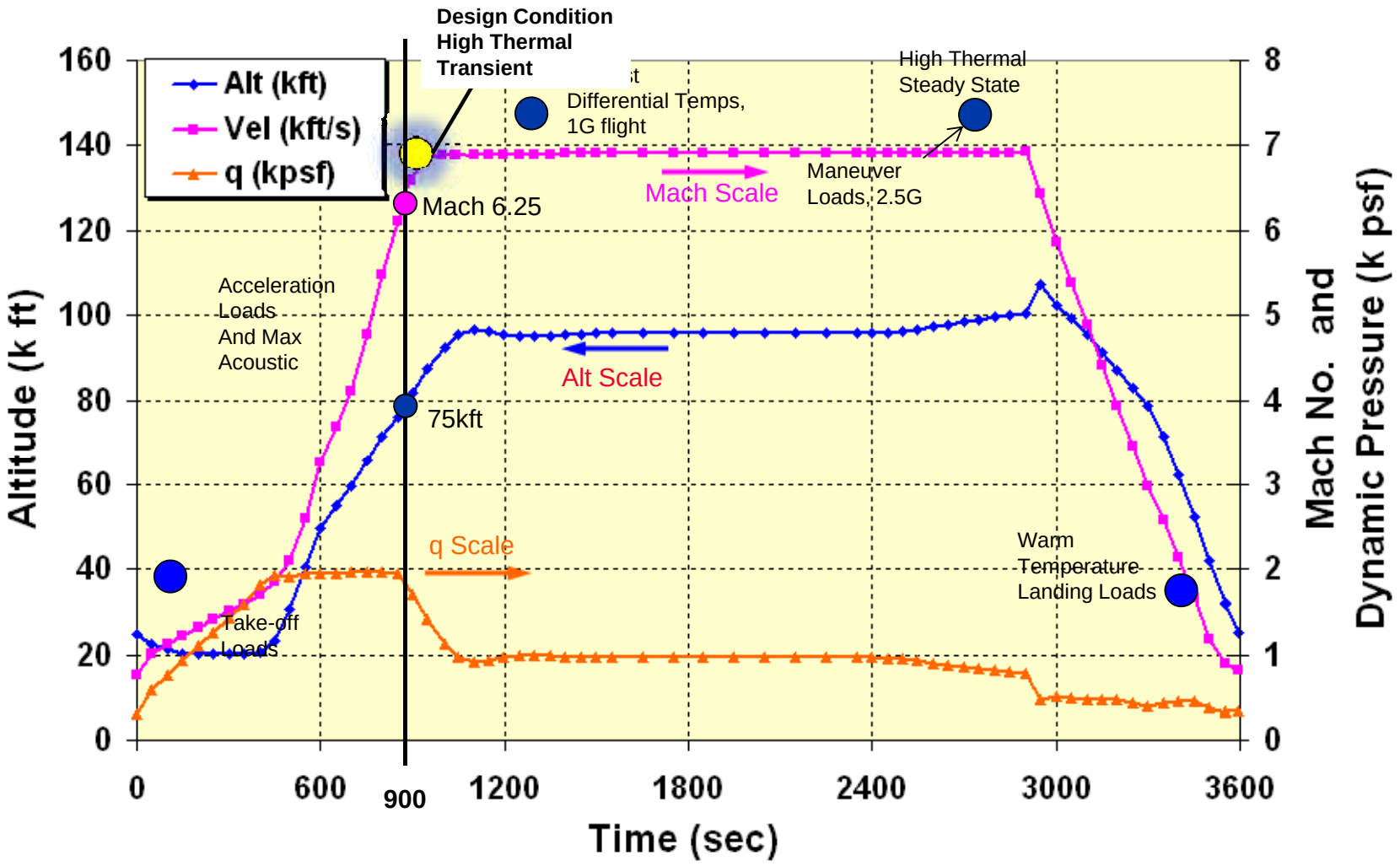

Approved for public release; distribution unlimited.

Panel Flutter Analysis for Hypersonic Aircraft

- **Two analysis methods are summarized:**
  - Empirically Derived Criteria
    - Fast
    - Approximate
    - Historically used on Tactical Aircraft Programs
  - High Fidelity Aeroelastic Analysis
    - More resource intensive
    - May address particular physics more directly
    - Relatively new technology

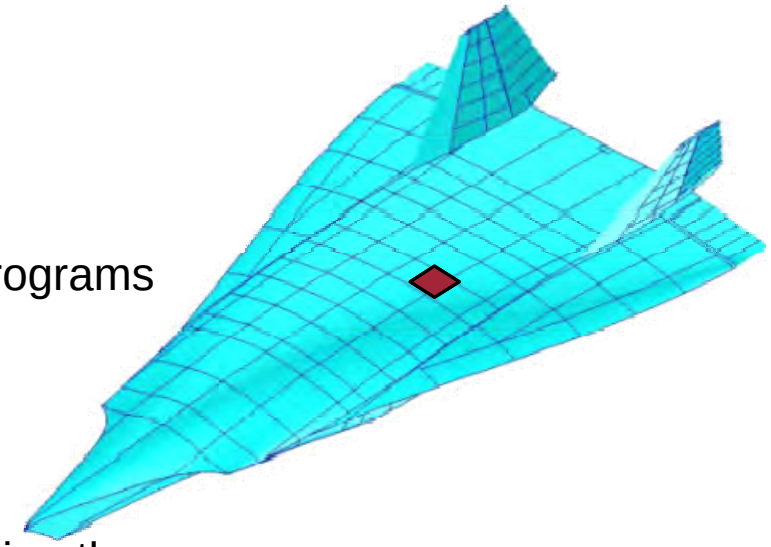

Approved for public release; distribution unlimited.

Empirical Panel Flutter Design Curves

- **Panel 816 lies well above the design curve for critical structure**
- **Design curves intended for flow at Mach 3 or less**
- **Panel flutter driven by stiffness, aspect ratio, and thickness**

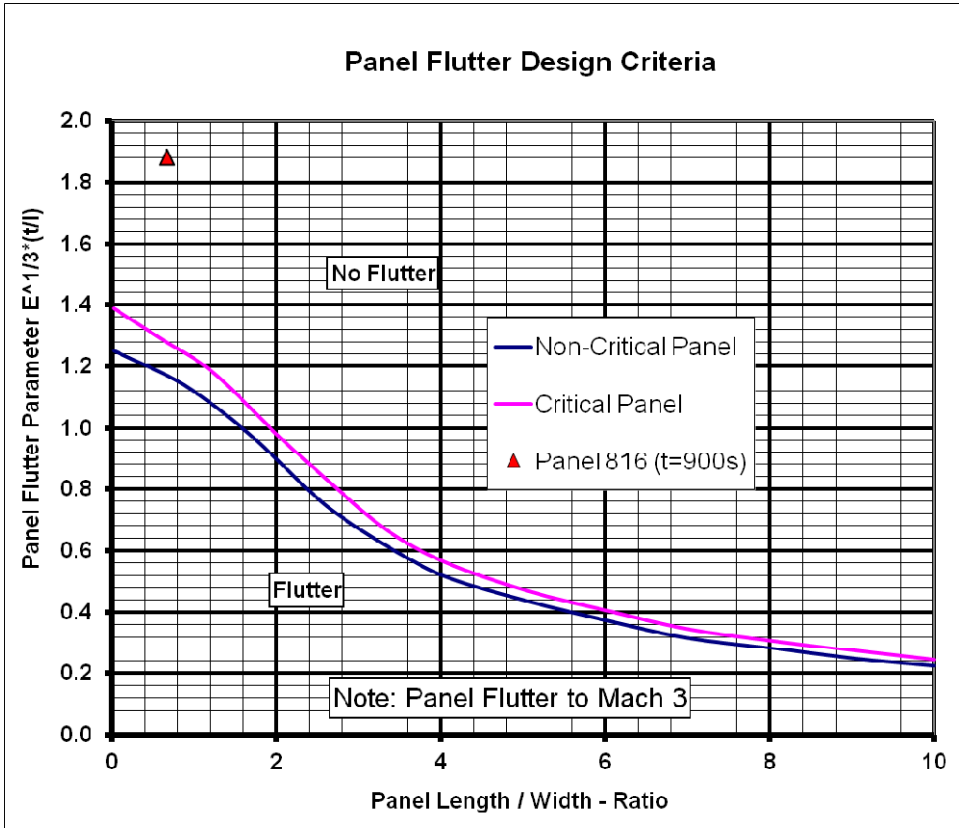

Note: Length is in flow direction

Approved for public release; distribution unlimited.

Empirically Derived Panel Flutter Design Criteria

Nondimensional Panel Flutter Parameter

$\Phi = [f(M) \times E / q]1/3 \times (t / l)$

where:

- Φ = Non-dimensional panel flutter parameter; a function of panel length-to-width ratio, l/w
- E = Young's modulus
- f(M) = Mach number correction factor; a function of Mach number and l/w ratio;
- l = Panel length (stream wise)
- q = Dynamic pressure
- t = Panel thickness
- w = Panel width

Correction Factors for:

- Curvature
- Mach Number
- Flow Angle
- In-plane stress
- Differential Pressure
- Differential Temperature

Revised F-18E/F Panel Flutter Desigh Requirement For Aluminum Structure

(Example)

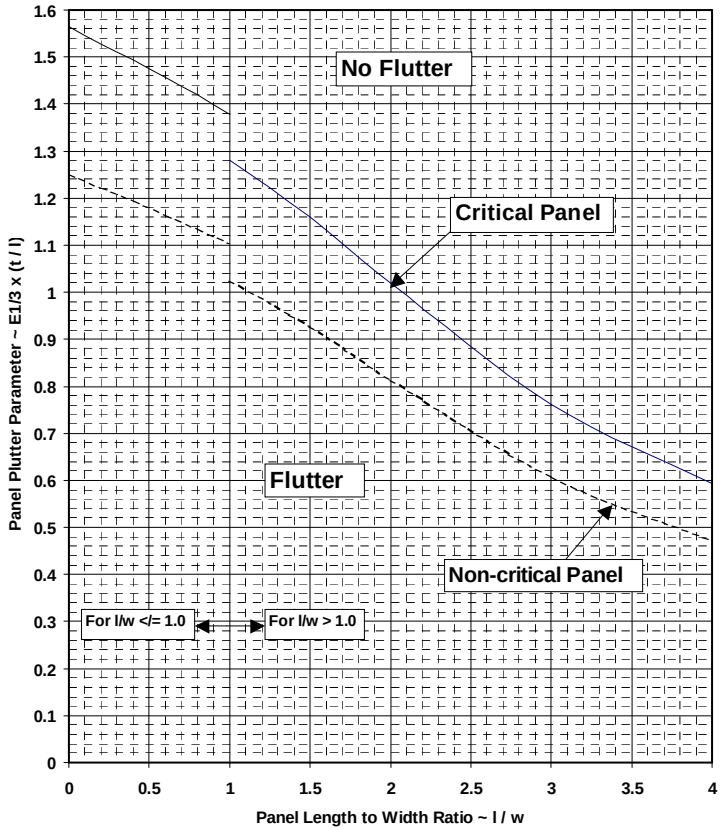

****** See accompanying References 1 & 2 ******

Approved for public release; distribution unlimited.

Aeroelastic FEA – Assumptions & Method

- **Method**
  - Piston Theory (Valid for high mach number)
  - Nastran Solution 145
- **Assumptions**
  - Use density factor of 0.5 for single-sided flow
  - 0.02 system damping,
    (flutter speed where VG curve exceeds 0.02 damping constant)
  - No preload from thermal or mechanical load cases
- **Flight Parameters**
  - Mach 6.25 @ 75,000 ft
  - Material properties adjusted for 900s thermal load

Approved for public release; distribution unlimited.

Aeroelastic FEA – Structural Model

- **Panel flutter model reduced from unit cell to entire upper surface including surrounding sandwich panels and the orthogrid stiffeners on panel 816**
- **Boundary conditions were imposed to get good approximation of unit cell modal frequencies**
- **Air flow in global X-direction**

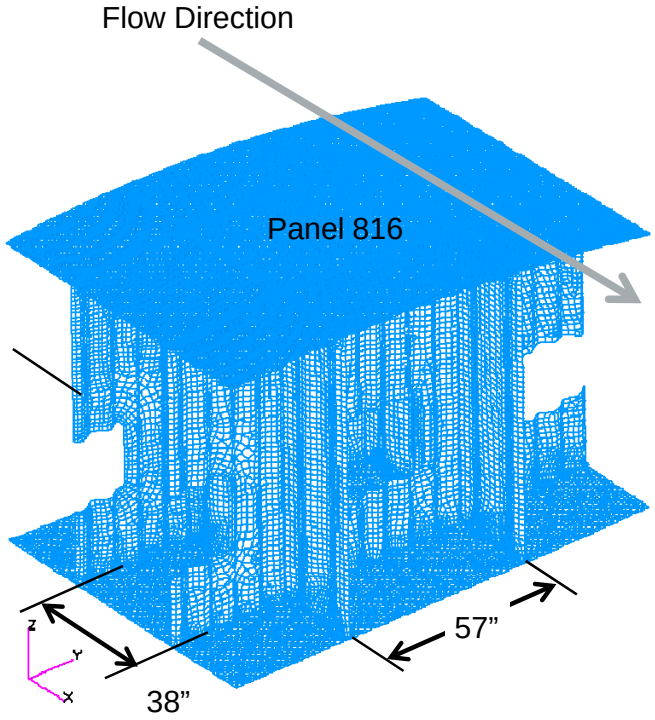

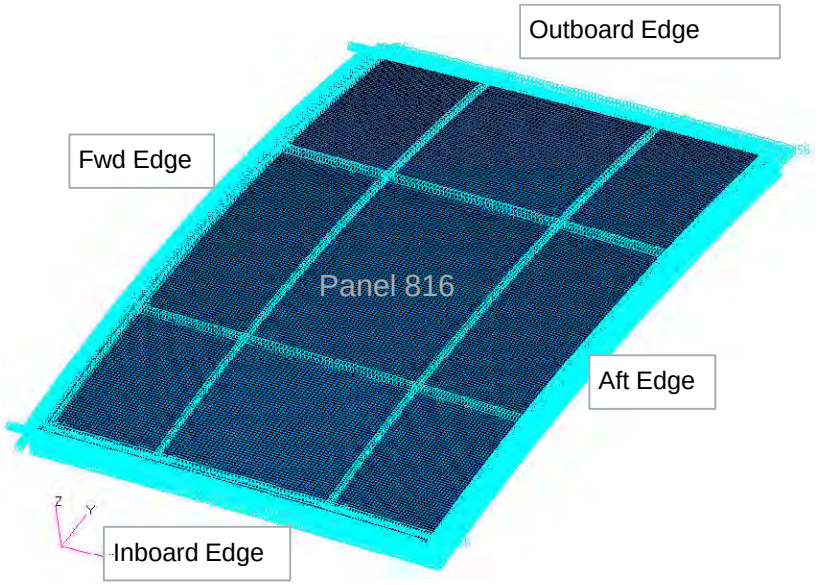

Panel Constraints:
Inboard and Outboard edges constrained in Ty, Rx, Rz
Forward and aft edges constrained in Tx, Ry, Rz
Skin to substructure attachment points constrained in Tz

Approved for public release; distribution unlimited.

Aeroelastic FEA – Aero Model

- **Panel defined by 10 CAERO5 entries in the chord or stream-wise direction**
- **Each CAERO divided into 20 span-wise strips**

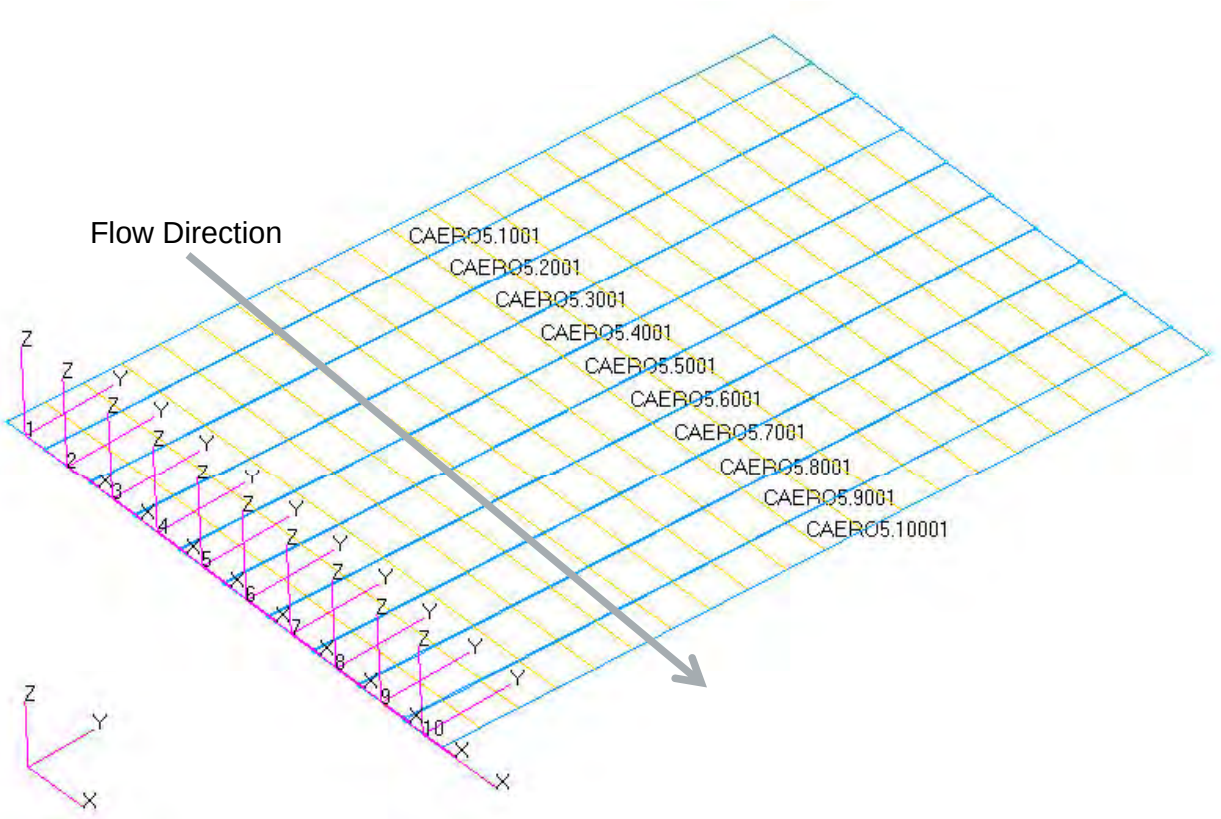

500
Approved for public release; distribution unlimited.

Aeroelastic FEA – Nastran Reference

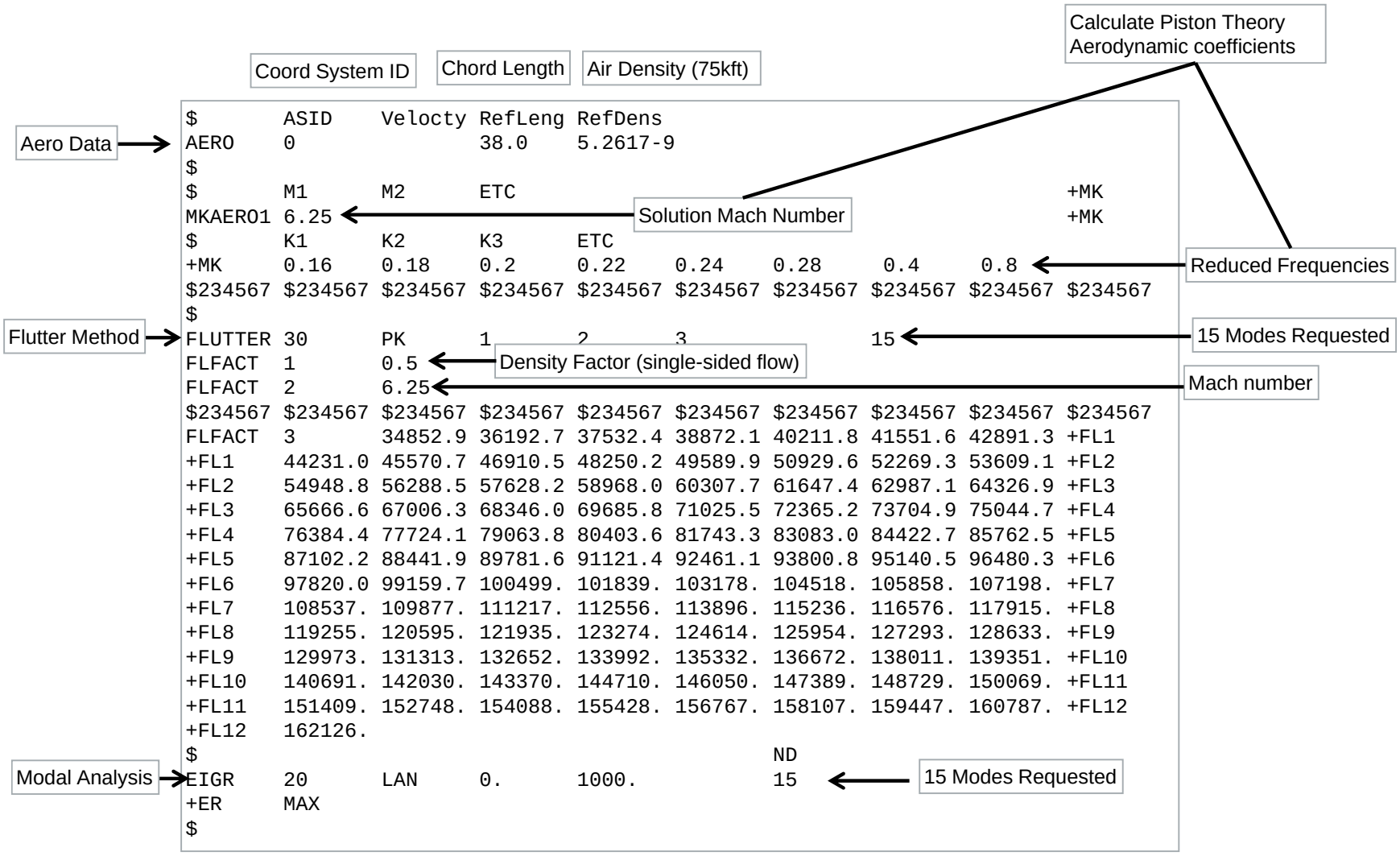


```
$        ASID     Velocty  RefLeng  RefDens
AERO     0                 38.0     5.2617-9
$
$        M1       M2       ETC                                          +MK
MKAERO1  6.25                                                          +MK
$        K1       K2       K3       ETC
+MK      0.16     0.18     0.2      0.22     0.24     0.28      0.4      0.8
$234567  $234567  $234567  $234567  $234567  $234567  $234567  $234567  $234567  $234567
$
FLUTTER  30       PK       1        2        3                  15
FLFACT   1        0.5
FLFACT   2        6.25
$234567  $234567  $234567  $234567  $234567  $234567  $234567  $234567  $234567  $234567
FLFACT   3        34852.9  36192.7  37532.4  38872.1  40211.8  41551.6  42891.3  +FL1
+FL1     44231.0  45570.7  46910.5  48250.2  49589.9  50929.6  52269.3  53609.1  +FL2
+FL2     54948.8  56288.5  57628.2  58968.0  60307.7  61647.4  62987.1  64326.9  +FL3
+FL3     65666.6  67006.3  68346.0  69685.8  71025.5  72365.2  73704.9  75044.7  +FL4
+FL4     76384.4  77724.1  79063.8  80403.6  81743.3  83083.0  84422.7  85762.5  +FL5
+FL5     87102.2  88441.9  89781.6  91121.4  92461.1  93800.8  95140.5  96480.3  +FL6
+FL6     97820.0  99159.7  100499.  101839.  103178.  104518.  105858.  107198.  +FL7
+FL7     108537.  109877.  111217.  112556.  113896.  115236.  116576.  117915.  +FL8
+FL8     119255.  120595.  121935.  123274.  124614.  125954.  127293.  128633.  +FL9
+FL9     129973.  131313.  132652.  133992.  135332.  136672.  138011.  139351.  +FL10
+FL10    140691.  142030.  143370.  144710.  146050.  147389.  148729.  150069.  +FL11
+FL11    151409.  152748.  154088.  155428.  156767.  158107.  159447.  160787.  +FL12
+FL12    162126.
$                                                                ND
EIGR     20       LAN      0.       1000.                       15
+ER      MAX
$
```


Approved for public release; distribution unlimited.

SOL 103 Panel Results (Flutter Analysis)

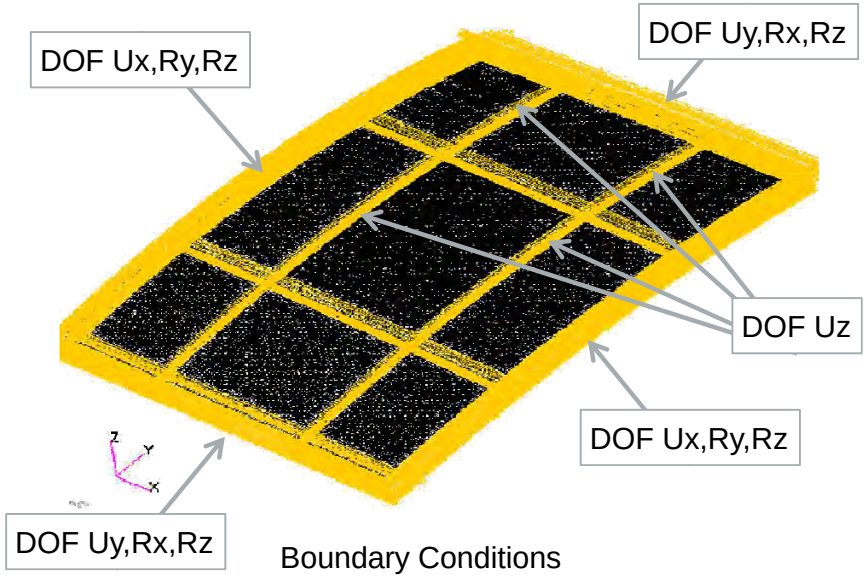

Boundary Conditions

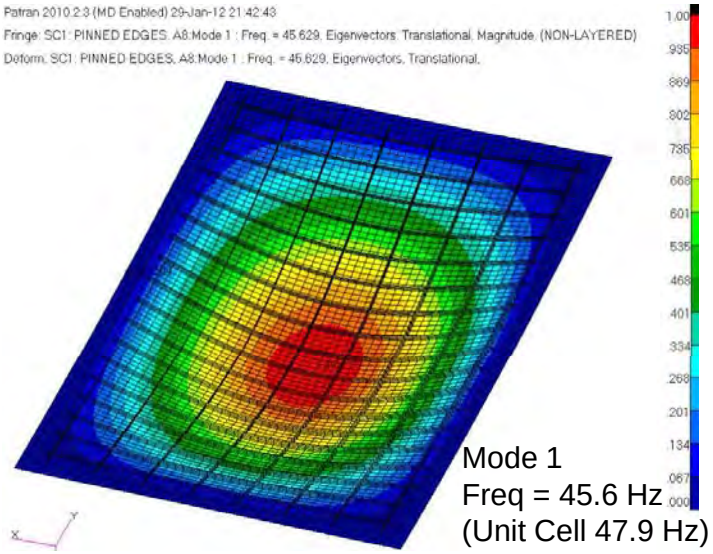

Mode 1
Freq = 45.6 Hz
(Unit Cell 47.9 Hz)

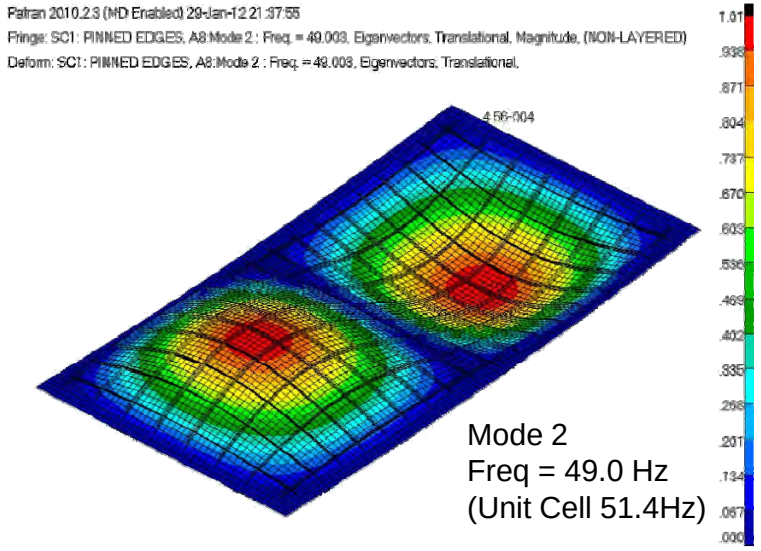

Mode 2
Freq = 49.0 Hz
(Unit Cell 51.4Hz)

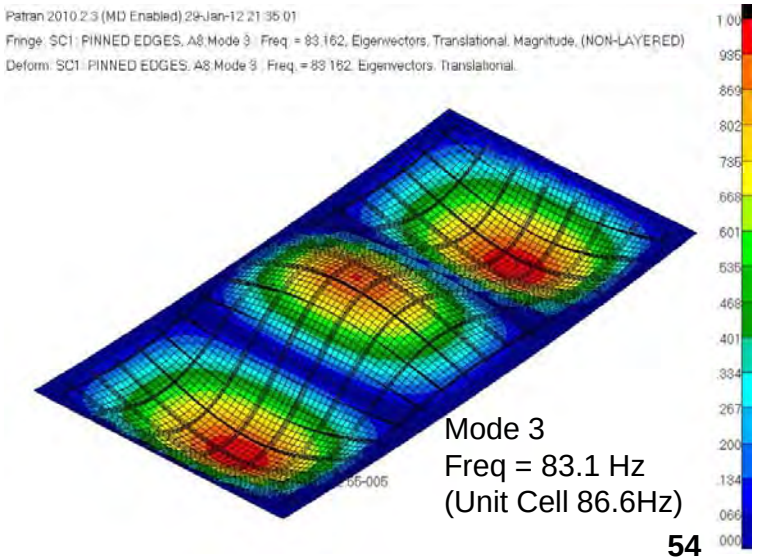

Mode 3
Freq = 83.1 Hz
(Unit Cell 86.6Hz)

Approved for public release; distribution unlimited.

Panel 816, Thermal Only (t=900s), Sea Level, Mach 7.5

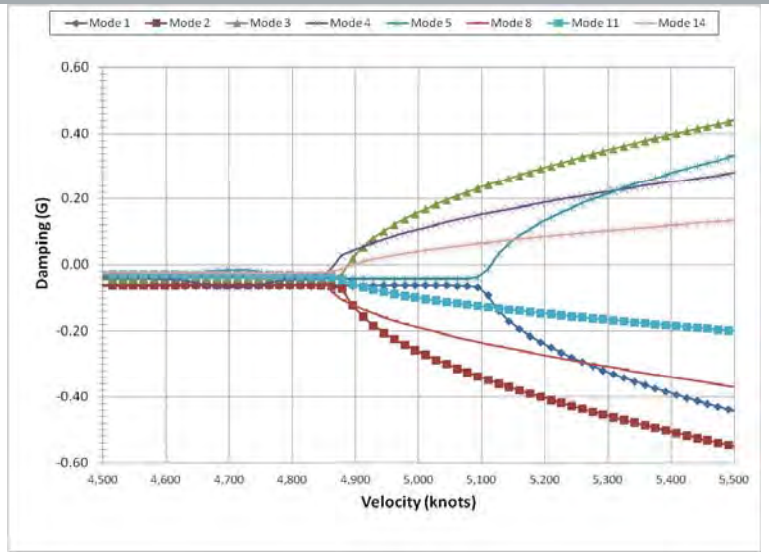

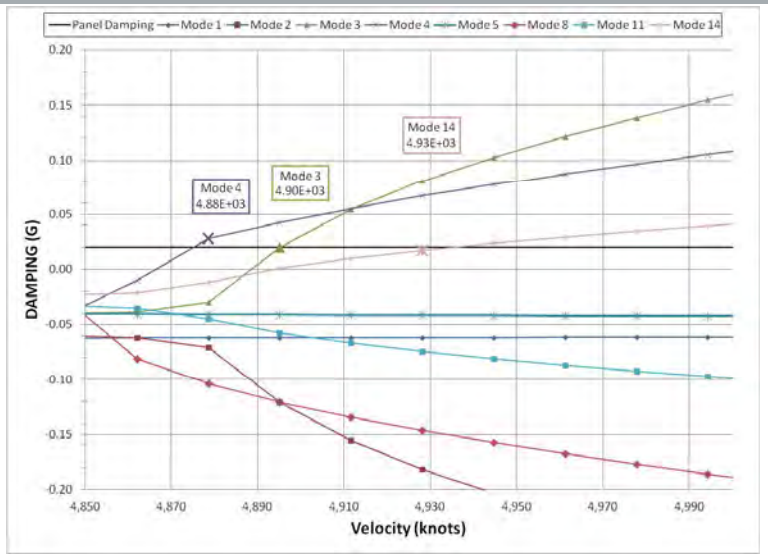

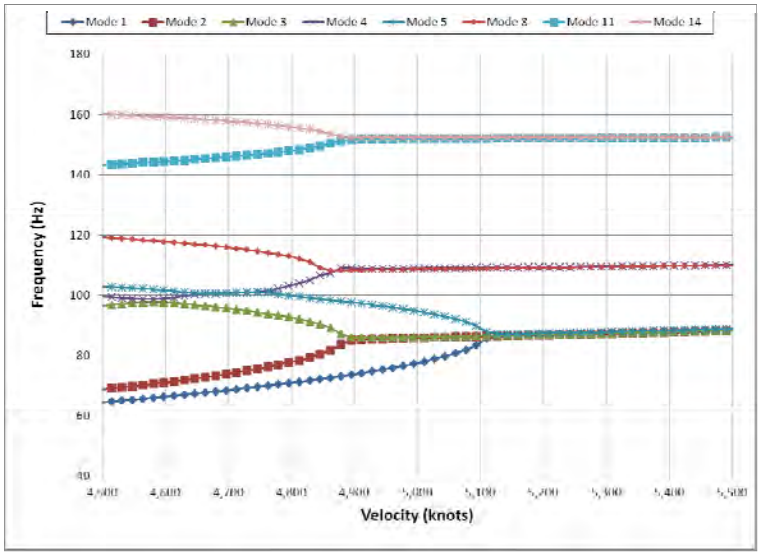

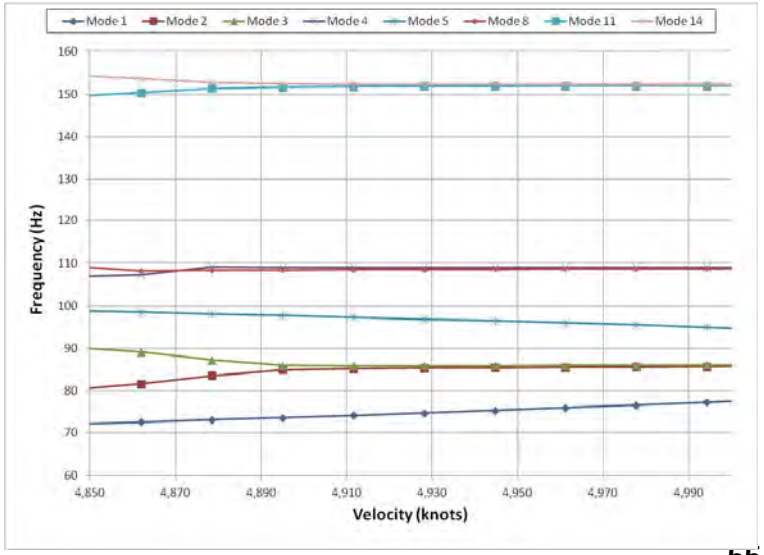

Approved for public release; distribution unlimited.

Panel 3, Thermal Only (t=900s), Sea Level, M6-M9

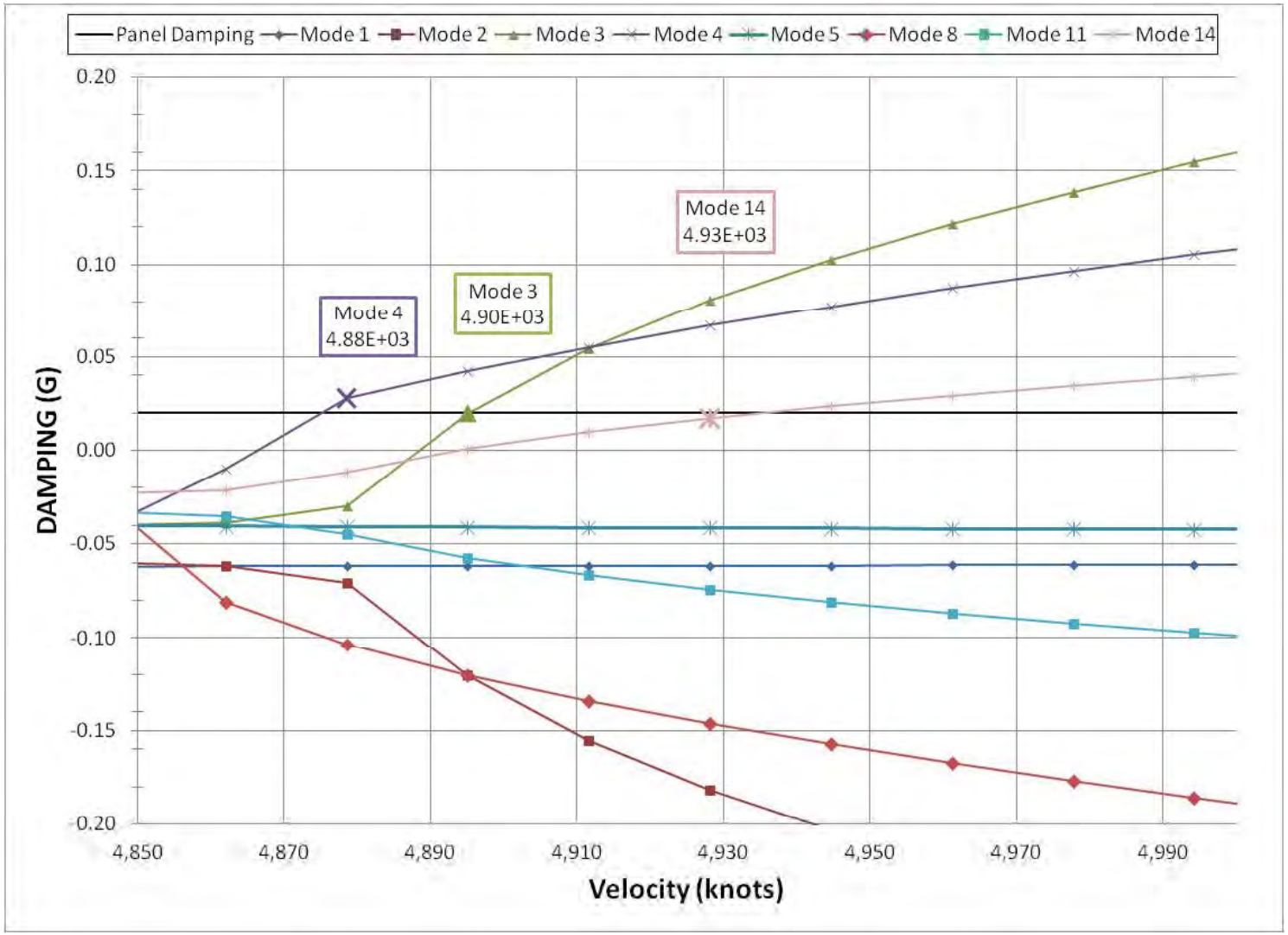

Approved for public release; distribution unlimited.

Flutter Model, Sea Level, Mach 7.5, Temp Adj. Material Properties

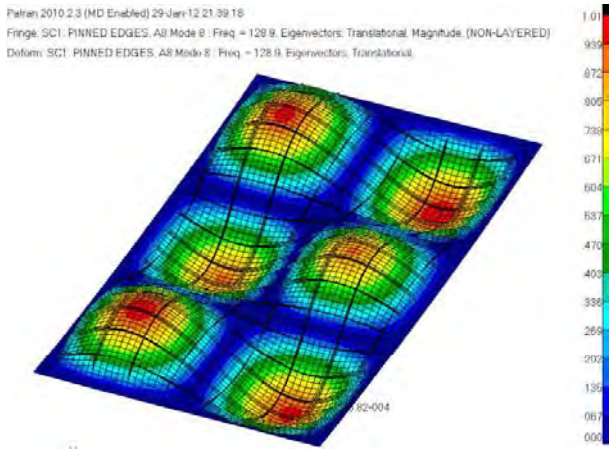

Panel Mode 8 with decreasing frequency

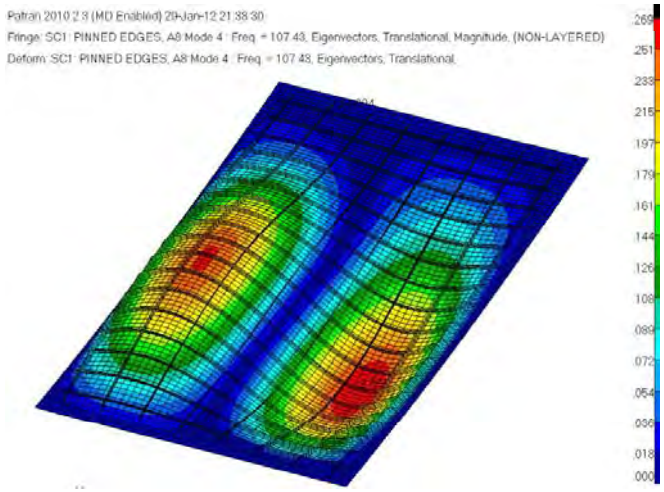

Panel Mode 4 with increasing frequency

As velocity increases:
- Mode 8 frequency decreases,
- Mode 4 frequency increases
- Panel becomes unstable at point where frequencies coincide

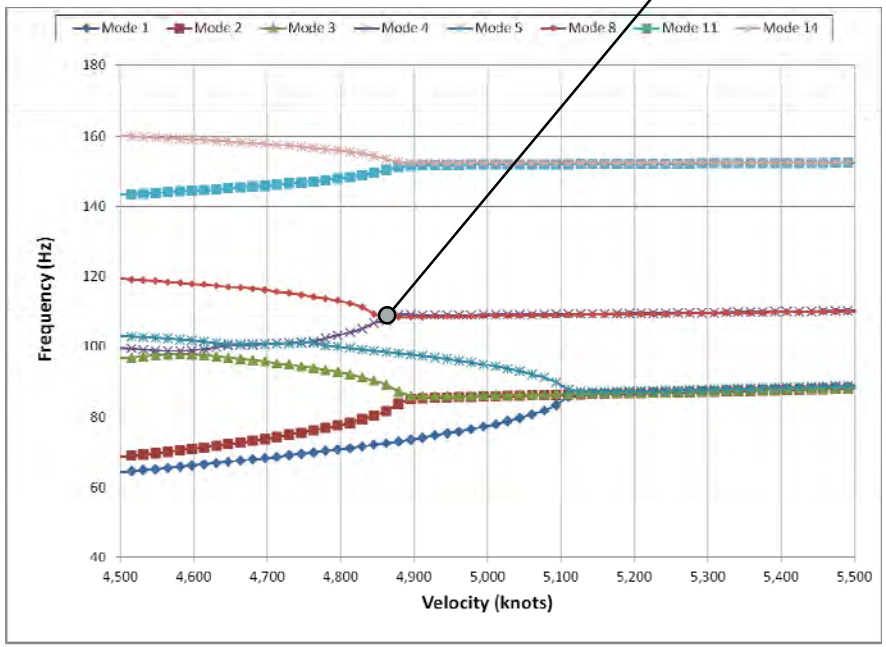

Approved for public release; distribution unlimited.

Panel 816 Flutter Analysis Summary

- **No flutter indicated at altitude up to air speeds equivalent to Mach 14**
- **Analysis indicates panel 816 has minimal risk of experiencing flutter**
- **Sea level flutter converges around Mach 7.5**
- **Thermal and mechanical load was not included for flutter analysis**

Altitude	Solution Mach Number	Velocity Range	Material Properties	Preload	First Flutter Mode	Frequency (Hz)	Flutter Speed (Knots)	Flutter Speed Mach Number
75,000 ft	6.25	M5 - M8	Room Temp	None	-----	-----	-----	-----
75,000 ft	6.25	M3 - M14	Room Temp	None	-----	-----	-----	-----
75,000 ft	6.25	M3 - M14	Temp Adj. (t=900s)	None	-----	-----	-----	-----
Sea Level	6.25	M5 - M8	Room Temp	None	-----	-----	-----	-----
Sea Level	6.25	M3 - M14	Room Temp	None	Mode 6	95.2	4961	7.50
Sea Level	6.25	M3 - M14	Temp Adj. (t=900s)	None	Mode 3	109	4498.2	6.80
Sea Level	7.5	M3 - M14	Temp Adj. (t=900s)	None	Mode 3	109	4961	7.50
Sea Level	7.5	M6 - M9	Temp Adj. (t=900s)	None	Mode 4	109.1	4879	7.38

506
Approved for public release; distribution unlimited.

Flutter Analysis Conclusions

- **The design curve and finite element analysis indicate large flutter margins for panel 816**
- **Design curves are a function of stiffness, panel aspect ratio, and panel thickness**
- **At high altitudes (low air density) panel stiffness and damping virtually constant as a function of velocity**
- **Empirical design curves would save time if their accuracy is proven for velocities and altitudes of this vehicle class**
- **Panel flutter can be calculated for panels at the unit cell level of fidelity**

507
Approved for public release; distribution unlimited.

Flutter Analysis Conclusions Continued

- **Aeroelastic Analysis Issues**
  - Analysis takes place down stream of configuration level sizing suggest adding empirical aeroelastic design curves to sizing routines at a high level
  - Requires an aero model that references grids on structural model, helps if structural model elements are aligned with flow direction(s) of interest
  - Results interrogation and visualization leaves something to be desired
    - Internal Boeing code used to plot damping and frequency vs. velocity.
    - Patran balked at importing modes from the CAERO5
  - Iterative process to determine correct flutter speed
    - Speeds away from the solution mach number are “approximations” and the solution must be iterated until flutter speed matches solution mach number

508
Approved for public release; distribution unlimited.

BACKUP CONTENT

509
Approved for public release; distribution unlimited.

Panel 816 Temperature History

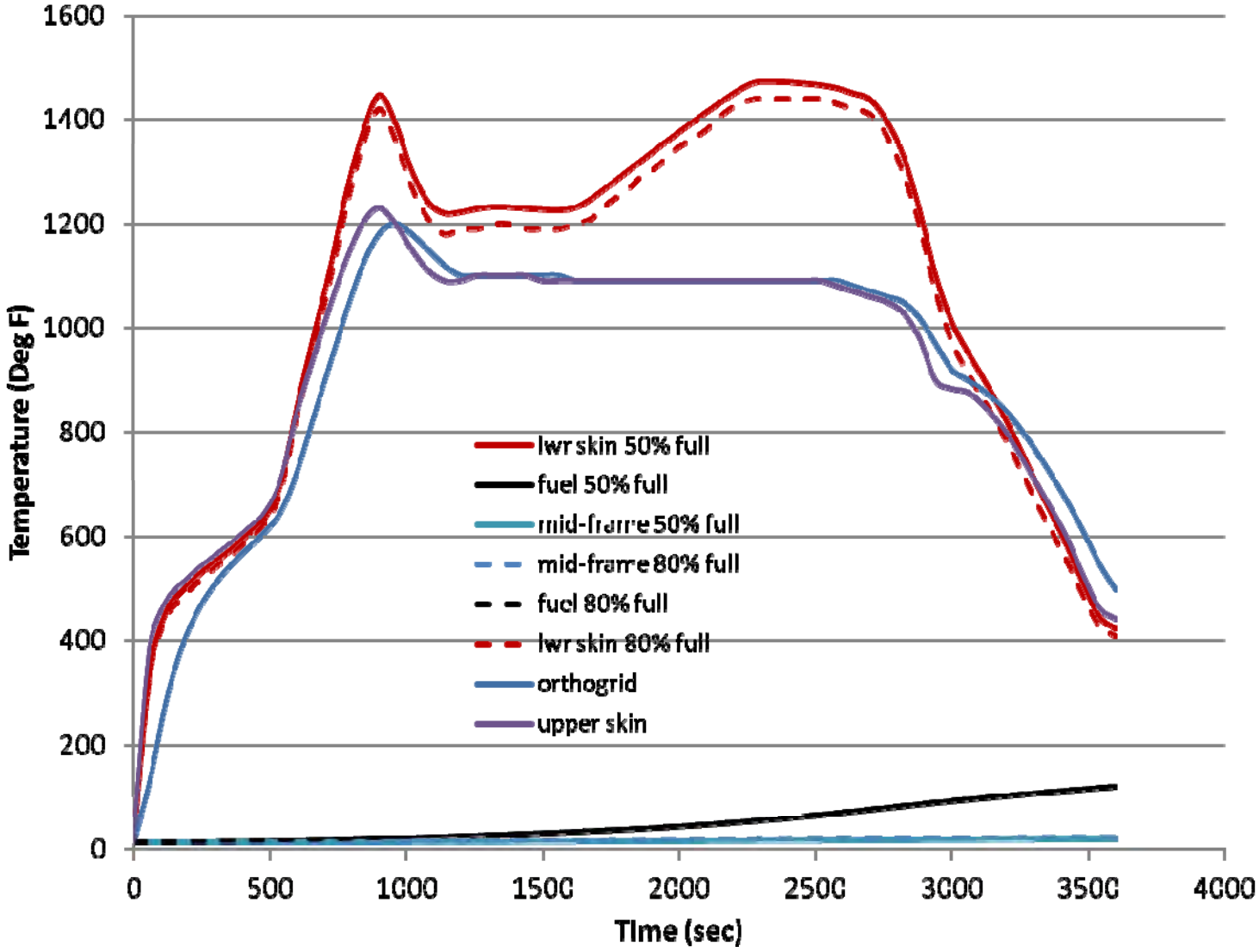

Approved for public release; distribution unlimited.

Analysis Issues

Issue	Approach	Source/Rationale
External Aero-acoustic Loads	Empirical with CFD guidance	Efimtsov Models, Boeing Best Practice, no hypersonic flight test data, or predictive capability available
Damping	Empirical Data	USAF Damping Design Guide, Boeing Best Practices, no inconel sine wave , iso-grid test data available
S-N Data for In 718	Convert Constant Amplitude Data to RMS Data, Adjust based for Temperature based on Strength	Mil-5, Best Practices, only source of reliable data
Sub-structure Modes	Filtered most Sub-structure modes	Concentrating on Panel Structure, also allows for quicker turn around
Choosing Worst Case Design Conditions	Using Max Thermal , matched to Max Acoustic for Fatigue Margin Checks	Dissimilar loads from different points in the trajectory, points are close, but not exact. This accounts for possible difference in trajectories
Combined Spectrum	Assuming a single trajectory	Don't have other trajectories, but a real vehicle will have many different possible missions.
Joint Allowables	Similarity to other material, joints	Boeing Best Practice, Need to test specific joints – welds, machine, fastened, etc…

Approved for public release; distribution unlimited.

ACOUSTIC MODEL DEVELOPMENT

512
Approved for public release; distribution unlimited.

Trajectory – Design Conditions of Interest

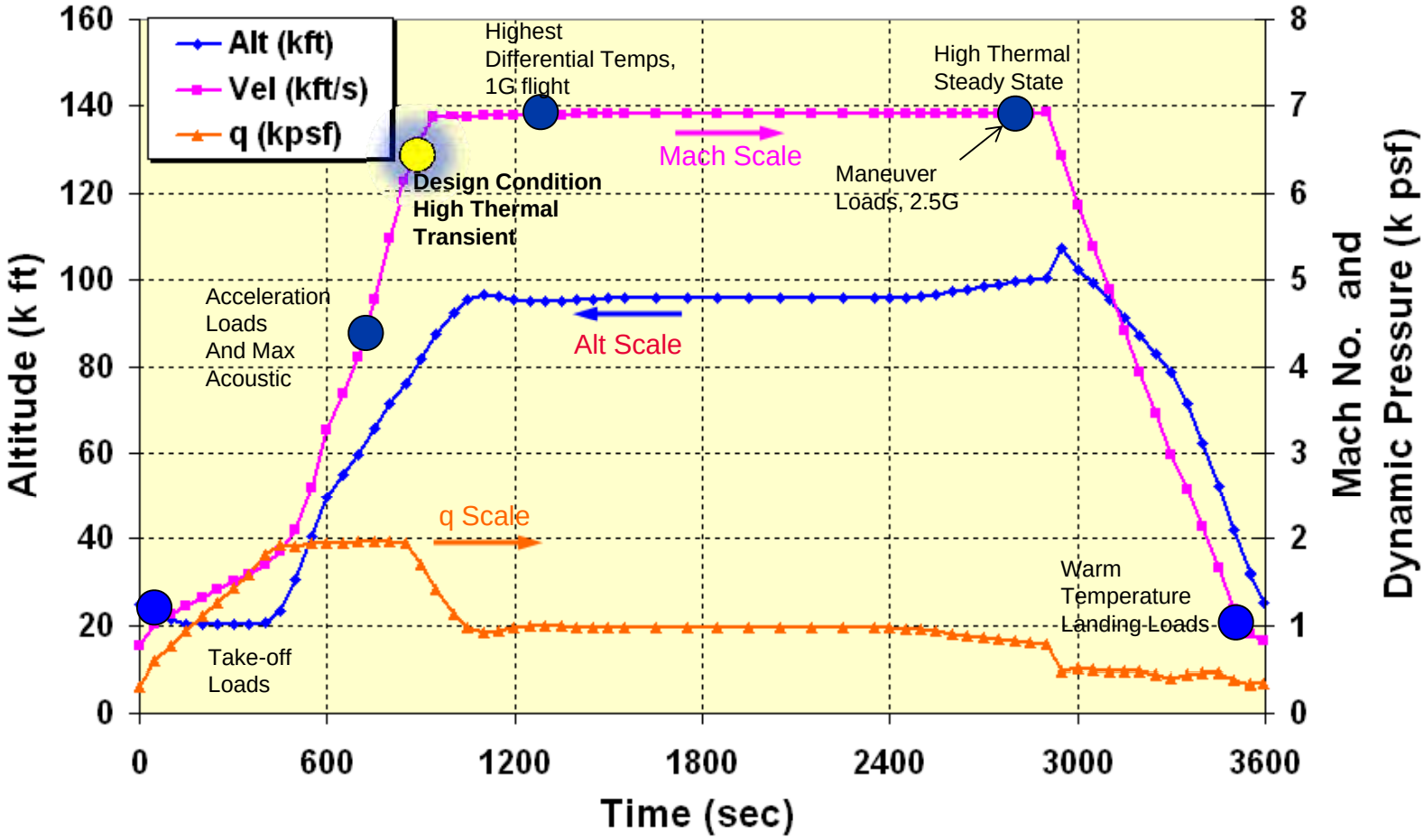

These are the Design Conditions of Interest for Dynamic & Fatigue Analysis.

513
Approved for public release; distribution unlimited.

Structural Damping

Frequency (Hz)	Damping Ratio, ζ
10	0.025
100	0.02
1000	0.01

```
$
TABDMP1  1        CRIT
         10.     .025     100.     .02       1000.
.01      ENDT
```

Nastran Damping Table Card

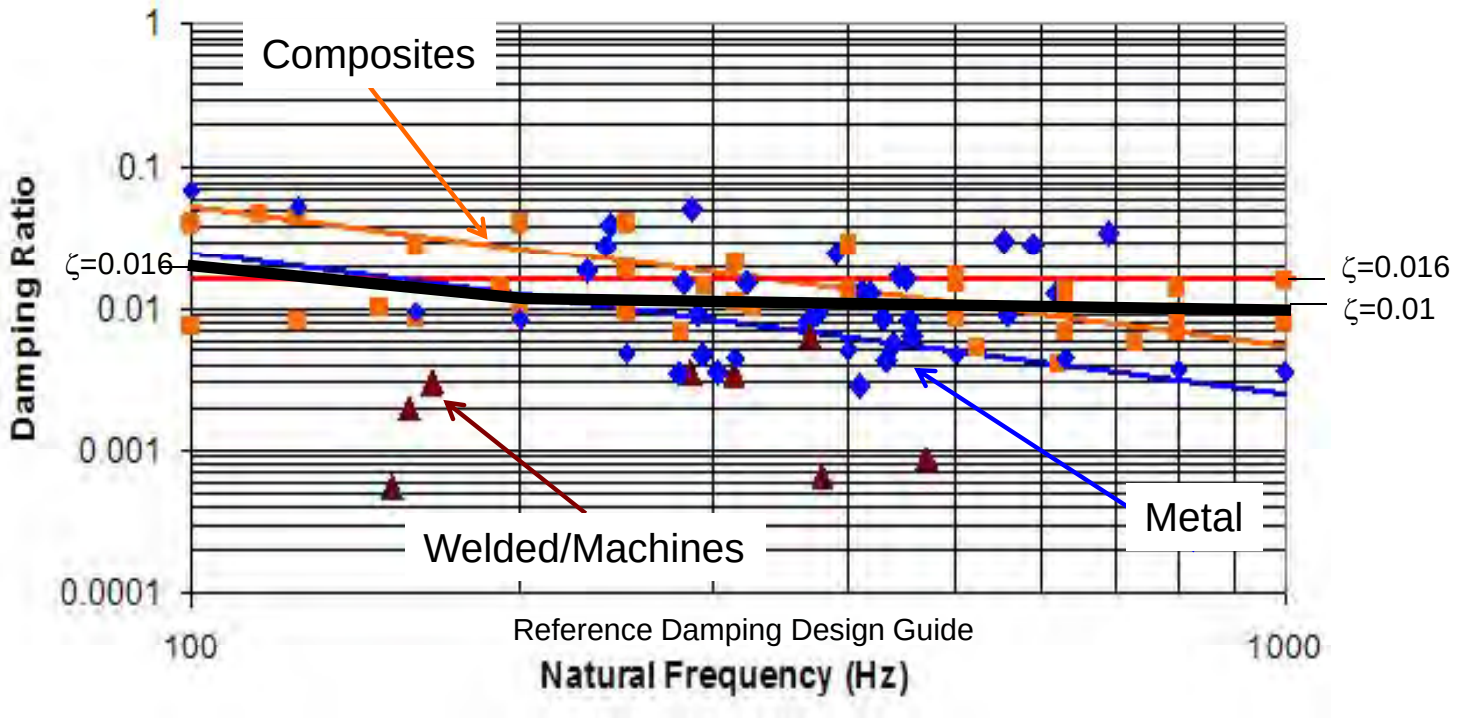

Dynamic Analysis uses the black curve

Approved for public release; distribution unlimited.

Panel 862 Location

Define acoustic levels for each panel and critical conditions:

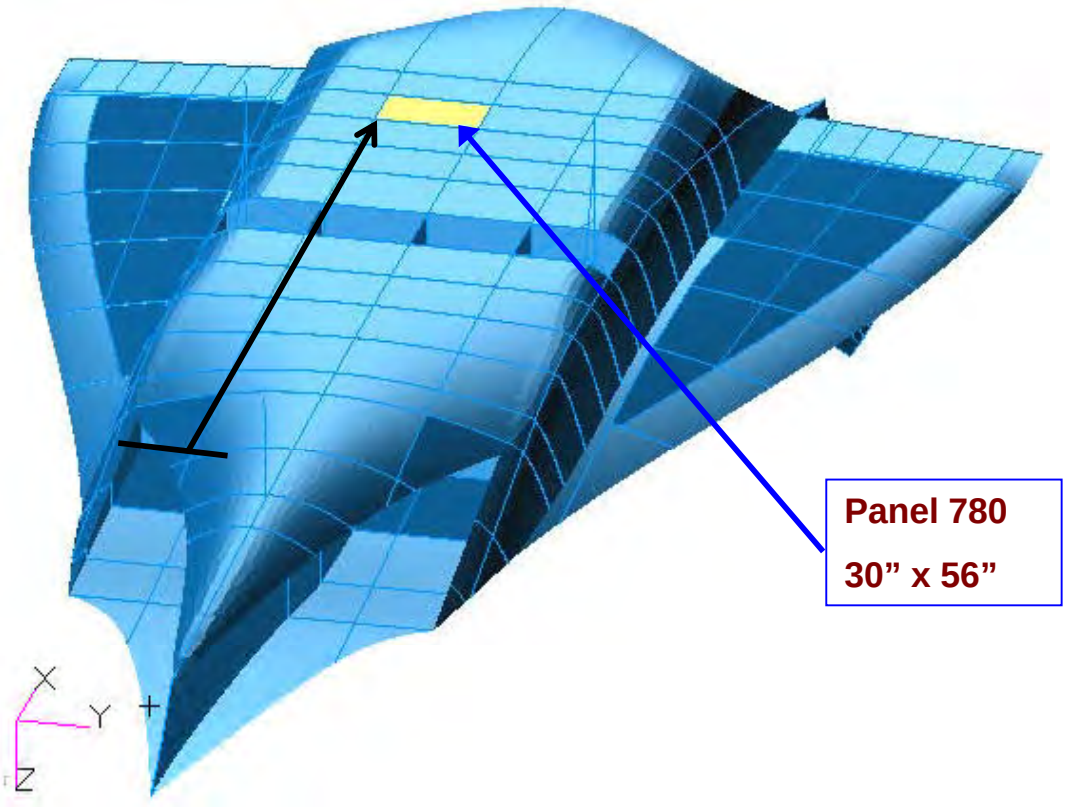

Distance from Lead Edge and Distance from Point of Separation are inputs to aero-acoustic models

Approved for public release; distribution unlimited.

CFD Results

CFD++ N-S Flow Field for M=7.0, α = 10 deg., Alt.=90Kft

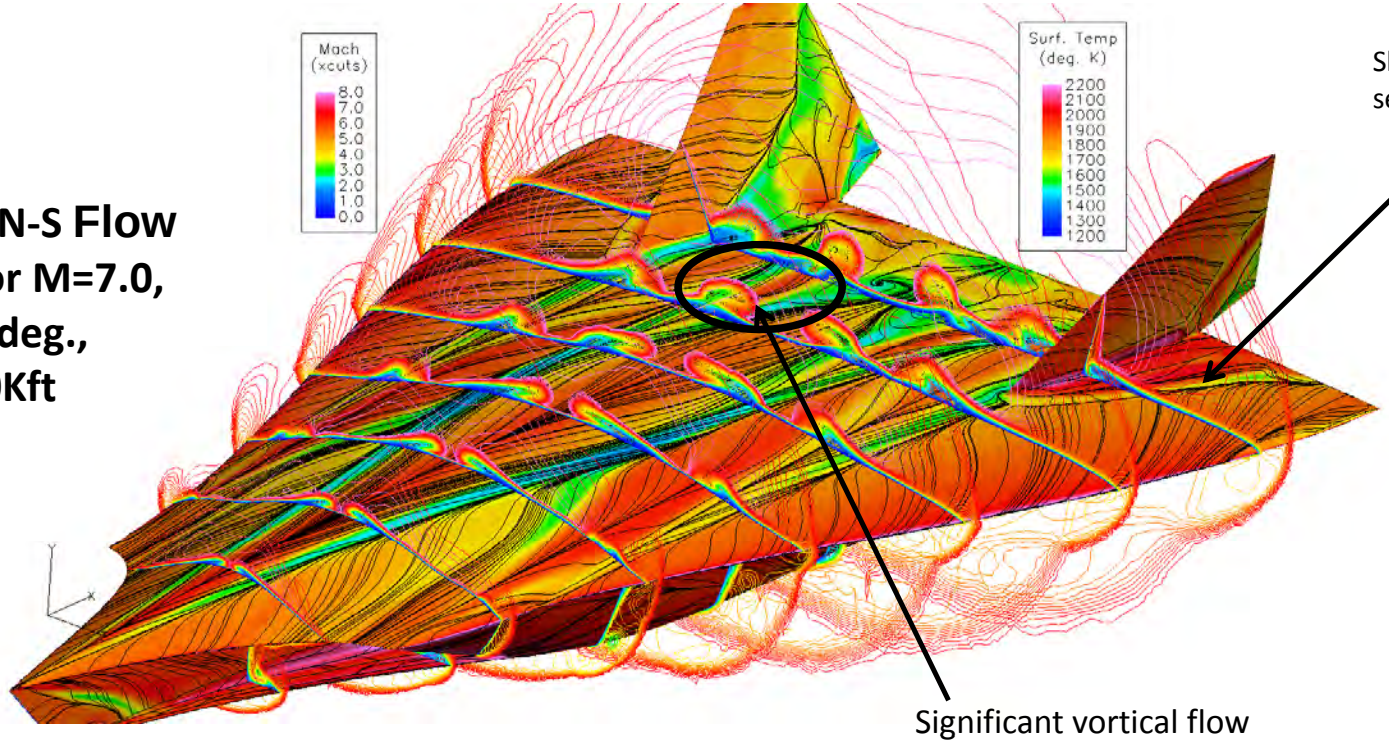

CFD was used to determine local flow features. This information was used in our Empirical models to predict acoustic loading spectrum

Approved for public release; distribution unlimited.

CFD Runs for Acoustic Loads

1.) Mach 7, 2.5g, AoA=10 deg, turn , Alt=90kft, q=1340 psf, Highest Maneuver and thermal loads (max G)

2.) Mach 7, 1.0g, AoA=4 deg, Cruise, Alt=100Kft, q=730 psf, High thermal loads and transient conditions (max T)

3.) Mach 6, 1.0g, AoA=6 deg, Accel, Alt= 75kft, q=2000 psf, Highest acoustic and thermal loads (max Q)

The load conditions for the detailed analysis was based on these are the three trajectory.

Approved for public release; distribution unlimited.

Required Data from CFD for Aero-acoustic Models

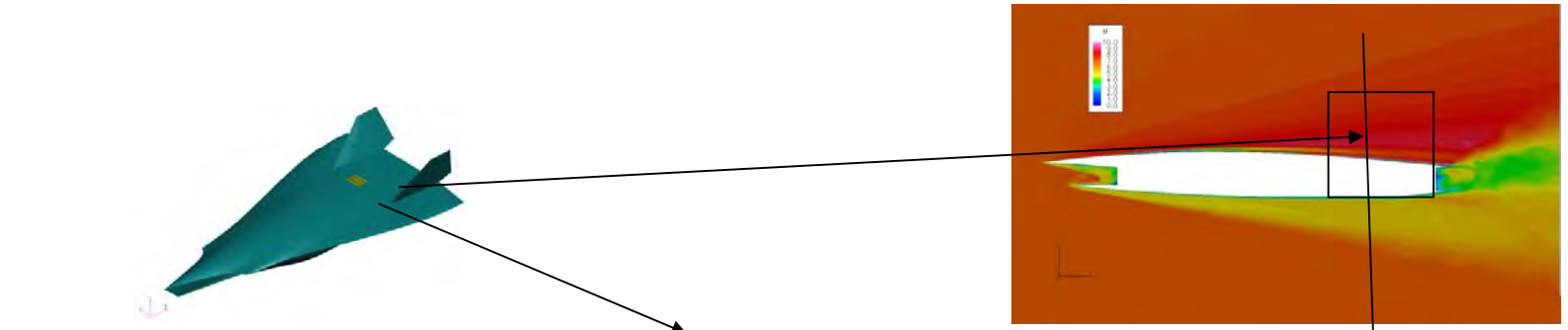

Streamline at center of panel

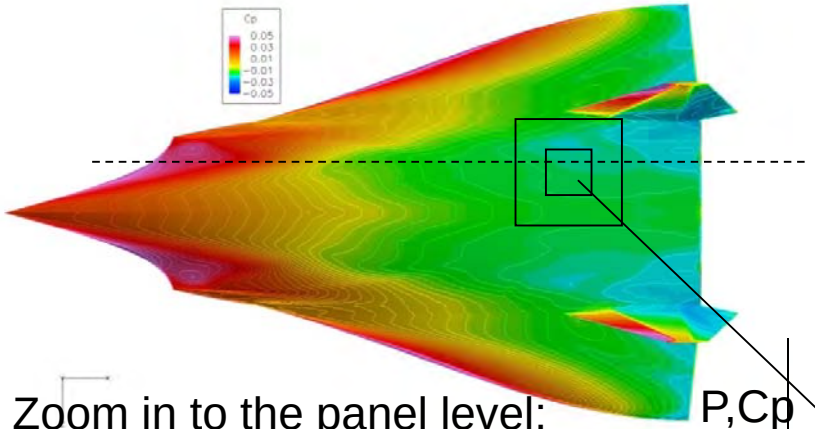

Zoom in to the panel level:

Graph of the pressure across
The panel at the Ctr line

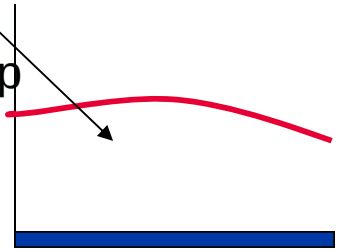

Velocity Profile

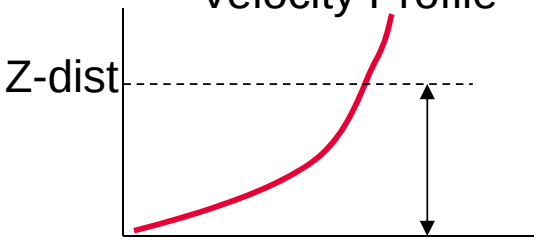

M,vel

An estimate of BL thick
At the leading edge of
the panel

Approved for public release; distribution unlimited.

CFD++ Computed Flow Field, M=6.0, a=6.0 deg., Alt.=75 Kft

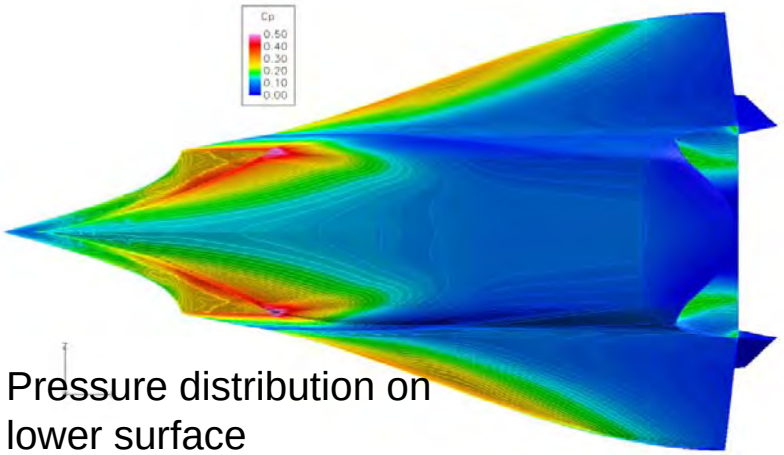

Pressure distribution on lower surface

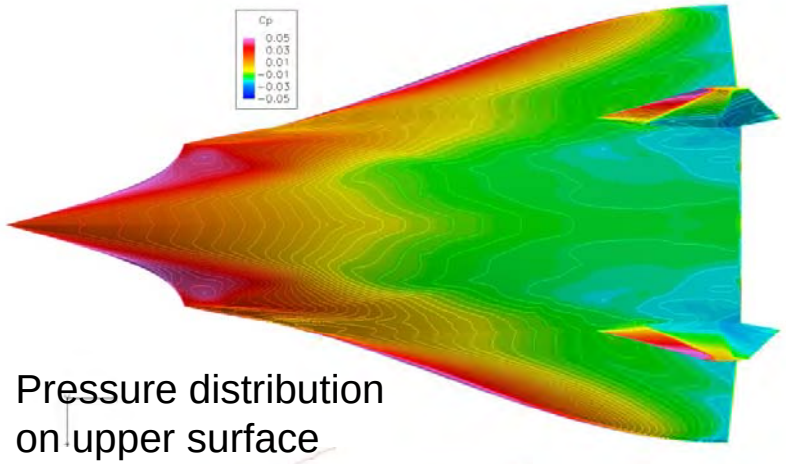

Pressure distribution on upper surface

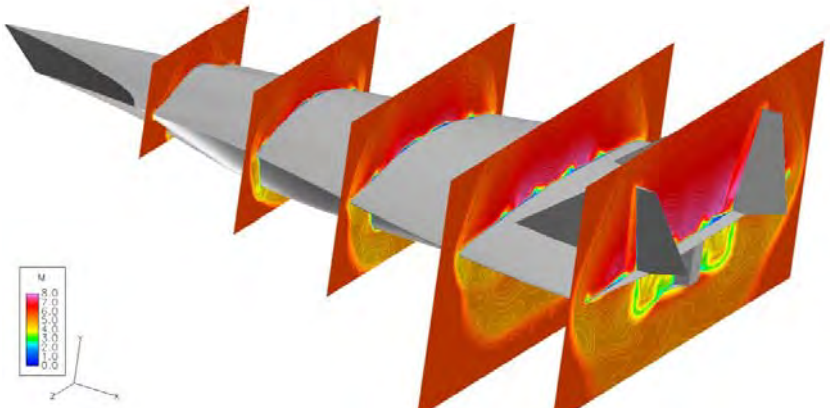

Mach No. at section cuts

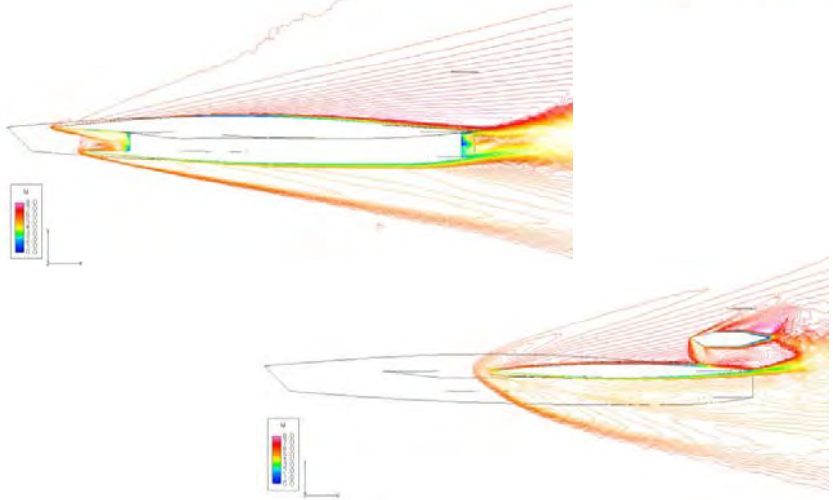

Approved for public release; distribution unlimited.

Computed Surface Pressures on the Panels

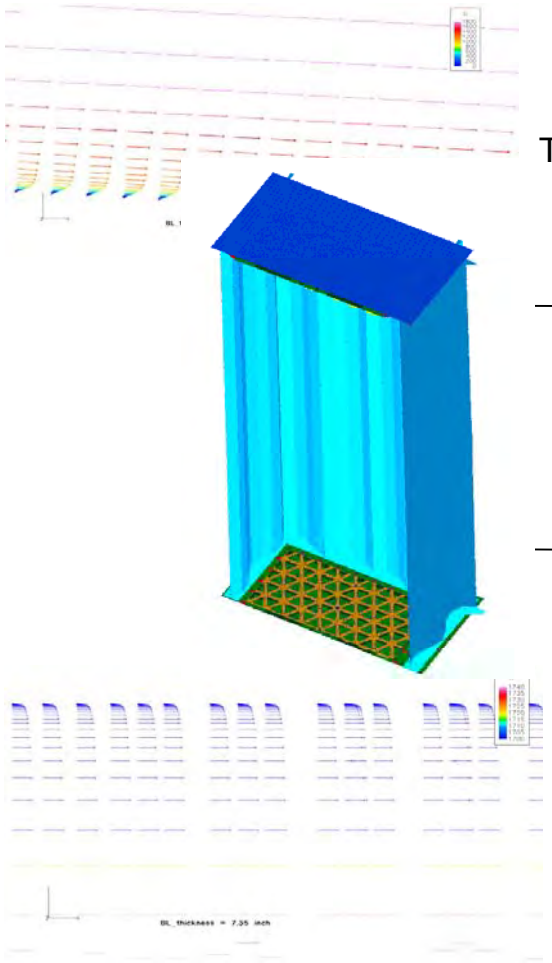

TBL_{ave}~11”

TBL_{ave}~7”

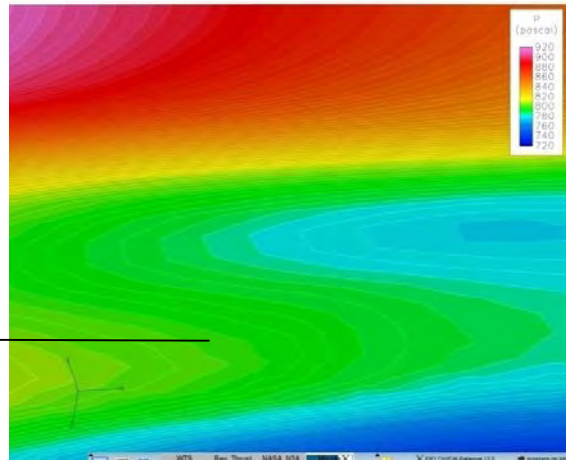

Panel 862
(Upper Surf)
ΔPy ~ 200 pa/m

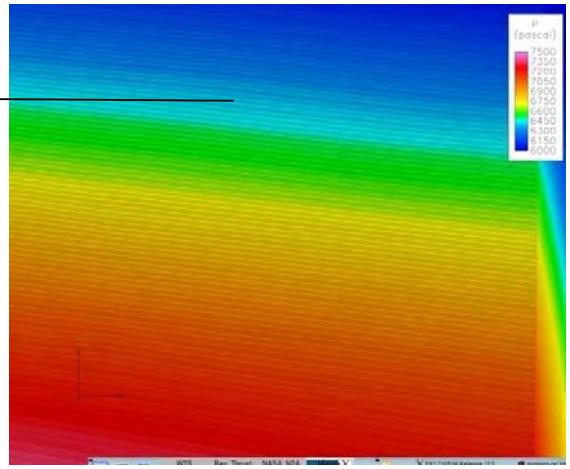

Panel 782
(Lower Surf)
ΔPy~1500 pa/m

Approved for public release; distribution unlimited.

Empirical Model Acoustic Prediction

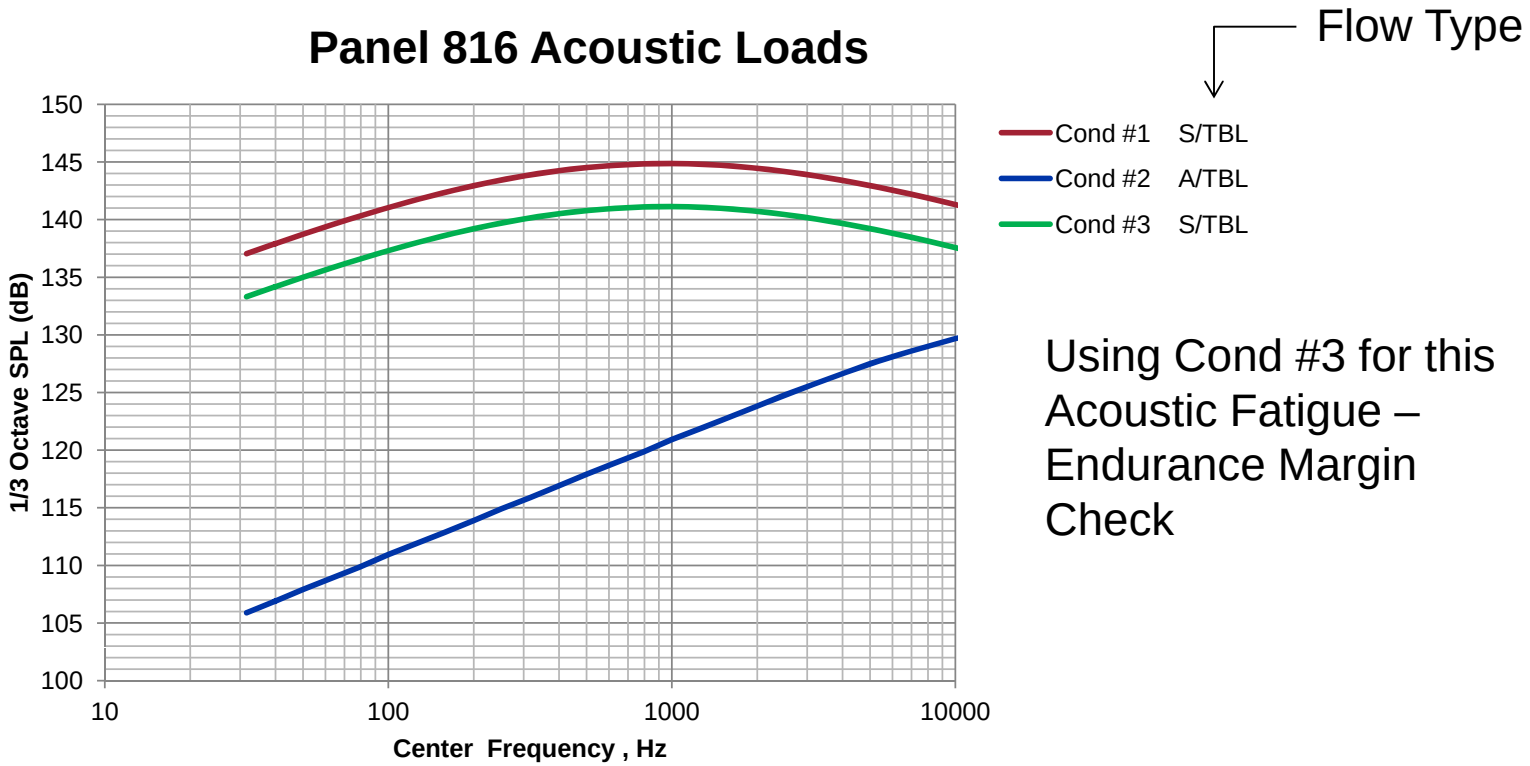

Using Cond #3 for this Acoustic Fatigue – Endurance Margin Check

Based on CFD input into Efimtsov TBL Models

Ref. R. Rackl, and A. Weston, "Modeling of Turbulent Boundary Layer Surface Pressure Fluctuation Auto and Cross Spectra - Verification and Adjustments Based on TU-144LL Data," NASA/CR-2005-213938.

521
Approved for public release; distribution unlimited.

Acoustic Damage Accumulation

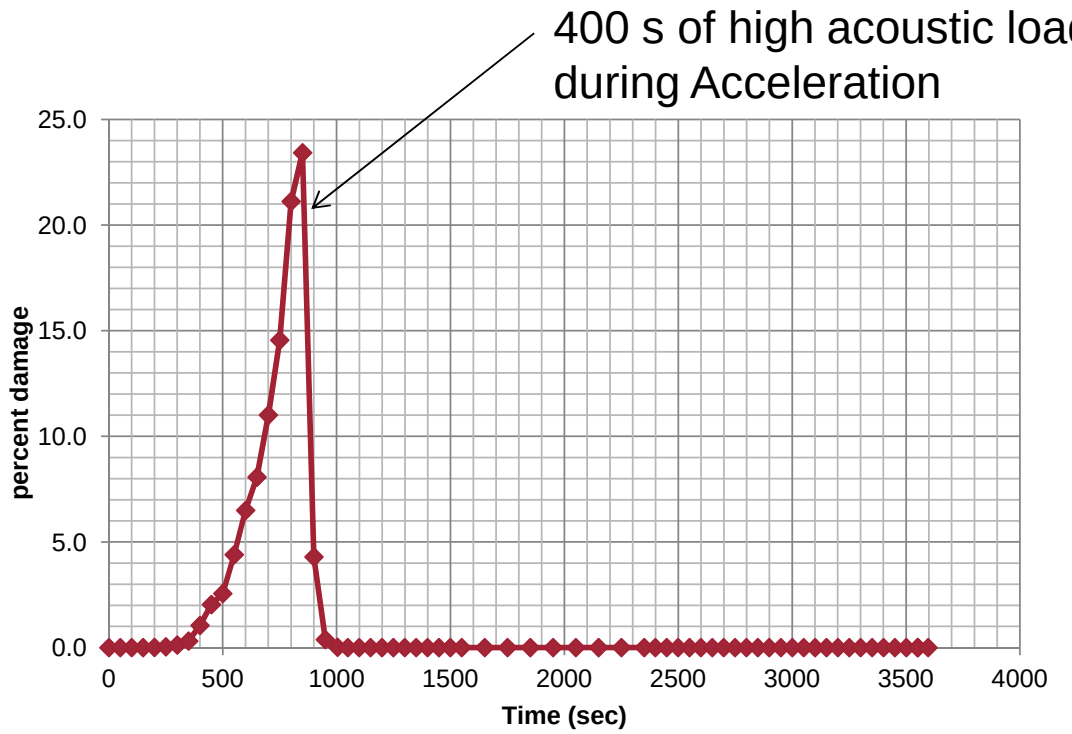

Acoustic Loads only critical during acceleration, add these stress cycles to fatigue spectrum

Approved for public release; distribution unlimited.

CAESAR DETAIL STRESS TOOL

523
Approved for public release; distribution unlimited.

CAESAR Description

- CAESAR (ComputAtional Engineering Structural Analysis Routines)
- CAESAR is a web based tool for determining detail stresses for open holes, filled holes, notches, fillets, etc
- User entered Input variables are submitted to stress check model templates which are executed on a remote server
- Results can be retrieved in multiple formats
- Details are given on stress check model and results calculations
- XML files and stress check model files can be saved for future runs

Approved for public release; distribution unlimited.

CAESAR Home Screen

Holes	Detail Stress Analysis	Notches, Fillets, etc.
Single Hole Cold Worked Single Hole Multi-Hole Multi-Loaded Holes Lug Rod End Cutout in Shear Reinforced Cutout (2D) Reinforced Cutout (3D) Reinforced Hole (3D) Nutplate	 *Please use Microsoft's Internet Explorer* Download SVG Install Package (Does not require admin privileges.)	Single Notch Double Notch Shallow Gradient Specimen Shoulder Fillet Web Fillet Stepped Flange (3D) Tension Fittings Multi-Hole Plate Buckling Reinforced Hole Plate Buckling Reinforced Cutout Plate Buckling
Questions or Problems? Email: CaesarSupport@Boeing.com Pager: 314-507-0531	First Time Users: Download Overview Charts	Change Log: • Functional change 12/19/2007

Approved for public release; distribution unlimited.

Example CAESAR INPUT – Single Hole Detail

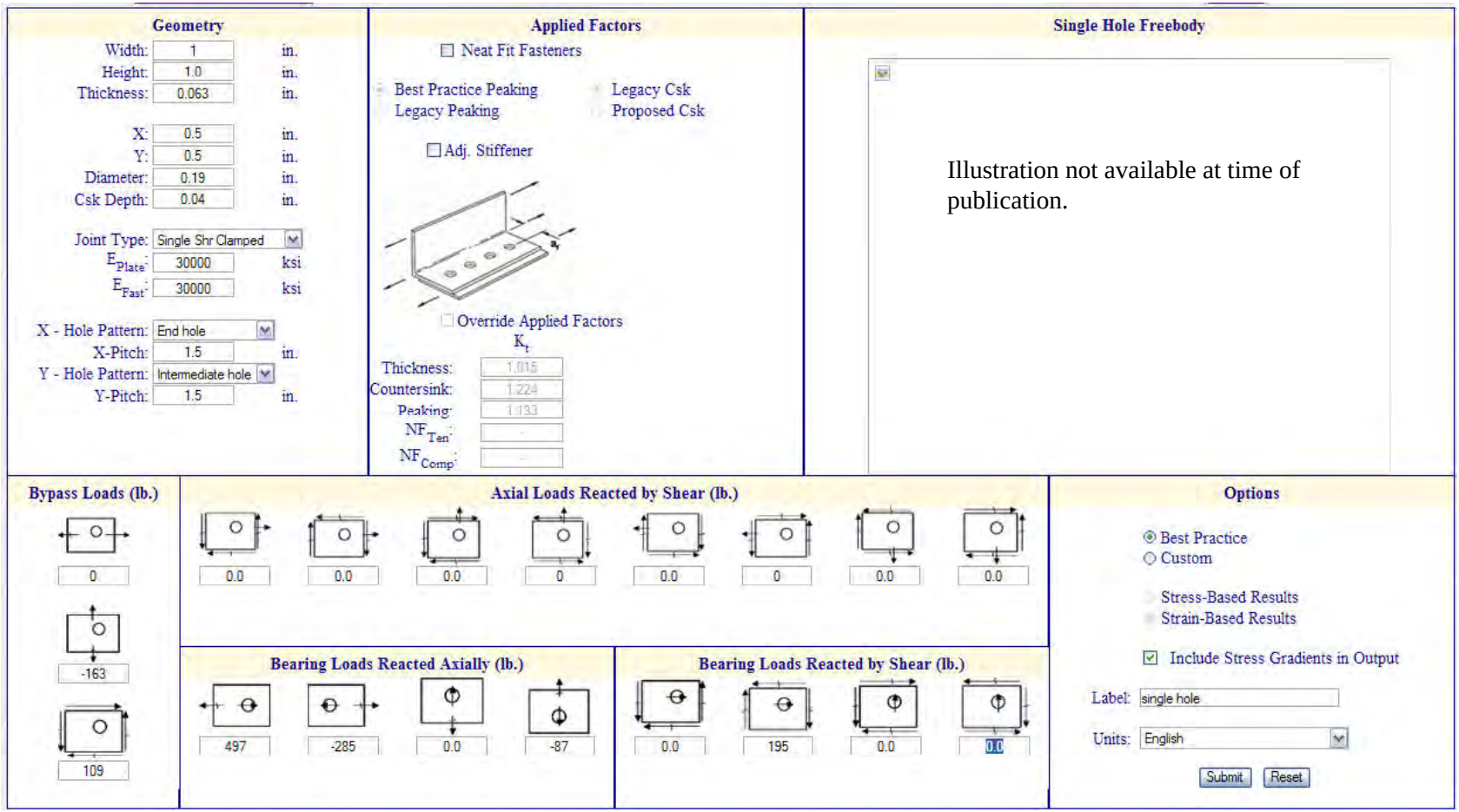

Approved for public release; distribution unlimited.

Example CAESAR Result – Single Hole Detail

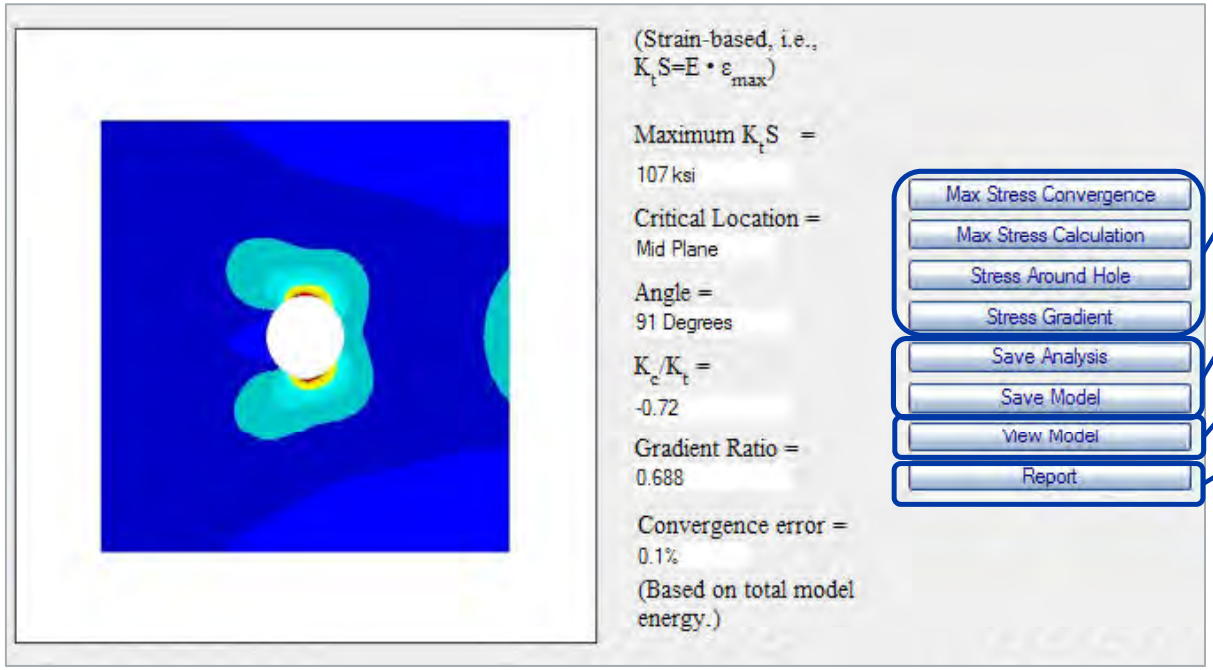

527
Approved for public release; distribution unlimited.

Engineering, Operations & Technology
Boeing Research & Technology

Panel 1074 Heat Transfer Analysis

January 17, 2012

Pete Keller
206-544-7528
peter.c.keller@boeing.com

Approved for public release; distribution unlimited.

Analysis Approach and Assumptions

- Transient analysis, temperature dependant material properties
- All structure modeled with shell elements: through-thickness gradients not significant
- Uniform initial temperature = recovery temperature at M=0.75, 25kft
- Aerothermal environment provided from MINIVER Mach 7 trajectory analysis
- Fuel assumed to occupy 80% of internal volume, modeled as lumped mass
- Uniform insulation thickness between fuel and simplified tank
- Internal radiation between the skin panels and substructure.

Approved for public release; distribution unlimited.

Panel 1074 Thermal Boundary Conditions

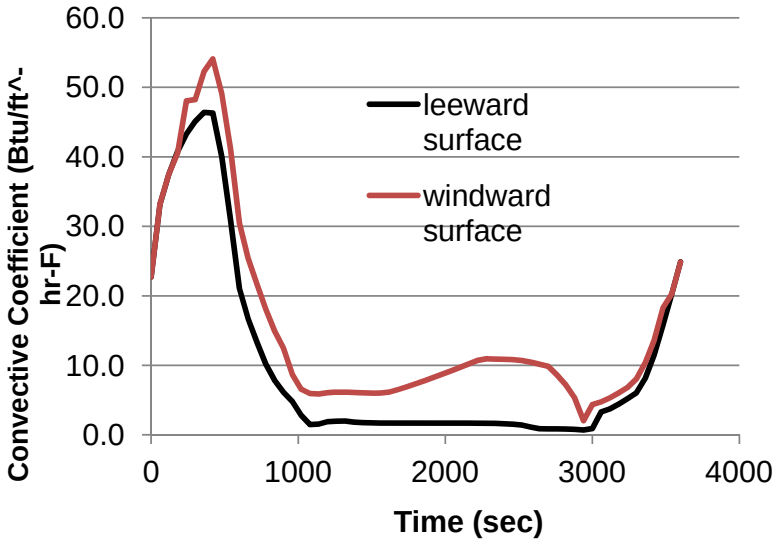

Panel 1074 Aerothermal Environment

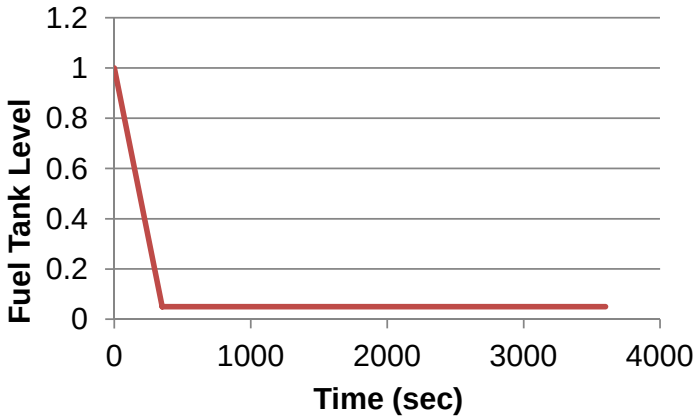

Wing Fuel Tank Schedule

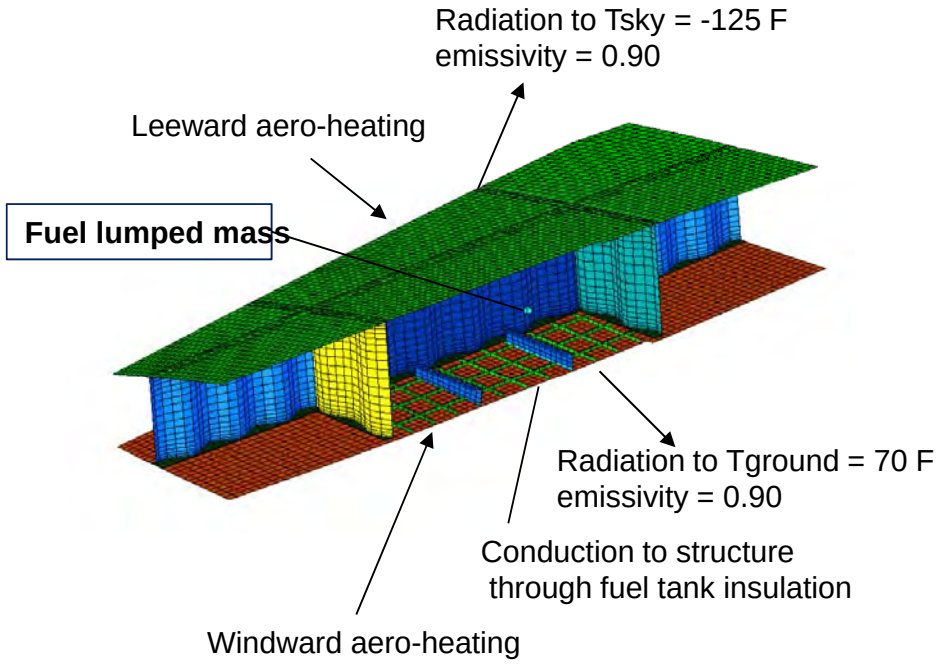

Initial temperature = 13 F
(recovery temperature at t=0)

Approved for public release; distribution unlimited.

Fuel Consumption Timeline

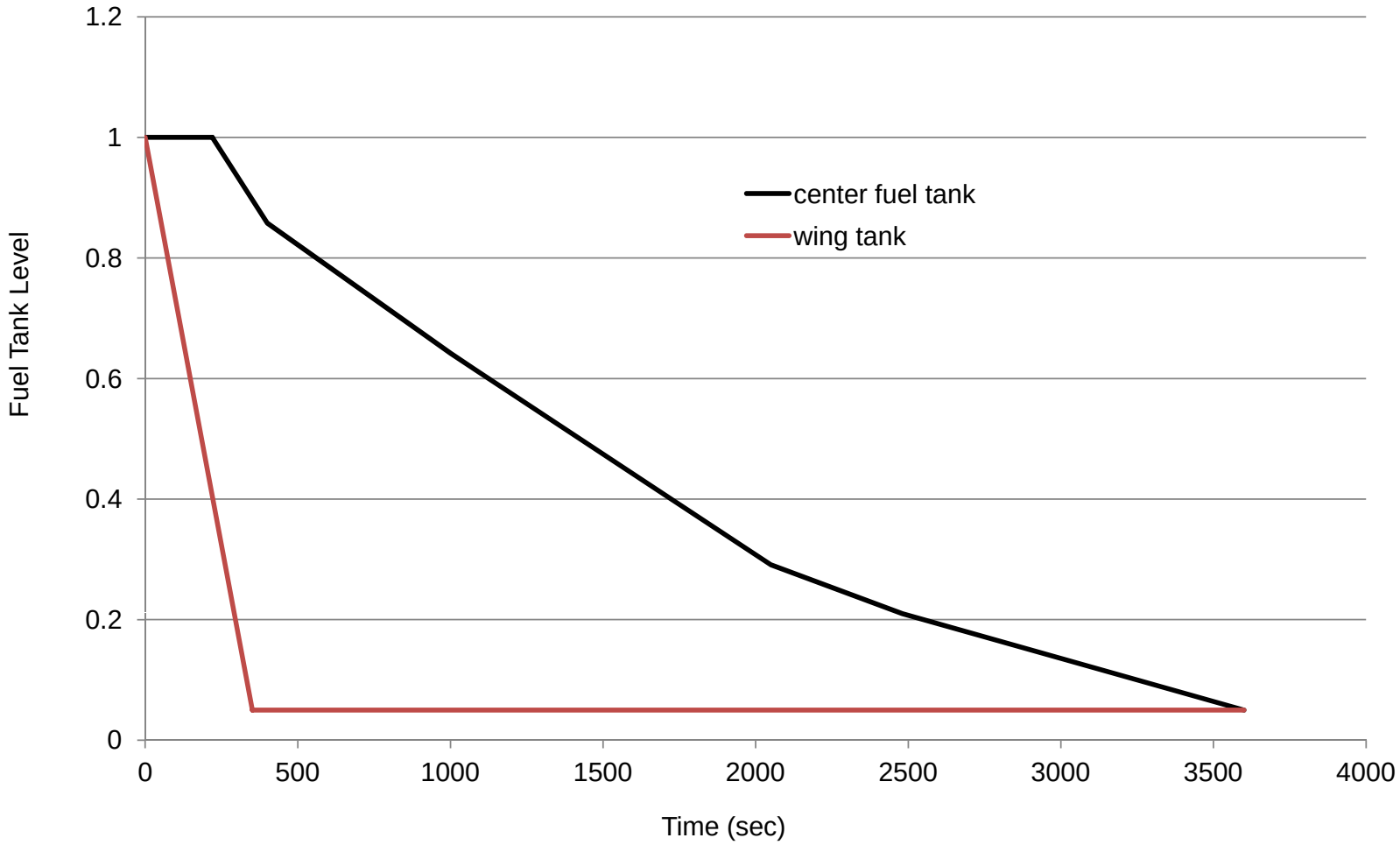

Approved for public release; distribution unlimited.

Panel 1074 Thermal Analysis

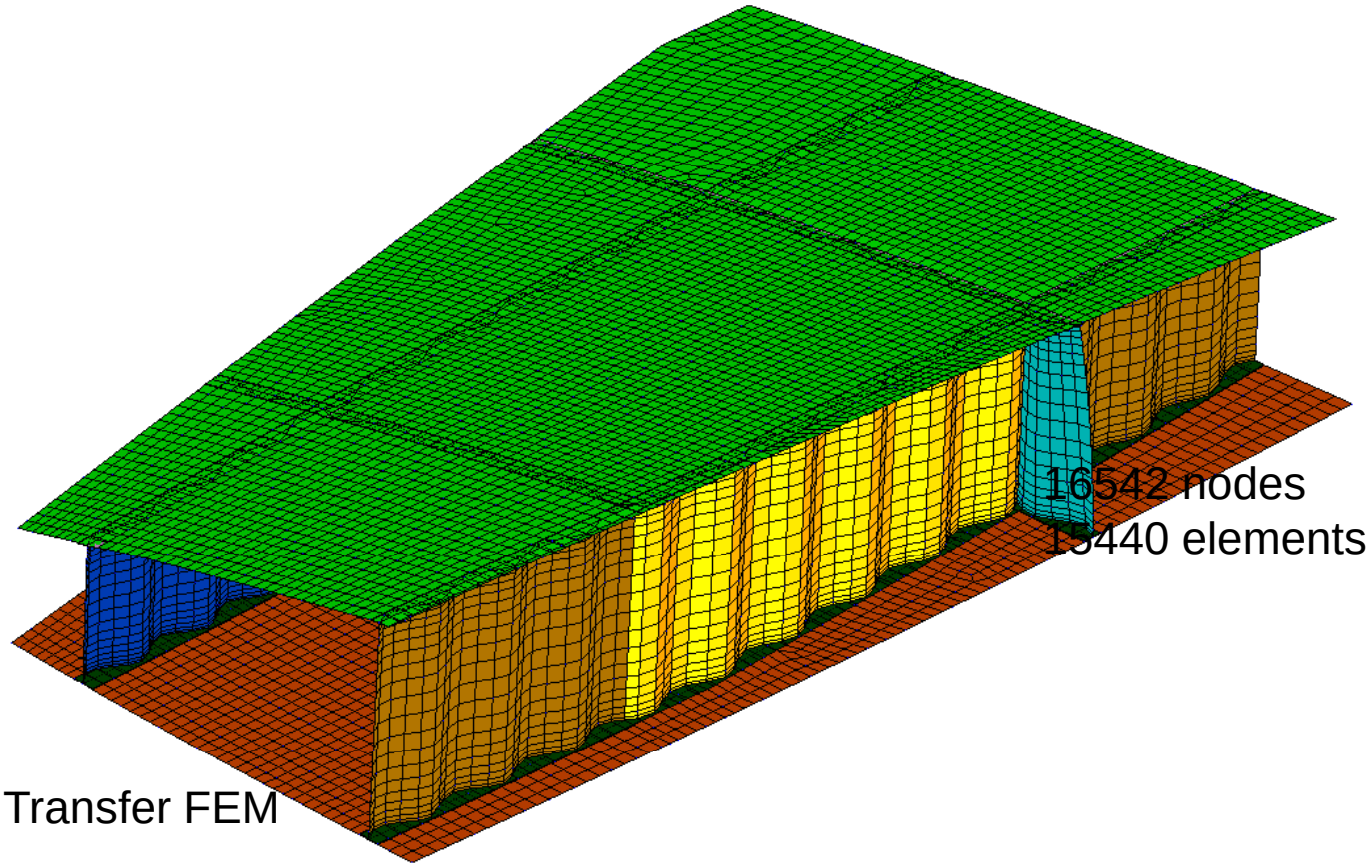

Heat Transfer FEM

Approved for public release; distribution unlimited.

Panel 1074 Temperature Distributions

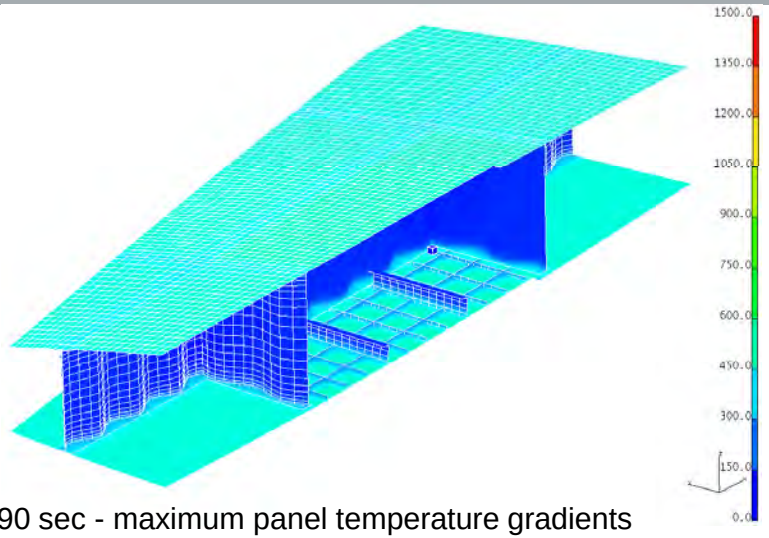

90 sec - maximum panel temperature gradients

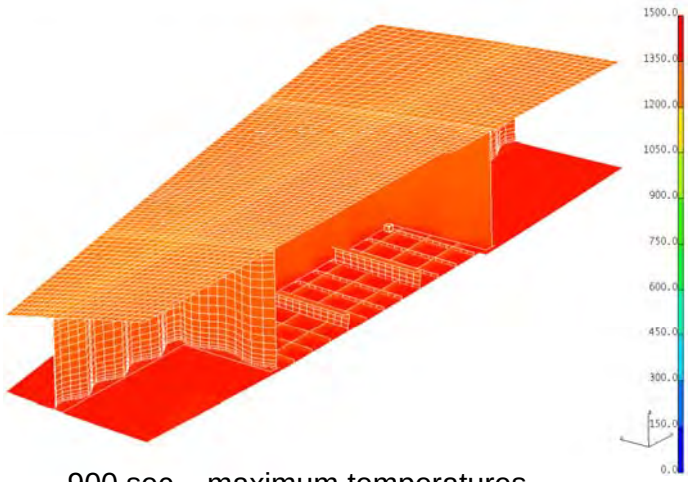

900 sec – maximum temperatures

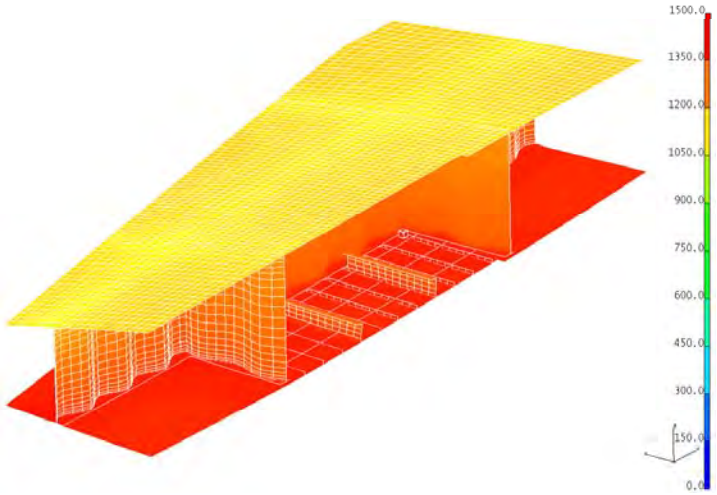

2700 sec – maximum substructure temperature gradient

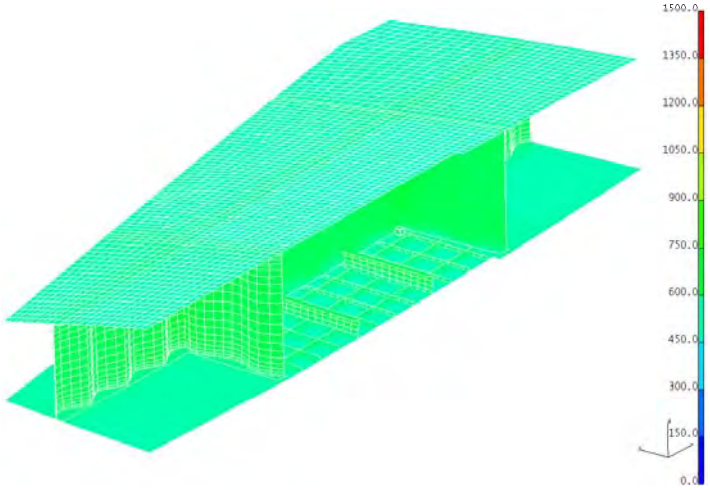

3540 sec – maximum negative temperature gradients

Approved for public release; distribution unlimited.

Panel 1074 Temperature History

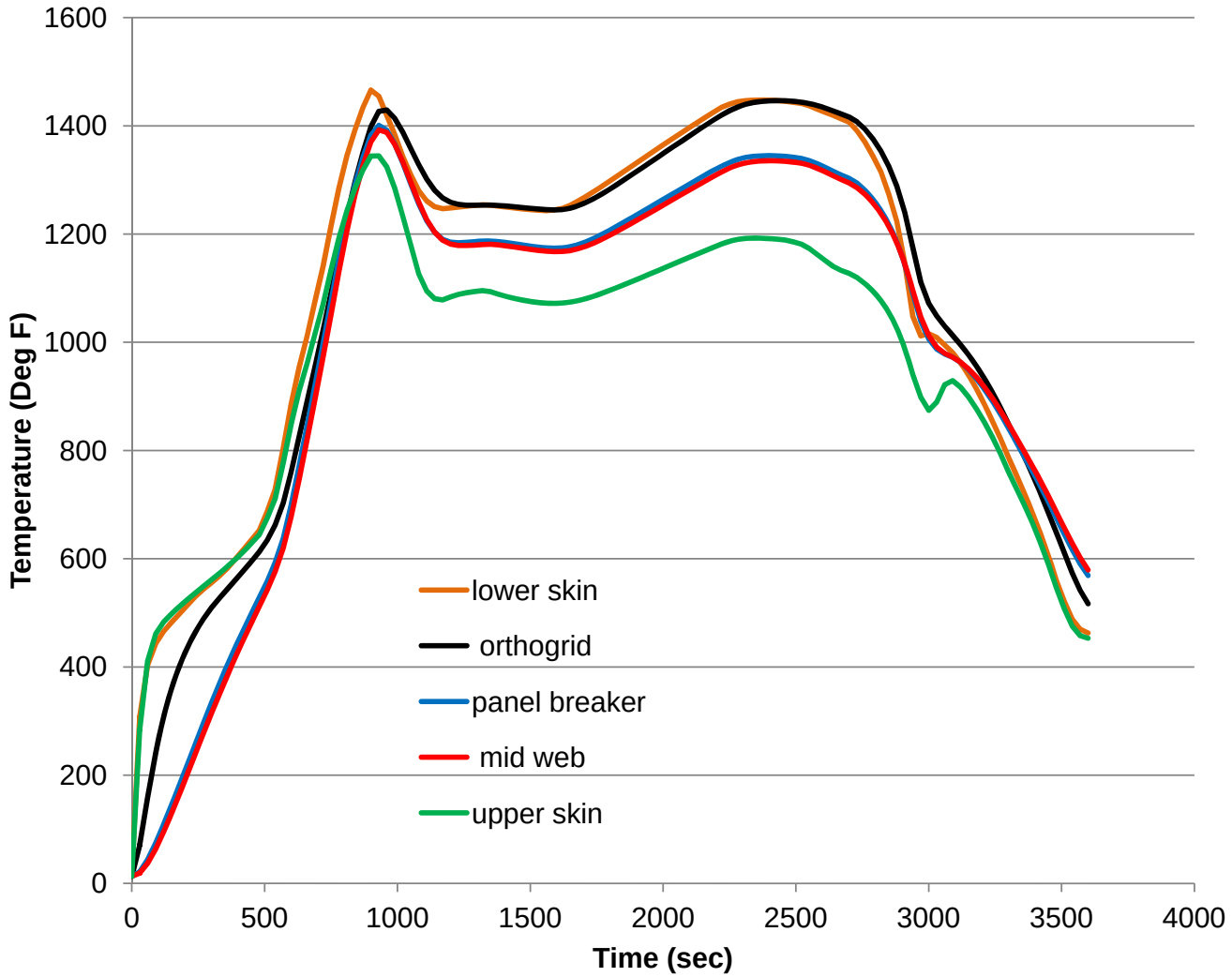

Approved for public release; distribution unlimited.

Panel 1074 Temperature Gradient History

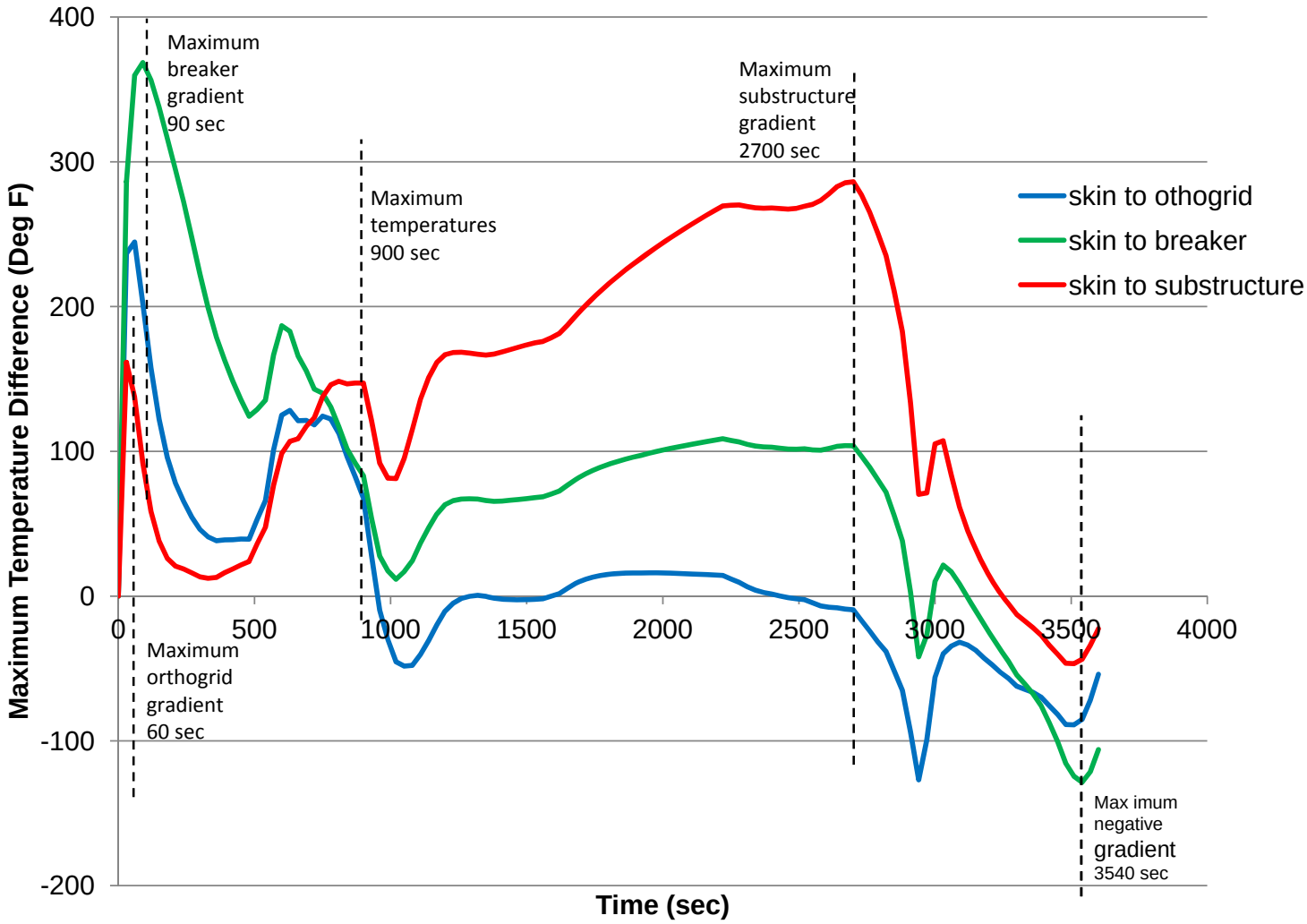

Approved for public release; distribution unlimited.

Summary of Results

- maximum skin temperatures = 1466 F at 90 sec
- maximum allowable fuel temperature = 120 F
- maximum temperature gradient in the panel = 369 F at 90 sec
- maximum temperature gradient between skin and substructure = 286 F at 2700 sec
- minimal effect of fuel since wing tanks empty during acceleration

Approved for public release; distribution unlimited.

Panel 4 (1074) Static Stress Analysis

January 25, 2012

Rob Quiroz
Robert.Quiroz@boeing.com
714-916-2577
BR&T Structures Technology

Approved for public release; distribution unlimited.

Panel Analysis Study

Unit Cell Static Analysis (linear): 2.5G ultimate (FS=1.5), no Temp

1. Mechanical loads from global model and SPC's to remove rigid-body motion; loads are balanced (reactions at supports ≈ zero)
2. Stress peaking at some load application points; does not affect interior panel

Unit Cell Static Analysis (linear): 2.5G ULT, T=2700s

1. Time step T=2700s is the critical condition, with max displacement and stress slightly higher than at max skin temp T=900s condition.

Panel local model Static Analyses:

Static linear: 2.5G ULT, T(900s)

1. Applied displacement from unit-cell model as boundary condition to center panel for 2.5G ULT + Temp=2700s
2. Good comparison with Unit Cell model

Static nonlinear: 2.5G ULT, T=900s

1. Displacement and overall stress are higher than linear analysis; nonlinear analysis reveals a different deformed shape resulting in a different critical locations.

Buckling analysis: 2.5G LIM (LF=1.15), T=900s

1. First panel eigenvalue << 1. First 35 buckling modes are local buckling. Combined local and global buckling eigenvalues are critical

Approved for public release; distribution unlimited.

Unit Cell Location

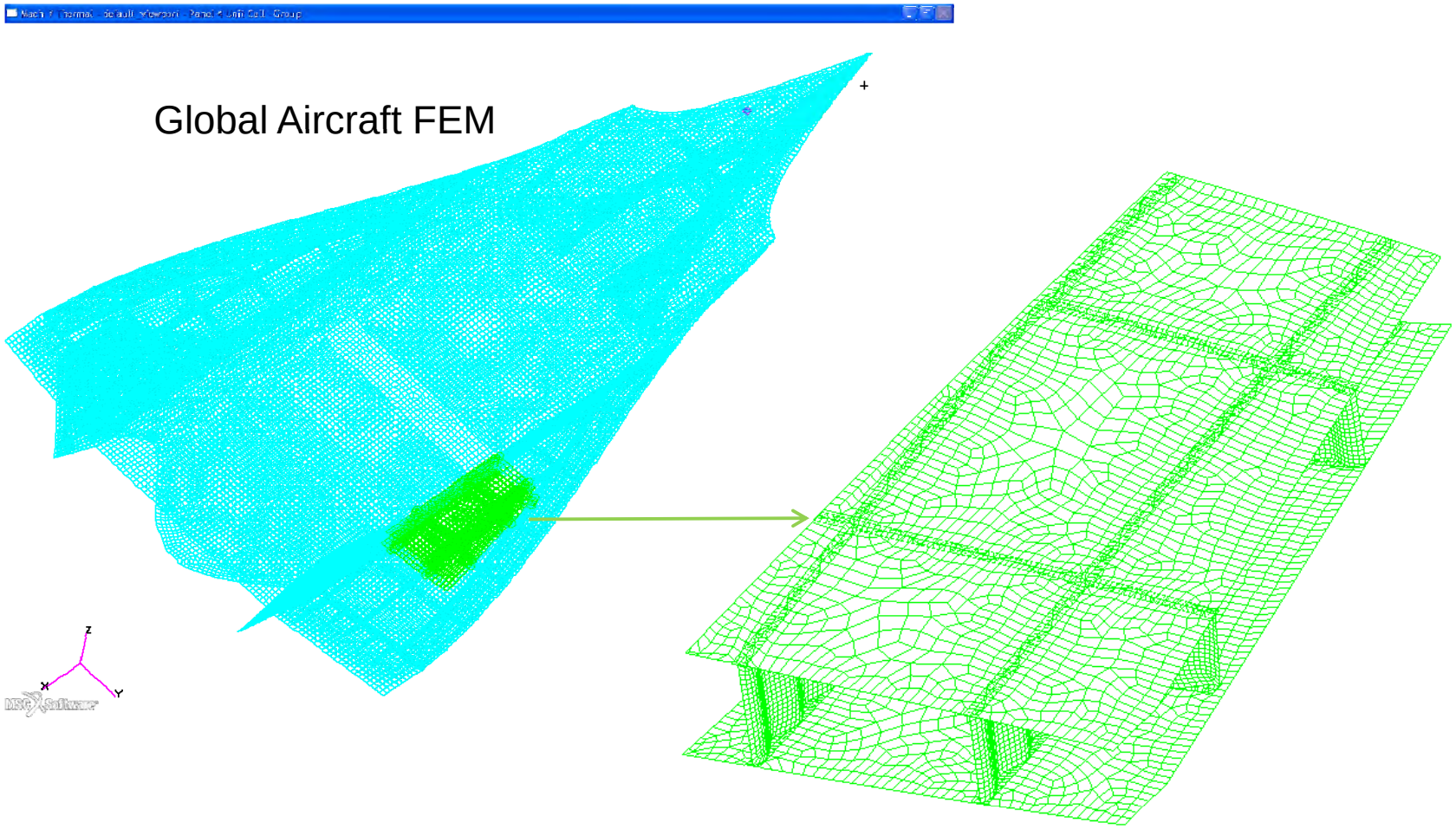

Approved for public release; distribution unlimited.

Model Constraints

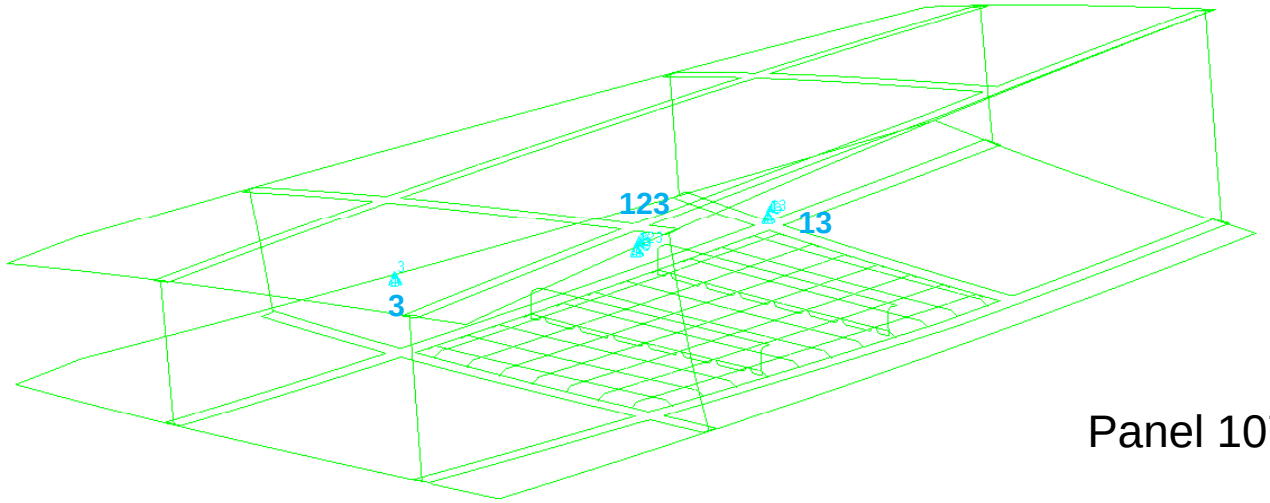

Panel 1074

Approved for public release; distribution unlimited.

Constraint Forces, 2.5g + T=2700s

Load case is balanced (RB motion constraint forces are small)

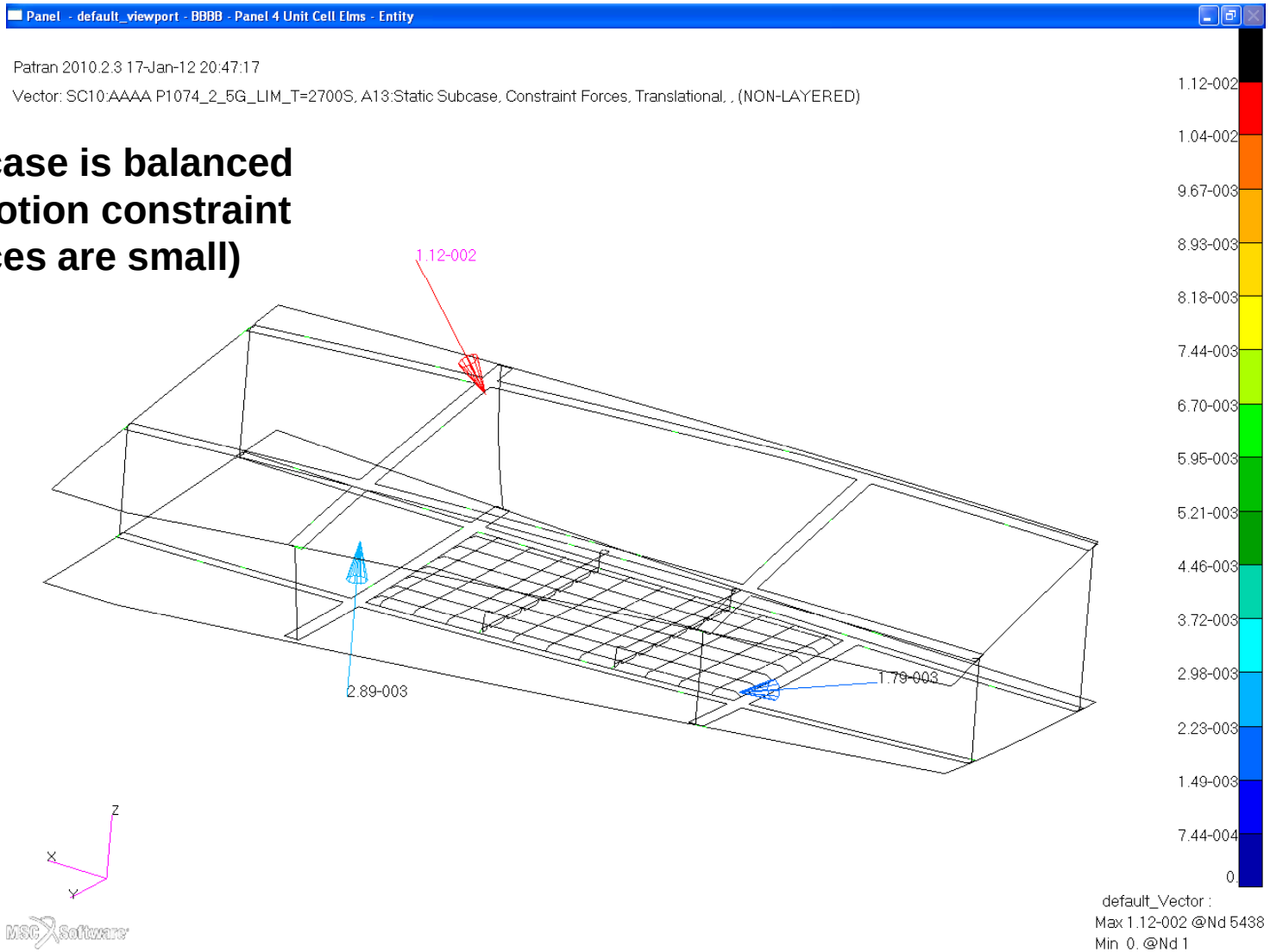

Approved for public release; distribution unlimited.

Panel 4 (1074) Unit Cell

Final Detailed FEM of Panel 1074 Unit Cell; Reflects sine wave ribs/spars, and Orthogrid structural details

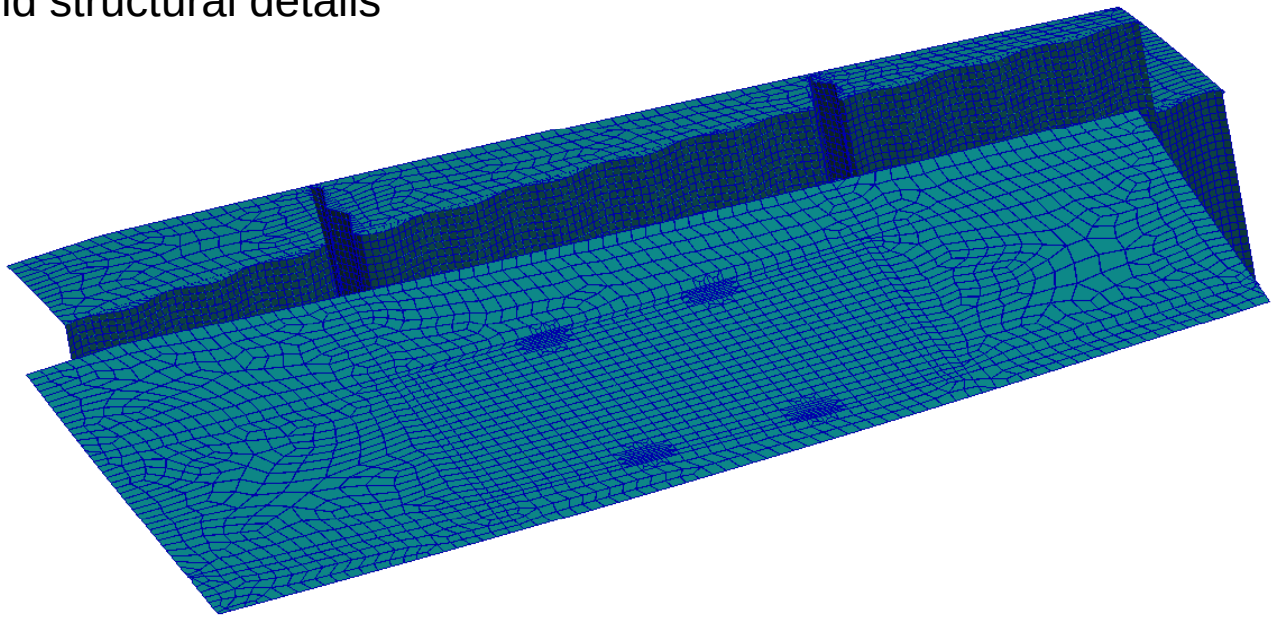

Approved for public release; distribution unlimited.

Temperature Profiles Panel 1074 Unit Cell

Approved for public release; distribution unlimited.

Temperature Profiles, Unit Cell, T=60s

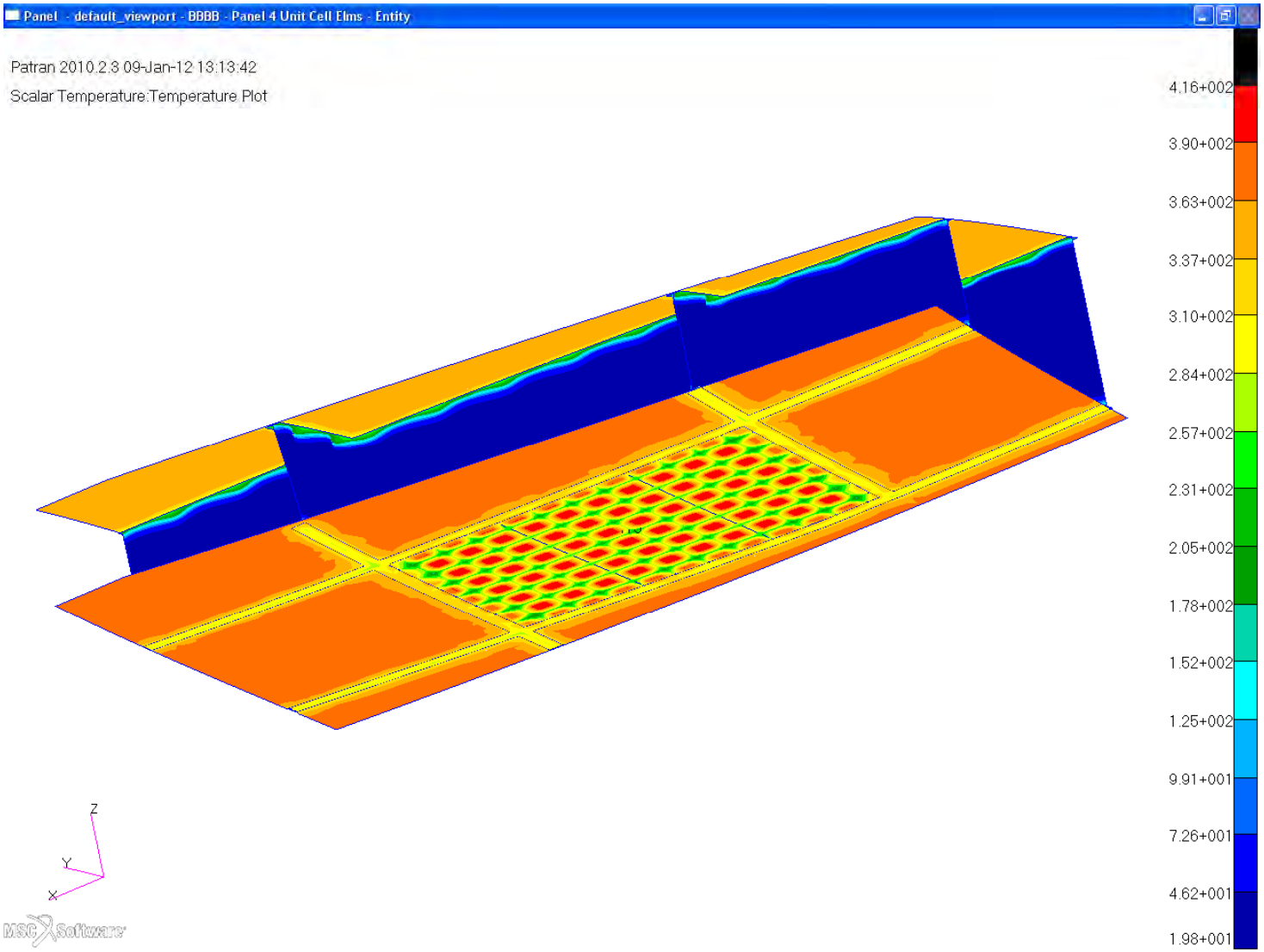

Approved for public release; distribution unlimited.

Temperature Profiles, Unit Cell, T=90s

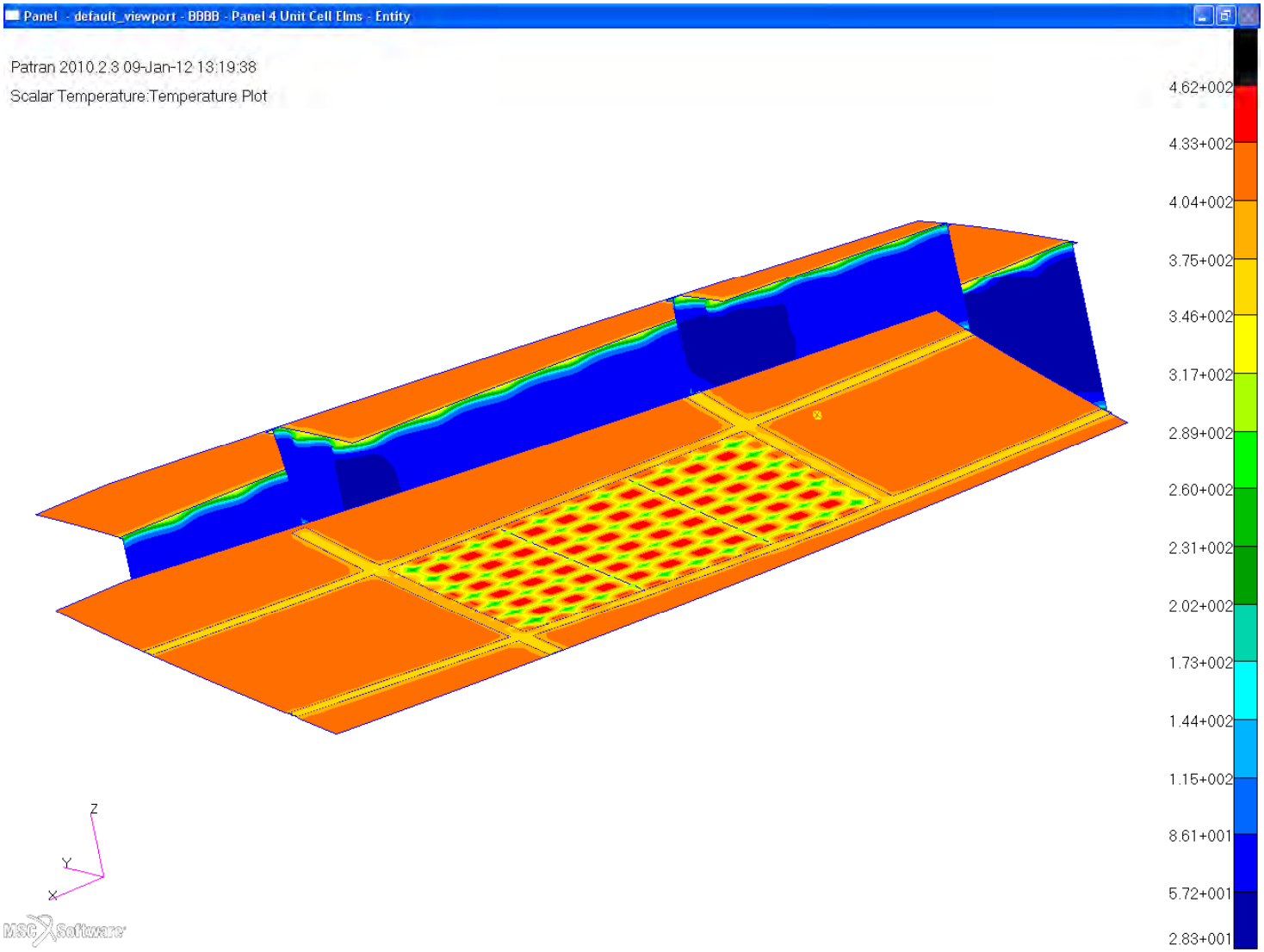

Approved for public release; distribution unlimited.

Temperature Profiles, Unit Cell, T=900s

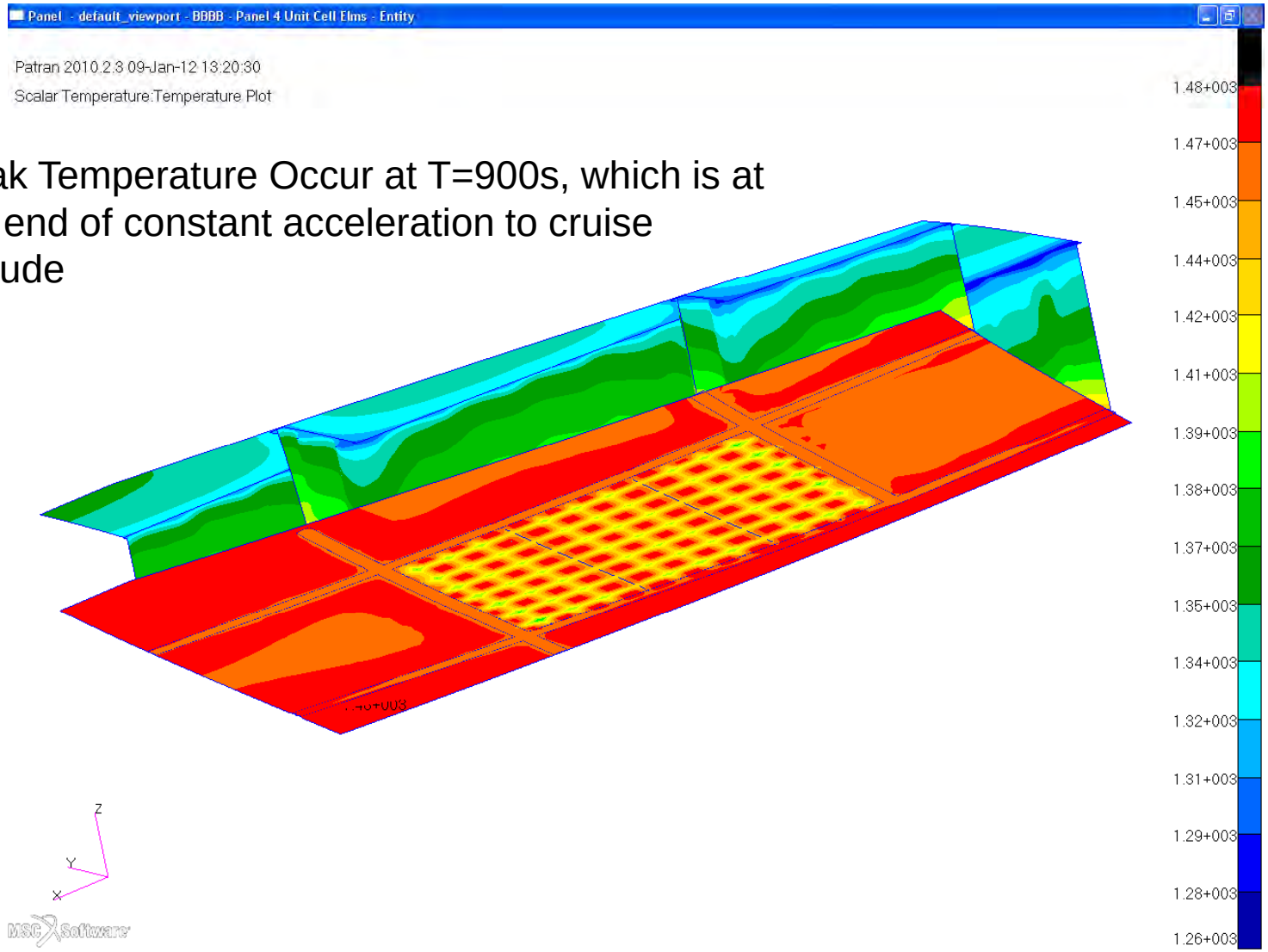

Peak Temperature Occur at T=900s, which is at the end of constant acceleration to cruise altitude

Approved for public release; distribution unlimited.

Temperature Profiles, Unit Cell, T=2700s

Max Gradient between skin and substructure occurs at T=2700s

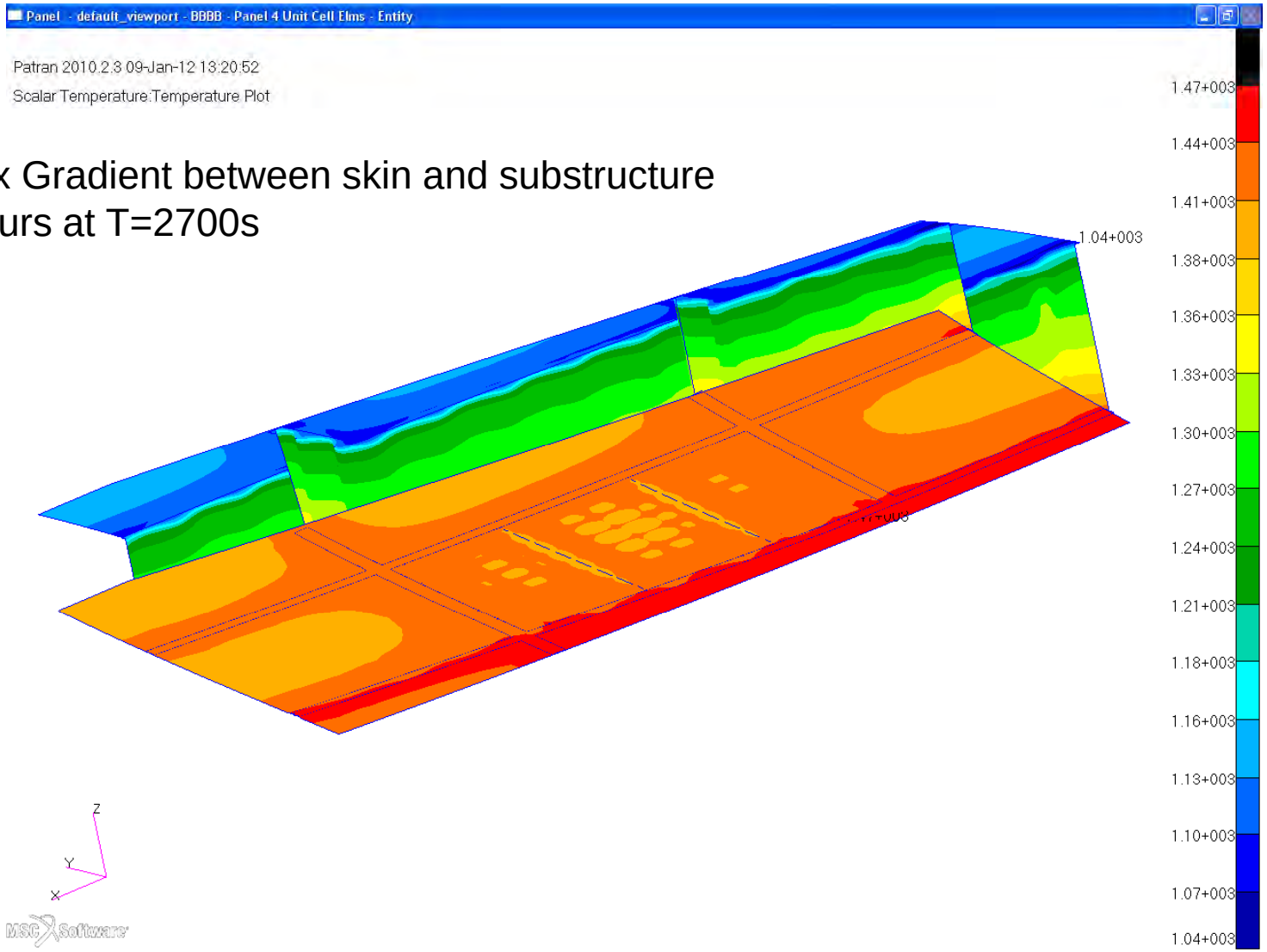

Approved for public release; distribution unlimited.

Temperature Profiles, Unit Cell, T=3540s

Temperature profile just prior to landing at T=3600s. Substructure is hotter than external skin.

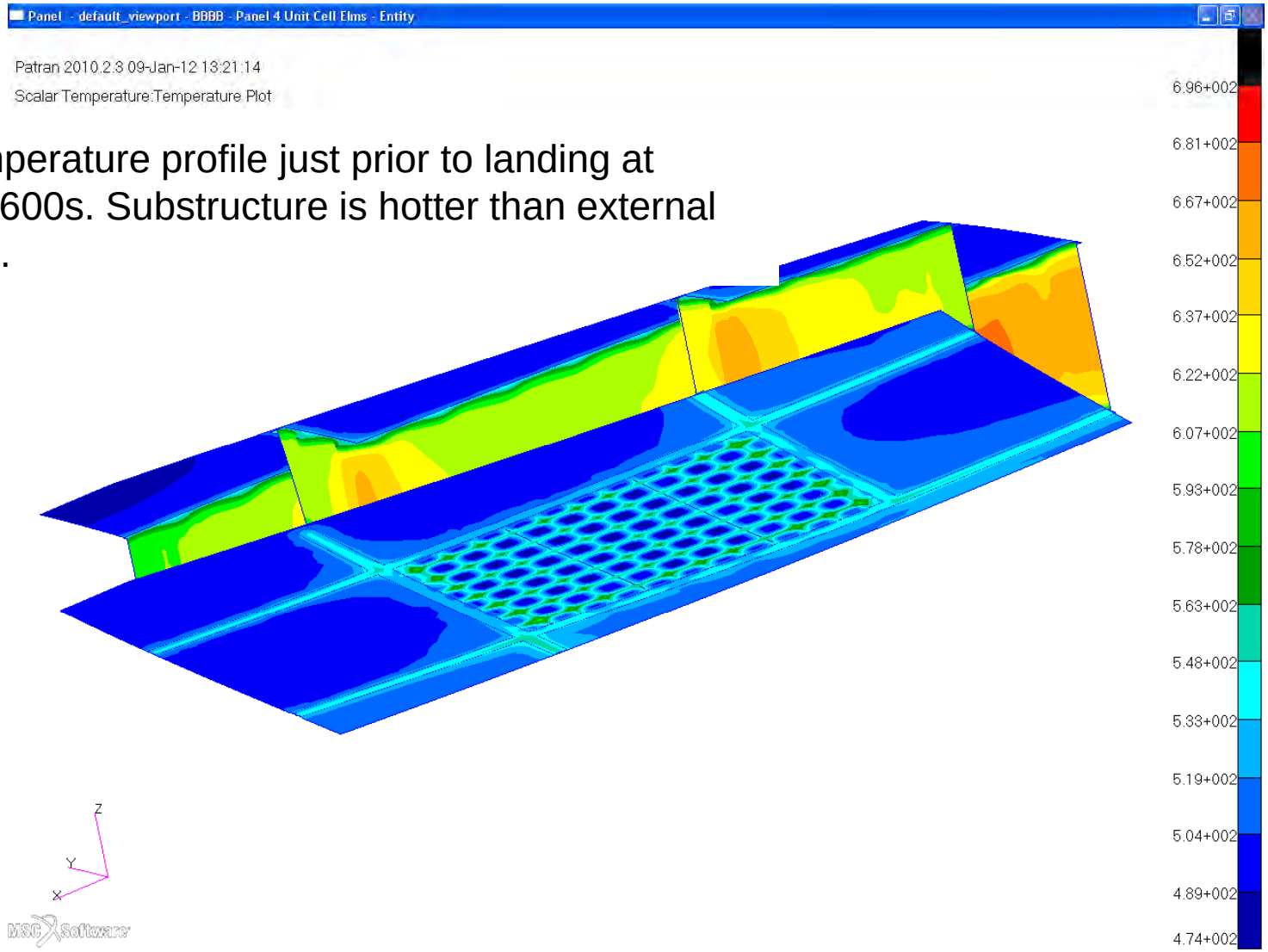

Approved for public release; distribution unlimited.

Temperature Profiles, Unit Cell

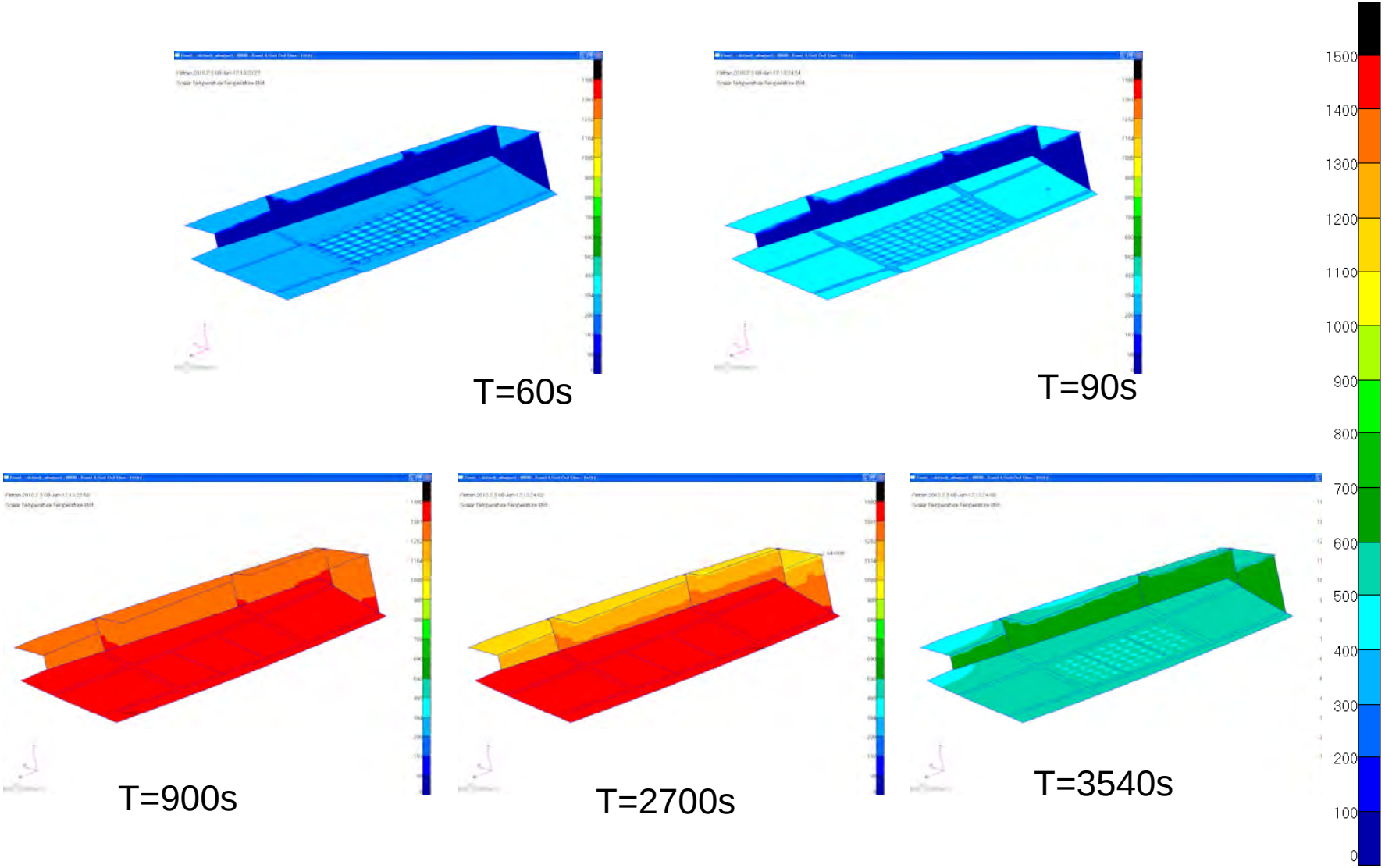

Approved for public release; distribution unlimited.

Temperatures on Panel 1074

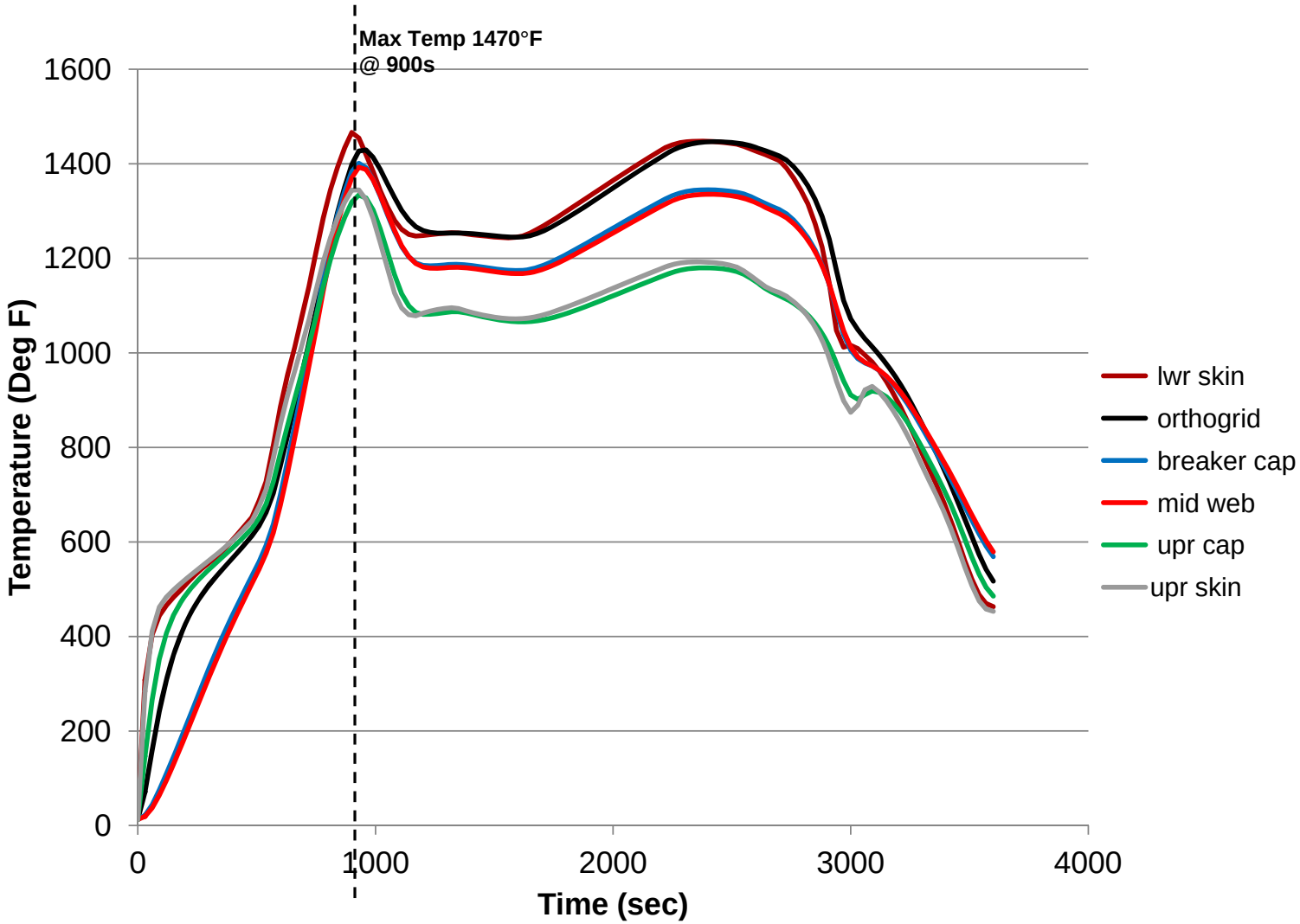

Approved for public release; distribution unlimited.

Panel 4 (1074) Temperature Load Cases

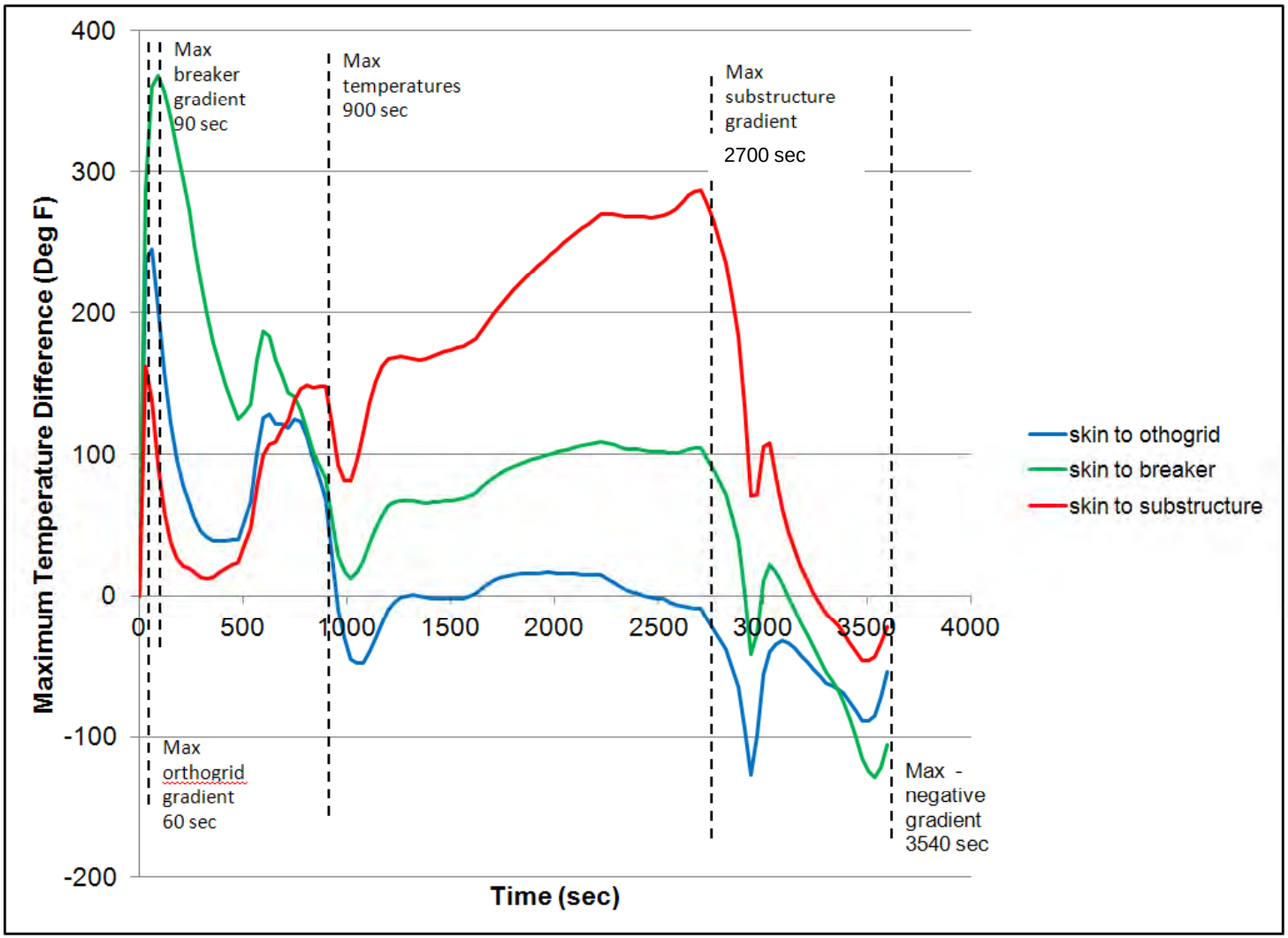

Approved for public release; distribution unlimited.

Inconel 718 Allowables @ 1470° F

MMPDS-05
1 April 2010

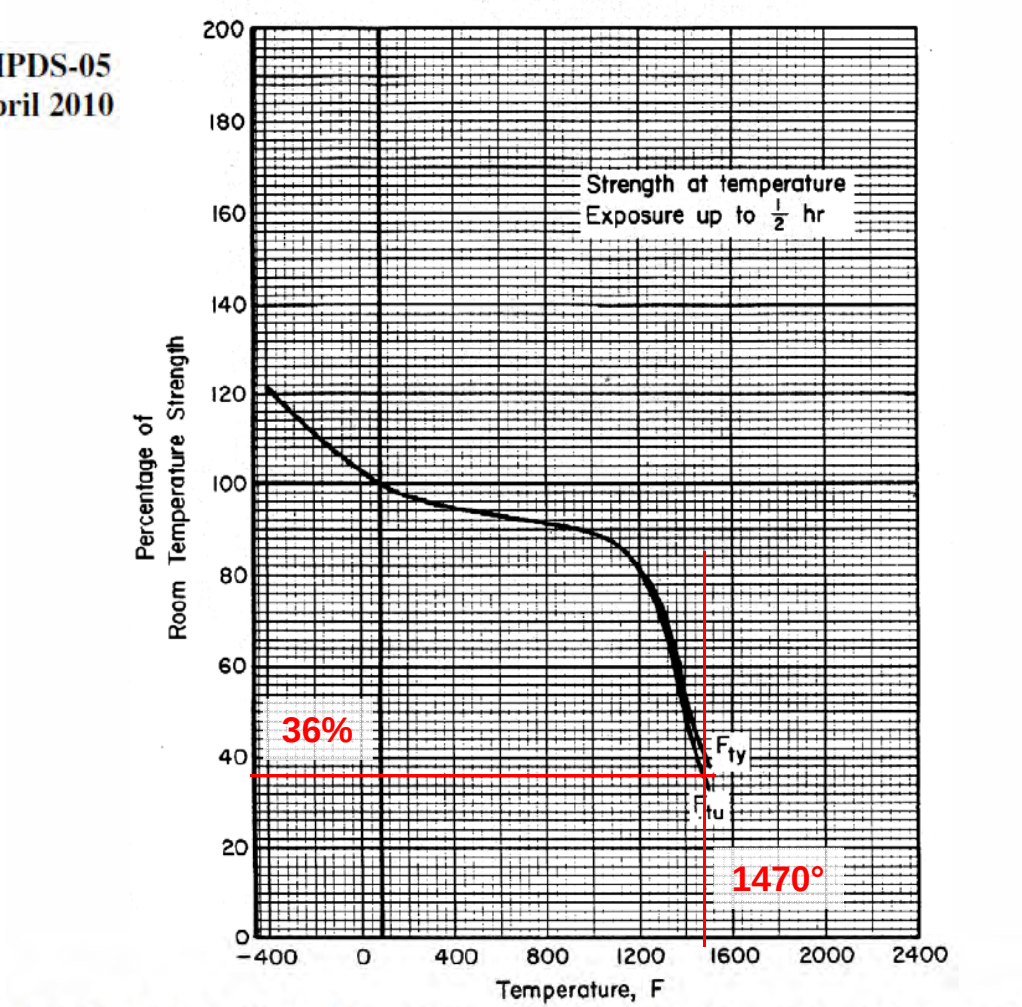

Figure 6.3.5.1.1. Effect of temperature on the tensile ultimate strength (F_{tu}) and tensile yield strength (F_{ty}) of solution-treated and aged Inconel 718.

Allowables @ 1470° F *36% knockdown*	
F_{tu}	**64.8 ksi**
F_{bru}	**111 ksi**

The reduction in material allowables is significant at high temperatures.

Approved for public release; distribution unlimited.

Temperature Profiles Panel 4 (1074)

Approved for public release; distribution unlimited.

Temperature Profiles, Panel, T=60s

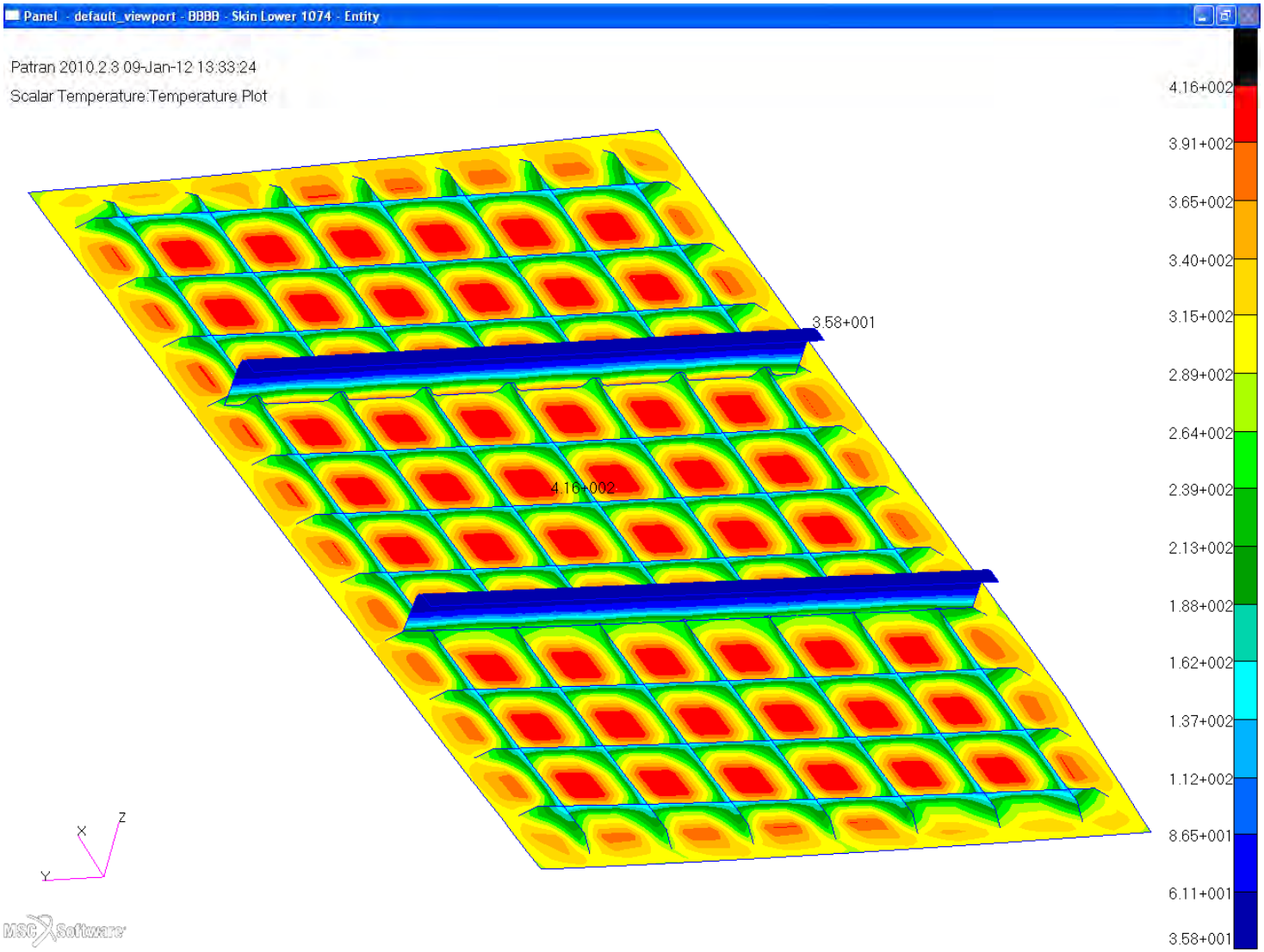

Approved for public release; distribution unlimited.

Temperature Profiles, Panel, T=90s

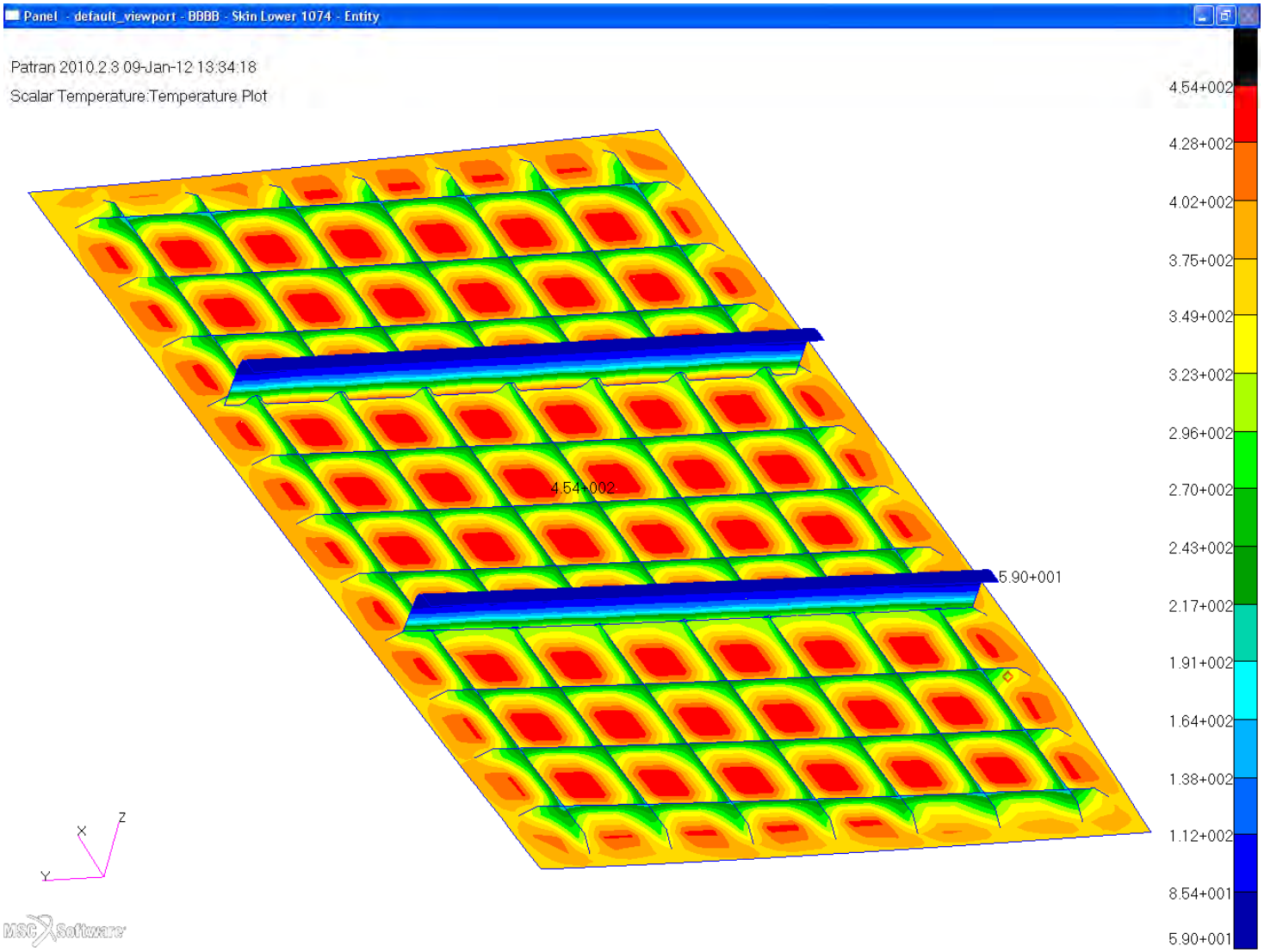

Approved for public release; distribution unlimited.

Temperature Profiles, Panel, T=900s

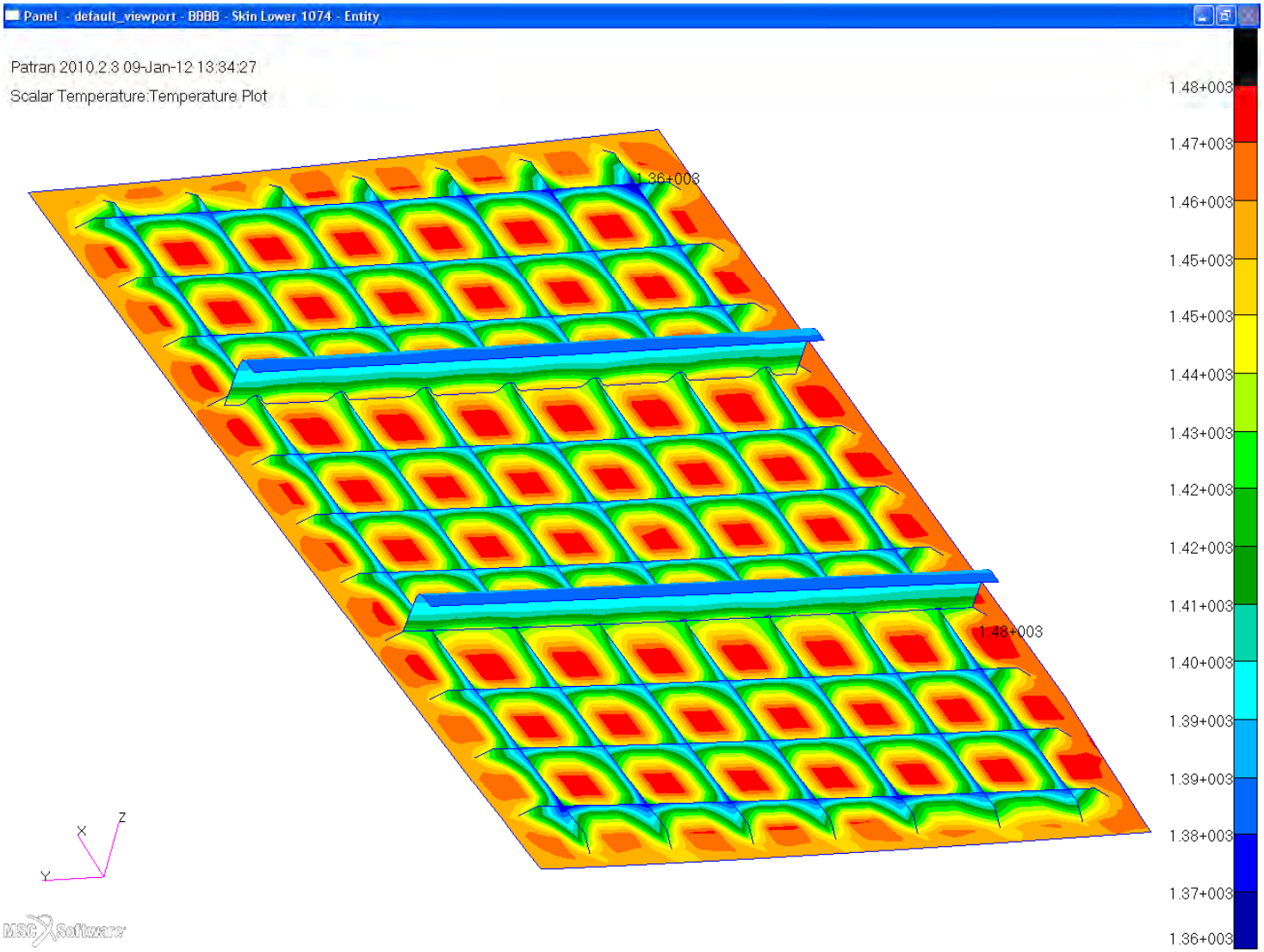

Approved for public release; distribution unlimited.

Temperature Profiles, Panel, T=2700s

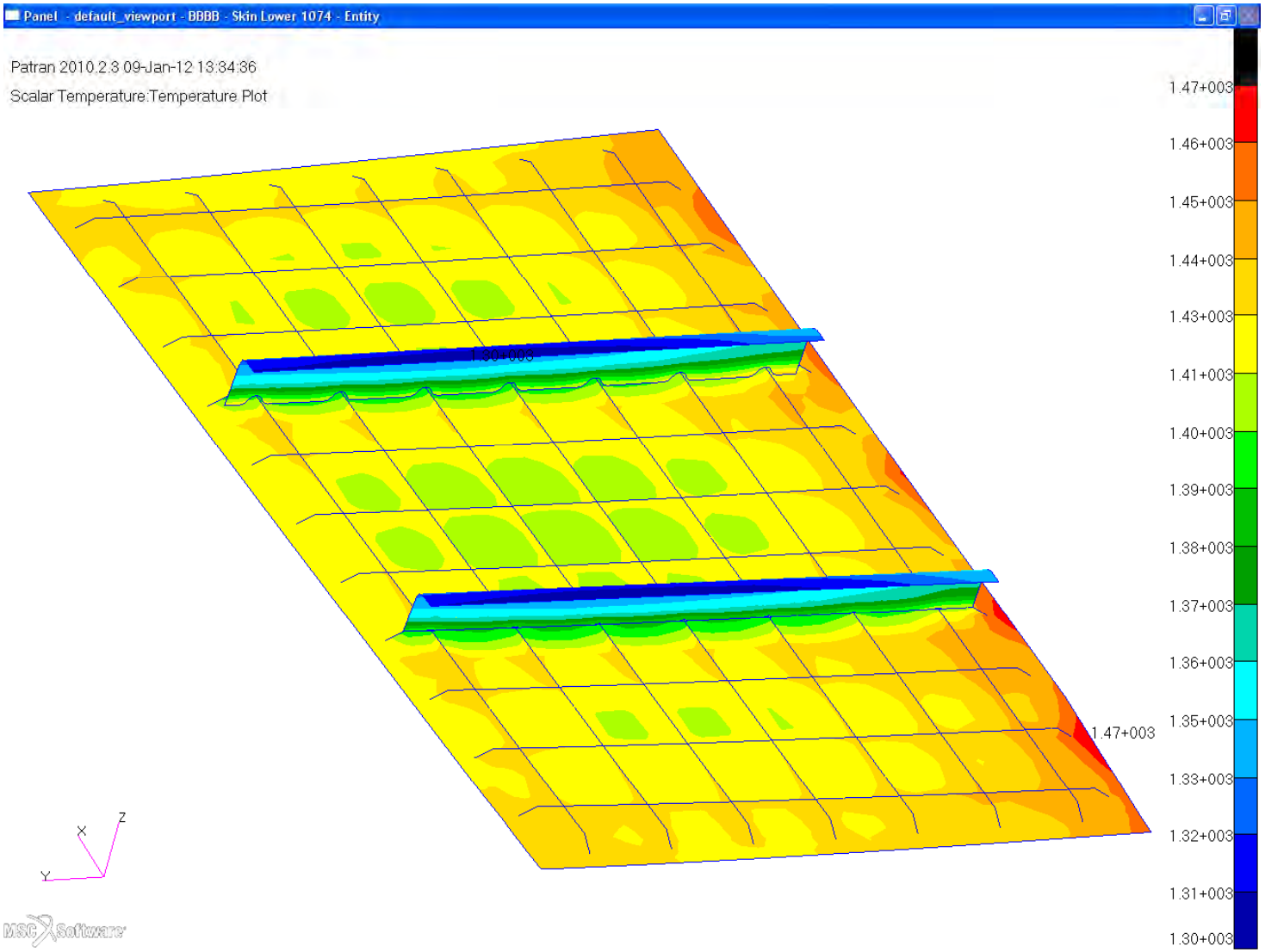

Approved for public release; distribution unlimited.

Temperature Profiles, Panel, T=3540s

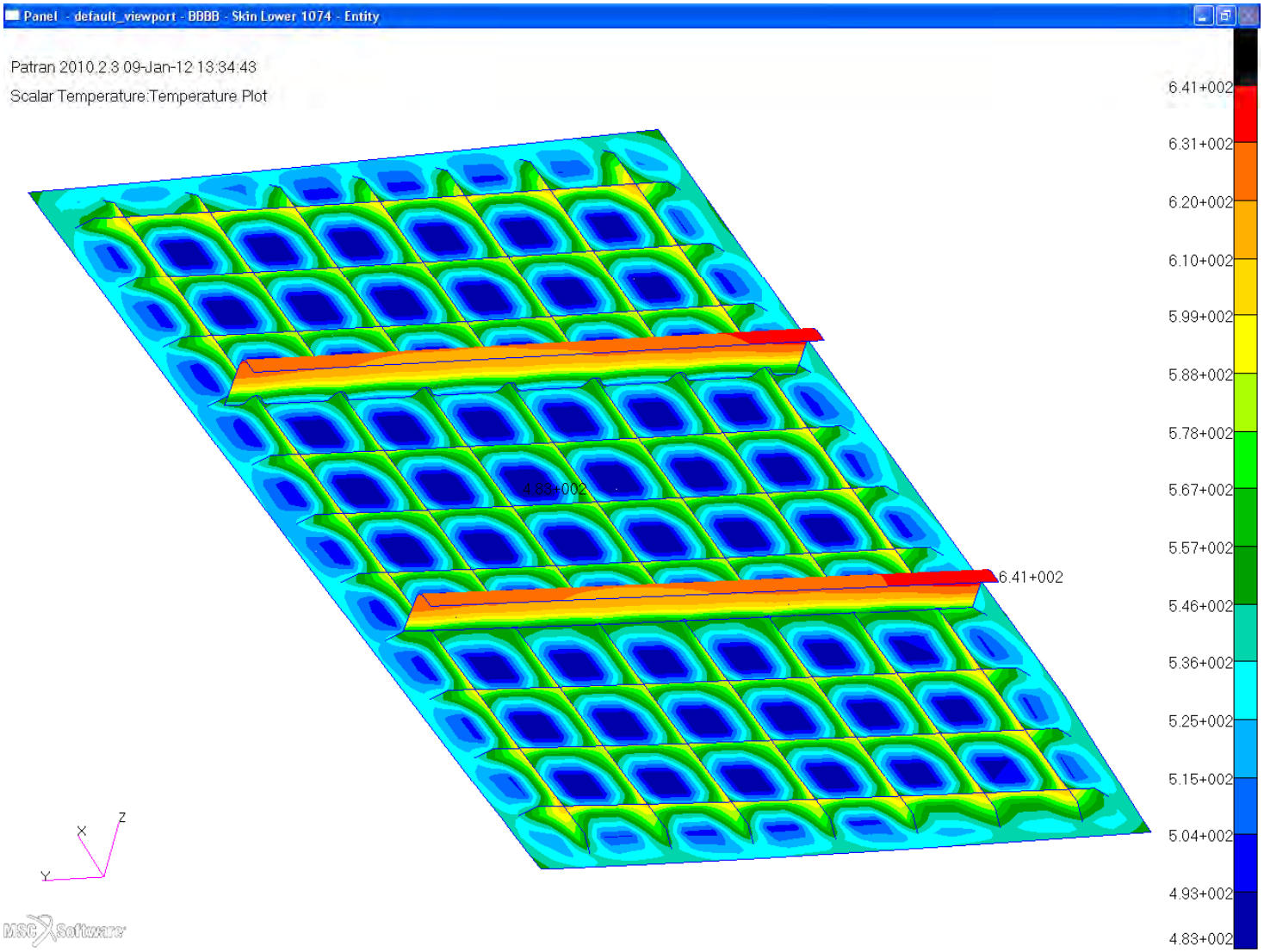

Approved for public release; distribution unlimited.

Temperature Profiles, Panel

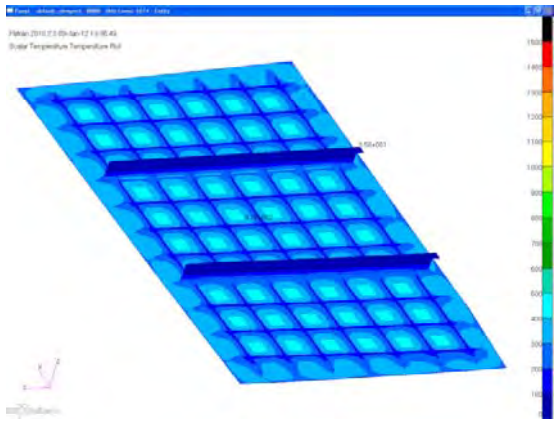

T=60s

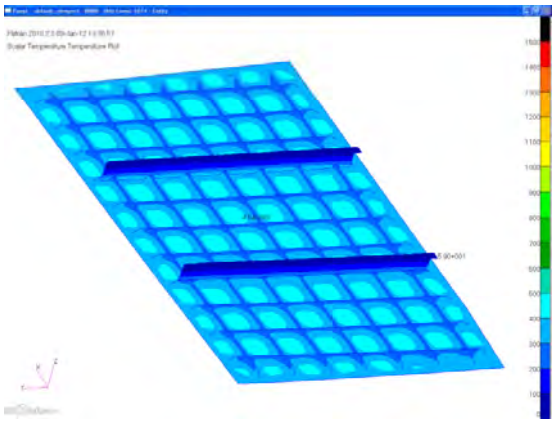

T=90s

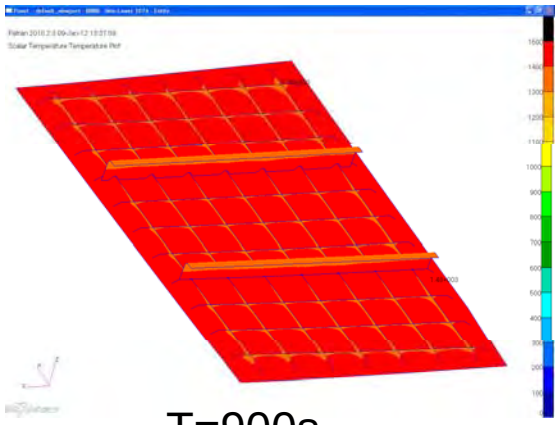

T=900s

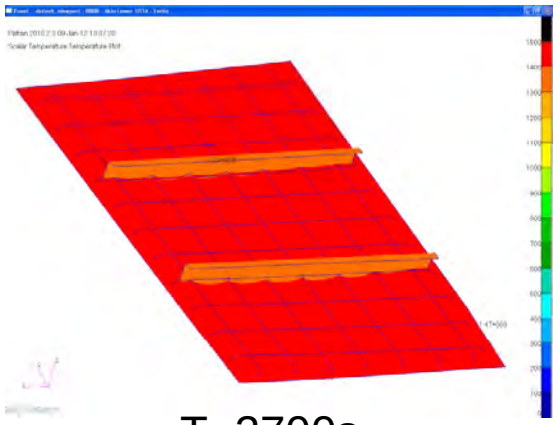

T=2700s

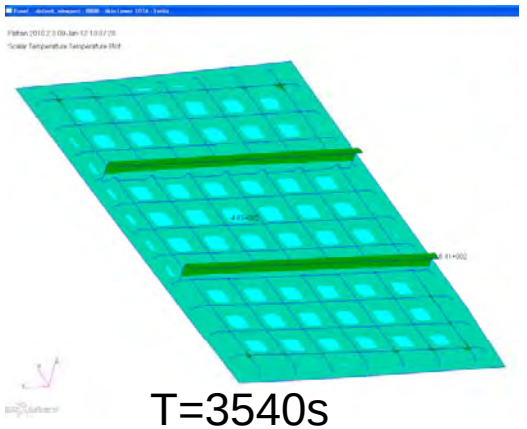

T=3540s

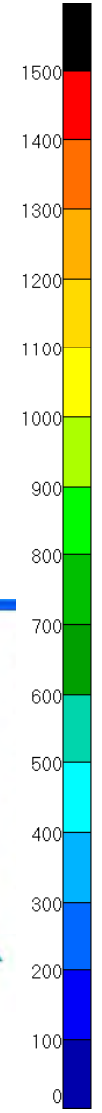

Approved for public release; distribution unlimited.

Displacements Thermal Loading Only Unit Cell

Approved for public release; distribution unlimited.

Displacements, Unit Cell, T=60s

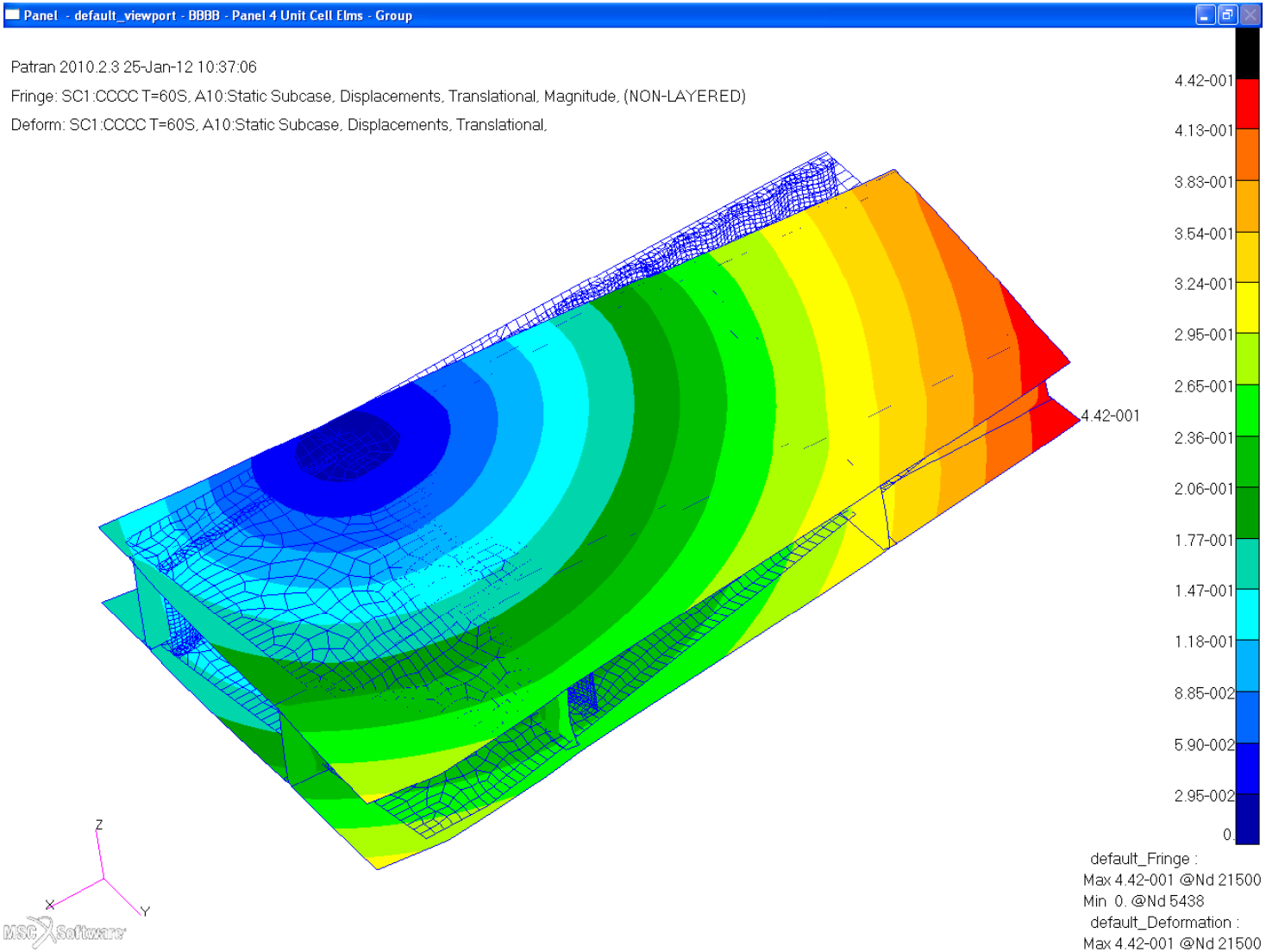

Approved for public release; distribution unlimited.

Displacements, Unit Cell, T=90s

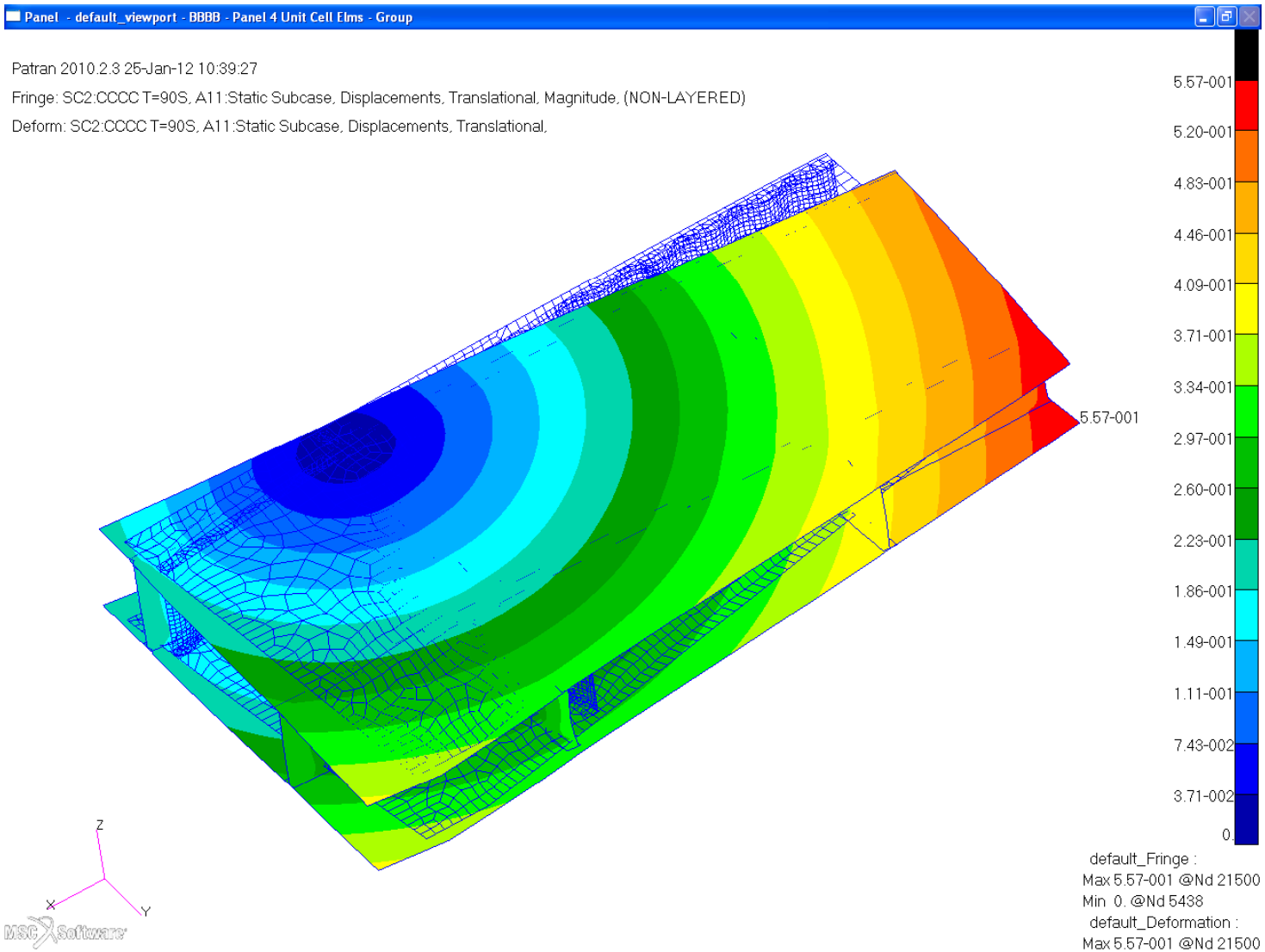

Approved for public release; distribution unlimited.

Displacements, Unit Cell, T=900s

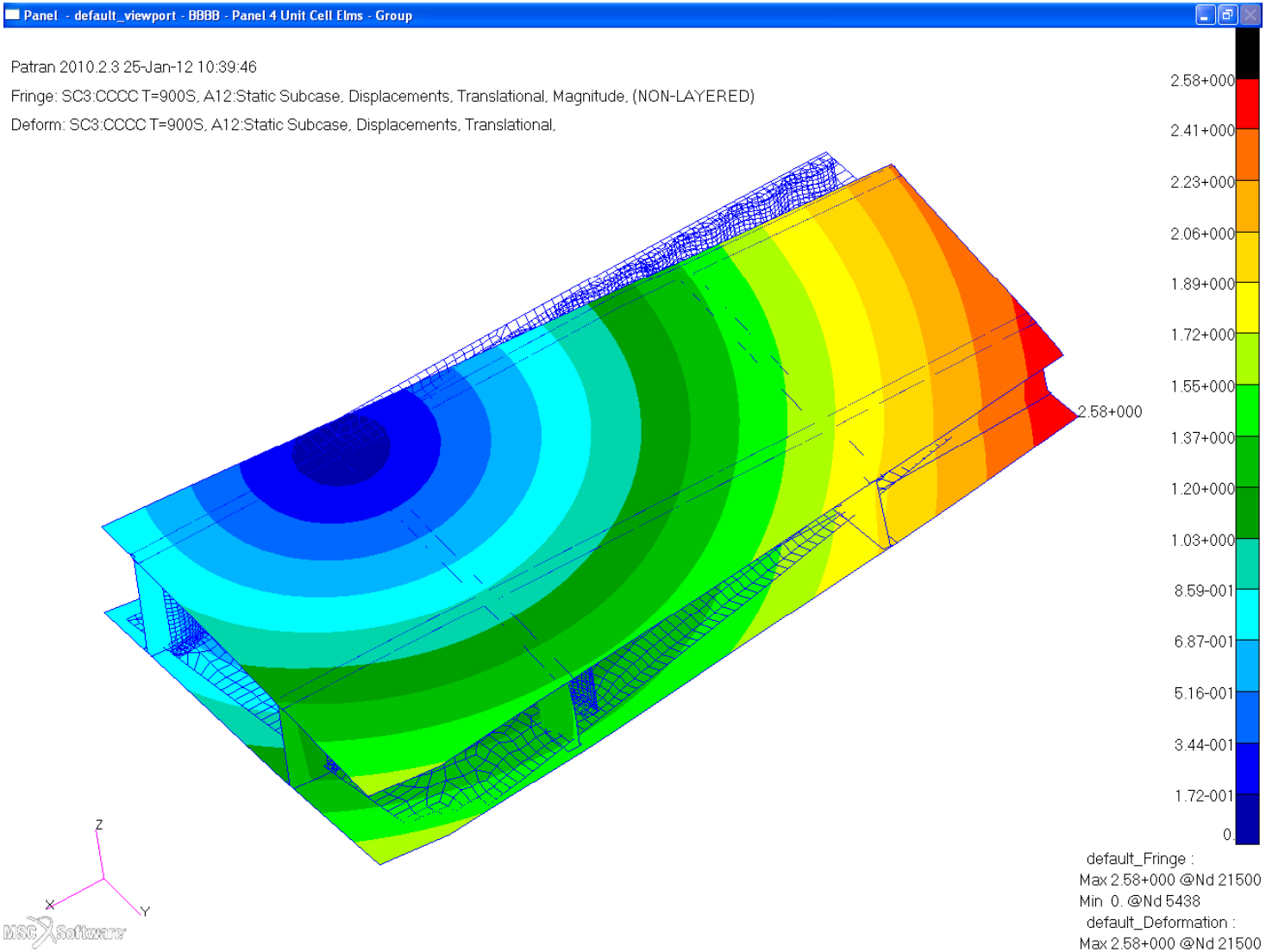

Approved for public release; distribution unlimited.

Displacements, Unit Cell, T=2700s

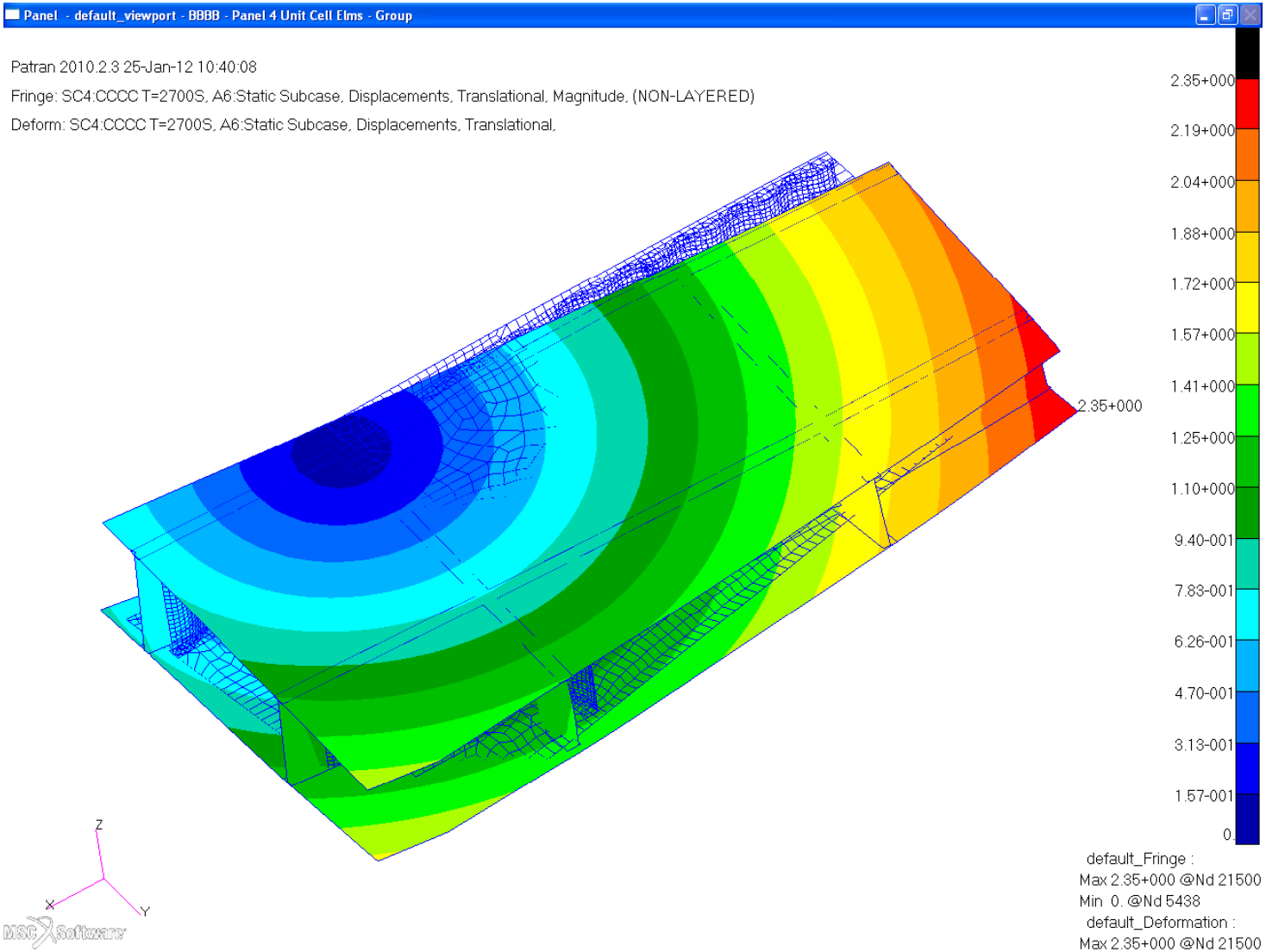

Approved for public release; distribution unlimited.

Displacements, Unit Cell, T=2700s, Mod Spc

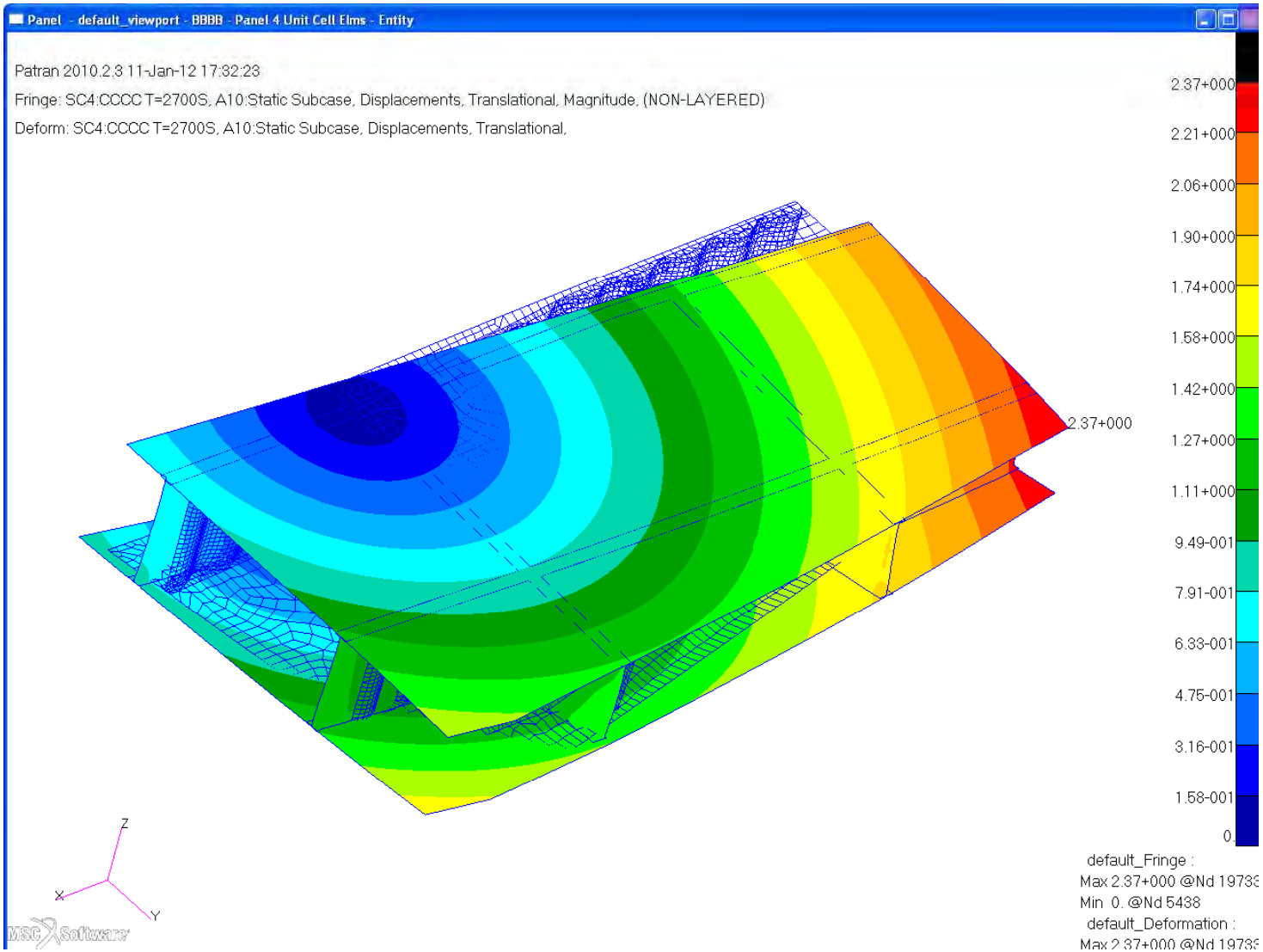

Approved for public release; distribution unlimited.

Displacements, Unit Cell, T=3540s

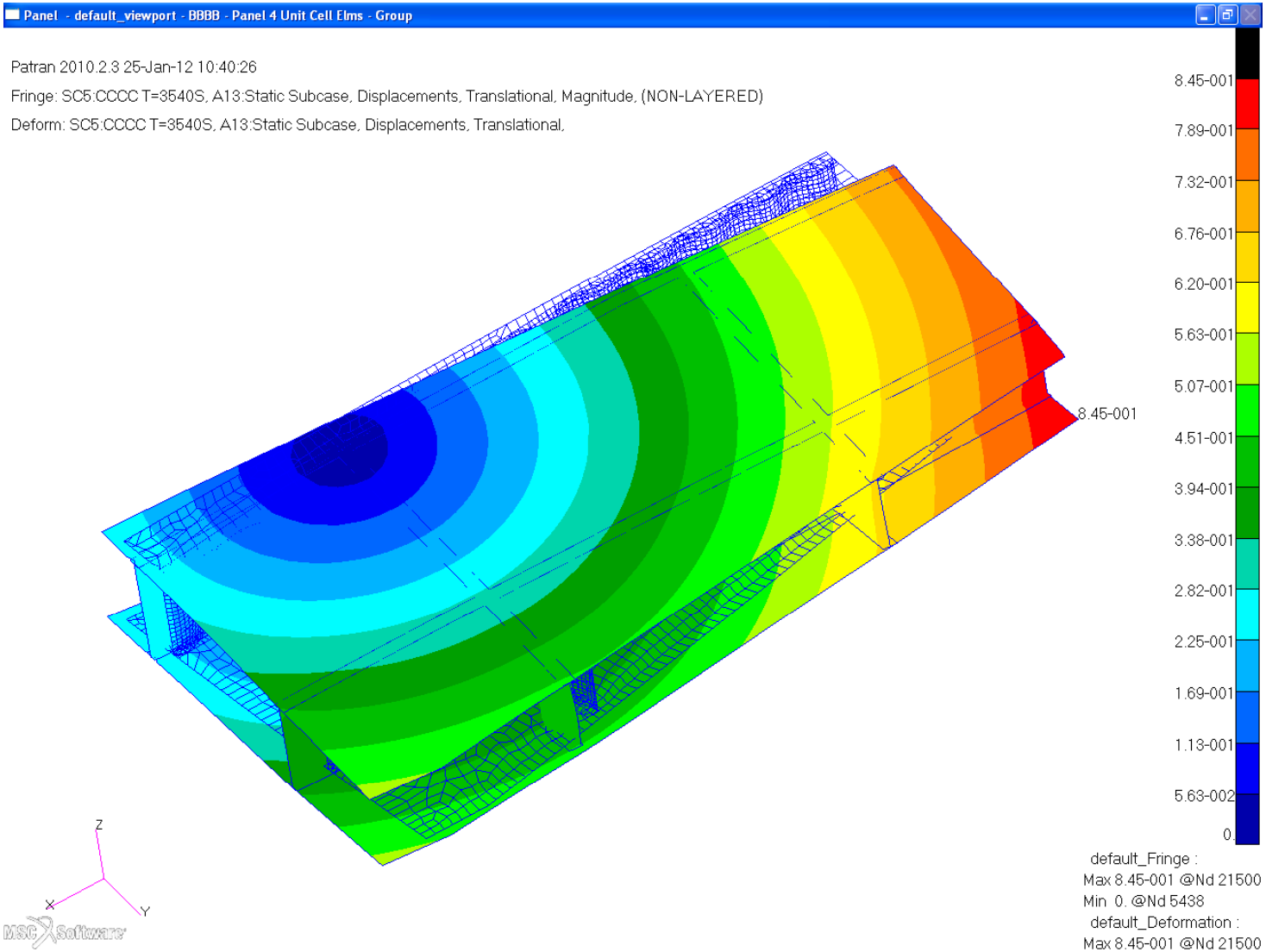

Approved for public release; distribution unlimited.

Displacements, Unit Cell

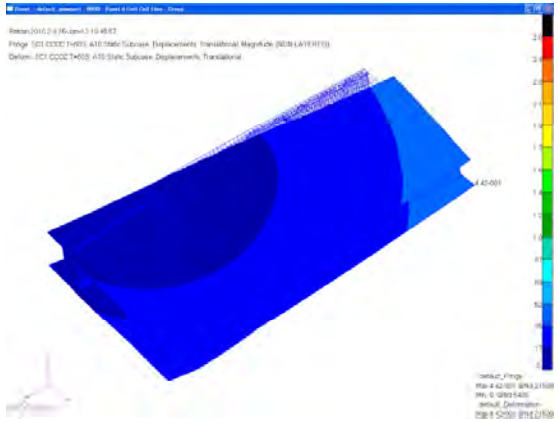

T=60s

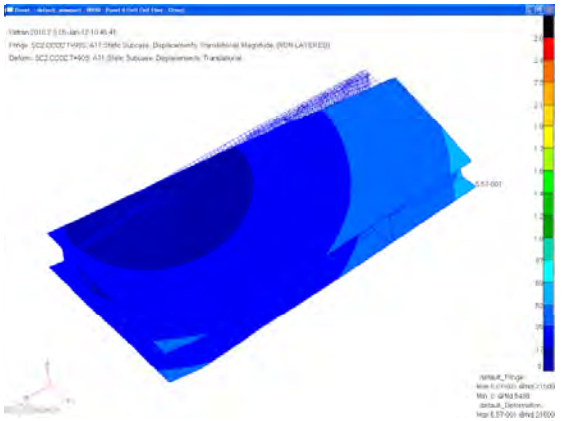

T=90s

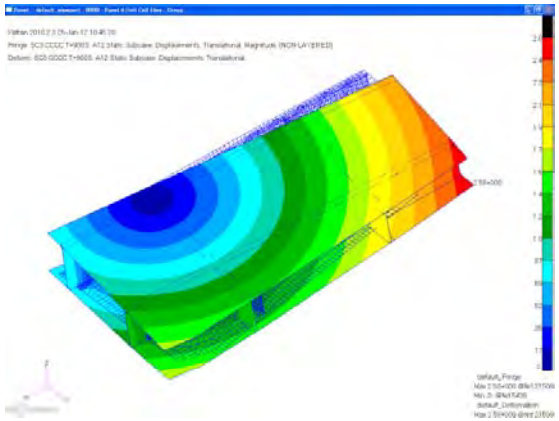

T=900s

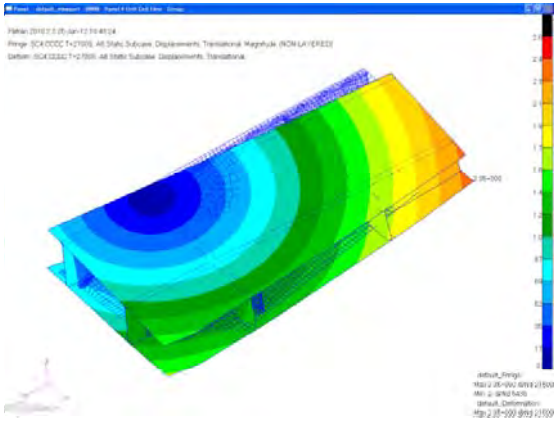

T=2700s

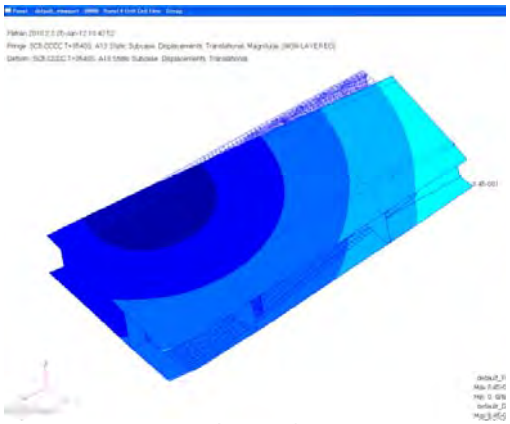

T=3540s

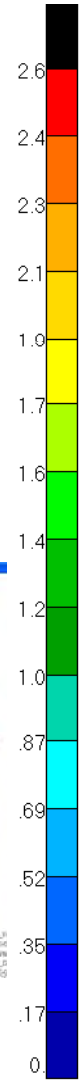

Approved for public release; distribution unlimited.

Z-Displacements from Unit Cell Analysis Thermal Loading Only Panel 4 (1074)

Approved for public release; distribution unlimited.

Z-Displacements, Unit Cell Analysis, T=60s

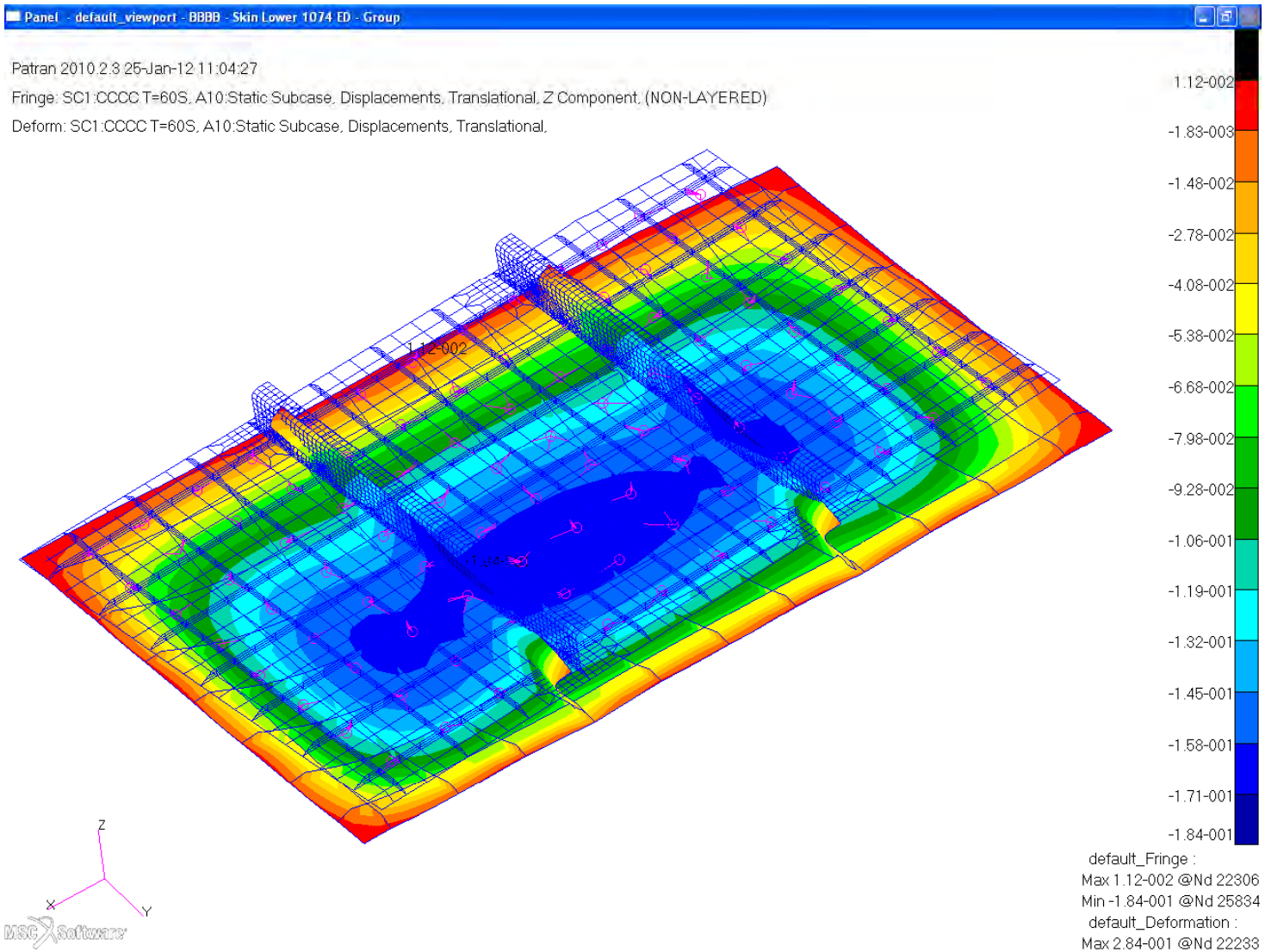

Approved for public release; distribution unlimited.

Z-Displacements, Unit Cell Analysis, T=90s

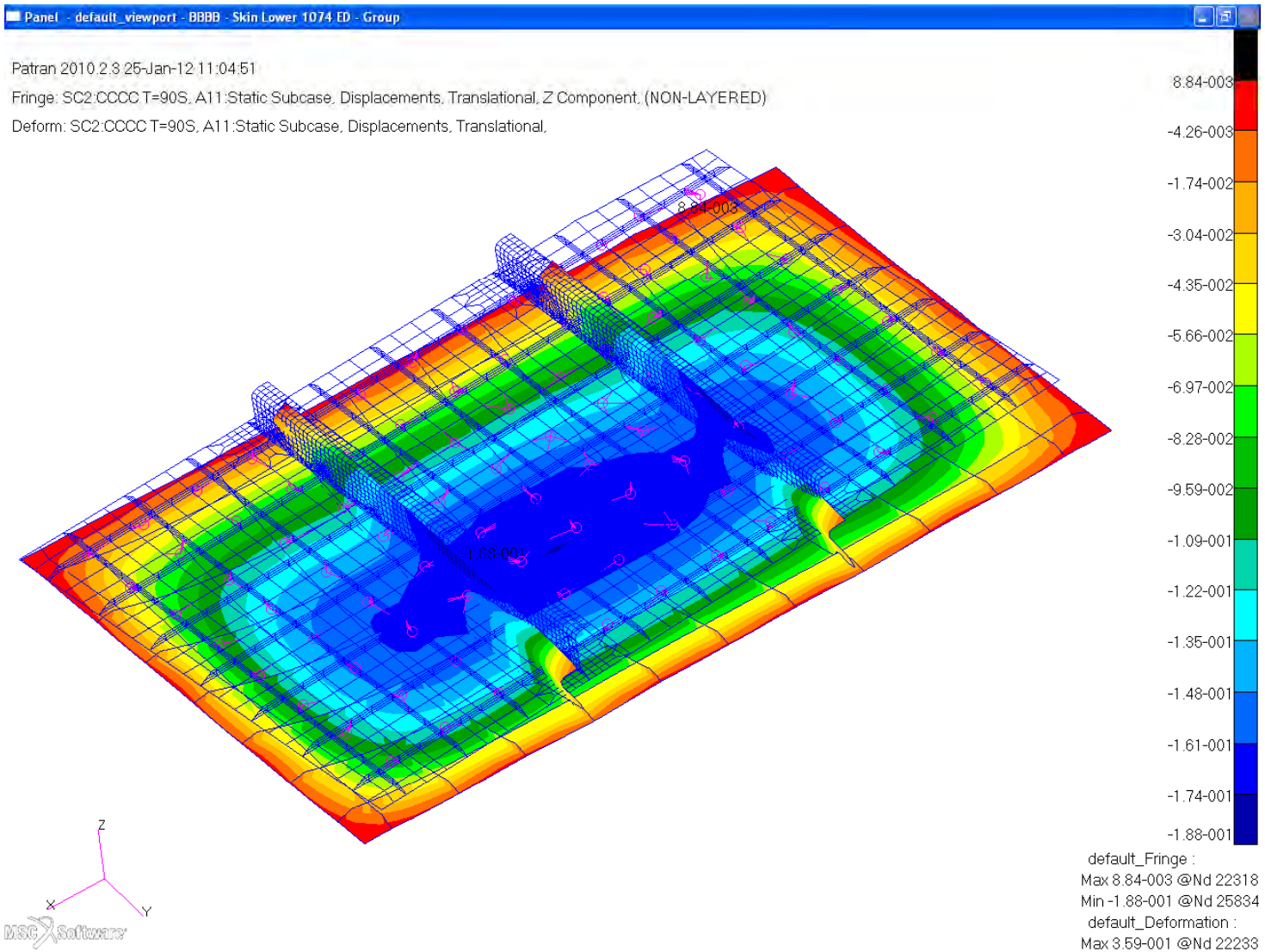

Approved for public release; distribution unlimited.

Z-Displacements, Unit Cell Analysis, T=900s

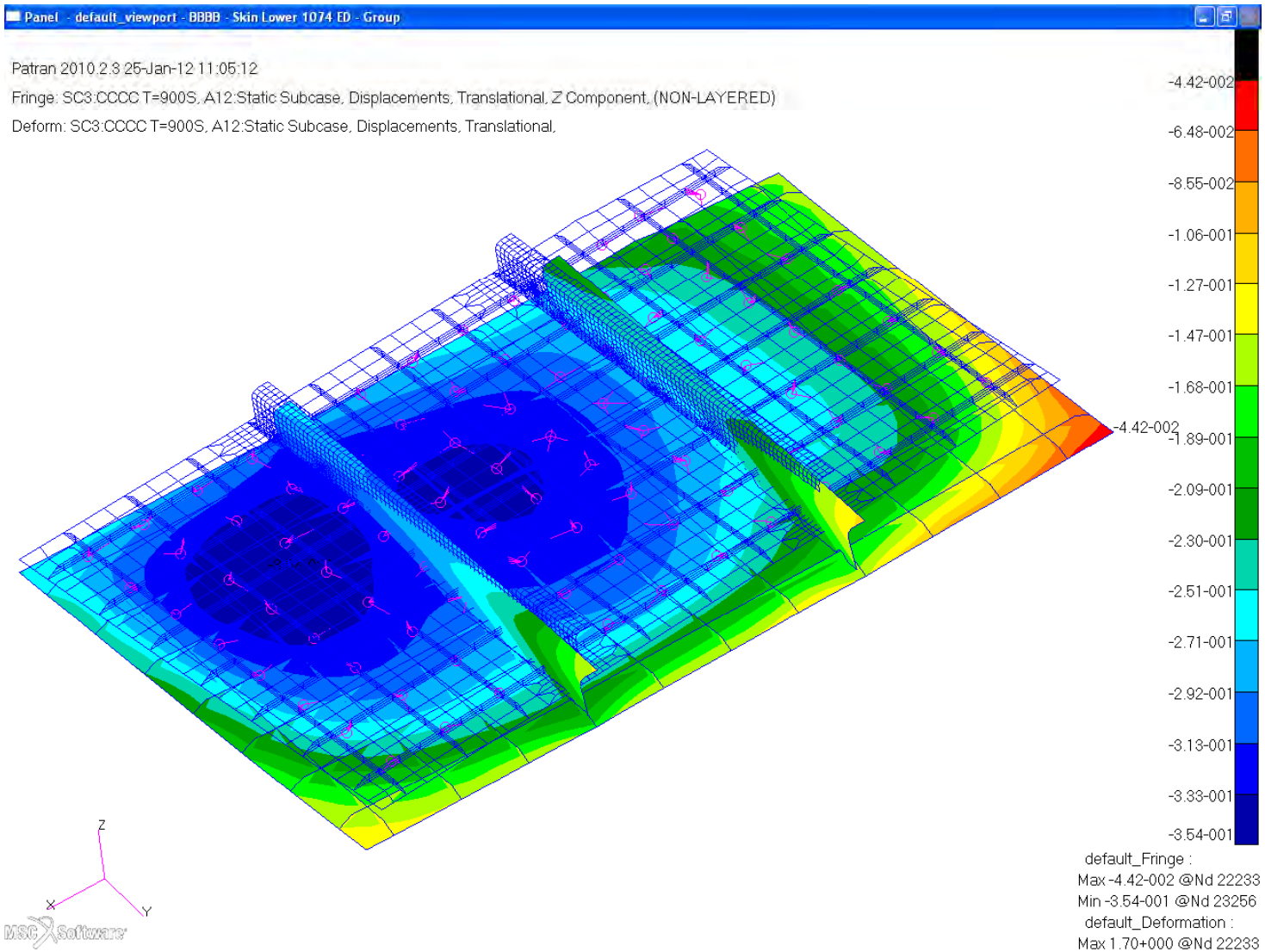

Approved for public release; distribution unlimited.

Z-Displacements, Unit Cell Analysis, T=2700s

Maximum flow-wise deflection:
0.372” – 0.048” = 0.324”`

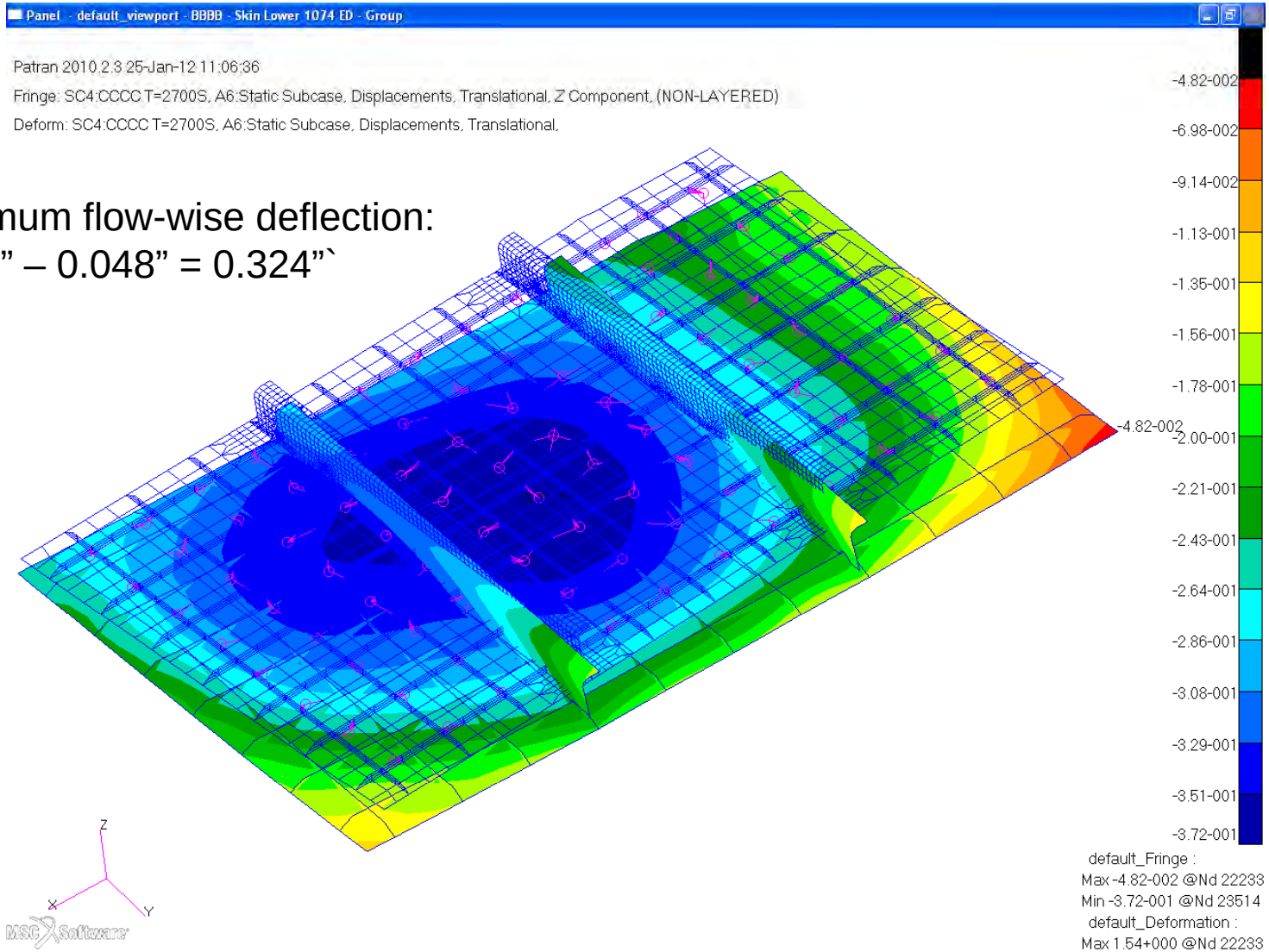

Approved for public release; distribution unlimited.

Z-Displacements, Unit Cell Analysis, T=3540s

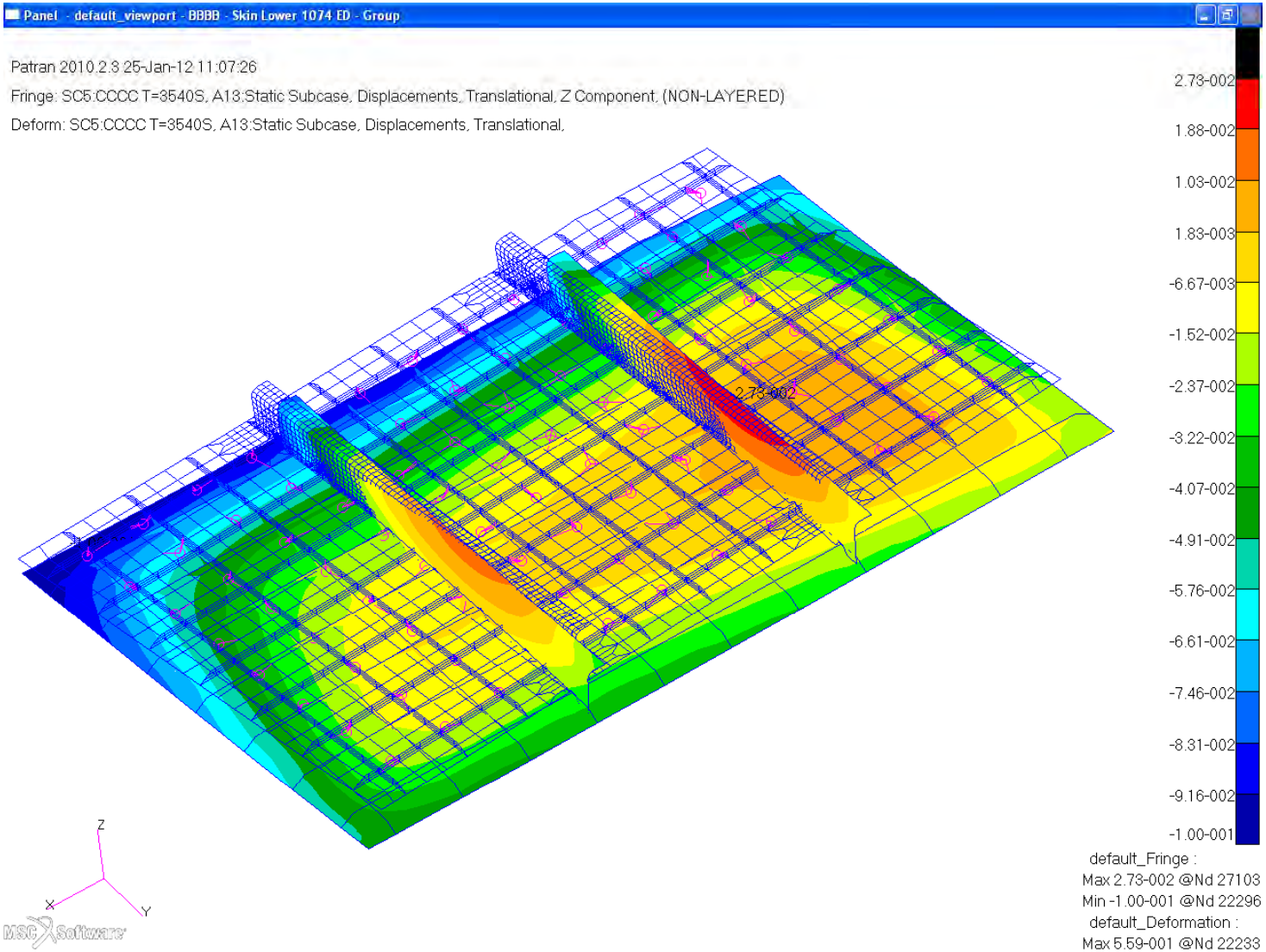

Approved for public release; distribution unlimited.

Z-Displacements, Unit Cell Analysis

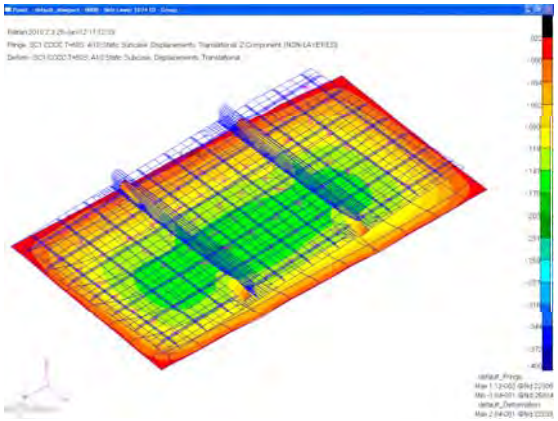

T=60s

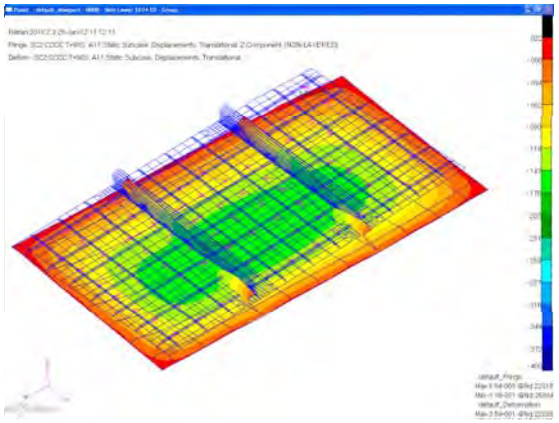

T=90s

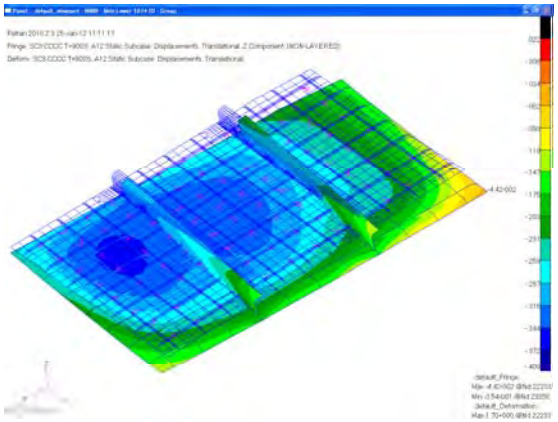

T=900s

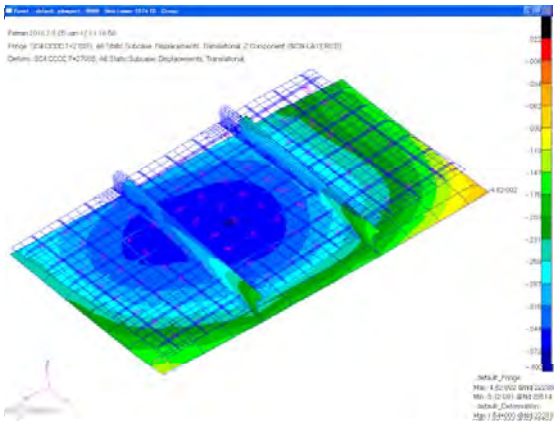

T=2700s

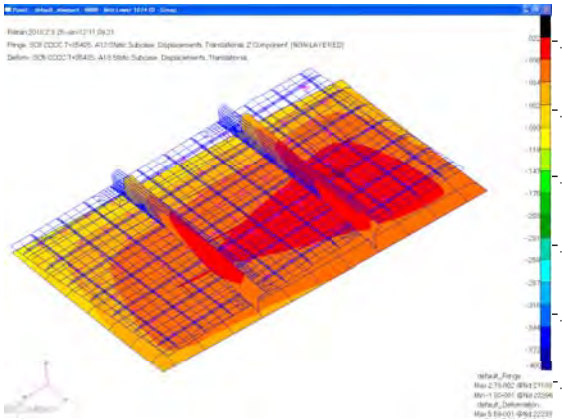

T=3540s

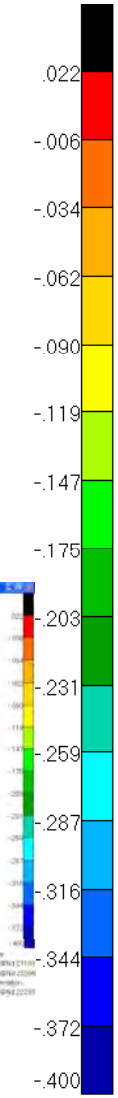

Approved for public release; distribution unlimited.

Von Mises Stress Thermal Loading Only Unit Cell

Approved for public release; distribution unlimited.

Von Mises Stress, Unit Cell, T=60s

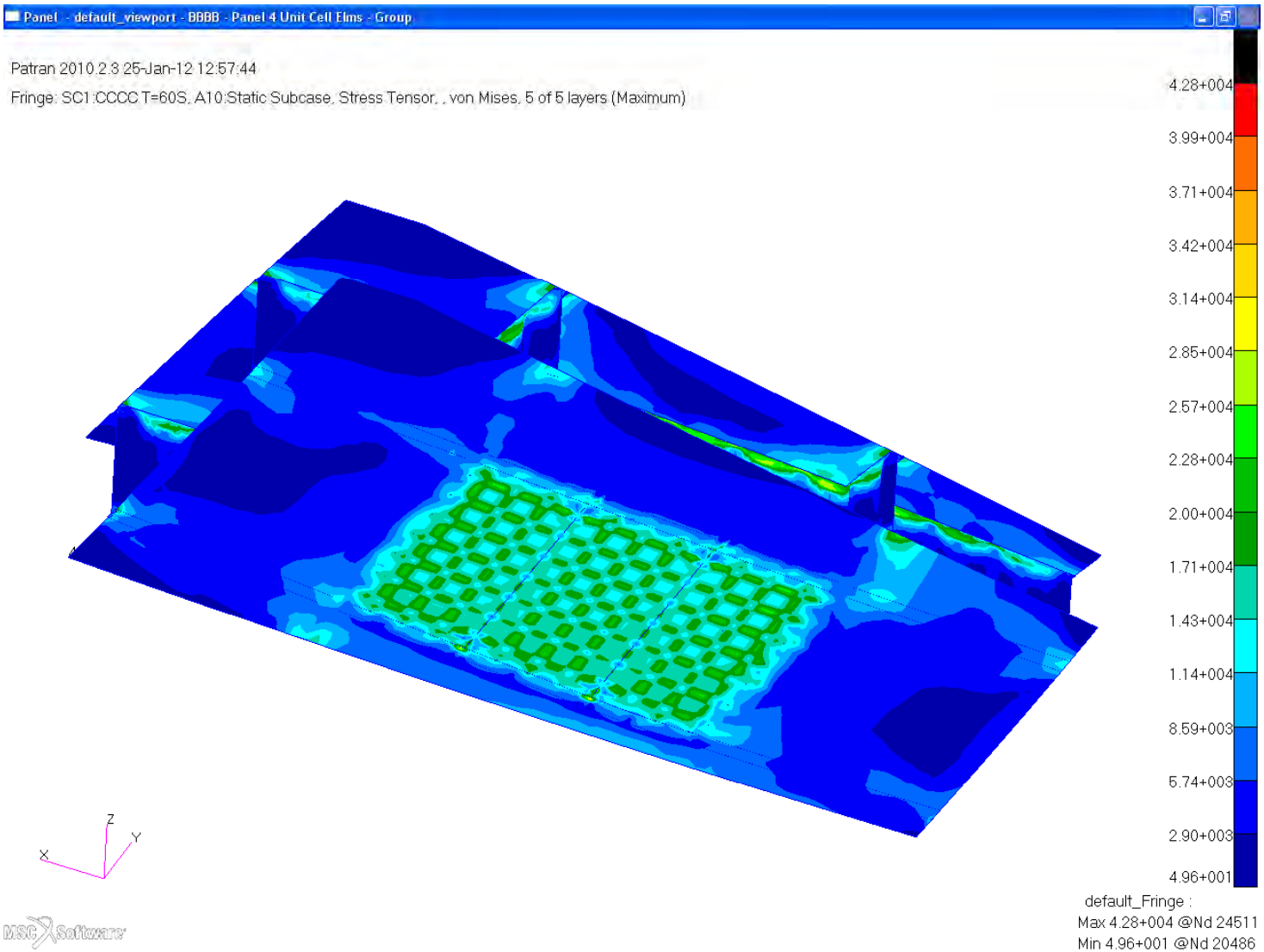

Approved for public release; distribution unlimited.

Von Mises Stress, Unit Cell, T=90s

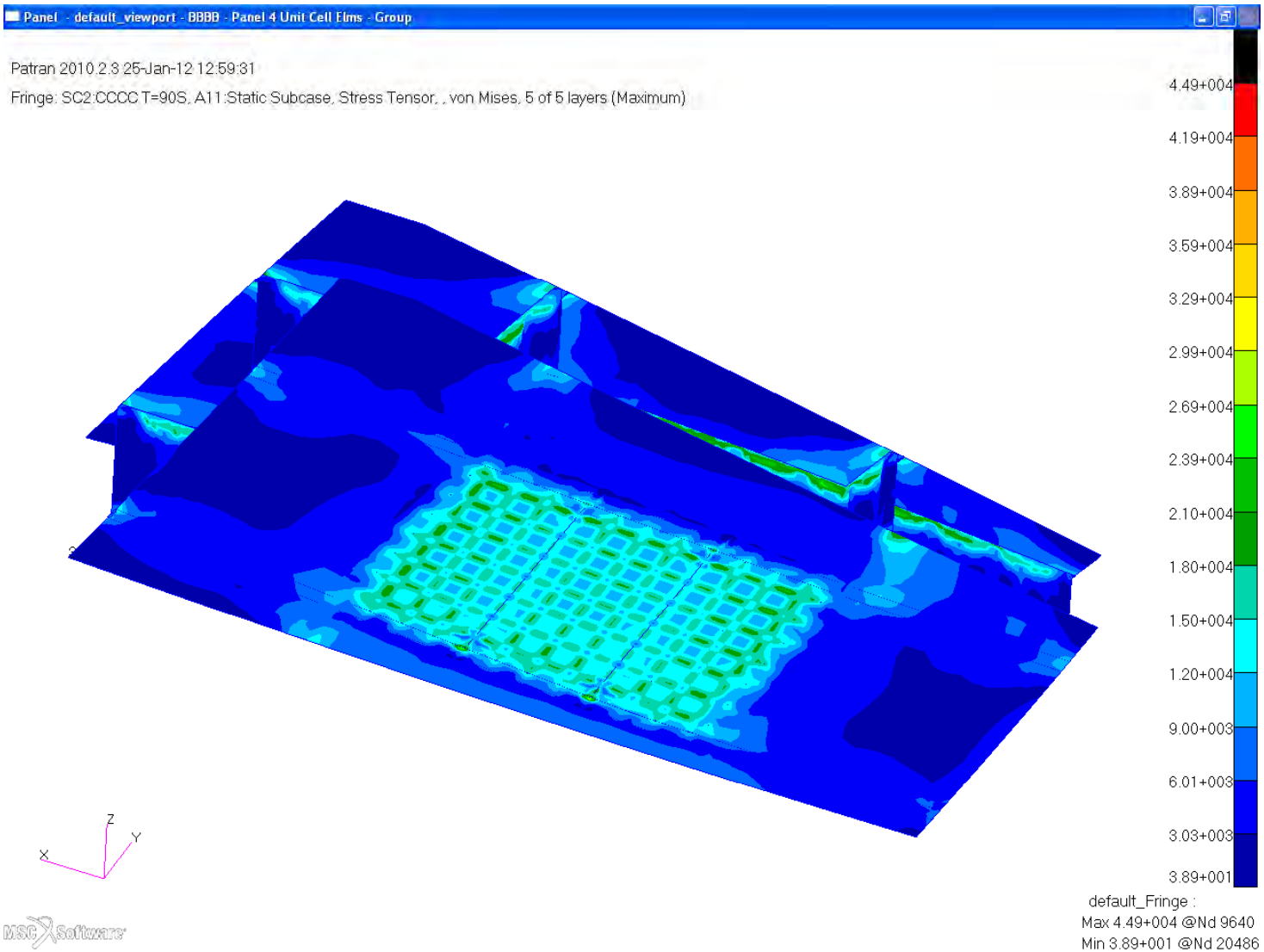

Approved for public release; distribution unlimited.

Von Mises Stress, Unit Cell, T=900s

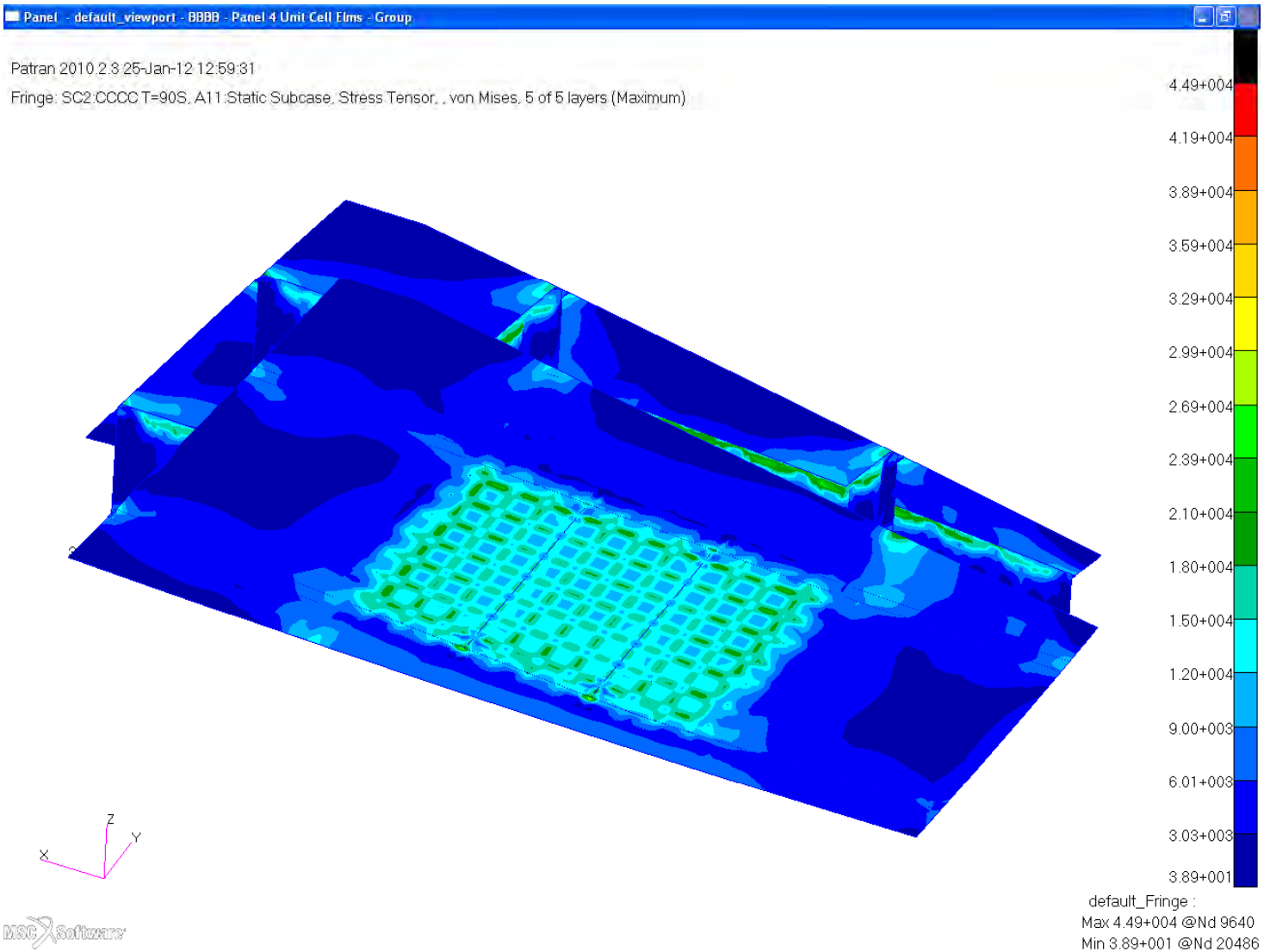

Approved for public release; distribution unlimited.

Von Mises Stress, Unit Cell, T=2700s

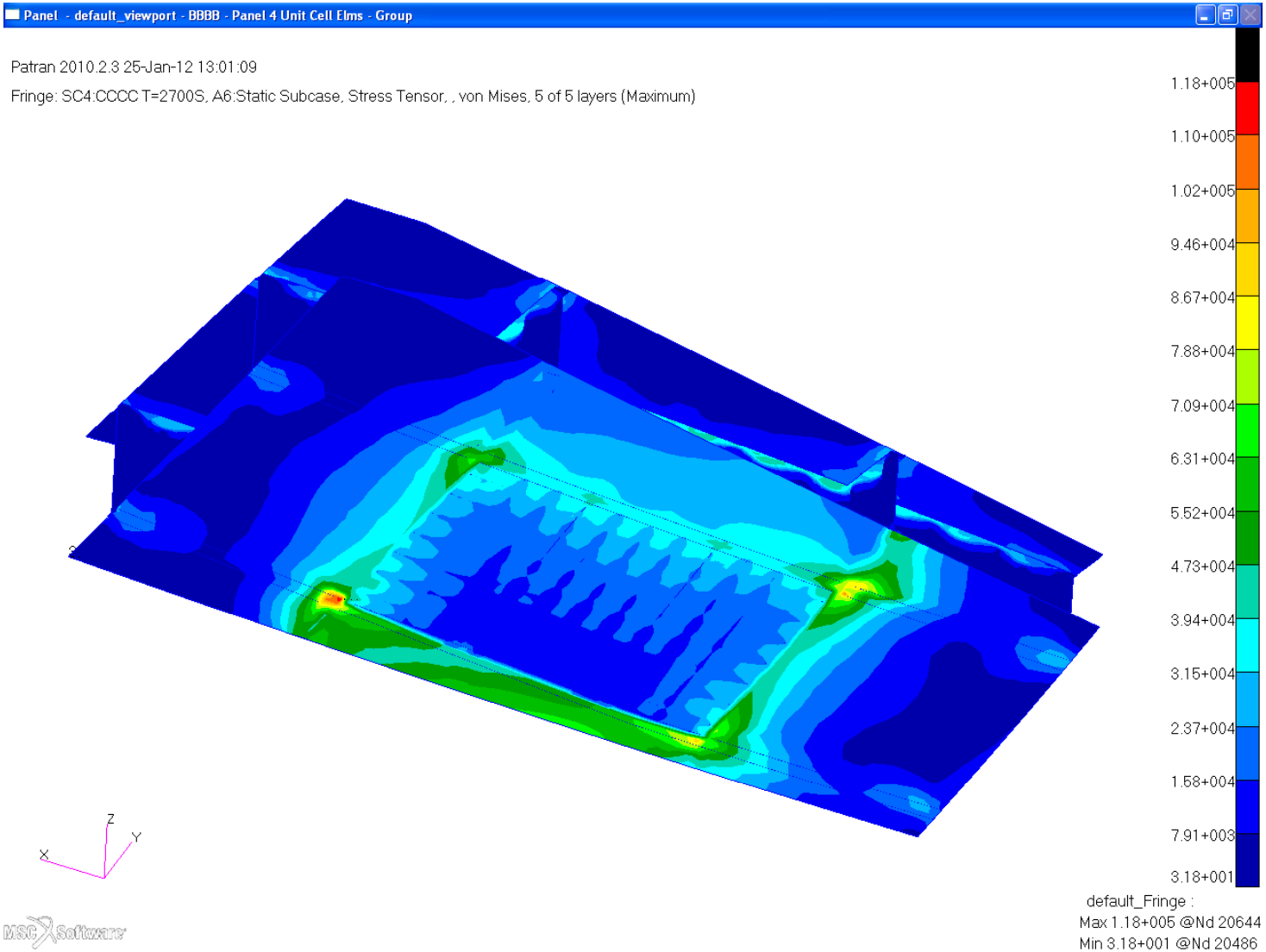

Approved for public release; distribution unlimited.

Von Mises Stress, Unit Cell, T=3540s

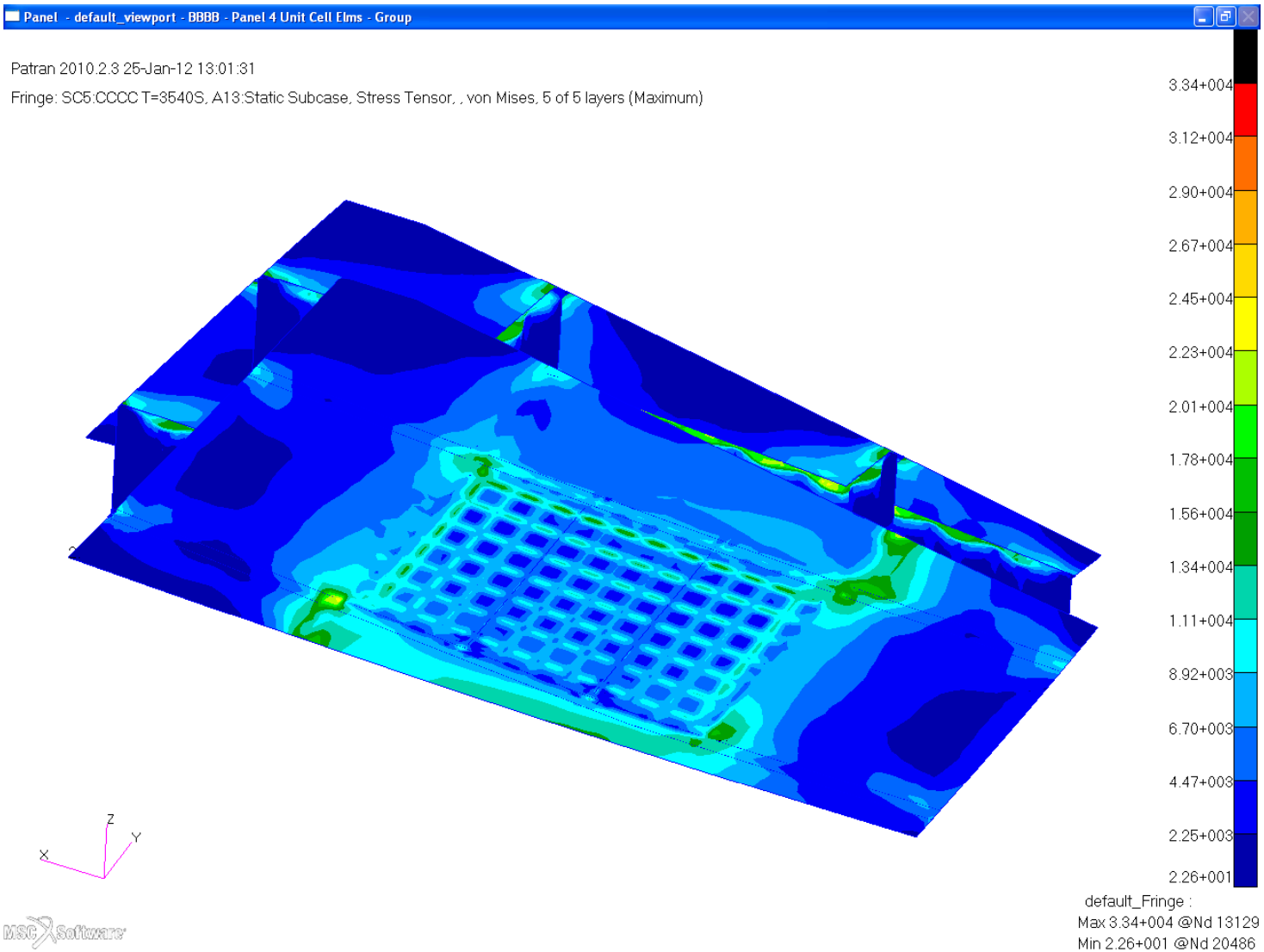

Approved for public release; distribution unlimited.

Von Mises Stress, Unit Cell

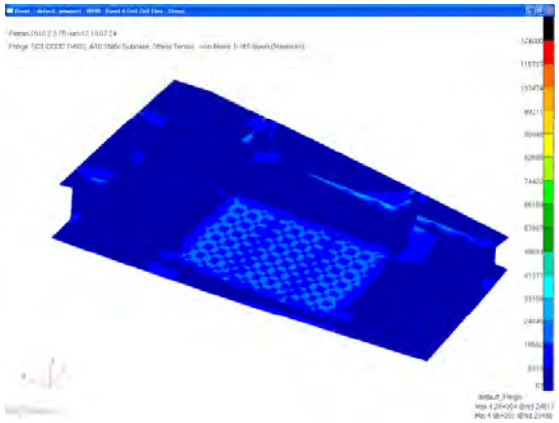

T=60s

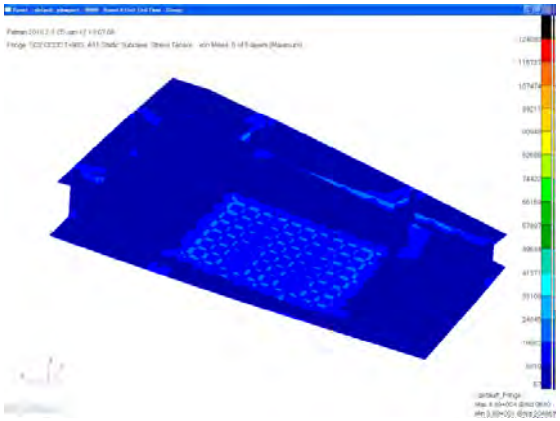

T=90s

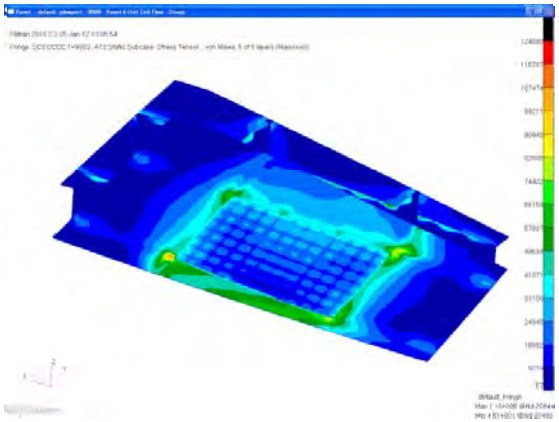

T=900s

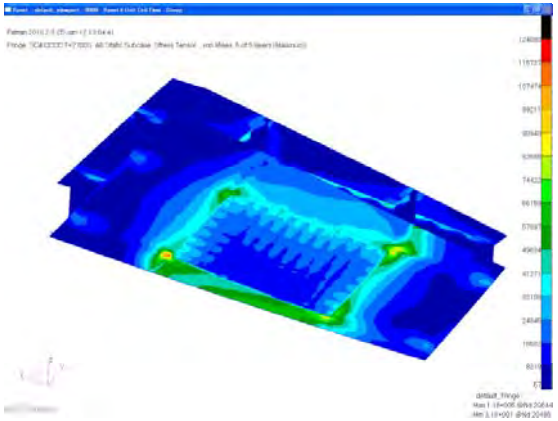

T=2700s

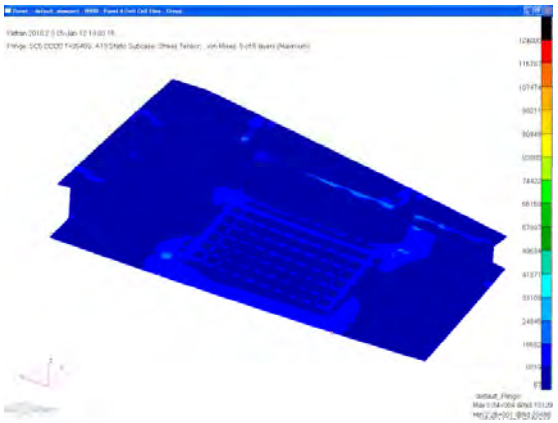

T=3540s

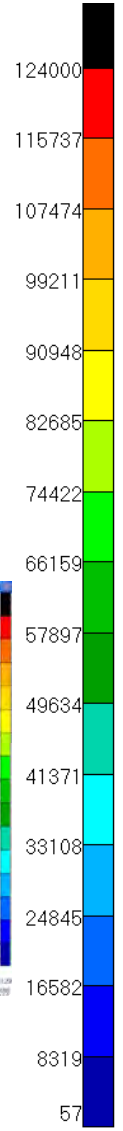

Approved for public release; distribution unlimited.

Von Mises Stress from Unit Cell Analysis Thermal Loading Only Panel 4 (1074)

Approved for public release; distribution unlimited.

Von Mises Stress, Unit Cell Analysis, T=60s

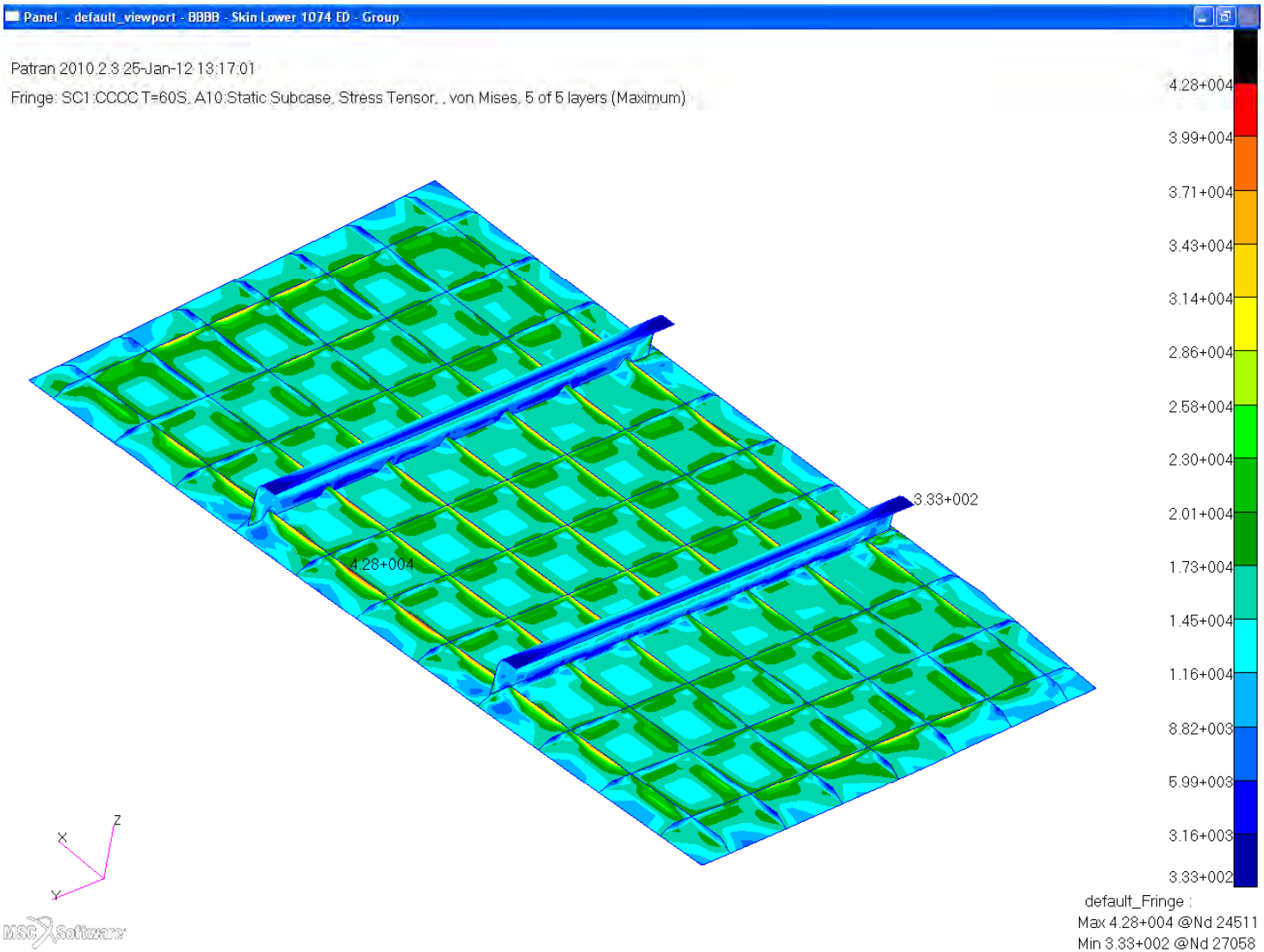

Approved for public release; distribution unlimited.

Von Mises Stress, Unit Cell Analysis, T=90s

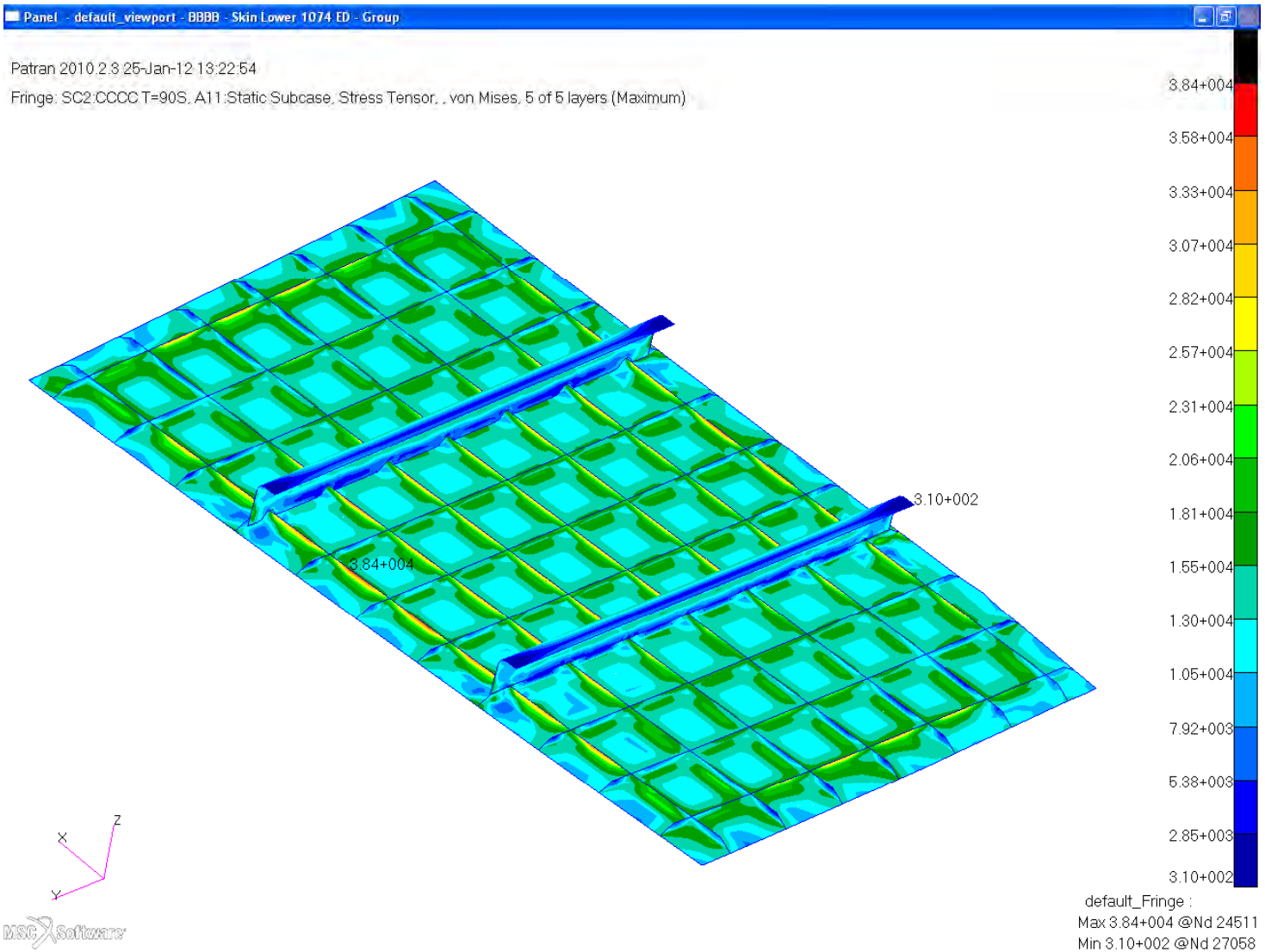

Approved for public release; distribution unlimited.

Von Mises Stress, Unit Cell Analysis, T=900s

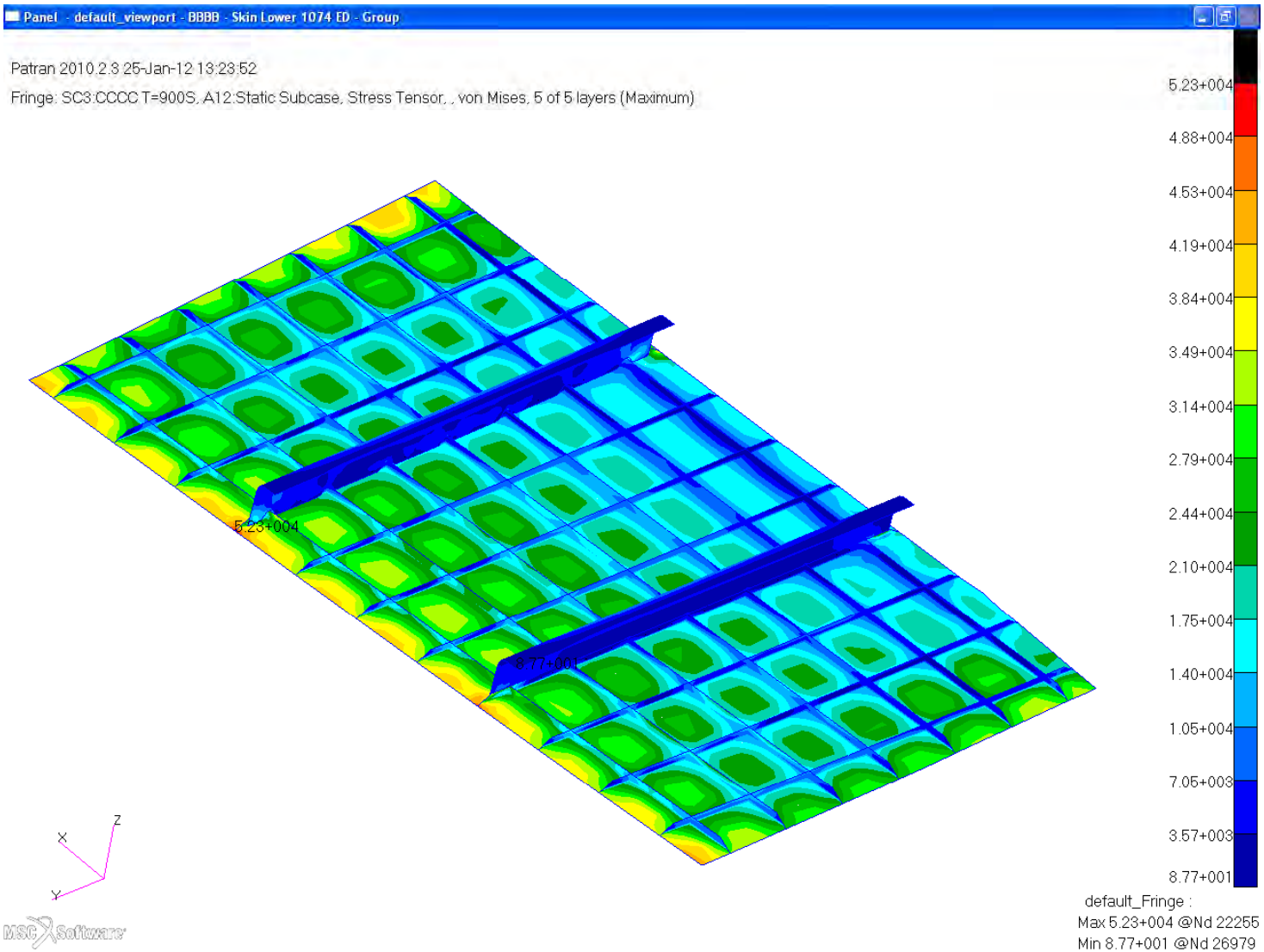

Approved for public release; distribution unlimited.

Von Mises Stress, Unit Cell Analysis, T=2700s

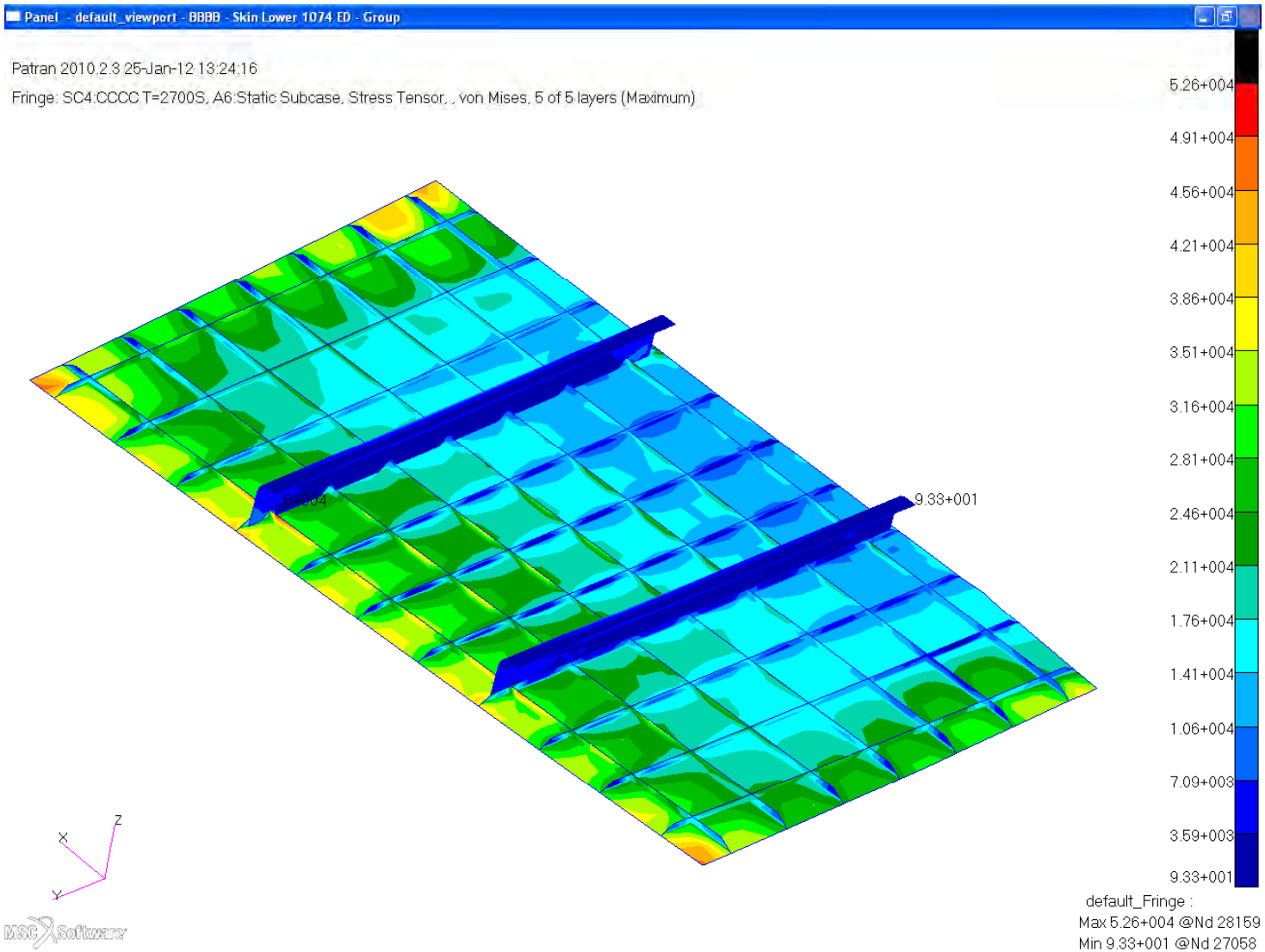

Approved for public release; distribution unlimited.

Von Mises Stress, Unit Cell Analysis, T=3540s

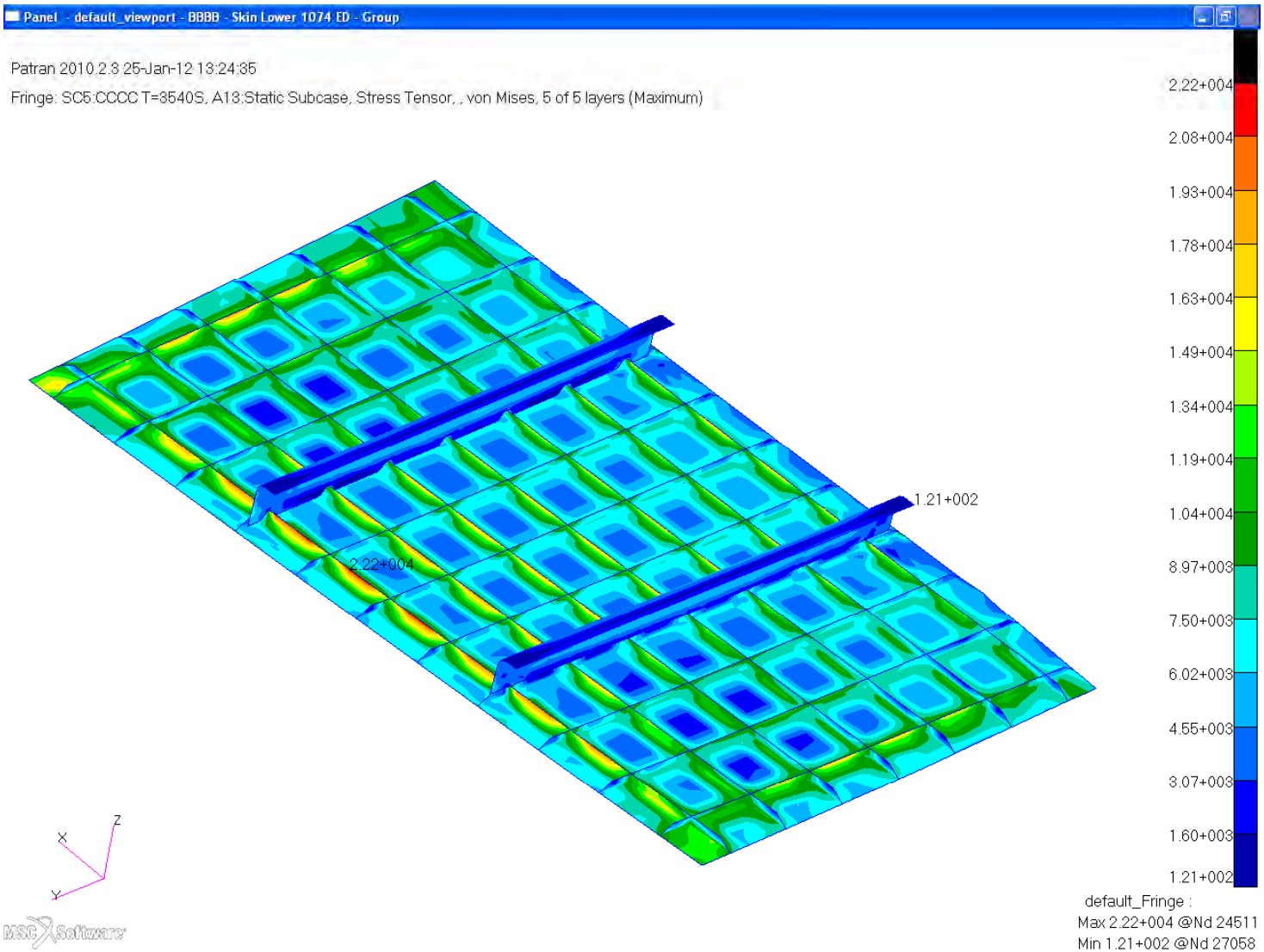

Approved for public release; distribution unlimited.

Von Mises Stress, Unit Cell

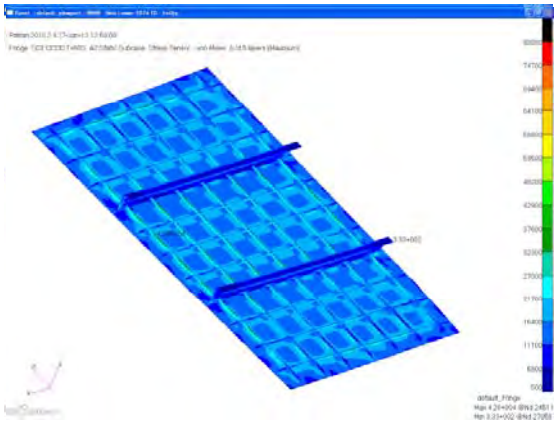

T=60s

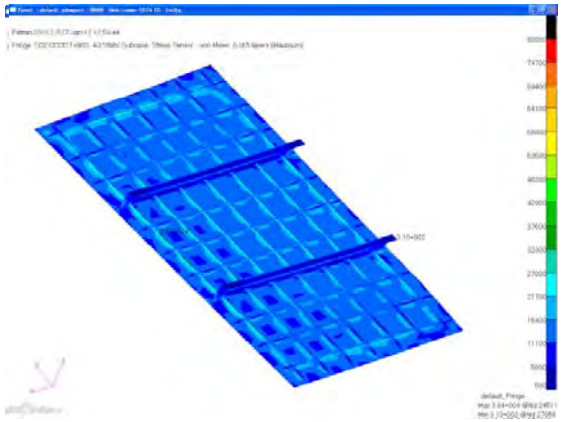

T=90s

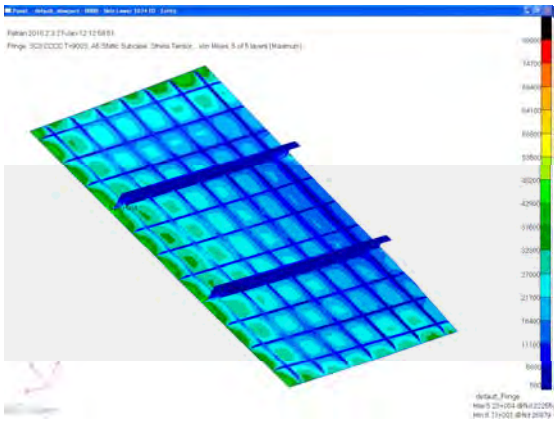

T=900s

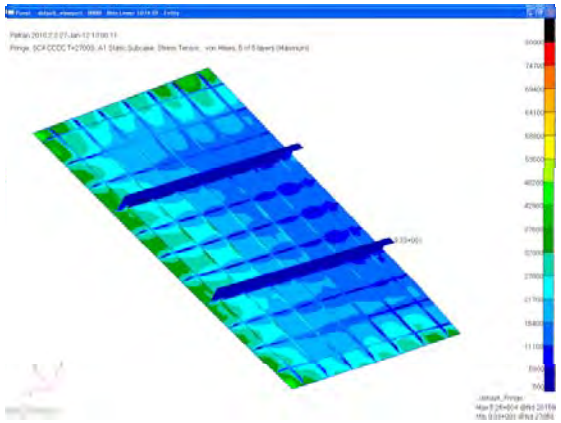

T=2700s

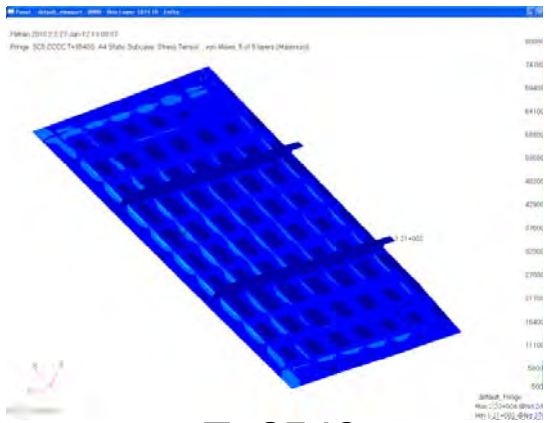

T=3540s

Approved for public release; distribution unlimited.

Displacements Mechanical Loading Only Unit Cell Analysis

Approved for public release; distribution unlimited.

Displacements, Unit Cell, 2.5G Ultimate 1.5

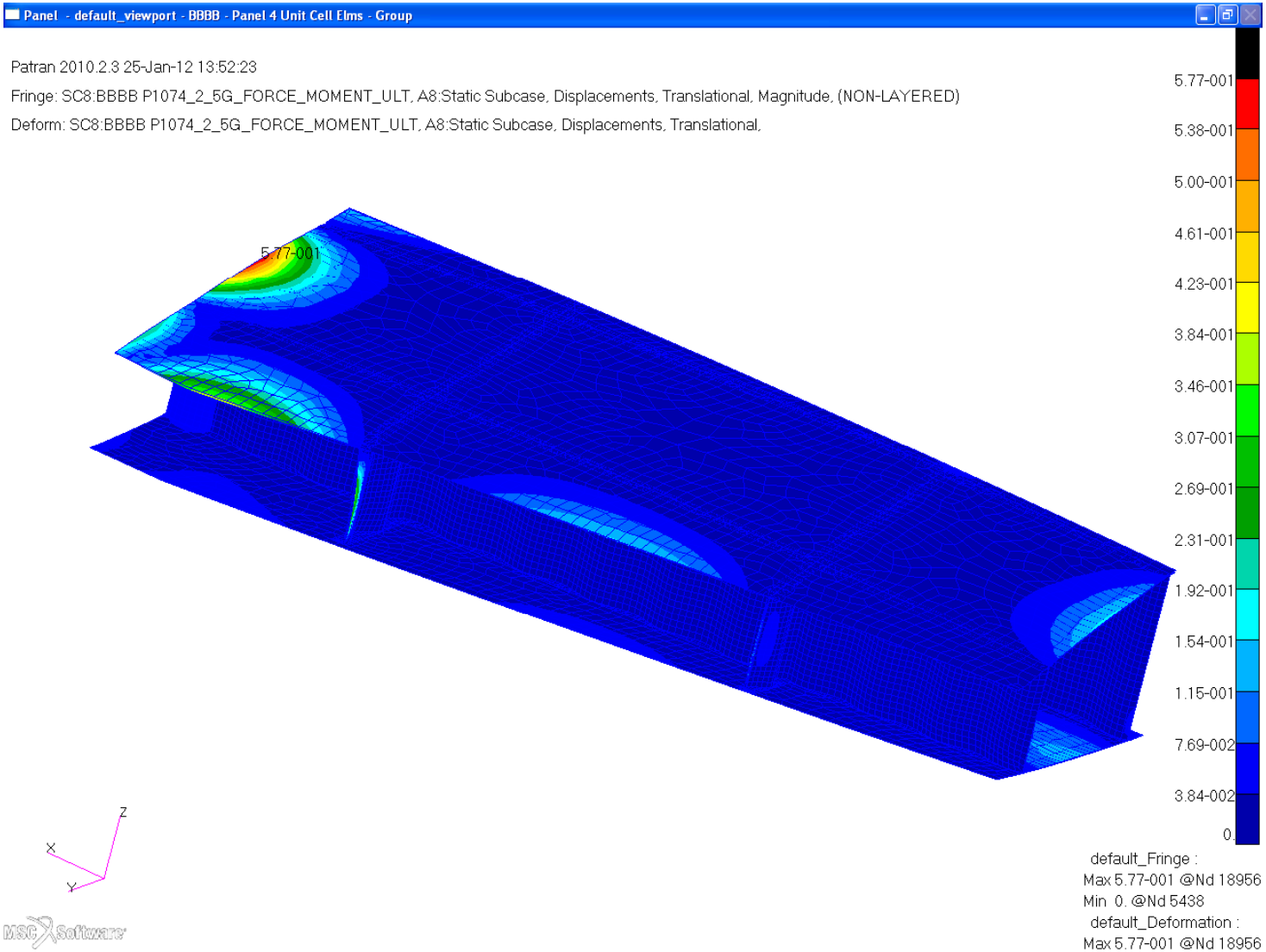

Approved for public release; distribution unlimited.

Z-Displacements, Unit Cell Analysis, 2.5G Ultimate 1.5

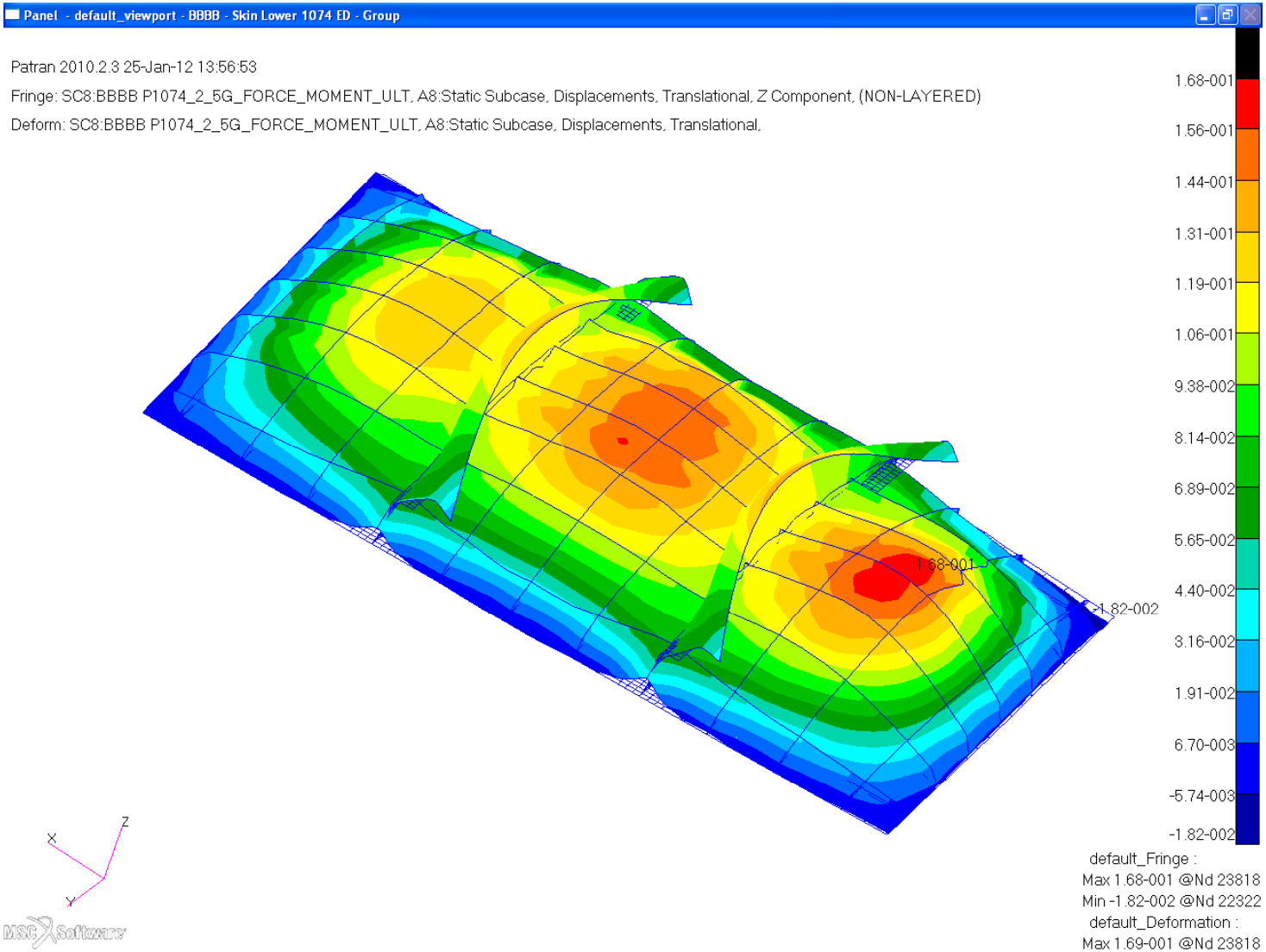

Approved for public release; distribution unlimited.

Z-Displacements, Unit Cell Analysis, 2.5G Limit 1.15

Maximum flow-wise deflection:
0.129” – 0.005” = 0.125”

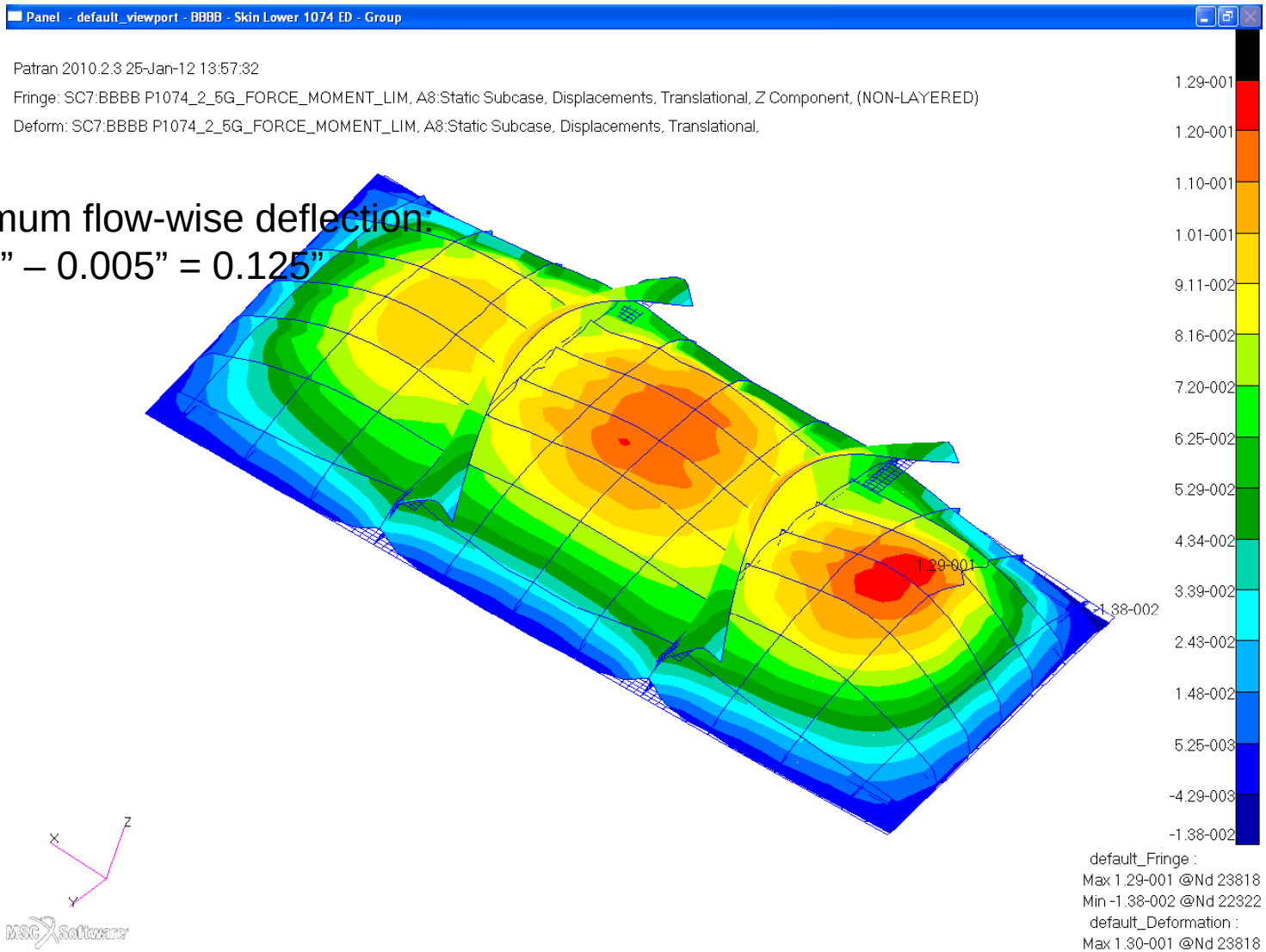

Approved for public release; distribution unlimited.

Von Mises Stress Mechanical Loading Only Unit Cell Analysis

Approved for public release; distribution unlimited.

Von Mises Stress, Unit Cell, 2.5G Ult 1.5

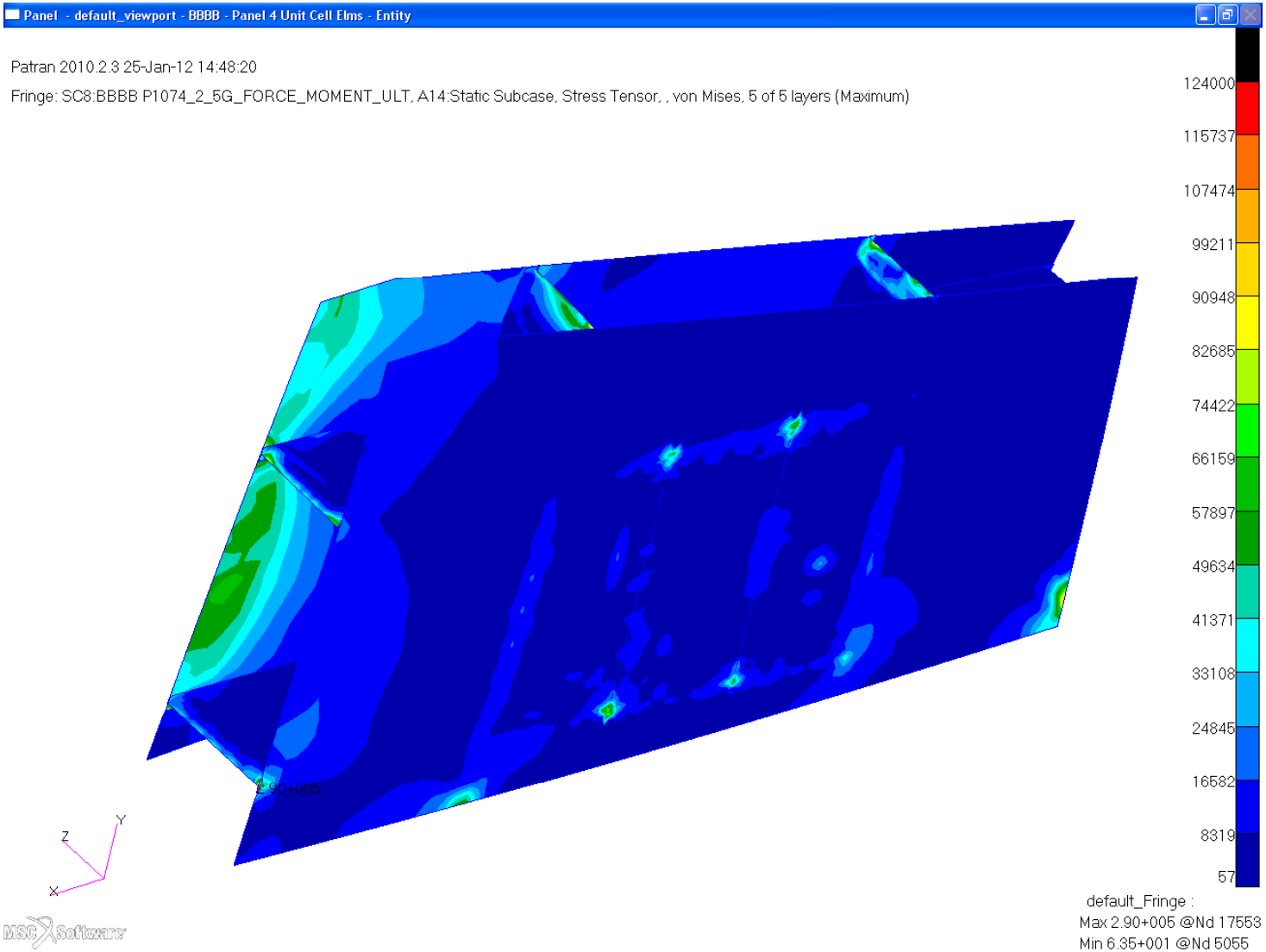

Approved for public release; distribution unlimited.

Von Mises Stress, Unit Cell, 2.5G Ult 1.5

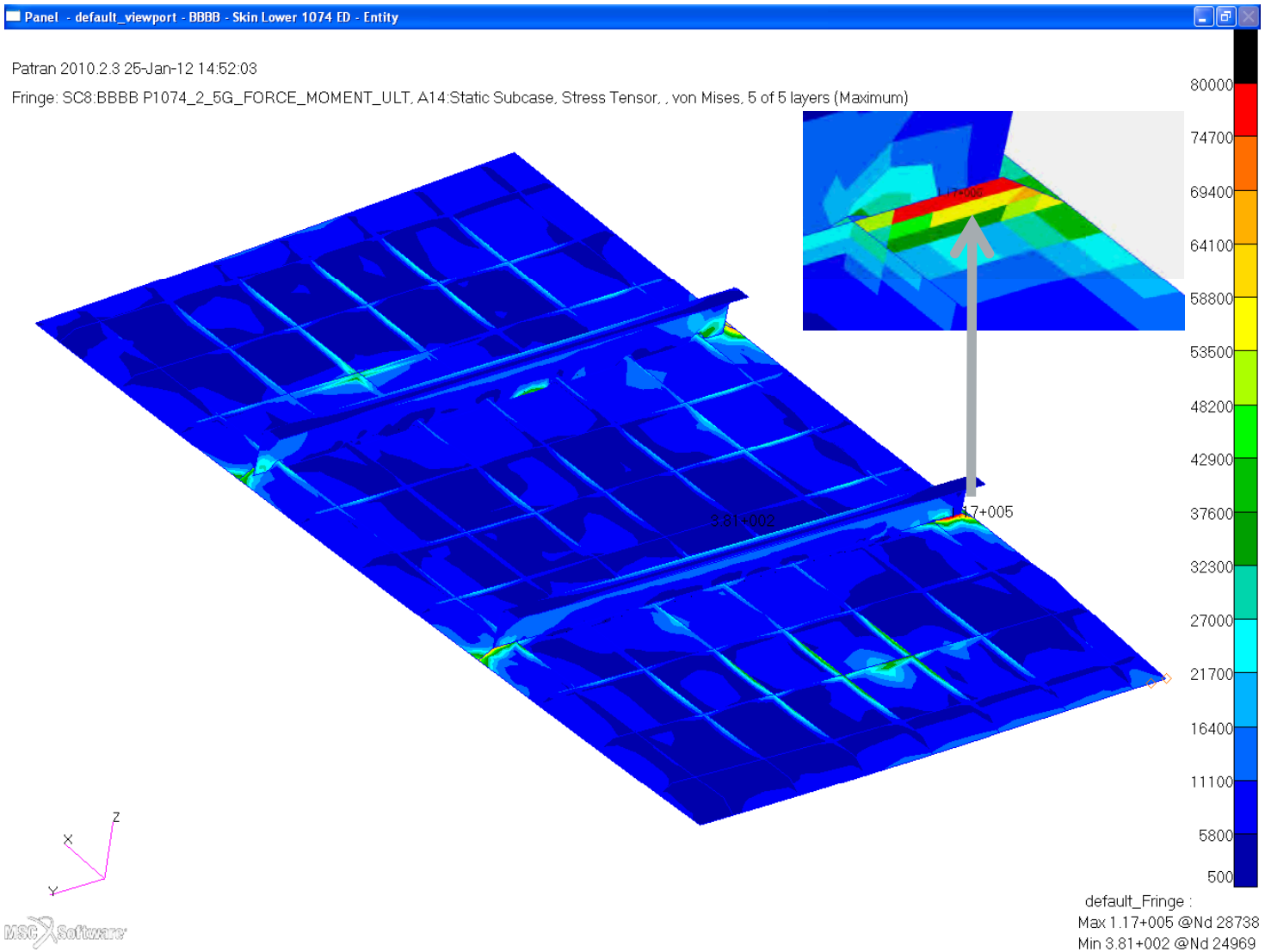

Approved for public release; distribution unlimited.

Von Mises Stress, Unit Cell, 2.5G Limit 1.15

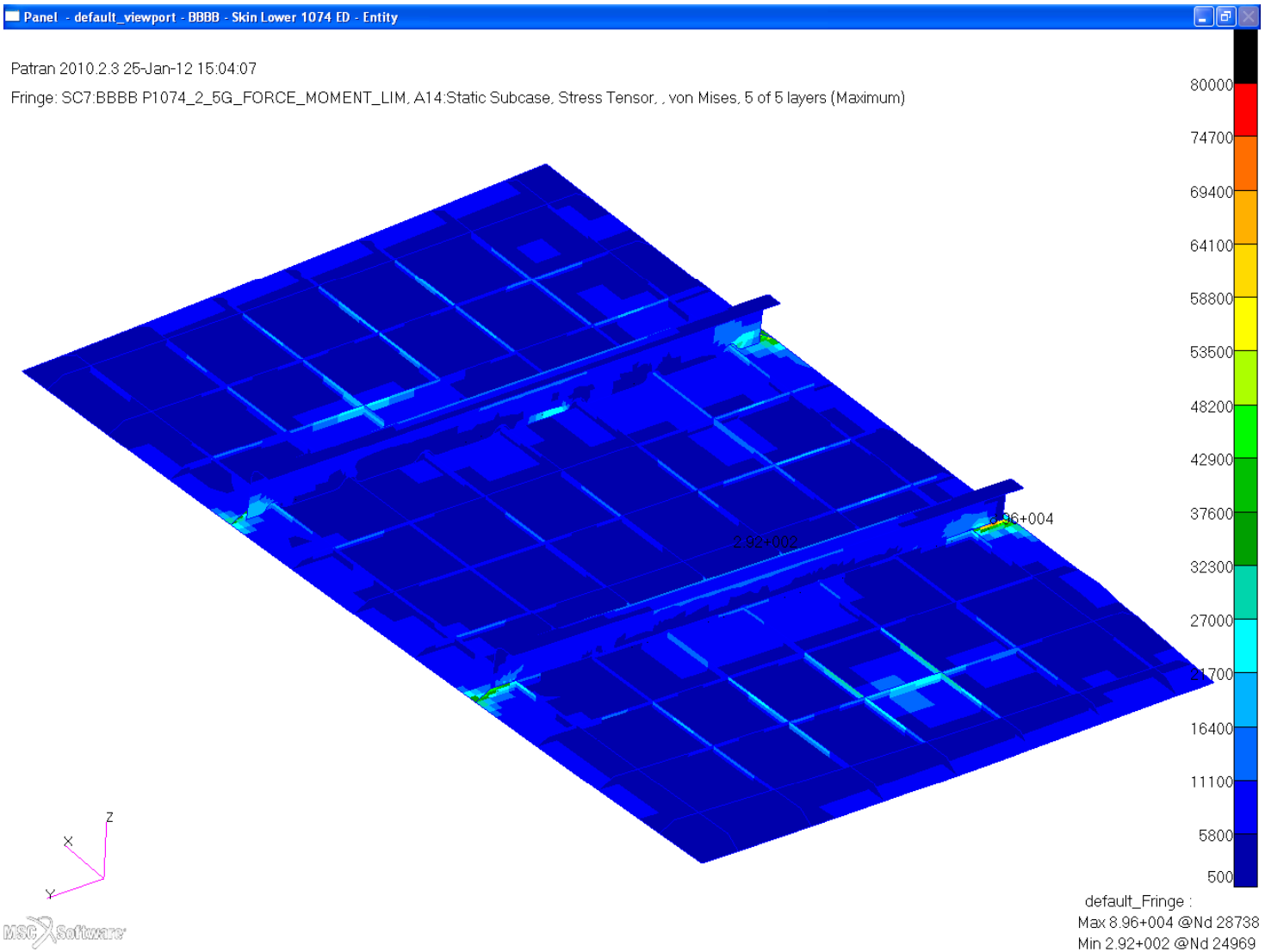

Approved for public release; distribution unlimited.

Displacements Combined Mechanical and Thermal T=900s Loading Unit Cell Analysis

Approved for public release; distribution unlimited.

Displacements, Unit Cell, 2.5G Ult 1.5+T=900s

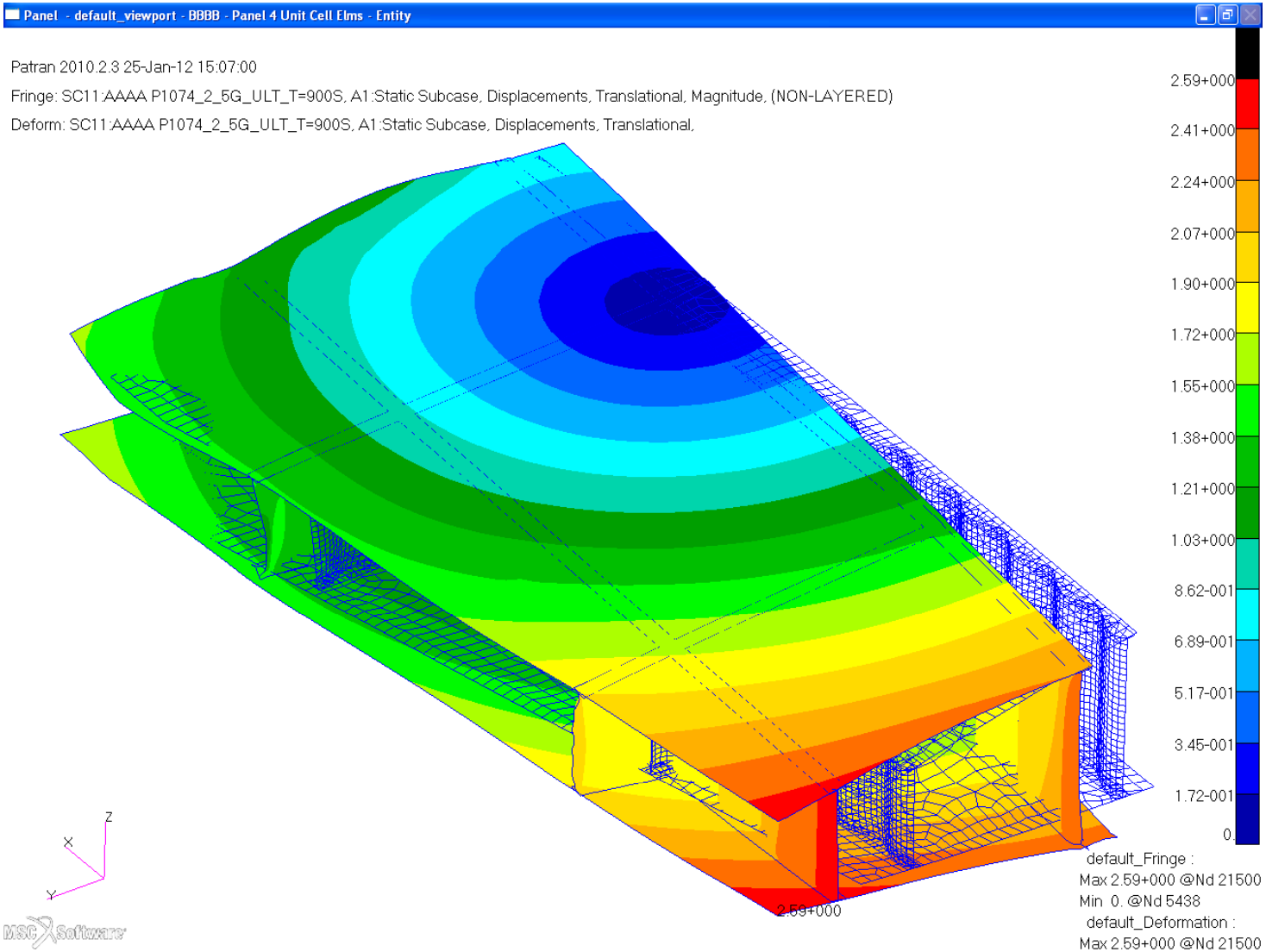

Approved for public release; distribution unlimited.

Z-Displacements, Unit Cell, 2.5G Ult 1.5+T=900s

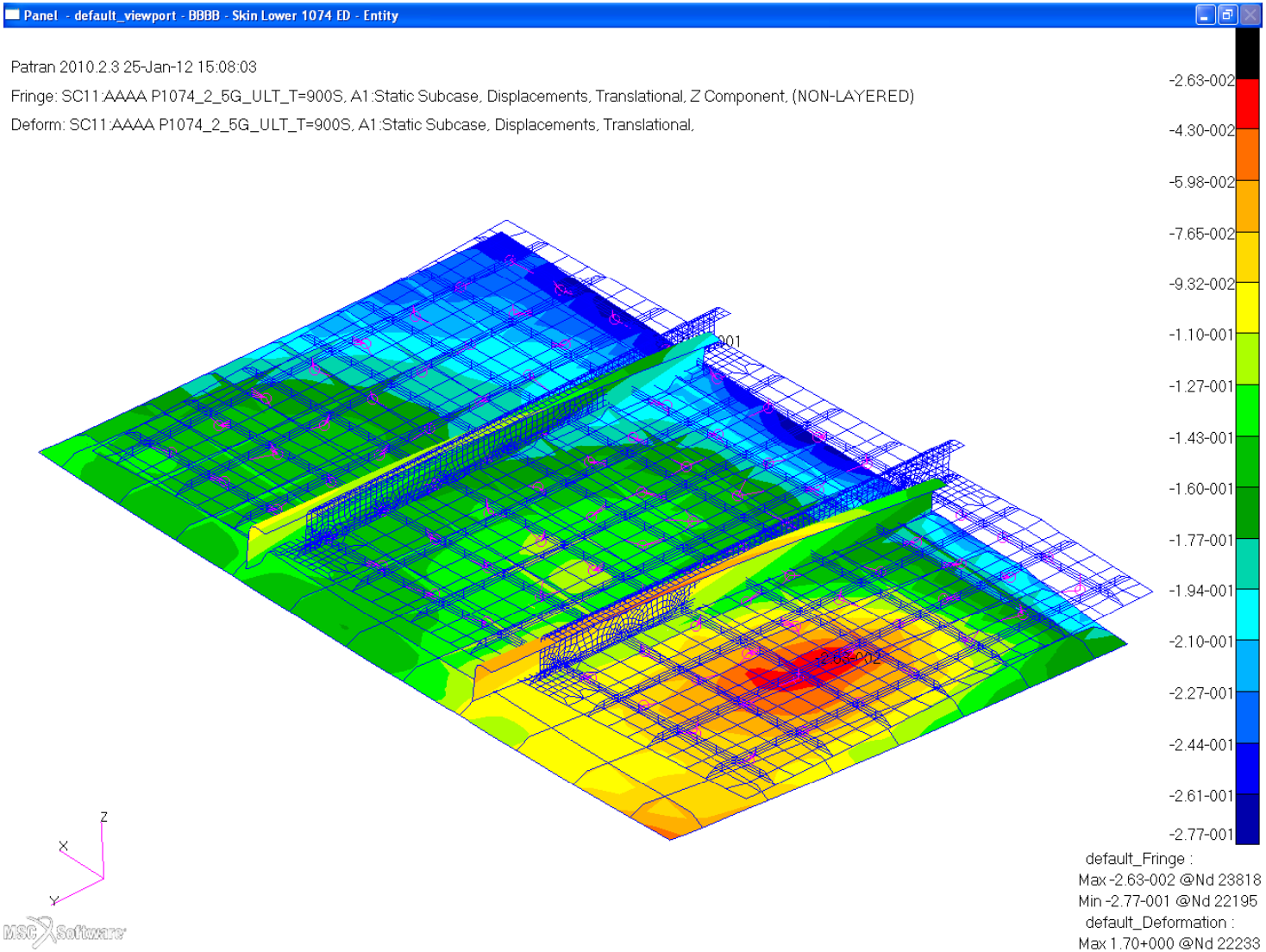

Approved for public release; distribution unlimited.

Z-Displacements, Unit Cell, 2.5G Lim 1.15+T=900s

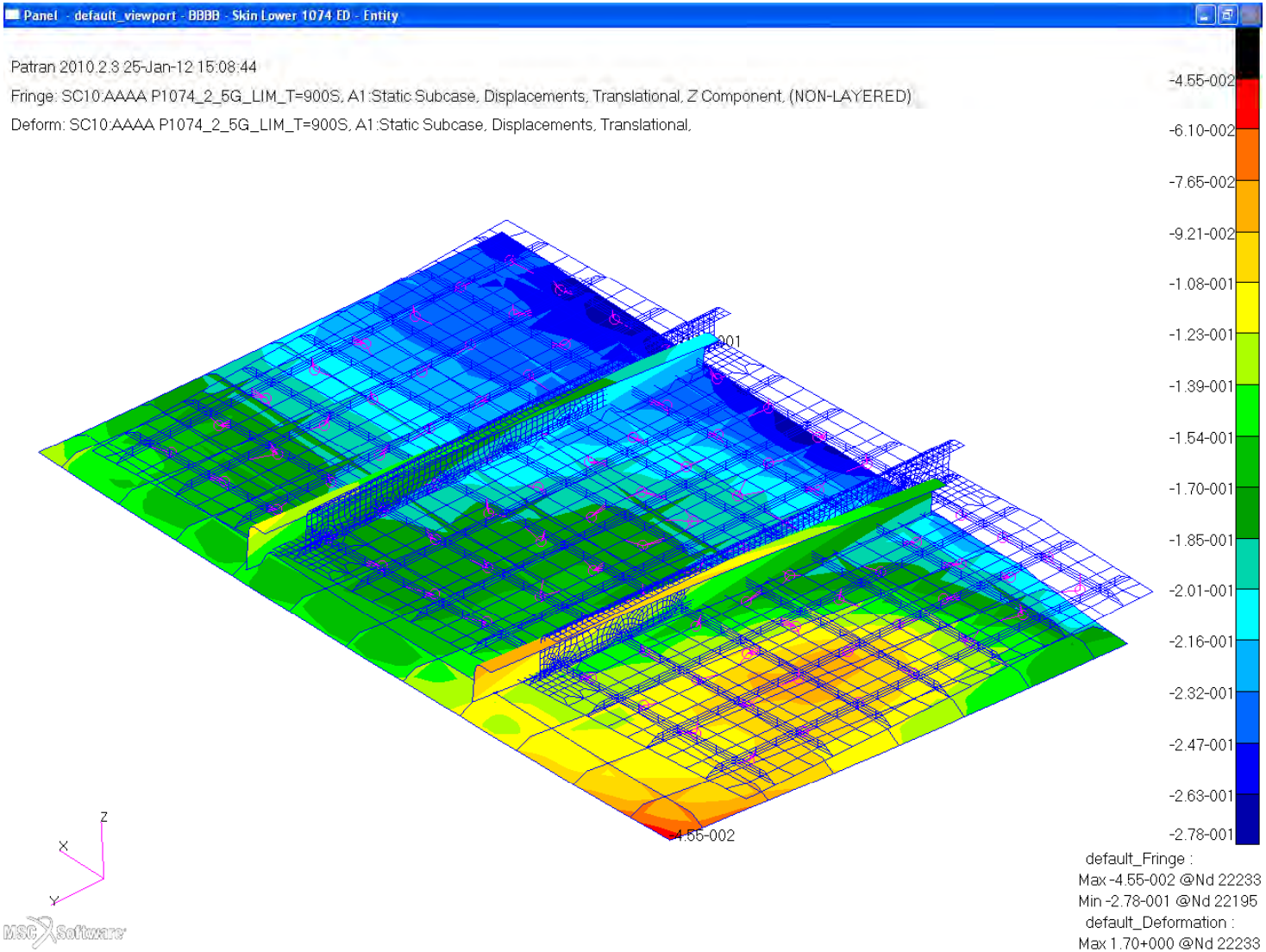

Approved for public release; distribution unlimited.

Von Mises Stress Combined Mechanical and Thermal T=900s Loading Unit Cell Analysis

Approved for public release; distribution unlimited.

Von Mises, Unit Cell, 2.5G Ult 1.5+T=900s

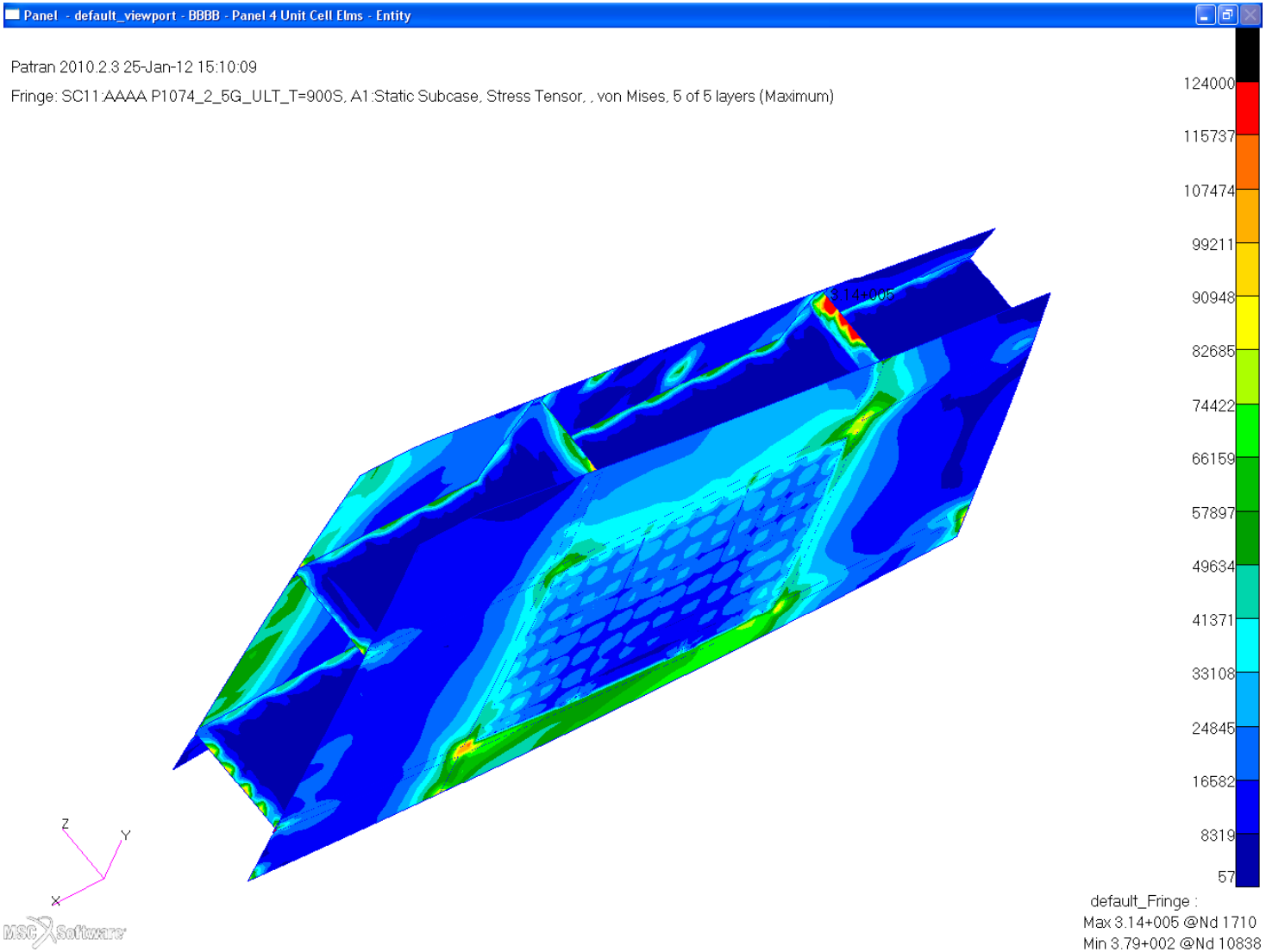

Approved for public release; distribution unlimited.

Von Mises, Unit Cell, 2.5G Ult 1.5+T=900s

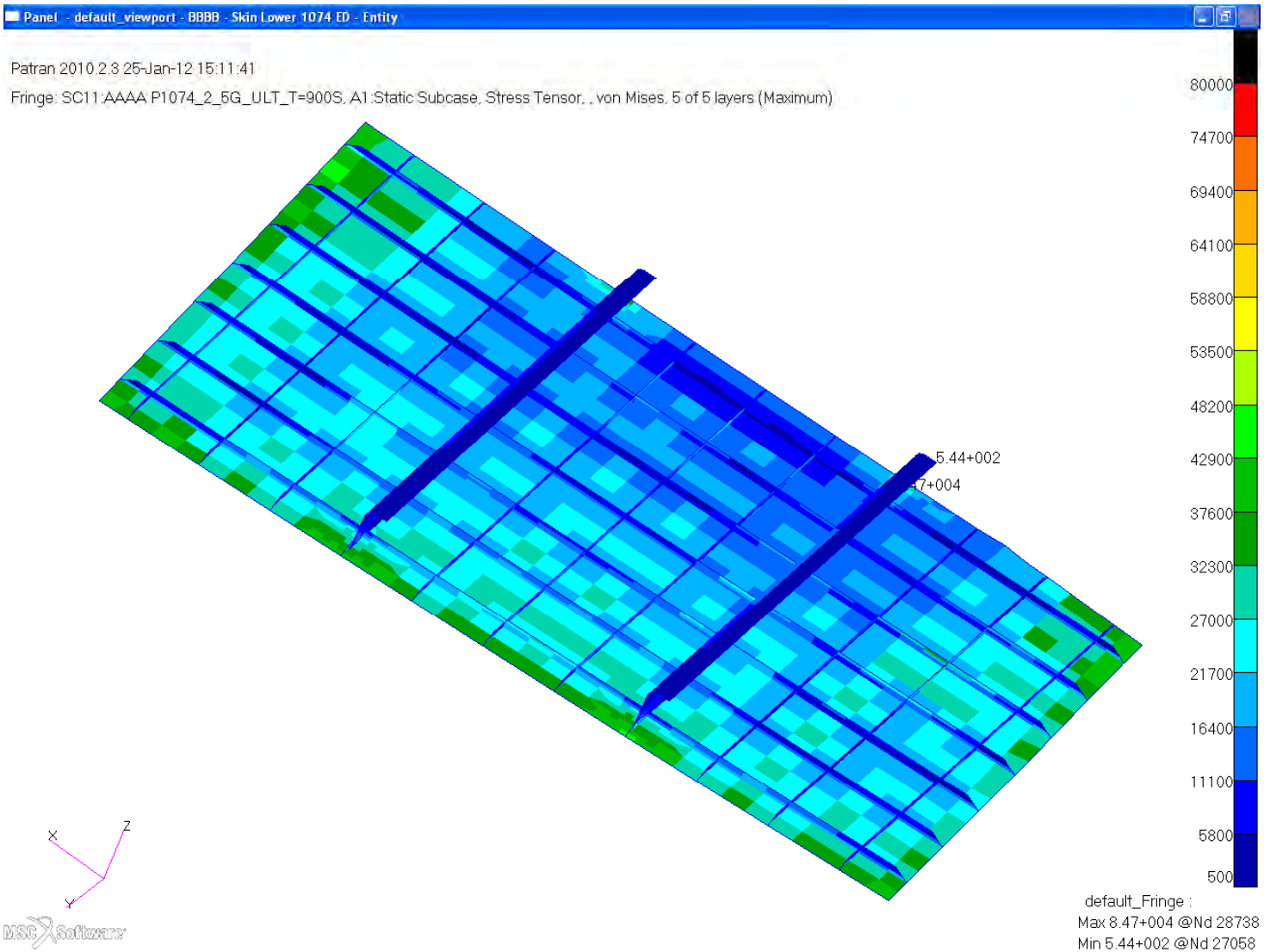

Approved for public release; distribution unlimited.

Von Mises, Unit Cell, 2.5G Lim 1.15+T=900s

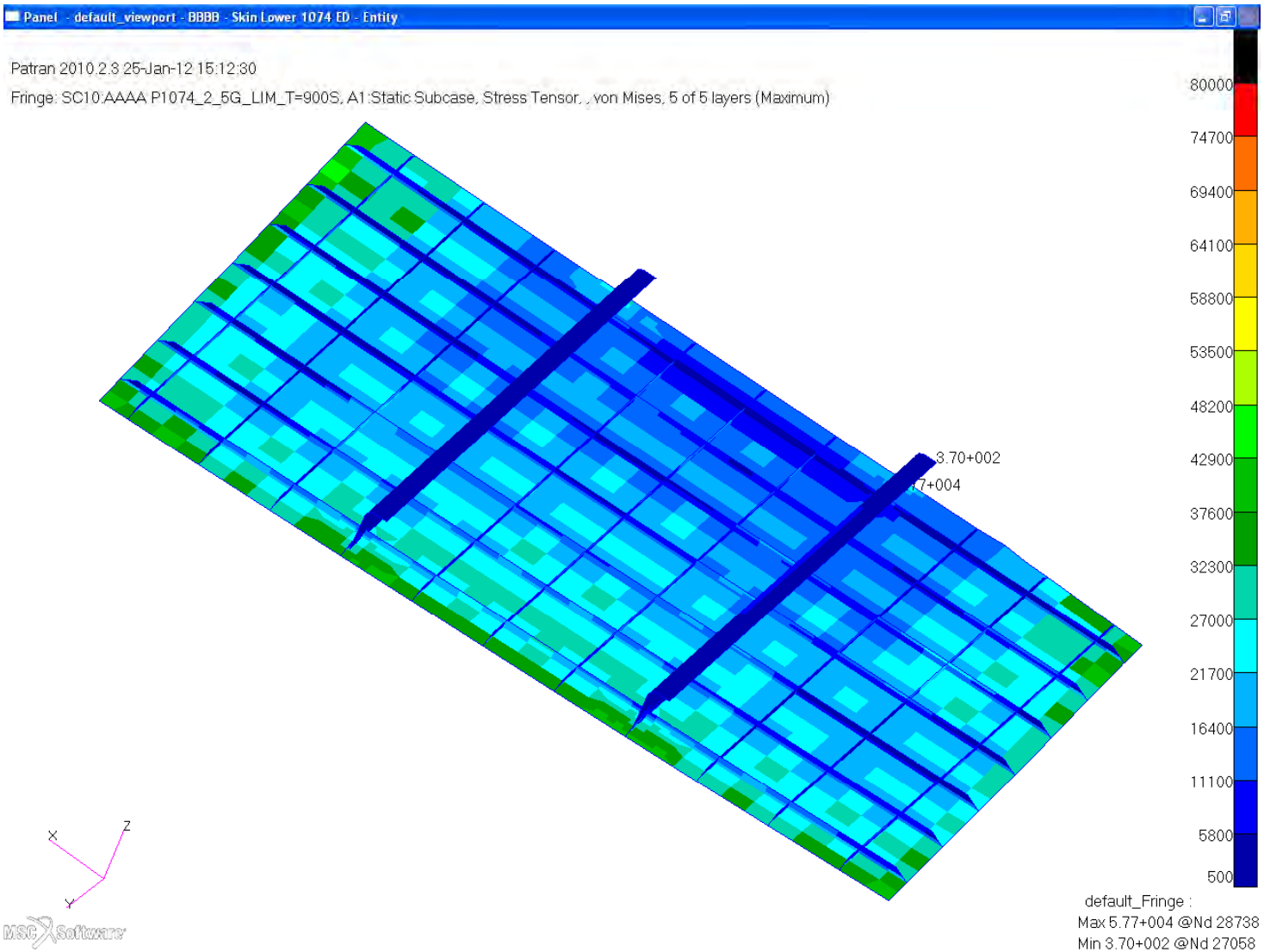

Approved for public release; distribution unlimited.

Displacements Combined Mechanical and Thermal T=2700s Loading Unit Cell Analysis

Approved for public release; distribution unlimited.

Displacements, Unit Cell, 2.5G Ult 1.5+T=2700s

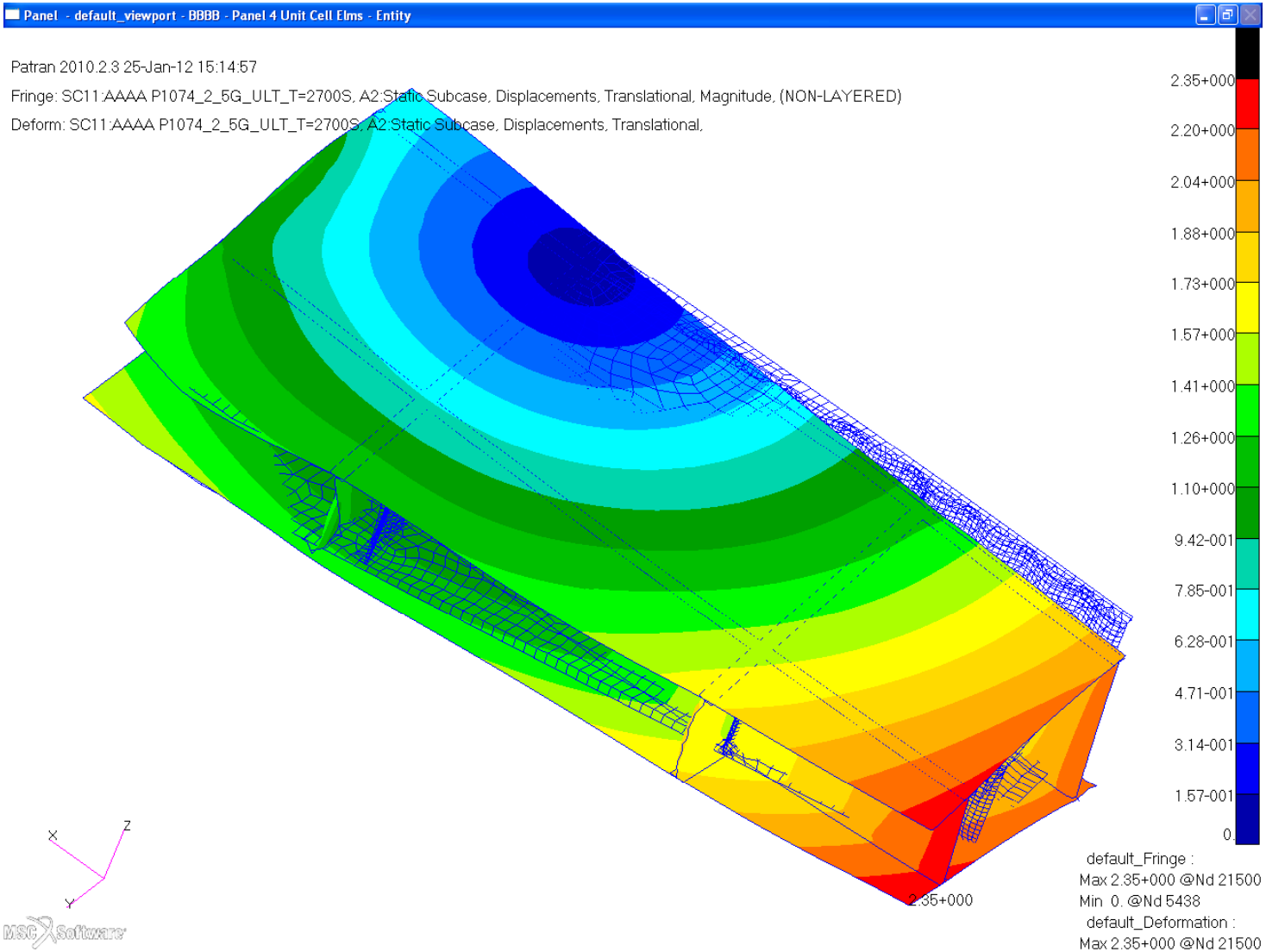

Approved for public release; distribution unlimited.

Z-Displacements, Unit Cell, 2.5G Ult 1.5+T=2700s

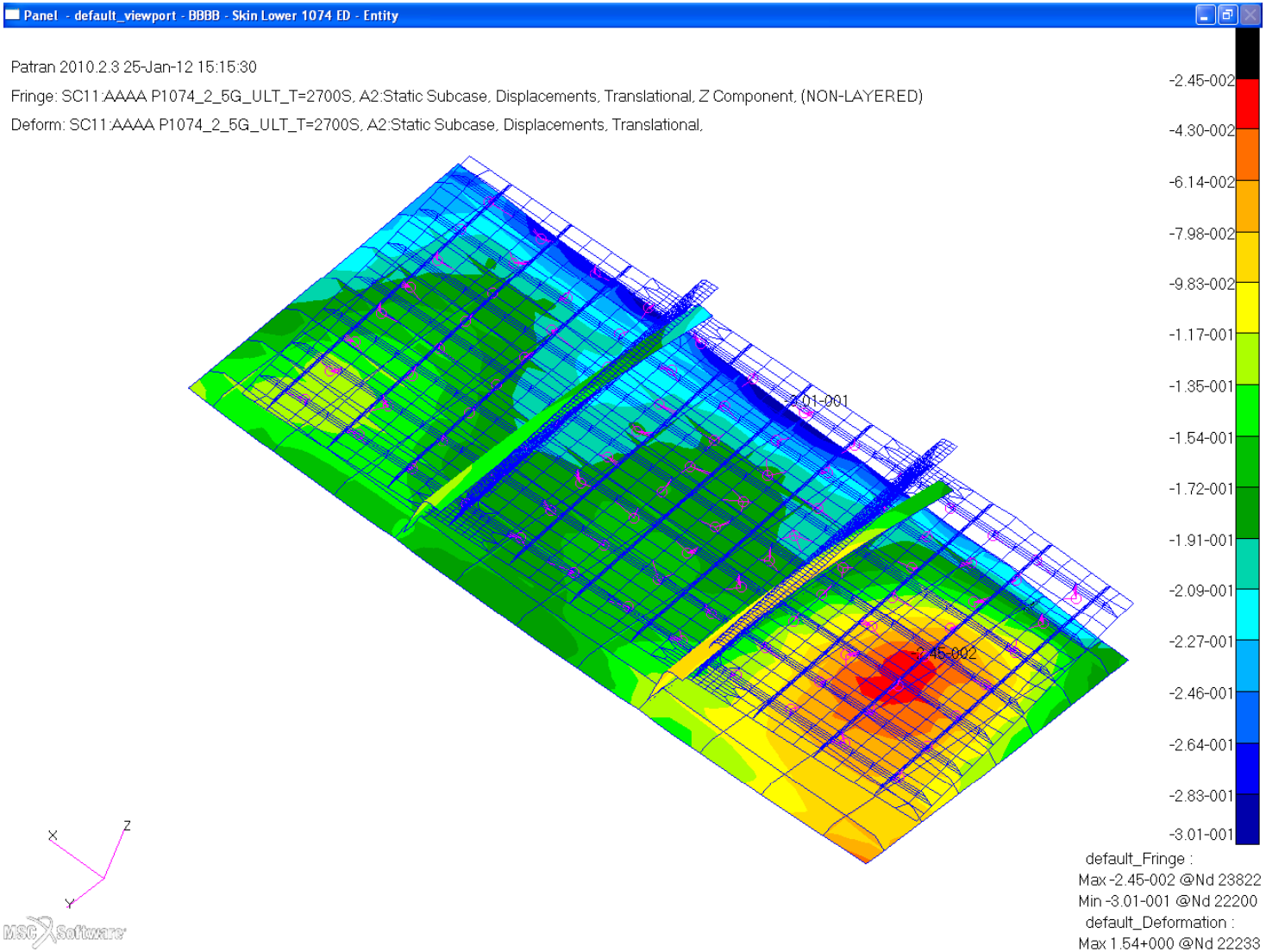

Approved for public release; distribution unlimited.

Z-Displacements, Unit Cell, 2.5G Lim 1.15+T=2700s

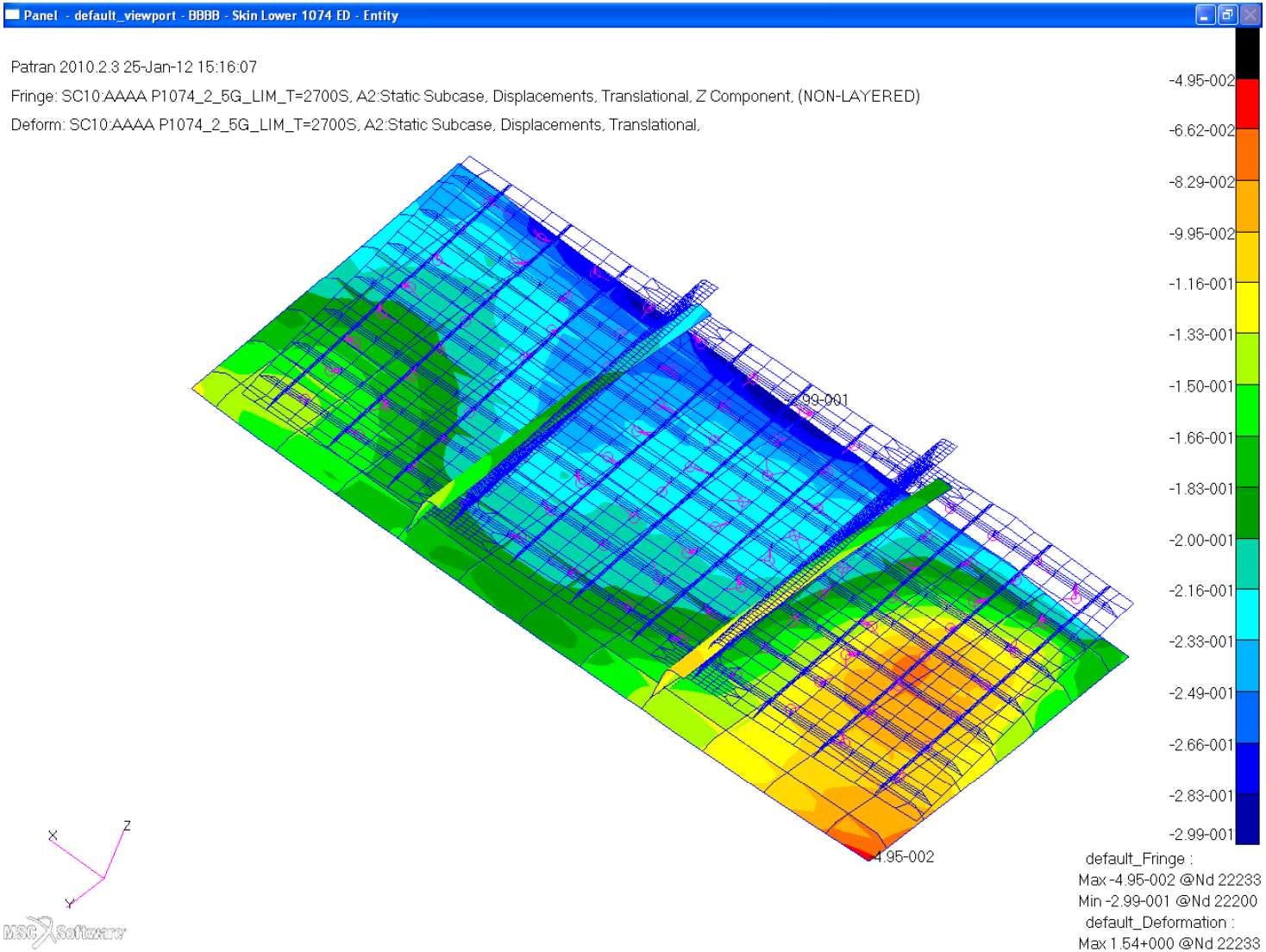

Approved for public release; distribution unlimited.

Von Mises Stress Combined Mechanical and Thermal T=2700s Loading Unit Cell Analysis

Approved for public release; distribution unlimited.

Von Mises, Unit Cell, 2.5G Ult 1.5+T=2700s

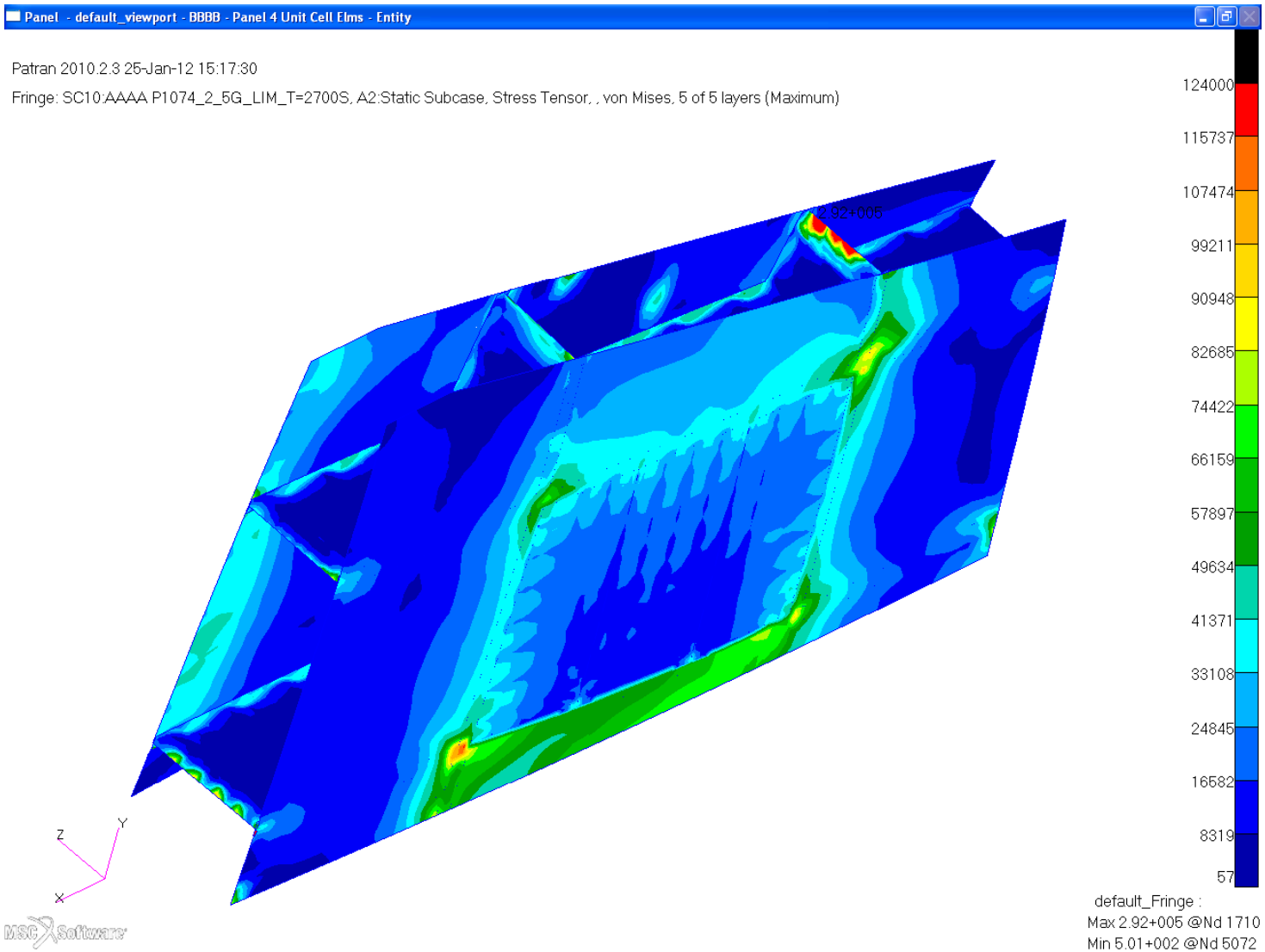

Approved for public release; distribution unlimited.

Von Mises, Unit Cell, 2.5G Ult 1.5+T=2700s

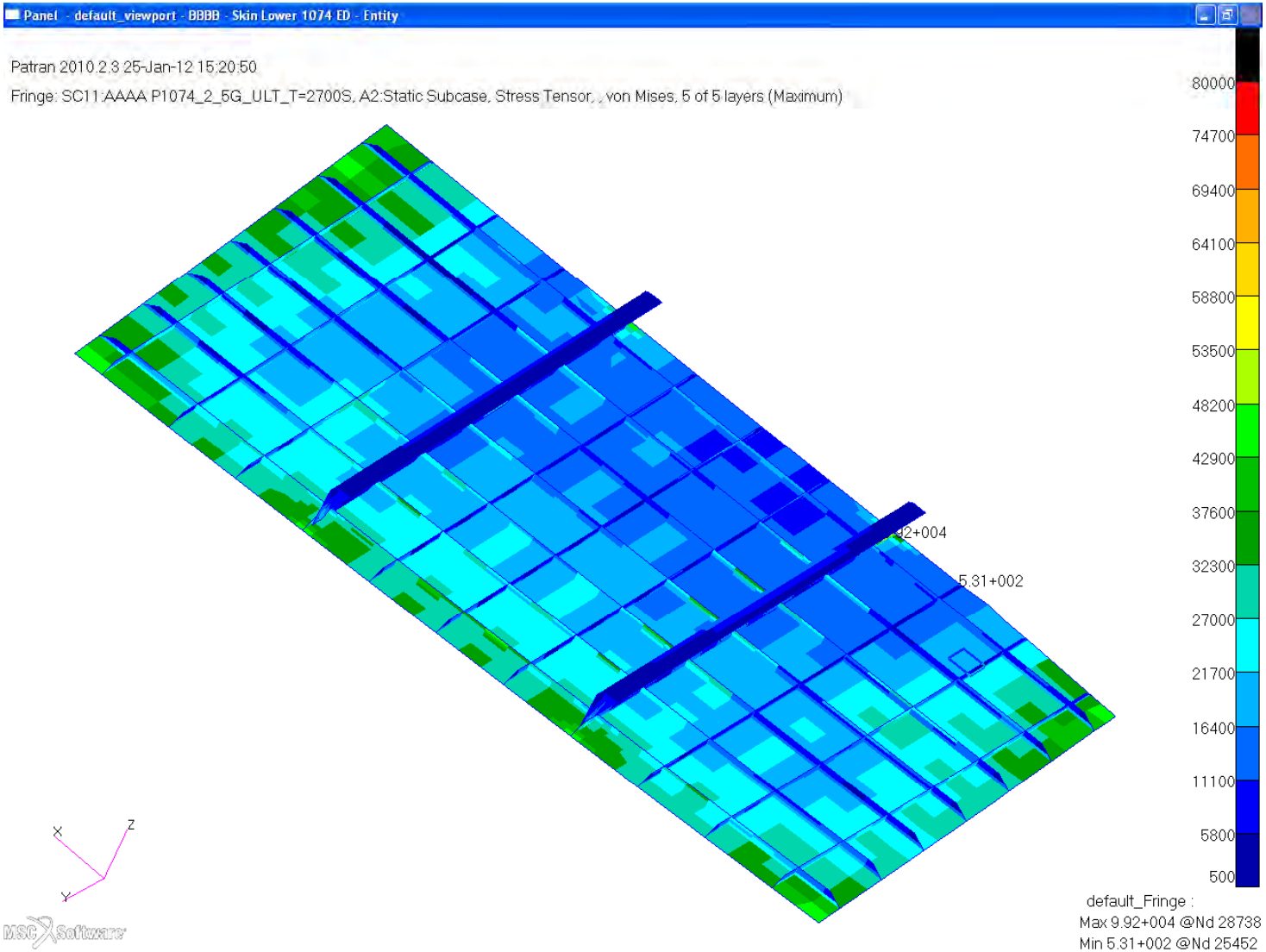

Approved for public release; distribution unlimited.

Von Mises, Unit Cell, 2.5G Lim 1.15+T=2700s

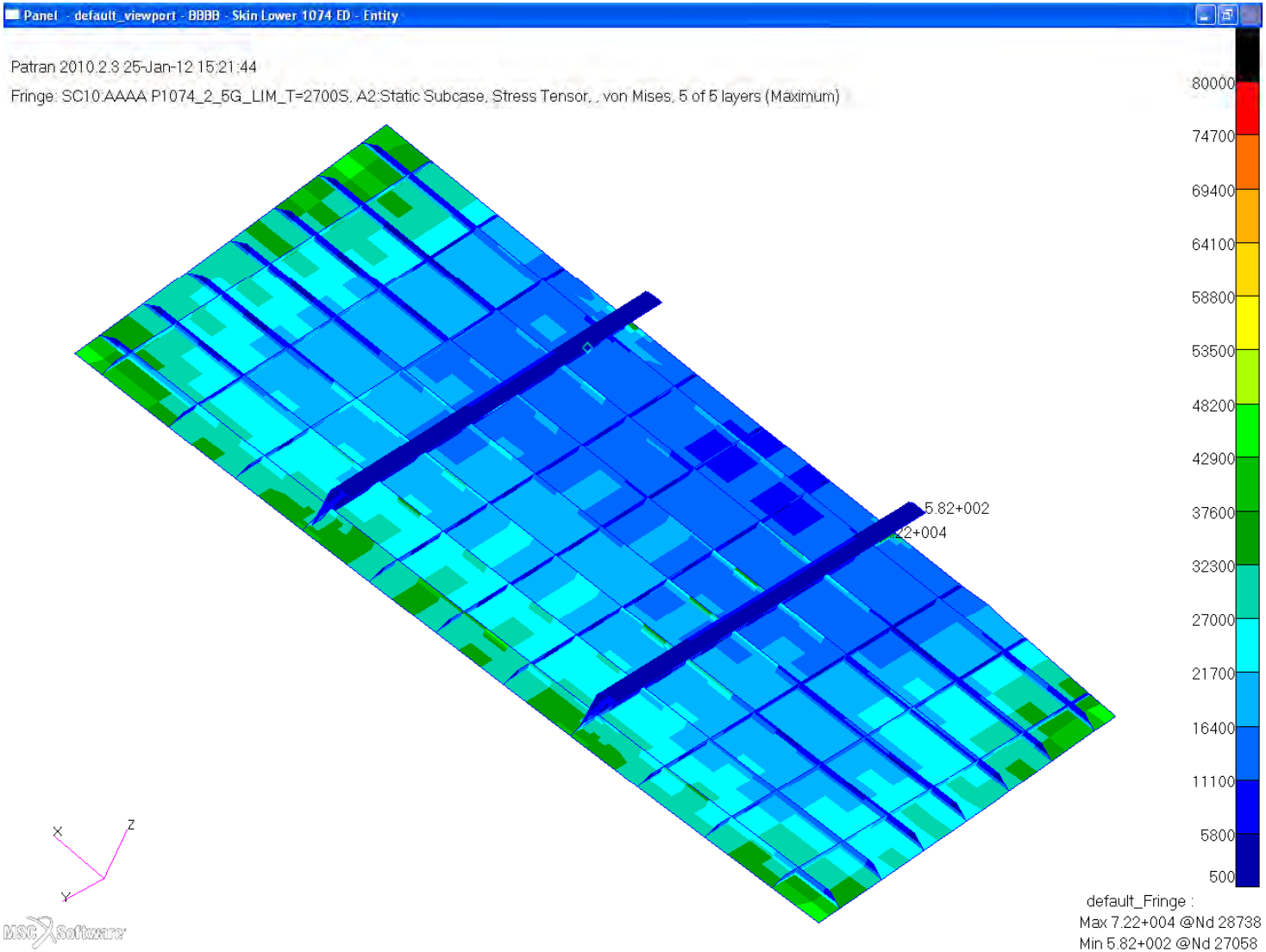

Approved for public release; distribution unlimited.

Displacements Combined Mechanical and Thermal T=2700s Loading Panel Analysis

Approved for public release; distribution unlimited.

Z-Disp, Panel Analysis, 2.5G Ult 1.5+T=2700s Linear

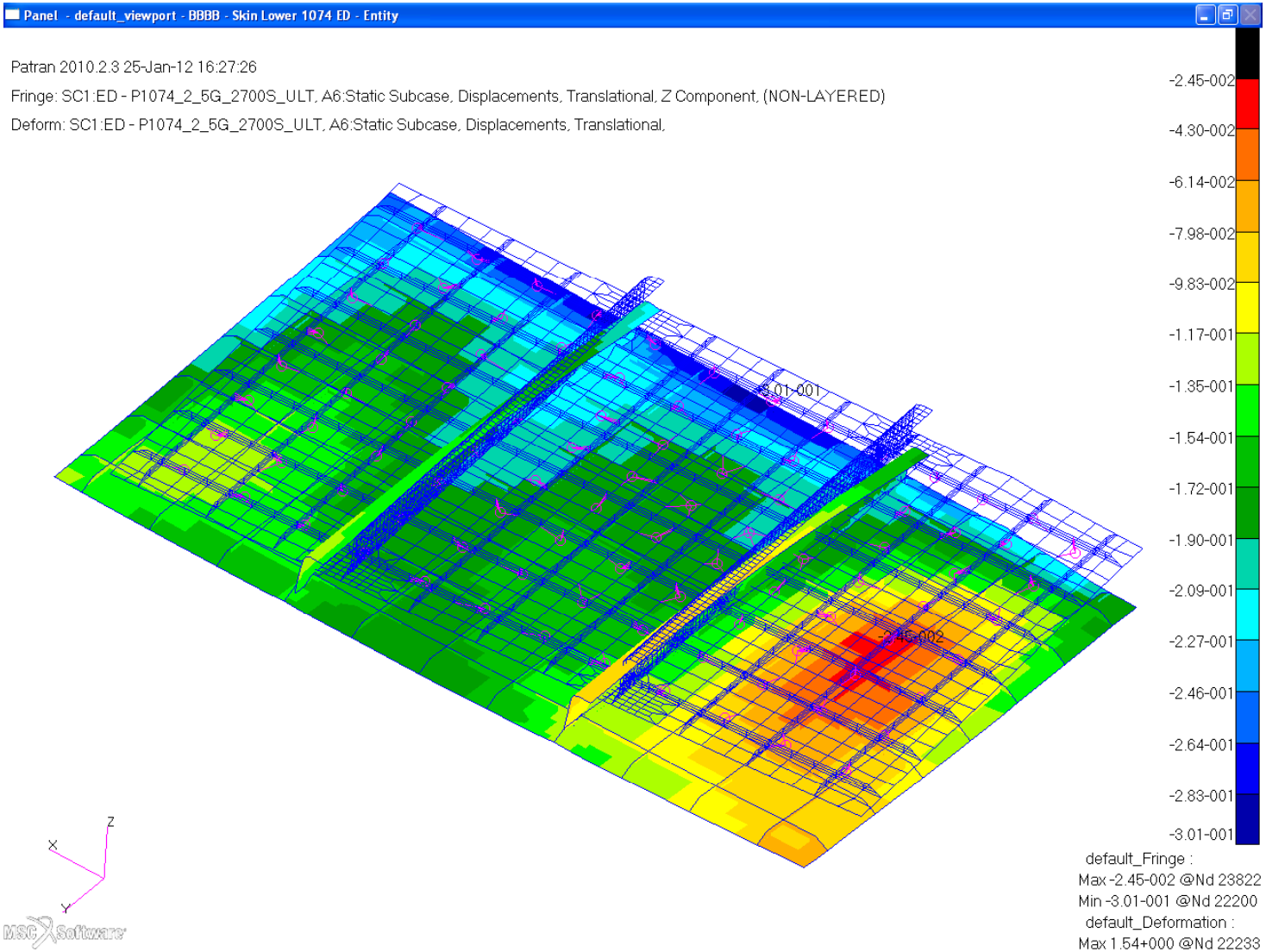

Approved for public release; distribution unlimited.

Z-Disp, Panel Analysis, 2.5G Lim 1.15+T=2700s Linear

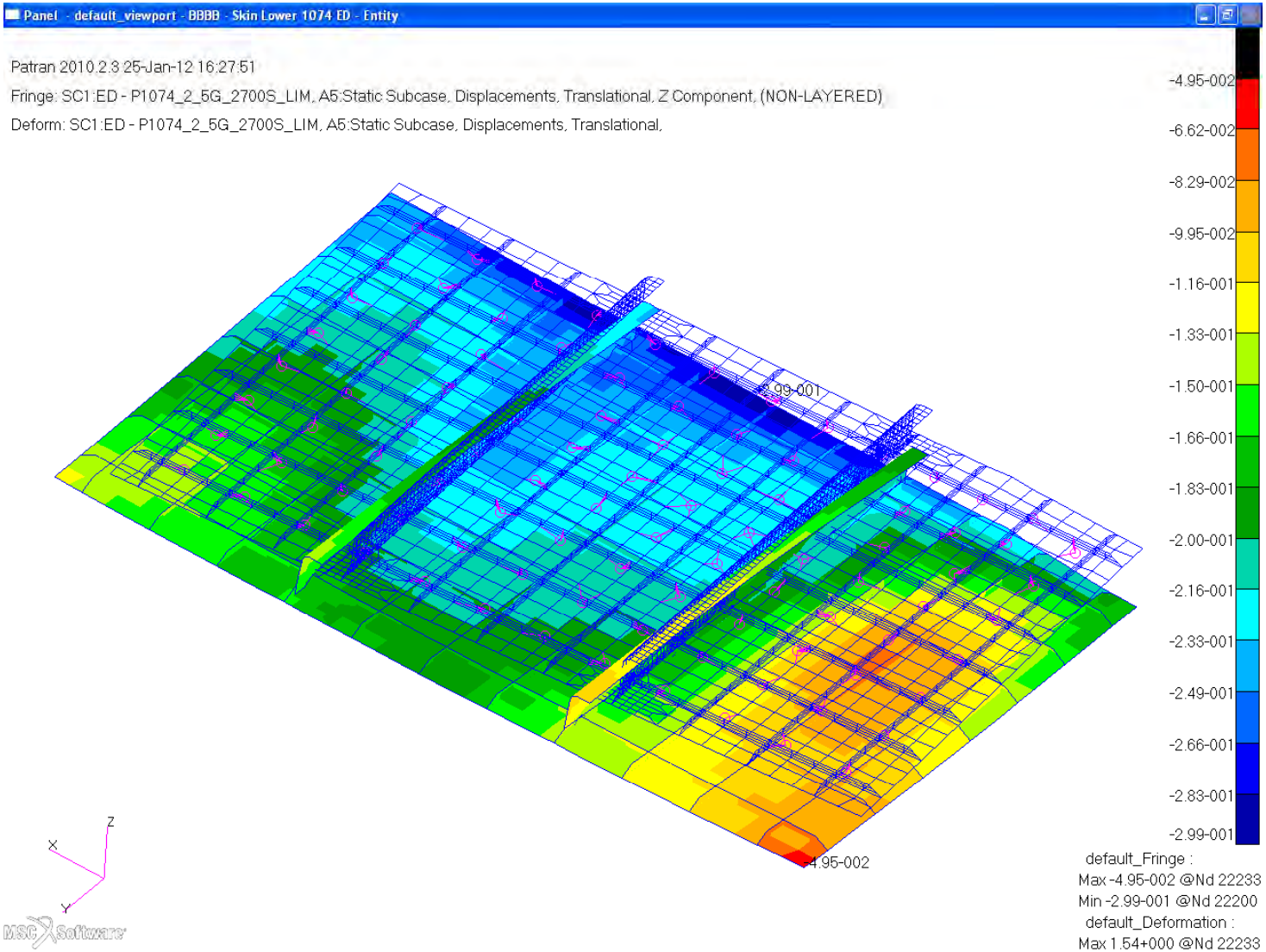

Approved for public release; distribution unlimited.

Z-Disp, Panel Analysis, 2.5G Ult 1.5+T=2700s Non-Linear

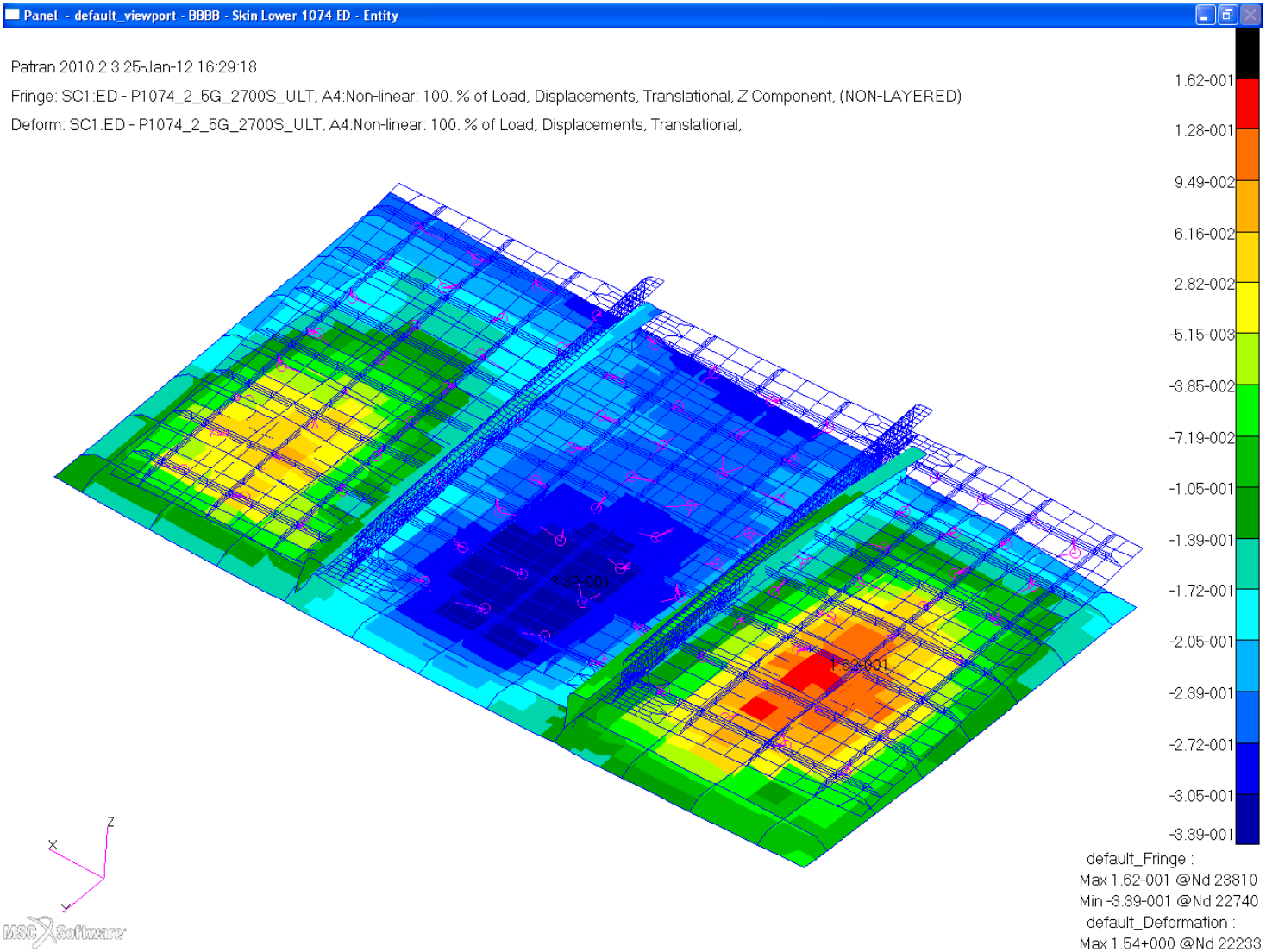

Approved for public release; distribution unlimited.

Z-Disp, Panel Analysis, 2.5G Lim 1.15+T=2700s Non-Linear

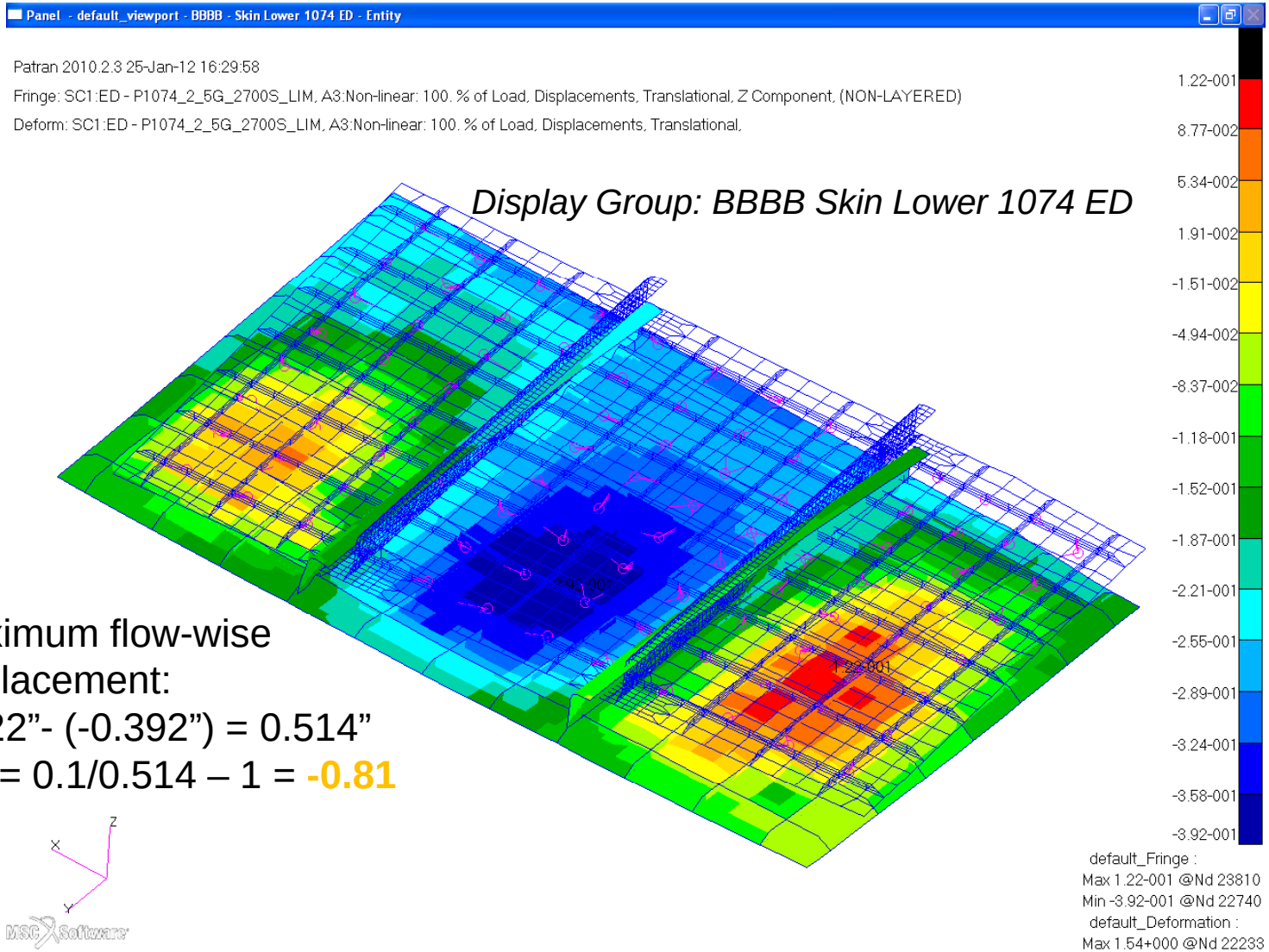

Display Group: BBBB Skin Lower 1074 ED

Maximum flow-wise displacement:
0.122”- (-0.392”) = 0.514”
MS = 0.1/0.514 – 1 = **-0.81**

Approved for public release; distribution unlimited.

Von Mises Stress Combined Mechanical and Thermal T=2700s Loading Panel Analysis

Approved for public release; distribution unlimited.

Von Mises, Panel Analysis, 2.5G Ult 1.5+T=2700s Linear

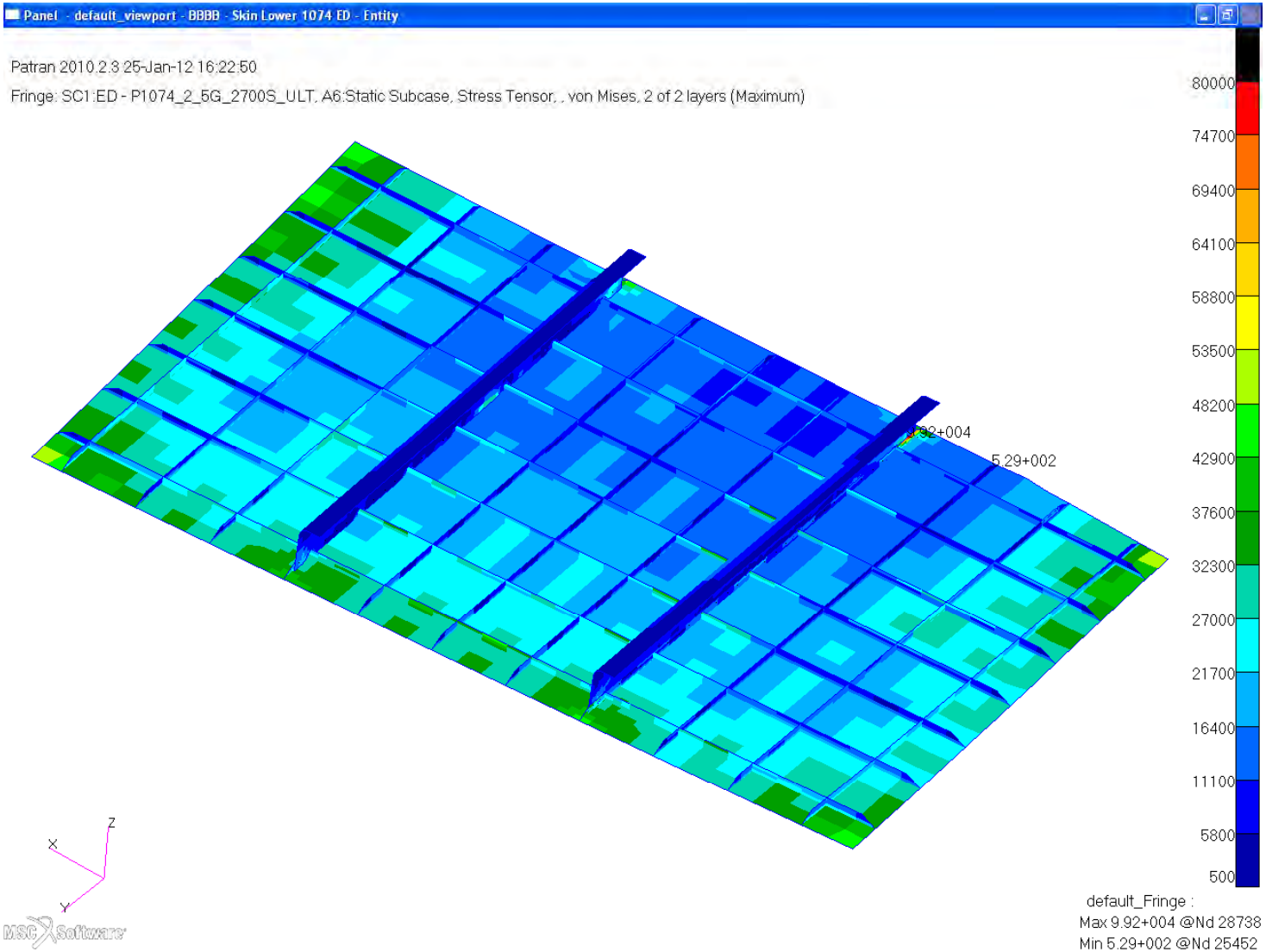

Approved for public release; distribution unlimited.

Von Mises, Panel Analysis, 2.5G Ult 1.5+T=2700s Non-Linear

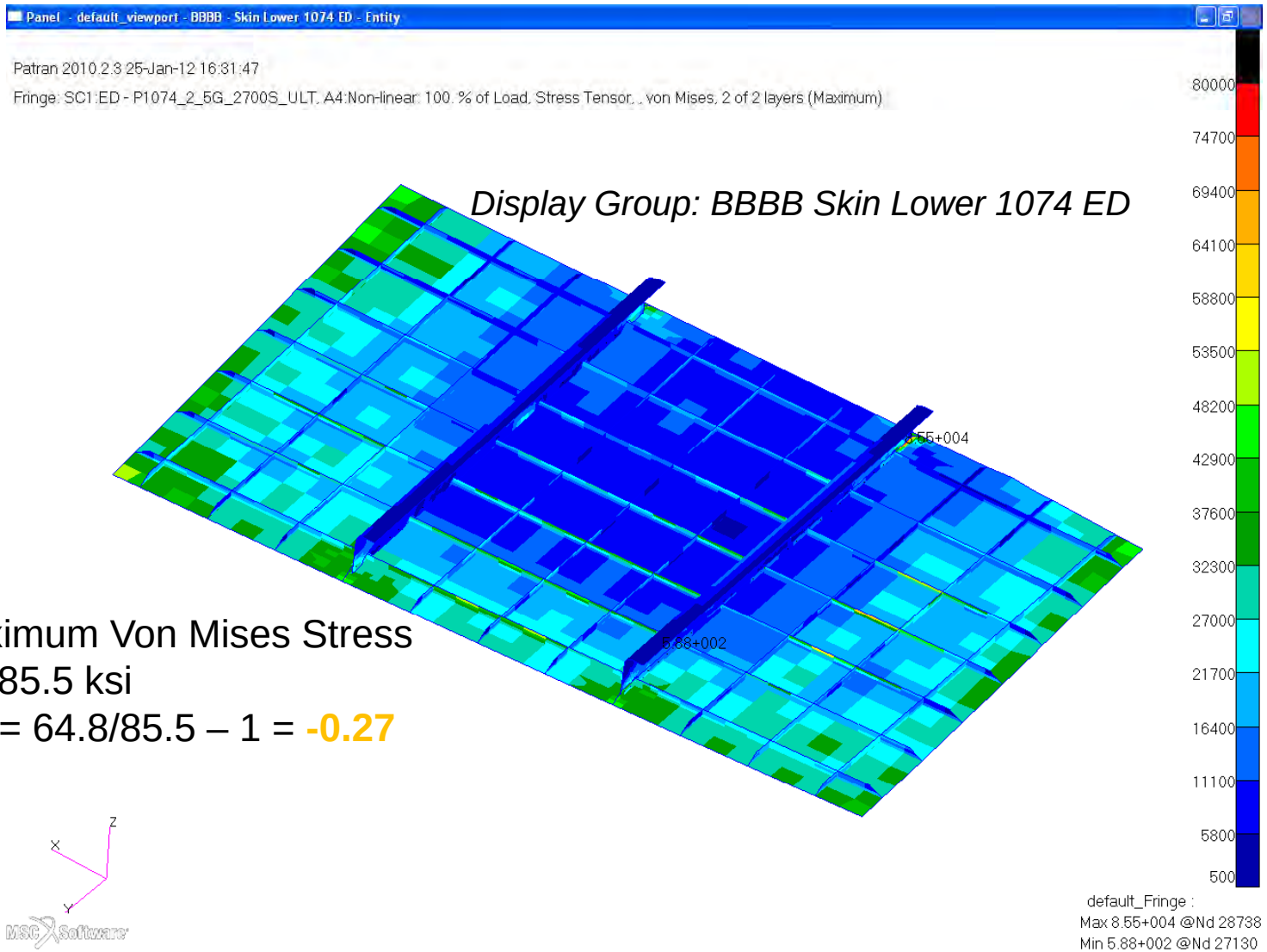

Maximum Von Mises Stress
σ = 85.5 ksi
MS = 64.8/85.5 – 1 = **-0.27**

Approved for public release; distribution unlimited.

Buckling Analysis Combined Mechanical and Thermal T=2700s Loading Panel Analysis

Approved for public release; distribution unlimited.

Buckling, Panel Analysis, 2.5G Lim 1.15+T=2700s

1st Combined Global and Local Mode:
Eigenvalue = 0.609
Ratio-to-Requirement = 0.609/1.0 = 0.609

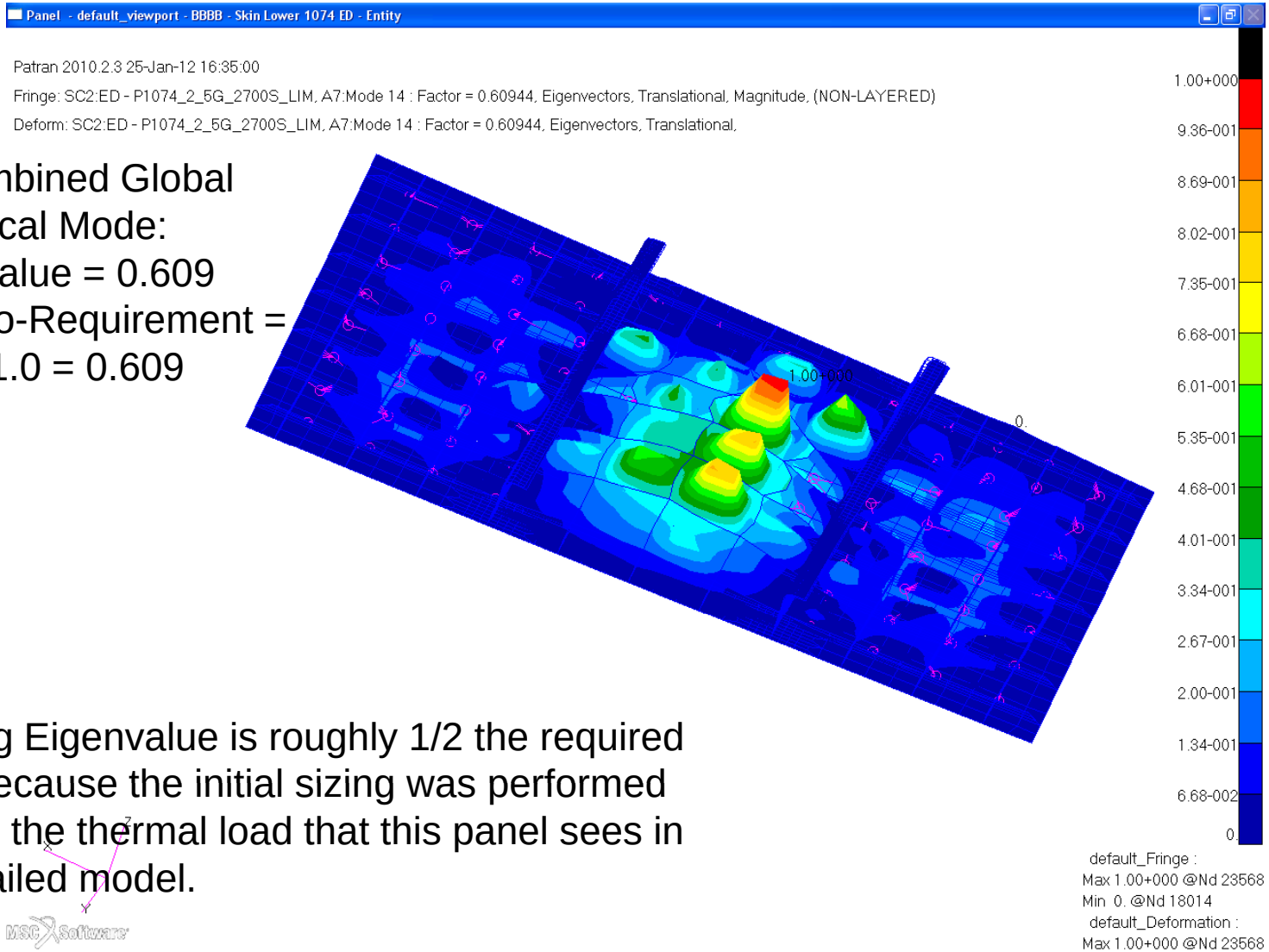

Buckling Eigenvalue is roughly 1/2 the required value because the initial sizing was performed with 1/6 the thermal load that this panel sees in the detailed model.

Approved for public release; distribution unlimited.

Buckling, Panel Analysis, 2.5G Lim 1.15+T=2700s

2nd Combined Global and Local Mode: Eigenvalue = 0.630

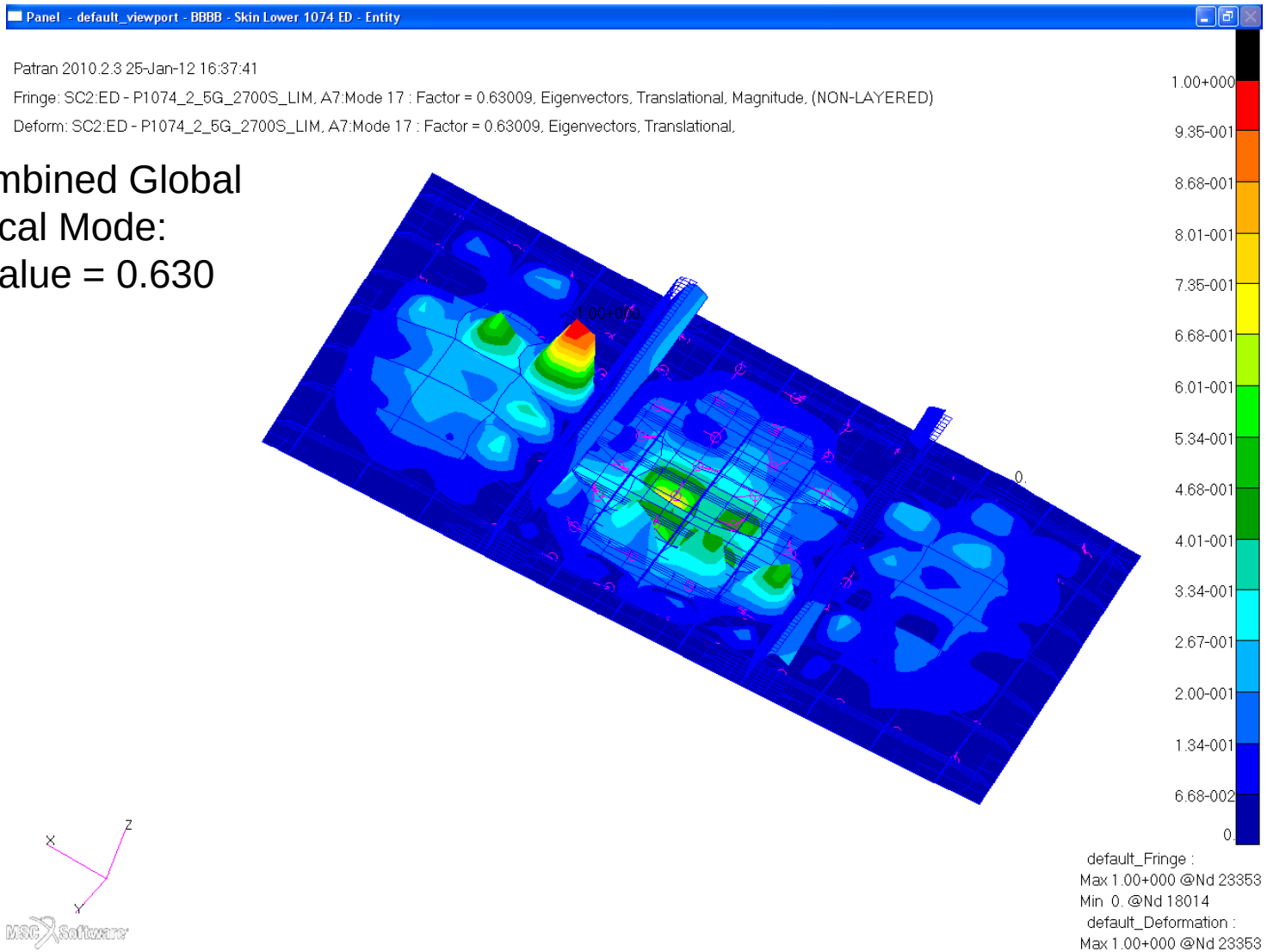

Approved for public release; distribution unlimited.

Buckling, Panel Analysis, 2.5G Lim 1.15+T=2700s

3rd Combined Global and Local Mode: Eigenvalue = 0.669

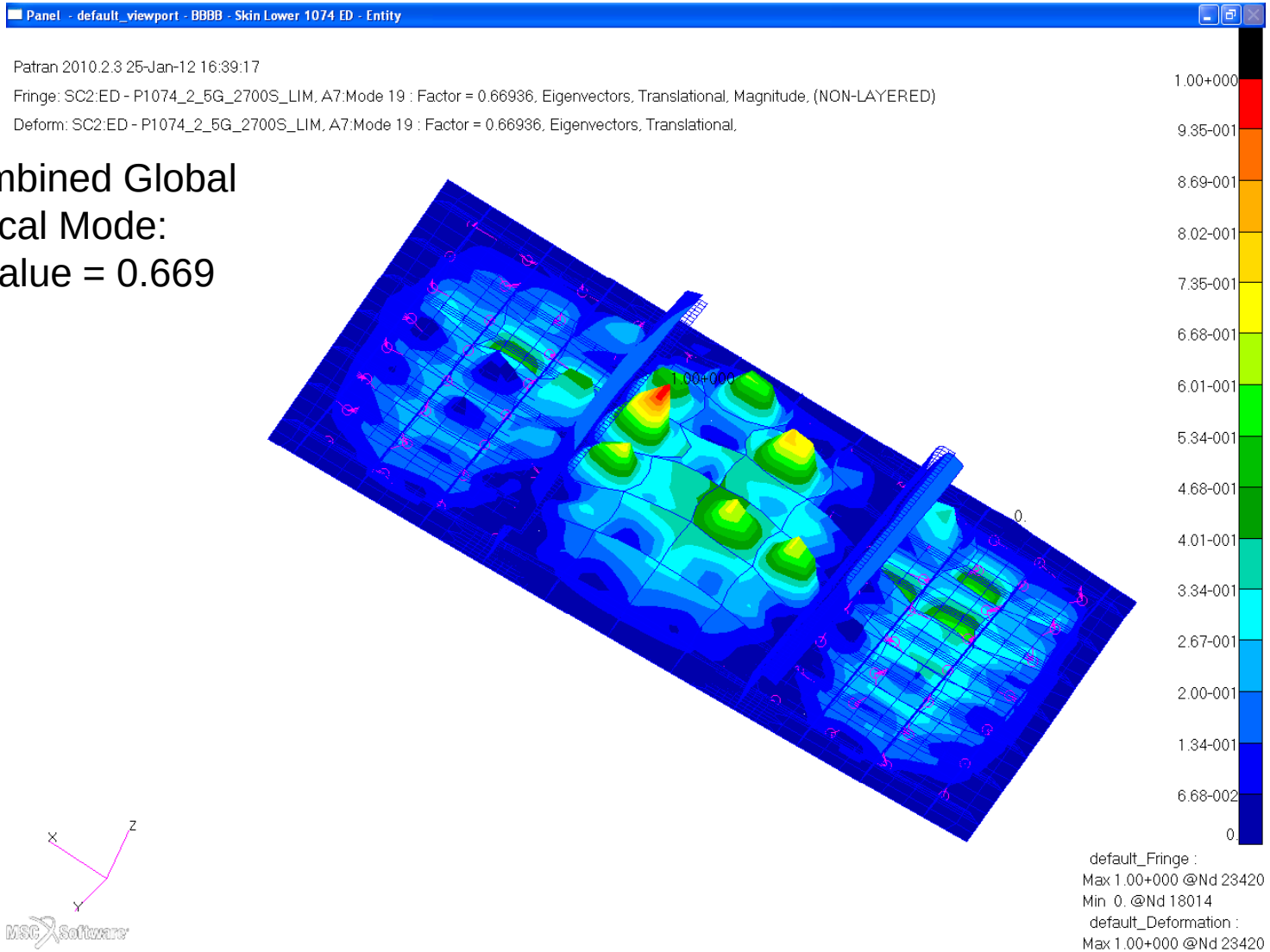

Approved for public release; distribution unlimited.

Bearing Analysis Combined Mechanical and Thermal T=2700s Loading Panel Analysis

Approved for public release; distribution unlimited.

Von Mises, Panel Analysis, 2.5G Ult 1.5+T=2700s Non-Linear

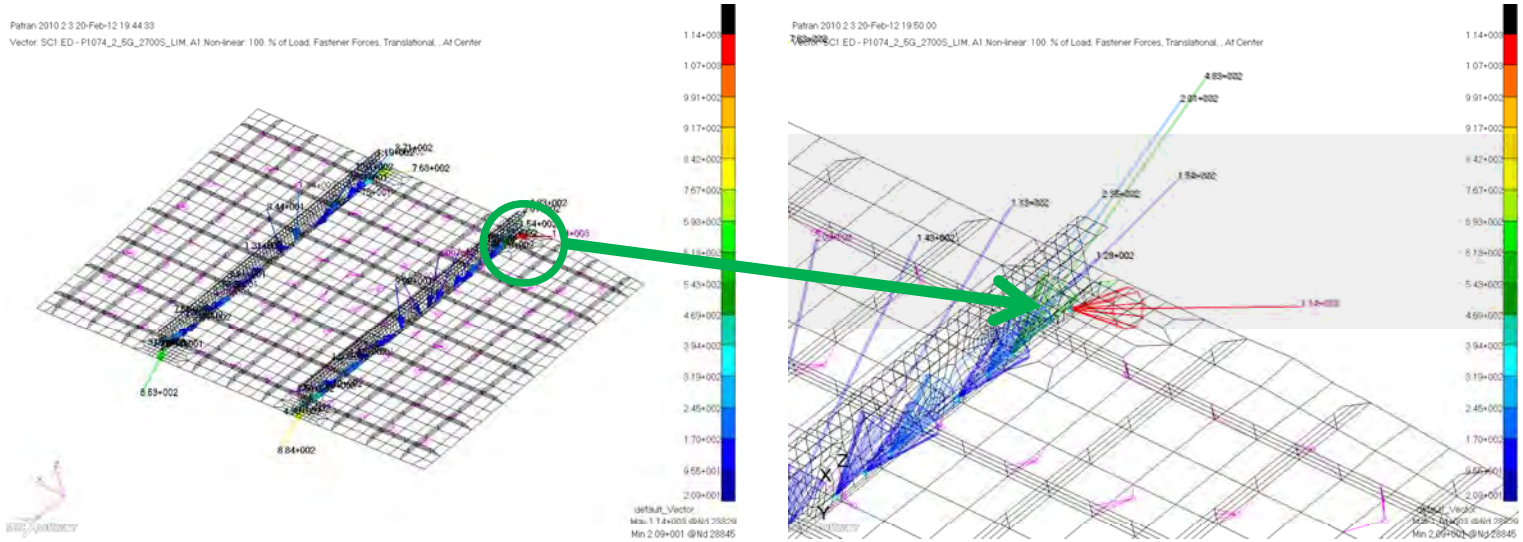

σ_{brg} = P/(d*t) = 1140 / (0.19*.063) = 95.2 ksi

MS = Allowable/Actual – 1 = 111/95.2 – 1 = 0.17

Approved for public release; distribution unlimited.

Thermal Loads Comparison T=2700s

Limit Edge Loads from Unit Cell Model

*Doesn't include internal loads

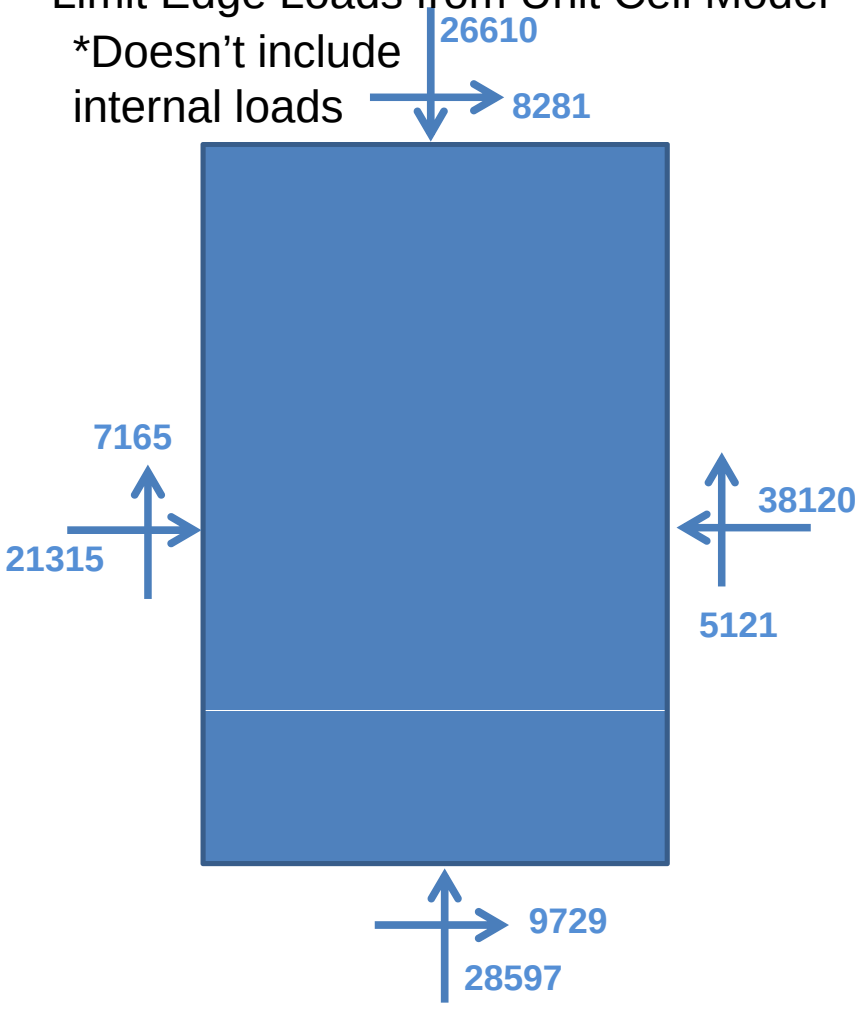

Limit Edge Loads from Hypersizer

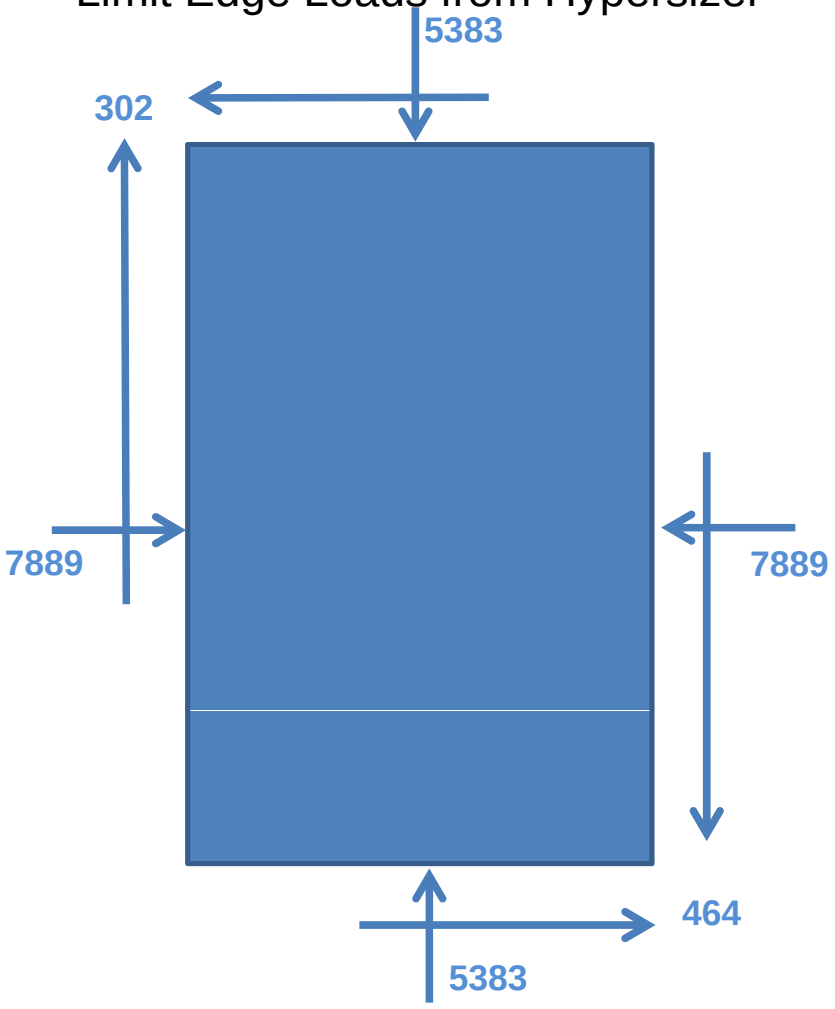

Initial thermal loads were based on Panel 2 thermal loads and reduced by 3.5 in proportion to Unit Cell Height

Approved for public release; distribution unlimited.

Margin of Safety Summary

Failure Mode	Solution Type	Thermal Load	Thermal F.S.	Mechanical Load	Mechanical F.S.	Allowable	Actual	Units	M.S./RR
Ultimate Material Failure	Non-Linear	T=2700s	1	2.5g	1.5	62.2	85.5	ksi	*-0.27*
Displacement	Non-Linear	T=2700s	1	2.5g	1.15	0.1	0.514	in.	*-0.81*
Buckling	Buckling	T=2700s	1	2.5g	1.15	1	.609	eigenvalue	*0.609*

- **Both severe underestimation of thermal loads during initial orthrogrid sizing and temperatures of 1470° F resulting in 36% of RT material allowables result in negative margins for static and buckling margins.**
- **Large normal displacements do not meet preliminary windward panel sizing criteria of 0.10". Non-Linear analysis reveals much higher deflections than Linear analysis (0.514” vs 0.25”) which is a result of such high temperatures.**
- **The maximum Von Mises stress is modest at 85.5 ksi occuring on an orthogrid stiffener. However, the temperature of this panel occur on a very steep portion of the material allowable thermal knockdown tables; roughly a 10% knock down for every 100 degrees.**
- **The buckling margin is very low due to the underestimation of thermal loads used for initial sizing resulting in 5” x 5” orthogrid pockets. A resizing with thermal loads 6x the initial loads would be required to achieve a buckling Ratio to Requirement > 1.0.**

Approved for public release; distribution unlimited.

PATRAN Database and NASTRAN Analysis Files

Approved for public release; distribution unlimited.

General Backup File Information

Location of files
Contact AFRL/RBSM Structural Sciences Center
WPAFB, OH, 45433

POC: Dr. S. Michael Spottswood, 937.904.6789, stephen.spottswood@wpafb.af.mil
PATRAN Database for Unit-Cell and Panel Models
Panel 4 r3.db

Flight Loads
Mach 7, +2.5g, symmetric pull up maneuver

Thermal
Temperature @
T = 60 sec, Maximum thermal gradient between panel skin and orthogrid stiffener
T = 90 sec, Maximum thermal gradient between panel and panel breaker
T = 900 sec, Maximum temperature
T = 2700 sec, Maximum thermal gradient between panel and substructure
T = 3450 sec, Maximum reverse thermal gradient

Boundary Conditions for Unit-Cell Model
Rigid Body Constraints

Approved for public release; distribution unlimited.

Linear Stress Analysis of Unit-Cell Model for 2.5G and Thermal (T=2700s)

Load Cases

UNITCELL

AAAA P1074_2_5g_T=2700s

2.5g * 1.0 (F.S.), Temp @ 2700s, Rigid body constraint

AAAA P1074_2_5g_Lim_T=2700s

2.5g * 1.15 (F.S.), Temp @ 2700s, Rigid body constraint

AAAA P1074_2_5g_Ult_T=2700s

2.5g * 1.5 (F.S.), Temp @ 2700s, Rigid body constraint

Analysis Files

P1074_Unit_Cell_2p5G_T2700s.dat

Results

P1074_Unit_Cell_2p5G_T2700s.xdb

631
Approved for public release; distribution unlimited.

Linear Stress Analysis of Unit-Cell Model for 2.5G only

Load Cases

UNITCELL

BBBB P1074_2_5g_Force_Moment

2.5g * 1.0 (F.S.), Rigid body constraints

BBBB P1074_2_5g_Force_Moment_Lim

2.5g * 1.15 (F.S.), Rigid body constraints

BBBB P1074_2_5g_Force_Moment_Ult

2.5g * 1.5 (F.S.), Rigid body constraints

Analysis Files

P1074_Unit_Cell_2p5G.dat

Results

P1074_Unit_Cell_2p5G.xdb

Approved for public release; distribution unlimited.

Linear Stress Analysis of Unit-Cell Model for Thermal only

Load Cases

UNITCELL

CCCC T=60s

Temp @ 60s, Rigid body constraint

CCCC T=90s

Temp @ 90s, Rigid body constraint

CCCC T=900s

Temp @ 900s, Rigid body constraint

CCCC T=2700s

Temp @ 2700s, Rigid body constraint

CCCC T=3540s

Temp @ 3540s, Rigid body constraint

Analysis Files

P1074_Unit_Cell_T60s.dat
P1074_Unit_Cell_T90s.dat
P1074_Unit_Cell_T900s.dat
P1074_Unit_Cell_T2700s.dat
P1074_Unit_Cell_T3540s.dat

Results

P1074_Unit_Cell_T60s.xdb
P1074_Unit_Cell_T90s.xdb
P1074_Unit_Cell_T900s.xdb
P1074_Unit_Cell_T2700s.xdb
P1074_Unit_Cell_T3540s.xdb

Approved for public release; distribution unlimited.

Linear Stress Analysis of Local Panel Model for 2.5G and Thermal (T=2700s)

Load Cases

LOCAL PANEL

ED - P1074_2_5g_2700s_Lim

2.5g * 1.15 (F.S.), Temp @ 2700s, Enforced displacements from Unit Cell at panel edges

ED - P1074_2_5g_2700s_Ult

2.5g * 1.5 (F.S.), Temp @ 2700s, Enforced displacements from Unit Cell at panel edges

Analysis Files

P1074_2p5G_2700s_Lim_ED_101.dat
P1074_2p5G_2700s_Ult_ED_101.dat

Results

P1074_2p5G_2700s_Lim_ED_101.xdb
P1074_2p5G_2700s_Ult_ED_101.xdb

Approved for public release; distribution unlimited.

Non-Linear Stress Analysis of Local Panel Model for 2.5G and Thermal (T=2700s)

Load Cases

LOCAL PANEL

ED - P1074_2_5g_2700s_Lim

2.5g * 1.15 (F.S.), Temp @ 2700s, Enforced displacements from Unit Cell at panel edges

ED - P1074_2_5g_2700s_Ult

2.5g * 1.5 (F.S.), Temp @ 2700s, Enforced displacements from Unit Cell at panel edges

Analysis Files

P1074_2p5G_2700s_Lim_ED_106.dat
P1074_2p5G_2700s_Ult_ED_106.dat

Results

P1074_2p5G_2700s_Lim_ED_106.dat
P1074_2p5G_2700s_Ult_ED_106.dat

Approved for public release; distribution unlimited.

Buckling Analysis of Local Panel Model for 2.5G and Thermal (T=2700s)

Load Cases

LOCAL PANEL

ED - P1074_2_5g_2700s_Lim

2.5g * 1.15 (F.S.), Temp @ 2700s, Enforced displacements from Unit Cell at panel edges

Analysis Files

P1074_2p5G_2700s_Lim_ED_105.dat

Results

P1074_2p5G_2700s_Lim_ED_105.xdb

Approved for public release; distribution unlimited.

Common Files

Unit Cell Files

P1074 Elements.bdf
P1074 Grids.bdf
P1074 RBEs.bdf
P1074 SPCs.bdf
P1074 TempLoads.bdf
P1074 Coords.bdf
P1074 Force.bdf

Panel Model Files

P1074 ED SPCs.bdf
P1074 ED Elements_2.bdf
P1074 ED Fasteners.bdf
P1074 ED Materials.bdf
P1074 ED RBEs.bdf
P1074 ED Grids.bdf
P1074 ED Forces.bdf
P1074 ED T2700s.bdf

Approved for public release; distribution unlimited.

Panel 4 (1074) Dynamic & Fatigue Analysis

January 31, 2012

Craig Masterson
314-232-9424
Craig.Masterson@boeing.com

Approved for public release; distribution unlimited.

Panel 1074 Dynamic Analysis

- Methods and Approach
- Analysis Assumptions
- Finite Element Model and Boundary Conditions
- Results
  - Modal
  - Response
  - Fatigue
  - Flutter
- Lessons Learned
- Summary

639
Approved for public release; distribution unlimited.

Panel 1074 Location

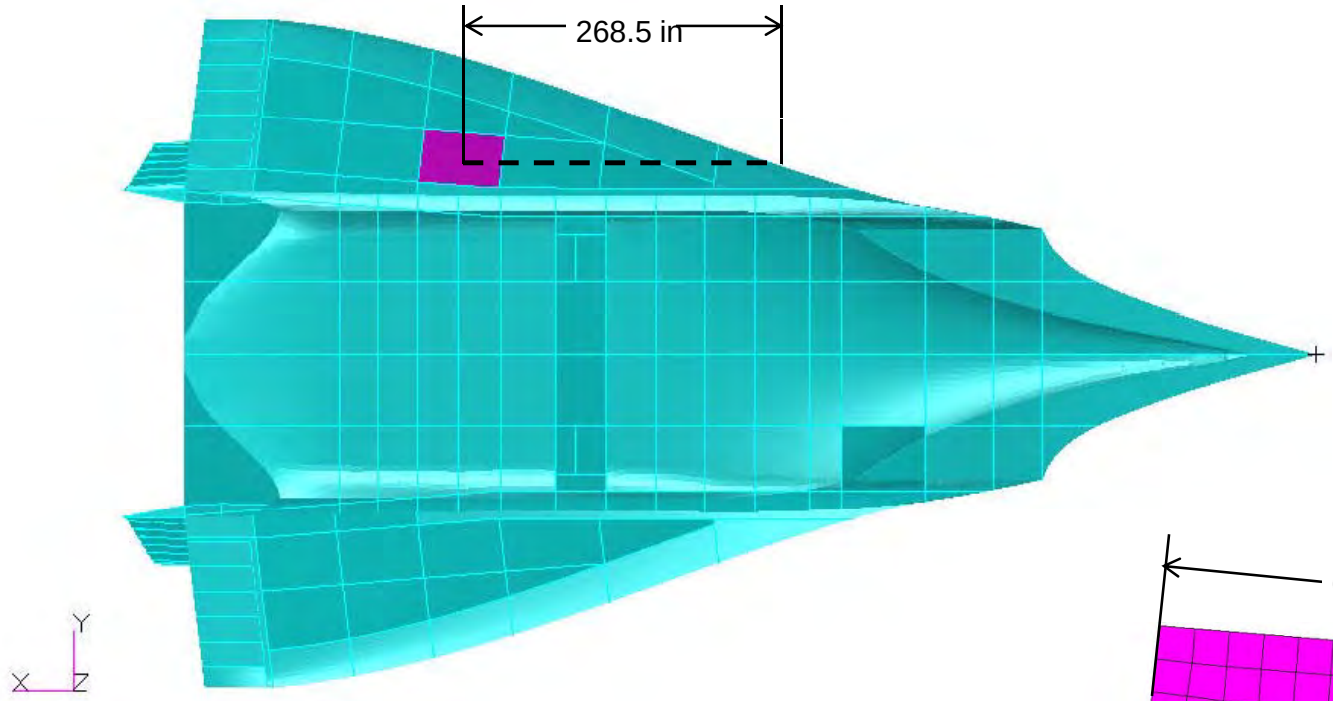

Bottom View of Vehicle

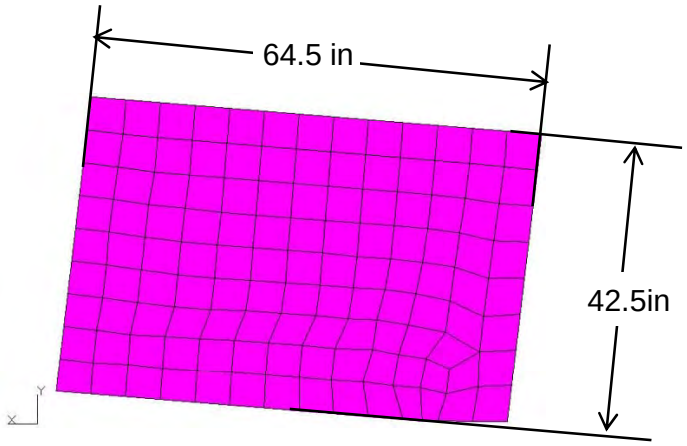

640
Approved for public release; distribution unlimited.

Unit Cell Model

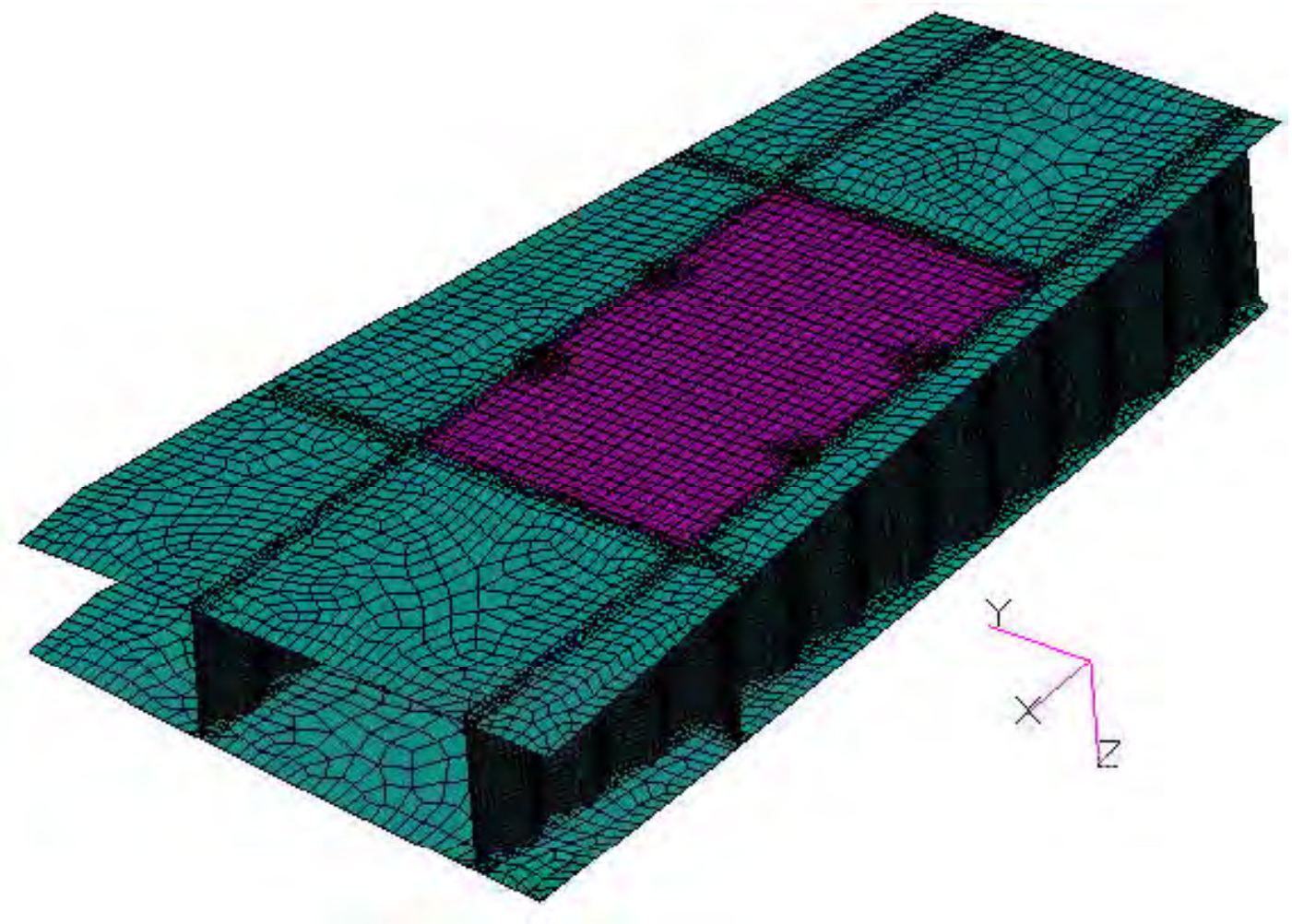

641
Approved for public release; distribution unlimited.

Panel 1074

- **Panel 1074 has a 0.050in acreage skin with 0.070in pad-up at skin to substructure fastened joints**
- **Panel stiffeners were sized to limit out of plane deformation and are roughly 3.5in tall with a 1.5in flange at 0.063in thick**
- **Orthogrid spacing is uniform in both direction at 5.625in**
- **Orthogrid stiffeners running in x-dir are 0.085in thick, y-dir stiffeners are 0.070in thick**
- **As a lesson learned from panel 780, mesh density is finer near panel stiffener terminations due to high stress gradient at that location**

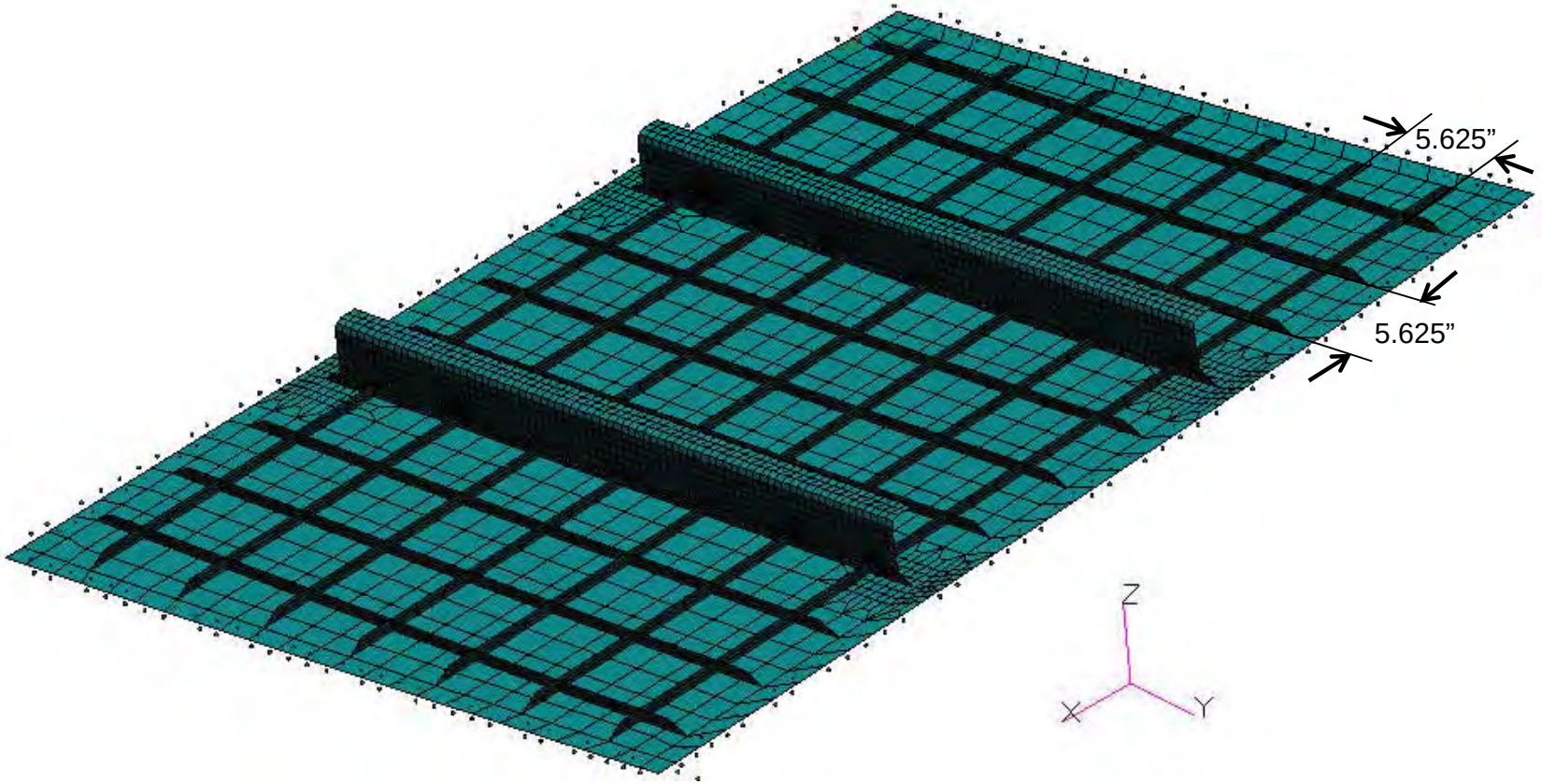

Approved for public release; distribution unlimited.

Fatigue Analysis Approach

- **Use Mil-hd-bk 5 Inconel 718 constant amplitude data**
- **Adjust for temperature and stress ratio if applicable**
- **Calculate design feature $k_t\sigma$ – holes, welds, radii**
- **Post-process results – references stress value**
- **Calculate Acoustic Margins – Compare predicted RMS Stress (KtS) to RMS Allowable (Endurance Limit)**
- **Assembly stress spectrum – Include maneuver loads, temperature for ground-air-ground (GAG) Cycles**
- **Calculate thermal-mechanical fatigue margins**
- **Perform acoustic damage (Dynamic Cycles) separate***
- **Calculate Total Fatigue Life – Combined Damage***

*A total fatigue life based on combined damage accumulation was not calculated for this panel
Margin of safety calculations will show panel is dominated by thermal-mechanical cyclic fatigue

643
Approved for public release; distribution unlimited.

General Fatigue Analysis Assumptions

- **Thermal-mechanical fatigue analysis was not performed for panel 1074 due to negative margins for static conditions**
- **A combined total fatigue life based on accumulated damage from aero-acoustic loads and cyclic thermal-mechanical fatigue was not performed for this panel (fatigue life dominated by thermal-mechanical stress)**
- **Thermal exposure effect on Fty is proportional to temperature effect on fatigue allowable**

644
Approved for public release; distribution unlimited.

Analysis Summary Table

Analysis Type	Preload	Load	Boundary Conditions	Output	Solution File(s)
Normal Modes (SOL 103)	None	Thermal (t=900s) Material Property Only	SPC at 5 nodes restricting rigid body motion and global vibration modes	> Normal Modes and Mode Shapes > Provides frequency range of interest for SOL 111	sol103_p1074_unit_cell_t900s_spc103.xdb
Non-linear Static (SOL 106)	None	Thermal (t=900s) Material + Load	SPC at 5 nodes restricting rigid body motion and global vibration modes	> Non linear stress and displacement > Preload for SOL111 > Stress results used as mean stress in fatigue calculations	panel4_sol106_0131-03_t900s.xdb
Frequency Response (SOL 111)	SOL 106	Thermal (t = 900s) Material Property Only	SPC at 5 nodes restricting rigid body motion and global vibration modes	> RMS stress	panel4_sol106_0131-03_t900s.MASTER panel4_sol106_0131-03_t900s.dball panel4_sol111_0131-06.xdb
Flutter (SOL 145)	None	Thermal (t = 900s) Material Property Only	SPC at 5 nodes restricting rigid body motion and global vibration modes	> Damping and modal frequency vs. velocity	P4UCt_XFlow_Temp900s_15Mds_M5to7_k1_32p5k.dat

645
Approved for public release; distribution unlimited.

Unit Cell Boundary Conditions

Linear Static Solution Boundary Conditions

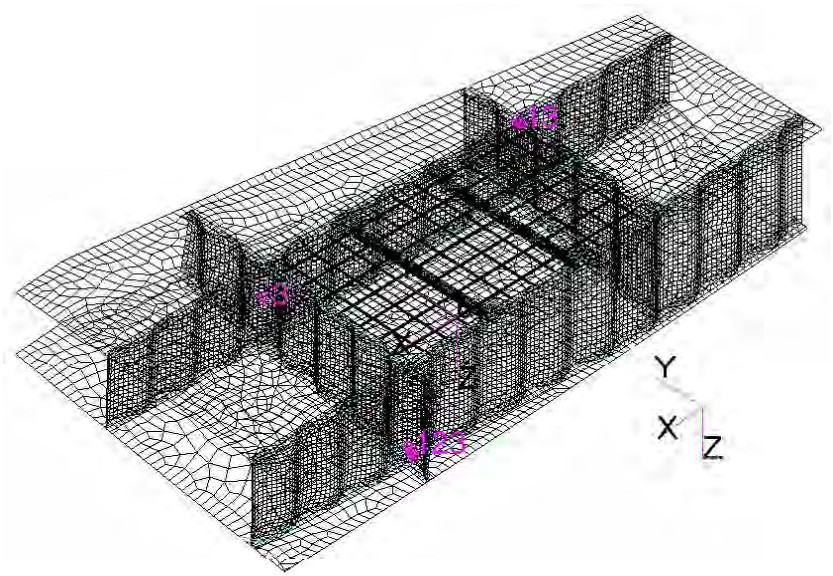

Constrained at 3 nodes on keel webs to prevent rigid body motion

Frequency Domain Boundary Conditions

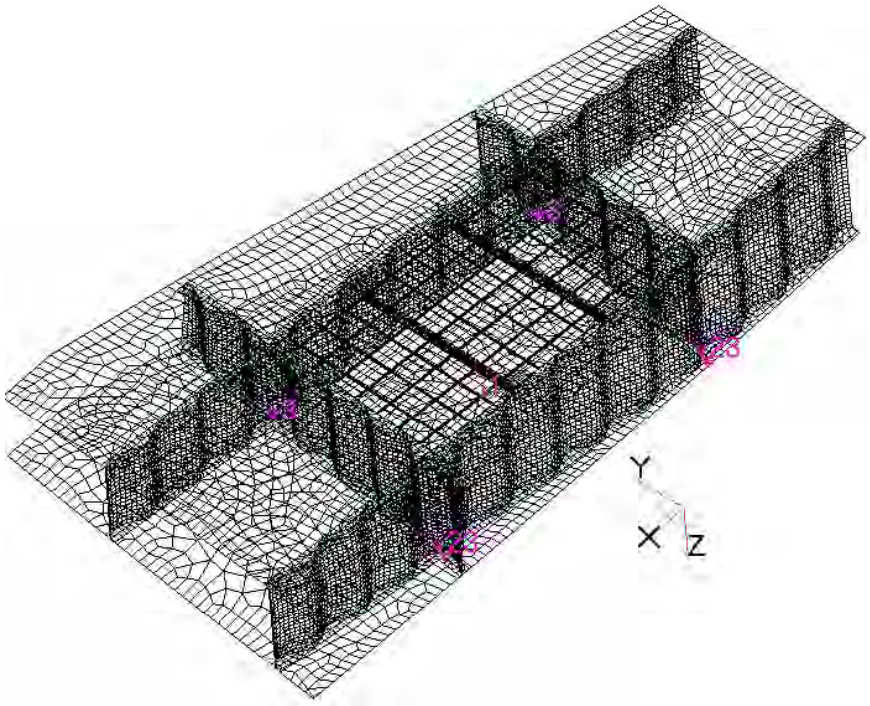

Constraints eliminate global vibration modes
- 4 frame nodes constrained in global Z
- 2 frame nodes constrained in global Y
- 1 upper skin node constrained in global X

646
Approved for public release; distribution unlimited.

MODAL ANALYSIS

647
Approved for public release; distribution unlimited.

SOL 103 Documentation

- **Preload**
  - None
- **Material Properties**
  - Inconel properties at mapped temperatures for t=900s thermal load
- **Boundary Conditions**
  - SPCs at 5 grids to prevent rigid body motion and global modes
- **SOL 103**
  - Group: ”AAAA - Panel 4 Unit Cell_NoMPCs”
  - Input File: SOL103_P1074_Unit_Cell_T900s_SPC103.dat
  - Results File: SOL103_P1074_Unit_Cell_T900s_SPC103.xdb

```
$ Normal Modes Analysis, Database
SOL 103
CEND
$ Direct Text Input for Global Case Control Data
ECHO = NONE
SUBCASE 3
$ Subcase name : CCCC T=900s
   SUBTITLE=CCCC T=900s
   SPC = 2
   METHOD = 1
   TEMPERATURE(MATERIAL) = 126
   VECTOR(PLOT,SORT1,REAL)=ALL
   SPCFORCES(PLOT,SORT1,REAL)=ALL
BEGIN BULK
$ Direct Text Input for Bulk Data
PARAM    POST    0
PARAM   PRTMAXIM YES
PARAM    WTMASS .0026
$
EIGRL    1      .1      1000.    15      0
MASS
$$$$$ CFAST TOLERANCE
swldprm,projtol,0.05
$$$$
include '.\inputFiles\P1074 Elements NoMass.bdf'
include '.\inputFiles\P1074 Grids.bdf'
$include 'P1074 RBEs.bdf'
include '.\inputFiles\P1074 SPCs.bdf'
include '.\inputFiles\P1074 TempLoads.bdf'
include '.\inputFiles\P1074 Coords.bdf'
$
```

Excerpt of SOL 103 Nastran Deck

Approved for public release; distribution unlimited.

SOL 103 Results

- **Modal solutions were run at various temperatures to see how temperature affected modal frequencies**
- **The maximum temperature case (t=900s) is of most interest for frequency response because it is in the envelope of maximum dynamic pressure, Q**

Temperature Case	Time (sec)	Skin Temp. (˚F)	Mode 1 Freq. (Hz)	Mode 2 Freq. (Hz)	Mode 3 Freq. (Hz)
Max Gradient between skin and orthogrid	60	416	83.3	95.2	101.5
Max gradient between skin and panel stiffener	90	462	83.0	94.9	101.1
Maximum Temperature	900	1480	73.8	84.2	89.3
Maximum Skin to substructure gradient	2700	1470	74.0	84.3	89.2
Maximum reverse gradient	3540	474	81.5	93.1	99.1

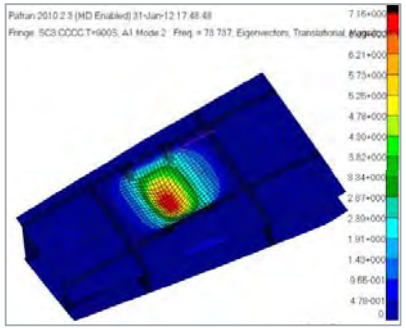

Mode 1: Freq = 73.8 Hz

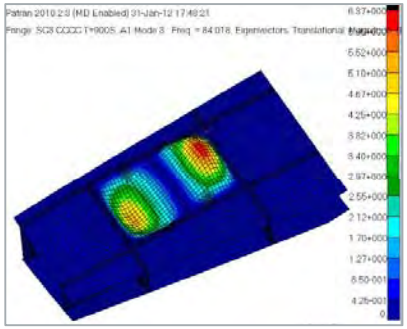

Mode 2: Freq = 84.2 Hz

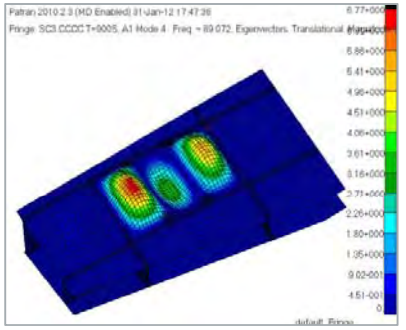

Mode 3: Freq = 89.3 Hz

Approved for public release; distribution unlimited.

AERO-ACOUSTIC FATIGUE

650
Approved for public release; distribution unlimited.

Acoustic Fatigue Analysis Approach

- **Use Mil-hdbk-5 Inconel 718 Constant Amplitude Data**
  - Adjust for Temperature and Stress Ratio
- **Calculate Design Feature Ktσ – Holes, Welds, Radii**
- **Post-process results – references stress value**
- **Calculate Margins – Compare predicted RMS Stress (KtS) to RMS Allowable (Endurance Limit)**

651
Approved for public release; distribution unlimited.

Acoustic Fatigue Analysis Assumptions

- **Mechanical Loads negligible during max Q flight envelope**
  - Limit Case of 1G * 1.15 did not affect stress results
- **Kt = 3.0 for filled fastener hole**
- **Thermal exposure effect on Fty is proportional to temperature effect on fatigue allowable**
- **Stress concentrations at orthogrid stiffener terminations will be ignored due to the time constraints of this study**

652
Approved for public release; distribution unlimited.

Dynamic Model - Loading & Boundary Conditions

- Preload
  - SOL 106: Panel4_SOL106_0131-03_t900s.dat
- Material Properties
  - Inconel properties at mapped temperatures for t=900s thermal load
- Boundary Conditions
  - SPCs at 5 points (Nodes: 1, 534, 3061, 5341, 20404)
- Acoustic Loads (3 - Zones)
  - Flow Direction – Uncorrelated (Panels vibrate independently)
  - Cross Flow – Fully Correlated (Panel vibration is in phase)
  - 1 psi plane wave acoustic load (Orthogonal to panel)
  - 0.1 to 250hz forcing frequency
  - Damping function of frequency
- SOL 111
  - Input Files: Panel4_SOL111_0131-06.bdf
  - Results File: Panel4_SOL111_0131-06.xdb

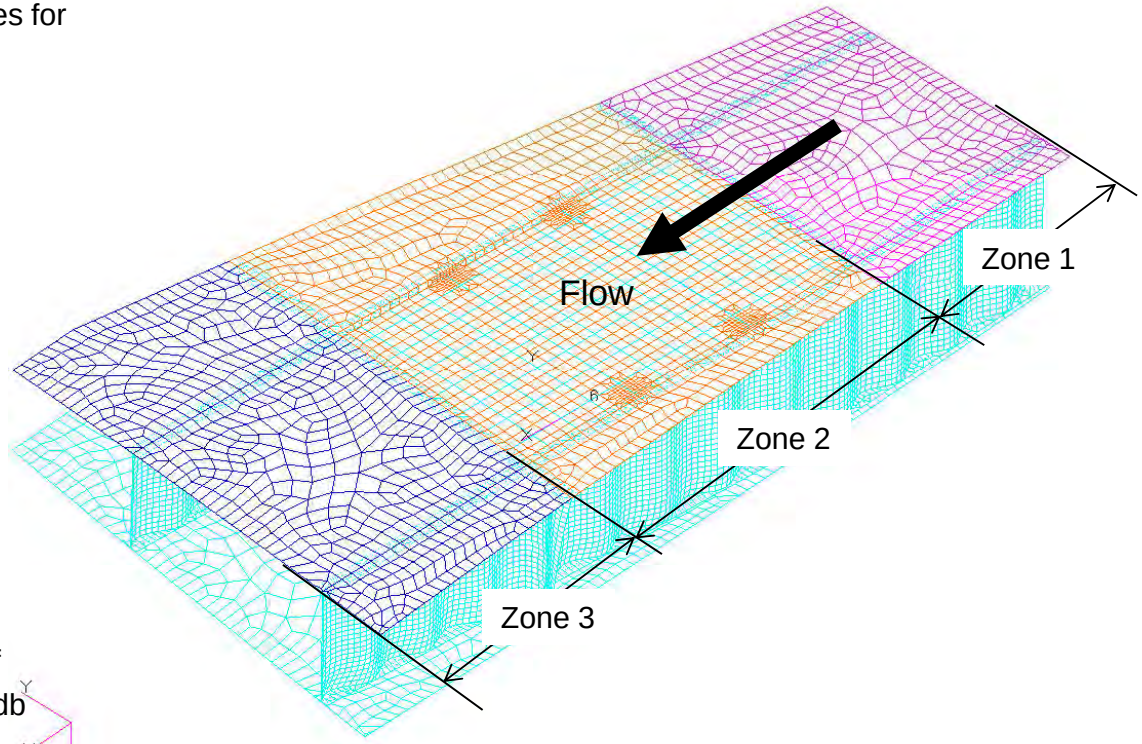

653
Approved for public release; distribution unlimited.

Acoustic Response – RMS Displacement Result

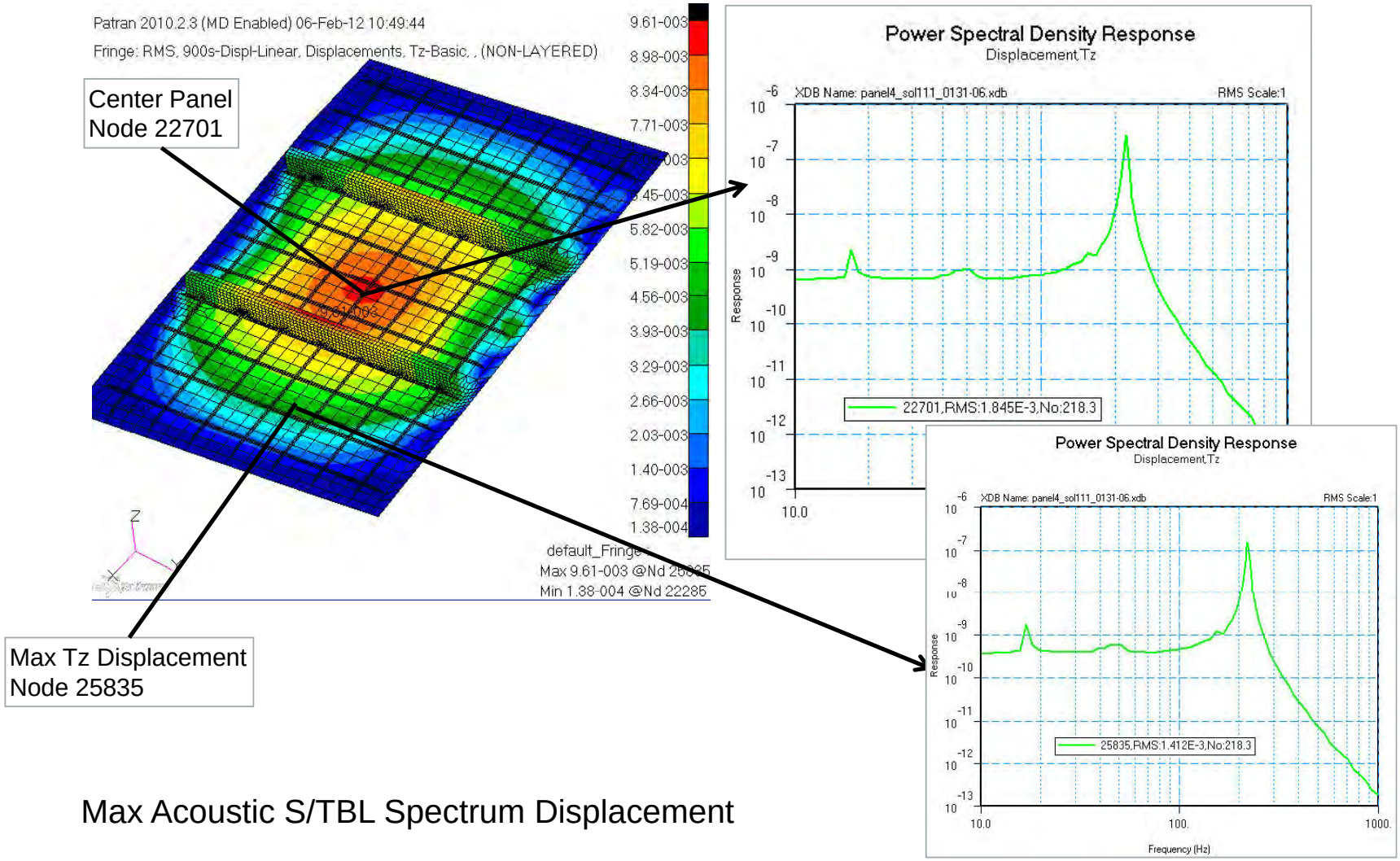

Max Acoustic S/TBL Spectrum Displacement

Approved for public release; distribution unlimited.

Unit Cell, Thermal Only (t900s), Acoustic Response – RMS Von Mises Stress Result

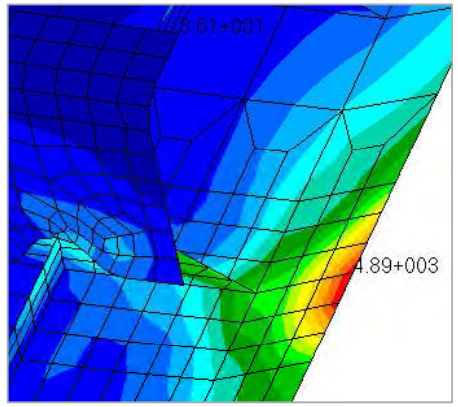

Large out of plane displacement near area of high stress

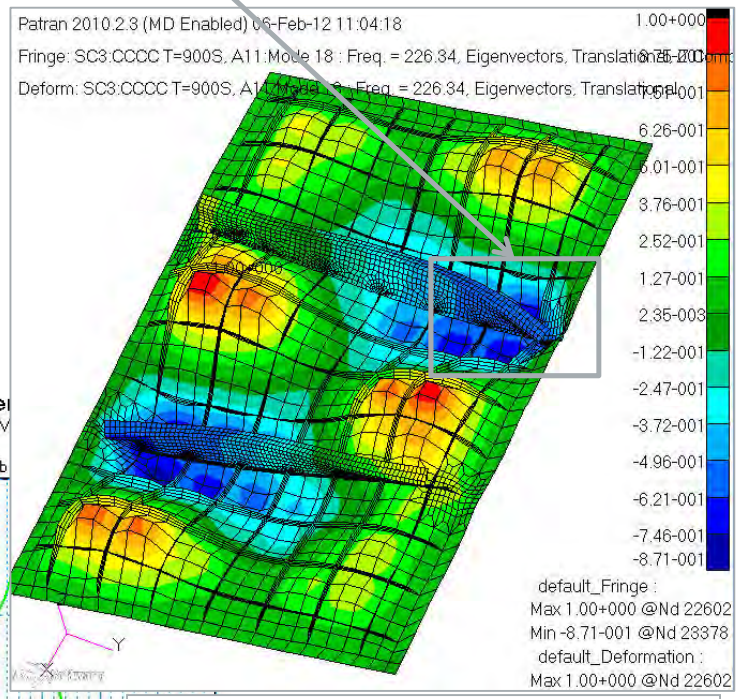

Nearest Mode Shape at 226Hz, Z-direction

Max Acoustic S/TBL Spectrum Von Mises Stress Plot

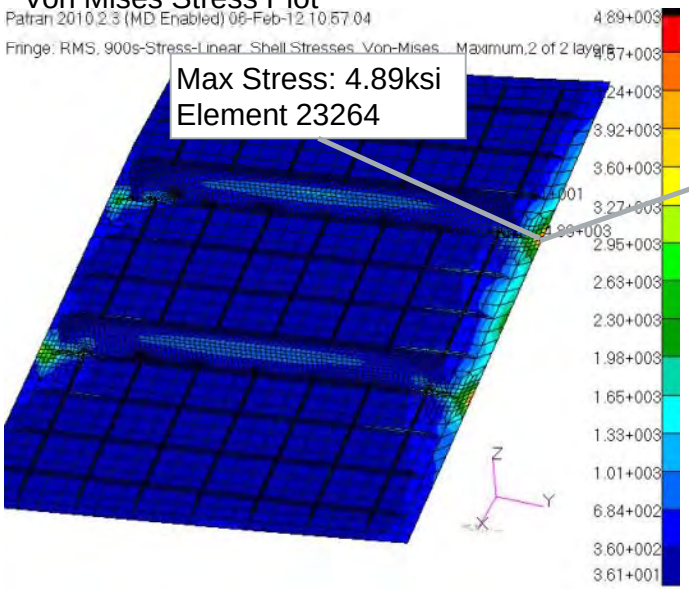

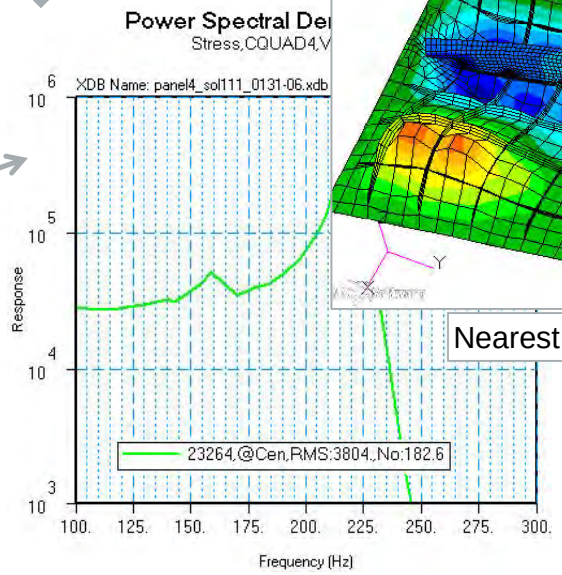

Approved for public release; distribution unlimited.

RMS Stress Allowable - Inconel 718

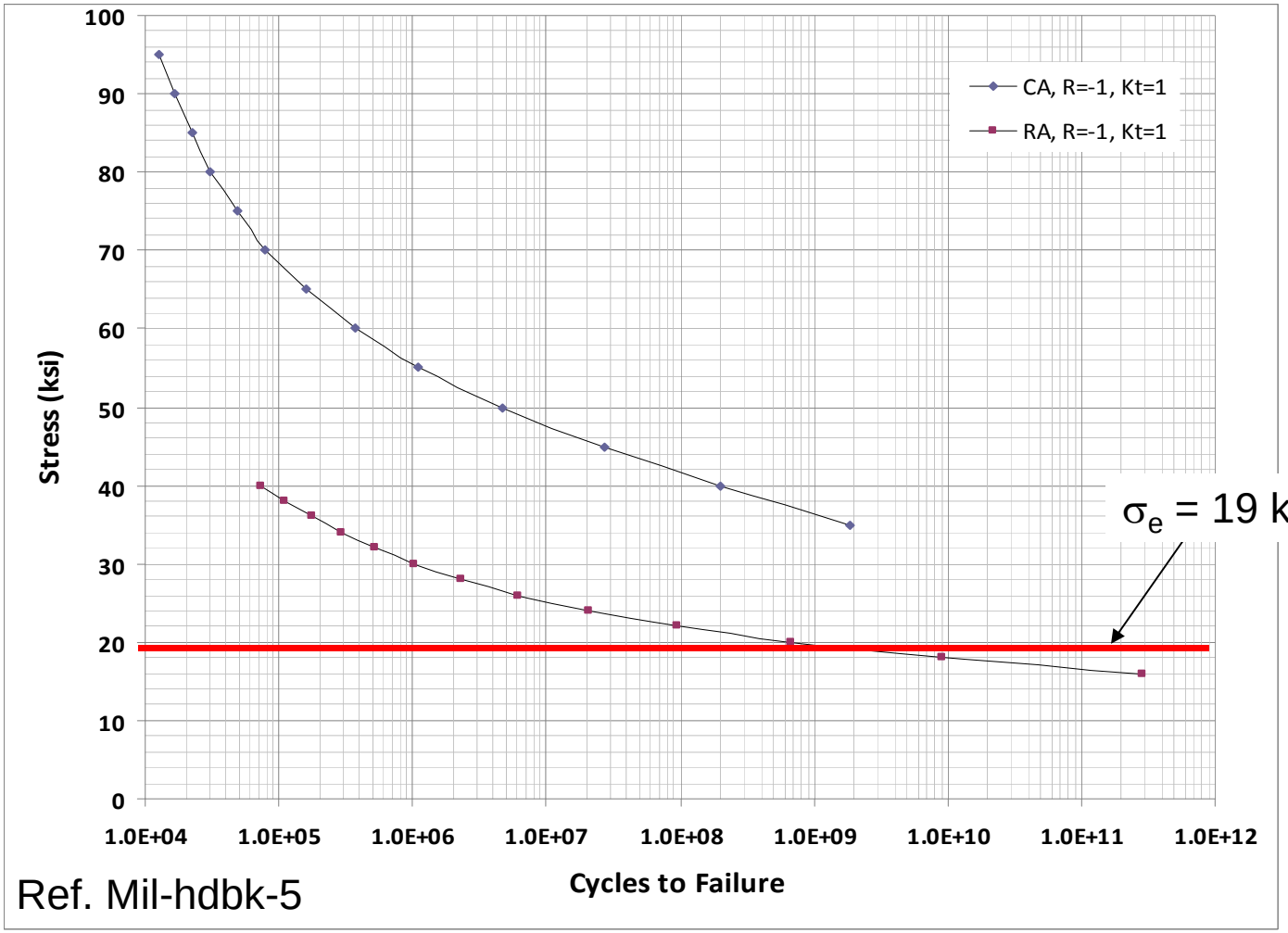

Approved for public release; distribution unlimited.

MMPDS – Inconel 718 – Fty v. Temp

- **Assume fatigue allowable follows trend of Fty as a function of temperature exposure**

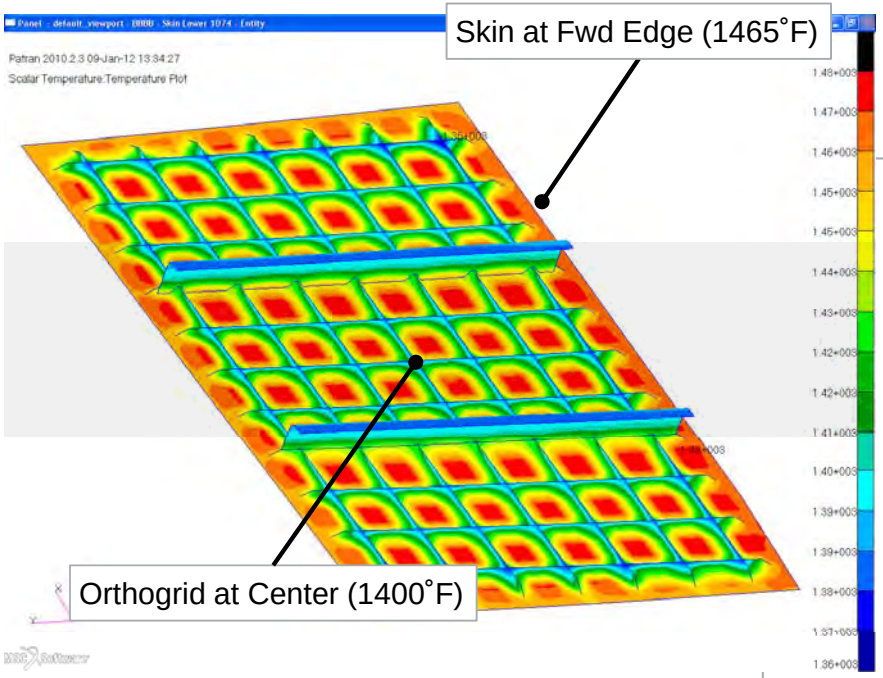

Applied Thermal Load for maximum panel to substructure gradient (t=900s)

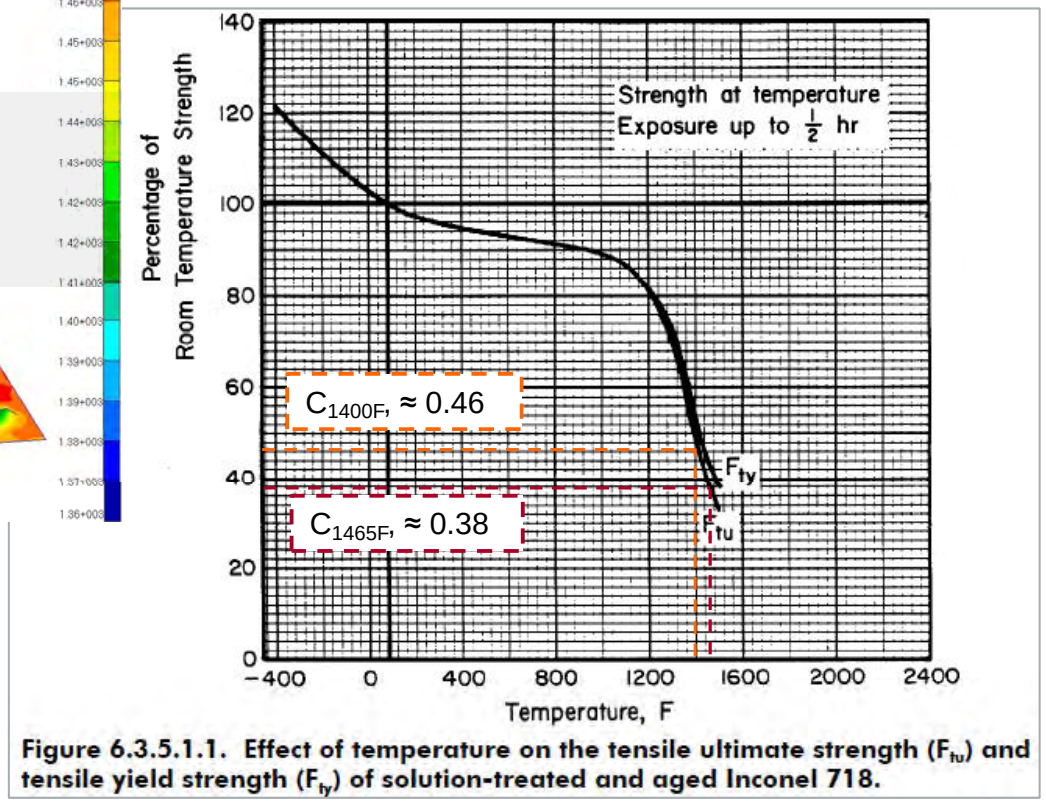

Figure 6.3.5.1.1. Effect of temperature on the tensile ultimate strength (F_{tu}) and tensile yield strength (F_{ty}) of solution-treated and aged Inconel 718.

657
Approved for public release; distribution unlimited.

MMPDS – Inconel 718 – S/N Curve

- **For locations with Kt > 1.5 use Fig 6.3.5.1.8.c (Best-fit S/N curves for un-notched Inconel 718 sheet at 1400F)**

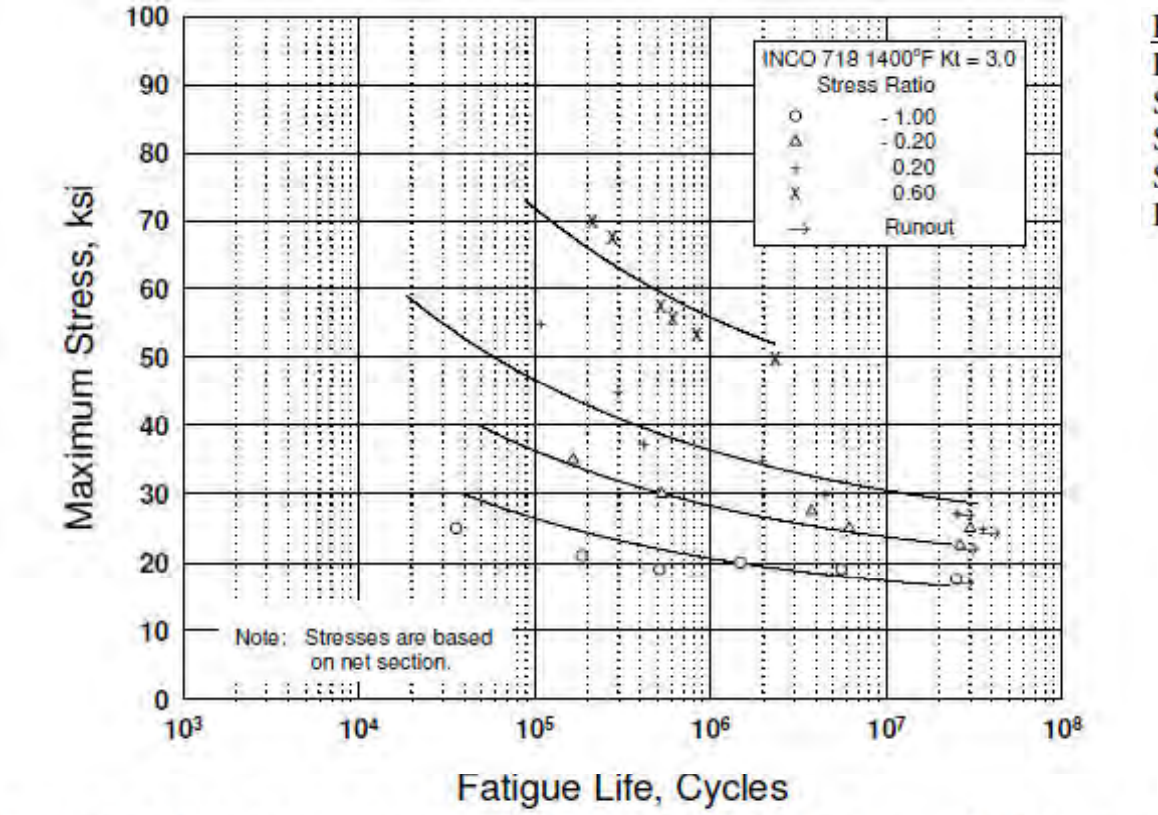

Equivalent Stress Equation:

$\text{Log } N_f = 10.29 - 4.02 \text{ Log } (S_{eq} - 20)$

$S_{eq} = S_{max}(1\text{-}R)^{0.62}$

Std. Error of Estimate, Log (Life) = 0.442

Standard Deviation, Log (Life) = 0.717

$R^2 = 62.0\%$

Figure 6.3.5.1.8(e). Best-fit S/N curves for notched, K_t = 3.0, Inconel 718 sheet at 1400°F, long transverse direction.

Approved for public release; distribution unlimited.

Unit Cell Model, Panel Results, Frequency Response, Thermal Only Preload (t=900s)

- **RMS stress plot shows peak stress at skin to substructure joint near termination of panel stiffeners**

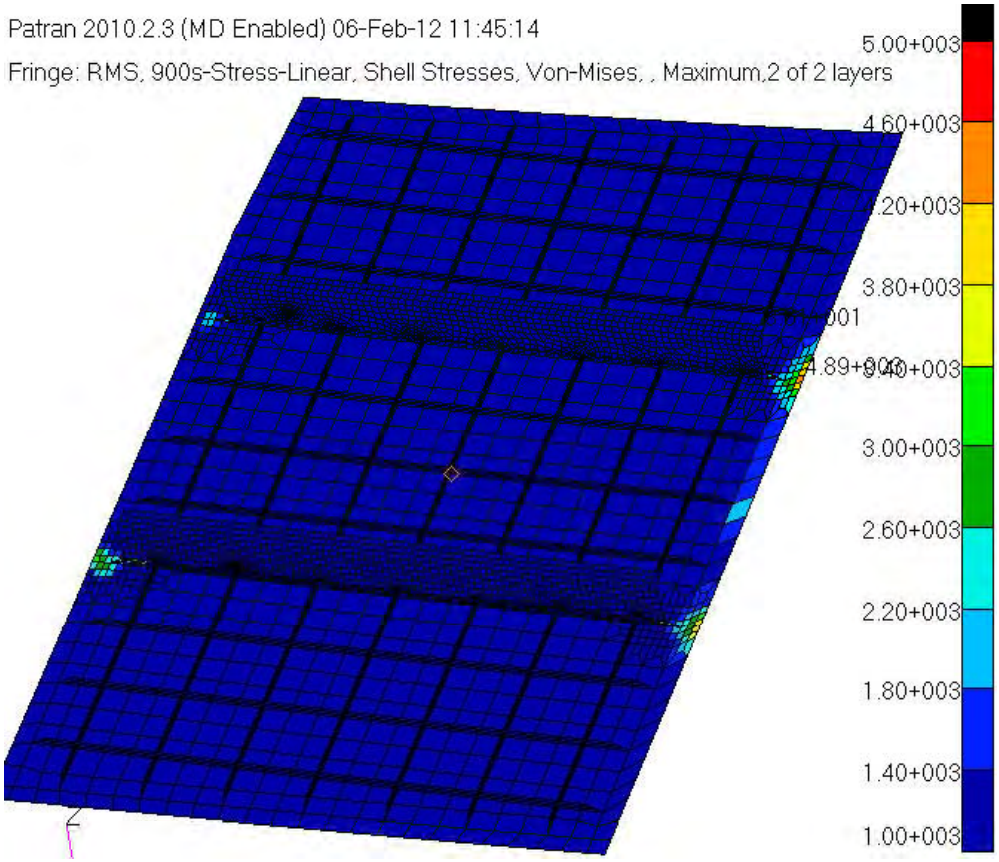

RMS Von Mises Stress Plot (element average) =4.89 ksi

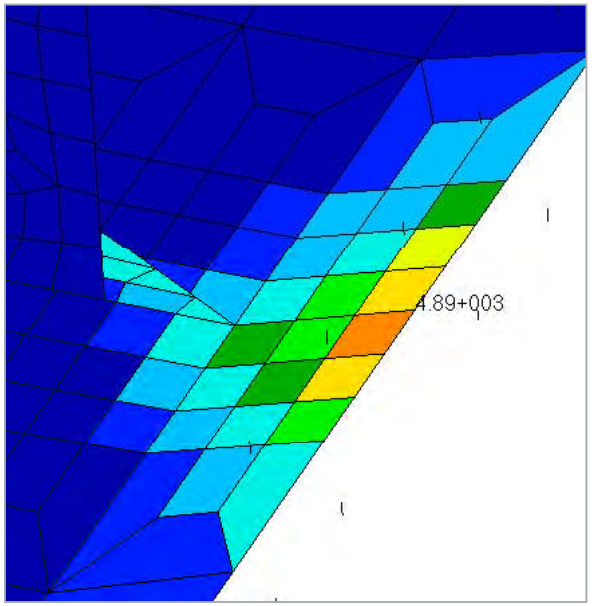

RMS Von Mises Stress (element average) =4.89 ksi

Approved for public release; distribution unlimited.

Skin to Substructure Fastener Hole near Panel Stiffener Termination

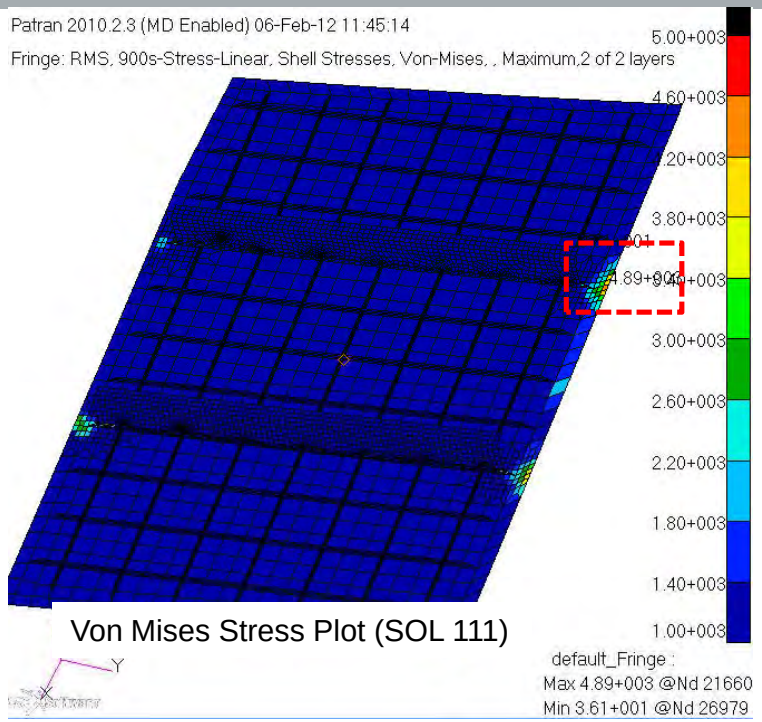

Von Mises Stress Plot (SOL 111)

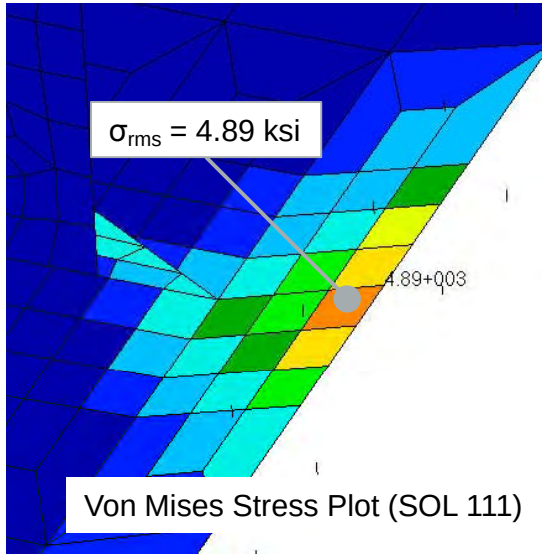

Von Mises Stress Plot (SOL 111)

$K_t = 3.0 \quad R = 0.86 \quad T = 1465^{\circ}F$

$$k_t\sigma'_e = \frac{\sigma_e \cdot C_T \cdot C_R}{k_t} = \frac{19.0 \cdot 0.38 \cdot 2.36}{3.0} = 5.68ksi$$

$$MS = \frac{k_t\sigma'_e}{\sigma_{rms}} - 1 = \frac{5.68}{4.90} - 1 = \underline{\underline{0.16}}$$

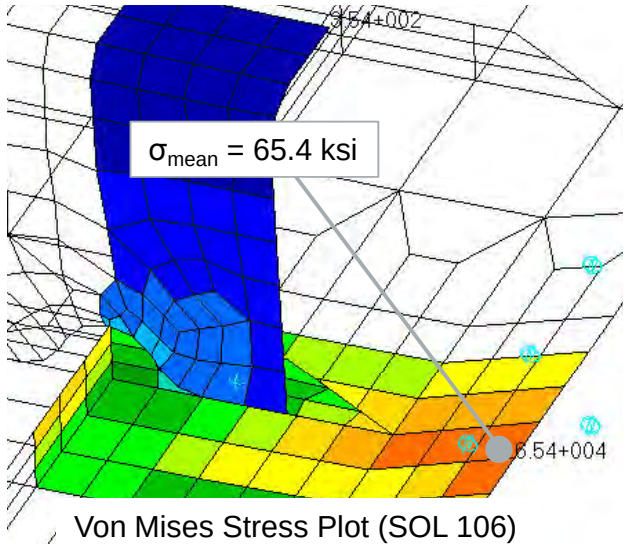

Von Mises Stress Plot (SOL 106)

Approved for public release; distribution unlimited.

Acoustic Fatigue Summary Table

Location of Stress Concentration	Stress Conc. Type	Struct. Temp (˚F)	Temp. Factor	Stress Ratio	Stress Ratio Factor	Kt	Allowable Stress* (ksi)	RMS Stress Result (ksi)	Mean Stress Thermal Load (ksi)	MS
Panel Skin to Substructure Near Stiffener Termination	Filled Holed	1465	0.38	0.86	2.36	3.0	5.7	4.89	65.4	0.16

* Baseline allowable = 19ksi (Kt=1,R=-1, T=RT)

Results file(s): panel4_SOL106_0131-03_t900s.dat
panel4_sol111_0131-06.xdb

•RMS stress from acoustic loads are small in magnitude compared to the thermal stress at t=900s.

$$R = \frac{-\sigma_{rms} + \sigma_{mean}}{\sigma_{rms} + \sigma_{mean}}$$

661
Approved for public release; distribution unlimited.

Aeroacoustic Fatigue Conclusions

- **Panel 1074 Conclusions**
  - Stresses due to acoustic response are negligible except at the skin to substructure joint near the panel stiffener termination
  - High temperatures drive down acoustic fatigue allowable stress significantly
  - High thermal stress (mean stress) makes stress ratios positive, increasing the RMS allowable stress
  - Due to the counteracting effects of positive stress ratios and material property knockdown, the max RMS stress of 4.89 gives a margin of safety of 0.16

662
Approved for public release; distribution unlimited.

THERMAL-MECHANICAL FATIGUE

663
Approved for public release; distribution unlimited.

Fatigue Analysis Approach for Thermal Mechanical Loads

- **Panel 1074 was not analyzed for thermal-mechanical fatigue due to the negative margins for static load conditions**

664
Approved for public release; distribution unlimited.

PANEL FLUTTER ANALYSIS

665
Approved for public release; distribution unlimited.

Trajectory – Design Conditions of Interest

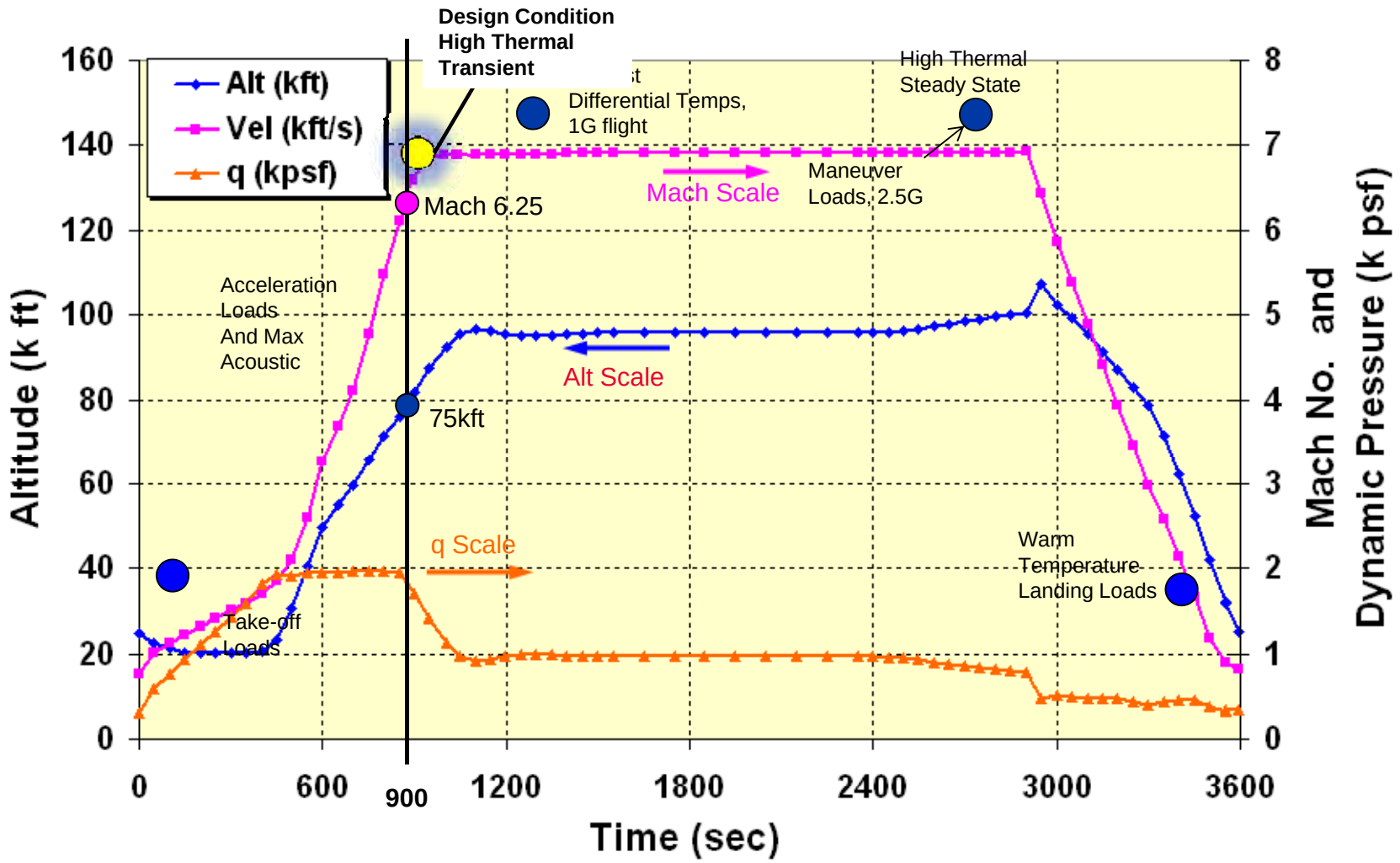

Approved for public release; distribution unlimited.

Panel Flutter Analysis for Hypersonic Aircraft

- **Two analysis methods are summarized:**
  - Empirically Derived Criteria
    - Fast
    - Approximate
    - Historically used on Tactical Aircraft Programs
  - High Fidelity Aeroelastic Analysis
    - More resource intensive
    - May address particular physics more directly
    - Relatively new technology

Approved for public release; distribution unlimited.

Empirical Panel Flutter Design Curves

- **Large MS indicated for panel 1074**
- **Panel temperature of 1450˚F**
- **Design curves intended for flow at Mach 3 or less**
- **Panel flutter driven by stiffness, aspect ratio, and thickness**

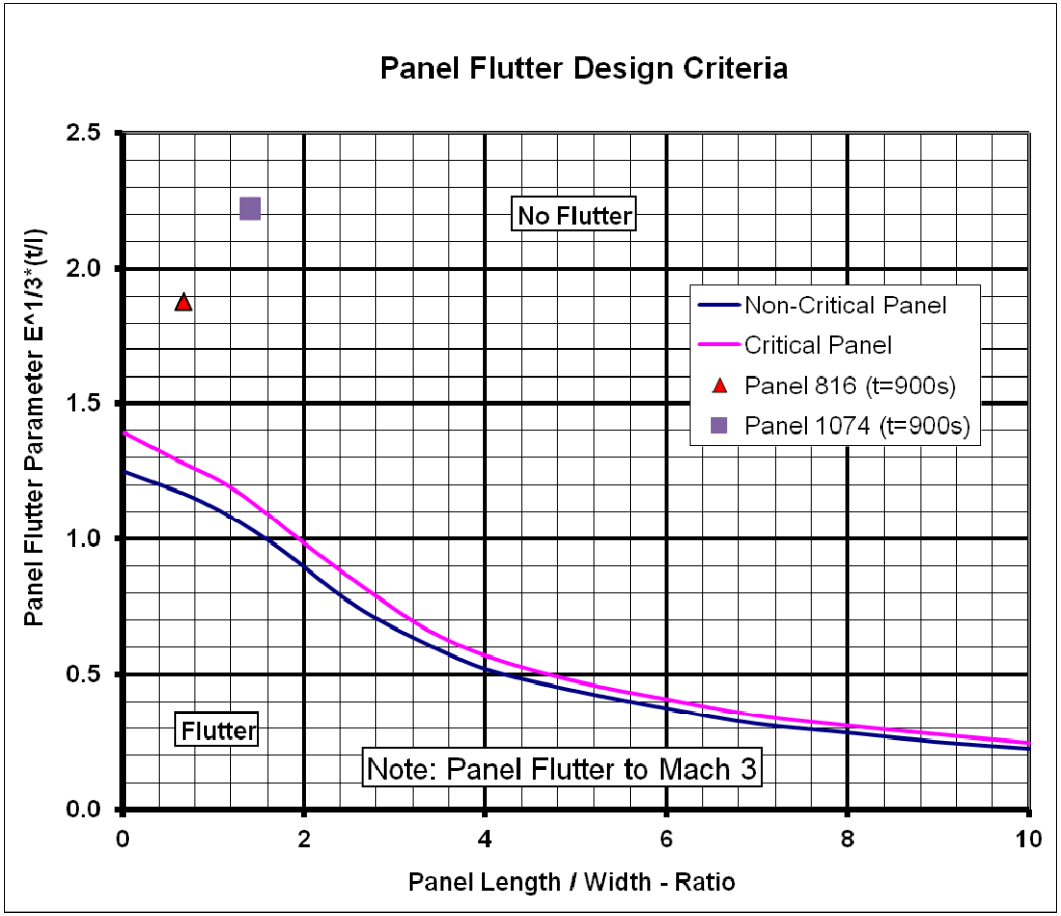

Note: Length is in flow direction

Approved for public release; distribution unlimited.

Empirically Derived Panel Flutter Design Criteria

Nondimensional Panel Flutter Parameter

$\Phi = [\, f(M) \times E / q \,]1/3 \times (t / l)$

where:

- Φ = Non-dimensional panel flutter parameter; a function of panel length-to-width ratio, l/w
- E = Young's modulus
- f(M) = Mach number correction factor; a function of Mach number and l/w ratio;
- l = Panel length (stream wise)
- q = Dynamic pressure
- t = Panel thickness
- w = Panel width

Correction Factors for:

- Curvature
- Mach Number
- Flow Angle
- In-plane stress
- Differential Pressure
- Differential Temperature

Revised F-18E/F Panel Flutter Desigh Requirement For Aluminum Structure

(Example)

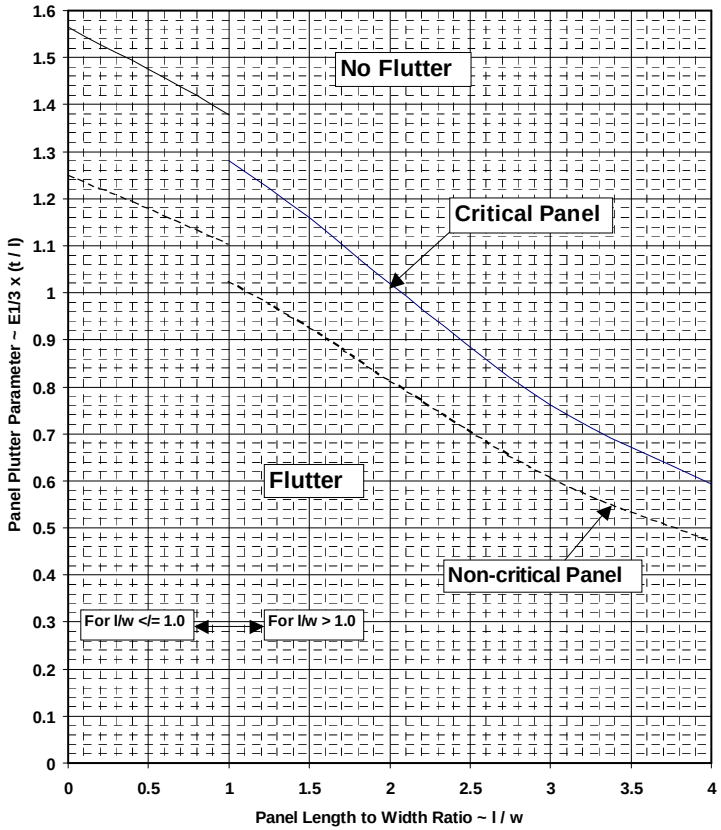

****** See accompanying References 1 & 2 ******

Approved for public release; distribution unlimited.

Aeroelastic FEA – Assumptions & Method

- **Method**
  - Piston Theory (Valid for high mach number)
  - Nastran Solution 145
- **Assumptions**
  - Use density factor of 0.5 for single-sided flow
  - 0.02 system damping,
    (flutter speed where VG curve exceeds 0.02 damping constant)
  - No preload from thermal or mechanical load cases
- **Flight Parameters**
  - Mach 6.25 @ 75,000 ft
  - Material properties adjusted for 900s thermal load

670
Approved for public release; distribution unlimited.

Aeroelastic FEA – Structural Model

- **Panel flutter structural model includes entire unit cell**
- **Air flow in global X-direction**
- **AERO model defined by 16 CAERO5 entries in the chord or stream-wise direction**

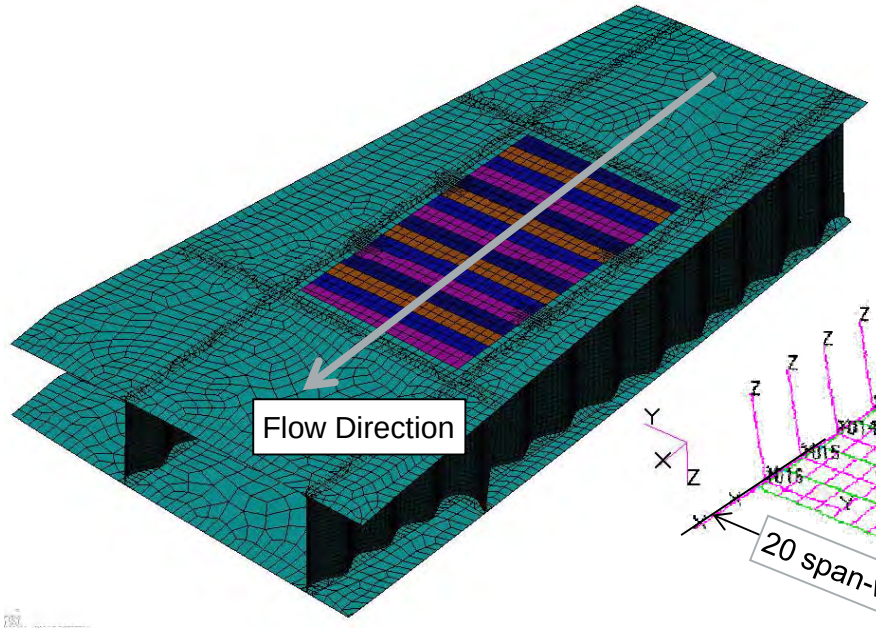

Structural FEM

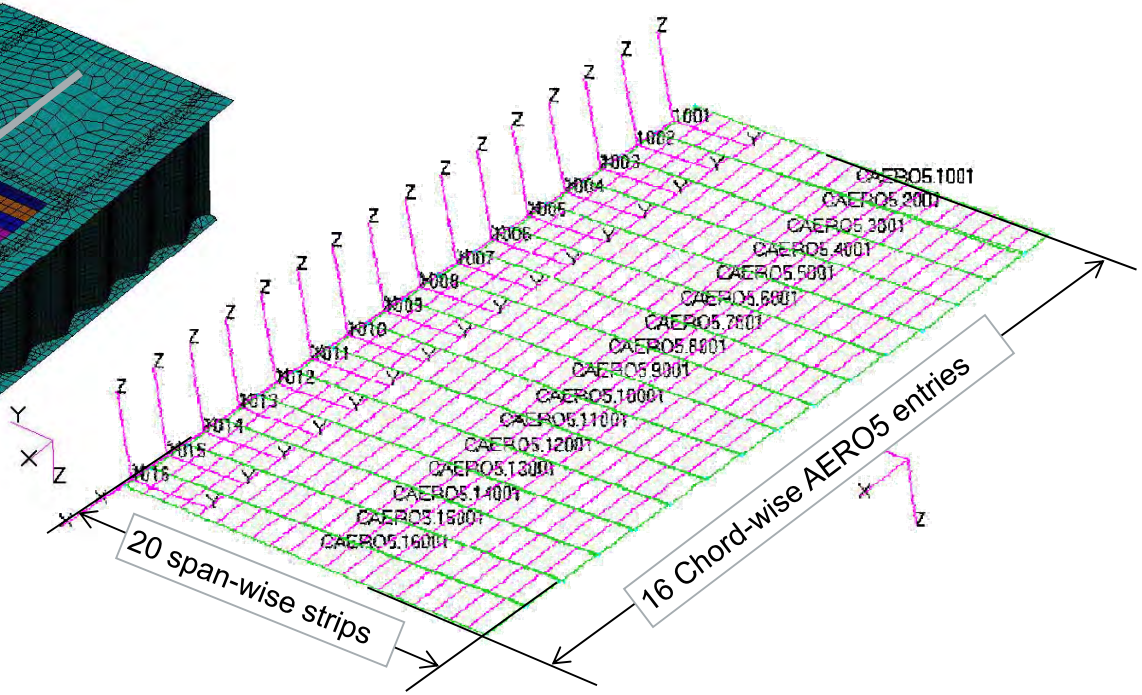

Panel 1074 AERO FEM

671
Approved for public release; distribution unlimited.

Panel 1074, Thermal Adj. Material Properties (t=900s),32.5kft, Mach 6.25

- **Piston theory flutter results for velocity range from Mach 5 to Mach 7**
- **Modes 1 and 2 interact to produce a unstable panel at Mach 6.25 at 32,500ft altitude**
- **Out of 30 modes in the solution, only modes 1 and 2 interact to produce a flutter condition at this combination of altitude and velocity**
- **Flight profile shows an altitude of ≈ 75,000ft at t=900s and Mach 6.25**
- **Using a 15% margin of safety there is a flutter margin of 31,250ft**

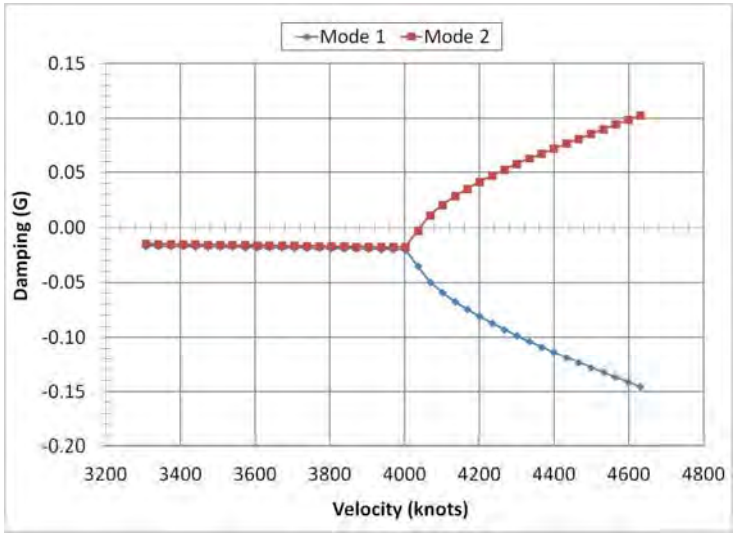

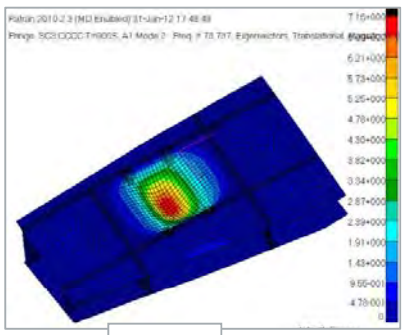

Mode 1

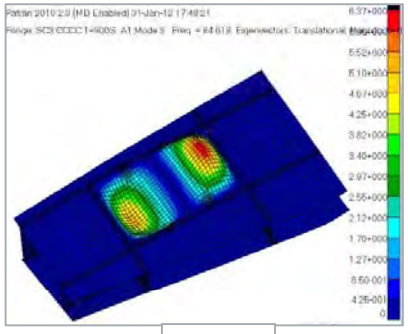

Mode 2

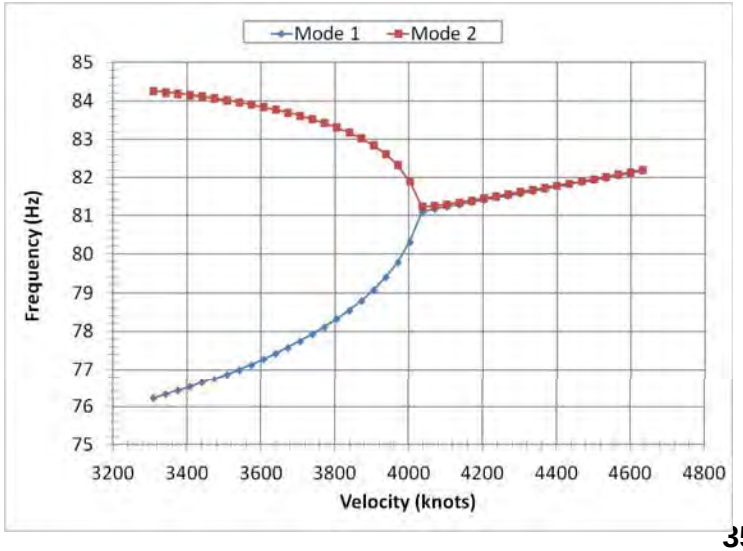

Approved for public release; distribution unlimited.

Panel 1074 Flutter Analysis Summary

- **Variables of angle of attack (AoA) and preload were explored for panel 1074 analysis (Analysis velocity held as a constant)**
- **Panel flutter analysis executed for panel with AoA = 0˚ and AoA = 6˚**
  - AoA had a moderate effect on panel flutter
  - Flutter at 32.5kft at m = 6.20 for AoA = 0
  - Flutter at 38.0kft at m = 6.20 for AoA = 6
- **A restart from a non-linear static solution was attempted (preload)**
  - The preload has negligible effect on the outcome of the panel flutter results
  - The preload should effect the stiffness of the panel that would be evident in flutter analysis
  - The preload process for panel flutter needs further investigation

Preload	Altitude (ft)	Air Density	Solution Mach Number	Velocity Range	Material Properties	Angle of Attack (deg)	Unstable Mode	Frequency (Hz)	Flutter Speed (Knots)	Flutter Speed Mach Number
No	75,000	5.262E-09	6.25	M3 - M14	Temp Adj. (t=900s)	0	None	-----	-----	-----
No	50,000	1.750E-08	6.25	M3 - M14	Temp Adj. (t=900s)	0	Mode 2	81.2	6086	9.2
No	35,000	3.549E-08	6.25	M3 - M14	Temp Adj. (t=900s)	0	Mode 2	81.3	4300	6.5
No	32,500	3.904E-08	6.25	M3 - M14	Temp Adj. (t=900s)	0	Mode 2	81.4	4161	6.3
No	30,000	4.286E-08	6.25	M3 - M14	Temp Adj. (t=900s)	0	Mode 2	81.4	3969	6
No	25,000	5.1338E-08	6.25	M3 - M14	Temp Adj. (t=900s)	0	Mode 2	81.4	3638	5.50
No	Sea Level	1.147E-07	6.25	M3 - M14	Temp Adj. (t=900s)	0	Mode 2	81.4	2448	3.70
No	**32,500**	**3.904E-08**	**6.25**	**M5-M7**	**Temp Adj. (t=900s)**	**0**	**Mode 2**	**81.3**	**4101**	**6.20**
No	50,000	1.750E-08	6.25	M3 - M14	Temp Adj. (t=900s)	6	Mode 2	81.2	5490	8.30
No	40,000	2.8299E-08	6.25	M3 - M14	Temp Adj. (t=900s)	6	Mode 2	81.3	4300	6.50
No	38,500	3.0414E-08	6.25	M5 - M7	Temp Adj. (t=900s)	6	Mode 2	81.3	4167	6.30
No	**38,000**	**3.1154E-08**	**6.25**	**M5 - M7**	**Temp Adj. (t=900s)**	**6**	**Mode 2**	**81.3**	**4101**	**6.20**
No	37,500	3.191E-08	6.25	M3 - M14	Temp Adj. (t=900s)	6	Mode 2	81.2	4101	6.20
No	37,500	3.191E-08	6.25	M5 - M7	Temp Adj. (t=900s)	6	Mode 2	81.3	4035	6.10
No	32,500	3.904E-08	6.25	M3 - M14	Temp Adj. (t=900s)	6	Mode 2	81.2	3638	5.50
No	37,500	3.191E-08	6.25	M3 - M14	Temp Adj. (t=900s)	6	Mode 2	81.2	4101	6.20
Yes	Sea Level	1.147E-07	6.25	M3 - M14	Temp Adj. (t=900s)	0	Mode 2	81.4	2448	3.70
Yes	Sea Level	1.147E-07	6.25	M3 - M14	Temp Adj. (t=900s)	6	Mode 2	81.4	2183	3.30

Approved for public release; distribution unlimited.

Flutter Analysis Conclusions

- **Empirical Design Curve Method**
  - The design curve and finite element analysis indicate healthy flutter margins for panel 1074
  - Design curve predicts higher MS for panel 1074 compared to panel 816. Finite element analysis indicated opposite was true
  - Empirical design curves would save time if their accuracy is proven for velocities and altitudes of this vehicle class
- **Finite Element Method**
  - Adequate flutter margin was calculated for panel 1074
  - At altitudes 30,000ft or greater, modes 1 and 2 are the only modes that interact to become unstable
  - Panel flutter can be calculated for panels at the unit cell level of fidelity
  - Panel pre-load did not change flutter results. The method for implementing pre-load into a flutter solution needs further investigation

674
Approved for public release; distribution unlimited.

Flutter Analysis Conclusions Continued

- **Aeroelastic Analysis Issues**
  - Analysis takes place down stream of configuration level sizing suggest adding empirical aeroelastic design curves to sizing routines at a high level
  - Requires an aero model that references grids on structural model, helps if structural model elements are aligned with flow direction(s) of interest
  - Results interrogation and visualization leaves something to be desired
    - Internal Boeing code used to plot damping and frequency vs. velocity.
    - Patran balked at importing modes from the CAERO5
  - Iterative process to determine correct flutter speed
    - Speeds away from the solution mach number are “approximations” and the solution must be iterated until flutter speed matches solution mach number

675
Approved for public release; distribution unlimited.

BACKUP CONTENT

676
Approved for public release; distribution unlimited.

Analysis Issues

Issue	Approach	Source/Rationale
External Aero-acoustic Loads	Empirical with CFD guidance	Efimtsov Models, Boeing Best Practice, no hypersonic flight test data, or predictive capability available
Damping	Empirical Data	USAF Damping Design Guide, Boeing Best Practices, no inconel sine wave , iso-grid test data available
S-N Data for In 718	Convert Constant Amplitude Data to RMS Data, Adjust based for Temperature based on Strength	Mil-5, Best Practices, only source of reliable data
Sub-structure Modes	Filtered most Sub-structure modes	Concentrating on Panel Structure, also allows for quicker turn around
Choosing Worst Case Design Conditions	Using Max Thermal , matched to Max Acoustic for Fatigue Margin Checks	Dissimilar loads from different points in the trajectory, points are close, but not exact. This accounts for possible difference in trajectories
Combined Spectrum	Assuming a single trajectory	Don't have other trajectories, but a real vehicle will have many different possible missions.
Joint Allowables	Similarity to other material, joints	Boeing Best Practice, Need to test specific joints – welds, machine, fastened, etc…

Approved for public release; distribution unlimited.

MATERIAL PROPERTIES

678
Approved for public release; distribution unlimited.

MMPDS – Inconel 718 – S/N Curve

- **For locations with Kt < 1.5 use Fig 6.3.5.1.8.c (Best-fit S/N curves for un-notched Inconel 718 sheet at 1000F)**

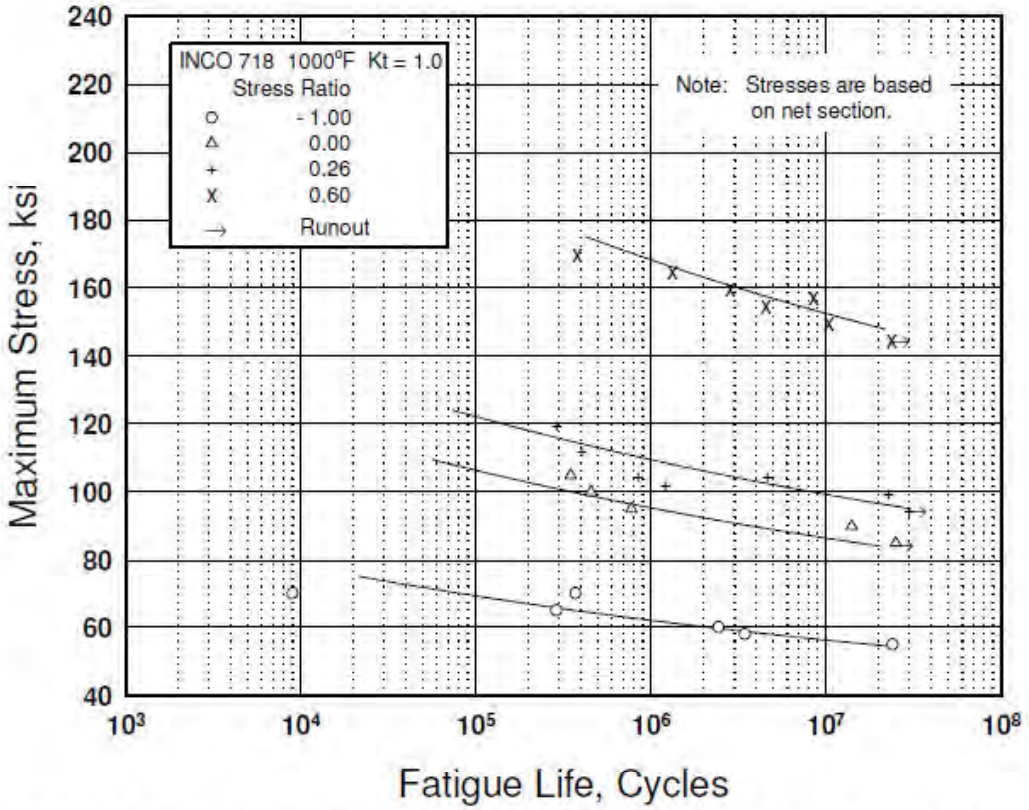

Equivalent Stress Equation:

$\text{Log } N_f = 23.51 - 10.57 \text{ Log } (S_{eq} - 50)$

$S_{eq} = S_{max}(1\text{-}R)^{0.62}$

Std. Error of Estimate, Log (Life) = 0.414

Standard Deviation, Log (Life) = 0.776

$R^2 = 71.5\%$

Figure 6.3.5.1.8(c). Best-fit S/N curves for unnotched Inconel 718 sheet at 1000°F, long transverse direction.

679
Approved for public release; distribution unlimited.

MMPDS – Inconel 718 – S/N Curve

- **For locations with Kt > 1.5 use Fig 6.3.5.1.8.c (Best-fit S/N curves for un-notched Inconel 718 sheet at 1000F)**

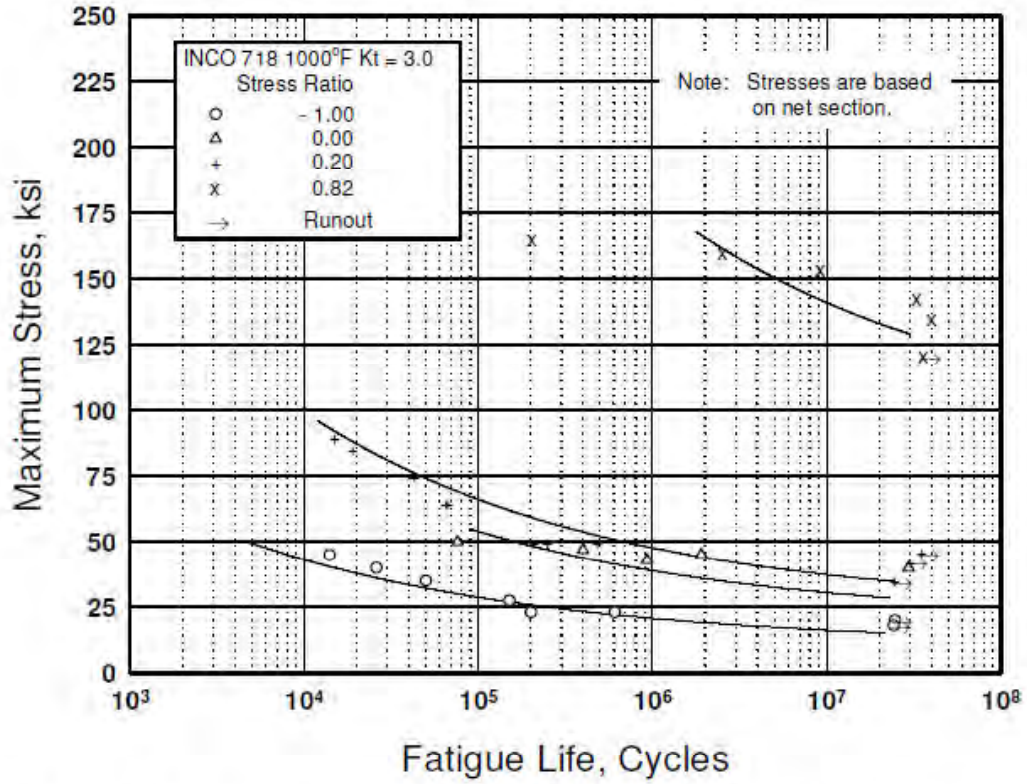

Equivalent Stress Equation:
$\text{Log } N_f = 11.02 - 3.93 \text{ Log } (S_{eq} - 20)$
$S_{eq} = S_{max}(1\text{-}R)^{0.91}$
Std. Error of Estimate, Log (Life) = 0.404
Standard Deviation, Log (Life) = 0.988
$R^2 = 83.3\%$

Sample Size = 23

[Caution: The equivalent stress model may provide unrealistic life predictions for stress ratios beyond those represented above.]

Figure 6.3.5.1.8(d). Best-fit S/N curves for notched, K_t = 3.0, Inconel 718 sheet at 1000°F, long transverse direction.

Approved for public release; distribution unlimited.

ACOUSTIC MODEL DEVELOPMENT

681
Approved for public release; distribution unlimited.

Trajectory – Design Conditions of Interest

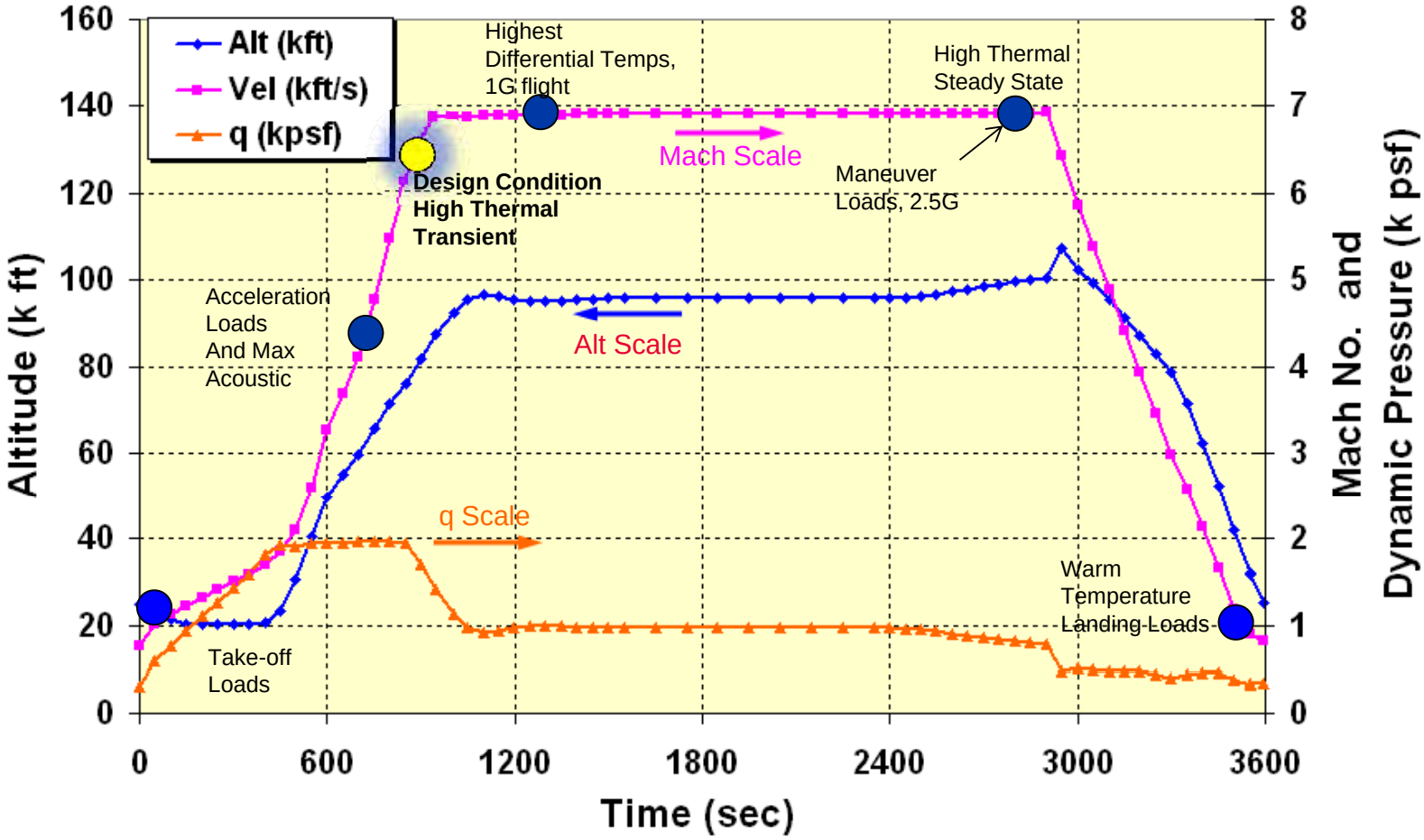

These are the Design Conditions of Interest for Dynamic & Fatigue Analysis.

682
Approved for public release; distribution unlimited.

Structural Damping

Frequency (Hz)	Damping Ratio, ζ
10	0.025
100	0.02
1000	0.01

```
$
TABDMP1  1        CRIT
         10.     .025     100.     .02       1000.
.01      ENDT
```

Nastran Damping Table Card

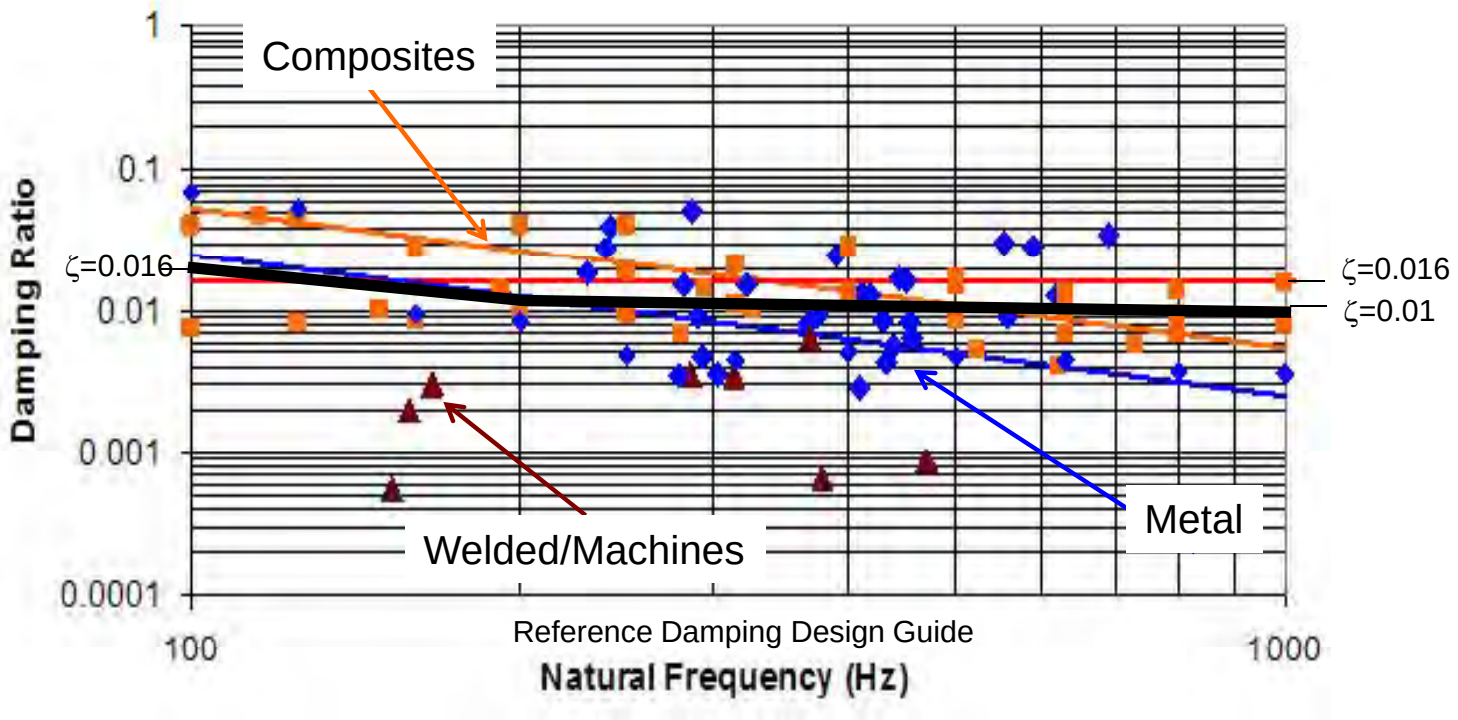

Dynamic Analysis uses the black curve

683
Approved for public release; distribution unlimited.

Panel 862 Location

Define acoustic levels for each panel and critical conditions:

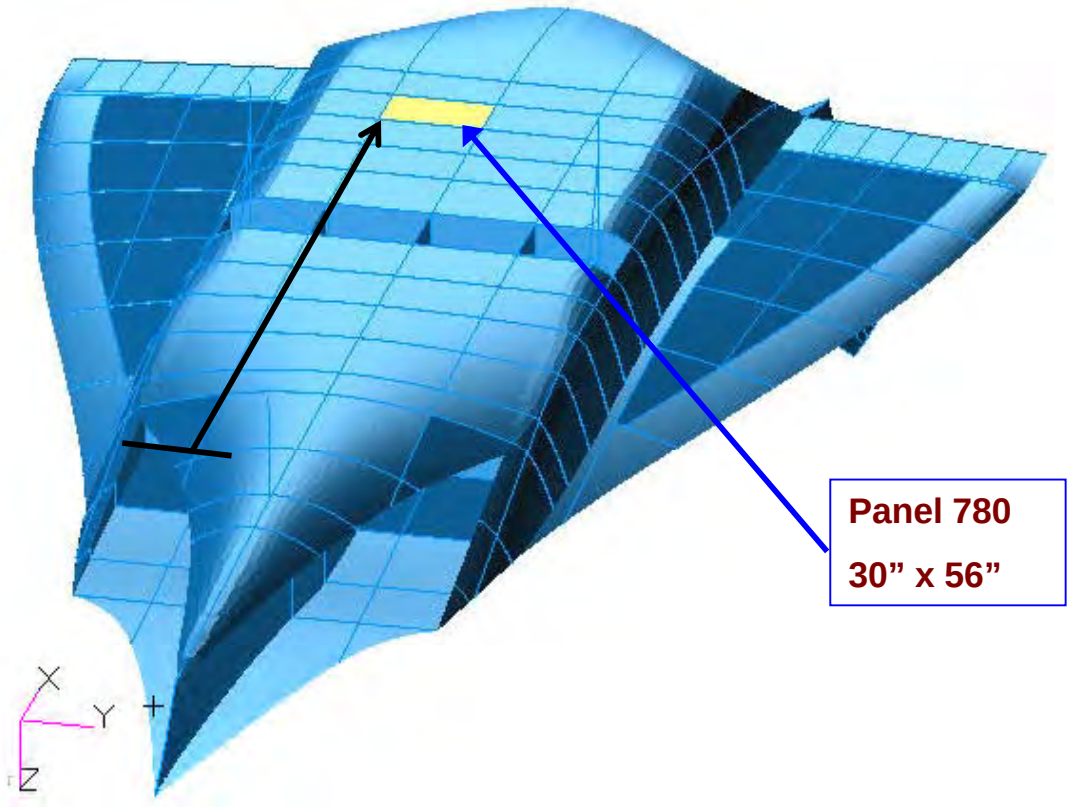

Distance from Lead Edge and Distance from Point of Separation are inputs to aero-acoustic models

Approved for public release; distribution unlimited.

CFD Results

CFD++ N-S Flow Field for M=7.0, α = 10 deg., Alt.=90Kft

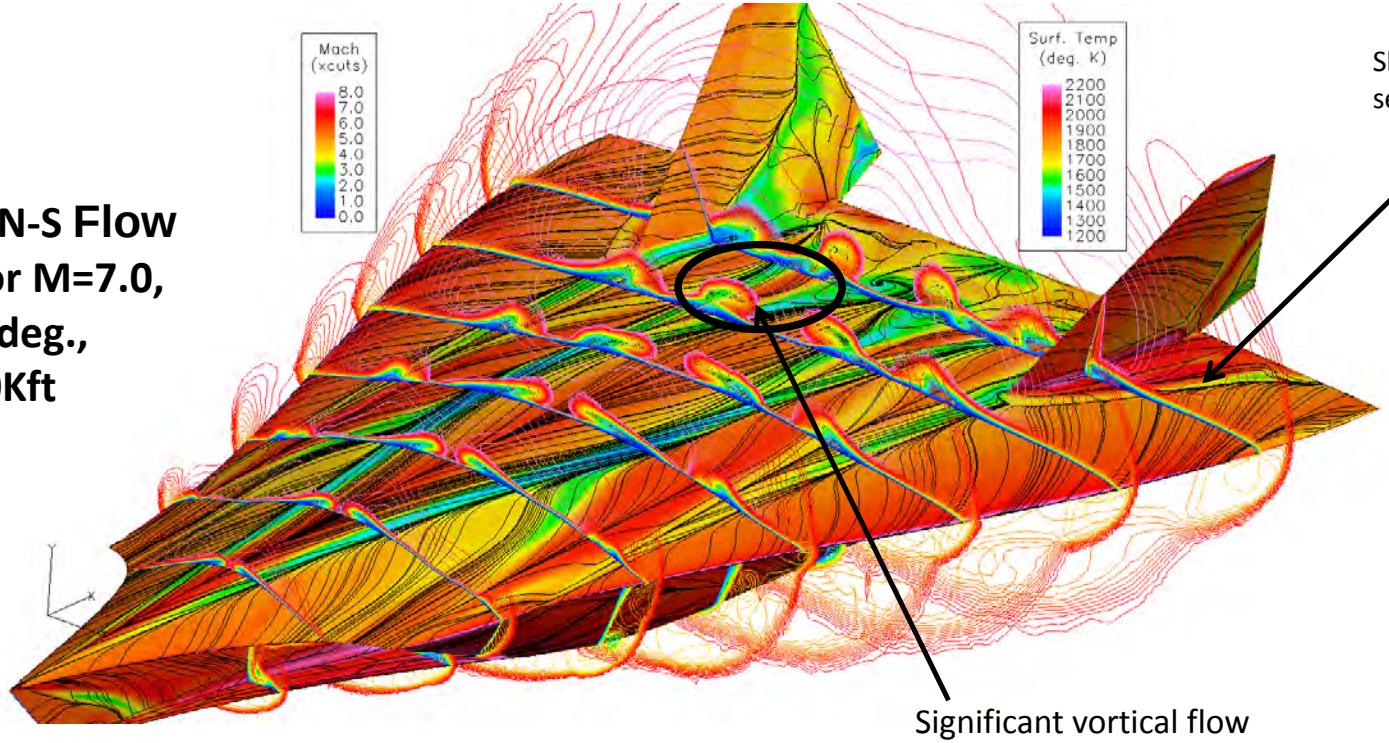

CFD was used to determine local flow features. This information was used in our Empirical models to predict acoustic loading spectrum

Approved for public release; distribution unlimited.

CFD Runs for Acoustic Loads

1.) Mach 7, 2.5g, AoA=10 deg, turn , Alt=90kft, q=1340 psf, Highest Maneuver and thermal loads (max G)

2.) Mach 7, 1.0g, AoA=4 deg, Cruise, Alt=100Kft, q=730 psf, High thermal loads and transient conditions (max T)

3.) Mach 6, 1.0g, AoA=6 deg, Accel, Alt= 75kft, q=2000 psf, Highest acoustic and thermal loads (max Q)

The load conditions for the detailed analysis was based on these are the three trajectory.

Approved for public release; distribution unlimited.

Required Data from CFD for Aero-acoustic Models

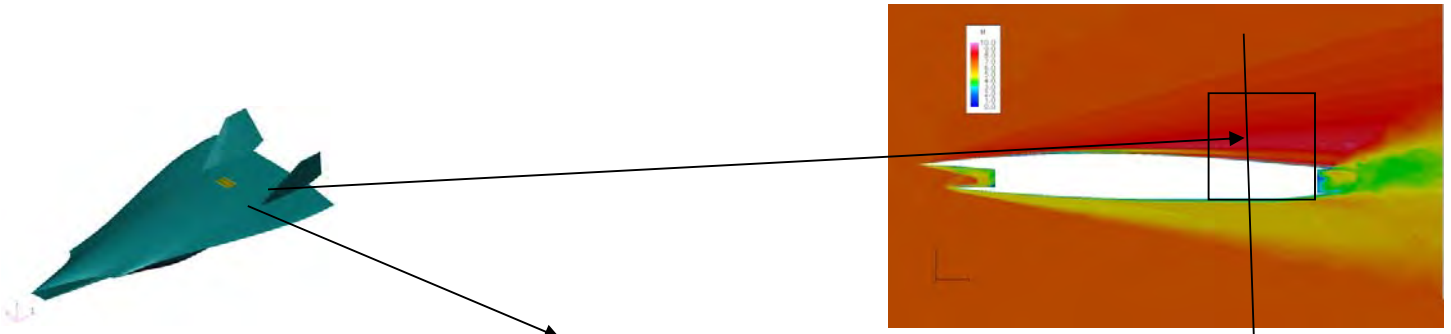

Streamline at center of panel

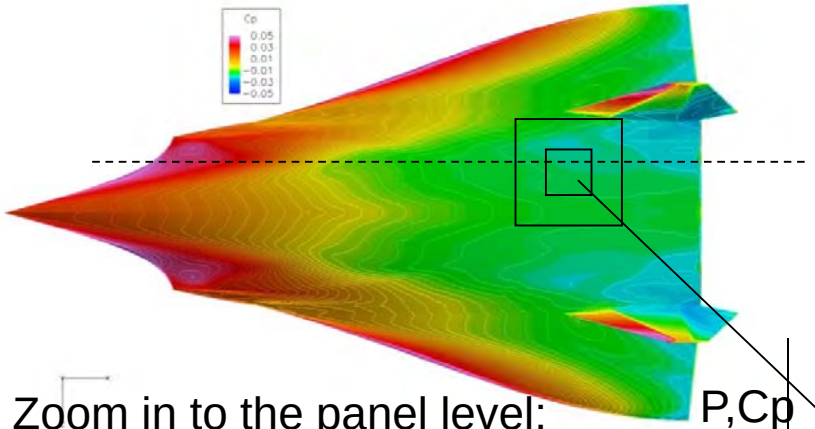

Zoom in to the panel level:

Graph of the pressure across
The panel at the Ctr line

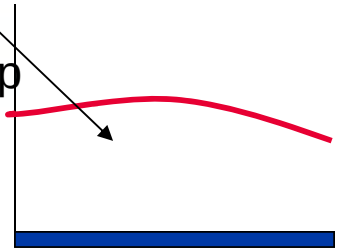

Velocity Profile

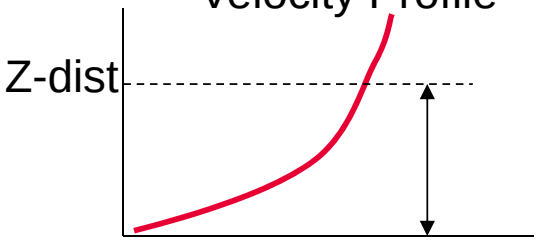

M,vel

An estimate of BL thick
At the leading edge of
the panel

Approved for public release; distribution unlimited.

CFD++ Computed Flow Field, M=6.0, a=6.0 deg., Alt.=75 Kft

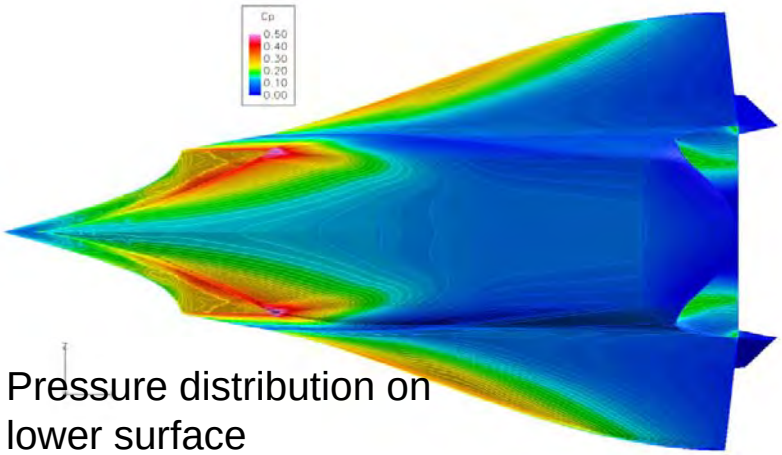

Pressure distribution on lower surface

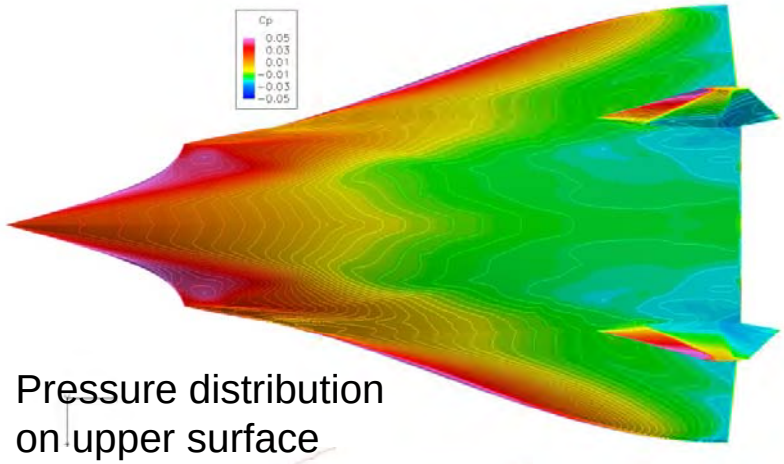

Pressure distribution on upper surface

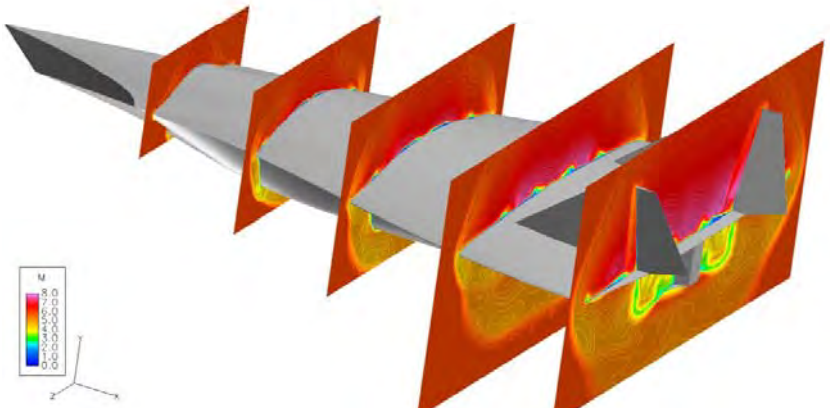

Mach No. at section cuts

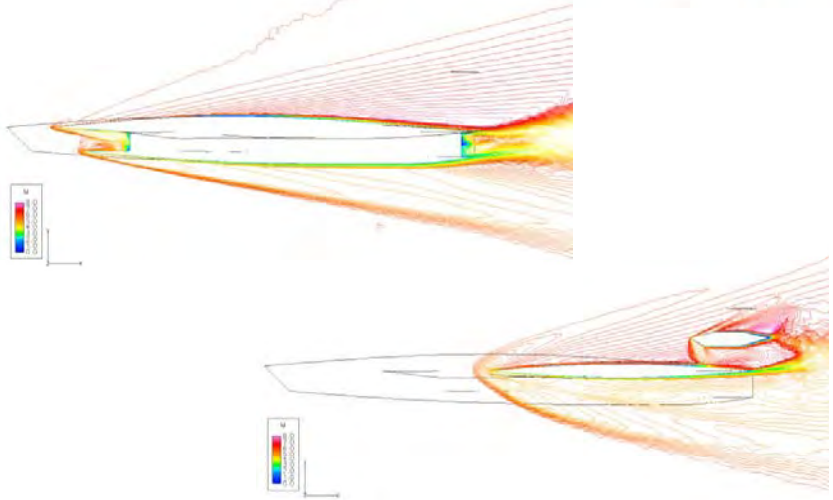

Approved for public release; distribution unlimited.

Computed Surface Pressures on the Panels

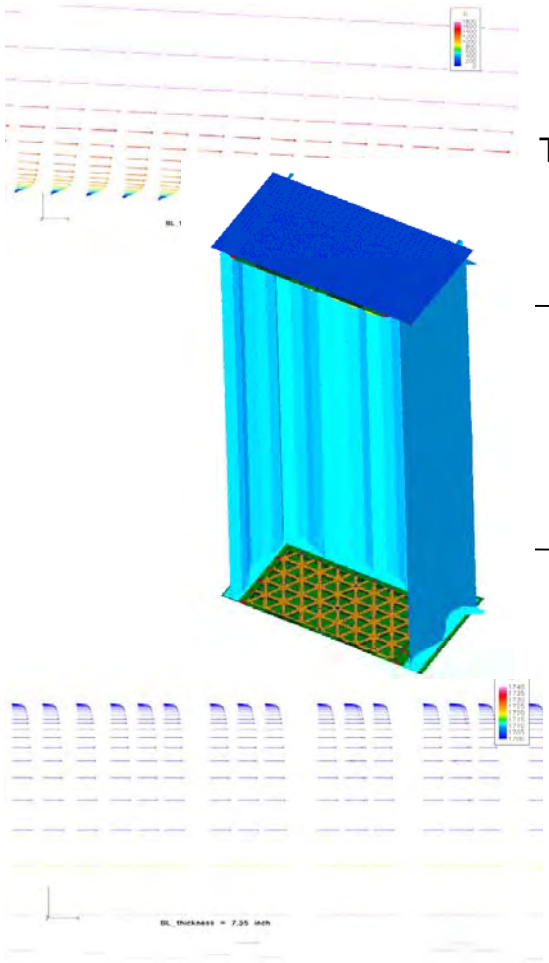

TBL_{ave}~11”

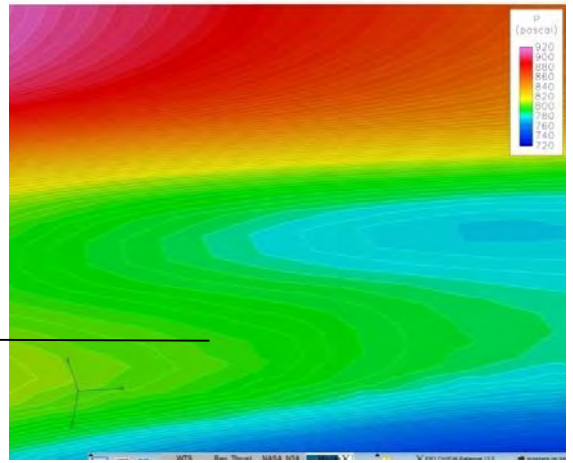

Panel 862
(Upper Surf)
ΔPy ~ 200 pa/m

TBL_{ave}~7”

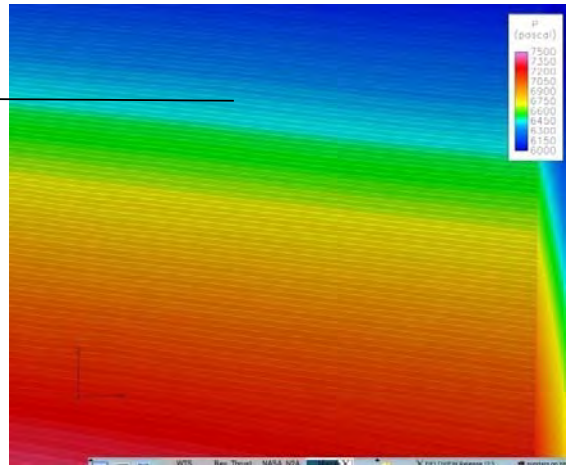

Panel 782
(Lower Surf)
ΔPy~1500 pa/m

Approved for public release; distribution unlimited.

Empirical Model Acoustic Prediction

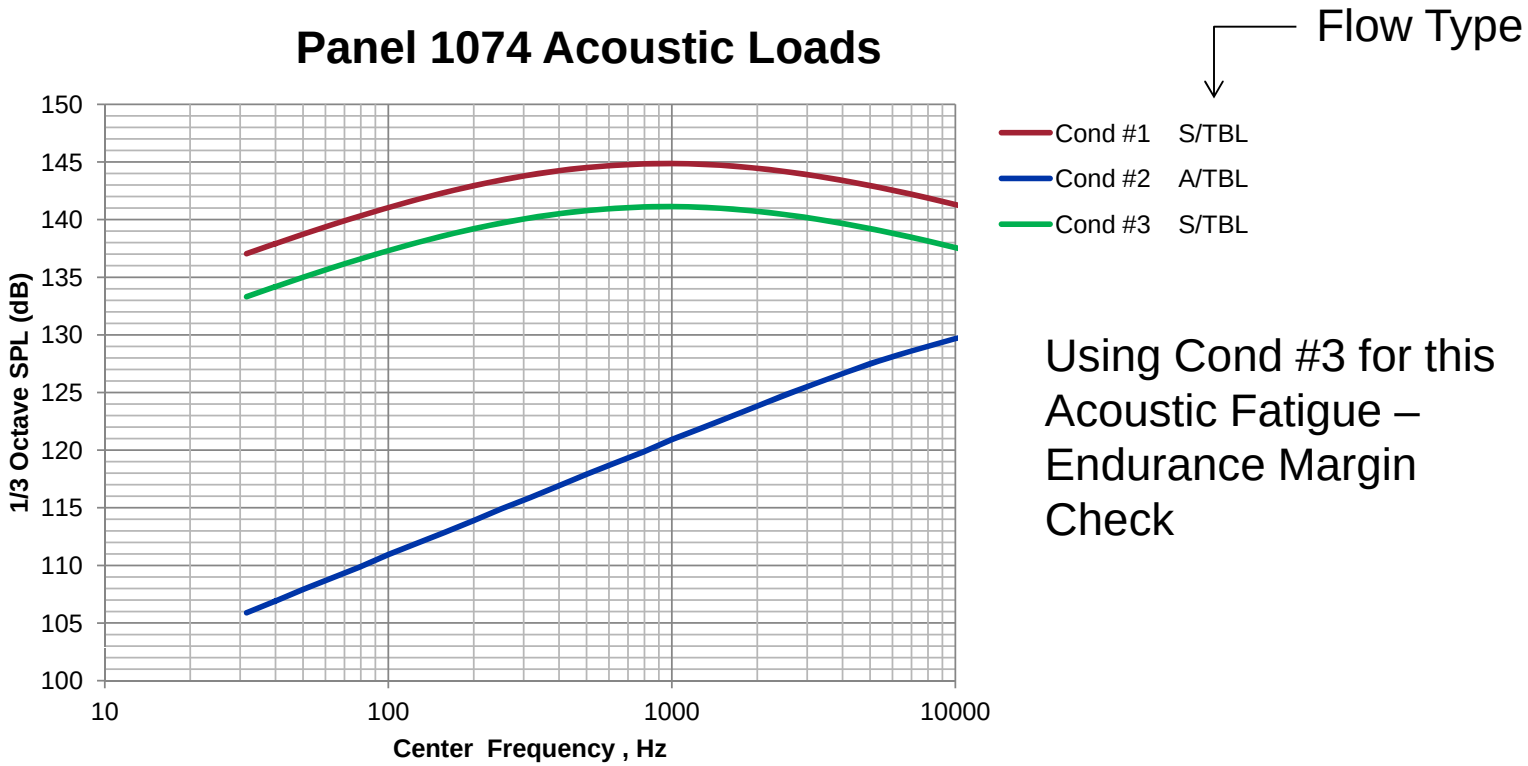

Using Cond #3 for this Acoustic Fatigue – Endurance Margin Check

Based on CFD input into Efimtsov TBL Models

Ref. R. Rackl, and A. Weston, "Modeling of Turbulent Boundary Layer Surface Pressure Fluctuation Auto and Cross Spectra - Verification and Adjustments Based on TU-144LL Data," NASA/CR-2005-213938.

Approved for public release; distribution unlimited.

Acoustic Damage Accumulation

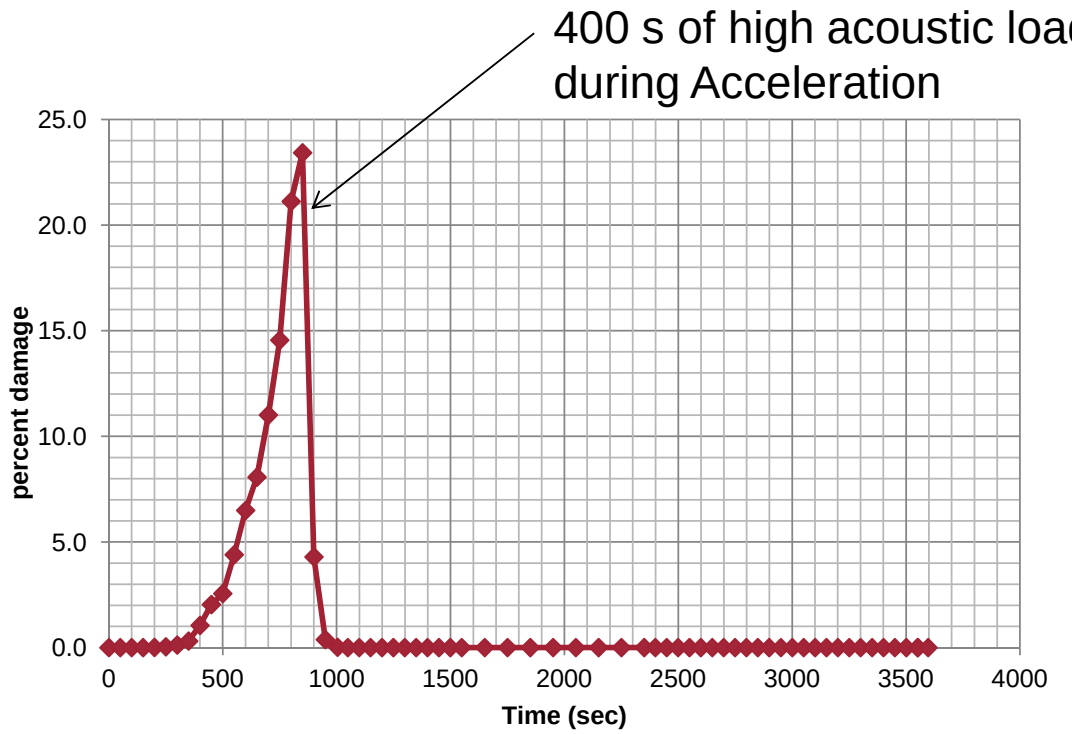

Acoustic Loads only critical during acceleration, add these stress cycles to fatigue spectrum

Approved for public release; distribution unlimited.

CAESAR DETAIL STRESS TOOL

692
Approved for public release; distribution unlimited.

CAESAR Description

- CAESAR (ComputAtional Engineering Structural Analysis Routines)
- CAESAR is a web based tool for determining detail stresses for open holes, filled holes, notches, fillets, etc
- User entered Input variables are submitted to stress check model templates which are executed on a remote server
- Results can be retrieved in multiple formats
- Details are given on stress check model and results calculations
- XML files and stress check model files can be saved for future runs

693
Approved for public release; distribution unlimited.

CAESAR Home Screen

Holes	Detail Stress Analysis	Notches, Fillets, etc.
Single Hole Cold Worked Single Hole Multi-Hole Multi-Loaded Holes Lug Rod End Cutout in Shear Reinforced Cutout (2D) Reinforced Cutout (3D) Reinforced Hole (3D) Nutplate	 *Please use Microsoft's Internet Explorer* Download SVG Install Package (Does not require admin privileges.)	Single Notch Double Notch Shallow Gradient Specimen Shoulder Fillet Web Fillet Stepped Flange (3D) Tension Fittings Multi-Hole Plate Buckling Reinforced Hole Plate Buckling Reinforced Cutout Plate Buckling
Questions or Problems? Email: CaesarSupport@Boeing.com Pager: 314-507-0531	First Time Users: Download Overview Charts	Change Log: • Functional change 12/19/2007

Approved for public release; distribution unlimited.

Example CAESAR INPUT – Single Hole Detail

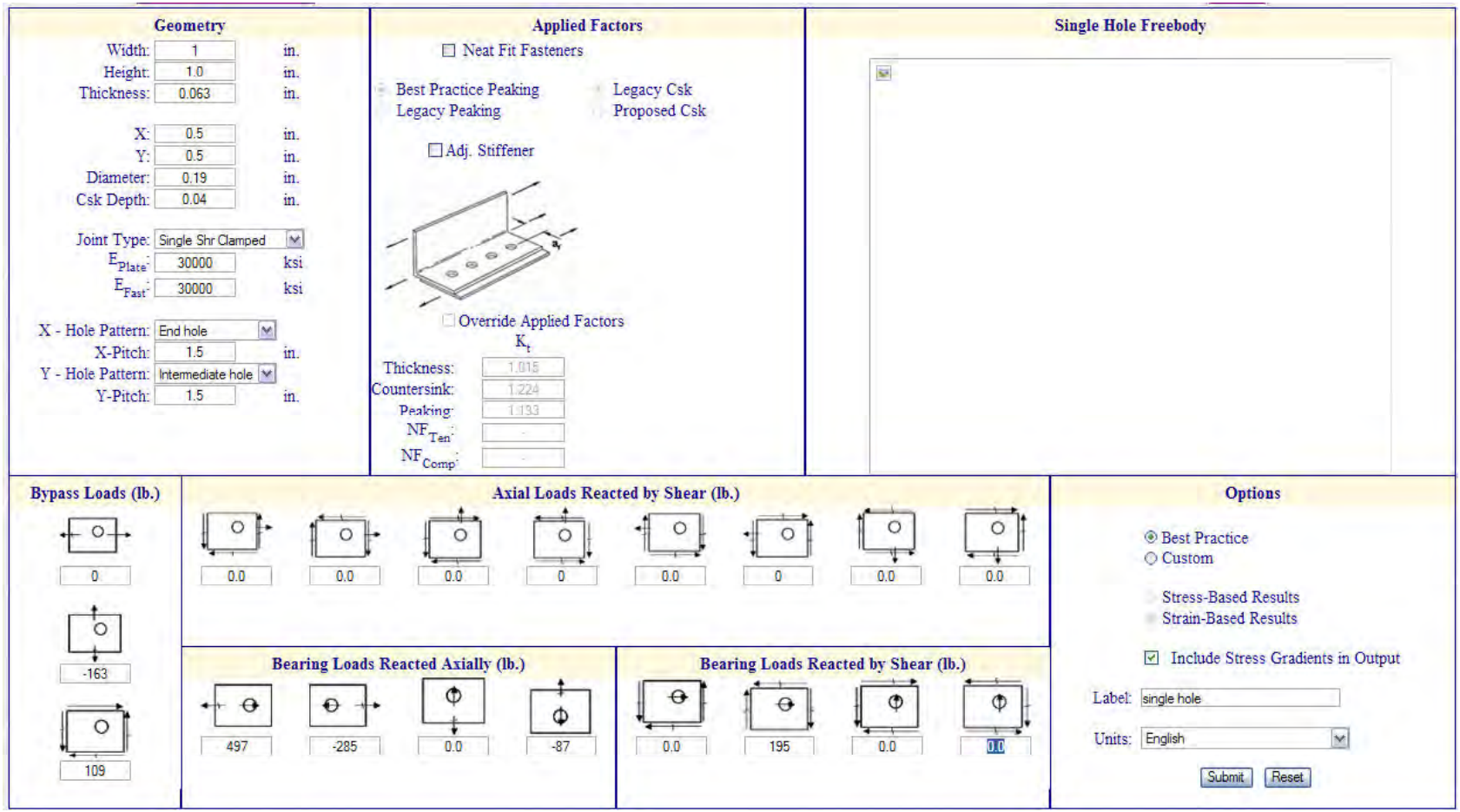

Approved for public release; distribution unlimited.

Example CAESAR Result – Single Hole Detail

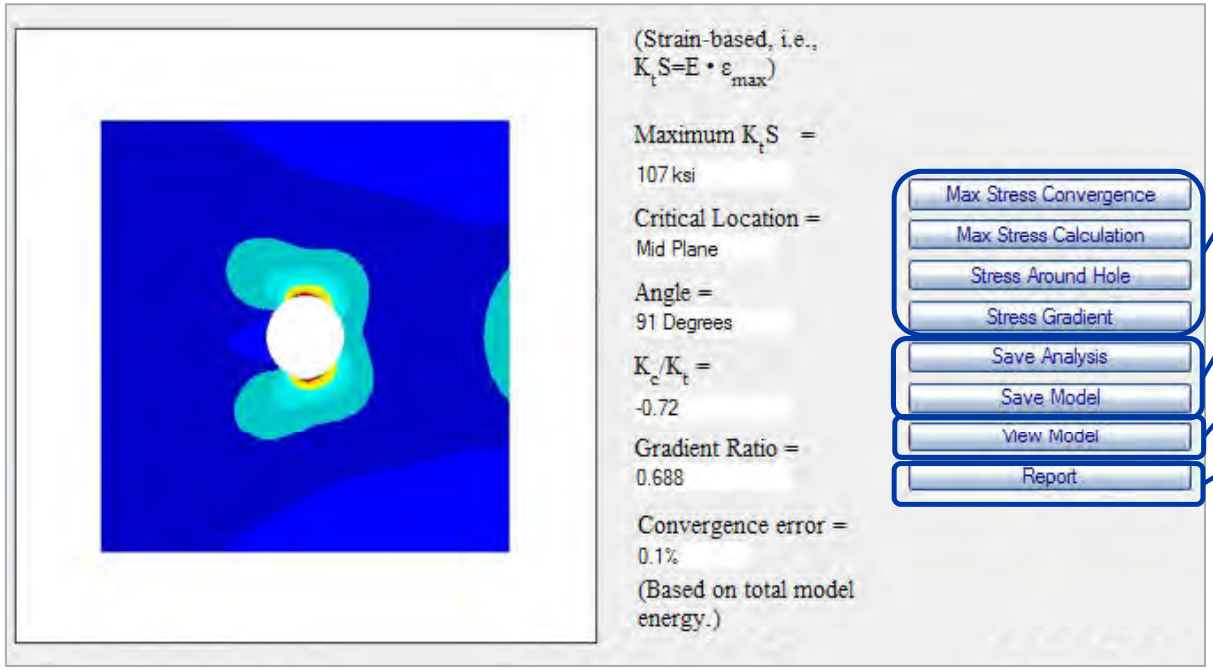

Details on solution and calculation of maximum stress

Options to save the solution or stress check model files

Interactive view of stress check model

Create a report in html or MS Word formats

696
Approved for public release; distribution unlimited.

Task 3: Verification Study with Explicit Dynamic Analysis

George Tzong and Sal Liguore

Approved for public release; distribution unlimited.

Objective and Approach

Objective:

Investigate the effects of Thermal Preload, Geometrical Nonlinearity, and Boundary Condition to thermal-acoustic response of acreage panel

Quantify gaps of current design analysis approach

Approach:

- Conduct explicit dynamic analysis with stationary thermal and time-history of acoustic pressure
- Quantify gaps with linear response analysis results
- Collaborate with co-simulation analysis by ATA Engineering

Approved for public release; distribution unlimited.

Content of Study

- Model selection: Panel 1 (Panel 862)
- Model revision and modal validation for explicit dynamics
- Validation by comparing static and quasi-dynamic analysis solutions
- Time history examples for hinged BC with thermal loads
- Comparisons of Mean, STDV and RMS
- PSD and effects of thermal loads, geometrical nonlinearity and BC to panel response

Approved for public release; distribution unlimited.

Panel Model Selection

- Panel 1 or Panel 862 is selected for verification study
  - Only surface panel is adopted for study
  - The static analysis model is revised by reducing No. of elements thru stiffener web from 5 to 3. A study showed minor differences in natural frequencies
  - Thermal loads and boundary displacements from unit-cell analysis are imposed prior to dynamic analysis
  - The temperature is considered stationary for 2-sec dynamic simulation

Approved for public release; distribution unlimited.

Analysis Approach

- Revise static analysis model more suitable for explicit dynamics, i.e., larger time step without compromising accuracy
- Apply thermal loads and corresponding boundary displacements at t=1,080 sec from analysis of unit-cell model to panel
- Define damping of panel
- Conduct quasi-dynamic analysis step to initiate explicit dynamics, i.e., applying preload (Initial step of 0.1 sec for thermal preloads)
- Apply 2-second time history of acoustic pressure, uniform and normal to panel surface.
- Four analysis cases were studied
  - Fixed boundary condition (BC) without thermal loads
  - Fixed BC with thermal loads
  - Hinged BC without thermal loads
  - Hinged BC with thermal loads

  All cases with temperature-dependent materials

Approved for public release; distribution unlimited.

Panel 1 Location

Panel 1 (Upper) in Unit-Cell Structure

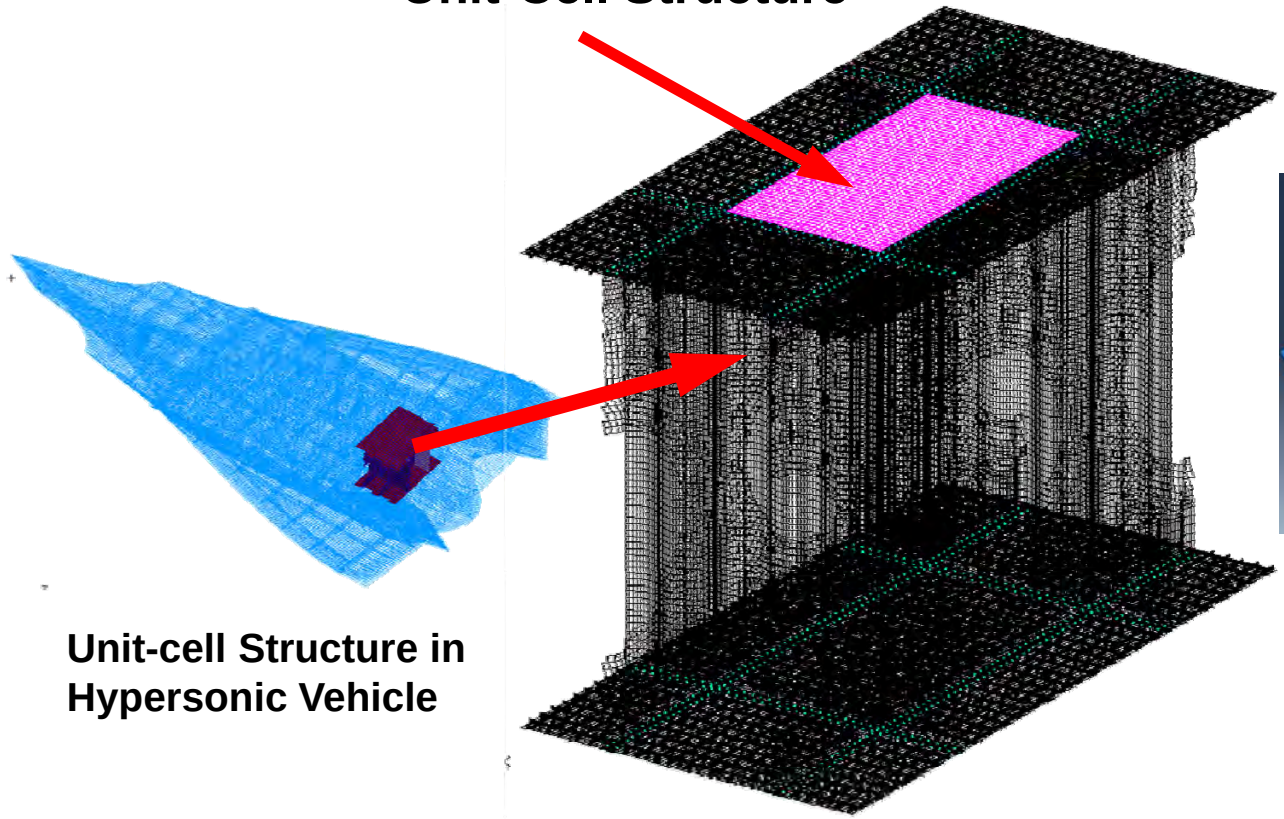

Unit-cell Structure in Hypersonic Vehicle

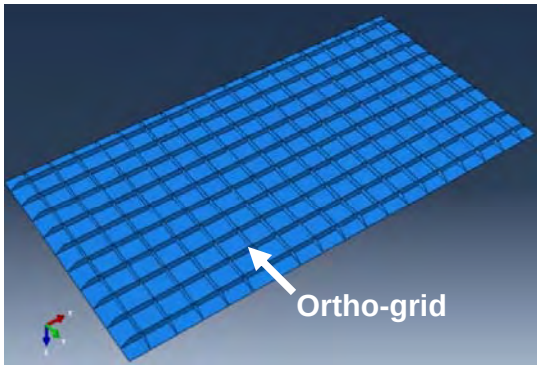

Panel Ortho-grid Construction

Approved for public release; distribution unlimited.

Temperature Distribution at t=1,080sec on Panel

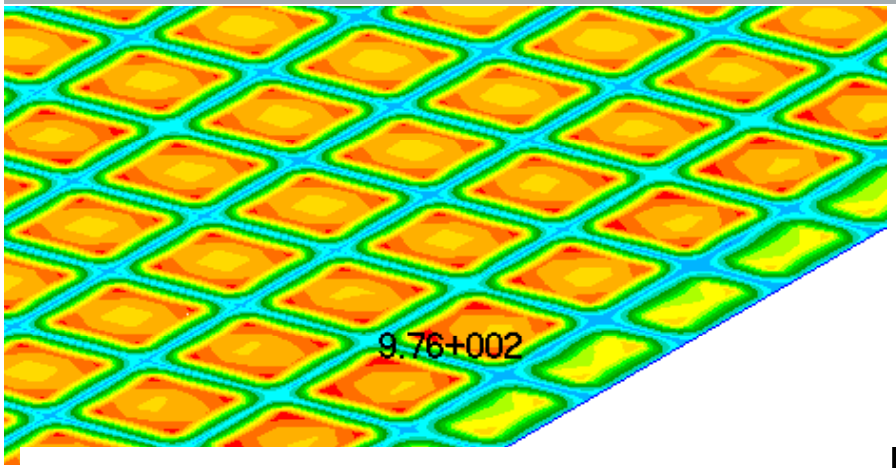

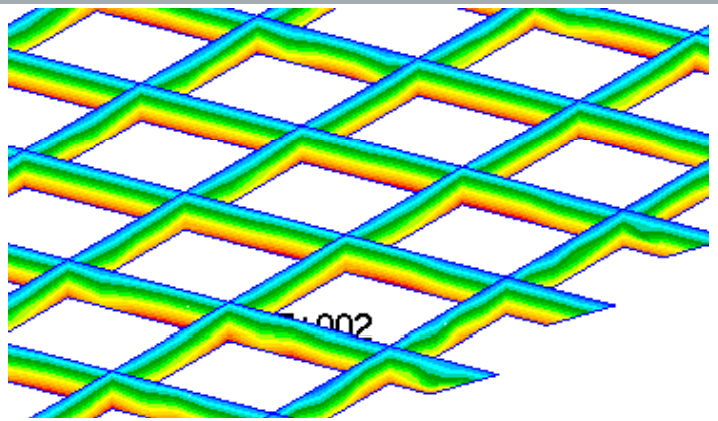

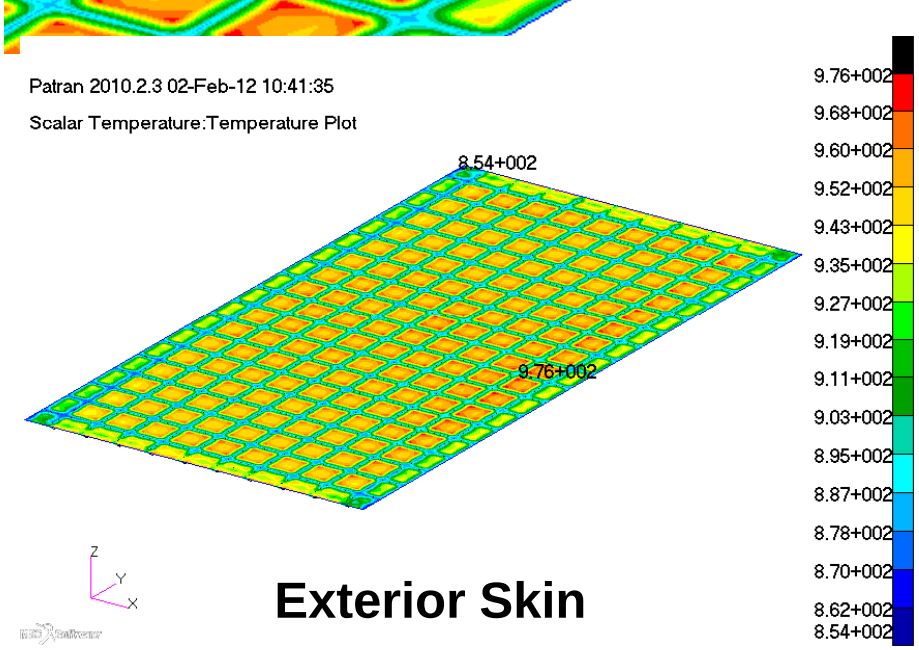

Exterior Skin

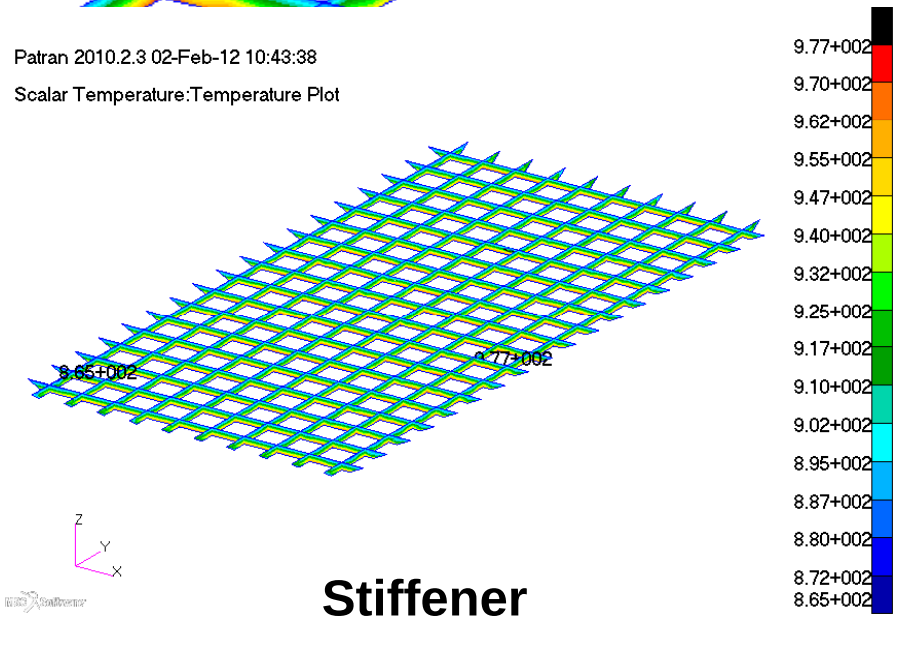

Stiffener

Approved for public release; distribution unlimited.

Mode Shapes of Panel 1

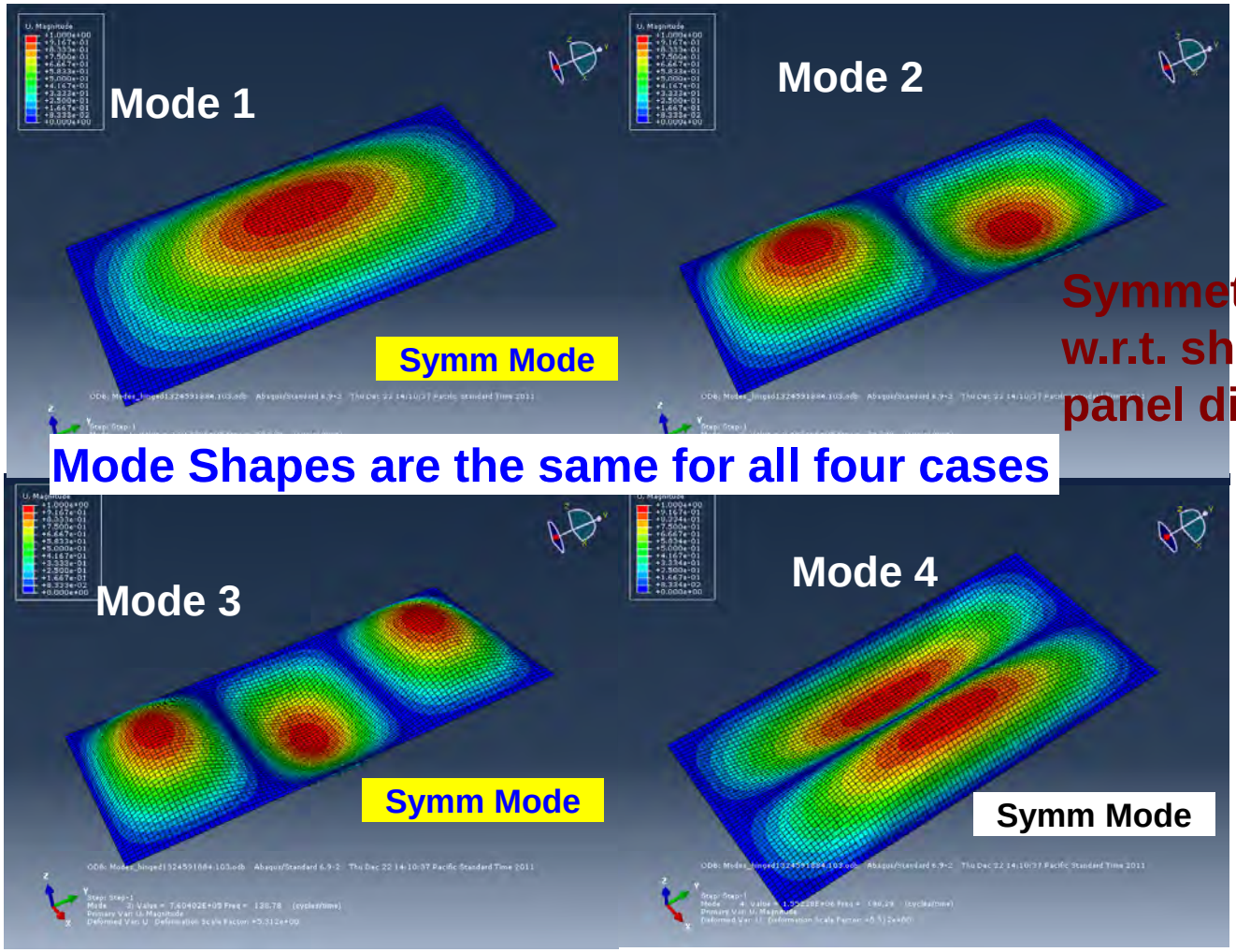

Approved for public release; distribution unlimited.

Mode Shapes of Panel 1 (cont.)

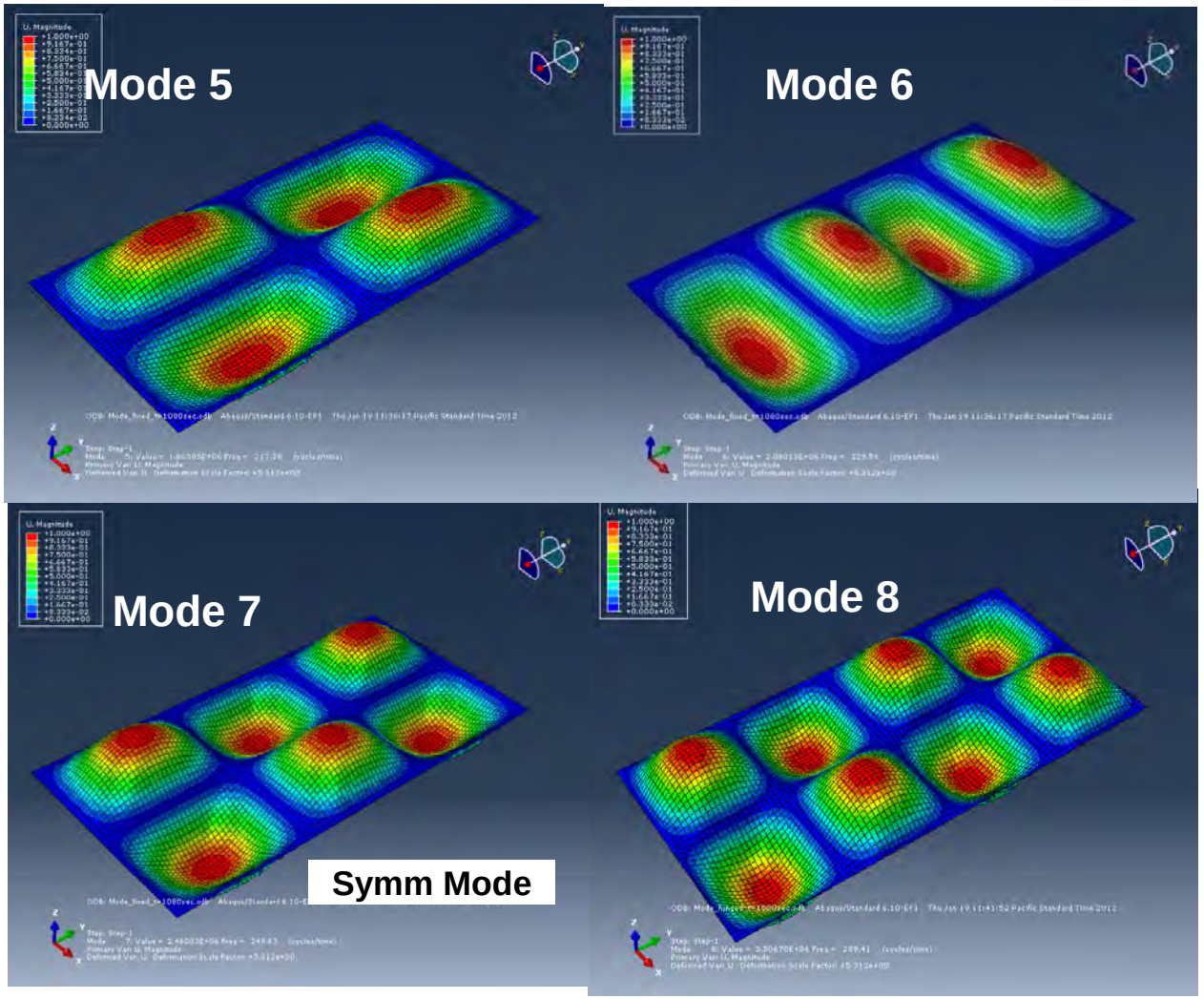

Approved for public release; distribution unlimited.

Mode Shapes of Panel 1 (cont.)

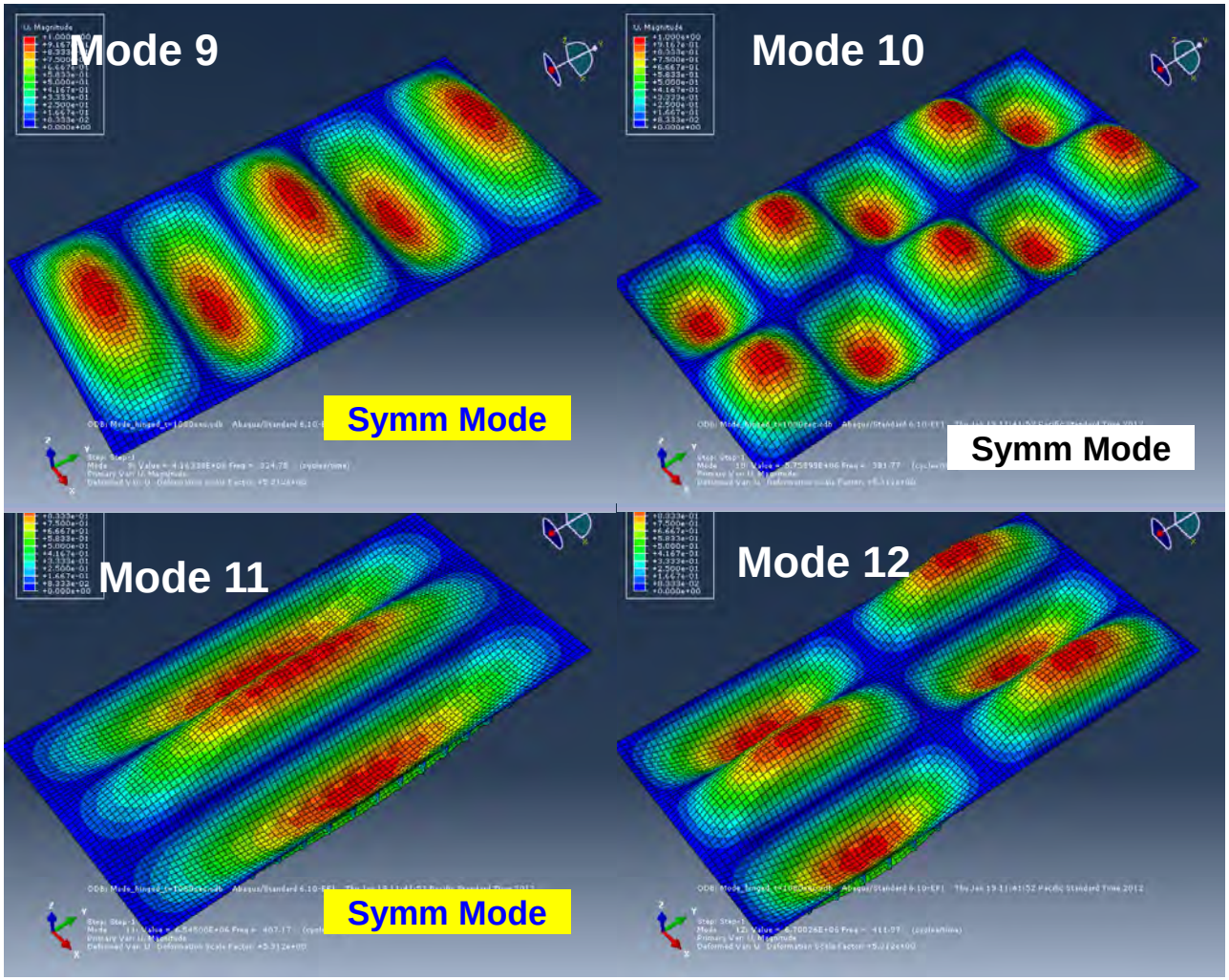

Approved for public release; distribution unlimited.

Comparison of Modes with Task 2; Temp-Dependent, No Preload

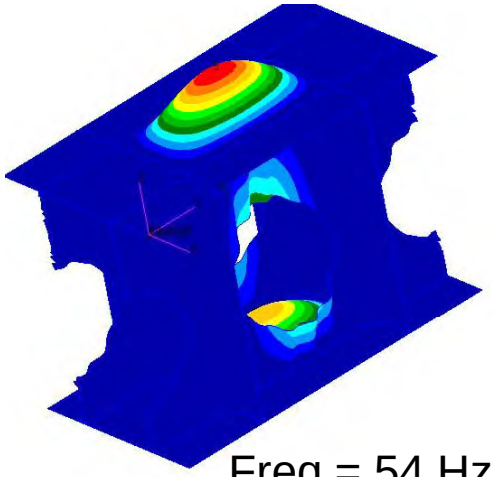

Freq = 54 Hz

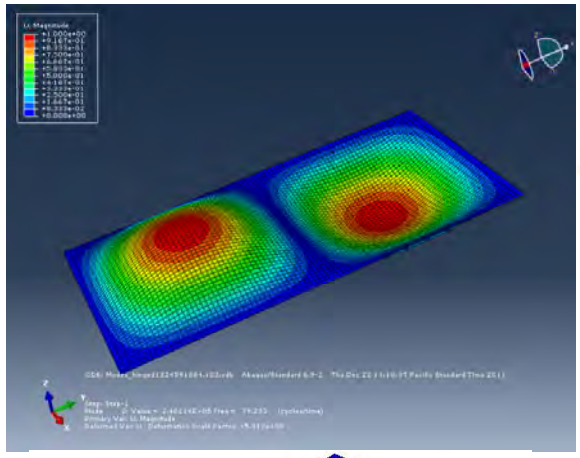

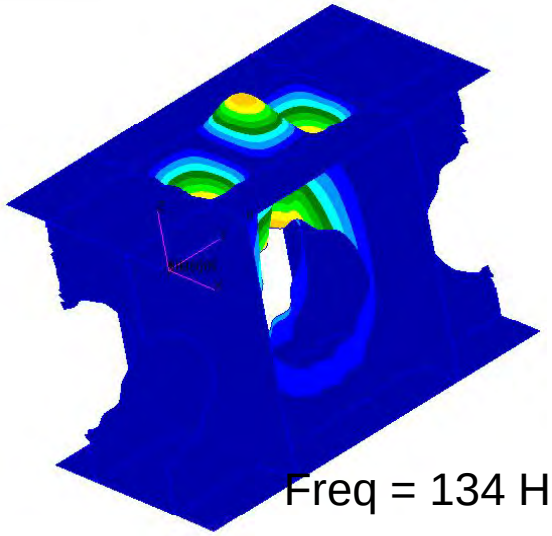

Freq = 134 Hz

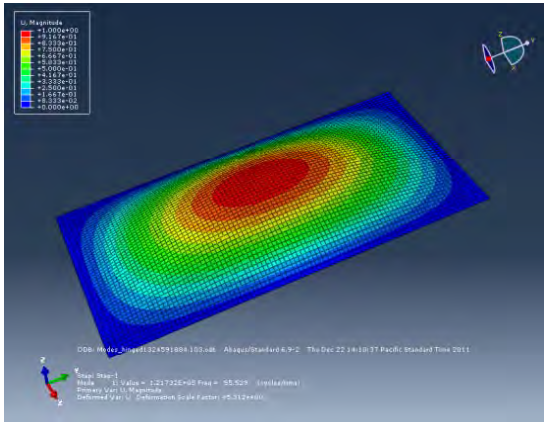

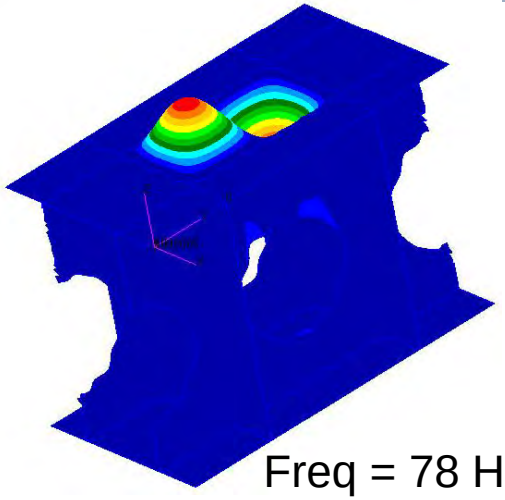

Freq = 78 Hz

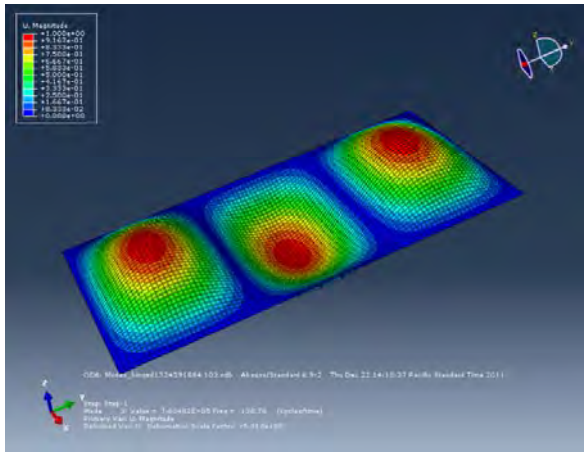

Approved for public release; distribution unlimited.

Comparison of Modal Frequencies

Mode No.	Hinged (Hz, T=75º)	Hinged (Hz, t=1080sec)	Fixed (Hz, T=75º)	Fixed (Hz, t=1080sec)	Linear Response w/ Unit-cell
1 (symm)	55.53	51.78	72.19	67.41	54
2	79.29	73.98	96.83	90.41	78
3 (symm)	138.78	129.51	155.49	145.16	134
4 (symm)	198.29	184.93	220.75	205.99	
5	209.56	195.47	232.82	217.28	
6	229.51	214.18	245.91	229.54	
7 (symm)	244.08	227.69	267.47	249.63	
8	310.19	289.41	333.03	310.82	
9 (symm)	347.96	324.75	364.45	340.17	
10 (symm)	409.13	381.77	431.30	402.54	
11 (symm)	436.54	407.17	463.51	432.43	
12	441.63	411.97	469.40	437.99	

Symm indicates symmetric modes w.r.t. short panel direction (x-axis)

Approved for public release; distribution unlimited.

Structural Damping

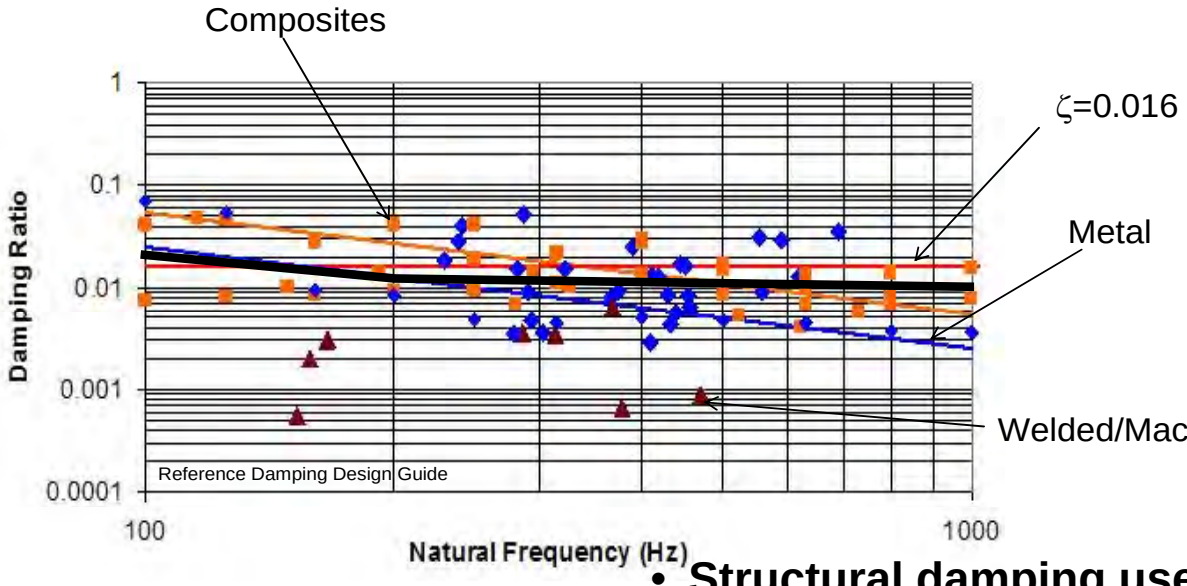

Frequency (Hz)	Damping Ratio
10	0.025
100	0.02
1000	0.01

Viscous Damping Matrix

$$\mathbf{C} = \alpha\mathbf{M} + \beta\mathbf{K}$$

$$\xi_n = \frac{1}{2}\left(\frac{\alpha}{\omega_n} + \beta\omega_n\right)$$

- **Structural damping used in Panel 1 linear response analysis was adopted**
- **Only the alpha term is used to generate damping matrix *C*, and only damping ratio of fundamental mode is used to generate Alpha. Therefore,**
  - **α =18.5 for fixed BC (ξ=0.0218)**
  - **α =14.8 for hinged BC (ξ=0.0227)**

Approved for public release; distribution unlimited.

Damping for Explicit Dynamic Analysis

Given, w_1, w_2, ξ_1, and ξ_2, a and b can be estimated from solving these two equations

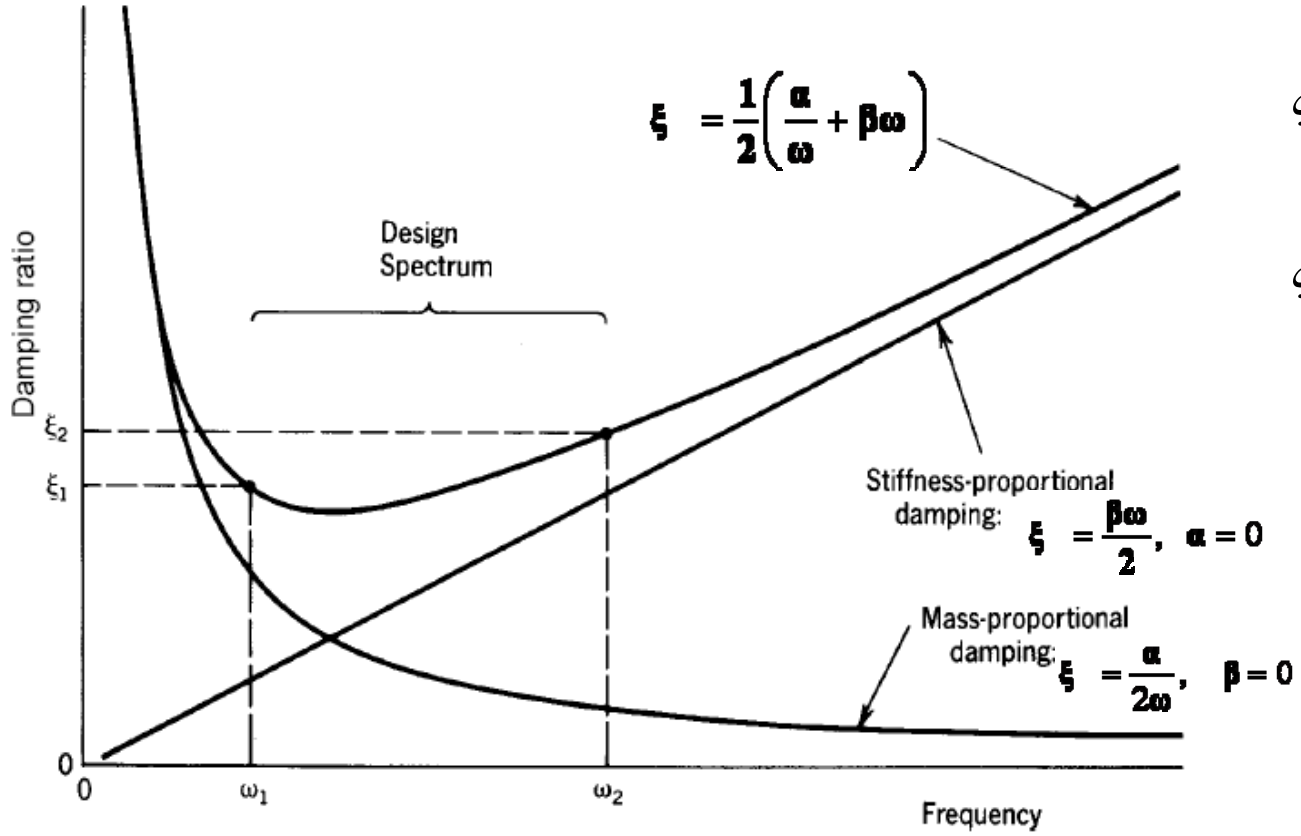

$$\xi_1 = \frac{1}{2}\left(\frac{\alpha}{\omega_1} + \beta\omega_1\right)$$

$$\xi_2 = \frac{1}{2}\left(\frac{\alpha}{\omega_2} + \beta\omega_2\right)$$

Approved for public release; distribution unlimited.

Comparison of Static and Quasi-dynamic: Total Displacements; Hinged BC; Thermal Loads

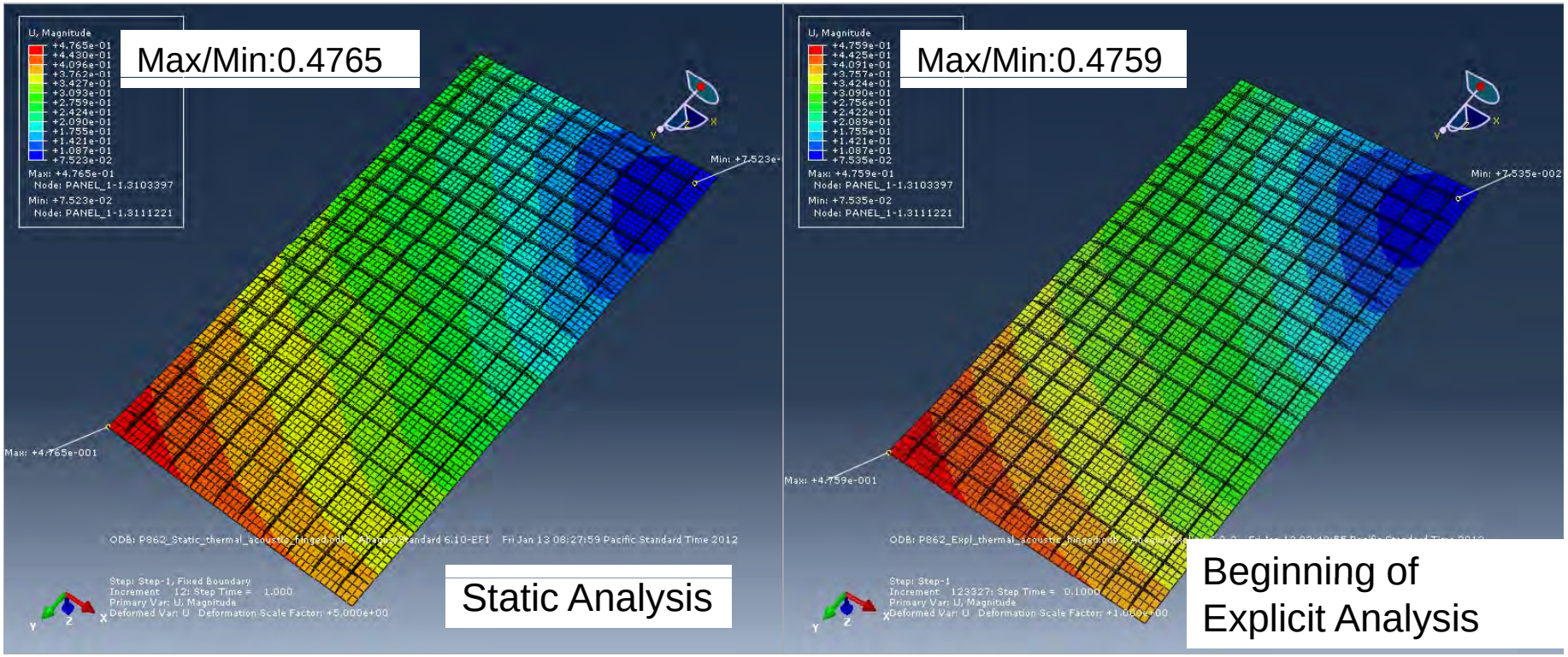

An Initial Time Step of 0.1 sec with ramped thermal preloads and boundary displacements to stabilize response

Approved for public release; distribution unlimited.

Comparison of Static and Quasi-dynamic: Normal Displacements; Hinged BC; Thermal Loads

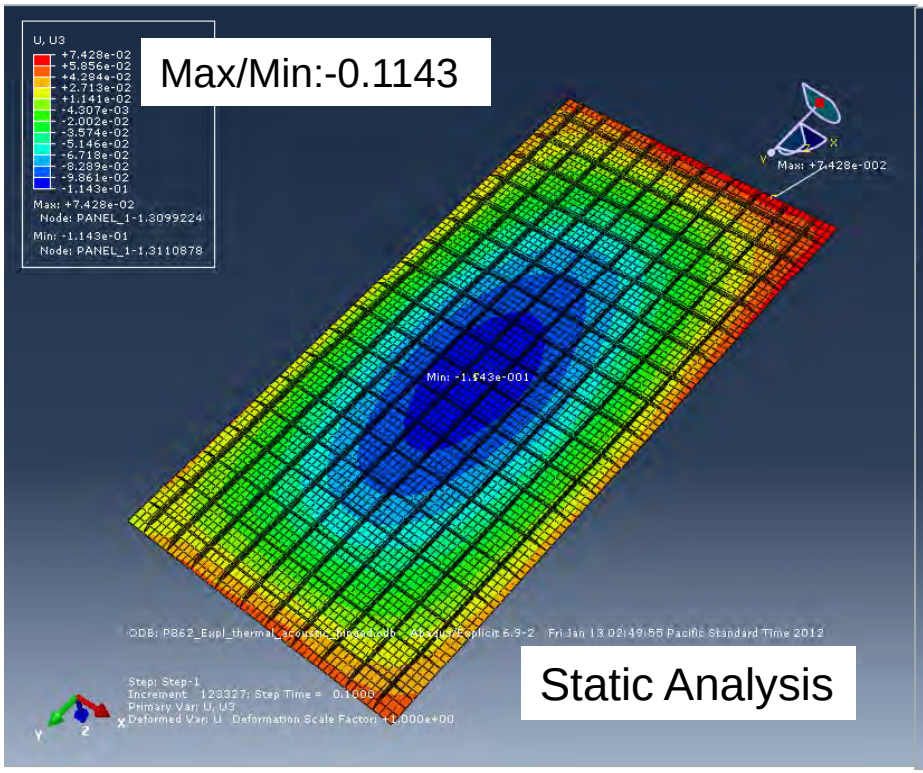

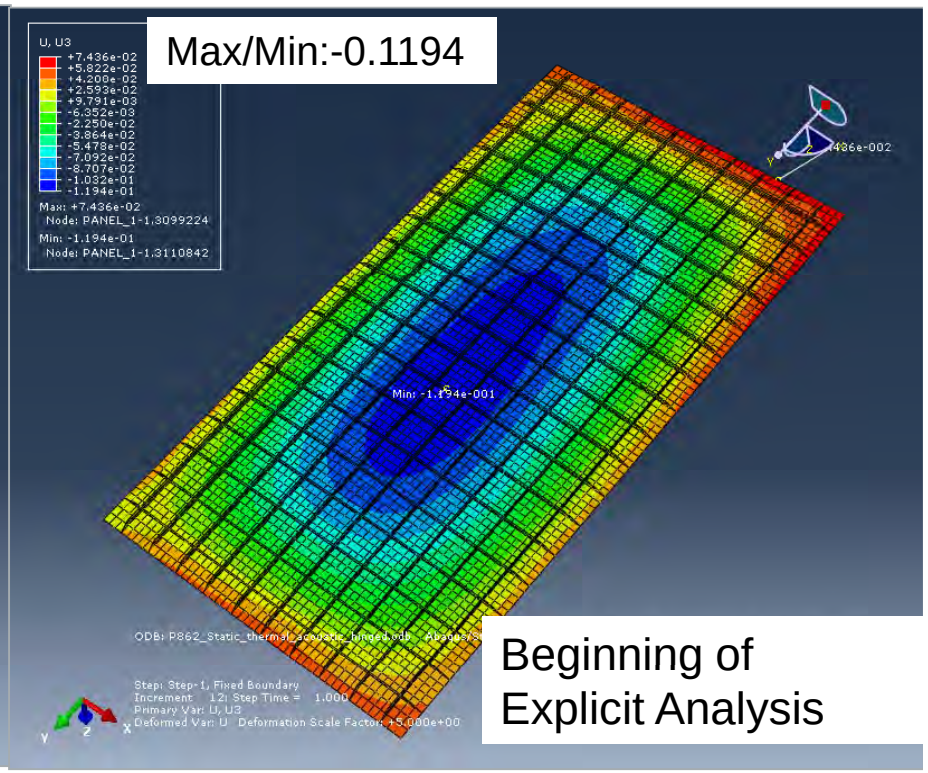

Difference of Normal displacements is ~4.5%

Approved for public release; distribution unlimited.

Comparison of Static and Quasi-dynamic: von Mises Stress; Hinged BC; Thermal Loads

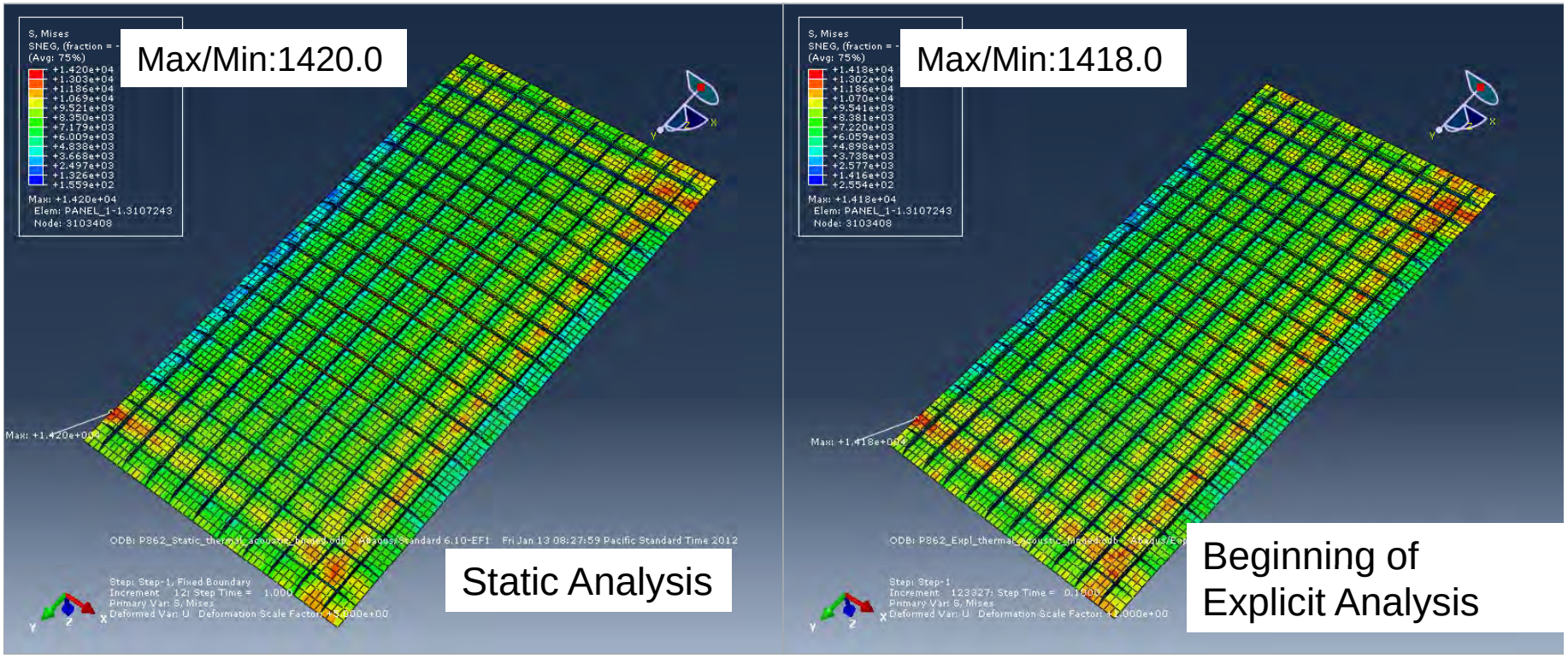

Difference of Max von Mises is less than 0.2%

Approved for public release; distribution unlimited.

Comparison of Static and Quasi-dynamic: Total Displacements; Fixed BC; Thermal Loads

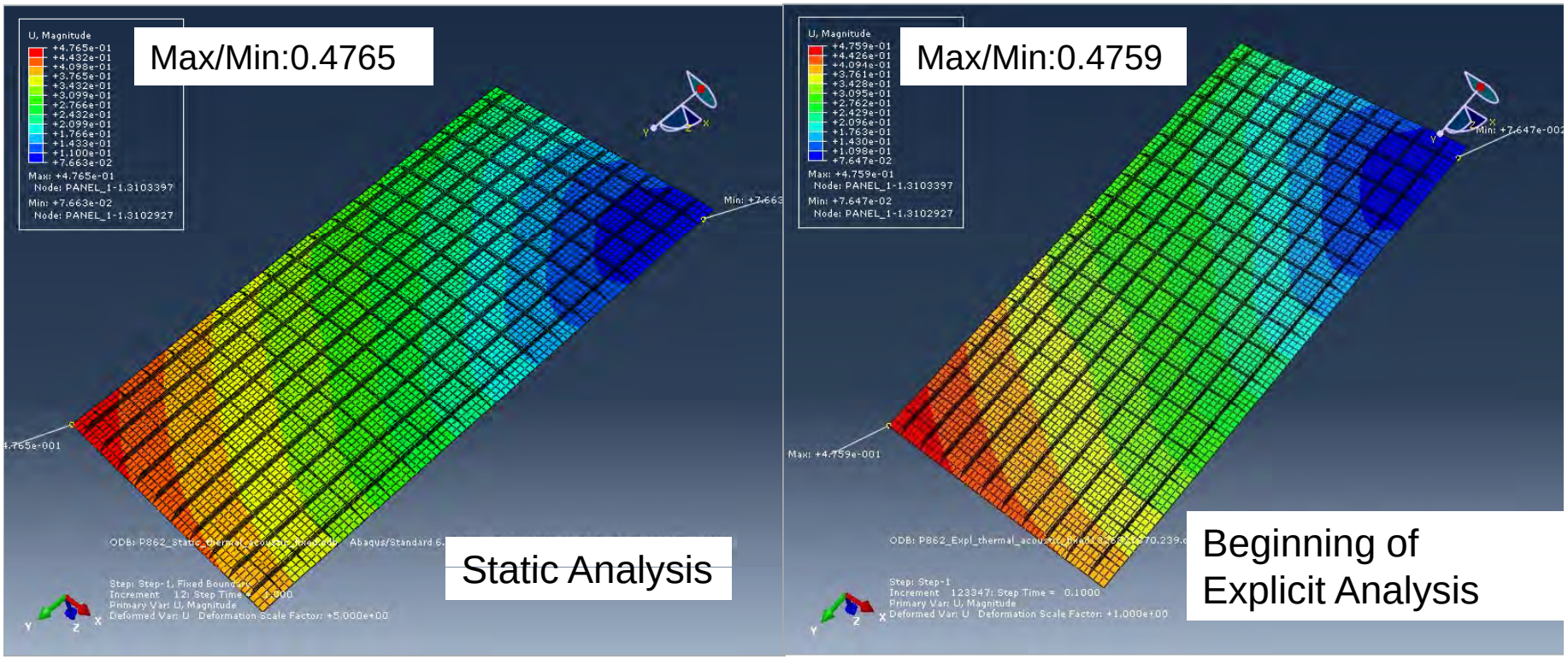

Approved for public release; distribution unlimited.

Comparison of Static and Quasi-dynamic; Normal Displacement; Fixed BC; Thermal Loads

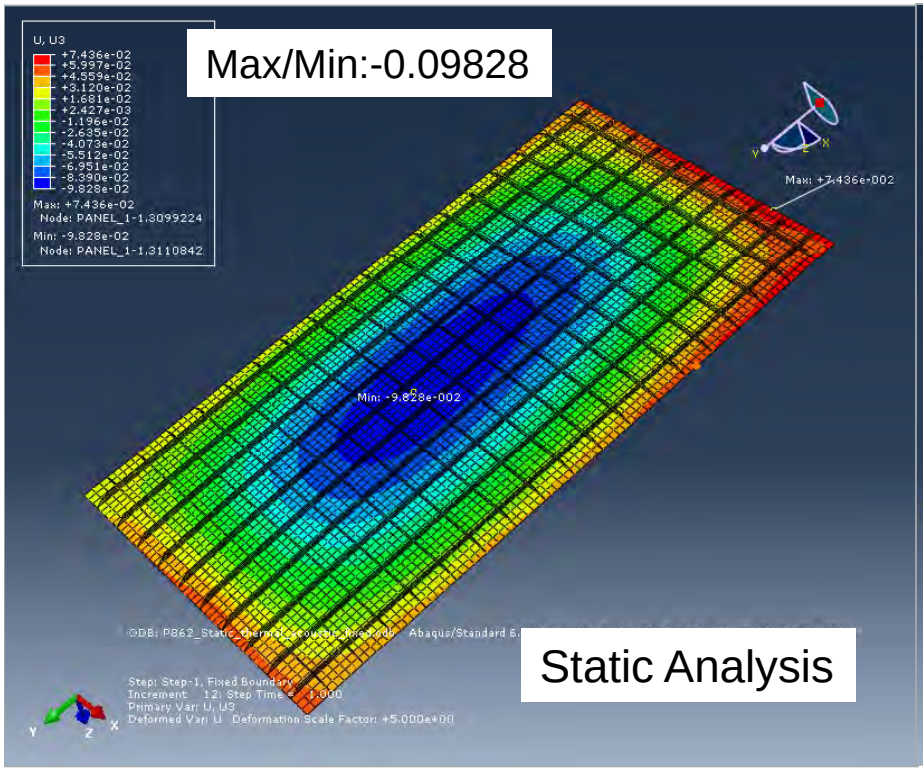

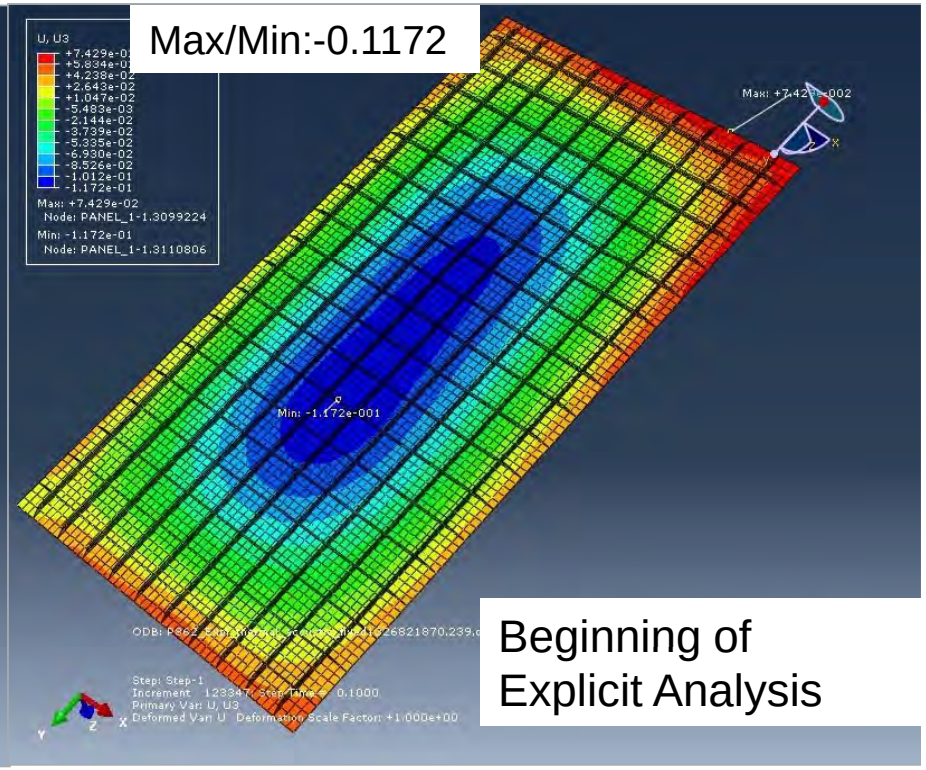

Difference of Normal displacements is ~19%

- Inertia effect in ramped thermal loads may not be fully stablized. A longer initial run time (>0.1 sec) may reduce the difference

Approved for public release; distribution unlimited.

Comparison of Static and Quasi-dynamic: von Mises Stress; Fixed BC; Thermal Loads

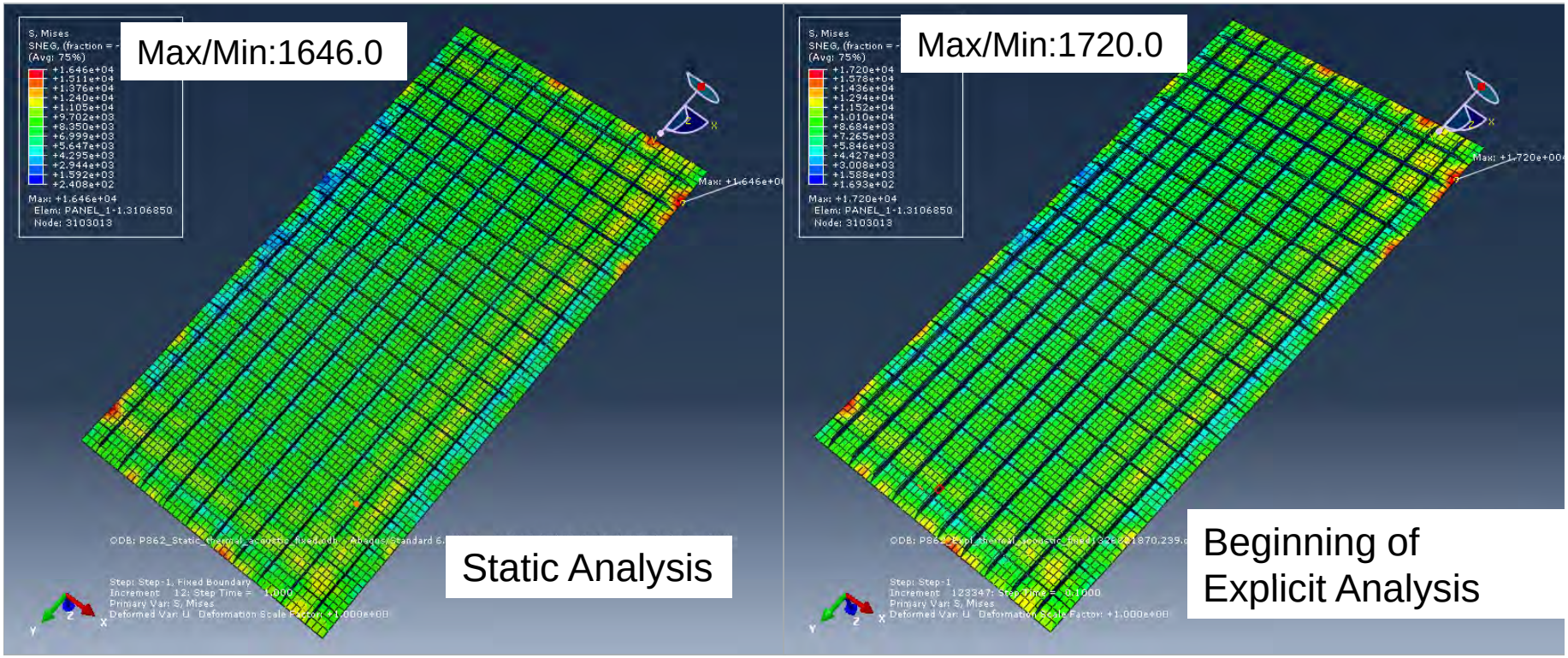

Difference of Max von Mises is ~4.5%

Approved for public release; distribution unlimited.

Principal Stresses due to Thermal Loads; Hinged BC

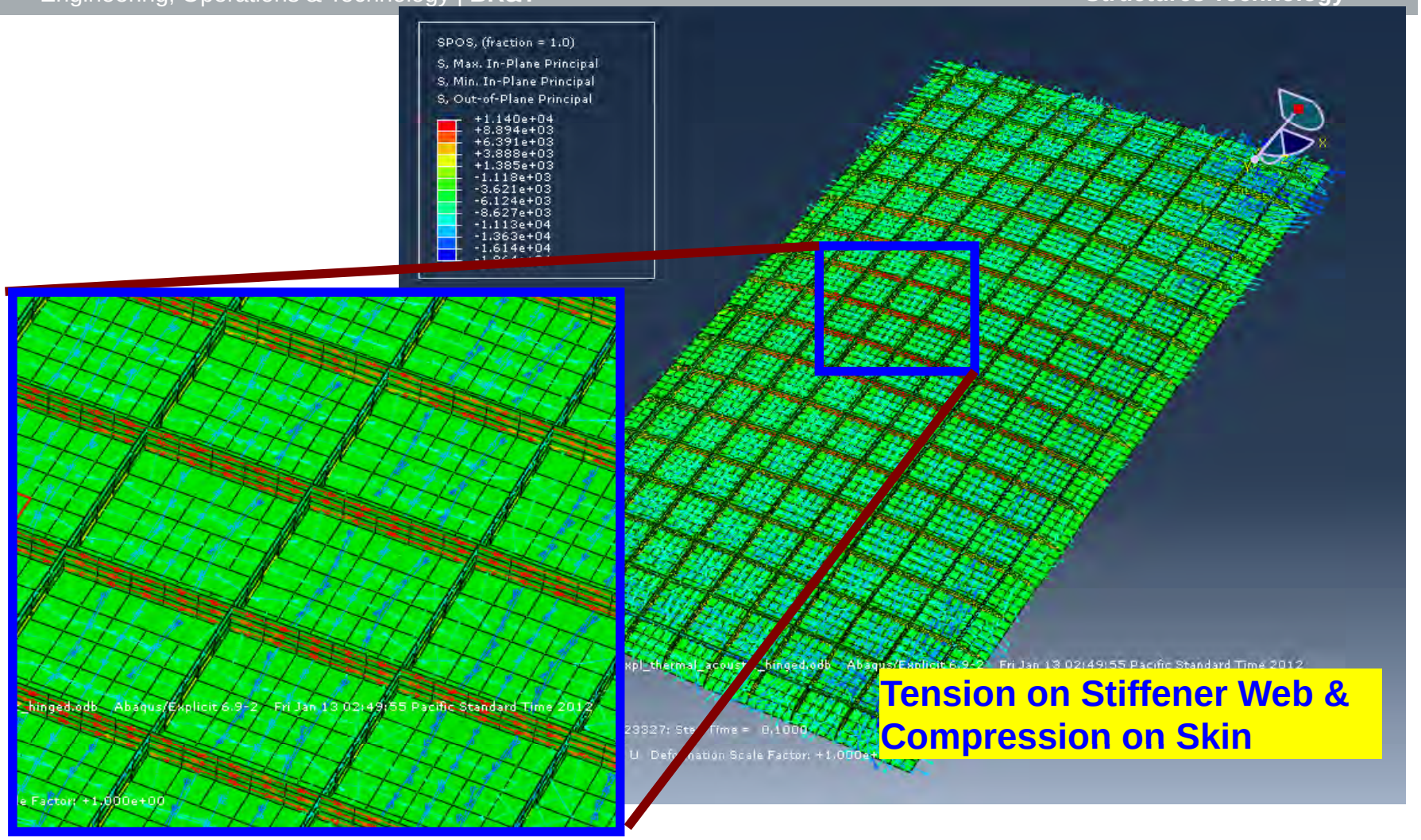

Approved for public release; distribution unlimited.

Principal Stresses due to Thermal Loads; Hinged BC

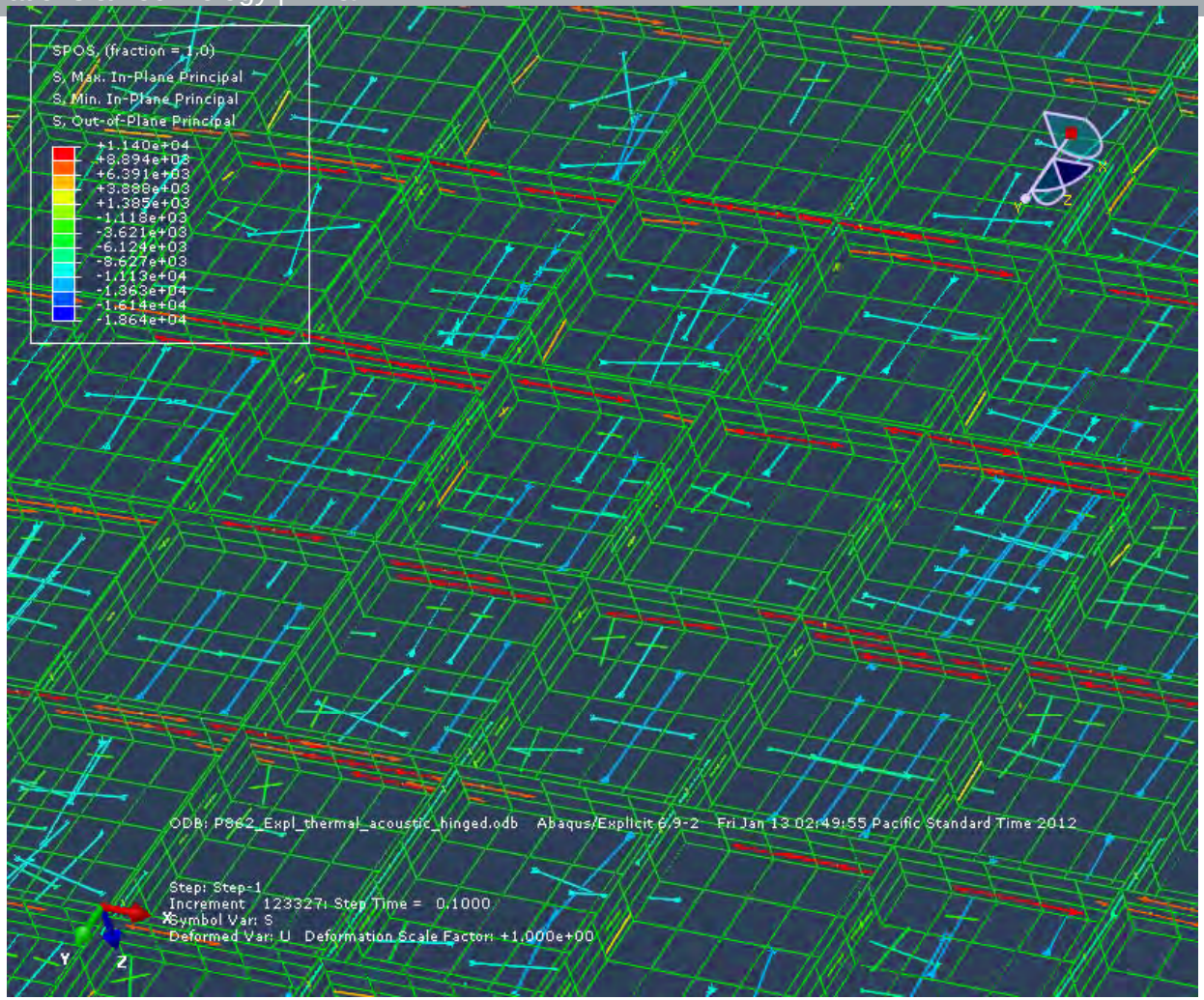

Approved for public release; distribution unlimited.

Principal Stresses due to Thermal Loads; Fixed BC

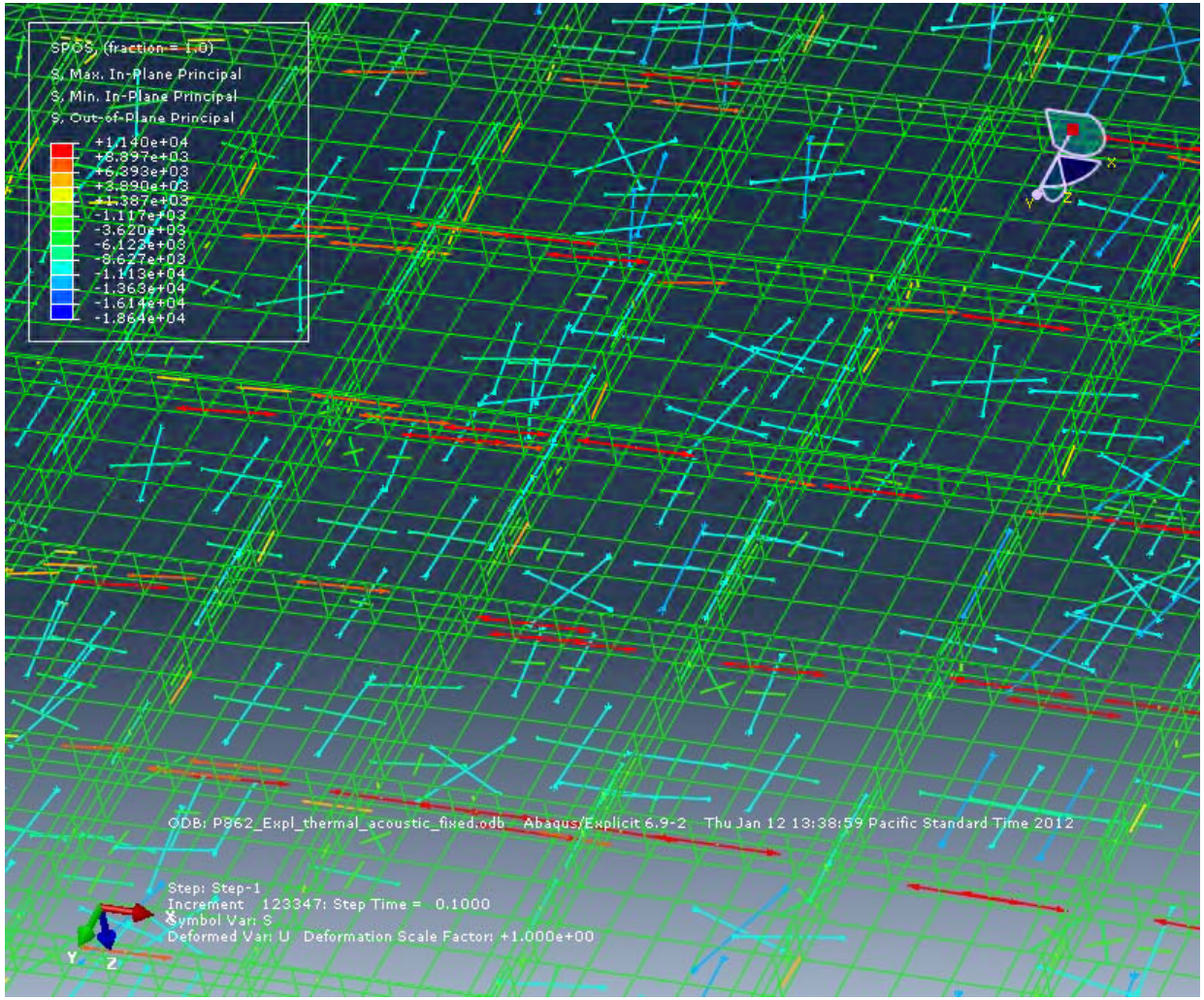

Approved for public release; distribution unlimited.

Time History of Acoustic Pressure

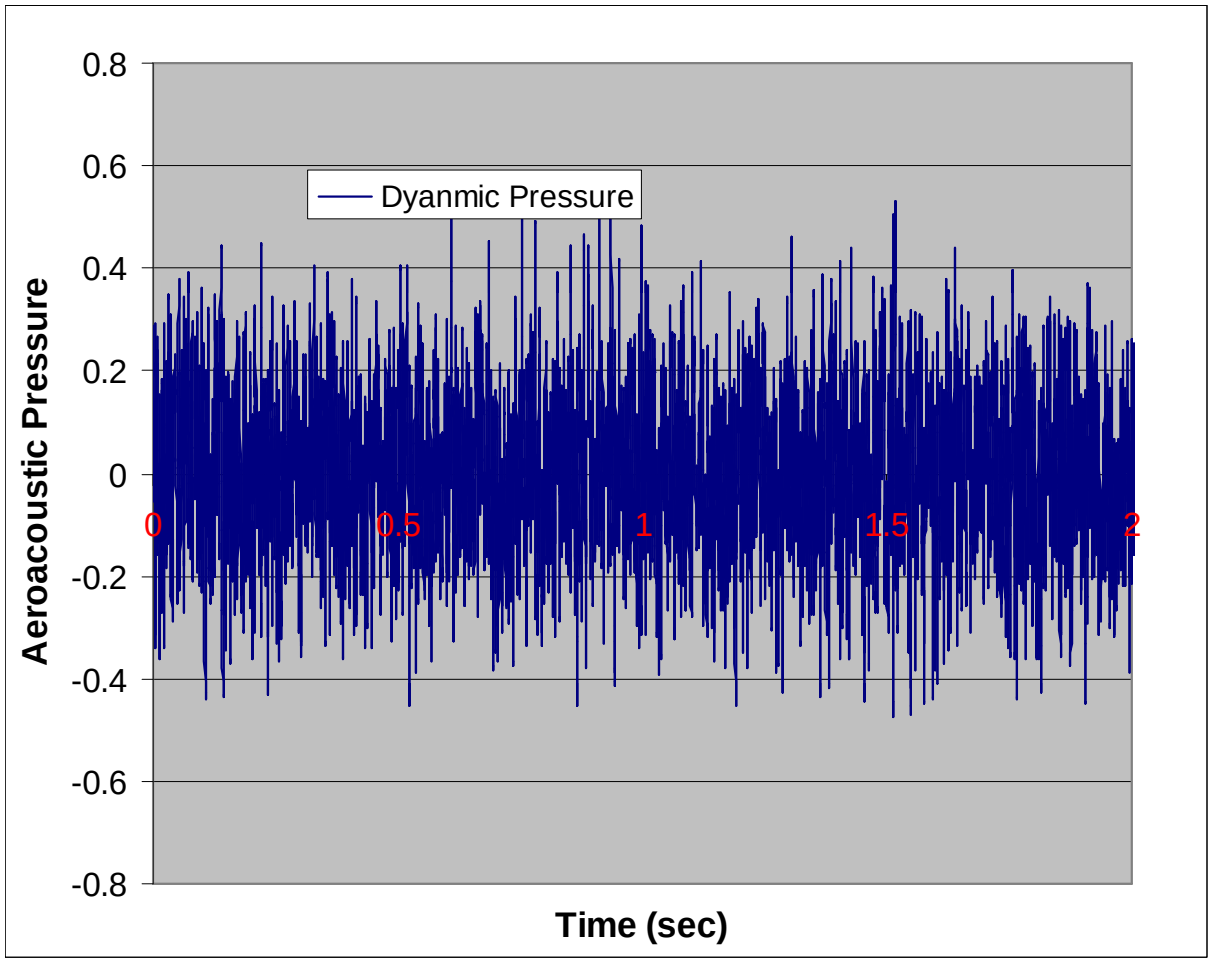

Approved for public release; distribution unlimited.

Normal Displacements for Acoustic Pressure; Thermal Loads, Hinged BC

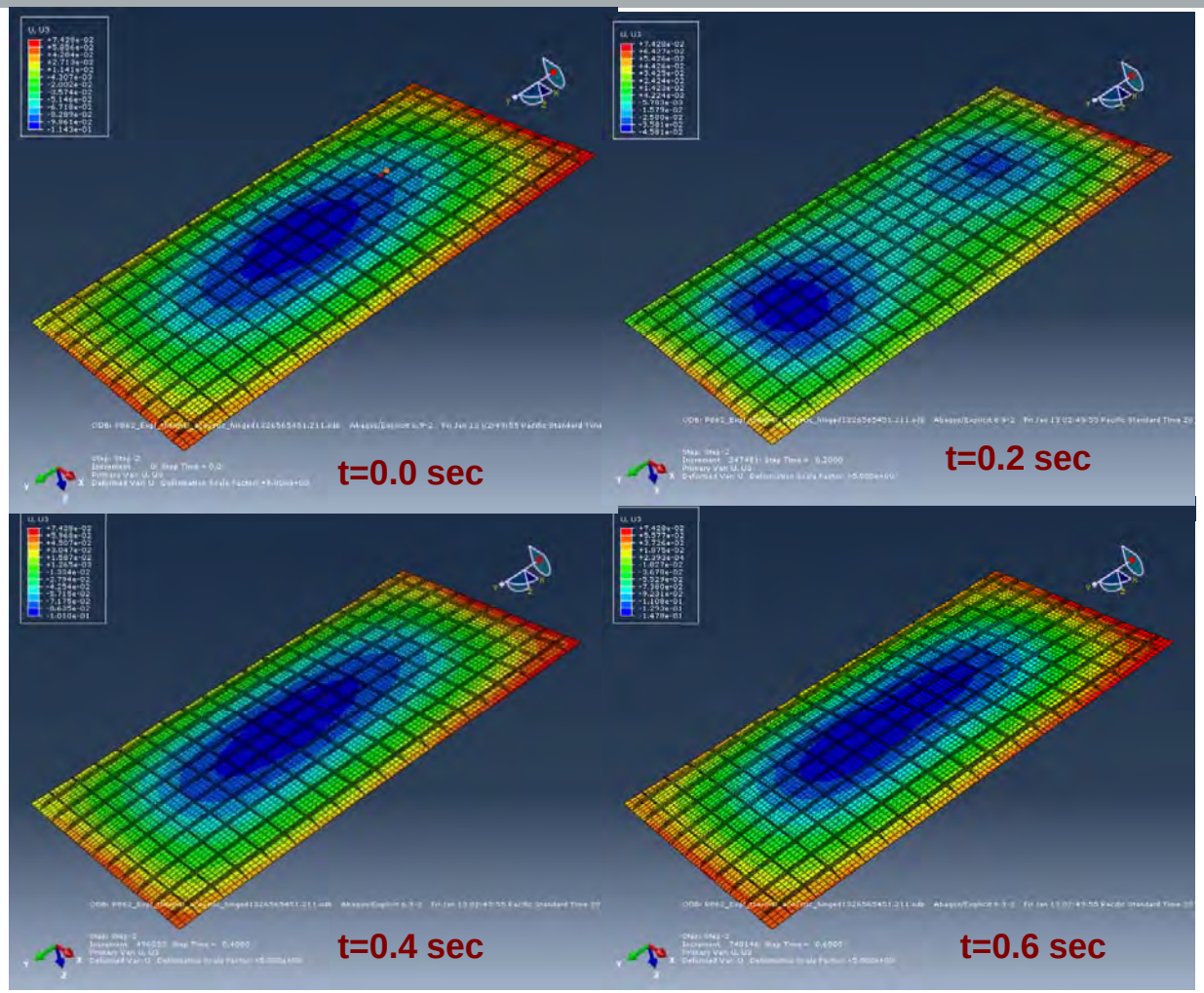

Approved for public release; distribution unlimited.

Normal Displacements for Acoustic Pressure; Thermal Loads, Hinged BC (cont.)

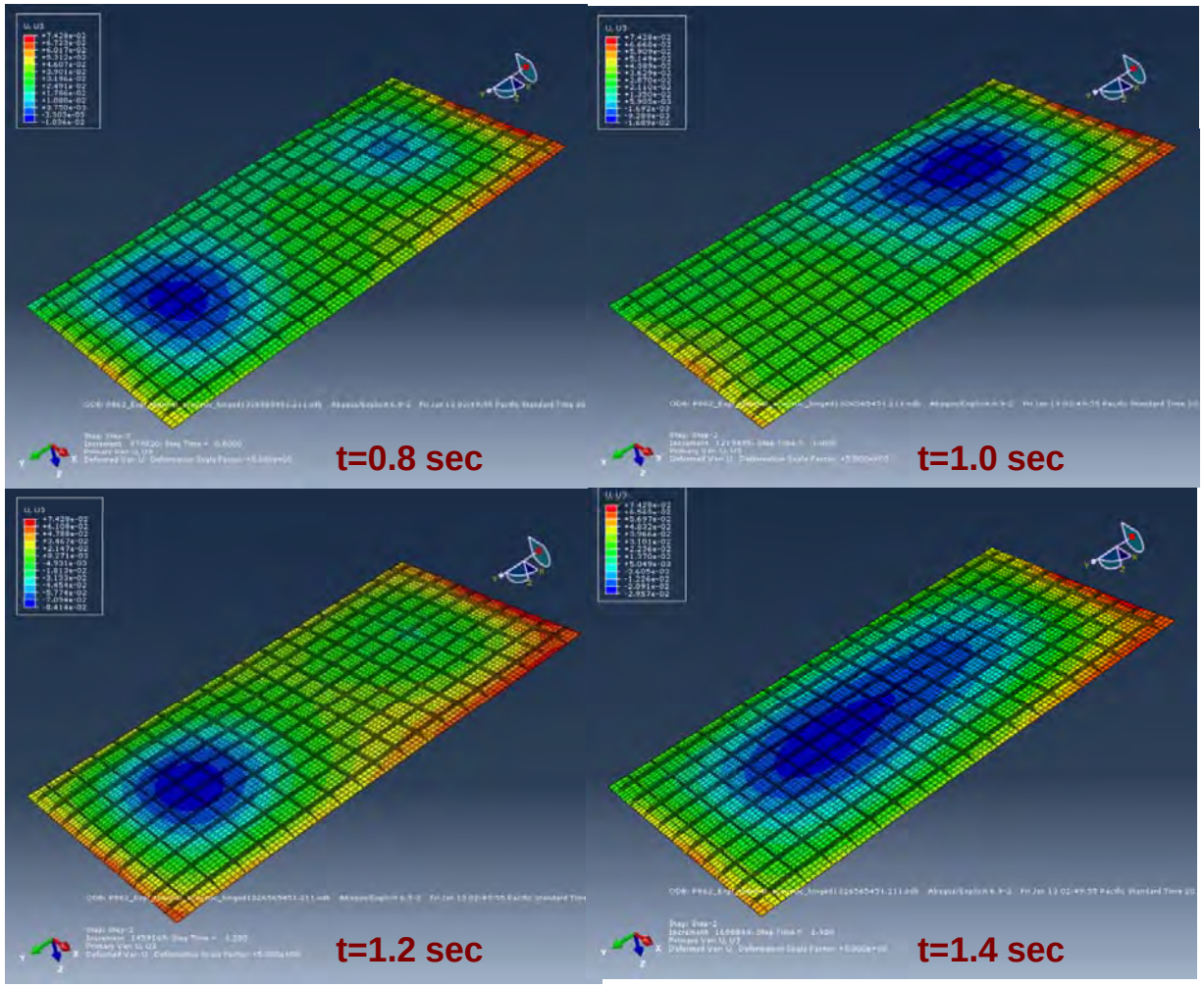

Approved for public release; distribution unlimited.

Normal Displacements for Acoustic Pressure; Thermal Loads, Hinged BC (cont.)

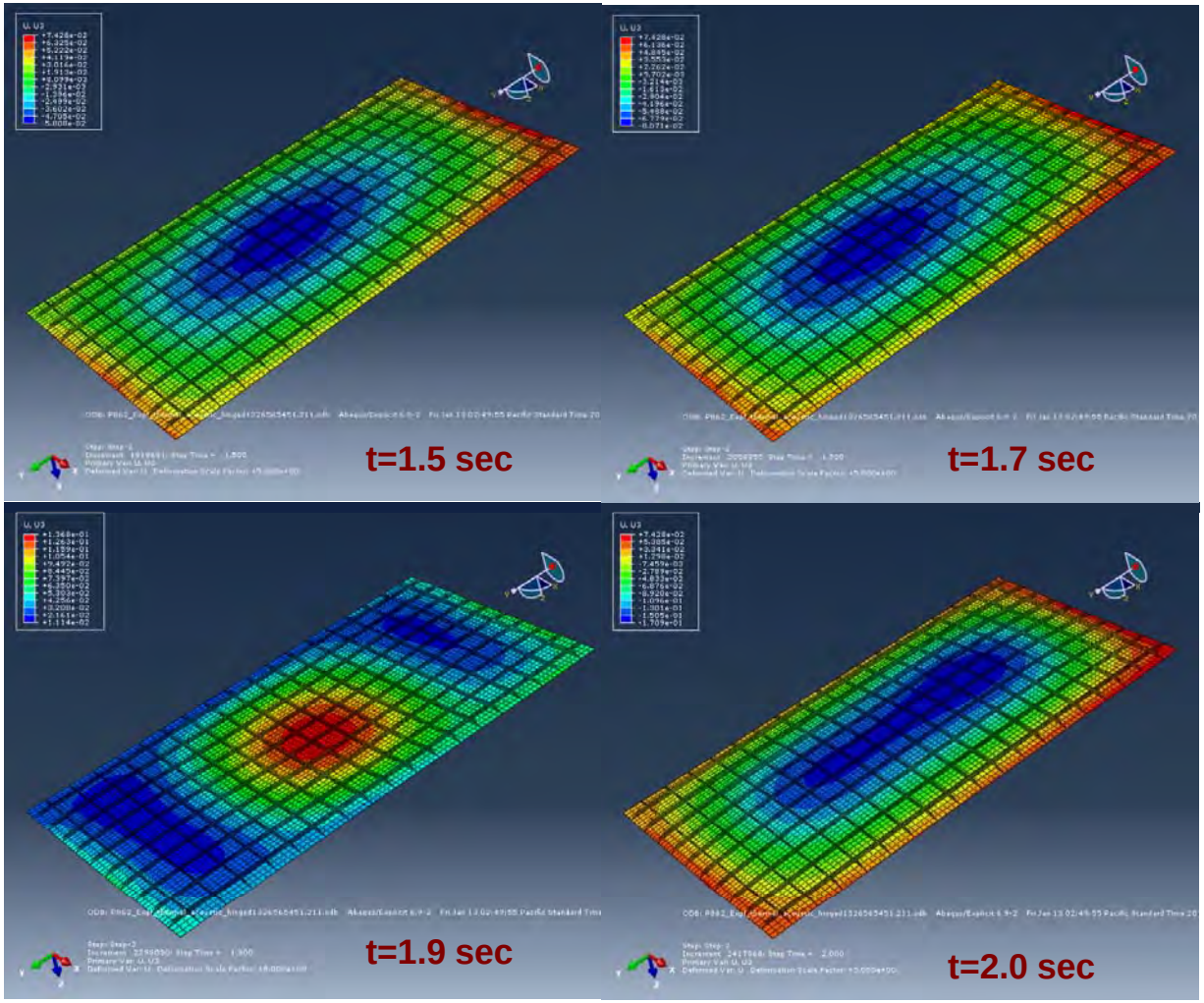

Approved for public release; distribution unlimited.

Hinged-BC Panel Vibrated under Combined Loading

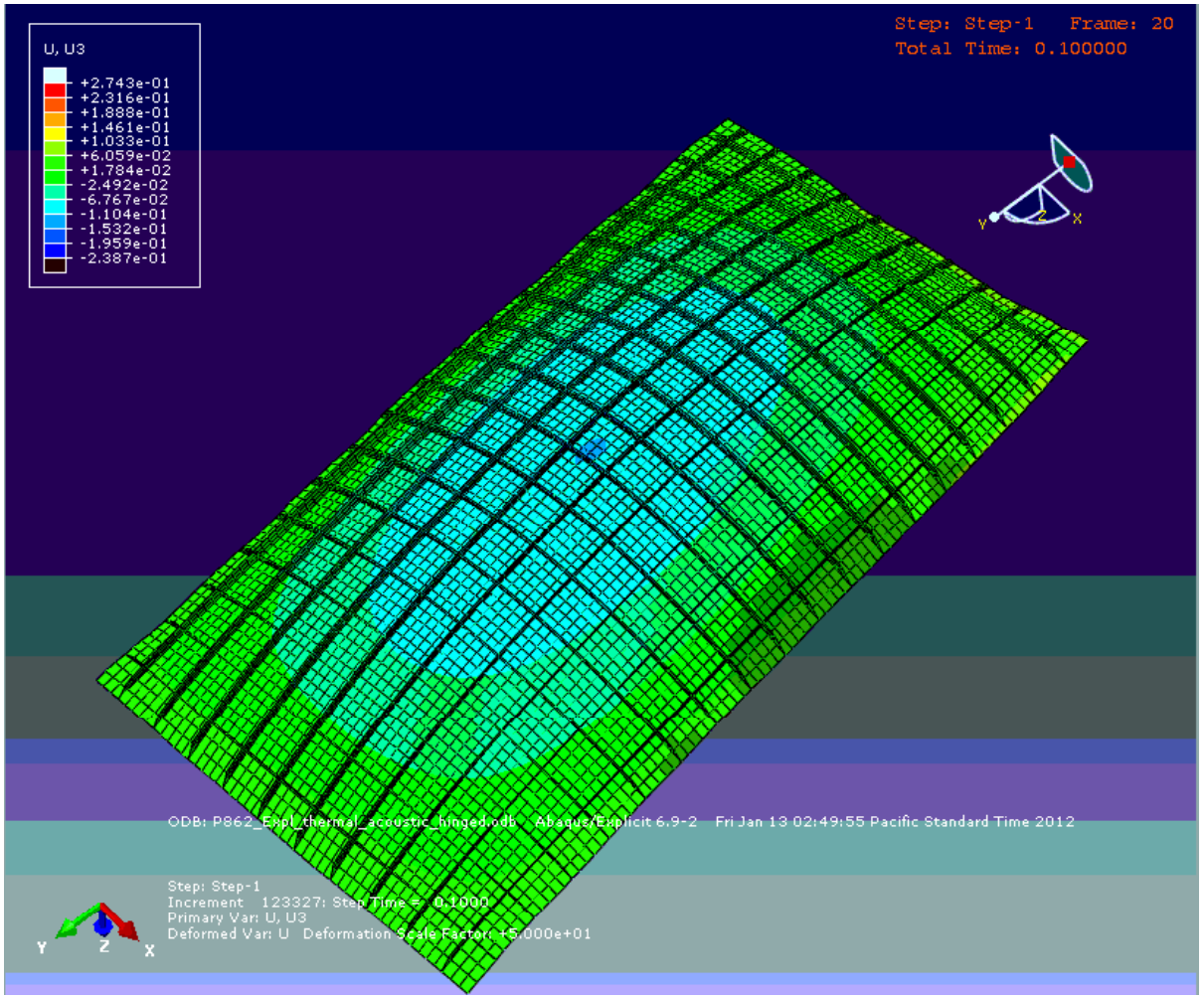

Approved for public release; distribution unlimited.

Node and Element Locations for Time History Result

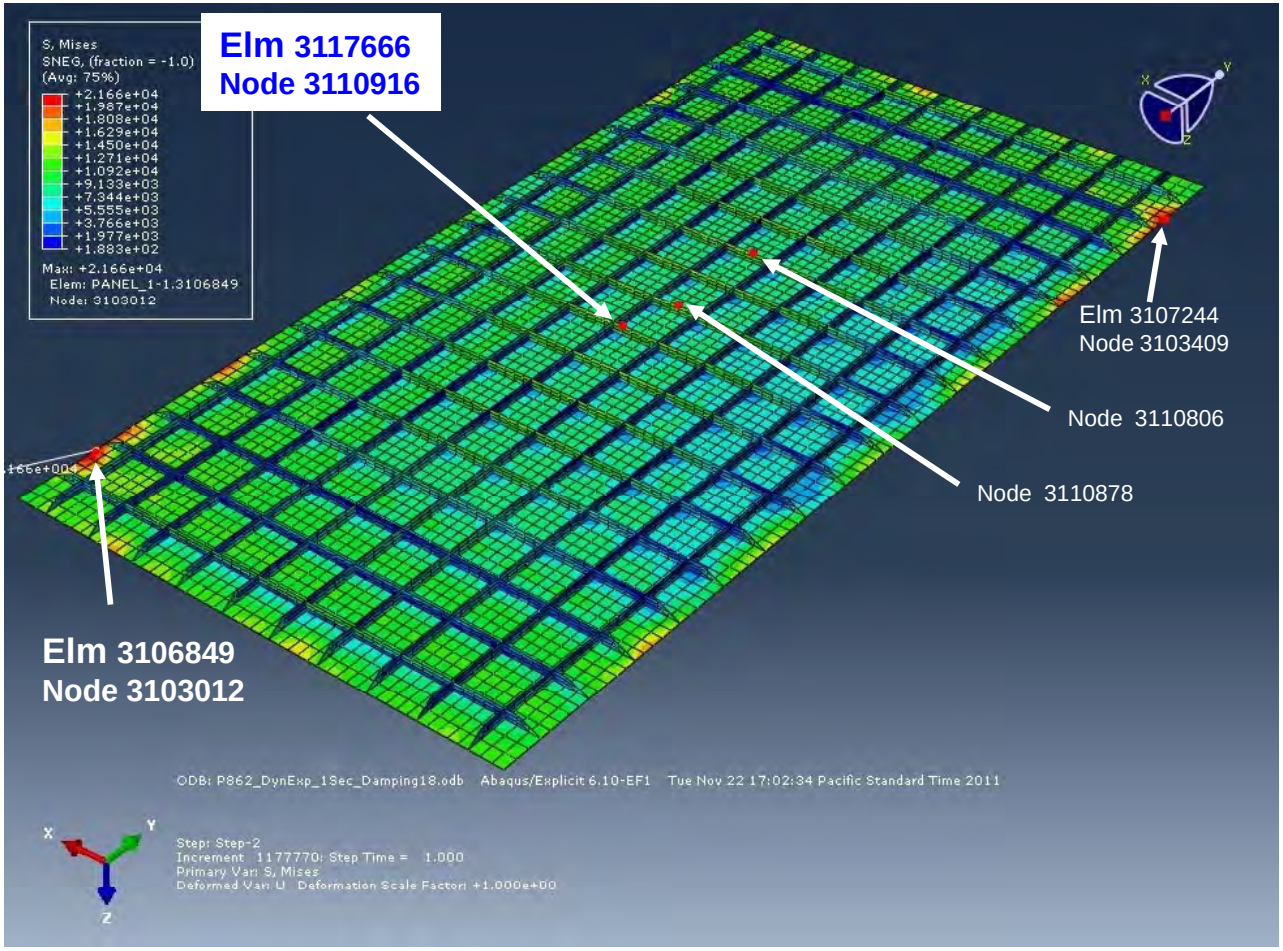

Approved for public release; distribution unlimited.

Dynamic Response of Normal Displacement; No Thermal Loads, Hinged BC

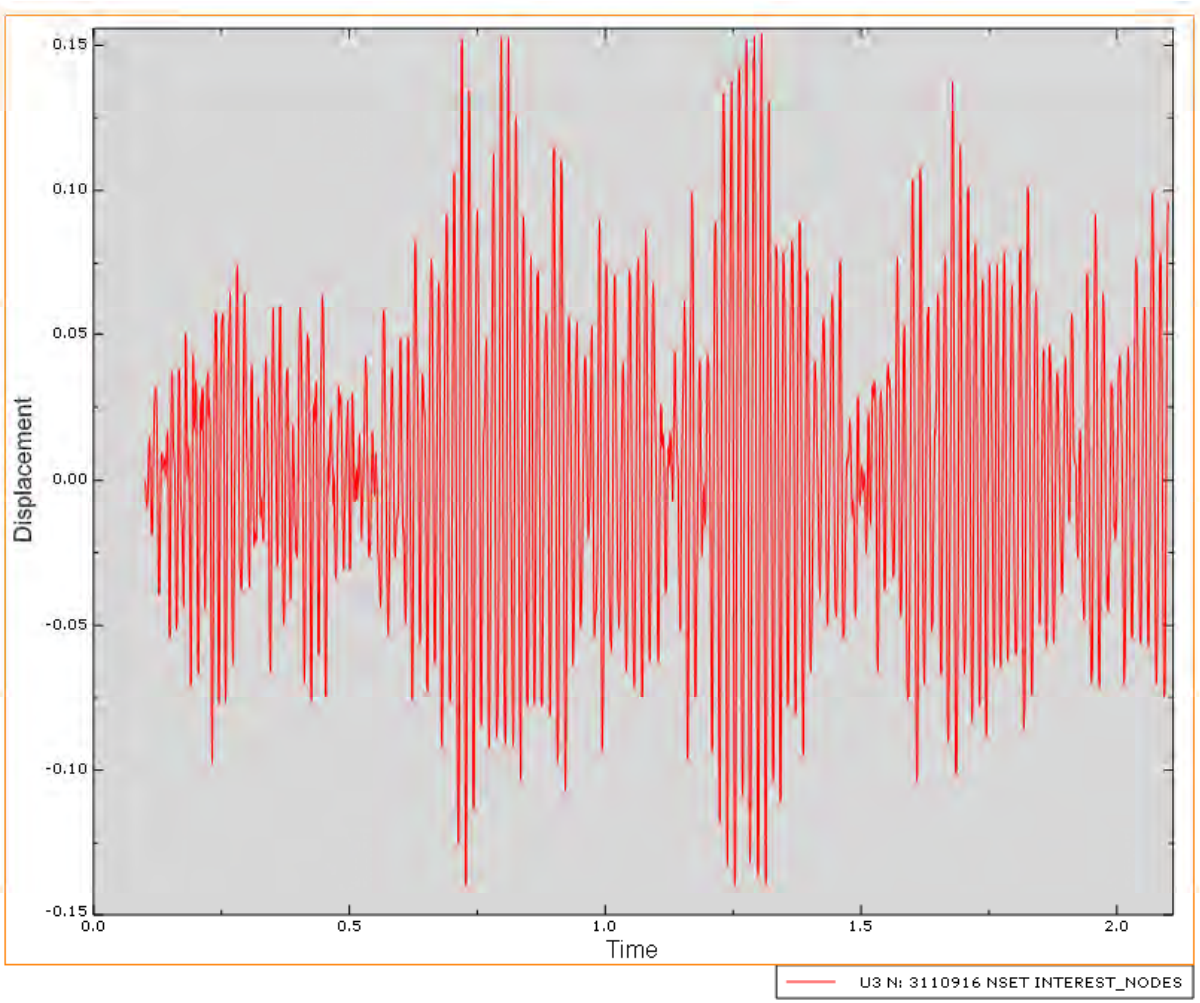

Approved for public release; distribution unlimited.

Dynamic Response of Normal Displacement; Thermal Loads, Hinged BC

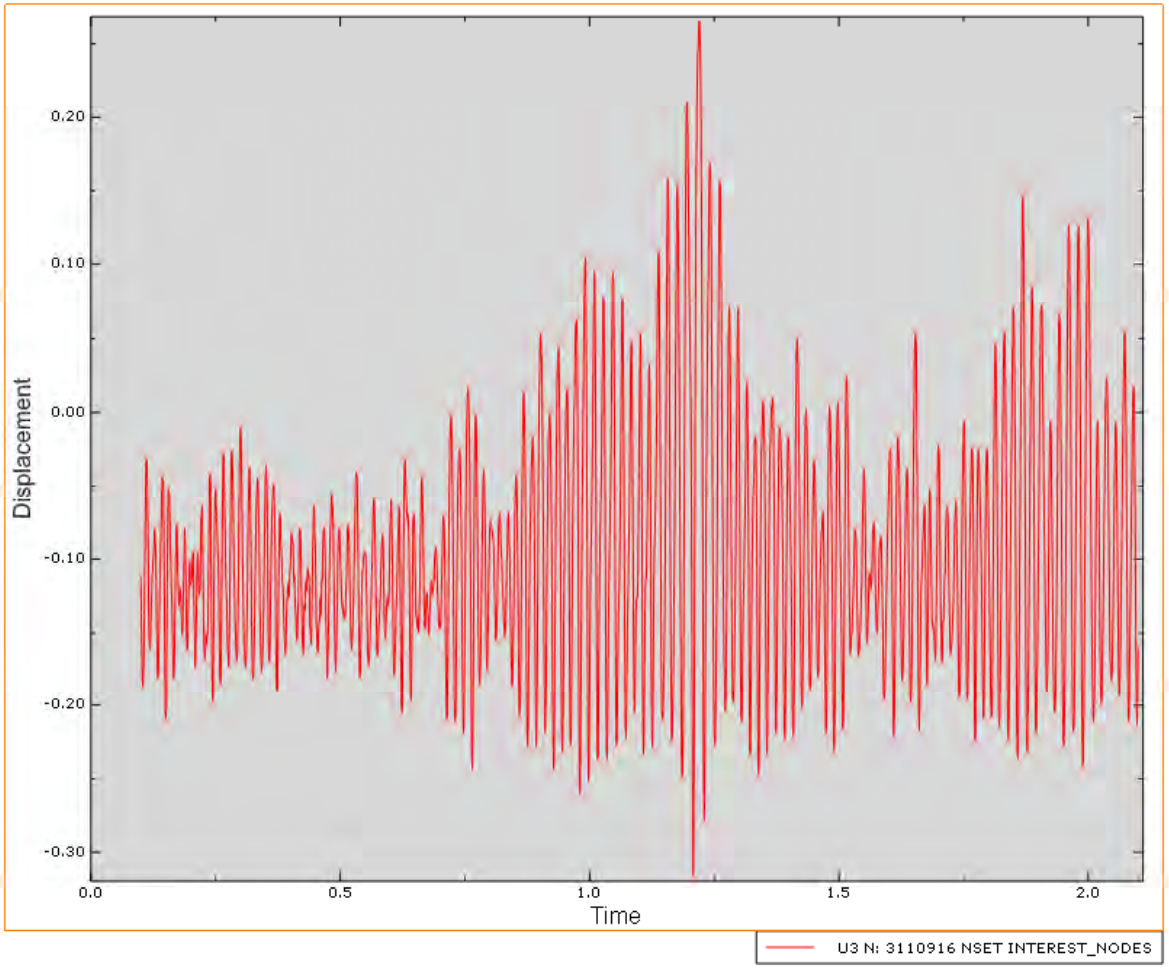

Approved for public release; distribution unlimited.

Time History of Stress S11 for Element 3117666; No Thermal Loads, Hinged BC

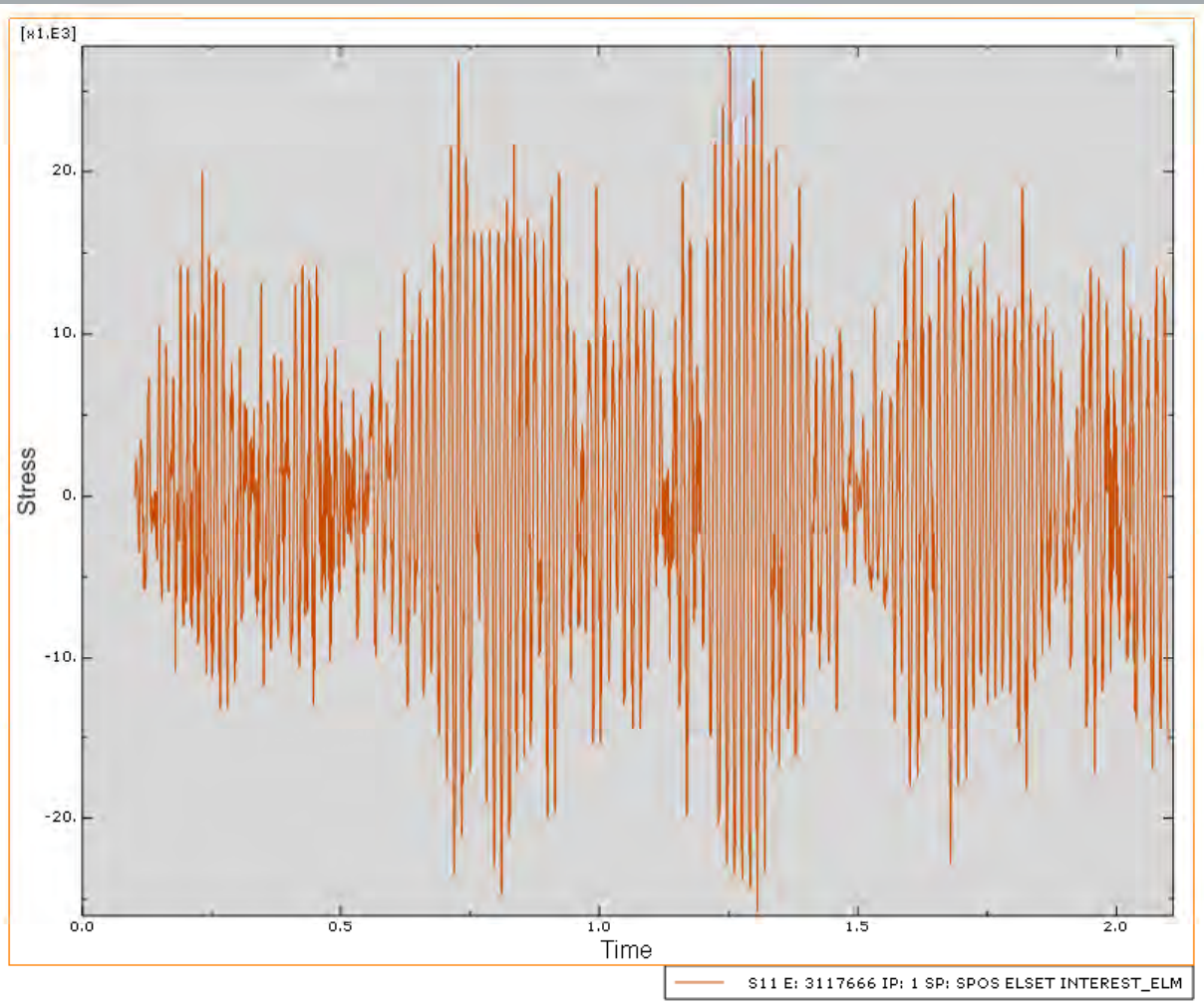

Approved for public release; distribution unlimited.

Time History of Stress S11 for Element 3117666; Thermal Loads, Hinged BC

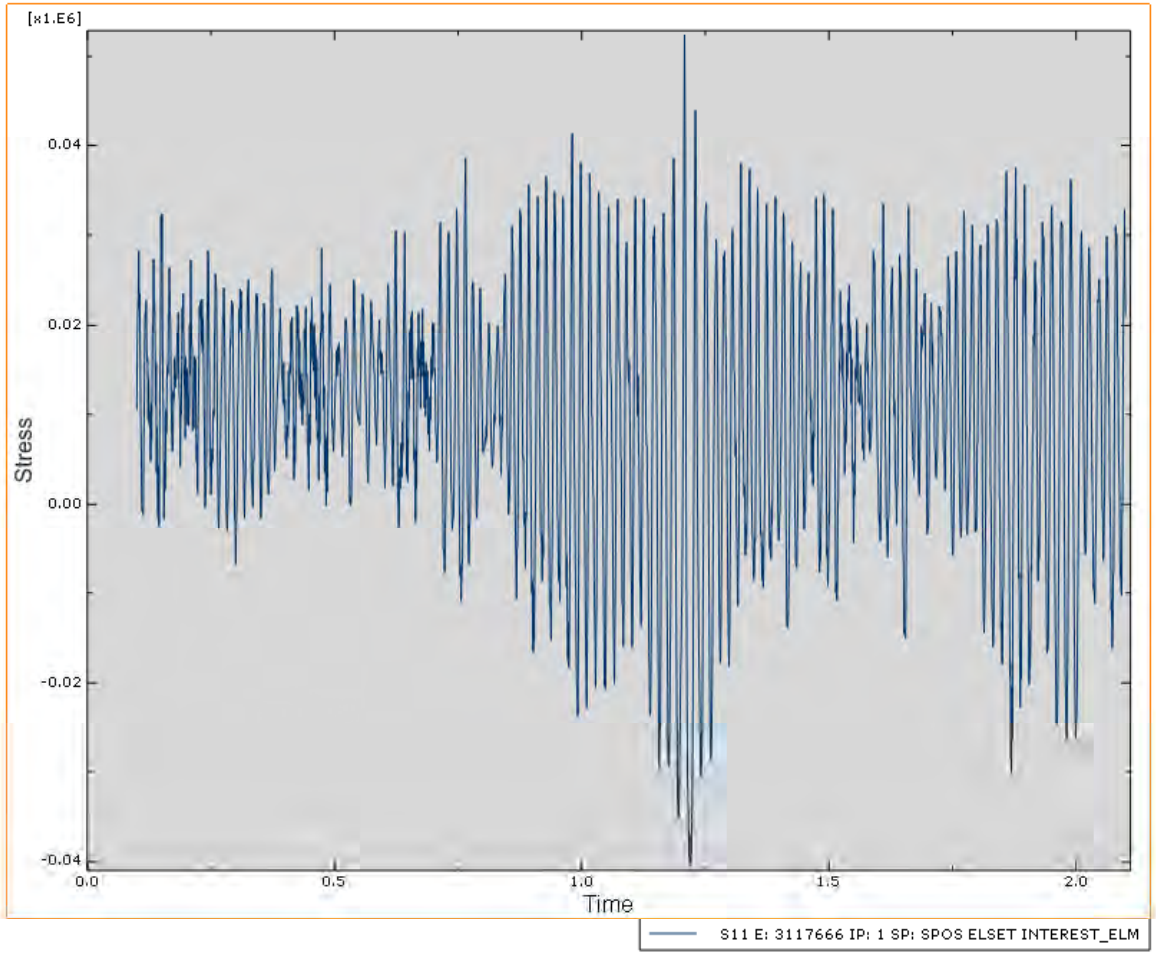

Approved for public release; distribution unlimited.

Comparison of Normal Displacement at Center of Panel

Analysis Condition	Mean	Standard Deviation	Root Mean Square
Fixed BC w/o Thermal Loads	.0027	0.051	.0511
Hinged BC w/o Thermal Loads	.0105	0.077	.0777
Fixed BC w/ Thermal Loads	-.0931	0.050	.1055
Hinged BC w/ Thermal Loads	-0.0941	0.084	.1262

Approved for public release; distribution unlimited.

Comparison of Stress S11 on Stiffener Web at Center of Panel

Analysis Condition	Mean	Standard Deviation	Root Mean Square
Fixed BC w/o Thermal Loads	-201	8681	8683
Hinged BC w/o Thermal Loads	-979	11440	11479
Fixed BC w/ Thermal Loads	9562	9554	13515
Hinged BC w/ Thermal Loads	9475	14198	17066

RMS Stress for the case with hinged BC and thermal loads is higher than 17 ksi (allowable for R=-1 @ T=1050^{o}F)

Approved for public release; distribution unlimited.

Comparison of Normal Displacement at Node 3110916 for Hinged & Fixed BC w/o Thermal Loads

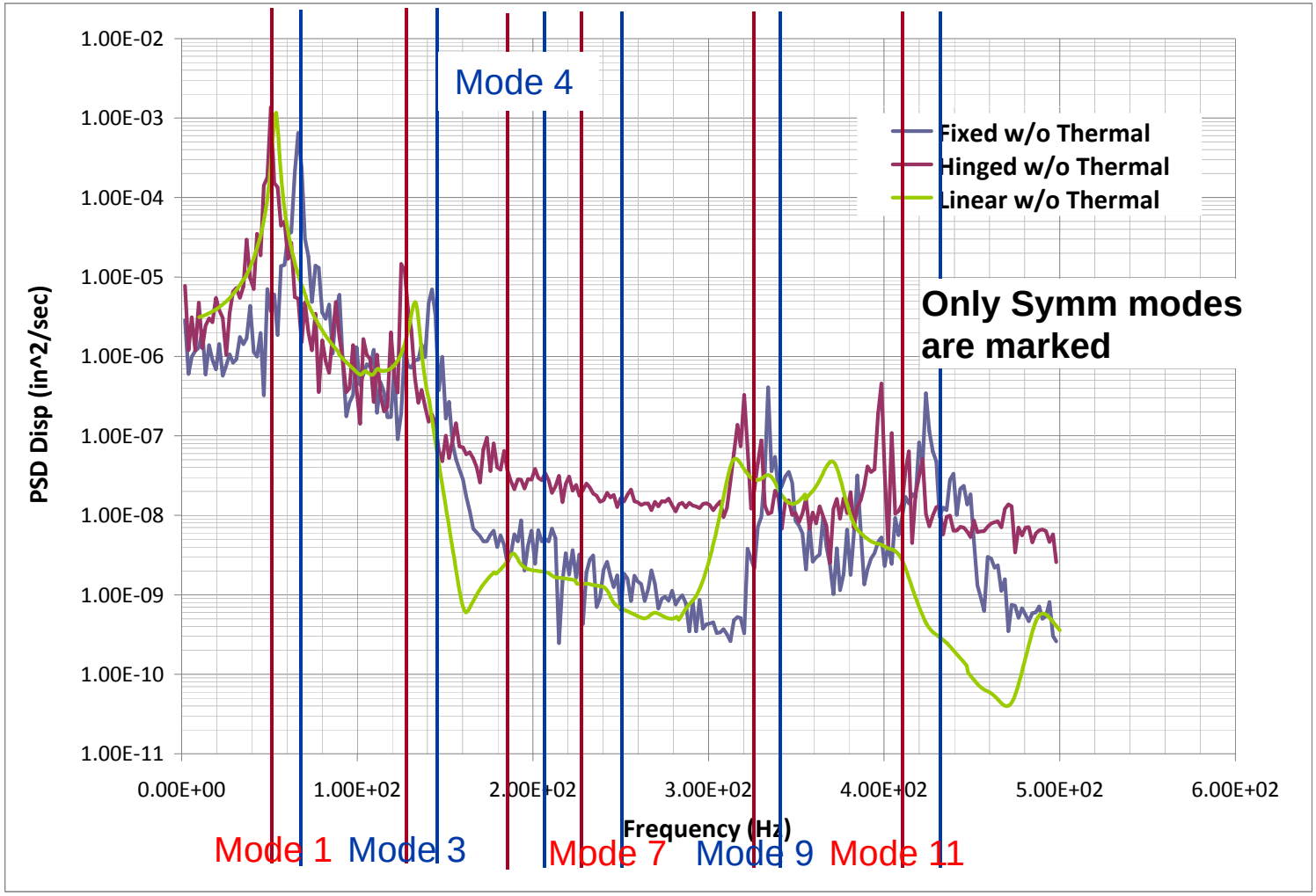

Approved for public release; distribution unlimited.

Comparison of Stress S11 at Element 311766 for Hinged & Fixed BC w/o Thermal Loads

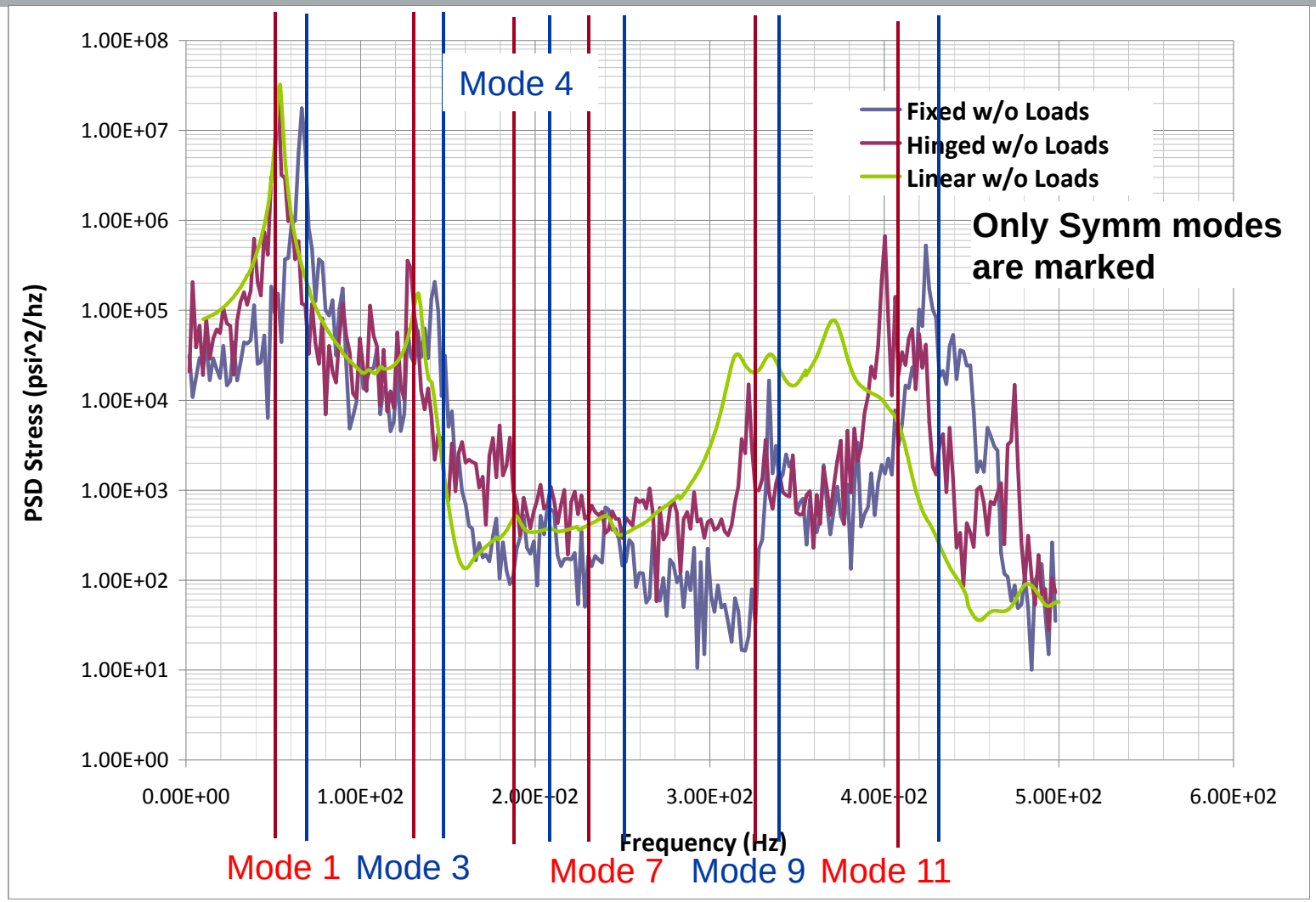

Approved for public release; distribution unlimited.

Notes from Observation

- The dominant PSD response of each case, i.e., hinged BC, fixed BC, and linear response analysis, matches their corresponding fundamental frequency. In other words, the system responds linearly to the acoustic pressure;
- The responses of fixed and hinged BC enclose that from linear response analysis;
- The acoustic pressure doesn't seem to excite the 2nd mode, which is the first anti-symmetrical mode of panel;
- Responses of 3rd mode also show that the linear response falls between two BC cases;
- The displacement response of fixed BC better correlates to the case of linear response for frequencies ranging from180Hz to 300Hz;
- Symmetric mode No. 4 and 7 are not excited by the acoustic pressure, which is due to the anti-symmetric nature of the modes in the long direction of panel;
- Peak response of both BC cases has minor shift in frequency, possibly due to the geometric nonlinearity of panel response;
- There are some noticeable responses for frequencies higher than 310 Hz, which correspond to Modes 9 and 11. The two modes are symmetric in both long and short directions of panel.

Approved for public release; distribution unlimited.

Comparison of Normal Displacement at Node 3110916 for Hinged & Fixed BC with Thermal Loads

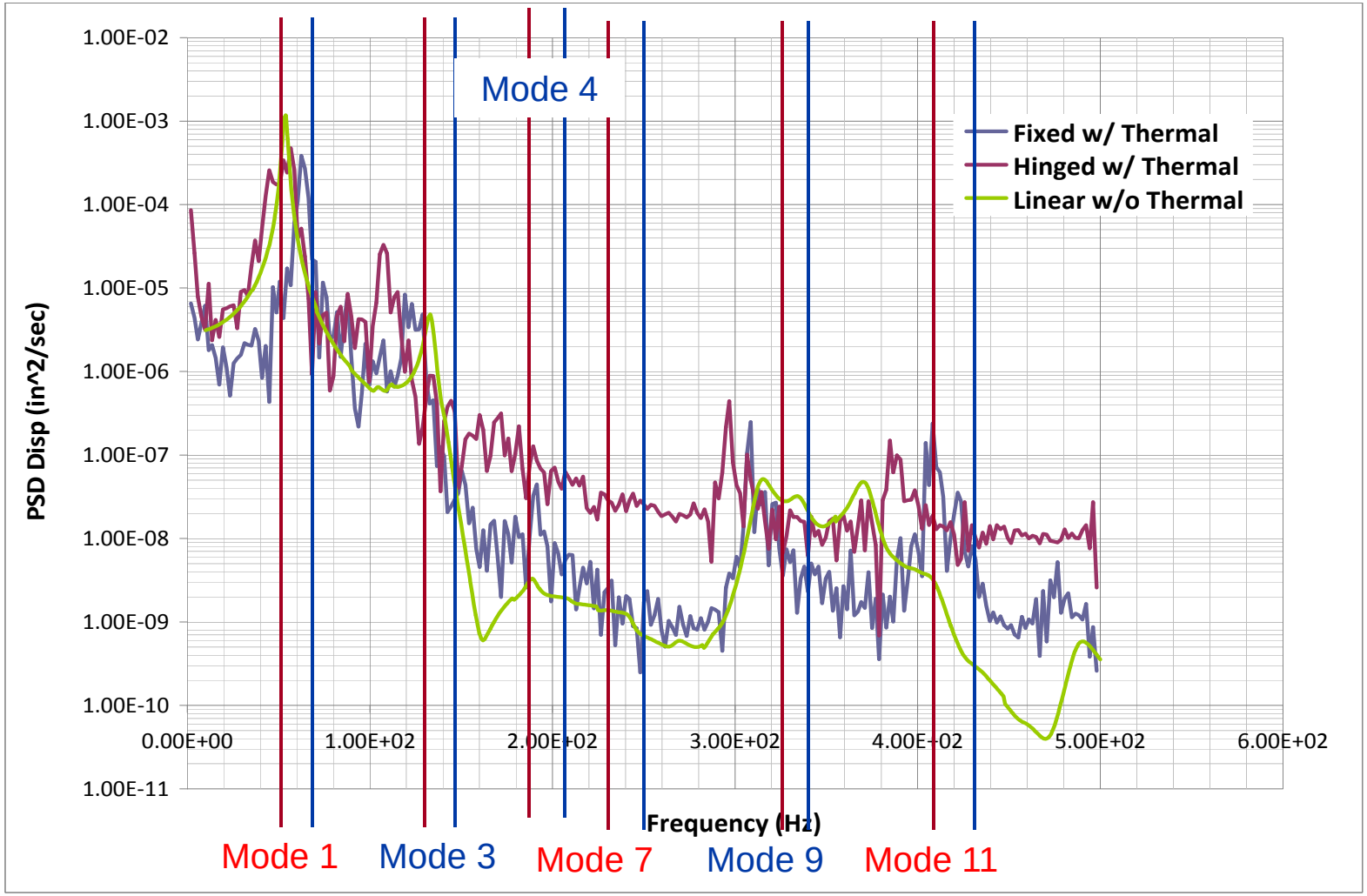

Approved for public release; distribution unlimited.

Comparison of Fiber Stress at Element 311766 for Hinged & Fixed BC w/ Thermal Loads

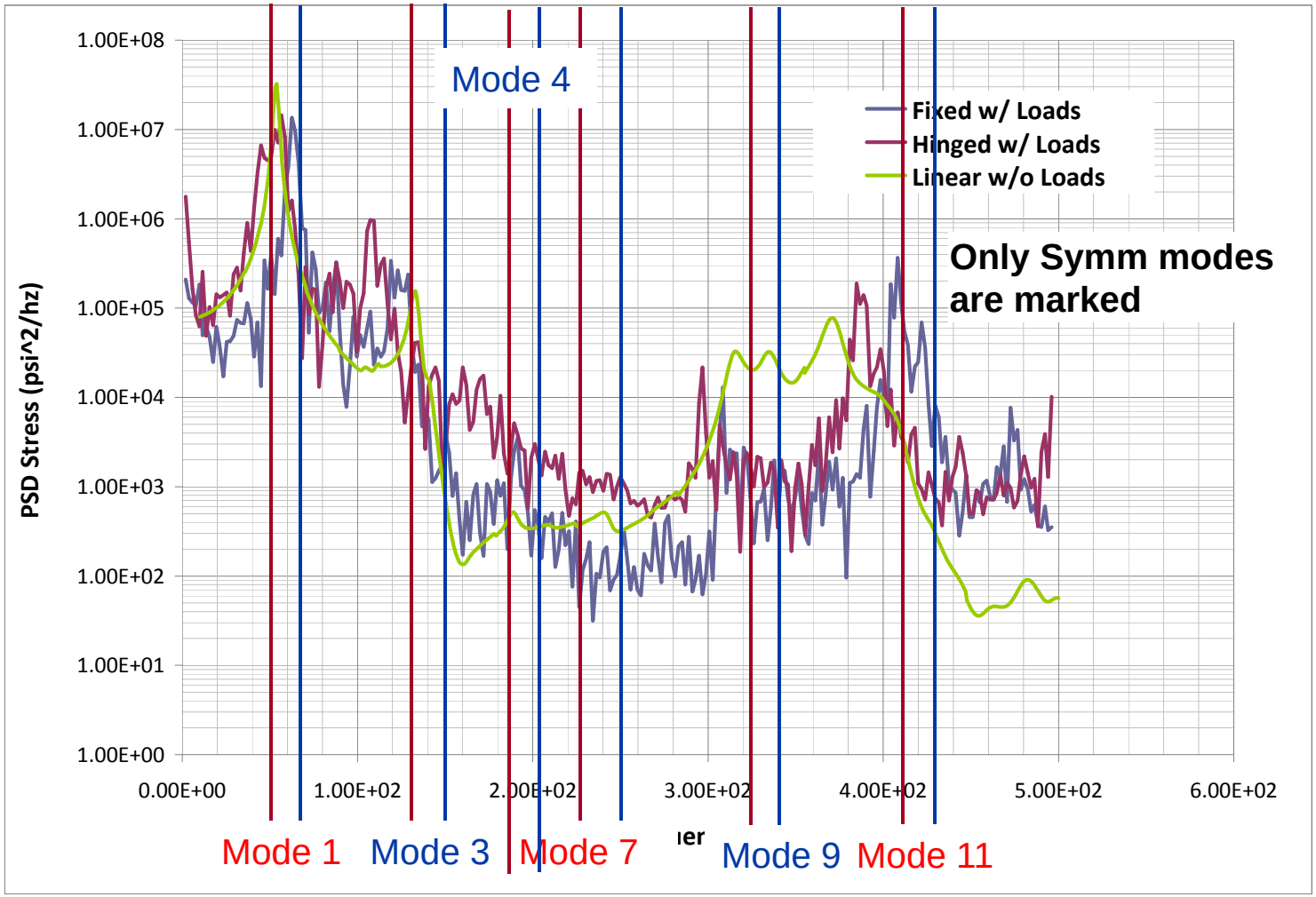

Approved for public release; distribution unlimited.

Notes from Observation

- The responses near the 1st mode for both BC still enclose that from the linear response analysis. However, the bandwidth of response for each BC is wider and the peak is lower than that without thermal loads, which is more obvious for hinged BC than for fixed BC. It is likely the result of the panel stiffness change due to geometric nonlinearity by thermal loads and geometrical stiffness effects, which are more significant for hinged BC than for fixed BC;
- The peak response of both BC shifts to lower frequency ranges as a result of geometric nonlinear effects, which is more significant for higher modes including the 3rd , 9th and 11th modes;
- A minor asymmetry of the system caused by the inclusion of boundary displacements may contribute to the difference between dynamic explicit and linear responses;
- There is a high response for very low frequencies for hinged BC.

Approved for public release; distribution unlimited.

Comparison of Normal Displacement at Node 3110916 for Hinged BC w/ & w/o Thermal Loads

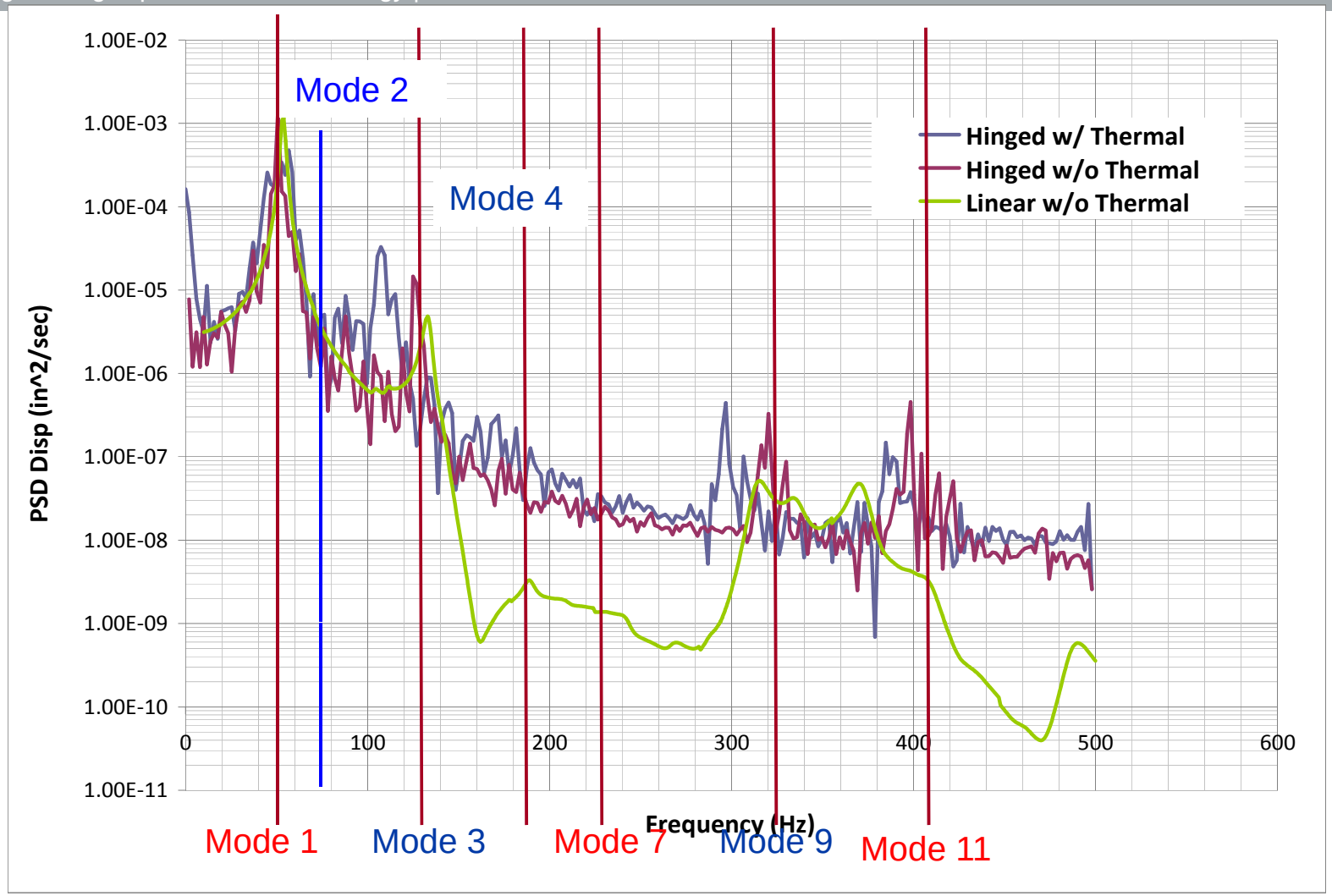

Approved for public release; distribution unlimited.

Comparison of Fiber Stress at Element 311766 for Hinged BC w/ & w/o Thermal Loads

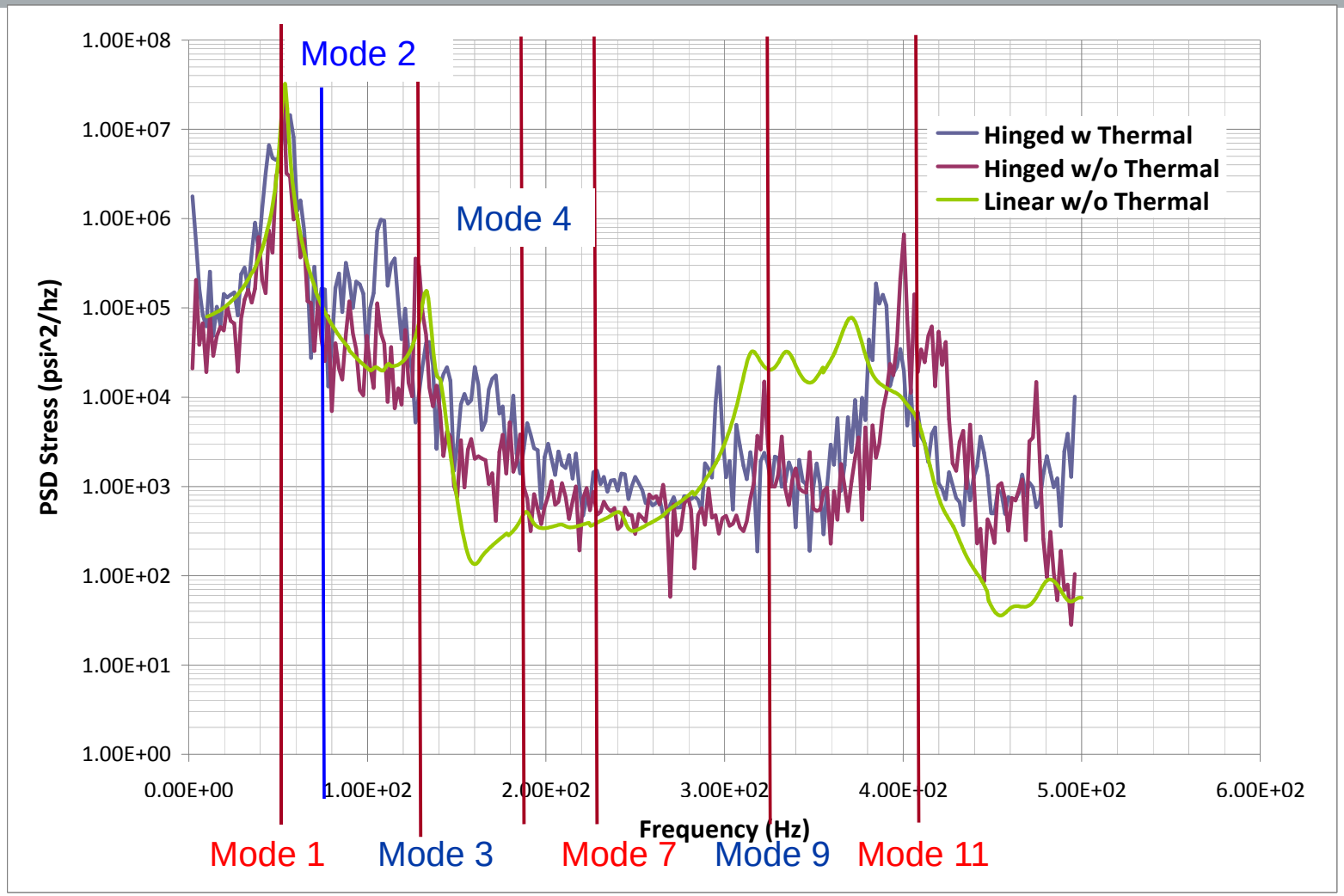

Approved for public release; distribution unlimited.

Notes from Observation

- The PSD plots show that the shift of peak response for 1st mode is relatively minor. This indicates that the stiffness softening due to compression of panel skin may offset stiffness increase due to geometric or deflection effect from thermal loads.
- The effects of thermal loads to the response of 1st mode include wider bandwidth and lower peak of the response;
- There is a noticeable shift of response corresponding to the 3rd mode from 129 Hz to about 107 Hz. Again a wider bandwidth of the response is observed;
- The displacement response of frequencies higher than 140 Hz deviates from the linear analysis result. Comparing with displacement response the stress is closer to the linear response analysis in the higher frequency range.

Approved for public release; distribution unlimited.

Comparison of Normal Displacement at Node 3110916 for Fixed BC w/ & w/o Thermal Loads

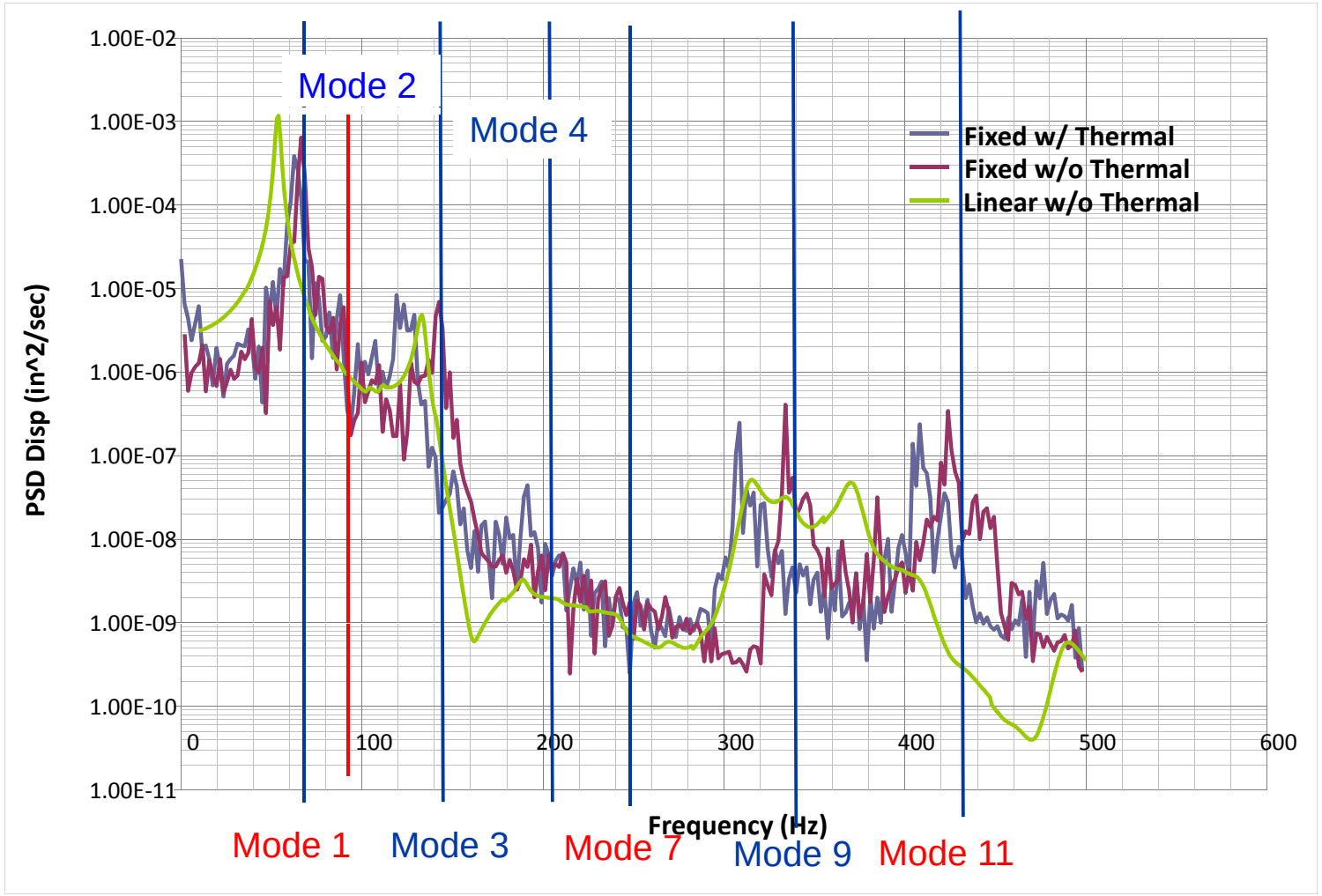

Approved for public release; distribution unlimited.

Comparison of Fiber Stress at Element 311766 for Fixed BC w/ & w/o Thermal Loads

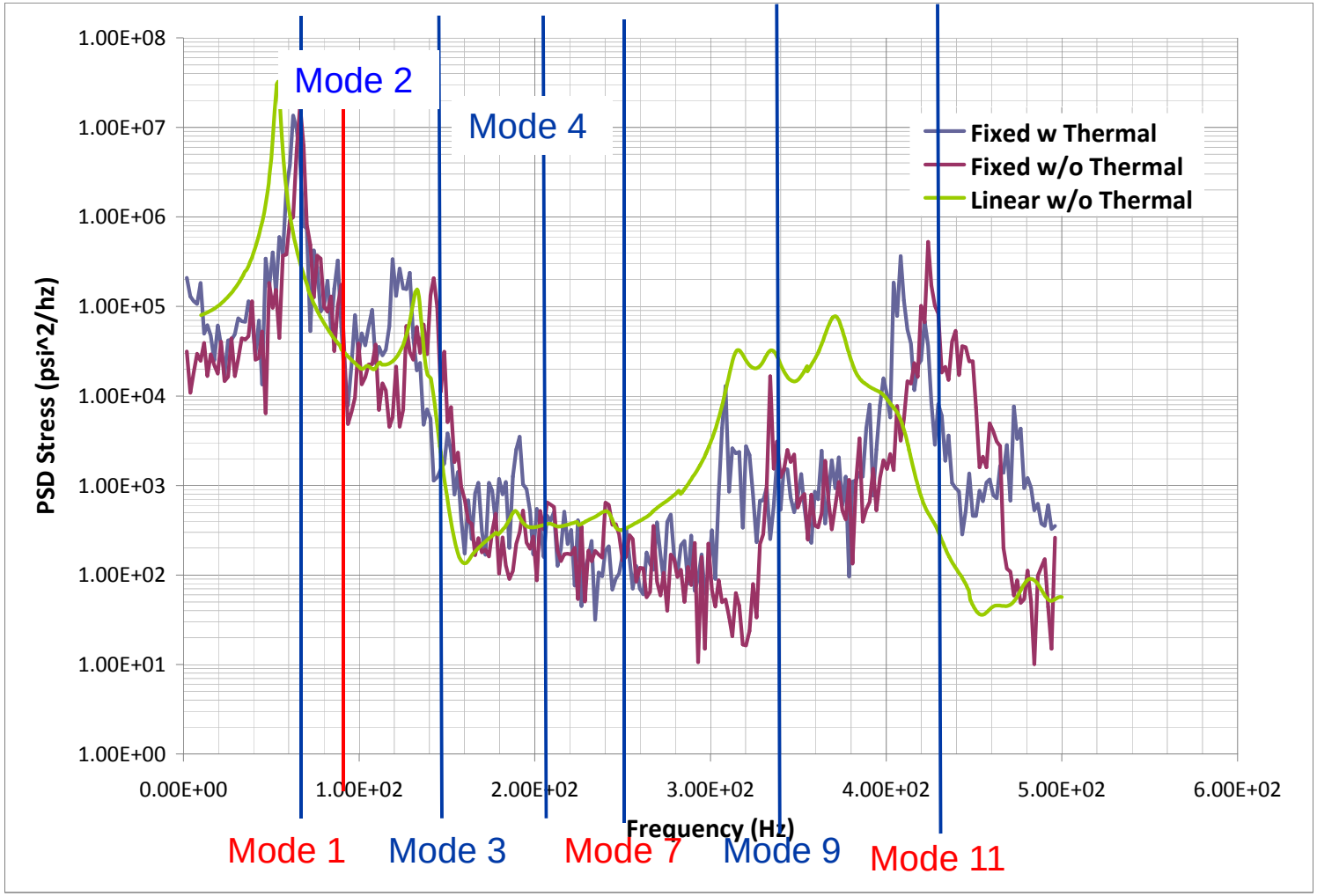

Approved for public release; distribution unlimited.

Notes from Observation

- For the 1st mode the shift of peak response is minor and is similar to the case of hinged BC. The bandwidth increase of fixed BC with thermal loads is not as much as that of hinged BC (due to smaller displacement effect). However, the shift of response for the 3rd mode is significant, and again is similar to the hinged BC case.
- For frequencies ranging from 180 to 290 Hz, the displacement responses for cases with and without thermal loads are closer than that for hinged BC. However, the stress response is not in good agreement;
- Higher responses at frequencies higher than 300 Hz are primarily contributed by Modes 9 and 11, both are symmetric in long and short directions of panel. The magnitude is however small compared to Mode 1.

Approved for public release; distribution unlimited.

Approved for public release; distribution unlimited.